



Sixth International Conference on Stochastic States and Uncertainty Relations

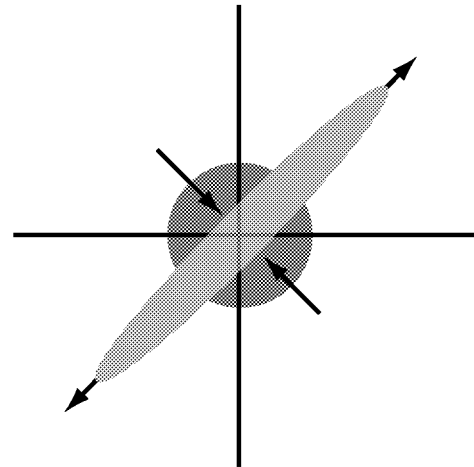
Kim, S. Solimeno, Editors

held at

1999

**Aeronautics and
Space Administration**

**Space Flight Center
Greenland 20771**



The NASA STI Program Office ... in Profile

Since its founding, NASA has been dedicated to the advancement of aeronautics and space science. The NASA Scientific and Technical Information (STI) Program Office plays a key part in helping NASA maintain this important role.

The NASA STI Program Office is operated by Langley Research Center, the lead center for NASA's scientific and technical information. The NASA STI Program Office provides access to the NASA STI Database, the largest collection of aeronautical and space science STI in the world. The Program Office is also NASA's institutional mechanism for disseminating the results of its research and development activities. These results are published by NASA in the NASA STI Report Series, which includes the following report types:

- **TECHNICAL PUBLICATION.** Reports of completed research or a major significant phase of research that present the results of NASA programs and include extensive data or theoretical analysis. Includes compilations of significant scientific and technical data and information deemed to be of continuing reference value. NASA's counterpart of peer-reviewed formal professional papers but has less stringent limitations on manuscript length and extent of graphic presentations.
- **TECHNICAL MEMORANDUM.** Scientific and technical findings that are preliminary or of specialized interest, e.g., quick release reports, working papers, and bibliographies that contain minimal annotation. Does not contain extensive analysis.
- **CONTRACTOR REPORT.** Scientific and technical findings by NASA-sponsored contractors and grantees.
- **CONFERENCE PUBLICATION.** Collected papers from scientific and technical conferences, symposia, seminars, or other meetings sponsored or cosponsored by NASA.
- **SPECIAL PUBLICATION.** Scientific, technical, or historical information from NASA programs, projects, and mission, often concerned with subjects having substantial public interest.
- **TECHNICAL TRANSLATION.** English-language translations of foreign scientific and technical material pertinent to NASA's mission.

Specialized services that complement the STI Program Office's diverse offerings include creating custom thesauri, building customized databases, organizing and publishing research results . . . even providing videos.

For more information about the NASA STI Program Office, see the following:

- Access the NASA STI Program Home Page at <http://www.sti.nasa.gov/STI-homepage.html>
- E-mail your question via the Internet to help@sti.nasa.gov
- Fax your question to the NASA Access Help Desk at (301) 621-0134
- Telephone the NASA Access Help Desk at (301) 621-0390
- Write to:
NASA Access Help Desk
NASA Center for AeroSpace Information
7121 Standard Drive
Hanover, MD 21076-1320

NASA/CP—2000—209899



Sixth International Conference on Squeezed States and Uncertainty Relations

Edited by

D. Han, NASA Goddard Space Flight Center, Greenbelt, Maryland

Y.S. Kim, University of Maryland, College Park, Maryland

S. Solimeno, University of Naples, Naples, Italy

National Aeronautics and
Space Administration

Goddard Space Flight Center
Greenbelt, Maryland 20771

July 2000

Available from:

NASA Center for AeroSpace Information
7121 Standard Drive
Hanover, MD 21076-1320
Price Code: A17

National Technical Information Service
5285 Port Royal Road
Springfield, VA 22161
Price Code: A10

PREFACE

These proceedings collect contributions from about 200 participants to the 6th International Conference on Squeezed States and Uncertainty Relations (ICSSUR'99) held in Naples from May 24–29, 1999, organized jointly by the University of Naples' "Federico II," the University of Maryland at College Park, and the Lebedev Institute, Moscow.

This was the sixth of a series of very successful meetings started in 1990 at the College Park Campus of the University of Maryland. The other meetings of the series were held in Moscow (1992), Baltimore (1993), Taiyuan P.R.C. (1995) and Balatonfüred, Hungary (1997). The present one was held at the campus Monte Sant' Angelo of the University "Federico II" of Naples.

The meeting aimed to provide a forum for updating and reviewing a wide range of quantum optics disciplines, including device developments and applications, and related areas of quantum measurements and quantum noise.

Over the years, the ICSSUR Conference evolved from a meeting on quantum measurement sector of quantum optics, to a wide range of quantum optics themes, including multifacet aspects of generation, measurement, and applications of nonclassical light (squeezed and Schrödinger cat radiation fields, etc.), and encompassing several related areas, ranging from quantum measurement to quantum noise.

ICSSUR'99 brought together about 250 people active in the field of quantum optics, with special emphasis on nonclassical light sources and related areas.

The Conference was organized in 8 Sections:

- A—Squeezed states and uncertainty relations;
- B—Harmonic oscillators and squeeze transformations;
- C—Methods of quantum interference and correlations;
- D—Quantum measurements;
- E—Generation and characterisation of non-classical light;
- F—Quantum noise;
- G—Quantum communication and information;
- H—Quantum-like systems.

In 2001 the Seventh International Conference will be hosted by the University of Boston. The meeting will take place in Boston.

The organizers of the Conference acknowledge the cooperation and the support of several Institutions. Among them, they wish to express special thanks to:

NASA's Goddard Space Flight Center
International Union Pure and Applied Physics (I.U.P.A.P.)
University of Naples "Federico II"
Phys. Dept. Univ. of Naples,
University of Maryland
Istituto Nazionale di Fisica Nucleare (I.N.F.N.)
Istituto Nazionale di Fisica della Materia (I.N.F.M.)

Particular thanks are due to the Soprintendente of the Archeological Museum of Naples for having organized and offered to all participants a guided tour of the most relevant collections originating from the Pompei and Herculaneum ruins.

In parallel to the Conference two short courses on “Optical quantum limits: From theory to engineering” and “Spectroscopic Methods for Quantum State Measurement” were delivered by Profs. Hans Bachor and Suhail Zubairy. These events were sponsored by the Istituto Nazionale di Fisica della Materia (I.N.F.M). and the Graduate School of Physics of Naples.

Sponsors

NASA’s Goddard Space Flight Center
International Union of Pure and Applied Physics (I.U.P.A.P.)
Università “Federico II,” Napoli
Dipartimento Scienze Fisiche, Università “Federico II,” Napoli
University of Maryland, College Park, Maryland
Istituto Nazionale Fisica Nucleare, Roma
Istituto Nazionale Fisica della Materia, Sez. A, Genova
Istituto Italiano per gli Studi Filosofici, Napoli
Gruppo Nazionale di Elettronica Quantistica e Plasmi, C.N.R., Roma
Sovrintendenza Archeologica, Museo Archeologico Nazionale, Napoli
Azienda Autonoma Soggiorno e Turismo, Napoli
Azienda Autonoma Soggiorno e Turismo, Pozzuoli
dB-Electronic Instruments, Milano
Technel, Napoli
Laser Source, Roma

Conference Organization

Organizing Committee

Salvatore Solimeno (Università di Napoli)–Chairman
Renato Fedele (Università di Napoli)
Jozsef Janszky (Institute of Solid State Physics and Optics, Budapest)
Young S. Kim (University of Maryland)
Leopoldo Milano (Università di Napoli)
Vladimir I. Man'ko (Lebedev Physical Institute, Moscow)
Enrico Santamato (Università di Napoli)
Francesco Zaccaria (Università di Napoli)

Local Committee

Marco Fiorentino (Marco.Fiorentino@na.infn.it)
Alberto Porzio (Alberto.Porzio@na.infn.it)

International Advisory Committee

G.S. Agarwal (Ahmedabad)
F.T. Arecchi (Firenze)
H. Bachor (Canberra)
B.A. Bambah (Chandigarh)
K. Boller (Kaiserslautern)
J.F. Cariñena (Zaragoza)
O. Castaños (Mexico City)
C.M. Caves (Albuquerque)

A. Chirkin (Moscow)
F. De Martini (Roma)
M.G. D'Ariano (Pavia)
C. Fabre (Paris)
G. Giacomelli (Firenze)
P. Grangier (Paris)
T.W. Haensch (Firenze Garching)
D. Han (NASA GSFC, Greenbelt)
C.K. Hong (Pohang, Korea)
V. Isakov (Moscow)
M. Kibler (Lyon)
M.S. Kim (Sogang, Korea)
J. Klauder (Florida)
P. Knight (London)
T. Kobayashi (Tokio)
P. Kumar (Evanston)
G. Leuchs (Erlangen)
U. Leonhardt (Ulm)
L. Lugiato (Milano)
M. Man'ko (Moscow)
N. Mukunda (Bangalore)
K. Peng (Taiyuan, P.R.C.)
R. Pike (London)
G. Pogosyan (Dubna)
E. Polzik (Aarus)
M.G. Raymer (Oregon)
M. Rubin (Baltimore)
B.E.A. Saleh (Boston)
W. Schleich (Ulm)
A. Sergienko (Boston)
Y. Shih (Baltimore)
S. Stringari (Trento)
E.C.G. Sudarshan (Austin)
M. Teich (Boston)
G. Tino (Napoli)
P. Tombesi (Camerino)
W. Vogel (Rostock)
A. Vourdas (Liverpool)
H. Walther (München)
D. Walls (Auckland)
D.G. Welsch (Jena)
K.B. Wolf (Cuernavaca)
Ling An Wu (Beijing)
C. Xie (Taiyuan, P.R.C.)
Y. Yamamoto (Palo Alto)
A. Zeilinger (Wien)
P. Zoller (Innsbruck)

Registered Participants

Surname	First name	Affiliation	mailing address(1)	mailing address(2)	mailing address(3)
Agarwal	G.S.	Physical Research Laboratory	Physical Research Laboratory, Navrangpura	Ahmedabad - 380 009	India
Aliaga	Jorge	Buenos Aires University	Phys. Dep. Buenos Aires University	Pab I, Ciudad Universitaria, (1428) Buenos Aires,	Argentina
Alodjants	Alexander	Vladimir State University	Department of Physics and Applied Mathematics	Gorky str.87, 600026 Vladimir	Russia
Altevogt	Torsten	Humboldt-Universität Berlin	Institut für Physik, Humboldt-Universität	Hausvogteiplatz 5-7, D-10117 Berlin	Germany
Anagnostakis	Emmanuel A.	Hellenic Army Academy	The Laboratory of Physics, Hellenic Army Academy	72 Cyprus Str., GR 112 57 Athens	Greece
Anderson	Dan	Department of Electromagnetics	Chalmers University of Technology	S-41296 Goteborg	Sweden
Andreev	Vladimir	Lebedev Institute	Optical Department, Lebedev Institute	Leninsky Prospect 53, 117924 Moscow	Russia
Ariunbold	Gombojav	Palacky University	Department of Optics Palacky University	17. Listopadu 50, Olomouc 77207	Czech Republic
Arnoldus	Henk F.	Mississippi State University	Department of Physics and Astronomy, Mississippi State University	P.O. Drawer 5167, Mississippi State, MS 39762	USA
Arvieu	Robert	Universite' de Grenoble	Institut Des sciences Nuclearies	53, Avenue des martyrs, 38026 Grenoble CEDEX	France
Arvind		Guru Nanak Dev University, Amritsar	Department of Physics, Guru Nanak Dev University, Amritsar	Amritsar, 143005 Punjab	India
Avram	Calin	West University of Timisoara, Phys. Dept.	University of Timisoara, Phys. dept.	Bv. Vasile Pirvan Nr.4	1900 TIMISOARA ROMANIA
Avram	Nicolae	West University of Timisoara, Phys. Dept.	University of Timisoara, Phys. dept.	Bv. Vasile Pirvan Nr.4	1900 TIMISOARA ROMANIA
Bachor	Hans	Australian National University	Physics Department, The Australian National University	Canberra ACT 0200	Australia

Ballesteros	Angel	Universidad de Burgos	Departamento de Fisica, Facultad de Ciencias, Universidad de Burgos	09001-Burgos	Spain
Bambah	Bindu	Centre for advanced studies in Mathematics	Dept. of Mathematics	Panjab University, Chandigarh	Chandigarh 160014, India
Banaszek	Konrad	Warsaw University	Instytut Fizyki Teoretycznej UW	Hoza 69	PL-00-681 Warszawa POLAND
Bandyopadhyay	Somshubhro	Bose Institute	Dept. of Physics, Bose Institute	93/1 A.P.C. Road	Calcutta - 700009 India
Banerji	J.	Physical Research Laboratory	Physical Research Laboratory	Navrangpura Ahmebad 380 009	INDIA
Barone	Antonio	Università di Napoli			
Bartlett	Stephen	University of Toronto	Department of Physics University of Toronto	60 Saint George Street	Toronto, Ontario, CANADA M5S 1A7
Bashkov	Victor	Kazan State University, Physical Department	Kazan State University, Physical Department	Kremlevskaya, 18, KAZAN	420008, RUSSIA
Baskal	Sibel	Middle East Technical University Ankara-Turkey	Department of Physics	Middle East Technical University	06531 Ankara-Turkey
Becher	Christoph	Universitaet Kaiserslautern			
Beckers	Jules	University of Liege	Institute of Physics (B.5)	University of Liege	B-4000 Liege 1 Belgium
Ben-Aryeh	Yacob	Technion-Israel Institute of Technology	Physics Department	Technion-Israel Institute of Technology	Haifa, 3200, ISRAEL
Berardi	Vincenzo	Università di Bari	Dipartimento Interateneo di Fisica, Università di Bari	Via E. Orabona n.4	70125 Bari (Italy)
Berkovich	Lev	Samara State University	Department of Mechanics & Mathematics	Acad. Pavlov, Str. , 1	443 011, Samara, Russia
Berlin	Guido	Buenos Aires University	Phys. Dep. Beunos Aires University	Pab I, Ciudad Universitaria	(1428) Buenos Aires, Argentina
Bessonov	Evgueni	Lebedev Physical Institute	Lebedev Physical Institute	Lebedev Physical Institute	117924, Moscow, Russia
Bouchoule	Isabelle	Laboratoire Kastler Brossel, ENS,	Laboratoire Kastler Brossel, ENS,	24 rue Lhomond, 75231 Paris	France
Brambilla	Enrico	Università di Milano	Dipartimento di Fisica, Sezione di Ottica Quantistica, Università di Milano	Via Celoria 16	20133 Milano

Brattke	Simon	Max Planck Insistute For Quantum Optics	Max Planck Insistute For Quantum Optics	Hans-Kopfermann str. 1 Garching bei Muenchen D-85748	Germany
Braunstein	Samuel L.	University of Wales	SEECs, Dean Street University of Wales	Bangor LL57 1UT	United Kingdom
Calarco	Tommaso	Universitaet Innsbruck	Institut fuer Theoretische Physik	Technikerstrasse 25/2, A-6020	Austria
Carinena	Josè F.	Universidad de Zaragoza	Departamento de Fisica Teorica, Universidad de Zaragoza	50.009, Zaragoza	Spain
Casado	Alberto	Universidad de Sevilla	Departamento de Fisica Aplicada, Universidad de Sevilla	Avenida de los Descubrimientos S/N	41092 Sevilla, Spain
Chaturvedi	Subhash	University of Hyderabad	School of Physics	University of Hyderabad	Hyderabad 500046 India
Chirkin	Anatoly	Lomonosov Moscow State University	Faculty of Physics,	Lomonosov Moscow State University Moscow 119899	Russia
Ciattoni	Alessandro	Università degli Studi de L'Aquila	Dipartimento di Fisica	via Vetoio	67100 Coppito, L'Aquila, Italy
Compagno	Giuseppe	Università di Palermo	Dipartimento di Scienze Fisiche ed Astronomiche, Università di Palermo	via Architrafì 36	90123 Palermo Italy
Courty	Jean-Michel	Laboratoire Kastler Brossel	Laboratoire Kastler Brossel, UPMC, Case 74	4, Place Jussieu, 75252 Paris 05	France
Crawford	Michael	University of Waterloo	Dept of Applied Math, U. of Waterloo	Waterloo, Ontario	Canada, N2L 3G1
Czachor	Marek	Arnold Sommerfeld Institute	Arnold Sommerfeld Institute	TU-Clausthal Leibniz str. 10	D-38678 Clausthal- Zellerfeld, Germany
D'Ariano	Giacomo Mauro	Università di Pavia	Dipartimento di Fisica "A. Volta"	Via Bassi 6, I-27100 Pavia	Italy
<i>De Martini</i>	<i>Francesco</i>	Università di Roma "La Sapienza"			Italy
De Martino	Salvatore	Università di Salerno	Dipartimento di Fisica, Università di Salerno	Baronissi (SA) - 84081	Italy
de Muyncck	Willem	Eindhoven University of Technology	Eindhoven University of Technology	POB 513	5600 MB Eindhoven, the Netherlands
De Siena	Silvio	Università di Salerno	Dipartimento di Fisica, Università di Salerno	Baronissi (SA) - 84081	Italy
De Zela	Francisco	Pontificia Universidad Catolica del Peru	Pontificia Universidad Catolica del Peru	Dpto. de Ciencias / Seccion Fisica	Ap. 1761 LIMA-PERU

Di Fidio	Christian	Universitaet Rostock	Arbeitsgruppe Quantenoptik, Fachbereich Physik, Universitaet Rostock	Universitaetsplatz 3	D-18051 Rostock, Germany
Di Virgilio	Angela	INFN Pisa	INFN, Sez. di Pisa	via Vecchia Livornese	56010 S. Piero a Grado (Pisa), Italy
Djordjevic	Goran	University of Nis	Department of Physics, University of Nis	P.O.Box 91	18001 Nis, Yugoslavia
Dodonov	Victor	Federal University of Sao Carlos	Departamento de Fisica, Universidade Federal de Sao Carlos	Via Washington Luiz, km 235,	13565-905 Sao Carlos, SP, Brasil
Doebner	H.-D.	Arnold Sommerfeld Institut	der TU Clausthal, Leibnizstraße 10	38678 Clausthal-Zellerfeld	Germany
Dowling	Jonathan	NASA Jet Propulsion Laboratory, California Institute of Technology	Quantum Information Project	Mail Stop 126-347, 4800 Oak Grove Drive	Pasadena, California 91109 USA
Draganescu	Gheorghe Eugen	West University of Timisoara, Phys. Dept.	University of Timisoara, Phys. dept.	Bv. Vasile Pirvan Nr.4	1900 TIMISOARA ROMANIA
Duerr	Stephan	Universitaet Konstanz	University of Konstanz	Department of Physics 78457 Konstanz	Germany
Duras	Maciej	Cracow University of Technology	Institute of Physics Cracow University of Technology	ulica Podchorazych 1	PL-30-084 Cracow, Poland
Dutra	Sergio M.	University of Leiden	Quantum Optica, Huygens Laboratorium, University of Leiden	Rijksuniversiteit Leiden, P.O. Box 9504	2300 RA Leiden, The Netherlands
Esslinger	Tilman	Universität München	Universität München Sektion Physik	Schellingstr. 4 80799 München	Germany
<i>Fabre</i>	<i>Claude</i>	Laboratoire Kastler-Brossel	Laboratoire Kastler-Brossel Département de Physique	24, rue Lhomond F-75231 Paris CEDEX 05	France
Facchi	Paolo	Università di Bari	Dipartimento di Fisica, Università di Bari	via Amendola 173	70126 Bari, Italy
Fedele	Renato	Università di Napoli	Dipartimento di Scienze Fisiche	Complesso Universitario di Monte Sant'Angelo	via Cintia 80126 Napoli, Italy
Feng	Yinqi	Quantum Processes Group, The Open University	Applied Mathematics Department, The Open University	Milton Keynes, MK7 6AA	UK

Fernandez C.	David J.	Physics Department, CINVESTAV	Physics Department, CINVESTAV	A.P. 14-740, O7000 Mexico D.F.	MEXICO
Ficek	Zbigniew	The University of Queensland	Department of Physics	The University of Queensland	Brisbane, Australia 4072
Fiorentino	Marco	Università di Napoli	Dipartimento di Scienze Fisiche	Complesso Universitario di Monte Sant'Angelo	via Cintia 80126 Napoli, Italy
Fort	Chiara	Università di Firenze, LENS	European Laboratory for non Linear Spectroscopy (LENS), University of Florence	Largo Enrico Fermi 2, 50125 Firenze	Italy
Fortunato	Mauro	Università di Camerino	Università di Camerino	Via Madonna delle Carceri	I-62032 Camerino (MC) Italy
Fu	Hongchen	The Open University	Applied Mathematics Department, The Open University	Milton Keynes, MK7 6AA	UK
Fujii	Mikio	Waseda University	Department of Physics, Waseda University	Ohkubo 3-4-1, Shinjuku	Tokyo, 169-0072, Japan
Garcia-Fernandez	Priscila	Instituto de Estructura de la Materia. CSIC	Instituto de Estructura de la Materia	CSIC C/ Serrano 123,	28006 Madrid, Spain
Garuccio	Augusto	Università di Bari	Dipartimento interateneo di Fisica - INFN sez. di Bari	Via Amendola 173, 70126 Bari	Italy
Gasparoni	Sara	Università di Napoli	Dipartimento di Scienze Fisiche	Complesso Universitario di Monte Sant'Angelo	via Cintia 80126 Napoli, Italy
Genovese	Marco	Istituto Elettrotecnico Nazionale Galileo Ferraris	IEN Metf	Str. delle Cacce 91	10135 Torino, Italy
Geron	Christine	University of Liege	Institute of Physics (B.5)	University of Liege	B-4000 Liege 1 Belgium
Gevorkyan	Ashot	Institute for high-performance computing and data base	Institute for high-performance computing and data base	P/O BOX 71	194291, St-Petersburg, Russia
Gianfrani	Livio	Università di Napoli	Dipartimento di Scienze Fisiche	Complesso Universitario di Monte Sant'Angelo	via Cintia 80126 Napoli, Italy
Graham	Robert	Universitaet Essen	Fachbereich Physik Universitaet	Essen	D 45117 Essen, Germany
Grangier	Philippe	Institut d'Optique, Orsay	Institut d'Optique	B.P. 147 - F91403 Orsay cedex	France
Granik	Alex	University of the Pacific	Physics Dept, UOP	Stockton	CA 95211, USA
Hansen	Hauke	University of Konstanz, Prof. J. Mlynek	Fakultaet fuer Physik Fach M696	Universitaet Konstanz	78457 Konstanz, Germany

Hermier	Jean - Pierre	Laboratoire Kastler Brossel	Laboratoire Kastler Brossel Tour 12 1er étage, case 74	Université Pierre et Marie Curie 4 place Jussieu	75252 Paris Cedex 05 France
Horoshko	Dmitri	Stepanov Institute of Physics, Minsk	Stepanov Institute of Physics, Minsk	F.Skarina Ave. 70	Minsk 220072 Belarus
Hradil	Zdenek	Palaky University	Department of Optics	17. listopadu 50, 772 00 Olomouc.	Czech Republic.
Hussin	Véronique	CRM, Université de Montréal	CRM, Université de Montréal	CP6128, Succursale Centre-Ville	Montréal, Québec H3C 3J7 CANADA
Ignatovich	Vladimir	Joint Institute for Nuclear Research	JINR, FLNP	Dubna Moscow region	141980 Russia
Illuminati	Fabrizio	Università di Salerno	Dipartimento di Fisica, Università di Salerno	I--84081 Baronissi (SA) Italia	
Isakov	Vladimir	Russian Academy of Sciences	P.N. Lebedev Physical Institute, Russian Academy of Sciences	Leninskii prosp. 53	Moscow 117924, Russia
Janszky	Jozsef				
Johansen	Lars M.	Buskerud College	Buskerud College	P.O. Box 251	N-3601 Kongsberg, Norway
Jonathan		Imperial College	Blackett Laboratory, Imperial College	London SW7 2BZ	Great Britain
Joosten	Krista	Leiden University	Huygens Laboratory, Leiden University	P.O. Box 9504	2300 RA Leiden, The Netherlands
Joshi	Amitabh	BARC	D-14, Ellora	Anushaktinagar	Bombay 400 094, India
Khan	Sameen A.	Universita di Padova, INFN-Padova	Dipartimento di Fisica Galileo Galilei, Università di Padova	Via Marzolo 8	Padova 35131 ITALY
Khodin	Alexander	National Academy of Sciences, Belarus	Institute of Electronics, National Academy of Sciences	Logoisky tract 22,	220090, Minsk, Republic of Belarus
Khrennikov	Andrei	Vaxjo Univetsity	Dept. Math., Stat. and Computer Sciences	University of Vaxjo	S35195,Vaxjo Sweden
Kim	Young S.	University of Maryland	University of Maryland	College Park, MD 20742	USA
Klimov	Vasily	P.N.Lebedev Physics Institute	P.N.Lebedev Physics Institute	Leninskii prospect, 53,	117924, Moscow, Russia
Korolkova	Natalja	Universität Erlangen-Nürnberg	Lehrstuhl für Optik Physikalisches Institut Universität Erlangen-Nürnberg	Staudtstr. 7/B2 91058 Erlangen	Germany

Kovacs	Amos	Technion	CEMA (T1)	P.O.Box 2250	Haifa 31021, Israel
Kretzschmar	Martin	Johannes-Gutenberg-University	Institut fuer Physik, Johannes-Gutenberg-University	55099 Mainz	Germany
Kulagin	Victor V.	Sternberg Astronomical Institute of Moscow State University	Sternberg Astronomical Institute of Moscow State University	Universitetsky prosp. 13	Moscow, 119899, Russia
Kumar	Prem	Northwestern University	ECE Department, Northwestern University	2145 N. Sheridan Rd., Evanston, IL 60208-3118	USA
Lahti	Pekka	University of Turku	Department of Physics	University of Turku	20014 Turku, Finland
Lam	Ping Koy				
Lantz	Eric				
Lugiato	Luigi	Università di Milano			Italy
Lukic	Dragan	INSTITUTE OF PHYSICS	INSTITUTE OF PHYSICS	PO BOX 57	11081 BELGRADE, YUGOSLAVIA
Luks		Palacky University	Faculty of Natural Sciences, Palacky University	Trida Svobody 26, 771 46 Olomouc	Czech Republic
Macchiavello	Chiara	Università di Pavia	Dipartimento di Fisica "A. Volta"	Via Bassi 6, I-27100 Pavia	Italy
Malakhaltsev	Mikhail	Kazan State University, Mathematical Department	Kazan State University, Mathematical Department	Kremlevskaya, 18, KAZAN	420008, RUSSIA
Maniscalco	Sabrina	Dipartimento di Scienze Fisiche ed Astronomiche	Dipartimento di Scienze Fisiche ed Astronomiche	via Archirafi 36	90123 Palermo Italy
Man'ko	Margarita	P.N. Lebedev Physical Institute	Lebedev Institute of Physics	Leninski pr. 53 , Moscow	Russia 117924
Man'ko	Olga	P.N. Lebedev Physical Institute	Lebedev Institute of Physics	Leninski pr. 53 , Moscow	Russia 117924
Man'ko	Vladimir	P.N. Lebedev Physical Institute	Lebedev Institute of Physics	Leninski pr. 53 , Moscow 117924	Russia
Marchioli	Marcelo A.	Universidade de Sao Paulo	Instituto de Fisica de Sao Carlos,	Grupo de Optica, Caixa Postal 369	13560-970 Sao Carlos, SP, Brazil
Mataloni	Paolo	Università "La Sapienza", Roma	Dipartimento di Fisica, Università di Roma "La Sapienza"	P.le A.Moro 2 ROMA	00185 ITALY
Maybourov	Sergey	Lebedev Institute of Physics	Lebedev Institute of Physics	Leninski pr. 53 , Moscow	Russia 117924
Messina	Antonino	Dipartimento di Scienze Fisiche ed Astronomiche	Dipartimento di Scienze Fisiche ed Astronomiche	via Archirafi 36	90123 Palermo Italy

Mizrahi	Salomon S.	Universidade Federal de Sao Carlos	Departamento de Fisica, CCET, Universidade Federal de Sao Carlos	via Washington Luiz km 235	13565-905 Sao Carlos, SP, Brasil
Moelmer	Klaus	University of Aarhus	Institute of Physics and Astronomy, University of Aarhus	Ny Munkegade, DK 8000 Aarhus C	Denmark
Moya-Cessa	Hector	Universita di Camerino	Universita di Camerino	Via Madonna delle Carceri	I-62032 Camerino (Mc) Italy
Mueller	Joerg Helge	INFN Unita' di Pisa	INFN Unita' di Pisa Universita' Dipartimento di Fisica Via Buonarroti 2	56127 Pisa	ITALY
Mukunda	N.	Indian Institute of Science	Centre for theoretical Studies	Indian Institute of Science, Bangalore 560012	India
Muminov	Khikmat	JINR	734025, Tajik State National University, Physics Department,	Rudaki street, 17,	Dushanbe, TAJIKISTAN
Napoli	Anna	Dipartimento di Scienze Fisiche ed Astronomiche	Dipartimento di Scienze Fisiche ed Astronomiche	via Archirafi 36	90123 Palermo Italy
Negrao da Silva Guerreiro	Ariel Ricardo	Centro de Fisica dos Plasmas	Instituto Superior Tecnico, Complexo Interdisciplinar, Centro de Fisica dos Plasmas	Av. Rovisco Pais	1096 Lisboa Codex, Portugal
Negro	Javier	Univ de Valladolid	Departemento de fisica teorica	Univ de Valladolid	47005 Valladolid, SPAIN
Nieto	Luis Miguel	Univ de Valladolid	Departemento de fisica teorica	Univ de Valladolid	47005 Valladolid, SPAIN
Nögel	Ulrich	Universität Kaiserslautern	Universität Kaiserslautern	Erwin-Schrödinger Straße	D-67663 Kaiserslautern, Germany
Obada	Abdel-Shafy Fahmy	Al-Azhar University	Departement of Mathematics, Faculty of Science	Nasr City 11884	Cairo, Egypt
O'Connel	Robert	Louisiana State University	Dept.of Physics	Baton Rouge	Louisiana 70803-4001,USA
Orlowski	Arkadiusz	Polish Academy of Sciences	Instytut Fizyki PAN	Aleja Lotnikow 32/46	02-668 Warszawa Poland
Orozco	Luis	State University of New York at Stony Brook	Dept. Physics and Astronomy, Sunvsb	Stony Brook	NY 11794-3800 USA
Palma	G. Massimo	Universita' di Palermo	Universita' di Palermo Phys. Dept	VIA ARCHIRAFI 36	90123 PALERMO, Italy

Paris	Matteo	Università di Pavia	Dipartimento di Fisica A. Volta		
Pascazio	Saverio	Università di Bari	Dipartimento di Fisica Università di Bari	Via Amendola 173, 70126 Bari	Italy
Pati	Arun Kumar	University of Wales	SEECs, Dean Street	University of Wales	Bangor LL 57 1UT, UK
Peng	Kunchi	Shanxi University	Institute of Opto-Electronics, Shanxi University	Taiyuan, Shanxi, 030006	P.R.China
Penson	Karol	Université Pierre et Marie Curie	Lab. Physique Theorique des Liquides , Université Paris 6	4, place Jussieu, Tour 16	75252 Paris Cedex 05, France
Perina	Jan	Palacky University	Faculty of Natural Sciences, Palacky University	Trida Svobody 26, 771 46 Olomouc	Czech Republic
Pinard	Michel	Laboratoire Kastler-Brossel	Laboratoire Kastler-Brossel Département de Physique	24, rue Lhomond F-75231 Paris CEDEX 05	France
Plastina	Francesco	Dip. Fisica Università della Calabria	Dip. Fisica Università della Calabria	87036 Arcavacata di Rende (CS)	Italy
Polzik	Eugene S.	Institute of Physics and Astronomy, Aarhus University	Institute of Physics and Astronomy, Aarhus University	8000, Aarhus,	Denmark
Porzio	Alberto	Università di Napoli	Dipartimento di Scienze Fisiche	Complesso Universitario di Monte Sant'Angelo	via Cintia 80126 Napoli, Italy
Rasetti	Mario	Politecnico di Torino	Politecnico di Torino	Corso Duca degli Abruzzi, 24, 10129 Torino	Italy
Rauch	Helmuth	Atominsttitut der Oesterreichischen Universitaeten	Atominsttitut der Oesterreichischen Universitaeten	Stadionallee 2	A-1020 Wien
Reznik	Benni	Tel Aviv University	School of Physics, Tel Aviv University	Tel-Aviv 69978	Israel
Rica da Silva	Amaro	Physics Dept. - I.S.T.	Dpto Fisica	Av. Rovisco Pais	1096 Lisboa Portugal
Richter	Thomas	Humboldt-Universitaet zu Berlin	Arbeitsgruppe "Nichtklassische Strahlung", Institut fuer Physik, Humboldt-Universitaet zu Berlin	Invalidenstr. 110	10115 Berlin, Germany
Rojo	Alberto	University of Michigan	Department of Physics, University of Michigan	2071 Randall Lab, Ann Arbor, MI 49109-1120,	USA
Romera	Elvira	Universidad de Granada	Instituto Carlos I de Fisica Teorica y Computacional	Avda. Fuentenueva s/n	E-18071 Granada Spain
Roncadelli	Marco	INFN, Pavia			

Rosas-Ortiz	J.Oscar	Universidad de Valladolid	Departamento de Fisica Teorica Facultad de Ciencias	Universidad de Valladolid	47011 Valladolid, Spain
Rosu	Hartet	GUANAJUATO UNIV., MEXICO	IFUG, APDO POSTAL E-143.	LEON, GTO, MEXICO	
Rubin	Morton H.	University of Maryland, Baltimore County	University of Maryland, Baltimore County	Physics Department 1000 Hilltop Circle	Baltimore, MD 21250, USA
Sakaguchi	Fuminori	Fukui University	Dept. of Electrical and Electronics Engineering Faculty of Engineering, Fukui University	3-9-1 Bunkyo	Fukui 910-8507 JAPAN
Saleh	Bahaa	Boston University	Departments of Electrical & Computer Engineering, Physics, and Biomedical Engineering	Boston University, 8 Saint Mary's Street, Boston, Massachusetts 02215-2421,	USA
Santamato	Enrico	Università di Napoli	Dipartimento di Scienze Fisiche	Complesso Universitario di Monte Sant'Angelo	via Cintia 80126 Napoli, Italy
Sapogin	Lev	Moscow T.U.	Physics Department, Technical University (MADI)	Leningradsky prospect 64	A-319, 125829, GSP Moscow, Russia
Saxena	G.M.				
Sazonova	Zoia S.	Moscow State Automobile & Road Construction Institute	Moscow State Automobile & Road Construction Institute (Technical University)	64, Leningradsky prospect, Moscow	Russia
Schamel	Hans	Universitaet Bayreuth	Universitaet Bayreuth	Theoretische Physik IV	D-95440 Bayreuth Germany
Schmidt	Eduard	Friedrich-Schiller Universitaet Jena	Theoretisch-Physikalisches Institut, Friedrich-Schiller Universitaet Jena	Max-Wien-Platz 1	D-07743, Jena, Germany
Sergienko	A.V.	Boston University Dept. of E.C.E	Boston University	8 Saint Mary's St. Boston, MA 02215-2421	USA
Seshadri	Sampath	Indian Institute of Technology	Department of Physics Indian Institute of Technology	Madras	Chennai 600036, India
Shatokhin	Vyatcheslav	National Academy of Sciences, Belarus	Institute of Physics National Academy of Sciences of Belarus	70, F.Scaryna Ave.	Minsk 220072, Belarus

Shih	Yanhua	University of Maryland	Department of Physics	University of Maryland, Baltimore County	Baltimore, MD 21250, USA
Shumovsky	Alexander	Bilkent Univerrcity	Department of Physics, Bilkent University	Bilkent	06533 Ankara Turkey
Sibilia	Concita	Universita' di Roam " La Sapienza"	Universita' di Roam " La Sapienza" Dip. di Energetica	Via Scaroa 16	00161 Roma Italy
Silvestrini	Paolo	CNR - Arco Felice			Italy
Simon	Rajiah	The Institute of Mathematical Sciences	C.I.T. Campus, Tharamani	Chennai (Madras) Tamilnadu - 600 113	India
Singh	Ranjit	Russian Accademy of Sciences	General Physics Institute of Russian Academy of Sciences	Wave Research Center, 38, Vavilov street	Moscow 117942, Russian Federation
Sintsova	Yulia	Kazan State University, Physical Department	Kazan State University, Physical Department	Kremlevskaya, 18, KAZAN	420008, RUSSIA
Sizmann	Andreas	Universität Erlangen-Nürnberg	Lehrstuhl für Optik Universität Erlangen-Nürnberg	Staudtstr. 7/B2 91058 Erlangen	Germany
Smerzi	Augusto	SISSA - Trieste	via Beirut 2/4	I-34014 Trieste	Italy
Sokolov	V.I	St.-Petersburg State University	Physics Institute, St.-Petersburg State University	198904 St. Petersburg , Petrodvotetz	Russia
Solimeno	Salvatore	Università di Napoli	Dipartimento di Scienze Fisiche	Complesso Universitario di Monte Sant'Angelo	via Cintia 80126 Napoli, Italy
Solomon	Allan	The Open University	Applied Mathematics Department	The Open University	Milton Keynes, MK7 6AA, UK
Sorensen	Anders	University of Aarhus	Institute of Physics and Astronomy, University of Aarhus	Ny Munkegade, DK 8000 Aarhus C	Denmark
Stergioulas	Lampros	Manchester University	Manchester School of Engineering, The University of Manchester	Simon Building, Oxford Road	Manchester, M13 9PL, UK
<i>Stringari</i>	<i>Sandro</i>	Università di Trento			
Sudarshan	George	University of Texas			USA
Swain	Stuart	Queen's University, Belfast	Applied Math. Dept., Queen's University	Belfast BTY 1NN, U.K.	
Takeuchi	Shigeki	ATRC, Mitsubishi Electric Corporation	ATRC, Mitsubishi Electric Corporation	Tsukaguchi-Hommachi, Amagasaki	Hyogo 661-8661 JAPAN

Tanas	Ryszard	Adam Mickiewicz University, Poznan, Poland	Nonlinear Optics Division, Institute of Physics, Adam Mickiewicz University.	Umultowska 85	61-614 Poznan, Poland
Teich	Malvin C.	Boston University	Departments of Electrical & Computer Engineering, Physics, and Biomedical Engineering	Boston University, 8 Saint Mary's Street, Boston, Massachusetts 02215-2421,	USA
Terra Cunha	Marcelo de O.	Universidade Federal de Minas Gerais	Departamento de Matematica, Universidade Federal de Minas Gerais	C.P. 702 Belo Horizonte - MG	30123-970 - Brazil
Tino	Guglielmo	Università di Napoli	Dipartimento di Scienze Fisiche	Complesso Universitario di Monte Sant'Angelo	via Cintia 80126 Napoli, Italy
Tittel	Wofgang	University of Geneva	Group of Applied Physics, University of Geneva	20, rue de l'Ecole de Medecine, CH-1211 Geneva 4	Switzerland
Tombesi	Paolo	Università di Camerino			Italy
Torelli	G.	Università di Pisa	Dipartimento di Fisica, Università di Pisa	Piazza Torricelli,2	I-56100 Pisa
Treps	Nicolas	Ecole Normale Superieure	Laboratoire Kastler Brossel, Ecole Normale Superieure	Tour 12, case 74, 4 place Jussieu	75252 Paris Cedex 05, France
Trueman	Colin	University of St. Andrews	School of Physics and Astronomy,	North Haugh, St. Andrews,	Fife, KY16 9SS, Scotland
Valishin	Fan	Kazan State University, Physical Department		27a, House 30, Mushtary st	Kazan, Russia 420015
Varcoe	Ben	Max Planck Insistute For Quantum Optics	Max Planck Insistute For Quantum Optics	Hans-Kopfermann str. 1 Garching bei Muenchen D-85748	Germany
Vidiella-Barranco	Antonio	Universidade Estadual de Campinas	Departamento de Eletronica Quantica	Insituto de Fisica "Gleb Wataghin"	13083-970 Campinas SP Brasil
Vogel	Werner	Universitaet Rostock	Arbeitsgruppe Quantenoptik, Fachbereich Physik, Universitaet Rostock	Universitaetsplatz 3, D-18051 Rostock	Germany
Volokhovsky	Vsevolod	M.V.Lomonosov Moscow State university	Department of General Physics and Wave Processes, Faculty of Physics	M.V.Lomonosov Moscow State university	Vorob'evy Gory, 119899, Moscow, Russia

von Klitzing	Wolf	Ecole Normale Superieure	Laboratoire Kastler Brossel, Ecole Normale Superieure	24 rue Lhomond	75231 Paris, France
Vourdas	A.	University of Liverpool	Department of Electrical Engineering and Electronics	Brownlow Hill Liverpool L69 3GJ	United Kingdom
Wan	Kong	University of St.Andrews	School of Physics and Astronomy, University of St.Andrews	North Haugh, St. Andrews,	Fife, KY16 9SS, Scotland
Weigert	Stephan	Institut de physique Neuchatel	Institut de physique	Rue A.-L. Breguet 1,CH-2000 Neuchatel	Switzerland
Weih	Gregor	Universitaet Wien	Institut fuer Experimentalphysik	Boltzmanngasse 5, A-1090 Wien	Austria
Welsch	Dirk Gunnar	Friedrich-Schiller-Universitaet Jena	Theoretisch-Physikalisches Institut, Friedrich-Schiller-Universitaet Jena	Max-Wien-Platz 1, D-07743 Jena	Germany
Wilkens	Martin	Universitaet Potsdam	Institut fuer Physik, Universitaet Potsdam	Am Neuen Palais 10, 14469 Potsdam	Germany
Wiseman	Howard	The University of Queensland	Physics Department	The University of Queensland	St Lucia 4072, AUSTRALIA
Wuensche	Alfred	Humboldt-University Berlin	Humboldt-Universitaet Berlin, Institut fuer Physik, Nichtklassische Strahlung	Invalidenstr. 110	10115 Berlin, Germany
Xie	Changde	Shanxi University	nstitute of Opto-Electronics, Shanxi University	Taiyuan, Shanxi, 030006	P.R.China
Zaccaria	Francesco	Università di Napoli	Dipartimento di Scienze Fisiche	Complesso Universitario di Monte Sant'Angelo	via Cintia 80126 Napoli, Italy
Zaitsev	Lev N.	JINR	Joint Institute for Nuclear Research	Jolio Curie 6	Dubna Moscow Region 141980 Russia
Zhou	Peng	Queen's University of Belfast	Dept. of Applied Mathematics & Theoretical Physics, The Queen's University of Belfast	Belfast, BT7 1NN	UK
Zubairy	M. Suhail	Quaid-i-Azam University	Department of Electronics, Quaid-i-Azam University	Islamabad	Pakistan

Zucchetti	Angelo	Universitaet Rostock	Arbeitsgruppe Quantenoptik, Fachbereich Physik, Universitaet Rostock	Universitaetsplatz 3	D-18051 Rostock, Germany
-----------	--------	-------------------------	---	----------------------	--------------------------------

SUB-POISSONIAN STATISTICS OF HIGHLY CORRELATED SQUEEZED PARAMETRIC SYSTEMS

M. Sebawe Abdalla

Mathematics Department, College of Science, King Saud University, P.O. Box 2455, Riyadh 11451, Saudi Arabia

Faisal A. A. El-Orany ¹ and J. Peřina

Department of Optics and Joint Laboratory of Optics, Palacký University, 17. Listopadu 50, 77207 Olomouc, Czech Republic

(1): Department of Mathematics and Computer Science, Faculty of Science, Suez Canal University, Ismailia, Egypt

Abstract

We introduce a new squeeze operator, which is related to the time-dependent evolution operator for Hamiltonian representing mutual interaction between three different modes. The effect of intermodal correlation between modes is discussed in terms of the variances of the photon-number sum and difference, the Glauber second-order correlation function and the violation of Cauchy-Schwarz inequality.

I. INTRODUCTION

Squeezed states of the electromagnetic field are purely quantum states and have several applications in quantum optics. There are two familiar squeeze operators to produce squeezed states; namely, single mode squeeze operator [1] and two-mode squeeze operator [2]. Here we introduce a highly correlated multidimensional squeeze operator as the evolution operator of an interaction part, in a slowly varying amplitudes, of the Hamiltonian representing three mode interaction (equation (1.5) in [3]), given as

$$\hat{S}(\underline{r}) = \exp[r_1(\hat{A}_1^\dagger \hat{A}_2^\dagger - \hat{A}_1 \hat{A}_2) + r_2(\hat{A}_1^\dagger \hat{A}_3^\dagger - \hat{A}_1 \hat{A}_3) + r_3(\hat{A}_3 \hat{A}_2^\dagger - \hat{A}_3^\dagger \hat{A}_2)], \quad (1.1)$$

where $r_j = \lambda_j t$, with $0 \leq r_j < \infty$, $j = 1, 2, 3$, λ_j are coupling constants, t is the time of interaction and $\underline{r} = (r_1, r_2, r_3)$. It is evident that this squeeze operator involves three different squeezing mechanisms and therefore it is more complicated than squeezing operators that have appeared in the literature earlier [1,2,4].

Squeezing property is the important phenomenon well distinguishing mechanism of correlation of systems, where squeezing can occur in combination of the quantum mechanical modes described by operators \hat{A}_1 , \hat{A}_2 and \hat{A}_3 , even if single modes are not themselves

squeezed. For more details about this the reader can consult [1]. In fact, the idea that quantum correlations can give rise to squeezing in the combination of mode operators has been shown true for multimode squeezed states of light [1,5] and for dipole fluctuations in multimode squeezed states [4].

The squeeze operator (1.1) provides a Bogoliubov transformation of the annihilation and creation operators that mixes the three modes as

$$\bar{A}_1 \equiv \hat{S}^{-1}(\underline{r})\hat{A}_1\hat{S}(\underline{r}) = \hat{A}_1 f_1 + \hat{A}_2^\dagger f_2 + \hat{A}_3^\dagger f_3, \quad (1.2a)$$

$$\bar{A}_2 \equiv \hat{S}^{-1}(\underline{r})\hat{A}_2\hat{S}(\underline{r}) = \hat{A}_2 g_1 + \hat{A}_3 g_2 + \hat{A}_1^\dagger g_3, \quad (1.2b)$$

$$\bar{A}_3 \equiv \hat{S}^{-1}(\underline{r})\hat{A}_3\hat{S}(\underline{r}) = \hat{A}_3 h_1 + \hat{A}_1^\dagger h_2 + \hat{A}_2 h_3, \quad (1.2c)$$

where f_j, g_j, h_j are functions in terms of $\sinh(\cdot)$ and $\cosh(\cdot)$ with argument $\mu = \sqrt{r_1^2 + r_2^2 - r_3^2}$ and $r_3^2 < r_1^2 + r_2^2$ (for exact forms see [7]).

We may point out that a strong correlation is built up between the three modes described by squeeze operator (1.1). This is quite obvious for the case of the parametric amplification when two mode waves are mixed to generate a third wave via nonlinear medium, e.g. in an optical crystal with nonlinear second-order susceptibility [1]. This can be demonstrated with the help of three-mode pure squeezed vacuum states $\hat{S}(\underline{r})\prod_{j=1}^3|0_j\rangle$, where $\hat{S}(\underline{r})$ is the squeeze operator (1.1). In this case the eigenstates of the three-mode photon-number difference $\hat{A}_1^\dagger\hat{A}_1 - \hat{A}_2^\dagger\hat{A}_2 - \hat{A}_3^\dagger\hat{A}_3$ correspond to zero eigenvalue, thus

$$\Delta(\hat{A}_1^\dagger\hat{A}_1 - \hat{A}_2^\dagger\hat{A}_2 - \hat{A}_3^\dagger\hat{A}_3)^2 = 0. \quad (1.3a)$$

However, the situation will be different for three-mode photon-number sum; after minor calculations we obtain

$$\begin{aligned} \Delta(\hat{A}_1^\dagger\hat{A}_1 + \hat{A}_2^\dagger\hat{A}_2 + \hat{A}_3^\dagger\hat{A}_3)^2 &= f_1^2(f_1^2 - 1) + g_3^2(1 + g_3^2) \\ &+ h_2^2(1 + h_2^2) + 2(f_1^2 g_3^2 + f_1^2 h_2^2 + h_2^2 g_3^2). \end{aligned} \quad (1.3b)$$

In the following section we employ the relations (1.2) to study the sub-Poissonian statistics for three-mode squeezed coherent states.

II. SUB-POISSONIAN STATISTICS FOR THREE-MODE SQUEEZED COHERENT STATES

Three-mode squeezed coherent states are defined formally by means of three-mode squeeze operator (1.1), in a sense similar to that of squeezed coherent states, as

$$|\underline{\alpha}, \underline{r}\rangle \equiv \hat{S}(\underline{r})|\alpha_1\rangle|\alpha_2\rangle|\alpha_3\rangle, \quad (2.1)$$

where $|\alpha_j\rangle$ are coherent states; for simplicity we have used $\underline{\alpha} = (\alpha_1, \alpha_2, \alpha_3)$.

Here we study the second-order correlation function, $g_j^{(2)}(0)$, for measuring the deviation from the Poisson statistics of the three-mode coherent states. Also we extend our investigation to include the violation of the Cauchy-Schwarz inequality.

The second-order normalized correlation function has been defined by

$$g_j^{(2)}(0) = 1 + \frac{\langle(\Delta\hat{n}_j)^2\rangle - \langle\hat{n}_j\rangle^2}{\langle\hat{n}_j\rangle^2}, \quad (2.2)$$

where $\langle(\Delta\hat{n}_j)^2\rangle$ and $\langle\hat{n}_j\rangle$ are the variance and average of the photon number for the j th mode, respectively. It can happen that $g_j^{(2)}(0) = 1$ for Poisson light (coherent states), or $g_j^{(2)}(0) < 1$ for sub-Poisson light (e.g. Fock states), otherwise we have super-Poisson light (e.g. chaotic field). In the following we restrict our discussion to the first mode 1, because

the other modes would have similar behaviour. So after calculating the required quantities in (2.2), in a straightforward way, we get

$$g_1^{(2)}(0) = 1 + \left[\frac{2(f_1^2 - 1)\langle \hat{n}_1 \rangle_{coh} - (f_1^2 - 1)^2}{\langle \hat{n}_1 \rangle_{coh}^2} \right], \quad (2.3)$$

where $\langle \hat{n}_1 \rangle_{coh} = |f_1\alpha_1 + f_2\alpha_2^* + f_3\alpha_3^*|^2 + f_2^2 + f_3^2$.

In phase space, squeezed coherent states $|\alpha, r\rangle$ are represented by a noise ellipse with the origin at α , and exhibit Poisson distribution at $r = 0$, and it is growing rapidly to superthermal distribution, i.e. $g^{(2)}(0) > 2$, and it persists for a large domain of r [8,9]. In our model, e.g. for mode 1, one can prove easily from equation (2.3) that the modes exhibit only partial coherence behaviour, i.e. $1 < g^{(2)}(0) < 2$. This is a consequence of intermodal correlations of the three-mode squeezed coherent states for $\alpha_j \neq 0$.

In quantum theory, the violation of Cauchy-Schwarz inequality can be represented by the factor [10]

$$I_{j,k} = \frac{[\langle \hat{A}_j^{2\dagger} \hat{A}_j^2 \rangle \langle \hat{A}_k^{2\dagger} \hat{A}_k^2 \rangle]^{\frac{1}{2}}}{\langle \hat{A}_j^\dagger \hat{A}_j \hat{A}_k^\dagger \hat{A}_k \rangle} - 1. \quad (2.4)$$

The negative values for the quantity $I_{j,k}$ mean that the intermodal correlation is larger than the correlation between the photons in the same mode [11] and this indicates strong violation of the Cauchy-Schwarz inequality. The quantity (2.4) may be used to investigate the anticorrelation (antibunching) between modes. We have concluded from the numerical analysis of (2.4) that there is a strong violation of Cauchy-Schwarz inequality between different modes, which means that the photons are more strongly correlated than it is possible classically. Further, we noted that the violation of this inequality is strongly sensitive to the values of squeeze parameters and coherent amplitudes.

It is known that the correspondence between quantum and classical theories can be established via Glauber-Sudarshan P -representation. But the P -representation does not have all the properties of a classical distribution function for quantum fields. So the violation of the Cauchy-Schwarz inequality provides explicit evidence of the quantum nature of intermodal correlations between modes, which implies that the P -distribution function possesses strong quantum properties [10].

III. Conclusion

In this contribution we have introduced new type of multidimensional squeeze operator which is more general than usually used. This operator yields from the time-dependent evolution operator for the Hamiltonian representing mutual interaction between three different modes of the field. We have shown that a strong correlation is built up between the three modes described by this operator and this is quite obvious for the case of the parametric amplification, when two-mode waves are mixed to generate a third wave via nonlinear medium. For the three-mode squeezed coherent state, we found that its second-order correlation function describes partially coherent field, so that one mechanism of squeezing is always surviving. Further we found strong violation for Cauchy-Schwarz inequality between some modes, i.e. the photons are more strongly correlated than it is allowed classically.

Acknowledgments

J. P. and F. A. A. E-O. acknowledge the partial support from the Project VS96028 of Czech Ministry of Education. One of us (M. S. A.) is grateful for the financial support from the project Math 1418/19 of the Research Centre, College of Science, King Saud University.

REFERENCES

- [1] D. Stoler, Phys. Rev. D **1**, 3217 (1970); H. P. Yuen, Phys. Rev. A **13**, 2226 (1976).
- [2] S. M. Barnett and P. L. Knight, J. Opt. Soc. Am. B **2**, 467 (1985).
- [3] M. S. Abdalla, M. M. A. Ahmed and S. AL-Homidan, J. Phys. A: Math. Gen. **31**, 3117 (1998).
- [4] S. M. Barnett and P. L. Knight, J. Mod. Opt. **34**, 841 (1987).
- [5] W. Vogel and D.-G. Welsch, Lectures on Quantum Optics (Academie, Berlin 1994).
- [6] S. M. Barnett and M. A. Dupertuis, J. Opt. Am. B **4**, 505 (1987).
- [7] M. S. Abdalla, F. A. A. El-Orany and J. Peřina, J. Opt. Soc. Am. B (accepted).
- [8] M. S. Kim, F. A. M. de Oliveira and P. L. Knight, Opt. Comm. **72**, 99 (1989).
- [9] M. S. Kim, F. A. M. de Oliveira and P. L. Knight, Phys. Rev. A **40**, 2494 (1989).
- [10] G. S. Agarwal, J. Opt. Soc. Am. B **5**, 1940 (1988).
- [11] L. Gilles and P. L. Knight, J. Mod. Opt. **39**, 1411 (1992).

LIGHT PULSE SQUEEZED STATE FORMATION IN MEDIUM WITH THE RELAXATION KERR NONLINEARITY

A.S. Chirkin*, F. Popescu

Faculty of Physics, Lomonosov Moscow State University, Moscow 119899, Russia

Abstract

The consistent theory of forming a pulsed squeezed state as a result of self-action of ultrashort light pulse in the medium with relaxation Kerr nonlinearity has been developed. A simple method to form the ultrashort light pulse with sub-Poissonian photon statistics is analyzed too.

I. INTRODUCTION

There are two groups of works in the quantum theory of self-action (or self-phase modulation) of ultrashort light pulses (USPs). In one group of the works (for example, [1]–[3]) the calculations of the nonclassical light formation at the self-action of pulses assume that the nonlinear response of the medium is instantaneous and that the relative fluctuations are small. The latter assumption is valid for the intense USP ordinarily used in experiments. However a finite relaxation time of the nonlinearity is of principal importance. The relaxation time of the nonlinearity determines a region of the spectrum of the quantum fluctuations that play a large role in the formation of squeezed light.

The inertia of the nonlinearity is taken into account in works [4]–[5]). The methods that have been developed in Refs. [4] and [5] differ in interaction Hamiltonians. The authors of Ref. [4] considered the interaction Hamiltonian using which one has to introduce thermal fluctuations to satisfy the commutation relations for time-dependent Bose-operators. For the case of the normally ordered interaction Hamiltonian [5] it is not necessary to include into consideration thermal fluctuations.

The results of the quantum theory of the USP self-action in the medium with the relaxation Kerr nonlinearity based on the normally ordered interaction Hamiltonian are presented below. Variances of the quadrature components and spectral distribution of the pulsed quadrature-squeezed light are calculated. Besides, propagation of such a pulse through a dispersive linear medium is analyzed. It is shown that in this case the pulse with sub-Poissonian photon statistics can be formed.

*chirkin@foton.ilc.msu.su, florentin_p@hotmail.com

II. QUANTUM THEORY OF SELF-ACTION OF LIGHT PULSE

We will describe the process under consideration by the following interaction Hamiltonian

$$\hat{H}_{int}(z) = \hbar\beta \int_{-\infty}^{\infty} dt \int_{-\infty}^t H(t-t_1) N[\hat{n}(t, z)\hat{n}(t_1, z)] dt_1, \quad (1)$$

where the coefficient β is determined by the nonlinearity of the medium, $H(t)$ is the nonlinear response function of the Kerr medium ($H(t) \neq 0$ for $t \geq 0$ and $H(t) = 0$ for $t < 0$); N is the normal ordering operator, $\hat{n}(t, z) = A^+(t, z)A(t, z)$ is the photon number density operator, and $A^+(t, z)$ and $A(t, z)$ are the Bose operators creating and annihilating photons in a given cross section z . The operator $\hat{n}(t, z)$ commutes with the Hamiltonian (1) and therefore $\hat{n}(t, z) = \hat{n}(t, z=0) = \hat{n}_0(t)$, where $z=0$ corresponds to the input of the nonlinear medium.

According to Eq. (1) the spatial evolution of the operator $A(t, z)$ is given by the equation

$$\frac{\partial A(t, z)}{\partial z} + i\beta q[\hat{n}_0(t)]A(t, z) = 0, \quad (2)$$

in the moving coordinate system, $z = z'$ and $t = t' - z'/u$ (u is the velocity of the pulse),

$$q[\hat{n}_0(t)] = \int_{-\infty}^{\infty} h(t_1)\hat{n}_0(t-t_1) dt_1 \quad (h(t) = H(|t|)).$$

The solution of Eq. (2) is

$$A(t, l) = \exp[-i\gamma q[\hat{n}_0(t)]]A_0(t). \quad (3)$$

Here $A_0(t) = A(t, 0)$, $\gamma = \beta l$, l is the length of the nonlinear medium. For $h(t) = 2\delta(t)$ and $A_0(t) = a_0$ expressions (2), (3) have a form corresponding to single-mode radiation.

To verify commutation relation $[A(t_1, l), A^+(t_2, l)] = \delta(t_1 - t_2)$ and to calculate the quantum characteristics of the pulse it is necessary to apply an algebra of time-dependent Bose operators [5], [7].

In accordance with Eq.(3) the photon number operator remains unchanged in the nonlinear medium. This fact has already used in Eq.(2). Therefore in the case of a self-action it is of greatest interest to study the fluctuations of the quadrature components. Here we restrict our consideration by the X -quadrature $\hat{X}(t, z) = [A^+(t, z) + A(t, z)]/2$. The correlation function of the X -quadrature is given by the formula [5]

$$R(t, t + \tau) = \frac{1}{4} \{ \delta(\tau) - \psi(t)h(\tau) \sin 2\Phi(t) + \psi^2(t)g(\tau) \sin^2 \Phi(t) \}, \quad (4)$$

where $\psi(t) = 2\gamma|\alpha_0(t)|^2$ is the nonlinear phase addition, $\alpha_0(t)$ is an eigenvalue of the operator $A_0(t)$ of a pulse in a coherent state, $\Phi(t) = \psi(t) + \phi(t)$ ($\phi(t)$ is the initial phase of the pulse). For the considered nonlinear response $h(\tau) = \tau_r^{-1} \exp(-|\tau|/\tau_r)$ and $g(\tau) = \tau_r^{-1}(1 + |\tau|/\tau_r) \exp(-|\tau|/\tau_r)$ (τ_r is the nonlinearity relaxation time). We took into consideration that the parameter $\gamma \ll 1$ and the pulse duration $\tau_p \gg \tau_r$.

According to Eq. (4) the spectral density of the quadrature fluctuations is

$$S(\omega, t) = \int_{-\infty}^{\infty} R(t, t + \tau) e^{i\omega\tau} d\tau = \frac{1}{4} [1 - 2\psi(t)L(\omega) \sin 2\Phi(t) + 4\psi^2(t)L^2(\omega) \sin^2 \Phi(t)], \quad (5)$$

where $L(\omega) = 1/[1 + (\omega\tau_r)^2]$. It follows from Eq.(5) that the level of the quadrature fluctuations, depending on the the value of the phase $\Phi(t)$, can be greater or less than the short noise one corresponding to $S^{(coh)}(\omega) = \frac{1}{4}$.

If the phase of the pulse is chosen optimal for a frequency ω_0 , $\phi_0(t) = 0.5 \arctan[(\psi(t)L(\omega_0))^{-1}] - \psi(t)$, then the spectral density at this frequency is minimal.

The calculated spectra at $t = 0$ for the case of $\omega_0 = \tau_r^{-1}$ are presented in Fig.1. It is obvious from Fig.1 that the frequency band in which the spectral density of the quadrature fluctuations is low than the shot noise level depends on the nonlinear phase addition $\psi(0)$.

III. SQUEEZED LIGHT PULSE IN DISPERSIVE LINEAR MEDIUM

We consider now the propagation of the quadrature-squeezed pulse through a dispersive linear medium in which the following operator transformation take place

$$B(t, z) = \int_{-\infty}^{\infty} G(t - t_1, z) A(t_1, l) dt_1 \quad (6)$$

Here $G(t, z)$ is the Green function for the medium, z is the distance and $A(t, l)$ is the input value of the operator (at $z = 0$) defined by Eq. (3).

Let us introduce the photon number operator over the measurement time T and the Mandel parameter $Q(t, z)$:

$$\hat{N}_T(t, z) = \int_{t-T/2}^{t+T/2} B^\dagger(t_1, z) B(t_1, z) dt_1, \quad Q(t, z) = \frac{\varepsilon(t, z)}{\langle \hat{N}_T(t, z) \rangle}, \quad (7)$$

$$\varepsilon(t, z) = \langle \hat{N}_T^2(t, z) \rangle - \langle \hat{N}_T(t, z) \rangle^2 - \langle \hat{N}_T(t, z) \rangle.$$

Let us assume that the initial light pulse has the form $\bar{n}_0(t) = \bar{n}_0 \exp(-t^2/\tau_p^2)$ and $G(t, z) = (-i2\pi k_2 z)^{-\frac{1}{2}} \exp\{-it^2/2k_2 z\}$. The coefficient k_2 characterises the dispersion of a group velocity. In the case of the normal dispersion $k_2 > 0$ and for the anormal dispersion $k_2 < 0$. When the phase self-modulation pulse passes through the dispersive linear medium a compression or a decompression of the pulse takes place. This effect can change the photon statistics of the pulse.

In the so called paraxial approximation we get [6]

$$\langle \hat{N}_T(t, z) \rangle = \bar{n}_0 T V^{-1}(z) \exp[-t^2/V^2(z)\tau_p^2], \quad V^2(z) = w^2(z) + \varphi^2(z),$$

$$Q(0, z) = - \left[\frac{T\psi_0}{\sqrt{\pi}\tau_p} \right] \cdot \frac{\sin[\arctan(\varphi(z)/w(z)) + 0.5\arctan[2\varphi(z)w(z)/(2\varphi(z)\varphi_d(z) - w^2(z))]]}{[w^4(z) - 2\varphi^2(z)w^2(z) + 4\varphi^4(z)]^{1/4}}, \quad (8)$$

$$w^2(z) = 1 - s\psi_0\varphi(z), \quad \varphi(z) = z/D, \quad \varphi_d(z) = z/d, \quad D = \tau_p^2/|k_2|, \quad d = \tau_r^2/|k_2|.$$

D and d are the characteristic dispersion lengths, $s = 1$ for $k_2 < 0$, and $s = -1$ for $k_2 > 0$.

It follows from Eq.(8) that the pulse with sub-Poissonian photon statistics ($Q(t, z) < 0$) can be obtained. Of particular interest is the compression of the phase self-modulation pulse ($s = 1, k_2 < 0$). The dependence of the Mandel parameter in this case is presented in Fig.2. One can see that the suppression of quantum fluctuation of the photon number becomes noticeable for the nonlinear phase $\psi_0 > 1$.

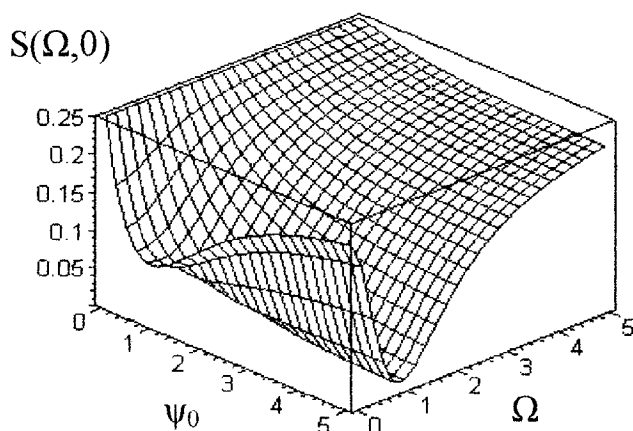


FIG. 1. Spectrum of the fluctuations of the squeezed quadrature of a pulse at time $t=0$ as a function of the maximum nonlinear phase ψ_0 and the reduced frequency $\Omega = \omega\tau_p$.

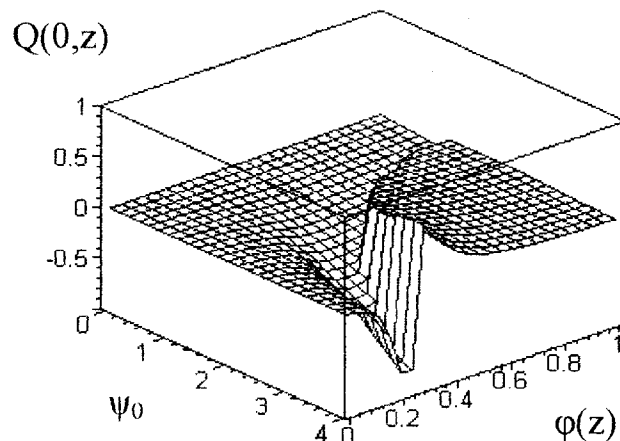


FIG. 2. Parameter $Q(0, z)$ as a function of the maximum nonlinear phase ψ_0 and the dispersion phase $\varphi(z)$.

IV. CONCLUSIONS

The basic results of the developed systematic theory are following. The spectral region with level of the quadrature fluctuations less than the shot noise one depends on relaxation time of the nonlinearity and the nonlinear phase addition. Choosing initial phase of pulse gives us possibility to control the frequency when the coefficient of squeezing is maximal. Propagation of the quadrature-squeezed light pulse through a dispersion linear medium (an optical fiber or optical copressor) can lead to formation of the pulse with sub-Poissonian photon statistics.

V. ACKNOWLEDGEMENT

One the authors (A.Ch.) acknowledges the Organizing Committee of ICSSUR'99 for financial support of participating in the Conference.

REFERENCES

- [1] N. Nishizawa, M. Hashiura, T. Horio et al., *Jpn. J. Appl. Phys., Part.2*, **37**, L792 (1998).
- [2] M. Shirasaki and H.A. Haus, *J. Opt. Soc. Am. B*, **7**, 30 (1990).
- [3] S.A. Akhmanov, V.A. Vysloukh and A.S. Chirkin, *Optics of Femtosecond Laser Pulses*, AIP, 1992.
- [4] L. Boivin, F.X. Kärtner, and H.A. Haus, *Phys. Rev. Lett.*, **73**, 240 (1994).
- [5] F. Popescu, A.S. Chirkin, *JETP Lett.*, **69**, 516 (1999).
- [6] F. Popescu, A.S. Chirkin, *Quantum Electron.*, **29**, N7 (1999).
- [7] K.J. Blow, R. Loudon, and S.J. Phoenix, *J.Opt.Soc.Am.B*, **8**, 1750 (1991).

DETECTION OF SQUEEZED PHONONS VIA STOKES–ANTI-STOKES CORRELATIONS

Alexander S. Shumovsky and Özgür E. Müstecaplıoğlu
Physics Department, Bilkent University, Bilkent, 06533 Ankara, Turkey

Abstract

A method of detection of number variance of Raman-active excitations in solids via measurement of Stokes–anti-Stokes correlations is proposed.

Recent progress in the field of quantum optics have stimulated the theoretical and experimental study of the so-called "nonclassical states of bosons" in solids (e.g., see [1–5]). Let us stress very important difference between the squeezed state of light and that of bosons in condensed matter. The former is usually a nonequilibrium state of radiation. The squeezed phonons which have been recently produced and detected [5] are similar to squeezed photons. At the same time, the squeezed states of bosons in solids can exist at thermal equilibrium [6]. The polariton excitations in an ionic crystal, for example, can be treated in terms of the "two-mode" squeezed thermal states [2]. Although the squeezing of quantum fluctuations cannot be observed in this case, the pairwise creation of phonons and photons leads to quite strong quantum fluctuations which can strongly influence the system at low temperature [2]. Among the other mechanisms leading to squeezed states of phonons the polaron-type interaction, exciton-phonon interaction, and phonon anharmonicity can be mentioned here [7].

In contrast to the case of nonclassical states of photons, there is no effective direct methods of measurements allowing the characterization of the quantum states of bosons in solids [3]. Here we propose a way of measurement of the number variance of Raman-active Bose-type excitations in solids (phonons, polaritons, etc.). It has been shown that the quantum statistical properties of a vibration mode can strongly influence the parameters of scattered light in the Stokes-type Raman process [8]. We show here that the measurement of Stokes–anti-Stokes photon correlations might be an effective way of investigation of the quantum statistical properties of vibration mode even at thermal equilibrium.

It is well known that the Raman-type process can be specified by the following Manley-Rowe relations [9,10]

$$\begin{aligned}\hat{N}_S + \hat{N}_A + \hat{N}_P &= \hat{C}_1, \\ \hat{N}_S - \hat{N}_A - \hat{N}_V &= \hat{C}_2\end{aligned}\tag{1}$$

where \hat{N}_X denotes the number operator for Stokes ($X = S$), anti-Stokes ($X = A$), and pumping ($X = P$) photons and for "vibration" excitations of medium ($X = V$). These

operators are determined in the Heisenberg representation at an arbitrary time, while $\hat{C}_{1,2}$ are some constant operators. If, for example, the S and A components are initially in the vacuum state, then $\hat{C}_1 = \hat{N}_P(0)$ and $\hat{C}_2 = \hat{N}_V(0)$. Consider the correlation function

$$\langle A; B \rangle = \langle AB \rangle - \langle A \rangle \langle B \rangle.$$

Since in the Heisenberg representation the evolution is provided by the time-dependent operators, the averaging should be performed with respect to the initial state of the system. Then, assuming the initial vacuum state of the components S and A , for the operators $\hat{N}_S(t)$ and $\hat{N}_A(t)$ we get

$$\begin{aligned} \langle \hat{N}_A(t); \hat{N}_S(t) \rangle = & \frac{1}{4} [V_0(N_P) - V_0(N_V) + V_t(N_P) - V_t(N_V) \\ & - 2\langle \hat{N}_P(0); \hat{N}_P(t) \rangle - 2\langle \hat{N}_V(0); \hat{N}_V(t) \rangle]. \end{aligned} \quad (2)$$

Here $V_t(X) \equiv \langle \hat{X}(t); \hat{X}(t) \rangle$ denotes the variance of a physical quantity described by the operator \hat{X} at time t . The equation (2) establishes an important connection between the $S - A$ correlations and quantum statistical properties of pump photons and excitations in solids (phonons). On making the further assumption that P -component is represented initially by a strong monochromatic coherent field, one can obtain

$$V_0(\hat{N}_P) = |\alpha|^2, \quad \langle \hat{N}_P(0); \hat{N}_P(t) \rangle = \alpha^* \langle [\hat{a}_P(0), \hat{N}_P(t)] \rangle$$

where α is the parameter of coherent state and a_P is the annihilation operator of P -type photon.

Let us stress that conventional quantum theory of Raman scattering [13,14] usually neglects the quantum properties of pump through the completely classical pump assumption. In view of (2) it means that \hat{N}_P is supposed to be independent of time so that

$$V_t(\hat{N}_P) + V_0(\hat{N}_P) - 2\langle \hat{N}_P(0); \hat{N}_P(t) \rangle = 0. \quad (3)$$

Then the $S - A$ correlation function (2) is related only to phonon (vibration modes) statistics. The condition (3) implies a time range to the problem during which any change in the pump intensity remains negligible [13,14]. However, it is not enough as far as the correlations of scattered photons are considered. As a matter of fact, the quantum statistical properties of the pump photons might be changed significantly in shorter time than the occurrence of a visible change in their intensity. To evaluate such a time, let us consider conventional parametric Raman model [13,14]

$$H = \sum_{\lambda=S,A} \omega_\lambda \hat{N}_\lambda + \sum_q \omega_{qV} \hat{N}_{qV} + \sum_q (g_{qS} \hat{a}_S^\dagger \hat{a}_{qV}^\dagger + d_{qA} \hat{a}_A^\dagger \hat{a}_{qV} + H.c.). \quad (4)$$

Here the operators \hat{a}_λ describe the photons of scattered light, \hat{a}_{qV} are the vibration-mode (phonon) Bose operators, and the complex coupling constants $g_{q\lambda}$ include the dependence on intensity of the classical pump. Summation over q in (4) permits us to take into account the Markoffian properties of phonons at thermal equilibrium [13,14]. One can expect, however, that phase-matching condition would have limited the number of active phonon modes to one.

Since the Hamiltonian (4) is a bilinear form in Bose operators, the Heisenberg equations for the scattered photons have the following general solution

$$\hat{a}_\lambda^+(t) = U_\lambda(t)\hat{a}_S^+(0) + V_\lambda(t)\hat{a}_A(0) + \sum_q W_{q\lambda}(t)\hat{a}_{qV}(0)$$

where the coefficients U, V , and W are some known functions of parameters of the Hamiltonian (4) and time. In view of this result and Eq. (3), the Eq. (2) can now be done in a straightforward manner to yield

$$\begin{aligned} \langle \hat{N}_S(t); \hat{N}_A(t) \rangle &= A(t) + \sum_{kq} B_{kq}(t) \langle \hat{a}_{kV}^+(0) \hat{a}_{qV}(0) \rangle \\ &+ \sum_{klpq} C_{klpq}(t) \langle \hat{a}_{kV}^+(0) \hat{a}_{qV}(0); \hat{a}_{lV}^+(0) \hat{a}_{pV}(0) \rangle \end{aligned} \quad (5)$$

so that the time evolution of $S - A$ correlation function is completely determined by the initial state of phonon sub-system. It is also straightforward to calculate the coefficients A, B , and C in terms of U, V , and W .

As usually, the summations in (5) can be converted into integrals involving phonon density of states. In the simplest case of perfectly phase-matched pump and phonon modes, the only phonon mode contributes in the right-hand side of (5) which yields

$$\langle \hat{N}_S(t); \hat{N}_A(t) \rangle = A(t) + B(t) \langle \hat{N}_V(0) \rangle + C(t) V_0 \langle \hat{N}_V \rangle. \quad (6)$$

Since $\langle \hat{N}_V(0) \rangle$ can be determined by measurement of either $\langle \hat{N}_S(t) \rangle$ or $\langle \hat{N}_A(t) \rangle$ [11] at short time, the Eq. (6) shows that $V_0 \langle \hat{N}_V \rangle$ can be determined by simultaneous measurement of the scattered light intensities and $S - A$ correlation function. The latter can be measured by standard homodyne detection scheme.

Similar result can be also obtained in the case of strong Van Hove singularities corresponding to the modes selected by Raman process which has been considered in [5] in the context of generation of squeezed phonons. In general, a relation similar to (6) can be obtained through the use of random-phase approximation under assumption that the phonon modes obeying Raman selection rules play the dominant role.

To estimate the time range of validity of the parametric approximation, one can use the sort-time approximation of the Heisenberg equations with the Hamiltonian (4) [13] up to the second order of t close to the beginning of interaction [2]. Using the condition $V_t \langle \hat{N}_P \rangle = \langle \hat{N}_P(t) \rangle$, we find the time range as $t \ll \tau_2$ where

$$\tau_2 = \frac{1}{4M(1 + \langle \hat{N}_V(0) \rangle)}. \quad (7)$$

Here M is some constant determined by the parameters of the Hamiltonian (4). It should be emphasized that $\tau_2 < \tau_1$ where

$$\tau_1 = \frac{1}{L_1 + L_2 \langle \hat{N}_V(0) \rangle}$$

is the conventional range of parametric approximation [15]. As an estimation, we may take $g_\lambda \approx 10^7 Hz$, giving the time ranges as $\tau_1 \approx 10 fs$ [15] and $\tau_2 \approx 3 fs$. This time range seems to

be available now due to remarkable recent progress in the field of femto-second spectroscopy [14]. Thus, it is shown that the variance of number of Raman-active excitations in solids can be detected even at thermal equilibrium via measurement of Stokes-anti-Stokes correlation function. It is clear that the measurement of quantum statistical properties of phonons can give an important information about microscopic interactions in solids [15]. The above obtained results can be also applied in the molecular Raman spectroscopy.

REFERENCES

- [1] M. Artoni and J.L. Birman, *Phys. Rev. B* **44**, 3736 (1991); *Optics Commun.* **104**, 319 (1994).
- [2] A.V. Chizhov, R.G. Nazmitdinov, and A.S. Shumovsky, *Quant. Optics* **3**, 1 (1991); *Mod. Phys. Lett. B* **7**, 1233 (1993).
- [3] X. Hu and F. Nori, *Phys. Rev. B* **53**, 2419 (1996); *Phys. Rev. Lett.* **76**, 2294 (1996).
- [4] Ö. E. Müstecaplıođlu and A.S. Shumovsky, *Appl. Phys. Lett.* **70**, 3489 (1997).
- [5] G.A. Garrett, A.G. Rojo, A.K. Sood, J.F. Whitaker, and R. Merlin, *Science* **175**, 1638 (1997).
- [6] M.S. Kim, F.A.M. de Olivera, and P.L. Knight, *Phys. Rev. A* **40**, 2494 (1989).
- [7] A.S. Shumovsky, in *Quantum Optics and the Spectroscopy of Solids*, edited by T. Hakioglu and A.S. Shumovsky (Kluwer, Dordrecht, 1997).
- [8] A.S. Shumovsky and B. Tanatar, *Phys. Rev. A* **48**, 4735 (1993); *Phys. Lett. A* **182**, 411 (1993).
- [9] Y.R. Shen, *The Principles of Non-Linear Optics* (Wiley, New York, 1984).
- [10] A.S. Shumovsky, in *Modern Nonlinear Optics Part I*, edited by M. Evans and S. Kielich (Wiley, New York, 1993).
- [11] D.F. Walls, *Z. Phys.* **237**, 224 (1970); *J. Phys. A* **6**, 496 (1973).
- [12] R. Loudon, *The Quantum Theory of Light* (Oxford University Press, Oxford, 1983).
- [13] J. Peřina, *Quantum Statistics of Linear and Nonlinear Optical Phenomena* (Reidel, Dordrecht, 1984).
- [14] J. Shah, *Ultrafast Spectroscopy of Semiconductors and Semiconductor Nanostructures* (Springer, Berlin, 1996).
- [15] A.S. Shumovsky and Ö. E. Müstecaplıođlu, *Phys. Rev. B* (1999) (to be published).

Two-level Atom in a Squeezed Vacuum with Finite Bandwidth: Master Equation versus Coupled-systems Approach

Ryszard Tanaś

*Nonlinear Optics Division, Institute of Physics, Adam Mickiewicz University, Umultowska 85,
61-614 Poznań, Poland*

Zbigniew Ficek

*Department of Physics and Centre for Laser Science, The University of Queensland, Brisbane,
Australia 4072*

Abstract

We address the question: how broad must be the squeezed vacuum to make the Markov approximation still applicable? We compare the resonance fluorescence spectra obtained using the Markovian master equation with the spectra calculated from the coupled-systems approach. We show that both approaches give very similar spectra up to realistic values of the squeezed vacuum bandwidth ($\sim 10\gamma$).

Broadband squeezed vacuum can be treated as a reservoir to an atom and a master equation in the Born and Markov approximation can be derived for the reduced density matrix of the atomic system. Realistic sources of squeezed field, such as the degenerate parametric oscillator (DPO), produce a squeezed vacuum with finite bandwidth. However, when the bandwidth of the DPO cavity is much larger than the atomic linewidth, one can still treat the squeezed vacuum as a reservoir to the atom and derive the Markovian master equation that describes the dynamics of the atomic variables only. If, moreover, the atom is driven by a classical coherent laser field one can perform the dressing transformation first and next apply the standard perturbation procedure to derive the master equation [1]. We have derived such a master equation [2,3], which in the frame rotating with the laser frequency ω_L can be written as

$$\begin{aligned}
 \dot{\rho} = & \frac{1}{2} i [(\delta \sigma_z - \Omega (\sigma_+ + \sigma_-)), \rho] \\
 & + \frac{1}{2} \gamma \tilde{N} (2 \sigma_+ \rho \sigma_- - \sigma_- \sigma_+ \rho - \rho \sigma_- \sigma_+) \\
 & + \frac{1}{2} \gamma (\tilde{N} + 1) (2 \sigma_- \rho \sigma_+ - \sigma_+ \sigma_- \rho - \rho \sigma_+ \sigma_-) \\
 & - \gamma \tilde{M} \sigma_+ \rho \sigma_+ - \gamma \tilde{M}^* \sigma_- \rho \sigma_-
 \end{aligned} \tag{1}$$

$$+ \frac{1}{4} i (\beta [\sigma_+, [\sigma_z, \rho]] - \beta^* [\sigma_-, [\sigma_z, \rho]]) ,$$

where

$$\begin{aligned} \tilde{N} &= N(\omega_L + \Omega') + \frac{1}{2} (1 - \tilde{\Delta}^2) \text{Re}\Gamma_- , \\ \tilde{M} &= M(\omega_L + \Omega') - \frac{1}{2} (1 - \tilde{\Delta}^2) \Gamma_- + i \tilde{\Delta} \delta_M e^{i\phi} , \\ \delta &= \Delta + \frac{\gamma}{2} (1 - \tilde{\Delta}^2) \text{Im}\Gamma_- + \gamma \tilde{\Delta} \delta_N , \\ \beta &= \gamma \tilde{\Omega} [\delta_N + \delta_M e^{i\phi} - i \tilde{\Delta} \Gamma_-] , \\ \Gamma_- &= N(\omega_L) - N(\omega_L + \Omega') - [M(\omega_L) - M(\omega_L + \Omega')] , \\ \delta_N &= \frac{1}{\pi} \mathcal{P} \int_{-\infty}^{\infty} \frac{N(x)}{x + \Omega'} dx , \quad \delta_M = \frac{1}{\pi} \mathcal{P} \int_{-\infty}^{\infty} \frac{|M(x)|}{x + \Omega'} dx , \\ \tilde{\Omega} &= \frac{\Omega}{\Omega'} , \quad \tilde{\Delta} = \frac{\Delta}{\Omega'} , \quad \Omega' = \sqrt{\Omega^2 + \Delta^2} , \end{aligned} \tag{2}$$

and the principal value terms for DPO have the form

$$\begin{aligned} \delta_N &= \Omega' \frac{\lambda^2 - \mu^2}{4} \left[\frac{1}{\mu (\Omega'^2 + \mu^2)} - \frac{1}{\lambda (\Omega'^2 + \lambda^2)} \right] , \\ \delta_M &= \Omega' \frac{\lambda^2 - \mu^2}{4} \left[\frac{1}{\mu (\Omega'^2 + \mu^2)} + \frac{1}{\lambda (\Omega'^2 + \lambda^2)} \right] , \\ \lambda &= \frac{\kappa}{2} + \epsilon \quad \mu = \frac{\kappa}{2} - \epsilon , \end{aligned} \tag{3}$$

where κ is the bandwidth of the DPO cavity and ϵ the amplitude of the pump field.

In the derivation of equation (1) we have included the divergent frequency shifts (the Lamb shift) to the redefinition of the atomic transition frequency. Moreover, we have assumed that the squeezed vacuum is symmetric about the central frequency ω_L , so that $N(\omega_L - \Omega') = N(\omega_L + \Omega')$, and a similar relation holds for $M(\omega)$. The atomic natural linewidth is γ , $\Delta = \omega_L - \omega_A$ is the detuning of the laser frequency of the atomic resonance, and Ω is the Rabi frequency of the coherent driving field.

The master equation (1) has the standard form known from the broadband squeezing approaches with the new effective squeezing parameters \tilde{N} and \tilde{M} . There are also new terms, proportional to β which are essentially narrow bandwidth modifications to the master equation. All the narrow bandwidth modifications are determined by the parameter Γ_- and the shifts δ_N and δ_M . These parameters become zero when the squeezing bandwidth goes to infinity.

As a reference for testing our master equation (1) we use the coupled-system (or cascaded-system) approach [4,5] in which output of the first system (DPO) drives the second system (atom) without any coupling back from the the second system to the first. In our case of an atom driven by a squeezed light from DPO and a coherent field with the Rabi frequency Ω , the corresponding master equation has the form [6].

$$\begin{aligned} \dot{\rho} = & \frac{1}{2} i [(\Delta\sigma_z - \Omega(\sigma_+ + \sigma_-) + (\epsilon a^{\dagger 2} - \epsilon^* a^2)), \rho] + \frac{\kappa}{2} \{2 a \rho a^\dagger - \rho a^\dagger a - a^\dagger a \rho\} \\ & - \sqrt{\eta\kappa\gamma} \{[\sigma_+, a \rho] + [\rho a^\dagger, \sigma_-]\} + \frac{\gamma}{2} \{2\sigma_- \rho \sigma_+ - \rho \sigma_+ \sigma_- - \sigma_+ \sigma_- \rho\}, \end{aligned} \quad (4)$$

where the parameter η ($0 < \eta \leq 1$) describes the matching of the incident squeezed vacuum to the modes surrounding the atom. For perfect matching $\eta = 1$, whereas $\eta < 1$ for an imperfect matching.

Since in (4) DPO is not treated as a reservoir but as a part of the system, equation (4) is applicable for any bandwidth of the squeezed vacuum produced by DPO. The advantage of the Markovian master equation (1) over equation (4), however, is the fact that the former allows for analytical solutions while the latter does not. When the DPO cavity bandwidth $\kappa \gg \gamma$, both equations are expected to give the same results. There is a question, however, how big really must be κ with respect to γ to make equation (1) still applicable. To

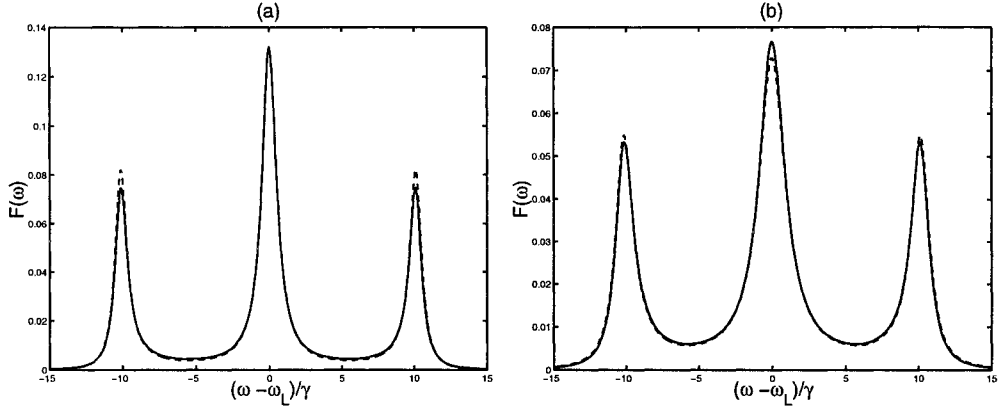


FIG. 1. Fluorescence spectra — coupled-systems (solid) and Markovian master equation (dash): $\epsilon = \kappa/8$ ($N = 0.26$, $M = 0.57$), $\Omega = 10$, $\varphi = 0$, $\Delta = 0$, $\eta = 0.98$ and (a) $\kappa = 10$, (b) $\kappa = 40$

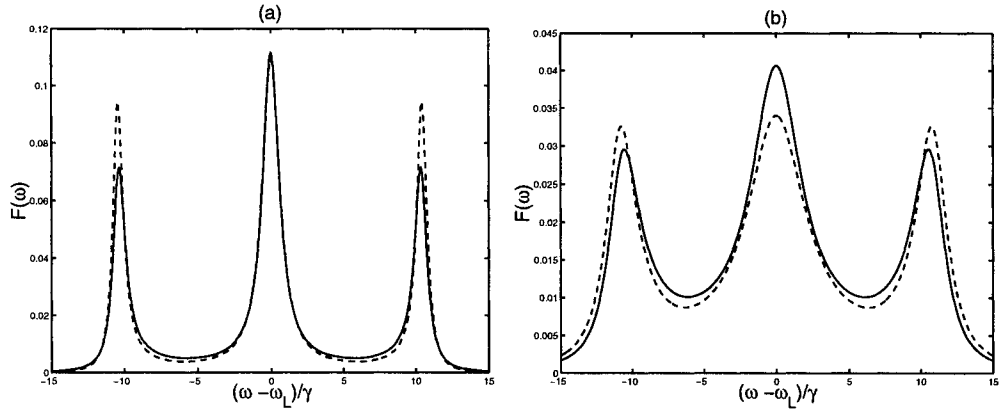


FIG. 2. Fluorescence spectra — coupled-systems (solid) and Markovian master equation (dash): $\epsilon = \kappa/4$ ($N = 1.78$, $M = 2.22$), $\Omega = 10$, $\varphi = 0$, $\Delta = 0$, $\eta = 0.98$ and (a) $\kappa = 10$, (b) $\kappa = 40$

answer this question we show in Figs. 1-3 few examples of the resonance fluorescence spectra obtained using both approaches. The width of the squeezed light κ as well as the amplitude of the pump field ϵ are given in units of the atomic linewidth of γ . In Figs. 1 and 2 there

are examples of the resonance fluorescence spectra for strong field ($\Omega = 10$ in units of γ). In Fig. 1 the squeezing is smaller than in Fig. 2. The well known squeezing parameters N and M (mean number of photons and the field correlation) are: for Fig. 1 $N = 0.26$, $M = 0.57$, and for Fig. 2 $N = 1.78$, $M = 2.22$. As it is seen from Fig. 1, for weak squeezing the agreement between the two approaches is perfect even for the squeezing bandwidth κ as small as 10. When the squeezing becomes more pronounced the agreement is worse for the same bandwidths of the squeezed vacuum, but it is still pretty good. We would like to emphasize that for $\kappa = \Omega = 10$ the squeezing bandwidth is the same as the Rabi frequency of the field, which shows explicitly that the Markovian approximation works well when the squeezing bandwidth is much broader than the atomic linewidth, but not necessarily larger than the Rabi frequency. This is an advantage of our master equation (1), which was derived by performing the dressing transformation first, and next coupling the atom to the reservoir.

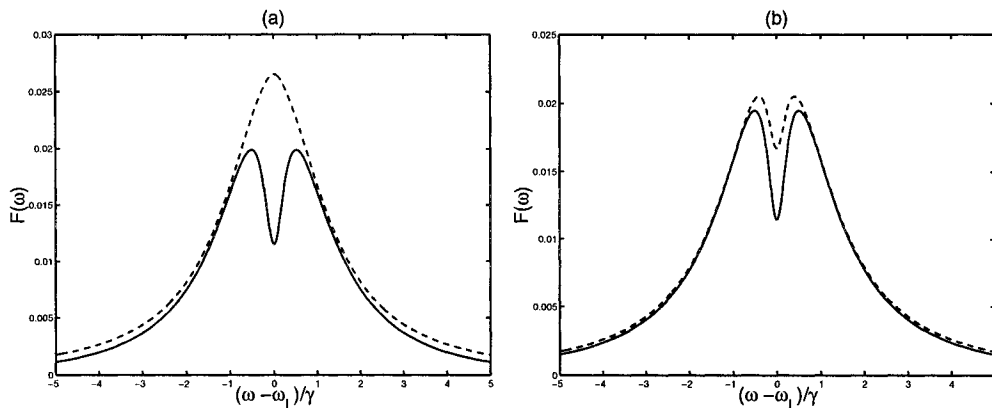


FIG. 3. Fluorescence spectra — coupled-systems (solid) and Markovian master equation (dash): $\epsilon = \kappa/8$ ($N = 0.26$, $M = 0.57$), $\Omega = 0.35$, $\varphi = 0$, $\Delta = 0$, $\eta = 0.98$ and (a) $\kappa = 20$, (b) $\kappa = 40$

In Fig. 3 we show examples of the spectra for a weak field ($\Omega = 0.35$). In this figure the Rabi frequency is chosen as to show a possibility to burn a hole in the spectrum. It is seen that for $\kappa = 10$ in this case the Markovian master equation does not reproduce the hole, and broader squeezing is needed to reproduce the feature, but for $\kappa = 40$ agreement is already quite good.

The results shown here convince us that the Markovian master equation (1) works quite well for the squeezing bandwidth which is ten times bigger than the atomic linewidth.

References

- [1] G. Yeoman and S. M. Barnett, *J. Mod. Optics* **43**, 2037 (1996).
- [2] R. Tanaś, Z. Ficek, A. Messikh, and T. El-Shahat, *J. Mod. Opt.* **45**, 1859 (1998).
- [3] R. Tanaś, *Acta Phys. Slovaca* **49**, 595 (1999).
- [4] H. J. Carmichael, *Phys. Rev. Lett.* **70**, 2273 (1993).
- [5] C. W. Gardiner, *Phys. Rev. Lett* **70**, 2269 (1993).
- [6] C. W. Gardiner and A. S. Parkins, *Phys. Rev. A* **50**, 1792 (1994).

Creation and Detection of Fock States in the Micromaser

B. T. H. Varcoe,^a S. Brattke,^{a,b} and H. Walther^{a,b}

^a*Max-Planck-Institut für Quantenoptik, 85748 Garching, Germany*

^b*Sektion Physik der Universität München, 85748 Garching, Germany*

Abstract

The recent observation of trapping state in the micromaser demonstrated that a maser field in a number state of Fock state can be generated in steady state. Additionally we have shown that Fock states in the micromaser can also be generated dynamically using state reduction of the pump atoms. In this case the purity of the Fock state can be probed by an additional atom sent into the cavity after the first.

The quantum treatment of the radiation field uses the number of photons in a particular mode to characterise the quantum states. The ground state of the quantum field is represented by the vacuum state consisting of field fluctuations with no residual energy. The states with fixed photon number are usually called Fock or number states. These states are also used as the basis for the quantum representation of all general radiation fields which are usually expressed in an expansion of number states. Fock states thus represent the most basic quantum states and are maximally distant from what one would call a classical field. So far Fock states of the radiation field have not been realised experimentally under steady state conditions since they are very fragile and very difficult to produce and maintain. In order to generate these states it is necessary that the mode considered has minimal losses. Additionally the thermal field, always present at finite temperatures, has to be eliminated since it causes photon number fluctuations. In this paper we demonstrate the presence of Fock states by probing the micromaser field using atoms to investigate the dynamics of the photon exchange.

In the micromaser highly excited Rydberg atoms, interact with a single mode of a superconducting cavity which can have a quality factor as high as 3×10^{10} , leading to a photon lifetime in the cavity of 0.2s. The steady state field generated in the cavity was the object of detailed studies of the sub-Poissonian statistical distribution of the field [1], the quantum dynamics of the atom-field photon exchange represented in the collapse and revivals of the Rabi nutation [2], atomic interference [3], bistability and quantum jumps of the field [4], atom-field and atom-atom entanglement [5].

The interaction of a two-level atom with a single mode of the cavity field is governed by the Jaynes-Cummings Hamiltonian [6]. In this system an atom in the presence of a resonant quantum field undergoes Rabi oscillations. At low temperatures of the cavity the number of blackbody photons in the cavity mode is reduced and under this condition, trapping states

begin to appear [11]. They occur in the micromaser when the atom field coupling, Ω , and the interaction time, t_{int} , are chosen such that in a cavity field with n_q photons each atom undergoes an integer number, k , of Rabi cycles. This is summarised by the condition,

$$\Omega t_{\text{int}} \sqrt{n_q + 1} = k\pi \quad (1)$$

When Eq.1 is fulfilled, each atom undergoes a full Rabi cycle leaving the cavity photon number unchanged after the interaction, hence the photon number is "trapped". This will occur over a long range of the atomic pump rates (N_{ex}). The trapping state is therefore characterised by the upper bound photon number n_q and the number of integer multiples of full Rabi cycles k . Trapping states are quantum features of the micromaser field that occur through the influence of Fock or number states of the electromagnetic field.

The experimental apparatus is presented in Fig. 1. The present setup has been described in detail previously [4,7]. Briefly a rubidium oven provides two collimated atomic beams; a main one passing directly into the cryostat which contains the maser cavity and a secondary one used to control the laser frequency. The cavity is cooled by the cryostat to 300mK which corresponds to a thermal photon number of 0.054. A frequency doubled dye laser ($\lambda = 294\text{nm}$) was used to excite rubidium (^{85}Rb) atoms to the Rydberg $63P_{3/2}$ state from the $5S_{1/2}(F = 3)$ ground state. The maser cavity is tuned to the $63P_{3/2}$ - $61D_{5/2}$ (21.4560 GHz) transition. Velocity selection is provided by angling the excitation laser towards the main atomic beam at 11° to the normal. The dye laser was locked to the reference beam, using an external computer control, to the $5S_{1/2}(F = 3) - 63P_{3/2}$ transition of the reference atomic beam excited under normal incidence. The natural velocity distribution of the atomic beam allowed the interaction time of the atoms with the cavity to be tuned from $40\mu\text{s}$ to $160\mu\text{s}$ by Stark shifting the reference frequency with a high quality programmable power supply. The detection of the Rydberg atoms is performed by field ionisation in two detectors set to different voltages so the upper and lower states, $63P_{3/2}$ and $61D_{5/2}$ respectively, can be counted separately. The cavity we used had a Q factor of 1.5×10^{10} for the trapping state measurement and 3.4×10^9 , for the dynamical measurement.

When a trapping state is realised by choosing a proper interaction time, the photon number distribution is strongly peaked in the range $n \leq n_q$. In which state the maser remains until a random event occurs, which changes the photon number in the cavity and violates the trapping state condition. In general during the steady state operation of a micromaser in a trapping state, the waiting time between two atoms in the lower state becomes longer and one should expect a general suppression of events in the lower state atom detector and an increase in the upper state detector [12]; a feature that should be preserved through increasing atomic pump rate N_{ex} [7].

A Fock state shows ideal sub-Poissonian statistics hence under the influence of a trapping state the atomic statistics (which are closely related to the photon statistics [9]) should also be sub-Poissonian. Consequently a first indication that the trapping states represented Fock states of the field was the observation of Sub-Poissonian Statistics when the maser was under conditions of a trapping state [7].

It has been shown theoretically [11] that fixed photon numbers may persist under steady state conditions of the micromaser when dissipation of the field is small and the thermal field in the cavity is reduced to photon numbers on the order of 10^{-2} , or below. This is the case for the following reason: normally the cavity field builds up from the initial thermal

distribution, the photon fluctuations are therefore determined by the initial field. If they are eliminated at low temperatures, the initial state is then the vacuum field. Successive emission events fill the cavity with photons until the photon number becomes "trapped", this being achieved when the emission probability of all subsequent atoms is reduced as all atoms perform complete Rabi cycles without releasing a photon.

Using a dynamical measurement we were able to observe the build up of the maser field using state reduction [13] of a detected atom to project the cavity field onto a Fock state and the Rabi oscillations of a probe atom to test the cavity state. In this way we have observed the Fock states of the maser field up to $n = 2$ [14].

In this paper we reported on the observation of trapping states in the micromaser and subsequent measurements of the maser field under the influence of a Fock state; the ultimate quantum states of a radiation field. The successful generation of Fock states makes many further experiments using these states possible. In the steady state Fock states can be used in quantum information, the observation of Schrödinger cat states and their decoherence and the investigation of nonlocal quantum phenomena such as the entanglement of atoms.

REFERENCES

- [1] G. Rempe and H. Walther, Phys. Rev. A **42**, 1650 (1990).
- [2] G. Rempe, H. Walther and N. Klein Phys. Rev. A **58**, 353 (1987).
- [3] G. Raithel, O. Benson and H. Walther, Phys. Rev. Lett. **75**, 3446 (1995).
- [4] O. Benson, G. Raithel and H. Walther, Phys. Rev. Lett. **72**, 3506 (1994).
- [5] B. Englert, M. Löffler, O. Benson, M. Weidinger, B. Varcoe, and H. Walther, Fortschr. Phys. **46**, 897 (1998)
- [6] E. T. Jaynes and F. W. Cummings, Proc.IEEE **51**, 89 (1963).
- [7] M. Weidinger, B. T. H. Varcoe, R. Heerlein and H. Walther, Phys. Rev. Lett. **82**, 3795 (1999).
- [8] P. Meystre, G. Rempe and H. Walther, Opt. Lett. **13**, 1078 (1988).
- [9] H.-J. Briegel et al., Phys. Rev. A **49**, 2962 (1994); G. Rempe, F. Schmidt-Kaler and H. Walther, Phys. Rev. Lett. **64**, 2783 (1990).
- [10] P. Filipowicz, J. Javanainen and P. Meystre, Phys. Rev. A **34**, 3077 (1986).
- [11] P. Meystre, G. Rempe and H. Walther, Opt. Lett. **13**, 1078 (1988).
- [12] C. Wagner, A. Schenzle and H. Walther, Opt. Comm. **107**, 318 (1994).
- [13] J. Krause, M. O. Scully, and H. Walther, Phys. Rev. A. **36**, 4547 (1987).
- [14] B. T. H. Varcoe, S. Brattke, H. Walther. In preparation.

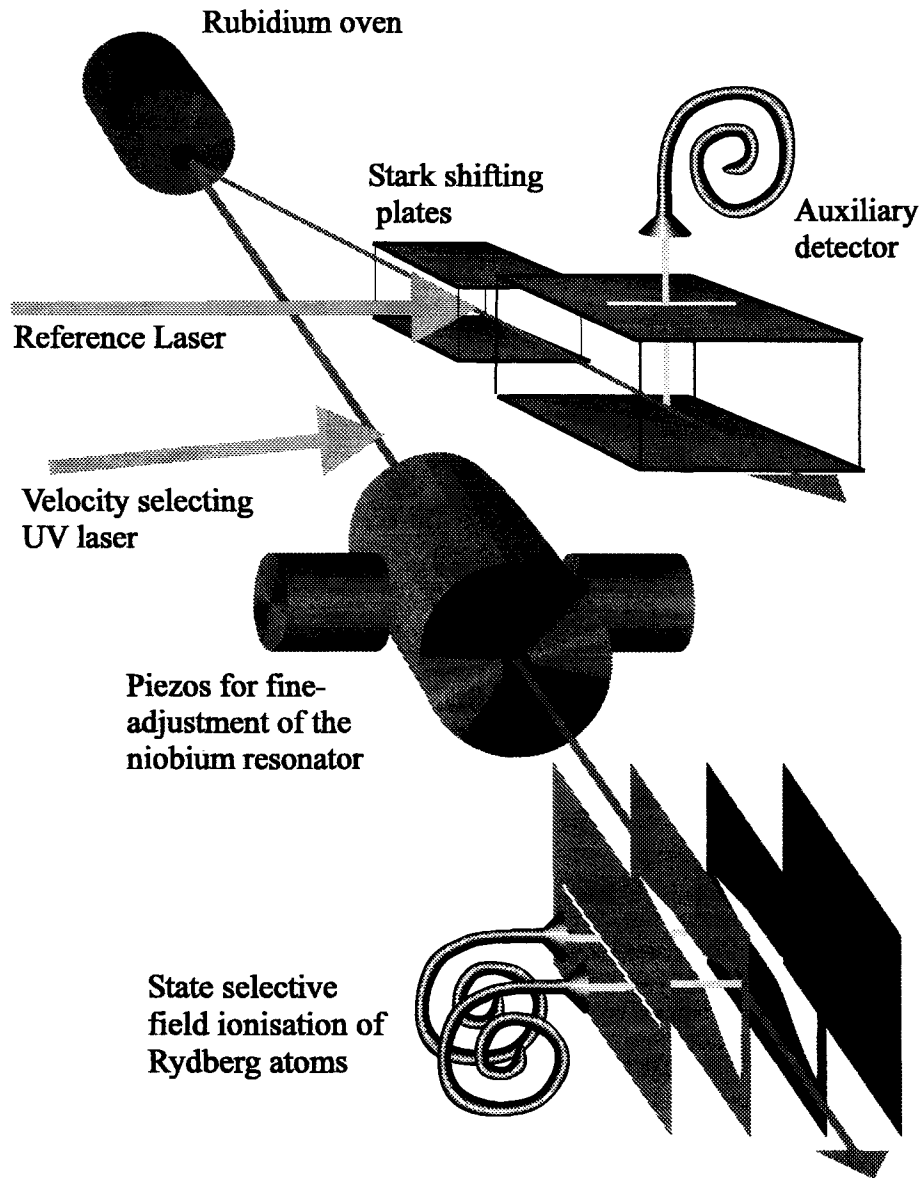


FIG. 1. The experimental setup. The atoms leaving the rubidium oven are excited into the $63P_{3/2}$ Rydberg state using a UV laser at an angle of 11° . After interacting with the cavity the atoms are detected using state selective field ionisation. Tuning of the cavity is performed using two piezo translators. The reference beam is used to stabilise the laser frequency to a Stark shifted atomic resonance. This allowed the velocity subgroup selected by excitation to be changed continuously within the range of the velocity distribution of the atoms.

Coherent instabilities within the thermal wave model as described by a generalized nonlinear Schroedinger equation

D.Anderson

Chalmers University of Technology, SE-41296 Göteborg, Sweden

R.Fedele and V.Vaccaro

Universita`"Federico II", Complesso Universitario di M.S.Angelo, Napoli,Italy

M.Lisak, A.Berntson and S.Johansson

Chalmers University of Technology, S-41259 Göteborg, Sweden

Abstract

Within the framework of the Thermal Wave Model description, an investigation is made of the longitudinal instability properties of a coasting high energy charged particle beam. The analysis, which is based on a nonlinear Schroedinger-like equation for the beam wave function, is shown to reproduce the characteristic features of the coherent instabilities as obtained previously by conventional techniques based on the Vlasov equation for the beam distribution in phase space.

Introduction. The thermal wave model (TWM) is a quantum-like description of classical charged particle beam dynamics. In the TWM description, the beam properties are described by a complex valued beam wave function, which satisfies a Schroedinger-like evolution equation with the beam emittance playing the role of Planck's constant, [1]. The square modulus of the beam wave function represents the beam density. The TWM has been used to analyze a number of linear as well as nonlinear collective effects that occur in charged particle beam dynamics. The approach has successfully reproduced many results of conventional analysis, but has also provided new insight and physical understanding for the propagation dynamics of charged particle beams, e.g. [2].

In the present analysis we will concentrate on an analysis of longitudinal coherent instabilities associated with particle beams. The dynamics of the beam wave function is determined by a Schroedinger equation where the potential is given in terms of a complex impedance, Z , which describes the self consistent interaction between the beam and its surroundings. The self consistency implies that Z is a nonlinear function of the beam wave function and the resulting equation becomes a generalized nonlinear Schroedinger equation.

A modulational instability analysis of a coasting particle beam is carried out for the general case of an impedance having both resistive and reactive parts and the results are shown to be fully consistent with the results of previous conventional analysis. An effort is also made to extend the modulational analysis to the case of bunched particle beams with a finite energy spread where Landau damping is known to be important. This effort is only partially successful in the sense that an increased region of stability in (Z_r, Z_i) space ($Z = Z_r + iZ_i$) is indeed obtained. However, this region is one-dimensional and, although of the correct extension in this dimension, does not reproduce the two-dimensional region of stability close to the origin in (Z_r, Z_i) space, which is found using Vlasov theory. On the other hand, in the limit of large instability growth rates (where Landau damping is negligible) there is again complete agreement between the TWM and Vlasov theories.

The question now arises whether the phenomenon of Landau damping is outside of the TWM as described by the characteristic model equation used. An indication that this is not the case is demonstrated as follows: If the analysis in configuration space, as expressed by the nonlinear

Schroedinger equation for the beam wave function, is generalized into a phase space description by means of a Wigner formalism, the TWM approach does indeed reproduce exactly the Landau damping phenomenon of the Vlasov formalism. Since the phase- and configuration -space descriptions are physically equivalent, Landau damping should be possible to regain also in configuration space, although it seems easier to obtain within a phase-space description.

Generalized nonlinear Schroedinger equation for the beam wave function.

Within the TWM description, the longitudinal dynamics of a charged particle beam is described by the following evolution equation for the beam wave function $\Psi(z,x)$, cf [2].

$$i\varepsilon \frac{\partial \Psi}{\partial z} = \frac{1}{2} \frac{\eta}{\beta^2} \varepsilon^2 \frac{\partial^2 \Psi}{\partial x^2} + \frac{\Psi}{(E_0/e)\beta c T_0} \int_0^x U(x', z) dx' \quad (1)$$

where the first term on the RHS accounts for the longitudinal spreading of the beam and the second term describes the interaction between the beam and its surroundings, as characterized by the self consistent voltage $U(z,x)$ which is related to the charge line density of the beam, $\lambda(z,x)$, according to $U(x,z) = e\beta c Z_r \lambda(x,z) + e\beta c R_0 (Z_i/n) \partial \lambda / \partial x$ where Z is the coupling impedance between the beam and its surroundings. Finally the system is closed by the relation between the charge line density $\lambda(z,x)$ and the beam density, viz. $\lambda(z,x) = N / (2\pi R_0) |\Psi(z,x)|^2$. The notation used here is standard see e.g. [2]. Combining eq. (1) with the definitions of U and λ , the following generalized nonlinear Schroedinger equation is obtained for the beam wave function

$$i\Psi_z = \alpha \Psi_{xx} + \kappa |\Psi|^2 \Psi + \mu \Psi \int_0^x |\Psi(x', z)|^2 dx' \quad (2)$$

where the coefficients are defined by

$$\alpha = \frac{\eta \varepsilon}{\beta^2} ; \quad \kappa = \frac{e^2 N}{2\pi \varepsilon E_0 T_0} \frac{Z_i}{n} ; \quad \mu = \frac{e^2 N}{2\pi \varepsilon E_0 T_0 R_0} Z_r \quad (3)$$

Modulational instability analysis. A convenient way of analyzing the stability properties of small perturbations on a background solution is to decompose the beam wave function as $\Psi(x, z) = A(x, z) \exp[i\Theta(x, z)]$ and to write eq.(2) as two coupled equations for A and θ

$$\begin{aligned} A_z &= \alpha (a A_x \Theta_x + A \Theta_{xx}) \\ -\Theta_z &= \alpha \left[\frac{1}{A} A_{xx} - (\Theta_x)^2 \right] + \kappa A^2 \end{aligned} \quad (4)$$

It is straightforward to show that a stationary solution of eq.(4) is given by $A(x,z) = A_0 = \text{constant}$; $\Theta(x, z) = \Theta_0(x, z) = -\kappa A_0^2 z - \mu A_0^2 x z + (1/3) \alpha \mu^2 A_0^4 z^3$. Considering small perturbations δA and $\delta \Theta$ on the amplitude and phase of the stationary background solution, the linear evolution of these perturbations are determined by the coupled system

$$\begin{aligned} \delta A_z &= \alpha (2\delta A_z \Theta_{0x} + A_0 \delta \Theta_{xx}) \\ -\delta \Theta_z &= \alpha \left(\frac{\delta A_{xx}}{A_0} - 2\Theta_{0x} \delta \Theta_x \right) + 2\kappa A_0 \delta A + 2\mu A_0 \int_0^x \delta A dx' \end{aligned} \quad (5)$$

The system (5) admits plane wave solutions of the form $\delta A, \delta \Theta \propto \exp[i(Kz + \mu \Omega A_0^2 z^2 - \Omega x)]$ which gives rise to the dispersion relation

$$K^2 = (\alpha \Omega^2)^2 \left(1 - \frac{2\kappa \Psi_0^2}{\alpha \Omega^2} - i \frac{2\mu \Psi_0^2}{\alpha \Omega^3}\right) \quad (6)$$

Neglecting the first dispersively stabilizing part, eq.(6) can be rewritten in physical quantities as

$$K^2 \approx -2\alpha \Omega^2 \Psi_0^2 \left(\kappa + i \frac{\mu}{\Omega}\right) = \left(\frac{n\omega_0}{\beta c}\right)^2 \frac{eI_0}{2\pi\beta^2 E_0} i \frac{\eta Z}{n} \quad (7)$$

in full agreement with conventional Vlasov results for the instability of a coasting beam cf e.g. [2]. In particular we note that if $Z_i \neq 0$, the beam is always unstable and writing $K = K_r + iK_i$, we can eliminate K_r from eq.(7) to express the dispersion relation in the form $Z_i = Z_i(Z_r; K_i)$. It is found that the level curves $Z_i = Z_i(Z_r; K_i)$ for constant K_i are parabolas of the form

$$\bar{Z}_i = 1 + \bar{K}_i^2 - \frac{1}{4\bar{K}_i^2} \bar{Z}_r^2 \quad (8)$$

where

$$\bar{Z}_i = \frac{2\kappa A_0^2}{\alpha \Omega^2} \propto \frac{Z_i}{\eta n} \quad ; \quad \bar{Z}_r = \frac{\mu A_0^2}{\alpha \Omega^3} \propto \frac{Z_r}{\eta n} \quad \text{and} \quad \bar{K}_i = \frac{K_i}{\alpha \Omega^2} \quad (9)$$

Modulational instability. We now generalize the situation to allow for a bunched beam, i.e. $A(x,0)=A_0(x)$. If we assume that the width of the beam bunch is large, the scale length for its change can be assumed much longer than that of the instability growth. Consequently, we can neglect the z-variation of the background profile and approximate $A_0(x,z) \approx A_0(x)$. Allowing however for the curvature of $A_0(x)$ we can approximate eq.(5) as

$$\begin{aligned} \left(\frac{\delta A}{A_0}\right)_z &= \alpha \left[2 \left(\frac{\delta A}{A_0}\right)_{xx} \Theta_{0x} + \delta \Theta_{xx} \right] \\ -\delta \Theta_z &= \alpha \left[\left(\frac{\delta A}{A_0}\right)_{xx} + \frac{A_{0xx}}{A_0} \frac{\delta A}{A_0} - 2\Theta_{0x} \delta \Theta_x \right] + 2\kappa A_0^2 \frac{\delta A}{A_0} + 2\mu A_0^2 \int_0^x \frac{\delta A}{A_0} dx' \end{aligned} \quad (10)$$

Here we can approximate further $A_{0xx}/A_0 \approx -F/a^2$, where a is the width of the beam and F is a form factor which depends on the actual shape, but is of the order of unity, e.g. if $A_0(x) = A_0 \cos(\pi x/2a)$ we have $A_{0xx}/A_0 = -\pi^2/4$. It can now easily be shown from eq.10) that the dispersion relation (6) is changed into

$$K^2 = (\alpha \Omega^2)^2 \left(1 + \frac{F}{a^2 \Omega^2} - \frac{2\kappa \Psi_0^2}{\alpha \Omega^2} - i \frac{2\mu \Psi_0^2}{\alpha \Omega^3}\right) \quad (11)$$

From eq.(11) we infer that the finite extension of the beam provides a further stabilizing effect. The corresponding level curves for constant growth rate are still parabolas, but are shifted by the new stabilizing term to read

$$\bar{Z}_i = \Gamma^2 + \bar{K}_i^2 - \frac{1}{4\bar{K}_i^2} \bar{Z}_r^2 \quad (12)$$

where $\Gamma^2 = 1 + F/(a^2\Omega^2)$. Clearly, the region of instability for $\bar{Z}_r = 0$ has been increased. However, conventional Vlasov theory predicts a two-dimensional region of stability close to the origin in the (Z_r, Z_i) plane and in the vicinity of this region, the level curves are deformed away from the simple parabolic form. For large growth rates though, the level curves regain their parabolic form. Thus, the present analysis based on the TWM reproduces all the characteristic features of the conventional analysis except for the small two-dimensional region of stability close to the origin in (Z_r, Z_i) space. Possible explanations for this discrepancy are the fact that the present analysis is based on the full nonlinear stationary solution and in particular that the analysis assumes that the scale length for the variation of the background solution is much longer than that of the instability. The latter assumption is clearly not valid in or close to the stability region.

Is there Landau damping in the TWM description ?

It is possible to go from configuration space (as described by the NLS equation for $\Psi(x, z)$) to phase space by introducing the Wigner-like function (p conjugate momentum to x)

$$\rho(z, x, p) \propto \int_{-\infty}^{+\infty} \Psi(x - \frac{y}{2}, z) \Psi^*(x + \frac{y}{2}, z) \exp(i \frac{py}{\epsilon\eta}) dy \quad (13)$$

If $\Psi(x, z)$ satisfies eq.(1), it can be shown that $\rho(z, x, p)$ satisfies the von Neuman equation

$$\left\{ \frac{\partial}{\partial z} + p \frac{\partial}{\partial x} + \frac{i}{\epsilon\eta} [U(x + i \frac{\epsilon\eta}{2} \frac{\partial}{\partial p}) - U(x - i \frac{\epsilon\eta}{2} \frac{\partial}{\partial p})] \right\} \rho = 0 \quad (14)$$

Expanding U for small values of ϵ and linearizing the corresponding equation around the equilibrium state $\rho_0(p)$, the dispersion relation becomes ($\alpha_0 = q^2 \beta c \eta \lambda_0 / (2\pi E_0 R_0)$)

$$1 = i\alpha_0 Z \int_{-\infty}^{+\infty} \frac{d\rho_0/dp}{Kp - \Omega} \quad (15)$$

which coincides with the dispersion relation of the conventional theory, including the phenomenon of Landau damping.

Conclusion. The present analysis has confirmed that the TWM provides a powerful new approach for analyzing the properties of high energy charged particle beams. In particular, the main properties of coherent longitudinal instabilities of a particle beam have been recovered although some additional analysis is needed to explain the two-dimensional stability region close to the origin in impedance space as found by classical Vlasov theory.

References.

- [1] R.Fedele and G. Miele, Il Nuovo Cimento D13,1527 (1991)
- [2] D.Anderson, R.Fedele, V.Vaccaro, M.Lisak, A.Berntson and S.Johanson, "Nonlinear and collective phenomena in beam physics 1998 Workshop", Editors S.Chattopadhyay, M.Cornacchia, C.Pellegrini, AIP Conf.Proc.468, 197 (1999)
- [3] M.Migliorati and L.Palumbo, in Quantum-like Models and Coherent Effects, Editors R.Fedele and P.Shukla (World Scientific Publ.) Singapore, 246 (1995) and R.Fedele, G.Miele, L.Palumbo and V.Vaccaro, Phys. Lett. A179, 263 (1995)

Complete Subsets of Coherent States and a Quantum Phase Operator

D. Arsenović

*Institute of Physics,
PO Box 57, Belgrade, Yugoslavia*

N. Burić

*Department of Mathematics and Physics, Faculty of Pharmacy,
Vojvode Stepe 450, Belgrade, Yugoslavia*

D. M. Davidović

*Laboratory of Theoretical Physics,
The Institute of Nuclear Sciences "Vinča",
PO Box 522, 11001 Belgrade, Yugoslavia*

Abstract

We use a subset of coherent states $\{|\alpha_k\rangle\}$, which is complete but not overcomplete, and its biorthogonal set $\{|w_k\rangle\}$, to define the action of the phase operator $\hat{\phi}_L$, introduced somewhat imprecisely by Lewis et al [Phys. Rev. Lett. **77**, 5157 (1996)], on a dense set of states. We show that its domain does not contain the number states so that the "no go" theorem for this putative phase operator does not apply, and we explain some misunderstandings related to it.

I. INTRODUCTION

It is well known that there is no self-adjoint operator with the domain containing the number states $|n\rangle$, which satisfies canonical commutation relations with the oscillator hamiltonian. This is the content of the well known "no go" theorem for the operator representing the phase variable of the quantum harmonic oscillator. It is usually ascribed to Susskind and Glogower [1], but it was probably noticed already by Dirac [2] as early as in 1931.

Recently, Lewis *et al.* [3] proposed the following expression:

$$\hat{\phi}_L = \frac{1}{2i}(\ln \hat{a}^+ - \ln \hat{a}), \quad (1)$$

where \hat{a}^+ and \hat{a} are the creation and annihilation operators, to represent the phase of the quantum harmonic oscillator. They proceeded, without a precise definition of the domain of the expression (2), to symbolically calculate its matrix elements in the overcomplete bases of the coherent states $|\alpha\rangle$. Furthermore they formally obtained the standard canonical commutation relations of $\hat{\phi}_L$ with the Hamiltonian. Somewhat later, Smith and Vacarro [4] claimed that the proposed expression $\hat{\phi}_L$ is equivalent to the one proposed by Turski [5]: $\hat{\phi}_T$, and for the later they explicitly showed that it does not satisfy the canonical commutation relations.

We show, by direct and simple, computation that the two expressions are not equivalent.

The conclusions of Smith and Vacarro are correct but they do not apply on the $\hat{\phi}_L$ by Lewis *at all*... Nevertheless, the analyses of Smith and Vacarro points to the one important aspect of the problem: If an expression, like (2), defined as a nonentire function of the creation and annihilation operators, is apparently changed by the unity $\int |\alpha\rangle\langle\alpha|d^2\alpha$, how should one correctly define its action on the states different from the coherent states. In the next section we give a constructive answer on this question

II. WHAT IS THE DOMAIN OF $\hat{\phi}_L$?

The subtlety of the problem with a putative phase operator is well illustrated by the example of the *Lewis et al.* expression (2), and the corresponding objections raised by Smith and Vacarro. *Lewis et al.* proposed the expression $\hat{\phi}_L$ given by (2) to represent the phase of the quantum harmonic oscillator, guided by the fact that its mean value in a coherent state $|\alpha\rangle$, $\alpha = \rho \exp(i\phi)$ is formally equal to the phase ϕ . They claim that in a (unspecified) domain $\hat{\phi}_L$ satisfies the canonical commutation relations with the Hamiltonian. Smith and Vacarro [4] acted on (2) by the unity expressed as $\mathbf{1} = \int |\alpha\rangle\langle\alpha|d^2\alpha$ to obtain:

$$\frac{1}{2i\pi} \left[\int |\alpha\rangle\langle\alpha|d^2\alpha \ln a^+ - \int \ln a |\alpha\rangle\langle\alpha|d^2\alpha \right] = \int \phi |\alpha\rangle\langle\alpha|d^2\alpha = \hat{\phi}_T \quad (2)$$

Then they showed that $\hat{\phi}_T$ does not satisfy the canonical commutation relations with the Hamiltonian, which, as they concluded, contradicts the claim by Lewis *at all*.

However, one should be careful in applying the resolution of unity given by the overcomplete set of coherent states on the symbolic expressions like (2). Indeed, remaining on the formal level of *Lewis at all*, the mean value of $\hat{\phi}_L$ in a coherent state $|\alpha\rangle$ is:

$$\langle\alpha|\hat{\phi}_L|\alpha\rangle = \langle\alpha|\ln \alpha^+ - \ln \alpha|\alpha\rangle = (\ln a^* - \ln a) \langle\alpha|\alpha\rangle = \phi \quad (3)$$

Let us suppose that $0 \leq \phi' < 2\pi$ and that $0 < \phi \leq \pi$. Since $|\langle\alpha|\alpha'\rangle|^2 = f(\rho', \cos(\phi' - \phi))$ we have:

$$\begin{aligned} \langle\alpha|\hat{\phi}_T|\alpha\rangle &= \int \phi' \langle\alpha|\alpha'\rangle \langle\alpha'|\alpha\rangle d\alpha' = \\ & \int_{-\phi}^{2\pi-\phi} (\phi + u) |\langle\alpha|\alpha'\rangle|^2 d\alpha' = \phi \int_{-\phi}^{2\pi-\phi} |\langle\alpha|\alpha'\rangle|^2 d\alpha' + \int_{-\phi}^{2\pi-\phi} u f(\rho', \cos u) du \rho' d\rho'. \end{aligned} \quad (4)$$

The first integral is equal to ϕ and the second can be split into a sum of two integrals, one on $(-\phi, \phi)$ and the other on $(\phi, 2\pi - \phi)$. Since $f(\rho', \cos u)$ is an even function of u the first

of these integrals is zero and the second is different from zero except when $\phi = \pi$. Thus, we have shown that

$$\langle \alpha | \hat{\phi}_L | \alpha \rangle \neq \langle \alpha | \hat{\phi}_T | \alpha \rangle . \quad (5)$$

So the claim by Smith and Vacarro can not be considered as proved since it is irrelevant for $\hat{\phi}_L$, although correct for $\hat{\phi}_T$.

These, apparently contradictory conclusions, about a putative phase operator are mathematically due to the facts that $\phi = i \ln(\alpha/\rho)$ is not an entire function of $\alpha \in \mathbf{C}$, and that the bases of the coherent states is overcomplete and nonorthogonal.

The difficulties with $\hat{\phi}_L$ can be circumvented by a more careful consideration of the states where the expression (2) gives convergent results. These states are obtained by picking up a discrete and complete, but not overcomplete, subset $\{|\alpha_k \rangle\}$ from the overcomplete set of all coherent states. Such states are first considered by J. von Neumann [6], and the exact completeness of $\{|\alpha_k \rangle\}$ was proved by Perelomov [7]. He also constructed the set of the corresponding biorthogonal states $\{|w_k \rangle\}$. The states $\{|\alpha_k \rangle\}$ are parameterised by points in a lattice in the complex plane. Namely, $\{|\alpha_k \rangle\} = \{|m\omega_1 + n\omega_2 \rangle\}$, where $(m, n) \neq (0, 0) \in \mathbf{Z} \times \mathbf{Z}$ are pairs of entire numbers except $(m, n) = (0, 0)$ and $\omega_1, \omega_2 \in \mathbf{C}$ are complex numbers. Furthermore, ω_1 and ω_2 are chosen such that the surface of the cell $S = Im(\omega_2 \omega_1^*)$ is equal to π . The latest condition is necessary and sufficient for the set of states to be complete and not overcomplete. In order to save on the notation we use single index k instead of the pair (m, n) . The biorthogonal basis $\{|w_k \rangle\}$ satisfies $\langle w_k | \alpha_l \rangle = \delta_{kl}$. Explicit relations for $\langle \alpha | w_k \rangle$, which shall not be used in this paper, are given in [7].

Using the sets $\{|\alpha_k \rangle\}$ and $\{|w_k \rangle\}$ we define the following expression:

$$\hat{\phi}_L = \sum_k \ln \alpha_k |\alpha_k \rangle \langle w_k| - \ln \alpha_k^* |\alpha_k \rangle \langle w_k| \quad (6)$$

to represent $\hat{\phi}_L$ when acting on the dense set of states represented as convergent sums of $|\alpha_k \rangle$:

$$|\psi \rangle = \sum_k c_k |\alpha_k \rangle, \quad c_k = \langle w_k | \psi \rangle . \quad (7)$$

The domain of $\hat{\phi}_L$ contains the dense set $\{|\alpha_k \rangle\}$, and in addition all the vectors represented as convergent sums (10) such that the action of $\hat{\phi}_L$ is also represented as a convergent sum (10). For example,

$$\langle \alpha_k | \hat{\phi}_L | \alpha_k \rangle = (\ln \alpha_k^* - \ln \alpha_k) = \phi_k . \quad (8)$$

in accord with *Lewis at all*. However $\hat{\phi}_L$ and $\hat{\phi}_T$, formally given by (2), could, and do, formally give different results when acting on the "redundant" coherent states $|\alpha \rangle \neq |\alpha_k \rangle$. Since the *Lewis at all* expression (2) has no properly defined domain, and in order to avoid multiplication of symbols, in what follows we shall always denote the operator $\hat{\phi}_L$ by $\hat{\phi}_L$, baring on mind the definition of its domain.

It is important to notice that the eigenstates of the Hamiltonian $|n \rangle$ can not be represented as a convergent sum (10), so that $\langle n | \hat{\phi}_L | n \rangle$ is not defined. Indeed, if $|n \rangle$ would

have been equal to $|n\rangle = \sum c_k |\alpha_k\rangle$ than, by applying $n+1$ times the annihilation operator, one would obtain $0 = \sum_k \alpha_k^{n+1} c_k |\alpha_k\rangle$, which can not be since $\{|\alpha_k\rangle\}$ are not overcomplete. This fact points out to a deep physical reason for the difficulties in the definition of the quantum phase.

III. DISCUSSION

Major impediment to a consistent definition of an operator representing the phase of the quantum harmonic oscillator is the well known "no go" theorem, mentioned in the introduction, which states that there is no hermitian operator \hat{O} on $L_2(\mathbf{R})$ with a domain containing the hermite functions and satisfying $[\hat{n}, \hat{O}] = i$, where \hat{n} is the number operator.

Our approach was to question the domain of the putative phase operator. Following Lewis et al. we introduced the expression (9) defined on a dense set of states, containing the complete subset of the coherent states, and we gave explicit rules how this expression should be used to give convergent results. The domain of the operator $\hat{\phi}_L$, given by (9), does not contain the number states, so that the "no go" theorem does not apply, and the canonical commutation relations could be satisfied. The operator $\hat{\phi}_L$ is based on a complete subset of the coherent states $|\alpha_k\rangle$, its biorthogonal set $|w_k\rangle$ and the $\ln \hat{a}$ function. The $\ln \hat{a}$ function was previously used in this context by *Lewis et al.*...but they remain on a formal, symbolic treatment of this quantity, which made possible, also formal, criticism of Smith and Vaccaro. However, $\hat{\phi}_L$ is an explicitly defined quantity, with a properly specified domain and action. Its action is defined by convergent series whenever it acts on a state which can be represented as a convergent series of $|\alpha_k\rangle$. Such states are dense in $L_2(\mathbf{R})$. However, $\hat{\phi}_L$ is not well defined in the number states $|n\rangle$, which is, in a way, in accord with the "no go" theorem.

REFERENCES

- [1] L. Susskind and J. Glogower J. Phys. **1**, 49 (1964).
- [2] D. A. Dubin, *private communication*.
- [3] H.R. Lewis, W.E. Lawrence and J. D. Harris Phys. Rev. Lett. **77**, 5157 (1996).
- [4] T. B. Smith and J. A. Vaccaro, Phys. Rev. Lett.
- [5] L.A. Turski, Physica **57**, 432 (1972).
- [6] J. von Neumann, *Mathematische Grundlagen der Quantenmechanik*, Springer, Berlin (1932).
- [7] A. Perelomov, *Generalised Coherent States and Their Applications* Springer, Berlin (1986).

Maximal squeezing, pure states, and squeezing amplification

Peng Zhou

*Department of Applied Mathematics and Theoretical Physics,
The Queen's University of Belfast, Belfast BT7 1NN, United Kingdom.*

Stuart Swain

*Department of Applied Mathematics and Theoretical Physics,
The Queen's University of Belfast, Belfast BT7 1NN, United Kingdom.*

We show that 100% squeezed output can be produced in the fluorescence from a driven two-level atom interacting with a squeezed vacuum, and that the atom evolves into a pure atomic state. The quadrature for which optimal squeezing occurs depends on the squeezing phase Φ . For small N , squeezing amplification may occur.

There have been several theoretical investigations of squeezing in resonance fluorescence, both in terms of the total variances and in terms of the fluctuation spectra of the phase quadratures. Single-mode or frequency-tunable two-mode squeezing with a finite bandwidth may be obtained, depending on the Rabi frequency and detuning [1].

Experimental observation of squeezing in the fluorescence field has proved a great challenge, one problem being that atomic motion produces phase shifts which destroy squeezing. This difficulty was surmounted in the recent experimental advances [2]. Recently, experiments carried out by Zhao *et al.* [3] have found some evidence of squeezing by measuring the phase-dependent fluorescence spectra of a coherently driven two-level atom with a long lifetime, stimulating the further exploration of squeezing in resonance fluorescence.

We have recently found that squeezing in resonance fluorescence can be greatly enhanced in a frequency-tunable cavity [4], or in a squeezed vacuum [5]. The latter works mainly in the regime over which anomalous spectra such as hole-burning and dispersive profiles [6] occur, where squeezing occurs in the *out-phase* quadrature of the fluorescent field.

Here we extend the study to the general case, and show that large squeezing occurs in *different phase* quadratures of the fluorescent field, depending upon the values of the parameters. The large squeezing is associated with an atomic pure state, and thereby with a large atomic coherence. Perfect fluorescent squeezing may only take place for the particular squeezing number $N = 1/8$.

For a two-level atom driven by a coherently laser field and damped by a broadband squeezed vacuum, the optical Bloch equations are of the form

$$\begin{aligned}\langle \dot{\sigma}_x \rangle &= -\gamma_x \langle \sigma_x \rangle - (\Delta + \gamma M \sin \Phi) \langle \sigma_y \rangle, \\ \langle \dot{\sigma}_y \rangle &= -\gamma_y \langle \sigma_y \rangle + (\Delta - \gamma M \sin \Phi) \langle \sigma_x \rangle - \Omega \langle \sigma_z \rangle, \\ \langle \dot{\sigma}_z \rangle &= -\gamma_z \langle \sigma_z \rangle + \Omega \langle \sigma_y \rangle - \gamma,\end{aligned}\tag{1}$$

where $\gamma_{x,y} = \Gamma \pm \gamma M \cos \Phi$, $\gamma_z = \gamma_x + \gamma_y$, $\Gamma = \gamma(N + 1/2)$, and $\Delta = \omega_A - \omega_L$ is the detuning, Ω the Rabi frequency and Φ the relative phase between the laser and the squeezed vacuum, N the squeezing photon number, and M the strength of the two-photon correlations in the squeezed vacuum which obeys $M \leq \sqrt{N(N + 1)}$; σ_x and σ_y are the in-phase (X) and out-of-phase (Y) quadrature components of the atomic polarization, respectively, and σ_z is the population inversion.

It has been shown that such a coherently driven two-level atom interacting with the squeezed vacuum reservoir can collapse into a steady-state which is a pure state, for the case $\Phi = 0$ or π [6], *i.e.*, $\Sigma = \langle \sigma_x \rangle^2 + \langle \sigma_y \rangle^2 + \langle \sigma_z \rangle^2 = 1$. We point out here that a steady pure state can, in fact, be achieved for other values of the squeezing phase as well, the requirement being that given Φ , Ω and Δ are chosen to satisfy $\Sigma = 1$. The general pure state has the form

$$|\Psi\rangle = \frac{\sqrt{M}|0\rangle - e^{i\alpha}\sqrt{N}|1\rangle}{(M + N)^{1/2}}. \quad (2)$$

where $\alpha = \arctan\left(\frac{\Gamma + \gamma M \cos \Phi}{\Delta + \gamma M \sin \Phi}\right)$. The conditions for the pure state (2) for a few specific cases are given below:

$$\Phi = 0, \quad \Delta = 0, \quad \Omega = \frac{\gamma\sqrt{M}}{\sqrt{N+1} + \sqrt{N}}, \quad (3)$$

$$\Phi = \frac{\pi}{2}, \quad \Delta = \Gamma - \gamma M, \quad \Omega = \frac{\gamma\sqrt{2M}}{\sqrt{N+1} + \sqrt{N}}, \quad (4)$$

$$\Phi = \pi, \quad \Delta \gg \Gamma - \gamma M, \quad \Omega = \frac{2\Delta\sqrt{M}}{\sqrt{N+1} - \sqrt{N}}. \quad (5)$$

Notice that for resonant excitation, a pure state is only possible if $\Phi = 0$. In general, the pure state (2) describes a completely polarized atom with the Bloch vector \mathbf{B} lying on the Bloch sphere with polar angles α and β ,

$$\mathbf{B} = \cos \alpha \sin \beta \mathbf{e}_x + \sin \alpha \sin \beta \mathbf{e}_y + \cos \beta \mathbf{e}_z \quad (6)$$

where $\beta = \arccos\left(-\frac{M-N}{M+N}\right)$. When Φ , Ω and Δ satisfy the condition (3), then $\alpha = \pi/2$, and the atomic Bloch vector (polarization) is in the Y-Z plane, whereas if the condition (5) holds, we have $\alpha = 0$ and the atom polarizes in the X-Z plane.

The total normally-ordered variances of the phase quadratures of the fluorescent field can be expressed in terms of the steady state solution of the Bloch equations (1) as

$$S_\theta = \langle : (\Delta E_\theta)^2 : \rangle = 1 + \langle \sigma_z \rangle - (\langle \sigma_x \rangle \cos \theta - \langle \sigma_y \rangle \sin \theta)^2, \quad (7)$$

where $E_\theta = e^{-i\theta}\mathcal{E}^{(+)} + e^{i\theta}\mathcal{E}^{(-)}$ is the θ -phase quadrature of the atomic fluorescence field, measured by homodyning with a local oscillator having a controllable phase θ relative to the driving laser. $E_{\theta=0}$ and $E_{\theta=\pi/2}$ are usually the in-phase (X) and out-of-phase (Y) quadratures of the fluorescent field, respectively. S_θ is the total normally-ordered variance of the θ -phase quadrature of the fluorescent field. The field is said to be squeezed when $S_\theta < 0$. The

normalization we have chosen is such that maximum squeezing corresponds to $S_\theta = -0.25$. Eq. (7) implies that the squeezing occurs at large values of the atomic coherences, $\langle\sigma_{x(y)}\rangle$.

It is not difficult to show that the total normally-ordered variances in the phase quadrature component of the fluorescent field reach their minimal value

$$S_{\theta_o} = 1 + \langle\sigma_z\rangle - \langle\sigma_x\rangle^2 - \langle\sigma_y\rangle^2 = \langle\sigma_z\rangle(1 + \langle\sigma_z\rangle) + 1 - \Sigma, \quad (8)$$

when the quadrature phase $\theta_o = \arctan\left(\frac{\Gamma + \gamma M \cos \Phi}{\Delta + \gamma M \sin \Phi}\right)$. (Note that only when $S_{\theta_o} < 0$ is the resonance fluorescence a noise-squeezed field.) Furthermore, if the atom is in a pure state, *i.e.*, $\Sigma = 1$, then S_{θ_o} reduces to

$$S_{\theta_o}^{PS} = \langle\sigma_z\rangle(1 + \langle\sigma_z\rangle) \leq 0, \quad (9)$$

showing that maximum squeezing occurs when $\langle\sigma_z\rangle = -1/2$. Therefore, a completely polarized atom always radiates a fluorescent field with θ_o -phase quadrature squeezing. The quadrature phase θ_o is same as the longitudinal angle α of the polarized atom in the Bloch sphere.

We may conclude that when $\Phi = 0$ and $\Delta = 0$, optimal squeezing in the fluorescent field always occurs in the out-of-phase (Y) quadrature component, *i.e.*, $\theta_o = \pi/2$ [5]. When $\Phi = \pi/2$ and $\Delta = \Gamma - \gamma M$, then $\theta_o = \pi/4$, and optimal squeezing takes place in the $\pi/4$ phase quadrature [3]. When $\Phi = \pi$ and $\Delta \gg \Gamma - \gamma M$, then $\theta_o = 0$, and optimal squeezing is always in the in-phase (X) quadrature [4].

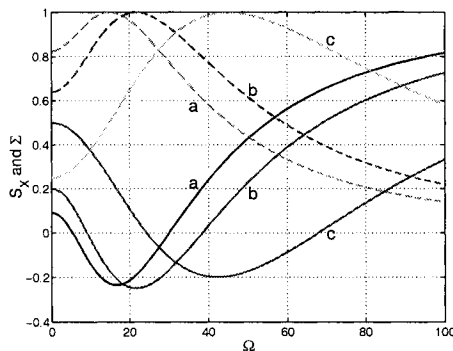


FIG. 1. S_X and Σ as functions of Ω , for $\gamma = 1$, $\Phi = \pi$, $\Delta = 12.5$ and (a): $N = 0.05$, (b): $N = 1/8$ and (c): $N = 0.5$. The solid and dashed lines represent respectively S_X and Σ .

Figure 1 shows that large squeezing in the resonance fluorescence of the two-level atom occurs for pure atomic states. When $N = 1/8$, maximal squeezing ($S_X = -0.25$) is achieved at the Rabi frequency $\Omega = 21.65\gamma$. The large squeezing is due to the large atomic coherence in the pure state.

When eq. (5) is satisfied, the atom is in the pure state (2) with $\alpha = 0$. The corresponding total, normally-ordered variance S_X of the in-phase quadrature of the fluorescent field is of the form

$$S_X^{PS} = \frac{N - M}{N + M + 1/2}. \quad (10)$$

When $N = 1/8$, $M = 3/8$. Then, from eq. (10) we have $S_X^{PS} = -0.25$ (100% squeezing). The corresponding value of the Rabi frequency is $\Omega = \sqrt{3}\Delta$.

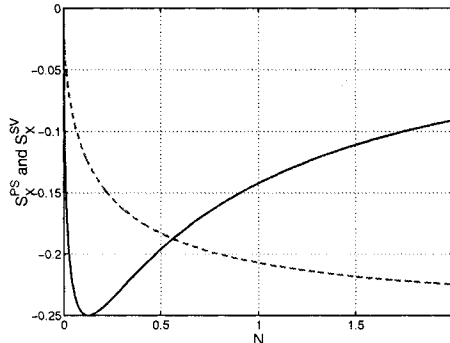


FIG. 2. S_X^{PS} and S_X^{SV} as functions of N , represented by the solid and dashed lines respectively.

We plot S_X^{PS} , indicated by the solid line, against N in Fig. 2, which demonstrates that large squeezing occurs for small photon numbers. For comparison, we also present the normally-ordered variance S_X^{SV} of the in-phase quadrature in the squeezed vacuum field, represented by the dashed line in this figure. It is clear that the squeezing of the output field (fluorescence) is greatly enhanced over the region $0 < N \leq 0.562$, compared with the squeezing of the input (squeezed vacuum) field. Hence, the atom may be applied as a nonlinear optical element to amplify squeezing.

Fluorescent field squeezing can also occur in other phase quadratures with the phase between 0 (in-phase) and $\pi/2$ (out-of-phase).

This work is supported by the United Kingdom EPSRC.

-
- [1] M. J. Collett, D. F. Walls, and P. Zoller, *Opt. Commun.* **52**, 145 (1984); P. Zhou and S. Swain, *Phys. Rev. A* **59**, 841 (1999).
 - [2] J. T. Hoffges, H. W. Baldauf, T. Eichler, S. R. Helmfrid, and H. Walther, *Opt. Commun.* **133**, 170 (1997).
 - [3] H. Z. Zhao, Z. H. Lu, and J. E. Thomas, *Phys. Rev. Lett.* **79**, 613 (1997); Z. H. Lu, S. Bali and J. E. Thomas, *Phys. Rev. Lett.* **81**, 3635 (1998).
 - [4] P. Zhou and S. Swain, *Phys. Rev. A* **59**, 1603 (1999).
 - [5] S. Swain and P. Zhou, *Opt. Commun.* **123**, 310 (1996); Z. Ficek and S. Swain, *J. Opt. Soc. Am. B* **14**, 258 (1997).
 - [6] Swain, *Phys. Rev. Lett.* **73**, 1493 (1994); S. Swain and P. Zhou, *Phys. Rev. A* **52**, 4845 (1995).

Squeezed light beam generated by injection locked VCSEL's

J.-P. Hermier, A. Bramati, and E. Giacobino

*Laboratoire Kastler Brossel, Ecole Normale Supérieure, CNRS, 4 place
Jussieu, 75252 Paris Cedex 05 (France)*

P. Schnitzer and K. J. Ebeling

*University of Ulm Optoelectronics Dept. Albert Einstein-Allee 45 D-89069
(Germany)*

Abstract

We have investigated the intensity noise properties of injection locked VCSEL's. This injection is realized with a laser diode in an external grating configuration. We observe a reduction of the intensity below the shot noise level with a reduction of the number of transverse oscillating modes.

I. INTRODUCTION

VCSEL's have been studied extensively in the past few years because of several useful characteristics and because they appear very promising both for industrial applications and for basic research. Indeed they show many advantages with respect to the previous standard semiconductor lasers architectures. They present a very low threshold, a high quantum efficiency and they can exhibit single longitudinal and transverse mode operation [1]. However, the maximum single mode power is limited by the onset of higher order transverse modes. Moreover, many changes are observed in the polarisation states of the emitted field as the driving current is increased [2,3].

In this paper, we investigate the intensity noise of high quantum efficiency oxide confined VCSEL's. We report generation of amplitude squeezed light by injection locked VCSEL's. This technique, already used to reduce the intensity noise of other semiconductor lasers [4] is applied with success to VCSEL's.

The material of the paper is organised as follows : after this introduction, we present the experimental setup in section II. In section III, we analyse the experimental results. Finally, in section IV, we summarize the results.

II. EXPERIMENTAL SETUP

We use oxide confined VCSEL's (made at the Department of Optoelectronics of the University of Ulm) with different active media diameters: 5, 7, 10, 12, 16 and 20 μm . They

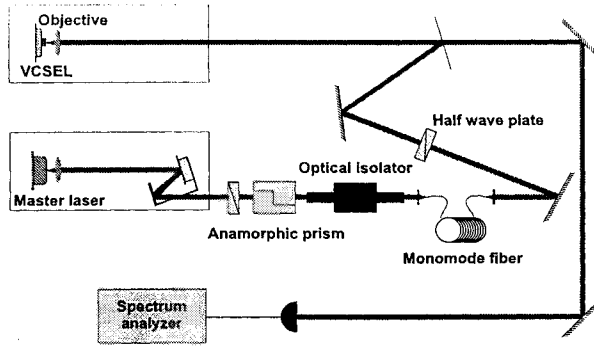


FIG. 1. Experimental setup for noise measurement on injection locked VCSEL's.

consist of carbon doped p-type AlGaAs/AlGaAs and silicon doped n-type AlAs/AlGaAs Bragg reflectors with pairs of quarter wavelength thick layers. The top (respectively bottom) mirror has a reflectivity of 99,8 % (respectively 99%). They are coated on each side of a cladding layer containing the three active 8 nm thick GaAs quantum wells and the oxide aperture which provides both current and optical confinement. The devices are attached to a copper plate using silver paste and the operation wavelength ranges from 820 to 850 nm.

Figure 1 shows the detail of the experimental setup. According to the principle of pump noise suppression [5], a low noise home made power supply with an appropriate LC filter provides the regulated electrical current which drives the VCSEL's. The VCSEL's are also thermally stabilised with an active temperature stabilisation. With this stabilisation, we were able to operate at a fixed temperature with a drift as small as 0.01°C per hour. The light beam is collimated by an antireflection coated microscope objective located at a distance of 2 mm from the laser output. This objective has a large numerical aperture ($\text{N.A.} = 0.6$) to avoid optical losses which would deteriorate the squeezing. To measure the intensity noise and the corresponding shot noise, the standard scheme consists in a pair of two high quantum efficiency balanced photodiodes: this is the usual homodyne detection. The sum of the two photocurrents is proportional to the intensity noise while the difference is proportional to the corresponding shot noise [6]. However, in our case, it is better to use only one photodiode (FND100, bandwidth 1-30 MHz, quantum efficiency of 90 %). Indeed, because of the multimode operation with two orthogonal linear polarisations, the shot noise obtained with a balanced detection would not be reliable and we preferred to use a separately calibrated shot noise. The shot noise reference is obtained by means of a laser diode beam which has a low intensity noise in the range of frequency of 1-30 MHz according to the above mentioned property. We carefully checked the linear dependence of the calibrated shot noise signal with the optical power incident on the photodiodes. The shot noise obtained

with this method was in agreement within 0.1 dB with the noise obtained by a thermal light generating the same DC current on the photodiode. The photodiode is connected via a low noise home made amplifier (with a CLC425) and electronic amplifier (Nucltude 4-40-1A) to a spectrum analyser (Tektronix 2753P). With this setup, the electronic noise was more than 6 dB below the signal we measured for a typical detected power of 1.5 mW.

We chose to inject the VCSEL's fundamental gaussian transverse mode TEM_{00} . We use a squeezed index guided quantum well GaAlAs laser diode operating at 850 nm as a master laser. Low noise operation is achieved by suppressing the side modes using feedback from an external grating in an extended cavity laser [6,7]. By tilting the grating, the laser diode wavelength can be tuned coarsely to match the wavelength of the VCSEL TEM_{00} mode. The grating is mounted on a piezoelectric ceramic to precisely tune the wavelength of the laser diode. Astigmatism in the beam is corrected by means of an anamorphic prism. Two optical isolators (for a total isolation of 50 dB) are used to prevent back reflection into the laser diode. A single mode optical fiber filters the laser diode beam: only the TEM_{00} mode gets out from the fiber. Hence we have same transverse geometry for the master beam and for the VCSEL transverse mode we want to inject. This ensures an efficient mode matching. Moreover the waists of the master beam and of the slave laser mode are about the same. A half wave plate enables to match the polarisation of the laser diode beam to the one of the VCSEL TEM_{00} mode. At last, the master laser beam is coupled to the VCSEL one with a beamsplitter. The injection locking is checked with a Fabry-Perot (FSR \sim 800 GHz, finesse \sim 100).

III. EXPERIMENTAL RESULTS

We were able to realize the injection locking of VCSEL's with various diameters. In figure 2, we have plotted the normalized intensity noise measured versus the noise frequency for a VCSEL of 7 μm diameter. In free-running operation this device always exhibits an excess noise. Curve (a) shows the normalized intensity noise in free-running operation while curve (b) shows the intensity noise of the VCSEL for the same driving current when it is injection locked (the injection power is equal to 2 % of the power of the free-running laser). The best squeezing (after correction for optical losses) obtained is about -0.8 dB. The VCSEL's with larger diameters present the same property: injection locking technique reduces the intensity noise. A spectral analysis shows that the intensity of the TEM_{00} mode is increased by injection locking. However, despite injection, several transverse modes still oscillate. The injection locking technique reduces the intensity noise but does not ensure single mode operation.

IV. CONCLUSION

In this paper, we have shown that the injection locking technique can be applied with success to reduce the intensity noise of the VCSEL's. We can obtain squeezed light with this technique from a laser which always shows an excess noise in free-running operation.

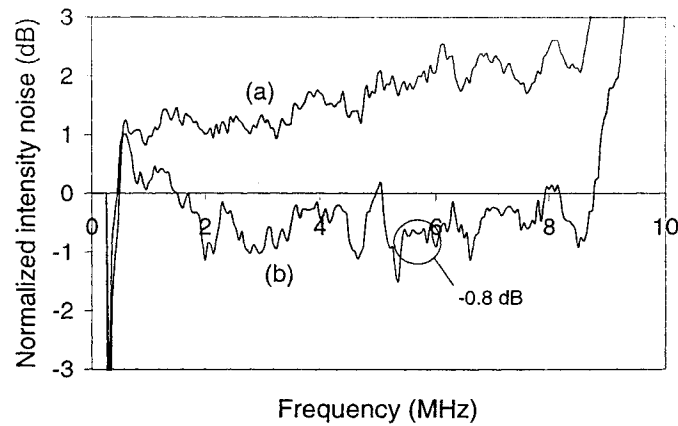


FIG. 2. Normalized intensity noise spectrum (0-10 MHz) for a $7 \mu\text{m}$ laser in free-running operation (curve (a)) and for the injection locked laser (curve (b)).

REFERENCES

- [1] D. Wiedenmann, P. Schnitzer, C. Jung, M. Grabherr, R. Jäger, R. Michalzik, and K.J. Ebeling, *Appl. Phys. Lett.* **73**, 717 (1998)
- [2] J. Martin-Regalado, S. Balle and M. San Miguel, *Opt. Lett.* **22** (7), 460 (1997)
- [3] J. Martin-Regalado, F. Prati, M. San Miguel and N. B. Abraham, *IEEE J. Quantum Electron.* **33** (5), 765 (1997)
- [4] F. Marin, A. Bramati, E. Giacobino, T.-C. Zhang, J.-Ph. Poizat, J.-F. Roch, P. Grangier, *Phys. Rev. Lett.* **75**, 4606 (1995)
- [5] Y. Yamamoto, S. Machida, and O. Nilsson, *Phys. Rev. A* **34** (5), 4025 (1986)
- [6] T.C. Zhang, J.-Ph. Poizat, P. Grelu, J.-F. Roch, P. Grangier, F. Marin, A. Bramati, V. Jost, M. D. Levenson and E. Giacobino, *Quantum Semiclass. Opt* **7**, 601 (1995)
- [7] H. Wang, M. J. Freeman and D. G. Steel, *Phys. Rev. Lett.* **71**, 3951 (1993)

Non-equivalence of photon flux and photocurrent in the presence of feedback

D.B.Horoshko* and S.Ya.Kilin
*Institute of Physics, Belarus National Academy of Sciences,
Minsk 220072 Belarus*

Abstract

We develop a theory of photodetection in the presence of feedback valid for arbitrary time delay in the feedback loop and any degree of field fluctuation. As a result we show that the statistical equivalence between photon flux and photocurrent in the feedback loop has no place at times exceeding the loop round-trip time.

Quantum theory of light detection was developed in 60's by Glauber [1] and Kelly and Kleiner [2]. The most important and widely used result of this theory is the expression connecting the photocurrent autocorrelation function and the normally ordered averages of the measured field:

$$\langle i(t)i(t') \rangle = \eta \langle E^+ E \rangle \delta(t - t') + \eta^2 \langle E^+(t') E^+(t) E(t) E(t') \rangle, \quad (1)$$

where the photocount charge is set to unity, η is the detector quantum efficiency and E is the positive-frequency part of the field, normalized so that the operator $\hat{I}(t) = E^+(t)E(t)$ has meaning of photon flux through the surface of the detector. For $\eta = 1$, using the commutation relations for free field: $[E(t), E^+(t')] = \delta(t - t')$, $[E(t), E(t')] = 0$, one can rewrite Eq. (1) as $\langle i(t)i(t') \rangle = \langle \hat{I}(t)\hat{I}(t') \rangle$, which, together with the relation $\langle i \rangle = \langle \hat{I} \rangle$, lets one speak about statistical equivalence of photon flux and photocurrent.

However, the deduction of Eq. (1), as well as the traditional theory of photodetection itself, is valid only when "the sources are assumed not to interact with the detector" [2]. Considerable effort has been made in the last years to developing a theory of photodetection in the presence of feedback between the detector and the sources. Shapiro et al. [3] proposed such a theory for linearized fields. In our early work [4] we considered feedback photodetection of intensity modulated coherent light. Wiseman and Milburn [5], [6] developed an operator formalism for describing feedback with zero time delay, which has been applied recently to many important problems of quantum optics [7]. Experimental investigations of feedback can be found in Ref. [8]. In the present work we develop a theory of photodetection in the presence of feedback valid for any degree of field fluctuation, any state of the field and arbitrary time delay in the loop.

Our starting idea is that in the presence of feedback the expression for photocount sequence probability has the same form as in the standard theory, but with field intensity explicitly depending on the times of the preceding counts of the in-loop detector:

$$p_{[0,t]}^{(k)}(\mathbf{T}_k) = \eta^k \left\langle \prod_{i=1}^k \hat{I}(t_i|\mathbf{T}_k) \exp \left\{ -\eta \int_0^t \hat{I}(\tau|\mathbf{T}_k) d\tau \right\} \right\rangle_N, \quad (2)$$

where $p_{[0,t]}^{(k)}(\mathbf{T}_k)$ is the probability density to observe in the time interval $[0, t)$ exactly k counts at times $\mathbf{T}_k \equiv t_1, \dots, t_k$, η is the detector quantum efficiency, $\hat{I}(t) = E^+(t)E(t)$ is the operator of field intensity on the surface of detector, and $\langle \dots \rangle_N$ stands for time-normally ordered averaging of field operators. The validity of Eq. (2) in the presence of feedback can be justified by the continuous photodetection theory [10], [11], [12].

The set of elementary probability densities given by Eq. (2) completely describes the stochastic point process of photocount arrivals. However, the correlation function of the photocurrent $i(t)$ is expressed via coincidence rates [9]:

$$\langle i(t)i(t_0) \rangle = w_1(t)\delta(t - t_0) + w_2(t, t_0), \quad (3)$$

where the function $w_l(t_1, \dots, t_l)$ is the probability density to observe l counts at times t_1, \dots, t_l , with possible counts at other times. These functions (coincidence rates) are related to elementary probability densities in the following way [9]:

$$w_l(t'_1, \dots, t'_l) \equiv \sum_{k=0}^{+\infty} \frac{1}{k!} \int_0^{t'_1} dt_1 \dots \int_0^{t'_l} dt_k p_{[0,t]}^{(k+l)}(t'_1, \dots, t'_l, \mathbf{T}_k). \quad (4)$$

In the absence of feedback such a transformation is trivial and results in a photocurrent correlation function given by Eq. (1). In the presence of feedback the calculation of coincidence rates can not be performed in general case and requires considering a concrete type of field intensity dependence on detector counts. Here we consider one rather general type of such a dependence, which in the P-representation of the field can be written as

$$I(\tau|\mathbf{T}_k) = I_0(t) + \sum_{i=1}^k F(t - t_i), \quad (5)$$

where $I_0(t)$ is the stochastic field intensity describing fluctuations of field not connected with feedback and $F(t)$ is the transmission function of the feedback loop ($F(t) = 0$ for $t < 0$). Substituting Eq. (5) into Eq. (2), rewritten in the P-representation, and averaging over photocount times according to Eq. (4), we arrive at a set of Volterra integral equations for coincidence rates, after resolving which we obtain ($t \geq t_0$):

$$w_1(t) = \eta \langle I(t) \rangle, \quad (6)$$

$$w_2(t, t_0) = \eta^2 \langle E^+(t_0)E^+(t)E(t)E(t_0) \rangle + R_F(t - t_0)w_1(t_0), \quad (7)$$

where $R_F(t)$ is the resolvent corresponding to the kernel $\eta F(t)$ [13]:

$$R_F(t) = \frac{1}{2\pi} \int_{-\infty}^{+\infty} \frac{\eta f(\omega)}{1 - \eta f(\omega)} e^{-i\omega t} d\omega, \quad (8)$$

where $f(\omega)$ is the Fourier transform of $F(t)$. The most important property of the resolvent is that if $F(t) = 0$ for $t < \tau_{del}$ (τ_{del} is the delay time of the loop), then $R_F(t)$ is also zero for $t < \tau_{del}$. Substituting Eqs. (6), (7) into Eq. (3), we obtain

$$\langle i(t)i(t_0) \rangle = \langle E^+ E \rangle G(t - t_0) + \eta^2 \langle E^+(t_0) E^+(t) E(t) E(t_0) \rangle, \quad (9)$$

where $G(\tau) = \eta\delta(\tau) + R_F(\tau) + R_F(-\tau)$ is the Green function of the feedback loop, describing the repeated round-trips of the signal in the loop. For no feedback $G(\tau) = \eta\delta(\tau)$ and Eq. (9) coincides with Eq. (1).

Eq. (9) is the main result of our theory. For unity quantum efficiency, applying the commutation relations for free field, we rewrite it in the form ($t \geq t'$):

$$\langle i(t)i(t') \rangle = \langle \hat{I}(t)\hat{I}(t') \rangle + R_F(t - t') \langle \hat{I} \rangle \quad (10)$$

showing that in the presence of feedback the statistical equivalence of photocurrent and photon flux has no place at times exceeding the delay time in the loop τ_{del} (for which R_F is not zero). This result is rather surprising for the intuitive representation of the photodetection process with unity quantum efficiency as a "direct conversion of photons into photocounts". However, the number of photons in some region of space is always equivalent to the number of photocounts in the corresponding time interval, as the integral of $\hat{I}(\tau)$ over time interval t has a sense of number of photons in some region of space only for $t \leq \tau_{pr}$, where τ_{pr} is the time of light propagation from the source to the detector, which is always less than τ_{del} .

It has been argued [3] that in the feedback loop the commutation relations of field operators are not the same as for free field. Let us show that no modification of that relations can preserve the statistical equivalence of the photon flux and the photocurrent. Indeed, for bosonic field the commutator must be a c-number. Then, to obtain $\langle i(t)i(t') \rangle = \langle \hat{I}(t)\hat{I}(t') \rangle$ we would need to combine Eq. (9) with the commutator

$$[E(t), E^+(t')] = \delta(t - t') + \frac{\langle E^+ E \rangle}{\langle E^+(t) E(t') \rangle} (R_F(t - t') + R_F(t' - t)), \quad (11)$$

which is unphysical, being state-dependent. In their approach Shapiro et al. [3] considered linearized fields, in which case Eq. (11) reduces to the relation

$$[E(t), E^+(t')] = G(t - t') \quad (12)$$

having a more physical appearance. However this trick is possible for linearized fields only.

In summary, we have shown, how the traditional theory of photodetection can be extended to the case of feedback between the detector and the source of radiation (Eq. (2)). For the case of additive feedback our approach allows to obtain an exact expression for the in-loop photocurrent autocorrelation function given by Eq. (9). This expression shows unambiguously that statistical equivalence between photon flux and photocurrent has no place in the feedback loop (even for unity quantum efficiency of the detector) at times exceeding the loop delay time τ_{del} .

This work was supported by INTAS, grant # 96-0167 and by Belarus Foundation for Basic Research, grant F 97-300.

REFERENCES

- * E-mail: horoshko@ifanbel.bas-net.by
- [1] R.J.Glauber, Phys. Rev. **130**, 2529 (1963); in *Quantum Optics and Electronics*, edited by C.De Witt, A.Blandin and C.Cohen-Tannoudji (Gordon and Breach, New York,1965).
 - [2] P.L.Kelley, and W.H.Kleiner, Phys. Rev. **136**, 316A (1964).
 - [3] J.H.Shapiro et al., J. Opt. Soc. Am. B **4**, 1604 (1987).
 - [4] D.B.Horoshko and S.Ya.Kilin, JETP **79**, 691 (1994).
 - [5] H.M.Wiseman and G.J.Milburn, Phys. Rev. A **49**, 1350 (1994).
 - [6] H.M.Wiseman, Phys. Rev. A **49**, 2133 (1994).
 - [7] D.B.Horoshko and S.Ya.Kilin, Phys. Rev. Lett. **78**, 840 (1997); D.Vitali, P.Tombesi, and G.J.Milburn, *ibid.* **79**, 2442 (1997); H.M.Wiseman, *ibid.* **81**, 3840 (1998); D.B.Horoshko and S.Ya.Kilin, Optics Express **2**, 347 (1998).
 - [8] Y.Yamamoto, N.Imoto, and S.Machida, Phys. Rev. A **33**, 3243 (1986); A.V.Masalov, A.A.Putilin, and M.V.Vasilyev, J. Mod. Opt. **41**, 1941 (1994).
 - [9] R.L.Stratonovich *Topics in the Theory of Random Noise* (Gordon and Breach, New York,1963).
 - [10] M.D.Srinivas and E.B.Davies, Opt. Acta **28**, 981 (1981).
 - [11] S.Ya.Kilin *Quantum Optics. Fields and their Detection* (Nauka i Tekhnika, Minsk, 1990).
 - [12] H.Carmichael *An Open System Approach to Quantum Optics* (Springer-Verlag, Berlin, 1993).
 - [13] J.A.Cochran *The Analysis of Linear Integral Equations* (McGraw-Hill, New York, 1972).

Squeezed States Production by Oscillating Boundary of Cold Relativistic Plasma

Anton S. Il'in, Vladimir A. Cherepenin

Institute of Radioengineering and Electronics RAS, Mohovaya 18, 103907, Moscow, Russia

Victor V. Kulagin

Sternberg Astronomical Institute, Moscow State University, Universitetsky prospect 13, 119899, Moscow, Russia, E-mail: kul@sai.msu.su

Abstract

The system with an overdense plasma produced from a solid target evaporated by an ultrashort high power laser pulse can provide a very large non-linearity at optical frequencies. In a field of a strong electromagnetic wave plasma boundary oscillates with double frequency of the field. Using an electron sheets model the statistical and dynamical characteristics of the reflected electromagnetic field are investigated. The squeezing coefficient for a fundamental mode at the frequency of the incident laser pulse is estimated.

Nonclassical states of light were generated in experiment more than ten years ago but hitherto the experimental squeezing coefficients were modest - about several units. At the same time applications of non-classical light seem to be very promising. Thus, for example, in experiments with probe bodies specifically in gravitational wave experiments the sensitivity of installation to external classical force can be considerably increased if the squeezed light is used for the pumping. Generally a gain in sensitivity can be proportional to the squeezing coefficient of the input light.

The systems with free electrons can be very perspective for squeezed states generation because of small dissipation and high nonlinearity of electron medium. Modern methods of creation of high charge density electron medium including an evaporation of targets by high-intensity ultrashort laser pulses and a possibility to tune the appropriate regime by changing a velocity of electrons give an expectation that a highly squeezed electromagnetic wave can be generated in the electron medium.

Let consider a thin layer of electrons with uniform density (electron mirror). Let the density of electrons N will be large enough for the reflection coefficient will be close to unity. Each electron in nonrelativistic limit moves along the figure of eight in the field of a strong electromagnetic wave with frequency ω_0 . Thus all electrons in the electron mirror move synchronously with frequency $2\omega_0$ in the direction of the wave vector of incident field. So for the reflection of the incident electromagnetic wave the parametric regime takes place [1].

In the linear approximation when $V \ll c$ the squeezing coefficient g of the reflected wave have the following value [1]

$$g = (1 - \nu)^{-1} \quad (1)$$

where $\nu = e^2 E_0^2 / (4m^2 c^2 \omega_0^2)$, e and m are electron charge and mass, E_0 is an amplitude of the field. Therefore the larger the value of ν the smaller the noise spectral density of the "silent" quadrature of reflected field. However the expression (1) is valid only for the small values of parameter ν therefore in the case of ν close to unity one have to take into account the higher nonlinearities in the system besides the relativistic equations for the electron motion have to be used.

It is useful to explore the microscopic model of electron medium for consideration of the relativistic mirror velocities. Electronic medium is modeled by a set of parallel planes with constant electron density N . Each plane has infinite dimensions in x and y directions. Thickness in z direction is considerably smaller than characteristic wavelength (wavelength of input electromagnetic wave). If the movement of the planes is without rotation then all variables depend only on coordinate z and time t and for a system with such a symmetry the (3+1) model can be used: the movement of the planes is described by three components of velocity $\beta_x = V_x/c$, $\beta_y = V_y/c$, $\beta_z = V_z/c$ and one coordinate z . This is the so called electron sheets model.

For a thin charged plane (electron sheet) charge density and current have the following form (σ is a surface charge density)

$$\rho(z, t) = \sigma \delta(z - Z(t)), \quad \vec{j}(z, t) = \sigma \vec{V}(z) \delta(z - Z(t)) \quad (2)$$

where $Z(t)$ is z coordinate of a sheet and the solutions for the fields have the form [2]

$$\begin{aligned} E_z(z, t) &= 2\pi\sigma \cdot \text{sign}(z - Z(t')) \\ \vec{E}_\perp(z, t) &= -2\pi\sigma \vec{V}_\perp(t') / [c - V_z(t') \text{sign}(z - Z(t'))] \\ \vec{H}(z, t) &= 2\pi\sigma \cdot \text{sign}(z - Z(t')) [\vec{V}_\perp(t'), \vec{e}_z] / [c - V_z(t') \text{sign}(z - Z(t'))] \end{aligned} \quad (3)$$

where $\vec{E}_\perp(z, t) = E_x \vec{e}_x + E_y \vec{e}_y$, $\vec{V}_\perp = V_x \vec{e}_x + V_y \vec{e}_y$ and t' is a retarded time: $c(t - t') = |z - Z(t')|$.

Let the movement of the plane in the z direction is defined by the following equation ($\beta_0 < 1$)

$$\beta_z(t) = \beta_0 \sin(2\omega_0 t), \quad (4)$$

This type of equation can be supported by the powerful electromagnetic wave incident normally at the plane. For the large surface charge density σ one can omit the dispersive term, in this case the charged plane becomes an ideal mirror with the reflectivity coefficient about 1.

Let the field incident at the plane have the form ($q = 0, 1 \dots$)

$$\begin{aligned} E_{iq} &= E_q \cos((2q + 1)\omega_0(t - z/c) + \varphi_q) \\ &= a_q \cos(2q + 1)\omega_0(t - z/c) - b_q \sin((2q + 1)\omega_0(t - z/c) \end{aligned} \quad (5)$$

where a_q and b_q are the quadrature components of the incident field. Then a reflected field E_r consists of a sum of odd harmonics of fundamental frequency ω_0 with frequencies $(2p+1)\omega_0, p = 0, 1 \dots$ and amplitudes defined by the following expression:

$$E_{qp} = -E_q(i)^p(A_{qp}(\beta_0)(-i)^q \exp(i\varphi_q) + B_{qp}(\beta_0)(i)^{q+1} \exp(-i\varphi_q)) \quad (6)$$

The coefficients A_{qp} and B_{qp} have the following form

$$A_{qp}(\beta_0) = \sum_{n=-\infty}^{\infty} (1 + 2(-n + p - q)/(2q + 1))J_n((2p + 1)\beta_0/2) \cdot J_{-n+p-q}((2q + 1)\beta_0/2)$$

$$B_{qp}(\beta_0) = \sum_{n=-\infty}^{\infty} (1 + 2(n - p - q - 1)/(2q + 1))J_n((2p + 1)\beta_0/2)J_{n-p-q-1}((2q + 1)\beta_0/2) \quad (7)$$

For the relative intensities of reflected harmonics one can obtain

$$|E_{qp}|^2 / E_q^2 = A_{qp}^2 + B_{qp}^2 - 2A_{qp}B_{qp} \sin 2\varphi_q \quad (8)$$

and for $A_{qp}B_{qp} \neq 0$ they depend on phase φ . So for the large velocity β_0 the scattering of input modes into output modes is phase sensitive.

The transformation of input noise from frequency $(2q+1)\omega_0$ into the frequency $(2p+1)\omega_0$ is defined by the following expressions

$$a_p = A_{qp}a_q + B_{qp}b_q$$

$$b_p = B_{qp}a_q + A_{qp}b_q \quad (9)$$

where a_q and b_q are the quadratures of the input field (cf. Eq. (5)) at frequency $(2q+1)\omega_0$ and a_p and b_p are the quadratures of the output field with frequency $(2p+1)\omega_0$. The output quadratures are correlated in this case. Introducing the new quadrature components "rotated" with respect to the old quadratures [1] and optimizing the angle of rotation one can obtain for the noise in the most "silent" quadrature

$$N_{0p}\nu_{qp} = N_{0q}(A_{qp} - B_{qp})^2 \quad (10)$$

where N_{0p} and N_{0q} are spectral densities of quadrature components for the field in the vacuum state at the frequencies $(2p+1)\omega_0$ and $(2q+1)\omega_0$, and ν_{qp} is the dimensionless noise suppression coefficient for scattering from frequency $(2q+1)\omega_0$ into the frequency $(2p+1)\omega_0$. Input noises at frequencies $(2q+1)\omega_0$ for different q are uncorrelated therefore for the whole noise at frequency $(2p+1)\omega_0$ one can obtain

$$\nu_p N_{0p} = N_{0p} \cdot \sum_{q=0}^{\infty} \nu_{qp} = \sum_{q=0}^{\infty} N_{0q}(A_{qp} - B_{qp})^2 \quad (11)$$

For scattering of the fundamental mode ω_0 into itself ($q = 0, p = 0$) without noises from other input frequencies the expressions for the elements of transformation matrix are the following

$$A_{00}(\beta_0) = \sum_{n=-\infty}^{\infty} (-1)^n J_n^2(\beta_0/2)$$

$$B_{00}(\beta_0) = \beta_0/2 \quad (12)$$

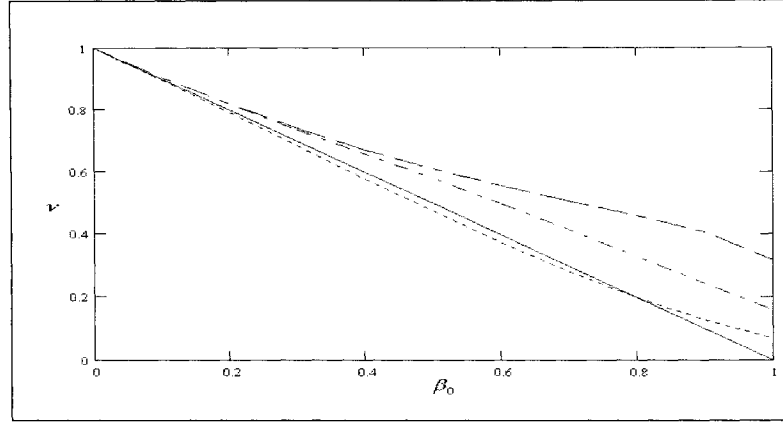


FIG. 1. Fluctuations ν (in units of vacuum spectral density) of "silent" quadrature of output (reflected) field at frequency ω_0 when only input fluctuations at frequency ω_0 are considered (dot); the same for input fluctuations at frequencies ω_0 and $3\omega_0$ (dash dot); the same for input fluctuations with frequencies $(2q + 1)\omega_0$, where $q = 0, 1 \dots 30$ (dash). The solid line - linear theory.

and for noise suppression coefficient one has (cf. the linear theory Eq.(1), $\beta_0 \ll 1$)

$$\nu_{00}(\beta_0) = \left[\sum_{n=-\infty}^{\infty} (-1)^n J_n^2(\beta_0/2) - \beta_0/2 \right]^2 \quad (13)$$

Therefore taking into consideration the nonlinearity change the coefficient $A_{00}(\beta_0)$ while the coefficient $B_{00}(\beta_0)$ remains unchanged (see fig. 1).

The noise suppression coefficient with consideration of vacuum noises at different number of input harmonics (maximum about 30) is shown in the figure 1. The contribution of the fluctuations of input odd harmonics into the fluctuations at the frequency ω_0 can be decreased with optical resonators or by using the electron mirror with appropriate thickness for the interference of harmonics would be destructive [2].

The considered mechanism of squeezed state generation can be useful only if the parameter ν will be close to unity. This condition can be met for very high amplitude of the laser light. Such high amplitude can be achieved in ultrashort laser pulses. Actually for input frequency ω_0 from the optical band and cross section of the light beam about 1 mm^2 the required instantaneous power of the laser have to be about 10^8 Wt that is easy enough to get in experiment. The excessive noises of laser light and the noises of electron medium have to be considered in more details for real experiment.

In conclusion the most advantage of the considered scheme is that the squeezing coefficient can be high and independent of frequency in the large frequency band.

REFERENCES

- [1] V. V. Kulagin, V. A. Cherepenin. In: *Laser Optics'98: Fundamental Problems of Laser Optics*, ed. N. N. Rosanov, Proc. of SPIE, **3685** (1999) 141.
- [2] A. S. Il'in, V. V. Kulagin, V. A. Cherepenin. *J. of Commun. Technology and Electronics* **42** (1999) 1158.

Sub-Poissonian light in integrated-optical systems

A. Karpati[†], P. Adam[†], J. Janszky[†], M. Bertolotti[‡], and C. Sibia[‡]

[†] *Research Institute for Solid State Physics and Optics, P. O. Box 49, H-1525 Budapest, Hungary;*

[‡] *Dipartimento di Energetica, Università di Roma I, Via Scarpa 16, 00161 Rome, Italy*

Abstract

General method is developed for analyzing the evolution of non-classical light in two-mode integrated-optical systems where linear and non-linear processes with quadratic Hamiltonians can take place simultaneously or successively. As an example, the evolution of sub-Poissonian light is analyzed in a non-linear coupler with degenerate and non-degenerate parametric amplification. It is shown that all-optical switching can be realized in this system.

I. GENERAL TWO-MODE PROCESS

Let us consider first the most general quadratic two-mode oscillator Hamiltonian in the interaction picture:

$$\hat{H}/\hbar = \frac{1}{2}\Delta_a \hat{a}^\dagger \hat{a} + \frac{1}{2}\Delta_b \hat{b}^\dagger \hat{b} + \frac{1}{2}\mu \hat{a} \hat{a} + \frac{1}{2}\nu \hat{b} \hat{b} + \lambda \hat{a} \hat{b} + \kappa \hat{a} \hat{b}^\dagger + \text{h.c.} \quad (1)$$

This Hamiltonian describes simultaneous linear coupling and non-degenerate parametric amplification (two-mode squeezing) of the modes, and degenerate parametric amplification (self-squeezing) of both of them. The parameters Δ_a and Δ_b describe the possible detuning values of the modes, κ is the linear coupling constant, λ is the non-degenerate amplification parameter, and μ and ν are the effective degenerate amplification parameters in the self-squeezing processes. The amplification parameters are proportional to the amplitudes of the corresponding pumping fields that are assumed to be classical and non-depleting.

By solving the Heisenberg-equations we have found the solution for the annihilation operators in the rotating interaction frame at a given moment t_{out} in the form

$$\begin{aligned} \hat{a}(t_{\text{out}}) &= \hat{a}_{\text{out}} = u\hat{a}_{\text{in}} + v\hat{b}_{\text{in}} + w\hat{a}_{\text{in}}^\dagger + z\hat{b}_{\text{in}}^\dagger, \\ \hat{b}(t_{\text{out}}) &= \hat{b}_{\text{out}} = U\hat{b}_{\text{in}} + V\hat{a}_{\text{in}} + W\hat{b}_{\text{in}}^\dagger + Z\hat{a}_{\text{in}}^\dagger \end{aligned} \quad (2)$$

where for example,

$$\begin{aligned} u(t_{\text{out}}) &= \frac{1}{\zeta_1 - \zeta_2} \left(-\cosh(\sqrt{\zeta_1}t_{\text{out}})(\Omega_a^2 + \zeta_2) + \cosh(\sqrt{\zeta_2}t_{\text{out}})(\Omega_a^2 + \zeta_1) + \right. \\ &\quad \left. + \frac{\sinh(\sqrt{\zeta_1}t_{\text{out}})}{\sqrt{\zeta_1}} [i\Delta_a(\Omega_a^2 + \zeta_2) - i\kappa^*A^* + i\lambda^*B] - \right. \\ &\quad \left. - \frac{\sinh(\sqrt{\zeta_2}t_{\text{out}})}{\sqrt{\zeta_2}} [i\Delta_a(\Omega_a^2 + \zeta_1) - i\kappa^*A^* + i\lambda^*B] \right) \end{aligned}$$

where

$$\begin{aligned}
A &= -(\Delta_a + \Delta_b)\kappa^* + \lambda\mu^* + \lambda^*\nu, & B &= -(\Delta_a - \Delta_b)\lambda - \kappa\nu + \kappa^*\mu, \\
\zeta_1 &= p + \sqrt{p^2 - q}, & \zeta_2 &= p - \sqrt{p^2 - q}, & p &= -\frac{1}{2}(\Omega_a^2 + \Omega_b^2), \\
q &= (|\lambda|^2 - |\kappa|^2)^2 + |\mu|^2|\nu|^2 - \Delta_a^2|\nu|^2 - \Delta_b^2|\mu|^2 - 2\Delta_a\Delta_b(|\lambda|^2 + |\kappa|^2), \\
&\quad -2\text{Re}(\mu\lambda^{*2}\nu + \kappa^2\mu^*\nu - 2(\Delta_a\lambda^*\kappa\nu + \Delta_b\mu^*\lambda\kappa)) + \Delta_a^2\Delta_b^2, \\
\Omega_a^2 &= \Delta_a^2 - |\mu|^2 + |\kappa|^2 - |\lambda|^2, & \Omega_b^2 &= \Delta_b^2 - |\nu|^2 + |\kappa|^2 - |\lambda|^2.
\end{aligned}$$

The obtained linear transformation generally holds for any integrated-optical four-port device [1-9] in which not only the general process of equation (1) but several successive quadratic processes are allowed. Equation (2) is also valid for phase-conjugate resonators [4]. The input and the output states can be completely described by the the two-mode Wigner function. The transformation formula between the input and the output Wigner functions is obtained as

$$W_{\text{out}}(\alpha) = \mathbf{W}_{\text{in}}(\mathbf{M}^{-1}\alpha) \quad (3)$$

where α denotes the vector $(\alpha, \alpha^*, \beta, \beta^*)$ and M^{-1} is the inverse of the parameter matrix:

$$M^{-1} = \begin{pmatrix} u & w & v & z \\ w^* & u^* & z^* & v^* \\ V & Z & U & W \\ Z^* & V^* & W^* & U^* \end{pmatrix}^{-1} =: \begin{pmatrix} a & c & b & d \\ c^* & a^* & d^* & b^* \\ B & D & A & C \\ D^* & B^* & C^* & A^* \end{pmatrix}. \quad (4)$$

II. PHOTON STATISTICS OF A COHERENT-STATE SUPERPOSITION INPUT

As it is well-known discrete coherent-state superpositions can approximate any quantum state of light with a high degree of accuracy [10]. Hence to describe the evolution of an arbitrary non-classical state of light in the considered integrated-optical systems it is usually sufficient to regard the following input states:

$$|\Psi\rangle = \sum_k c_k |\alpha_k\rangle_a \otimes |0\rangle_b \quad (5)$$

where $|\alpha_k\rangle$ are the coherent states in the superposition and the coefficients c_k can be obtained for a given non-classical state using the method presented in [10]. Here the vacuum state is chosen for the input state of the mode 'b'.

In the following we present the results only for the mode 'a'. Using the results of the previous section and equation (5) the following expression can be derived for the output Wigner function of the mode 'a':

$$\begin{aligned}
W_a^{\text{out}}(\alpha) &= \frac{4}{\pi} \frac{1}{\sqrt{R_a^2 - |s_a|}} \sum_{k,l} K_a^{kl} \times \\
&\quad \times \exp\left(-R'_a|\alpha|^2 + \frac{1}{2}(s'_a\alpha^{*2} + s_a'^*\alpha^2) + \lambda_a^{kl}\alpha + \nu_a^{kl}\alpha^*\right) \quad (6)
\end{aligned}$$

where

$$\begin{aligned}
K_a^{kl} &= c_k^* c_l \exp \left(-\frac{1}{2} |\alpha_k|^2 - \frac{1}{2} |\alpha_l|^2 - \alpha_k^* \alpha_l + \frac{R_a f_a^{kl} g_a^{kl} + \frac{1}{2} (s_a f_a^{kl2} + s_a^* g_a^{kl2})}{R_a^2 - |s_a|^2} \right), \\
s_a' &= -4(ca^* + DB^*) + \frac{2R_a y_a x_a^* + s_a y_a^2 + s_a^* x_a^{*2}}{R_a^2 - |s_a|^2}, \\
\lambda_a^{kl} &= 2(a\alpha_k^* + c^* \alpha_l) + \frac{R_a f_a^{kl} y_a^* + R_a x_a g_a^{kl} + s_a f_a^{kl} x_a + s_a^* g_a^{kl} y_a^*}{R_a^2 - |s_a|^2}, \\
\nu_a^{kl} &= 2(c\alpha_k^* + a^* \alpha_l) + \frac{R_a y_a g_a^{kl} + R x_a^* f_a^{kl} + s_a f_a^{kl} y + s_a^* g_a^{kl} x_a^*}{R_a^2 - |s_a|^2}, \\
R_a' &= 2(|a|^2 + |c|^2 + |B|^2 + |D|^2) - \frac{R_a(|x_a|^2 + |y_a|^2) + s_a x_a y_a + s_a^* x_a^* y_a^*}{R_a^2 - |s_a|^2}, \\
R_a &= 2(|b|^2 + |d|^2 + |A|^2 + |C|^2), \quad f_a^{kl} = 2(b\alpha_k^* + d^* \alpha_l), \quad g_a^{kl} = 2(d\alpha_k^* + b^* \alpha_l), \\
s_a &= -4(db^* + CA^*), \quad x_a = -2(bc^* + d^* a + D^* A + BC^*), \\
y_a &= -2(ba^* + cd^* + AB^* + C^* D). \tag{7}
\end{aligned}$$

Knowing the Wigner function any physical quantity can be determined. For example, the photon number distribution's expression can also be calculated analytically.

III. EVOLUTION OF AMPLITUDE SQUEEZED STATES

Using this method we have analyzed the time-evolution of amplitude squeezed states [11] in simultaneous non-degenerate parametric amplifier and linear coupling processes, that correspond to parameters $\Delta_a = \Delta_b = \mu = \nu = 0$ in the Hamiltonian (1). We have found that the time-evolution in this system will be periodic if $|\lambda| < |\kappa|$. For $|\lambda| > |\kappa|$ the mean photon number will diverge.

We have shown that sub-Poissonian statistic emerges in the mode 'b' only for small amplification. At a fixed coupling κ there exists a critical amplification λ_{crit} where the Mandel Q parameter of the mode 'a' is exactly zero through the whole process. The parameter λ_{crit} depends on the parameters of the input state.

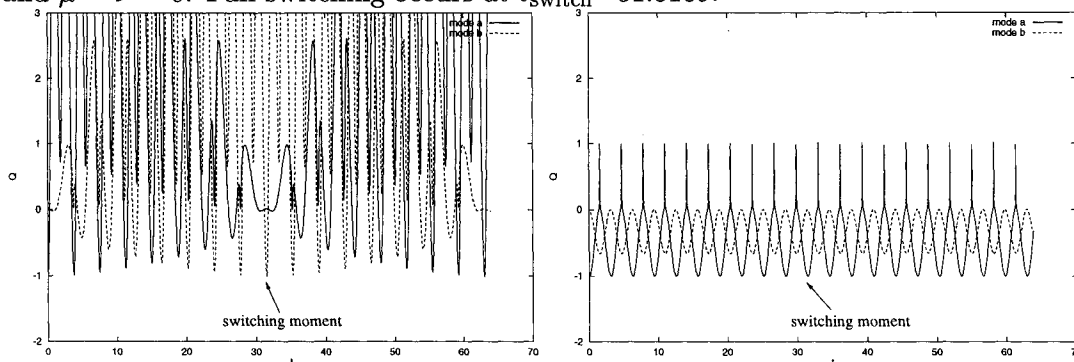
It is an interesting effect that there is a maximal value of amplitude squeezing such that the less squeezed states get more amplitude squeezed during the evolution in the mode 'a' for certain time intervals. At any coupling constant κ one can find an optimal amplification λ_{opt} for which the amount of amplitude squeezing enhancement is maximal, and the minimal Mandel Q parameter does not depend on the coupling constant κ , only on the input state.

IV. ALL-OPTICAL SWITCHER

Introducing degenerate parametric amplification for both modes in the previous system, and assuming the symmetric case ($\mu = \nu$), it is easy to see that two oscillating frequencies will appear in the time-evolution of the system when $|\mu| + |\lambda| < |\kappa|$. This fact results in a beating effect in the time-evolution of physical quantities. It can be shown that for

certain moments complete switching of the input coherent-state superposition signal into the mode 'b' occurs without additional noise. Figure 1 shows the time-evolution of the Mandel Q parameters for an input amplitude squeezed state. The switching moment is indicated in the figure. For certain parameter values it can be realized that in the system without degenerate parametric amplification ($\mu = \nu = 0$) the original input state emerges at these moments (see figure 1). Having a four-port device with outputs corresponding to the switching moment, an all-optical switcher is realized since the degenerate amplification parameters μ and ν can be changed by adjusting the corresponding optical pump fields.

FIG. 1. Time-evolution of the Mandel Q parameter for an amplitude squeezed state in the process $\lambda = 0.08078$, $\kappa = 1$ and $\mu = \nu = 0.5227$, and on the right side in the process $\lambda = 0.08078$, $\kappa = 1$ and $\mu = \nu = 0$. Full switching occurs at $t_{\text{switch}}=31.5189$.



ACKNOWLEDGMENTS

This work was supported by the National Scientific Research Fund (OTKA) of Hungary, under Contracts No. T023777 and No. F023617.

-
- [1] Janszky J *et al* 1991 *J. Mod. Opt.* **38** 2467
 - [2] Janszky J *et al* 1995 *Quantum Opt.* **7** 509
 - [3] Perina J Jr. and Perina J 1997 *Quantum Opt.* **9** 443
 - [4] Agarwal G S *et al* 1993 *Phys. Rev. A* **47** 597
 - [5] Abdalla M S 1993 *J. Mod. Opt.* **40**, 1369
 - [6] Yeoman G and Barnett S M 1993 *J. Mod. Opt.* **40** 1497
 - [7] Louis A and Perina J 1996 *Phys. Rev. A* **53** 1886
 - [8] Petrossian K G 1997 *Opt. Commun.* **134** 99
 - [9] Janszky J *et al* 1992 *Quantum Opt.* **4** 163
 - [10] Szabo S *et al* 1995 *Phys. Rev. A* **53** 2698
 - [11] Szabo S *et al* 1994 *Quantum Opt.* **6** 527

Complete quenching of fluorescence in a narrowband squeezed vacuum

Stuart Swain

*Department of Applied Mathematics and Theoretical Physics,
The Queen's University of Belfast, Belfast BT7 1NN, United Kingdom.*

We consider a single two-level atom driven by the output from a degenerate optical parametric oscillator. For squeezing bandwidths of the order of the natural atomic width and smaller, we report remarkable spectral profiles for the scattered light, including the existence of a narrow hole at line-centre.

In 1986, Gardiner [1] predicted that a two-level atom interacting with an ideal squeezed vacuum exhibited different decay rates for the real and imaginary parts of the atomic dipole moment, one part having a supernatural, and the other part a subnatural, linewidth. As the intensity of the squeezed field is increased, the value of the reduced decay rate tends to zero. The difficulty in observing this very narrow linewidth predicted for a strong squeezed vacuum is that *all* the modes with which the atom interacts must be squeezed. Here we consider a two-level atom driven by an ideal, but weak squeezed vacuum, and we show that for squeezing bandwidths of the order of the natural linewidth, unusual fluorescence spectra can be obtained, including spectra which exhibit complete quenching of fluorescence at line centre. We also show that pronounced line narrowing can occur even in this weak field case. However, unlike the regime considered by Gardiner, it does not require a nonclassical field or 4π coupling. Full references are cited in the papers [2,3], where details of the calculations presented here may also be found. A recent review on atom/squeezed light interactions is given by Dalton et al. [4].

We consider a single two-level atom, of transition frequency ω_a , driven by the output of a degenerate optical parametric oscillator (DOPO) operating below threshold, using the cascaded-systems approach given by Gardiner, and Gardiner and Parkins [5,6]. The interaction is described through the master equation

$$\begin{aligned} \dot{\rho} = & E/2 [a^{\dagger 2} - a^2, \rho] \\ & + \kappa/2 (2a\rho a^{\dagger} - a^{\dagger}a\rho - \rho a^{\dagger}a) \\ & - (\lambda r \kappa \gamma)^{1/2} \{[\sigma^+, a\rho] + [\rho a^{\dagger}, \sigma^-]\} \\ & + \gamma/2 (2\sigma^- \rho \sigma^+ - \sigma^+ \sigma^- \rho - \rho \sigma^+ \sigma^-), \end{aligned} \tag{1}$$

with E being the pump amplitude (assumed real), $\kappa = \kappa_a + \kappa_b$, λ the fraction of modes surrounding the atom which are squeezed, r the fraction of output from the DOPO which drives the atom and γ is the natural width of the atom. In general, Eq. (1) must be solved numerically.

The output field from a DOPO operating below threshold is squeezed vacuum light, characterized by the two parameters, $N(\omega)$ and $M(\omega)$, where

$$\begin{aligned}\langle a^\dagger(\omega) a(\omega') \rangle &= N(\omega) \delta(\omega - \omega') \\ \langle a(\omega) a(\omega') \rangle &= M(\omega) \exp(i\phi_s) \delta(\omega + \omega')\end{aligned}\quad (2)$$

and $a(\omega)$ destroys a photon of frequency $\omega_s + \omega$, ω_s being the centre frequency of the squeezed vacuum. The N and M functions are related as follows

$$M^2(\omega) = \eta(\omega) N(\omega) [N(\omega) + 1], \quad (3)$$

where

$$\eta(\omega) = r \frac{(\kappa^2/4 + E^2 + \omega^2)^2}{(\kappa^2/4 + E^2 + \omega^2)^2 + (1-r)(E\kappa)^2}. \quad (4)$$

If $r = 1$ (i.e. $\kappa = \kappa_a$) then $\eta(\omega) = 1$. This maximum possible value of η is attained when the OPO cavity is single-ended, and represents *ideal squeezing*.

We also consider an alternative system, in which the atom is driven by arbitrarily correlated light of arbitrary bandwidth, and we find different spectral features depending whether we require the driving field to have *classical* or *non-classical* characteristics.

In 1986 Gardiner made the *broadband assumption*, that $N(\omega)$ and $M(\omega)$ are constant (independent of ω). He showed that the real and imaginary parts of the dipole moment $p \propto \sigma_1 + i\sigma_2$ of the two-level atom have different decay rates, one much faster and one much slower than the natural decay rate $\gamma/2$:

$$\begin{aligned}\langle \dot{\sigma}_1 \rangle &= -\gamma_L \langle \sigma_1 \rangle; & \gamma_L &= \gamma \left(N + \frac{1}{2} + M \right) \geq \gamma/2, \\ \langle \dot{\sigma}_2 \rangle &= -\gamma_S \langle \sigma_2 \rangle; & \gamma_S &= \gamma \left(N + \frac{1}{2} - M \right) \leq \gamma/2.\end{aligned}\quad (5)$$

For $N \gg 1$ and the *ideal case*, $\eta = 1$, or $M^2 = N(N+1)$, we have

$$\gamma_S = \frac{\gamma}{8N} \rightarrow 0 \text{ as } N \rightarrow \infty. \quad (6)$$

Pronounced line narrowing is thus possible, and the larger the value of N , the narrower the line.

On the other hand, the greatest value of M that a field with a classical analogue can take is $M = N$ [2,3]. Such fields are often called *classically-squeezed fields*. So $\alpha = N/(N+1)$ is the fraction of correlations reproducible classically. Clearly $\alpha \rightarrow 0$ as $N \rightarrow 0$ and $\alpha \rightarrow 1$ as $N \rightarrow \infty$. The most pronounced quantum effects are therefore expected for small N (and $\eta = 1$). This is the regime we consider here, and of course we also allow for the finite bandwidth of the driving field.

The steady state fluorescence spectrum for the two-level atom is

$$S(\omega) = \int_{-\infty}^{\infty} d\tau e^{-i\omega\tau} \langle \sigma^+(0) \sigma^-(\tau) \rangle_{ss} \quad (7)$$

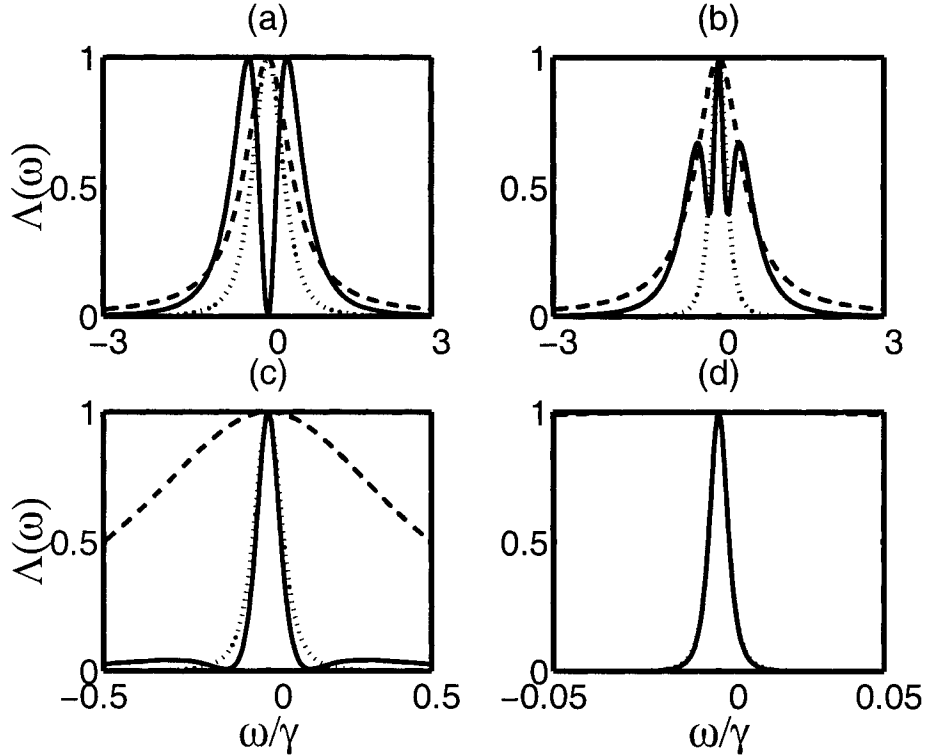


FIG. 1. Fluorescence spectrum emitted by a two-level atom driven by finite-bandwidth squeezed light from a degenerate parametric oscillator (D.O.P.O.). Parameters are $E = \kappa/100$ and $\lambda = 1$. The solid curves in (a),(b),(c) and (d) are for $\kappa/\gamma = 1, 0.5, 0.15$, and 0.01 respectively. The dashed curve in each frame is a normalized Lorentzian of width γ , whilst the dotted curve is $N_{out}(\omega)/N_{out}(0)$.

where

$$\langle \sigma^+(0) \sigma^-(\tau) \rangle_{ss} = \lim_{t \rightarrow \infty} \langle \sigma^+(t) \sigma^-(t + \tau) \rangle. \quad (8)$$

The results presented have been obtained via numerical solution of the master equation.

Frame (a) of Figure 1 shows that complete quenching of the fluorescence occurs at line centre for an atom driven by an ideal squeezed vacuum when $\kappa = \gamma$. The quenching persists for arbitrarily weak driving fields, but vanishes for classical fields. In Frame (b), it is demonstrated that the hole is gradually filled in as κ is reduced. In Frame (c), we see that the fluorescence linewidth is less than both the natural linewidth and the linewidth of the driving field, and in the final frame the fluorescence is essentially that of the incident driving field.

In Figure 2, we demonstrate that the quenching at line centre requires a quantum driving field, by employing the alternative system, which allows us to vary the value of M for a fixed N , and thus the quantum or classical nature of the field.

To summarize, we have considered the fluorescence spectrum resulting from a two-level atom driven by fields with finite bandwidths, which may be of a classical or nonclassical nature. A variety of distinctive spectral features have been shown to exist in the regime of weak narrowband atomic excitation. Nonclassical light is essential for the appearance of a narrow hole at line-centre, and for an ideal squeezed vacuum, the fluorescence at line-centre vanishes. Complete fluorescence quenching requires 4π solid angle squeezing.

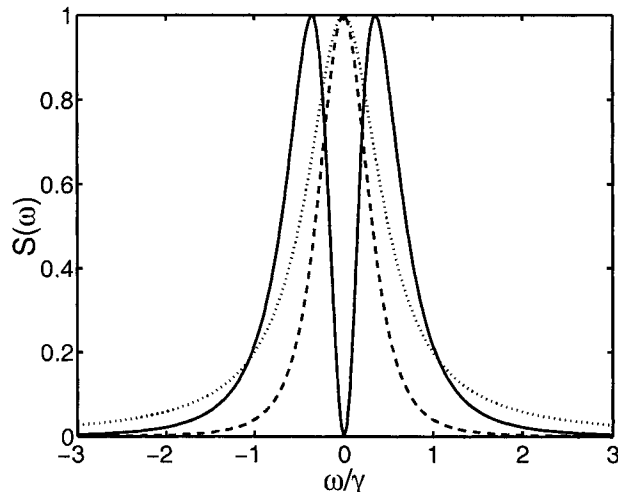


FIG. 2. Fluorescence spectrum emitted by a two-level atom driven by the finite-bandwidth light from the alternative physical system. The solid line corresponds to an ideal squeezed vacuum, the dashed line to a classically-squeezed field ($M = N$), and the dotted line represents the spectrum of the driving field.

We also report that line narrowing can be achieved with both classical and non-classical driving sources. The bandwidths which give rise to optimal narrowing coincide with readily accessible experimental values. The early predictions of spectral narrowing for this system required an intense, ideally squeezed field with bandwidth very much larger than the atomic transition linewidth, and 4π solid angle squeezing. By contrast, the line-narrowing we describe here requires weak, narrowband driving, and crucially, does not require 4π solid angle squeezing.

Acknowledgements.

This research was supported by the UK EPSRC.

-
- [1] C. W. Gardiner *Physical Review Letters* **56**, 1917 (1986).
 - [2] W. S. Smyth and S. Swain, *Phys. Rev. A* **59**, R2579, (1999).
 - [3] W. S. Smyth and S. Swain, *J. Mod. Optics*, **46**, 1233, (1999).
 - [4] B. J. Dalton, Z. Ficek and S. Swain *J. Mod. Optics*, **46**, 379.
 - [5] C. W. Gardiner, *Physical Review Letters* **70**, 2269 (1993).
 - [6] C. W. Gardiner and A. S. Parkins, *Physical Review* **A50**, 1792 (1994).

PARTIAL COHERENCE EFFECTS IN POLARIZATION-SQUEEZED LIGHT FORMATION AT FREQUENCY DOUBLING

Vsevolod V. Volokhovskiy

*Department of General Physics and Wave Processes, Faculty of Physics, M.V. Lomonosov
Moscow State university, Moscow, 119899, Russia*

Abstract

Influence of partial coherence of laser radiation upon a nonclassical light formation during second harmonic generation by mixing was considered. The analysis was made in terms of mean values and variances of the Stokes parameters under short time approximation. It was shown that partial coherence decreased the degree of polarization squeezing, but in the involved process it was possible to suppress both coherent and thermal fluctuations.

I. INTRODUCTION

Recently a set of nonlinear optical processes which lead to polarization - squeezed (PS) light formation has been studied thoroughly. This type of nonclassical light is characterized by suppressed fluctuation of the Stokes parameters which are used to describe the polarization state of radiation.

PS light formation in type II second harmonic generation was considered in [1,2]. To estimate the real fluctuation suppression in experiment taking into account the real properties of light and media is necessary. Influence of dissipation and thermal noise was analyzed in [3]. The another important factor influencing the fluctuation suppression is partial coherence of laser radiation.

The quadrature nonlinear media have comparatively strong nonlinearities. In such a medium it is possible to achieve high conversion coefficients. Due to these reasons the χ^2 medium most likely seem to reveal the PS light in the experiment. The main aim of this work is to analyze the influence of fundamental radiation partial coherence upon the PS light formation at frequency doubling by type II.

II. QUANTUM DESCRIPTION OF SHG PROCESS

Let us consider the type II second harmonic generation. In this process the PS light formed due to simultaneous annihilation of quanta in two orthogonally polarized modes of

fundamental radiation which makes these modes correlated. The interaction Hamiltonian for this case has the form

$$H_{int} = \hbar\tilde{\gamma}(a_1^\dagger a_2^\dagger a_3 + a_1 a_2 a_3^\dagger), \quad (1)$$

here $a_j(a_j^\dagger)$ are the j -th fundamental ($j=1,2$) mode and second harmonic ($j=3$) photon annihilation (creation) operators, $\tilde{\gamma}$ is nonlinear coupling coefficient.

The Hamiltonian (1) leads to the following system of operator equations

$$\frac{da_1}{dt} = i\tilde{\gamma}a_2^\dagger a_3, \quad \frac{da_2}{dt} = i\tilde{\gamma}a_1^\dagger a_3, \quad \frac{da_3}{dt} = i\tilde{\gamma}a_1 a_2. \quad (2)$$

The system under consideration does not have an analytical solution. Thus the short time approximation was employed. Then the time dependence of operators has the form

$$a_j(t) = a_{j0} + i\tilde{\gamma}t a_{k0}^\dagger a_{30} + 0.5\tilde{\gamma}^2 t^2 (a_{j0} a_{30}^\dagger a_{30} - a_{j0} a_{k0}^\dagger a_{k0}),$$

here the subscript 0 denotes the value of corresponding operator at medium input (at $t=0$).

III. PARTIALLY COHERENT PUMP

Let the initial state of each of the two fundamental modes is given by density matrix $\rho(0)$ with Fock matrix elements

$$\rho_{m,k}(0) = \langle m | \rho(0) | k \rangle = \int \frac{\beta^{*m} \beta^k}{\sqrt{m!k!}} \exp(-(|\beta|^2)) P(\beta) d^2\beta,$$

here $P(\beta)$ is Glauber- Shudarshan quasidistribution function. For partially coherent radiation of fundamental modes it has the form

$$P(\beta) = \frac{1}{\pi N} \exp\left(-\frac{|\beta - \alpha|^2}{N}\right).$$

At medium input ($t=0$) the polarization modes were assumed uncorrelated then the initial state of the whole field was given by the matrix

$$\rho(0) = \sum |m_1\rangle\langle m_2| \rho_{m_1, k_1}(0) \rho_{m_2, k_2}(0) \langle k_1 | \langle k_2 |.$$

IV. STATISTICAL PROPERTIES OF THE STOKES PARAMETERS

We used the radiation polarization state description by means of the Stokes operators which in the given basis has the form

$$\begin{aligned} S_0(t) &= a_1^\dagger(t)a_1(t) + a_2^\dagger(t)a_2(t), \\ S_1(t) &= a_1^\dagger(t)a_1(t) - a_2^\dagger(t)a_2(t), \\ S_2(t) &= a_2^\dagger(t)a_1(t)e^{i\phi} + a_1^\dagger(t)a_2(t)e^{-i\phi}, \\ S_3(t) &= i(a_2^\dagger(t)a_1(t)e^{i\phi} - a_1^\dagger(t)a_2(t)e^{-i\phi}). \end{aligned} \quad (3)$$

The operators satisfy commutation relation of $SU(2)$ algebra

$$[S_m, S_n] = 2i\epsilon_{nml}S_l$$

which leads to the following uncertainty relation

$$V_m V_n \geq |\epsilon_{nml}\langle S_l \rangle|^2,$$

where V_m is the parameter S_m fluctuation variance, ϵ_{mnl} is antisymmetric Levi - Civita tensor.

Having determined the operators time dependence one can get the statistical characteristics of Stokes operators by applying the usual averaging procedure $\langle A(t) = Tr(A(t)\rho(0)) \rangle$ where $A(t)$ should be substituted by $S_j(t)$ and $S_j^2(t)$. Then for Stokes operators variances one can obtain

$$\begin{aligned} V_0 &= \sigma_{10}^2 + \sigma_{20}^2 + 4\gamma^2\langle n_{10} \rangle\langle n_{20} \rangle - 4\gamma^2\langle n_{10} \rangle\sigma_{20}^2 - 4\gamma^2\langle n_{20} \rangle\sigma_{10}^2, \\ V_1 &= \sigma_{10}^2 + \sigma_{20}^2, \\ V_{2,3} &= G_1 + G_2 - 2N_1N_2 - 2\gamma^2\langle n_{10} \rangle\sigma_{20}^2 - 2\gamma^2\langle n_{20} \rangle\sigma_{10}^2 + 2\gamma^2(N_1 + N_2)(\langle n_{10} \rangle - \langle n_{20} \rangle - N_1N_2), \end{aligned} \quad (4)$$

Here $G_j = \langle n_{j0} \rangle(1 + 2N_k + 2\gamma^2(N_2^2 - N_1N_2))$, $\langle n_{j0} \rangle = |\alpha_j|^2 + N_j$ is the j-th mode photon mean value, $|\alpha_j|^2$ and N_j are the coherent and thermal photon number, respectively; $\sigma_{j0}^2 = |\alpha_j|^2(1 + 2N_j) + N_j + N_j^2$ is the initial photon number variance, $\gamma = \tilde{\gamma}t$.

V. SUPPRESSION OF POLARIZATION FLUCTUATIONS

As it can be seen from (4) in case of completely coherent radiation the variances have the simple form [1] ($\bar{n}_{j0} = |\alpha_j|^2$).

$$V_1 = \bar{n}_{10} + \bar{n}_{20}, \quad V_0 = V_2 = V_3 = \bar{n}_{10} + \bar{n}_{20} - 4\gamma^2\bar{n}_{10}\bar{n}_{20}.$$

Thus, it can also be seen from (4) that partial coherence of the pump causes the presence of additional terms in variances dependencies. These terms decrease the efficiency of fluctuation suppression. To illustrate this effect the values of variances $v_j = V_j/\langle S_0 \rangle$ normalized by the fundamental field intensity are the most appropriate. The coefficient of conversion into the second harmonic is given by the relation $\eta = \hbar 2\omega n_{sh}/\hbar\omega n_0$ where n_0 and n_{sh} are mean photon number of fundamental radiation and second harmonic, respectively. Then for the fundamental field intensity one can obtain $\langle S_0 \rangle = n_0(1 - \eta(1 + 4r + 4r^2) + 2r)$. Taking into account the real properties of laser field ($r = N/n_0 \ll 1, N + N_j$) the normalized variances can be expressed in the form

$$v_1 = (1 + 2N)\frac{1}{1 - \eta}, \quad v_0 = v_2 = v_3 = (1 + 2N)\frac{1 - 2\eta}{1 - \eta}. \quad (5)$$

It should be noted that this result is valid for comparatively low conversion coefficients ($\eta < 0.5$) since the short time approximation was used to determine the operator time dependence (for details see [4]).

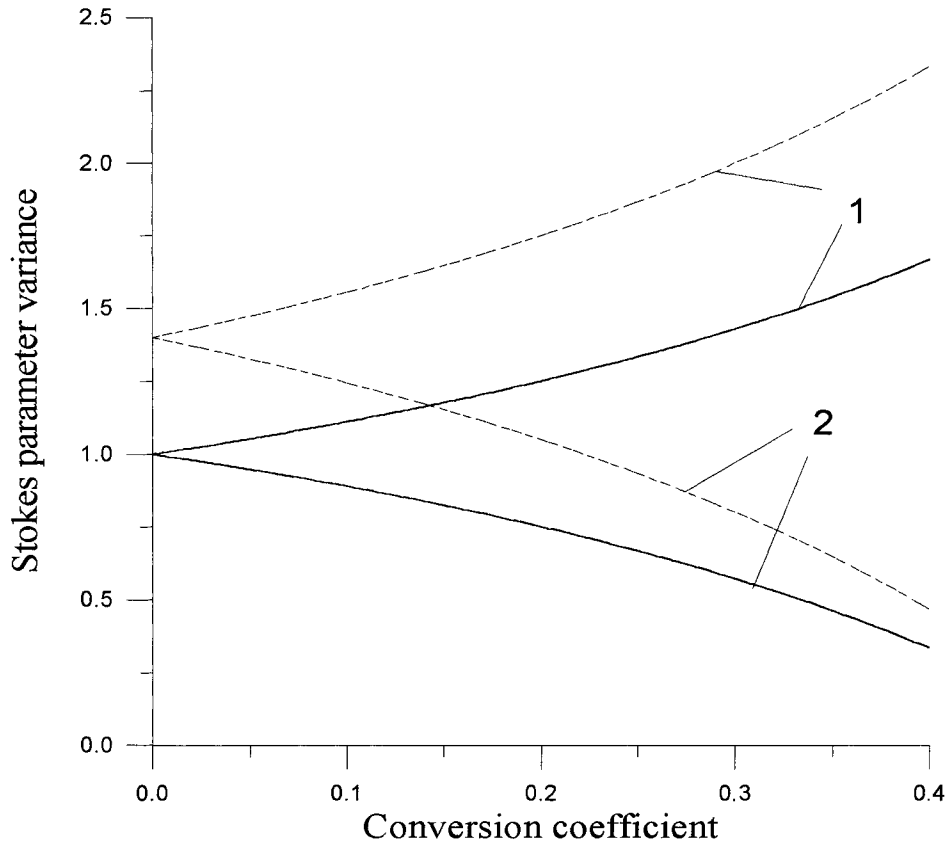


FIG. 1. The Stokes parameters variances $v_1(1)$ и $v_{0,2,3}(2)$ as functions of conversion coefficient η . Partially coherent radiation with $N = 0.2$ – dotted lines, completely coherent radiation — solid lines.

VI. CONCLUSIONS

The analysis made allows to conclude that partial coherence of the radiation decreases the efficiency of polarization - squeezed light formation as it was expected. Besides, during the PS light formation process both the coherent and thermal fluctuation could be suppressed. Also it can be seen that for partial coherence of laser radiation not to influence dramatically the fluctuation suppression process the number of noise photons should be less than 0.1. This value limits the thermal fluctuation level to generate the PS light.

The author acknowledges the Organizing Committee of ICSSUR'99 for financial support and Prof. A.S.Chirkin for useful discussion.

REFERENCES

- [1] Beskrovniy V.N, Chirkin A.S., *Quantum Electron.*, **23**, 843 (1996).
- [2] Beskrovniy V.N., Chirkin A.S., *Quantum Semiclas. Opt*, **10**, 263 (1998).
- [3] Volokhovskiy V.V., Chirkin A.S., *Quantum Electron.*, **28**, 1022 (1998).
- [4] Volokhovskiy V.V., *Laser Physics*, **9**, 669 (1999).

The Optical Stark Effect With Squeezed Radiation Field

T. Altevogt, H. Puff, and R. Zimmermann

*Institut für Physik der Humboldt-Universität Berlin, Arbeitsgruppe Halbleitertheorie,
Hausvogteiplatz 5-7, D-10117 Berlin, Germany,
e-mail: altevogt@physik.hu-berlin.de*

Abstract

The optical Stark effect in a pump-probe setup is expected to show new features if the quantization of the pump field becomes important. For example, the lineshape of a Stark-shifted resonance is strongly modified when squeezing the pump field. Moreover, nonclassical gain occurs at low pump detuning. A quantitative calculation of these effects in terms of a density matrix approach is presented.

I. INTRODUCTION

The optical Stark effect is a well-known phenomenon in modern spectroscopy. It is due to the dynamic coupling of two energy levels by a near-resonant pump field which shifts the levels with respect to their original positions. One common detection scheme is a pump-probe setup, where the pump-induced optical Stark-shift of a two-level system (TLS) is observed in the absorption spectrum of an additional probe field [1,2,3].

In this scheme, new additional features are expected if the quantization of the pump field is of importance [4]. In section II, we will discuss two of these features, i. e. the influence of a squeezed pump field on the lineshape and nonclassical gain. In section III, we give an outline of a density matrix approach (DMA) which allows an approximate but reliable calculation of the Stark-shifted probe absorption with low numerical effort.

II. PROBE ABSORPTION SPECTRUM FOR A SQUEEZED PUMP FIELD

The system under consideration consists of N identical two-level systems (TLS) which are strongly coupled to a near-resonant pump field of frequency ω_p . The coupling constant g is enhanced by confining the pump mode within a cavity. Moreover, a probe field at frequency ω being non-resonant to a cavity mode is irradiated. Its absorption spectrum displays the pump-induced optical Stark-shift.

The pump field is assumed to be in a squeezed state defined by

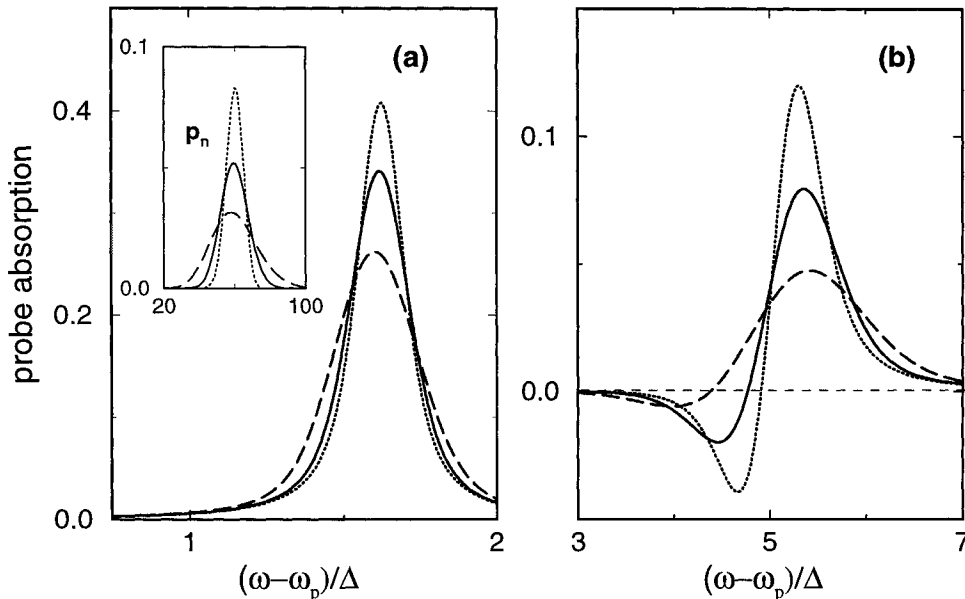


FIG. 1. Probe absorption for pump detuning (a) $\Delta=12g$ and (b) $\Delta=3g$. Solid curves: $\xi=0$, dotted curves: $\xi=0.5$, dashed curves: $\xi=-0.5$. The inset figure shows corresponding photon statistics. Other parameters: $N=10$, $\langle n \rangle=60$.

$$|\alpha; \xi\rangle = D(\alpha)S(\xi)|0\rangle$$

$$\text{with } S(\xi) = \exp\left(-\frac{1}{2}(\xi a^{\dagger 2} - \xi^* a^2)\right); D(\alpha) = \exp(\alpha a^\dagger - \alpha^* a) \quad (1)$$

where α and ξ are c-numbers [5].

In Fig. 1a, the Stark-shifted probe absorption spectrum for a pump detuning Δ of the order of the (mean) Rabi frequency $\Omega = 2g\sqrt{\langle n \rangle}$ ($\langle n \rangle$: mean pump photon number) is shown for three different types of squeezed states. The first type is a coherent state ($\xi=0$), while the second type with ξ being positive is a state with suppressed fluctuations of the pump photon number. The third type for negative ξ is a state with suppressed phase fluctuations. If the lineshapes of the Stark-shifted resonances are compared to the various photon statistics of these three states shown in the inset of Fig. 1a, it becomes apparent that the lineshape directly displays the pump photon statistics. The results of Fig. 1 have been obtained by exact diagonalization of the Hamiltonian that will be discussed in the next section.

For smaller pump detuning, a probe gain occurs within the Stark-shifted resonance (Fig. 1b). As this gain would not appear when treating the pump field classically, we refer to it as nonclassical gain. Although the lineshape does not directly display the pump photon statistics here, it still strongly depends on the latter, as can also be seen in Fig. 1b.

III. DENSITY MATRIX APPROACH (DMA)

In this section, we briefly describe a density matrix approach that allows the calculation of the Stark-shifted probe absorption. The starting point is a Hamiltonian describing the coupling between N two-level systems (TLS) ($|g_\nu\rangle, |e_\nu\rangle$; $\nu = 1, \dots, N$) and the two fields (pump and probe) which reads in rotating wave approximation

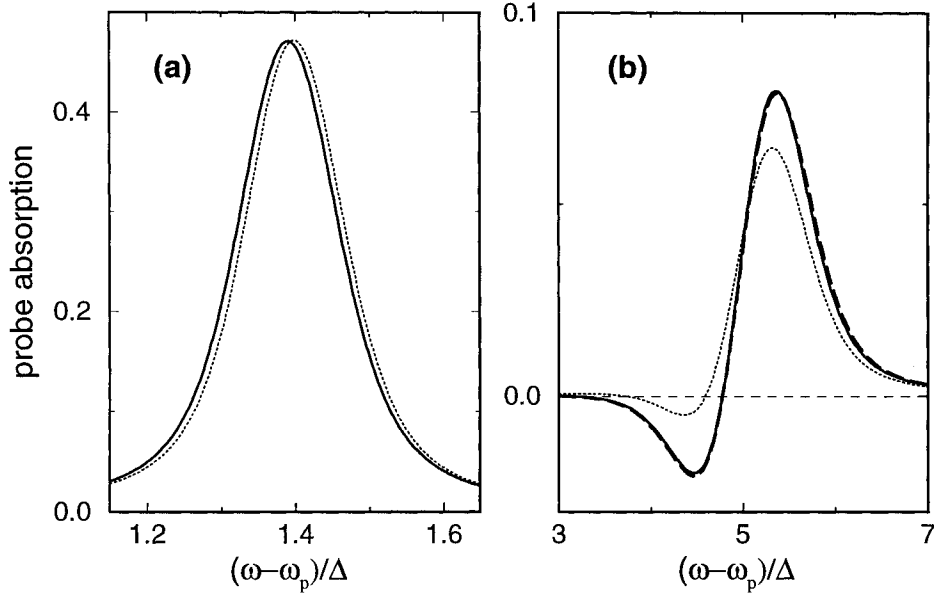


FIG. 2. Probe absorption for (a) $\Delta=16g$, $N=5$ and (b) $\Delta=3g$, $N=10$ for $\xi=0$. Solid curves: exact, dotted curves: DMA, dashed curves: improved DMA. Other parameters: $\langle n \rangle=60$.

$$\mathcal{H} = \hbar\omega_p \mathcal{K} + \hbar\Delta J_3 + \hbar g(J_+ a + a^\dagger J_-) + \hbar\tilde{g}(J_+ A e^{-i\omega t} + h.c.). \quad (2)$$

Here, a and a^\dagger are annihilation and creation operators of pump photons. The J -operators defined by

$$\begin{aligned} J_+ &= \sum_{\nu=1}^N J_{\nu,+} = \sum_{\nu=1}^N |e_\nu\rangle\langle g_\nu|; \quad J_- = (J_+)^\dagger; \\ J_3 &= \sum_{\nu=1}^N J_{\nu,3} = \frac{1}{2} \sum_{\nu=1}^N (|e_\nu\rangle\langle e_\nu| - |g_\nu\rangle\langle g_\nu|) \end{aligned} \quad (3)$$

are collective operators of the N TLS that are well-known from the Dicke-model [6]. Moreover, we have introduced the excitation number operator \mathcal{K} as $\mathcal{K} \equiv a^\dagger a + J_3 + N/2$. \mathcal{K} commutes with \mathcal{H} and counts pump photons and excited TLS. The c-number A denotes the amplitude of the probe field which can be treated classically due to weak coupling [7].

The linear probe absorption is determined by the linear probe-induced polarization which is proportional to $\langle J_-(t) \rangle^{(1)}$. If an initial state with all the TLS being in their ground states is assumed, $\langle J_-(t) \rangle^{(1)}$ can be decomposed as

$$\langle J_-(t) \rangle^{(1)} = \sum_{n=0}^{\infty} p_n \langle J_-(t) \rangle_n^{(1)}, \quad (4)$$

where p_n is the pump photon statistics and $\langle \dots \rangle_n$ refers to an initial state with n pump photons.

The density matrix equations for $\langle J_-(t) \rangle_n^{(1)}$ directly follow from the Heisenberg equations of motion. One obtains, as usual, an infinite set of equations. In order to truncate the hierarchy, we approximately decouple terms which describe correlations between different two-level systems, for example $\langle J_{3,\nu} J_{-\nu'} \rangle_n$ for $\nu \neq \nu'$. For pump detunings of the order of

the (mean) Rabi frequency, the results of the DMA agree with the exact results apart from a small shift (Fig. 2a). Nevertheless, this first approach is inappropriate for a quantitative calculation in the regime of nonclassical gain (dotted curve in Fig. 2b).

In order to improve the DMA, terms which include pair correlations between different TLS are fully taken into account. A finite set of equations is then obtained by decoupling terms which describe correlations between three different TLS, for example $\langle J_{-, \nu} J_{3, \nu'} J_{3, \nu''} \rangle_n$ with ν , ν' , and ν'' being pairwise different. This improved approach then gives an accurate description of nonclassical gain (dashed curve in Fig. 1b).

The advantage of the DMA is that it allows the calculation of the Stark-shifted probe absorption for even high numbers of TLS N as its numerical effort is independent of N in contrast to an exact diagonalization of \mathcal{H} .

IV. SUMMARY

In this paper, we have shown that a squeezed pump field can alter the lineshape of a Stark-shifted resonance. For a pump detuning of the order of the (mean) Rabi frequency, the lineshape directly displays the squeezed photon statistics. An efficient way to calculate the probe absorption spectra is given by a density matrix approach in which higher-order correlations between different TLS are approximated. The advantage of the density matrix approach is that its numerical burden is independent on TLS number N . Moreover, an extension of the density matrix approach to describe the optical Stark effect in more complex systems as, for example, impurity-bound excitons in semiconductors is possible [8].

ACKNOWLEDGMENTS

This work was supported by the DFG (Deutsche Forschungsgemeinschaft).

V. REFERENCES

1. F. Y. Wu, S. Ezekiel, M. Ducloy, and B. R. Mollow, *Phys. Rev. Lett.* **38**, 1073 (1977).
2. Ph. Tamarat, B. Lounis, J. Bernard, S. Kummer, R. Kettner, S. Mais, Th. Basché, *Phys. Rev. Lett.* **75**, 1514 (1995).
3. A. Mysrowicz, D. Hulin, A. Antonetti, A. Migus, W. T. Masselink, H. Moroc, *Phys. Rev. Lett.* **56**, 274 (1986).
4. T. Altevogt, H. Puff, R. Zimmermann, *Phys. Rev. A* **56**, 1592 (1997).
5. D. F. Walls, G. J. Milburn; *Quantum Optics*, Springer-Verlag (1994).
6. R. H. Dicke, *Phys. Rev.* **93**, 99 (1954).
7. S. M. Dutra, P. L. Knight, H. Moya-Cessa, *Phys. Rev. A* **49**, 1993 (1994).
8. T. Altevogt, H. Puff, R. Zimmermann, *phys. stat. sol. (b)*, **206**, 87 (1998).

Nonclassical states in a model of micromaser with unified Jaynes–Cummings interaction

G. Ariunbold

*Department of Optics, Palacký University, 17. listopadu 50, 772 07 Olomouc, Czech Republic;
Department of Theoretical Physics, National University of Mongolia, 210646 Ulaanbaatar,
Mongolia*

J. Peřina

*Department of Optics, Palacký University, 17. listopadu 50, 772 07 Olomouc, Czech Republic;
Joint Laboratory of Optics of Palacký University and Physical Institute of Academy of Sciences
of Czech Republic, 17. listopadu 50, 772 07 Olomouc, Czech Republic*

Ts. Gantsog

*Department of Theoretical Physics, National University of Mongolia, 210646 Ulaanbaatar,
Mongolia*

Abstract

The lossless micromaser-type models with the various versions of the Jaynes–Cummings (JC) interaction are treated in a unified formalism based on the oscillator algebra. It is proposed that the vacuum in the cavity with injected atomic coherence evolves to pure states when atom–field interaction is weak.

We consider a monokinetic beam of individual two–level atoms which are prepared in the same coherent superposition of the upper and lower states and injected into a lossless cavity in such a rate that at most one atom at a time is present inside the cavity, in order to generate a maser field [1]. However, from the theoretical point of view, the similarities among the algebraic manipulations used in the various micromaser-type systems [2–4] in the weak interaction regime (WIR) suggest that there would be a unified approach predicting the production of arbitrary states, that is based on the generalized bosonic oscillator (GBO) algebra. The most general form of the JC Hamiltonian is given, in the dipole and rotating–wave approximations and in the interaction picture, by [5]

$$\hat{H} = \hbar g(\hat{a}\hat{\sigma}_+ + \hat{a}^\dagger\hat{\sigma}_-), \quad (1)$$

where $\hat{\sigma}_\pm$ are the standard spin–1/2 operators, g is the atom–cavity mode coupling, the frequency of the cavity mode coincides with the atomic transition frequency and the operators \hat{a}, \hat{a}^\dagger constitute the GBO algebra basis $\{\hat{1}, \hat{a}, \hat{a}^\dagger, \hat{n}\}$ which satisfies the relations,

$$\hat{a}^\dagger\hat{a} = \hat{\Psi}(n), \quad \hat{a}\hat{a}^\dagger = \hat{\Psi}(n+1), \quad [\hat{a}, \hat{n}] = \hat{a}, \quad [\hat{a}^\dagger, \hat{n}] = -\hat{a}^\dagger, \quad (2)$$

where \hat{n} being the excitation number operators and real non-negative structure function $\Psi(n)$ ($\Psi(n) \geq 0, \forall n \geq 0$) characterizes the given system. We assume that system (2) has a unique vacuum state $|0\rangle$ such that $\hat{a}|0\rangle = 0, \Psi(n) > 0, \forall n > 0$, the spectrum of \hat{n} is taken to be $\{0, 1, 2, \dots\}$ [6]. The micromaser cavity field density matrix $\hat{\rho}$ evolves according to

$$\hat{\rho}_N = \text{Tr}_A[e^{-i\hat{H}\tau/\hbar}\hat{\rho}_A \otimes \hat{\rho}_{N-1}e^{i\hat{H}\tau/\hbar}]. \quad (3)$$

Here $\hat{\rho}_N$ is the density matrix of the field after N atoms have passed through the cavity with the constant flight time τ , Tr_A stands for the trace over the atomic variables. Thus the recursion relation for the density matrix elements can be written as

$$\begin{aligned} \rho_N(n, n') &= [\alpha^2 C_{n+1} C_{n'+1} + \beta^2 C_n C_{n'}] \rho_{N-1}(n, n') \\ &+ \beta^2 S_{n+1} S_{n'+1} \rho_{N-1}(n+1, n'+1) + \alpha^2 S_n S_{n'} \rho_{N-1}(n-1, n'-1) \\ &+ i\alpha\beta e^{i\phi} C_{n+1} S_{n'+1} \rho_{N-1}(n, n'+1) + i\alpha\beta e^{-i\phi} C_n S_{n'} \rho_{N-1}(n, n'-1) \\ &- i\alpha\beta e^{i\phi} S_n C_{n'} \rho_{N-1}(n-1, n') - i\alpha\beta e^{-i\phi} S_{n+1} C_{n'+1} \rho_{N-1}(n+1, n'), \end{aligned} \quad (4)$$

with an input state $\rho_{N=0}(n, n') = \rho_0(n, n')$, where $C_n = \cos(g\tau\sqrt{\Psi(n)})$, $S_n = \sin(g\tau\sqrt{\Psi(n)})$ and $\rho_{aa} = \alpha^2$, $\rho_{bb} = \beta^2$, $\rho_{ab} = \alpha e^{i\phi}\beta$, $\rho_{ba} = \alpha e^{-i\phi}\beta$, ($\alpha^2 + \beta^2 = 1$) are the atomic parameters. We also suppose that the input state be constructed from the vacuum using the sole operators in (2). However, the case of the input ordinary coherent state does lead to the generation of the two-photon state [7] in the two-photon micromaser system [2], which is not considered here. The solution of the recursion relation (4) can be found by the same method which was adopted in [2-4] to be

$$\rho_N(n, n') \simeq \sum_{k=0}^n \sum_{k'=0}^{n'} G_k^{(n-k)}(z) G_{k'}^{(n'-k')}(z^*) \rho_0(n-k, n'-k'), \quad (5)$$

under the conditions $\alpha, \beta \neq 0, N \gg 1, g\tau\sqrt{\Psi(n)} \ll 1, n + n' + \frac{nn'}{\beta^2} \ll N, |z| < 1$, where $z = ie^{i\phi}\alpha\beta g\tau N$, $G_k^{(n)}(z) = \frac{(-z)^k}{k!} \sqrt{\Psi(n+k)!/\Psi(n)!}$, $\Psi(0)! \equiv 1$. Of course, this solution has been written for those systems in which the structure function be chosen in such a way that the function $G_k^{(n-k)}(z)$ to be convergent for finite z . If the micromaser system starts from a pure state $|\psi_{in}\rangle$, then the cavity field evolves also to the pure state $|\psi_{out}\rangle$, from (5),

$$\langle n|\psi_{out}\rangle \simeq \sum_{k=0}^n G_k^{(n-k)}(z) \langle n-k|\psi_{in}\rangle. \quad (6)$$

Particularly, for the input vacuum $\langle n-k|\psi_{in}\rangle = \delta_{n-k,0}$, it becomes $\langle n|\psi_{out}\rangle \simeq G_n^{(0)}(z)$, while for an initial state with an amplitude z_0 and a certain normalization coefficient, it conserves its form, but with the displaced amplitude $\langle n|\psi_{out}\rangle \propto G_n^{(0)}(z_0 + z)$. This means that perfect echo may occur when the phase difference of the amplitudes z_0 and z is π . These approximate analytical calculations performed when $|z| < 1$, since the normalization coefficient does not appear in both expressions, while the numerical calculation of the recursion relation (4) in the WIR provides the production of a transformed state for not only small displacement z . In Table 1. we summarize the results of the numerical calculation of the various micromaser-type systems in the WIR. Furthermore, we believe that the proposed procedure can suggest

TABLE I. Nonclassical states in the micromaser-type systems with Hamiltonians \hat{H} , operators \hat{a} , \hat{n} and functions $\Psi(x)$ for the various version of the Jaynes-Cummings model.

Model	Hamiltonian \hat{H}	\hat{a}	\hat{n}	$\Psi(x)$	States
Micromaser	$\hbar g(\hat{b}\hat{\sigma}_+ + \hat{b}^\dagger\hat{\sigma}_-)$	\hat{b}	$\hat{b}^\dagger\hat{b}$	x	Displaced [2]
Two-photon system	$\hbar g(\hat{b}^2\hat{\sigma}_+ + \hat{b}^{\dagger 2}\hat{\sigma}_-)$	\hat{b}^2	$\frac{\hat{b}^\dagger\hat{b}}{2}$	$2x(2x-1)$	Squeezed [2]
Two-mode system	$\hbar g(\hat{b}_1\hat{b}_2\hat{\sigma}_+ + \hat{b}_1^\dagger\hat{b}_2^\dagger\hat{\sigma}_-)$	$\hat{b}_1\hat{b}_2$	$\frac{\hat{b}_1^\dagger\hat{b}_1 + \hat{b}_2^\dagger\hat{b}_2}{2}$	x_1x_2	Squeezed [3]
ID ^a system	$\hbar g(\hat{b}(\hat{b}^\dagger\hat{b})^{\frac{1}{2}}\hat{\sigma}_+ + (\hat{b}^\dagger\hat{b})^{\frac{1}{2}}\hat{b}^\dagger\hat{\sigma}_-)$	$\hat{b}(\hat{b}^\dagger\hat{b})^{\frac{1}{2}}$	$\hat{b}^\dagger\hat{b}$	x^2	HPTS ^b [4]

^aIntensity Dependent

^bHolstein-Primakoff $SU(1,1)$ transformed state

the production of pure states in the cavity system associated with the structure function which leads to the divergence of the function $G_n^{(0)}(z)$ for finite z . Therefore, from the computational point of view, to make a probable convergent approximation to the pure states generated in the cavity associated with any structure function, we introduce new states as

$$\langle n|\psi\rangle \propto \frac{G_n^{(0)}(z)}{f(n)!} = \frac{(-z)^n}{n!} \left(\frac{\sqrt{\Psi(n)!}}{f(n)!} \right), \quad (7)$$

where the deformation function $f(x)$ is always unity if $G_n^{(0)}(z)$ is a convergent, otherwise, it is not unity (let $f(x) \neq 0$, see, FIG. 1). In fact, these states are included in the class of

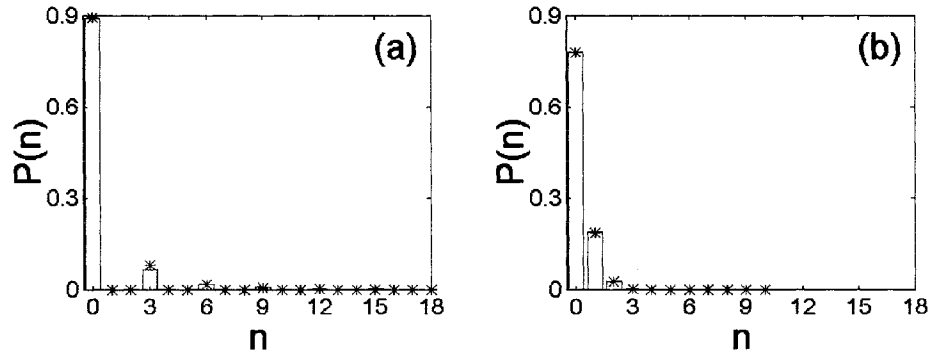


FIG. 1. The photon-number distributions (a) for the three-photon system (bars) with parameters $\alpha = \beta = 1/2$, $\phi = 3\pi/2$, $g\tau = 0.00001$, $N = 30000$ so that $\alpha\beta g\tau N = 0.15$ (input vacuum) and for the multiphoton state (stars) $\langle mn|\psi\rangle \propto \frac{(-z_m)^n}{m^n n!} \frac{\sqrt{\Psi(n)!}}{f_m(n)!}$ with $\Psi(n) = \frac{(mn)!}{(mn-m)!}$, $f_m(n) \begin{cases} = 1 & \text{if } m = 1, 2 \\ \neq 1 & \text{otherwise} \end{cases}$ for $m = 3$ and $f_3(n) = \sqrt{n}$, $z_3 = \tanh r = 0.6366$ with $r = 0.7524$; (b) for the q -deformed [9] system (bars) with the same α, β, ϕ as in (a), $g\tau = 0.0001$, $N = 10000$ to get $\alpha\beta g\tau N = 0.5$ and for the state (stars) $\langle n_q|\psi\rangle \propto \frac{(-z)^n}{n!} \frac{\sqrt{\Psi(n)!}}{f(n)!}$ with $\Psi(n) = [n]_q = \frac{q^n - q^{-n}}{q - q^{-1}}$, $q = 2$, $f(n) = \begin{cases} 1 & \text{if } n < n_0 \\ \infty & \text{otherwise.} \end{cases}$ Here n_0 makes truncation establishing the probability amplitude $\langle n_q|\psi\rangle$ to be convergent, where $n_0 = 10$, $z = 0.49$.

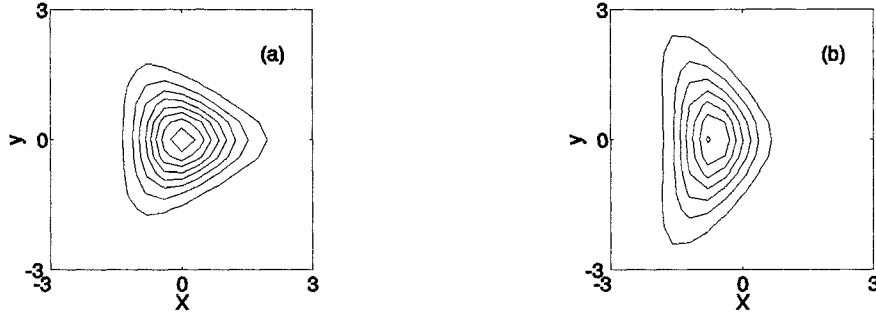


FIG. 2. 'Generalized squeezing' [10]; the Husimi Q -function contour plots for the generated field states (a) the same as in FIG. 1a; (b) the same as in FIG. 1a, but $\phi = \pi$, with input coherent state $|1\rangle$.

nonlinear coherent states [8], where in the framework of our model, the $f(x)$ does only assist to ensure that the 'tail' of the probability amplitude $\langle n|\psi\rangle$ is convergent. The physical reason why we use the deformation function is that the divergence is the result of the parametric approximation—that is of the assumption that the pump beam is classical and undepleted. If the pump beam is quantum and treated dynamically, the energy is conserved and there is no divergence so that the $f(x)$ may reflect a role of the pump depletion.

ACKNOWLEDGEMENTS

This work was supported by Complex Grant No VS96028 of the Czech Ministry of Education.

REFERENCES

- [1] J. Krause, M.O. Scully and H. Walther, Phys. Rev. A **34**, 2032 (1986).
- [2] G. Ariunbold, J. Peřina and Ts. Gantsog, J. Opt. B: Quant. Semiclass. Opt. **1**, 219 (1999).
- [3] G. Ariunbold, J. Peřina, Ts. Gantsog and F.A.A. El-Orany, Acta Phys. Slov. **49**, 627 (1999).
- [4] G. Ariunbold and J. Peřina Acta Phys. Slov. **48**, 315 (1998).
- [5] D. Bonatsos, C. Daskaloyannis and G.A. Lalassisis, Phys. Rev. A **47**, 3448 (1993).
- [6] P. Shanta, S. Chaturvedi, V. Srinivasan and R. Jagannathan, J. Phys. A: Math. Gen. **27**, 6433 (1994).
- [7] J. Peřina, 1991, *Quantum Statistics of Linear and Nonlinear Optical Phenomena*, 2nd edn (Kluwer:Dordrecht).
- [8] V.I. Man'ko, G. Marmo, F. Zaccaria and E.C.G. Sudarshan, 1996, *Proceedings of the 4th Wigner Symposium*, ed. by Ataishiyev N, Seligman T and Wolf K B (World Scientific: Singapore); R.L. de Matos Filho and W. Vogel, Phys. Rev. A **54** 4560 (1996).
- [9] A.J. Macfarlane, J. Phys. A: Math. Gen. **22**, 4581 (1989); L.C. Biedenharn, *ibid*, L873.
- [10] S.L. Braunstein and R.I. McLachlan, Phys. Rev. A **35**, 1659 (1987).

COMBINATORIAL SOLUTION FOR THE PHOTON INTENSITY CORRELATIONS IN A CAVITY AT FINITE TEMPERATURE

Henk F. Arnoldus and Qiuhan Xue

*Department of Physics and Astronomy, Mississippi State University,
P.O. Drawer 5167, Mississippi State, MS 39762, USA
arnoldus@ra.msstate.edu*

Radiation in a single-mode cavity will evolve from some given initial state to thermal equilibrium with the cavity mirrors. The temporal, time-dependent, photon intensity correlation functions have been obtained to all orders. The result is a sum over combinatorial products connecting the detection times. In the limit of zero temperature we recover a well-known expression.

When radiation in a single-mode cavity is prepared in an initial state, described by the density operator $\rho(0)$, then the interaction with the mirrors will lead to relaxation of the radiation to the unique thermal equilibrium state, which is determined by the temperature only. The transient state density operator $\rho(t)$ obeys the Liouville equation

$$i \frac{d\rho}{dt} = L\rho, \quad (1)$$

with the Liouvillian L defined by

$$L\rho = \omega_c [a^\dagger a, \rho] - \frac{1}{2} i K n_{\text{eq}} (aa^\dagger \rho + \rho aa^\dagger - 2a^\dagger \rho a) - \frac{1}{2} i K (n_{\text{eq}} + 1) (a^\dagger a \rho + \rho a^\dagger a - 2\rho a^\dagger a). \quad (2)$$

Here, ω_c is the cavity frequency, K is the cavity damping rate, and n_{eq} is the number of photons in thermal equilibrium. This last parameter represents the temperature in the usual way. We are interested in the statistical photon correlations of this radiation during the time evolution towards equilibrium. Let $I_k(t_1, \dots, t_k) dt_1 \dots dt_k$ be the probability for the detection of a photon in $[t_1, t_1 + dt_1]$ and ... and the detection of a photon in $[t_k, t_k + dt_k]$, irrespective of detections at other times. Assuming that the detection does not significantly disturb the radiation itself, these photon correlations are proportional to the field intensity correlations

$$I_k(t_1, \dots, t_k) = \zeta^k \langle a^\dagger(t_1) \dots a^\dagger(t_k) a(t_k) \dots a(t_1) \rangle, \quad k = 1, 2, \dots, \quad (3)$$

where ζ is an overall detection efficiency parameter. Here, $t_k > \dots > t_2 > t_1$.

In order to evaluate the intensity correlations, we first transform expression (3) to the Schrödinger picture, which yields

$$I_k(t_1, \dots, t_k) = \zeta^k \text{Tr} \mathbf{D} e^{-iL(t_k - t_{k-1})} \mathbf{D} \dots \mathbf{D} e^{-iL(t_2 - t_1)} \mathbf{D} \rho(t_1). \quad (4)$$

The Liouville operator \mathbf{D} is defined by

$$\mathbf{D}\rho = a\rho a^\dagger, \quad (5)$$

giving its effect on an arbitrary density operator ρ . In order to clarify the significance of expression (4), we first notice that for $k = 1$ we have

$$I_1(t_1) = \zeta \text{Tr} \mathbf{D} \rho(t_1) = \zeta \sum_{n=0}^{\infty} \langle n | a \rho(t_1) a^\dagger | n \rangle = \zeta \sum_{n=0}^{\infty} n \langle n | \rho(t_1) | n \rangle = \zeta \sum_{n=0}^{\infty} n p_n(t_1) , \quad (6)$$

with $p_n(t) = \langle n | \rho(t) | n \rangle$ the probability to find n photons in the cavity at time t . Therefore,

$$I_1(t_1) = \zeta \bar{n}(t_1) , \quad (7)$$

which is ζ times the average number of photons in the cavity at time t_1 . The intensity $I_1(t_1)$ is the uncorrelated photon detection rate. The interpretation of expression (4) for $I_k(t_1, \dots, t_k)$ is then as follows: First the system evolves from $t = 0$ to t_1 , and the state is represented by $\rho(t_1)$. Action of operator \mathbf{D} then corresponds to the detection of the first photon at time t_1 . Then the system evolves to time t_2 by means of the evolution operator $\exp[-iL(t_2-t_1)]$. Then \mathbf{D} acts again, indicating the detection of the second photon, and so on.

Working out expression (4) in the same fashion as I_1 gives for $k = 2, 3, \dots$

$$I_k(t_1, \dots, t_k) = \zeta^k \sum_{n_k=0}^{\infty} \dots \sum_{n_2=0}^{\infty} \sum_{n_1=0}^{\infty} n_k \dots n_2 n_1 \\ \times X_{n_k, n_{k-1}}(t_k - t_{k-1}) \dots X_{n_2, n_1}(t_2 - t_1) p_{n_1}(t_1) . \quad (8)$$

Here, $X_{n,m}(t)$ is the propagation matrix for the probability distribution:

$$p_n(t) = \sum_{m=0}^{\infty} X_{n,m}(t) p_m(0) , \quad (9)$$

which can be computed explicitly from the equation of motion (1). The result is^{1,2}

$$X_{n,m}(t) = \frac{u^n}{(1+u)^{n+1}} \left(\frac{1+v}{1+u} \right)^m \sum_k \frac{(m+n-k)!}{(n-k)! k! (m-k)!} \left[-\frac{v(1+u)}{u(1+v)} \right]^k , \quad (10)$$

with $u = n_{\text{eq}} \{ 1 - \exp(-Kt) \}$ and $v = n_{\text{eq}} - (n_{\text{eq}} + 1) \exp(-Kt)$.

It then remains to perform the summations in (8). It appears to be convenient to express the result in terms of the factorial moments $s_k(t)$ of the photon distribution, rather than the probabilities. At any time t the relation is

$$s_k(t) = \sum_{n=k}^{\infty} \frac{n!}{(n-k)!} p_n(t) . \quad (11)$$

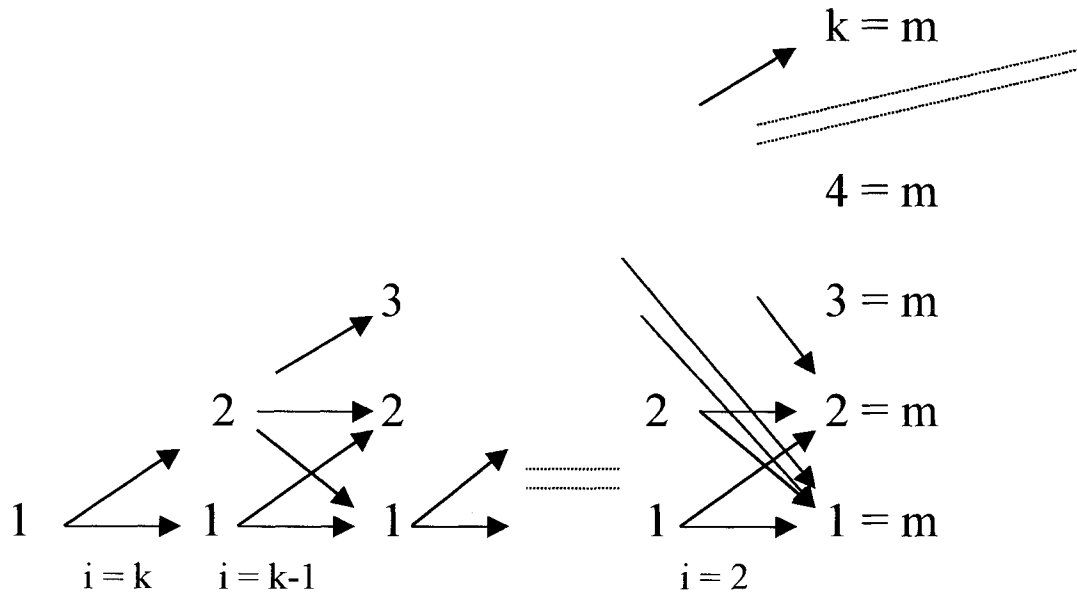
Moreover, the result simplifies considerably if we express the intensity correlations in terms of the factorial moments at time t_1 , rather than time $t = 0$. It follows by inspection that the result can be written in the form

$$I_k(t_1, \dots, t_k) = \zeta^k \sum_{m=1}^k n_{eq}^{k-m} s_m(t_1) \tilde{Z}_{k,m}(t_1, \dots, t_k) . \quad (12)$$

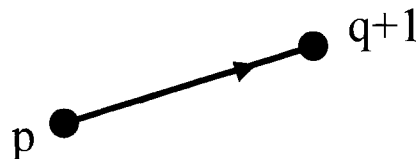
In this expression, the functions $\tilde{Z}(t_1, \dots, t_k)$ are independent of n_{eq} and the state of the field at time t_1 . They are combinatorial functions of the k time variables, and nothing else. Hence, expression (12) displays the temperature dependence, and the dependence on the state of the system at time t_1 . For the combinatorial functions we have found the following result:

$$\tilde{Z}_{k,m}(t_1, \dots, t_k) = \sum_{\substack{\text{all paths} \\ 1 \rightarrow m}} \prod_{i=k}^2 \left(\frac{p!}{q!} \right)^2 \frac{1}{(p-q)!} \left(1 - e^{-K(t_i - t_{i-1})} \right)^{p-q} e^{-qK(t_i - t_{i-1})} . \quad (13)$$

The summation runs over all paths on the lattice shown below. We start at "1" in the lower left



corner, and go in unit steps to the desired m value on the right. In each step you can go up one level, remain horizontal, or go down by an arbitrary number of levels. Each step determines a factor in the product. The values of p and q follow from the numbers on the lattice that are connected, according to the following diagram:



The factorial moments $s_m(t_1)$ can be expressed in terms of the factorial moments at $t = 0$, as derived in Ref. 2. The general result is

$$s_m(t) = \sum_{\ell=0}^m \left(\frac{m!}{\ell!} \right)^2 \frac{1}{(m-\ell)!} u^{m-\ell} e^{-\ell Kt} s_{\ell}(0) . \quad (14)$$

Combining (14) and (12) then shows that the intensity correlations can also be expressed as

$$I_k(t_1, \dots, t_k) = \zeta^k \sum_{n=0}^k n_{\text{eq}}^{k-n} s_n(0) Z_{k,n}(t_1, \dots, t_k) , \quad (15)$$

in terms of different combinatorial functions $Z_{k,n}$. The relation between the two representations is then found to be

$$Z_{k,n}(t_1, \dots, t_k) = \sum_{m=n}^k \tilde{Z}_{k,m}(t_1, \dots, t_k) \left(\frac{m!}{n!} \right)^2 \frac{1}{(m-n)!} \left(1 - e^{-Kt_1} \right)^{m-n} e^{-nKt_1} , \quad (16)$$

where we have set $\tilde{Z}_{k,0} = 0$.

For $k = 1$ the lattice reduces to one point, and we have $\tilde{Z}_{1,1} = 1$. This gives $Z_{1,0} = 1 - \exp(-Kt_1)$ and $Z_{1,1} = \exp(-Kt_1)$, and then

$$I_1(t_1) = \zeta s_1(t_1) = \zeta \left(n_{\text{eq}} (1 - e^{-Kt_1}) + \bar{n}(0) e^{-Kt_1} \right) , \quad (17)$$

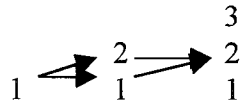
which is the same as expression (7). For $k = 2$ the lattice is $1 \rightleftarrows 1 \xrightarrow{2}$ so that each product in (13) has one factor and each summation has one term. This yields

$$\tilde{Z}_{2,1} = 1 - \exp(-K(t_2 - t_1)) , \quad \tilde{Z}_{2,2} = \exp(-K(t_2 - t_1)) , \quad (18)$$

and then, for instance

$$Z_{2,0} = (1 - \exp(-K(t_2 - t_1)))(1 - \exp(-Kt_1)) + 2 \exp(-K(t_2 - t_1))(1 - \exp(-Kt_1))^2 . \quad (19)$$

For $k > 2$ the expressions become more involved very rapidly. For instance, the possible paths for the function $\tilde{Z}_{3,2}$ are



For zero temperature, the only contribution comes from $\tilde{Z}_{k,k}$, and therefore from only one path on the lattice. We then obtain

$$I_k(t_1, \dots, t_k) = \zeta^k s_k(0) e^{-Kt_k} \dots e^{-Kt_2} e^{-Kt_1} . \quad (20)$$

1. B. Ya. Zel'dovich, A. M. Perelomov and V. S. Popov, Sov. Phys. JETP 28 (1969) 308
2. H. F. Arnoldus, J. Opt. Soc. Am. B 13 (1996) 1099

Single-beam blue-detuned optical trap for cold atoms

L. Cacciapuoti, G. Cennini, M. de Angelis ^{*}, P. Maddaloni, M. Prevedelli [†],
L. Ricci [‡] and G. M. Tino

*Dipartimento di Scienze Fisiche, Università degli Studi di Napoli "Federico II", INFN
Complesso Universitario di Monte S. Angelo, via Cintia, I-80126 Napoli (Italy)*

Abstract

We report a new optical scheme for the confinement of ultracold atoms in blue-detuned dipole traps. Three dimensional confinement can be achieved with a single laser beam. Long coherence times can be expected for Bose-Einstein condensed atoms.

Optical traps for neutral atoms have recently attracted increasing interest. After the demonstration of efficient cooling of atoms at ultralow temperatures down to Bose-Einstein condensation [1], the requirements for trap depth are greatly reduced. On the other hand, for several experiments it is important to achieve a long confinement and coherence time in a pure optical potential. Although magnetic traps represent an excellent tool to obtain Bose-Einstein condensation through the evaporative cooling technique, they can limit the studies of some atomic properties. Only the atoms in weak-field seeking states can be confined in a magnetic trap so that it is impossible, for example, to realize samples of unpolarized atoms.

These problems are overcome using far detuned optical dipole traps [2]. The trapping potential originates from the light shift induced on atomic levels by a far-off-resonance field. The use of highly detuned laser beams has two advantages: first of all, heating processes such as spontaneous scattering of photons, inelastic collisions induced by light or radiation trapping are strongly reduced; then, with detunings greatly exceeding the hyperfine splitting of the ground state, the trapping potential is completely independent of F and m_F quantum numbers. In red-detuned optical traps atoms are confined where the light field is maximum. This limits the trap lifetime and moreover, as the atoms spend most of their time in a strong radiation field, energy levels are deeply perturbed by the AC Stark effect. Long trap coherence times and very little perturbations on hyperfine atomic levels can be achieved in blue-detuned optical dipole traps. Using a radiation field detuned to the high frequency side

^{*}Istituto di Cibernetica del CNR, Napoli.

[†]Dipartimento di Fisica, Laboratorio LENS, Università di Firenze.

[‡]Dipartimento di Fisica, Università di Trento.

of an atomic transition it is possible to confine the atoms in low field intensity regions. So, the main problem is the realization of a laser beam geometry where a dark region is surrounded by light. Different methods have been developed to produce the required repulsive optical walls: light sheets by an elliptical focused laser beam can be used to realize nearly flat optical walls [3,4]; hollow laser beams geometries obtained by diffractive [5,6] or holographic methods [7] can provide spatial confinement in two or three dimensions; evanescent waves trapping [8,9,10] is realized by total reflection on the surface of a dielectric medium.

In this paper we study the generation of a single-beam blue-detuned optical trap using an axicon lens. We are planning to employ this field geometry for optical confinement of ^{87}Rb atomic samples, cooled down to Bose-Einstein condensation, first by evaporatively cooling the atoms in a magnetic trap and then by transferring them into the optical potential. Evaporative cooling reduces atomic temperatures well below $1\ \mu\text{K}$ so that only some milliwatts of laser power are needed for the optical confining beam. This approach allows us to minimize all heating mechanisms proportional to the field intensity and depending on amplitude fluctuations of the laser beam.

The axicon [11] is an excellent tool for the generation of hollow beam geometries. It is an optical element with a shape given by any figure of revolution that, by reflection or refraction or both, produces a line focus rather than a point focus from an incident collimated light beam along the symmetry axis of the system. Our axicon is a flat cone with a base angle $\alpha \simeq 10\ \text{mrad}$ realized on a plexiglass substrate. We use as a test a diode laser ($\lambda = 780\ \text{nm}$). The output beam is expanded to a waist $w = 5\ \text{mm}$. An axicon illuminated by a collimated beam produces a cone of light with an aperture angle $\theta = 2\alpha(n-1)$ where n is the refraction index of the optical medium ($n = 1.492$ for plexiglass). A converging lens before the axicon can be used to focus this beam on its back focal plane where, with a *CCD* camera, it is possible to observe a ring shaped intensity distribution. A typical picture is shown in Fig.1. The ring radius R in the focal plane depends on the distance d between the focusing lens and the axicon:

$$R = \alpha(n-1)(f-d)$$

where f is the focal length. With this configuration it is very easy to obtain ring diameters

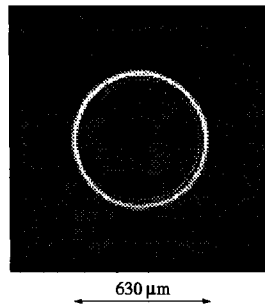


FIG. 1. Intensity distribution of the hollow beam in the back focal plane of the input lens observed with a *CCD* camera ($f = 20\ \text{cm}$ and $d = 13\ \text{cm}$).

around $100\ \mu\text{m}$. The transverse intensity distribution is well approximated by a gaussian profile [12] whose typical width is $1.65\lambda f/\pi w$ that is comparable with the limit imposed by diffraction on the focusing of a gaussian beam by a simple lens. Moving the *CCD* camera around the focal plane of the input lens it is possible to study the evolution of the beam profile along the direction of propagation (z axis). The ring radius increases with the distance from the focal plane: this reveals the expected funnel-like propagation of the hollow laser beam. However, on distances around one millimeter the ring radius is almost constant.

The hollow beam provides a good two dimensional confinement only if the core region is extremely dark. Compared to the peak intensity, we measured a 1% of scattered light in the trap center. This value can be reduced further on by obscuring the inner region with a dark spot in the back focal plane of the input lens and by using another lens to image the ring shaped intensity distribution [6]. Another improvement to the optical system is possible using a couple of axicons [13]. A divergent and a convergent axicon with the same base angle in a telescopic mounting turn a collimated incident beam into a collimated tube of light. In this case, by varying the axicons separation it is possible to change the trapping volume.

A far detuned hollow laser beam is an efficient tool for bidimensional confinement (2D trap). The restoring force along the z axis can be obtained by adding two "plugging" laser beams (3D trap) or crossing two tubes of light around the sample of ultracold atoms. We are studying a novel scheme to confine atoms in a blue-detuned optical dipole trap that uses a single laser beam. In the experimental set up (Fig.2) a collimated laser beam crosses a converging lens, enters the axicon and comes out from a second converging lens. A similar scheme was reported by L. A. Orozco in [14]. The input lens and the axicon produce a virtual ring shaped intensity distribution which is focused by the output lens. Around the plane of image of the second lens it is possible to observe a dark region surrounded by light. If G_y is the magnification of the output lens, the ring shaped intensity distribution in the plane of image has a radius

$$R = G_y \alpha (n - 1)(d - f)$$

where d is the distance between the axicon and the first lens and f is its focal length. Using this scheme we have realized an optical trap with a diameter of $300\ \mu\text{m}$ and an axial length of 3 mm. In Fig.3 we report the intensity profile along the propagation direction of the laser beam (z axis). In the radial direction a ring shaped intensity distribution provides the required repulsive walls to trap atoms in the dark region.

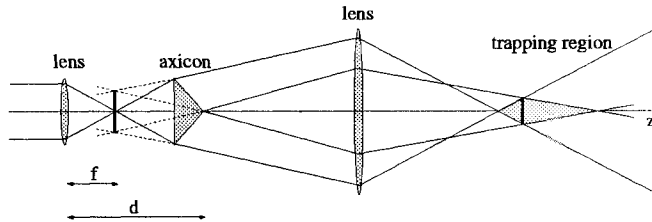


FIG. 2. Experimental set up for the generation of a single-beam blu-detuned optical trap.

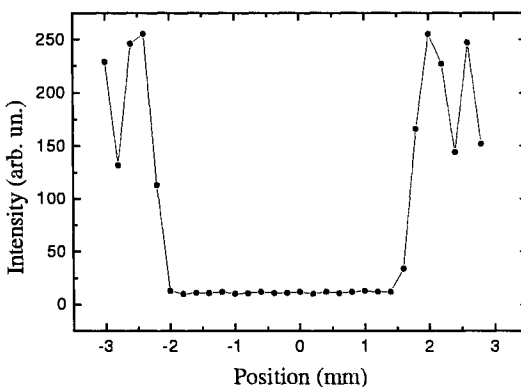


FIG. 3. Intensity profile of the single-beam blu-detuned optical trap along the axial direction (z axis).

We have developed a new scheme to realize a blue-detuned dipole trap of variable size using an axicon lens. In particular, the single-beam optical trap simplifies the alignment and the trap geometry offering new opportunities in the study of a Bose-condensed gas.

The authors acknowledge useful discussions with C. Altucci, C. De Lisio and P. Maddalena.

REFERENCES

- [1] For a review on recent experiments on Bose-Einstein condensation see, for example, G. M. Tino and M. Inguscio, *La Rivista del Nuovo Cimento*, **22**, n.4 (1999).
- [2] R. Grimm, M. Weidemüller, and Y. B. Ovchinnikov (to be published) and references therein.
- [3] N. Davidson, H. J. Lee, C. S. Adams, M. Kasevich, and S. Chu, *Phys. Rev. Lett.* **74**, 1311 (1995).
- [4] H. J. Lee, C. S. Adams, M. Kasevich, and S. Chu, *Phys. Rev. Lett.* **76**, 2658 (1996).
- [5] T. Kuga, Y. Torii, N. Shiokawa, and T. Hirano, *Phys. Rev. Lett.* **78**, 4713 (1997).
- [6] I. Manek, Y. B. Ovchinnikov, and R. Grimm, *Opt. Commun.* **147**, 67 (1998).
- [7] R. Ozeri, L. Khaykovich, and N. Davidson, *Phys. Rev. A* **59**, R1750 (1999).
- [8] R. J. Cook and R. K. Hill, *Opt. Commun.* **43**, 258 (1982).
- [9] H. Ito, K. Sakaki, W. Jhe, and M. Ohtsu, *Phys. Rev. A* **56**, 712 (1997).
- [10] Y. B. Ovchinnikov, I. Manek, and R. Grimm, *Phys. Rev. Lett.* **79**, 2225 (1997).
- [11] J. H. McLeod, *J. Opt. Soc. Am.* **44**, 592 (1954).
- [12] P. A. Bélanger and M. Rioux, *Appl. Opt.* **17**, 1080 (1978).
- [13] M. Rioux, R. Tremblay, and P. A. Bélanger, *Appl. Opt.* **17**, 1532 (1978).
- [14] L. A. Orozco, poster presented at the *XIV International Conference on Laser Spectroscopy, Innsbruck (1999)*.

PHOTON GENERATION AND SQUEEZING IN A CAVITY WITH VIBRATING WALLS

V.V. Dodonov and M.A. Andreato

Depto. de Física, Univ. Federal de São Carlos, 13565-905 São Carlos, SP, Brazil

Abstract

We discuss the squeezing properties and the photon distribution functions of the electromagnetic field modes excited from vacuum due to the non-stationary Casimir effect in an ideal one-dimensional Fabry–Perot cavity with vibrating walls, provided the frequency of vibrations is close to a multiple frequency of the fundamental unperturbed electromagnetic mode.

Many authors considered recently the phenomena related to the quantum properties of the electromagnetic fields created due to the motion of boundaries, which are known under the names *nonstationary Casimir effect* (NSCE) [1], *dynamical Casimir effect* [2], or *mirror (motion) induced radiation* [3, 4]. Here we report on a progress in studying the NSCE in a cavity with *resonantly vibrating* boundaries. It was suggested as far back as in [5] that a significant amount of photons could be created from vacuum provided the boundaries of a high-Q cavity perform small oscillations at a frequency proportional to some cavity eigenfrequency. Approximate calculations in the short- and long-time limits, performed in the frameworks of different schemes, confirmed this conjecture [6-8]. Recently, analytical solutions to the problem were found [9, 10] for a small amplitude of the wall vibrations (this limitation is quite unessential under realistic conditions). These solutions, which hold for any moment of time, enable to calculate the number of photons created from an arbitrary initial state and to take into account the effects of detuning from the strict resonance [10].

Here we apply the new solutions to calculate the effects of *squeezing* and to find the photon distribution function. Although a possibility of squeezing the electromagnetic field in a cavity with moving boundaries due to the NSCE was discussed for the first time in [5], the concrete calculations of the variances of the field quadrature components were made only in the short-time [5, 11] and long-time [12] limits. As to the photon statistics, this question was not discussed at all until now.

We confine ourselves to the special case of a 1D ideal cavity, assuming that the left boundary is fixed at the point $x = 0$ (this condition is not significant [10]), whereas the right one performs small oscillations in the (quasi)resonance regime (at $t > 0$), according to the law $L(t) = L_0(1 + \varepsilon \sin[p\omega_1(1 + \delta)t])$, with $p = 1, 2, \dots$, $\omega_1 = \pi/L_0$ (we assume $c = \hbar = 1$) and $|\varepsilon|, |\delta| \ll 1$. The field operator in the Heisenberg picture $\hat{A}(x, t)$ must satisfy the wave equation $\hat{A}_{tt} - \hat{A}_{xx} = 0$ and the boundary conditions $\hat{A}(0, t) = \hat{A}(L(t), t) = 0$. Remembering the standard decomposition of the field operator for $t < 0$ (when the wall was at rest), $\hat{A}(x, t) = \sum_{n=1}^{\infty} (2/\sqrt{n}) [\hat{b}_n \sin(n\pi x/L_0) \exp(-in\omega_1 t) + \text{h.c.}]$, $[\hat{b}_n, \hat{b}_m^\dagger] = \delta_{nm}$, we write, for

$t \geq 0$, $\hat{A}(x, t) = \sum_{n=1}^{\infty} (2/\sqrt{n}) [\hat{b}_n \psi^{(n)}(x, t) + \text{h.c.}]$, and expand each function $\psi^{(n)}(x, t)$ in a series with respect to the *instantaneous basis*

$$\psi^{(n)}(x, t) = \sqrt{L_0/L(t)} \sum_{k=1}^{\infty} [\rho_k^{(n)} e^{-ik\omega_1(1+\delta)t} - \rho_{-k}^{(n)} e^{ik\omega_1(1+\delta)t}] \sin[\pi kx/L(t)]. \quad (1)$$

Then the boundary conditions are satisfied automatically. The coefficients $\rho_k^{(n)}(t)$ obey an infinite system of coupled ordinary differential equations, which is equivalent to the wave equation. This system was solved under the resonance conditions in [10].

The nonzero coefficients $\rho_k^{(n)}$ form p independent subsets ($j = 0, 1, \dots, p-1$)

$$\begin{aligned} \rho_{j+mp}^{(j+np)}(\tau) &= - \frac{\Gamma(-m-j/p) \Gamma(1+n+j/p) \sin[\pi(m+j/p)]}{\pi \Gamma(1+n-m)} \\ &\times (\sigma\kappa)^{n-m} \lambda^{m+n+2j/p} F(n+j/p, -m-j/p; 1+n-m; \kappa^2) \end{aligned} \quad (2)$$

where $F(a, b; c; z)$ is the Gauss hypergeometric function, $\sigma \equiv (-1)^p$, $\tau = \frac{1}{2}\varepsilon\omega_1 t$, and

$$\kappa = \frac{\sinh(ap\tau)}{\sqrt{a^2 + \sinh^2(ap\tau)}}, \quad a = \sqrt{1-\gamma^2}, \quad \lambda = \sqrt{1-\gamma^2\kappa^2 + i\gamma\kappa}, \quad \gamma = \delta/\varepsilon.$$

If the wall comes back to its initial position L_0 after some time T , the coefficients $\rho_{\pm k}^{(n)}$ become time independent at $t > T$, but the initial operators \hat{b}_n and \hat{b}_n^\dagger cease to be ‘physical’, due to the contribution of the terms $\rho_{-k}^{(n)} \exp(ik\omega_1 t)$ with ‘incorrect signs’ in the exponentials. The ‘physical’ annihilation operator \hat{a}_m , which can be introduced according to the ‘standard decomposition’ $\hat{A} = \sum_{m=1}^{\infty} (2/\sqrt{m}) \sin(\pi mx/L_0) [\hat{a}_m e^{-im\omega_1(t+\delta T)} + \text{h.c.}]$ at $t \geq T$, is related to the operators \hat{b}_n and \hat{b}_n^\dagger by means of the Bogoliubov transformation $\hat{a}_m = \sum_{n=1}^{\infty} \sqrt{m/n} [\hat{b}_n \rho_m^{(n)}(\tau_T) - \hat{b}_n^\dagger \rho_{-m}^{(n)*}(\tau_T)]$.

The quadrature operators and their (co)variances are defined as (hereafter $\omega_1 \equiv 1$) $\hat{q}_m = (\hat{a}_m + \hat{a}_m^\dagger)/\sqrt{2}$, $\hat{p}_m = (\hat{a}_m - \hat{a}_m^\dagger)/(i\sqrt{2})$, $U_m = \langle \hat{q}_m^2 \rangle - \langle \hat{q}_m \rangle^2$, $V_m = \langle \hat{p}_m^2 \rangle - \langle \hat{p}_m \rangle^2$, $Y_m = \frac{1}{2} \langle \hat{p}_m \hat{q}_m + \hat{q}_m \hat{p}_m \rangle - \langle \hat{p}_m \rangle \langle \hat{q}_m \rangle$. For the vacuum initial state, $\hat{b}_n |0\rangle = 0$, we have

$$\left. \begin{aligned} U_m \\ V_m \end{aligned} \right\} = \frac{m}{2} \sum_{n=1}^{\infty} \frac{1}{n} \left| \rho_m^{(n)}(\tau_T) \mp \rho_{-m}^{(n)}(\tau_T) \right|^2, \quad Y_m = \sum_{n=1}^{\infty} \frac{m}{n} \text{Im} \left[\rho_m^{(n)*}(\tau_T) \rho_{-m}^{(n)}(\tau_T) \right]. \quad (3)$$

Calculating the derivatives of the variances with respect to the ‘slow final time’ $\tau_T \equiv \tau$, we find $dU_m/d\tau = dV_m/d\tau = 2\sigma m \text{Re}(\rho_m^{(j)} \rho_{-m}^{(p-j)})$, $dY_m/d\tau = 0$, for all numbers m , excepting the ‘principal’ modes with the numbers $m = \mu \equiv p(k+1/2)$, $k = 0, 1, 2, \dots$ (provided p is even). There is no squeezing in the ‘nonprincipal’ modes, since $Y_m = 0$, and the quadrature variances $U_m = V_m = \mathcal{N}_m + 1/2$ (where \mathcal{N}_m is the mean photon number) monotonously increase in time for $\gamma \leq 1$, with asymptotical linear dependence $d\mathcal{N}_{j+pq}/d\tau \approx 2ap^2 \sin^2(\pi j/p) / [\pi^2(j+pq)]$ at $ap\tau \gg 1$. If $\gamma > 1$, then $-1/\gamma \leq \kappa \leq 1/\gamma$, and the variances oscillate in time with amplitudes inversely proportional to $\gamma^2 - 1$, being always greater than (or equal to) $1/2$.

Squeezing can be achieved only in the ‘principal’ μ -modes, for which we have

$$\left. \begin{aligned} dU_\mu/d\tau \\ dV_\mu/d\tau \end{aligned} \right\} = \mp \mu \text{Re} \left(\left[\rho_\mu^{(p/2)} \mp \rho_{-\mu}^{(p/2)} \right]^2 \right), \quad dY_\mu/d\tau = \mu \text{Im} \left(\left[\rho_\mu^{(p/2)*} \right]^2 + \left[\rho_{-\mu}^{(p/2)} \right]^2 \right). \quad (4)$$

In the resonance case $\gamma = 0$, all the coefficients $\rho_m^{(n)}$ are real, so $dU_\mu/d\tau \leq 0$ and $Y_\mu = 0$.

In the important special case $p = 2$ we have simple expressions at $\tau \rightarrow 0$ and $\tau \rightarrow \infty$:

$$\left. \begin{array}{l} U_{2m+1} \\ V_{2m+1} \\ Y_{2m+1} \end{array} \right|_{\tau \rightarrow 0} = \begin{array}{l} 1/2 - a_m \tau^{2m+1} [1 - b_m \tau + \dots] \\ 1/2 + a_m \tau^{2m+1} [1 + b_m \tau + \dots] \\ -2(2m+1)\gamma a_m \tau^{2(m+1)} + \dots \end{array}, \quad \begin{array}{l} a_m = [(2m-1)!!/m!]^2, \quad a_0 = 1 \\ b_m = (2m+1)/(m+1)^2 \end{array}$$

$$\left. \begin{array}{l} U_{2m+1} \\ V_{2m+1} \\ Y_{2m+1} \end{array} \right|_{\tau \rightarrow \infty} \approx \frac{8a\tau}{\pi^2(2m+1)} \times \begin{cases} 2 \sin^2 [(m+1/2)\phi] \\ 2 \cos^2 [(m+1/2)\phi] \\ -\sin[(2m+1)\phi] \end{cases}, \quad \phi = \arcsin \gamma, \quad \gamma < 1$$

If $\gamma \neq 0$, then $Y_m \neq 0$, so the field goes to the *correlated* state [13]. In this case the variances U_m, V_m, Y_m rapidly oscillate with the frequency $2\omega_m$, therefore it is better to characterize the squeezing properties by means of the *minimal* and *maximal* variances [14]

$$\left. \begin{array}{l} u_m \\ v_m \end{array} \right\} = \frac{1}{2} \left[U_m + V_m \mp \sqrt{(U_m - V_m)^2 + 4Y_m^2} \right]. \quad (5)$$

In the special case $p = 2$ and $\mu = 1$ the coefficients $\rho_{\pm 1}^{(1)}$ can be written in terms of the complete elliptic integrals [10], $\rho_1^{(1)} = 2\lambda(\kappa)\mathbf{E}(\kappa)/\pi$, $\rho_{-1}^{(1)} = 2[\tilde{\kappa}^2\mathbf{K}(\kappa) - \mathbf{E}(\kappa)]/(\pi\kappa)$, where $\tilde{\kappa} \equiv \sqrt{1 - \kappa^2}$, and equations (4) can be integrated exactly [15]:

$$\left. \begin{array}{l} U_1 \\ V_1 \end{array} \right\} = \frac{2}{\pi^2\kappa} \left[2(\kappa \mp \beta)\mathbf{K}(\kappa)\mathbf{E}(\kappa) \pm \tilde{\kappa}^2(\beta \mp \kappa)\mathbf{K}^2(\kappa) \pm \beta\mathbf{E}^2(\kappa) \right], \quad (6)$$

$$Y_1 = \frac{2\gamma}{\pi^2} \left[\mathbf{E}^2(\kappa) - 2\mathbf{K}(\kappa)\mathbf{E}(\kappa) + \tilde{\kappa}^2\mathbf{K}^2(\kappa) \right], \quad (7)$$

where $\beta \equiv \text{Re}\lambda = \sqrt{1 - \gamma^2\kappa^2}$. Then the minimal and maximal variances (5) read

$$\left. \begin{array}{l} u_1 \\ v_1 \end{array} \right\} = \frac{2}{\pi^2\kappa} \left[2(\kappa \mp 1)\mathbf{K}(\kappa)\mathbf{E}(\kappa) \pm \tilde{\kappa}^2(1 \mp \kappa)\mathbf{K}^2(\kappa) \pm \mathbf{E}^2(\kappa) \right]. \quad (8)$$

Asymptotically the minimal variance tends to the unique limit $u_1(\infty) = 2/\pi^2$ for any $\gamma \leq 1$ (only the rate of the evolution depends on γ). Moreover, this asymptotical value does not depend on the initial (nonvacuum) state of the field, provided the initial density matrix was diagonal in the Fock basis (in particular, for the thermal of Fock states) [15].

The field appears in a mixed quantum state, and $\text{Tr}\hat{\rho}_m^2 = [4(U_m V_m - Y_m^2)]^{-1/2} \rightarrow 0$ as $\kappa \rightarrow 1$ (where $\hat{\rho}_m$ is the statistical operator of the m th mode), due to strong intermode interactions caused by the Doppler effect. The total energy $\mathcal{E}(\tau) \equiv \sum_m m\mathcal{N}_m(\tau)$ (normalized by $\hbar\omega_1$) of the initially vacuum state equals [10] $\mathcal{E}^{(vac)}(\tau) = (p^2 - 1)\sinh^2(pa\tau)/(12a^2)$.

The knowledge of the quadrature variances enables to find the photon distribution in each mode, provided initially the field was in a multimode Gaussian state (which include, as special cases, vacuum, coherent, squeezed, and thermal states). Indeed, it was shown in [7, 16] that the field evolution can be described in the framework of the Schrödinger picture, with a *quadratic* multidimensional time-dependent Hamiltonian. But it is known [17] that

the evolution governed by quadratic Hamiltonians transform any Gaussian state to another Gaussian state. And it is also known that the Gaussian state is determined completely by the average values of quadratures and its variances. Using the general formula for the photon distribution function $f_m(n) \equiv \langle n | \hat{\rho}_m | n \rangle$ derived in [18], we get, in the special case of the initial vacuum state and the exact resonance, the expression

$$f_m(n) = 2 \frac{[(2U_m - 1)(2V_m - 1)]^{n/2}}{[(2U_m + 1)(2V_m + 1)]^{(n+1)/2}} P_n \left(\frac{4U_m V_m - 1}{\sqrt{(4U_m^2 - 1)(4V_m^2 - 1)}} \right), \quad (9)$$

where $P_n(x)$ is the Legendre polynomial. In ‘non-principal’ modes we have the Planck distributions $f_m(n) = [2V_m(\tau) - 1]^n / [2V_m(\tau) + 1]^{n+1}$. For the ‘principal’ μ - modes, one can simplify (9) for $n \gg 1$ and $V_\mu(\tau) \gg 1$: $f_\mu(n) \approx (\pi n V_\mu)^{-1/2} [(2V_\mu - 1) / (2V_\mu + 1)]^n$. The Mandel parameter $Q \equiv \sigma_n / \bar{n} - 1$ is positive for all values of τ and m , so the statistics is super-Poissonian. For the other recent results on NSCE see [19-23] and references therein.

Acknowledgment: VVD thanks the Brazilian agency FAPESP for the travel grant 1999/1098-5. MAA thanks Brazilian agency CNPq for the support (project 110524/97-7).

References

- [1] V.V. Dodonov, A.B. Klimov and V.I. Man’ko, Phys. Lett. A **142**, 511 (1989).
- [2] J. Schwinger, Proc. Natl. Acad. Sci. USA **90**, 958, 2105, 4505, 7285 (1993).
- [3] G. Barton and C. Eberlein, Ann. Phys. (NY) **227**, 222 (1993).
- [4] A. Lambrecht, M.-T. Jaekel and S. Reynaud, Phys. Rev. Lett. **77**, 615 (1996).
- [5] V.V. Dodonov, A.B. Klimov and V.I. Man’ko, Phys. Lett. A **149**, 225 (1990).
- [6] V.V. Dodonov, A.B. Klimov and D.E. Nikonov, J. Math. Phys. **34**, 2742 (1993).
- [7] C.K. Law, Phys. Rev. A **49**, 433 (1994); **51**, 2537 (1995).
- [8] C.K. Cole and W.C. Schieve, Phys. Rev. A **52**, 4405 (1995).
- [9] V.V. Dodonov and A.B. Klimov, Phys. Rev. A **53**, 2664 (1996).
- [10] V.V. Dodonov, J. Phys. A **31**, 9835 (1998).
- [11] A.V. Chizhov, G. Schrade and M.S. Zubairy, Phys. Lett. A **230**, 269 (1997).
- [12] V.V. Dodonov and A.B. Klimov, Phys. Lett. A **167**, 309 (1992).
- [13] V.V. Dodonov, E.V. Kurmyshev and V.I. Man’ko, Phys. Lett. A **79**, 150 (1980).
- [14] V.V. Dodonov, V.I. Man’ko and P.G. Polynkin, Phys. Lett. A **188**, 232 (1994).
- [15] V.V. Dodonov and M.A. Andreatta, J. Phys. A (to be published).
- [16] R. Schützhold, G. Plunien and G. Soff, Phys. Rev. A **57**, 2311 (1998).
- [17] V.V. Dodonov and V.I. Man’ko, in *Invariants and the Evolution of Nonstationary Quantum Systems*, edited by M. A. Markov, Proceedings of Lebedev Physics Institute, Vol. **183** (Nova Science, Commack, 1989), p. 263.
- [18] V.V. Dodonov, O.V. Man’ko and V.I. Man’ko, Phys. Rev. A **49**, 2993 (1994).
- [19] V.V. Dodonov, Phys. Lett. A **244**, 517 (1998); Phys. Rev. A **58**, 4147 (1998).
- [20] J.P.F. Mendonça, P.A. Maia Neto and F.I. Takakura, Opt. Comm. **160**, 335 (1999).
- [21] F. Miri and R. Golestanian, Phys. Rev. A **59**, 2291 (1999).
- [22] Y. Wu, M.-C. Chu and P.T. Leung, Phys. Rev. A **59**, 3032 (1999).
- [23] D.A.R. Dalvit and F.D. Mazzitelli, Phys. Rev. A **59**, 3049 (1999).

ON SOME JAYNES-CUMMINGS HAMILTONIAN SUPERSYMMETRIC FEATURES

C. GERON¹

Theoretical and Mathematical Physics,
Institute of Physics (B.5),
University of Liège,
B-4000 LIEGE 1 (Belgium)

Abstract

The degeneracies of the Jaynes-Cummings Hamiltonian are studied by underscoring operators explaining the non-degeneracy or the degeneracy of some eigenstates. These operators are supercharges and we thus display the supersymmetry underlying the Jaynes-Cummings model. Two extensions of the Hamiltonian are also considered.

1 Introduction

The Jaynes-Cummings Hamiltonian (H_{JC}) [1] is associated with a model describing the interaction between a spin- $\frac{1}{2}$ particle and a one-mode magnetic field having an oscillating component along one axis and a constant component along another axis [2]. This model, extensively used in quantum optics [3] is one of the simplest examples of quantum systems combining bosons and fermions, a typical feature of supersymmetry [4].

This model has been widely studied (see for example Ref.[2], [5], [6], [7]). Some supersymmetric characteristics of H_{JC} have also already been pointed out [7]. We propose here another approach of some H_{JC} supersymmetric features [8].

So we underscore the energy spectrum and the eigenstates of H_{JC} (Section 2). These states are degenerated only for one value of energy. We explain this fact through supersymmetry or more precisely through the existence of supercharges which explain the non-degeneracy or the degeneracy of some eigenstates (Section 3). We also reconsider two generalizations [6] of H_{JC} to show the unicity of their supercharges (Section 4).

Our units are taken with the constant \hbar equal to unity.

2 Energy spectrum and eigenstates of H_{JC}

The Jaynes-Cummings model can be described by the Hamiltonian [1]

$$H_{JC} = \omega(a^\dagger a + \frac{1}{2}) + \frac{\omega_0}{2}\sigma_3 + g(a^\dagger\sigma_- + a\sigma_+), \quad (2.1)$$

¹E-mail: Christine.Geron@ulg.ac.be

where a^\dagger and a are respectively the creation and annihilation operators of the bosonic harmonic oscillator and where $\sigma_\pm = \sigma_1 \pm \sigma_2$, σ_3 refer to the Pauli matrices.

If we note Δ the difference between the two angular frequencies ω and ω_0 , we can summarize the eigenstates and the energy spectrum of H_{JC} in the basis of the vectors

$$\begin{pmatrix} 0 \\ |n\rangle \end{pmatrix} = |n, -\rangle \quad \text{and} \quad \begin{pmatrix} |n\rangle \\ 0 \end{pmatrix} = |n, +\rangle$$

as follows [8] :

a) for all the values of g , we have to distinguish two cases

(i) either $E = \frac{\Delta}{2}$ and the corresponding eigenstate is

$$|E_0\rangle = |0, -\rangle; \quad (2.2)$$

(ii) or $E = \omega k \pm \frac{\Delta}{2} r(k)$, $k \in \mathbb{N}_o$, and the corresponding eigenstates are

$$|E_k^+\rangle = \frac{1}{R(k)} (g\sqrt{k} |k-1, +\rangle + \frac{\Delta}{2} (r(k)+1) |k, -\rangle), \quad (2.3)$$

$$|E_k^-\rangle = \frac{1}{R(k)} (\frac{\Delta}{2} (r(k)+1) |k-1, +\rangle - g\sqrt{k} |k, -\rangle), \quad (2.4)$$

where

$$r(k) = (1 + \frac{4g^2k}{\Delta^2})^{\frac{1}{2}} \quad (2.5)$$

and

$$R(k) = (\frac{\Delta^2}{2} r(k)(1+r(k)))^{\frac{1}{2}}; \quad (2.6)$$

b) if there exists $k \in \mathbb{N}_o$ such as $\frac{\Delta}{2} = \omega k + \frac{\Delta}{2} r(k)$, Δ has to be negative and g has to take the values

$$g = \pm \sqrt{\omega(\omega k - \Delta)}. \quad (2.7)$$

Then the corresponding eigenstates are

$$|E_k^\mp\rangle = \sqrt{\frac{\omega k}{2\omega k - \Delta}} (|k-1, +\rangle \mp \sqrt{\frac{\omega k - \Delta}{\omega k}} |k, -\rangle) \quad (2.8)$$

with respect to the signs of g in (2.7).

c) if there exists $k \in \mathbb{N}_o$ such as $\frac{\Delta}{2} = \omega k - \frac{\Delta}{2} r(k)$, Δ has to be positive and, also here, g has to take the values

$$g = \pm \sqrt{\omega(\omega k - \Delta)}.$$

Then the corresponding eigenstates are also (2.8).

In the particular case where $\Delta = 0$ and $g = 0$, the results are, as expected, those of the supersymmetric harmonic oscillator [4].

3 Explanation of the degeneracy

The non-degeneracy of the $H_{JC} + c$ -eigenstates in the general case, when $\Delta = 0$, c being a positive constant ensuring the positive nature of the energies, can be explained through the existence of a supercharge

$$Q = \sqrt{\omega}a\sigma_+ + \sqrt{\omega}a^\dagger\sigma_- + \frac{1}{2}\frac{g}{\sqrt{\omega}}I, \quad (3.1)$$

which is unique because of the presence of the generators of the Clifford algebra Cl_2 .

The degeneracy of the eigenstates corresponding to $E = c$ is due to the existence [8] of two operators P and P^\dagger connecting these degenerated eigenstates and satisfying the typical relations of the supersymmetric quantum mechanics characterizing the Lie superalgebra $\text{sqm}(2)$, but only on the space generated by the degenerated eigenstates. On the whole Fockspace, the relations of $\text{sqm}(2)$ are not ascertained.

Because the two operators connecting degenerated eigenstates only act on the above-mentioned space of these eigenstates, the unicity of $Q = (3.1)$ is not in the balance again.

4 Two generalizations of H_{JC} in the case $\Delta = 0$

In the first generalization, the Hamiltonian $H + c$ resulting from the superposition of a second Hamiltonian H_2 [6]

$$H_2 = \omega(a^\dagger a + \frac{1}{2} + \frac{1}{2}\sigma_3) + ig(a^\dagger\sigma_- - a\sigma_+) \quad (4.1)$$

with H_{JC} , has a supercharge given by

$$Q = \sqrt{\omega}a\xi_+ + \sqrt{\omega}a^\dagger\xi_- + \frac{g}{2\sqrt{\omega}}\eta \quad (4.2)$$

where

$$\xi_+ = \begin{pmatrix} 0 & 0 & 0 & -i \\ 0 & 0 & 0 & 0 \\ 0 & 1 & 0 & 0 \\ 0 & 0 & 0 & 0 \end{pmatrix}, \quad \xi_- = \begin{pmatrix} 0 & 0 & 0 & 0 \\ 0 & 0 & 1 & 0 \\ 0 & 0 & 0 & 0 \\ i & 0 & 0 & 0 \end{pmatrix}, \quad \eta = \begin{pmatrix} 0 & 0 & 1 & 0 \\ 0 & 0 & 0 & -i \\ 1 & 0 & 0 & 0 \\ 0 & i & 0 & 0 \end{pmatrix}. \quad (4.3)$$

These matrices (4.3) are three generators of the Lie superalgebra $\text{osp}(2/2)$ [8] whose representation with 4 by 4 matrices is unique up to a unitary transformation [9]. Therefore $Q = (4.2)$ is the only supercharge of $H + c$.

In the second extension, obtained by adding a positive constant Δ' to $H + c$, we can prove [8] that the Hamiltonian has also only one supercharge given by

$$Q^{\Delta'} = Q + \sqrt{\Delta'}R \quad (4.4)$$

where $Q = (4.2)$ and

$$R = \begin{pmatrix} 0 & 0 & i & 0 \\ 0 & 0 & 0 & 1 \\ -i & 0 & 0 & 0 \\ 0 & 1 & 0 & 0 \end{pmatrix}. \quad (4.5)$$

Acknowledgements

I am extremely grateful to Dr. N. DEBERGH for very useful and fruitful discussions. I would also like to thank Prof. A.I. SOLOMON for interesting discussions and for bringing Ref. [7] to my attention.

References

- [1] JAYNES E.T. and CUMMINGS F.W., Proc.IEEE 51, 89 (1963).
- [2] BERUBE-LAUZIERE Y., HUSSIN V. and NIETO L.M., Phys.Rev.A50, 1725 (1994).
- [3] NAROZHNY N.B., SANCHEZ-MONDRAGON J.J. and EBERLY J.H., Phys.Rev.A23, 236 (1981).
- [4] WITTEN E., Nucl.Phys.B188, 513 (1981).
RAVNDAL F. : in Proceedings of the 1984 CERN School of Physics, LOFTHUS, Norway, CERN 85-11, Genève, p.300 (1985).
- [5] KOCHETOV E.A., J.Phys.A25, 411 (1992).
- [6] ANDREEV V.A. and LERNER P.B., Phys.Lett.A134, 507 (1989).
- [7] BUZANO C., RASETTI M.G. and RASTELLO M.L., Phys.Rev.Lett.62, 137 (1989).
SOLOMON A.I. and DASKALOYANNIS C., "Jaynes-Cummings Variants" in Proceedings of the Third International Workshop on Symmetry Methods in Physics, DUBNA, Russia (1995).
- [8] GERON C., "On the Jaynes-Cummings Hamiltonian supersymmetric characteristics" to be published in Bulletin de la Société Royale des Sciences de Liège (1999).
- [9] CORNWELL J.F. : Group Theory in Physics, vol III, Academic Press, N.Y. (1989).

Probing colored noise of a cavity on strongly driven two-level atoms

Salomon S. Mizrahi¹ * G.A. Prata², V.V. Dodonov¹ and J.R. Brinati³

¹*Departamento de Física, CCET, Universidade Federal de São Carlos, CP 676, São Carlos, 13565-905, SP, Brasil.*

²*Optical Sciences Centre, University of Arizona, Tucson-AZ-85721, USA*

³*Instituto de Física, Universidade Federal do Rio de Janeiro, 21945-970, Rio de Janeiro, RJ, Brasil.*

Abstract

The effects of a colored-noise reservoir on the index of refraction of a strongly driven two-level atoms system (gas), probed by a weak field, are analyzed. For high Rabi frequencies, Ω , a simple analytic expression results for the susceptibility function (with respect to the probe) when $\nu \approx \Omega$, where ν is the detuning between driving and probe fields frequencies. Several features are revealed in that function when compared to the one resulting from a reservoir with a white-noise spectrum.

1. Introduction In many quantum systems interacting with an environment the evolution of the density operator can be described in the framework of a master equation

$$id\rho(t)/dt = [H, \rho(t)] + \int_0^t K(t-t')\rho(t')dt', \quad (1)$$

where H is the Hamiltonian of reservoir, system and its interaction with external fields; $K(t-t')$ is a superoperator embodying the interaction of the system with reservoir, whose ‘width’ is called *memory time*. Although any real evolution is, strictly speaking, non-Markovian, the corrections due to a finite memory time are in many cases very small [1]. In other cases a nonzero memory time, or a frequency-dependent **colored noise spectrum**, leads to significant changes in the dynamical properties of the system: Atoms inside a high-Q EM cavity [2]. In particular, when an atom in a cavity is strongly driven by an external radiation (the pump) the phenomenon of dynamical suppression of spontaneous emission occurs [3]. Also, it was shown that if an atom is strongly pumped at a frequency nearby a two-level transition frequency and is probed by a weak field (probe), then depending on the functional form of the cavity-reservoir spectrum, the absorption spectrum changes significantly, compared to the Markovian approximation [4]. Yet as another instance, for

*E-mail: salomon@power.ufscar.br

a low density atomic gas confined into a cell or a cavity, when the coupling between the atoms and the cell modes prevails over the vacuum-atom coupling, the absorption lineshape function changes from one to two-bump shape beyond some critical temperature [5]. More recently it was verified [6] that “memory” effects on the atomic absorption lineshape function are significantly enhanced when the atoms are strongly driven and that colored noise leaves a signature which is characterized by a linear increasing, as function of Rabi frequency, of the heights of the peaks of the absorption lineshape function. Analyzing the dependence of the atomic susceptibility function χ' on the Rabi frequency Ω and the detuning between probe and pump fields ν one could infer about the nature of the coupling between atom and cavity (cell) colored noise. For high values of Ω and $\Omega \approx \nu$, the measurement of the modified atomic decay rate and the dynamic frequency shift for several values of Ω and ν could permit determining the frequency spectrum of the cell-reservoir.

2. Stationary solution to the master equation The density matrix of a two-level atom is

$$\rho = W_1|1\rangle\langle 1| + W_2|2\rangle\langle 2| + W_3|1\rangle\langle 2| + W_4|2\rangle\langle 1|. \quad (2)$$

For the rotating wave coupling between the atomic variables and the external (pump and probe) fields, the Hamiltonian reads $H = \frac{1}{2}\omega_0\sigma_0 + (F_1e^{-i\omega_1t}\sigma_+ + F_2e^{-i\omega_2t}\sigma_+ + h.c.)$ where ω_0 is the atomic transition frequency, F_1 (F_2) and ω_1 (ω_2) are the coupling constant and frequency of the driving (probe) field and we consider $|F_1| \gg |F_2|$. The coupling constants can be expressed in terms of the vector dipole matrix element between the excited and ground atomic states $\vec{\mu}_{12}$ and the electric field strengths \vec{E}_i as $F_i = -\vec{\mu}_{12} \cdot \vec{E}_i$, $i = 1, 2$.

The reservoir is assumed being made of an infinite number of oscillator modes interacting resonantly with the driven two-level atom, the superoperator kernel $K(t-t')$ is written as [6] $K(t-t') \cdot = \text{Tr}_R [V_{SR}, e^{-iL_0(t-t')} [V_{SR}, \rho_R \cdot]]$ where $L_0 \cdot \equiv [H_0, \cdot]$ is the Liouvillian operator, H_0 is the free (atom plus reservoir) hamiltonian, $V_{SR} = \int \sqrt{g(\omega - \omega_0)}(b_\omega^\dagger \sigma_- + h.c.)d\omega$ is the atom-reservoir resonant interaction term, the function $g(\omega - \omega_0) = D(\omega - \omega_0)|\kappa(\omega - \omega_0)|^2$ combines the reservoir spectrum $D(\omega - \omega_0)$ and the coupling constant $\kappa(\omega - \omega_0)$ that may be frequency dependent, and ρ_R is the density operator of the reservoir at thermal equilibrium.

The solution to (1) with the above Hamiltonian can be written as $\rho(t) = \rho_0(t) + \Delta\rho(t)$, where $\Delta\rho(t)$ is a small correction term to the density matrix $\rho_0(t)$ of the driven atom due to the weak probe field, thus the functions $W_i(t)$, $i = 1, 2, 3, 4$, at the stationary regime read

$$W_1(t) = W_1^\infty + \Delta W_1(t), \quad W_2(t) = W_2^\infty - \Delta W_1(t), \quad W_3(t) = \overline{W_3}^\infty e^{-i\omega_1 t} + \Delta W_3(t), \quad (3)$$

and $W_4(t) = W_3^*(t)$, W_1^∞ (W_2^∞) is the unperturbed (by the probe) population of the upper (lower) atomic level, $\overline{W_3}^\infty$ its c.c. are the coherence coefficients; the terms with the prefix Δ correspond to the corrections due to the probe. Taking into account the first Floquet harmonics, we can write [7],

$$\Delta W_1(t) = \delta W_1 + \eta e^{-i\nu t} + \eta^* e^{i\nu t}, \quad \Delta W_3(t) = e^{-i\omega_1 t} (\delta W_0 + \delta W_+ e^{-i\nu t} + \delta W_-^* e^{i\nu t}), \quad (4)$$

where $\nu = \omega_2 - \omega_1$ is the detuning of the probe from the driving field frequency. Inserting (2), (3)-(4) into (1) leads to a set of algebraic equations that are solved for the reservoir at 0K and $\omega_1 = \omega_0$ (resonance condition), thus we determine the coefficients δW_1 , η , δW_0 , δW_+ and δW_- .

3. The atomic susceptibility function The susceptibility function with respect to the probe field for N atoms per unit volume is [6],

$$\chi(\nu, \Omega) = -\frac{N}{3} |\vec{\mu}_{12}|^2 \delta W_+ / F_2 = -\frac{N \lambda_0^3}{32\pi^3} \delta \tilde{W}_+(\nu, \Omega), \quad (5)$$

where $\lambda_0 = 2\pi c / \omega_0$ is the wavelength of the atomic transition, and $\delta \tilde{W}_+(\nu, \Omega) \equiv \hbar \gamma \delta W_+(\nu, \Omega) / F_2$ is the dimensionless coherence function (it does not depend on the probe field and its modulus is less or of the order of the unity), which depends on two frequencies: the detuning between the pump and probe frequencies ν and the Rabi frequency $\Omega = 2|F_1|$. The square of the matrix dipole element $|\vec{\mu}_{12}|^2$ is replaced by the natural (vacuum) atomic decay constant $\gamma = (4\omega_0^3 |\vec{\mu}_{12}|^2) / (3\hbar c^3)$, and

$$\delta \tilde{W}_+(\nu, \Omega) = \frac{i(W_2^\infty - W_1^\infty) \left[\Omega^2 \left(1 - \frac{Z^*(-\nu)}{Z^*(0)} \right) - 2Q(\nu)Z^*(-\nu) \right]}{\Omega^2 [Z(\nu) + Z^*(-\nu)] - 2Q(\nu)Z(\nu)Z^*(-\nu)}, \quad (6)$$

with $W_2^\infty - W_1^\infty = 2\Gamma^2(0) / (2\Gamma^2(0) + \Omega^2)$. $Z(x) \equiv ix - \Gamma(x)$, $Q(x) = -Z(x) + \Gamma^*(x)$, and

$$\Gamma(x) = \int_0^\infty \frac{ig(\omega - \omega_0)}{x + \omega_0 - \omega + i\epsilon} d\omega \approx \pi g(x) - i\mathcal{P} \int_{-\infty}^\infty \frac{g(\omega)}{\omega - x} d\omega, \quad (7)$$

$g(\omega - \omega_0)$ is nearly an even function of its argument, the approximation is quite reasonable since the atom and reservoir exchange energy resonantly. Hereafter we express all the quantities having the dimension of frequency (like $\Gamma(x)$, ν , Ω) in units of γ . Expression (6) can be simplified in the case of a strong pumping field, $\Omega \gg 1$, the real part of (6) attains its larger value at $\nu = \nu_m$, slightly shifted from the Rabi frequency,

$$\nu_m = \Omega + \frac{3}{2} \Gamma_I(\Omega) + O\left(\frac{1}{\Omega}\right). \quad (8)$$

The subscripts (R, I) stand for real and imaginary parts. For the frequencies close to ν_m , the real part of the susceptibility function changes its behavior when compared to the usual situation of a two-level atom probed without pumping, namely, the real part acquires the Lorentzian shape:

$$\text{Re} \delta \tilde{W}_+(\nu, \Omega) = \left\{ 12\Omega \Gamma(0) \Gamma_R(\Omega) \left[1 + \frac{4(\nu - \nu_m)^2}{9\Gamma_R^2(\Omega)} \right] \right\}^{-1}. \quad (9)$$

By varying Ω it should be possible to determine experimentally the real part of the function $\Gamma(\Omega)$ since the width of the Lorentzian shape is $\Delta\nu = 3\Gamma_R(\Omega)$. The shift of ν_m from Ω , $3\Gamma_I(\Omega)/2$, could also be determined. Thus, varying Ω it should be possible to determine the complex function $\Gamma(\Omega)$.

To illustrate the above general results, suppose an effective spectral function $g(\omega - \omega_0) = g_0 + g_c [1 + \tau^2(\omega - \omega_0)^2]^{-1}$. The first term, g_0 , is the coupling constant between atom and the vacuum white noise, the second is for the cavity modes when a Lorentzian shape is assumed. τ is a correlation time and g_c (that can be positive or negative) is an effective coupling constant of the atom with the cavity modes. For $\tau = 0$ one gets the

vacuum+cavity white noise. Then, with $\Gamma(x) = \frac{1}{2} \left[\gamma + \gamma_c \frac{1+ix\tau}{1+(x\tau)^2} \right]$, $\gamma_c = 2\pi g_c$, the point of maximum of $\text{Re}\delta\tilde{W}_+(\nu, \Omega)$ is

$$\nu_m = \Omega + \frac{3\gamma_c\tau\Omega}{4(1 + \tau^2\Omega^2)} + O\left(\frac{1}{\Omega}\right), \quad (10)$$

thus due to the colored noise the shift $|\nu_m - \Omega|$ attains its largest value, $3|\gamma_c|/8$, at $\tau\Omega = 1$; so, by varying Ω until the shift attaining its larger value, it should be possible to determine experimentally γ_c and τ . Disregarding terms $O(1/\Omega)$ in (10) $\nu_m - \Omega > 0$ ($\nu_m - \Omega < 0$) means a positive (negative) γ_c . The width of the line is

$$\Delta\nu = \frac{3}{2} \left[\gamma + \gamma_c (1 + \tau^2\Omega^2)^{-1} \right], \quad (11)$$

and it tells that γ_c can assume values only in the open interval $(-\gamma, \infty)$, thus two different situations may happen for an atom in a cavity ($\gamma_c \neq 0$): **i)** For $\gamma_c < 0$ the linewidth $\Delta\nu$ is always narrower than natural linewidth ($3\gamma/2$) and it becomes broader with increasing Ω although $\Delta\nu < 3\gamma/2$. **ii)** For $\gamma_c > 0$ the linewidth is always broader than $3\gamma/2$ and it becomes narrower with increasing Ω .

In sum, the modified lineshape differs from the one in free space ($\gamma_c = 0$) in **three aspects** for a finite τ and $\gamma_c < 0$ ($\gamma_c > 0$):

- a) a shift of the point of maximum to the left (right) of $\nu = \Omega$,
- b) a narrowing (broadening) of the width $\Delta\nu$ (although it is wider the larger is Ω),
- c) a decrease (increase) in the height of the curve.

These effects worth be verified experimentally and an experimental setup is reported in [8].

Acknowledgments. SSM, VVD and GAP thank FAPESP for financial support

References

1. K. Wódkiewicz and J.H. Eberly, *Ann. Phys. (N.Y.)* **101**, 574 (1976).
2. T.W. Mossberg and M. Lewenstein, in *Cavity Quantum Electrodynamics* (Advances in Atomic, Molecular and Optical Physics, Supplement 2), ed. P.R. Berman (Academic, New York, 1994), p. 171.
3. M. Lewenstein, T.W. Mossberg and R.J. Glauber, *Phys. Rev. Lett.* **59**, 775 (1987); M. Lewenstein and T.W. Mossberg, *Phys. Rev. A* **37**, 2048 (1988); M. Lewenstein, J. Zakrzewski and T.W. Mossberg, *Phys. Rev. A* **38**, 808 (1988); Y. Zhu, A. Lezama, T.W. Mossberg and M. Lewenstein, *Phys. Rev. Lett.* **61**, 1946 (1988).
4. An.V. Vinogradov, *Opt. Spektrosk.* **67**, 12 (1989) [*Opt. Spectrosc. (USSR)* **67**, 6 (1989)]; O. Kocharovskaya and Y.V. Radeonychev, *Quantum Semiclass. Opt.* **8**, 7 (1996).
5. J.R. Brinati, S.S. Mizrahi and G.A. Prataviaera, *Phys. Rev. A* **50**, 3304 (1994); *Phys. Rev. A* **52**, 2804 (1995).
6. J.R. Brinati, S.S. Mizrahi and G.A. Prataviaera, *Phys. Rev. A* **56**, 322 (1997).
7. B.R. Mollow, *Phys. Rev. A* **5**, 2217 (1972).
8. G.A. Prataviaera, S.S. Mizrahi, V.V. Dodonov and J.R. Brinati, to appear in *Phys. Rev. A*.

A Method of Quantum State Reconstruction for a Dissipative Cavity

H. Moya-Cessa

*INAOE, Coordinación de Óptica, Apdo. Postal 51 y 216, 72000 Puebla, Pue., Mexico and
Dipartimento di Matematica e Fisica, Università di Camerino, Camerino (MC), Italy*

J.A. Roversi, S.M. Dutra, and A. Vidiella-Barranco

*Instituto de Física “Gleb Wataghin”, Universidade Estadual de Campinas, 13083-970 Campinas
SP Brazil*

Abstract

We present a feasible scheme for reconstructing the quantum state of a field prepared inside a lossy cavity. Quantum coherences are normally destroyed by dissipation, but we show that at zero temperature we are able to retrieve enough information about the initial state, making possible to recover its Wigner function.

Methods to reconstruct quantum states of light are of great importance in quantum optics and there have been several proposals using different techniques to achieve such reconstructions.¹ However, it is well known that dissipation has destructive effects in most schemes which makes of importance to study methods of reconstruction which take into account decoherence.²

We present a method of reconstruction of the density operator of the cavity radiation field after the destructive action of dissipation has taken place. We consider a single mode high- Q cavity where we suppose that a (nonclassical) field state $\hat{\rho}(0)$ is previously prepared. The first step of our method consists in driving the generated quantum state by a coherent pulse. The reconstruction of the field state may be accomplished after turning-off the driving field, i.e., at a time in which the cavity field has already suffered decay. This is a generalization of a method previously presented by us where, although we took into account losses, we did not consider them while the displacement of the initial state took place.² We will show below

¹see for instance: U. Leonhardt, *Measuring the Quantum State of Light* (Cambridge: CUP) 1997, and references therein

²H. Moya-Cessa, S.M. Dutra, J.A. Roversi and A. Vidiella-Barranco, *J. of Mod. Optics* **46**, 555 (1999)

that by displacing the initial state (even while it is decaying) we turn its quantum coherences robust enough to allow its experimental determination, at a later time, despite dissipation. The evolution of the cavity field is such that it directly yields the Wigner function of the initial nonclassical field from the measurement of field statistics. For that we make direct use of the series representation of quasiprobability distributions.³

The master equation in the interaction picture for the reduced density operator $\hat{\rho}$ relative to a driven cavity mode, taking into account cavity losses at zero temperature and under the Born-Markov approximation is given by

$$\frac{\partial \hat{\rho}}{\partial t} = -i\hbar[\hat{H}, \hat{\rho}] + \frac{\gamma}{2} \left(2\hat{a}\hat{\rho}\hat{a}^\dagger - \hat{a}^\dagger\hat{a}\hat{\rho} - \hat{\rho}\hat{a}^\dagger\hat{a} \right), \quad (1)$$

with

$$\hat{H} = i \left(\alpha^* \hat{a} - \alpha \hat{a}^\dagger \right), \quad (2)$$

where \hat{a} and \hat{a}^\dagger are the annihilation and creation operators, γ the (cavity) decay constant and α the amplitude of the driving field.

We define the superoperators $\hat{\mathcal{R}}$ and $\hat{\mathcal{L}}$ by their action on the density operator⁴

$$\hat{\mathcal{R}}\hat{\rho} = (\alpha^* \hat{a} - \alpha \hat{a}^\dagger)\hat{\rho} - \hat{\rho}(\alpha^* \hat{a} - \alpha \hat{a}^\dagger), \quad (3)$$

and

$$\hat{\mathcal{L}}\hat{\rho} = \gamma\hat{a}\hat{\rho}\hat{a}^\dagger - \frac{\gamma}{2} \left(\hat{a}^\dagger\hat{a}\hat{\rho} + \hat{\rho}\hat{a}^\dagger\hat{a} \right). \quad (4)$$

It is not difficult to show that

$$[\hat{\mathcal{R}}, \hat{\mathcal{L}}]\hat{\rho} = \frac{\gamma}{2}\hat{\mathcal{R}}\hat{\rho}, \quad (5)$$

and the formal solution of Eq. (1) can then be written as

$$\hat{\rho}(t) = \exp \left[(\hat{\mathcal{R}} + \hat{\mathcal{L}})t \right] \hat{\rho}(0) = \exp(\hat{\mathcal{L}}t) \exp \left[-\frac{2\hat{\mathcal{R}}}{\gamma}(1 - e^{\gamma t/2}) \right] \hat{\rho}(0). \quad (6)$$

After driving the initial field during a time t_d , the resulting field density operator will read

$$\hat{\rho}(t_d) = e^{\hat{\mathcal{L}}t_d} \hat{\rho}_{\beta; t_d}(0), \quad (7)$$

where

$$\hat{\rho}_{\beta}(0) = \hat{D}^\dagger(\beta)\hat{\rho}(0)\hat{D}(\beta), \quad (8)$$

³H. Moya-Cessa and P.L. Knight, Phys. Rev. A **48**, 2479 (1993)

⁴see for instance S.M. Barnett and P.L. Knight, Phys. Rev. A **33**, 2444 (1986)

and with

$$\beta = -2\alpha \frac{1 - e^{\gamma t_d/2}}{\gamma}. \quad (9)$$

This means that if we drive the initial field while it decays, during a time t_d , this is equivalent to having the field driven by a coherent field with an effective amplitude β given in Eq. (9).

The driving of the initial field is carried out during a time t_d . This procedure enables us to obtain information about all the elements of the initial density matrix from the diagonal elements of the time-evolved displaced density matrix only. As diagonal elements decay much slower than off-diagonal ones, information about the initial state stored this way becomes robust enough to withstand the decoherence process. We will now show how this robustness can be used to obtain the Wigner function of the initial state after it has already started to be dissipated. Once the injection of the coherent pulse is completed, the cavity field is left to decay, so that its dynamics will be governed by the master equation in Eq. (1) without the first (driving) term in its right-hand-side. Therefore, the cavity field density operator will be, at a time t , given by

$$\hat{\rho}_\beta(t) = e^{(\hat{J} + \hat{L})t} \hat{\rho}_\beta(0), \quad (10)$$

with

$$\hat{J}\hat{\rho} = \gamma\hat{a}\hat{\rho}\hat{a}^\dagger, \quad \hat{L}\hat{\rho} = -\frac{\gamma}{2}(\hat{a}^\dagger\hat{a}\hat{\rho} + \hat{\rho}\hat{a}^\dagger\hat{a}). \quad (11)$$

The next step is to calculate the diagonal matrix elements of $\hat{\rho}_\beta(t) = \exp[(\hat{J} + \hat{L})t] \hat{\rho}_\beta$ in the number state basis, or

$$\langle m | \hat{\rho}_\beta(t) | m \rangle = \frac{e^{-m\gamma t}}{q^m} \sum_{n=0}^{\infty} q^n \binom{n}{m} \langle n | \hat{\rho}_\beta(0) | n \rangle, \quad (12)$$

where $q = 1 - e^{-\gamma t}$.

Now we multiply those matrix elements by powers of the function

$$\chi(s; t) = 1 + \frac{2e^{\gamma t}}{s - 1}. \quad (13)$$

If we sum over m the resulting expression we obtain the following simple sum

$$F(\beta, s) = \frac{2}{\pi} \sum_{m=0}^{\infty} \chi^m(s; t) \langle m | \hat{\rho}_\beta(t) | m \rangle = -\frac{2}{\pi(s - 1)} \sum_{n=0}^{\infty} \left(\frac{s + 1}{s - 1} \right)^n \langle n | \hat{\rho}_\beta | n \rangle. \quad (14)$$

The expression in Eq. (14) is the s -parametrized quasiprobability distribution^{5 6} corresponding to $\hat{\rho}$ (the initial field state) at the point specified by the complex amplitude

⁵for $s = -1$ one obtains the Q -function, $s = 0$ the Wigner function and for $s = 1$ the Glauber-Sudarshan P -function

⁶K.E. Cahill and R.J. Glauber, Phys. Rev. **177**, 1882 (1969)

β . Therefore we need simply to measure the diagonal elements of the dissipated displaced cavity field $P_m(\beta; t) = \langle m | \hat{\rho}_\beta(t) | m \rangle$ for a range of β 's, the transformation in Eq. (14) in order to obtain, for instance, the Wigner function of the initial state for this range. We note that after performing the sum, the time-dependence cancels out completely, leaving us a constant s -parametrized quasiprobability distribution function. Therefore the initial state may be reconstructed, at least in principle, at an arbitrary later time. In practice, however, the decay of the field energy will impose a limitation on the times in which we will be able to measure the photon distribution (12) (for a method, see for instance reference 2).

Eq. (14) also implies that, although one needs to know all the density matrix elements (diagonal and off-diagonal) to have complete information of a given state, in our case it is only needed to know the diagonal elements of the displaced and decayed density matrix to know the initial field state.

In conclusion, we have presented a method for reconstructing the Wigner function of an initial nonclassical state at times when the field would have normally lost its quantum coherence. In particular, even at times such that the Wigner function would have lost its negativity, reflecting the decoherence process. The most important point in our approach is the driving of the initial field immediately after preparation, which stores quantum coherences in the diagonal elements of the time evolved displaced density matrix, making them robust. We have therefore shown that the initial displacement transfers the robustness of a coherent state against dissipation to any initial state, allowing the full reconstruction of the field state under less than ideal conditions.

A natural application of our method would be the measurement of quantum states in cavities, where dissipation is difficult to avoid. Moreover, the application of the driving pulse at different times after the generation of a field state, would allow the “snapshooting” of the Wigner function as the state is dissipated. This means that valuable information about the (mixed) quantum state as well as about the decay mechanism itself could be retrieved while it suffers decay. The possibility of reconstructing quantum states even in the presence of dissipation may be also relevant for applications in quantum computing. Loss of coherence associated to dissipation is likely to occur in those devices, and our method could be used, for instance, as a scheme to refresh the state of a quantum computer in order to minimize the destructive action of dissipation.⁷ Application of our scheme to reconstruct a Schrödinger cat state will be presented elsewhere.⁸

This work was partially supported by FAPESP (Brazil), CONACYT (México), and CNPq (Brazil).

⁷A. Ekert and C. Macchiavello, *Acta Phys. Polon. A* **93**, 63 (1998)

⁸H. Moya-Cessa, S.M. Dutra, J.A. Roversi and A. Vidiella-Barranco, *Phys. Rev. A*, in press

A classical experiment of atom optics with a Bose-Einstein Condensate

J.H. Müller

INFM UdR Università di Pisa, Dipartimento di Fisica, Via Buonarroti, 2 56127 Pisa, Italy

Y.B. Ovchinnikov, E.J.D. Vredenburg, M.R. Doery, K. Helmerson, S.R. Rolston, and
W.D. Phillips

Atomic Physics Division, PHYS A-167, NIST, Gaithersburg MD20899, USA

Abstract

Diffraction of atoms by a pulsed standing light wave is a classical experiment of atom optics. We repeat this experiment with sodium atoms in a Bose-Einstein condensate released from a magnetic trap. For the first time we give clear experimental evidence of periodic focusing and collimation of the atomic momentum distribution in the thick grating limit of normal incidence diffraction. Numerical simulation of the diffraction with our experimental parameters, suggests that we achieve true squeezing of the atomic wavefunction at the minima of the periodic potential.

The advent of Bose-Einstein condensation in dilute atomic vapours provides sources of cold atoms with unprecedented brightness and coherence. Many experiments in atom optics so far limited by the imperfections of the source can now be performed with much higher precision allowing for stringent tests of the underlying physical models [2, 3, 4, 5]. We study normal incidence diffraction of atoms from a standing light wave [1]. In contrast to former experiments [6] the momentum spread of our sample far below a single recoil momentum and its small spatial extension together with the use of a large pulsed standing light wave guarantees clear separation of the various diffraction orders and uniform interaction conditions over the whole sample. Varying the interaction time of the atoms with the periodic potential we explore the thick grating limit of diffraction, where the interaction time becomes comparable or larger than the classical oscillation period in the potential wells.

We consider the interaction of two-level atoms with a plane standing light wave pulse with an electric field amplitude $E(z, t) = 2E_0 f(t) \cos(kz) \sin(\omega t)$, where the function $f(t)$ describes the unit step-like envelope of the pulse of duration τ , $k = 2\pi/\lambda$ is the wave number. We assume the magnitude of the detuning, $|\Delta| = |\omega - \omega_0| \gg \Omega_0, \Gamma$. Here ω is the standing wave frequency, ω_0 is the frequency of the resonant atomic transition, $\Omega_0 = \mu E_0/\hbar$ is the traveling wave Rabi frequency, μ is the dipole matrix element and Γ is the natural width of the transition. In the limit of large detuning the light shift potential can be written as

$$U(z) = U_0 \cos^2(kz), \quad (1)$$

where $U_0 = \hbar\Omega_0^2/\Delta$. Atoms near the nodes experience an approximately harmonic potential, with an oscillation frequency of

$$\omega_{ho} = \sqrt{\frac{4\Omega_0^2}{|\Delta|}}\omega_r, \quad (2)$$

where $\omega_r = \hbar k^2/2M$ is the recoil frequency, and M is the mass of the atom.

In a classical picture atoms oscillate in the wells of the standing wave potential and experience cyclic focusing and defocusing with a period of about π/ω_{ho} . This leads to a complementary breathing of the atomic momentum distribution. Classically one expects rapid dephasing of these breathing oscillations due to the strong anharmonicity of the single potential wells. In a full quantum treatment of the motion inside the periodic potential, however, this feature can reappear, if the potential depth is chosen such that the initial momentum distribution projects onto only a few - ideally two - allowed energy bands. Here the oscillation of the momentum distribution arises from the interference between equal momentum states in different energy bands governed by the differential phase accumulated during the interaction time with the periodic potential. The maximum possible momentum transferred to an atom in the potential (1) is $p_{max} = \sqrt{2|U_0|M}$, which corresponds to a maximum significantly populated diffraction order [5] $n_{max} = \sqrt{|U_0|/(4\hbar\omega_r)}$.

In the experiment we produced with a combination of laser and evaporative cooling a condensate consisting of about 10^6 sodium atoms in the $3S_{1/2}(F = 1, m_F = -1)$ state in a time magnetic trap. Subsequently, the spring constants of the trap were adiabatically decreased in order to decrease the momentum spread of condensate. The final size of the adiabatically expanded cloud was about $60 \mu\text{m}$. The standing light wave used for diffracting the BEC was produced by a single-mode dye laser, frequency-locked at $\Delta = -42\Gamma$. A spatially filtered beam was expanded to a diameter of 2.8 mm ($1/e^2$ intensity level), passed through the vacuum chamber containing the BEC, and retroreflected by a flat mirror. The total power in the laser beam was about 1 mW corresponding to a peak Rabi frequency $\Omega_0/2\pi \simeq 16 \text{ MHz}$. In all experiments the BEC was suddenly released from the magnetic trap and allowed to expand for 2 ms , to minimize interaction effects. To produce diffraction a short pulse of horizontal standing wave light was then applied. After an additional time of flight of 10 ms the horizontal spatial distribution of the diffracted atoms was detected using a standard absorption imaging method [7]. As a detector a standard 8-bit CCD camera was used. Analysing the optical depth information encoded in the images we can extract the number of atoms in the various diffraction peaks and by looking at the width of individual peaks we can deduce the momentum spread of the original sample, which amounts to $p_{rms}^{(i)} = 0.02 \pm 0.002 \hbar k$ in our case. The number of observed diffraction orders ($n_{max} = 2$) is in accordance with the calculated value for our experimental parameters. Shown in Fig. 1(a) is the dependence of the relative number of atoms in the $n = 0$ and in each of the $n = 1$ and $n = -1$ diffraction peaks as a function of the duration of the standing wave pulse. One can observe three collapses of the BEC motion, manifested as an absence of splitting of the BEC at $\tau = 3.2, 6.5$ and $10 \mu\text{s}$. The maximum number of atoms in the $n = \pm 1$ peaks [Fig. 1(b)] was observed between these times. This behavior can be explained as an alternating sequence of squeezing of the whole atomic distribution in coordinate (focusing) and momentum (collimation) space in a standing wave potential

with period $t_c \simeq 3.2 \mu\text{s}$. In order to understand in more detail the dependence of the intensities of the main diffracted peaks on the duration of the standing wave pulse, we solved numerically the linear Schrödinger equation for a two-level atom in a periodic potential with our experimental parameters. These calculations agree very well with the experimentally-obtained curves of Fig. 1, yielding $t_c = 3.2 \mu\text{s}$. The calculated minimum rms spatial width of the focused atomic ensemble in a single well of the optical potential is $z_{rms} \simeq 20 \text{ nm}$ at $\tau = 1.54 \mu\text{s}$. Furthermore, the calculated phase space density of these atoms satisfies $z_{rms}p_{rms} \simeq \hbar/2$ near values of τ for which atoms are maximally focused. A calculation of the spatial extent of the groundstate wavefunction of an harmonic oscillator corresponding to the potential near the nodes of the standing wave yields $a_{ho} = 45 \text{ nm}$. We thus prepare at times near maximal focusing an array of truly squeezed wavepackets. One should keep in mind, though, that the calculations are based on the linear Schrödinger equation, i.e. interaction between the atoms whether groundstate or mediated by the light field is neglected. Calculations taking into account the mean-field interaction show, however, that none of the experimentally observed quantities are altered with respect to the linear model [9]. Atom stimulated scattering into the various diffraction orders or creation of new diffraction peaks is strongly suppressed, since in our 1-D geometry energy and momentum conservation cannot be satisfied for those processes.

Making use of the standard methods of solid state physics we also calculated the energies of the eigenstates and their populations for the atoms in the standing wave potential with a total depth $U_0 = -19.26 \hbar\omega_r$. There are only 3 bands (labeled $v = 0, 1, 2$) of allowed states below the potential barrier. Due to the very narrow initial momentum distribution, the atoms are projected onto states near the center of the Brillouin zone of only the three, lowest-energy, even bands. The energies and occupations of these states are $E_0 = -15.14 \hbar\omega_r$, $W_0 = 59.1\%$; $E_2 = -2.28 \hbar\omega_r$, $W_2 = 38.2\%$; $E_4 = 7.37 \hbar\omega_r$, $W_4 = 2.7\%$. We thus expect strongly nonclassical behaviour, since the system consists mainly of two populated vibrational states, with a beat period of $2\pi\hbar/(E_0 - E_2) = 3.1 \mu\text{s}$ between them. This is in very good agreement with the experimentally observed period of atomic motion t_c and the fact that multiple collapses of the diffraction pattern are observable.

This conceptually simple experiment allowed to test the physical models behind diffraction of matter waves by light waves. Future experiments will go beyond those simple models and look specifically for effects related to the backaction of a dense sample on the light field or to the interaction between the atoms.

1. Yu.B. Ovchinnikov et al., Phys. Rev. Lett. **83**, 284 (1999).
2. S. Altshuler, L.M. Frantz, and R. Braunstein, Phys. Rev. Lett. **17**, 231 (1966).
3. R.J. Cook, A.F. Bernhardt, Phys. Rev. A **18**, 2533 (1978).
4. A.P. Kazantsev, G.I. Surdutovich, and V.P. Yakovlev, Pis'ma ZhETF **31**, 542 (1980) [JETP Lett. **31**, 509 (1980)]. Appl. Phys. **B 59**, 217 (1994).
5. A.F. Bernhardt, and B.W. Shore, Phys. Rev. A **23**, 1290 (1981); E. Arimondo, A. Bambini, S. Stenholm, Phys. Rev. A **24**, 898 (1981).

6. E. Arimondo, H. Lew, T. Oka, Phys. Rev. Lett. **43**, 753 (1979). P.E. Moskowitz et al, Phys. Rev. Lett. **51**, 370 (1983); P.E. Moskowitz, P.L. Gould, and D.E. Pritchard, J. Opt. Soc. Am. **B2**, 1784 (1985); P.L. Gould, G.E. Ruff, and D.E. Pritchard Phys. Rev. Lett. **56**, 827 (1986); P.J. Martin et al, Phys. Rev. A **36**, 2495 (1987); P.L. Gould et al, Phys. Rev. A **43**, 585 (1991).
7. M.H. Anderson et al, Science **269**, 198 (1995).
8. Y. Castin, R. Dum, Phys. Rev. Lett. **77**, 5315 (1996).
9. M. Trippenbach, Y.B. Band, and P.S. Julienne, OPTICS EXPRESS **3**, 530 (1998).

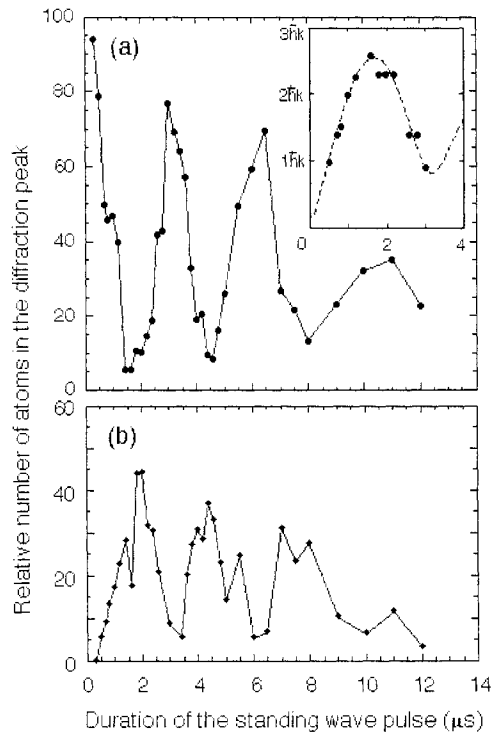


FIG. 1. Relative number of atoms in $n = 0$ (a) and $n = 1$ (b) diffraction orders as a function of the interaction time with the standing wave. The inset shows rms momentum width p_{rms} of the diffracted atoms for different standing wave pulse duration.

The Haroche-Ramsey experiment as a generalised measurement

Willem M. de Muynck

*Theoretical Physics, Eindhoven University of Technology, P.O.B. 513,
5600 MB Eindhoven, the Netherlands*

Abstract

It is demonstrated that the Haroche-Ramsey experiment is a generalised measurement that can be interpreted as a joint measurement of incompatible interference and path observables. Complementarity is studied on the basis of the Martens inequality. From this point of view a phase measurement is seen to be preferable over the photon number measurement that was actually performed.

In the atomic-beam interference experiment by Brune et al. (to be referred to as the Haroche-Ramsey experiment) [1] a Rb atom is sent through three cavities, R_1 , R_2 and C , of which the first two are resonant with a particular transition between two Rydberg states $|e\rangle$ and $|g\rangle$ of the atom. Finally it is determined whether the atom is in $|e\rangle$ or $|g\rangle$. Whereas the experiment without cavity C is a pure interference experiment, already performed by Ramsey [2], the introduction of cavity C provides the possibility to obtain also “which way” information by measuring some observable of the cavity C field. In the Haroche-Ramsey experiment the “which way” information is not about trajectories in configuration space, but about trajectories in the Hilbert space of the internal states of the atom.

Restricting to $\pi/2$ pulses, the atom experiences the following transitions in cavities R_1 and R_2 : $|e\rangle \rightarrow |p_-\rangle = \frac{1}{\sqrt{2}}(|e\rangle - i|g\rangle)$, $|g\rangle \rightarrow |p_+\rangle = \frac{1}{\sqrt{2}}(|e\rangle + i|g\rangle)$. In cavity C there is a phase change of the field according to $|e\rangle \otimes |\gamma\rangle \xrightarrow{C} |e\rangle \otimes |\gamma e^{i\Phi}\rangle$, $|g\rangle \otimes |\gamma\rangle \xrightarrow{C} |g\rangle \otimes |\gamma e^{-i\Phi}\rangle$, $|\gamma\rangle$ being the initial coherent state of the field. From this it is straightforward to calculate the final state $|\Psi_f\rangle$ starting from the initial state $|\Psi_{in}\rangle = |\psi_{in}\rangle \otimes |\gamma\rangle$, $|\psi_{in}\rangle = \alpha|e\rangle + \beta|g\rangle$.

Measuring an arbitrary observable $\{\mathbf{R}_n\}$ of the cavity C field in coincidence with the measurement of the final state of the atom, we can determine the positive operator-valued measure $\{\mathbf{M}_{en}, \mathbf{M}_{gn}\}$ representing the experiment, by relating the detection probabilities p_{en} and p_{gn} to the initial state $|\psi_{in}\rangle$ of the atom according to

$$p_{en} = \langle \Psi_f | |e\rangle \langle e| \otimes \mathbf{R}_n | \Psi_f \rangle = \langle \psi_{in} | \mathbf{M}_{en} | \psi_{in} \rangle, \quad p_{gn} = \langle \Psi_f | |g\rangle \langle g| \otimes \mathbf{R}_n | \Psi_f \rangle = \langle \psi_{in} | \mathbf{M}_{gn} | \psi_{in} \rangle.$$

We find

$$\mathbf{M}_{en} = \frac{1}{4} \begin{pmatrix} \langle v_e | \mathbf{R}_n | v_e \rangle & -i \langle v_e | \mathbf{R}_n | v_g \rangle \\ i \langle v_g | \mathbf{R}_n | v_e \rangle & \langle v_g | \mathbf{R}_n | v_g \rangle \end{pmatrix}, \quad \mathbf{M}_{gn} = \frac{1}{4} \begin{pmatrix} \langle v_g | \mathbf{R}_n | v_g \rangle & -i \langle v_g | \mathbf{R}_n | v_e \rangle \\ i \langle v_e | \mathbf{R}_n | v_g \rangle & \langle v_e | \mathbf{R}_n | v_e \rangle \end{pmatrix},$$

with $|v_e\rangle = |\gamma e^{i\Phi}\rangle - |\gamma e^{-i\Phi}\rangle$, $|v_g\rangle = |\gamma e^{i\Phi}\rangle + |\gamma e^{-i\Phi}\rangle$.

We shall first consider an experiment in which the phase Φ of the cavity C field is measured by means of balanced homodyning, having $\{|\alpha\rangle\langle\alpha|\pi\}$, $|\alpha\rangle$ coherent states, as a POVM [3]. By coarsening this POVM according to $\mathbf{R}_\pm = \frac{1}{\pi} \int_{C^\pm} d^2\alpha |\alpha\rangle\langle\alpha|$ (in which

the integrations are over the upper and lower halves of the complex plane) we restrict to measuring whether Φ is positive or negative. Moreover, in this measurement we take $|\Phi| = \pi/2$. For this value the Ramsey experiment (corresponding to $\gamma = 0$) is a measurement of the interference observable $\{|e\rangle\langle e|, |g\rangle\langle g|\}$.

In order to be able to interpret the experiment for $\gamma \neq 0$ as a joint measurement of incompatible observables it is necessary to order the four operators $\mathbf{M}_{e\pm}, \mathbf{M}_{g\pm}$ in a bivariate way. Thus,

$$(\mathbf{R}_{mn}) := \begin{pmatrix} \mathbf{M}_{e+} & \mathbf{M}_{g+} \\ \mathbf{M}_{e-} & \mathbf{M}_{g-} \end{pmatrix}.$$

For the marginals of this bivariate POVM we find

$$\begin{aligned} \begin{pmatrix} \mathbf{M}_{e+} + \mathbf{M}_{e-} \\ \mathbf{M}_{g+} + \mathbf{M}_{g-} \end{pmatrix} &= \frac{1}{2} \overbrace{\begin{pmatrix} 1 + C_1 & 1 - C_1 \\ 1 - C_1 & 1 + C_1 \end{pmatrix}}^{(\lambda_{mm'})} \begin{pmatrix} |e\rangle\langle e| \\ |g\rangle\langle g| \end{pmatrix}, \\ \begin{pmatrix} \mathbf{M}_{e+} + \mathbf{M}_{g+} \\ \mathbf{M}_{e-} + \mathbf{M}_{g-} \end{pmatrix} &= \frac{1}{2} \overbrace{\begin{pmatrix} 1 + A & 1 - A \\ 1 - A & 1 + A \end{pmatrix}}^{(\mu_{nn'})} \begin{pmatrix} |p_+\rangle\langle p_+| \\ |p_-\rangle\langle p_-| \end{pmatrix}, \end{aligned}$$

with $C_1 = e^{-2\gamma^2}$ and $A = \text{erf}(\gamma)$. These relations show that the experiment can be interpreted as a joint non-ideal measurement [4] of the incompatible observables $\{|e\rangle\langle e|, |g\rangle\langle g|\}$ and $\{|p_+\rangle\langle p_+|, |p_-\rangle\langle p_-|\}$. Because of the analogy of the present experiment with the neutron interference experiment carried out by Summhammer et al. [5], which can be interpreted as a joint non-ideal measurement of interference and path [6], the latter observable will be referred to as the path observable. The matrices $(\lambda_{mm'})$ and $(\mu_{nn'})$ are the non-ideality matrices, expressing complementarity in the sense of mutual disturbance in a joint measurement of incompatible observables. Thus, if $\gamma = 0$ the interference observable is measured ideally since $C_1 = 1$ implies $(\lambda_{mn}) = (\delta_{mn})$, whereas the other marginal becomes uninformative. For $\gamma \rightarrow \infty$ we have $A = 1$; then path is measured ideally, whereas the interference marginal is uninformative. More generally, taking the average row entropy $J_{(\lambda)} = -\frac{1}{N} \sum_{mm'} \lambda_{mm'} \ln \frac{\lambda_{mm'}}{\sum_{m''} \lambda_{mm''}}$ as a measure of the non-ideality of the non-ideality matrix $(\lambda_{mm'})$ (and analogously for $(\mu_{nn'})$), it is possible [4] to derive for two observables having eigenvectors $|a_m\rangle$ and $|b_n\rangle$, respectively, the following inequality (to be referred to as the Martens inequality):

$$J_{(\lambda)} + J_{(\mu)} \geq -2 \ln \{ \max_{mn} |\langle a_m | b_n \rangle| \}.$$

If the observables are incompatible, then the right-hand side of this inequality is positive, thus prohibiting that $J_{(\lambda)}$ and $J_{(\mu)}$ can simultaneously be small. For the joint non-ideal measurement of the interference and path observables we get

$$\begin{aligned} J_{(\lambda)} &= -\frac{(1+C_1)}{2} \ln\left(\frac{1+C_1}{2}\right) - \frac{(1-C_1)}{2} \ln\left(\frac{1-C_1}{2}\right), \\ J_{(\mu)} &= -\frac{(1+A)}{2} \ln\left(\frac{1+A}{2}\right) - \frac{(1-A)}{2} \ln\left(\frac{1-A}{2}\right). \end{aligned}$$

A parametric plot of $J_{(\lambda)}$ versus $J_{(\mu)}$ as a function of γ (cf. figure) clearly exhibits complementarity in the sense that the plot remains outside the shaded area that is forbidden by the Martens inequality.

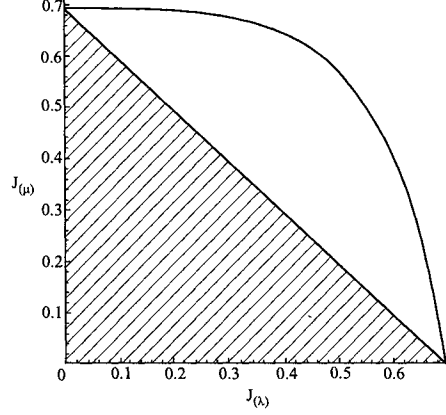


Figure 1: Parametric plot of $J_{(\lambda)}$ versus $J_{(\mu)}$, for $0 \leq \gamma < \infty$.

In the experiment performed by Brune et al. [1] a different measurement of the cavity C field was performed. A second atom, starting in state $|e\rangle$, was used as a probe of the field [7]. Also for this second atom it is determined whether it is in state $|e\rangle$ or $|g\rangle$ after leaving cavity R_2 . Once again the POVM of the experiment can be found by relating the detection probabilities $p_{e_1 e_2} = \langle \Psi'_f | |e_1\rangle \langle e_1| \otimes |e_2\rangle \langle e_2| | \Psi'_f \rangle$, etc., in the final state $|\Psi'_f\rangle$ to the initial state $|\psi_{in1}\rangle \otimes |e_2\rangle \otimes |\gamma\rangle$, $|\psi_{in1}\rangle = \alpha|e_1\rangle + \beta|g_1\rangle$ (and analogously for the other probabilities). Allowing Φ to be arbitrary, we straightforwardly find

$$\mathbf{M}_{e_1 e_2} = \frac{1}{16} \begin{pmatrix} \| |v'_g\rangle - 2|\gamma\rangle \|^2 & -i(\langle v'_g | v'_e \rangle - 2\langle \gamma | v'_e \rangle) \\ i(\langle v'_e | v'_g \rangle - 2\langle v'_e | \gamma \rangle) & \| |v'_e\rangle \|^2 \end{pmatrix}, \text{ etc.},$$

with $|v'_e\rangle = |\gamma e^{i2\Phi}\rangle - |\gamma e^{-i2\Phi}\rangle$, $|v'_g\rangle = |\gamma e^{i2\Phi}\rangle + |\gamma e^{-i2\Phi}\rangle$.

Defining a bivariate POVM according to

$$\mathbf{R}_{mn} := \begin{pmatrix} \mathbf{M}_{e_1 e_2} & \mathbf{M}_{e_1 g_2} \\ \mathbf{M}_{g_1 g_2} & \mathbf{M}_{g_1 e_2} \end{pmatrix},$$

we can straightforwardly determine its marginals. These can be seen to represent non-ideal measurements of incompatible observables (that will not be reproduced here), with non-ideality matrices given by

$$(\lambda_{mm'}) = \begin{pmatrix} \lambda & 1 - \lambda \\ 1 - \lambda & \lambda \end{pmatrix}, \quad (\mu_{nn'}) = \begin{pmatrix} \mu & 1 - \mu \\ 1 - \mu & \mu \end{pmatrix},$$

with

$$\lambda = \frac{1}{2}(1 + e^{-2\gamma^2 \sin^2 \Phi}),$$

$$\mu = \frac{1}{2} + \frac{1}{4}[\{1 + e^{-2\gamma^2 \sin^2 2\Phi} \cos(\gamma^2 \sin 4\Phi)\}^2 + e^{-4\gamma^2 \sin^2 2\Phi} \sin^2(\gamma^2 \sin 4\Phi)]^{1/2}.$$

For the non-ideality measures we obtain

$$J_{(\lambda)} = -\{\lambda \ln(\lambda) + (1 - \lambda) \ln(1 - \lambda)\}, \quad J_{(\mu)} = -\{\mu \ln(\mu) + (1 - \mu) \ln(1 - \mu)\}.$$

For $\gamma = 0$ we get $\lambda = \mu = 1$, and, hence, $J_{(\lambda)} = J_{(\mu)} = 0$. This shows that there is no complementarity in this limit. Evidently, in this limit the field measurement of the second atom does not yield information on the initial state of the atom that is complementary to the one obtained from the first atom. The reason for this is that as a measurement of the cavity C field, the second atom is not a phase measurement, but a (non-ideal) measurement of photon number. This can be seen by calculating the POVM of the measurement of the state of the atom, interpreted as a measurement of an observable of the cavity C field. For the initial state $|\Psi_{in}\rangle = |e\rangle \otimes |\gamma\rangle$ of atom and cavity C field ($|\gamma\rangle$ an arbitrary coherent state) we get as the final state

$$|\Psi_f\rangle = \frac{1}{2}[|e\rangle|v_e\rangle - i|g\rangle|v_g\rangle].$$

Then the POVM is derived by equating

$$\left. \begin{aligned} p_e &= \langle \Psi_f | e \rangle \langle e | \Psi_f \rangle = \langle \gamma | \mathbf{R}_e | \gamma \rangle \\ p_g &= \langle \Psi_f | g \rangle \langle g | \Psi_f \rangle = \langle \gamma | \mathbf{R}_g | \gamma \rangle \end{aligned} \right\}.$$

This gives

$$\left. \begin{aligned} p_e &= \frac{1}{4} \langle v_e | v_e \rangle = \frac{1}{4} \langle \gamma | 2 - e^{2i\Phi a^\dagger a} - e^{-2i\Phi a^\dagger a} | \gamma \rangle \\ p_g &= \frac{1}{4} \langle v_g | v_g \rangle = \frac{1}{4} \langle \gamma | 2 + e^{2i\Phi a^\dagger a} + e^{-2i\Phi a^\dagger a} | \gamma \rangle \end{aligned} \right\},$$

from which the POVM is easily found as $\{\mathbf{R}_e = \sin^2 \Phi a^\dagger a, \mathbf{R}_g = \cos^2 \Phi a^\dagger a\}$, or

$$\begin{aligned} \mathbf{R}_e &= \sum_{n=0}^{\infty} \lambda_{en} |n\rangle \langle n|, \quad \lambda_{en} = \sin^2 \Phi n, \\ \mathbf{R}_g &= \sum_{n=0}^{\infty} \lambda_{gn} |n\rangle \langle n|, \quad \lambda_{gn} = \cos^2 \Phi n. \end{aligned}$$

References

- [1] M. Brune, E. Hagley, J. Dreyer, X. Maître, A. Maali, C. Wunderlich, J. M. Raimond and S. Haroche, *Phys. Rev. Lett.* **77**, 4887 (1996).
- [2] Norman F. Ramsey, *Molecular Beams*, Oxford at the Clarendon Press, First published 1956, Reprinted lithographically in Great Britain from corrected sheets of the first edition 1963, 1969.
- [3] H.P. Yuen, J.H. Shapiro, *IEEE Trans. Inform. Theory* **IT-26**, 78 (1980).
- [4] H. Martens and W. de Muynck, *Found. of Phys.* **20**, 255, 357 (1990).
- [5] J. Summhammer, H. Rauch, and D. Tuppinger, *Phys. Rev.* **A36**, 4447 (1987).
- [6] W.M. de Muynck and H. Martens, *Phys. Rev.* **42A**, 5079 (1990).
- [7] L. Davidovich, M. Brune, J. M. Raimond and S. Haroche, *Phys. Rev. A* **53**, 1295 (1996).

Radiation pressure effects in a high-finesse optical cavity

M. Pinard, Y. Hadjar, P.F. Cohadon, A. Heidmann
*Laboratoire Kastler Brossel, Université Pierre et Marie Curie et CNRS,
Case 74, 4 place Jussieu, Paris Cedex 05, France*

Abstract

We study the optomechanical coupling in a high-finesse cavity with a mirror coated on a mechanical resonator. We observed the thermal motion of the mirror with a sensitivity of $2 \times 10^{-19} \text{ m}/\sqrt{\text{Hz}}$ and cooled the resonator by laser radiation pressure.

The optomechanical coupling between a movable mirror and a light beam is based on two complementary effects. The first one is the phase shift of the light due to the mirror motion. The second one is the mirror response to radiation pressure which induces quantum correlations between its position and the light intensity. These effects can be enhanced using a high finesse optical cavity that is very sensitive to mirror displacements and it has recently been proposed to use such a device to generate squeezed states [1,2], to realize QND measurements [3,4], or to study the Standard Quantum Limit in interferometric measurements [5]. In this paper, we present the recent progress of our experiment in which a laser beam is sent into a high-finesse cavity with a movable mirror. We have observed the Brownian motion of the mirror and cooled the mirror by radiation pressure. We also discuss the quantum limit of this cooling process.

The experimental set-up is shown in Figure 1. The light source is a titane-sapphire laser working at 810 nm and frequency-locked to a resonance of the high-finesse cavity by monitoring the residual light transmitted by the cavity. The beam is intensity-stabilized by a variable attenuator composed of an electro-optic modulator and a polarizer, and it is spatially filtered by a mode cleaner. One gets a 100- μW incident beam on the high-finesse cavity, which is composed of a coupling mirror and a totally reflecting back mirror coated on the plane side of a plano-convex resonator made of silica. The two mirrors are mounted in a rigid cylinder at a distance of 1 mm from each other. The phase of the beam reflected by the cavity is measured by homodyne detection. The reflected beam is mixed on two photodiodes with a 10-mW local oscillator and a servoloop monitors the length of the local oscillator arm so that we measure the phase fluctuations of the reflected beam.

For a resonant cavity, this signal is very sensitive to mirror displacements which are due to the excitation of internal acoustic modes of the resonator. More precisely, a displacement δx of the mirror induces a phase shift $\delta\varphi_{out}$ of the reflected beam equal to

$$\delta\varphi_{out} = \delta\varphi_{in} + \frac{8\mathcal{F}}{\lambda}\delta x, \quad (1)$$

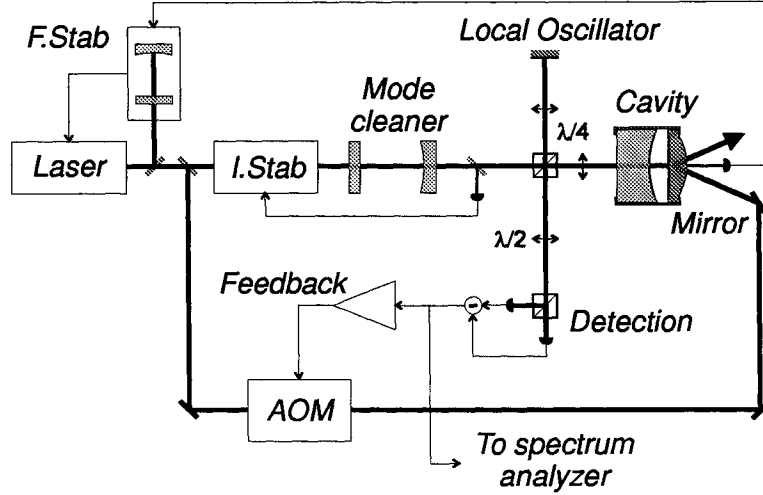


FIG. 1. Experimental set-up. A light beam provided by a frequency (F.Stab) and intensity (I.Stab) stabilized titane-sapphire laser is sent into a high-finesse cavity composed of a coupling mirror and a highly-reflecting mirror coated on a mechanical resonator. Phase fluctuations of the reflected beam are measured by homodyne detection. This signal is fed back to the mirror via the radiation pressure exerted by an auxiliary beam with modulated intensity (AOM)

where $\delta\varphi_{in} = 1/2\sqrt{I_{in}}$ is the quantum phase noise of the incident beam, \mathcal{F} is the cavity finesse, λ is the optical wavelength and I_{in} is the mean incident intensity counted as a number of photons per second. The sensitivity of the displacement measurement is given by the minimum displacement δx_{min} which induces a signal equal to the noise :

$$\delta x_{min} = \frac{\lambda}{16\mathcal{F}\sqrt{I_{in}}}. \quad (2)$$

To cool the mirror, we use a 500-mW auxiliary beam derived from the laser and reflected from the rear of the back mirror. This beam is intensity-modulated by an acousto-optic modulator driven by the the amplified output of the homodyne detection (see Figure 1). The mirror motion can be described by its Fourier transform $\delta x [\Omega]$ at frequency Ω , which is proportional to the applied forces

$$\delta x [\Omega] = \chi [\Omega] (F_T [\Omega] + F_{rad} [\Omega]), \quad (3)$$

where $F_T [\Omega]$ is the thermal Langevin force and $F_{rad} [\Omega]$ is the radiation pressure of the auxiliary beam. If we assume that the mechanical response of the resonator is harmonic, the susceptibility has a lorentzian shape

$$\chi [\Omega] = \frac{1}{M(\Omega_M^2 - \Omega^2 - i\Gamma\Omega)}, \quad (4)$$

characterized by a mass M , a resonance frequency Ω_M and a damping Γ . If we neglect the quantum phase noise $\delta\varphi_{in}$, the signal $\delta\varphi_{out}$ is proportional to the mirror position δx . We choose the gain of the servoloop in such a way that the radiation pressure is proportional to the speed $v = i\Omega\delta x$ of the mirror :

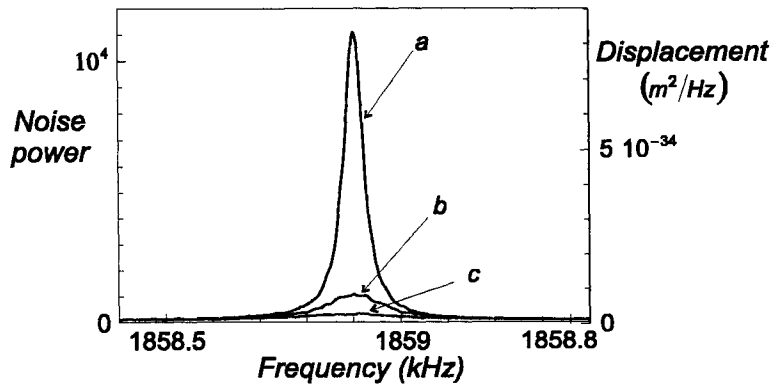


FIG. 2. Phase noise spectrum of the reflected field normalized to the shot-noise level (vertical scale on the left) and equivalent displacement (vertical scale on the right) for a frequency span of 1 kHz around the fundamental resonance frequency of the mirror. The peak reflects the Brownian motion of the mirror without feedback (a) and with feedback for increasing gains of the loop (b and c).

$$F_{rad}[\Omega] = igM\Omega\delta x[\Omega], \quad (5)$$

where g is related to the electronic gain. The radiation pressure exerted by the auxiliary beam is thus equivalent to an additional viscous force and the resulting motion is given by

$$\delta x[\Omega] = \frac{1}{M(\Omega_M^2 - \Omega^2 - i(\Gamma + g)\Omega)} F_T[\Omega]. \quad (6)$$

This equation shows that there is an increase of the damping without any change of the thermal Langevin force. This corresponds to a cold damping of the mirror, the resulting motion being equivalent to a thermal equilibrium at a temperature T_{eff} equal to $T/(1+g/\Gamma)$.

Figure 2 shows the cooling obtained in our experiment. The curves represent the phase noise spectrum of the reflected field normalized to the shot-noise level for a frequency span of 1 kHz around the fundamental resonance frequency of the mirror. Curve (a) is obtained at room temperature without feedback. The peak reflects the thermal excitation of the fundamental mode of the mirror. The vertical scale on the right corresponds to the equivalent displacement in m^2/Hz . The sensitivity δx_{min} reached in our experiment is equal to $2 \times 10^{-19} m/\sqrt{Hz}$ [6].

Curves (b) and (c) show the effect of the feedback loop. The thermal peak is strongly reduced, while its width is increased. The total area of the peak is decreased, corresponding to a reduction of the effective temperature T_{eff} by a factor larger than 10 for curve (c) [7].

Up to now, we have neglected the effect of quantum noise in the description of the cooling mechanism. As a consequence, we predict that the effective temperature T_{eff} can be arbitrarily small for large gain. This will be no longer true if we take into account the contribution of the quantum phase noise $\delta\varphi_{in}$ to the feedback signal $\delta\varphi_{out}$. The feedback control $F_{rad}[\Omega]$ and the resulting motion have then additional terms associated with $\delta\varphi_{in}$:

$$F_{rad}[\Omega] = igM\Omega \left(\delta x[\Omega] + \frac{\lambda}{8\mathcal{F}} \delta\varphi_{in} \right), \quad (7a)$$

$$\delta x[\Omega] = \frac{F_T[\Omega]}{(1/\chi - igM\Omega)} + \frac{igM\Omega}{(1/\chi - igM\Omega)} \frac{\lambda}{8\mathcal{F}} \delta\varphi_{in}. \quad (7b)$$

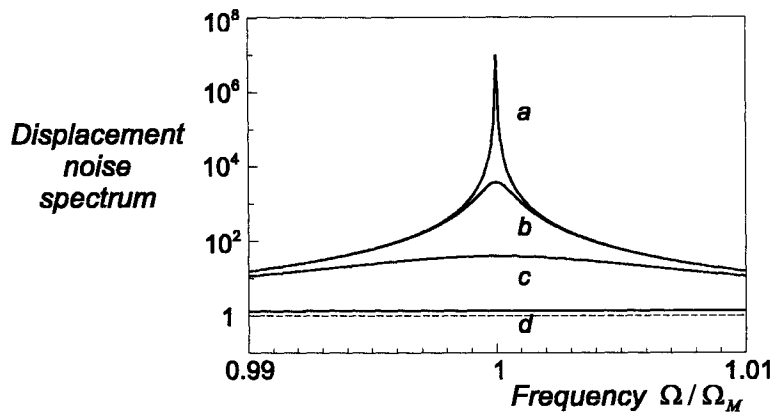


FIG. 3. Displacement noise spectrum $S_x [\Omega]$ normalized to the minimum observable displacement S_{min} . Curves (a) to (d) correspond to increasing values of the gain g (0, 50, 500 and 5000, respectively).

Figure 3 shows the theoretical evaluation of the displacement noise spectrum $S_x [\Omega]$ for different values of the gain g . The spectrum is normalized to $S_{min} = \delta x_{min}^2$ which represents the minimum observable displacement (eq. 2). For large gain, the displacement reduces to the sensitivity δx_{min} , and the displacement noise spectrum is flat and equal to S_{min} (dashed line in Figure 3).

In conclusion, we have observed the Brownian motion of internal acoustic modes of a mirror with a very high sensitivity. We have cooled the fundamental mode of the resonator using the radiation pressure exerted by an auxiliary beam, and we have observed a reduction of the temperature by a factor larger than 10. The cooling reduction is theoretically limited by the contribution of the quantum phase fluctuations to the feedback signal. The feedback signal $\delta\varphi_{out}$ can become arbitrarily small for very large gains so that the mirror displacement reproduces the quantum noise of the measurement. Note that the mirror is no longer at thermal equilibrium since the resulting displacement fluctuations correspond to a white noise related to the sensitivity of the measurement.

REFERENCES

- [1] C. Fabre, M. Pinard, S. Bourzeix, A. Heidmann, E. Giacobino and S. Reynaud, Phys. Rev. A **49**, 1337 (1994)
- [2] M. Pinard, Y. Hadjar, A. Heidmann, quant-ph/9901057, to be published in Eur. Phys. J. D
- [3] K. Jacobs, P. Tombesi, M.J. Collett, D.F. Walls, Phys. Rev. A **49**, 1961 (1994)
- [4] A. Heidmann, Y. Hadjar, M. Pinard, Appl. Phys. B **64**, 173 (1997)
- [5] M.T. Jaekel, S. Reynaud, Europhys. Lett. **13**, 301 (1990)
- [6] Y. Hadjar, P.F. Cohadon, C.G. Aminoff, M. Pinard, A. Heidmann, quant-ph/9901056, to be published in Europhys. Lett.
- [7] P.F. Cohadon, A. Heidmann, M. Pinard, quant-ph/9903094

QED in the Presence of Arbitrary Kramers–Kronig Dielectric Media

Stefan Scheel and Dirk–Gunnar Welsch

*Theoretisch-Physikalisches Institut, Friedrich-Schiller-Universität Jena,
Max-Wien-Platz 1, D-07743 Jena, Germany*

The phenomenological Maxwell field is quantized for arbitrarily space- and frequency-dependent complex permittivity. The formalism takes account of the Kramers–Kronig relation and the dissipation-fluctuation theorem and yields the fundamental equal-time commutation relations of QED. Applications to the quantum-state transformation at absorbing and amplifying four-port devices and to the spontaneous decay of an excited atom in the presence of absorbing dielectric bodies are discussed.

I. INTRODUCTION

Quantization of the electromagnetic field in dispersive and absorbing dielectrics requires a concept which is consistent with both the principle of causality and the dissipation-fluctuation theorem and which necessarily yields the fundamental equal-time commutation relations of QED. In order to achieve this goal, several approaches are possible. The microscopic approach starts from the exact Hamiltonian of the coupled radiation–matter system and integrates out, in some approximation, the matter degrees of freedom to obtain an effective theory for the electromagnetic field. Since the procedure can hardly be performed for arbitrary media, simplified model systems are considered. A typical example is the use of harmonic-oscillator models for the matter polarization and the reservoir variables together with the assumption of bilinear couplings [1]. In the macroscopic approach, the phenomenological Maxwell theory, in which the effect of the medium is described in terms of constitutive equations, is quantized. Since this concept does not use any microscopic description of the medium, it has the benefit of being universally valid, at least as long as the medium can be regarded as a continuum.

Here we study the problem of quantization of the phenomenological Maxwell theory for nonmagnetic but otherwise arbitrary linear media at rest, starting from the classical Green function integral representation of the electromagnetic field. The method was first established for one-dimensional systems [2] and simple three-dimensional systems [3] and later generalized to arbitrary inhomogeneous dielectrics described in terms of a spatially varying permittivity which is a complex function of frequency [4].

In Sec. II we briefly review the quantization scheme and give an extension to anisotropic dielectrics (including amplifying media), which complete the class of nonmagnetic (local) media. In Sec. III we apply the method to the problem of quantum-state transformation at absorbing and amplifying four-port devices, and in Sec. IV we give an application to the problem of spontaneous decay of an excited atom in the presence of absorbing bodies.

II. QUANTIZATION SCHEME

Let us first consider the electromagnetic field in isotropic dielectrics without external sources. The (operator-valued) phenomenological Maxwell equations in the temporal Fourier space read

$$\nabla \cdot \hat{\mathbf{B}}(\mathbf{r}, \omega) = 0, \quad \nabla \times \hat{\mathbf{E}}(\mathbf{r}, \omega) = i\omega \hat{\mathbf{B}}(\mathbf{r}, \omega), \quad (1)$$

$$\nabla \cdot [\epsilon_0 \epsilon(\mathbf{r}, \omega) \hat{\mathbf{E}}(\mathbf{r}, \omega)] = \hat{\rho}(\mathbf{r}, \omega), \quad \nabla \times \hat{\mathbf{B}}(\mathbf{r}, \omega) = -i(\omega/c^2) \epsilon(\mathbf{r}, \omega) \hat{\mathbf{E}}(\mathbf{r}, \omega) + \mu_0 \hat{\mathbf{j}}(\mathbf{r}, \omega). \quad (2)$$

From the principle of causality it follows that the complex-valued permittivity $\epsilon(\mathbf{r}, \omega) = \epsilon_R(\mathbf{r}, \omega) + i\epsilon_I(\mathbf{r}, \omega)$ satisfies the Kramers–Kronig relations. Hence, it is a holomorphic function in the upper complex frequency plane without poles and zeros and approaches unity in the high-frequency limit. Consistency with the dissipation–fluctuation theorem requires the introduction of an operator noise charge density $\hat{\rho}(\mathbf{r}, \omega)$ and an operator noise current density $\hat{\mathbf{j}}(\mathbf{r}, \omega)$ satisfying the equation of continuity. Quantization is performed by introducing bosonic vector fields $\hat{\mathbf{f}}(\mathbf{r}, \omega)$,

$$\hat{\mathbf{j}}(\mathbf{r}, \omega) = \omega \sqrt{\hbar \epsilon_0 \epsilon_I(\mathbf{r}, \omega) / \pi} \hat{\mathbf{f}}(\mathbf{r}, \omega), \quad (3)$$

which play the role of the fundamental variables of the theory. All relevant operators of the system such as the electric and magnetic fields and the matter polarization can be constructed in terms of them. For example, the operator of the electric field is given by the integral representation

$$\hat{E}_k(\mathbf{r}) = i\mu_0 \sqrt{\hbar \epsilon_0 / \pi} \int_0^\infty d\omega \int d^3 \mathbf{r}' \omega^2 \sqrt{\epsilon_I(\mathbf{r}', \omega)} G_{kk'}(\mathbf{r}, \mathbf{r}', \omega) \hat{f}_{k'}(\mathbf{r}', \omega) + \text{H.c.}, \quad (4)$$

with $G_{kk'}(\mathbf{r}, \mathbf{r}', \omega)$ being the classical dyadic Green function. This representation together with the fundamental relation

$$\int d^3 \mathbf{s} (\omega/c)^2 \epsilon_I(\mathbf{s}, \omega) G_{ik}(\mathbf{r}, \mathbf{s}, \omega) G_{jk}^*(\mathbf{r}', \mathbf{s}, \omega) = \text{Im} G_{ij}(\mathbf{r}, \mathbf{r}', \omega), \quad (5)$$

which follows directly from the partial differential equation for the dyadic Green function, leads to the equal-time commutation relation [3]

$$[\epsilon_0 \hat{E}_k(\mathbf{r}), \hat{B}_l(\mathbf{r}')] = (\hbar/\pi) \epsilon_{lmk'} \partial_m' \int_{-\infty}^\infty d\omega (\omega/c^2) G_{kk'}(\mathbf{r}, \mathbf{r}', \omega). \quad (6)$$

Using general properties of the Green function, it can be shown [4] that Eq. (4) reduces, for arbitrary $\epsilon(\mathbf{r}, \omega)$, to the well-known QED commutation relation

$$[\epsilon_0 \hat{E}_k(\mathbf{r}), \hat{B}_l(\mathbf{r}')] = i\hbar \epsilon_{klm} \partial_m' \delta(\mathbf{r} - \mathbf{r}') \quad (7)$$

The extension to anisotropic and amplifying media is straightforward, since we may assume the medium to be reciprocal, so that the permittivity tensor $\epsilon_{ij}(\mathbf{r}, \omega)$ is necessarily symmetric. In particular, $\epsilon_{ij}(\mathbf{r}, \omega)$ can be diagonalized by an orthogonal matrix $O_{kl}(\mathbf{r}, \omega)$. With regard to amplifying media, we note that amplification requires the role of the noise creation and annihilation operators to be exchanged. The calculation then shows that the fundamental relation (3) can be generalized to

$$\hat{j}_i(\mathbf{r}, \omega) = \omega \sqrt{\hbar \epsilon_0 / \pi} [\gamma_{ij}^-(\mathbf{r}, \omega) \hat{f}_j(\mathbf{r}, \omega) + \gamma_{ij}^+(\mathbf{r}, \omega) \hat{f}_j^\dagger(\mathbf{r}, \omega)], \quad (8)$$

with

$$\gamma_{ij}^\mp(\mathbf{r}, \omega) = O_{ik}(\mathbf{r}, \omega) \sqrt{|\tilde{\epsilon}_{kl I}(\mathbf{r}, \omega)|} O_{lj}^{-1}(\mathbf{r}, \omega) \Theta[\pm \tilde{\epsilon}_{kl I}(\mathbf{r}, \omega)], \quad (9)$$

$$\tilde{\epsilon}_{ij I}(\mathbf{r}, \omega) = \delta_{ij} \epsilon_I^{(i)}(\mathbf{r}, \omega) = O_{ik}^{-1}(\mathbf{r}, \omega) \epsilon_{kl I}(\mathbf{r}, \omega) O_{lj}(\mathbf{r}, \omega). \quad (10)$$

Equation (8) completes the quantization scheme for the electromagnetic field in arbitrary linear, nonmagnetic (local) media.

III. QUANTUM-STATE TRANSFORMATIONS BY ABSORBING AND AMPLIFYING FOUR-PORT DEVICES

Let us first apply the theory to the problem of quantum-state transformation at absorbing and amplifying four-port devices such as beam-splitter-like devices. Specifying the formulas to the one-dimensional case for simplicity and rewriting the integral representation (7) in terms of amplitude operators $\hat{a}_j(\omega)$ and $\hat{b}_j(\omega)$ for the incoming and outgoing waves ($j=1, 2$), the action of an absorbing device can be given by the (vector) operator transformation

$$\hat{\mathbf{b}}(\omega) = \mathbf{T}(\omega)\hat{\mathbf{a}}(\omega) + \mathbf{A}(\omega)\hat{\mathbf{g}}(\omega), \quad (11)$$

where $\hat{g}_j(\omega)$ are the operators of device excitations and $\mathbf{T}(\omega)$ and $\mathbf{A}(\omega)$ are the characteristic transformation and absorption matrices of the device given in terms of its complex refractive-index profile [5]. Note that $\hat{a}_j(\omega)$ and $\hat{g}_j(\omega)$ are independent bosonic operators. Further, it can be shown that the relation $\mathbf{T}(\omega)\mathbf{T}^+(\omega) + \mathbf{A}(\omega)\mathbf{A}^+(\omega) = \mathbf{I}$ is satisfied, which ensures bosonic commutation relations for $\hat{b}_j(\omega)$. In order to construct the unitary transformation, we introduce some auxiliary (bosonic) device variables $\hat{h}_j(\omega)$, combine the two-vectors $\hat{\mathbf{a}}(\omega)$ and $\hat{\mathbf{g}}(\omega)$ to the four-vector $\hat{\boldsymbol{\alpha}}(\omega)$, and accordingly $\hat{\mathbf{b}}(\omega)$ and $\hat{\mathbf{h}}(\omega)$ to $\hat{\boldsymbol{\beta}}(\omega)$. The four-vectors $\hat{\boldsymbol{\alpha}}(\omega)$ and $\hat{\boldsymbol{\beta}}(\omega)$ are related to each other as

$$\hat{\boldsymbol{\beta}}(\omega) = \boldsymbol{\Lambda}(\omega)\hat{\boldsymbol{\alpha}}(\omega), \quad \boldsymbol{\Lambda}(\omega) \in \text{SU}(4). \quad (12)$$

Introducing the positive Hermitian matrices $\mathbf{C}(\omega) = \sqrt{\mathbf{T}(\omega)\mathbf{T}^+(\omega)}$ and $\mathbf{S}(\omega) = \sqrt{\mathbf{A}(\omega)\mathbf{A}^+(\omega)}$, the four-matrix $\boldsymbol{\Lambda}(\omega)$ can be written in the form [6]

$$\boldsymbol{\Lambda}(\omega) = \begin{pmatrix} \mathbf{T}(\omega) & \mathbf{A}(\omega) \\ -\lambda\mathbf{S}(\omega)\mathbf{C}^{-1}(\omega)\mathbf{T}(\omega) & \mathbf{C}(\omega)\mathbf{S}^{-1}(\omega)\mathbf{A}(\omega) \end{pmatrix} \quad (13)$$

($\lambda=1$). The input-output relation (12) can then be expressed in terms of a unitary operator transformation $\hat{\boldsymbol{\beta}}(\omega) = \hat{U}^\dagger \hat{\boldsymbol{\alpha}}(\omega) \hat{U}$. Equivalently, \hat{U} can be applied to the density operator of the input quantum state $\hat{\rho}_{\text{in}}[\hat{\boldsymbol{\alpha}}(\omega), \hat{\boldsymbol{\alpha}}^\dagger(\omega)]$, and tracing over the device variables yields

$$\hat{\rho}_{\text{out}}^{(\text{Field})} = \text{Tr}^{(\text{Device})} \left\{ \hat{\rho}_{\text{in}} \left[\boldsymbol{\Lambda}^+(\omega)\hat{\boldsymbol{\alpha}}(\omega), \boldsymbol{\Lambda}^T(\omega)\hat{\boldsymbol{\alpha}}^\dagger(\omega) \right] \right\}. \quad (14)$$

To give an example, let us consider the case when one input channel is prepared in an n -photon Fock state and the device and the second input channel are left in vacuum, i.e., $\hat{\rho}_{\text{in}} = |n, 0, 0, 0\rangle\langle n, 0, 0, 0|$. Applying Eq. (14), after some algebra we derive for the density operator of the i -th output channel

$$\hat{\rho}_{\text{out},i}^{(\text{Field})} = \sum_{k=0}^n \binom{n}{k} |T_{i1}|^{2k} (1 - |T_{i1}|^2)^{n-k} |k\rangle\langle k|. \quad (15)$$

Next, let us assume that the two input channels are prepared in single-photon Fock states, i.e., $\hat{\rho}_{\text{in}} = |1, 1, 0, 0\rangle\langle 1, 1, 0, 0|$. We derive for the density operator of the i -th output channel

$$\begin{aligned} \hat{\rho}_{\text{out},i}^{(\text{Field})} &= \left[1 - |T_{i1}|^2(1 - |T_{i2}|^2) - |T_{i2}|^2(1 - |T_{i1}|^2) \right] |0\rangle\langle 0| \\ &+ \left(|T_{i1}|^2 + |T_{i2}|^2 - 4|T_{i1}|^2|T_{i2}|^2 \right) |1\rangle\langle 1| + 2|T_{i1}|^2|T_{i2}|^2 |2\rangle\langle 2|. \end{aligned} \quad (16)$$

The extension to amplifying devices is straightforward. One has to replace the annihilation operators $\hat{g}_j(\omega)$ in Eq. (11) by the corresponding creation operators $\hat{g}_j^\dagger(\omega)$. This leads again to an input-output relation of the form (12) but with $\lambda = -1$ in Eq. (13), the matrix $\boldsymbol{\Lambda}(\omega)$ being now an element of the noncompact group $\text{SU}(2,2)$.

IV. SPONTANEOUS DECAY NEAR DIELECTRIC BODIES

Spontaneous decay of an excited atom is a process that is directly related to the quantum vacuum noise, which in the presence of absorbing bodies is drastically changed and so is the rate of spontaneous decay, because of the additional noise introduced by absorption. To study a radiating (two-level) atom in the presence of dielectric media, we start from the following Hamiltonian in dipole and rotating wave approximations:

$$\hat{H} = \int d^3\mathbf{r} \int_0^\infty d\omega \hbar\omega \hat{\mathbf{f}}^\dagger(\mathbf{r}, \omega) \cdot \hat{\mathbf{f}}(\mathbf{r}, \omega) + \sum_{\alpha=1}^2 \hbar\omega_\alpha \hat{A}_{\alpha\alpha} - [i\omega_{21} \hat{A}_{21} \hat{\mathbf{A}}^{(+)}(\mathbf{r}_A) \cdot \mathbf{d}_{21} + \text{H.c.}] . \quad (17)$$

Here, the atomic operators $\hat{A}_{\alpha\alpha'} = |\alpha\rangle\langle\alpha'|$ are introduced, and $\hat{\mathbf{A}}^{(+)}(\mathbf{r}_A)$ is the (positive-frequency part of the) vector potential (in Weyl gauge) at the position of the atom. Note that the first term in Eq. (17) is the (diagonal) Hamiltonian of the system that consists of the electromagnetic field and the medium (including the dissipative system) and is expressed in terms of the fundamental variables $\hat{\mathbf{f}}(\mathbf{r}, \omega)$. Solving the resulting equations of motion in Markov approximation, the well-known Bloch equations for the atom are recognized, where the decay rate is given by [7]

$$\Gamma = 2\omega_A^2 \mu_k \mu_{k'} / (\hbar\epsilon_0 c^2) \text{Im} G_{kk'}(\mathbf{r}_A, \mathbf{r}_A, \omega_A) \quad (18)$$

$[\mu_k \equiv (d_{21})_k, \omega_A \equiv \omega_{21}]$. Note that from Eq. (4) together with Eq. (5) it follows that

$$\text{Im} G_{kk'}(\mathbf{r}, \mathbf{r}', \omega) \delta(\omega - \omega') = \pi\epsilon_0 c^2 / (\hbar\omega^2) \langle 0 | [\hat{\underline{E}}_k(\mathbf{r}, \omega), \hat{\underline{E}}_{k'}^\dagger(\mathbf{r}', \omega')] | 0 \rangle \quad (19)$$

in full agreement with the dissipation-fluctuation theorem.

Equation (18) is valid for any absorbing dielectric body. For example, when the atom is sufficiently near to an absorbing planar interface, then purely nonradiative decay is observed, with [8]

$$\Gamma = \Gamma_0 \left(1 + \frac{\mu_z^2}{\mu^2} \right) \frac{\epsilon_I(\omega_A)}{|\epsilon(\omega_A) + 1|^2} \frac{3c^3}{(2\omega_A z)^3}, \quad (20)$$

where z is the distance between the atom and the interface, and Γ_0 is the spontaneous emission rate in free space (for a guest atom embedded in an absorbing dielectric, see [7]).

Acknowledgement

This work was supported by the Deutsche Forschungsgemeinschaft.

-
- [1] B. Huttner and S.M. Barnett, Phys. Rev. A **46**, 4306 (1992).
 - [2] T. Gruner and D.-G. Welsch, Phys. Rev. A **53**, 1818 (1996).
 - [3] Ho Trung Dung, L. Knöll, and D.-G. Welsch, Phys. Rev. A **57**, 3931 (1998).
 - [4] S. Scheel, L. Knöll, and D.-G. Welsch, Phys. Rev. A **58**, 700 (1998).
 - [5] T. Gruner and D.-G. Welsch, Phys. Rev. A **54**, 1661 (1996).
 - [6] L. Knöll, S. Scheel, E. Schmidt, D.-G. Welsch, and A.V. Chizhov, Phys. Rev. A **59**, 4716 (1999).
 - [7] S. Scheel, L. Knöll, D.-G. Welsch, and S.M. Barnett, Phys. Rev. A **60** (1999), in press; S. Scheel, L. Knöll, and D.-G. Welsch, submitted to Phys. Rev. A. (quant-ph/9904015).
 - [8] S. Scheel, L. Knöll, and D.-G. Welsch, Acta Phys. Slov. **49** (special issue), 585 (1999).

Squashed States of Light and Atomic Line-Narrowing

H. M. Wiseman

*Centre for Laser Science, The Department of Physics,
The University of Queensland, Queensland 4072 Australia.*

Feedback can reduce the fluctuations in one quadrature of an in-loop field without increasing those in the other. I show that a two-level atom coupled to the in-loop light responds to broad-band “squashed” fluctuations, resulting in line-narrowing. For a finite feedback bandwidth the effect is reduced. With perfect broadband squeezing in one quadrature and perfect broadband squashing in the other, atomic decay can be completely suppressed.

I. INTRODUCTION

Squeezed states of light are nonclassical. The foremost consequence of this is that they can produce a homodyne photocurrent having a noise level below the shot-noise limit.

There is, however, a simple way to produce a sub-shot-noise photocurrent without squeezed light: modulating the light incident on the photodetector by a current originating from that very detector. This was first observed [1,2] around the same time as the first incontestable observation of squeezing [3].

The sub-shot noise spectrum of an in-loop photocurrent is not regarded as evidence for squeezing for two reasons. First, the two-time commutation relations for an in-loop field are not those of a free field [4]. Second, attempts to remove some of the supposedly low-noise light by a beam splitter yields only above shot-noise light, as verified experimentally [1,5].

Because of these differences, the presence of a sub-shot noise photocurrent spectrum for in-loop light has by and large been omitted from discussions of squeezing. However, recent results have shown that the in-loop noise suppression (called “squashing” in Ref. [6]) can sometimes be useful for the same reasons that squeezing is [6–8]. In particular, I recently showed [7,8] that a two-level atom coupled to the in-loop field can exhibit linewidth narrowing exactly analogous to that produced by squeezed light [9].

In this paper I present the results from Refs. [7,8], and also, for the first time, the in-loop photocurrent noise spectrum and the effect of non-Markovian feedback on the line-narrowing. To begin I discuss conventional squeezing and its effect on an atom.

II. SQUEEZING

Consider first a single-mode field described by annihilation and creation operators satisfying $[a, a^\dagger] = 1$, so that $a^\dagger a$ is the photon number. This field has quadrature operators $x = a + a^\dagger$ and $y = -ia + ia^\dagger$ limited by the Heisenberg uncertainty relation $V_x V_y \geq |[x, y]/2|^2 = 1$. For coherent states $V_x = V_y = 1$, while for squeezed states we have, for example, $V_x < 1$ so that $V_y > 1$.

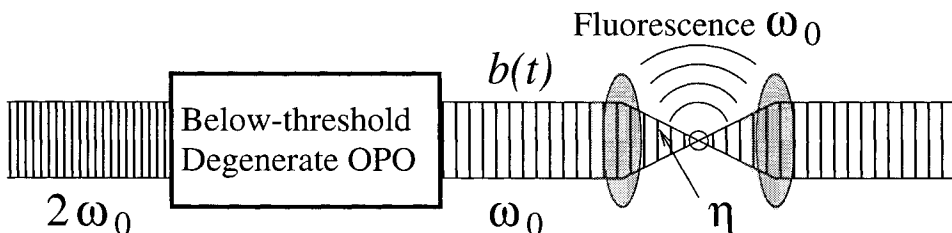
Analogous properties can be defined for a continuum field described by $b(t), b^\dagger(t)$ such that $[b(t), b^\dagger(t')] = \delta(t - t')$ so that $b^\dagger b$ is the photon flux. This field has quadrature operators $X(t) = b(t) + b^\dagger(t)$ and $Y(t) = -ib(t) + ib^\dagger(t)$, limited by the uncertainty relation $S^X(\omega)S^Y(\omega) \geq 1$, where the quadrature noise spectrum is

$$S^X(\omega) = \langle \tilde{X}_{ss}(\omega) X_{ss} \rangle - \langle \tilde{X}_{ss}(\omega) \rangle \langle X_{ss} \rangle. \quad (1)$$

Coherent states of the continuum field have, for all ω , $S^X(\omega) = S^Y(\omega) = 1$, the shot-noise limit. Squeezed states can have, for some ω , $S^X(\omega) < 1$ so that $S^Y(\omega) > 1$.

III. ATOM IN SQUEEZED LIGHT

Broad-band squeezed light has, for all ω inside some “broad” bandwidth B , $S^X(\omega) = \bar{S}^X$ and $S^Y(\omega) = \bar{S}^Y$. This is a good approximation to the output of a below-threshold degenerate optical parametric oscillator in the bad-cavity limit. Consider a resonant 2-level atom with decay rate $\gamma \ll B$. Let $b(t)$ be mode-matched into the atom with efficiency η :



The Hamiltonian coupling the atom to the squeezed field b and the vacuum field ν is

$$H = \sqrt{\gamma} \sigma^\dagger \left[\sqrt{\eta} b(t) + \sqrt{1 - \eta} \nu(t) \right] + \text{H.c.}$$

From this model, Gardiner [9] showed that the atomic dynamics are

$$\frac{\partial}{\partial t} \langle \sigma_x \rangle = -\gamma_x \langle \sigma_x \rangle; \quad \frac{\partial}{\partial t} \langle \sigma_y \rangle = -\gamma_y \langle \sigma_y \rangle; \quad \frac{\partial}{\partial t} \langle \sigma_z \rangle = -\gamma_z \langle \sigma_z \rangle - C \quad (2)$$

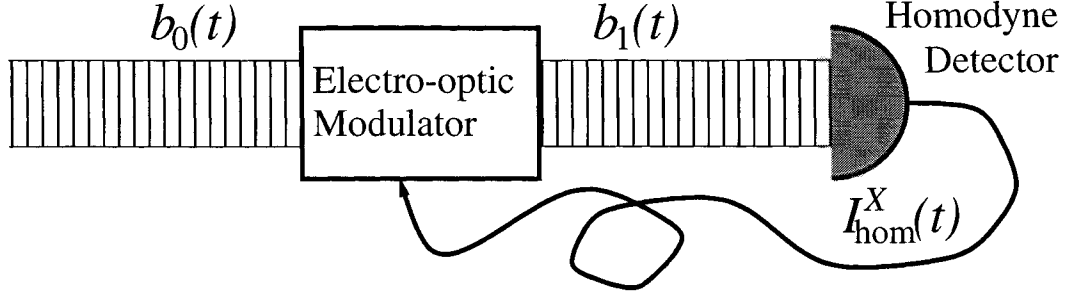
where

$$\gamma_x = \frac{1}{2} \gamma [(1 - \eta) + \eta \bar{S}_X]; \quad \gamma_y = \frac{1}{2} \gamma [(1 - \eta) + \eta \bar{S}_Y]; \quad \gamma_z = \gamma_x + \gamma_y; \quad C = 1. \quad (3)$$

That is to say, the atomic quadrature decay rates are directly proportional to level of noise in the corresponding light quadratures. In particular, for a squeezed input field the atomic decay in one quadrature can be suppressed, giving line narrowing.

IV. SQUASHING

As noted in the introduction, a sub-shot-noise spectrum can also be achieved using an electro-optical feedback loop:



Here the field exiting the modulator is related to that entering by $b_1(t) = b_0(t) + \frac{1}{2}\chi(t)$, where added coherent field is

$$\chi(t) = \int_{\tau}^{\infty} g(s) I_{\text{hom}}^X(t-s) ds. \quad (4)$$

Here the homodyne photocurrent is represented (for unit-efficiency detectors) by the operator $I_{\text{hom}}^X(t) = X_1(t) = b_1(t) + b_1^\dagger(t)$.

Now let the feedback be broad-band, and say we are only interested in frequencies $\omega \ll B$, the bandwidth. This allows us to set $e^{i\omega\tau} \rightarrow 1$, $\tilde{g}(\omega) \rightarrow g$, giving

$$\tilde{X}_1(\omega) = \tilde{X}_0(\omega) + \frac{e^{i\omega\tau} \tilde{g}(\omega) \tilde{X}_0(\omega)}{1 - e^{i\omega\tau} \tilde{g}(\omega)} \rightarrow \frac{\tilde{X}_0(\omega)}{1 - g}. \quad (5)$$

The noise spectrum of the in-loop X quadrature is thus given by $S_1^X(\omega) = 1/(1-g)^2$, so that we have *squashing* for $g < 0$ (negative feedback). The in-loop Y quadrature is unaffected: $\tilde{Y}_1(\omega) = \tilde{Y}_0(\omega)$. Thus the usual uncertainty relations are violated: $S_1^X(\omega)S_1^Y(\omega) = 1/(1-g)^2 < 1$ for $g < 0$. That is, the phase space area has apparently been compressed (squashed), rather than merely squeezed out of one quadrature and into the other.

V. ATOM IN SQUASHED LIGHT

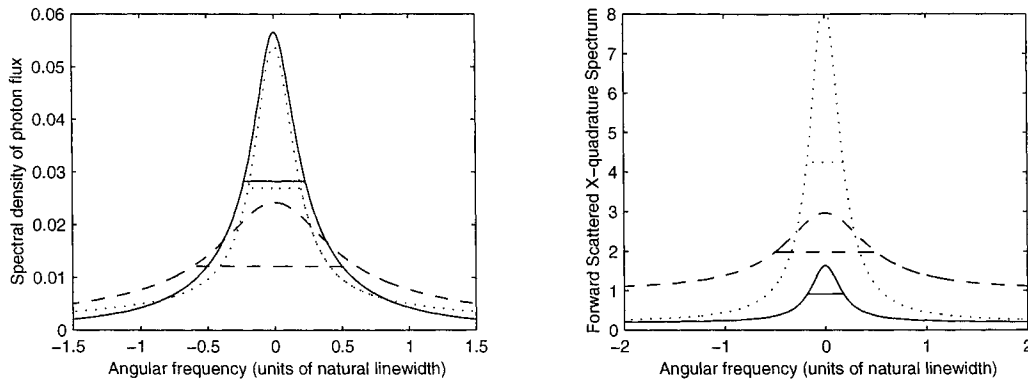
Now consider coupling an atom to the squashed field b_1 just as we earlier considered coupling it to a squeezed field. In the broad-band limit $B \gg \gamma$ the atomic dynamics are again as in Eq. (2), but with

$$\gamma_x = \frac{1}{2}\gamma[(1-\eta) + \eta/(1-g)^2]; \quad \gamma_y = \frac{1}{2}\gamma; \quad \gamma_z = \gamma_x + \gamma_y; \quad C = \gamma[1 + g\eta/(1-g)]. \quad (6)$$

That is, the atomic quadrature decay rates are *still* directly proportional to the level of high-frequency noise in the light quadratures. The reduction in the x -quadrature decay rate by squashed light can be seen as line-narrowing in the power spectrum $P(\omega)$ of resonance fluorescence into the vacuum modes [7,8], or in the in-loop photocurrent noise spectrum

$$S_2^X(\omega) = \frac{1}{(1-g)^2} \left[1 + \eta \left(1 - \frac{C^2}{\gamma_z \gamma} \right) \frac{2\gamma_x}{\gamma_x^2 + \omega^2} \right], \quad (7)$$

which goes to $1/(1-g)^2$ at high frequencies. Both $P(\omega)$ and $S_2^X(\omega)$ are shown below for $\eta = 0.8$ and squashing $\bar{S}^X = 0.2$, $\bar{S}^Y = 1$. The analogous results for squeezing ($\bar{S}_X = 0.2$, $\bar{S}_Y = 5$, \dots) and for classical noise ($\bar{S}_X = 1$, $\bar{S}_Y = 5$, $--$) are also shown.



VI. EXTENSIONS

The effect of non-unit efficiency photodetectors was considered in Refs. [7,8] and I will not recapitulate that here. The other obvious effect to consider is when the feedback is not infinitely broad band. Assuming nevertheless that $\epsilon = \gamma/B$ is small, the perturbation approach for finite bandwidth feedback in Ref. [10] is applicable. The form of the dynamics is again as in Eq. (2), but the changed parameters (indicated by the prime) are

$$\gamma'_x = \gamma_x - \frac{g\eta}{1-g} \left(\frac{\gamma}{2} - C \right) \epsilon; \quad \gamma'_z = \gamma_z + \frac{g\eta}{1-g} \frac{\gamma}{2} \epsilon; \quad C' = C - \frac{g\eta}{1-g} (\gamma_x - C) \epsilon \quad (8)$$

In the limit of large squashing, $g \rightarrow -\infty$, it is evident that $\gamma'_x = \gamma_x + \gamma\eta(\eta - 1/2)\epsilon$ so that for $\eta > 1/2$ there is less linewidth narrowing than in the broad-band case.

In addition to considering non-Markovian feedback, there are some obvious extensions of the work presented here. For example, it is possible to squash light which is already squeezed in the other quadrature. As shown in Ref. [8], in the limit where the light is perfectly squeezed in one quadrature and perfectly squashed in the other, the atomic decay can be completely inhibited. That is, the atom would remain frozen in its initial state. Another generalization would be to consider squashed cross-correlations between two beams of light, and the effect of this on a three level atom. This will be a topic for future work, as will be the effect of a finite bandwidth in the non-perturbative limit.

- [1] J.G. Walker and E. Jakeman, Proc. Soc. Photo-Opt. Instrum. Eng. **492**, 274 (1985).
- [2] S. Machida and Y. Yamamoto, Opt. Commun. **57**, 290 (1986).
- [3] R.E. Slusher *et al.*, Phys. Rev. Lett. **55**, 2409 (1985).
- [4] J.M. Shapiro *et al.*, J. Opt. Soc. Am. B **4**, 1604 (1987).
- [5] Y. Yamamoto, N. Imoto and S. Machida, Phys. Rev. A **33**, 3243 (1986).
- [6] B.C. Buchler *et al.* Optics Letters **24**, 259 (1999).
- [7] H.M. Wiseman, Phys. Rev. Lett. **81**, 3840 (1998).
- [8] H.M. Wiseman, to be published in J.E.O.S. B (1999).
- [9] C.W. Gardiner, Phys. Rev. Lett. **56**, 1917 (1986).
- [10] H.M. Wiseman, Phys. Rev. A **49**, 2133 (1994).

Quantum beats in the fluorescence intensity of a three-level atom driven by a detuned squeezed vacuum

Z. Ficek^{1,2}

¹*Department of Physics, The University of Queensland, Brisbane, Australia 4072*

²*Department of Applied Mathematics and Theoretical Physics, The Queen's University of
Belfast, Belfast BT7 1NN, Northern Ireland*

Abstract

Excitation of three-level atoms in a cascade configuration with a detuned squeezed vacuum results in quantum beats in the intensity of the emitted fluorescence field. We show that the quantum beats are not present for a classically correlated field and persist even for very small coupling efficiencies of the squeezed field with the atoms.

The interaction of squeezed light with atoms leads to novel physical effects not obtainable with conventional radiation sources [1]. The origin of these effects is in quantum correlations between pairs of photons in the squeezed field which reduce quantum fluctuations in one quadrature component of the field below the ordinary vacuum level. Since the reduction of the fluctuations is a nonclassical effect, it is obvious that this feature will lead to intrinsically quantum effects in the atom-squeezed field interaction.

In contrast to the significant theoretical advances in this area [1,2], experimental work has proven to be extremely difficult with only one experiment so far demonstrating a purely non-classical effect in the spectroscopy with squeezed light [3a]. The experiment has demon-

strated the linear dependence on intensity of the population of the upper state of a three-level cascade atom, which is in contrast to the quadratic dependence with classical field. Additional attempts to observe squeezing effects in quantum interference [3b], and spontaneous decay of the atomic polarization [3c] have not convincingly demonstrated that these effects arise from the nonclassical character of the squeezed field.

A general difficulty in the experimental realisation of the predicted nonclassical effects is their strong dependence on the coupling efficiency η of the squeezed field with the atom. In the experiments [3] the squeezed field was coupled only to a small fraction of the modes surrounding the atom and the estimated coupling efficiency η was very small ($\eta \approx 0.05$). For such small values of η most of the predicted nonclassical effects disappears [1]. In the experiment [3a] the nonclassical linear dependence on intensity of the population was observed in accordance with the theoretical prediction [2] that the population changes linearly with intensity independent of η .

In this paper, we show that the time evolution of the population of the upper state of a cascade three-level atom driven by a detuned squeezed vacuum can exhibit quantum beats which are not sensitive to η and are absent for a classically correlated squeezed field.

We consider a three-level atom in the cascade configuration with the ground state $|1\rangle$, the intermediate state $|2\rangle$ and the upper state $|3\rangle$ driven by a squeezed vacuum field whose the carrier frequency ω_s is detuned from the average atomic transition frequency $\omega_0 = (\omega_1 + \omega_2)/2$ by $\Delta = \omega_0 - \omega_s$. The bandwidth of the squeezed field is assumed to be much larger than the atomic spontaneous emission rates Γ_3 and Γ_2 of the excited levels $|i\rangle$ ($i = 3, 2$). In this case the time evolution of the atomic populations is given by the following set of coupled equations of motion [2]

$$\begin{aligned}
\dot{\rho}_{33} &= -(\tilde{N} + 1)\Gamma_3\rho_{33} + \tilde{N}\Gamma_3\rho_{22} - \frac{1}{2}|\tilde{M}|\Gamma_{32}(\rho_{13}e^{i\phi_s} + \rho_{31}e^{-i\phi_s}), \\
\dot{\rho}_{22} &= \tilde{N}\Gamma_2 - [\tilde{N}\Gamma_3 + (2\tilde{N} + 1)\Gamma_2]\rho_{22} + [(\tilde{N} + 1)\Gamma_3 - \tilde{N}\Gamma_2]\rho_{33} \\
&\quad + |\tilde{M}|\Gamma_{32}(\rho_{13}e^{i\phi_s} + \rho_{31}e^{-i\phi_s}), \\
\dot{\rho}_{31} &= (\dot{\rho}_{13})^* = -\frac{1}{2}\Gamma_{32}\tilde{M} - \left\{ \frac{1}{2}[\tilde{N}\Gamma_2 + (\tilde{N} + 1)\Gamma_3] - 2i\Delta \right\} \tilde{\rho}_{31} + \frac{3}{2}\Gamma_{32}\tilde{M}\rho_{22},
\end{aligned} \tag{1}$$

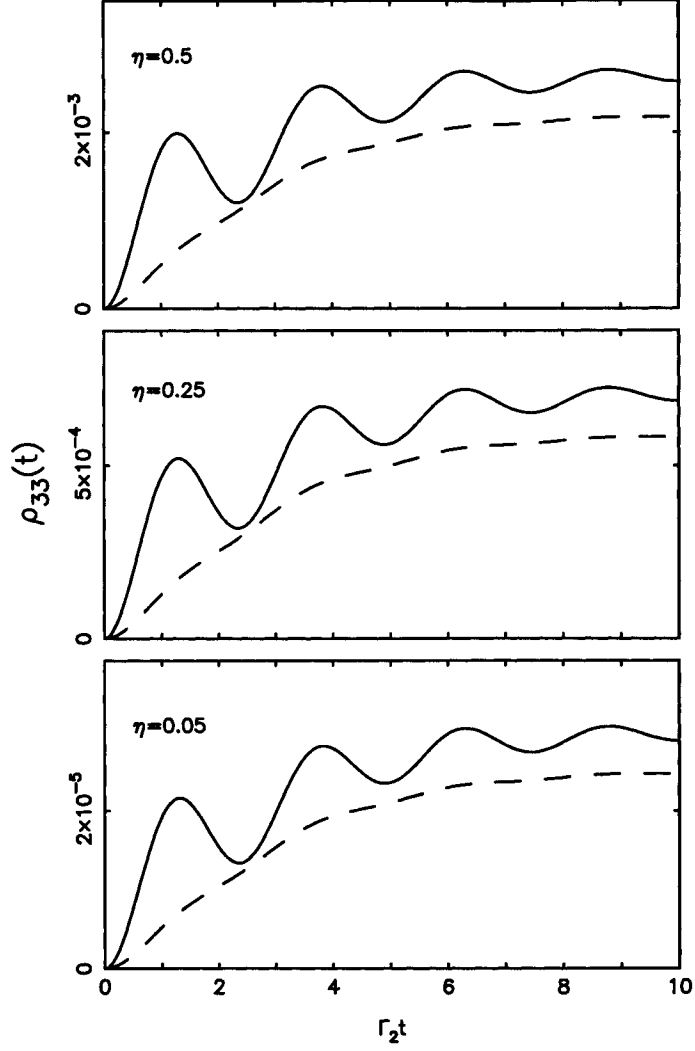


FIG. 1. Time evolution of the population $\rho_{33}(t)$ for $N = 0.1, \Gamma_3/\Gamma_2 = 0.5, \Delta = 2.5\Gamma_2$, $|M| = \sqrt{N(N+1)}$ (solid line), $|M| = N$ (dashed line), and different η .

where $\Gamma_{32} = \sqrt{\Gamma_3\Gamma_2}$, $\tilde{N} = \eta N$, $\tilde{M} = \eta M$ and the parameters N and $M = |M|e^{i\phi_s}$ characterize squeezing intensity and the magnitude of the two-mode correlations, respectively, and ϕ_s is the squeezing phase. For classically correlated fields the squeezing parameters N and $|M|$ are related by the inequality $|M| \leq N$, whereas for quantum fields $|M| \leq \sqrt{N(N+1)}$.

We will show that the excess of the correlations over the maximum classical value $|M| = N$ can produce dramatic changes in the time evolution of the population $\rho_{33}(t)$, which can be regarded as nonclassical. In order to analyse the time evolution of the atomic population, we write the set of equations (1) in a matrix form and solve it for $\rho_{33}(t)$ by the matrix

inversion. In Fig. 1, we plot the population for three different values of η and two values of $|M|$: $|M| = \sqrt{N(N+1)}$ corresponding to the maximum quantum squeezing and $|M| = N$ of the maximum classical squeezing. When the atom is driven by a quantum squeezed vacuum, the time evolution exhibits a sinusoidal modulation (quantum beats). However, the classical analog does not show quantum beats. The lack of quantum beats for the classical squeezed field can be explained by the fact that for $|M| = N$ the two-photon correlations are much weaker than for the corresponding quantum field. In Fig. 1, we plot the population for $N = 0.1$. In this case $|M| = 0.1$ for the classical field, whereas $|M| = 0.332$ for the quantum field.

Moreover, it is seen from Fig. 1 that the quantum beats are not affected by η . A small coupling efficiency diminishes only the value of the population in the state $|3\rangle$. The parameter values $N = 0.1$, $\Gamma_3/\Gamma_2 = 0.5$ and $\eta = 0.05$ correspond to those in the experiments [3], and therefore the quantum beats are experimentally accessible with the present technology. It should be possible to observe this effect without the necessity to squeeze a majority of the vacuum modes coupled to the atom.

- [1] A.S. Parkins, in *Modern Nonlinear Optics, Part II*, eds. M. Evans and S. Kielich (Wiley, New York, 1993) p. 607;
For a recent review on spectroscopy with squeezed light fields see: B.J. Dalton, Z. Ficek and S. Swain, *J. Mod. Opt.* **46**, 379 (1999).
- [2] Z. Ficek and P.D. Drummond, *Phys. Rev. A* **43**, 6247 (1991); **43**, 6258 (1991); *Physics Today* **50**, 34 (1997).
- [3] (a) N.Ph. Georgiades, E.S. Polzik, K. Edamatsu, H.J. Kimble and A.S. Parkins, *Phys. Rev. Lett.* **75**, 3426 (1995); (b) N.Ph. Georgiades, E.S. Polzik and H.J. Kimble, *Phys. Rev. A* **55**, R1605 (1997); **59**, 676 (1999); (c) Q.A. Turchette, N.Ph. Georgiades, C.J. Hood, H.J. Kimble and A.S. Parkins, *Phys. Rev. A* **58**, 4056 (1998).

Micromaser Atomic Correlations beyond the RWA

F. De Zela

*Pontificia Universidad Católica del Perú, Dpto. de Ciencias -
Sección Física*

Ap. 1761, Lima -Perú, e-mail: fdezela@fisica.pucp.edu.pe

Abstract

We study the possibility of using the micromaser as a tool for testing the validity of the rotating wave approximation (RWA). We predict that the so-called counter-rotating terms, which are neglected within the RWA, can give rise to physically observable effects for the parameter range accessible to current experiments. We focus on atomic correlations, as the atoms exiting the micromaser cavity constitute the only physical entity that can be subjected to measurements. Although the predictions we have made do not include the less than 100% efficiency of the atom detectors, they should serve as a first indication of the capability of the micromaser for testing the range of validity of the Jaynes-Cummings model in the microwave domain.

I. INTRODUCTION

It has been generally assumed that the Jaynes-Cummings model correctly describes the atom-photon interaction in a micromaser cavity. Any departure from the RWA is expected to occur well beyond the range of parameter values typical of current micromaser experiments. On the other hand, the range of validity of the RWA still remains unclear and it has been the subject of recent theoretical investigations [1]. The so-called counter-rotating terms, which are neglected within the RWA, could give rise to physically observable effects like the Bloch-Siegert shift or high-frequency modulation of Rabi oscillations. Early studies assumed that such effects could be experimentally observed by going from the optical to the microwave domain. However, in spite of having developed the micromaser as a tool for exploring such a domain, no attempts were made, to our knowledge, to go beyond the RWA in the interpretation and planning of micromaser experiments.

In a previous work [2], we undertook the study of the micromaser dynamics by going beyond the RWA. We calculated linewidths and second-order field correlations, comparing the standard results with those obtained beyond the RWA. Differences appeared for parameter values within the range accessible to current experiments. However, as we limited ourselves to predictions that involved the photon field only, there was no possibility for proposing a comparison between theory and experiment. The reason is that the photon field itself

cannot be sensed directly but through the exiting two-level atoms, which so play a double role: they serve to pump the maser field as well as to probe it. By measuring the state in which the atoms leave the cavity, conclusions can be drawn about the photon field. The back-action of the measurement process must be properly taken into account, as the atom and the cavity field constitute an entangled state. Atomic correlations can thus be used to study different features of the field dynamics. In the present work we have focussed on these correlations.

II. MASTER EQUATION BEYOND THE RWA

We consider the Hamiltonian given by

$$H = \hbar\omega_0\left(\frac{1}{2} + \sigma_z\right) + \hbar\omega(a^\dagger a + 1/2) + \hbar(a + a^\dagger)(g\sigma_+ + g^*\sigma_-), \quad (1)$$

for the description of the atom-field interaction. We remark that, even at resonance ($\omega_0 = \omega$), the RWA breaks down when g/ω becomes large enough. For current micromaser experiments, e. g. those performed at Garching, $g/\omega \sim 10^{-6}$, and the effects stemming from the counter-rotating terms ($a\sigma_-$ and $a^\dagger\sigma_+$), are expected to be negligible. By going slightly out of resonance ($\omega_0 - \omega \sim 1MHz$) the RWA is expected to remain valid as long as g/ω is kept small enough: a detuning of $1MHz$ is still much smaller than the hyperfine splitting of the Rb $21GHz$ transition employed in the Garching experiments, which is of -approximately- $50MHz$. However, our results indicate that this is not the case: we find differences between the predictions made within the RWA and those obtained by including the counter-rotating terms.

In the present work we deduce the master equation for the steady-state photon distribution beyond the RWA. To this end, we have employed continued-fractions techniques, as developed by Swain [3]. They allow us to go to the desired order of approximation in the relevant parameter, which in our case is g/ω . By using Swain's approach we obtain transition probabilities that the RWA do not include, such as $P_{a,n\pm 2}^{a,n}$ and $P_{b,n-1}^{a,n}$. Here, a and b mean, respectively, the upper and lower atomic energy levels, whereas n denotes the photon number. Within the RWA the only allowed transitions are $P_{a,n}^{a,n}$ and $P_{b,n+1}^{a,n}$, the so-called energy-conserving transitions. Of course, all transitions conserve energy, as long as the complete Hamiltonian is time-independent. However small, the additional transitions we have included are real, physical ones. They can give rise to -in principle - measurable effects that we predict in the present work. In general, $P_f^i(t) = |\langle f|i(t) \rangle|^2 = |\langle f|\exp(-iHt/\hbar)|i \rangle|^2$, where the transition probability $P_f^i(t)$ can be put in the form [3]: $P_f^i(t) = \left| \frac{1}{2\pi i} \oint L_f^i(E) \exp(-iEt) dE \right|^2$, with

$$L_f^i(E) = \sum_{\xi} \frac{\langle f|\xi \rangle \langle \xi|i \rangle}{E - E_{\xi}} \quad (2)$$

It is the calculation of these last quantities which can be accomplished through continued-fractions techniques. In our case, we need the quantities $L_{a,n}^{a,n}$, $L_{a,n\pm 2}^{a,n}$, $L_{b,n\pm 1}^{a,n}$, which can be readily calculated. It is then straightforward to obtain the part of the master equation for the photon field, which corresponds to the evolution of the field when it interacts with the atom. Calling $T(\tau)$ the evolution operator which results from tracing

the whole atom-field evolution operator over the atomic degrees of freedom, we have: $T(\tau)\rho = Tr_{atoms}\{\exp(-iHt/\hbar)\rho\exp(iHt/\hbar)\}$, with $\rho = \sum_{a,n;b,m} \rho_{an,bm}|a,n\rangle\langle b,m|$. As usual, we take the initial atom-field state as an uncorrelated one, with atoms entering the cavity in their excited state: $\rho = \rho_{field} \otimes |a\rangle\langle a|$. After neglecting the coherences of the resulting photon density matrix in comparison with the populations, we obtain the following relationship:

$$p_n(\tau + t_i) = P_{a,n}^{a,n+2} p_{n+2}(t_i) + P_{b,n}^{a,n+1} p_{n+1}(t_i) + [P_{a,n}^{a,n} p_n(t_i) + P_{b,n}^{a,n-1} p_{n-1}(t_i)] + P_{a,n}^{a,n-2} p_{n-2}(t_i) \quad (3)$$

Within the RWA only the terms in brackets on the r. h. s. would appear. Now, during the time when no atom is inside the cavity, the photon distribution decays as described by the well-known master equation

$$\frac{dp}{dt} = -\gamma_d L_c p, \quad (4)$$

with γ_d the cavity decay rate, and the Liouvillian operator L_c on the right being defined through

$$(L_c)_{nm} = (n_b + 1)[n\delta_{nm} - (n+1)\delta_{n+1,m}] + n_b[(n+1)\delta_{nm} - n\delta_{n-1,m}]. \quad (5)$$

Here, n_b means the average number of thermal photons. For atoms arriving at times following a Poisson distribution it is possible to describe the evolution of the photon field through a differential equation encompassing both evolutions, as given in Eqs.(3) and (4):

$$\frac{dp}{dt} = -\gamma_d L_c p + r(M-1) \equiv -\gamma_d L p, \quad (6)$$

where $L = L_c - N_{ex}(M-1)$, and with $N_{ex} \equiv r/\gamma_d$; r being the rate of atomic injection. N_{ex} means therefore the number of atoms passing the cavity in a single decay time. The matrix M is defined through the r. h. s. of Eq.(3).

III. CORRELATION LENGTHS

The photon steady-state can be obtained by putting the r. h. s. of Eq.(6) equal to zero. With such a photon distribution we can calculate different quantities related to atomic measurements [4] like, for example, the conditional probability that an excited atom decays to the ground state in the cavity. It is given by

$$P(-) = \sum_n P_{b,n}^{a,n+1} p_{n+1} + P_{b,n}^{a,n-1} p_{n-1} \quad (7)$$

With $P(+) = 1 - P(-)$ we can then calculate the average inversion $\langle s \rangle = P(+) - P(-)$. Here, $+(-)$ means the upper (lower) atomic state. If we now define $P_k(i, j)$, with i, j taking the values \pm , as the joint probability for observing a first atom in the i -state and the second in the j -state, with k unobserved atoms in-between, one can show that, besides $\langle s \rangle$ there

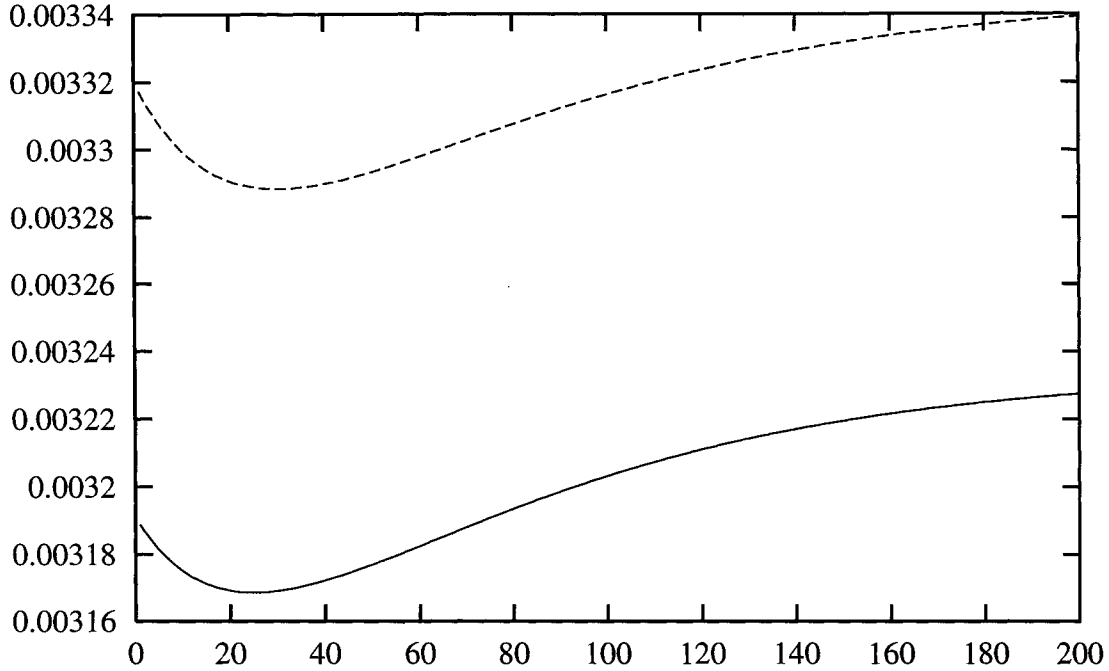


FIG. 1. Correlation length, γ_k , as a function of the number of undetected atoms. The upper line corresponds to the calculation beyond the RWA

is only one two-point correlation, namely $\langle ss \rangle_k = 1 - 4P_k(i, j)$. From it, we can define the normalized correlation function as

$$\gamma_k = \frac{\langle ss \rangle_k - \langle s \rangle^2}{1 - \langle s \rangle^2} \quad (8)$$

It is for this quantity that we have compared the results obtained with and without the RWA. Fig. 1 shows a representative example of a case where they differ from each other, even for parameter values of current experiments. The parameters are: $\omega = 21.5 \text{ GHz}$, $\omega_0 - \omega = 1 \text{ MHz}$, $g = 44 \text{ KHz}$, $n_b = 10^{-4}$, $r = 3500$, $N_{ex} = 700$, $\tau = 80 \mu\text{sec}$.

The differences between the γ_k -values obtained with and without the RWA are quite small. Whether they lie or not within the experimental accuracy of current technology, that is a question we hope to address in the next future.

REFERENCES

- [1] C. F. Lo, K. L. Liu and K. M. Ng, *Europhys. Lett.* 42, 1 (1998)
- [2] F. De Zela, E. Solano, A. Gago, *Opt. Comm.* 142, 106 (1997)
- [3] S. Swain, *J. Phys. A: Math., Nucl. Gen.*, 6, 1919 (1973)
- [4] P. Elmfors, B. Lautrup and B-S. Skagerstam, CERN/TH 95-333 (atom-ph/9601004) (1996)

Conditional field measurements in cavity QED

G. T. Foster, D. Greenbaum, L. A. Orozco

Department of Physics and Astronomy, State University of New York at Stony Brook, Stony Brook NY 11794-3800, U. S. A.

H. J. Carmichael

Department of Physics, University of Oregon, Eugene, OR 97403-1274, U. S. A.

Abstract

We study the conditional evolution of the field in a strongly coupled cavity QED system in the optical regime using a combination of photon counting and homodyne detection techniques. We show experimental and theoretical results of our laboratory realization.

Nonclassical intensity fluctuations of a light beam are detected by two principal methods: measurement of a second-order intensity correlation function, $g^{(2)}(\tau)$, that shows antibunching or some related feature, or measurement of a photon counting distribution that is sub-Poissonian. The intensity correlation function is obtained from a conditional measurement, and its nonclassical features are insensitive to detection efficiency. A sub-Poissonian counting distribution on the other hand is sensitive to detection efficiency; the measured sub-Poissonian character of the distribution is reduced as the efficiency is decreased. The traditional scheme for detecting quadrature squeezing essentially measures the variance of a photon counting distribution. The observed nonclassical effect also decreases with decreasing detection efficiency.

The intensity correlation function can probe some of the dynamical processes involved in producing the light. The photon correlator does not directly measure the evolution of the electric field, however a modification of the detection system allows a more complete exploration of the field.

We have measured the correlation function of the photons escaping from a strongly coupled cavity QED system formed by a high finesse interferometer traversed by a beam of N optically pumped Rb atoms [1]. Figure 1 shows an intensity correlation function for weak resonant excitation. The system is characterized by the single atom cooperativity parameter $C_1 \approx 6$ and the photon saturation number $n_0 \approx 0.2$, placing it in the strong coupling regime [1–3]. The oscillatory exchange of excitation between the atoms and the cavity is evident in the figure as well as are the non-classical features of antibunching ($g^{(2)}(0) < g^{(2)}(0^+)$) and sub-Poissonian statistics ($g^{(2)}(0) < 1$). The escape of a single photon has a dramatic effect in the system, because the saturation phonon number is so small [4]. The jump occurs because

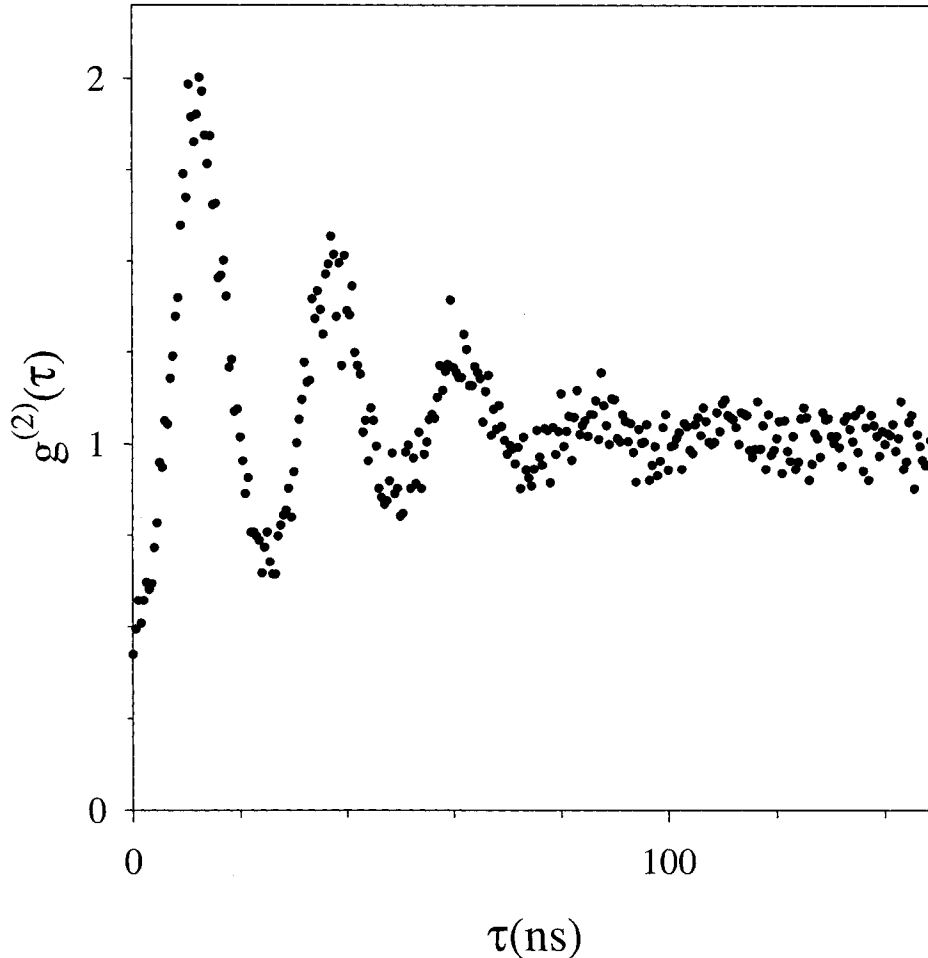


FIG. 1. Experimentally measured second order correlation function $g^{(2)}(\tau)$ of the intensity in a strongly coupled cavity QED system.

the polarization of the medium increases when a photon leaves the cavity. The collective cavity enhancement of the dipole decay rate is reduced in the ratio $(N - 1)/N$ and this increases the polarization amplitude (which is inversely proportional to the damping rate).

We have modified our detection apparatus in a way that permits us to measure the conditional evolution of the electromagnetic field escaping out of the cavity QED system (see figure 2). Our detector starts with a beam splitter. One arm has an avalanche photodiode. The second arm has a balanced homodyne detector. The detection of a photon in the diode triggers a fast digitizer that records the photocurrent output of the homodyne detector. The detection of the first photon projects the state in a well defined initial condition that then evolves back to steady state. The photocurrent of the balanced homodyne detector provides information about the state of the electromagnetic field escaping the cavity. We can sample the two quadratures of the signal field with phase reference to a local oscillator beam. The time record of the photocurrent, in coincidence with the avalanche photon detections, permits the reconstruction of the field of the cavity QED system.

Although the underlying dynamics involves quantum jumps, our detection scheme cannot resolve there. The averaging process necessary to extract the signal out of the shot noise of the homodyne detector eventually evens out the time asymmetry. The resulting field is

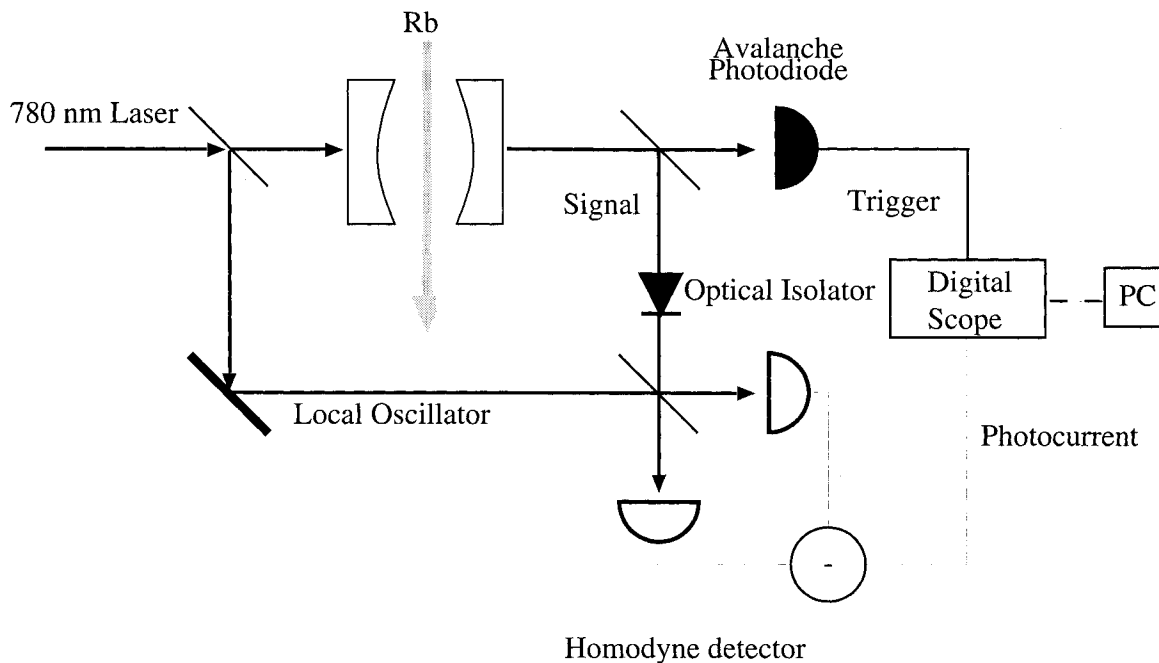


FIG. 2. Diagram of the experimental apparatus.

time symmetric with respect to the conditional trigger.

Initial measurements have detected the conditional field magnitude from the cavity, and show a relation with a bunched second order correlation function. We get additional information by varying the local oscillator phase. This measurement technique should allow observation of the evolution of the field of a single photon triggered by the detection of first photon escaping out of the cavity QED system.

This conditional measurement scheme for electromagnetic field amplitudes detects the nonclassical correlations underlying squeezing in an efficiency insensitive way [5]. The measurement is in effect a third order correlation function in the field. The correlator response involves two operators, the photon flux operator governing the response of the “start” detector, and the field amplitude operator for the quadrature selected by the phase of the local oscillator in the homodyne detector.

We are interested in the regime of large quantum fluctuations observed in Ref. [1]. We are pursuing a measurement of such correlation functions in cavity QED, where violations of the classical inequalities underlie the nonclassical intensity correlations discussed in Refs. [2] and [4]. A similar approach is presently followed by the group of Mlynek in their study of the state reconstruction of parametric down-converted photon pairs [6], but the time scales of the evolution are much faster than in cavity QED.

We will use this technique to characterize the evolution of the state of the cavity field. By sampling the variance of the field at a given time and at a set of phases, tomographic reconstruction techniques can be used to obtain a density matrix of the field.

This work is supported in part by ONR and NSF.

REFERENCES

- ¹ S. L. Mielke, G. T. Foster, and L. A. Orozco, Phys. Rev. Lett. **80**, 948 (1998).
- ² G. Rempe, R. J. Thompson, R. J. Brecha, W. D. Lee, and H. J. Kimble, Phys. Rev. Lett. **67**, 1727 (1991).
- ³ For a review of the field of cavity QED see for example: P. Berman, ed., *Cavity Quantum Electrodynamics*, Supplement 2 of Advances in Atomic, Molecular and Optical Physics series (Academic Press, Boston, 1994).
- ⁴ H. J. Carmichael, R. J. Brecha, and P. R. Rice, Opt. Commun. **82**, 73 (1991).
- ⁵ H. J. Carmichael, G. Foster, and L. A. Orozco, in preparation.
- ⁶ H. Hansen, S. Schiller, and J. Mlynek, Sixth International Conference on Squeezed States and Uncertainty Relations, Book of Abstracts, p. 29, Napoli, Italia, May 24-29, 1999.

Two-Photon Fluorescence Spectrum from Atom+Dielectric Microsphere System

V.V. Klimov*

P. N. Lebedev Physical Institute, Russian Academy of Sciences

V.S.Letokhov

Institute of Spectroscopy, Russian Academy of Sciences

Abstract

Within framework of quantum electrodynamics the strong resonance interaction between an atom and a dielectric microsphere is considered. As initial conditions we choose the case when both an atom and a resonance mode of a microsphere are excited simultaneously. Two-photon fluorescence spectrum depends strongly on the way of an excitation of a microsphere resonance mode, that is it depends on distribution of photon energy over space. The most characteristic feature of two-photon fluorescence spectrum is the emitted photons have strong correlations on energy. These correlations are described by ellipse equation $(\omega_1 + \omega_2 - 2\omega_A)^2 + 3(\omega_1 - \omega_2)^2 = 4\Omega_{Rabi}^2$

The connection of results with dressed state picture is discussed.

Dielectric microsphere is of great interest because it is a high quality resonator with a low mode density in optical range and with a small effective volume of mode[1-3]. Now there has been proposed a number of applications and interesting experiments using dielectric microsphere. In particular the laser with very low lasing threshold is already developed on the base of microsphere[4].

To describe the two-photon fluorescence spectrum it is necessary to build a quantum theory of resonance interaction of an excited atom with a resonance mode of a microsphere, excited by a single photon. Such theory was considered in [5] for the case of first excited manifold. Here we consider the case of second excited manifold. Within rotating wave approximation it is a self-consistent problem. As approximation of second excited manifold we shall consider n ($n \rightarrow \infty$) quantized modes of electromagnetic field with frequencies $\omega_i = i\pi c/\Lambda, i = 1..n$ (Λ -radius of quantization sphere)[5].

To find two-photon spectrum it is necessary to solve a system of Shrödinger equations for probability amplitudes of different states. The vector of probability amplitudes of different states of second excited manifold has a following structure:

*E-mail:klimov@rim.phys.msu.su

$$\left[\underbrace{\Psi_1^A(t), \dots, \Psi_n^A(t), \dots}_{1} \underbrace{\Psi_{1,1}^{Ph}(t), \dots, \Psi_{n,n}^{Ph}(t), \dots}_{2} \underbrace{\Psi_{1,2}^{Ph}(t), \dots, \Psi_{n-1,n}^{Ph}(t), \dots}_{3} \right] \quad (1)$$

Here, the first group describes probability amplitudes of finding an atom and one quantized mode of electromagnetic field in the excited states. The second group describes probability amplitudes of finding an atom in ground state and two photons in one quantized mode. Finally, the last group describes probability amplitudes of finding an atom in ground state and two photons in different quantized modes. To solve Shrödinger equations it is necessary to choose the initial conditions. Here we shall consider the case when two-photon states are not occupied at initial instant of time, $\Psi_{i,j}^{Ph}(t=0) = 0$, $\Psi_i^A(t=0) \neq 0$. In other words, as wave functions of initial state we shall consider a direct product of wave function of an excited atom and wave function of photon field. As wave function of photon field we will consider a superposition of one-photon states with energies, falling into the contour of a resonance mode of a microsphere (whispering gallery mode).

In frequency domain Shrödinger equation is reduced to system of linear equations:

$$\begin{aligned} (\omega - \omega_i - \omega_A) \Psi_i^A(\omega) &= i\Psi_i^A(t=0) + \sum_{s \neq i} V_s \Psi_{i,s}^{Ph}(\omega) + \sqrt{2}V_i \Psi_{i,i}^{Ph}(\omega) \\ (\omega - 2\omega_i) \Psi_{i,i}^{Ph}(\omega) &= \sqrt{2}V_i^* \Psi_i^A(\omega) \\ (\omega - \omega_i - \omega_j) \Psi_{i,j}^{Ph}(\omega) &= V_i^* \Psi_j^A(\omega) + V_j^* \Psi_i^A(\omega), \quad i \neq j \end{aligned} \quad (2)$$

Here ω_A is atom frequency, which may be considered as equal to resonance frequency of a microsphere ω_{res} , ω_i is frequency of i-th quantized modes, $\Psi_i^A(t=0)$ are atomic amplitudes at initial instant. V_i is a matrix element of dipole interaction of an atom with i-th quantized mode:

$$V_i = V(\omega_i) = -\frac{d_{rad} e_{rad}(l, m=0, \nu_i, \mathbf{r})}{i\hbar\sqrt{2}} \quad (3)$$

Here d_{rad} - dipole moment, $e_{rad}(l, m, \nu_i, \mathbf{r})$ -electric field of quantized mode [5]. This matrix element has resonance behaviour near microsphere resonance frequency ω_{res} [5]:

$$V(\omega_i) \propto \frac{1}{\omega_i - \omega_{res} + i\Gamma_{res}/2} \quad (4)$$

Excluding the photon amplitudes from (2) leads to a system of n linear equations for the probability amplitudes of finding an atom and one photon in the excited states:

$$\begin{aligned} (\omega - \omega_i - \omega_A) \Psi_i^A(\omega) &= i\Psi_i^A(t=0) + \\ \sum_s \frac{V_s V_s^* \Psi_i^A(\omega) + V_s V_i^* \Psi_s^A(\omega)}{(\omega - \omega_i - \omega_s + i\epsilon)} \end{aligned} \quad (5)$$

If $\Psi_i^A(t=0) \propto V_i^*$, the average square of electrical field will be maximum at atom position. Such excitation of a microsphere we shall call optimum excitation. If $\Psi_i^A(t=0) \propto V_i$, the average square of electrical field will be minimum at atom position. Such excitation

of a microsphere we shall call anti-optimum excitation. The rest kinds of excitation will have intermediate nature.

After the solution of (5) is found there is no need to return to the time domain to find fluorescence spectrum. It happens due to the fact that probability amplitudes of two-photon states at $t \rightarrow \infty$ are expressed through frequency components of atomic amplitudes with the help of the expressions:

$$\begin{aligned}\Psi_{i,j}^{Ph}(t \rightarrow \infty) &= V_i^* \Psi_j^A(\omega_i + \omega_j) + V_j^* \Psi_i^A(\omega_i + \omega_j), \quad i \neq j \\ \Psi_{i,i}^{Ph}(t \rightarrow \infty) &= \sqrt{2} V_i^* \Psi_i^A(2\omega_i)\end{aligned}\quad (6)$$

From these expressions one can easily see that the final two-photon states are entangled. So we can expect the appearance of strong correlation between final photon states. In its turn two-photon fluorescence spectrum can be expressed through asymptotic expressions for two-photon amplitudes:

$$P(\omega_i, \omega_j) = \frac{|\Psi_{i,j}^{Ph}(t \rightarrow \infty)|^2}{\Delta\omega^2}\quad (7)$$

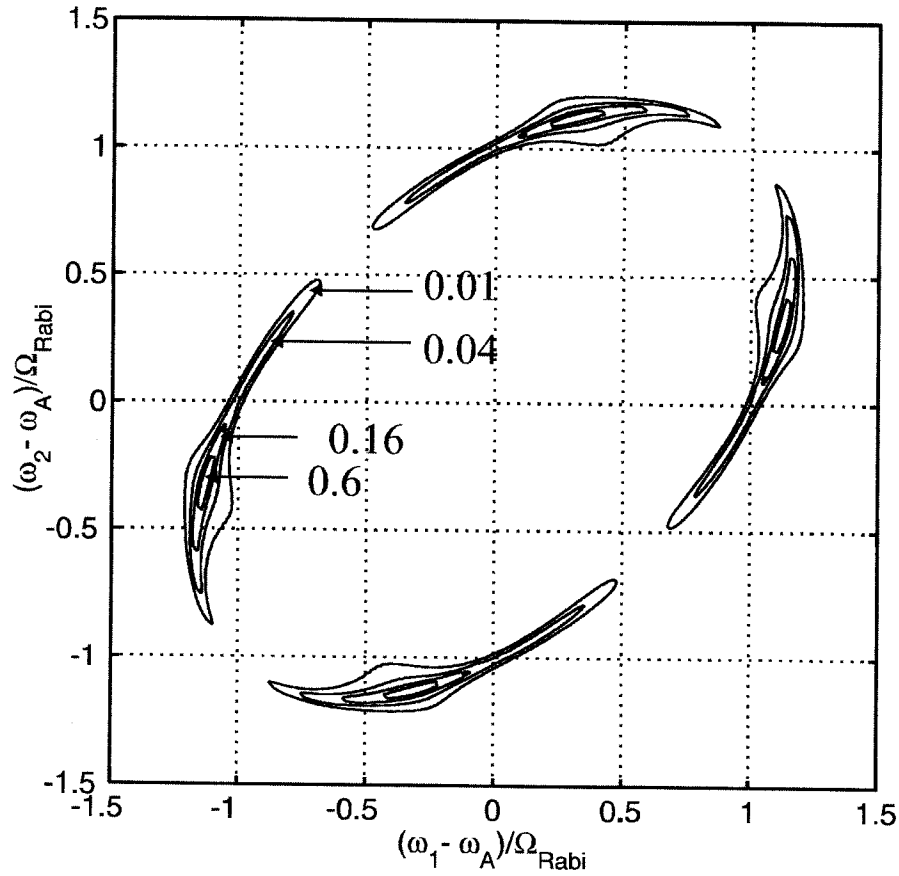


Fig.1. Two-photon fluorescence spectrum from atom+ dielectric microsphere system timum excitation, $\Psi_i^A(t=0) \propto V_i^$, $\Psi_{i,j}^{Ph}(t=0)$, $\Omega_{Rabi}/\Gamma_{res} = 3$.*

The result of solution of a Schrödinger equation for optimum excitation of microsphere is shown in Fig.1.

First of all in this figure one can see that photon frequencies are situated on the ellipse, that is they are strongly correlated. Radial width of the ellipse is essentially less in comparison with the width of microsphere resonance Γ_{res} . In the limit of strong interaction ($\Omega_{Rabi} \gg \Gamma_{res}$) the equation of ellipse has the following form

$$(\omega_1 + \omega_2 - 2\omega_A)^2 + 3(\omega_1 - \omega_2)^2 = 4\Omega_{Rabi}^2 \quad (8)$$

Here Rabi frequency Ω_{Rabi}^2 is determined through relation

$$\Omega_{Rabi}^2 = \sum_i |V_i|^2 \quad (9)$$

Secondly, the four peaks are present on the ellipse. These peaks are close to difference frequency peaks arising in dressed state picture ($\omega_1 = \omega_A \pm \Omega_{Rabi}$, $\omega_2 = \omega_A \pm (\sqrt{2} - 1)\Omega_{Rabi}$) [6]. Important difference of our results from the dressed-state picture is that we do not observe the peaks with sum frequencies ($\omega_1 = \omega_A \pm \Omega_{Rabi}$, $\omega_2 = \omega_A \pm (\sqrt{2} + 1)\Omega_{Rabi}$).

To test experimentally the existence of the elliptical correlations between energies of emitted photons it is insufficiently to measure one-photon spectrum, because the main features of two-photon spectrum are lost here. For full reconstruction of elliptical structures one should measure the spectrum of one of the photons provided the energy of second photon is fixed.

In conclusion, we have shown that in two-photon fluorescence spectrum from the atom+microsphere system the emitted photons have strong energy correlations. These correlations are expressed through appearance of elliptical structures in two-dimensional spectrum. The obtained results are applicable to other cases of two-photon fluorescence spectrum from an atom+ resonator systems.

The authors thank the Russian Basic Research Foundation for financial support of this work.

REFERENCES

1. V.B. Braginsky, M.L. Gorodetsky and V.S. Ilchenko, Phys. Lett A. **137**, 393(1989).
2. L. Collot , V.Lefevre , M.Brune, J.-M. Raimond and S. Haroche, Euro. Phys. Lett. **23**, 327(1993).
3. M.L. Gorodetsky , A.A. Savchenkov and V.S. Ilchenko, Opt. Lett. **21**, 453 (1996).
4. V. Sandoghdar , F. Treussart , J. Hare, V. Lefevre-Seguin , J.-M.Raimond and S. Haroche, Phys. Rev.A **54**, R1777(1996).
5. V.V. Klimov , M. Ducloy , V.S. Letokhov, Phys. Rev.A. **59**, 2996(1999).
6. M. Löffler, G.M. Meyer, H.Walther. Phys.Rev.A **55**, 3923(1997).

Macroscopic observable effects induced by the granularity of the vibrational states of a trapped ion

S. Maniscalco

Dipartimento di Scienze Fisiche ed Astronomiche, via Archirafi 36, 90123 Palermo, Italy

A. Messina

Dipartimento di Scienze Fisiche ed Astronomiche, via Archirafi 36, 90123 Palermo, Italy

A. Napoli

Dipartimento di Scienze Fisiche ed Astronomiche, via Archirafi 36, 90123 Palermo, Italy

Abstract

The occurrence of nonclassical effects in the dynamics of an ion confined in a isotropic bidimensional trap is demonstrated. We find that the variances of a simple observable undergoes macroscopic variations when the total initial number of vibrational quanta is increased or decreased by one unit only.

Very recently it has been demonstrated that a single ion can be confined in a electromagnetic trap and cooled down near to its zero point energy [1]. Such a system is describable as a quantum particle in a harmonic potential in the sense that the center of mass (c.m.) motion can be quantized as harmonic oscillator. Moreover, appropriately driving the confined ion by classical laser beams, its internal and external degrees of freedom can be coupled [2-4]. Thus, simply controlling the configuration of the driving lasers, becomes it possible guiding the vibrational motion of the trapped ion. It is moreover of particular relevance the fact that, if the Lamb-Dicke limit is satisfied and the driving field is tuned to one of the vibrational sidebands of the atomic transition, then the quantum dynamics of such systems may be deduced from generalised nonlinear Jaynes-Cummings models wherein the quantized radiation field is obviously replaced by the quantized c.m. motion of the ion [5]. In this sense the growing development in laser cooling and trapping techniques has opened a new research field for experimentally testing fundamental features either of atomic physics and quantum optics.

In this paper we investigate on the dynamics of a single ion confined in a bidimensional trap. We will show that appropriately choosing both the configuration of the external laser beams and the initial conditions of the system, the time evolution of some simple ionic observables exhibits peculiar nonclassical properties which may be traced back to the granularity of the vibrational states.

Consider a two-level ion of mass M confined in a bidimensional isotropic harmonic potential characterised by a trap frequency ν . Indicate by \hat{a} (\hat{a}^\dagger) and \hat{b} (\hat{b}^\dagger) the annihilation (creation) operators of vibrational quanta relative to the oscillatory motion along the X and Y axes of the trap respectively. Accordingly the position and momentum operators can be written as

$$\hat{X} = \sqrt{\frac{\hbar}{2\nu M}} (\hat{a}^\dagger + \hat{a}) \quad \hat{Y} = \frac{1}{\sqrt{2\nu M}} (\hat{b}^\dagger + \hat{b}) \quad (1)$$

$$\hat{P}_x = i\sqrt{\frac{\hbar\nu M}{2}} (\hat{a}^\dagger - \hat{a}) \quad \hat{P}_y = i\sqrt{\frac{\hbar\nu M}{2}} (\hat{b}^\dagger - \hat{b}) \quad (2)$$

The bidimensional harmonic oscillator can be also described, in the well known Schwinger representation, introducing a generalised angular momentum operator $\hat{J} \equiv (J_x, J_y, J_z)$ in the form

$$\hat{J}_x = \frac{\hat{a}^\dagger \hat{b} + \hat{b}^\dagger \hat{a}}{2} \quad \hat{J}_y = \frac{\hat{a}^\dagger \hat{b} - \hat{b}^\dagger \hat{a}}{2i} \quad \hat{J}_z = \frac{\hat{a}^\dagger \hat{a} - \hat{b}^\dagger \hat{b}}{2} \quad (3)$$

We assume that the ion is driven by two laser beams applied along directions with an angle $\pi/4$ and $3\pi/4$ relative to the X axis respectively, having phases $\phi_x = 0$ and $\phi_y = \pi$ and equal intensity and wavelength. It is possible to demonstrate that [6], if the laser beams are both tuned to the second lower vibrational sideband, the physical system under scrutiny can be described, in the Lamb-Dicke limit, by the following effective Hamiltonian

$$\hat{H} = \hbar\nu(\hat{a}^\dagger \hat{a} + \hat{b}^\dagger \hat{b}) + \hbar\nu\hat{\sigma}_z + g \left[(\hat{a}\hat{b})\hat{\sigma}_+ + (\hat{a}^\dagger \hat{b}^\dagger)\hat{\sigma}_- \right] \quad (4)$$

where $\hat{\sigma}_z = |+\rangle\langle+| - |-\rangle\langle-|$, $\hat{\sigma}_+ = |+\rangle\langle-|$, $\hat{\sigma}_- = |-\rangle\langle+|$ are internal ionic operators with $|+\rangle$ and $|-\rangle$ ionic excited and ground states respectively. In eq. (4) g measures the strength of the interaction between the internal and external degrees of freedom and depends on physical parameters such as laser intensity, wavelength and amplitude of oscillation of the ionic center of mass.

It is easy to verify that the total number of excitations $\hat{N} = \hat{a}^\dagger \hat{a} + \hat{b}^\dagger \hat{b} + \hat{\sigma}_z + 1$ and the difference of vibrational quanta, relative to X and Y harmonic motion, $\hat{a}^\dagger \hat{a} - \hat{b}^\dagger \hat{b} = 2\hat{J}_z$ are constants of motion. Let's denote with $|n_a, n_b\rangle \equiv |n_a\rangle|n_b\rangle$ the simultaneous eigenstates of $\hat{a}^\dagger \hat{a}$ and $\hat{b}^\dagger \hat{b}$ such that:

$$\hat{a}^\dagger \hat{a} |n_a, n_b\rangle = n_a |n_a, n_b\rangle \quad \hat{b}^\dagger \hat{b} |n_a, n_b\rangle = n_b |n_a, n_b\rangle \quad (5)$$

We suppose to prepare the ion at $t = 0$ in the state $|\psi(0)\rangle = |\tau = 1, j_0 = \frac{N}{2}\rangle|-\rangle$, where

$$\begin{aligned} |\tau = 1, j_0 = \frac{N}{2}\rangle &\equiv |\tau, j_0\rangle \equiv \frac{1}{2^{N/2}} \sum_{k=0}^N \binom{N}{k}^{1/2} |N-k, k\rangle \equiv \\ &\equiv \sum_{k=0}^N P_k |N-k, k\rangle \end{aligned} \quad (6)$$

is a SU(2) coherent state. Very recently, Fock states of the ion motion along the X direction of an electromagnetic trap have been experimentally realized by the researchers of the

National Institute for Standards and Technologies [7]. Of course the applicability of this method is by no means restricted to oscillations along the X axis only. As pointed out by Gou and Knight [8], then, the generation of the initial state $|\tau = 1, j_0\rangle$ of a bidimensionally confined ion, amounts at realizing a Fock state of the ion motion along the direction with an angle $\pi/4$ relative to the X axis. The states $|N - k, k\rangle$ appearing in eq. (6) are eigenstates of the operator $(\hat{a}^\dagger \hat{a} + \hat{b}^\dagger \hat{b})$ all pertaining to the common eigenvalue $N = 2j_0$, representing the initial total number of vibrational quanta. Observing that \hat{J}_y is a purely imaginary hermitian operator and that, in the coordinate representation, the initial state $|\Psi(0)\rangle$ is real, it is easy to convince oneself that necessarily

$$\langle \tau = 1, j_0 | \hat{J}_y | \tau = 1, j_0 \rangle = \frac{N}{2} \langle \tau = 1, j_0 | \hat{J}_y | \tau = 1, j_0 \rangle = 0 \quad (7)$$

Moreover a straightforward calculation gives that the initial variance of \hat{J}_y is $\frac{N}{4}$.

If we turn on, at $t = 0$, the laser fields which realize the Hamiltonian model (4), then at any subsequent instant of time t the state of the system can be exactly determined in the form [9]

$$|\Psi(t)\rangle = |\varphi_-(t)\rangle |-\rangle - i |\varphi_+(t)\rangle |+\rangle \quad (8)$$

with

$$\begin{aligned} |\varphi_-(t)\rangle &= \sum_{k=0}^N P_k \cos(f_k t) |N - k, k\rangle \\ |\varphi_+(t)\rangle &= \sum_{k=1}^{N-1} P_k \sin(f_k t) |N - k - 1, k - 1\rangle \end{aligned} \quad (9)$$

where $f_k = 2g\sqrt{(N - k)k}$ are the Rabi frequencies. Eq. (8) shows the occurrence of entanglement between the internal and external degrees of freedom in the time evolution of the system. It is of relevance to emphasise that, as a consequence of the specific coupling mechanism adopted in this paper, the bosonic states $|\varphi_-(t)\rangle$ and $|\varphi_+(t)\rangle$, given by eqs. (9), in the coordinate representation, are real at any time t this implying

$$\langle \Psi(t) | \hat{J}_y | \Psi(t) \rangle = 0 \quad (10)$$

in view of the fact that \hat{J}_y is a bosonic operator. As easily deducible from eqs. (1-3), the operator \hat{J}_y is proportional to the z -component of the ionic angular momentum operator $L_z \equiv \hat{X} \hat{P}_y - \hat{Y} \hat{P}_x \equiv i\hbar (\hat{a}^\dagger \hat{b} - \hat{b}^\dagger \hat{a})$. Thus eq. (10) assumes a simple physical meaning saying that the expectation value of L_z vanishes at any t . Since, however, \hat{J}_y does not commute with \hat{H} , useful information on the physical behaviour of this observable may be achieved investigating on the time evolution of its variance $(\Delta J_y)^2$ here coincident with $\langle \Psi(t) | \hat{J}_y^2 | \Psi(t) \rangle$. We have exactly and analytically calculated this quantity and figure 1 displays its time dependence for (a) $N = 20$ and (b) $N = 21$, respectively.

These plots clearly evidence that our system possesses an inherent peculiar nonclassical sensitivity to the parity of the initial total number N of vibrational quanta. In fact, there exists an instant of time t_s at which the variance of \hat{J}_y assumes values strongly dependent on

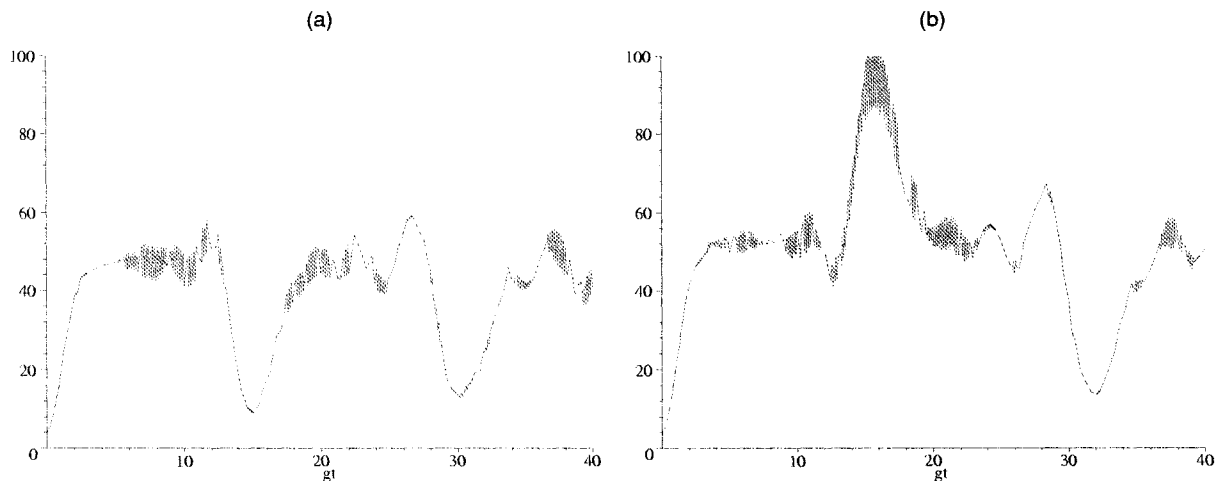


FIG. 1. Time evolution of $(\Delta J_y)^2$ for (a) $N = 20$ and (b) $N = 21$ respectively.

the evenness or oddness of N . We have analytically proved by lengthy calculations that, at the N -dependent instant of time $t_s = \frac{\pi N}{4g}$ that, the quantity under scrutiny may be written as

$$(\Delta J_y)^2 = \begin{cases} \frac{N^2}{4} & \text{if } N \text{ is odd} \\ \frac{N}{4} & \text{if } N \text{ is even} \end{cases} \quad (11)$$

This result suggests the possibility of controlling the fluctuations of a physically interesting observable, that is L_z , simply varying the initial total number of vibrational quanta. More in detail, we may claim that at $t = t_s$ the z component of the angular momentum manifests macroscopically different fluctuations as a consequence of the variation of only one vibrational quantum in the initial conditions. This means that the degree of precision associated to the measurement of this highly interesting and simple physical observable may be macroscopically influenced by the discreteness of the quantum states of the harmonic oscillator.

In conclusion we have demonstrated that the interaction mechanism envisaged in this paper as well as the particular initial condition imposed on the system, doubtless in the grasp of the experimentalists, lead to a nonclassical macroscopic effect directly stemming from the granularity of the vibrational states of the trapped ion.

References

- [1] C. Monroe, D.M. Meekhof, B.E. King, J.R. Jefferts, W.M. Itano and D. J. Wineland, Phys. Rev. Lett. **75**, 4011 (1995)
- [2] C.A. Blockley, D.F. Walls and H. Risken, Europhys. Lett. **17**, 509 (1992)
- [3] J.I. Cirac, R. Blatt, A.S. Parkins and P. Zoller, Phys. Rev. A **49**, 1202 (1994)
- [4] H. Zeng and F. Lin, Phys. Rev. A **52**, 809 (1995)
- [5] W. Vogel and R.L. de Matos Filho, Phys. Rev. A **52**, 4214 (1995)
- [6] S.-C. Gou, J. Steinbach and P.L. Knight Phys. Rev. A **54**, R1014 (1996)
- [7] D.M. Meekhof, C. Monroe, B.E. King, W.M. Itano and D. J. Wineland, Phys. Rev. Lett. **76**, 1796 (1996)
- [8] S.-C. Gou and P.L. Knight Phys. Rev. A **54**, 1682 (1996)
- [9] A. Napoli and A. Messina J. Mod. Opt. **43**, 649 (1996)

Generation of vibrational Schrödinger cats of an ion confined in a bidimensional trap

S. Maniscalco

Dipartimento di Scienze Fisiche ed Astronomiche, via Archirafi 36, 90123 Palermo, Italy

A. Messina

Dipartimento di Scienze Fisiche ed Astronomiche, via Archirafi 36, 90123 Palermo, Italy

A. Napoli

Dipartimento di Scienze Fisiche ed Astronomiche, via Archirafi 36, 90123 Palermo, Italy

Abstract

A scheme for generating quantum superpositions of macroscopically distinguishable states of the vibrational motion of a bidimensionally trapped ion is reported. We show that these states possess highly nonclassical properties controllable by an adjustable parameter simply related to the initial condition of the confined system

An ion confined in an electromagnetic trap is describable as a particle in a harmonic potential in the sense that its center of mass (c.m.) can be quantized as harmonic oscillator [1]. Appropriately driving the trapped ion by classical laser beams, its internal and external degrees of freedom can be coupled. It is of particular relevance the fact that, if the Lamb-Dicke limit is satisfied and the driving field is tuned to one of the vibrational sidebands of the atomic transition, then the quantum dynamics of such systems may be deduced from generalized nonlinear Jaynes-Cummings models wherein the quantized radiation field is obviously replaced by the quantized c.m. motion of the ion [2]. The advantages of testing the rich dynamics predicted by these models using trapped ions instead of cavities stem from the circumstance that typical dissipative effects strongly limiting the performance of experiments in cavities, in the optical as well as in the microwave regime, can be significantly suppressed for the ion motion thanks to the extremely weak coupling between the vibrational modes and the external environment. It is thus not surprising that ions confined by electromagnetic fields are eligible systems for producing, for example, specific nonclassical vibrational states. Several schemes for the generation of Fock states, coherent states and squeezed states have been, in fact, reported and realized in this contest [3]. Quite recently, Monroe et al. [4] have proposed an experimental scheme for generating and detecting a Schrödinger cat-like state of a trapped ion providing insight into the fuzzy boundary between the classical and quantum worlds. Over the last few years, some interesting methods for creating generalized coherent

states of the bidimensional vibrational c.m. motion have also been reported [5-7]. In this paper we present an original scheme aimed at generating quantum superpositions of bosonic SU(2) macroscopically distinguishable coherent states exploiting the wave packet reduction method. In particular, we show that these states possess nonclassical properties controllable by an adjustable parameter simply related to the initial condition imposed on the confined system. Consider a two-level ion of mass M confined in a bidimensional isotropic harmonic potential characterized by a trap frequency ν . Denote by \hat{X} , \hat{Y} , \hat{P}_x and \hat{P}_y the position operators and their relative conjugate momenta. Then, as usual, the operators \hat{a} (\hat{a}^\dagger) and \hat{b} (\hat{b}^\dagger) defined as

$$\hat{a} = \frac{1}{\sqrt{2}} \left(\sqrt{\frac{M\nu}{\hbar}} \hat{X} + i \frac{1}{\sqrt{M\nu\hbar}} \hat{P}_x \right) \quad \hat{b} = \frac{1}{\sqrt{2}} \left(\sqrt{\frac{M\nu}{\hbar}} \hat{Y} + i \frac{1}{\sqrt{M\nu\hbar}} \hat{P}_y \right) \quad (1)$$

are the annihilation (creation) operators of vibrational quanta in the X and Y directions respectively. It has been shown [6] that irradiating the trapped ion with an appropriate configuration of laser beams, if the Lamb-Dicke limit is satisfied, the physical system under scrutiny can be studied, in the interaction picture, by the following Hamiltonian model

$$\hat{H} = \hbar\nu(\hat{a}^\dagger\hat{a} + \hat{b}^\dagger\hat{b}) + \frac{\hbar\nu}{2}\hat{\sigma}_z + g \left[(\hat{a}\hat{b})\hat{\sigma}_+ + (\hat{a}^\dagger\hat{b}^\dagger)\hat{\sigma}_- \right] \quad (2)$$

where $\hat{\sigma}_z = |+\rangle\langle+| - |-\rangle\langle-|$, $\hat{\sigma}_+ = |+\rangle\langle-|$, $\hat{\sigma}_- = |-\rangle\langle+|$ describe the internal degrees of freedom, $|+\rangle$ and $|-\rangle$ being the ionic excited and ground states respectively. Let's denote with $|n_a, n_b\rangle = |n_a\rangle|n_b\rangle$ the simultaneous eigenstates of $\hat{a}^\dagger\hat{a}$ and $\hat{b}^\dagger\hat{b}$ such that $\hat{a}^\dagger\hat{a}|n_a, n_b\rangle = n_a|n_a, n_b\rangle$ and $\hat{b}^\dagger\hat{b}|n_a, n_b\rangle = n_b|n_a, n_b\rangle$. We suppose that the initial state of the ion has the form $|\Psi(0)\rangle = |\tau = 1, j_0 = \frac{N}{2}\rangle|-\rangle$ where

$$|\tau = 1, j_0 = \frac{N}{2}\rangle \equiv \frac{1}{2^{N/2}} \sum_{k=0}^N \binom{N}{k}^{1/2} |N-k, k\rangle \equiv \sum_{k=0}^N P_k |N-k, k\rangle \quad (3)$$

is known as $SU(2)$ coherent state and may be prepared exploiting a method recently proposed by Knight et al. [7]. The states $|N-k, k\rangle$ appearing in Eq. (3) are eigenstates of the operator $(\hat{a}^\dagger\hat{a} + \hat{b}^\dagger\hat{b})$ all pertaining to the eigenvalue $N = 2j_0$ representing the initial total number of vibrational quanta. The state of the system, at a generic time t , can be written down as [8]

$$\begin{aligned} |\Psi(t)\rangle &= \sum_{k=0}^N P_k \cos(f_k t) |N-k, k\rangle|-\rangle - i \sum_{k=1}^{N-1} P_k \sin(f_k t) |N-k-1, k-1, +\rangle|+\rangle \\ &\equiv |\varphi_-(t)\rangle|-\rangle - i|\varphi_+(t)\rangle|+\rangle \end{aligned} \quad (4)$$

where $f_k = 2g\sqrt{(N-k)k}$ are the Rabi frequencies. Starting from the factorized state $|\Psi(0)\rangle$, the Hamiltonian model (2) leads to entanglement between the external and internal degrees of freedom of the trapped ion giving rise to far-reaching interesting dynamical consequences. In order to appreciate the meaning of this statement, we focus our attention on the time evolution of the vibrational entropy defined as $S_v(t) = -Tr[\rho_v(t) \ln \rho_v(t)]$, ρ_v being the reduced density operator describing the external motion of the ion. We have analitically

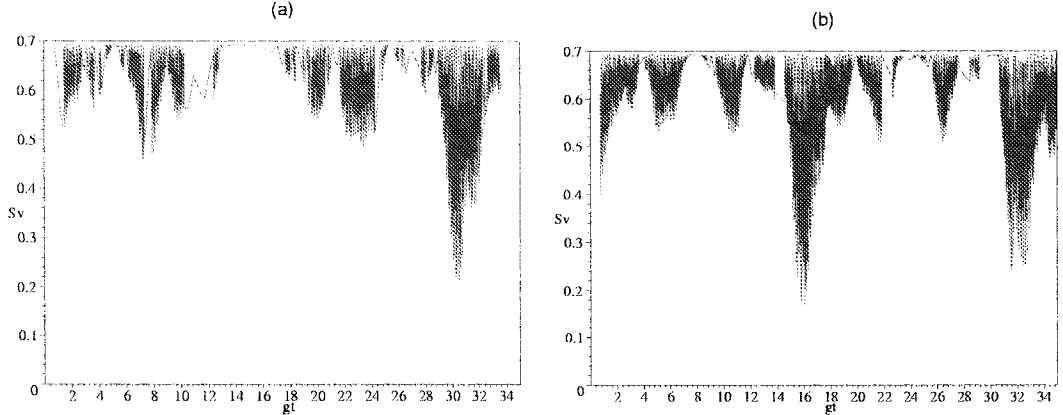


FIG. 1. Time evolution of the vibrational entropy S_v , (a) for $N = 20$ and (b) $N = 21$

demonstrated that there exist N -dependent instants of time at which the internal and external degrees of freedom of the trapped ion are disentangled or maximally entangled. More in detail we have obtained that, if $N \gg 1$ is even, the vibrational entropy S_v reaches its maximum value at $t_e = \frac{\pi N}{4g}$ thus implying that the vibrational and electronic degrees of freedom are maximally entangled at this instant of time. On the contrary, if $N \gg 1$ is odd, at the instant $t_o = t_e - \frac{\pi}{4gN} \simeq t_e$, $S_v(t)$ reaches its absolute minimum $\simeq 0.2$, as shown in fig. 1. In this case, the internal and external degrees of freedom manifest a marked tendency to disentangle each other. This means that there exists a N -dependent instant of time t_e at which the system under scrutiny exhibits different quantum behaviours dependent on the parity of N . The physical origin of this peculiar sensitivity to the granularity of the initial total number of vibrational quanta, directly stems from the specific two-boson coupling mechanism envisaged in this paper (Eq. (2)).

In order to bring to the light the link between the quantum dynamics followed by our system and the occurrence of such a nonclassical feature we study the time evolution of the SU(2) Q -function defined as $Q^{(j)}(\tau) = \langle \tau, j | \rho_v | \tau, j \rangle$, where $|\tau, j\rangle$ is a generic SU(2) coherent state. For what follows it is of relevance to underline that the total excitation number operator $\hat{N} = \hat{a}^\dagger \hat{a} + \hat{b}^\dagger \hat{b} + 2\hat{S}_z + 1$ is a constant of motion and that the initial state of our system $|\Psi(0)\rangle$ is an eigenstate of \hat{N} correspondent to the eigenvalue $n = 2j_0$ with $j_0 = \frac{N}{2}$. Observing that $|\tau, j\rangle$ is orthogonal to $|n_a, n_b\rangle$ when $2j \neq n_a + n_b$, then it is easy to convince oneself that $|\varphi_-(t)\rangle$ ($|\varphi_+(t)\rangle$) can be expressed as quantum superposition of different SU(2) coherent states $|\tau, j = j_0 = \frac{N}{2}\rangle$ ($|\tau, j = j_0 - 1 = \frac{N-2}{2}\rangle$), obtained varying τ . This circumstance directly leads to consider the Q -functions $Q^{(j=j_0)}(\tau)$ or $Q^{(j=j_0-1)}(\tau)$ only. In particular we fix our attention on the quasiprobability function $Q^{(j_0)}(\tau)$. Figure 2 displays, for (a) $N = 20$ and (b) $N = 21$, $Q^{(j=j_0)}(\tau)$ at $t = t_e$ and $t = t_o$ respectively. A careful analysis of this figure suggests that, detecting at these N -dependent instants of time the electronic state of the trapped ion in its ground state $|-\rangle$, projects the c.m. motion into the state $|\Psi\rangle = N_- |\varphi_-\rangle$ which is a superposition of two macroscopically distinguishable SU(2) coherent states. In addition we find that such a superposition exhibits a high sensitivity to the parity of the total number of vibrational quanta present at $t = 0$, in accordance with the conclusions previously deduced on the basis of the properties of S_v .

In fact figure 2 strongly suggests that, after a successful measurement of the internal state of the ion, the two components of the vibrational state are $|\tau = 1, j = \frac{N}{2}\rangle$ and

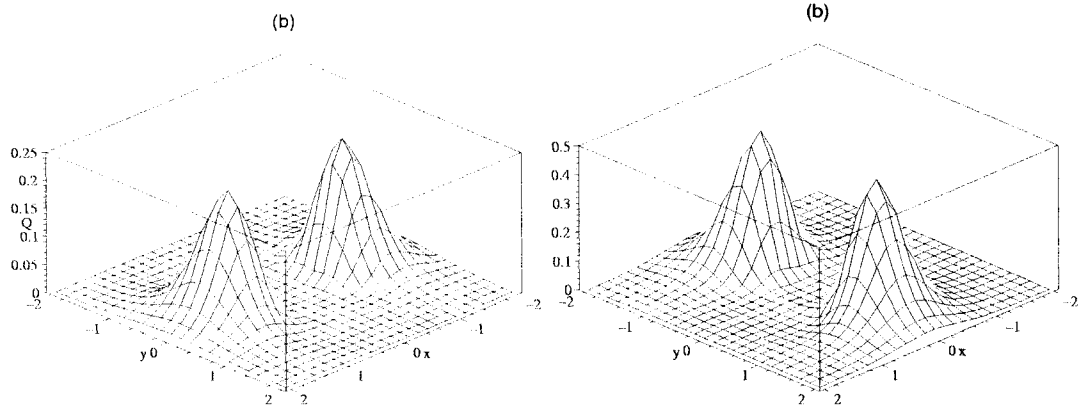


FIG. 2. Plot of $Q^{j=j_0}(x = \text{Re}[\tau], y = \text{Im}[\tau])$ for $N = 20$ and $N = 21$, in correspondence with (a) $t = t_e$ and (b) $t = t_o$ respectively

$|\tau = -1, j = \frac{N}{2}\rangle$ if N is even, or $|\tau = i, j = \frac{N}{2}\rangle$ and $|\tau = -i, j = \frac{N}{2}\rangle$ if N is odd. Of course it is very difficult to guess the exact form of the vibrational state, after the measurement of the electronic state, from this kind of analysis of the $Q^{(j)}(\tau)$ plots. For this reason, in order to reach more quantitative conclusions, we have performed an exact analytical calculation proving that, provided that the measurement is made at $t = t_e$ when N is even, the state $|\psi\rangle$ has the form of even or odd $SU(2)$ coherent state in correspondence with $\frac{N}{2}$ even or odd respectively. On the contrary, for N odd, the two states $|\psi\rangle$, obtained measuring at $t = t_o$ the internal state of the ion as $|-\rangle$, may be called Yurke-Stoler like states with a relative quantum phase of $\frac{\pi}{2}$ or $\frac{3\pi}{2}$ in correspondence with $\frac{N-1}{2}$ even or odd respectively.

Summarizing, in the contest of our scheme, the total number of excitation N present in the initial state of the ion center of mass motion, behaves as an adjustable parameter allowing the realization of vibrational states possessing very different nonclassical bosonic number distributions.

It is worth to emphasize that, whatever the parity of N is, the states discussed in this paper are quantum superpositions of two macroscopically distinguishable $SU(2)$ coherent states of a bidimensional isotropic harmonic oscillator.

References

- [1] C.A. Blockley, D.F. Walls and H. Risken, *Europhys. Lett.* **17**, 509 (1992)
- [2] W. Vogel and R.L. de Matos Filho, *Phys. Rev. A* **52**, 4214 (1995)
- [3] J.I. Cirac, R. Blatt, A.S. Parkins and P. Zoller, *Phys. Rev. Lett.* **70**, 762 (1993)
- [4] D.M. Meekhof, C. Monroe, B.E. King, W.M. Itano and D. J. Wineland, *Phys. Rev. Lett.* **76**, 1796 (1996); J.I. Cirac, A.S. Parkins, R. Blatt and P. Zoller, *ibid.* **70**, 556 (1993); C. Monroe, D.M. Meekhof, B.E. King and D.J. Wineland, *Science* **212**, 1131 (1996)
- [5] C.C. Gerry, S.-C. Gou, and J. Steinbach, *Phys. Rev A* **55**, 630 (1997)
- [6] S.-C. Gou, J. Steinbach and P.L. Knight *Phys. Rev. A* **54**, R1014 (1996)
- [7] S.-C. Gou and P.L. Knight *Phys. Rev. A* **54**, 1682 (1996)
- [8] A. Napoli, A. Messina, *J. Mod. Opt.* **43**, 649 (1996)

Measuring Vibrational Quantum States of Diatomic Molecules

A. Zucchetti, W. Vogel

*Arbeitsgruppe Quantenoptik, Fachbereich Physik, Universität Rostock, Universitätsplatz 3,
D-18051 Rostock, Germany*

D.-G. Welsch

*Theoretisch-Physikalisches Institut Friedrich-Schiller-Universität Jena, Max-Wien-Platz 1,
D-07743 Jena, Germany*

I. A. Walmsley

The Institute of Optics, University of Rochester, New York 14627

Abstract

A pump-probe heterodyne detection scheme is proposed, which allows one to infer the vibronic quantum state of diatomic molecules from the intensity of the resulting interference signal. In particular, it is shown that direct measurement of the vibrational wave-packet in the excited electronic state is possible.

Many methods for determining the quantum state of light and matter have been recently developed¹. In particular for molecular systems, methods for recovering the vibrational quantum state from time and frequency resolved emission spectra by use of tomographic reconstruction have been experimentally realized² and further developed for applications to anharmonic vibrations³. Other experimental schemes have been theoretically studied such as a Raman experiment⁴, which allows one to directly measure the Wigner function in harmonic approximation, and a holographic approach⁵, which applies beyond the harmonic approximation but requires the application of numerical inversion procedures.

¹For a recent review of the topic, see D.-G. Welsch, W. Vogel, and T. Opatrny, *Homodyne Detection and Quantum State Reconstruction*, in: *Progress in Optics*, Vol. 39, ed. by E. Wolf.

²T. J. Dunn, I. A. Walmsley and S. Mukamel, *Phys. Rev. Lett.* **74**, 884 (1995).

³L. J. Waxer, I. A. Walmsley, and W. Vogel *Phys. Rev. A.* **56** R2491 (1997).

⁴L. Davidovich, M. Orszag, and N. Zagury, *Phys. Rev. A.* **57**, 2544 (1998).

⁵C. Leichtle and W. Schleich, I. Sh. Averbukh, and M. Shapiro, *Phys. Rev. Lett.* **80**, 1418 (1998); I.Sh. Averbukh, M. Shapiro, C. Leichtle, and W. Schleich, *Phys. Rev. A* **59** 2163 (1999).

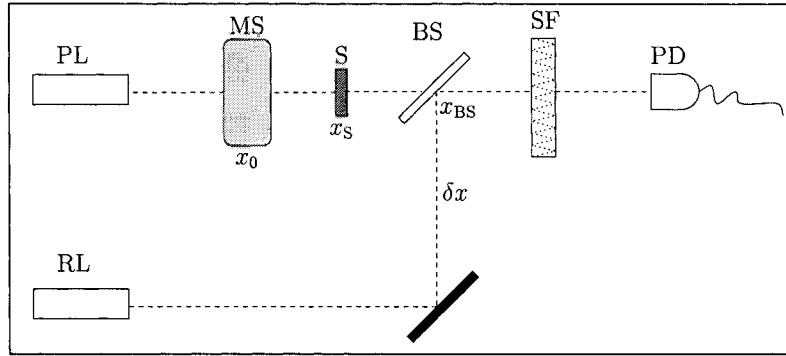


FIG. 1. Experimental scheme for the heterodyne state measurement. A pump laser (PL) at position $x = 0$ is used to prepare the quantum state of a molecular sample (MS) at x_0 . A shutter (S) at x_s separates the source signal of the molecular sample from the pump pulse. This signal is superimposed by a beam splitter (BS) at position x_{BS} with a test pulse from a reference laser (RL), δx being the path-length difference between PL and RL. The heterodyne signal is transmitted through a spectral filter (SF) and recorded by a photodetector (PD).

In this work a heterodyne experimental set-up is proposed which allows one to measure directly the vibrational quantum state of a diatomic molecule. The experimental set-up is shown in Fig. 1. An ensemble of diatomic molecules is prepared in a particular vibronic quantum state by a pump laser. This laser is switched on at position $x=0$ at time $t=0$. The duration of the preparation process is τ_P . The pump-laser pulse reaches a molecule located at position x_0 at time x_0/c and the shutter at time x_s/c . The shutter is used to suppress the influence of the preparation process on the measured signal. After the preparation the shutter is turned on. The outgoing source field is then mixed with a reference field by a beam splitter. The reference field is a pulse of few femtoseconds duration centered at time τ_R at position $-\delta x$, with δx being the path-length difference between the pump and reference lasers. The total field is spectrally filtered and detected by a photodetector at position x .

The photoelectron-count difference, defined as the difference between the number of measured photoelectrons and the number of photoelectrons measured by detecting the reference field alone, can be written in frequency domain as⁶,

$$\Delta N = -\frac{\xi}{2\pi} \int d\omega \langle \hat{E}_s^{(-)}(x, \omega) \hat{E}_{\text{ref}}^{(+)}(x, \omega) \rangle + c.c., \quad (1)$$

where $\hat{E}_s^{(\pm)}(x, \omega)$ and $\hat{E}_{\text{ref}}^{(\pm)}(x, \omega)$ are the source and the reference field, respectively, at position x . The constant factor ξ is proportional to the quantum efficiency η of the photodetector. Taking into account the effect of the optical devices in the experiment, these fields can be related to the reference field at the laser source $\hat{\mathcal{E}}_{\text{ref}}^{(\pm)}(\omega)$ and to the source field $\hat{\mathcal{E}}_s^{(\pm)}(\omega)$ passing through the switch device. This gives for the measured photocount difference

$$\Delta N = -\frac{\xi'}{2\pi} \int d\omega |T(\omega)|^2 \langle \hat{\mathcal{E}}_s^{(-)}(\omega) \hat{\mathcal{E}}_{\text{ref}}^{(+)}(\omega) \rangle e^{i\omega(\frac{x_0 + \delta x}{c})} + c.c., \quad (2)$$

where $T(\omega)$ describes the spectral filtering operated by the spectrometer and $\xi' = \xi \mathcal{R} \mathcal{T}^*$ (\mathcal{R} and \mathcal{T} are the reflection and transmission coefficients of the beam splitter, respectively).

⁶W.Vogel, D.-G. Welsch and B. Wilhelmi, Phys. Rev. A **37**, 3825 (1988).

The reference pulse can be described by a multimode coherent field, which allows one to replace the reference-field operator in Eq. (2) with the corresponding complex function defined as

$$\mathcal{E}_{\text{ref}}^{(+)}(\omega) = \mathcal{A}(\omega - \omega_L) e^{i(\omega - \omega_L)\tau_R}, \quad (3)$$

where $\mathcal{A}(\omega)$ is an envelope function and ω_L the central frequency of the laser. On the other hand, the source field is related to the vibronic quantum state of the diatomic molecule by the following equation

$$\langle \hat{\mathcal{E}}_s^{(-)}(\omega) \rangle = \sum_{nm} g_{12}^{mn} \tilde{\varrho}_{12}^{mn}(\omega) e^{-i\omega \frac{x_0}{c}}, \quad (4)$$

where the coefficients g_{12}^{mn} are proportional to the corresponding Franck-Condon factors and the phase factor arises from the spatial retardation. The Fourier transformed density matrix elements $\tilde{\varrho}_{12}^{mn}(\omega)$ (the indices 1 and 2 label the lower and upper electronic state, respectively, and the indices n and m the corresponding vibrational level) are defined as

$$\tilde{\varrho}_{12}^{mn}(\omega) = \int_{\tau_P=t_p}^{+\infty} dt \varrho_{12}^{mn}(t) \exp[-i\omega t]. \quad (5)$$

To evaluate $\tilde{\varrho}_{12}^{mn}(\omega)$, the density matrix elements $\varrho_{12}^{mn}(t)$ must be known for $t \geq \tau_P$. Solving the corresponding master equation (including radiative damping), the following result is obtained

$$\varrho_{12}^{mn}(t) = \varrho_{12}^{mn}(\tau_P) e^{-\Gamma_n(t-\tau_P)} e^{i\omega_{21}^{nm}(t-\tau_P)} \quad (t \geq \tau_P), \quad (6)$$

where Γ_n is the radiative damping rate of the n -th vibrational level in the upper electronic state.

Inserting the previous results in Eq. (2) and performing the resulting double integral, taking into account that the envelope function $\mathcal{A}(\omega)$ is slowly varying with respect to the spectral filter function $T(\omega)$, we obtain the following expression for the difference signal

$$\Delta N = \sum_{n,m} K_{12}^{mn}(\omega_F) |\varrho_{12}^{mn}(\tau_P)| \cos[(\omega_{21}^{nm} - \omega_L) \delta t - \phi_{12}^{mn}(\tau_P)], \quad (7)$$

where $\phi_{12}^{mn}(\tau_P)$ is the phase of the matrix element $\varrho_{12}^{mn}(\tau_P)$ and the time delay δt is defined as $\delta t = \tau_R - \tau_P + \delta x/c$. The kernel function $K_{12}^{mn}(\omega_F)$ is given by

$$K_{12}^{mn}(\omega_F) \simeq \xi' g_{12}^{mn} \mathcal{A}(\omega_F - \omega_L) |T(\omega_{21}^{nm} - \omega_F)|^2, \quad (8)$$

under the condition that the time delay δt is chosen to be longer than the characteristic time of the spectrometer and shorter than the characteristic damping time of the system.

The measured photocount difference depends linearly on the density matrix elements $\varrho_{12}^{mn}(\tau_P)$. These elements can be recovered by measuring the difference heterodyne spectrum for different values of the experimental parameters, such as ω_F and δt and inverting the obtained linear set of equations using, e. g., least-squares inversion. Moreover, the signal is proportional to the intensity of the reference laser which can be chosen large enough to assure a optimal signal to noise ratio.

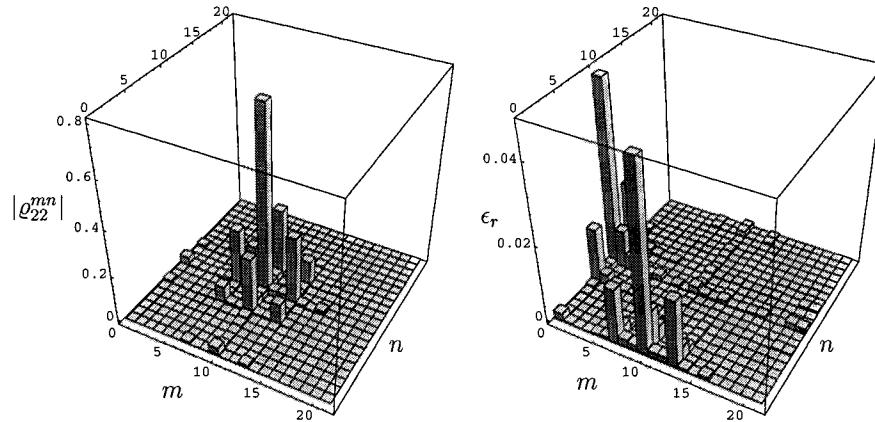


FIG. 2. Absolute values of the reconstructed density-matrix elements $\rho_{22}^{nm} = c_2^{n*} c_2^m$ and relative deviations ϵ_r from the theoretical values.

Equation (7) above shows also that a direct measurement of the vibrational wave-packet in the upper electronic state is possible. The necessary physical conditions are that the molecule before the preparation is cooled down to its vibrational ground state and that the pump pulse is weak enough so that the populations of the excited vibrational levels in the lower electronic state are negligible. Under such conditions the vibrational state in the energy eigenstate representation is given by

$$|\psi(\tau_P)\rangle = c_1^0(\tau_P)|1, 0\rangle + \sum_n c_2^n(\tau_P)|2, n\rangle, \quad (9)$$

and Eq. (7) reduces to

$$\Delta N = K_{12}^{0n}(\omega_{21}^{0n})|\rho_{12}^{0n}(\tau_P)| \cos [(\omega_{21}^{0n} - \omega_L) \delta t - \phi_{12}^{0n}]. \quad (10)$$

The real and the imaginary part of the density matrix elements can be directly measured from the photocount difference for a particular choice of the time delay δt . For a pure state these elements are also the unnormalized coefficients of the vibrational wave-packet in the upper electronic state, i. e.

$$c_2^n(\tau_P) = \frac{|\rho_{12}^{0n}(\tau_P)|}{c_1^{0*}(\tau_P)} e^{-i\phi_{12}^{0n}}. \quad (11)$$

The unknown coefficient $c_1^0(\tau_P)$ can be chosen real and determined from the normalization.

For example, measurements have been numerically simulated for an ensemble of Sodium dimers. A particular quantum state is prepared using a train of three laser pulses of time duration of 60 fs, and a delay between them of 103 fs tuned on the vibronic transition $|1, 0\rangle \leftrightarrow |2, n\rangle$. The measurements are simulated by taking into account the shot noise. In Fig. (2) the norm of the reconstructed density matrix of the vibrational wave-packet in the upper electronic state is shown together with the relative deviation from the theoretical values.

In conclusion, an experiment has been proposed which allows one to directly measure the vibrational wave packet of a diatomic molecule. This applies for general anharmonic potentials and does not require complicated and instable reconstruction methods.

This work was supported by the Deutsche Forschungsgemeinschaft.

Squeezed angular momentum coherent states : construction and time evolution

R. ARVIEU

Institut des Sciences Nucléaires - F 38026 - Grenoble Cédex - France

e-mail address: arvieu@isn.in2p3.fr

P. ROZMEJ

University Marie Curie Sklodowska - PL 20-031 - Lublin - Poland

e-mail address: rozmej@tytan.umcs.lublin.pl

Abstract

A family of angular momentum coherent states on the sphere is constructed using previous work by Aragone et al. These states depend on a complex parameter which allows an arbitrary squeezing of the angular momentum uncertainties. The time evolution of these states is analyzed assuming a rigid body hamiltonian. The rich scenario of fractional revivals is exhibited with cloning and many interference effects.

In this contribution we will concentrate on a family of coherent states on the sphere which can be proposed for the description of the rotation of quantum simple systems like rigid diatomic molecules or rigid nuclei. The relevant hamiltonian depends then only on the angular momentum I and the energy spectrum is expressed in terms of a frequency ω_0 by $E_I = \hbar\omega_0 I(I + 1)$. A general wave packet (WP) of the family depends on a parameter η and of a real integer number k and will be denoted as $\Psi_{\eta k}(\theta, \phi)$. The states with k different from 0 are deduced from a parent state $\Psi_{\eta 0}$ defined as

$$\Psi_{\eta 0}(\theta, \phi) = \sqrt{\frac{N}{2\pi \sinh 2N}} e^{N \sin \theta (\cos \phi + i\eta \sin \phi)} \quad (1)$$

For real η the angular spread of the latter depends only on N while the average value of L_z is given by

$$\langle L_z \rangle = \eta(N \coth(2N) - \frac{1}{2}) \xrightarrow{N \gg \frac{1}{2}} \eta(N - \frac{1}{2}) \quad (2)$$

The states with $k \neq 0$ are obtained from (1) by application on $\Psi_{\eta 0}$ of an operator $(\mathcal{L}_+)^k$. The operator \mathcal{L}_+ and two other ones which form an SU(2) algebra are defined by

$$\mathcal{L}_3 = \frac{L_x + i\eta L_y}{\sqrt{1 - \eta^2}}, \quad \mathcal{L}_{\pm} = \pm \left(\frac{\eta L_x + iL_y}{\sqrt{1 - \eta^2}} \right) - L_z \quad (3)$$

Up to a normalization factor we have

$$\Psi_{\eta k}(\theta, \phi) = (\mathcal{L}_+)^k \Psi_{\eta 0}(\theta, \phi) \quad (4)$$

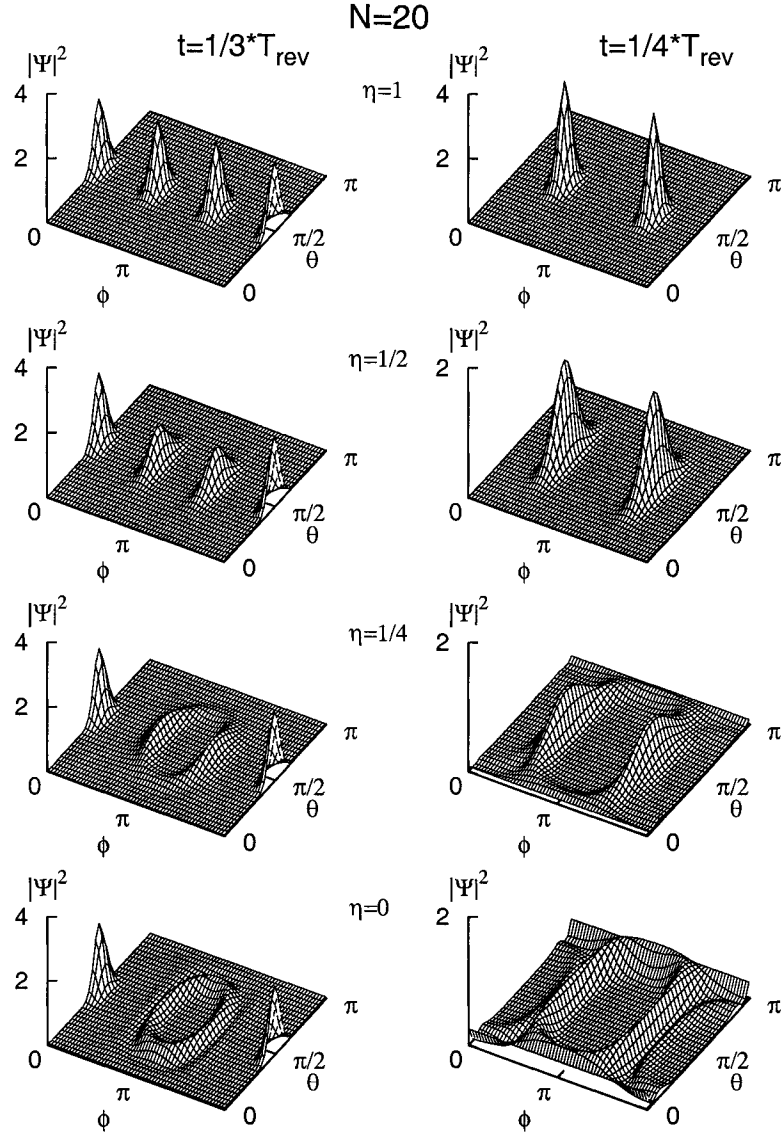


FIG. 1. Transition of fractional wave packets from exact clones ($\eta = 1$) through developing crescents ($\eta = 1/2, \eta = 1/4$) to ring topology ($\eta = 0$) is demonstrated for two fractional revival times $t = 1/3 * T_{\text{rev}}$ (left) and $t = 1/4 * T_{\text{rev}}$ (right). The fractional waves called mutants are clearly seen in the lower rows of the figure.

The states $\Psi_{\eta k}$ have the following properties:

1. They are eigenstates of \mathcal{L}_3

$$\mathcal{L}_3 \Psi_{\eta k} = k\sqrt{1 - \eta^2} \Psi_{\eta k} \quad (5)$$

2. The parameter $\eta = |\eta| \exp(i\alpha)$ is a squeezing parameter since one has

$$|\eta|^2 = \frac{\Delta L_x^2}{\Delta L_y^2} \quad (6)$$

3. If η is real the WP are minimum uncertainty states and in general we have

$$\Delta L_x^2 \Delta L_y^2 = \frac{1}{4} [\langle L_z \rangle^2 + |\langle \{L_x, L_y\} \rangle - \langle L_x \rangle \langle L_y \rangle|^2] = \frac{1}{4} \frac{\langle L_z \rangle^2}{\cos^2 \alpha} \quad (7)$$

4. Changing k enable to change the average values of all the components of L.

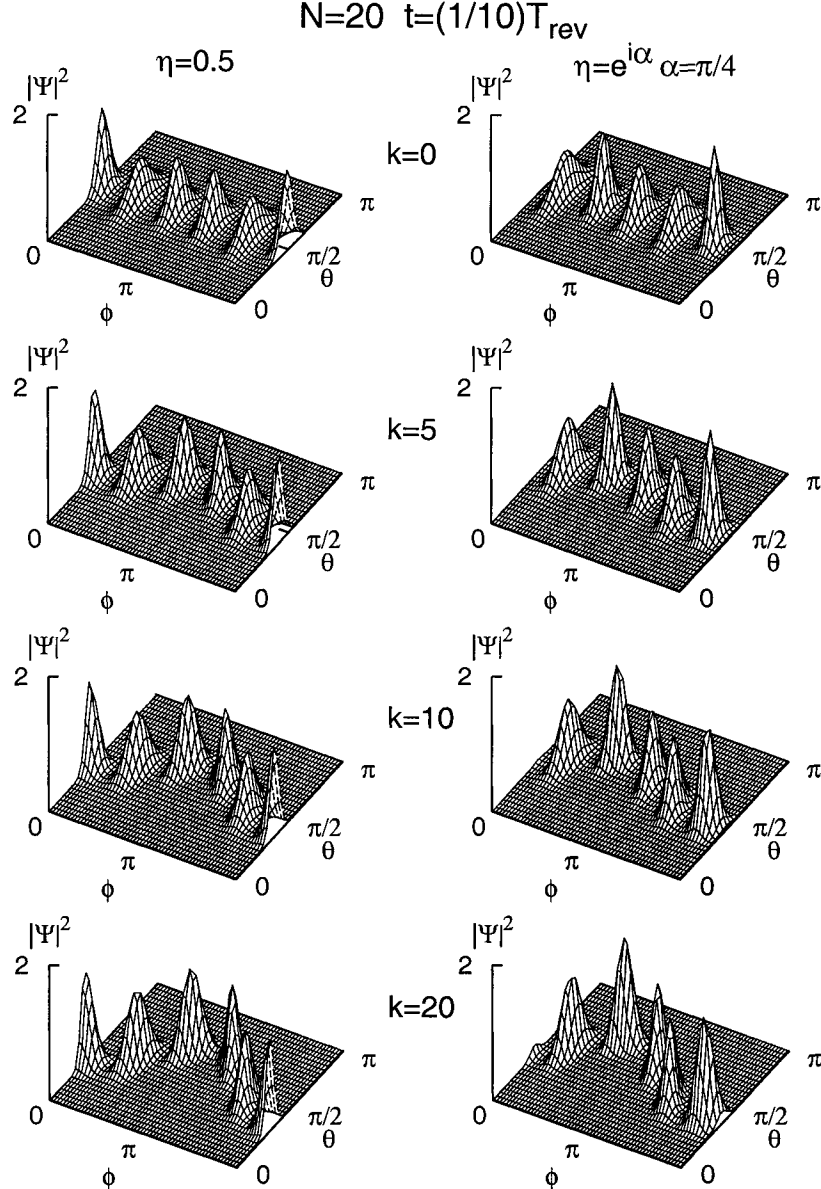


FIG. 2. Shapes of wave packets with $N = 20$ at fractional revival time $t = (1/10) T_{\text{rev}}$ for real $\eta = 0.5$ (left column), and $\eta = \exp(i\alpha)$, $\alpha = \pi/4$ (right column) and $k = 0, 5, 10, 20$ as functions of angular variables for a rigid molecule. Clones and mutants are clearly visible. Note that with increasing k the classical trajectory becomes more and more tilted with respect to Oxy plane.

There exist intensive analytical studies devoted to the eigenstates of L^2 and \mathcal{L}_3 . When η is real they are called intelligent spin states [1] and quasi intelligent spin states if η is complex [2]. These states extend the well known work of [3]. Ref. [2] has discussed fully the use of the SU(2) algebra (3). Obviously our WP are not eigenstates of L^2 but can be expanded in such a basis of intelligent or quasi intelligent spin states with the freedom, by a convenient choice of N , to concentrate the WP on the sphere. More details on these WP can be found in our recent papers [4] and [5].

Let us now sketch briefly the dynamics which take place if one take these WP as initial WP at time zero and if we let them evolve assuming a rigid body spectrum. Here we rely fully on the work of Averbukh and Perelman [6]. For times of the form $t = (m/n)T_{\text{rev}}$ ($T_{\text{rev}} = 2\pi/\omega_0$) the WP is subdivided into q fractional WP ($q = n$ if n is odd, $q = n/2$ if n is even), the shape of these WP depends on the squeezing parameter η . By changing η and k one can modify the quantum angular spread and make it different for the variable θ and for the variable ϕ . For $\eta = \pm 1$ and for all m/n the fractional WP are all clones of the initial one (upper part of Fig. 1 for $m/n = 1/3$ and $1/4$). For different values their shape changes (we have called these WP mutants). These shapes are shown in the lower part of Fig. 1 and on Fig. 2.

The differences between real and imaginary η are not very significant as shown in Fig. 2. Therefore there exist numerous possibilities for constructing angular coherent states using these intelligent and quasi intelligent spin states. Obviously the choice made in (1) of an exponential WP does not exhaust all possible ones. These remarks illustrate the richness of the rotation of a rigid body in quantum mechanics. The internal rotational degree of freedom (i.e. the use of D_{MK}^I functions instead of Y_M^I) can be studied on a similar footing [5].

This work extends to the rigid rotor in three dimensions the revival mechanism discussed in [7] for the hydrogen atom. The cloning mechanism, valid in our case only for $\eta = \pm 1$, was already investigated in ref [8] for an infinite square well. A review of the evolution of localized WP is found in [9].

REFERENCES

- [1] Aragone C et al. 1974 J. Phys. A : Math. Nucl. Gen. 17 L149;
Aragone C et al. 1976 J. Math. Phys. 17 1963.
- [2] Rashid M A 1978 J. Math. Phys 19 1391, 1397.
- [3] Radcliffe J M 1971 J. Phys. A4 313.
- [4] Arvieu R and Rozmej P 1999 J. Phys. A: Math. Gen. 32 2645.
- [5] Rozmej P and Arvieu R 1998 Phys Rev. A 58 4314.
- [6] Averbukh I Sh and Perelman NF 1989 Phys. Lett. A 139 449.
- [7] Dačić-Gaeta Z and Stroud CR 1990 Phys. Rev. A 42 6308.
- [8] Aronstein DI and Stroud CR 1997 Phys. Rev. A 55 4526.
- [9] Bluhm R et al. 1996 Am. J. Phys. 64 944.

Some applications of group-theoretical methods in geometric optics

José F. Cariñena

*Departamento de Física Teórica, Universidad de Zaragoza,
50009, Zaragoza, Spain*

Javier Nasarre

*Seminario de Matemáticas, I.E.S. Miguel Catalán
50009, Zaragoza, Spain*

A mathematical prelude

Dynamical evolution is described by systems of time-dependent first order differential equations $dx^i/dt = F^i(t, x)$, $i = 1, \dots, n$. The autonomous systems, for which F^i do not depend on t , can be considered as those determining the integral curves of a vector field $X = F^i(x) \frac{\partial}{\partial x^i}$. Similarly, the previous non-autonomous system determines the integral curves of the time-dependent vector field $X = F^i(x, t) \frac{\partial}{\partial x^i}$. The simplest case would be $dx^i/dt = A^i_j(t) x^j$, $i = 1, \dots, n$, which is written in matrix form $\dot{x} = A(t)x$, with A time-independent for autonomous systems.

We know that in the simplest case of an autonomous system the general solution can be written as a linear combination $x(t) = c_1 x_{(1)} + \dots + c_n x_{(n)}$ of n independent particular solutions and that the solution determined by $x(0)$ is $x(t) = \Phi(t)x(0)$, from which $\dot{\Phi}(t)\Phi^{-1}(t) = A$, with $\Phi(0) = 0$, and therefore $\Phi(t) = e^{At}$. We remark that $\Phi(t)$ can be found without computing the exponential when a set of n particular solutions are known, because if $X(t) = e^{At}X(0)$ then $e^{At} = X(t)X(0)^{-1}$.

For linear time-dependent systems, the relation between $x(t_0)$ and $x(t)$ depends on both t and t_0 and not only on $t - t_0$ and $\Phi(t, t_0) \neq e^{A(t-t_0)}$. If $[A(t), A(t')] = 0$, $\forall t, t'$, then $\Phi(t, t_0) = \exp\left(\int_{t_0}^t A(t') dt'\right)$, but how to find Φ when $[A(t), A(t')] \neq 0$? The equation $\dot{\Phi}(t, t_0)\Phi^{-1}(t, t_0) = A(t)$ cannot be easily solved in the general case, but if n solutions are known, then $\Phi(t, t_0) = X(t)X(t_0)^{-1}$. For some linear systems it suffices to know $k < n$ solutions for obtaining the general solution. For instance, for Frenet equations only one solution is necessary.

Therefore, the questions to be answered are: Are there other differential equation systems admitting a nonlinear superposition principle and allowing us to write the general solution in terms of some known particular solutions? How the knowledge of particular solutions can be used to simplify or, even more, to find the general solution?

Remark that for the linear autonomous case $\Phi(t) = e^{At}$ implies that $\dot{\Phi}(t)\Phi^{-1}(t) = A$ with $A \in \mathfrak{gl}(\mathbb{R}, n)$ and that the mentioned simplification in the non-autonomous case arises when A takes values in a subalgebra of $\mathfrak{gl}(\mathbb{R}, n)$, for instance A in the Frenet case A is skew-symmetric.

The main result is due to Lie [1]:

Theorem Given a non-autonomous system of n first order differential equations $dx^i/dt = X^i(x^1, \dots, x^n, t)$, $i = 1, \dots, n$, a necessary and sufficient condition for the existence of a function $\Phi : \mathbb{R}^{n(m+1)} \rightarrow \mathbb{R}^n$ such that the general solution is $x = \Phi(x_{(1)}, \dots, x_{(m)}; k_1, \dots, k_n)$, with $\{x_{(a)} \mid a = 1, \dots, m\}$ being a set of particular solutions of the system and k_1, \dots, k_n , n arbitrary constants, is that the system can be written as $dx^i/dt = Z_1(t)\xi^{1i}(x) + \dots + Z_r(t)\xi^{ri}(x)$, where Z_1, \dots, Z_r , are r functions depending only on t and $\xi^{\alpha i}$, $\alpha = 1, \dots, r$, are functions of $x = (x^1, \dots, x^n)$, such that the r vector fields in \mathbb{R}^n given by $Y^{(\alpha)} \equiv \sum_{i=1}^n \xi^{\alpha i}(x^1, \dots, x^n) \frac{\partial}{\partial x^i}$, $\alpha = 1, \dots, r$, close on a real finite-dimensional Lie algebra, i.e. $\{Y^{(\alpha)}\}$ are linearly independent and there are r^3 real numbers, $f^{\alpha\beta\gamma}$, such that $[Y^{(\alpha)}, Y^{(\beta)}] = \sum_{\gamma=1}^r f^{\alpha\beta\gamma} Y^{(\gamma)}$. The number r satisfies $r \leq mn$.

Particular examples are the linear systems $dx^i/dt = A^i_j(t)x^j$ for which the (linear) superposition principle is $\Phi(x_{(1)}, \dots, x_{(n)}; k_1, \dots, k_n) = k_1x_{(1)} + \dots + k_nx_{(n)}$. In this case $m = n$ and there are n^2 vector fields, $Y^{ij} = x^j \frac{\partial}{\partial x^i}$, which close on the $\mathfrak{gl}(n, \mathbb{R})$ algebra, $[Y^{ij}, Y^{kl}] = \delta^{il}Y^{kj} - \delta^{kj}Y^{il}$, to be compared with the commutation relations of the $\mathfrak{gl}(n, \mathbb{R})$ algebra, $[E_{ij}, E_{kl}] = \delta_{jk}E_{il} - \delta_{il}E_{kj}$, with $(E_{ij})_{kl} = \delta_{ik}\delta_{jl}$.

Another prototypical example is the Riccati equation $\dot{x} = c_2(t)x^2(t) + c_1(t)x(t) + c_0(t)$. The superposition principle comes from the relation $\frac{x-x_1}{x-x_2} : \frac{x_3-x_1}{x_3-x_2} = k$. In this case the vector fields $Y^{(1)}$, $Y^{(2)}$ and $Y^{(3)}$ are given by $Y^{(1)} = \frac{\partial}{\partial x}$, $Y^{(2)} = x \frac{\partial}{\partial x}$ and $Y^{(3)} = x^2 \frac{\partial}{\partial x}$, which close on a three-dimensional real Lie algebra, with defining relations $[Y^{(1)}, Y^{(2)}] = Y^{(1)}$, $[Y^{(1)}, Y^{(3)}] = 2Y^{(2)}$, and $[Y^{(2)}, Y^{(3)}] = Y^{(3)}$, i.e. the $\mathfrak{sl}(2, \mathbb{R})$ algebra (see e.g. [2]).

Notice that if the system cannot be written in the form of the statement of the Theorem the general solution cannot be written in terms of an arbitrary set of particular solutions. The solution should be obtained by approximation methods [3]. When the system can be written as proposed, the problem reduces to find a curve in a Lie group G with Lie algebra \mathfrak{g} starting from the neutral element and given by an equation $\dot{g}(t)g(t)^{-1} = X(t) \in \mathfrak{g}$. Such equation in the group can be solved using a generalization of the method proposed by Wei and Norman [4] for linear systems, i.e. writing $g(t)$ in terms of the second kind canonical coordinates w.r.t. a basis $\{a_\alpha \mid \alpha = 1, \dots, r\}$, $g(t) = \prod_{\alpha=1}^r \exp(u_\alpha(t)a_\alpha) = \exp(u_1(t)a_1) \cdots \exp(u_r(t)a_r)$, and transforming the equation into a differential equation system for the $u_\alpha(t)$. This last system may be even more difficult but we only need a particular solution. Moreover, the problem of finding $g(t)$ can be simplified when we know particular solutions of the original system: there exist reduction theorems and group based procedures for simplifying it.

The second class coordinates $u_\alpha(t)$ can be found using

$$X(t) = \sum_{\alpha=1}^r b_\alpha(t)a_\alpha = \sum_{\alpha=1}^r \dot{u}_\alpha(t) \left[\prod_{\beta=\alpha+1}^r \exp(u_\beta(t) \text{ad } a_\beta) \right] a_\alpha$$

with $u_\alpha(0) = 0$, $\alpha = 1, \dots, r$. It is quite simple to use it for the inhomogeneous linear equation $\frac{dx}{dt} = c_1(t)x + c_0(t)$ with associated vector field: $X = c_1(t)x \frac{\partial}{\partial x} + c_0(t) \frac{\partial}{\partial x} = c_1(t)L_1 + c_0(t)L_0$, $L_0 = \frac{\partial}{\partial x}$ and $L_1 = x \frac{\partial}{\partial x}$, which close on the Lie algebra, $[L_0, L_1] = L_0$, and there exist two orderings for $g(t)$; $g(t) = \exp(u_1(t)L_1) \exp(u_0(t)L_0)$ gives rise to the linear superposition principle. $x(t) = C_1x^1(t) + C_2x^2(t)$, $C_1 = (1-x_0)$, $C_2 = x_0$, and using the second order, $g(t) = \exp(v_0(t)L_0) \exp(v_1(t)L_1)$ it is found that $x(t) = e^{\int dt c_1(t)} (x_0 + \int dt c_0(t) e^{-\int dt' c_1(t')})$. Similarly, for Riccati Equation $g(t)$ takes values in the group $SL(2, \mathbb{R})$ and satisfies $\dot{g}(t)g(t)^{-1} = [c_0(t)L_0 + c_1(t)L_1 + c_2(t)L_2]$, $g(0) = I$, where L_α

are generating a Lie algebra isomorphic to $\mathfrak{sl}(2, \mathbb{R})$, $L_0 = \frac{\partial}{\partial x}$, $L_1 = x \frac{\partial}{\partial x}$ and $L_2 = x^2 \frac{\partial}{\partial x}$. There will be six orderings, the first one being $g(t) = \exp(u_1 L_1) \exp(u_2 L_2) \exp(u_0 L_0)$ giving rise to the following equations:

$$\begin{aligned}\dot{u}_0(t) &= a_0(t) + a_1(t)u_0(t) + a_2(t)u_0^2(t) \\ \dot{u}_1(t) &= a_1(t) + 2a_2(t)u_0(t) \\ \dot{u}_2(t) &= a_2(t) - a_1(t)u_2(t) - 2a_2(t)u_0(t)u_2(t)\end{aligned}$$

with initial conditions $u_0(0) = u_1(0) = u_2(0) = 0$.

Applications in geometric optics

Not only linear systems, but Riccati equations too, appear very often in Physics, mainly as a consequence of Lie reduction theory when taking into account that dilations are symmetries of second order differential equations [5], and then it may be useful for solving Schrödinger equation for stationary states. For other applications, see e.g. [6] and [7]. Furthermore, it is a condition for the superpotential W in the factorization of H

$$H - c = \left(-\frac{d}{dx} + W \right) \left(\frac{d}{dx} + W \right)$$

and it plays a relevant role in the search for Shape Invariant potentials (Infeld and Hull Factorization method). It may appear every time the group $SL(2, \mathbb{R})$ plays a role (see e.g. [8]) and because of the isomorphism of the Lie algebras of $SL(2, \mathbb{R})$ and the linear symplectic group, it will be useful in the linear approximation of Symplectic transformations.

Radiative transfer equation for polarized light

The intensity and the state of polarization of a partially polarized beam of light are completely determined by the four Stokes parameters. The Stokes vector [9] $\mathbf{I} = (Q, U, V, I)$ satisfies the Stokes criterion $Q^2 + U^2 + V^2 \leq I^2$, what allows us to define the degree of polarization $p = \frac{1}{I} \sqrt{Q^2 + U^2 + V^2}$. The state of polarization changes because of the interaction between the radiation beam and the media itself. Using the terminology borrowed from relativity, Stokes criterion establishes that \mathbf{I} is a time-like vector and according to a well-known result [10], the fact that this time-like character is preserved in the evolution means that the change of the state of polarization is described by an element of the Weyl group [11], $T_4 \odot (D \otimes \mathcal{L})$. At the infinitesimal level, the transfer equation for polarized light, [12] introduced by Unno and completed by Rachkowsky will be $\frac{d}{dz} \mathbf{I} = -K \mathbf{I} + \mathbf{J}$ where z is the geometrical path, K is a matrix of the homogeneous Weyl algebra and \mathbf{J} is the emission term. Additional assumptions on the characteristics of media restrict even more the form of the 4×4 matrix K describing absorption in presence of Zeeman effect. So, for nondepolarizing media $I'^2 - Q'^2 - U'^2 - V'^2 = I^2 - Q^2 - U^2 - V^2$, the group reduces to Poincaré group and K lies in the Lie algebra of it.

Application in symplectic optics

The evolution of rays in optical phase space, which is endowed with a symplectic structure [13], is not linear but described by Hamilton equations and this gives rise to aberrations. The optical Hamiltonian is given by $h = -\sqrt{n^2(z, q) - p^2}$, the associated symplectic maps are $\xi(z) = \mathcal{M}(z, z_0)\xi(z_0)$, where $\xi = (\mathbf{q}, \mathbf{p})$, and \mathcal{M} satisfy $\dot{\mathcal{M}} = \mathcal{M}H$, and $\mathcal{M}(0) = I$, with H being the vector field $H = \{\cdot, h\}$. When H takes values in a Lie algebra we can use the theory

we mentioned in the previous section, otherwise we should use approximation methods. The simplest case is when the refractive index is constant, $H = \frac{p}{\sqrt{n^2 - p^2}} \frac{\partial}{\partial q}$. Then the results of Fer and Magnus approximation methods coincide. In the case of a z -dependent refraction index, if $n = n(z)$, using Taylor development for the Hamiltonian $h = -\sqrt{n^2(z) - p^2} = -n(z) + \frac{1}{2n(z)}p^2 + \frac{1}{8n^3(z)}p^4 + \frac{1}{16n^5(z)}p^6 + \dots$, we can see that the three methods of Fer, Magnus and Dragt-Forest, give the same results in the paraxial approach: $q(z) = q_0 + \mathcal{N}(z)p_0$, $p(z) = p_0$, with $\mathcal{N}(z) = \int_{z_0}^z dz' \frac{1}{n(z')}$. The Hamiltonian for the third order aberration is $h = -n(z) + \frac{1}{2n(z)}p^2 + \frac{1}{8n^3(z)}p^4$, and then $H = \left(\frac{1}{n(z)}p + \frac{1}{2n^3(z)}p^3 \right) \frac{\partial}{\partial q}$. Once again the three methods coincide $p = p_0$, $q(z) = q_0 + p_0\mathcal{N}(z) + \frac{1}{2}p_0^3\mathcal{R}(z)$, with $\mathcal{R}(z) = \int_{z_0}^z dz' \frac{1}{n^3(z')}$.

Finally, the most interesting case is that of q and z -dependent refractive index. If $h = h_0 + h_2 + h_4 + \dots$, with

$$h_0 = -\alpha_0(z), \quad h_2 = \frac{1}{2\alpha_0(z)}p^2 - \alpha_2(z)q^2, \quad h_4 = \frac{1}{8\alpha_0^3(z)}p^4 - \frac{\alpha_2(z)}{2\alpha_0^2(z)}p^2q^2 - \alpha_4(z)q^4.$$

The paraxial approach is $H = \frac{1}{\alpha_0(z)}p \frac{\partial}{\partial q} + 2\alpha_2(z)q \frac{\partial}{\partial p}$.

Using Wei-Norman method, $U(z) = \exp(u_1 L_1) \exp(u_2 L_2) \exp(u_0 L_0)$, we find

$$\begin{aligned} \dot{u}_0(z) &= \frac{1}{\alpha_0(z)} - 2\alpha_2(z)u_0^2(z) \\ \dot{u}_1(z) &= -4\alpha_2(z)u_0(z) \\ \dot{u}_2(z) &= -2\alpha_2(z) + 4\alpha_2(z)u_0(z)u_2(z). \end{aligned}$$

This gives the action

$$\begin{aligned} q(z) &= (1 - u_0 u_2) e^{\frac{1}{2}u_1} q_0 + u_0 e^{-\frac{1}{2}u_1} p_0 \\ p(z) &= -u_2 e^{\frac{1}{2}u_1} q_0 + e^{\frac{1}{2}u_1} p_0. \end{aligned}$$

REFERENCES

- [1] Lie S. and Scheffers G., *Vorlesungen über kontinuierlichen Gruppen mit geometrischen und anderen Anwendungen*, Teubner, Leipzig (1893).
- [2] Cariñena J.F., and Ramos A., *Int. J. Mod. Phys.* **14**, 1935 (1999).
- [3] Dragt A.J. and Forest E., *J. Math. Phys.* **24**, 2734 (1983)
- [4] Wei J. and Norman E., *J. Math. Phys.* **4**, 575 (1963).
- [5] Cariñena J.F., Marmo G. and Nasarre J., *Int. J. Mod. Phys.* **13**, 3601 (1998).
- [6] Bel L., gr-qc 9702028
- [7] Barata J.C.A., math-ph/9903041,
- [8] Schopohl N., cond-math/9804064
- [9] Kim Y.S., Contribution in these Proceedings (1999)
- [10] Zeeman E.C., *J. Math. Phys.* **5**, 490 (1964).
- [11] Boya L.J., Cariñena J.F. and Santander M., *J. Math. Phys.* **16**, 1813 (1975).
- [12] Landi degl'Innocenti E. and Landi degl'Innocenti M., *Nuovo Cim.* **62 B** 1 (1981).
- [13] Cariñena J.F. and Nasarre J., *Forts. der Phys.* **44**, 181 (1996)

Trilinear Quantum Optical Hamiltonians Through $su_q(2)$ Perturbation Theory

Angel Ballesteros

*Departamento de Física, Universidad de Burgos
Pza. Misael Bañuelos, E-09001-Burgos, Spain*

Sergei M. Chumakov

*Departamento de Física, Universidad de Guadalajara
Corregidora 500, 44420, Guadalajara, Jal., México*

Abstract

The quantum algebra $su_q(2)$ is shown to be the approximate dynamical symmetry algebra of trilinear boson interactions in Quantum Optics. As a consequence, the spectrum and eigenvectors of a certain hamiltonian defined on $su_q(2)$ can be used to solve the dynamics of such models. In particular, a perturbative approach to the obtention of the ground state energy in the case of second harmonics generation is presented.

I. DYNAMICAL $su_q(2)$ SYMMETRY IN QUANTUM OPTICS

Its well-known that quantum optical hamiltonians describing Raman and Brillouin scattering, the processes of three and four-wave mixing, the second and the third-harmonics generation or the interaction of atomic systems with a quantized radiation field in an ideal cavity (Dicke model) can be presented in a block-diagonal form. Each block is a finite dimensional subspace where the Hamiltonian acts as a matrix (usually, of very high dimension) of the form (see [1]-[6] and references therein)

$$H = \begin{pmatrix} 0 & A_l & 0 & \dots & 0 \\ A_l & 0 & A_{l-1} & \dots & 0 \\ \dots & \dots & \dots & \dots & \dots \\ 0 & \dots & A_{-l+2} & 0 & A_{-l+1} \\ 0 & \dots & 0 & A_{-l+1} & 0 \end{pmatrix}. \quad (1.1)$$

In [4-5] it was noticed that, for certain dynamical regimes, such hamiltonians can be approximated by the $J_x = (J_+ + J_-)/2$ generator of the $su(2)$ algebra. This fact allows the use of a $su(2)$ perturbation theory in order to analyse the dynamics associated to (1.1). In this contribution we show that the $su_q(2)$ quantum algebra (see [7]-[9]) can be also used to

define a Hamiltonian of the type (1.1) in a natural way. Moreover, the use of a quantum algebra provides an additional (deformation) parameter that enlarges the range of dynamical regimes for which the perturbation theory can be applied and improves the accuracy of the model.

We recall that the quantum algebra $\text{su}_q(2)$ [7]-[9] is a deformation of the $\text{su}(2)$ algebra given by the following deformed commutation rules:

$$[J_z, J_\pm] = \pm J_\pm, \quad [J_+, J_-] = [2 J_z], \quad (1.2)$$

where $[x] := \frac{q^x - q^{-x}}{q - q^{-1}}$ and $q = e^{z/2}$. Obviously, ‘‘classical’’ (undeformed) results are obtained when the limit $q \rightarrow 1$ ($z \rightarrow 0$) is considered. In the ‘‘bare’’ basis of eigenvectors of J_z ,

$$2J_z|l, m\rangle = 2m|l, m\rangle, \quad (1.3)$$

the $(2l + 1)$ -dimensional irreducible representation of $\text{su}_q(2)$ is given by (1.3) and

$$J_\pm|l, m\rangle = \sqrt{[l \mp m][l \pm m + 1]}|l, m \pm 1\rangle. \quad (1.4)$$

Let us consider the following operator defined on $\text{su}_q(2)$ [10]:

$$H_q = q^{J_z/2} (J_+ + J_-) q^{J_z/2}. \quad (1.5)$$

The connection between (1.5) and trilinear quantum optical hamiltonians is immediate provided we consider the $(2l + 1)$ -dimensional representation D_l for H_q , that takes the form (1.1) with

$$A_m(q) = q^{m-1/2} \sqrt{[l+m][l-m+1]}. \quad (1.6)$$

In particular, when $l = 1$ we have,

$$D_1(H_q) = \begin{pmatrix} 0 & q^{1/2}\sqrt{[2]} & 0 \\ q^{1/2}\sqrt{[2]} & 0 & q^{-1/2}\sqrt{[2]} \\ 0 & q^{-1/2}\sqrt{[2]} & 0 \end{pmatrix}. \quad (1.7)$$

A straightforward computation shows that the spectrum of this operator is $[2], 0, -[2]$. The corresponding normalized eigenvectors are

$$|\underline{1}, \pm 1\rangle = \frac{1}{\sqrt{2[2]}} \begin{pmatrix} q^{1/2} \\ \pm\sqrt{[2]} \\ q^{-1/2} \end{pmatrix}, \quad |\underline{1}, 0\rangle = \frac{1}{[2]} \begin{pmatrix} q^{-1/2}\sqrt{[2]} \\ 0 \\ -q^{1/2}\sqrt{[2]} \end{pmatrix}. \quad (1.8)$$

By making use of the Hopf algebra structure of the $\text{su}_q(2)$ algebra, this result can be generalized to arbitrary dimensions. It turns out that the spectrum of H_q for a given l is anharmonic and given by the q -numbers $[2m]$, with $m = -l, \dots, l$. Moreover, arbitrary eigenvectors can be also constructed, as well as Clebsch-Gordan coefficients for both the bare and the dressed basis [10].

II. DICKE/SHG HAMILTONIAN AND $su_q(2)$ PERTURBATION THEORY

Let us consider the Dicke model, which describes the interaction of a system of $N = 2l$ two-level atoms with the quantum radiation field in an ideal cavity. The Dicke hamiltonian can be written in the matrix form (1.1) with the matrix elements

$$A_m^D = \sqrt{(l+m)(l+1-m)(s+1-m)}, \quad (2.1)$$

where $s \geq l$ is a fixed parameter ($2s$ is just the excitation number, which is a constant of the motion in this model [4]-[5]). In particular, the case $s = l$ represents the highest nonlinearity, and is mathematically equivalent to the second harmonics generation (SHG) hamiltonian. Moreover, we will be mainly interested in the limit of large l (high photon numbers).

Let us try to approximate the Dicke hamiltonian H^D through a zeroth-order hamiltonian

$$H_0 = \Omega H_q, \quad (2.2)$$

with H_q (1.5) belonging to $su_q(2)$. It is immediate to realize that we have two free parameters (q and Ω) in order to get the closest H_0 that will optimize a further perturbation approach. The simplest way to do this is to choose both parameters in such a way that the matrix elements A_m^D of the three-wave Hamiltonian H^D and the matrix elements

$$\tilde{A}_m(q) = \Omega \langle l, m+1 | H_q | l, m \rangle = \Omega q^{m-1/2} \sqrt{[l-m][l+m+1]} \quad (2.3)$$

of the Hamiltonian H_0 coincide in their maxima. This choice gives rise (for $s = l$) to the following relations involving both parameters and the number of atoms N :

$$\alpha = N \log q = \frac{3}{2} \log \frac{\sqrt{5}-1}{2} \approx -0.7218, \quad (2.4)$$

$$\Omega = \frac{4(N+1)^{3/2}}{\sqrt{27}[N+1]}. \quad (2.5)$$

In this way, both the maxima of A_m^D and $\tilde{A}_m(q)$ (considered as functions of m) occur in the point $m_0 = -(l-1)/3$.

Now, around such a maximum we can approximate the Dicke/SHG matrix elements as:

$$A_m^D \approx \Omega \tilde{A}_m(q) \phi(m), \quad \phi(m) = 1 + \phi_1 \Delta - \phi_2 \Delta^2 + \phi_3 \Delta^3, \quad \Delta = m - m_0. \quad (2.6)$$

We thus restrict the expansion up to the third-order polynomial $\phi(m)$. The coefficients ϕ_j can be explicitly found and read:

$$\phi(\Delta) = 1 - \left(\frac{27}{8} - \frac{2\alpha^2}{\tanh^2 \alpha} \right) \left(\frac{\Delta}{N+1} \right)^2 + \left(\frac{27}{8} + \frac{4\alpha^3}{\tanh^2 \alpha} \right) \left(\frac{\Delta}{N+1} \right)^3 + O(N^{-4}). \quad (2.7)$$

Now we may substitute $\Delta = m - m_0 = J_z + (l-1)/3$ and rewrite (2.6) in the matrix form:

$$H^D \approx \Omega [J_+ \phi(J_z - m_0) + \phi(J_z - m_0) J_-] = 2 \Omega \{H_q, f(J_z)\}. \quad (2.8)$$

Here $J_{\pm,z}$ are generators of $su_q(2)$ and $\{A, B\} = AB + BA$. The new function $f(J_z)$ is also a polynomial of degree three, whose coefficients f_k can be easily obtained. Now the ground state energy of H^D can be approximately given as

$$\langle \underline{-l, l} | H^D | \underline{-l, l} \rangle \approx -\Omega [2l] \sum_{k=0}^3 f_k \langle \underline{-l, l} | (J_z)^k | \underline{-l, l} \rangle, \quad (2.9)$$

where $|\underline{-l, l}\rangle$ is the ground state for the H_q hamiltonian in the dressed basis. Therefore, we have reduced the problem to the calculation of averages of the powers of the operators J_z (the moments) in the eigenstates of the operator H_q , and this problem can be solved for arbitrary eigenstates.

Comparing these results with the numerical computations, it turns out that the accuracy for the energy of the ground state is 1.5% for 100 atoms ($N = 100$) and 0.35% for 400 atoms. Note that the correct asymptotic behaviour when $N \rightarrow \infty$ (large photon numbers) is obtained without considering higher degree expansions. It is also worth mentioning that this method produces much better accuracy than both the analogous $su(2)$ perturbation theory (see [4],[5],[11]) or than the variational method with the $su(2)$ coherent states as probe states introduced in [12]. Therefore, quantum algebras seem to provide a new suitable analytic approach to the dynamics of nonlinear quantum optical processes.

Acknowledgements

This work was partially supported by CONACYT, Mexico (Project No. 465100-5-3927PE) and by Junta de Castilla y León, España (Project CO2/399). We thank V.P. Karassiov, A.B. Klimov and K.B. Wolf for interesting discussions.

REFERENCES

- [1] L. Mandel and E. Wolf, *Optical Coherence and Quantum Optics* (Cambridge University Press, Cambridge, 1995).
- [2] V.P. Karassiov and A.B. Klimov, Phys. Lett. A **189**, 43 (1994).
- [3] V.P. Karassiov, J. Sov. Laser Research **13**, 188 (1992).
- [4] S.M. Chumakov and M. Kozierowski, Quant. Semiclas. Optics **8**, 775 (1996).
- [5] M. Kozierowski, A.A. Mamedov and S.M. Chumakov, Phys. Rev. A **42**, 1762 (1990).
- [6] G. Drobný, A. Bandilla and I. Jex, Phys. Rev. A **55**, 78 (1997).
- [7] P. Kulish and N. Reshetikhin, J. Soviet. Math. **23**, 2435 (1983).
- [8] V.G. Drinfel'd, in *Quantum Groups*, Proceedings of the International Congress of Mathematics, (MRSI, Berkeley, 1986).
- [9] M. Jimbo, Lett. Math. Phys. **10**, 63 (1985).
- [10] A. Ballesteros and S.M. Chumakov, J. Phys. A **32**, (1999) (to appear). LANL preprint quant-ph/9810061.
- [11] S.M. Chumakov, A.B. Klimov and J.J. Sánchez-Mondragón, Phys. Rev. A **49**, 4972 (1994).
- [12] V.P. Karassiov, Phys. Lett. A **238**, 19 (1998).

Ray Optics and Sheared States as Representations of Symplectic Groups

S. Bařkal *

Department of Physics, Middle East Technical University, 06531 Ankara, Turkey

Y. S. Kim †

Department of Physics, University of Maryland, College Park, Maryland 20742, U.S.A.

Abstract

The shear representations of the $Sp(2)$ group is derived from the theory of ray optics. Sheared states in Fock space are constructed and are discussed as two-photon or two-phonon coherent states. It is shown that these states can be described in terms of squeezed states which are already well-established.

I. INTRODUCTION

Shear transformations receive wide attention in applied physics, most significantly in the context of condensed matter [1] and in optics [2], both geometric and quantum. Here, our attempt is to contribute to the theoretical aspect of this interdisciplinary concept. We point out that shear transformations are the representations of the $Sp(2)$ or $SU(1,1)$ groups, which are locally isomorphic. We first introduce the two by two transformation matrices of $Sp(2)$ in the framework of ray optics. We then construct shear states in Fock space and discuss them in connection with squeezed states of light.

II. RAY OPTICS AS REPRESENTATIONS OF $SP(2)$

We formulate the $Sp(2)$ symmetry by studying a concrete physical example. For this purpose, we introduce the fundamental equations of para-axial ray optics [3]. The para-axial theory of ray optics consists of straight lines of the form

$$y = sx + b \tag{1}$$

*electronic mail: baskal@newton.physics.metu.edu.tr

†electronic mail: yskim@physics.umd.edu

on the xy coordinate system, where s and b are the slope and the y value at $x = 0$ respectively. The y coordinate measures the distance from the x axis. The above equation can be written in the matrix form as

$$\begin{pmatrix} y \\ s \end{pmatrix} = \begin{pmatrix} 1 & x \\ 0 & 1 \end{pmatrix} \begin{pmatrix} 0 \\ s \end{pmatrix}. \quad (2)$$

Let us consider a thin convex lens which changes the slope of the ray. The change depends on the focal length and the distance from the axis. For the para-axial rays,

$$s' = s - \frac{y}{f}. \quad (3)$$

This formula can also be converted to a matrix form

$$\begin{pmatrix} y' \\ s' \end{pmatrix} = \begin{pmatrix} 1 & 0 \\ -1/f & 1 \end{pmatrix} \begin{pmatrix} y \\ s \end{pmatrix}. \quad (4)$$

The above two-by-two matrix is called the lens matrix.

III. TWO DIFFERENT REPRESENTATIONS OF $SP(2)$

The translation and lens matrices of the preceding section are generated by

$$X_1 = \begin{pmatrix} 0 & i \\ 0 & 0 \end{pmatrix}, \quad X_2 = \begin{pmatrix} 0 & 0 \\ i & 0 \end{pmatrix}. \quad (5)$$

If we take the commutation relation,

$$[X_1, X_2] = iX_3, \quad (6)$$

with

$$X_3 = \begin{pmatrix} i & 0 \\ 0 & -i \end{pmatrix}. \quad (7)$$

This new generator satisfies the following commutation relations with X_1 and X_2

$$[X_1, X_3] = -2iX_1, \quad [X_2, X_3] = 2iX_2. \quad (8)$$

Thus the commutation relations in Eq.(6) and Eq.(8) form a closed set, and the matrices X_1, X_2 and X_3 generate a Lie group. If we make the following linear combinations of the above three generators

$$L = \frac{1}{2}(X_2 - X_1), \quad B_1 = \frac{1}{2}X_3, \quad B_2 = \frac{1}{2}(X_2 + X_1) \quad (9)$$

with their matrix form as

$$L = \frac{1}{2} \begin{pmatrix} 0 & -i \\ i & 0 \end{pmatrix}, \quad B_1 = \frac{1}{2} \begin{pmatrix} i & 0 \\ 0 & -i \end{pmatrix}, \quad B_2 = \frac{1}{2} \begin{pmatrix} 0 & i \\ i & 0 \end{pmatrix} \quad (10)$$

we immediately recognize the $Sp(2)$ group, where L generates rotations while, B_1 and B_2 generate squeezes. We therefore have two different representations of $Sp(2)$, which we call them the "shear-squeeze" and the "rotation-squeeze" representations.

In the sequel we will observe that the Iwasawa decomposition theorem [4] finds a worthy application in constructing sheared states. The transformation matrices obtained from X_1 and X_2 decompose as:

$$\begin{pmatrix} 1 & \alpha \\ 0 & 1 \end{pmatrix} = \begin{pmatrix} \cos(\psi_-/2) & \sin(\psi_-/2) \\ -\sin(\psi_-/2) & \cos(\psi_-/2) \end{pmatrix} \begin{pmatrix} e^{\lambda/2} & 0 \\ 0 & e^{-\lambda/2} \end{pmatrix} \begin{pmatrix} \cos(\psi_+/2) & -\sin(\psi_+/2) \\ \sin(\psi_+/2) & \cos(\psi_+/2) \end{pmatrix}, \quad (11)$$

and

$$\begin{pmatrix} 1 & 0 \\ \beta & 1 \end{pmatrix} = \begin{pmatrix} \cos(\phi_+/2) & \sin(\phi_+/2) \\ -\sin(\phi_+/2) & \cos(\phi_+/2) \end{pmatrix} \begin{pmatrix} e^{\rho/2} & 0 \\ 0 & e^{-\rho/2} \end{pmatrix} \begin{pmatrix} \cos(\phi_-/2) & -\sin(\phi_-/2) \\ \sin(\phi_-/2) & \cos(\phi_-/2) \end{pmatrix}, \quad (12)$$

respectively. The shear parameters α and β are related to the rotation and squeeze parameters in similar forms:

$$\begin{aligned} \psi_+ &= \cot^{-1}(\alpha/2), & \psi_- &= \pi - \cot^{-1}(\alpha/2), & \lambda &= \cosh^{-1}(1 + \alpha^2/2), \\ \phi_+ &= \cot^{-1}(\beta/2), & \phi_- &= \pi - \cot^{-1}(\beta/2), & \rho &= \cosh^{-1}(1 + \beta^2/2). \end{aligned} \quad (13)$$

IV. SHEARED STATES

We are now interested in constructing sheared states in the Fock space. For this purpose we shall make use of the "squeeze-rotation" generators of $SU(1,1)$, which are already available in the literature [5,6]:

$$L = -\frac{1}{4}(a^\dagger a + a a^\dagger), \quad B_1 = -\frac{i}{4}(a a - a^\dagger a^\dagger), \quad B_2 = -\frac{1}{4}(a a + a^\dagger a^\dagger). \quad (14)$$

In view of Eq.(9) the "shear-squeeze" representation is written as:

$$X_1 = -\frac{1}{4}(a - a^\dagger)^2, \quad X_2 = -\frac{1}{4}(a + a^\dagger)^2, \quad X_3 = -\frac{i}{2}(a a - a^\dagger a^\dagger). \quad (15)$$

The most general sheared states in Fock space are constructed with the application of the shear transformations to the vacuum state:

$$\begin{aligned} \exp(-i\alpha X_1) |0\rangle &= \exp\left\{i\frac{\alpha}{4}(a - a^\dagger)^2\right\} |0\rangle, \\ \exp(-i\beta X_2) |0\rangle &= \exp\left\{i\frac{\beta}{4}(a + a^\dagger)^2\right\} |0\rangle \end{aligned} \quad (16)$$

and they can be expanded in power series as:

$$\sum \frac{1}{n!} \left(\frac{i\alpha}{4}\right)^n (a - a^\dagger)^{2n} |0\rangle, \quad \sum \frac{1}{n!} \left(\frac{i\beta}{4}\right)^n (a + a^\dagger)^{2n} |0\rangle, \quad (17)$$

respectively. It is possible to construct the series, but it is not straight-forward to compute $(a \pm a^\dagger)^{2n} |0\rangle$. One easy way to look at this problem is to decompose the shear operator into squeeze and rotation operators. For this purpose we refer to Eq.(11) and Eq.(12), which can be expressed in compact forms as

$$\begin{aligned}\exp(-i\alpha X_1) &= \exp(i\psi_- L) \exp(-i\lambda B_1) \exp(-i\psi_+ L), \\ \exp(-i\beta X_2) &= \exp(i\phi_+ L) \exp(-i\rho B_1) \exp(-i\phi_- L),\end{aligned}\tag{18}$$

respectively.

With this preparation sheared states are expressed in a more revealing form:

$$\begin{aligned}\exp(-i\alpha \hat{X}_1) &= \exp\{i\alpha(a - a^\dagger)^2/4\} = \exp(i\psi_- \hat{L}) \exp(-i\lambda \hat{B}_1) \exp(-i\psi_+ \hat{L}), \\ \exp(-i\beta \hat{X}_2) &= \exp\{i\beta(a + a^\dagger)^2/4\} = \exp(i\phi_+ \hat{L}) \exp(-i\rho \hat{B}_1) \exp(-i\phi_- \hat{L}).\end{aligned}\tag{19}$$

If these operators are applied to the vacuum state, $\exp(-i\psi_+ \hat{L})$ and $\exp(-i\phi_- \hat{L})$ become $\exp(i\psi_+/4)$ and $\exp(i\phi_-/4)$ respectively. Thus, the sheared vacuum states are

$$\begin{aligned}\exp(-i\alpha \hat{X}_1) |0\rangle &= \exp(i\psi_+/4) \exp(i\psi_- \hat{L}) \exp(-i\lambda \hat{B}_1) |0\rangle, \\ \exp(-i\beta \hat{X}_2) |0\rangle &= \exp(i\phi_-/4) \exp(i\phi_+ \hat{L}) \exp(-i\rho \hat{B}_1) |0\rangle.\end{aligned}\tag{20}$$

According to these equations, the sheared vacuum is a squeezed vacuum followed by a rotation.

- [1] G. A. Garret, A. G. Rojo, A. K. Sood, J. F. Whitaker, R. Merlin, *Science* 275 (1997) 1638.
- [2] A. W. Lohmann, *J. Opt. Soc. Am. A* 10 (1993) 2181.
- [3] M. Nazarathy and J. Shamir, *J. Opt. Soc. Am.* 72 (1982) 356
- [4] R. Simon and N. Mukunda, *J. Opt. Soc. Am. A*, 55 (1998) 2146
- [5] Y. S. Kim and L. Yeh, *J. Math. Phys.* 33 (1992) 1237
- [6] Y. S. Kim and M. E. Noz, *Phase Space Picture of Quantum Mechanics* (World Scientific, Singapore, 1991)

$Sp(2, R) \sim SU(1, 1)$ in quantum optics and $Sp(4, R)$ with subgroups for two modes

Alfred Wünsche

*Humboldt-Universität, Institut für Physik, Nichtklassische Strahlung,
Invalidenstr. 110, 10115 Berlin, Germany
e-mail: awuensche@physik.hu-berlin.de*

Abstract

We consider the symplectic groups $Sp(2n, R)$ of an n -mode system in quantum mechanics and discuss, in particular, $Sp(2, R) \sim SO(2, 1)$ for a single mode and $Sp(4, R) \sim SO(3, 2)$ with some of its important subgroups such as $SU(2)$ and $SU(1, 1) \sim Sp(2, R)$ in quantum optics (squeezing, beamsplitter, light polarization). The root diagrams, different realizations of $Sp(2, R)$ and the unitary and nonunitary irreducible representations are shortly discussed.

I. INTRODUCTION

The symplectic groups $Sp(n, R)$ are the groups of homogeneous linear transformations which preserve the structure of classical Hamiltonian mechanics as well as of quantum mechanics of canonically quantized systems of n degrees of freedom (outer automorphism groups). The group of inner automorphisms which are the displacement groups are different in both regions because the quantum-mechanical displacement groups (Heisenberg-Weyl groups) are, in contrast to the classical displacement groups, noncommutative ones which, however, in addition to the noncommutative irreducible representation possess commutative ones. This determines the relations between classical Hamiltonian and canonical quantum mechanics. Since I have submitted a paper with some content of my lecture to the special issue of JOPB [1], I treat here only some problems which mainly complement this paper.

II. SYMPLECTIC GROUPS IN QUANTUM MECHANICS

Quantum mechanics is very important for the treatment of symplectic groups $Sp(2n, R)$ as it provides a concrete realization by quadratic combinations of canonical or of boson operators and in addition a natural basis of their Lie algebras for the construction of the fundamental $2n$ -dimensional representations. For an n -mode system with the boson annihilation and creation operators (a_i, a_i^\dagger) obeying the commutation relations $[a_i, a_j^\dagger] = i\hbar\delta_{ij}I$, $[a_i, a_j] = [a_i^\dagger, a_j^\dagger] = 0$, we consider the following $n(2n + 1)$ quadratic combinations of boson operators

$$\begin{aligned}
K_0^{(i)} &\equiv \frac{1}{4} (a_i a_i^\dagger + a_i^\dagger a_i), & K_-^{(i)} &\equiv \frac{1}{2} a_i^2, & K_+^{(i)} &\equiv \frac{1}{2} a_i^{\dagger 2}, & (i = 1, \dots, n), \\
K_{--}^{(ij)} &\equiv a_i a_j, & K_{-+}^{(ij)} &\equiv a_i a_j^\dagger, & K_{+-}^{(ij)} &\equiv a_i^\dagger a_j, & K_{++}^{(ij)} &\equiv a_i^\dagger a_j^\dagger, & (j > i = 1, \dots, n).
\end{aligned} \tag{1}$$

The operators in (1) form a convenient basis of the Lie algebra $sp(2n, \mathbb{R})$. The n operators $K_0^{(i)}$, ($i = 1, \dots, n$) commute with each other and can be taken as an n -dimensional basis of the Cartan subalgebra ($sp(2n, \mathbb{R})$ has rank n). Then one has the following commutation relations with the basis operators of the Cartan subalgebra

$$\begin{aligned}
[K_0^{(i)}, K_0^{(j)}] &= 0, & [K_0^{(i)}, K_-^{(j)}] &= -\delta_{ij} K_-^{(j)}, & [K_0^{(i)}, K_+^{(j)}] &= +\delta_{ij} K_+^{(j)}, \\
[K_0^{(i)}, K_{--}^{(jk)}] &= -\frac{1}{2} (\delta_{ij} + \delta_{ik}) K_{--}^{(jk)}, & [K_0^{(i)}, K_{++}^{(jk)}] &= +\frac{1}{2} (\delta_{ij} + \delta_{ik}) K_{++}^{(jk)}, \\
[K_0^{(i)}, K_{-+}^{(jk)}] &= -\frac{1}{2} (\delta_{ij} - \delta_{ik}) K_{-+}^{(jk)}, & [K_0^{(i)}, K_{+-}^{(jk)}] &= +\frac{1}{2} (\delta_{ij} - \delta_{ik}) K_{+-}^{(jk)}.
\end{aligned} \tag{2}$$

The chosen basis operators are solutions of the root equations for the operators $K_0^{(i)}$ and (2) contains all informations of the root diagrams of these Lie algebras (see [1] for $sp(4, \mathbb{R})$). We do not write down the remaining commutation relations. The symplectic groups $Sp(2n, \mathbb{R})$ contain interesting subgroups, for example, the n -fold direct product $(Sp(2, \mathbb{R}))^n$ of groups $Sp(2, \mathbb{R})$ and the groups $SU(n)$ and $U(n) = U(1) \times SU(n)$ (Jordan-Schwinger realization).

III. UNITARY IRREDUCIBLE REPRESENTATIONS OF TWO-DIMENSIONAL SYMPLECTIC GROUP

The Lie algebra $sp(2, \mathbb{R}) \sim su(1, 1)$ in the basis (K_-, K_0, K_+) is given by

$$[K_0, K_-] = -K_-, \quad [K_0, K_+] = +K_+, \quad [K_-, K_+] = 2K_0, \quad (K_\mp \equiv K_1 \mp iK_2). \tag{3}$$

As a noncompact group, $Sp(2, \mathbb{R})$ possesses only infinite-dimensional unitary irreducible representations (irreps) but finite-dimensional nonunitary ones. The unitary irreps in the basis $|k, n\rangle$ of eigenstates of K_0 with a lowest state $|k, 0\rangle$ ('vacuum') which is annihilated by K_- are constructed in [2] (slightly different notation there; our notation see, e.g. [3]). The parameter $k > 0$ is a label of the irrep. In unitary irreps with the label $k > 0$, one can construct $SU(1, 1)$ -coherent states $|k, z\rangle; z \in \mathbb{C}$ which are normalizable within the unit disk $|z| < 1$ [1-3]. For integer $l = 2k$, they are states with negative binomial number distributions.

IV. SINGLE-MODE REALIZATIONS OF TWO-DIMENSIONAL SYMPLECTIC GROUP

There are other realizations of $sp(2, \mathbb{R})$ in comparison to the standard one contained in (1). We give here single-mode realizations. With $N \equiv a^\dagger a$ the number operator, there are the following realizations with arbitrary fixed parameters $k > 0$ acting onto Fock states $|sn + j\rangle; (s = 1, 2, \dots; j = 0, 1, \dots, s - 1)$ (in general form represented in [1], see also [4])

1. applied to $|n\rangle$

$$K_- \equiv \sqrt{N + 2kI} a, \quad K_0 \equiv N + kI, \quad K_+ = K_-^\dagger, \tag{4}$$

2. applied to $|2n\rangle$ and $|2n+1\rangle$, correspondingly

$$K_- \equiv \frac{1}{2} \sqrt{\frac{N+4kI}{N+I}} a^2, \quad K_0 = \frac{1}{2}(N+2kI), \quad K_+ = K_-^\dagger, \quad (5)$$

$$K_- \equiv \frac{1}{2} \sqrt{\frac{N+(4k-1)I}{N+2I}} a^2, \quad K_0 = \frac{1}{2}(N+(2k-1)I), \quad K_+ = K_-^\dagger, \quad (6)$$

3. applied to $|3n\rangle$, $|3n+1\rangle$ and $|3n+2\rangle$, correspondingly

$$K_- \equiv \frac{1}{2} \sqrt{\frac{N+6kI}{(N+2I)(N+I)}} a^3, \quad K_0 = \frac{1}{3}(N+3kI), \quad K_+ = K_-^\dagger, \quad (7)$$

$$K_- \equiv \frac{1}{2} \sqrt{\frac{N+(6k-1)I}{(N+3I)(N+I)}} a^3, \quad K_0 = \frac{1}{3}(N+(3k-1)I), \quad K_+ = K_-^\dagger, \quad (8)$$

$$K_- \equiv \frac{1}{2} \sqrt{\frac{N+(6k-2)I}{(N+3I)(N+2I)}} a^3, \quad K_0 = \frac{1}{3}(N+(3k-2)I), \quad K_+ = K_-^\dagger. \quad (9)$$

The case $k = \frac{1}{2}$ of (4) leads to coherent phase states as $SU(1,1)$ -coherent states. The cases $k = \frac{1}{4}$ in (5) and $k = \frac{3}{4}$ in (6) lead to the realization (1). It acts in the Hilbert spaces of even and odd Fock states as different unitary irreps of $SU(1,1)$. The corresponding $SU(1,1)$ -coherent states are squeezed vacuum states and Fock state $|1\rangle$ squeezed.

V. FUNDAMENTAL REPRESENTATION OF TWO-DIMENSIONAL SYMPLECTIC GROUP

The fundamental representation of $Sp(2, \mathbb{C})$ (we consider here the complexification of $Sp(2, \mathbb{R})$) is two-dimensional and uses the basis (a, a^\dagger) for its construction. With the mapping

$$x \leftrightarrow X = e^{ix} \equiv \exp(\xi K_- + i2\eta K_0 - \zeta K_+) \rightarrow \hat{X} = e^{i\hat{x}}, \quad (10)$$

one finds for the two-dimensional complex unimodular matrices \hat{X}

$$\begin{pmatrix} \kappa & \lambda \\ \mu & \nu \end{pmatrix} = \begin{pmatrix} \text{ch } \varepsilon - i\eta \frac{\text{sh } \varepsilon}{\varepsilon} & \xi \frac{\text{sh } \varepsilon}{\varepsilon} \\ \zeta \frac{\text{sh } \varepsilon}{\varepsilon} & \text{ch } \varepsilon + i\eta \frac{\text{sh } \varepsilon}{\varepsilon} \end{pmatrix}, \quad \varepsilon \equiv \sqrt{\xi\zeta - \eta^2}, \quad \kappa\nu - \lambda\mu = 1. \quad (11)$$

Together with its inversion (nonuniqueness due to multiplicity of $\text{Arsh}(z)$ by $\pm i2\pi l$)

$$(\xi, \eta, \zeta) = \left(\lambda, i \frac{\kappa - \nu}{2}, \mu \right) \frac{\text{Arsh } \vartheta}{\vartheta}, \quad \vartheta \equiv \sqrt{\left(\frac{\kappa + \nu}{2}\right)^2 - 1} = \sqrt{\left(\frac{\kappa - \nu}{2}\right)^2 + \lambda\mu}, \quad (12)$$

it allows to solve all composition and decomposition problems, for example

$$\exp(\xi K_- + i2\eta K_0 - \zeta K_+) = \exp\left(-\frac{\mu}{\kappa} K_+\right) \exp(-2(\log \kappa) K_0) \exp\left(\frac{\lambda}{\kappa} K_-\right). \quad (13)$$

The quantity $-\varepsilon^2 \equiv \eta^2 - \xi\zeta$ is coordinate-invariant (group scalar product, Killing form). The inverse transition $\hat{X} \rightarrow X$ from the matrices \hat{X} to the operators X brings an additional nonuniqueness in dependence on the label k of the irrep (metaplectic groups). By using (K_-, K_0, K_+) instead of (a, a^\dagger) as a basis of the representation, one can construct the three-dimensional regular (or adjoint) representation.

VI. FOUR-DIMENSIONAL SYMPLECTIC GROUP

The 4-dimensional symplectic group $Sp(4, \mathbb{R})$ possesses 10 real parameters corresponding to 10 basis operators of the Lie algebra $sp(4, \mathbb{R})$ which can be chosen, for example, according to (1) with $i, j = 1, 2$. There is a remarkable isomorphism to the pseudo-orthogonal group $SO(3, 2)$ (de Sitter group) [5]. By the substitutions in (1) (upper indices (12) can be omitted)

$$K_0 \equiv K_0^{(1)} + K_0^{(2)} = \frac{1}{2}(N_1 + N_2 + I), \quad J_3 \equiv K_0^{(1)} - K_0^{(2)} = \frac{1}{2}(N_1 - N_2), \quad (14)$$

and $K_{--} \equiv K_-, K_{++} \equiv K_+, K_{-+} \equiv J_-, K_{+-} \equiv J_+$, one finds two interesting (genuine two-mode) subgroups of $Sp(4, \mathbb{R})$, the group $SU(1, 1)$ spanned by the operators (K_0, K_-, K_+) of its Lie algebra and $SU(2)$ spanned by the operators (J_-, J_+, J_3) of its Lie algebra. The root diagrams of $sp(4, \mathbb{R})$ together with some of their subgroups are given in Fig.1.

The subgroup $SU(1, 1)$ of $Sp(4, \mathbb{R})$ describes two-mode squeezing, whereas the subgroup $U(2)$ describes the unitary transformations between two inputs and two outputs of a device with conservation of the total photon number (beam splitter, light polarization).

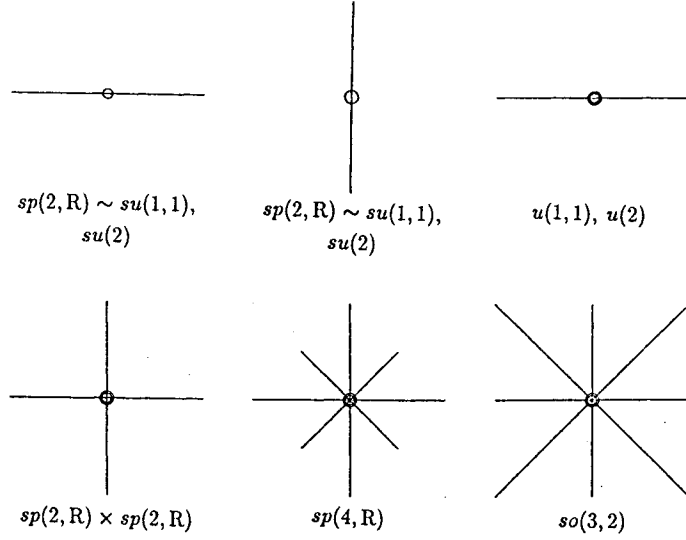


Fig.1: Root diagrams to $Sp(4, \mathbb{R}) \sim SO(3, 2)$ and to some of their subgroups

VII. CONCLUSION

In addition to [1], we have considered here some special problems for the symplectic groups $Sp(2n, \mathbb{R})$ and their special cases $Sp(2, \mathbb{R})$ and $Sp(4, \mathbb{R})$.

REFERENCES

- [1] A. Wünsche, JOPB: Quantum Semicl. Opt., submitted July 1999.
- [2] A. Perelomov, *Generalized Coherent States and Their Applications*, Springer-Verlag, Berlin 1986.
- [3] A. Vourdas, A. Wünsche, J. Phys. A: Math. Gen. **31**, 9341 (1998)
- [4] G.M. D'Ariano, M.G. Rasetti, J. Katriel, and A.I. Solomon, in *Squeezed and Nonclassical Light*, Eds. P. Tombesi and E.R. Pike, p. 301, Plenum Press, New York 1989.
- [5] Y.S. Kim, M.E. Noz, *Phase Space Picture of Quantum Mechanics*, World Scientific, Singapore 1991.

Klauder's coherent states in energy degenerate systems: The hydrogen atom

Michael G.A. Crawford*

*Department of Applied Mathematics, University of Waterloo,
Waterloo, Ontario, Canada, N2L 3G1*

Abstract

Klauder's recent generalization of the harmonic oscillator coherent states is applicable only in non-degenerate systems, requiring some additional structure when applied to systems with degeneracies. The author suggests how this structure could be added, and applies the complete method to the hydrogen atom problem. To illustrate how a certain degree of freedom in the construction may be exploited, states are constructed which are initially localized and evolve semi-classically, and whose long time behaviour exhibits "fractional revivals".

I. INTRODUCTION

Due to the many useful mathematical and physical properties of the harmonic oscillator coherent states [1], many generalizations appear in the literature. Each generalization tends to preserve a small number of the properties of the original states in the general scheme at the expense of the remaining properties. A recent generalization due to Klauder [2] preserves many, at the expense of few. Klauder's generalization gives states which (a) are continuously parameterized, (b) evolve in time among themselves, and (c) admit a resolution of the identity. As such, no reservations are made for "semi-classical" properties such as minimum uncertainty, though a certain degree of freedom to be discussed below remains within the construction which may be optimized according additional concerns. Two studies have since appeared [3,4] proposing fourth conditions which eliminate this degree of freedom: These will not be herein considered.

As initially presented, Klauder's construction was appropriate for systems without energy degeneracies: With no additional structure, the resolution of the identity fails for degenerate systems. Energy degeneracies arise when independent operators commute with the Hamiltonian which suggests a Lie algebraic approach to imposing the necessary additional structure. Thus in the presence of degeneracies, excepting those few cases of truly "accidental" degeneracies, the Perelomov approach to constructing coherent states for the degeneracy group is an obvious and general path to take [5].

*E-mail address: mgacrawf@barrow.uwaterloo.ca

II. THE CONSTRUCTION

Readers are urged to consult the original paper [2] for a comparison with the non-degenerate construction. In the degenerate case presented here, (in atomic units) the coherent states are given by

$$|s, \gamma, x\rangle = N(s^2) \sum_{n=0}^{\infty} \frac{s^n \exp(-i\gamma e_n)}{\sqrt{\rho_n}} \sqrt{d_n} |n, x\rangle, \quad (1)$$

where $s \geq 0$ and γ is real. The sum is over the bound energy levels of a Hamiltonian \hat{H} with energy e_n , each with degeneracy d_n . The states $|n, x\rangle$ are the Perelomov coherent states for the degeneracy group G , and $N(s^2)$ ensures normalization. The factors ρ_n are the moments of a function $\rho(u) > 0$, $u \geq 0$. The choice of $\rho(u)$ is the remaining degree of freedom up to the following restrictions: All the moments ρ_n exist and states must be normalizable for all s . Such functions $\rho(u)$ are known to exist: In the harmonic oscillator, $\rho(u) = e^{-u}$ gives rise to the standard harmonic oscillator coherent states.

Regarding properties, the states $|s, \gamma, x\rangle$ clearly are (a) continuously parameterized. The states (b) exhibit temporal stability: $\exp(-i\hat{H}t)|s, \gamma, x\rangle = |s, \gamma + t, x\rangle$. Further, given $\rho(u)$ and $N^2(u)$, let $k(u)$ be defined by $k(u)N^2(u) = \rho(u)$. Then, the coherent states (c) satisfy the resolution of the identity,

$$\hat{1} = \int d\mu(s, \gamma, x) |s, \gamma, x\rangle \langle s, \gamma, x|, \quad (2)$$

with

$$\int d\mu(s, \gamma, x) = \lim_{\Gamma \rightarrow \infty} \frac{1}{2\Gamma} \int_0^\infty ds^2 k(s^2) \int_{-\Gamma}^\Gamma d\gamma \text{vol}(H) \int_X d\eta(x), \quad (3)$$

in which H is the isotropy subgroup relative to the fiducial vector in the construction of the Perelomov coherent states, $X = G/H$ is the quotient space formed by the degeneracy group with the isotropy subgroup, and the measure $d\eta$ is induced from the Haar measure on the degeneracy group. The limit is necessary to accommodate possible incommensurabilities of energy levels. These three properties in concert make these states useful in the representation of arbitrary, bound, time evolved states.

A construction by Majumdar and Sharatchandra [3] also makes use of the Perelomov coherent states for the degeneracy group, though d_n is incorporated into the measure after the summation of the state, an operation of questionable justifiability. Klauder's construction [2], using an adaptation of $\text{SO}(3)$ coherent states, incorporates d_n into the states after, and therefore affecting, normalization. This present construction suffers neither of these problems.

III. SPECIAL CASE: THE HYDROGEN ATOM

The group theoretical treatment of the hydrogen atom is standard in the literature [6]. Here, the degeneracy group $\text{SO}(4)$ is realized as the direct product of two $\text{SO}(3)$ groups generated by \hat{M}_j and \hat{N}_j , the sum and difference of the angular momentum and the quantum

Runge-Lenz vectors respectively. Expressed as the direct product of two SO(3) coherent states, the SO(4) coherent states are given by ($n = 2j + 1$ so $n \geq 1$)

$$|n, \zeta_1, \zeta_2\rangle = \sum_{m_1, m_2 = -j}^j \frac{(2j)! \zeta_1^{j+m_1} \zeta_2^{j+m_2} |j, m_1\rangle |j, m_2\rangle}{[(j+m_1)!(j-m_1)!(j+m_2)!(j-m_2)!]^{1/2} (1+|\zeta_1|^2)^j (1+|\zeta_2|^2)^j}. \quad (4)$$

The direct product states may be related to the standard $|n, \ell, m\rangle$ states with Clebsch-Gordon coefficients as usual. Using the above states, the hydrogen atom coherent states are given by

$$|s, \gamma, \zeta_1, \zeta_2\rangle = N(s^2) \sum_{n=0}^{\infty} \frac{s^n \exp(-i\gamma e_{n+1})}{\sqrt{\rho_n}} |n+1, \zeta_1, \zeta_2\rangle \quad (5)$$

which satisfy the resolution of the identity

$$\hat{1}_B = \frac{1}{\pi^2} \int d\mu(s, \gamma) \int \frac{d^2\zeta_1 d^2\zeta_2}{(1+|\zeta_1|^2)^2 (1+|\zeta_2|^2)^2} |s, \gamma, \zeta_1, \zeta_2\rangle \langle s, \gamma, \zeta_1, \zeta_2|, \quad (6)$$

where the subscripted B is included to emphasize that this is more appropriately regarded as a projection operator into the bound portion of the Hilbert space. In the specific example of $\rho(u) = e^{-u}$, with moments $\rho_n = n!$, explicit form may be given to $N(s^2)$ and $k(u)$ by $N(s^2) = e^{-s^2/2} (1 + 3s^2 + s^4)^{-1/2}$, and $k(u) = 1 + 3u + u^2$.

IV. DYNAMICS

To illustrate how the above recipe may be adapted to one's purposes using the freedom granted by $\rho(u)$, we now construct states which remain restricted to Keplerian orbits and exhibit fractional revivals. Fractional revivals are a universal phenomenon exhibited by wave functions with large quantum numbers provided corrections of order larger than two to a polynomial approximation to the energy eigenvalues are not large over contributing states to the wave function [7]. For the hydrogen atom, considering a Taylor series of the energy level, expanding about $n = \bar{n}$, one readily observes that states not satisfying $\Delta n \ll \langle n \rangle$ will not be expected to exhibit revivals. Further, linear corrections to equal energy spacing become multiples of 2π , signaling the occurrence of a revival, when $t = T_r = \frac{2\pi}{3} \langle n \rangle^4$. Note that $T_r = T_{rev}/2$ in Averbukh and Perelman's notation.

With $\rho(u) = e^{-u}$, one obtains a distribution in eigenlevels characterized by

$$\langle n \rangle = s^2 \frac{s^4 + 5s^2 + 4}{s^4 + 3s^2 + 1} \quad \text{and} \quad (\Delta n)^2 = s^2 \frac{s^8 + 6s^6 + 14s^4 + 10s^2 + 4}{s^8 + 6s^6 + 11s^4 + 6s^2 + 1}, \quad (7)$$

so that, taking leading order behaviour, $\Delta n \sim \sqrt{\langle n \rangle}$. Hence, strong revivals would be expected for very large $\langle n \rangle$, and weak or non-existent revivals for small $\langle n \rangle$. Considering instead $\rho(u) = \exp(-u^\alpha)$ for some constant $\alpha > 0$, the moments are $\rho_n = \Gamma((n+1)/\alpha)/\alpha$. Though the expressions for $\langle n \rangle$ and $(\Delta n)^2$ are not summable in closed form for general α , they may be approximated by recognizing the scalings necessary to map expressions with general α onto those with $\alpha = 1$: $n+1 \rightarrow (n+1)/\alpha$, and $s \rightarrow s^\alpha$. Hence, one

obtains to leading order (large values of s will eventually be involved) $\langle n \rangle \sim \alpha s^{2\alpha}$, and $\Delta n \sim \alpha s^\alpha$, so that $\Delta n \sim \sqrt{\alpha \langle n \rangle}$. Clearly, a small α may permit the observation of revivals for lower $\langle n \rangle$. Without discussing the effect of changing α any further, there will be a tradeoff between large and small α : Large α will introduce many significantly contributing energy levels for a given $\langle n \rangle$ yielding good spatial localization but weak or non-existent revivals, whereas small α yields strong revivals of poorly localized states. Numerical studies bear out these conclusions. As a typical example, a state centred at $\langle n \rangle = 160$ with $\alpha = 1/32$ and $s = 2.23 \times 10^{59}$ has a width of $\Delta n = \sqrt{5}$. The full revival occurs at $t = T_r = 1.31 \times 10^9$ at which time the autocorrelation function peaks at approximately 0.83. No significant full revival occurs for a state with $\langle n \rangle = 160$ and $\alpha = 1$.

V. ACKNOWLEDGMENTS

The author is grateful for the support provided by the Natural Sciences Engineering Research Council of Canada. The author also wishes to acknowledge useful discussions with Dr. E.R. Vrscaj and Dr. J. Paldus, both of the Department of Applied Mathematics, University of Waterloo.

1. J. R. Klauder and B.-S. Skagerstam, editors. *Coherent States: Applications in Physics and Mathematical Physics*. World Scientific, Singapore, 1985.
2. J. R. Klauder. Coherent states for the hydrogen atom. *J. Phys. A*, 29(12):L293–L298, 1996.
3. P. Majumdar and H. S. Sharatchandra. Coherent states for the hydrogen atom. *Phys. Rev. A*, 56(5):R3322–R3325, 1997.
4. J. P. Gazeau and J. R. Klauder. Coherent states for systems with discrete and continuous spectrum. *J. Phys. A*, 32:123–132, 1999.
5. A. M. Perelomov. *Generalized Coherent States and Their Applications*. Springer-Verlag, London, 1986.
6. B. G. Adams, J. Čížek, and J. Paldus. Lie algebraic methods and their applications to simple quantum systems. In *Advances in Quantum Chemistry, Vol 19*. Academic Press, 1988.
7. I. S. Averbukh and N. F. Perelman. Fractional revivals: Universality in the long-term evolution of quantum wave packets beyond the correspondence principle dynamics. *Phys. Lett. A*, 139(9):449–453, 1989.

Squeezed Coherent States for the Morse Oscillator

C. N. Avram*, Gh. E. Drăgănescu, N. M. Avram

*Department of Physics, West University of Timișoara, Bv. V. Pârvan, Nr. 4, 1900 Timișoara,
Romania*

Abstract

In this paper we consider a one-dimensional Morse oscillator and build a set of creation and annihilation operators for this system. We also establish the corresponding squeezed coherent states. We also calculate also the average values of some observables in these squeezed coherent states.

I. INTRODUCTION

In the last years the properties and the squeezed states was intensively studied, due their future applications [1-4], and due to their applications to the new coherent radiation sources [2].

In this paper we consider the problem of squeezed coherent states for an anharmonic oscillator, described by the Morse potential.

II. THE ALGEBRA OF THE MORSE OSCILLATOR

We consider the one-dimensional Morse oscillator described by the Hamiltonian [5-9]:

$$H = \frac{p^2}{2m} + V_0(e^{-2\alpha x} - 2e^{-\alpha x}), \quad (1)$$

where V_0 represents the force constant of the oscillator, α a constant ($V_0 > 0$, $\alpha > 0$), x the relative position, m reduced mass, and p momentum operator of oscillator.

We will use the y variable and the notations:

$$\nu = \sqrt{\frac{8mV_0}{\alpha^2\hbar^2}} \quad s = \sqrt{\frac{-2mE}{\alpha^2\hbar^2}}, \quad y = \nu \exp(-\alpha x). \quad (2)$$

The eigenfunctions of the Hamiltonian are the discrete eigenenergy levels ($E \in [-V_0, 0]$) are written in term of confluent hypergeometric functions:

*E-MAIL: acalin@galileo.uvt.ro

$$\psi_n(y) = \frac{1}{\Gamma(\nu - 2n)} \sqrt{\frac{\Gamma(\nu - n)}{n!}} y^{\mu - n} \exp\left(-\frac{y}{2}\right) F(-n, \mu - 2n; y) \quad (3)$$

Solutions are possible for $2s + 1 - \nu = -2n$, where $n \in N$. The quantum number n can take values $n = 0, 1, 2, \dots, N_{max} = [\mu]$ where $[\mu]$ represents the entire part of $\mu = (\nu - 1)/2$.

In a previous paper we have established a realisation of the creation and annihilation operators b_{\pm} , and b_0 operator, with the aid of an analytical method [10,11,12].

The action of these operators on eigenfunctions are given by:

$$b_- \psi_n = -\sqrt{n(\nu - n)} \psi_{n-1}, \quad (4)$$

$$b_+ \psi_n = \sqrt{(n+1)(\nu - n - 1)} \psi_{n+1}, \quad (5)$$

$$b_0 \psi_n = \left(n - \frac{\nu - 1}{2}\right) \psi_n. \quad (6)$$

The commutation relations for these operators are:

$$[b_-, b_+] = 2b_0 \quad [b_0, b_-] = -b_- \quad [b_0, b_+] = b_+. \quad (7)$$

The Hamiltonian of the oscillator can be expressed in terms of these operators

$$H = -\frac{4V_0}{\nu^2} b_0^2 = -\hbar\Omega b_0^2, \quad (8)$$

where $\Omega = 4V_0/\mu^2$.

We can see that by hermitic conjugation results:

$$b_+^\dagger = -b_- \quad b_-^\dagger = -b_+. \quad (9)$$

We can define also the "number" operator

$$N = b_0 + \frac{\nu - 1}{2}, \quad (10)$$

and the harmonic oscillator like operators:

$$a = -b_- \frac{1}{\sqrt{\nu - N}} \quad a^\dagger = \frac{1}{\sqrt{\nu - N}} b_+, \quad (11)$$

which obey the commutator $[a, a^\dagger] = 1$.

The Hamiltonian of the system can be expressed in terms of $\{a, a^\dagger\}$:

$$H = -\hbar\Omega \left(a^\dagger a - \frac{\nu - 1}{2}\right)^2 \quad (12)$$

and the "number" operator is $N = a^\dagger a$. Due to the Hamiltonian (8), the temporal evolution of the observables is not identical to those of the standard harmonic oscillator.

III. THE SQUEEZED COHERENT STATES

With the aid of the unitary operator

$$D(\beta) = \exp[i(\beta b_+ - \beta^* b_-)] \quad (13)$$

where $\alpha \in C$ and with the squeeze operator

$$S(z) = \exp[i(z \lambda b_+^2 - z^* b_-^2)] \quad (14)$$

where $z \in C$, we build the coherent states:

$$|\beta\rangle = D(\beta)|0\rangle, \quad (15)$$

and the squeezed coherent states:

$$|z, \beta\rangle = S(z)D(\beta)|0\rangle. \quad (16)$$

We can calculate the average values of different observables of a system, corresponding to the coherent states $|\beta\rangle$.

Unfortunately the calculation of the average values of the observables in the squeezed states can be not obtained in a closed form.

In order to establish calculable quantities we use the $\{a^\dagger, a\}$ representation of the system, given by (11).

We can to define the displacement operator

$$\mathcal{D}(\alpha) = \exp[\alpha a_+ - \alpha^* a_-], \quad \alpha \in C \quad (17)$$

and the squeeze operator:

$$\mathcal{S}(z) = \exp[i(z a_+^2 - z^* (a^\dagger)^2)]. \quad (18)$$

The new set of coherent states $|\alpha\rangle$ and new squeezed coherent states $|z\alpha\rangle$, are:

$$|\alpha\rangle = \mathcal{D}(\alpha)|0\rangle \quad |z, \alpha\rangle = \mathcal{S}(z)\mathcal{D}(\alpha)|0\rangle. \quad (19)$$

The average values of the observables a and a^\dagger in a squeezed coherent state are:

$$\begin{aligned} \langle a(t) \rangle_{SC} &= \langle z\alpha | a(t) | z\alpha \rangle = \\ &= \cosh r \alpha e^{i(2|\alpha|^2-1)\Omega t} - e^{i\theta} \sinh r \alpha^* e^{-i(2|\alpha|^2+1)\Omega t}, \end{aligned} \quad (20)$$

$$\begin{aligned} \langle a^\dagger(t) \rangle_{SC} &= \langle z\alpha | a^\dagger(t) | z\alpha \rangle = \\ &= \cosh r \alpha^* e^{i(-2|\alpha|^2+1)\Omega t} - e^{i\theta} \sinh r \alpha e^{i(2|\alpha|^2-1)\Omega t}. \end{aligned} \quad (21)$$

We obtain also the evolution of the average values of the observables a^2 and $a^{\dagger 2}$ in a squeezed coherent state:

$$\begin{aligned}
& \langle a(t)^2 \rangle_{SC} = \langle z\alpha | a^2(t) | z\alpha \rangle = \\
& = \cosh^2 r \alpha^2 e^{i(2|\alpha|^2-1)2\Omega t} + e^{i2\theta} \sinh^2 r \alpha^{*2} e^{-i(2|\alpha|^2+1)2\Omega t} - \sinh r \cosh r e^{i\theta} (2|\alpha|^2 + 1), \quad (22)
\end{aligned}$$

$$\begin{aligned}
& \langle a^{\dagger 2}(t) \rangle_{SC} = \langle z\alpha | a^{\dagger 2}(t) | z\alpha \rangle = \\
& = \cosh^2 r \alpha^{*2} e^{i(-2|\alpha|^2+1)2\Omega t} + e^{i2\theta} \sinh^2 r \alpha^2 e^{i(2|\alpha|^2-1)2\Omega t} - \sinh r \cosh r (2|\alpha|^2 + 1). \quad (23)
\end{aligned}$$

ACKNOWLEDGMENTS

We want to thank National Council of University Scientific Research (Bucharest) for financial support of this work under grant 39560/11.09.98

REFERENCES

- [1] H. P. Yuen, Phys. Rev., **13**, 2226 (1976)
- [2] M. O. Scully, M. S. Zubairy, *Quantum Optics*, Cambridge Univ. Press, Cambridge, 1997
- [3] G. M. D' Ariano, M. F. Sacchi, Mod. Phys. Lett. B, **11**, 1283 (1997)
- [4] D. A. Trifonov, J. Math. Phys, **35**, 2297 (1994)
- [5] C. C. Gerry, Phys. Rev. A, **33**, 2207, (1986); Phys. Rev. A, **31**, 2721, (1985)
- [6] R. Cordero, Hojman, Lett. Nuovo Cim., **4**, 1123 (1970)
- [7] M. Berrondo, A. Palma, J. Phys., **A13**, 773 (1980)
- [8] N. Bessis , G. Bessis, Phys. Rev. A, **50**, 4506, (1994)
- [9] A. E. Kondo, R. Truax, J. Math. Phys., **29**, 1396 (1988)
- [10] N. M. Avram, Gh. E. Drăgănescu, Int. Journ. Quant. Chemistry, **65** 655 (1997)
- [11] Gh. Drăgănescu, N. M. Avram, Zeitschr. Phys. Chem., **200 S**, 51 - 56 (1997)
- [12] Gh. Drăgănescu, N. M. Avram, Canad. J. Phys., **76**, 273 (1998)

Vibrational Coherent States for Morse Oscillator

N. M. Avram*, Gh. E. Drăgănescu, C. N. Avram

Department of Physics, West University of Timișoara, Bv. V. Pârvan, Nr. 4, 1900 - Timișoara, România

Abstract

In order to study strong vibrations of diatomic molecules we use the model of three-dimensional Morse oscillator, of which dynamic group are $\{K_{\pm i}, K_{0i}\}$ ($i = 1, 2, 3$), where $K_{\pm i}$ represents the creation and annihilation operators.

For this system it has been builded the coherent states and calculated the dynamic modifications of the refractive index of the molecules as the results of interaction of a laser beam with them.

I. INTRODUCTION

The algebraic study of the one-dimensional Morse oscillator was suggested by Wybourne [1] and has been obtained, by Gerry [2] using the $SU(1, 1)$ group. In a previous paper [3,4] we have established a method of construction of the creation and annihilation operators for one-dimensional Morse oscillator, based on an analytical method and on the properties of the confluent hypergeometric functions.

The aim of this paper is to consider a three-dimensional Morse oscillator model for which will establish the creation and annihilation operators and construct the coherent states.

Also, we will establish the variation of the refractive index of the diatomic molecules due to the interaction of the Morse coherent states with the coherent radiation field.

II. THE THREE - DIMENSIONAL MORSE OSCILLATOR

We consider a three-dimensional Morse oscillator obtained by superposition of three one-dimensional isotropic Morse oscillators:

$$H_0 = H_{01} + H_{02} + H_{03}$$

where:

*E-MAIL: avram@quasar.uvt.ro

$$H_{0i} = \frac{p_i^2}{2m} + V_0(e^{-2\alpha x_i} - 2e^{-\alpha x_i}), \quad (1)$$

where $i = 1, \dots, 3$, x_i - is the displacement from the equilibrium position along the direction i , m - the reduced mass, p_i the i component of the momentum operator. The eigenenergy will be $E_n = E_{01} + E_{02} + E_{03}$.

We use the notations and the variables y_i :

$$\nu = \sqrt{\frac{8mV_0}{\alpha^2\hbar^2}}, \quad s_i = \sqrt{\frac{-2mE_{0i}}{\alpha^2\hbar^2}}, \quad y_i = \nu \exp(-\alpha x_i)$$

The eigenfunctions for the H_{0i} 's Hamiltonian will be:

$$\psi_{n_i}^i(y_i) = \frac{1}{\Gamma(\nu - 2n_i)} \sqrt{\frac{\Gamma(\nu - n_i)}{n_i!}} y_i^{\mu - n_i} \exp(-\frac{y_i}{2}) F(-n_i, \mu - 2n_i; y_i) \quad (2)$$

where $F(-n_i, 2s_i + 1; y_i)$ is the confluent hypergeometric function. Solutions are possible for:

$$2s_i + 1 - \nu = -2n_i \quad (3)$$

where $n \in \mathbb{N}$, and for discrete energy levels $E \in [-V_0, 0]$, the quantum numbers must be:

$$n_i = 0, 1, 2, \dots, N_{max} = [\mu] \quad (4)$$

where $[\mu]$ represents the entire part of $\mu = (\nu - 1)/2$.

The eigenfunctions for the Hamiltonian H_0 will be $|n_1 n_2 n_3 \rangle = \psi_{n_1}^1 \psi_{n_2}^2 \psi_{n_3}^3$.

III. THE ALGEBRA OF THE MODEL

The operators of algebra for the model of three-dimmmensional Morse oscillator are:

$$\begin{aligned} K_{+i} &= (2s_i - 1) \frac{d}{dy_i} + \frac{s_i(2s_i - 1)}{y_i} - \frac{\nu}{2} \\ K_{-i} &= (2s_i + 1) \frac{d}{dy_i} - \frac{s_i(2s_i + 1)}{y_i} + \frac{\nu}{2} \end{aligned} \quad (5)$$

$$K_{0i} = y_i \frac{d^2}{dy_i^2} + \frac{d}{dy_i} - \frac{s_i^2}{y_i} - \frac{y_i}{2} - n_i + \frac{1}{2}$$

These operators have the properties

$$\begin{aligned} K_{-i} \psi_{n_i} &= k_{-i} \psi_{n_i-1} = -\sqrt{n_i(\nu - n_i)} \psi_{n_i-1}, \\ K_{+i} \psi_{n_i} &= k_{+i} \psi_{n_i+1} = \sqrt{(n_i + 1)(\nu - n_i - 1)} \psi_{n_i+1}, \end{aligned} \quad (6)$$

$$K_{0i} \psi_{n_i} = k_{0i} \psi_{n_i} = (n_i - \frac{\nu - 1}{2}) \psi_{n_i}$$

and satisfy the commutation relations will be:

$$[K_{-i}, K_{+i}] = 2K_{0i}, \quad [K_{0i}, K_{-i}] = -K_{-i}, \quad [K_{0i}, K_{+i}] = K_{+i}. \quad (7)$$

The Hamiltonian of the system of diatomic molecules are

$$H_0 = -\frac{4V_0}{\nu^2}(K_{01}^2 + K_{02}^2 + K_{03}^2) = -\hbar\Omega(K_{01}^2 + K_{02}^2 + K_{03}^2). \quad (8)$$

($\Omega = 4V_0/(\nu^2\hbar)$) and the evolution operator is:

$$U(t) = \exp[i(K_{01}^2 + K_{02}^2 + K_{03}^2)\Omega t].$$

IV. COHERENT STATES

Because the eigenfunctions space of the system is finite - dimensional in order to build the coherent states we will define an unitary operator with the form:

$$D(\lambda_1, \lambda_2, \lambda_3) = \exp\left[i \sum_{m=1}^3 (\lambda_m K_{+m} - \lambda_m^* K_{-m})\right] \quad (9)$$

where $\lambda_1, \lambda_2, \lambda_3$ are complex valued parameters.

The coherent states can be defined in the parametrization $\lambda_m, m = 1, \dots, 3$:

$$|\lambda_1 \lambda_2 \lambda_3 \rangle = D(\lambda_1 \lambda_2 \lambda_3) |000 \rangle \quad (10)$$

With the coherent states (10), we can obtain the mean values for the operators $K_{\pm m}$, $K_{\pm m}^2$ and K_{0m} and the temporal evolution of the observable. For example, we have

$$\langle K_{0m} \rangle_\lambda = -\frac{\nu-1}{2} \cos(2|\lambda_m|), \quad (11)$$

$$\langle K_{0m}^2 \rangle_\lambda = \frac{\nu-1}{4} [\sin^2(2|\lambda_m|) + (\nu-1) \cos^2(2|\lambda_m|)] \quad (12)$$

$$D^\dagger K_{+m} D = \frac{i|\lambda_m|}{\lambda_m} \sin(2|\lambda_m|) K_{0m} + \frac{|\lambda_m|^2}{2\lambda_m^2} [\cos(2|\lambda_m|) - 1] K_{-m} + \frac{1}{2} [\cos(2|\lambda_m|) + 1] K_{+m}$$

$$\langle K_{+m} \rangle_\lambda = -\frac{\nu-1}{2} \frac{i|\lambda_m|}{\lambda_m^*} \sin(2|\lambda_m|), \quad (13)$$

$$\langle K_{+m}^2 \rangle_\lambda = -\frac{|\lambda_m|^2}{\lambda_m^2} \frac{(\nu-1)(\nu-2)}{4} \sin^2(2|\lambda_m|). \quad (14)$$

The temporal evolution of the $K_{\pm m}$ will be:

$$K_{\pm m}(t) = K_{\pm m} e^{\pm i\Omega t(2K_{0m} \pm 1)}. \quad (15)$$

The time dependent refractive index in the coherent states is:

$$n_2(t) = \frac{qi\beta}{\sqrt{V}} \sqrt{\frac{k}{2}} \sum_{n=1}^{\infty} \sum_{i=1}^3 \frac{1}{n} \{ \cos \delta_i$$

$$\times \left[c_n \lambda_i \exp\left[i\Omega t \left(-2\frac{\nu-1}{2} \cos(2|\lambda_i|) - 1\right)\right] + d_n \lambda_i^* \exp\left[i\Omega t \left(-2\frac{\nu-1}{2} + \cos(2|\lambda_i|)\right)\right] + c_n \right]^n$$

$$\times e^{-i\omega t} - c.c\}.$$

Results the refractive index have an oscillatory manifestation with very fast frequency.

ACKNOWLEDGMENTS

We want to thank National Council of University Scientific Research (Bucharest) for financial support of this work under grant 39560/11.09.98

REFERENCES

- [1] R. G. Wybourne, *Classical Groups for Physicists*, Wiley, New York, 1974
- [2] C. C. Gerry, Phys. Rev. A, **33**, 2207, (1986); **31**, 2721, (1985)
- [3] N. M. Avram, Gh. E. Drăgănescu, Int. Journ. Quant. Chemistry, **65** 655 (1997)
- [4] Gh. Drăgănescu, N. M. Avram, Canad. J. Phys., **76**, 273 (1998)

Coherent States for the Dirac Hydrogenlike Atom

Gh. E. Drăgănescu*, N. M. Avram, C. N. Avram

Department of Physics, West University of Timișoara, Bv. V. Párvan, Nr. 4, 1900 Timișoara, Romania

Abstract

In this paper there are established the coherent states for the radial wavefunction, corresponding to the $su(2)$ algebra and for angular wavefunction. We calculate also the average values of some observables.

I. INTRODUCTION

The problem of coherent states for the atom is of a great interest due to the fact that are possible to consider the spin effects.

In the literature there exists a series of papers devoted to the coherent states of the relativistic harmonic oscillator [1,2].

Due to the difficulties, the problem of coherent states for Dirac hydrogen atom is not studied, but there exists algebraic studies of the Dirac hydrogen atom [3,4].

In this paper we use the creation and annihilation operator for the radial wavefunction of the Dirac hydrogen atom established in [3,4].

II. THE ALGEBRA OF THE RADIAL WAVE FUNCTION

We consider the hydrogenlike atom, described by the Dirac Hamiltonian:

$$H_D = \boldsymbol{\alpha}\mathbf{p} + m\beta - \frac{Ze^2}{r},$$

where m represents the mass of the electron, \mathbf{p} the momentum, $r \in R_+$ the radial variable, Ze the charge of the nucleus. $\boldsymbol{\alpha}$, β and $\boldsymbol{\sigma}$ represents the Dirac matrix, and with Ψ the eigenfunction (in (r, θ, ϕ) variables):

$$\boldsymbol{\alpha} = \begin{pmatrix} 0 & \boldsymbol{\sigma} \\ \boldsymbol{\sigma} & 0 \end{pmatrix}, \quad \beta = \begin{pmatrix} 1 & 0 \\ 0 & 1 \end{pmatrix}, \quad \Psi(r, \theta, \phi) = \begin{pmatrix} \frac{1}{r}F(r)Y_{lm} \\ \frac{1}{r}G(r)Y'_{jm} \end{pmatrix},$$

*E-MAIL: ghed@quasar.uvt.ro

where Y_{jm}, Y'_{jm} are the spinor spherical harmonics of opposite parity.

We use the dynamic group obtained in [3,4], and the notations:

$$k = \sqrt{m^2 - E^2} \quad q = Ze^2 \quad \mu = \frac{qE}{k} + 1,$$

where E is the energy level. The radial functions F and G can be written:

$$F = \sqrt{m - E}(\psi_- + \psi_+), \quad G = \sqrt{m - E}(\psi_- - \psi_+).$$

In order to express the radial eigenfunctions we will introduce the the variable $x \in R$:

$$\rho = kr = \exp(x),$$

an extra phase variable ξ , and the quantities (quantum numbers) ω and μ [3]:

$$\omega = j(j+1) - q^2 \quad \mu \geq \sqrt{\frac{\omega}{2}}. \quad (1)$$

With the aid of these notations the radial functions $\psi_{\pm}(x)$ can be expressed

$$\psi_+(x) = P_{\omega}^{\mu}(x), \quad \psi_-(x) = P_{\omega}^{\mu-1}(x) \quad (2)$$

and the eigenstates $|\omega\mu\rangle$

$$|\omega\mu\rangle = e^{i\mu\xi} \mathcal{P}_{\omega}^{\mu}(x), \quad (3)$$

where the particular polynomial $\mathcal{P}_{\omega}^{\mu}$ is:

$$\mathcal{P}_{\omega}^{\mu} = \frac{2^{\omega-\frac{1}{2}}}{\sqrt{\Gamma(2\omega-1)}} e^{(\omega-\frac{1}{2})x} \exp(-e^x). \quad (4)$$

It must to prove that the minimal value of μ is:

$$\mu_{min} = \sqrt{\frac{\omega}{2}} = s + \frac{1}{2} = \sqrt{(j + \frac{1}{2})^2 - q^2}.$$

representing a real quantity.

It was found that the eigenfunctions verify the orthogonality condition:

$$\langle \omega\mu | \omega'\mu' \rangle = \delta_{\omega\omega'} \delta_{\mu\mu'}.$$

For the radial wavefunctions can be defined the operators:

$$K_{\pm} = e^{\pm i\xi} \left(\frac{\partial}{\partial x} \mp e^x \mp i \frac{\partial}{\partial \xi} + \frac{1}{2} \right) \quad (5)$$

$$K_z = -i \frac{\partial}{\partial \xi} \quad (6)$$

The action of the operators $\{K_{\pm}, K_z\}$ on the eigenstates $|\omega\mu\rangle$ is given by [3]:

$$K_{\pm} |\omega\mu\rangle = \pm \sqrt{\mu(\mu \pm 1) - \mu_{min}(\mu_{min} - 1)} |\omega\mu \pm 1\rangle \quad (7)$$

$$K_z |\omega\mu\rangle = \mu |\omega\mu\rangle. \quad (8)$$

From (7) results that the states $|\omega\mu\rangle$ can be obtained from $|\omega\omega\rangle$ (see (4)) as the result of repeated action of (7).

These operators obey the commutation relations, corresponding to $su(2)$ algebra:

$$[K_z, K_{\pm}] = \pm K_{\pm}, \quad [K_+, K_-] = 2K_z \quad (9)$$

It can be proved that to the hermitian conjugation operation of the operators becomes:

$$K_{\pm}^{\dagger} = -K_{\mp} \quad K_z^{\dagger} = K_z \quad (10)$$

Finally we must observe that the minimal value of the quantum number μ is μ_{min} have the value:

$$\mu_{min} = \mu_0 = \sqrt{\frac{\omega}{2}} = s + \frac{1}{2} + n \quad n = 0, 1, 2, 3, \dots$$

Results that μ have one of the values:

$$\mu = \mu_0, \mu_0 + 1, \mu_0 + 2, \dots, \mu_0 + k, \dots$$

III. THE COHERENT STATES

We can to define the Glauber coherent states $|z\rangle$ as the states that are eigenfunctions for the operator K_- :

$$K_- |z\rangle = z |z\rangle, \quad z \in C, \quad (11)$$

z being a complex variable.

We use the notation $(a)_n = a(a+1)(a+2)\dots(a+n-1)$.

From the calculations results, after normation

$$|z\rangle = \frac{1}{\sqrt{{}_0F_1(2\mu_0, |z|^2)}} \sum_{n=0}^{\infty} \frac{(-1)^n z^n K_-^n}{n!(2\mu_0)_n} |\omega, \mu_0\rangle, \quad (12)$$

Results that the states $|z\rangle$ can be obtained from the state $|\omega, \mu_0\rangle$, applying the H linear operator:

$$|z\rangle = H(2\mu_0, -zK_+) |\omega, \mu_0\rangle, \quad (13)$$

where the operator H is

$$H(2\mu_0, -zK_+) = \frac{1}{\sqrt{{}_0F_1(2\mu_0, |z|^2)}} {}_0F_1(2\mu_0, -zK_+), \quad (14)$$

where we have denoted by ${}_0F_1$ the hypergeometric function of $-zK_+$ variable, of form ${}_pF_q(a_1, a_2, \dots, a_p; b_1, \dots, b_q; x)$.

We can calculate the average values of different observables corresponding to the coherent states. Results after calculations:

$$\begin{aligned}
 \langle K_- \rangle_z &= \langle z|K_-|z \rangle = z & \langle K_+ \rangle_z &= \langle z|K_+|z \rangle = z^* \\
 \langle K_-^2 \rangle_z &= z^2 & \langle K_+^2 \rangle_z &= z^{*2} \\
 \langle K_z \rangle_z &= \frac{1}{{}_0F_1(2\mu_0, |z|^2)} \sum_{n=0}^{\infty} \frac{|z|^{2n}(\mu_0 + n)}{n!(2\mu_0)_n}, & (15) \\
 \langle K_z^2 \rangle_z &= \frac{1}{{}_0F_1(2\mu_0, |z|^2)} \sum_{n=0}^{\infty} \frac{|z|^{2n}(\mu_0 + n)^2}{n!(2\mu_0)_n}
 \end{aligned}$$

It must be noted that the average values $\langle K_z \rangle_z$ and $\langle K_z^2 \rangle_z$ can be also written in terms of hypergeometric functions of higher p, q orders.

ACKNOWLEDGMENTS

We want to thank National Council of University Scientific Research (Bucharest) for financial support of this work under grant 39560/11.09.98

REFERENCES

- [1] V. Aldaya, J. Guerro, Preprint, Univ. Granada, 1995
- [2] Y. Nogami, F. M. Toyama, *Canad. J. Phys.*, **74**, 114 (1996)
- [3] R. P. Martinez-y-Romero, A. L. Salas-Brito, J. Saldana-Vega, *J. Phys. A*, **31**, L157 (1998)
- [4] R. P. Martinez-y-Romero, J. Saldana-Vega, A. L. Salas-Brito, *J. Math. Phys.*, **30**, 2324 (1999)
- [5] O. L. de Lange, *J. Math. Phys.*, **30**, 858 (1989);

Generalized minimum uncertainty relation and a new class of super-squeezed states

Véronique Hussin

CRM, Université de Montréal, CP 6128 Succursale Centre-Ville, Montréal, H3C 3J7, Canada

Abstract

The Schrödinger-Robertson uncertainty relation will be the starting point of a classification of minimum uncertainty states associated with supermomentum and superposition operators. These operators are connected with an annihilator that generalizes the one of the supersymmetric harmonic oscillator. Such operators may be correlated and uncorrelated and give coherent and squeezed states.

For two Hermitian operators X and P satisfying the commutator $[X, P] = iC$, we know that the variances ΔX^2 and ΔP^2 satisfy the Schrödinger-Robertson uncertainty relation:

$$\Delta X^2 \Delta P^2 \geq \frac{1}{4} (\langle C \rangle^2 + \langle F \rangle^2), \quad (1)$$

where $F = \{X - \langle X \rangle, P - \langle P \rangle\}$. When there is a correlation between X and P , i.e. $\langle F \rangle \neq 0$, such a relation is a generalization of the usual one

$$\Delta X^2 \Delta P^2 \geq \frac{1}{4} \langle C \rangle^2 \quad (2)$$

and gives new results when, for example, C is not a multiple of the identity.

The so-called coherent and squeezed states are obtained when the equality is realized [1,2,3]. Let us recall that such an equality is satisfied for states which are solutions of the eigenvalues equation

$$(X + i\lambda P)|\psi\rangle = \frac{\beta}{\sqrt{2}}|\psi\rangle, \quad \lambda, \beta \in \mathbf{C}. \quad (3)$$

As a consequence we have the following relations:

$$\Delta X^2 = |\lambda| \Delta, \quad \Delta P^2 = \frac{1}{|\lambda|} \Delta, \quad \text{with} \quad \Delta = \frac{1}{2} \sqrt{\langle C \rangle^2 + \langle F \rangle^2}. \quad (4)$$

Note that $\langle C \rangle$ and $\langle F \rangle$ can be expressed in terms of the variances as, for example,

$$\langle C \rangle = 2\text{Re}\lambda \Delta P^2, \quad \langle F \rangle = 2\text{Im}\lambda \Delta P^2. \quad (5)$$

It is then clear from (4) that if $|\lambda| = 1$, we have coherent states and if $|\lambda| \neq 1$, they are squeezed.

In this work, we start with a supersymmetric annihilation operator $A = \begin{pmatrix} \mu a & \tau \\ 0 & \mu a \end{pmatrix}$ where $\mu, \tau \in \mathbf{C}$ and a is as usual the annihilation operator for the harmonic oscillator. Indeed A is the generalized form of an annihilator for the supersymmetric harmonic oscillator which has been first considered by Aragone and Zypman [4]. It is then easy to see that the Hermitian operators

$$X = \frac{1}{\sqrt{2}}(A + A^\dagger), \quad P = \frac{i}{\sqrt{2}}(A^\dagger - A) \quad (6)$$

satisfy the commutation relation $[X, P] = i(|\mu|^2\sigma_0 + |\tau|^2\sigma_3) = iC$. Since C is not necessarily a multiple of the identity, the Schrödinger-Robertson uncertainty relation gives us a new understanding of what are the coherent and squeezed states for the supersymmetric harmonic oscillator. In the following, we will completely solve the eigenvalues equation (3), give a classification of the corresponding coherent and squeezed states and compute the variances ΔX^2 and ΔP^2 in those states.

To solve the eigenvalues equation (3) with X and P given by (6) it is convenient to use the Fock-Bargmann representation (see [5]), i.e $a \rightarrow \frac{d}{dz}$, $a^\dagger \rightarrow z$. We then get

$$\begin{cases} (1 + \lambda)\mu \frac{d\psi_1}{dz} + ((1 - \lambda)\bar{\mu}z - \beta)\psi_1(z) + (1 + \lambda)\tau\psi_2(z) = 0, \\ (1 + \lambda)\mu \frac{d\psi_2}{dz} + ((1 - \lambda)\bar{\mu}z - \beta)\psi_2(z) + (1 - \lambda)\bar{\tau}\psi_1(z) = 0, \end{cases} \quad (7)$$

where $|\psi\rangle = \begin{pmatrix} \psi_1(z) \\ \psi_2(z) \end{pmatrix}$. The resolution then deals with three different cases depending on the values of the parameters.

1) $\mu = 0, \lambda \neq -1$ and $\tau = 1$: we get generalized spin-1/2 squeezed states based on the $su(2)$ algebra since $X + i\lambda P = \frac{1}{\sqrt{2}}((1 + \lambda)\sigma_+ + (1 - \lambda)\sigma_-)$. This is a particular case of the general approach by Brif [6]. Taking

$$\frac{1 - \lambda}{1 + \lambda} = \delta e^{i\phi}, \quad \delta \in \mathbf{R}^+, \quad \phi \in [-\frac{\pi}{2}, 3\frac{\pi}{2}[, \quad (8)$$

we can write the normalized eigenstates as

$$|\psi_+\rangle = \frac{1}{\sqrt{1 + \delta}} \begin{pmatrix} 1 \\ \delta^{1/2} e^{i\phi/2} \end{pmatrix}, \quad |\psi_-\rangle = \frac{1}{\sqrt{1 + \delta}} \begin{pmatrix} -1 \\ \delta^{1/2} e^{i\phi/2} \end{pmatrix}, \quad (9)$$

with eigenvalues $\beta_+ = \sqrt{1 - \lambda^2}$ and $\beta_- = -\sqrt{1 - \lambda^2}$ respectively. Since we have $[X, P] = i\sigma_3$ and $\{X, P\} = 0$, it is easy to see that in these states

$$\langle C \rangle_\pm = \frac{1 - \delta}{1 + \delta}, \quad \langle F \rangle_\pm = \frac{-2\delta}{(1 + \delta)^2} \sin \phi \quad (10)$$

and

$$\Delta = \frac{\sqrt{\delta^4 - 2\delta^2 \cos 2\phi + 1}}{2(\delta + 1)^2}. \quad (11)$$

Finally, we have

$$\Delta X^2 = \frac{1}{2} \left(1 - \frac{4\delta}{(\delta+1)^2} \cos^2 \frac{\phi}{2} \right), \quad \Delta P^2 = \frac{1}{2} \left(1 - \frac{4\delta}{(\delta+1)^2} \sin^2 \frac{\phi}{2} \right). \quad (12)$$

Let us observe that the coherent states appear for $\phi = \pm \frac{\pi}{2}$. For $\phi \in]\frac{\pi}{2}, \frac{3\pi}{2}[$, P is squeezed while for $\phi \in]-\frac{\pi}{2}, \frac{\pi}{2}[$, it is X that is squeezed. In [3], $\delta=1$ so that $\langle C \rangle = 0$.

2) $\mu = 1$, $\lambda = 1$: the solutions of (3) are now coherent states (or supercoherent states like in [4]) for which $\langle F \rangle = 0$, so they satisfy

$$\Delta X^2 = \Delta P^2 = \frac{1}{2} \langle C \rangle. \quad (13)$$

Those states may be written as a linear combination of the orthogonal and normalized states (with $\alpha = \frac{\beta}{2}$)

$$|\psi_0\rangle = \frac{1}{\sqrt{\pi}} e^{-|\alpha|e^{\alpha z}} \begin{pmatrix} 1 \\ 0 \end{pmatrix}, \quad |\psi_1\rangle = \frac{|\tau|^2}{\sqrt{\pi(1+|\tau|^2)}} e^{-|\alpha|e^{\alpha z}} \begin{pmatrix} z - \bar{\alpha} \\ -1/\tau \end{pmatrix}. \quad (14)$$

The mean value of $\langle C \rangle$ in these pure states is given by

$$\langle C \rangle_0 = (1 + |\tau|^2), \quad \langle C \rangle_1 = \frac{1 + |\tau|^4}{1 + |\tau|^2}. \quad (15)$$

It is interesting to mention that the state $|\psi_0\rangle$ constitutes the more classical-like state for the standard harmonic oscillator [4]. Indeed, for the usual position and momentum operators $x = \frac{1}{\sqrt{2}}(a + a^\dagger)$ and $p = \frac{i}{\sqrt{2}}(a^\dagger - a)$, we have

$$(\Delta x^2)_0 = (\Delta p^2)_0 = \frac{1}{2}. \quad (16)$$

A new point is that $|\psi_1\rangle$ constitutes the more classical-like state for the supersymmetric harmonic oscillator since, for $|\tau| = 1$, we get from (13) and (15)

$$(\Delta X^2)_1 = (\Delta P^2)_1 = \frac{1}{2}. \quad (17)$$

3) $\mu = 1$, $\lambda \neq \pm 1$: we will produce a completely new set of solutions which will give squeezed and coherent states. The general solution of (3) can now be written as

$$|\psi\rangle = e^{p(z)} \begin{pmatrix} v(z) \\ -\frac{1}{\tau} v'(z) \end{pmatrix}, \quad \text{where} \quad p(z) = \frac{1}{1+\lambda} \left(\beta z - \frac{1}{2} (1-\lambda) z^2 \right) \quad (18)$$

and $v(z)$ satisfies the linear equation

$$v''(z) + kv(z) = 0 \quad \text{for} \quad k = - \left(\frac{1-\lambda}{1+\lambda} \right) |\tau|^2. \quad (19)$$

The general solution of (19) is a linear combination of pure states given by

$$|\psi_{\pm}\rangle = N_{\pm} e^{q_{\pm}(z)} \left(\mp \frac{|\tau|}{\tau} \delta^{1/2} e^{i\phi/2} \right), \quad (20)$$

where N_{\pm} is a normalization factor and

$$q_{\pm}(z) = \left(\frac{1}{2} \beta(1 + \delta e^{i\phi}) \pm |\tau| \delta^{1/2} e^{i\phi/2} \right) z - \frac{1}{2} \delta e^{i\phi} z^2, \quad (21)$$

with δ and ϕ given by (8) in terms of λ . Note that the norm of $|\psi_{\pm}\rangle$ is defined by

$$\langle \psi_{\pm} | \psi_{\pm} \rangle = |N_{\pm}|^2 (1 + \delta) \int_{-\infty}^{+\infty} \exp \left[-|z|^2 + q_{\pm}(z) + \bar{q}_{\pm}(\bar{z}) \right] dz d\bar{z} \quad (22)$$

and the integrability condition is $\text{Re } \lambda > 0$ which is equivalent to $0 \leq \delta < 1$. The limit case $\delta = 0$ (or equivalently $\lambda = 1$) does not give the complete solution (14) and then must be excluded. It is easy to compute the mean value of C and we deduce the one of F from that of C using (5)

$$\langle C \rangle_{\pm} = \frac{1 - \delta}{1 + \delta} \left(\frac{1 + \delta}{1 - \delta} + |\tau|^2 \right), \quad \langle F \rangle_{\pm} = \frac{-2\delta \sin \phi}{(1 + \delta)^2} \left(\frac{1 + \delta}{1 - \delta} + |\tau|^2 \right), \quad (23)$$

for normalized states. Finally, we have

$$\Delta = \frac{\sqrt{\delta^4 - 2\delta^2 \cos 2\phi + 1}}{2(\delta + 1)^2} \left(\frac{1 + \delta}{1 - \delta} + |\tau|^2 \right) \quad (24)$$

and

$$\Delta X^2 = \frac{1}{2} \left(1 - \frac{4\delta}{(\delta + 1)^2} \cos^2 \frac{\phi}{2} \right) \left(\frac{1 + \delta}{1 - \delta} + |\tau|^2 \right), \quad (25)$$

$$\Delta P^2 = \frac{1}{2} \left(1 - \frac{4\delta}{(\delta + 1)^2} \sin^2 \frac{\phi}{2} \right) \left(\frac{1 + \delta}{1 - \delta} + |\tau|^2 \right). \quad (26)$$

This work has been partially supported by research grants from NSERC of Canada and FCAR du Gouvernement du Québec.

References

- [1] V.V. Dodonov, E.V. Kurmyshev and V.I. Man'ko, Phys. Lett. A **79**, 150 (1980).
- [2] D.A. Trifonov, J. Math. Phys. **35**, 2297 (1994).
- [3] R.R. Puri, Phys. Rev. A **49**, 2178 (1994).
- [4] C. Aragone and F. Zypman, J. Phys. A **19**, 2267 (1986).
- [5] A. Perelomov, *Generalized coherent states and their applications*, Springer-Verlag, Berlin (1986).
- [6] C. Brif, Int. J. Theor. Phys. **36**, 1651 (1997).

New Creation and Annihilation Operators for Hydrogenlike Potentials

J. Negro, L.M. Nieto and O. Rosas-Ortiz*
Departamento de Física Teórica, Universidad de Valladolid
47011 Valladolid, Spain

Abstract

The factorization technique is shown to be a powerful algebraic tool to show general properties of some integrable physical systems in Quantum Mechanics. The method by itself gives rise to a wide set of raising and lowering operators changing the azimuthal as well as the principal quantum number used in the study of radial hydrogenlike potentials.

I. INTRODUCTION

After the separation of the angular variables, the stationary radial Schrödinger equation for the Coulomb potential in N dimensions takes the form

$$H^\ell \psi_E^\ell = \left\{ -\frac{d^2}{dr^2} + \frac{(2\ell + N - 3)(2\ell + N - 1)}{4r^2} - \frac{2}{r} \right\} \psi_E^\ell = E \psi_E^\ell, \quad (1)$$

where the constants \hbar, m, e have been conveniently reabsorbed. The values of the orbital angular momentum are positive integers $\ell = 0, 1, 2, \dots$. We shall henceforth consider exclusively the two-dimensional case $N = 2$ that (together with $N = 3$) is the most interesting one. Therefore we shall think of the potential $V^\ell(r)$ as given by

$$V^\ell(r) = \frac{(2\ell + 1)(2\ell - 1)}{4r^2} - \frac{2}{r}. \quad (2)$$

The computation of the discrete spectrum associated to the bounded states of H^ℓ can be easily obtained by means of the conventional factorizations [1]

$$H^\ell = X_\ell^+(r)X_\ell^-(r) - q(\ell) = X_{\ell-1}^-(r)X_{\ell-1}^+(r) - q(\ell-1), \quad (3)$$

$$X_\ell^\pm(r) = \mp \frac{d}{dr} - \frac{2\ell + 1}{2r} + \frac{2}{2\ell + 1}, \quad q(\ell) = \frac{-1}{(\ell + 1/2)^2}. \quad (4)$$

*On leave of absence from *Departamento de Física, CINVESTAV-IPN, A.P. 14-740, 07000 México D.F., Mexico.*

Some properties that can immediately be derived are enumerated below.

i) Spectrum. The lowest energy of the fundamental state is precisely $E_\ell = q(\ell) = -1/(\ell + 1/2)^2$. The corresponding eigenfunction, denoted by ψ_ℓ^ℓ is determined by the equation $X_\ell^-(r)\psi_\ell^\ell = 0$. The energy of the excited states ψ_n^ℓ is given by $E_n = -1/(2n + 1/2)^2$, with $n = \ell, \ell + 1, \dots$

ii) The operators X^\pm . Let us design by $\mathcal{H}^\ell = \langle \{\psi_n^\ell\}_{n=\ell}^{+\infty} \rangle$ the Hilbert space spanned by the bounded states of H^ℓ , for $\ell = 0, 1, \dots$. The operators X_ℓ^\pm connect these spaces as

$$\begin{aligned} X_\ell^- : \mathcal{H}^\ell &\rightarrow \mathcal{H}^{\ell+1} & X_\ell^+ : \mathcal{H}^{\ell+1} &\rightarrow \mathcal{H}^\ell \\ X_\ell^-(r)\psi_n^\ell(r) &\propto \psi_n^{\ell+1}(r), & X_\ell^+(r)\psi_n^{\ell+1}(r) &\propto \psi_n^\ell(r). \end{aligned} \quad (5)$$

Remark that they preserve the label n , that is, they connect eigenfunctions with the same energy E_n . We can define the free-index linear operators $\{X^\pm, L\}$ acting on the direct sum $\oplus_{\ell=0}^{+\infty} \mathcal{H}^\ell$ by means of

$$X^-\psi_n^\ell := X_\ell^-\psi_n^\ell, \quad X^+\psi_n^{\ell+1} := X_\ell^+\psi_n^{\ell+1}, \quad L\psi_n^\ell := \ell\psi_n^\ell, \quad (6)$$

where one must have in mind (5). The action on any other vector can be obtained from (6) by linearization, but we shall never need it.

Formally we can allow the label ℓ to take also negative integer values since $V^\ell(r) = V^{-\ell}(r)$ in (2). Therefore we shall henceforth assume $\mathcal{H} = \oplus_{\ell=-\infty}^{+\infty} \mathcal{H}^\ell$ as the total Hilbert space. This space can be written as another direct sum $\mathcal{H} = \oplus_{n=0}^{+\infty} \mathcal{H}_n$, where $\mathcal{H}_n = \langle \{\psi_n^\ell\}_{\ell=-n}^n \rangle$. Each subspace \mathcal{H}_n , of dimension $2n + 1$, is generated by eigenfunctions with the same energy E_n and is invariant under the operators $\{X^\pm, L\}$.

Taking into account the previous considerations it is straightforward to arrive at the following commutators,

$$[L, X^\pm] = \mp X^\pm, \quad [X^+, X^-] = q(L) - q(L-1). \quad (7)$$

where, for the hydrogen potential the function $q(L)$ was given in (4).

It is clear that the operators $\{X^\pm, L\}$ do not close a Lie algebra; at this level we can only speak of an associative algebra. Of course, formally we could make a change of basis, inside the enveloping algebra, so that the new generators $\{\tilde{X}^\pm, \tilde{L}\}$ would close in fact an $su(2)$ Lie algebra. In the next section we will show that there can be more factorizations leading to larger operator algebras exhibiting further properties of the wavefunction space.

II. GENERAL FACTORIZATIONS

Once the discrete spectrum E_n of H^ℓ is known, we propose a somewhat more general factorization than that already displayed in (3). We shall write

$$B_{n,\ell}(r)A_{n,\ell}(r) - \phi(n, \ell) = h_{n,\ell}(r) [H^\ell - E_n], \quad (8)$$

$$A_{n,\ell}(r)B_{n,\ell}(r) - \phi(n, \ell) = h_{\tilde{n},\tilde{\ell}}(r) [H^{\tilde{\ell}} - E_{\tilde{n}}]. \quad (9)$$

This must be understood as a series of relationships valid for all the allowed values of the (n, ℓ) parameters. Here $B_{n,\ell}(r), A_{n,\ell}(r)$ are first order differential operators, $h_{n,\ell}(r)$

design functions, and $\phi(n, \ell)$ are constants. The problem of finding solutions to this kind of factorizations becomes more involved because we have additional functions $h_{n, \ell}(r)$ to be determined. The important point is that the operators $B_{n, \ell}(r), A_{n, \ell}(r)$ share similar properties with their analogs $\{X^\pm\}$ presented in Section I:

$$\begin{aligned} A_{n, \ell} : \mathcal{H}^\ell &\rightarrow \mathcal{H}^{\tilde{\ell}} & B_{n, \ell} : \mathcal{H}^{\tilde{\ell}} &\rightarrow \mathcal{H}^\ell \\ A_{n, \ell}(r)\psi_n^\ell(r) &\propto \psi_{\tilde{n}}^{\tilde{\ell}}(r), & B_{n, \ell}(r)\psi_{\tilde{n}}^{\tilde{\ell}}(r) &\propto \psi_n^\ell(r). \end{aligned} \quad (10)$$

In this case the most important difference is that $B_{n, \ell}(r), A_{n, \ell}(r)$ do not keep the energy eigenvalue, so that they could change both labels: $(n, \ell) \rightarrow (\tilde{n}, \tilde{\ell})$, where $(\tilde{n}, \tilde{\ell}) = F(n, \ell) := (F_1(n, \ell), F_2(n, \ell))$, being F an invertible function. Indeed, when $n = \tilde{n}$ and $h_{n, \ell}(r) = 1$ we recover the conventional case. We can define the free-index operators $\{A, B, L, N\}$ as before (the latter is defined by $N\psi_n^\ell = n\psi_n^\ell$), satisfying the following commutation rules

$$\begin{aligned} [L, A] &= \tilde{L} - L, & [L, B] &= \tilde{L}^{-1} - L, & [B, A] &= \phi(N, L) - \phi(\tilde{N}^{-1}, \tilde{L}^{-1}) \\ [N, A] &= \tilde{N} - N, & [N, B] &= \tilde{N}^{-1} - N, & [N, L] &= 0. \end{aligned} \quad (11)$$

where $\tilde{N} = F_1(N, L)$, $\tilde{L} = F_2(N, L)$, $\tilde{N}^{-1} = (F^{-1})_1(N, L)$, and $\tilde{L}^{-1} = (F^{-1})_2(N, L)$.

We must also notice that the equation $A_{n, \ell}(r)\psi_n^\ell(r) = 0$ does not necessarily give an eigenfunction of H^ℓ ; this happens to be the case only when $\phi(n, \ell) = 0$. Finally we want to remark that $\{A, B\}$ are not shape invariant potential operators, they should rather be called ‘shape invariant eigenequation operators’.

III. APPLICATION TO THE HYDROGEN POTENTIAL

In this section the general factorization above introduced will be applied to the hydrogen Hamiltonians H^ℓ of equation (1) with potential (2). We shall consider the simplest nontrivial type of functions $h_{n, \ell}(r) \propto r$. In this way we obtain two independent solutions $\{A^i, B^i\}_{i=1,2}$, displayed in Table I.

TABLE I. Explicit expressions for first order operators.

$\left\{ \begin{aligned} B_{n, \ell}^1(r) &= (2n + 1)^{1/2} \left(\frac{r^{1/2}}{2} \frac{d}{dr} + \frac{r^{1/2}}{2n+1} + \frac{\ell}{2r^{1/2}} \right) \left(\frac{2n+1}{2n+2} \right)^{1/2} D \left(\frac{2n+2}{2n+1} \right) \\ A_{n, \ell}^1(r) &= D \left(\frac{2n+1}{2n+2} \right) \left(\frac{2n+2}{2n+1} \right)^{1/2} (2n + 1)^{1/2} \left(\frac{r^{1/2}}{2} \frac{d}{dr} - \frac{r^{1/2}}{2n+1} - \frac{2\ell+1}{4r^{1/2}} \right) \end{aligned} \right.$
$\left\{ \begin{aligned} B_{n, \ell}^2(r) &= (2n + 1)^{1/2} \left(\frac{r^{1/2}}{2} \frac{d}{dr} + \frac{r^{1/2}}{2n+1} - \frac{\ell}{2r^{1/2}} \right) \left(\frac{2n+1}{2n+2} \right)^{1/2} D \left(\frac{2n+2}{2n+1} \right) \\ A_{n, \ell}^2(r) &= D \left(\frac{2n+1}{2n+2} \right) \left(\frac{2n+2}{2n+1} \right)^{1/2} (2n + 1)^{1/2} \left(\frac{r^{1/2}}{2} \frac{d}{dr} - \frac{r^{1/2}}{2n+1} + \frac{2\ell+1}{4r^{1/2}} \right) \end{aligned} \right.$

The symbol D in Table I is for the dilation operator, $D(\mu)\psi(r) = \psi(\mu r)$. For the first couple $\{A^1, B^1\}$ we have $(\tilde{n}, \tilde{\ell}) = (n + 1/2, \ell + 1/2)$, while for the second pair $\{A^2, B^2\}$,

$(\tilde{n}, \tilde{\ell}) = (n + 1/2, \ell - 1/2)$. The general factorizations obtained from these solutions read as follows

$$B_{n,\ell}^1(r)A_{n,\ell}^1(r) + \ell + n + 1 = -\frac{(2n+1)r}{4} [H^\ell(r) - E_n], \quad (12)$$

$$B_{n,\ell}^2(r)A_{n,\ell}^2(r) - \ell + n + 1 = -\frac{(2n+1)r}{4} [H^\ell(r) - E_n]. \quad (13)$$

The nonvanishing commutators among these operators are

$$\begin{aligned} [N, A^1] &= \frac{1}{2}A^1, & [N, B^1] &= \frac{-1}{2}B^1, & [L, A^1] &= \frac{1}{2}A^1, & [L, B^1] &= \frac{-1}{2}B^1, & [A^1, B^1] &= I, \\ [N, A^2] &= \frac{1}{2}A^2, & [N, B^2] &= \frac{-1}{2}B^2, & [L, A^2] &= \frac{-1}{2}A^2, & [L, B^2] &= \frac{1}{2}B^2, & [A^2, B^2] &= I, \end{aligned} \quad (14)$$

In other words, we have a set of two independent boson operator algebras. The problem with these operators is that they change the quantum numbers (n, ℓ) in half-units, so that they do not keep inside the sector of physical wavefunctions. To avoid this problem we can build quadratic operators [2] $\{A^i A^j, B^i A^j, B^i B^j\}_{i,j=1,2}$ satisfying this requirement; such second-order operators close the Lie algebra $sp(4, \mathbf{R})$ [3]. It includes the subalgebras $su(2)$ (whose generators connect eigenstates with the same energy but different ℓ 's) and $su(1, 1)$ (relating states with the same ℓ but different energies E_n). This is called a 'singleton representation' of $so(3, 2) \approx sp(4, \mathbf{R})$, where there is one lowest weight eigenvector ψ_0^0 from which all the representation space is generated by applying raising operators. A more evident situation arises with the (radial) oscillator potential [4]. We have restricted our considerations to the $N=2$ space dimensions which is the simplest one; for $N \geq 3$ the same treatment still holds valid, but with some special features which will not be discussed here [5].

Starting from the $so(3, 2)$ Lie structure of the second order operators one can build coherent states from a group theoretical approach in a standard way [6]. However, the physics is given by the Hamiltonian (which is not among the second order operators), its spectrum and the degeneration labels. Therefore, in this sense, Klauder's construction [7] is closer to physical requirements.

This work was performed under the auspices of CONACyT (Mexico) and DGES project PB94-1115 from Ministerio de Educación y Cultura (Spain), as well as by Junta de Castilla y León (CO2/197). ORO acknowledges the ICSSUR'99 Organizing Committee for partial financial support.

References

- [1] W. Miller Jr., *Lie Theory and Special Functions*, Mathematics in Science and Engineering **43** (Academic Press, N. Y., 1968)
- [2] Y.F. Liu, Y.A. Lei and J.Y. Zeng, Phys. Lett A **231**, 9 (1997)
- [3] Y. Alhassid, F. Gürsey and F. Iachello, Ann. Phys. **148**, 346 (1983).
- [4] D.J. Fernández C., J. Negro and M.A. del Olmo, Ann. Phys. **252**, 386 (1996)
- [5] J. Negro, L M Nieto, O Rosas-Ortiz, Preprint UVA (1999)
- [6] A. Perelomov, *Generalized Coherent States and their Applications*, (Springer-Verlag, Berlin, 1986)
- [7] J.R. Klauder, J. Phys A **29**, L293 (1996). P. Majumdar and H.S. Sharatchandra, Phys. Rev. A **56**, R3322 (1997). P. Bellomo and C.R. Stroud, Phys. Rev. A **59**, 900 (1999)

On the annihilation-creation relation and the number states related to the minimum-uncertainty states between the position and the inverse of the momentum

Fuminori SAKAGUCHI

Department of Electrical and Electronics Engineering

Faculty of Engineering, Fukui University, 3-9-1 Bunkyo, Fukui-shi, 910-8507 Japan

tel: +81-776-27-8912, fax: +81-776-27-8749, e-mail: saka@dignet.fuee.fukui-u.ac.jp

Abstract

The annihilation/creation relation and the number states related to the minimum-uncertainty states between the position and the inverse of the momentum are investigated. A non-linear type of the re-ordering relation between the annihilation and creation operator is derived.

The eigenvectors of the linear operator $Q - ikP^{-1}$ [5-8] (Q : position op. and P : momentum op., k : positive integer) are the minimum uncertainty states between Q and P^{-1} , and their eigenfunction system in the position representation is the over-complete wavelet system made of Cauchy wavelets[5-8]. This relation is analogous to the coherent states which are the eigenvector system of the boson annihilation operator. In this case, it is well known that this operator is the step-down operator (down-ladder) of the eigenfunction of the boson number operator.

In this paper, the similar relation to this will be investigated for the Cauchy wavelet case, where the operator $Q - ikP^{-1}$ itself is not but the Cayley transform of $Q - ikP^{-1}$ is the analogue of the annihilation operator. What is the analogue of the 'number operator' will be shown there. Moreover, the re-ordering relation between the analogues of the annihilation and creation operators will be investigated.

Let Q and P be the position-coordinate operator and the momentum operator which satisfy $[Q, P] = iI$ (I : identity op.). For a fixed positive integer k , define the operator

$$A_k := Q - ikP^{-1}. \quad (1)$$

Because A_k is not hermitian, it has complex eigenvalues, and the eigenvectors are not orthogonal. The eigenvector $|\alpha\rangle_{A_k}$ of A_k is a minimum uncertainty states between the Q and P^{-1} in the sense that $(\Delta Q)^2 \cdot (\Delta P^{-1})^2 = (1/4) | \langle i[Q, P^{-1}] \rangle |^2$ is satisfied. It is easily shown that the eigenfunction in the position-coordinate representation with the eigenvalue α is

$$h_k^{(\alpha)}(x) := {}_Q \langle x | \alpha \rangle_{A_k} = \frac{G_k^{(\alpha)}}{(x - \alpha)^{k+1}} \quad (2)$$

with the normalization constant $G_k^{(\alpha)}$, and the eigenfunction system is over-complete[6,8]. For non-real α , this function is a complex-valued square-integrable wavepacket localized almost around $x = \text{Re } \alpha$.

Let b be the real part of the normalized eigenvalue α and a be the imaginary part of α . Then, we have

$$h_k^{(b+ia)}(x) = \frac{1}{|a|^{1/2}} h_k^{(i)}\left(\frac{x-b}{a}\right), \quad (3)$$

because $x - \alpha = a\left(\frac{x-b}{a} - i\right)$ and $G_k^{(\alpha)} = |a|^{k+1/2} G_k(i)$. This relation shows that the eigenfunction system of the operator A_k defined in (1) is just a wavelet system [1-4] with continuous parameters made from the basic wavelet $h_k^{(i)}(x)$. This wavelet system is often called Cauchy wavelet system. (NB: $h_k^{(i)}(x)$ has the vanishing moments from 0-th to $(k-1)$ -th order)

By making the Fourier transform of these eigenfunctions where the calculation is made by residue calculus, we obtain the wavefunctions of them in the momentum representation

$$H_k^{(\alpha)}(p) := {}_P\langle p|\alpha\rangle_{A_k} = \begin{cases} (\text{const.}) \cdot |\text{Im } \alpha|^{1/2} (-ip)^k e^{-i\alpha p} & (\text{if } p \text{ Im } \alpha < 0) \\ 0 & (\text{if } p \text{ Im } \alpha \geq 0). \end{cases} \quad (4)$$

This shows that the Fourier transform of the Cauchy wavelet has the support only in the positive-momentum part (if $a < 0$) or only in the negative-momentum part (if $a > 0$).

From now, we are introducing the analogue of the annihilation operator. Define

$$a_{k\pm} := (A_k \mp iI)^{-1} (A_k \pm iI) \quad (+, -). \quad (5)$$

Because the Cauchy wavelets are the eigenfunctions of A_k as mentioned above, the eigenfunctions (in the position representation) of the operator $a_{k\pm}$ with the eigenvalue $(\alpha \pm 1)/(\alpha \mp 1)$ is the Cauchy wavelet $h_k^{(\alpha)}(t)$. (NB. a_{k+}/a_{k-} is bounded for the positive/negative-momentum component of a signal.)

The analogue to the number operator is defined in wavelet version as follows; Define

$$N_{k\pm} := \mp \frac{1}{2} (A_k \pm iI)^\dagger P (A_k \pm iI). \quad (6)$$

We restrict the domain of N_{k+} to the positive-momentum components and the negative-momentum components. $N_{k\pm}$ is hermitian, and, as will be shown below, $N_{k\pm}$ has the eigenvalues 0, 1, 2, 3, ... In the special case with $k = 1$, the operator $\pm 2N_{k\pm} \pm 3I$ is mathematically equivalent to the Hamiltonian given in p.41 of Daubechies' textbook[3]. For general k , the corresponding 'Hamiltonian' in our notation is defined by $H_k := QPQ + k^2 P^{-1} + P$, and the relation to $N_{k\pm}$ is $N_{k\pm} = \mp \frac{1}{2} H_k - (k + \frac{1}{2})I$.

In the momentum representation, by defining $\Phi_\lambda^{(k\pm)}(p) := {}_P\langle p|\lambda\rangle_{K_{k\pm}}$, the characteristic equation of the operator $K_{k\pm} := e^P P^{-k} N_{k\pm} P^k e^{-P}$ is

$$\mp \frac{1}{2} \left[p \frac{d^2}{dp^2} + (2k + 1 - 2p) \frac{d}{dp} \right] \Phi_\lambda^{(k\pm)}(p) = \lambda \Phi_\lambda^{(k\pm)}(p) \quad (7)$$

Because this equation is rewritten into the associated Laguerre differential equation with orders λ , $2k$ by the change of variable $\eta = \pm 2p$, this equation has polynomial solutions

$$\Phi_\lambda(p)^{(k\pm)} = \begin{cases} (\text{const.}) L_\lambda^{2k}(\pm 2p) & (\text{if } \pm p \geq 0) \\ 0 & (\text{otherwise}) \end{cases} \quad (8)$$

only when $\lambda = 0, 1, 2, 3, \dots$, where $L_n^m(x)$ denotes the associated Laguerre polynomial (or Sonine polynomial) with orders n, m . Since the momentum operator P is the scalar p in the momentum representation, the above result shows that $N_{k\pm}$ has the eigenvalues $0, 1, 2, 3, \dots$ and the eigenfunction $\Psi_\lambda^{(k\pm)}(p) (:= {}_P\langle p|n\rangle_{N_{k\pm}})$ with the eigenvalue $\lambda = n$ is

$$\Psi_n^{(k\pm)}(p) = \begin{cases} C_n^{(k\pm)} e^{\mp p} (\pm p)^k L_n^{2k}(\pm 2p) & (\text{if } \pm p \geq 0) \\ 0 & (\text{otherwise}). \end{cases} \quad (9)$$

($C_n^{(k\pm)}$ is the normalization constant.) The eigenfunction in the position-coordinate representation $\psi_n^{(k\pm)}(x) := {}_Q\langle x|n\rangle_{N_{k\pm}}$ is the inverse Fourier transform of $\Psi_n^{(k\pm)}(p)$. It is easily shown that the eigenfunction in the position representation is

$$\psi_n^{(k\pm)}(x) = (\text{const.}) \sum_{r=0}^n (-2i)^{m-r} m \frac{(n+2m-r)!}{r!(m-r)!(n-m-r+1)!} (x \pm i)^{-(n+m-r+1)}. \quad (10)$$

It is interesting that this expansion is made of a finite number of the cauchy wavelets $h_\ell^{(\mp i)}(x)$ in (2) with various ℓ 's. And the eigenfunction with $n = 0$ (in other words, the vacuum) is identical to the basic wavelet $h_k^{(i)}(x)$, which is quite parallel to the relation that the vacuum state of the boson number operator is identical to the coherent state with the eigenvalue 0 (Note that $h_k^{(i)}(x)$ is the eigenfunction of a_{k-} with the eigenvalue 0 as well as the eigenfunction of A_k with the eigenvalue i). Since $N_{k\pm}$ is hermitian and the eigenvalues are not degenerated, the eigenfunction system $\{\psi_n^{(k\pm)}(x)|n = 0, 1, 2, \dots\}$ in the position representation is also orthogonal.

In the following, it will be shown that $a_{k\pm}$ defined in (5) and its adjoint are the step-down and step-up operators of this eigenfunction system; From (1),(5),(6) and the relations $[Q, P^{-1}] = -iP^{-2}$, $[P, A_k] = -iI$, $[A_k, A_k^\dagger] = 2kP^{-2}$, we have

$$[A_k, N_{k\pm}] = \pm k P^{-2} P (A_k \pm iI) \pm \frac{i}{2} (A_k \pm iI)^\dagger (A_k \pm iI) \pm \frac{i}{2} I = \pm \frac{i}{2} (A_k^2 + I) \quad (11)$$

$$[a_{k\pm}, N_{k\pm}] = \pm \frac{i}{2} (A_k \mp iI)^{-1} (A_k^2 + I) \mp \frac{i}{2} (A_k \mp iI)^{-2} (A_k^2 + I) (A_k \pm iI) = a_{k\pm}. \quad (12)$$

By operating this relation on the eigenvector $|n\rangle_{N_{k\pm}}$ of the operator $N_{k\pm}$ (with the eigenvalue n), we have

$$N_{k\pm} a_{k\pm} |n\rangle_{N_{k\pm}} = a_{k\pm} N_{k\pm} |n\rangle_{N_{k\pm}} - a_{k\pm} |n\rangle_{N_{k\pm}} = (n-1) a_{k\pm} |n\rangle_{N_{k\pm}}. \quad (13)$$

This relation shows that $a_{k\pm} |n\rangle_{N_{k\pm}}$ is the eigenvector of $N_{k,\pm}$ with the eigenvalue $n-1$.

Because we can show $a_{k\pm}^\dagger N_{k\pm} a_{k\pm} = -N_{k\mp}$ and $N_{k\pm} = -N_{k\mp} - (2k+1)I$ from (5) and (6), we have $a_{k\pm}^\dagger \{N_{k\pm} + (2k+1)I\} a_{k\pm} = N_{k\pm}$. From this relation and (13), we have

$$\begin{aligned} & \{(n-1) + (2k+1)\} {}_{N_{k\pm}} \langle n | a_{k\pm}^\dagger a_{k\pm} | n \rangle_{N_{k\pm}} \\ &= {}_{N_{k\pm}} \langle n | a_{k\pm}^\dagger \{N_{k\pm} + (2k+1)I\} a_{k\pm} | n \rangle_{N_{k\pm}} = {}_{N_{k\pm}} \langle n | N_{k\pm} | n \rangle_{N_{k\pm}} = n. \end{aligned} \quad (14)$$

However, from (13) and the non-degeneracy of the eigenvalues of $N_{k\pm}$, by choosing the phase factor of $|n\rangle_{N_{k\pm}}$ appropriately, we obtain the annihilation/creation relations

$$a_{k\pm} |n\rangle_{N_{k\pm}} = \sqrt{\frac{n}{n+2k}} |n-1\rangle_{N_{k\pm}}, \quad a_{k\pm}^\dagger |n\rangle_{N_{k\pm}} = \sqrt{\frac{n+1}{n+2k+1}} |n+1\rangle_{N_{k\pm}}. \quad (15)$$

From the orthonormality of the eigenfunction system of $N_{k\pm}$ and the relations (15), we have

$$a_{k\pm}^\dagger a_{k\pm} = N_{k\pm} (N_{k\pm} + 2kI)^{-1}, \quad a_{k\pm} a_{k\pm}^\dagger = (N_{k\pm} + I) (N_{k\pm} + (2k+1)I)^{-1}, \quad (16)$$

and hence, by eliminating N , the non-linear re-ordering relations

$$a_{k\pm} a_{k\pm}^\dagger = (a_{k\pm}^\dagger a_{k\pm} - (2k+1)I)^{-1} ((2k-1)a_{k\pm}^\dagger a_{k\pm} + I) \quad (17)$$

$$a_{k\pm}^\dagger a_{k\pm} = (a_{k\pm} a_{k\pm}^\dagger + (2k-1)I)^{-1} ((2k+1)a_{k\pm} a_{k\pm}^\dagger - I) \quad (18)$$

are derived. These relations are, different from the boson case ($a^\dagger a = n$, $aa^\dagger = n+I$, $a^\dagger a = aa^\dagger + I$), non-linear type of re-ordering relations.

These relations are special case of the $\text{su}(1,1)$ -annihilation/creation relation [10] with $\lambda = 2k+1$, $E_0 = -i(PQ + QP)$, $E_+ = iP$, $E_- = -i(QPQ + k^2P^{-1})$.

REFERENCES

- [1] Daubechies, I. *IEEE Trans. Information Theory*, **36**, 961- (1990).
- [2] Grossman, A. et al., in *Wavelets* (Combes, J.M. et al. eds.), Springer, 2- (1989).
- [3] Daubechies, I. *Ten Lectures on Wavelets*, SIAM (1992).
- [4] Meyer, Y., *Wavelets: Algorithms & Applications* (Ryan, R.D. tr.), SIAM.
- [5] Daubechies, I. & Paul, T., *Proc. 8th Int. Congr. Math. Phys., Marseilles*, 675- (1986).
- [6] Paul, T. & Seip, K., in *Wavelets and Its Applications* (Ruskai, M.B. et al eds.) Jones and Bartlett Pub., 303 (1992).
- [7] Falomir, H. et al., *J. Math. Phys.*, **35**, 1939- (1994).
- [8] Sakaguchi, F., *RIMS Kokyuroku, Kyoto University*, **885**, 8- (1994); *Proc. ICCS/ISITA'94, Sydney*, 303- (1994); *ibid.*, 309-; *Proc. IEEE-SP International Symposium on Time-Frequency and Time-Scale Analysis (TFTS'96), Paris*, 85- (1996).
- [9] Sakaguchi, F., *Proc. IEEE-SP International Symposium on Time-Frequency and Time-Scale Analysis (TFTS'98), Pittsburgh*, 133- (1998).
- [10] Sakaguchi, F. & Hayashi, M. E-print quant-ph/9905066 (1999)

On the eigenvector problem and the uncertainty relation with respect to the squeezing parameters of squeezed states

Fuminori SAKAGUCHI

Department of Electrical and Electronics Engineering, Fukui University, 910-8507, Japan
e-mail:saka@dignet.fuee.fukui-u.ac.jp

Masahito HAYASHI

Department of Mathematics, Kyoto University, 606-8502, Japan
e-mail:masahito@kusm.kyoto-u.ac.jp

Abstract

The over-complete eigenvector system of the operator $Q^{-1}P$ (Q :position, P :momentum) consists of the squeezed states $|0; \mu, \nu\rangle$ with various μ and ν . This eigenvalue problem is investigated from the viewpoint of the annihilation and creation relations and the generalized squeezed states related to the algebra $\text{su}(1,1)$.

It is known well that the squeezed state is the eigenvector $|\alpha; \mu, \nu\rangle$ of the operator $b_{\mu, \nu} := \mu a_b + \nu a_b^*$ ($|\mu|^2 - |\nu|^2 = 1$) (where $a_b := (1/2)^{1/2}(Q + iP)$, Q :position, P :momentum) associated with the eigenvalue α [1]. The eigenvalue α indicates the center of the localization of the wave packet in the phase plane, and the coefficients μ and ν do the squeezing properties. By multiplying $b_{\mu, \nu}|0; \mu, \nu\rangle = 0$ by Q^{-1} from the left, we have

$$Q^{-1}P|0; \mu, \nu\rangle = i\frac{\mu+\nu}{\mu-\nu}|0; \mu, \nu\rangle. \quad (1)$$

This relation is another kind of characteristic equation of the squeezed states, which is very convenient for investigating the uncertainty relation and the quantum estimation problem only with respect to the squeezing parameters, because the operator $Q^{-1}P$ itself does not but the eigenvalue does depend on μ and ν .

The operator $Q^{-1}P$ is not self-adjoint, and the self-adjoint part and the skew-adjoint part of $Q^{-1}P$ are $(Q^{-1}P + PQ^{-1})/2$ and $Q^{-2}/2$, respectively. Therefore $|0; \mu, \nu\rangle$ is a minimum-uncertainty state between these parts in the sense that it attains the lower bound given by the following inequality called the uncertainty relation¹[6];

$$(\Delta(Q^{-1}P + PQ^{-1}))^2 \cdot (\Delta(Q^{-2}))^2 \geq \frac{1}{4} \left| i\langle \psi | [Q^{-1}P + PQ^{-1}, Q^{-2}] | \psi \rangle \right|^2 \quad (2)$$

¹This uncertainty is concerning about the width of wave packet, not about the measurement error.

These eigenvector relations are closely related to the Lie algebra $\text{su}(1,1)$, because the three generators of the displacement of the squeezing parameters satisfy the commutation relations of this algebra. The above squeezed states $\{ |0; \mu, \nu\rangle \mid \mu, \nu: \text{complex}, |\mu|^2 - |\nu|^2 = 1 \}$ are generalized coherent states[2] associated with the Lie group generated by these generators. In this paper, by the Möbius transform of $Q^{-1}P$, we will derive the annihilation/creation relations and the number operators related to the algebra $\text{su}(1,1)$.

First, we will start with more general algebraic formalism. If the triplet of the skew-adjoint operators E_0, E_+ and E_- on a Hilbert space \mathcal{H} satisfies the commutation relations $[E_0, E_{\pm}] = \pm 2E_{\pm}$ and $[E_+, E_-] = E_0$, it is called the unitary representation of the Lie algebra $\text{su}(1,1)$. Define another triplet of the operators $L_0 := i(E_- - E_+)$ and $L_{\pm} := (E_0 \pm i(E_+ + E_-))/2$. ($E_0 = L_+ + L_-$ and $E_{\pm} = \pm(L_0 \mp L_{\pm})/2$). Then the same type of commutation relations $[L_0, L_{\pm}] = \pm 2L_{\pm}$, $[L_+, L_-] = L_0$ hold, and these are another basis of the same Lie algebra. However, in this basis system, L_0 is self-adjoint while L_{\pm} are neither self-adjoint nor skew-adjoint, and $(L_{\pm})^* = -L_{\mp}$. In this paper, we investigate only the cases where the representation is irreducible and is not trivial. Then the corresponding Casimir operator should be a scalar by the Schur's lemma,

$$C := L_0^2 + 2(L_+L_- + L_-L_+) = \beta \quad (= L_0^2 \pm 2L_0 + 4L_{\mp}L_{\pm} = E_0^2 \pm 2E_0 + 4E_{\mp}E_{\pm}). \quad (3)$$

where the scalar parameter β depends on the representation of the Lie algebra. If v is the eigenvector of L_0 associated with the eigenvalue value κ , then $L_0(L_{\pm}v) = L_{\pm}(L_0 \pm 2)v = (\kappa \pm 2)(L_{\pm}v)$, from the commutation relations. From this relation and the self-adjoint property of L_0 , the eigenvector system of L_0 is an orthogonal system, and the eigenvalues of L_0 are the real numbers spaced uniformly. The irreducibility and the unitarity imply that the dimension of the kernel of L_{\pm} should be not more than one and the dimension of the kernel either of L_- or of L_+ is zero. From now, we are investigating the case where $\dim \text{Ker } L_+ = 0$ and $\dim \text{Ker } L_- = 1$. Let v_0 be the unit vector in $\text{Ker } L_-$, from the above relation, v_0 should be the eigenvector of L_0 associated with the minimum eigenvalue λ (otherwise the existence of a smaller eigenvalue were contradictory to $L_-v_0 = 0$). Then the characteristic equation

$$L_0((L_+)^n v_0) = (\lambda + 2n)((L_+)^n v_0) \quad (4)$$

holds. It is known well that this constant λ determine the representation of the algebra $\text{su}(1,1)$ uniquely. In this case, the unitarity means that $\lambda > 0$ [5]. From the irreducibility and the self-adjointness of L_0 , the set $\{(L_+)^n v_0\}_{n=0}^{\infty}$ is a CONS of \mathcal{H} . From the relation(3) and $L_-v_0 = 0$ and $L_0v_0 = \lambda v_0$, we have $\beta = \lambda(\lambda - 2)$. Now, we define the $\text{su}(1,1)$ -number operator N and $\text{su}(1,1)$ -number states vector $|n\rangle_N$

$$N := \frac{1}{2}(L_0 - \lambda), \quad |n\rangle_N := \sqrt{\frac{\Gamma(\lambda)}{n! \Gamma(\lambda+n)}} L_+^n v_0. \quad (5)$$

Then, the equation (4) and the definition (5) imply that $N|n\rangle_N = n|n\rangle_N$. The relations (3) and $L_+^* = -L_-$ show that the vector $|n\rangle_N$ defined in (5) is an unit vector [8].

Next we will define the $\text{su}(1,1)$ -annihilation operator a . The relation (4) implies that $(L_0 - \lambda)|n\rangle_N$ belongs to the range of L_+ for any n . Because $\dim \text{Ker}(L_+) = 0$, we can define the annihilation operator a as the bounded operator

$$a|n\rangle_N := \frac{1}{2}L_+^{-1}(L_0 - \lambda)|n\rangle_N = \sqrt{\frac{n}{n+\lambda-1}} |n-1\rangle_N, \quad (6)$$

(where we mean $a|0\rangle_N = 0$ by the second equality of (6) in the case of $\lambda = 1$ and $n = 0$.) The second equality of (6) is derived from (4) and (5). From the relations (5) and (6), we have $[a, N] = a$. Thus the creation operator can be defined as the adjoint operator a^* , and

$$a^*|n\rangle_N = \sqrt{\frac{n+1}{n+\lambda}} |n+1\rangle_N. \quad (7)$$

Therefore, from the completeness and orthogonality of the eigenvectors of L_0 , we have

$$a^*a = (N + \lambda - 1)^{-1}N, \quad aa^* = (N + \lambda)^{-1}(N + 1) \quad (8)$$

in the case of $\lambda \neq 1$. By eliminating N from these, we have the re-ordering relation between the annihilation operator a and the creation operator a^*

$$aa^* = -(a^*a + \lambda - 2)^{-1}(\lambda a^*a - 1), \quad a^*a = (aa^* - \lambda)^{-1}((2 - \lambda)aa^* - 1) \quad (9)$$

in the case of $\lambda \neq 1$. In the case of $\lambda = 1$, we have $aa^* = 1$, $a^*a = 1 - |0\rangle_N \langle 0|$. These relations are important for the calculating the quantum characteristic function.

With the unitary displacement operator $D(\xi) := \exp(\xi L_+ - \bar{\xi} L_+^*)$, define the $\text{su}(1,1)$ -coherent state

$$v(\zeta) := D\left(\frac{1}{2}e^{i\arg\zeta} \ln \frac{1+|\zeta|}{1-|\zeta|}\right) |0\rangle_N = \exp(\zeta L_+) \exp\left(\frac{1}{2} \ln(1 - |\zeta|^2) L_0\right) \exp(\bar{\zeta} L_-) |0\rangle_N \quad (10)$$

(for $|\zeta| < 1$). The latter ‘‘normal-order’’ form of the right hand side is obtained from the relations given in pp.73-74 of [2]. Because $\exp\left(\frac{1}{2} \ln(1 - |\zeta|^2) L_0\right) \exp(\bar{\zeta} L_-) |0\rangle_N = (1 - |\zeta|^2)^{\lambda/2} |0\rangle_N$ and $[a, \exp(\zeta L_+)] = \zeta \exp(\zeta L_+)$ [8], we have

$$av(\zeta) = \exp(\zeta L_+) a |0\rangle_N + \zeta \exp(\zeta L_+) |0\rangle_N = \zeta v(\zeta). \quad (11)$$

These relations show that the vector $v(\zeta)$ is the eigenvector of a associated with the eigenvalue ζ . Thus we can denote $v(\zeta)$ by $|\zeta\rangle_a$, and the set of eigenvalues of a is the unit disk.

From the relations (3),(6) and the relation $[L_0, L_+^{-1}] = L_+^{-1}[L_+, L_0]L_+^{-1} = -2L_+^{-1}$, we can show the relation $(E_0 - \lambda)(a - 1) = -2iE_+(a + 1)$ [8]. If the dimension of the kernel of E_+ is not 0, then this representation becomes trivial by the relation (3) and the unitarity. Since we can show that $(E_0 - \lambda)|n\rangle_N$ belongs to the range of E_+ [8], we can define the operator

$$A := \frac{1}{2}E_+^{-1}(E_0 - \lambda) = -i(a + 1)(a - 1)^{-1}, \quad (12)$$

whose domain is dense in \mathcal{H} . Hence $A|\zeta\rangle_a = -i\frac{\zeta+1}{\zeta-1}|\zeta\rangle_a$, which shows that the vector $|\zeta\rangle_a$ can be denoted by $\left|-i\frac{\zeta+1}{\zeta-1}\right\rangle_A$. Since $-i$ doesn't belong to the spectrum of A , the latter relation in (12) indicates that

$$a = (A + i)^{-1}(A - i). \quad (13)$$

Since a is given by the Möbius transform of A , the set of eigenvalues of A is the upper half plane, and they are mapped to the unit disk by the Möbius transform.

Next, we will interpret the eigenfunction problem (1) from the algebraic structure discussed above. For this, we have only to choose the representation

$$E_0 = i(PQ + QP)/2, \quad E_+ = iQ^2/2, \quad E_- = -iP^2/2. \quad (14)$$

Then we have $L_0 = n_b + \frac{1}{2}$, $L_+ = -(1/2)a_b^{*2}$, $L_- = (1/2)a_b^2$, where $n_b := 1/2(Q^2 + P^2 - 1) = a_b a_b^*$. The Casimir operator is $\beta = C = -(PQ + QP)^2/4 + (Q^2P^2 + P^2Q^2)/2 = -\frac{3}{4}$. From $\beta = \lambda(\lambda + 2)$, λ should be $1/2$ or $3/2$. These two solutions are corresponding to the two function spaces of the representation. When we choose the function space with even parity $L_{\text{even}}^2 := \{f(q) \in L^2(R) | f(-q) = f(q)\}$, then $\lambda = 1/2$. From (5),(6) and (12),

$$A = Q^{-1}P, \quad a = a_b^{*-1}a_b, \quad N = \frac{1}{4}(Q^2 + P^2 - 1) = \frac{1}{2}n_b. \quad (15)$$

Then, from (13) and (15), the characteristic equation (1) for the squeezed states $|0; \mu, \nu\rangle$ can be regarded as the characteristic equation of the $\text{su}(1,1)$ -annihilation operator, and we have $|0; \mu, \nu\rangle = \left| \frac{\nu}{\mu} \right\rangle_a = \left| i \frac{\mu + \nu}{\mu - \nu} \right\rangle_A$. Moreover, $|n\rangle_N = (-1)^n |2n\rangle_{n_b}$, where $|n\rangle_{n_b}$ denotes the boson number state. From (6) and (7), we have the annihilation and creation relations

$$a|n\rangle_N = \sqrt{\frac{2n}{2n-1}} |n-1\rangle_N, \quad a^*|n\rangle_N = \sqrt{\frac{2n+2}{2n+1}} |n+1\rangle_N, \quad (16)$$

and the non-linear re-ordering relations

$$aa^* = -(2a^*a - 3)^{-1}(a^*a - 2), \quad a^*a = (2aa^* - 1)^{-1}(3aa^* - 2). \quad (17)$$

On the other hand, when we choose the function space with odd parity, then $\lambda = 3/2$. In this case, $A = PQ^{-1}$, $a = a_b a_b^{*-1}$, $N = \frac{1}{2}(n_b - 1)$, and the $\text{su}(1,1)$ -coherent states are obtained by squeezing the boson number states with $n = 1$ [8].

Another example is the annihilation/creation relation related to the Cauchy wavelets[3,4], with $E_0 = -i(PQ + QP)$, $E_+ = iP$, $E_- = -i(QPQ + k^2P^{-1})$ ($k > -1/2$) [8].

References

- [1] H.P.Yuen, Phys. Rev. **A13**, 2226 (1976).
- [2] A.Perelomov, 'Generalized Coherent States and Their Applications', Springer (1986).
- [3] I.Daubechies & T.Paul, Proc. 8th. Int. Congr. Math. Phys., Marseilles, 675 (1986).
- [4] F.Sakaguchi, Proc. IEEE-SP Int. Symp. Time-Frequency & Time-Scale Anal., Pittsburgh, 133 (1998).
- [5] R.Howe & E.C.Tan, 'Non-Abelian Harmonic Analysis', Springer.
- [6] A.S.Holevo, 'Probabilistic and Statistical aspects of Quantum Theory', North-Holland (1982).
- [7] M.Hayashi, 'On simultaneous measurement for non-commutative observables' to appear in RIMS Koukyuroku, Kyoto University (In Japanese).
- [8] F.Sakaguchi & M.Hayashi, E-print, quant-ph/9905066.

Embedding Classical Models in Quantum Mechanics

S. D. Bartlett and D. J. Rowe

Department of Physics, University of Toronto, Toronto, Ontario, Canada M5S 1A7
bartlett@physics.utoronto.ca

Abstract

For models with an algebraic structure, the classical dynamics is embedded in the quantum model as a constrained subsystem. This result is applied to the theory of quantization, and gives insight into what are the closest-to-classical quantum states. Applications involving harmonic oscillator coherent states and squeezed states are discussed.

If one holds the philosophy that quantum mechanics is fundamental, a classical model must somehow be embedded in its quantal counterpart. The process of obtaining a classical model from a quantum one is referred to as **dequantization**. It was Dirac [1] who noted that classical mechanics provides a framework through which quantum mechanics can be interpreted.

The coherent states of the harmonic oscillator exemplify how dequantization is envisioned: the coherent states are minimum uncertainty states, and the expectation values of the observables in these states evolve according to classical equations of motion. The coherent state construction has been generalized to an arbitrary Lie group by Perelomov [2], Gilmore [3] and Onofri [4], who also showed that some coherent state manifolds have properties of classical phase spaces. These methods were combined with Dirac's theory of constrained quantum mechanics [5] by Rowe, Ryman and Rosensteel [6] to show that, under specified conditions, constrained quantum systems exhibit classical behavior. However, it is known that there are situations when these methods do not work. Thus, despite the many significant contributions, the theory of dequantization remains incomplete.

In this paper, it is shown how a classical model may be embedded in a quantal one as a constrained subsystem. The examples used to illustrate these concepts include motion of a particle in a Euclidean space (with the Heisenberg-Weyl algebra as the relevant algebra) and breathing-mode vibrations or squeezed states (using an $sp(2)$ algebra). Although these models possess the same Hilbert space of square-integrable functions on the real line, they each describe different dynamics and lead to distinctly different results when viewed as a classical model. As a result, the concept of "closest-to-classical state" does not necessarily satisfy the same criteria for both systems, and one is led to the question of what quantum state (or mixture of quantum states) is appropriate. Further details will be given in a paper to follow.

I. EXAMPLE: A CANONICAL SYSTEM

Consider the standard quantum mechanics for a particle moving in one dimension on the real line \mathbb{R} . The Hilbert space is $\mathbb{H} = \mathcal{L}^2(\mathbb{R}; dx)$. This Hilbert space is the carrier space for a unitary irrep of the Heisenberg-Weyl group $HW(1)$, for which the infinitesimal generators are the linear operators $\{\hat{x}, \hat{p}, \hat{I}\}$, where

$$[\hat{x}\psi](x) = x\psi(x), \quad [\hat{p}\psi](x) = -i\hbar\frac{\partial}{\partial x}\psi(x), \quad [\hat{I}\psi](x) = \psi(x). \quad (1)$$

The Hamiltonian is the linear operator

$$\hat{H} = \frac{\hat{p}^2}{2m} + \hat{V}, \quad (2)$$

where \hat{V} is a function of \hat{x} (and possibly \hat{p}). The full quantal algebra of observables consists of Hermitian operators on \mathbb{H} , with commutator as Lie bracket.

Let $|\phi\rangle$ denote some chosen state vector with wavefunction $\phi \in \mathbb{H}$. The coherent state manifold \mathcal{M} in the projective Hilbert space $\mathbb{P}\mathbb{H}$ (where states equivalent to within a phase are identified) is defined to be

$$\mathcal{M} = \left\{ |x, p\rangle = \exp\left(\frac{i}{\hbar}(p\hat{x} - x\hat{p})\right)|\phi\rangle \right\}. \quad (3)$$

This expression endows \mathcal{M} with coordinates (x, p) . A general state $|\phi\rangle$ is an eigenstate only of the operator $\hat{I} \in \mathfrak{hw}(1)$, and thus \hat{I} does not appear in this expression. The generic orbit \mathcal{M} is 2-dimensional with the geometry of \mathbb{R}^2 , and is symplectic. It seems reasonable, then, to associate a coherent state $|x, p\rangle \in \mathcal{M}$ with the classical state (x, p) .

The coherent state manifold \mathcal{M} is embedded in the projective Hilbert space $\mathbb{P}\mathbb{H}$, and has the properties of a classical phase space. However, under quantum evolution (following the Schrödinger equation), a coherent state will remain a coherent state only for exceptional Hamiltonians (such as the harmonic oscillator Hamiltonian). By constraining the dynamics [5,6] to \mathcal{M} , classical mechanics is assured. For functions on \mathcal{M} of the form

$$F(x, p) = \langle x, p | \hat{F} | x, p \rangle, \quad (4)$$

constraining the dynamics to \mathcal{M} defines a Poisson bracket on \mathcal{M} to be

$$\{F, G\}(x, p) = \left(\frac{\partial F}{\partial x} \frac{\partial G}{\partial p} - \frac{\partial F}{\partial p} \frac{\partial G}{\partial x} \right). \quad (5)$$

The resulting dynamics is given by the classical equations of motion

$$\frac{d}{dt}F = \{F, H\}, \quad (6)$$

where H is the function on \mathcal{M} given by the expectation value of the quantum Hamiltonian

$$H(x, p) = \langle x, p | \hat{H} | x, p \rangle. \quad (7)$$

Thus, the quantum mechanics of this system constrained to any orbit of the Heisenberg-Weyl group leads to classical dynamics.

II. EXAMPLE: “SQUEEZED” STATES

The Hilbert space $\mathbb{H} = \mathcal{L}^2(\mathbb{R}; dx)$ given above is also the carrier space for an unitary representation of the Lie group $Sp(2, \mathbb{R})$. The Lie algebra $sp(2)$ is spanned by the linear operators $\{\hat{A}, \hat{B}, \hat{C}\}$ which act on wavefunctions $\psi \in \mathbb{H}$ as

$$[\hat{A}\psi](x) = \left[\frac{1}{4}(\hat{x}^2 + \hat{p}^2)\psi\right](x), \quad [\hat{B}\psi](x) = \left[\frac{1}{4}(\hat{x}^2 - \hat{p}^2)\psi\right](x), \quad [\hat{C}\psi](x) = \left[\frac{1}{4}(\hat{x}\hat{p} + \hat{p}\hat{x})\psi\right](x). \quad (8)$$

It is straightforward to check that these operators satisfy the commutation relations for an $sp(2)$ algebra; they are

$$[\hat{A}, \hat{B}] = -i\hbar\hat{C}, \quad [\hat{A}, \hat{C}] = i\hbar\hat{B}, \quad [\hat{B}, \hat{C}] = i\hbar\hat{A}. \quad (9)$$

It should be noted that, unlike the operators \hat{x} and \hat{p} of the Heisenberg-Weyl algebra, the expectation values of these operators give information on the width and spreading of a quantum wavefunction. By choosing this algebra for dequantization, the classical observables will be different than those of the canonical system.

As with the Heisenberg-Weyl group of the previous example, a coherent state manifold can be constructed using the representation of the group $Sp(2, \mathbb{R})$. Choose a state vector $|\phi\rangle$ in the Hilbert space, and define the (generalized) coherent state manifold \mathcal{M}' in the projective Hilbert space $\mathbb{P}\mathbb{H}$ to be

$$\mathcal{M}' = \{ |a, b, c\rangle = \exp\left(\frac{i}{\hbar}(a\hat{A} + b\hat{B} + c\hat{C})\right)|\phi\rangle \}. \quad (10)$$

The parameters $\{a, b, c\}$ serve as coordinates on \mathcal{M}' .

For a general state $|\phi\rangle$, the coherent state manifold \mathcal{M}' will be three-dimensional and thus cannot be a classical phase space. However, for judicious choice of $|\phi\rangle$, one of these dimensions can be made small or even degenerate. For example, if $|\phi\rangle = |0\rangle$, the ground state of the harmonic oscillator, one has the identity

$$\hat{A}|0\rangle = |0\rangle. \quad (11)$$

Thus, the coordinate a is only a phase term; the manifold $\mathcal{M}' \subset \mathbb{P}\mathbb{H}$ corresponding to $|0\rangle$ is a two dimensional manifold, and is in fact a phase space. The coordinates b and c become canonical coordinates (as seen by the expectation value $\langle 0|[\hat{B}, \hat{C}]|0\rangle$), and a Poisson bracket for functions on \mathcal{M}' can be found to be

$$\{F, G\}(b, c) = 4 \left(\frac{\partial F}{\partial b} \frac{\partial G}{\partial c} - \frac{\partial F}{\partial c} \frac{\partial G}{\partial b} \right). \quad (12)$$

This Poisson bracket is proportional to that of eqn. (5), with coordinates (b, c) replacing (x, p) .

However, the resulting classical model is not equivalent to that of the previous example. Instead, it is the classical model of a “breathing mode;” the coordinates (observables) on the phase space describe the width and spreading (the momentum associated to the width) of a classical object (a compressible fluid, for example).

III. CONCLUSIONS

It has been shown, for the simplest example, that classical phase spaces are embedded in a quantum model. This result is general. One can use the methods of Perelomov [2] to create coherent state manifolds in a quantum Hilbert space which have the properties of a classical phase space. The full quantum (Schrödinger) evolution will in general cause the system to leave the classical manifold; a coherent state will remain a coherent state only for exceptional Hamiltonians. However, by constraining quantum dynamics to this coherent state manifold, the resulting dynamics is classical.

The coherent state manifold, and thus the resulting classical phase space, depends critically on the algebra of observables chosen to generate the manifold. This choice of observables will serve as coordinates for the classical phase space, and all other observables can be expressed as functions of these basic ones. As illustrated in these examples, the simplest quantum model with Hilbert space $\mathbb{H} = \mathcal{L}^2(\mathbb{R}; dx)$ can yield a classical model for a point particle moving in one dimension, or a classical “breathing mode” system where the basic observables are the width and its spreading. Note also that the classical manifold for each example depends on the choice of base vector $|\phi\rangle$, and that different choices lead to different results. The result is that the map from quantum mechanics to classical mechanics is not one-to-one; many classical models can arise from a single quantal one.

Dequantization can be used to address the inverse process of quantization: how does one construct a quantum model from a given classical one? The results given here imply that a quantum model must carry a unitary representation of the algebra of “basic” observables. These concepts can be defined rigorously using *spectrum generating algebras* (see [7]).

Finally, these results provide insight into the concept of “minimum uncertainty ” or “closest to classical” states. It is not a requirement of the dequantization process that the coherent states satisfy any sort of minimum uncertainty relation; in fact, such a relation would depend on what the chosen basic observables are.

IV. REFERENCES

1. P. A. M. DIRAC, “The Principles of Quantum Mechanics,” Oxford University Press, 1958.
2. A. PERELOMOV, “Generalized Coherent States and their Applications,” Springer, Berlin, 1986.
3. R. GILMORE, *Ann. Phys. (N.Y.)* **74** (1972), 391.
4. E. ONOFRI, *J. Math. Phys.* **16** (1975), 1087.
5. P. A. M. DIRAC, “Lectures on Quantum Mechanics,” Belfer Graduate School of Science Monograph Series 2, 1964.
6. D.J. ROWE, A. RYMAN, AND G. ROSENSTEEL, *Phys. Rev.* **A22** (1980), 2362.
7. D.J. ROWE, *Prog. Part. Nucl. Phys.* **37** (1996), 265.

Bäcklund-type superposition and free particle n -susy partners

O. Rosas-Ortiz^{1,2}, B. Mielnik^{1,3}, and L.M. Nieto²

¹*Departamento de Física, CINVESTAV-IPN, AP 14-740, México 07000, DF, Mexico*

²*Departamento de Física Teórica, Universidad de Valladolid, 47011 Valladolid, Spain*

³*Institute of Theoretical Physics, Warsaw University, Hoza 69 Warsaw, Poland*

Abstract

The higher order susy partners of Schrödinger Hamiltonians can be explicitly constructed by iterating a nonlinear difference algorithm coinciding with the Bäcklund superposition principle used in soliton theory. As an example, it is applied in the construction of new higher order susy partners of the free particle potential, which can be used as a handy tool in soliton theory.

Recent studies confirm that the higher order supersymmetric (susy) partners of Schrödinger Hamiltonians are most easily constructed by a simple algebraic tool named intertwining technique [1]. One of the keys of this method is an algebraic nonlinear expression which links solutions of different Riccati equations (see, e.g. [2–4]). In a previous paper [3], we have studied the application of this method to the free particle potential. The ‘building blocks’ of some of the resulting potentials are the well known soliton solutions of the Korteweg-de Vries (KdV) equation: $\kappa^2 \text{sech}^2[\kappa(x-a)]$ and $\kappa^2 \text{csch}^2[\kappa(x-a)]$. In this work we shall sketch the main steps of the approach in order to present some of the potentials derived in [3].

First, consider the intertwining relationship $H_1 A_1 = A_1 H_0$, where the intertwiner A_1 is the first order differential operator $A_1 = \frac{d}{dx} + \beta_1(x, \epsilon)$. All the available information concerning the Hamiltonians $H_0 = -\frac{1}{2} \frac{d^2}{dx^2} + V_0(x)$ and $H_1 = -\frac{1}{2} \frac{d^2}{dx^2} + V_1(x, \epsilon)$ is encoded in the beta function, which satisfies the Riccati equation

$$-\beta_1'(x, \epsilon) + \beta_1^2(x, \epsilon) = 2[V_0(x) - \epsilon]. \quad (1)$$

The arbitrary integration constant ϵ plays the role of a *factorization energy*. It is very simple to check that the potentials are related by the first order susy relationship

$$V_1(x, \epsilon) = V_0(x) + \beta_1'(x, \epsilon). \quad (2)$$

Equations (1) and (2) are necessary and sufficient conditions for the Hamiltonians to be factorized as $H_0 - \epsilon = (1/2) A_1^\dagger A_1$, and $H_1 - \epsilon = (1/2) A_1 A_1^\dagger$. Suppose now that $V_0(x)$ is a known solvable potential with eigenvalues E_n and eigenfunctions ψ_n , $n = 0, 1, 2, \dots$. Let us assume that we have found a general solution of (1) for a given factorization energy $\epsilon_1 \neq E_n, \forall n$. Then, the potential $V_1(x, \epsilon_1)$ is also given [1–3]. The iteration of this procedure

starts by considering now $V_1(x, \epsilon_1)$ as the known solvable potential and looking for a new one $V_2(x, \epsilon_1, \epsilon)$ satisfying the second order susy relationship

$$V_2(x, \epsilon_1, \epsilon) = V_1(x, \epsilon_1) + \beta_2'(x, \epsilon_1, \epsilon). \quad (3)$$

Therefore, the new beta function must fulfill the Riccati equation

$$-\beta_2'(x, \epsilon_1, \epsilon) + \beta_2^2(x, \epsilon_1, \epsilon) = 2[V_1(x, \epsilon_1) - \epsilon], \quad (4)$$

where ϵ is again an arbitrary factorization energy. The corresponding solution is given by

$$\beta_2(x, \epsilon_1, \epsilon) = -\beta_1(x, \epsilon_1) - \frac{2(\epsilon_1 - \epsilon)}{\beta_1(x, \epsilon_1) - \beta_1(x, \epsilon)}. \quad (5)$$

The finite difference expression (5) is a nonlinear superposition of two general solutions of (1), one for each factorization energy ϵ_1 and ϵ , transforming equation (1) into (4) by the change of $V_0(x)$ by $V_1(x, \epsilon_1)$, and $\beta_1(x, \epsilon)$ by $\beta_2(x, \epsilon_1, \epsilon)$. This transformation can be used to link the higher order susy partners of $V_0(x)$ with the first order superpotentials $\beta_1(x, \epsilon)$, just by solving (1) for different values of the factorization energy ϵ . For instance, providing n different general solutions of (1), one for each ϵ_k , $k = 1, 2, \dots, n$, we are able to iterate $n - 1$ times the algorithm (5) acquiring a new beta function in each step, given by

$$\beta_k(x, \epsilon_k) = -\beta_{k-1}(x, \epsilon_{k-1}) - \frac{2(\epsilon_{k-1} - \epsilon_k)}{\beta_{k-1}(x, \epsilon_{k-1}) - \beta_{k-1}(x, \epsilon_k)}, \quad k = 2, 3, \dots, n. \quad (6)$$

We have adopted here an abbreviated notation making explicit only the dependence of β_k on the factorization constant introduced in the very last step, keeping implicit the dependence on the previous factorization constants (henceforth, the same criterion will be used for any other symbol depending on k factorization energies). Therefore, given any initial potential V_0 , the corresponding n -susy partner potential V_n can be written as

$$V_n(x, \epsilon_n) = V_0(x) + \sum_{k=1}^n \beta_k'(x, \epsilon_k), \quad (7)$$

provided that the master equations for β_k and V_k are given by

$$-\beta_k'(x, \epsilon_k) + \beta_k^2(x, \epsilon_k) = 2[V_{k-1}(x, \epsilon_{k-1}) - \epsilon_k], \quad k = 1, 2, \dots, n, \quad (8)$$

$$V_k(x, \epsilon_k) = V_{k-1}(x, \epsilon_{k-1}) + \beta_k'(x, \epsilon_k), \quad k = 1, 2, \dots, n. \quad (9)$$

Now, let us stress that every general solution of the Riccati equation (1), for a given ϵ , depends on an additional implicit integration parameter α , hence, the process acumulates as many of these integration parameters as many general solutions of (1) have been used.

Observe the coincidence of our nonlinear algorithm (6) and the Wahlquist and Estabrook superposition principle expression (see equation (16) of [5]), derived from the Bäcklund transformation (BT) of the KdV equation $w_t = 6w_x^2 - w_{xxx}$; subscripts t and x denote partial derivatives. The method has been typically used to generate new, multisoliton solutions $w_{12}, \dots, w_{(n)}$ of the KdV equation from a given one-soliton solution $w \equiv w_1$ of the same

equation. It is thus quite interesting that the validity of the same algorithm in the intertwining problem (supersymmetry) is much easier to demonstrate without worrying at all about the nonlinear equations! Moreover, its physical applicability in susy seems much wider. Thus, e.g., the singular solutions of KdV (singular water waves) would be of marginal physical interest. The singular potentials in the Schrödinger equation are not! Therefore, the possibility of reducing the n -th intertwining iteration to the multiple applications of the Bäcklund superposition principle means that n -susy could be a universal method generating the “multisoliton deformations” of any initial potential.

We shall now focus on the vacuum case, presenting some simplifications which the method offers in deriving the n -susy partners for the potential $V_0(x) = 0$. In this case, the Riccati equation (1) has the general solution

$$\beta_1(x, \epsilon) = -\sqrt{2\epsilon} \cot[\sqrt{2\epsilon}(x - \alpha)], \quad (10)$$

where α is an integration constant (in general complex). It is well known that the superpotential (10) gives four different first order susy partners of $V_0(x) = 0$ by taking different values of ϵ and α . This information is summarized in Table I.

TABLE I. The four different real superpotentials β_1 coming out from (10), depending on the values of ϵ and the integration parameter α . In each case S means singular, R regular, P periodic, and N null. The parameters a and b are arbitrary real numbers.

Case	ϵ	$\sqrt{2\epsilon}$	α	$\beta_1(x, \epsilon)$
S	$\epsilon < 0$	$i\sqrt{2 \epsilon } = i\kappa$	a	$-\kappa \coth[\kappa(x - a)]$
R	$\epsilon < 0$	$i\sqrt{2 \epsilon } = i\kappa$	$-b - \frac{i\pi}{2\kappa}$	$-\kappa \tanh[\kappa(x + b)]$
P	$\epsilon > 0$	$\sqrt{2\epsilon} = k$	a	$-k \cot[k(x - a)]$
N	0	0	a	$-\frac{1}{x - a}$

As an example, notice that the regular case (R) leads to the well known modified Pöschl-Teller type susy partner $V_1^R(x, \epsilon) = -\kappa^2 \text{sech}^2[\kappa(x + b)]$, while the null case (N) leads to the potential barrier $V_1^N(x, 0) = (x - a)^{-2}$. Now, in order to give an example of second order susy partner potentials $V_2(x, \epsilon)$, let us consider the superpotentials R and S as given in Table I. By introducing them in (5) and (3) we get

$$V_2(x, \epsilon_2) = -(\kappa_1^2 - \kappa_2^2) \frac{\kappa_1^2 \text{csch}^2[\kappa_1(x + b)] + \kappa_2^2 \text{sech}^2[\kappa_2(x - a)]}{(-\kappa_1 \coth[\kappa_1(x + b)] + \kappa_2 \tanh[\kappa_2(x - a)])^2}. \quad (11)$$

The potential (11) has two finite wells which can be modulated by changing the values of κ_1 and κ_2 under the condition $\kappa_2 < \kappa_1$. A Taylor expansion of (11) shows a singularity at $x = a$ when $\kappa_2 > \kappa_1$. The case $\kappa_2 = \kappa_1$ gives a potential $V_2(x, \epsilon_1) = 0$.

Let us remark that, for the periodic superpotentials β_1 in Table I, equation (7) leads to a natural classification of two kinds of potentials depending on the parity of n . For n even, the periodic superpotential β_1 does not appear as a separate term in (7), affecting only one of denominators. The resulting susy partners have only a finite quantity of singularities. This fact has been used by Stalhofen [8] by constructing potentials with bound states embedded in the continuum. On the other hand, for n odd, the function β_1 is a separate term in the sum (7) and its global effect is not canceled by any similar term. The corresponding susy partners become singular periodic potentials.

In conclusion, the nonlinear difference algorithm (6) allows the construction of higher order susy partners of any initial potential $V_0(x)$, provided that a certain number of solutions of (1) have been given. This finite difference algorithm generalizes the superposition principle reported in [5] extending its applications to the susy construction of new solvable potentials. In particular, the higher order susy partners $V_n(x, \epsilon_n)$ of the free particle potential represent a wide set of transparent wells in the terms discussed in [7–9], as well as multisoliton solutions of the KdV equation as given in [5].

This work was performed under the auspices of CONACyT (Mexico) and DGES project PB94-1115 from Ministerio de Educación y Cultura (Spain), as well as by Junta de Castilla y León (CO2/197). BM and ORO acknowledge the kind hospitality at Departamento de Física Teórica, Universidad de Valladolid (Spain). ORO wishes to acknowledge partial financial support from the ICSSUR'99 Organizing Committee.

References

- [1] D.J. Fernández C, *Int. J. Mod. Phys. A* **12**, 171 (1997);
D.J. Fernández C., M.L. Glasser and L.M. Nieto, *Phys. Lett. A* **240**, 15 (1998)
- [2] D.J. Fernández C., V. Hussin and B. Mielnik, *Phys. Lett. A* **244**, 1 (1998);
J.O. Rosas-Ortiz, *J. Phys. A* **31**, L507 (1998); *J. Phys. A* **31**, 10163 (1998);
D.J. Fernández C. and V. Hussin, *J. Phys. A* **32**, 3603 (1999)
- [3] B. Mielnik, L.M. Nieto and O. Rosas-Ortiz, *The finite difference algorithm for higher order supersymmetry*, Universidad de Valladolid *Preprint*, Spain (1998)
- [4] V. E. Adler, *Physica D* **73**, 335 (1994)
- [5] H. D. Wahlquist and F. B. Estabrook, *Phys. Rev. Lett.* **31**, 1386 (1973)
- [6] C. S. Gardner, J. M. Greene, M. D. Kruskal and R. Miura, *Phys. Rev. Lett.* **19**, 1095 (1967)
- [7] V.B. Matveev and M.A. Salle, *Darboux Transformations and Solitons*, Springer-Verlag, Berlin (1991)
- [8] A. Stalhofen, *Phys. Rev. A* **51**, 934 (1995)
- [9] B.N. Zakhariev and V. M. Chabanov, *Inverse Problems* **13**, R47 (1997)

m-SUSY Coherent States

David J. Fernández C.

Depto. de Física, CINVESTAV, A.P. 14-740, 07000 México D.F., MEXICO

Véronique Hussin

*Département de Mathématiques et Centre de Recherches Mathématiques, Université de Montréal
C.P. 6128, Succ. Centre-Ville, Montréal (Québec), H3C 3J7 CANADA*

Abstract

Anharmonic oscillator potentials derived from the standard harmonic oscillator by means of iterations of the first order intertwining transformation possess a *natural* pair of ladder operators obeying polynomial non-linear algebras. Those operators can be partially linearized, and the coherent states construction can be performed in the non-linear and linearized cases.

1. In supersymmetric quantum mechanics (SUSY QM) a realization of the SUSY algebra with two generators Q_1, Q_2 [1-3]

$$[Q_i, H_{ss}] = 0, \quad \{Q_i, Q_j\} = \delta_{ij} H_{ss}, \quad i, j = 1, 2, \quad (1)$$

is constructed from supercharges $Q_1 = (Q^\dagger + Q)/\sqrt{2}$, $Q_2 = (Q^\dagger - Q)/i\sqrt{2}$, where:

$$Q = \begin{pmatrix} 0 & 0 \\ B & 0 \end{pmatrix}, \quad Q^\dagger = \begin{pmatrix} 0 & B^\dagger \\ 0 & 0 \end{pmatrix}, \quad H_{ss} = \{Q, Q^\dagger\} = \begin{pmatrix} B^\dagger B & 0 \\ 0 & BB^\dagger \end{pmatrix} = \begin{pmatrix} H^+ & 0 \\ 0 & H^- \end{pmatrix}. \quad (2)$$

If B and B^\dagger are first-order differential operators

$$B \equiv A_1 = \frac{1}{\sqrt{2}} \left[\frac{d}{dx} + \alpha_1(x, \epsilon) \right], \quad B^\dagger \equiv A_1^\dagger = \frac{1}{\sqrt{2}} \left[-\frac{d}{dx} + \alpha_1(x, \epsilon) \right], \quad (3)$$

H_{ss} becomes linear in $H^p = \begin{pmatrix} \tilde{H} & 0 \\ 0 & H \end{pmatrix}$:

$$H_{ss} = H^p - \epsilon, \quad (4)$$

where H and \tilde{H} are intertwined to each other by B and B^\dagger [3-4]:

$$\tilde{H}B^\dagger = B^\dagger H, \quad H = -\frac{1}{2} \frac{d^2}{dx^2} + V(x), \quad \tilde{H} = -\frac{1}{2} \frac{d^2}{dx^2} + \tilde{V}(x). \quad (5)$$

There is a natural relationship between V , \tilde{V} and α_1 :

$$\alpha_1'(x, \epsilon) + \alpha_1^2(x, \epsilon) = 2[V(x) - \epsilon], \quad \tilde{V}(x) = V(x) - \alpha_1'(x, \epsilon). \quad (6)$$

The value of the *factorization energy* ϵ is crucial for the behaviour of $\tilde{V}(x)$. For the harmonic oscillator potential $V(x) = x^2/2$, in order to avoid singularities of $\tilde{V}(x)$ at some $x \in (-\infty, \infty)$ we must have $\epsilon < 1/2$, where $1/2$ is the oscillator ground state energy [4].

2. Now, if instead of the first-order operators A_1 and A_1^\dagger of (3) one substitutes B and B^\dagger by the m th-order operators B_m and B_m^\dagger resulting of m iterations of the first-order transformation (3,5-6), one is led to the m -SUSY QM in which H_{ss} is a m th order polynomial of H^p [5-9]:

$$H_{ss} = (H^p - \epsilon_1) \dots (H^p - \epsilon_m), \quad (7)$$

where the $\epsilon_i, i = 1, \dots, m$ are ordered as $\epsilon_{i+1} < \epsilon_i < 1/2$. The final potential $\tilde{V}(x)$ is of kind:

$$\tilde{V}(x) = \frac{x^2}{2} - \sum_{i=1}^m \alpha'_i(x, \epsilon_i). \quad (8)$$

The $(i+1)$ th superpotential $\alpha_{i+1}(x, \epsilon_{i+1})$ depends of the previous one at ϵ_{i+1} and ϵ_i :

$$\alpha_{i+1}(x, \epsilon_{i+1}) = -\alpha_i(x, \epsilon_i) - 2 \frac{(\epsilon_i - \epsilon_{i+1})}{\alpha_i(x, \epsilon_i) - \alpha_i(x, \epsilon_{i+1})}, \quad i = 1, \dots, m-1. \quad (9)$$

Thus, the main role is played by m solutions $\alpha_i(x, \epsilon_i), i = 1, \dots, m$ (preferably general) to the initial Riccati equation (6). It turns out that for the harmonic oscillator it can be gotten the general solution for an arbitrary ϵ [10-11]:

$$\alpha_1(x, \epsilon) = -x + \frac{d}{dx} \left\{ \ln \left[{}_1F_1 \left(\frac{1-2\epsilon}{4}, \frac{1}{2}; x^2 \right) + 2\nu \frac{\Gamma(\frac{3-2\epsilon}{4})}{\Gamma(\frac{1-2\epsilon}{4})} x {}_1F_1 \left(\frac{3-2\epsilon}{4}, \frac{3}{2}; x^2 \right) \right] \right\}. \quad (10)$$

The spectrum of $\tilde{V}(x)$ is composed by one infinite ladder of equally spaced energies starting from $1/2$ plus m additional levels at arbitrary positions below $1/2$.

3. There is a natural pair of annihilation and creation operators for the m -parametric family of potentials (8), whose action is squematically drawn in figure 1 [4,12-13]:

$$D = B^\dagger a B, \quad D^\dagger = B^\dagger a^\dagger B, \quad (11)$$

where a and a^\dagger are the oscillator annihilation and creation operators. It turns out that D, D^\dagger and \tilde{H} close a polynomial algebra of $(2m)$ th order [13]

$$[\tilde{H}, D] = -D, \quad [\tilde{H}, D^\dagger] = D^\dagger, \quad [D, D^\dagger] = N(\tilde{H} + 1) - N(\tilde{H}), \quad (12)$$

where $N(\tilde{H})$ is a generalized number operator [14] given by:

$$N(\tilde{H}) \equiv D^\dagger D = \left(\tilde{H} - \frac{1}{2} \right) \prod_{i=1}^m (\tilde{H} - \epsilon_i - 1) (\tilde{H} - \epsilon_i). \quad (13)$$

The eigenstates $|\tilde{\psi}_{\epsilon_i}\rangle$ of \tilde{H} associated to $\epsilon_i, i = 1, \dots, m$ are annihilated by both D and D^\dagger . The ones $|\tilde{\psi}_n\rangle$ associated to $E_n, n = 1, 2, \dots$ are linked to two neighbours $|\tilde{\psi}_{n-1}\rangle$ and $|\tilde{\psi}_{n+1}\rangle$ by D and D^\dagger . The extremal state $|\tilde{\psi}_0\rangle$ is linked with $|\tilde{\psi}_1\rangle$ by D^\dagger and it is annihilated by D .

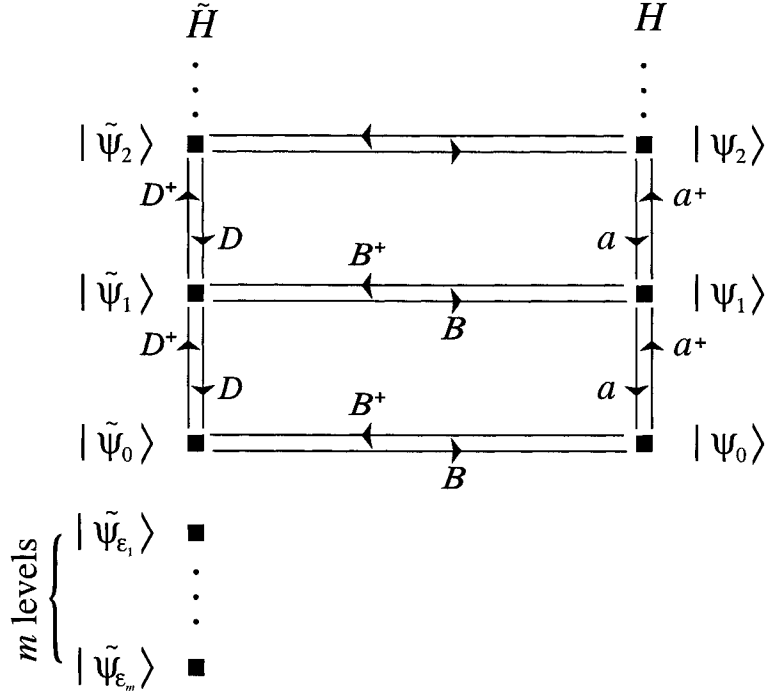


FIG. 1. Schematic representation of the m th order intertwining operators B , B^\dagger and the annihilation and creation operators a , a^\dagger , D , D^\dagger for the Hamiltonians H and \tilde{H} .

4. We notice that the nonlinear algebra (11-13) can be partially linearized, i.e., there is a pair of creation and annihilation operators D_L and D_L^\dagger satisfying the Heisenberg-Weyl algebra on the subspace associated to the levels $E_n = n + 1/2$, $n = 0, 1, \dots$ [13,15]. Those operators and their action onto $\{|\tilde{\psi}_n\rangle, n = 0, 1, \dots\}$ are given by:

$$D_L = B^\dagger \left[\prod_{i=1}^m (N - \epsilon_i + \frac{1}{2})(N - \epsilon_i + \frac{3}{2}) \right]^{-1/2} aB, \quad (14)$$

$$D_L^\dagger = B^\dagger a^\dagger \left[\prod_{i=1}^m (N - \epsilon_i + \frac{1}{2})(N - \epsilon_i + \frac{3}{2}) \right]^{-1/2} B, \quad (15)$$

$$D_L |\tilde{\psi}_n\rangle = \sqrt{n} |\tilde{\psi}_{n-1}\rangle, \quad D_L^\dagger |\tilde{\psi}_n\rangle = \sqrt{n+1} |\tilde{\psi}_{n+1}\rangle, \quad [D_L, D_L^\dagger] |\tilde{\psi}_n\rangle = |\tilde{\psi}_n\rangle. \quad (16)$$

We see that the explicit expressions for the nonlinear annihilation and creation operators (11) are simpler than the linear expressions (14,15). However, the action of the linear operators onto the states $\{|\tilde{\psi}_n\rangle, n = 0, 1, \dots\}$ is simpler than the corresponding nonlinear action. This characteristic will be seen once again in the coherent states construction.

5. It is quite natural to construct the coherent states (CS) as eigenstates of D and D_L . In the *nonlinear* case we have ($D|z\rangle = z|z\rangle$) [13]:

$$|z\rangle = \sum_{n=0}^{\infty} \frac{\sqrt{\prod_{i=1}^m \Gamma(-\epsilon_i + \frac{1}{2}) \Gamma(-\epsilon_i + \frac{3}{2})} z^n |\tilde{\psi}_n\rangle}{\sqrt{n! {}_2F_2(-\epsilon_1 + \frac{1}{2}, \dots, -\epsilon_m + \frac{1}{2}, -\epsilon_1 + \frac{3}{2}, \dots, -\epsilon_m + \frac{3}{2}; r^2) \prod_{i=1}^m \Gamma(n - \epsilon_i + \frac{1}{2}) \Gamma(n - \epsilon_i + \frac{3}{2})}} \quad (17)$$

where $\Gamma(x)$ is the gamma function, $z \in \mathbf{C}$, $r = |z|$, and ${}_pF_q$ is a generalized hypergeometric function. On the other hand, in the *linear* case we get ($D_L|z\rangle = z|z\rangle$):

$$|z\rangle = e^{-\frac{r^2}{2}} \sum_{n=0}^{\infty} \frac{z^n}{\sqrt{n!}} |\tilde{\psi}_n\rangle. \quad (18)$$

Due to the CS (17,18) involve just the eigenstates of \tilde{H} associated to the levels $E_n = n + 1/2, n = 0, 1, \dots$, they evolve in time as for the harmonic oscillator:

$$|z, t\rangle \equiv e^{-i\tilde{H}t}|z\rangle = e^{-it/2}|z(t)\rangle, \quad z(t) = e^{-it}z. \quad (19)$$

The resolution of the identity needs to take into account the existence of the atypical orthogonal coherent states $|\tilde{\psi}_{\epsilon_i}\rangle$ [12-13,15]:¹

$$I = \sum_{i=1}^m |\tilde{\psi}_{\epsilon_i}\rangle\langle\tilde{\psi}_{\epsilon_i}| + \int |z\rangle\langle z|d\mu(z). \quad (20)$$

In the nonlinear case the measure $d\mu_{NL}(z)$ takes the form [13]:

$$d\mu_{NL}(z) = {}_0F_{2m}\left(-\epsilon_1 + \frac{1}{2}, \dots, -\epsilon_m + \frac{1}{2}, -\epsilon_1 + \frac{3}{2}, \dots, -\epsilon_m + \frac{3}{2}; r^2\right) h(r^2) r dr d\varphi, \quad (21)$$

where $h(x)$ is proportional to a Meijer G -function:

$$h(x) = \frac{G_{0}^{2m+1} \begin{smallmatrix} 0 \\ 2m+1 \end{smallmatrix} (x|0, -\epsilon_1 - \frac{1}{2}, \dots, -\epsilon_m - \frac{1}{2}, -\epsilon_1 + \frac{1}{2}, \dots, -\epsilon_m + \frac{1}{2})}{\pi \prod_{i=1}^m \Gamma(-\epsilon_i + \frac{1}{2}) \Gamma(-\epsilon_i + \frac{3}{2})}. \quad (22)$$

In the linear case the measure $d\mu_L(z)$ becomes the standard one:

$$d\mu_L(z) = \pi^{-1} r dr d\varphi. \quad (23)$$

In conclusion, from both the algebraic and practical viewpoints it is convenient to work with the linear annihilation and creation operators and their corresponding coherent states.

Acknowledgements.

DJFC acknowledges support by CONACyT (México), project 26329-E. VH acknowledges support by research grants from NSERC of Canada and FCAR du gouvernement du Québec.

References

1. E. Witten, Nucl. Phys. B **188**, 513 (1981).
2. M.M. Nieto, Phys. Lett. B **145**, 208 (1984).
3. A.A. Andrianov, N.V. Borisov and M.V. Ioffe, Phys. Lett. A **105**, 19 (1984).
4. B. Mielnik, J. Math. Phys. **25**, 3387 (1984).
5. A.A. Andrianov, M.V. Ioffe and V. Spiridonov, Phys. Lett. A **174**, 273 (1993).
6. V.G. Bagrov and B.F. Samsonov, Theor. Math. Phys. **104**, 1051 (1995).
7. D.J. Fernández C., M.L. Glasser and L.M. Nieto, Phys. Lett. A **240**, 15 (1998).
8. D.J. Fernández C., V. Hussin and B. Mielnik, Phys. Lett. A **244**, 309 (1998).
9. J.O. Rosas-Ortiz, J. Phys. A **31**, L507 (1998); *ibid* **31**, 10163 (1998).
10. C.V. Sukumar, J. Phys. A **18**, 2917 (1985).
11. G. Junker and P. Roy, Ann. Phys. **270**, 155 (1998)
12. D.J. Fernández C., V. Hussin and L.M. Nieto, J. Phys. A **27**, 3547 (1994).
13. D.J. Fernández C. and V. Hussin, J. Phys. A **32**, 3603 (1999).
14. V.M. Eleonsky and V.G. Korolev, J. Phys. A **28**, 4973 (1995).
15. D.J. Fernández C., L.M. Nieto and O. Rosas-Ortiz, J. Phys. A **28**, 2693 (1995).

¹Notice that $z = 0$ is a $(m+1)$ th degenerate eigenvalue of D and D_L because $D|\tilde{\psi}_{\epsilon_i}\rangle = D_L|\tilde{\psi}_{\epsilon_i}\rangle = 0, i = 1, \dots, m$, and from (17,18) we have $|z = 0\rangle = |\tilde{\psi}_0\rangle$ and $D|\tilde{\psi}_0\rangle = D_L|\tilde{\psi}_0\rangle = 0$.

New Pöschl-Teller susy partners

L.M. Nieto, J. Negro, and O. Rosas-Ortiz*

Departamento de Física Teórica, Universidad de Valladolid, 47005 Valladolid, Spain

Abstract

The supersymmetric problem related to the modified Pöschl-Teller potential is solved in closed form. Some of the new potentials present singularities, but it is also possible to find some others free of singular points, and with interesting physical features.

In the last years there has been remarkable progress in the study of new exactly solvable problems in quantum mechanics. The topic has been developed along different lines: Darboux transformation, Infeld-Hull factorization, Mielnik factorization, susy quantum mechanics, and inverse scattering theory, among others [1]. All of them can be embraced in the elegant algebraic approach called *intertwining technique*, which has been successfully applied in the construction of higher order susy partners of the harmonic oscillator[2] and hydrogen-like radial potentials [3]. Using the intertwining technique, we are going to analyze the susy problem associated with the modified Pöschl-Teller potential in order to determine new families of susy partner potentials directly related to it.

Let us consider the well known one-dimensional two-parametric modified Pöschl-Teller potential [4], written in the following equivalent forms:

$$V(\alpha, x) = -\alpha^2 \frac{\lambda(\lambda - 1)}{\cosh^2 \alpha x} = -\frac{g\alpha}{2 \cosh^2 \alpha x}, \quad \alpha > 0, \quad (1)$$

where we take $\lambda > 1$ or $g > 0$ in order to have an attractive potential. The parameters α , λ and g are related by

$$\lambda = \frac{1}{2} \left(1 + \sqrt{1 + \frac{2g}{\alpha}} \right) > 1. \quad (2)$$

The bound states ($E < 0$) for this potential are

$$\begin{aligned} \psi(x) = (\cosh \alpha x)^\lambda & \left[A {}_2F_1(a, b; 1/2; -\sinh^2 \alpha x) \right. \\ & \left. + B (\sinh \alpha x) {}_2F_1(a + 1/2, b + 1/2; 3/2; -\sinh^2 \alpha x) \right], \end{aligned} \quad (3)$$

*On leave of absence from *Departamento de Física, CINVESTAV-IPN, A.P. 14-740, 07000 México D.F., Mexico.*

with $2a = \lambda - \sqrt{|E|}/\alpha$, $2b = \lambda + \sqrt{|E|}/\alpha$, and the discrete energy spectrum is given by $E_n = -\alpha^2(\lambda - 1 - n)^2$, $n \in \mathbf{N}$, $0 \leq n < \lambda - 1$. Observe that the energy for $n = 0$ always belongs to the discrete spectrum of $V(\alpha, x)$. The corresponding normalized wave function is precisely

$$\psi_0(x) = \sqrt{\frac{\alpha \Gamma(\lambda - 1/2)}{\sqrt{\pi} \Gamma(\lambda - 1)}} (\cosh \alpha x)^{1-\lambda}. \quad (4)$$

We look now for a first order differential operator $A = \frac{d}{dx} + \beta(x)$ and a partner potential $\tilde{V}(\alpha, x)$ such that the following intertwining relationship holds:

$$\left[-\frac{d^2}{dx^2} + \tilde{V}(\alpha, x) \right] A = A \left[-\frac{d^2}{dx^2} + V(\alpha, x) \right]. \quad (5)$$

The new potential $\tilde{V}(\alpha, x)$ is related to $V(\alpha, x)$ through the following susy relationships

$$\tilde{V}(\alpha, x) = V(\alpha, x) + 2\beta'(x), \quad \beta^2(x) - \beta'(x) = V(\alpha, x) - \epsilon, \quad (6)$$

with ϵ an integration constant, which turns out to be the factorization energy. We can find two different particular solution of the Riccati equation (6) in the form

$$\beta_0^\pm(\alpha, x) = D^\pm \tanh \alpha x, \quad D^+ = -\alpha\lambda, \quad D^- = -\alpha(1 - \lambda), \quad (7)$$

associated with two different factorization energies $\epsilon^\pm = -(D^\pm)^2$. The general solutions of the Riccati equation (6) can be found to be

$$\beta_{C^\pm}^\pm(\alpha, x) = D^\pm \tanh \alpha x - \frac{d}{dx} \ln \left(1 - C^\pm \int^x (\cosh \alpha y)^{2D^\pm/\alpha} dy \right), \quad (8)$$

where C^\pm are two new different integration constants; when they are zero, the particular solutions $\beta_0^\pm(x)$ are recovered. We have two different families of intertwining operators $A_{C^+}^+$, $A_{C^-}^-$, generating two different families of susy partners of the potential (1). Since the begining of susy quantum mechanics, it has been usual to consider only the susy partners of a given potential constructed by using only particular solutions of the Riccati equation. We are going to analyze now the results coming out when the general solutions (8) are taken into account. The integrals appearing there can be expressed in a closed form as

$$\int^x (\cosh \alpha y)^q dy = -\frac{2^{-q} e^{-\alpha q x}}{\alpha q} {}_2F_1 \left(-\frac{q}{2}, -q; 1 - \frac{q}{2}; -e^{2\alpha x} \right) + \text{constant}. \quad (9)$$

Let us analyze first the family of potentials $\tilde{V}_\zeta^+(\alpha, x)$. In this case the definite integral (9) exists in the whole real axis, and we can define

$$M(\lambda, \alpha, x) = \int_0^x (\cosh \alpha y)^{-2\lambda} dy = \frac{2^{2\lambda} e^{2\alpha\lambda x}}{2\alpha\lambda} {}_2F_1 \left(\lambda, 2\lambda; 1 + \lambda; -e^{2\alpha x} \right) - \frac{\sqrt{\pi} \Gamma(\lambda)}{2\alpha \Gamma(\lambda + 1/2)}.$$

This function is odd in the variable x , and it is monotonically increasing from its minimum value $M(\lambda, \alpha, -\infty) = -\sqrt{\pi} \Gamma(\lambda)/(2\alpha \Gamma(\lambda + 1/2))$ to $M(\lambda, \alpha, +\infty) = |M(\lambda, \alpha, -\infty)|$. Defining now the function

$$\Omega_{\zeta}^{+}(\lambda, \alpha, x) := \frac{(\cosh \alpha x)^{-2\lambda}}{1 - \zeta M(\lambda, \alpha, x)} = -\frac{1}{\zeta} \frac{d}{dx} \ln [1 - \zeta M(\lambda, \alpha, x)], \quad (10)$$

we can evaluate the associated susy partner potential, which turns out to be

$$\tilde{V}_{\zeta}^{+}(\alpha, x) = -\alpha^2 \frac{1 + \frac{g}{2\alpha} + \sqrt{1 + \frac{2g}{\alpha}}}{\cosh^2 \alpha x} - 4\lambda\alpha\zeta \Omega_{\zeta}^{+}(\lambda, \alpha, x) \tanh \alpha x + 2(\zeta \Omega_{\zeta}^{+}(\lambda, \alpha, x))^2. \quad (11)$$

The typical features of these potentials can be seen in [5]. It can be proved that the function $\tilde{V}_{\zeta}^{+}(\alpha, x)$ is free of singularities in the following range of values of the parameter ζ

$$|\zeta| < \frac{1}{M(\lambda, \alpha, +\infty)} = \frac{2\alpha \Gamma(\lambda + 1/2)}{\sqrt{\pi} \Gamma(\lambda)}. \quad (12)$$

Working in this interval, the potential (11) corresponds to the following family of almost isospectral Hamiltonians

$$\tilde{H}_{\zeta}^{+} := -\frac{d^2}{dx^2} + \tilde{V}_{\zeta}^{+}(\alpha, x) = A_{\zeta}^{+} (A_{\zeta}^{+})^{\dagger} + \epsilon^{+}; \quad H = -\frac{d^2}{dx^2} + V(\alpha, x) = (A_{\zeta}^{+})^{\dagger} A_{\zeta}^{+} + \epsilon^{+}. \quad (13)$$

Due to the fact that $\epsilon^{+} = E_{-1}$ is an energy level not allowed in the spectrum of the initial Hamiltonian H , the eigenfunctions of \tilde{H}_{ζ}^{+} can be constructed by acting with the operator A_{ζ}^{+} on the eigenfunctions ψ_n of H :

$$\tilde{\psi}_n^{+}(\zeta, x) = (E_n - \epsilon^{+})^{-1/2} A_{\zeta}^{+} \psi_n(x), \quad n = 0, 1, \dots, \quad (14)$$

plus an extra “missing state” $\tilde{\varphi}^{+}(\zeta, x)$ satisfying $(A_{\zeta}^{+})^{\dagger} \tilde{\varphi}^{+}(\zeta, x) = 0$, which is

$$\tilde{\varphi}^{+}(\zeta, x) = \sqrt{\frac{1 - \zeta^2 M^2(\lambda, \alpha, +\infty)}{2 M(\lambda, \alpha, +\infty)}} (\cosh \alpha x)^{\lambda} \Omega_{\zeta}^{+}(\lambda, \alpha, x). \quad (15)$$

The non-singularity condition (12) appears here again, although in this case it is required for the missing state to be normalizable. Note also from (13) that $\tilde{\varphi}^{+}(\zeta, x)$ is clearly the eigenfunction of \tilde{H}_{ζ}^{+} with eigenvalue ϵ^{+} . This is the reason why we named it missing state. The spectrum of \tilde{H}_{ζ}^{+} is $\{E_n; n = 0, 1, \dots\}$ plus a new level at $\epsilon^{+} = E_{-1}$. The conclusion is immediate: the family of potentials $\tilde{V}_{\zeta}^{+}(\alpha, x)$ is not strictly isospectral to its susy partner $V(\alpha, x)$: it has the same levels plus an additional one which is placed below all of them.

The study of the other family of potentials $\tilde{V}_{\xi}^{-}(\alpha, x)$ arising from (8) can be done according to the lines already followed, although there are important differences between the final results. Let us introduce a function similar to $M(\lambda, \alpha, x)$, let us call it $L(\lambda, \alpha, x)$:

$$L(\lambda, \alpha, x) = -\frac{e^{-2\alpha(\lambda-1)x}}{2^{2(\lambda-1)} 2\alpha(\lambda-1)} {}_2F_1\left(1 - \lambda, 2 - 2\lambda; 2 - \lambda; -e^{2\alpha x}\right) + \frac{\sqrt{\pi} \Gamma(2 - \lambda)}{2\alpha(\lambda - 1) \Gamma(\frac{3}{2} - \lambda)}.$$

This function is also odd and takes arbitrary positive values for $x > 0$ and arbitrary negative values for $x < 0$. We use $L(\lambda, \alpha, x)$ to define the function

$$\Omega_{\xi}^{-}(\lambda, \alpha, x) := \frac{(\cosh \alpha x)^{2(\lambda-1)}}{1 - \xi L(\lambda, \alpha, x)} = -\frac{1}{\xi} \frac{d}{dx} \ln [1 - \xi L(\lambda, \alpha, x)], \quad (16)$$

from where we compute the new susy partner potential

$$\tilde{V}_\xi^-(\alpha, x) = -\alpha^2 \frac{1 + \frac{g}{2\alpha} - \sqrt{1 + \frac{2g}{\alpha}}}{\cosh^2 \alpha x} + 4\alpha(\lambda - 1)\xi \Omega_\xi^-(\lambda, \alpha, x) \tanh \alpha x + 2(\xi \Omega_\xi^-(\lambda, \alpha, x))^2.$$

Due to the behaviour of $L(\lambda, \alpha, x)$, it is quite clear that for any choice of $\xi \neq 0$ the potential $\tilde{V}_\xi^-(\alpha, x)$ presents a singular point, in contradistinction to the previous case of $\tilde{V}_\xi^+(\alpha, x)$. The presence of this singularity forces the results to be interpreted according to [6]: the susy partner potentials are not directly related by isospectrality to the original potential $V(\alpha, x)$, but to a different problem consisting of this modified Pöschl-Teller potential plus an infinite barrier potential placed precisely at the position where $\tilde{V}_\xi^-(\alpha, x)$ has its singular point.

The case $\xi = 0$ is interesting enough to be considered separately. It gives just the particular solution $\tilde{V}_0^-(\alpha, x)$, which is free of singularities. The susy partner potentials are directly connected to the factorization energy $\epsilon^- = E_0$ through (6). The eigenfunctions of \tilde{H}_0^- are given by

$$\tilde{\psi}_n^-(x) = (E_n - \epsilon^-)^{-1/2} A_0^- \psi_n(x). \quad n = 1, 2, \dots, \quad (17)$$

In the present case it can be proved that there is no missing state. The spectrum of \tilde{H}_0^- is given simply by $\{E_n; n = 1, 2, \dots\}$. Remark that, like in the previous case, this new Hamiltonian is not either strictly isospectral to H , although the reason is just the opposite: now the susy process eliminates one state of H without creating a new one which can substitute it, while in the previous situation a new state was created, but keeping the initial spectrum.

More details on the results reported here and their connection with the Dirac delta well potential can be seen in [5].

This work has been supported by a DGES project (PB94-1115) from Ministerio de Educación y Cultura (Spain), and also by Junta de Castilla y León (CO2/197). ORO acknowledges financial support from CONACyT (Mexico) and from the ICSSUR'99 Organizing Committee.

- [1] G. Darboux, C. R. Acad. Sci. Paris **94**, 1456 (1882); L. Infeld and T.E. Hull, Rev. Mod. Phys. **23**, 21 (1951); B. Mielnik, J. Math. Phys. **25**, 3387 (1984); D.J. Fernández C., Lett. Math. Phys. **8**, 337 (1984); E. Witten, Nucl. Phys. B **188**, 513 (1981); B.N. Zakhariev and A.A. Suzko, *Direct and Inverse Problems*, Springer-Verlag, New York (1990).
- [2] D.J. Fernández C., M.L. Glasser and L.M. Nieto, Phys. Letts A **240**, 15 (1998); D.J. Fernández C., V. Hussin and B. Mielnik, Phys. Lett. A **244**, 309 (1998).
- [3] J.O. Rosas-Ortiz, J. Phys. A **31**, L507 (1998); J. Phys. A **31**, 10163 (1998).
- [4] L.D. Landau and E.M. Lifshitz, *Quantum Mechanics*, Pergamon (1965). S. Flügge, *Practical Quantum Mechanics*, Springer-Verlag, New York (1974).
- [5] J.I. Díaz, J. Negro, L.M. Nieto and O. Rosas-Ortiz, *The supersymmetric modified Pöschl-Teller and delta-well potentials*, Preprint Univ. de Valladolid (1999).
- [6] I.F. Márquez, J. Negro, and L.M. Nieto, J. Phys. A **31**, 4115 (1998).

Quantum precise interferometry and ellipsometry with ultimate polarization states of light

Alexander P. Alodjants and Sergei M. Arakelian

Department of Physics and Applied Mathematics, Vladimir State University, Vladimir, 600026, Russia. Tel.: (0922)233334, 279621; Fax: (0922) 232575 E-mail: laser@vpti.vladimir.su and/or arak@vpti.vladimir.su

Abstract

The principles of high-precision interferometry including the ellipsometry, polarimetry based on the measurements with nonclassical polarization states of light are discussed. Formation of polarization-squeezed light and description of the ultimate measurement procedure in the Mach-Zehnder and/or Michelson interferometers are considered for the first time to make a precise gravitational radiation detection. Another type of interferometric measurement based on simultaneous measurement of the all four polarization Stokes parameters in a special type of multichannel interferometer-polarimeter are considered as well.

1. INTRODUCTION

At present the problem of nonclassical properties of light in polarization parameters has been a subject of intensive study in quantum optics [1-3]. The discussion has generally focused on suppression of quantum fluctuations of the Hermitean Stokes parameters that obey to the SU(2) algebra. In our previous papers [2,3] we discussed the procedure of quantum nondemolition measurement of the Stokes parameters of light. From the standpoint of application of nonclassical polarization light in high-precision measurements the SU(2) interferometers have a special interest[4,5]. In fact, it is well known that such interferometers play an essential role for gravitational radiation detection [5]. The problem is under our study in the paper.

2. QUANTUM DESCRIPTION OF THE LIGHT POLARIZATION

Let us describe the polarization characteristics of quantized optical field by the Hermitian Stokes operators S_j ($j = 0, 1, 2, 3$):

$$S_0 = a_x^+ a_x + a_y^+ a_y, \quad S_1 = a_x^+ a_x - a_y^+ a_y, \quad (1a, b)$$

$$S_2 = a_x^+ a_y e^{i\psi} + a_y^+ a_x e^{-i\psi}, \quad S_3 = i \left(-a_x^+ a_y e^{i\psi} + a_y^+ a_x e^{-i\psi} \right), \quad (1c, d)$$

where ψ is the classical phase shift (see Fig.1); $a_{x,y}$ and $a_{x,y}^+$ are the annihilation and creation operators, respectively, of two orthogonally polarized modes. In general case the operator a of total optical field can be expressed via two operators a_x and a_y for elliptically polarized light as [1]:

$$a = e_x^* a_x + e_y^* a_y, \quad (2)$$

where complex c-numbers $e_{x,y}$ determine the polarization characteristics of optical field. They can be written in the terms of two phase parameters η and θ in 3D-space of the Poincare sphere:

$$e_x = \cos \eta \cos \theta - i \sin \eta \sin \theta, \quad e_y = \cos \eta \sin \theta + i \sin \eta \cos \theta. \quad (3a, b)$$

In fact, the phase parameters 2η and 2θ determine the ellipticity and azimuth of the polarization state of light, respectively. Formation of nonclassical polarization states of light in different optical interferometers is the subject under discussion in our paper. The presence of fluctuations of both phases and amplitudes for two orthogonally polarized modes, which are unavoidable in quantum approach, results in principal uncertainty for light in polarization Stokes parameters and also for the phase angles η and θ in ellipsometric measurements [2].

3. FORMATION OF POLARIZATION-SQUEEZED LIGHT IN NONLINEAR MACH-ZEHNDER INTERFEROMETER

The 3D-dependence for normalized variance $\sigma_3^2 = \langle (\Delta S_3)^2 \rangle / \bar{n}$ vs input polarization state of light, i.e. vs the phase angles η and θ is shown in Fig.2. The quantum interference of two polarization modes results in formation of polarization-squeezed light with suppressed fluctuations of the S_3 -Stokes parameter at output of the Mach-Zehnder interferometer. The minimal value of σ_3^2 corresponds to the case of circularly polarized light at the input of optical fiber being used as a nonlinear medium to form the squeezed light. The suppression of fluctuations of the S_3 -Stokes parameter depends on the interferometer characteristics as well (cf.[1]). In Fig.3 the normalized variance σ_3^2 is shown as a function of the $r = \gamma_2/\gamma_1$ parameter (where the γ_2 and γ_1 magnitudes depends on the nonlinearity and length of optical fiber in two arms of interferometer, consequently). The value of σ_3^2 is minimal for $r = -1$.

4. ACCURACY OF THE MEASUREMENT FOR MICHELSON INTERFEROMETER

We have also considered an application of light in different polarization states for precise phase measurement in two interferometric schemes, i.e. based on the Mach-Zehnder and Michelson interferometers. The best accuracy of the phase shift measurement can be achieved with polarization-squeezed light at input of the measurement system, i.e. when $\delta\phi_c/\delta\phi_{sq} \simeq \kappa$, where $\delta\phi_c = 1/\sqrt{\bar{n}}$ and $\delta\phi_{sq} = 1/\sqrt{\langle \Delta S_2^2 \rangle}$ are the errors of the measured phase difference in the interferometer for coherent and polarization-squeezed states of light at the input of interferometer, respectively, κ determine the squeezing parameter before the interferometer.

Finally, the experimental set up with polarization-squeezed light for the precise gravitational radiation detection using the Michelson interferometer has been discussed as well. The necessary power requirements to reach a best sensitivity of the measurements by such a procedure is much smaller for polarization-squeezed light than for coherent light and/or for quadrature squeezed light being generated by parametric oscillator being used at input of the interferometer (cf.[5]).

5. QUANTUM ELLIPSOMETRIC MEASUREMENT

Another type of interferometric (ellipsometric) measurements is connected with new direction in quantum optics and ultimate measurements based on quantum ellipsometry, polarimetry and profilometry [3] – see Fig.4. In the case the procedure of the measurement of the matter characteristic (in condensed or atomic and/or molecular systems) is limited by quantum properties (fluctuations) of the light polarization and ellipsometric parameters as well. The basic scheme of quantum ellipsometer includes the source of polarization-squeezed light for precise measurements of the phase angles η and θ . The original eight-port polarization interferometer-polarimeter for simultaneous homodyne detection of both the Stokes parameters of light and the polarization phase operators (ellipsometric parameters) is proposed by us for the first time as a final step of the ellipsometric measurement.

ACKNOWLEDGEMENTS

This work has been supported by the Deutscher Akademischer Austauschdienst (DAAD) and partly by Russian Fund of Basic Researches. One of authors (A.P.A.) is grateful to Professor G.Leuchs for useful discussions.

REFERENCES

- [1] G.S.Agarwal, R.R.Puri Phys.Rev.A, **40**, 5179 (1988); R.Tanas, S.Kielich J.Mod.Opt. **37**, 1935 (1990)
- [2] A.S.Chirkin, A.A.Orlov, D.Yu.Paraschuk Sov.J.Quant.Electron. **23**, 870 (1993); A.P. Alodjants, S.M. Arakelian, A.S. Chirkin. Quantum and Semiclassical Optics, part B, **9**, 311 (1997); A.P. Alodjants, S.M. Arakelian, A.S. Chirkin. Applied Physics B, **66**, 53 (1998)
- [3] A.P.Alodjants, S.M.Arakelian JETP **113**, 1235 (1998); A.P.Alodjants, S.M.Arakelian J.Mod.Optics **46**, 475 (1999)
- [4] B.Yurke, S.L.McCall, J.R.Klauder Phys.Rev.A **33**, 4033 (1986); M.Hillery, L.Mlodinow Phys.Rev.A **48**, 1548 (1993)
- [5] C.M.Caves Phys.Rev.D **23**, 1693 (1981); P.Grangier, R.E.Slusher, B.Yurke, A.LaPorta Phys.Rev.Letts. **59**, 2152 (1987)

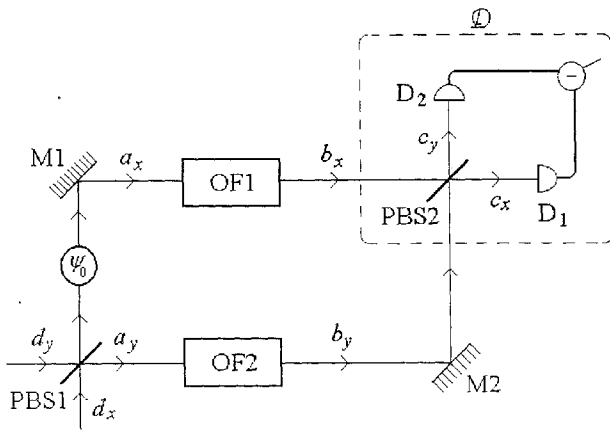


FIG.1. The Mach-Zehnder interferometer set-up to observe the polarization squeezed light; PBS1 and PBS2 are the polarization beam splitters, OF1, OF2 are the optical fibers with third order nonlinearity; \mathcal{D} is the detection system contains two photodetectors $D_{1,2}$; ψ denotes a classical phase shift between two polarized modes at input of optical fiber.

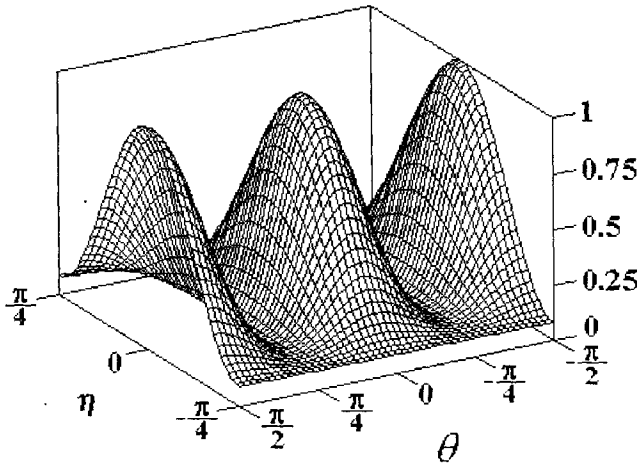


FIG.2. 3D-dependences for normalized variances $\sigma_3^2 \equiv \langle \Delta S_3^2 \rangle / n$ of the Stokes parameter S_3 vs the polarization phase parameters η and θ . The magnitudes of the parameters used for calculations are optimal. The value $\sigma_3^2 = 1$ corresponds to the coherent light.

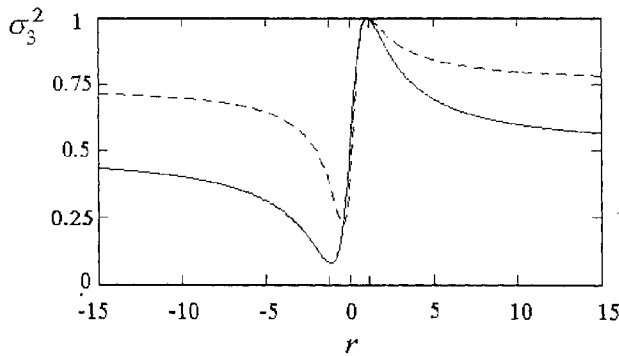


FIG.3. The dependences for suppressed variance σ_3^2 of the Stokes parameter for circularly polarized light (solid curve) and elliptically polarized light (dashed curve) as a function of the r -parameter; nonlinear phase shift $\kappa = \pi$.

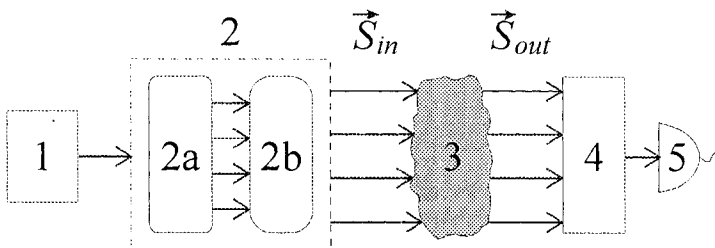


FIG.4. Scheme of the quantum ellipsometric measurement. Here we denote: 1 - laser source, 2 - generator of nonclassical polarization state \vec{S}_{in} (2a is a linear system, 2b is a nonlinear media both needed for polarization-squeezed light formation); 3 - sample, 4 - polarimeter for the all Stokes parameters (\vec{S}) detection, 5 - electronic scheme of detection

Atom Interferometric Tests of Complementarity

Stephan Dürr, Thomas Nonn, and Gerhard Rempe
Fakultät für Physik, Universität Konstanz, 78457 Konstanz, Germany

Abstract

We report on several which-way experiments performed with an atom interferometer. The internal atomic state serves as a which-way marker. With which-way information stored, the interference fringes are lost. It is a peculiarity of this experiment that Heisenberg's position-momentum uncertainty relation cannot explain the loss of spatial interference fringes. In addition, we can vary the parameters of the experiment such that only incomplete which-way information is stored. In this case, a reduced fringe visibility is observed. For a given fringe visibility, the amount of which-way information which can be obtained is limited by the recently discovered duality relation. With this atom interferometer, we have performed the first experimental test of the duality relation.

Introduction

The principle of complementarity refers to the ability of quantum-mechanical objects to behave as particles or waves under different experimental conditions. For example, in the famous double-slit experiment, a single atom can apparently pass through both apertures simultaneously, forming an interference pattern which reveals the atom's wave nature. But if a which-way detector is employed to determine the atom's way, the interference pattern is destroyed. In this case, each atom passes through only one of the slits, just like a classical particle. Complementarity expresses the fact that it is impossible to observe the wave and particle properties simultaneously.

The usual explanation for the loss of interference in a which-way experiment is based on Heisenberg's position-momentum uncertainty relation. This has been illustrated in famous *gedanken* experiments like Einstein's recoiling slit [1] or Feynman's light microscope [2]. However, Scully, Englert, and Walther [3] have recently proposed a new *gedanken* experiment, where the loss of the interference pattern is not related to Heisenberg's position-momentum uncertainty relation. Instead, the correlations between the which-way detector and the atomic beams are responsible for the loss of interference fringes.

We have performed a which-way experiment with an atom interferometer. A microwave field is used to store the which-way information in internal atomic states. A careful analysis of the experiment shows that Heisenberg's position-momentum uncertainty relation cannot explain the loss of interference fringes. Instead, correlations between the which-way detector and the atomic motion destroy the interference fringes.

The Atom Interferometer

We start with a brief description of the atom interferometer, which has been presented in more detail in Refs. [4–6]. Figure 1 shows a scheme of the setup, which uses Bragg reflection

of atoms from standing light waves. A first standing light wave splits the incoming atomic beam, A, into two beams, B and C, of equal atomic flux. After free propagation, a second standing light wave splits each atomic beam into two components. Now two beams, D and E, are travelling to the left, while beams F and G are travelling to the right. In the far field, each pair of overlapping beams produces a spatial interference pattern. The envelope of the interference pattern is given by the collimation properties of the incoming atomic beam. For detection, the atoms are illuminated with laser light and the fluorescence photons are observed. Figure 3(a) shows the experimentally observed interference pattern.

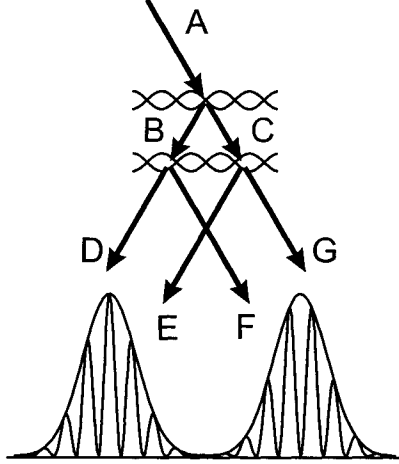


FIG. 1. Scheme of the atom interferometer. Bragg reflection from a standing light wave splits the incoming atomic beam, A, into two beams, B and C. A second standing light wave splits the beams again. In the far-field, a spatial interference pattern is observed.

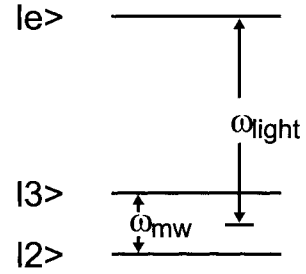


FIG. 2. Level scheme. The ground state is split into two hyperfine components, $|2\rangle$ and $|3\rangle$. The light frequency is chosen midway between the corresponding resonances to the excited state $|e\rangle$.

Storing Which-Way Information

The experiment employs a beam of ^{85}Rb atoms, whose ground state is split into two hyperfine components with total angular momentum $F=2$ and $F=3$, labeled $|2\rangle$ and $|3\rangle$, respectively. In these long-lived internal states, which-way information can be stored. For that purpose, the frequency of the standing light wave, ω_{light} , is tuned halfway between the $|2\rangle \leftrightarrow |e\rangle$ and $|3\rangle \leftrightarrow |e\rangle$ transition (see Fig. 2). Hence atoms in state $|2\rangle$ ($|3\rangle$) see a red (blue) detuned light field creating a negative (positive) ac-Stark shift potential, corresponding to an optically thicker (thinner) medium. In analogy to light optics one therefore expects [4] that the wave experiences a π phase shift if reflected from an optically thicker medium, *i.e.* if an atom is Bragg reflected in state $|2\rangle$. However, a detailed calculation [5] shows that here this π phase shift occurs if an atom is transmitted in state $|2\rangle$.

This phase shift is converted into a population difference between states $|2\rangle$ and $|3\rangle$ by applying a microwave field, at frequency ω_{mw} , resonant with the $|2\rangle \leftrightarrow |3\rangle$ transition. Two $\pi/2$ -pulses of the microwave are required. They form a Ramsey scheme: one is applied before and one after the first standing light wave. The internal atomic state is initially prepared in state $|2\rangle$ and then converted to the superposition state $(|2\rangle + |3\rangle)/\sqrt{2}$ by the first microwave pulse. Next, the standing light wave splits the beam, so that the state vector is changed to

$$|\psi\rangle \propto |\psi_B\rangle \otimes (|3\rangle + |2\rangle) + |\psi_C\rangle \otimes (|3\rangle - |2\rangle), \quad (1)$$

where the minus sign is due to the π phase shift, and $|\psi_B\rangle$ and $|\psi_C\rangle$ denote the state vectors of the center-of-mass motion for the reflected and transmitted beams (B and C in Fig. 1),

respectively. The second microwave pulse, acting on both beams (B and C), converts the state vector to

$$|\psi\rangle \propto |\psi_B\rangle \otimes |3\rangle - |\psi_C\rangle \otimes |2\rangle, \quad (2)$$

Obviously, the atom's internal and external degrees of freedom are entangled. This entanglement is the key point for the storage of which-way information. If later a measurement of the internal state is performed, the result of this measurement reveals in which of the beams the atom is: if the internal state is found to be $|3\rangle$, the atom was Bragg reflected, otherwise transmitted. Eq. (2) indicates that full which-way information is stored.

Interferometer with Which-Way Information

After considering a single beam splitter, we now return to the complete interferometer. Sandwiching the first Bragg beam splitter between two microwave $\pi/2$ pulses stores the which-way information in the internal atomic state, as described above. Figure 3(b) shows the atomic distribution with which-way information stored. Obviously, the interference fringes are lost. The mechanical effects of the which-way detection were analyzed in detail in Ref. [4]. We found that Heisenberg's position-momentum uncertainty relation cannot explain the loss of fringes.

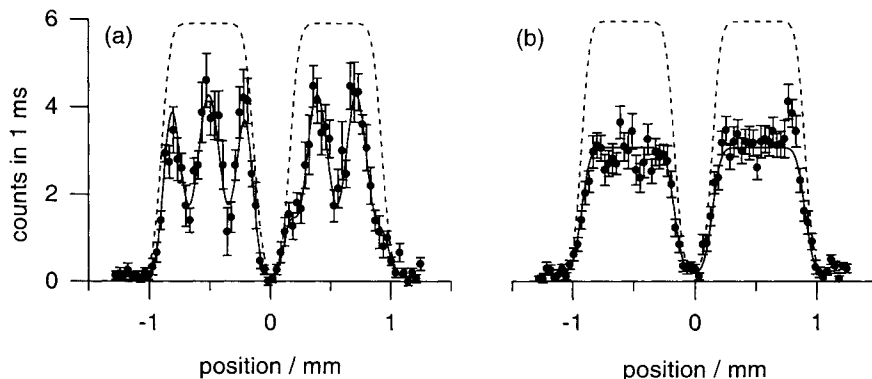


FIG. 3. Experimental results. (a) Interference pattern obtained with the atom interferometer. (b) Storing which-way information destroys the interference fringes.

In order to investigate why the interference fringes are lost, we consider the state vector for this interaction sequence. The state vector after the interaction with the first beam splitter sandwiched between the two microwave pulses is given in Eq. (2). The second beam splitter transforms this state vector into

$$|\psi\rangle \propto |\psi_D\rangle \otimes |3\rangle - |\psi_E\rangle \otimes |2\rangle + |\psi_F\rangle \otimes |3\rangle + |\psi_G\rangle \otimes |2\rangle. \quad (3)$$

The sign of $|\psi_G\rangle$ is positive due to the π phase shift during the transmission through the second beam splitter.

In the far field the atomic position distribution under the left peak of the envelope is given by

$$P(z) \propto |\psi_D(z)|^2 + |\psi_E(z)|^2 - \psi_D^*(z)\psi_E(z)\langle 3|2\rangle - \psi_E^*(z)\psi_D(z)\langle 2|3\rangle, \quad (4)$$

because here the spatial wave functions $\psi_F(z)$ and $\psi_G(z)$ vanish. The first two terms describe the mean intensity under the envelope. Interference could only be created by the last two terms, but they vanish because $\langle 2|3\rangle = 0$. Precisely the same entanglement that was required to store the which-way information is now responsible for the loss of interference. In other words: the correlations between the which-way detector and the atomic motion destroy the interference, as discussed in Ref. [3].

Incomplete Which-Way Information

These correlations need not always be perfect. In our experiment, we can adjust the degree of correlation by varying the pulse area φ of the microwave pulses. In general, a later measurement performed on the which-way detector yields only incomplete which-way knowledge. In order to quantify, how much which-way information is available from such a measurement, one typically uses the distinguishability, D . With incomplete which-way information stored, one obtains interference fringes with a reduced visibility, V , which is limited by the so-called duality relation [7,8]

$$D^2 + V^2 \leq 1. \quad (5)$$

This fundamental limit can be regarded as a quantitative statement about wave-particle duality.

The first experimental test of the duality relation was reported in Ref. [9]: For various values of φ , D and V were measured independently. The results shown in Fig. 3 are in good agreement with the duality relation.

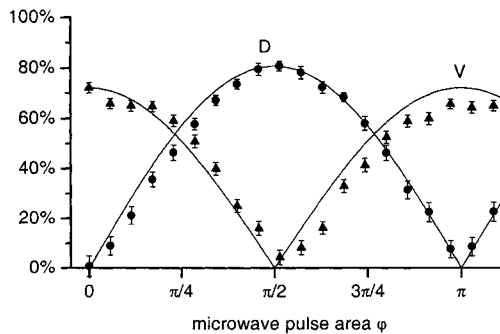


FIG. 4. Fringe visibility V (triangles) and path distinguishability D (dots) as a function of the pulse area φ of the microwave pulses which are applied to store which-way information. The solid lines display the theoretical expectations (see Ref. [9]).

- [1] N. Bohr, in *Albert Einstein: Philosopher-Scientist*, edited by P. A. Schilpp (Library of Living Philosophers, Evanston, 1949), pp. 200-241.
- [2] R. P. Feynman, R. B. Leighton, and M. Sands, in *The Feynman Lectures on Physics* (Addison Wesley, Reading, 1965), Vol. III, Chap. 1.
- [3] M. O. Scully, B.-G. Englert, and H. Walther, *Nature* **351**, 111 (1991).
- [4] S. Dürr, T. Nonn, and G. Rempe, *Nature* **395**, 33 (1998).
- [5] S. Dürr and G. Rempe, in *Advances in Atomic, Molecular, and Optical Physics*, edited by B. Bederson and H. Walther (Academic Press, New York, in press), Vol. 42.
- [6] S. Kunze, S. Dürr, K. Dieckmann, M. Elbs, U. Ernst, A. Hardell, S. Wolf, and G. Rempe, *J. Mod. Opt.* **44**, 1863 (1997).
- [7] G. Jaeger, A. Shimony, and L. Vaidman, *Phys. Rev. A* **51**, 54 (1995).
- [8] B.-G. Englert, *Phys. Rev. Lett.* **77**, 2154 (1996).
- [9] S. Dürr, T. Nonn, and G. Rempe, *Phys. Rev. Lett.* **81**, 5705 (1998).

Generation of non-classical light with diode and solid-state lasers

C. Becher, and K.-J. Boller

*Fachbereich Physik, Universität Kaiserslautern,
Erwin-Schrödinger-Str.46, 67663 Kaiserslautern, Germany
e-mail: cbecher@rhrk.uni-kl.de*

Abstract

We show that the generation of squeezed light from diode lasers is strongly affected by spectrally asymmetric mode-correlation effects. The experimental results correspond closely to the predictions of a quantum-mechanical Langevin multi-mode rate equation model. Using the squeezed diode laser as a pump source the intensity noise of a Nd:YVO₄ microchip laser was reduced to 0.5 dB above the quantum noise limit at low frequencies.

I. INTRODUCTION

In recent years there has been considerable interest in laser sources for applications in laser-based high-sensitivity metrology and communication technologies. Examples are high-precision interferometry, e.g. the detection of gravitational waves, high-sensitivity spectroscopy, and the transmission of information with the highest possible channel capacity. The demand for a high signal-to-noise ratio in such applications requires laser sources with a high output power and an intensity noise close to the standard quantum noise limit (SQL) or even below. Diode lasers have been shown to offer the potential to reach and go below this limit by a reduction of pump current fluctuations below the SQL [1,2]. Solid-state lasers have been proposed to emit non-classical light with photon number squeezing if they are pumped with a pump source which shows sub-Poissonian intensity fluctuations [3].

The major goals of our investigations are the realization and characterization of a diode laser source of non-classical light with photon-number squeezing and the optical pumping of high-stability, single frequency solid-state lasers with this pump source. The detailed investigation of both the diode laser's and the solid-state laser's intensity noise characteristics is an indispensable basis for the generation of non-classical light with diode-laser pumped solid-state lasers, which has not been demonstrated by now.

II. INTENSITY NOISE MEASUREMENTS

Diode laser sources for non-classical light were realized with SDL 5410-C single mode, quantum well AlGaAs diode lasers with wavelengths around 810 nm. The pump current noise was reduced by driving the diode lasers with a high-impedance constant current source. The generation of non-classical light required a suppression of the competing diode laser side modes to a high degree (> 35 dB). A diode laser, which was stabilized by the technique of injection-locking [4], emitted light with an intensity noise of 2.4 dB (42%) below the SQL with an output power of 100 mW [5], whereas without injection-locking (free emitting laser) the noise was 1-2 dB above the SQL. The stabilization of a second diode laser by the feedback of an external Littrow grating [6] provided wavelength-tunable radiation with a noise suppression of 2.2 dB (40%) below the SQL with an output power of 80 mW [7].

With these pump sources the intensity noise of a solid-state laser optically pumped with non-classical light was investigated for the first time [5,8]. The extremely low intensity noise of the diode laser pump source allowed for an observation of the solid-state laser's internal noise sources, i.e. the quantum noise characteristics. Nd:YVO₄ microchip lasers with a low lasing threshold of less than 0.5 mW and a high quantum efficiency of up to 66% were used for the investigation of these noise characteristics. By pumping with non-classical light the intensity noise of the microchip lasers at low frequencies below the relaxation oscillation resonance was reduced by more than 20 dB compared to pumping with a free emitting diode laser. Fig. 1 (trace (i)) shows the microchip laser intensity noise spectrum, measured with a balanced homodyne detector, for the case of pumping with squeezed light from the grating feedback diode laser. The minimum intensity noise was 0.5 dB (12%) above the SQL in the low frequency range (250 kHz). This is the lowest intensity noise of an optically pumped laser in that range at present [8].

III. FUNDAMENTAL NOISE PROCESSES

The measured intensity noise spectra of the Nd:YVO₄ microchip lasers were compared with the predictions of a quantum mechanical Langevin rate equation model (see trace (ii) of Fig. 1), whose parameters were experimentally determined in independent measurements. The comparison shows that the microchip laser intensity noise is higher than the predictions in the low frequency range below the relaxation oscillations and is lower than the calculated values in the relaxation oscillation frequency range.

From the difference between experimental and theoretical data in the low frequency range a noise source for the solid-state laser can be identified, which has not been taken into account so far: The emission of photon number squeezed light by a diode laser results from an anticorrelation between the fluctuations of the diode laser main mode and the fluctuations of a large number of weakly excited side modes. As the solid state laser does not absorb all the modes which participate in this anticorrelation, its effective pump noise is higher than the total (spectrally integrated) diode laser intensity noise.

In order to investigate the mode correlation effect, the diode laser radiation was spectrally filtered with a grating spectrometer [7]. The results showed that the generation of nonclassical light with the diode laser always results from a cancellation of the anticorrelated fluctuations of the main mode and up to 150 side modes, where the latter number depends

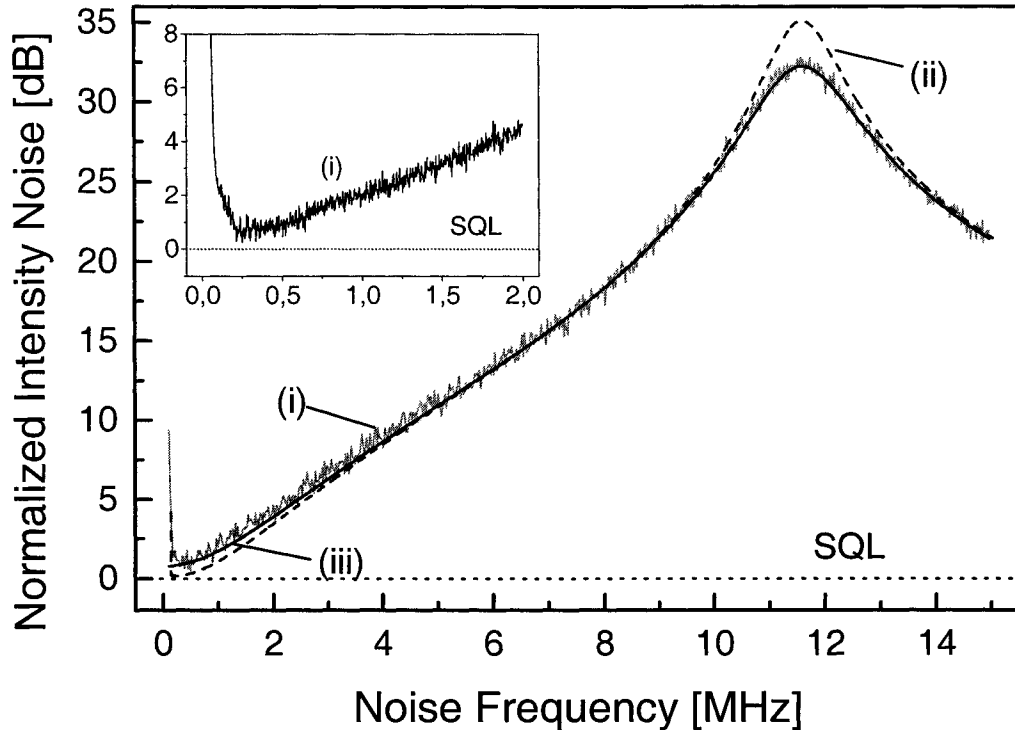


FIG. 1. Intensity noise spectrum of the Nd:YVO₄ microchip laser pumped with the grating feedback laser, normalized to the SQL. Trace (i): experimental data as measured with the homodyne detector; trace (ii): spectrum calculated from the Langevin rate equation model; trace (iii): theoretical spectrum with consideration of measured effective pump noise and enhanced damping of the relaxation oscillations.

on the side mode suppression. Additionally, for the first time, an asymmetric contribution of long- and short-wavelength side modes to the total intensity noise was demonstrated. The experimental results could be modeled to a high degree of correspondence with a quantum mechanical Langevin multimode rate equation model taking into account nonlinear gain effects in the diode laser [7]. As physical origin for the asymmetric intensity and intensity noise distribution we identified a nonlinear dynamic self saturation of each mode by its own fluctuations as well as a nonlinear cross-correlation of the modes, introduced by mode beating effects and population pulsations. According to this model, the cancellation of the mode fluctuations in the total intensity noise depends on the degree of mode anticorrelation and subsequently on the nonlinear gain contributions in the diode laser.

In order to independently determine the effective microchip laser pump noise, the diode laser intensity noise which is contained in the spectral interval of the microchip laser absorption bandwidth was measured by a spectral filtering with the grating spectrometer [8]. The measured effective pump noise agrees well with the theoretical noise obtained from a fit of the Langevin noise model to the measured microchip laser intensity noise spectra. This agreement directly proves that the effective microchip laser pump noise is determined by mode correlation effects in the diode pump laser.

The difference of the experimentally microchip laser noise spectra and the data calculated

from the Langevin model in the relaxation oscillation frequency range can be explained by nonlinear gain effects in the microchip laser which increase the relaxation oscillation damping constant. As physical origin a gain saturation by the finite lifetime of the lower laser level $^4I_{11/2}$ of 620 ps and the resulting non-zero occupation of this level were identified [8].

Trace (iii) of Fig. 1 shows the microchip laser noise spectrum calculated from the Langevin rate equation model taking into account the measured effective pump noise and the enhanced damping of the relaxation oscillations. This calculated noise spectrum now shows an excellent agreement with the experimentally measured noise spectrum (trace (i)) over the entire range of noise frequencies. This agreement proves that the quantum noise characteristics of the microchip laser are understood completely now.

As a result, our investigations show that a diode laser pumped solid state laser offers the potential for the generation of photon number squeezed light. The currently best possible combination of a diode and a solid state laser is the diode laser with grating feedback and the Nd:YVO₄ microchip laser. Here, the generation of squeezed light from the microchip laser is prohibited by an increase of the diode laser intensity noise above the SQL in the low frequency range below 1 MHz, which is caused by mode correlation effects in the pump diode laser. In order to generate squeezed light from the microchip laser, it has to be pumped with a source which shows sub-Poissonian intensity fluctuations at low frequencies. This can be achieved by a single-frequency emission of the diode laser, corresponding to a side mode suppression of much more than 55 dB.

In summary, the presented results extend and clarify the picture of squeezed light generation in diode lasers and diode-laser-pumped solid-state lasers.

REFERENCES

- [1] S. Machida, Y. Yamamoto, and Y. Itaya, *Phys.Rev.Lett.* **58**, 1000 (1987).
- [2] Y. Yamamoto, S. Machida, and W.H. Richardson, *Science* **255**, 1219 (1992).
- [3] Y.M. Golubev, and I.V. Sokolov, *Sov. Phys. JETP* **60**, 234 (1984).
- [4] H. Wang, M.J. Freeman, and D.G. Steel, *Phys.Rev.Lett.* **71**, 3951 (1993).
- [5] C. Becher, and K.-J. Boller, *Opt. Commun.* **147**, 366 (1998).
- [6] M.J. Freeman, H. Wang, D.G. Steel, R. Craig and D.R. Scifres, *Opt.Lett.* **18**, 2141 (1993).
- [7] C. Becher, E. Gehrig, and K.-J. Boller, *Phys. Rev. A* **57**, 3952 (1998).
- [8] C. Becher, and K.-J. Boller, *J. Opt. Soc. Am. B* **16**, 286 (1999).

Green lasing in microspheres at very low pump powers

W.von Klitzing, E. Jahier, R. Long, F. Lissillour,
V. Lefèvre-Seguin, J. Hare, J.-M. Raimond, S. Haroche
Laboratoire Kastler Brossel de l'Ecole Normale Supérieure
24 rue Lhomond, 75231 Paris 05, France

Abstract

A green room temperature up-conversion laser is being demonstrated in a 120 μm diameter microsphere of Er^{3+} doped ZBLAN. Lasing occurs around 540 nm with a 801 nm diode laser pump. The lasing threshold of only 30 μW of absorbed power is over two orders of magnitude lower than the lowest previously observed [1].

A low-cost green laser would have considerable impact on telecommunications, optical data storage, and medicine. Here we demonstrate an Er^{3+} microsphere laser with an extremely low threshold. This type of laser might, by the virtue of its small size and ease of fabrication, be an useful tool in the characterisation of laser glasses or as a highly monochromatic seed source for fibre lasers.

Lasing in Er^{3+} : The energy level diagram and pumping scheme can be seen in Figure 1. A diode laser operating at 801 nm pumps the ions from their fundamental level $^4I_{15/2}$ to $^4I_{9/2}$, from where they decay rapidly by non-radiative processes to the meta-stable level $^4I_{11/2}$ and from there to $^4I_{13/2}$. A second photon transfers the ion to either $^4F_{5/2}$ or $^2H_{11/2}$. These levels decay very rapidly to the lasing level $^4S_{3/2}$. Inversion can be achieved between this level and the upper Stark levels of the ground state $^4I_{15/2}$. The splitting of the Stark levels is only of the order of a few tens of cm^{-1} [2] thus guaranteeing a rapid thermalisation.

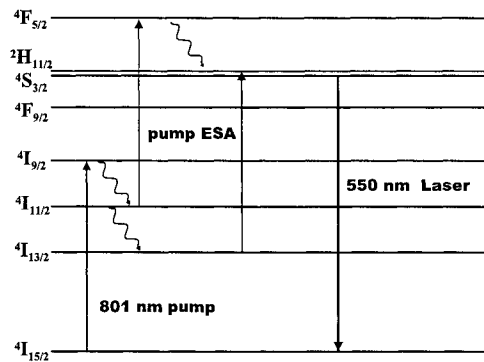


FIG. 1. Level diagram of Er^{3+} in ZBLAN

The laser resonators here are similar to our earlier experiments [3] microspheres of a diameter between 40 μm and 120 μm made from Erbium doped silica or ZBLAN. Light within such a dielectric spheres can be confined to so called whispering gallery modes (WGMs) which are formed under the appropriate resonance conditions by successive total internal reflections of the light at the surface of the sphere [4] and have the shape of a thin ring at the equator of the sphere. In order to feed light into this modes one has use evanescent wave coupling. This can be done by approaching a dielectric surface close to the sphere. Radiation can then be coupled into such a mode by optical tunneling through the gap between the sphere and for example a high refractive index prism. The rate of coupling of the WGMs into the prism can be adjusted by changing the distance between the prism and the sphere, e.g. with a PZT. The mode volume of the WGMs is about a thousand cubic wavelengths thus leading to field strengths of 10^3 V/m for a *single* photon in the mode. A quality factor of 10^9 corresponding to cavity damping times of one half of a microsecond are readily achieved in non-doped spheres. [5] Clearly such a system is ideally suited to examine laser materials, especially if taking into account the ease of production from very little material.

Spheres made from either ZBLAN or silica glass doped with Erbium are used here. The ZBLAN spheres have a diameter of between 60 μm and 120 μm and are doped to 800 ppm Er^{3+} . At the Laboratoire d'Optique, Lannion, the ZBLAN glass [6] is ground to a fine powder. This is then dropped through a microwave plasma torch where it is heated and subsequently cooled in free fall. The spheres form due to the surface tension of the molten material. For ease of manipulation the spheres are then attached to the tip of a glass fibre using UV-curing glue.

The silica microspheres are formed by laser fusion at the end of a silica fibre to which they remain attached. The final spheres have a diameter of between 30 μm and 100 μm and are doped to 500 ppm Er^{3+} . In order to produce these an optical fibre [7] is eroded down to its 20 μm diameter Er^{3+} doped core. Using a CO_2 laser a length of fibre of 2 mm is then fused onto a thicker silica stem which serves as a holder. Finally the tip of the doped fibre is carefully heated near the focus of the CO_2 laser so that the molten glass might form a sphere due to the surface tension [8].

Experimental set-up: The pump radiation from a 801 nm, 40 mW diode laser is coupled into a monomode fibre guides the light to the launching optics. A coupling efficiency of 25%, i.e. a few milli Watt of absorbed power, is readily achieved. The part of the light reflected by the prism and the light coupled out of WGMs of the sphere is collimated using a high aperture lens. Once a sphere has been coupled a Si-diode can be used to measure the absorbed pump power and the quality factor (Q) of the pump mode. The green radiation created in the upconversion of the pump radiation can be investigated by a monochromator [Jobin Yvon HR230; Resolution ~ 0.08 nm] followed by photo-multiplier.

Experimental results: The width of the pump modes is about 300 MHz in doped silica and 400 MHz in doped ZBLAN and agree with the ones calculated from the respective bulk absorption coefficients. The lifetime of the population of the $^4S_{3/2}$ state has been investigated by mechanically chopping the intensity of the pump beam and measuring the exponential decay of the green fluorescence. The measured values of 0.55(5) ms for ZBLAN is close to the value of 0.43 ms measured in fluoindate glass doped to 1 mol% [9]. In silica the $^4S_{3/2}$ level is known to relax in about 700 ns [10]. The large difference in the life times between the two glasses originates in the lower energy of the phonons in ZBLAN as compared to

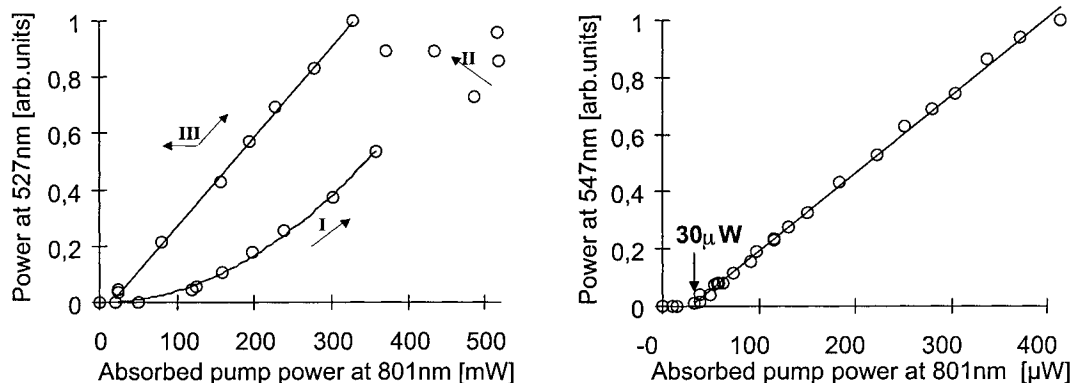


FIG. 2. a) The 'apprenticeship' b) After the 'apprenticeship'

silica [11]. This explains why lasing in Er^{3+} doped silica can not be achieved at the pump powers available here.

Lasing in the ZBLAN spheres has been achieved in one sphere of $120 \mu\text{m}$ diameter. Figures 2–3 show the intensity the 547 nm radiation coupled out of the WGMs as a function of the pump intensity at 801 nm. At each point of the measurement the wavelength of the pump laser was adjusted to coincide with the resonance of the WGM. The width of the gap between the sphere and the prism and thus the coupling rate between the pump beam and the sphere was verified to be constant throughout the experiment.

Figures 2–3 show the intensity of the green light coupled out of the mode via the prism versus the absorbed pump power. Upon starting with a virgin sphere (Fig.2a) one finds that at first (I) on increasing the pump intensity the green intensity follows a quadratic curve, as one might expect for a two photon process. However, at higher intensities a time dependent component appears. Most notably the green intensity increases even without an increase in pump intensity (II). After a few minutes of 'apprenticeship' the green emission stabilises. If one now reduces the pump power the green emission follows a linear regime (III). Decreasing the intensity further makes the lasing threshold of only $30 \mu\text{W}$ apparent. Upon increasing the intensity again one stays in the linear lasing regime, even if starting again from zero Watt (Fig.2b). The exceedingly low lasing threshold has its origin in a combination of small mode volume and high finesse. Taking into account the strong confinement of the pumping radiation in the WGMs it agrees well with the thresholds measured elsewhere [12,13]. It should also be noted that the laser output remains linear with respect to the pump power even ten times above threshold. The green emission returns to the quadratic regime only after a period of about two hours of absence of pump radiation. In fibre lasers this effect has been observed [14,13] before, albeit at far higher pump powers.

It is interesting to observe that we have not observed this temporary transition between the quadratic and linear regime in absence of lasing. Figure 3 shows the radiation from a virgin sphere exhibiting no 'apprenticeship' at all. Even after absorbed $2200 \mu\text{W}$ power into the pump mode for a duration of twenty minutes the green intensity retraces the original curve. One possible interpretation of the 'apprenticeship', put forward by D. Piehler [13], is photo darkening observed in rare-earth doped fibres.

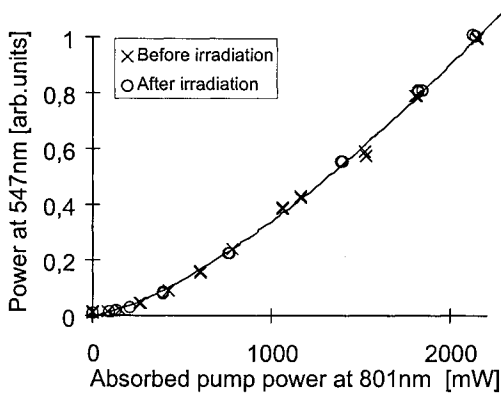


FIG. 3. Certain spheres do not show any ‘apprenticeship’.

Conclusion : We have succeeded in demonstrating an Erbium doped green microlaser with a threshold of only $30 \mu\text{W}$ which is about 300 times lower than the lowest in Er^{3+} [12] and 100 times lower than the previous lowest IR to visible up-conversion laser in any material [1]. An ‘apprenticeship’ of the green laser emission has been observed.

Acknowledgements: The authors gratefully acknowledge the support of the CEE TMR network (Microlasers and microcavities) and of the CNRS-Ultimatech program.

REFERENCES

- [1] D. Funk, J. Eden, J. Osinski, and B. Lu, *El.Lett.* **33**, 1958 (1997).
- [2] E. Desurvire and J. Simpson, *Optics Letters* **15**, 547 (1990).
- [3] V. Sandoghdar, F. Treussart, J. Hare, V. LefevreSeguin, J. Raimond, and S. Haroche, *PRA* **54**, R1777 (1996).
- [4] F. Treussart, N. Dubreuil, J. Knight, V. Sandoghdar, J. Hare, V. LefevreSeguin, J. Raimond, and S. Haroche, *Ann.Telecom.* **52**, 557 (1997).
- [5] F. Treussart, V. Ilchenko, J. Roch, P. Domokos, J. Hare, V. Lefevre, J. Raimond, and S. Haroche, *Journal Of Luminescence* **76-7**, 670 (1998).
- [6] M. Poulain, Personal Communication (1998).
- [7] J. Bayon, Personal Communication (17-12-1996).
- [8] W. von Klitzing, V. Ilchenko, J. Hare, V. Lefevre, J. Raimond, and S. Haroche (unpublished).
- [9] T. Catunda, L. Nunes, and A. Florez, *PRB* **53**, 6065 (1996).
- [10] C. Layne and M. Weber, *PRB* **16**, 3259 (1977).
- [11] C. Layne, W. Lowdermilk, and M. Weber, *PRB* **16**, 10 (1977).
- [12] J. Massicott, M. Bierley, R. Wyatt, S. Davey, and D. Szebesta, *El.Lett.* **29**, 2119 (1993).
- [13] D. Pihler and D. Craven, *El.Lett.* **30**, 1759 (1994).
- [14] T. Whitley, C. Millar, R. Wyatt, M. Bierley, and D. Szebesta, *El.Lett.* **27**, 1785 (1991).

Parametric Free Particle Lasers

E.G.Bessonov

Lebedev Physical Institute AS, 117924, Leninsky prospect 53, Moscow, Russia

E-mail: bessonov@sgi.lpi.msk.su

Abstract

The main objective of the work is the discussion of the physics of the undulatory radiation sources and parametric free-particle lasers. Some features of such sources based on ion beams will be considered.

According to Maxwell electrodynamics a particle nonuniformly moving in the external electromagnetic field emit the electromagnetic radiation. The properties of the emitted radiation are determined by the trajectory of the particle. Monochromatic radiation is emitted in the external field which perform a periodic (undulatory) trajectory along some axis. The broadband radiation is emitted when the particle trajectory has a single bend or a system of bends of the opposite polarity irregularly located along a straight line.

Electromagnetic radiation sources based on the emission of charged particles in undulators are named undulator radiation (UR) sources. UR sources can be classified to spontaneous incoherent, spontaneous coherent and induced UR sources. Spontaneous coherent and induced UR sources are named free-particle lasers (FPLs) as well. The nature of radiation emitted in the undulator is determined by quality (emittance) and features of the particle beam (homogeneous, prebunched), availability of the external wave, feedback (resonator).

Spontaneous incoherent UR sources and FPLs are devices made of an accelerator or storage ring and an undulator (wiggler). The accelerator and storage ring are devices which produce relativistic charged particle bunches. The undulator is a device which make particles go along specially periodic trajectories relative to some axis. The most typical undulators produce spatially periodic magnetic fields. Different electromagnetic fields can perform the same trajectories. For example, helical trajectory can be performed by either homogeneous magnetic field produced by solenoid or by helical magnetic field produced by a helical undulator. Helical trajectories are performed by circular polarized electromagnetic waves as well. Sine-like, helical, elliptical in the transverse plane and more complicated trajectories can be used. When an optical resonator storing the produced radiation is inserted in the undulator of a FPL then the successive particle bunches periodically enter the undulator such a way that they copropagate with the stored optical wavepackets.

In ordinary FPLs the particle bunches are not bunched on the scale of the emitted wavelength at the entrance of the undulator. Then under the action of the combined fields of the undulator and the stored wavepacket the particle beam is continuously self-microbunched on the scale of the emitted wavelength and emit coherent radiation. In the parametric FPLs (PFPLs) the previously microbunched particle bunches are used.

The generated wavelength of the spontaneous UR sources and FPLs is a continuous function of the electron incoming energy and the undulator field amplitude which are the operating parameters. That is why such sources are intrinsically tunable devices.

Particle beam in undulator is a system of moving excited oscillators which is the active medium of the UR sources. Particle bunches that is active medium are continuously renewed, so that FPLs are expected to support high power devices.

All particles of microbunches in PFPLs emit in definite directions electromagnetic waves of the same phase. The power of the emitted radiation in this case is proportional to the square of the number of particles in one microbunch or the square of the bunch current. Such lasers does not need in the external or stored in optical resonator electromagnetic wave. That is why they can work without resonators (mirrors) both in the longwavelength and in a hard X-ray region. It follows that PFPLs represent the ultimate in the capabilities of FPLs. The main problem of PFPLs is the problem of bunchers which produce beams microbunched on the scale of the emitted wavelength.

When the external field is a special periodic transverse magnetic field of an undulator then this field can be considered as an equivalent electromagnetic wave field which shake the particles with the same special period and the same value of strength as the undulator field. From this point of view any periodical real electromagnetic wave (in general case non-monochromatic) can be considered as a kind of an undulator.

A complex charged particle (not fully stripped ion, nucleus) emit UR the same way as a simple one when the frequency of the equivalent wave in a coordinate system connected with the particle is far from the resonance frequency of the particle corresponding to any transitions between levels of the particle. The scattering (emission) cross-section of the electromagnetic radiation in this case is determined by Thompson (Compton) cross section $\sigma_T = 3\pi r_p^2/8$, where $r_p = q^2/m_p c^2$ is the classical particle radius, q and m_p charge and mass of the particle, c light velocity. The charge $q = -e$ for electrons and $q = en^+$ for ions, where n^+ is the number of the ion charge state. When the frequency of the particle oscillation is near to resonance one then the cross section is highly increased and determined by the Rayleigh scattering cross section $\sigma_R = \lambda_r^2 g_1/2\pi g_2$, where λ_r is the transition wavelength between two electronic states in the particle rest frame, g_i the degeneracy factor of the state i . The ratio $\sigma_R/\sigma_T \sim (\lambda/r_e)^2 \sim 10^{10} \div 10^{15}$. This means that sources of the electromagnetic radiation based on Rayleigh scattering of equivalent or real photons by not fully stripped ion beams in undulators or in backward directed laser waves can appear on the level with UR sources based on electron beams.

The foundations of the theory of UR sources and PFPLs are in [1] - [3]. Below we will consider some features of such sources based on ion beams.

1. Backward Rayleigh scattering sources. Depending on the energy of a storage ring and type of ions the energy of backward Rayleigh scattered monochromatic polarized photons can lie in a wide range of energies of X-Ray to hard γ -Ray regions. The power of such sources can be very high [4], [5].

A scheme of a short period relativistic multilayer ion mirror can be produced in the form of a series of narrow flat layers transverse to the direction of beam propagation [6], [7]. This geometry is similar to that of a dielectric stack mirror. Such mirror can reflect both spontaneous incoherent and spontaneous coherent radiation with high efficiency and in a such a way to transform monochromatic IR or optical radiation to monochromatic X-ray

radiation with low divergence.

2. *Free-ion lasers (FILs)*. Under conditions of equal relativistic factors which define the hardness of the emitted radiation, ion beams possess many orders of magnitude higher stored energy and much less emittance than electron beams. For example, the electron beam of the Advanced Photon Source (APS) possess two orders higher emittance and five orders less stored energy than proton beams of storage rings LHC and SSC (project). The relativistic factors of electrons and protons are nearly the same in this cases [8]. The beam stored energy of the LHC will exceed the value 500 MJ. It follows that under conditions of optimal deflecting parameters of undulators used in free-particle lasers and equal efficiencies for both electron and ion beams the limiting power of FILs will be many orders higher than that of FELs. Possible parameters of the FILs are presented in the paper [3].

3. *Particle accelerators*. Cooled Super-high power high current ion beams of the energy ~ 10 GeV and based on such beams cm-to mm FILs can be used for the excitation of accelerator structures of Linear Colliders [6].

4. *Grasers and axion sources*. By analogy with the emission of the electromagnetic radiation the ion beams of FPLs emit gravitational radiation with the same energy of gravitons and angular divergence. The efficiency of the graviton production is proportional to the square of the ion mass. The transformation of gravitons into photons in the magnetic field can be used in detectors of gravitational radiation. Some schemes of gravitational experiments based on stimulated emission of gravitons by ion beams in undulators (under conditions of suppression of the photon emission at the same time) are presented in [9].

The transformation of axions into photons and back in the magnetic field takes place as well [10]. It means that the same or similar schemes can be used in experiments on search of axions.

UR sources, backward Compton scattering sources based on electron beams and free-electron lasers (FELs) are widespread sources now [11] - [13]. The UR of ions is more hard than synchrotron radiation (in contradiction to UR of electrons). This feature permit to produce ion beam diagnostic in accelerators and storage rings [14], [15].

UR sources and FPLs based on proton and ion beams [16], [17] are based on the same principle as UR sources based on electron beams and the Free-Electron Lasers (FELs) [18], [19]. However they have specific peculiarities that can lead to their adoption as superhigh power and/or ultrashort wavelength sources of the electromagnetic radiation. The peculiarities are connected with unique parameters of the proton and ion beams in existing or planned storage rings. The spontaneous radiation of proton and ion beams in undulators installed in straight sections of rings would be diffraction dominated as particle beam emittances in the rings are smaller than light beam emittances. In the case of protons and ions of the energy more than 10 TeV/nucleus the synchrotron radiation will lead to decrease of emittances and hence to more unique quality of proton and ion beams. Similar effect can be obtained by using three-dimensional laser cooling of not fully stripped ion beams [20], [21].

FILs can be next generation machines which will offer performance levels significantly beyond that which are available now. These performance levels follow from the fact that up-to-date technology can make ion beams that possess much smaller emittances and much greater total stored energy than the electron beams of the same relativistic factor.

REFERENCES

- [1] D.F.Alferov, Yu.A.Bashmakov, E.G.Bessonov, Sov. Phys. Tech. Phys., Vol.18, (1974), 1336; Proc. Lebedev. Phys. Inst., Ser. 80, (Synchrotron Radiation), Ed. N.G.Basov, (New York Consultant Bureau), (1976), p.97.
- [2] E.G.Bessonov, Proc. Lebedev. Phys. Inst., Ser. 214, (Undulator radiation, Free-Electron Lasers), Ed. P.A.Cherenkov, M.: Nauka, (1993), 3; Nucl. Instr. Meth., 1989, A282, p.442; *ibid*, 1994, v.A341, p.335.
- [3] E.G.Bessonov, Proc. of the 15th Int. Free-Electron Laser Conference FEL94, Nucl. Instr. Meth. v.A358, (1995), pp. 204.
- [4] E.G.Bessonov, K.-J.Kim, Proc. of the 1995 Part. Accel. Conf. and Int. Conf. on High-Energy Accelerators, p.2895.
- [5] E.G.Bessonov, K.-J.Kim, Proc. 5th European Particle Accelerator Conference, Sitges, Barcelona, 10-14 June 1996, v.2, pp. 1196.
- [6] E.G.Bessonov, Proc. Sixth Internat. Workshop on Linear Colliders LC95, Tsukuba Center for Institutes, March 27-31,1995, p.1227.
- [7] E.G.Bessonov, Proc. MICRO BUNCHES WS, Upton, New York, Sept 1995, p.367.
- [8] Samir K.Dutt, Proc of the Workshop on Fourth Generation Light Sources, SSRL/SLAC, February 24-27, 1992, p.170.
- [9] E.G.Bessonov, Proc. of the ICFA Beam Dynamics Workshop on Quantum aspects of beam Physics, Monterey, CA, January 4-9, 1998, World Scientific, USA, p.330 (rough version is in: <http://xxx.lanl.gov/abs/physics/9802037>).
- [10] Yu.N.Gnedin, Astrophysics and Space Science, 1997, v. 252, p. 95.
- [11] D.Attwood, K.Halbach, K-Je Kim, Science, 1985, v.228, p.1265.
- [12] K-Je Kim, A. Sessler, Science, 1990, v.250, p.88.
- [13] J.Feldhaus, B.Sonntag, Synchrotron Radiation News, v.11, No 1, 1988, p.20.
- [14] Coisson R., Opt. Commun., 1977, v.22, No 2, p.135.
- [15] D.F.Alferov, E.G.Bessonov, Proc. 10 Int. Conf. on High Energy Accel., Protvino, 1977, p.387, USSR.
- [16] R.Coisson, SSC as a powerful coherent source of radiation from X-ray to IR written in Dec. 1991 in response to a question H.Winic (private communication).
- [17] E.G.Bessonov, Ya.A.Vazdik, Proc. of the 15th Int. Accel. Conf., Hamburg, July 20-24, 1992, Vol.1, p.540.
- [18] Charles A.Brau, "Free-Electron Lasers". Academic Press Inc., 1250, Sixth Avenue, San Diego, CA 92101, 1990.
- [19] E.G.Bessonov, A.V.Vinogradov, Sov. Phys. USPEKHI, Vol.32, (9), (1989), p.806.
- [20] E.G.Bessonov, Kwang-Je Kim, Phys. Rev. Lett., 1996, v.76, No 3, p.431.
- [21] E.G.Bessonov, Kwang-Je Kim, F.Willeke, physics/9812043.

Finite Energy States for Periodically Kicked Nonlinear Media

W. Leoński and R. Tanaś

*Nonlinear Optics Division, Institute of Physics, A. Mickiewicz University,
ul. Umultowska 85, 61-614 Poznań, Poland*

Abstract

We study nonlinear media (nonlinear oscillator) located inside a one mode cavity and interacting with the cavity field. We assume, that the cavity is permanently kicked by a series of ultra-short coherent pulses. We show that for some values of the parameters describing the system its evolution is restricted to a finite set of n -photon states.

Quantum engineering of the electromagnetic field states has been a subject of numerous papers during the past years. Among a large variety of the systems discussed, models involving nonlinear oscillator are of the great importance ([1-12] and the references quoted therein). This paper is devoted to such kind of system that comprises nonlinear oscillator located inside a one-mode, high-Q cavity that is irradiated by a series of ultra-short coherent pulses. This system is governed by the following Hamiltonian (in units of $\hbar = 1$):

$$\hat{H} = \hat{H}_{NL} + \hat{H}_p , \quad (1)$$

where

$$\hat{H}_{NL} = \frac{\chi}{2} \hat{a}^{\dagger 2} \hat{a}^2 \quad (2)$$

and

$$\hat{H}_p = \epsilon(\hat{a}^\dagger + \hat{a}) \sum_{k=0}^{\infty} \delta(t - nT) . \quad (3)$$

The parameter χ appearing above denotes the nonlinearity parameter, ϵ corresponds to the strength of the cavity – external field coupling, whereas T denotes the time between two subsequent pulses.

We neglect all damping processes from the model discussed in this paper. It seems that due to the lack of damping the permanent excitation by external pulses should lead to the quantum dynamics with higher and higher mean number of photons. However, for some values of the parameters describing our system its evolution can be practically restricted to finite set of number states.

In this communication we are interested in the short-time regime, *i.e.* we assume that the time $T \ll 1/\chi$. For this case we perform numerical calculations enabling us to investigate

dynamics of our system. Our calculations are based on the method applied in the papers [8,10-12]. Assuming that the damping processes are absent we are able to describe the evolution of our system using the following wave-function (in n -photon basis):

$$|\Psi(t)\rangle = \sum_{n=0}^{\infty} a_n(t) |n\rangle . \quad (4)$$

The history of the system can be determined by the unitary evolution operators. They are defined using the Hamiltonians \hat{H}_{NL} and \hat{H}_p . One can notice that the whole evolution can be divided on two stages. The first one is the evolution during the times between two subsequent pulses. For these times the wave-function evolution is governed by the operator:

$$\hat{U}_{NL} = e^{-i\frac{\chi T}{2}(\hat{a}^\dagger)^2 \hat{a}^2} . \quad (5)$$

Owing to the fact that external excitation is modeled by the series of Dirac delta functions we are in a position to determine the unitary evolution operator acting on the wave-function during the pulse in the following form:

$$\hat{U}_p = e^{-i\epsilon(\hat{a}^\dagger + \hat{a})} . \quad (6)$$

In consequence, the evolution of the system from the time just after j -th pulse to the time just after $(j+1)$ -th pulse is determined by the operator $\hat{U} = \hat{U}_p \hat{U}_{NL}$. Hence, assuming that the system was initially in the vacuum state $|0\rangle$, the state corresponding to the time just after k -th pulse can be written as:

$$|\Psi_k\rangle = \sum_{n=0}^{\infty} a_n(k) |n\rangle = (\hat{U}_p \hat{U}_{NL})^k |0\rangle . \quad (7)$$

Applying this formula we determine the evolution of the wave-function and hence, the time dependence of mean values of various operators. In Fig.1a we plot the mean number of photons $\langle n \rangle = \langle \Psi | \hat{a}^\dagger \hat{a} | \Psi \rangle$ as a function of time. We see that $\langle n \rangle$ oscillates in a regular way between 0 and ~ 85 exhibiting the periodic behavior of the oscillations. Fig.1b shows the evolution of the probabilities $|a_n(t)|^2$ corresponding to the times just after the first 200 subsequent pulses. It is seen that the field state starts its evolution from the vacuum state $|0\rangle$. Then the wave-packet in the space of n -photon states is formed. This packet moves toward higher and higher Fock states reaching the states corresponding to $n \sim 95$. After that the packet comes back to lower values of n and for $t \sim 0.12$ transforms itself to its initial form corresponding to the vacuum state. Next, the probabilities evolve in a similar way as for the times between $t = 0$ and $t \sim 0.12$ exhibiting periodic character of the dynamics of the system.

This behavior can be explained on the basis of the well known Q -function. Thus, Figure 2 depicts contour plots of this function corresponding to the times just after the first 25 subsequent pulses. We see that for the time $t = 0$ the Q -function corresponds to the vacuum state and is located at the origin of the coordinate system. Then, after ~ 5 pulses

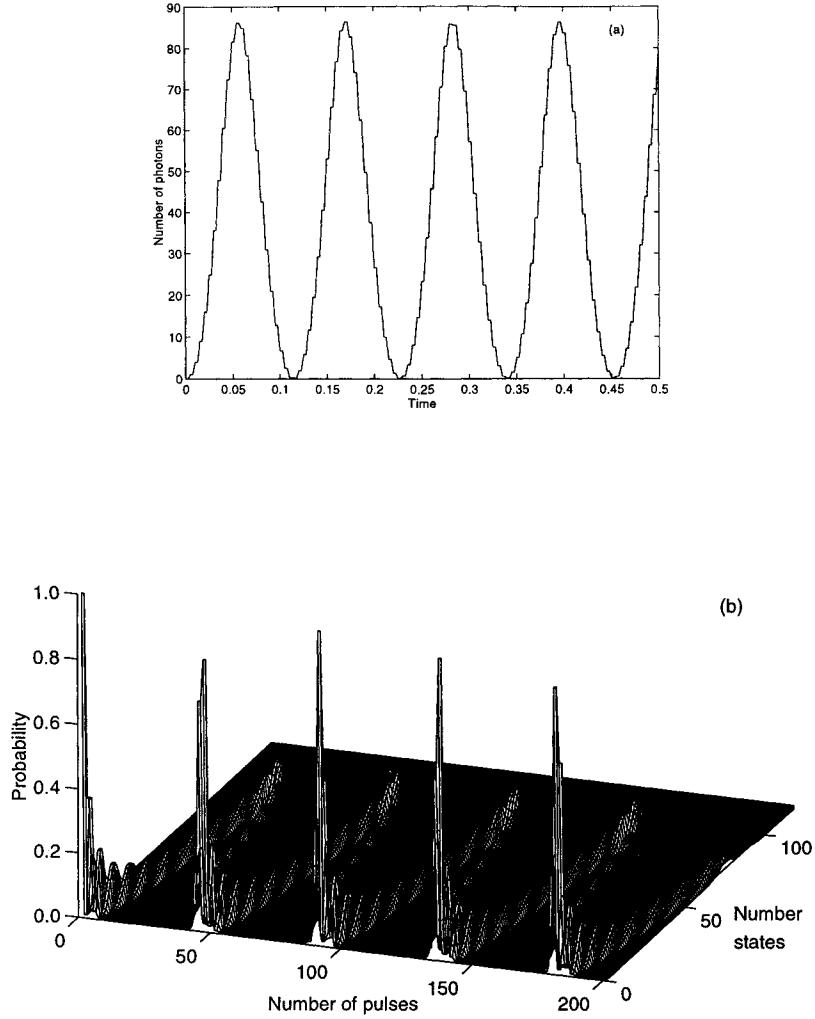


FIG. 1. Mean number of photons $\langle \Psi | \hat{a}^\dagger \hat{a} | \Psi \rangle$ (Fig. 1a) and the probabilities for n -photon states (Fig. 1b) as a function of time. The time between two subsequent pulses $T = 0.005$, the other parameters are: $\epsilon = 1$ and $\chi = 1$.

this function is translated on the complex α plane toward negative values of $\text{Im}(\alpha)$. As the parameter $|\alpha^2| = \langle n \rangle$ reaches sufficiently high values, the Q -function changes its character from that reminding a coherent state to that of a crescent type. For those times the unitary operator \hat{U}_{NL} starts to play a significant role in the whole evolution operator \hat{U} (\hat{U}_{NL} contains a factor proportional to n^2 and becomes dominant when we compare it with the factors proportional to \sqrt{n} and n). In consequence, the nonlinear evolution takes the leading role and the Q -function peak is rotated around the center of the system. Due to this rotation the peak is shifted above the point $(0, 0)$. Then, subsequent pulses shift it down, toward the point of the initial position. Moreover, during the last stage, the Q -function is transformed close to its initial form corresponding to the vacuum state. This mechanism leads to evolution of the system within a finite set of n -photon states and, in consequence, to the generation of states with finite energy. Moreover, the field state, and the mean values plotted in Fig. 2 have periodic character.

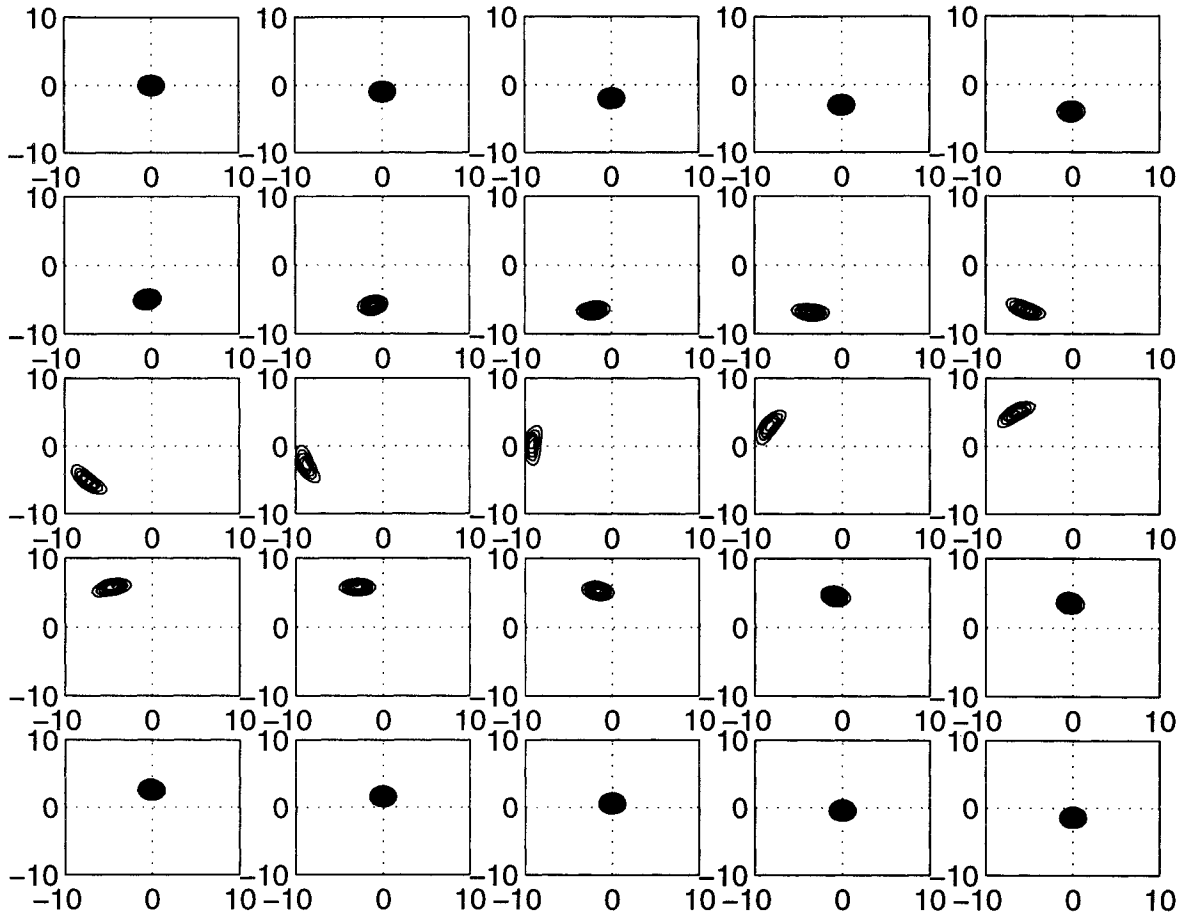


FIG. 2. The Q function evolution for the first 25 pulses. All parameters are the same as in Fig.2.

References

- [1] R. Tanaś, Phys. Lett. A **141**, 217 (1989)
- [2] J. R. Kukliński, Phys. Rev. Lett. **64**, 2507 (1990)
- [3] A. Miranowicz, R. Tanaś and S. Kielich, Quant. Opt. **2**, 253 (1990)
- [4] A. D. Wilson-Gordon, V. Bužek, and P.L. Knight, Phys. Rev. A **44**, 7647 (1991)
- [6] G. J. Milburn and C. A. Holmes, Phys. Rev. A **44**, 4704 (1991)
- [7] P Szlachetka, K. Grygiel and J. Bajer, Phys. Rev. E **48**, 101 (1993)
- [8] W. Leoński and R. Tanaś, Phys. Rev. A **49**, R20 (1994)
- [9] V. Peřinová, V. Vrana, A. Lukš, and J. Křepelka, Phys. Rev. A **51**, 2499 (1995)
- [10] W. Leoński, S. Dyrting, and R. Tanaś, J. Mod. Opt. **44**, 2105 (1997)
- [11] W. Leoński, Phys. Rev. A **54**, 3369 (1996)
- [12] W Leoński, Physica **223**, 365 (1996)

Frequency noise reduction of a DFB diode laser at 1393 nm

L. Gianfrani^{*}, G. Gagliardi, G. Rusciano, and A. Sasso
*INFN, Unità di Napoli, and Dipartimento di Scienze Fisiche,
Università "Federico II" di Napoli
Complesso Universitario di Monte S. Angelo, Via Cintia, I-80125 Napoli, Italy*

Abstract

The frequency of a 1393-nm distributed feedback diode laser was stabilized to a high finesse Fabry-Perot cavity by means of the Pound-Drever-Hall method. Short term stability was determined through measurements of the Allan variance for different integration times. We found a minimum root Allan variance of about 20 KHz, for an integration time of 1 ms.

Line narrowing in diode laser is always a topic of big interest. This is due to the fact that in several fields, such as high resolution spectroscopy, optical communications, optical precision measurements and laser cooling, improvements of the diode laser coherence are often required. Recently, new diode lasers have been developed, namely distributed feedback (DFB) and distributed Bragg reflector (DBR) diode lasers [1], operating in the relevant spectral region between 1 and 2 μm . They offer improved performances in terms of spectral purity and frequency tuning, with respect to previous generations of diode lasers. Nevertheless, the emission line width still ranges from few MHz up to few tens of MHz. Line narrowing is possible using a mirror-extended cavity configuration [2]. A further stabilization can be achieved by using a FM sideband technique [3]. This method has been successfully applied to 1.5- μm DFB [3] and 1.08- μm DBR [4] diode lasers.

In this work, we have reduced the frequency noise of a DFB diode laser at 1393 nm down to few tens of KHz. Our motivation is the sensitive detection of water vapour roto-vibrational lines using an optical cavity as a common gas cell. Direct measurements of absorption losses inside the passive resonator can be performed through measurements of changes in the cavity transmission [5]. For the best signal-to-noise ratios, a stable coupling of the laser radiation inside the resonator is necessary [6]. This requires a narrowing of the laser emission. For these proceedings, we will emphasise the experimental results concerning frequency-noise reduction of our laser source.

We mounted a 1393-nm DFB diode laser (Sensors Unlimited mod. SU1393-DFB-TE) in a mirror-extended cavity configuration, by using a 50% beamsplitter. In this configuration the laser line width was reduced from 20 MHz down to about 2 MHz. Continuous frequency scans were possible by varying the injection current and the extended cavity length by means of a piezoelectric actuator. The reference cavity is a confocal Fabry-Perot resonator formed by an invar tube and two identical concave 10-cm-radius mirrors, with a reflectivity of 99.7 %, for this spectral region. We facilitated the mode matching into the cavity using beam-shaping optics to partially correct the astigmatism and the asymmetry of the spatial mode, and a 30-cm focal length lens. The resulting coupling efficiency, measured on cavity reflection, was about 30 %. The laser source was frequency locked to the cavity using the Pound-Drever-Hall method [7]. Small sidebands at 24 MHz were impressed on the laser beam through an electro-

^{*} Also at Dipartimento di Scienze Ambientali, Seconda Università di Napoli, Caserta, Italy.

optic modulator. As shown in Fig. 1, heterodyne detection of the cavity reflected beam furnished a dispersion signal, with a sharp zero in correspondence of a cavity resonance, which was used as an error signal to actively control both the diode injection current and extended cavity length. A two path servo loop was built: a *slow* loop, acting on the extended cavity length within an electronic bandwidth of about 1 KHz, and a *fast* loop, controlling the injection current in a 150-KHz wide band. The integrators of both loops have the same electronic design, similar to that reported in ref. 8.

First, we analyzed the performance of our frequency-locking system recording the Fourier spectrum of the error signal in different situations. Fig. 2 shows the noise spectrum of the error signal for different values of the *fast* loop gain. The electronic bandwidth, in which corrections of the servo take place, increases with the gain. At these Fourier frequencies, the AM noise imposed on the error signal is drastically reduced.

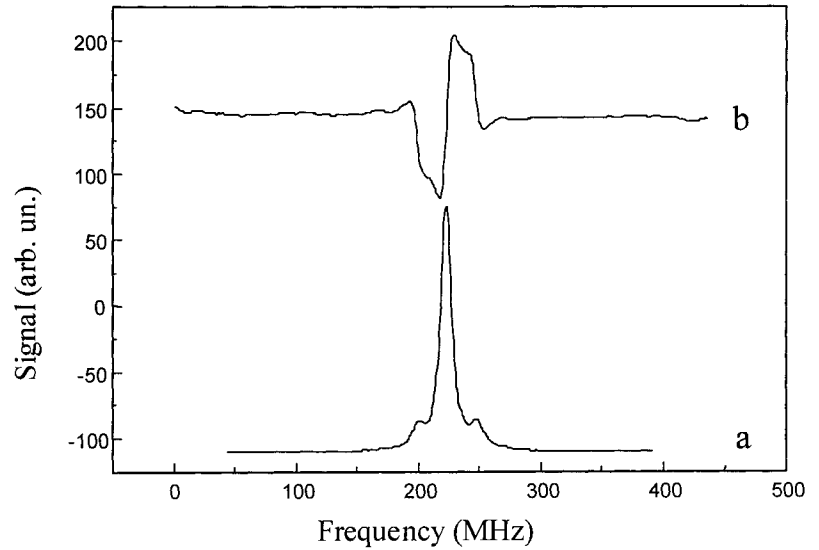


Fig. 1. Trace "a" is the spectrum recorded on cavity transmission during a cavity scan around a resonance frequency. Trace "b" is the error signal used to feed back the diode laser injection current and extended cavity length.

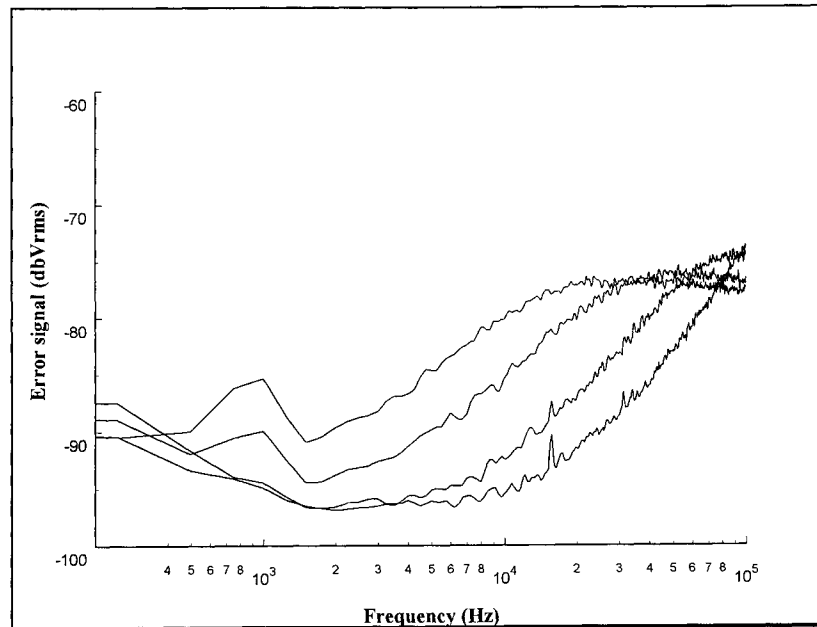


Fig. 2. Noise spectral density of the error signal for increasing servo gains.

At the maximum gain, the system starts to auto-oscillate at a frequency of about 150 KHz. When the laser is locked, the noise spectral density of the error signal provides information on phase and frequency fluctuations of the laser with respect to the cavity resonance frequency. In other words, the Allan variance can be evaluated for different integration times τ . At time scales longer than the optical storage time of the high finesse cavity (≈ 150 ns), the Allan variance quantifies laser frequency fluctuations. At shorter time scales, it is possible to get information about the laser phase variations and laser line width.

In general, the average angular frequency $\Omega_\tau(t)$ of a simple oscillator is defined as [9]:

$$\Omega_\tau(t) = \frac{1}{\tau} [\Phi(t + \tau) - \Phi(t)].$$

Here τ is the integration time. So the Allan variance $\sigma^2(\tau)$ is given by:

$$\sigma^2(\tau) = \langle \Omega_\tau(t)^2 \rangle - \langle \Omega_\tau(t) \rangle^2$$

The experimental procedure, which we adopted to measure the Allan variance, is as follows. With the laser locked to the cavity, we low-pass filtered the error signal and recorded its variations as a function of the time, using a digital oscilloscope. Calibration of the error signal in terms of frequency was possible from Fig. 1. Near resonance, the error signal is proportional to the laser frequency offset from the resonance frequency. Hence, the calibrating factor is immediately deduced from a comparison of the error signal around the zero line with the trace “a”.

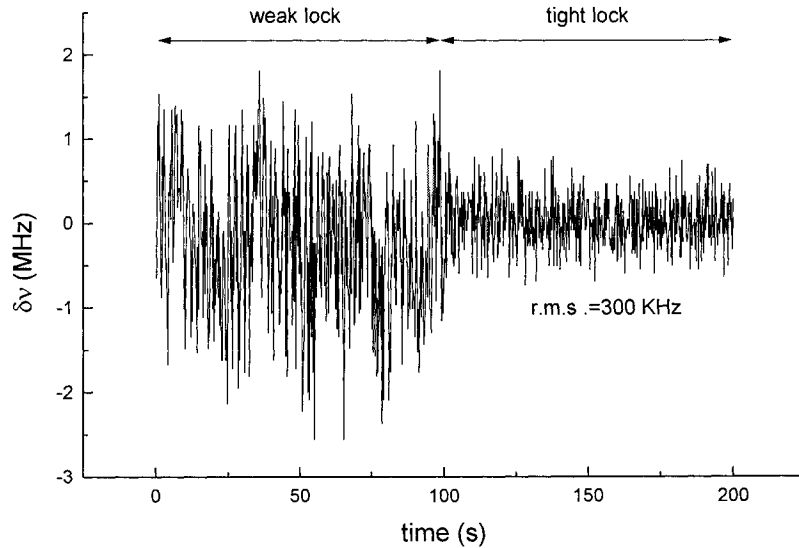


Fig. 3. Time trace of the error signal while the laser was weakly and tightly locked to the cavity. The integration time is $1 \mu\text{s}$. Frequency fluctuations are about 3 times greater in the case of a weak lock.

Examples are reported in Fig. 3, in the case of a loose lock (at low gain) and a tight lock (at the maximum gain). The root of the Allan variance is furnished by the root mean square of the trace. Note the larger fluctuations in the case of a loose lock. These measurements, for a tight lock, were repeated at different integration times, ranging from 40 ns to 3 s. The results are reported in fig. 4. A minimum of about 20 KHz was found for $\tau = 1$ ms, while for $\tau = 40$ ns, i.e. below the cavity storage time, we measured about 320 KHz.

The results above reported will be of great importance for our experiments of ultra-high resolution spectroscopy of H₂O roto-vibrational lines. Possible improvements of the system efficiency, actually limited by the current driver bandwidth, could be achieved if high frequency servo corrections were fed back directly to the diode laser cathode, through a bias-tee connection.

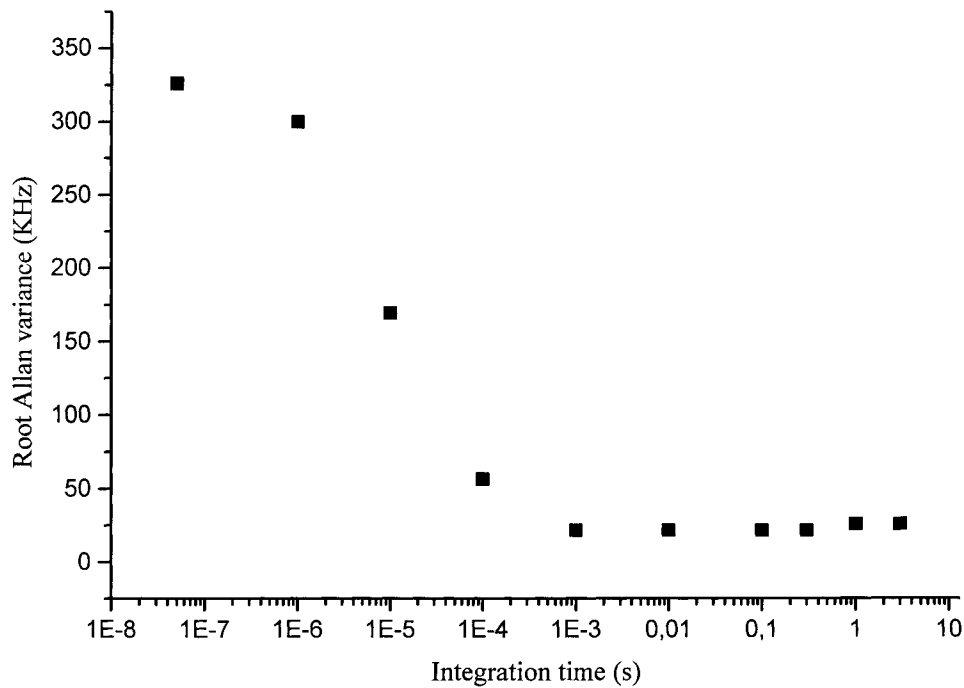


Fig. 4. Experimental values of the root Allan variance for different integration times. Below 150 ns, we found a value of about 320 KHz.

References

- [1] D.E. Cooper and R.U. Martinelli, Laser Focus World, 133, Nov. 1992
- [2] M. Prevedelli et al., Opt. Comm. 125, 231 (1996)
- [3] K. Nakagawa et al., Opt. Lett. 17, 934 (1992)
- [4] G. Bianchini et al., Appl. Phys. B 66, 407 (1998)
- [5] L. Gianfrani, R.W. Fox, and L. Hollberg, J. Opt. Soc. Am. B, to be published
- [6] J. Ye, L.-S. Ma, J. L. Hall, J. Opt. Soc. Am. B15, p. 6, 1998.
- [7] R. W. P. Drever et al., Appl. Phys. B 31, 97 (1983)
- [8] R.W. Fox, L. Gianfrani, and L. Hollberg: SPIE volume 3491, 794 (1998)
- [9] D. W. Allan, Proc. of the IEEE 54, 221 (1966)

The quadrature-phase squeezed state field generated by the ultrahigh Q single-mode laser

Mikio Fujii

*Department of Physics, Waseda University
Ohkubo 3-4-1, Shinjuku, Tokyo, 169-0072, Japan
Tel +81-3-5286-3440, Fax +81-3-3200-2567
E-mail: 697L5226@mn.waseda.ac.jp*

Abstract

The quadrature-phase squeezed states satisfying the detailed balance condition on the photon number state is suggested as the ansatz for the Scully-Lamb laser master equation. In a laser cavity with the extremely high quality factor Q , the squeezed states are shown to be kept squeezed long compared to the observation time.

In steady-state laser operation above threshold, the laser field is known to become a state quite similar to the Glauber's coherent state spontaneously. In the quantum theory of the laser in density operator approach, the field state is expressed by the density matrix on the photon number basis, where the detailed balance condition on the photon number state is satisfied [1]. But the laser field suggested by M. O. Scully and W. E. Lamb, Jr. in their original paper [1] is not the only field state satisfying the detailed balance condition. The squeezed states satisfying the detailed balance condition are newly suggested by using the *phase order parameter*, and time evolution of those initially squeezed states is numerically calculated in this presentation. The suggested squeezed states are the quadrature-phase squeezed states whose photon number statistics is just the same as that of the Scully-Lamb field. It is shown that those initially squeezed states are kept squeezed long compared to the observation time (assuming of the order 10^{-3}) in a laser cavity with extremely high Q quality factor.

In density operator approach developed in [1], the master equation for the single-mode laser field is given by

$$\frac{1}{C} \frac{d\rho_{n,n-k}}{dt} = -\frac{\left(n+1-\frac{k}{2}+\frac{k^2}{8\beta}\right)\left(\frac{\alpha\beta}{C}\right)}{\beta+n+1-\frac{k}{2}+\frac{k^2}{16\beta}}\rho_{n,n-k} + \frac{\sqrt{n(n-k)}\left(\frac{\alpha\beta}{C}\right)}{\beta+n-\frac{k}{2}+\frac{k^2}{16\beta}}\rho_{n-1,n-1-k} - \left(n-\frac{k}{2}\right)\rho_{n,n-k} + \sqrt{(n+1)(n+1-k)}\rho_{n+1,n+1-k}. \quad (1)$$

In Eq.(1) α is variable on pumping rate, β is a constant related to decay rates of the lasing levels, given as $\beta = 3 \times 10^7$ and C is the decay constant given by $C = \nu/Q = c(1-R)/L$, where ν is the mode angular frequency, L is the length of the one-dimensional laser cavity, c is light velocity, and R is reflectance of mirrors at the ends of the cavity [2]. For

the ultrahigh Q laser where $L = 3 \times 10^3 \text{m}$, $R = 0.9999$ and $\nu = 2\pi \times 10^{15} \text{Hz}$, Q is given as $Q = 3 \times 10^{14}$ and C is given as $C = 1 \times 10^{15} \text{s}^{-1}$.

From the steady-state solution of diagonal elements for Eq.(1), off-diagonal elements with the phase factor is given as

$$\rho_{n,n-k}(t) = \frac{\exp(-\beta - \bar{n})(\beta + \bar{n})^{\beta+n-\frac{k}{2}}}{\sqrt{(\beta+n)!(\beta+n-k)!}} e^{i(\theta_n - \theta_{n-k})} T_{n,k}(t) \quad \left(\frac{\alpha}{C} > 1\right), \quad (2)$$

$$T_{n-k,-k}(t) = T_{n,k}(t)^* \quad (t \geq 0), \quad (3)$$

$$T_{n,k}(0) = 1. \quad (4)$$

The pumping parameter α is fixed so that the average photon number \bar{n} is given as $\bar{n} = 1 \times 10^8$. The initial photon state is determined using the "phase order parameter" Δ , defined by

$$\Delta \equiv (\theta_{n+2} - \theta_{n+1}) - (\theta_{n+1} - \theta_n). \quad (5)$$

Δ is a squeezing parameter which determines the degree of squeezing and the argument of the phaser in the range of $|\Delta| \leq \bar{n}^{-1}$. The solution for (1) is found in the form

$$T_{n,k}(t) = \exp[(-p_{n,k} + iq_{n,k})t], \quad (6)$$

where

$$p_{n,k} = C \left\{ \frac{\left(n+1 - \frac{k}{2} + \frac{k^2}{8\beta}\right)(\beta + \bar{n})}{\beta + n + 1 - \frac{k}{2} + \frac{k^2}{16\beta}} + \left(n - \frac{k}{2}\right) - \left[\frac{\sqrt{n(n-k)(\beta+n)(\beta+n-k)}}{\beta + n - \frac{k}{2} + \frac{k^2}{16\beta}} + \sqrt{\frac{(n+1)(n+1-k)}{(\beta+n+1)(\beta+n+1-k)}}(\beta + \bar{n}) \right] \cos(k\Delta) \right\} \quad (7)$$

and

$$q_{n,k} = C \left[\sqrt{\frac{(n+1)(n+1-k)}{(\beta+n+1)(\beta+n+1-k)}}(\beta + \bar{n}) - \frac{\sqrt{n(n-k)(\beta+n)(\beta+n-k)}}{\beta + n - \frac{k}{2} + \frac{k^2}{16\beta}} \right] \sin(k\Delta), \quad (8)$$

when $T_{n-1,k} \simeq T_{n,k} \simeq T_{n+1,k}$.

For the Hermitian amplitude operators $\hat{X} \equiv (\hat{a} + \hat{a}^\dagger)/2$ and $\hat{Y} \equiv (\hat{a} - \hat{a}^\dagger)/(2i)$, we find

$$\begin{aligned} & \langle (\Delta X)^2 \rangle(\Theta, t) \\ &= \frac{1}{4} \left\{ 1 + 2 \sum_{n=0}^{\infty} \exp(-\beta - \bar{n}) \frac{(\beta + \bar{n})^{\beta+n+1}}{(\beta+n)!} \sqrt{\frac{(n+2)(n+1)}{(\beta+n+2)(\beta+n+1)}} \right\} \end{aligned}$$

$$\begin{aligned}
& \times \exp(-p_{n+2,2}t) \cos[2\Theta + \Delta(2n+1) + q_{n+2,2}t] \\
& + 2\bar{n} \\
& -4 \left[\sum_{n=0}^{\infty} \exp(\beta - \bar{n}) \frac{(\beta + \bar{n})^{\beta+n}}{(\beta+n)!} \sqrt{\frac{(\beta + \bar{n})(n+1)}{\beta+n+1}} \right. \\
& \quad \left. \times \exp(-p_{n+1,1}t) \cos(\Theta + \Delta n + q_{n+1,1}t) \right]^2 \Big\}, \tag{9}
\end{aligned}$$

$$\langle (\Delta Y)^2 \rangle (\Theta, t) = \langle (\Delta X)^2 \rangle \left(\Theta - \frac{\pi}{2}, t \right), \tag{10}$$

where $\Theta \equiv \theta_1 - \theta_0$ is an arbitrary phase constant. $\Theta_0(t)$ is defined to satisfy

$$\langle (\Delta X)^2 \rangle (\Theta_0(t), t) \leq \langle (\Delta X)^2 \rangle (\Theta, t), \tag{11}$$

for all Θ . If $\sqrt{\langle (\Delta X)^2 \rangle (\Theta_0(t), t)} < 1/2$, the field is a squeezed state at time t . Fig.1. shows that the squeezed state at the initial time is kept squeezed for times $0 \leq t \ll C^{-1}$.

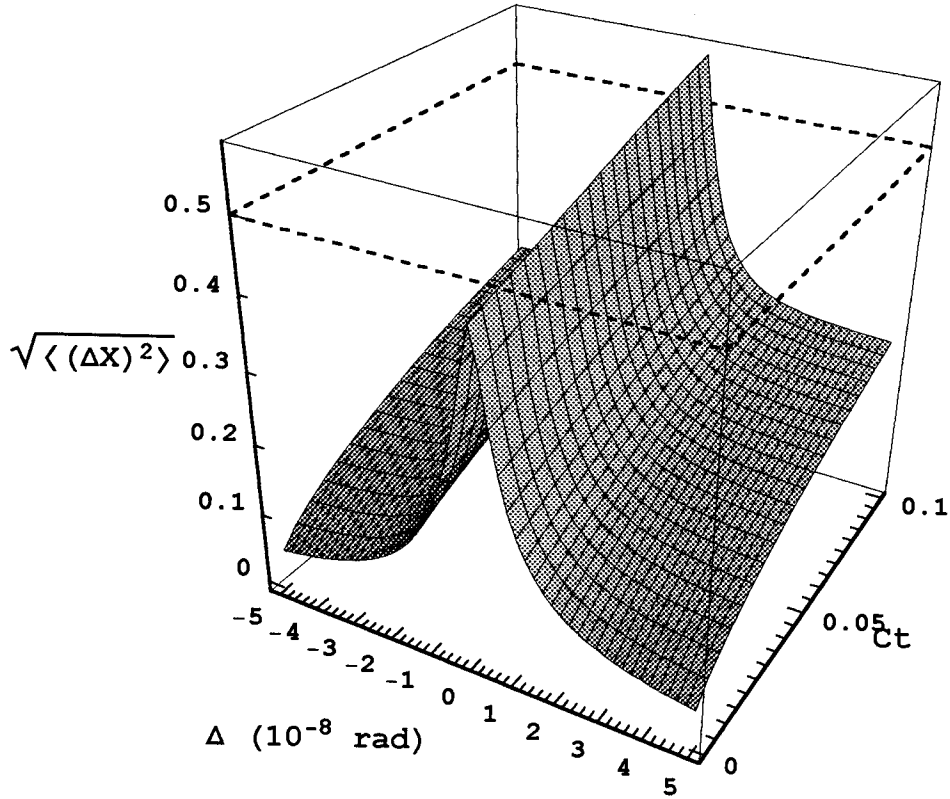


FIG. 1.

References

- [1] M. O. Scully and W. E. Lamb, Jr., Phys. Rev. **159**, 208 (1967).
- [2] Rodney Loudon, *The Quantum Theory of Light, second edition*, (Oxford University Press, New York 1983).

SQUEEZED LIGHT PUMPED Cs BEAM ATOMIC CLOCK

G. M. SAXENA, A. AGARWAL, A.CHATTERJEE AND B.S.MATHUR.
*NATIONAL PHYSICAL LABORATORY, DR.K.S.KRISHNAN ROAD,
NEW DELHI-110012 INDIA*

The optically pumped Cesium (Cs) atomic beam Clock is the Primary Time and Frequency Standard. The frequency stability of the optically pumped Cs standard is ultimately limited by the atomic shot noise. However, the frequency fluctuations due to the quantum noise in the laser light used for the optical pumping ($F = 3 \rightarrow F' = 3, \pi$; $F = 4 \rightarrow F' = 4, \sigma$) and detection ($F = 4, m_F = 0 \rightarrow F' = 5, m_{F'} = 0$) also affect the performance of the standard. We shall discuss in this paper the application of the squeezed light for obtaining higher optical pumping rate and narrower resonance fluorescence lineshape. The optical pumping is used for the particle preparation, which plays an important role in determining the S/N and the frequency stability of the standard. In the detection region the application of the squeezed light results in line narrowing of the resonance fluorescence of the Cs atom-squeezed light interaction. We have theoretically found that the resonance fluorescence signal linewidth may be reduced by 1/5th on squeezing the light. The use of the squeezed light for optical pumping and detection may improve the frequency stability of the optically pumped Cs Clock almost by one order of magnitude.

1 Introduction

The optically pumped Cs atomic beam clock [1-3] is being used as national Time and Frequency Standard in several countries. Even after controlling the technical noises and evaluating the deterministic frequency shifts, the frequency stability of the Standard is affected by several factors like laser frequency fluctuations and the photon detection noise. However, the ultimate frequency stability is restricted by the atomic shot noise [4].

In this paper we shall discuss the application of the squeezed light for reducing the laser frequency fluctuations arising due to the quantum noise. The application of the squeezed states will be both for the optical pumping and resonance fluorescence detection.

The schematic diagram of the optically pumped Cs atomic beam Time and Frequency Standard is shown in Fig. 1. We shall briefly describe in Section 2 the Cs atomic beam tube of the Cs atomic beam clock, on which critically depends the performance of the standard. Section 3 describes the interaction of Cesium atoms with the squeezed light. In Section 4, the frequency stability of the Cs clock with squeezed light is discussed. Finally, we summarize our results in Sec. 5.

2 The Cs atomic beam tube

The Cs atomic beam tube of the optically pumped Cs atomic beam frequency standard has three distinct regions. In the first region we have a Cs oven at temperature of about 90° C which produces the ribbon shaped Cs atomic beam. The beam is collimated by multi-channel array of crinkled nickel foils. The oven is followed by a Ramsey microwave cavity. In the region between the oven and Ramsey cavity optical pumping of Cs atoms takes place. The two lasers are used for obtaining large population inversion. The optical pumping transitions between $F = 3 \rightarrow F' = 3, \pi$ and $F = 4 \rightarrow F' = 4, \sigma$ yield large population in the desired ground state hyperfine sublevel $F = 3, m_F = 0$. The population of this optically pumped sublevel is a function of the light intensity, interaction time and linewidth of the pumping light. In the second region Cs atoms undergo the microwave transition in the Ramsey cavity. The Ramsey cavity is of copper and works in the transverse magnetic field mode. The cavity length is 1 m and its $Q = 5000$. On the both sides of the cavity, holes are drilled for the Cs beam to pass through. After the microwave interaction in the Ramsey cavity, Cs atoms are transferred to the ground state hyperfine sublevel $F = 4, m_F = 0$. The length of the field free region or the time of interaction between the microwave and Cs atoms determines the linewidth of the Ramsey fringes on which depends the frequency stability of the clock. In the third region which is the detection region these atoms interact with the orthogonal optical beam of intensity 3mW cm^{-2} tuned and locked, using saturation absorption cell, to $F = 4 \rightarrow F' = 5$ cyclic transition for detecting the number of Cs atoms which undergo the microwave transitions. The resonance fluorescence signal of the atom-light interaction is collected and focussed onto a silicon photodiode by the means of a spherical mirror and two aspherical lenses. The collection efficiency of the detection system is about 50%. The frequency fluctuations due to the quantum noise in the detection laser light get coupled to the atomic beam via lightshift and scattering. The linewidth of the resonance fluorescence signal is determined by the quantum noise in the probe or detection light. However, The non-classical source of the detection light may improve the S/N and thus narrow down the linewidth of the resonance fluorescence signal [5].

3 Interaction of Cs atoms with Squeezed light

We consider the interaction of the Cs atomic beam with a squeezed light. The schematic diagram of the experimental set-up is shown in the Fig. 2. While considering the atom-squeezed light interaction we make the following assumptions:

1. The collisions between the Cs atoms are very small and neglected. Cs atoms are mono-kinetic. As the Cs atomic beam and the squeezed detection light are at right angle to each other, the first order Doppler shift is absent. However, the second order Doppler or the relativistic frequency shift is still present. The squeezed light will be generated using the optical parametric oscillator (OPO) [6]. The correction for the second order Doppler frequency shift is applied by suitably shifting the OPO pump frequency.

2. The squeezed light linewidth is of the order of the natural linewidth of the frequency of transitions between $S_{1/2} \rightarrow P_{3/2}$ levels of the Cs atoms.

3. The intensity of the squeezed light for optical pumping and detection is small.

4. We consider the Cs atom to be a two level atom for the detection of the cyclic transition between the levels $S_{1/2}F = 4 \rightarrow P_{3/2}F' = 5$. While for the optical pumping with two lasers, we take a three level ($S_{1/2}F = 3, F = 4; P_{3/2}F' = 3$ and $S_{1/2}F = 4, F = 3; P_{3/2}F' = 4$.) approximation with the lambda configuration.

We shall describe the optical pumping of the Cs atoms, and the detection of the atoms undergoing the microwave transitions.

3.1 Optical Pumping of Cs Atoms with Squeezed light

In the conventional optically pumped Cs atomic beam frequency standard two diode lasers of wavelength 852nm and intensity 3mW cm^{-2} are used for the efficient optically pumping of atoms to the ground state sublevel $F = 3, m_F = 0$. The diode lasers are tuned to the levels $F = 3 \rightarrow F' = 3, \pi$ and $F = 4 \rightarrow F' = 4, \sigma$ respectively. The particle preparation has significant impact on the S/N of the clock signal. If the particle preparation is not perfect then the laser frequency fluctuations may add to the atomic shot noise and the S/N of the clock signal in the detection region is degraded for a particle flux above 10^8 atom/sec. The effect of the laser frequency fluctuations on the particle preparation and hence on the clock S/N may be reduced by the use of squeezed light. It has been shown [7] that the use of the squeezed light enhances the pumping rate, compared to the case when coherent light is used, leading to the better particle

preparation. While using the squeezed light for the particle preparation it is assumed that it has low intensity, the coupling between the atoms and squeezed light is weak except in the cavity environment and the bandwidth of the pump light is comparable to the natural linewidth of the atomic transitions. The enhancement in the pumping rate largely depends on the coupling coefficient. The improvement in the S/N will depend on the squeeze factor.

3.2 Detection of the Resonance Fluorescence Signal

We shall now discuss the interaction of the squeezed light with the Cs atomic beam in the detection region of the atomic beam tube. We shall assume that the squeezed light is of linewidth comparable to the natural linewidth of the atomic transitions so that leakages to neighboring levels is negligible and we have effectively two-level atomic system approximation for the cyclic transition $F = 4 \rightarrow F' = 5$. The correction for the second order Doppler frequency shift due to the Maxwellian velocity distribution of the moving Cs atoms is incorporated by shifting the frequency of the OPO pump. For the cyclic transition $F = 4 \rightarrow F' = 5$ the stationary line shape of the resonance fluorescence signal is given by the expression [5,8] :

$$I = \frac{1}{2}\mu(N + M)\frac{\frac{1}{2}\Gamma + \mu}{(\frac{1}{2}\Gamma + \mu)^2 + \Delta^2} + \frac{1}{2}\lambda(N - M)\frac{\frac{1}{2}\Gamma + \lambda}{(\frac{1}{2}\Gamma + \lambda)^2 + \Delta^2}. \quad (1)$$

where γ is the spontaneous decay rate into the normal vacuum modes of the Cs atoms, $\Delta = \omega_L - \omega_0$ is the detuning, ω_L is the second order Doppler shifted frequency of the squeezed radiation and ω_0 is the Cs atomic transition frequency ($F = 4 \rightarrow F' = 5$). N and M are the parameters pertaining to the squeezing. They are related to the parameters μ and λ which determine the linewidth of the squeezed field and also determine the degree of squeezing. The relationship among these parameters is given below.

$$N - M = -\frac{\lambda^2 - \mu^2}{2\lambda^2}. \quad (2)$$

$$N + M = \frac{\lambda^2 - \mu^2}{2\mu^2}. \quad (3)$$

where $\mu = 1/2\gamma - \epsilon$, $\lambda = 1/2\gamma + \epsilon$; γ is the damping constant of the OPO and ϵ is its amplification parameter. It is observed from the Eq. 1 that the resonance fluorescence line shape is made up of two terms. For $M > N$ the contribution of the second term in the equation is negative. This results in the narrowing of the line shape of the resonance fluorescence. Our theoretical calculations [8] have shown that with squeezed light, under the optimum experimental conditions, the resonance fluorescence line width may be

narrowed by about 1/5th of the Lorentzian linewidth $(1/2\gamma + \mu)$ (Fig.3). The narrowing of the linewidth will be reflected in the improvement in the frequency stability of the optically pumped Cs atomic frequency and time standards because of the higher clock S/N.

4 Frequency Stability of Cs Clock

The frequency stability of a optically pumped frequency standard is given by [9]

$$\sigma(\tau) \approx \frac{\delta\nu \tau^{-1/2}}{\nu (S/N)}. \quad (4)$$

here ν is the microwave clock transition frequency (9.192 GHz), $\delta\nu$ is its linewidth, τ is the sampling time and S/N is the clock signal to noise ratio. The clock S/N represents the effect of all noise processes including the atomic shot noise, laser frequency fluctuations, photon shot noise and the noise of the detection system. The use of the squeezed light for the particle preparation reduces contribution of the pumping light frequency fluctuations to the atomic shot noise. In the detection region, use of the squeezed light, as a probe, reduces the noise bandwidth of the detection system because of narrowing of the resonance fluorescence signal. The overall enhancement in the clock S/N and the lowering of the minimum detectable signal level due to the use of the squeezed light for the optical pumping and detection will depend on the squeeze factor and degree of coupling between the squeezed mode of light and the Cs atoms. The optical cavity environment will increase the coupling coefficient [7]. An improvement by one order in the frequency stability of the standard may be expected with the application of the squeezed light. However, much depends on the coupling of the squeezed light to the Cs atoms.

5 Conclusion

In this paper we have studied the application of the squeezed light for the optical pumping of the Cs atoms and their detection. We expect that frequency stability of the Cs atomic clock may be improved by an order. However, it depends on the coupling of the squeezed light with atoms. The ultimate frequency stability will depend on the atomic shot noise or the projection noise. The atomic shot noise can also be manipulated by the squeezed light [10]. However, the experimental realization of the tunable source of the squeezed light is a prerequisite for its successful application to the Cs clock.

6 Acknowledgements

The discussions on squeezed states with Prof. C.L.Mehta, I.I.T. Delhi are gratefully acknowledged. The authors are thankful to NIST, USA for the financial support for this work under the US-India fund project code NIST G040

References

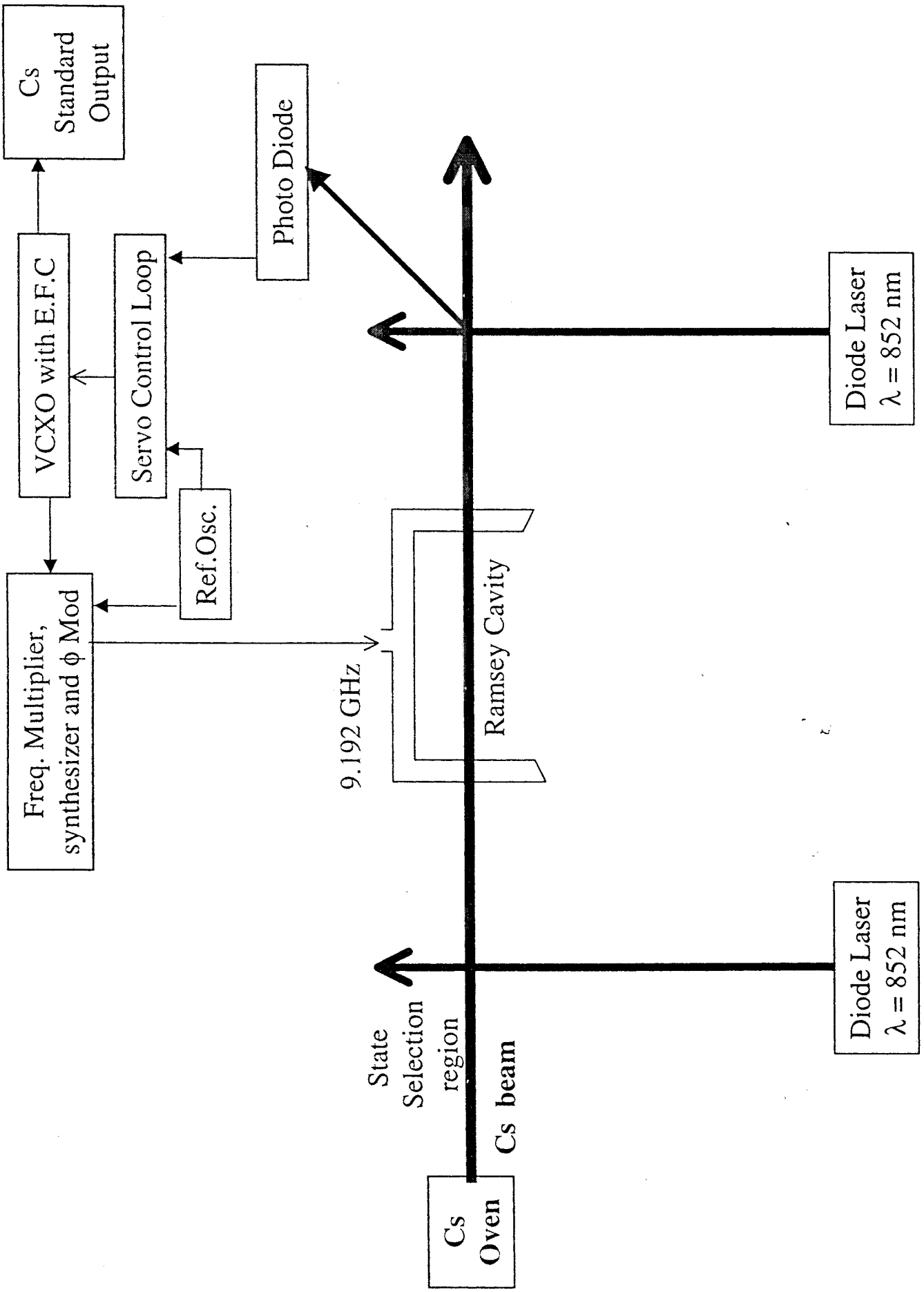
- [1] R.E.Drullinger, D.J.Glaze, J.P.Lowe and J.H.Shirley, IEEE Tran. Instru. Meas. **40**, 162 (1991).
- [2] E.de Clercq, G.D.Rovera, S.Bouzig and A.Clairon, IEEE Tran. Instru. Meas. **42**, 457 (1993).
- [3] R.E.Drullinger, J.H.Shirley, J.P.Lowe and D.J.Glaze, IEEE Tran. Instru. Meas. **42**, 453 (1993).
- [4] N.Dimarco, V.Giordano, P.Cerez and G.Theobald, IEEE Tran. Instru. Meas. **42**, 115 (1993).
- [5] Z.Ficek, J.Seke, R.Kralicek and G.Adam, Opt. Commun. **147**, 289 (1998).
- [6] E.S.Polzik, J.Carri and H.J.Kimble, Appl. Phys. B **55**, 279 (1992).
- [7] A.S.Parkins, Phys. Rev. A **53**, 2893 (1996).
- [8] A.Agarwal, B.S.Mathur and G.M.Saxena, 16th Int'l Conf. on CODATA, New Delhi-India, Abs.91, 8-12 Nov.1998.
- [9] J.Vernier and C.Audoin, in *The Quantum Physics of Atomic Frequency Standards* (Adam Hilger, Bristol, U.K 1989).
- [10] J.L.Sresen, J.Hald and E.S.Polzik, Phys. Rev. Lett. **80**, 3487 (1998).

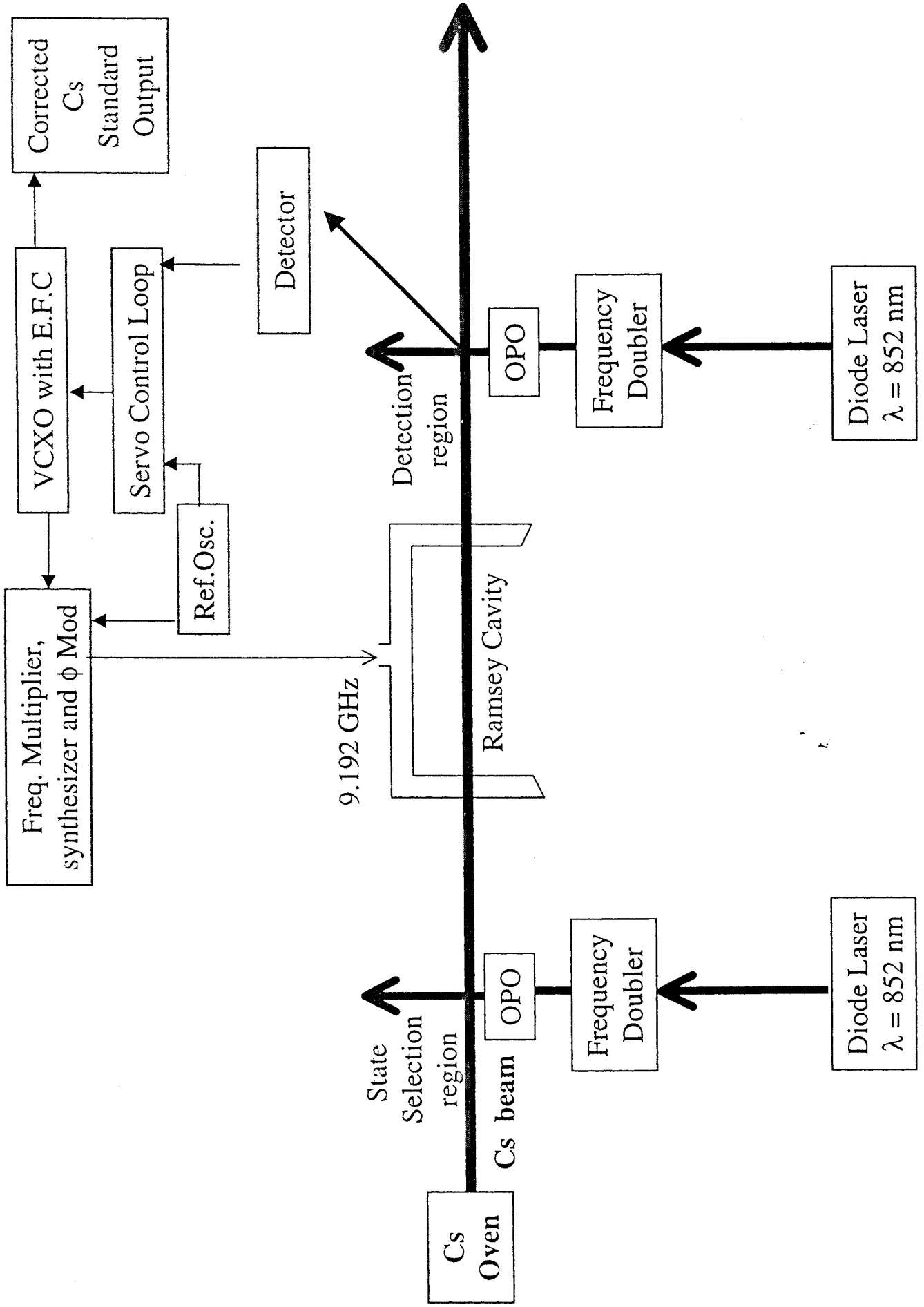
Figure Captions

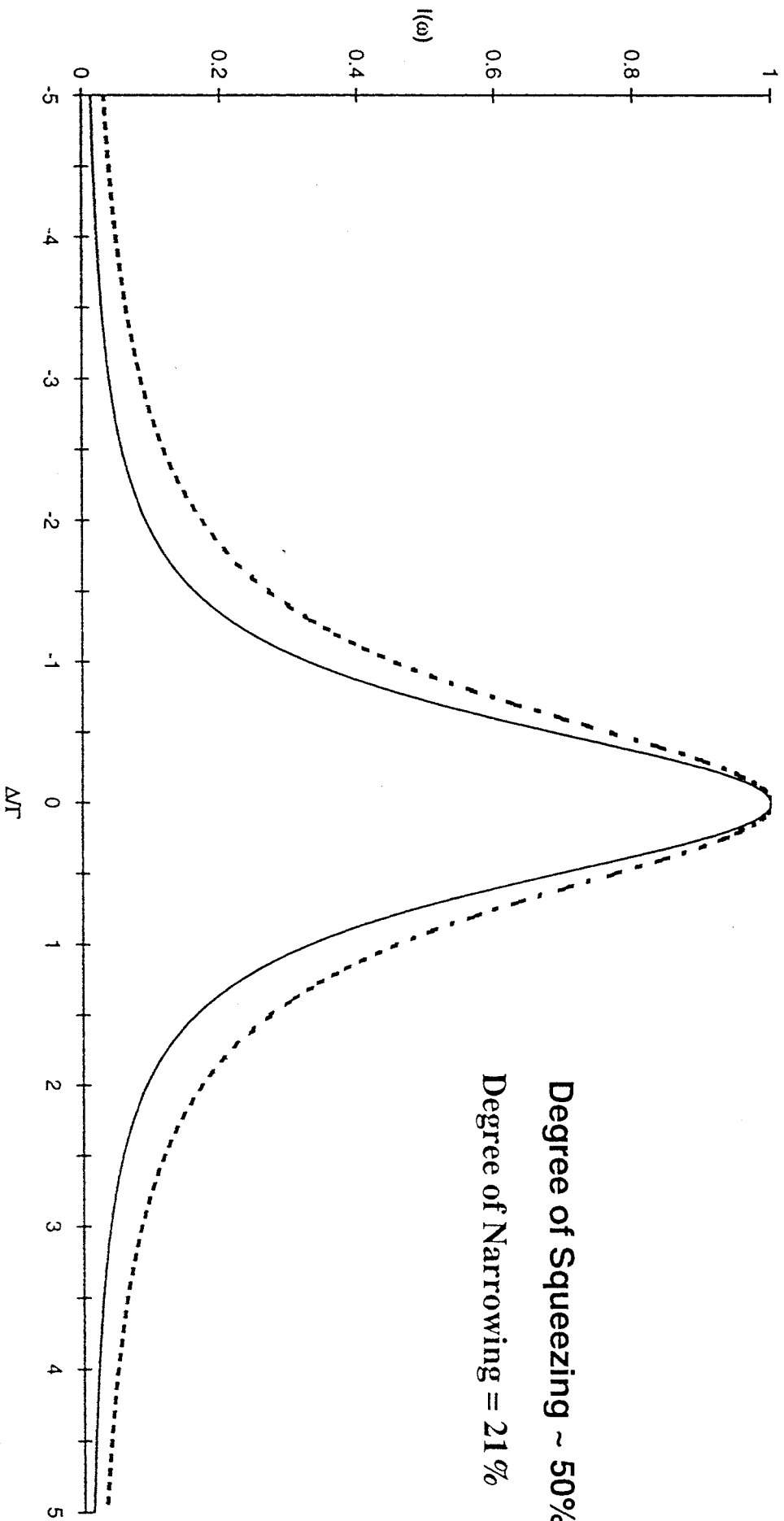
Fig. 1. Schematic diagram of the optically pumped Cesium frequency standard.

Fig. 2. Schematic diagram of the squeezed light pumped Cesium frequency standard

Fig. 3. Narrowing of the stationary lineshape (solid curve) as a function of Δ/Γ for $N = 1/8$, $M = 3/8$, $\epsilon/\gamma_c = 0.0858$ and $\gamma_c/\Gamma = 1.0$. The dotted curve is the Lorentzian of width $\Gamma/2 + \mu$.







Degree of Squeezing ~ 50%

Degree of Narrowing = 21%

Cascaded optical homodyne detection

Z. Kis, T. Kiss, J. Janszky and P. Adam

*Department of Nonlinear and Quantum Optics, Institute for Solid State Physics and Optics, P.
O. Box 49, H-1525 Budapest, Hungary*

S. Wallentowitz and W. Vogel

*Arbeitsgruppe Quantenoptik, Fachbereich Physik, Universität Rostock, Universitätsplatz 3,
D-18051 Rostock, Germany*

Abstract

In our proposal two different kinds of homodyne arrangements are applied in cascade, in order to locally sample the phase-space distribution of a one mode radiation field.

I. INTRODUCTION

Optical homodyning [1], both in balanced [2] and unbalanced [3] form, has recently been used in experiments to reconstruct the quantum state of a single mode travelling light field. In the unbalanced scheme the phase space is scanned locally. The point of interest is chosen by the complex amplitude of the local oscillator. A technical difficulty in the unbalanced scheme stems from the lack of proper photon counters. On the other hand, very sensitive reconstruction of the photon statistics is possible with a phase randomized balanced homodyne detector [4]. In order to combine advantages of both methods we have recently proposed a cascaded scheme [5], where balanced and unbalanced arrangements are employed one after the other. In this way one can keep the local nature of the reconstruction, which means the point in phase space to be measured is selected by a physical process and not by an indirect numerical algorithm. The second part may seem to be a rather complicated photon counter, however, in recent experiments [6] balanced homodyne detection was proven to be the first method sensitive enough to measure the fine structure in the photon statistics of a single mode weak squeezed vacuum field.

II. THE SCHEME

The cascaded optical homodyne scheme is depicted in Fig. 1. The working principle of the scheme can be understood in two ways. One may think of it either as an unbalanced homodyne reconstruction scheme with a special photon counter or as balanced homodyning with an additional preparation step.

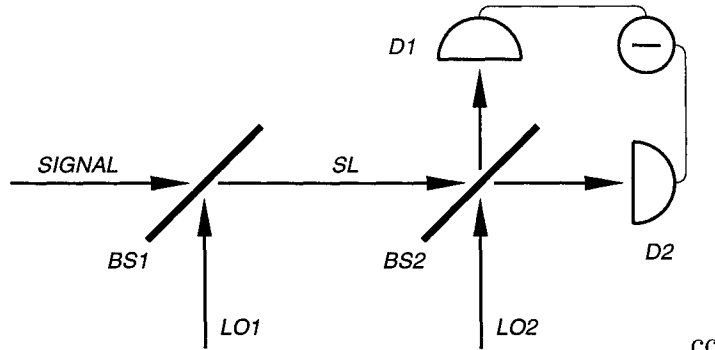


FIG. 1. Setup for cascaded optical homodyning. The first beam splitter $BS1$, with high transmission and low reflection, mixes the signal with the first local oscillator $LO1$. Then the transformed signal SL enters a phase-randomized balanced homodyne detector consisting of the beam splitter $BS2$ and the second local oscillator $LO2$ with random phase. The difference signal of the two linear photodiodes $D1$ and $D2$ provide the measured data $p(x; \alpha, \eta)$.

In the first approach one may start from the reconstruction formula [3]

$$W(\alpha; s) = \frac{2}{\pi(1-s)} \sum_{n=0}^{\infty} (-\xi)^n P_n(\alpha, \eta). \quad (1)$$

Here $P_n(\alpha, \eta)$ is the photon statistics of the intermediate signal SL , and the reconstructed quantity $W(\alpha; s)$ is the s parametrized quasiprobability of the signal. The $\epsilon = R/T \ll 1$ parameter characterizes the first beam splitter $BS1$, where R is the coefficient of amplitude reflection and $|T|^2 + |R|^2 = 1$. The complex amplitude β of the first local oscillator $LO1$ determines the complex variable ($\alpha = -\epsilon\beta$) of the quasiprobability function. The parameter $\xi = \xi(s, \eta)$ accounts for the detection losses and the ordering parameter of the desired quasiprobability distribution, it is given by $\xi(s, \eta) = (2 - \eta(1 - s))/(\eta(1 - s))$. The overall quantum efficiency η includes transmission losses at $BS1$ and other linear losses due to inefficient detection and e.g. mode mismatch. The photon statistics of the intermediate signal is provided by the theory of balanced homodyne detection [7] which requires an averaging of the measured difference photocurrent signal of detectors $D1$ and $D2$ $p(x; \alpha, \eta)$ with phase randomized local oscillator $LO2$ with respect to a so-called pattern function

$$P_n(\alpha, \eta) = \int_{-\infty}^{\infty} dx f_{nn}(x) p(x; \alpha, \eta). \quad (2)$$

The pattern function $f_{nn}(x)$ is characteristic for the given Fock state n , and has a non-trivial expression with the regular and irregular stationary solutions of the corresponding Schrödinger equation $f_{nn}(x) = \frac{\partial}{\partial x} [\psi_n(x)\varphi_n(x)]$. Combining equations (1) and (2) the integration and summation can be interchanged (if convergence is kept) and one arrives at the expression

$$W(\alpha; s) = \int_{-\infty}^{\infty} dx S(x; s, \eta) p(x; \alpha, \eta), \quad (3)$$

where S is a sampling function, given by the infinite sum of the pattern functions

$$S(x; s, \eta) = \frac{2}{\pi(1-s)} \sum_{n=0}^{\infty} [-\xi(s, \eta)]^n f_{nn}(x). \quad (4)$$

The limit of this series can be determined, and we have found a surprisingly simple analytical expression by exploiting the properties of the pattern functions [5]

$$S(x; s, \eta) = \eta / [\pi(\eta(1-s) - 1)] f_{00} \left(x / (\sqrt{\eta(1-s) - 1}) \right), \quad (5)$$

where the scaled zeroth pattern function occurs, which can be evaluated quite easily by using Dawson's integral $F(x)$ [8], as $f_{00}(x) = 2 - 4xF(x)$.

The second way to look at this scheme is to realize that the effect of the first beam splitter BS1 is essentially a displacement in phase space with an additional small smoothing due to the deviation from unit transparency [3]. The second part, a balanced homodyne detector, effectively measures the value of the transformed signal Wigner function in the origo of the phase space $W_{SL}(0) = W(\alpha)$. The phase averaged quadrature distributions measured by an ideal balanced homodyne detector $p(x; \alpha, \eta) = \frac{1}{\pi} \int_0^\pi \text{pr}(x, \theta) d\theta$ are related to the marginals of the Wigner function (with real variables) $\text{pr}(q, \theta) = \int_{-\infty}^{\infty} W_{SL}(q \cos \theta - p \sin \theta, q \sin \theta + p \cos \theta) dp$ (for simplicity, we do not include here in the derivation the detector efficiency, it can be treated as part of the overall quantum efficiency η). The Radon transformation in the previous expression may be inverted by filtered back projection. By Fourier transforming both sides with respect to q , inverting the occurring two-dimensional Fourier transform of the Wigner function and changing to polar coordinates, one derives the basic formula of filtered back projection

$$W(q, p) = \frac{1}{(2\pi)^2} \int_0^\pi d\theta \int_{-\infty}^{\infty} d\xi \int_{-\infty}^{\infty} dq' \text{pr}(q', \theta) e^{-i\xi(q' - q \cos \theta - p \sin \theta)} f(\xi), \quad (6)$$

where $f(\xi) = |\xi|$. In order to cut the high frequencies it is usual to introduce a filter function of the form $f(\xi) = |\xi| \Phi(\xi)$ where $\Phi(\xi)$ is a low pass window. In optical homodyne tomography it is advantageous to use a Gaussian window function, $\Phi_s(\xi) = e^{s\xi^2/4}$ with which the filter reads $f_s(\xi) = |\xi| e^{s\xi^2/4}$, s is a small real negative parameter. The Gauss filtered back projection yields the s -parametrized quasiprobability [9], i. e. a smoothed version of the Wigner function. Collecting the above results we find for the s parametrized quasiprobability in the origo $W_{SL}(0; s) = \int_{-\infty}^{\infty} dx p(x; \alpha, \eta) S(x; s)$ where $S(q'; s) = \frac{1}{4\pi} \int_{-\infty}^{\infty} d\xi e^{-i\xi q'} f_s(\xi)$. We have here inserted the definition of the phase averaged quadrature distribution, measured by the phase randomized homodyne detector. The Fourier transformed filter function serves as sampling function denoted by $S(x; s)$, which can be calculated by evaluating the above integral, yielding the same expression (5) as in the previous paragraph. The overall quantum efficiency can be included in his formula in a similar way as previously. By setting $s = -1$ we can reconstruct the Q function of the intermediate signal in the origo, which is nothing else than the vacuum Fock state probability $Q_{SL}(0, 0) = \langle 0 | \rho | 0 \rangle$. This fact explains why the scaled zeroth pattern function serves as the sampling function for the cascaded scheme, since the zero Fock state coincides with the zero coherent state.

It is interesting to note that the point-by-point reconstruction of the quasiprobability functions can help to directly find the density operator. For example, from the Q function

one can find the Glauber's analytic R function. The R function is defined by the relation $R(\alpha^*, \beta) = e^{\frac{1}{2}(|\alpha|^2 + |\beta|^2)} \langle \alpha | \hat{\rho} | \beta \rangle$. It can be expressed through the Q function as an analytic continuation by exchanging the two real variables by complex ones with the rule: $q \rightarrow \frac{1}{\sqrt{2}}(\alpha^* + \beta)$, $p \rightarrow \frac{1}{i\sqrt{2}}(-\alpha^* + \beta)$. The density operator is then obtained as

$$\hat{\rho} = \frac{1}{\pi} \int d^2\alpha d^2\beta e^{-\frac{1}{2}(|\alpha|^2 + |\beta|^2) + \alpha^*\beta} |\alpha\rangle Q\left(\frac{1}{\sqrt{2}}(\alpha^* + \beta), \frac{1}{i\sqrt{2}}(\beta - \alpha^*)\right) \langle \beta|. \quad (7)$$

The analytic continuation of a function requires its knowledge in an analytic form, which can be achieved by interpolating with some algorithm between reconstructed points of the Q function. This can be particularly useful if the general structure of the Q function is known, and thus the interesting regions in the phase space can be scanned systematically.

III. CONCLUSIONS

The cascaded homodyning scheme seems to be an experimentally feasible method for the local measurements in phase space. The sampling function we calculated analytically has a simple structure and is universal in the sense that it does not depend on the particular point where the quasiprobability function is reconstructed. Our simulations indicate that a rather low number of measurements is enough to check for negativities of a quasiprobability, distinguishing the superposition of two coherent states from a statistical mixture.

We acknowledge the support of a joint program of the DAAD (Deutscher Akademischer Austauschdienst) and MÖB (Magyar Ösztöndíj Bizottság). This work was partially supported by the National Research Fund of Hungary (OTKA) under Contracts T023777 and T020202.

References

- [1] U. Leonhardt, *Measuring the Quantum State of Light* (Cambridge University Press, Cambridge, 1997).
- [2] K. Vogel and H. Risken, Phys. Rev. A **40**, 2847 (1989); D. T. Smithey, M. Beck, M. G. Raymer, and A. Faridani, Phys. Rev Lett. **70**, 1244 (1993).
- [3] S. Wallentowitz and W. Vogel, Phys. Rev. A **53**, 4528 (1996); K. Banaszek and K. Wódkiewicz, Phys. Rev. Lett. **76**, 4344 (1996); K Banaszek, C. Radzewicz, K. Wódkiewicz, and J. S. Krasinski, Phys. Rev. A **60**, 674 (1999).
- [4] G. Breitenbach, S. Schiller, and J. Mlynek, Nature (London) **387**, 471 (1997).
- [5] Z. Kis, T. Kiss, J. Janszky, P. Adam, S. Wallentowitz, and W. Vogel, Phys. Rev. A **59** R39 (1999).
- [6] S. Schiller, G. Breitenbach, S. F. Pereira, T. Müller, and J. Mlynek, Phys. Rev. Lett. **77**, 2933 (1996).
- [7] U. Leonhardt, M. Munroe, T. Kiss, M.G. Raymer, and Th. Richter, Opt. Commun. **127**, 144 (1996).
- [8] For an efficient numerical calculation of Dawson's integral, $F(x) = \exp(-x^2) \int_0^x dt \exp(t^2)$, see Chap. 6.10 of W.H. Press, S.A. Teukolsky, W.T. Vetterling, and B.P. Flannery, *Numerical Recipes in C* (Cambridge University Press, 1995).
- [9] T. Kiss, *PhD thesis* Budapest, 1999.

Interferometers with Phase-Conjugate Mirrors and Light States

A. Garuccio, V.L. Lepore, D. Picca

Dipartimento Interateneo di Fisica and INFN - Sezione di Bari, Via. E. Orabona 4, 70126 Bari

V. Berardi, M. Dabbicco

INFN - Unitá di Bari and Dipartimento Interateneo di Fisica, Via E. Orabona 4, 70126 Bari

Abstract

The non usual behavior of an Michelson interferometer with phase conjugate mirrors (MIPCM) when classical and quantum light states impinge into the apparatus is described and discussed. Starting from the limits of the theoretical and experimental analysis of this device, a research program is presented whose attempt is to perform a more complete study of this interferometer. Moreover, the connections between the unexpected behaviors of MIPCM and the foundations of quantum mechanics will be carefully investigated.

I. Introduction

In the recent years the behavior of a Michelson interferometer with phase conjugate mirrors (MIPCM) has been investigated both theoretically and experimentally. This apparatus consists of a Michelson interferometer (Fig. 1) in which one metallic mirror is substituted for a phase conjugate mirror (*PCM*). A *PCM* is a non linear medium that performs a complex conjugation on the spatial part of the complex amplitude of an impinging electromagnetic field. The effect is to reflect the impinging wave back in the direction of propagation while changing the phase from α to $-\alpha$. Consequently, the *PCM* maintains the polarization state of the incident wave and, more precisely, a linear polarized wave is reflected as a linear polarized wave, while a circular polarized wave is reflected with identical circular polarization [1]. This behavior (different from that of a conventional mirror) has an interesting consequence on the visibility of the interference in the phase-conjugate interferometer as we will show in the next sections. Another interesting property is the so called "phase compensating effect" which consists of the independence of interference pattern of the length of the arm of the interferometer in which the *PCM* is placed.

Many of these effects are a function of the impinging state of light and therefore the *MIPCM* has attracted the interest of the researchers working on foundations of quantum theories. In this context, a recent proposal[2] to use a such a device to test the intrinsic non-locality of quantum mechanics has given rise to an interesting discussion on the possibility to produce interference when impinging states of light with few and well defined number of photons are used.

FIGURES

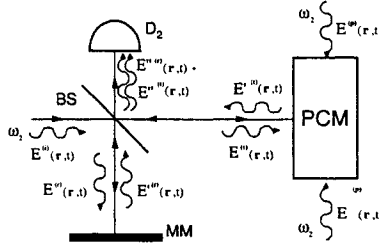


FIG. 1. The modified Michelson interferometer. One of two metallic mirrors is replaced with the phase-conjugate mirror *PCM*.

In the next section we will briefly resume the results of a classical analysis of a *MIPCM* and the results of experiments confirming these predictions, while the section III will be devoted to present the main results of a quantum study of this device.

In section IV we will present the main topics of a research program on this subject that our group is planning to perform in the next year.

II. Michelson interferometer with PCM: a classical analysis.

Let us consider an electromagnetic wave with wave vector \mathbf{k}_z and frequency $\omega/2\pi$ incident upon the beamsplitter *BS* of Michelson interferometer (Fig. 1) along the positive direction of *z*-axis $\mathbf{E}^{(i)}(\mathbf{r}, t) = \mathbf{e}A \exp[i(\mathbf{k}_z \cdot \mathbf{r} - \omega t)]$, where \mathbf{e} is the complex unit polarization vector satisfying the condition $\mathbf{e} \cdot \mathbf{e}^* = 1$.

The reflected beams at the two mirrors *PCM* and *MM* are:

$$\mathbf{E}'^{(t)}(\mathbf{r}_{PCM}, t) = \mu \mathbf{e}^* t^* A^* \exp[i(-\mathbf{k}_z \cdot \mathbf{r}_{PCM} - \omega t - S_{PCM})], \quad (1)$$

$$\mathbf{E}'^{(r)}(\mathbf{r}_{MM}, t) = -e r A \exp[i(-\mathbf{k}_y \cdot \mathbf{r}_{MM} - \omega t + S_{MM})], \quad (2)$$

were S_{PCM} and S_{MM} are the phase shifts due to the two arms, t and r are the complex transmission and reflection coefficients of the beamsplitter satisfying the conditions $t \cdot t^* + r \cdot r^* = 1$ and $t \cdot r^* - r \cdot t^* = 0$, and μ is the complex reflectivity of the mirror which depends on the intensity of the pumping beams, the strength of the coupling between pumping beams via the nonlinear susceptibility, and the length of the *PCM*. In general $|\mu|$ is less than 1, but it can be equal to or greater than 1 under well defined conditions[1].

The superposition of the two field after the second reflection in *BS* results in a total field traveling in the direction of detector D_2 with a total light intensity at the detector

$$I(r, t) = |\mathbf{e}^2| |A(i)|^2 (1 + |\mu|^2)/4 + 2|\mu| |\mathbf{e}^2| |A(i)|^2 \cos([\mathbf{k}_y \cdot \mathbf{r}_{D_2} + 2S_{MM}] - \phi + \delta + 2\alpha)/2, \quad (3)$$

where we have assumed that $\mu = |\mu| \exp[i\phi]$, $A = |A| \exp[i\alpha]$, $\mathbf{e}^2 = |\mathbf{e}^2| \exp[i\delta]$, $t = 1/\sqrt{2}$ and $r = i1/\sqrt{2}$.

The visibility of the interference results in $V = \frac{2|\mu||\mathbf{e}^2|}{1+|\mu|^2}$, and it exhibits a maximum when $|\mu| = 1$ and $|\mathbf{e}^2| = 1$. If we make $|\mu| = 1$, and if the impinging wave is linearly polarized, we have $\delta = 0$ and the scalar product \mathbf{e}^2 equal to 1; therefore the visibility of the interference V is equal to 1. Vice versa, if the impinging light is right-handed [left-handed] polarized, the

polarization vector is $\mathbf{e} = (\mathbf{i} + \mathbf{j})/\sqrt{2}$ [$\mathbf{e} = (\mathbf{i} + \mathbf{j})/\sqrt{2}$], and the scalar product \mathbf{e}^2 is equal to zero. Consequently $V = 0$ and the interference effect vanishes.

Moreover, it is worth to note that formula (3) depends on double of the phase α of the impinging field, on the phase shift $2S_{MM}$ introduced from the length of the arm with the metallic mirror, but does not depends on the length of the arm with the *PCM*. However, this "phase compensating propriety" holds only for perfect monochromatic waves[3].

Mandel, Wolf, and co-authors[4] confirmed these predictions with an experiment in which a linearly polarized laser beam was sent in the interferometer and a phase shifter was introduced in different positions in order to vary the phase of the incident and pumping waves. Unfortunately the experiment did not check the property of *MIPCM* to cancel any interference effect when a circularly polarized beam impinge on it.

III Michelson interferometer with PCM: a quantum analysis

The behavior of a *MIPCM* changes dramatically when the impinging state is a photon number state. In order to see better this different behavior it is necessary to perform a quantum analysis of the apparatus.

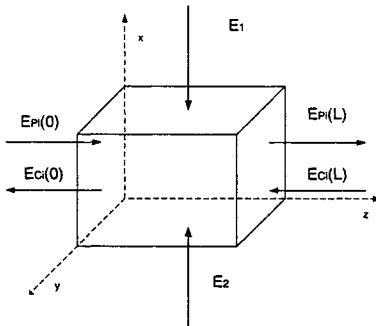


FIG. 2. The nonlinear medium, of length L , is pumped by two classical beams of the same frequency as the impinging wave and with opposite directions.

Let us consider a nonlinear material with high susceptibility $\chi^{(3)}$ and length L pumped by two classical fields E_1 and E_2 (see Fig. 2). If $i = \hat{x}, \hat{y}$ are the two possible state of linear polarizations for the impinging and conjugate fields, the annihilation operators are:

$$\hat{a}_i^{(t)}(L) = \frac{|k|}{k} \alpha \hat{a}_i^{(t)\dagger}(L) + \beta \hat{a}_i^{(t)}(0), \quad \hat{a}_i^{(t)}(0) = \beta \hat{a}_i^{(t)}(L) + \frac{k^*}{|k|} \alpha \hat{a}_i^{(t)\dagger}(L), \quad (4)$$

where $\alpha = -i \tan(|k|L)$, $\beta = \frac{1}{\cos(|k|L)}$, and $K^* = \omega/2\sqrt{\frac{\mu}{\epsilon}}\chi^{(3)}E_1E_2$. It is easy to see that the *PCM* preserves the propriety to reflect circular polarized light with the same polarization if the impinging field.

Inserting this description of a *PCM* in a quantum analysis of the interferometer, the main results can be resume as follow:

- When a coherent field impinge into the interferometer, the field at the detector is a superposition of a coherent field and a chaotic field depending on $|\mu|^2$ [5];
- The "phase compensating" propriety holds only if the impinging beam is a plane wave[3];
- The minimum theoretical number of photon in the impinging beam must be at least 2 in order to distinguish the signal from the noise[6];

- If the impinging field is a Fock state, the field in the two arms of the interferometer are statistically uncorrelated and no interference occurs[5],[7].

IV Conclusions

We would briefly comment the last result of previous section. The operator electric field $\mathbf{E}''(\mathbf{r}_{D_2})$ at D_2 can be written as a sum of two field. One is the field reflected on metallic mirror $\mathbf{E}''^{(r)}(\mathbf{r}_{D_2})$, which is proportional to $\sum_{j=1}^2 \sigma_{ij} \hat{a}_j$, where \hat{a}_j is the field operator associated with the incident field of polarization j , and the complex number σ_{ij} allows for a possible polarization change of this field inside the interferometer. The other is the field $\mathbf{E}''^{(t)}(\mathbf{r}_{D_2})$ reflected in *PCM*, which is proportional to $\sum_{j=1}^2 \tau_{ij} \hat{a}_j^\dagger$, where τ_{ij} accounts for polarization and phase changes in the arm with the *PCM*. Then, the intensity of photon detection in D_2 $\langle \mathbf{E}''(\mathbf{r}_{D_2})^\dagger \mathbf{E}''(\mathbf{r}_{D_2}) \rangle$ will result proportional to

$$\sum_{j=1}^2 \sum_{k=1}^2 [\sigma_{ij} \sigma_{ik}^* \langle \hat{a}_k^\dagger \hat{a}_j \rangle + \sigma_{ik}^* \tau_{ij} \langle \hat{a}_k^\dagger \hat{a}_j^\dagger \rangle + \sigma_{ij} \tau_{ik}^* \langle \hat{a}_k \hat{a}_j \rangle + \tau_{ik}^* \tau_{ij} \langle \hat{a}_k \hat{a}_j^\dagger \rangle]. \quad (5)$$

The second and third terms of (5) express the interference modulation in photon counting and vanish for any input state of the field with a well defined number of photons. This however does not mean that the apparatus does not exhibit any interference when a well defined photon number is injected, because it is possible to prove[8] that there are some physical optical states, as the photon pairs produced in degenerate parametric down-conversion process, which produce in a *MIPCM* interference with maximum visibility.

Moreover, even if the *MIPCM* has been studied theoretically both from a classical and quantum point of view, not all the unexpected behaviors of this object have been experimentally tested, therefore a more accurate experimental analysis of the apparatus is worth to be performed.

On the other side, most of the theoretical analyses and the experimental tests of the behavior of a *PCM* assume that the pumping beam is a coherent state (classical field) produced in a laser and the possibility to use different pumping states (as squeezed or number states) has not been yet investigated.

References

- [1] D. M. Pepper, Nonlinear optical phase conjugation in *Laser Handbook, Vol. IV*, edited by M.L. Stitch and M. Bass, North-Holland, Amsterdam (1985)
- [2] A. Garuccio, in "Quantum Interferometry", pag. 315, eds. De Martini, Denardo, and Shih, VCH, Weinheim (1996)
- [3] Z.Y. Ou, S. Bali, and L. Mandel, Phys. Rev. A **39**, 2509, (1989)
- [4] R.W. Boyd, T.M. Habashy, A.A. Jacobs, L. Mandel, M. Nieto-Vesperinas, W.R. Tompkin, and E. Wolf, Opt. Lett. **12**, 42, (1987)
- [5] G.S. Agarwal, J. Opt. Soc. Am. **4**, 1806 (1987)
- [6] N.F. Andreev, V.I. Bespalov, M.A. Dvoretzky, and G.A. Pasmanik, IEEE Jour. of Quant. El. **25**, 346-350 (1989)
- [7] K. Furuya, P.W. Milonni, A.M. Steinberg, M. Wolinsky Phys. Lett. A **251**, 294 (1999)
- [8] A. Garuccio, V. Berardi, V.L. Lepore: *Anticoherence, vacuum states and phase-conjugate mirrors*, Bari preprint (1999)

BEYOND THE COHERENT STATES IN INTERFEROMETRY, HOW AND WHY?

V. Peřinová and A. Lukš

*Laboratory of Quantum Optics, Faculty of Natural Sciences,
Palacký University, Třída Svobody 26,
771 46 Olomouc, Czech Republic*

Abstract

Fisher's measure of information is compared with the usual measure of sensitivity of the SU(2) interferometer. The states of optimum Fisher measure of information and prescribed mean photon-number difference are defined and properties of these states are studied in this interferometer.

I. INTRODUCTION

The optical interferometry is known to provide high precision measurements of various physical quantities. The enhancement of precision can be connected with the use of strong input fields, but this could damage the device. Therefore, in the framework of quantum optics, the optimization of the input state has been considered with the subsidiary condition that the mean total number of the photons on the input is prescribed. The phase-shift measurement scheme was devised by Caves [1, 2].

The SU(2) group representation of the Mach–Zehnder interferometer has been shown to be advantageous [3]. A phase sensitivity measure has been introduced to assess the precision of the measurements. In the course of time, the assumption of the input coherent states has been replaced by that of the input squeezed light and special quantum states. In the connection with the group theoretical approach, the constraint of the prescribed mean photon number has been simplified to the assumption that the total photon number is prescribed.

In this paper, we utilize the Cramér–Rao lower bound as an alternative of the usual sensitivity measure. As usual, we concentrate on the Fisher measure of information, which is an important constituent of the lower bound. Even though the question of the attainment of the lower bound is left open and the usual regularity assumptions are reformulated, the main result of this paper is seen in the study of special states which render the Fisher measure of information maximum.

II. SU(2) INTERFEROMETER, STANDARD SENSITIVITY MEASURE, AND GENERALIZED COHERENT STATES

Yurke, McCall, and Klauder [3] were first to emphasize the importance of the Mach–Zehnder interferometer as well as the role of the Heisenberg and Schrödinger pictures for

its description. The Heisenberg picture resembles the classical description in that it relates the output annihilation operators $\hat{a}_{j\text{out}}$, $j = 1, 2$, to the input ones $\hat{a}_{j\text{in}}$, $j = 1, 2$, leaving the state of physical system unchanged. The equivalent Schrödinger picture consists in a transformation of the input state to the output state, whereas the operators which are to be averaged do not evolve.

The beam splitters and the phase-shift imparted by the measured medium as well as the detectors can be described using the following operators

$$\hat{J}_1 = \frac{1}{2}(\hat{a}_1^\dagger \hat{a}_2 + \hat{a}_2^\dagger \hat{a}_1), \quad \hat{J}_2 = \frac{1}{2i}(\hat{a}_1^\dagger \hat{a}_2 - \hat{a}_2^\dagger \hat{a}_1), \quad \hat{J}_3 = \frac{1}{2}(\hat{a}_1^\dagger \hat{a}_1 - \hat{a}_2^\dagger \hat{a}_2), \quad (1)$$

$$\hat{N} = \hat{a}_1^\dagger \hat{a}_1 + \hat{a}_2^\dagger \hat{a}_2. \quad (2)$$

In the Mach-Zehnder interferometer the output state $|\text{out}\rangle$ is related to the input state $|\text{in}\rangle$ as follows

$$|\text{out}\rangle = \hat{U}_2 \hat{U}(\phi) \hat{U}_1 |\text{in}\rangle, \quad (3)$$

with

$$\hat{U}_1 = \exp\left(-i\frac{\pi}{2}\hat{J}_1\right), \quad \hat{U}(\phi) = \exp\left(-i\phi\hat{a}_1^\dagger \hat{a}_1\right), \quad \hat{U}_2 = \hat{U}_1^\dagger, \quad (4)$$

where the unitary operators \hat{U}_j , $j = 1, 2$, describe operation of beamsplitters and the unitary operator $\hat{U}(\phi)$ describes the phase shift ϕ imparted in one arm of the interferometer. Using the relation $\hat{a}_1^\dagger \hat{a}_1 = \frac{1}{2}\hat{N} + \hat{J}_3$ and exploiting the group formalism, we can rewrite (3) in the form

$$|\text{out}\rangle = \exp\left(-i\frac{\phi}{2}\hat{N}\right) \exp\left(-i\phi\hat{J}_2\right) |\text{in}\rangle. \quad (5)$$

On the output the operator \hat{J}_3 is measured. Naturally, it means that the photon-number difference is measured. The assumption that the total photon number is known is then equivalent to the knowledge of photon number on both the output ports. The phase sensitivity or the minimum detectable phase shift (the uncertainty of the phase measurement) depends on the unknown phase shift (to be measured), and on the assumption of small phase shifts which are most interesting it can be restricted to the value for $\phi = 0$. It is then determined by

$$(\delta\phi)^2 = \frac{\langle(\Delta\hat{J}_3)^2\rangle}{\langle\hat{J}_1\rangle^2}, \quad \langle\hat{J}_1\rangle \neq 0, \quad (6)$$

where the expectation values are computed for the input state. Assuming that the interferometer is fed with the Glauber coherent state $|\alpha_1\rangle_1 |\alpha_2\rangle_2$, it can be found that the optimal choice among the coherent states with $|\alpha_j|$, $j = 1, 2$, fixed is a coherent state with $\text{Im}(\alpha_1^* \alpha_2) = 0$.

Among the eigenstates of the total photon-number operator belonging to the eigenvalue $2j$, the SU(2) generalized coherent states $|j, \zeta\rangle$ are the most important [4]

$$(\hat{N} + \hat{1})|j, \zeta\rangle = (2j + 1)|j, \zeta\rangle. \quad (7)$$

Slightly more refined calculations than in the case of ordinary coherent state show that the phase uncertainty is minimum for $\text{Im} \zeta = 0$ when minimized under the constraint that $|\zeta|$ is fixed.

For any input state

$$|\text{in}\rangle = \sum_{n_1=0}^{2j} c_{n_1} |n_1\rangle_1 |2j - n_1\rangle_2 \quad (8)$$

from the $\text{SU}(2)$ -irreducible invariant space of the states $|\psi\rangle$ obeying the equation

$$(\hat{N} + \hat{1})|\psi\rangle = (2j + 1)|\psi\rangle, \quad (9)$$

we can formulate a criterion of optimality. It holds that the expectation value $\langle\psi|(\Delta\hat{J}_3)^2|\psi\rangle$ comprises only the products $|c_k||c_l|$, whereas $\langle\psi|\hat{J}_1|\psi\rangle^2$ depends only on $\text{Re}(c_k^*c_{k+1})$. It can be derived that these are terms with the sign plus each. Therefore, among the states which have the moduli $|c_k|$ fixed the optimum ones have real c_k , such that $c_1 \gtrless 0, c_2 > 0, \dots, c_{2j} > 0$ for $2j$ even and $c_{2j} \gtrless 0$ for $2j$ odd if $c_0 > 0$ is chosen. This rule relates to a phase difference. Invoking the theory of quantum phase, we can call such states partial phase states with the preferred phase either 0 (the upper relation) or π (the lower relation) [5]. Similarly as in the above case of the input coherent state, this phase is rather the phase difference.

III. FISHER'S MEASURE OF INFORMATION

The Fisher measure of information [6] is a good alternative measure of sensitivity since it measures directly the rate of change of the probability distribution in dependence on a parameter. Mathematically this measure of information is introduced as a constituent of the Cramér–Rao lower bound for the variance (sometimes mean-square deviation) of any estimate of the parameter. Since the number of photons N_1 on the first output port is a discrete random variable, we assume a discrete random variable which takes on the values $0, \dots, 2j$. The Fisher measure of information on the parameter ϕ contained in the photon number N_1 is

$$I(\phi) = \sum_{n=0}^{2j} \left[\frac{c^*(n, \phi)}{|c(n, \phi)|} c'(n, \phi) + \frac{c(n, \phi)}{|c(n, \phi)|} c'^*(n, \phi) \right]^2, \quad (10)$$

where

$$c(n, \phi) = {}_1\langle n | {}_2\langle 2j - n | \text{out} \rangle, \quad c'(n, \phi) \equiv \frac{\partial}{\partial \phi} c(n, \phi). \quad (11)$$

We try optimal input states with real coefficients. From the fact that the operator $(-i\hat{J}_2)$ has real matrix elements, we have, up to a common phase factor, real coefficients $c(n, \phi)$. Among the states which have the $|c_k|$ fixed, the optimum states have real c_k such that $c_0 > 0, c_2 < 0, c_4 > 0, \dots, c_{2j} > 0$ for $2j \equiv 0 \pmod{4}$, $c_{2j} < 0$ for $2j \equiv 2 \pmod{4}$, $c_{2j-1} > 0$ for $2j \equiv 1 \pmod{4}$, $c_{2j-1} < 0$ for $2j \equiv 3 \pmod{4}$ if $c_0 > 0$ is chosen, whereas $c_1 \gtrless 0, c_3 \gtrless 0, c_5 \gtrless 0$, etc.

As we have mentioned above, it is reasonable to optimize the sensitivity of measurement under the constraint that the mean photon numbers on both the input ports are known. Making use of the optimality of the input states with real coefficients, we may reduce the relation (10) to the form

$$I(\phi) = 4 \sum_{n=0}^{2j} [c'(n, \phi)]^2. \quad (12)$$

Employing further the assumption of a compensation measurement [3], we obtain that

$$I(0) = 4 \langle \hat{J}_2^2 \rangle. \quad (13)$$

Assuming that the input states are related to a representation of the group SU(2) and that the constraint can be formulated in terms of $\langle \hat{J}_3 \rangle$, we arrive at the eigenvalue problem

$$(\hat{J}_3 - \gamma \hat{J}_2^2)|\psi\rangle = \lambda|\psi\rangle \quad (14)$$

by a standard variational argument. The real parameter γ is to be determined as a function of the quantum expectation $\langle \hat{J}_3 \rangle$. All the eigenvalues $\lambda_l^{(j)}(\gamma)$ are real and they are numbered from zero to $2j$ in increasing order.

We have compared the values of Fisher's measure of information for the Yurke–McCall–Klauder quality state and the optimum state of the same mean photon-number difference, $\langle \hat{J}_3 \rangle = \frac{1}{2}$. The former is described asymptotically by $4\kappa_{\text{YMK}}j^2$ and the latter behaves asymptotically as $4\kappa_{\text{opt}}j^2$, with $1 = \kappa_{\text{opt}} > \kappa_{\text{YMK}} = \frac{1}{2}$. The optimum input states have $l = 2j$ and γ values negative.

REFERENCES

- [1] C. M. Caves, Phys. Rev. Lett. **45**, 75 (1980).
- [2] C. M. Caves, Phys. Rev. D **23**, 1693 (1981).
- [3] B. Yurke, S. L. McCall, and J. R. Klauder, Phys. Rev. A **33**, 4033 (1986).
- [4] A. M. Perelomov, *Generalized Coherent States and their Applications* (Springer-Verlag, Berlin, 1986).
- [5] D. T. Pegg and S. M. Barnett, Phys. Rev. A **39**, 1665 (1989).
- [6] R. A. Fisher, Proc. Cambridge Phil. Soc. **22**, 700 (1925).

Quantum computation, entanglement and phase transitions in mesoscopic boson-like systems with non-classical polarization states

A.P.Alodjants, A.Yu.Leksin, A.V.Prokhorov, S.M.Arakelian

Department of Physics and Applied Mathematics, Vladimir State University, Vladimir, 600026, Russia. Tel.: 7-(0922)233334, 279621; Fax: 7-(0922) 232575 E-mail: laser@vpti.vladimir.su and/or arak@vpti.vladimir.su

Abstract

The problem of formation of macroscopic (mesoscopic) coherent superposition of polarization states of boson-like systems are discussed for the first time. The quantum interference of two (and/or more) orthogonally polarized coherent states in such systems results in non-classical behavior of the polarization states of light being described by different parameters: the Wigner quasi-distribution function, the boson statistics and the entropy of quantum states. The phase transition from classical to quantum state occurs in such a correlated ("frozen") mesoscopic system. The Wigner function in the area of the phase transition demonstrates the fractal-like structure. The application of considered coherent superposition of quantum states and induced phase transition in mesoscopic systems to construct the optical quantum logical controlled-NOT gates for quantum computation are discussed as well. For that non-local quantum properties of the entangled coherent states resulting in quantum bits are studied.

1.INTRODUCTION

At present, the study of non-classical states of many-body boson-like systems are very rapidly developed area in quantum and atomic optics. Here we are speaking about experimental observation of the Bose- Einstein condensation [1], and also about the demonstration of quantum computation in the ion traps and some other electronic and optical systems [2].

In our previous papers [3] we developed the theory of formation of non-classical polarization states and also discussed the accurate measurement procedure (i.e. quantum non-demolition, simultaneous, continuous etc. measurements) for polarization characteristics of such quantum system. We have obtained that this type of quantum states demonstrates a new non-classical behavior as a result of quantum interference in optical field.

In present paper we consider for the first time the possibility to formate the coherent superposition of two selected quantum states for orthogonally (linear and/or circular) polarized optical wave packets (the Schroedinger cat states) in boson-like systems (under

condition of boson condensate). In contrast with previous consideration namely the polarization non-classical macroscopic (mesoscopic) states of light is a principal item of our discussion.

2. QUANTUM INTERFERENCE OF MACROSCOPIC LOCALIZED POLARIZATION STATES

First, we have examined the superposition of two coherent circularly polarized states $|\zeta\rangle = K(|+\rangle + |-\rangle)$, where K is determined by the state normalization condition (cf. [4]). The polarization characteristics closely depend on two phase angles θ and η those are azimuth and ellipticity of polarization state correspondingly. The probability to detect the m particles in a single polarization mode is described by the sub-poissonian distribution function of photons being strongly oscillated vs m . For linear polarization (when $\theta = \eta = 0$) the distribution function is the Poissonian. Both the wave functions and the distribution functions of two hermitian quadratures demonstrate the two well separated areas of localization as a result of interference of the condensates that corresponds to two quantum states of different (orthogonal) polarizations. The distance between two maxima of them is determined by the phase parameters θ and η . The quantum effect of tunneling for bosons takes place due to quantum interference. The similar result we obtained for the Wigner quasi-distribution functions. In last case we deal with the polarization interference in a phase space. The computer simulation demonstrates the areas with purely quantum (negative) behavior of the Wigner functions being varied vs the parameters θ and η .

For qualitative description of the measurement procedure in Hermitian quadratures (coordinate and momentum of the wave packets) for such a mesoscopic system we introduce the entropy parameters $S_Q = -\int_{-\infty}^{\infty} W_Q \ln(W_Q) dQ$, $S_P = -\int_{-\infty}^{\infty} W_P \ln(W_P) dP$ of the polarization states, where W_Q and W_P characterize the probability function distribution of localization for coordinate Q and momentum P of the wave packet. Physically two parameters S_Q and S_P can be interpreted as a degree of the information loss due to the measurement procedure. These quantities demonstrate the "squeezing" effect for information about the object during the measurement procedure vs η and θ - see Fig.1.

3. CRITICAL PHENOMENA IN MESOSCOPIC BOSE-SYSTEMS

We have considered the phase transition in optical mesoscopic systems, i.e. in analogy with superfluid and/or superconductor boson-like systems. For these states of the matter the number of particles is a large enough but the degrees of freedom are frozen at the same time as a result of their quantum correlation. The main characteristics of similar systems are connected with spontaneously broken gauge symmetry [5]. The phase transition in such a mesoscopic system demonstrates the linear superposition $|N\rangle = u|n_c\rangle + \nu e^{i\phi}|n_c + 1\rangle$ of the Fock states with neighborhood values of the boson numbers n_c ; $u, \nu > 0$, ϕ are the some real parameters of the problem, $n_c \gg 1$ is a critical average number of particles which results in phase transition - see [5]. The sharp switching effect from positive to negative values of the quasi-distribution (Wigner) function can be associated with the phase transition - see Fig.2a,b. The intermediate values being both positive and negative describe the intrinsic

structure of the phase transition (Fig.2c). For this case the projection of the Wigner function on the coordinate-momentum phase plane has a fractal-like structure and the average number of particles is essentially fractional. Physically the fact can be interpreted as a macroscopic transition from quantum (classical) to classical (quantum) behavior of the mesoscopic system in the phase space. In this approach the negative values of the quasi-distribution function correspond directly to quantum domains in contrast with the positive values which are associated with classical states.

4. ENTANGLED POLARIZATION COHERENT STATES IN QUANTUM LOGIC XOR-GATE

We have proposed the quantum logical XOR-gate using the mesoscopic (macroscopic) systems under consideration. We showed that for linear coherent superposition of two modes the XOR-operation is reduced to entanglement of the coherent orthogonal polarization states being the two qubits in polarization parameters of the boson system. We also introduced the first- and second-order correlation functions for the qubits. Their behavior demonstrates the strong anticorrelation between target and control qubits vs variation of the polarization phase angles of control mode – Fig.3. The Einstein-Podolsky-Rosen correlation effect can be analyzed for such an entanglement of coherent qubits.

For practical realization of predicted effects for quantum computation we are considering the multiparticle boson-like systems in quantum and atomic optics. For these purposes the non-linear Lipkin model with standard spin-spin interaction is using to describe the mesoscopic properties of the systems. The problem of decoherence for such consideration is discussed as well.

ACKNOWLEDGEMENTS

This work has been partly supported by Russian Fund of Basic Researches.

REFERENCES

- [1] M.H.Anderson et al., Science **269**, 198 (1995); K.B.Davis, et al, Phys.Rev.Letts. **75**, 3969 (1995); C.C.Bradly et al, Phys.Rev.Letts. **75**, 1687 (1995)
- [2] D.P.DiVincenzo Science **270**, 255 (1995); L.Davidovich, M.Brune, J.M.Raimond, S.Haroche Phys.Rev.A **53**, 1295 (1996); M.Brune, E.Hagley, J.Dreyer, X.Maitre, A.Maali, C.Wunderlich, J.M.Raimond, S.Haroche Phys.Rev.Letts. **77**, 4887 (1996); D.M.Meekhof, G.Monroe, B.E.King, W.M.Itano, D.Wineland Phys.Rev.Lett. **76**, 1796 (1996);
- [3] A.P.Alodjants, S.M.Arakelian, A.S.Chirkin Appl.Phys.B **66**, 53 (1998); A.P.Alodjants, S.M.Arakelian Russian JETP **113**, 1235 (1998); A.P.Alodjants, S.M.Arakelian J.of Mod.Optics **46**, 475 (1999)
- [4] W.Schleich, M.Pernigo, Fam Le Kien Phys.Rev.A **44**, 2172 (1991)
- [5] Andreev A F Russian Usp.Fiz.Nauk **168** 655 (1998)

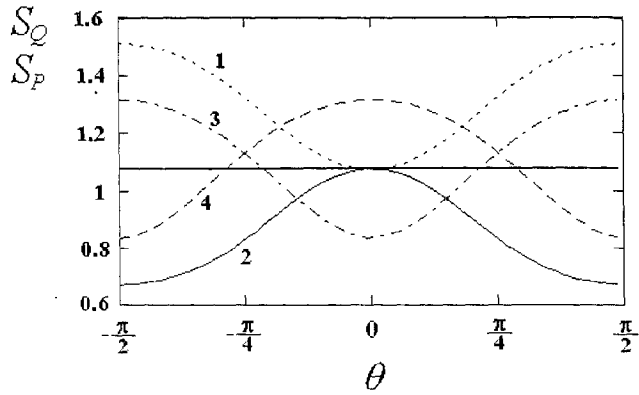


FIG.1. Dependence for entropy in measuring quadratures S_Q and S_P as the functions of polarization angle θ . Figure introduces symbols of curves: (1) - S_P , (2) - S_Q when $\eta = 0$; (3) - S_P , (4) - S_Q when $\eta = \pi/4$. The value of amplitude of the each polarization state $|\alpha| = 1$. The values $S_Q = S_P = 0.5 \ln(\pi e) \approx 1.072$ correspond to the measurements with coherent wave packets.

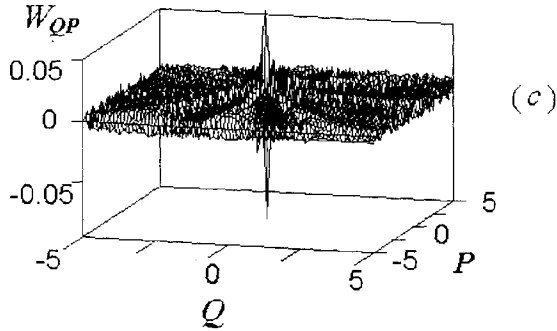
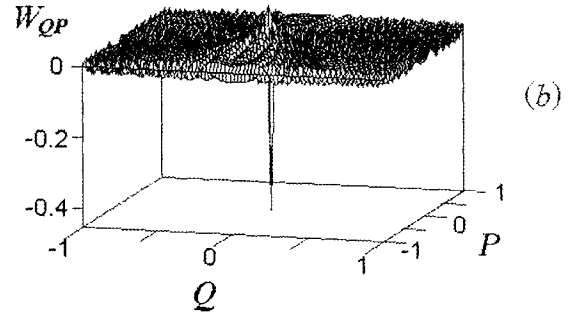
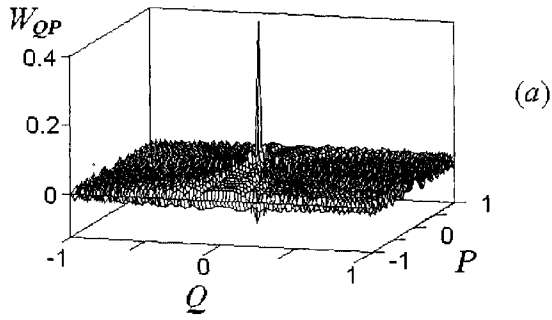


FIG.2. 3-D dependence for the Wigner function W_{QP} under condition of the phase transition with the change of the number of particles n_c per unit from $n_c = 1000$ to $n_c = 1001$. The parameters values are: $\phi = \pi/3$; (a) $u = 1$, $v = 0$; (b) $u = 0$, $v = 1$; (c) $u = 0.7$.

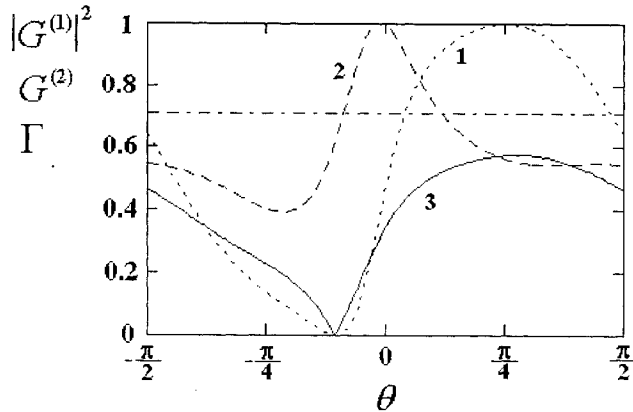


FIG.3. Dependences of normalized correlation functions $|G^{(1)}|^2$, $G^{(2)}$ and the value Γ as the functions of polarization angle θ . Symbols of curves are: 1 - $|G^{(1)}|^2$, 2 - $G^{(2)}$, 3 - Γ . The parameter values are: $\eta = 0$, $\psi = 0$, $\phi = -\pi/4$. The amplitudes of the state of each qubit are equal, i.e. $|\alpha|^2 = |\beta|^2 = 1$. The value $\Gamma = 1/\sqrt{2} \approx 0.71$ guarantees the maximum level of solving of Bell's inequalities.

Ultracold atoms for quantum computation

T. Calarco^{1,2}, D. Jaksch¹, J.I. Cirac¹, and P. Zoller¹

¹*Institut für Theoretische Physik, Universität Innsbruck, Technikerstr. 25, A-6020 Innsbruck, Austria*

²*ECT*, European Centre for Theoretical Studies in Nuclear Physics and Related Areas
Villa Tambosi, Strada delle Tabarelle 286, I-38050 Villazzano (Trento), Italy*

Abstract

Recent proposals for realizing a quantum logical gate by entangling neutral atoms via cold controlled collisions are presented. The possibility of implementing them with present-day experimental techniques is quantitatively discussed. The examples of optical lattices and magnetic microtraps, to be loaded with atoms from Bose–Einstein condensates, are analyzed.

Entanglement is one of the most intriguing features of Quantum Mechanics. It leads to paradoxes, like the Einstein–Podolsky–Rosen one, and has certain applications, like quantum cryptography or quantum computing [1]. However, there are very few physical systems in which entanglement can be systematically studied in a controlled way. Those systems include ion-traps, cavity QED, photons, solid state systems, and molecules in the context of NMR. Very recently, we have identified a new way of entangling neutral atoms by using *cold controlled collisions* [2]. Given the impressive experimental advances made so far in the fields of neutral atom trapping and cooling, and in the studies of Bose Einstein condensation (BEC) of ultracold gases, that proposal opens a new perspective to several experimental groups who so far have concentrated their efforts in other fields of Atomic Physics. In this paper we review some of the basic concepts of this method to entangle atoms, and analyze them in two different scenarios: atoms in dipole traps and in magnetic micro-traps [3].

Consider two neutral atoms 1 and 2 with two internal states confined in traps. We will show how by changing selectively the trapping potentials one can implement a fundamental two-qubit gate of the form

$$|0\rangle_1|0\rangle_2 \rightarrow |0\rangle_1|0\rangle, |0\rangle_1|1\rangle_2 \rightarrow |0\rangle_1|1\rangle, |1\rangle_1|0\rangle_2 \rightarrow |1\rangle_1|0\rangle, |1\rangle_1|1\rangle_2 \rightarrow -|1\rangle_1|1\rangle_2. \quad (1)$$

Here, $|0\rangle$ and $|1\rangle$ denote two internal states of the atoms, and the phase-shift is obtained as a consequence of the atomic collision. If one can additionally perform single-qubit rotations, that is, change the internal state of each of the atoms independently (using a laser, for example), then by concatenating such operations with the fundamental gate (1) one can manipulate the quantum state of the atoms at will [1]. In particular, one can create arbitrary entangled states. Note that instead of changing the sign of the state $|1\rangle|1\rangle$ one could change the sign of any other state (see below).

We consider two bosonic atoms 1 and 2 with internal states $|a\rangle_{1,2}$ and $|b\rangle_{1,2}$ trapped by conservative potentials $V^{\beta_i}(\mathbf{x}_i, t)$ whose functional dependence on the coordinate \mathbf{x}_i , with

$i = 1, 2$ the particle index, depends on the internal state of the particle $\beta_{1,2} = a, b$. Initially, the two particles are in the ground state of the trapping potentials and the centers of the two potential wells are sufficiently far apart so that the particles do not interact. Then the form of the potential wells is changed such that there is some overlap of the wave functions of the two atoms; the particles interact with each other, and then the potential is restored to the original situation. We describe the interaction between the atoms in two given internal states β_1 and β_2 by a contact potential

$$u^{\beta_1\beta_2}(\mathbf{x}_1 - \mathbf{x}_2) = \frac{4\pi a_s^{\beta_1\beta_2} \hbar^2}{m} \delta^3(\mathbf{x}_1 - \mathbf{x}_2), \quad (2)$$

where $a_s^{\beta_1\beta_2}$ is the s -wave scattering length for the corresponding internal states describing elastic collisions and m is the mass of the particles. We treat the interaction perturbatively. The phase accumulated due to the interaction in the time interval $[-\tau, \tau]$ is

$$\phi^{\beta_1\beta_2} = \frac{1}{\hbar} \int_{-\tau}^{\tau} dt \langle \psi^{\beta_1\beta_2}(t) | u^{\beta_1\beta_2} | \psi^{\beta_1\beta_2}(t) \rangle, \quad (3)$$

where $|\psi^{\beta_1\beta_2}(t)\rangle$ is the symmetrized state for two particles in internal states β_1 and β_2 in the time dependent potential $V^{\beta_1} \otimes V^{\beta_2}$.

One way of controlling the interaction between the particles is to move the center position of the potentials $V^{\beta_i}(\mathbf{x}_i, t) = V(\mathbf{x}_i - \bar{\mathbf{x}}_i^{\beta_i}(t))$ towards each other in a state-dependent way while leaving the shape of the potential unchanged (left part of Fig. 1). By moving the potential we get two kinds of phase shifts: a kinetic phase which is a single-particle phase due to the kinetic energy of the particles and an interaction phase due to coherent interactions between two atoms. The first one can be easily calculated by ignoring the effects of collisions to lowest order. The second one is responsible for the entanglement. If the motion of the potential is slow enough such that the atoms always remain in the ground state, depending on the initial internal atomic states we have: $|a\rangle_1|a\rangle_2 \rightarrow e^{-i2\phi^a}|a\rangle_1|a\rangle_2$, $|a\rangle_1|b\rangle_2 \rightarrow e^{-i(\phi^a+\phi^b+\phi^{ab})}|a\rangle_1|b\rangle_2$, $|b\rangle_1|a\rangle_2 \rightarrow e^{-i(\phi^a+\phi^b)}|b\rangle_1|a\rangle_2$, $|b\rangle_1|b\rangle_2 \rightarrow e^{-i2\phi^b}|b\rangle_1|b\rangle_2$, where the motional states remain unchanged. The kinetic phases ϕ^β and the collisional phase ϕ^{ab} can be easily calculated. The ϕ^β are (trivial) one-particle phases that, as long as they are known, can always be incorporated in the definition of the states $|a\rangle$ and $|b\rangle$. If we identify the states $|0\rangle$ and $|1\rangle$ appropriately, this realizes the fundamental two-qubit quantum gate (1) for $\phi^{ab} = \pi$ (but with the change of sign in the state $|1\rangle|0\rangle$).

The interaction between the particles can be controlled also in another way, for example by changing with time the shape of the potentials depending on the particles' internal states (right part of Fig. 1). We consider two atoms initially trapped in two displaced wells. At a certain time the barrier between the wells is suddenly removed in a selective way for atoms in state $|b\rangle$, whereas it remains unchanged for atoms in state $|a\rangle$. The atoms are allowed to oscillate for some time, and then the barrier is raised again suddenly such as to trap them back at the original positions. As before, during the process they will acquire both a kinematic phase due to the oscillations within their respective wells, and an interaction phase due to the collision. These phase-shifts will depend on the number of oscillations and the initial conditions. On the other hand, if the effect of the deformation of the wavefunctions due to the interaction is negligible, we will have that after the atoms come back to the

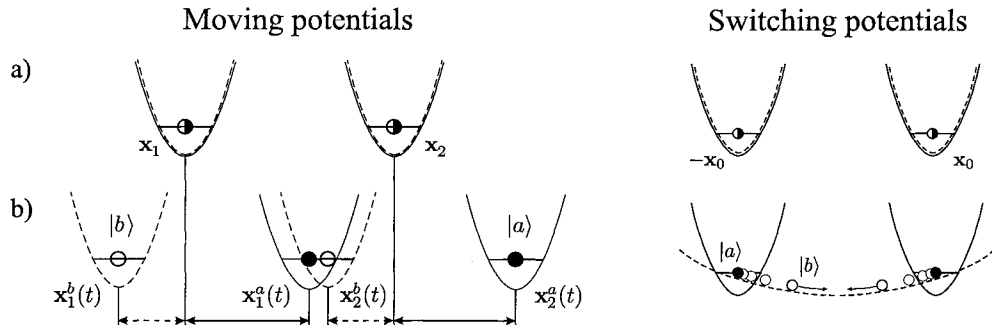


FIG. 1. Configurations at times $\pm\tau$ (a) and at t (b) for moving (left) and switching potentials (right). The solid (dashed) curves show the potentials for particles in the internal state $|a\rangle$ ($|b\rangle$).

original situation. If the phases are known and the phase difference $\phi^{bb} - 2\phi^{ab}$ is adjusted to $\pm\pi$ by a proper choice of the trap parameters, we obtain (1).

A physical implementation of the scenarios described here requires an interaction which produces internal-state-dependent conservative trap potentials and the possibility of manipulating these potentials independently. The choice of the internal atomic states $|a\rangle$ and $|b\rangle$ has to be such that they are elastic (i.e. the internal states do not change after the collision).

We consider first that the atoms are trapped in an optical lattice (one can similarly consider trapping in other optical fields), and we show how to move the optical potentials [3,4]. We consider the example of alkali atoms with a nuclear spin equal to $3/2$ (^{87}Rb , ^{23}Na) trapped by standing waves in three dimensions. The internal states of interest are hyperfine levels corresponding to the ground state $S_{1/2}$. Along the z axis, the standing waves are in the lin \angle lin configuration (two linearly polarized counter-propagating traveling waves with the electric fields \vec{E}_1 and \vec{E}_2 forming an angle 2θ). The total electric field is a superposition of right and left circularly polarized standing waves (σ^\pm) which can be shifted with respect to each other by changing θ . The lasers are tuned between the $P_{1/2}$ and $P_{3/2}$ levels so that the dynamical polarizabilities $\alpha_{\pm\mp}$ of the two fine structure $S_{1/2}$ states corresponding to $m_s = \pm 1/2$ due to the laser polarization σ^\mp vanish ($\alpha_{+-} = \alpha_{-+} = 0$), whereas the polarizabilities $\alpha_{\pm\pm}$ due to σ^\pm are identical ($\alpha_{++} = \alpha_{--} \equiv \alpha$). We choose for the states $|a\rangle$ and $|b\rangle$ the hyperfine structure states $|a\rangle \equiv |F=1, m_f=1\rangle$ and $|b\rangle \equiv |F=2, m_f=2\rangle$. Due to angular momentum conservation, these states are stable under collisions. On the other hand, by varying the angle θ from $\pi/2$ to 0 , the corresponding potentials V^b and V^a move in opposite directions until they completely overlap. Then, going back to $\theta = \pi/2$ the potentials return to their original positions.

We now consider the implementation of a switching potential by means of electromagnetic trapping forces. The interaction between the magnetic dipole moment of an atom in some hyperfine state $|F, m_F\rangle$ and an external static magnetic field \vec{B} entails an energy $U_{\text{magn}} \approx g_F \mu_B m_F |\vec{B}|$ depending on the atomic internal state via the quantum number m_F (here μ_B is the Bohr magneton and g_F is the Landé factor). On the other hand, the Stark shift induced on an atom by an electric field \vec{E} gives a state-independent energy $U_{\text{el}} \approx \frac{1}{2} \alpha |\vec{E}|^2$, where α is the atomic polarizability. The interplay between these two effects can be exploited in order to obtain a trapping potential whose shape depends on the atomic internal state. As

an example, we consider an atomic mirror with an external magnetic field [5], providing confinement along two directions with trapping frequencies which can range from a few tens of kHz up to some MHz. Microscopic electrodes can be plugged on the mirror's surface [6], thus allowing for the design of a potential with the characteristics described above. In order to perform the gates, we choose for the states $|a\rangle$ and $|b\rangle$ the same hyperfine structure states of ^{87}Rb considered before, which are low-magnetic field seekers.

We use the minimum fidelity F to characterize the quality of the gate $F = \min_{\varphi} \left\{ \text{tr}_{\text{ext}} \left[\langle \tilde{\varphi} | \mathcal{U} S (|\varphi\rangle\langle\varphi| \otimes \rho_{\text{ext}}) S^\dagger \mathcal{U}^\dagger | \tilde{\varphi} \rangle \right] \right\}$, where $|\varphi\rangle$ is an arbitrary internal state of both atoms, and $|\tilde{\varphi}\rangle$ is the state resulting from $|\varphi\rangle$. The trace is taken over motional states, \mathcal{U} is the evolution operator for the internal states coupled to the external motion (including the collision), S is an operator expressing symmetrization under particle interchange, and ρ_{ext} is the density operator corresponding to both atoms being at a temperature T at time $t = -\tau$ [2,3]. In both the schemes considered here we obtain a $F \approx 0.99$ assuming reasonable values for the trapping parameters.

We have shown how to perform quantum gates between neutral atoms using cold controlled collisions. We have analyzed two different setups, one based on optical lattices and the other on magnetic traps. It is clear that, at the present time, most of the experimental requirements have yet to be realized, before one can implement quantum information processing. There are, however, recent achievements in cooling and trapping of atoms in optical lattices and in magnetic microtraps which make it seem possible that some of these elements could be implemented in the laboratory in the near future. There are short-term and long-term perspectives. Essential for all quantum information experiments is a successful *cooling* of the atoms to the ground state of a three dimensional lattice. Under these circumstances, one could perform interesting Ramsey-type spectroscopic studies of the fidelity of multi-particle entanglement as discussed in Ref. [3]. To do this, neither single-atom addressability is required nor are regular filling structures. When the latter requirements can be realized, on the other hand, coding experiments can be done and a quantum memory be implemented. Finally, if one can find three-level schemes with different scattering phases for the logical states, universal computations can be performed. The parallelism of the lattice could then be exploited for efficient implementations of fault-tolerant quantum computing.

We thank E. Hinds and J. Schmiedmayer for many useful discussions. One of us (T. C.) thanks M. Traini and S. Stringari for the kind hospitality at the Physics Department of Trento University, and the INFN (Gruppo Collegato di Trento). This work was supported in part by the Österreichischer Fonds zur Förderung der wissenschaftlichen Forschung, the European Community under the TMR network ERB-FMRX-CT96-0087, the Institute for Quantum Information GmbH, and by the Schwerpunktsprogramm "Quanten-Informationsverarbeitung" der Deutschen Forschungsgemeinschaft.

1. See, for example, A. Ekert and R. Josza, Rev. Mod. Phys. **68**, 733 (1996).
2. D. Jaksch *et al.*, Phys. Rev. Lett. **82**, 1975 (1999)
3. H.-J. Briegel *et al.*, J. Mod. Opt. (submitted).
4. G.K. Brennen, C.M. Caves, P.S. Jessen, and I.H. Deutsch, Phys. Rev. Lett. **82**, 1060 (1999).
5. E.A. Hinds, Phil. Trans. Roy. Soc. **357**, 1 (1999).
6. J. Schmiedmayer, Eur. Phys. J. D **4**, 57 (1998).

The experimental demonstration of quantum computation using linear optics

Shigeki Takeuchi

In JST-PRESTO project,

Mitsubishi Electric Corporation A.T.R.C.

takeuchi@bio.crl.melco.co.jp

Abstract

An experimental demonstration of the Deutsch-Jozsa quantum computation algorithm of 3-qubit using linear optics is described. The quantum algorithm was implemented by use of linear (passive) optics which acted as unitary transformations on the polarization and modes of photons as quantum registers. The result was given by 'a single quantum computation' in the experiment.

Quantum computation is a new concept which utilizes quantum superposition states for ultra-fast parallel processing. There have been several proposals for the actual realization of quantum computers. Among them, only the nuclear magnetic resonance(NMR) quantum computation[1] has played the role of a test-bed for the algorithms. Some mechanisms for quantum computation, however, cannot be tested by the NMR quantum computers because the result of the NMR computation is always given by the average of the huge number of quantum computations. Here we report an demonstration of the Deutsch-Jozsa quantum computation algorithm[2] of 3-qubit using linear optics and single-photons, which has been proposed as an alternative test-bed for quantum computation[3].

Our quantum computer solves the problem with 4-bit inputs, for which three qubits are required in the Deutsch-Jozsa algorithm; two qubits are used as the address register and one as the accumulator for the given oracle. The schematic experimental setup is shown in Fig. 1. In our computer, four optical paths are used for the address register and the polarization of the photon is used for the accumulator. Our quantum computer was used by following procedure. First, the optical length of each path was adjusted one by one to have suitable phase parameters. Second, 'the oracle' (a 4-bit digit) was given to the computer and is converted to the appropriate voltage signal applied to the E/O modulators in the system. Then, we put a single-photon with vertical polarization to the input port of this 'quantum computer'. In the experiment, we used weak coherent light which was attenuated to 0.5pW so that the each detection signal was given by single photon interference. Then, we observed the detector at the output port to find whether it detects the photon or not. When the photon was detected, it meant the answer was that 'the given oracle $\{f(i)\}$ is not even.' When not, the answer was 'the given oracle $\{f(i)\}$ is not uniform[4].' We emphasize that the answer was given by a single quantum computation (a single event of photon detection)

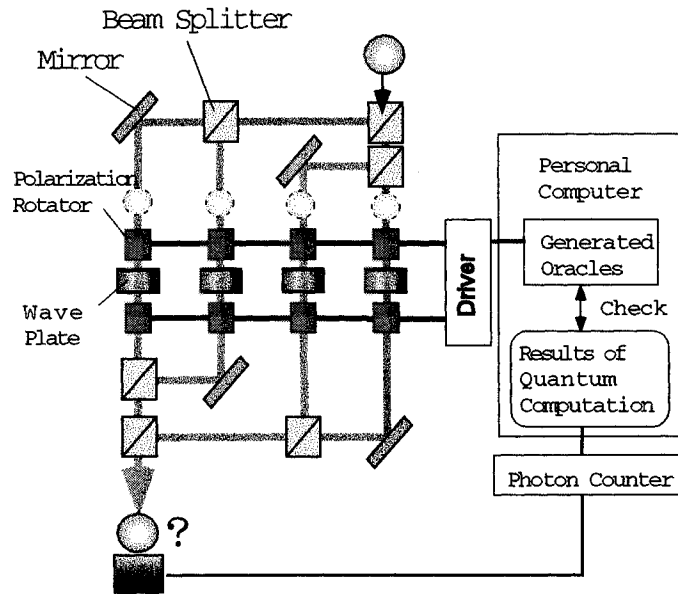


FIG. 1. The schematic diagram of the experiment.

in this experiment[5].

The detailed explanation of the transformations given by each optics was given in the reference[3]. The first three beam splitters, the E/O modulators, the wave plates, and the last three beam splitters correspond to the unitary transformation A , $U(f)$, S , and A^\dagger used in the reference[2] respectively. The details of the experiment is given elsewhere[6].

As the experimental result, we could determine whether the statement 'the given oracle $\{f(i)\}$ is not even' or 'the given oracle $\{f(i)\}$ is not uniform' is correct with the small average error rates of 2.7% and 4.0% respectively by the observation of a single-photon. These errors might be caused by the imperfect initialization and the decoherence caused by the wave front distortion caused by the optics.

On the quantum computation using linear optics, Reck showed that the any unitary transformation can be realized by linear optics[7]. After the first proposal of the quantum computation using linear optics[3], Cerf described the method to realize any quantum logic by linear optics[8]. This was the first experiment of 3 qubits using linear optics. The weak point of linear optics quantum computation is that we need 2^N modes to implement an algorithm with N qubits. However, the algorithm with small number of qubits(say ten qubits, which is supposed to be a limit for NMR quantum computation) will be possible with today's experimental technique. In addition, it is possible to demonstrate an algorithm in which the result should be given by a single computation. Quantum computation using linear optics will be an alternative test bed as shown here.

We thank Dr. Toshiro Isu for his helpful comments.

- [1] N. A. Gershenfeld, and I. Chuang, *Science* **275**, 350(1997); N. Linden, H. Barjat, and R. Freeman, *Chem. Phys. Lett.*, **296** 61-67(1998)
- [2] D. Deutsch and R. Jozsa, *Proc. R. Soc. Lond. A* **439**, 553 (1992).
- [3] S. Takeuchi, in *Proceedings of Fourth Workshop on Physics and Computation: PhysComp96* (ed. Toffoli, T.), 299-302 (1996) (New England Complex Systems Institute).
- [4] When the weak coherent light was used, we could set other 3 detectors at the rest of the output ports of the lower three beam splitters. We would consider the signal from these three detector as 'not detected'. In the experiment, we did not observe these three output ports but we calculated error rates by assuming the dark counts from these additional detectors.
- [5] The original Deutsch Jozsa problem is devised so that we can have the result by a single quantum computation.
- [6] S. Takeuchi, submitted to *Phys. Rev. Lett.*
- [7] M. Reck and A. Zeilinger, *Phys. Rev. Lett.* **73** 58 (1994).
- [8] N. J. Cerf, C. Adami, and P. G. Kwiat, *Phys. Rev. A* **57**, R1477 (1998).

Cloning transformations for qubits

Chiara Macchiavello

*Dipartimento di Fisica 'Alessandro Volta' and INFN-Unità di Pavia,
Via A. Bassi 6, I-27100 Pavia, Italy*

Abstract

We derive bounds on the efficiency of approximate cloning transformations for two-dimensional quantum systems. We consider three different types of cloners and compare the corresponding fidelities.

The laws of quantum mechanics do not allow the realisation of a perfect cloning machine for quantum states that are *a priori* unknown [1]. It is intuitive to expect that perfect cloning transformations can be approximated with increasing efficiency by increasing the amount of *a priori* information on the set of allowed input states. We analyse here approximate cloning for two-dimensional states and show bounds on its efficiency for three possible classes of inputs. We study the efficiency of a cloning transformation in terms of the fidelity $F = \langle \psi | \rho_{out} | \psi \rangle$ of the density operator ρ_{out} describing the state of each output copy with respect to the original pure input state $|\psi\rangle$.

We will first consider the most general case where the input state is completely unknown (the class of allowed input states corresponds to the whole two-dimensional Hilbert space of a qubit). We will investigate universal cloning transformations, namely transformations whose efficiency does not depend on the form of the input state. Universal $N \rightarrow M$ quantum cloning is a unitary transformation acting on an extended input which contains N original qubits all in the same unknown pure state $|\psi\rangle$, $M - N$ “blank” qubits and K auxiliary systems in an arbitrary state, and giving M output clones together with the auxiliary K systems. We describe the state of each qubit in terms of its Bloch vector representation $\rho = (\mathbb{1} + \vec{s} \cdot \vec{\sigma})/2$, where $\mathbb{1}$ is the 2×2 identity matrix, \vec{s} is the Bloch vector (with unit length for pure states) and σ_i are the Pauli matrices. By requiring that all input states must be treated in the same way (universality condition) it has been shown [2] that the reduced density operator of each of the M output qubits is related to the input one by a shrinking transformation in the Bloch vector representation, namely $\rho_{out} = (\mathbb{1} + \eta_u(N, M)\vec{s} \cdot \vec{\sigma})/2$. Notice that the shrinking factor is simply related to the fidelity as $F_u(N, M) = (1 + \eta_u(N, M))/2$.

In order to optimise the fidelity $F_u(N, M)$, or equivalently the shrinking factor $\eta_u(N, M)$, universal cloning has been related to state estimation [3] by the following equality

$$F_{est}^{opt}(N) = F_u^{opt}(N, \infty) \quad . \quad (1)$$

$F_{est}^{opt}(N)$ is the fidelity corresponding to optimal state estimation of N unknown pure input qubit states and was found to be $F_{est}^{opt}(N) = (N + 1)/(N + 2)$ [4].

Moreover, it can be shown [3] that the shrinking factors of universal cloning machines multiply, namely the shrinking factor of a universal $N \rightarrow L$ cloner composed of a sequence

of an $N \rightarrow M$ cloner followed by an $M \rightarrow L$ cloner is the product of the two shrinking factors: $\eta_u(N, M) \cdot \eta_u(M, L)$. By exploiting the above concatenation property and Eq. (1) the following upper bound for an $N \rightarrow M$ cloner can be derived [3]:

$$\eta_u(N, M) \leq \frac{\eta_u^{opt}(N, \infty)}{\eta_u^{opt}(M, \infty)} = \frac{N(M+2)}{M(N+2)}. \quad (2)$$

The above bound is achieved by the cloning transformations proposed in [5].

We now start restricting the class of input states and consider only states of the form $|\psi_\phi\rangle = (|0\rangle + e^{i\phi}|1\rangle)\sqrt{2}$, where $\phi \in [0, 2\pi)$. We are interested in cloning transformations that treat each input state belonging to this class in the same way, namely whose efficiency does not depend on the value of the phase ϕ . Cloning transformations satisfying the above condition will be called phase covariant.

It can be shown [7] that phase covariant cloning transformations for input states $|\psi_\phi\rangle$ correspond to a shrinking of the Bloch vector by a factor $\eta_{pc}(N, M)$ and that the sequence of two covariant cloners, the first taking N states $|\psi_\phi\rangle$ and giving M output copies, and the second taking the M output copies as input and generating L output copies, can be viewed as an $N \rightarrow L$ phase covariant cloner with shrinking factor $\eta_{pc}(N, M) \cdot \eta_{pc}(M, L)$.

Moreover, similarly to the case of universal cloning, the following link between phase covariant cloning and phase estimation on qubits of the form $|\psi_\phi\rangle$ can be proved [7]

$$F_{pc}^{opt}(N, \infty) = F_{ph}^{opt}(N), \quad (3)$$

where $F_{ph}^{opt}(N)$ is fidelity of the reconstructed reduced density operator after performing optimal covariant phase estimation on N qubits in the pure state $|\psi_\phi\rangle$. The fidelity for optimal covariant phase estimation for qubits in state $|\psi_\phi\rangle$ takes the form [6]

$$F_{ph}^{opt}(N) = \frac{1}{2} + \frac{1}{2^{N+1}} \sum_{l=0}^{N-1} \sqrt{\binom{N}{l} \binom{N}{l+1}}. \quad (4)$$

As for phase covariant cloners, the fidelity of covariant phase estimation is simply related to the shrinking factor as $F_{ph}(N) = (1 + \eta_{ph}(N))/2$ and therefore the equality (3) holds also for the corresponding shrinking factors.

By concatenating an $N \rightarrow M$ and an $N \rightarrow \infty$ phase covariant cloners and exploiting Eq. (3) we can find the following upper bound on the fidelity of an $N \rightarrow M$ phase covariant cloner [7]

$$\eta_{pc}^{opt}(N, M) \leq 2^{(M-N)} \frac{\sum_{l=0}^{N-1} \sqrt{\binom{N}{l} \binom{N}{l+1}}}{\sum_{j=0}^{M-1} \sqrt{\binom{M}{j} \binom{M}{j+1}}}. \quad (5)$$

Note that while in the case of the universal cloning we know the explicit form of the cloning map which achieves the bound (2), in the case of phase covariant cloners we know that the above bound can be achieved for the simplest case of the $1 \rightarrow 2$ cloner [7], but we do not know yet whether it can be achieved for any values of N and M . Notice that the bound (5) is always greater than the optimal shrinking factor for the universal cloner (2), as expected.

Finally, we further restrict the class of input states and consider the smallest non trivial one, namely a set of two nonorthogonal pure states, parametrised as

$$|a\rangle = \cos\theta|0\rangle + \sin\theta|1\rangle, \quad |b\rangle = \sin\theta|0\rangle + \cos\theta|1\rangle, \quad (6)$$

where $\theta \in [0, \pi/4]$. The set of the two input states can equivalently be specified by means of their scalar product $S = \langle a|b\rangle = \sin 2\theta$.

We will present here a lower bound for the fidelity of an optimal $N \rightarrow M$ cloning transformation that operates on N input states of the form $|x\rangle^{\otimes N}$, with $x = a, b$, generalising the results presented in [2] for the $1 \rightarrow 2$ case. The resulting transformation is also called state dependent cloner, because its form depends explicitly on the form of the initial states, namely on the parameter θ . We will consider a unitary operator V_{NM} acting on the Hilbert space of M qubits and define the final states $|\alpha_{NM}\rangle$ and $|\beta_{NM}\rangle$ as

$$|\alpha_{NM}\rangle = V_{NM}(|a\rangle^{\otimes N} \otimes |0\rangle^{\otimes M-N}), \quad |\beta_{NM}\rangle = V_{NM}(|b\rangle^{\otimes N} \otimes |0\rangle^{\otimes M-N}). \quad (7)$$

Unitarity gives the constraint $\langle \alpha_{NM} | \beta_{NM} \rangle = S^N$ on the scalar product of the final states.

As a convenient criterion for optimality of the cloning transformation, we maximize the global fidelity $F_g(N, M)$ of both final states $|\alpha_{NM}\rangle$ and $|\beta_{NM}\rangle$ with respect to the perfect cloned states $|a^M\rangle \equiv |a\rangle^{\otimes M}$ and $|b^M\rangle \equiv |b\rangle^{\otimes M}$, namely

$$F_g(N, M) = \frac{1}{2} \left(|\langle \alpha_{NM} | a^M \rangle|^2 + |\langle \beta_{NM} | b^M \rangle|^2 \right). \quad (8)$$

It can be easily shown [8] that the above fidelity is maximized when the states $|\alpha_{NM}\rangle$ and $|\beta_{NM}\rangle$ lie in the two-dimensional space \mathcal{H}_{a^M, b^M} which is spanned by vectors $\{|a^M\rangle, |b^M\rangle\}$ and the maximum fidelity takes the form

$$F_g(N, M) = \frac{1}{2} (1 + S^{N+M} + \sqrt{1 - S^{2N}} \sqrt{1 - S^{2M}}). \quad (9)$$

We can also derive the fidelity of each output copy to compare it with the previous cases and it turns out to be [8]

$$F_{sd}(N, M) = \langle a | \rho_\alpha | a \rangle = A^2(1 + S^2 + 2S^M) + B^2(1 + S^2 - 2S^M) + 2AB(1 - S^2), \quad (10)$$

where ρ_α is the reduced density operator corresponding to input state $|a\rangle$ and $A = \frac{1}{2} \sqrt{\frac{1+S^N}{1+S^M}}$, $B = \frac{1}{2} \sqrt{\frac{1-S^N}{1-S^M}}$. (By the symmetry of the transformation the fidelity of the output state ρ_β with respect to the input $|b\rangle$ leads to the same result.)

Notice that the fidelities for the cloner of nonorthogonal states (10) are just a lower bound. Actually, in order to find the optimal state dependent cloner to be compared with the universal and phase covariant ones, the fidelity $F_{sd}(N, M)$ should be maximised explicitly, and in general additional auxiliary systems interacting with the M qubits should be considered in the definition of the cloning transformation V_{NM} . In Ref. [2] it was shown that for the $1 \rightarrow 2$ case the maximisation of $F_{sd}(1, 2)$ leads to a different cloning transformation than the one considered here, where the global fidelity is maximised. However, the value of the resulting optimal fidelity is only slightly different from the fidelity reported corresponding to Eq. (10). It can be easily verified that the fidelities (10) always correspond to considerably higher values than the ones for universal and covariant cloning.

REFERENCES

- [1] W. K. Wootters and W. H. Zurek, *Nature* **299**, 802 (1982).
- [2] D. Bruss, D.P. DiVincenzo, A. Ekert, C.A. Fuchs, C. Macchiavello and J.A. Smolin, *Phys. Rev. A* **57**, 2368 (1998).
- [3] D. Bruß, A. Ekert, C. Macchiavello, *Phys. Rev. Lett.* **81**, 2598 (1998).
- [4] S. Massar and S. Popescu, *Phys. Rev. Lett.* **74**, 1259 (1995).
- [5] N. Gisin and S. Massar, *Phys. Rev. Lett.* **79**, 2153 (1997).
- [6] R. Derka, V. Buzek, A. Ekert, *Phys. Rev. Lett.* **80**, 1571 (1998).
- [7] D. Bruß, M. Cinchetti, G.M. D'Ariano and C. Macchiavello, unpublished.
- [8] C. Macchiavello, unpublished.

Quantum Cloning machines and linear superposition of multiple clones

Arun Kumar Pati*

SEECs, Dean Street, University of Wales, Bangor LL 57 1UT, U. K.

and

Theoretical Physics Division, BARC, Mumbai-400 085, India.

(July 22, 1999)

Abstract

We ask the existence of a novel quantum cloning machine which can produce a linear superposition of multiple copies of the input state. We show that a novel cloning machine can exist if and only if the states are linearly independent. Unlike the other cloning machines the novel cloning machine treats the ‘number’ of clones as a quantum variable. We derive a general bound on the success probability of the novel cloning machine.

In one hand quantum mechanical principles enhance the possibility of information processing and on the other they put some limitations. That an unknown quantum state can not be perfectly copied is a consequence of linearity of quantum theory. This was realised by Wootters-Zurek [1] and Dieks [2]. After the seminal paper on quantum “no-cloning” theorem there is an ongoing interest [3–15] in the investigation of the problem of approximate and exact cloning of non-orthogonal quantum states.

In the literature various authors have asked the question: If we have an unknown state $|\psi\rangle$ is there a device which will produce either $|\psi\rangle \rightarrow |\psi\rangle^{\otimes 2}$, $|\psi\rangle \rightarrow |\psi\rangle^{\otimes 3}$, $|\psi\rangle \rightarrow |\psi\rangle^{\otimes M}$ or $|\psi\rangle^{\otimes N} \rightarrow |\psi\rangle^{\otimes M}$ copies of an unknown state in a deterministic or probabilistic fashion. This is a “classicalised” way of thinking about a quantum cloning machine. With a classical Xerox machine if we feed a paper with some amount of information we can either get $1 \rightarrow 2$, or $1 \rightarrow 3$, or $1 \rightarrow M$ copies by pressing the number of copies we want. In the light of above remark I feel that all the quantum cloning machines discussed so far are not “fully quantum”. If a real quantum cloning machine would exist it should exploit one basic feature of the quantum world and it should produce simultaneously $|\psi\rangle \rightarrow |\psi\rangle^{\otimes 2}$, $|\psi\rangle \rightarrow |\psi\rangle^{\otimes 3}$, and $|\psi\rangle \rightarrow |\psi\rangle^{\otimes M}$ copies. A more general question to ask is if it is possible by some physical process to produce an output state of an unknown quantum state which will be *in a linear superposition of all possible multiple copies each in the same original state*, i.e.,

$$|\Psi\rangle|00\dots 0\rangle \rightarrow c_1|\Psi\rangle|\Psi\rangle|0\rangle\dots|0\rangle + c_2|\Psi\rangle|\Psi\rangle|\Psi\rangle\dots|0\rangle + \dots + c_M|\Psi\rangle|\Psi\rangle\dots|\Psi\rangle. \quad (1)$$

*email:akpati@sees.bangor.ac.uk

A device that can perform this task we call “novel quantum cloning machine” (NQCM). We [16] have recently shown that *an ideal novel cloning machine based on unitarity of quantum theory which succeeds all the time cannot exist.*

Here we discuss the state-dependent exact novel cloning machines. Consider an unknown input state $|\psi_i\rangle$ from a set \mathcal{S} which belongs to a Hilbert space $\mathcal{H}_A = C^{N_A}$. Let $|\Sigma\rangle_B$ be the state of the ancillary system B (analogous to bunch of blank papers) which belongs to a Hilbert space \mathcal{H}_B of dimension $N_B = N_A^M$, where M is the total number of blank states each having dimension N_A . In fact we can take $|\Sigma\rangle_B = |0\rangle^{\otimes M}$. Let there be a probe state of the cloning device which can measure the number of copies that have been produced and $|P\rangle$ be the initial state of the probing device. Let $|P_1\rangle, \dots, |P_M\rangle, \dots, |P_{N_C}\rangle$ are orthonormal basis states of the probing device. The set $\{|P_n\rangle\} \in \mathcal{H}_C = C^{N_C}$ such that $N_C > M$. If a novel cloning machine exist, then it should be represented by a linear, unitary operator that acts on the combined states of the composite system.

We find that if the cloning machine fails some time and the failure branch is described by a state independent of the input state [17] then it is possible to create a linear superposition of multiple clones. Our theorem says:

Theorem : There exists a unitary operator U such that for any unknown state chosen from a set $\mathcal{S} = \{|\psi_i\rangle\} (i = 1, 2, \dots, k)$ the device can create a linear superposition of multiple clones together with failure copies given by

$$U(|\psi_i\rangle|\Sigma\rangle|P\rangle) = \sum_{n=1}^M \sqrt{p_n^{(i)}} |\psi_i\rangle^{\otimes(n+1)} |0\rangle^{\otimes(M-n)} |P_n\rangle + \sum_{l=M+1}^{N_C} \sqrt{f_l^{(i)}} |\Psi_l\rangle_{AB} |P_l\rangle, \quad (2)$$

if and only if the states $|\psi_1\rangle, |\psi_2\rangle, \dots, |\psi_k\rangle$ are linearly independent. In the above equation $p_n^{(i)}$ and $f_l^{(i)}$ are success and failure probabilities for the i th input state to produce n exact copies and to remain in the l th failure component, respectively. The states $|\Psi_l\rangle_{AB}$'s are normalised states of the composite system AB and they are not necessarily orthogonal. The proof can be found in [17].

Since this machine produces exact clones the local fidelity in each branch of the output state is unit. However, the global fidelity may not be unit. If the non-orthogonal states are chosen with certain probability η_i , then the global fidelity can be defined as

$$F = \sum_i \eta_i |\langle \Psi^{ideal} | \Psi^{out} \rangle|^2 = \sum_i \eta_i P_i^2, \quad (3)$$

where $|\Psi^{ideal}\rangle = \sum_{n=1}^M \sqrt{p_n^{(i)}} |\psi_i\rangle^{\otimes(n+1)} |0\rangle^{\otimes(M-n)} |P_n\rangle$ and $|\Psi^{out}\rangle$ is given in (2). The probability $P_i = \sum_n p_n^{(i)}$. One may try to optimise the global fidelity and see if one can do better (in terms of information gain) with a novel cloning machine in contrast to universal, optimal cloning machines.

After the input state chosen from the set \mathcal{S} undergo unitary evolution in order to know how many copies are produced by the novel cloning machine, one needs to do a von Neumann measurement onto the probe basis. This can be thought of as a measurement of a Hermitian operator. We introduce such an operator, which is called “Xerox number” operator N_X , defined as

$$N_X = \sum_{n=1}^M n |P_n\rangle \langle P_n|. \quad (4)$$

The probe states $|P_n\rangle$ are eigenstates of the Xerox number operator with eigenvalue n where n is the number of clones produced with a probability distribution $p_n^{(i)}$. The novel cloning machine would produce $1 \rightarrow 2$ copies with probability p_1 , $1 \rightarrow 3$ copies with probability p_2 , ...and $1 \rightarrow M + 1$ copies with probability p_M in accordance with the usual rules of quantum mechanics.

Our result is consistent with the known results on cloning. In the unitary evolution if one of the positive number in success branch is one and all others (including failure branches) are zero, then we have $U(|\psi_i\rangle|\Sigma\rangle|P\rangle) = |\psi_i\rangle^{\otimes(n+1)}|0\rangle^{\otimes(M-n)}|P_n\rangle$. This tells us that the matrix equation would be $G^{(1)} = G^{(n+1)}$ since $A_n = I$. This will be possible only when the states chosen from a set are orthogonal to each other. Thus a single quanta in an orthogonal state can be perfectly cloned [4]. An interesting result also follows from our proposed cloning machine. If the state are orthogonal and all $p_n^{(i)}$'s are non-zero, then unitarity allows us to have a *linear superposition of multiple copies of orthogonal states* as the matrix equation is always satisfied.

The tight bound on the individual success probability for cloning of two distinct non-orthogonal states is given by

$$\frac{1}{2} \sum_n (p_n^{(i)} + p_n^{(j)}) (1 - |\langle\psi_i|\psi_j\rangle|^{n+1}) \leq (1 - |\langle\psi_i|\psi_j\rangle|). \quad (5)$$

The above bound is related to the distinguishable metric of the quantum state space. Since the "minimum-normed-distance" [18] between two non-orthogonal states $|\psi_i\rangle$ and $|\psi_j\rangle$ is $D^2(|\psi_i\rangle, |\psi_j\rangle) = 2(1 - |\langle\psi_i|\psi_j\rangle|)$ and the "minimum-normed-distance" between $n+1$ clones is $D^2(|\psi_i\rangle^{\otimes n+1}, |\psi_j\rangle^{\otimes n+1}) = 2(1 - |\langle\psi_i|\psi_j\rangle|^{n+1})$, the tight bound can be expressed as

$$\sum_n p_n D^2(|\psi_i\rangle^{\otimes n+1}, |\psi_j\rangle^{\otimes n+1}) \leq D^2(|\psi_i\rangle, |\psi_j\rangle), \quad (6)$$

where we have defined total success probability p_n for n th clones as $p_n = \frac{1}{2}(p_n^{(i)} + p_n^{(j)})$. The above bound can be interpreted physically as the sum of the weighted distance between two distinct states of $n+1$ clones is always bounded by the the original distance between two non-orthogonal states. Our bound is consistent with the known results on cloning. For example, if we have $1 \rightarrow 2$ cloning, then in the evolution we have $p_1^{(i)}$ and $p_1^{(j)}$ are non-zero and all others are zero. In this case our bound reduces to $\frac{1}{2}(p_1^{(i)} + p_1^{(j)}) \leq \frac{1}{1+|\langle\psi_i|\psi_j\rangle|}$, which is the Duan-Guo bound [12]. Similarly if we have $1 \rightarrow M$ cloning, then in the evolution we have $p_M^{(i)}$ and $p_M^{(j)}$ are non-zero and all others are zero. In this case our bound reduces to $\frac{1}{2}(p_M^{(i)} + p_M^{(j)}) \leq \frac{1-|\langle\psi_i|\psi_j\rangle|}{1-|\langle\psi_i|\psi_j\rangle|^M}$, which is the Chefles-Barnett [14] bound. Both these bounds can be interpreted as the *ratio of the distance function between two non-orthogonal state* before and after (ideal) cloning operation.

It would be interesting to construct a novel cloning for unknown mixed states. We conjecture that if one can construct such a machine, then the success probabilities of producing superposition of multiple copies of the mixed states chosen from a set $\{\rho_i\}$ would obey the bound given by

$$\frac{1}{2} \sum_n (p_n^{(i)} + p_n^{(j)}) (1 - [\text{tr}(\rho_i\rho_j)]^{\frac{n+1}{2}}) \leq (1 - [\text{tr}(\rho_i\rho_j)]^{\frac{1}{2}}). \quad (7)$$

We show that the probabilistic cloning machine discussed by Duan and Guo [13] can be considered as a special case of the general novel cloning machine. To see that from our machine Duan-Guo machine follows as a special case, let us take one of the $p_n^{(i)}$ is non-zero and all others are zero in the unitary transformation (2). Then we have the following evolution for the non-orthogonal states

$$U(|\psi_i\rangle|\Sigma\rangle|P\rangle) = \sqrt{p_2^{(i)}}|\psi_i\rangle^{\otimes 2}|P_2\rangle + \sum \sqrt{f_l^{(i)}}|\Psi_l\rangle_{AB}|P_l\rangle. \quad (8)$$

where we have assumed that there is only one blank state. This is nothing but Duan-Guo type of probabilistic machine for producing $1 \rightarrow 2$ copies. If one does a measurement of the probe with a postselection of the measurement results, then this will yield two exact copies of the unknown quantum states. Since all other deterministic cloning machines are special cases of Duan-Guo machine, we can say, in fact, that all deterministic and probabilistic cloning machines are special cases of our novel cloning machines.

In conclusion, we have asked an important question: whether it is possible to create a linear superposition of multiple clones. We proved that unitarity allows us to create linear superposition of multiple clones of non-orthogonal states along with a failure term if and only if the states are linearly independent. We derived a tight bound on the success probability of passing two non-orthogonal states through our novel cloning machine and shown that all known bounds follow from our tight bound. The present idea can be applied to universal cloning machine, state-dependent, approximate quantum cloning machines and so on. We hope that the linear superposition of multiple clones will have potential application in the easy preservation of important quantum information, quantum error correction and parallel storage of information in a quantum computer.

I thank S. L. Braunstein and L. M. Duan for very useful discussions. I thank A. Chefles for useful comments. I gratefully acknowledge financial support by EPSRC.

REFERENCES

- [1] W. K. Wootters and W. H. Zurek, *Nature* **299**, 802 (1982).
- [2] D. Dieks, *Phys. Lett. A* **92**, 271 (1982).
- [3] L. Susskind and J. Uglun, *String Physics and Black holes*, *Nuclear Phys. (Proc. Suppl.)* **45 B, C**, 115 (1996).
- [4] H. P. Yuen, *Phys. Lett. A* **113**, 405 (1986).
- [5] G. M. D'Ariano and H. P. Yuen, *Phys. Rev. Lett.* **76**, 2832 (1996).
- [6] H. Barnum, C. M. Caves, C. A. Fuchs, R. Josza, and B. Schumacher, *Phys. Rev. Lett.* **76**, 2818 (1996).
- [7] V. Bužek and M. H. Hillery, *Phys. Rev. A* **54**, 1844 (1996).
- [8] V. Bužek, S. L. Braunstein, M. H. Hillery, D. Bruß, *Phys. Rev. A* **56**, 3446 (1997).
- [9] N. Gisin and S. Massar, *Phys. Rev. Lett.* **79**, 2153 (1997).
- [10] D. Bruß, et al, *Phys. Rev. A* **57**, 2368 (1998).
- [11] V. Bužek, V. Vedral, M. B. Plenio, P. L. Knight, and M. H. Hillery, *Phys. Rev. A* **55** 3327 (1997).
- [12] L. M. Duan and G. C. Guo, *Phys. Lett. A* **243**, 261 (1998).
- [13] L. M. Duan and G. C. Guo, *Phys. Rev. Lett.* **80**, 4999 (1998).
- [14] A. Chefles and S. M. Barnett, *J. Phys. A* **31**, 10097 (1998).
- [15] A. K. Pati, "*Assisted cloning*" and "*orthogonal complementing*" of unknown states, quant-ph/9904068.
- [16] A. K. Pati, *Multiple quantum clones cannot be superposed*, (Preprint, 1999).
- [17] A. K. Pati, *Quantum superposition of multiple clones and the novel cloning machine*, quant-ph/9903038.
- [18] A. K. Pati, *Phys. Lett. A* **159**, 105 (1991).

Imaging of faint phase objects at Heisenberg limit with quadrature squeezed light

Ivan V. Sokolov

Physics Institute, St. Petersburg University, 198904 Petrodvorets, St. Petersburg, Russia

Email: sokolov@is2968.spb.edu

Abstract

We evaluate the limiting sensitivity of imaging of a two-dimensional faint phase object, placed into an interferometer. We consider the case when both input ports of the interferometer are illuminated by spatially-multimode quadrature squeezed light. In optimum case one can minimize both noise contributions to the observed signal: the beatings between the coherent and the squeezed components of pump and the self-beatings of squeezed pump. We demonstrate that this provides the Heisenberg-limited sensitivity of the measurement of the spatial phase distribution in the object. The optimum choice of space-time scales of the system and the resolving power of the measurement in space and time are discussed.

The measured phase shift is introduced by a two-dimensional faint phase object, placed into the Mach-Zehnder interferometer. The observed signal is the spatial variation in the output light power. If the interferometer (the pump port) is illuminated by classical monochromatic wave, the minimum measured phase shift $\delta\varphi^{(sh)}$ is limited by the photon (shot) noise, $\delta\varphi^{(sh)} = 1/\sqrt{n}$. Here n is the mean number of photons, detected during the measurement cycle. For $n \gg 1$ this estimate is far from the ultimate Heisenberg limit to the minimum measured phase difference $\delta\varphi^{(H)} \sim 1/n$.

The shot-noise-limited estimate is significantly improved when the quadrature squeezed states of light are used. This was shown in a number of papers (see e.g., a comprehensive paper by Caves [1]). By the illumination of the normally unused (idle) port of the interferometer with quadrature squeezed light and for the optimum choice of the phase and the degree of squeezing the sensitivity of the phase measurement is limited by the value $\delta\varphi^{(sq)} \sim 1/n^{3/4}$. For $n \gg 1$ these estimates are ranged as $\Delta\varphi^{(H)} \ll \Delta\varphi^{(sq)} \ll \Delta\varphi^{(sh)}$. A clear physical explanation of the improvement in the signal-to-noise ratio is based on the wave picture. The main noise source for $n \gg 1$ and not very large degree of squeezing is due to the beatings (interference) between the classical wave from the input port 1 (pump port) and the in-phase quadrature component of the squeezed light from the input port 2 (idle port). With the decreasing amplitude of the in-phase quadrature component the observed noise also decreases.

The first phase measurements beyond the shot noise limit were done in [2,3]. The possi-

bility to improve the sensitivity of measurements for two-dimensional phase objects (images) was demonstrated theoretically in [4,5] for the objects with faint phase modulation in space and time and in [6] for the case of phase modulation of any amplitude. The sensitivity predicted in [4 - 6] is limited by the estimate similar to $\delta\varphi^{(sq)}$.

The problem of Heisenberg-limited phase measurements attracts now significant interest. One can mention the proposal to use for such measurements the de Broglie wavelength Mach-Zehnder interferometer [7], the discussion of the phase properties of the entangled (equipartition) states of two electromagnetic oscillators [8,9] etc.

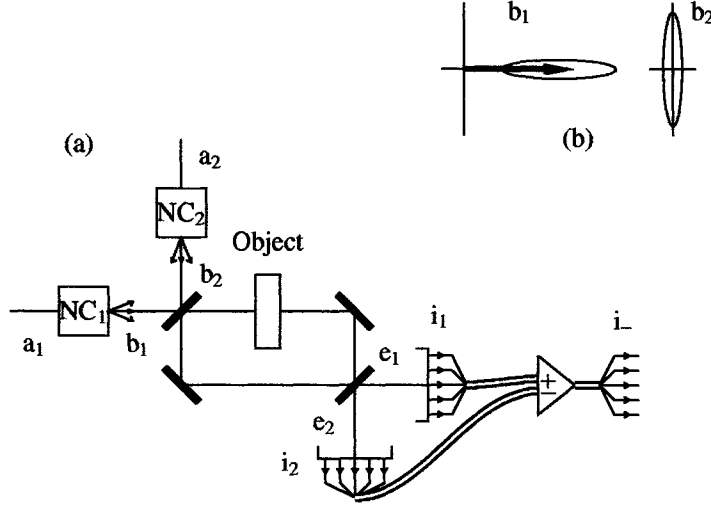


FIG.1. (a) Schematic diagram of the optical scheme for imaging of a faint phase object; (b) optimum phase matching of classical and squeezed components of the illuminating light fields.

The optical scheme for imaging of a faint phase object is shown in Fig.1. A two-dimensional phase object is placed into Mach-Zehnder interferometer with plane mirrors. The input port 1 of the interferometer is illuminated by the light wave in a spatially-multimode squeezed state, generated in non-linear crystal NC_1 . The light field amplitude has an average (classical) component b_1^c . This component describes a plane wave, which produces the average response of the device to the phase shift $\varphi(\vec{\rho}, t) \ll 1$ in the object (here $\vec{\rho} = (x, y)$). The input port 2 is illuminated by the light wave in the state of spatially-multimode squeezed vacuum, produced by the non-linear crystal NC_2 .

The squeezing transformation of the field amplitudes, performed by non-linear crystals, is given by

$$b_p(\vec{q}, \Omega) = U_p(\vec{q}, \Omega)a_p(\vec{q}, \Omega) + V_p(\vec{q}, \Omega)a_p^+(-\vec{q}, -\Omega), \quad (1)$$

where \vec{q}, Ω are the Fourier arguments, $\vec{\rho}, t \rightarrow \vec{q}, \Omega$. The coefficients U, V of the squeezing transformation determine the standard parameters of squeezed state:

$$\psi_p(\vec{q}, \Omega) = \frac{1}{2} \arg \{U_p(\vec{q}, \Omega)V_p(-\vec{q}, -\Omega)\}, \quad e^{\pm r_p(\vec{q}, \Omega)} = |U_p(\vec{q}, \Omega)| \pm |V_p(\vec{q}, \Omega)|, \quad (2)$$

where $\psi_p(\vec{q}, \Omega)$ is the orientation angle of the major axis of squeezing ellipse in the complex plane of field amplitude, and $e^{\pm r_p(\vec{q}, \Omega)}$ gives the degree of stretching and squeezing of the uncertainty region.

The state of the light fields at the inputs of non-linear crystals is coherent for the plane wave, propagating in z direction at the input 1, and vacuum for all other degrees of freedom. We assume that in absence of the object the interferometer is precisely balanced and is equivalent to the 1:1 beamsplitter.

The output light fields are detected with the use of dense arrays of effective photon counters with quantum efficiency $\eta \leq 1$. The measured quantities are the output photocurrent densities $i_n(\vec{\rho}, t)$ (without multiplication by the elementary charge), where $n = 1, 2$.

The observed quantity is the difference photocurrent density $i_-(\vec{\rho}, t) = i_1(\vec{\rho}, t) - i_2(\vec{\rho}, t)$. The response of the scheme to the phase shift in the object (i.e. the signal) is found in the form $\langle i_-(\vec{\rho}, t) \rangle \approx |b_1^c|^2 \varphi(\vec{\rho}, t)$. Since both the signal and the quantum fluctuations are assumed to be small, we evaluate quantum noise of the observable in absence of the signal.

With the use of Glauber's photodetection theory we relate the photocurrent correlation functions to the correlation functions of the input fields a_p . The spectral power of space-time fluctuations in the observed difference photocurrent density is found after some calculations in the form

$$\left(\delta i_-^2\right)_{\vec{q}, \Omega} = \langle i_+ \rangle (1 - \eta) + \left(\delta i_-^2\right)_{\vec{q}, \Omega}^{(cs)} + \left(\delta i_-^2\right)_{\vec{q}, \Omega}^{(ss)}. \quad (3)$$

Here η is the quantum efficiency of a pixel. There are three main contributions to the noise spectrum (3):

1. The term, proportional to the sum of the mean photocurrent densities $\langle i_+ \rangle = \langle i_1 \rangle + \langle i_2 \rangle$, is responsible for residual shot noise in the case of non-ideal photodetection, $\eta < 1$.

2. The contribution

$$\left(\delta i_-^2\right)_{\vec{q}, \Omega}^{(cs)} = |b_1^c|^2 \eta^2 \left\{ \exp(2r_2(\vec{q}, \Omega)) \cos^2 \theta_{12}(\vec{q}, \Omega) + \exp(-2r_2(\vec{q}, \Omega)) \sin^2 \theta_{12}(\vec{q}, \Omega) \right\}, \quad (4)$$

proportional to the surface power $|b_1^c|^2$ of the classical plane wave (in photon units), is related to the beatings between the classical wave at the input port 1 and the in-phase quadrature component of the light wave in the spatially-multimode squeezed state at the input port 2. The power of the beatings is determined by the difference angle $\theta_{12}(\vec{q}, \Omega) = \psi_2(\vec{q}, \Omega) - \arg b_1^c$ between the main axis of the squeezing ellipse and the complex amplitude of the classical wave. This contribution to the noise power is minimized by the phase matching $\theta_{12}(\vec{q}, \Omega) = \pm \pi/2$.

3. The term

$$\left(\delta i_-^2\right)_{\vec{q}, \Omega}^{(ss)} = \eta^2 \frac{1}{(2\pi)^3} \int d\vec{q}' d\Omega' \left\{ \sinh^2(r_1(\vec{q} - \vec{q}', \Omega - \Omega') + r_2(\vec{q}', \Omega')) \times \right. \\ \left. \cos^2(\psi_1(\vec{q} - \vec{q}', \Omega - \Omega') - \psi_2(\vec{q}', \Omega')) + \right. \quad (5)$$

$$\left. \sinh^2(r_1(\vec{q} - \vec{q}', \Omega - \Omega') - r_2(\vec{q}', \Omega')) \sin^2(\psi_1(\vec{q} - \vec{q}', \Omega - \Omega') - \psi_2(\vec{q}', \Omega')) \right\},$$

gives the spectral power of the cross-beatings between two multimode squeezed light waves. This term is determined by the space-time spectral convolution. Here one can easily identify contributions, proportional to $\exp(\pm r_1 \pm r_2)$, each due to the cross-beatings between given pair of squeezed or stretched quadrature components of input light fields. The power of each

contribution is determined by *sin* or *cos* of the difference angle $\psi_1(\vec{q}-\vec{q}', \Omega-\Omega')-\psi_2(\vec{q}', \Omega')$ between the main axes of squeezing ellipses for the input light waves.

The major contribution to the noise power (5) due to the beatings between the *stretched* quadrature components of two squeezed light fields is eliminated by the relative phase shift $\psi_1-\psi_2=\pm\pi/2$. The optimum matching of the degrees of squeezing of two squeezed input light waves $r_1=r_2$, eliminates the noise contribution (5) completely.

Consider the low-frequency value of the noise power in the case of degenerate and collinear phase matching in the non-linear crystals. Assume that the photons are collected by the effective ($\eta=1$) elementary detectors (pixels) of area $S_d \geq S_{coh}$ during the sampling time $T_d \geq T_{coh}$, where $S_{coh}=(2\pi/\Delta q)^2$ and $T_{coh}=2\pi/\Delta\Omega$ are the coherence area and the coherence time of squeezed light at input port 2. Here Δq and $\Delta\Omega$ are the widths of the frequency bands of effective squeezing. In the case of large degree of squeezing, $r_2 \gg 1$, we arrive to the estimate

$$\delta\varphi(\vec{\rho}, t) \approx \frac{1}{2\sqrt{n^c n^{sq}}} \left(\frac{S_d T_d}{S_{coh} T_{coh}} \right)^{1/2}, \quad (6)$$

where n^c and n^{sq} are the mean numbers of photons in the coherent and the squeezed waves. Let us evaluate the limiting sensitivity of phase measurement by given overall number of photons n in the classical and the two squeezed light waves, detected during the measurement cycle $n=n^c+2n^{sq}$. In the case $S_d T_d \geq S_{coh} T_{coh}$ we obtain, up to a numerical factor, the Heiseberg-limited value. But if the time-space scales of the detection procedure and the squeezed input light waves are not matched, $S_d T_d \gg S_{coh} T_{coh}$, the limiting sensitivity is degraded by the factor $(S_d T_d / S_{coh} T_{coh})^{1/2} \gg 1$.

Physically this can be explained in a following way. Since the mean number of photons in squeezed light waves per measurement cycle is limited by n , the number of photons collected at the coherence area during the coherence time is limited by the value $n S_{coh} T_{coh} / S_d T_d$. The smaller coherence volume $S_{coh} T_{coh}$, the smaller is the number of photons in elementary field degree of freedom, the amount of squeezing in illuminating light and the noise suppression.

REFERENCES

1. C.M.Caves, Phys. Rev. A **23**, 1693 (1981).
2. Min Xiao, Ling-An Wu and H.J.Kimble, Phys. Rev. Lett. **59**, 278 (1987).
3. P.Grangier, R.E.Slusher, B.Yurke and A.LaPorta, Phys. Rev. Lett. **59**, 2153 (1987).
4. I.V.Sokolov, Opt. Spectrosc. (USSR) **70**, 393 (1991).
5. M.I.Kolobov and P.Kumar, Opt. Lett. **18**, 849 (1993).
6. I.V.Sokolov, Sov. Phys. JETP **73**, 431 (1991).
7. J.Jacobson, G.Björk, I.Chuang and Y.Yamamoto, Phys. Rev. Lett. **74**, 4835 (1995).
8. Björk G, Trifonov A, Tsegaye T and Söderholm J, Journ. of Opt. B: Quant. and Semicl. Opt. **10**, 705 (1998).
9. Trifonov A, Tsegaye T, Björk G, Goobar E and Söderholm J, Opt. Spectrosc. (USSR), in press (1999).

Quantum Limits in the Measurement of Very Small Displacements in Optical Images

C. Fabre, A. Maître, M. Vaupel

*Laboratoire Kastler Brossel, Université Pierre et Marie Curie, Case 74,
75252 Paris cedex 05, France*

Abstract

We consider the problem of the measurement of very small displacements in the transverse plane of an optical image using a split-photodetector. We show that the standard quantum limit for such a measurement, equal to the diffraction limit divided by the square root of the number of photons used in the measurement, can be overcome, not by using "ordinary" single mode squeezed light, but by nonclassical transverse multimode light. We present an experiment aiming at producing such states.

Up to now, Quantum Optics has been mainly interested in measurements involving the total intensity of light beams. But classical optics is not limited to the study of a single information extracted from light : it is mainly interested in *images*, which are now recorded by very efficient detectors such as CCD cameras or photodetector arrays, which sample the transverse variation of the light intensity on their pixels. Improving the quality of image recording is of paramount importance in many areas, such as astronomy, microscopy, holography, According to the Rayleigh criterion, the resolution in optical images is limited by diffraction. This classical criterion, based on the capabilities of the human visual system, is violated when one uses modern photodetectors which are able to resolve image details much smaller than the size of a diffraction spot [1]. The quality and resolution of image recording is then limited by the quantum fluctuations of the light affecting each pixel [2]. We will here recall the standard quantum limit in image recording, and then determine what are the best nonclassical states of light which can allow us to go beyond it.

Let us first assume that the incident beam is described by a *single mode quantum state* in a given transverse mode $u_1(x, y)$ (where x and y are the coordinates in the transverse plane). Let N_A and N_B be the photocurrent measured on two photodetectors A and B of areas S_A and S_B , expressed in units of number of photons recorded during the measurement time. A straightforward calculation based on standard photodetection theory gives the following result for the quantity $C_{N_A N_B} = \langle N_A N_B \rangle - \langle N_A \rangle \langle N_B \rangle$, equal to the correlation function when $A \neq B$, and to the intensity noise variance ΔN_A^2 when $A = B$

$$C_{N_A N_B} = N_{S_A \cap S_B} + \frac{\langle N_A \rangle \langle N_B \rangle}{\langle N_{tot} \rangle^2} (\Delta N_{tot}^2 - \langle N_{tot} \rangle) \quad (1)$$

where $N_{S_A \cap S_B}$ is the mean intensity measured by a photodetector covering the intersection between the two areas S_A and S_B . $\langle N_{tot} \rangle$ and ΔN_{tot}^2 are respectively the mean and the

variance of the total photocurrent, measured by a detector covering the entire transverse plane. If the quantum state describing the single mode beam is a coherent state, formula (1) shows that the photocurrent fluctuations are at the shot noise level on all the pixels, whatever their size and position, and that the fluctuations at two different pixels are uncorrelated. This result is consistent with the simple picture that a coherent state is 'composed' of photons which are randomly distributed not only in time, but also in the transverse plane inside the beam area. If the beam is in a sub-Poissonian state, like the ones produced by some semiconductor lasers, one can easily show from this formula that there is less noise reduction in partial photodetection than in the entire beam. When the pixel size is decreased, the noise increases exactly in the same way as when one inserts an absorbing medium in a squeezed beam which reduces the mean intensity by the same factor. For a single mode beam, a partial detection is thus equivalent to a loss mechanism. This property can be simply pictured by asserting that a single mode sub-Poissonian beam is composed of photons which are somehow antibunched in time, but still completely randomly distributed in the transverse plane, like in a coherent state : transverse randomness is therefore associated to the single mode nature of the field, and not to its coherent or quasi-classical nature.

Let us now consider a two-mode state, spanned on two transverse modes u_1 and u_2 . It is also possible in this case to derive a formula giving the local noise and correlations of the different pixels. We will not give here its lengthy expression, which can be found in [3]. Let us simply say that in this case, partial photodetection cannot be assimilated to a simple loss mechanism, as in the single mode case. In the case of multimode laser beams having excess noise, for example, one can find in [4] and [5] examples of nontrivial noise variations in partial photodetection, providing a precious information on the laser used in the experiment.

In order to give precise assessments of the quantum limits in transverse measurements, we will focus our attention on a precise problem, namely the measurement of very small displacements in an optical image. Let us consider more precisely a configuration which is very often used by experimentalists, for example in atomic force microscopy [6] or in single molecule tracking in biology [7] : the photodetector array is a two-pixel photodetector ("split detector"), delivering two photocurrents N_A and N_B proportional to the light intensities integrated over the two halves of the transverse plane ($A: x > 0; B: x < 0$). A light beam of intensity $I(x, y)$, assumed symmetrical with respect to the pixel boundary, is incident on the split photodetector. If the beam is initially centered on the detector, the mean value of the photocurrent difference $N_- = N_A - N_B$ is directly proportional to the relative lateral displacement D of the whole beam with respect to the initial symmetrical configuration, at least for displacements small compared to the beam size. The noise affecting this quantity, sometimes called "position noise", limits the accuracy in the measurement of D . When the light beam is in a coherent state, the displacement D_{sql} providing a value of $\langle N_- \rangle$ equal to this noise is the standard quantum limit in the measurement of a small transverse displacement. One finds from Eq(1)

$$D_{sql} = \frac{\Delta}{\sqrt{\langle N_{tot} \rangle}} \quad (2)$$

where Δ is an effective beam width, equal for example to $0.63w_0$ for a TEM_{00} Gaussian beam of waist w_0 . Within some numerical factor of order one, Δ gives the Rayleigh, or diffraction,

limit in this specific measurement. The fact that the standard quantum limit can be much smaller than the optical wavelength even with light beams of moderate intensities, is often used in optical transverse measurements.

Let us now use nonclassical states of light and see whether they can improve this kind of transverse measurement. As already stated, it will not be useful to replace the single mode coherent beam by a single mode nonclassical beam. It is easy to show from Formula (1) that the minimum measurable displacement is still given by expression (2) for any single mode state of light. The standard quantum limit can be overcome only if one uses a multi-transverse mode nonclassical state of light. Ref([3]) gives an example of a two-mode state allowing us to reduce by a large amount the variance in the measurement of the intensity difference between the two half planes. This state is nevertheless difficult to propagate over some distance because it contains high spatial Fourier components. Other non-classical states, less sensitive to propagation effects, can be envisioned. They consist of appropriate superpositions of many different transverse TEM_{pq} modes in nonclassical states. In this respect parametric interaction in an optical cavity with a great number of degenerate transverse modes seems a very promising source of nonclassical transverse states of light. In particular the quasi-planar configuration has been shown in [8] to produce below threshold a field with almost identical quantum intensity fluctuations at points symmetrical with respect to the cavity axis. This device is indeed likely to increase by a large factor the ultimate sensitivity in the measurement of a small displacement.

We have developed an experimental set-up to produce such multimode nonclassical states of light. It consists of a non degenerate, c.w., triply resonant Optical Parametric Oscillator pumped by a high power (1.8W) source of light at 532nm of high spectral purity and stability [9]. The OPO cavity is operated close to its confocal position, so that many different transverse modes of the signal and idler modes can be coupled by the parametric interaction. Figure 1 shows the pump threshold for the OPO oscillation as a function of the resonator length. For lengths longer than the confocal configuration, the threshold is roughly 40mW, corresponding to a single mode OPO. For lengths smaller than this value, the threshold dramatically increases by more than a factor 5. The different pictures inserted in the figure show the corresponding near field transverse distribution of the signal mode. In the region where the threshold is high, the signal near field exhibits a ring structure, consisting of a bright small center, surrounded by wide concentric rings and thin fringes. This is the first experimental evidence of a pattern formation in OPOs. We have shown that in this experimental configuration, the OPO oscillates on a coherent superposition of roughly 25 transverse modes. This highly multi-transverse mode configuration is a good candidate to generate light fields with nonclassical transverse distribution of quantum fluctuations likely to increase the transverse resolution in optical images. We are currently studying the noise properties of the observed optical patterns.

We thank L. Lugiato, A. Gatti and M. Kolobov for many enlightening discussions. This work has been partially funded by an E.C. TMR network "QSTRUCT". Laboratoire Kastler Brossel, from Ecole Normale Supérieure and Université P.M. Curie, is associated to CNRS.

REFERENCES

- [1] for a survey, see for example : A. den Dekker, A. van den Bos, J. Opt. Soc. Am. A **14**, 547 (1994)
- [2] for a review, see for example : L. Lugiato, A. Gatti, H. Wiedemann, Les Houches Session LXIII, p. 431, North-Holland (1997), and M. Kolobov, "the spatial behavior of quantum noise", to be published in Rev. Mod. Physics (1999)
- [3] C. Fabre, J.B. Fouet, A. Maître, "Quantum limits in the measurement of very small displacements in optical images", preprint, to be published
- [4] M. Levenson, W. Richardson, S. Perlmutter, Opt. Lett. **14**, 779 (1990)
- [5] J-P. Poizat, T-J. Chang, O. Ripoll, P. Grangier, J. Opt. Soc. Am.B **15**, 1757 (1998)
- [6] C. Putman, B. De Grooth, N. Van Hulst, J. Greve J. Appl. Phys. **72**, 6 (1992)
- [7] S. Kamimura, Applied Opt. **26**, 3425 (1987)
- [8] I. Marzoli, A. Gatti, L. Lugiato, Phys. Rev. Lett. **78**, 2092 (1997)
- [9] M. Vaupel, A. Maître, C. Fabre, "Observation of pattern formation in Optical Parametric Oscillators", preprint, submitted

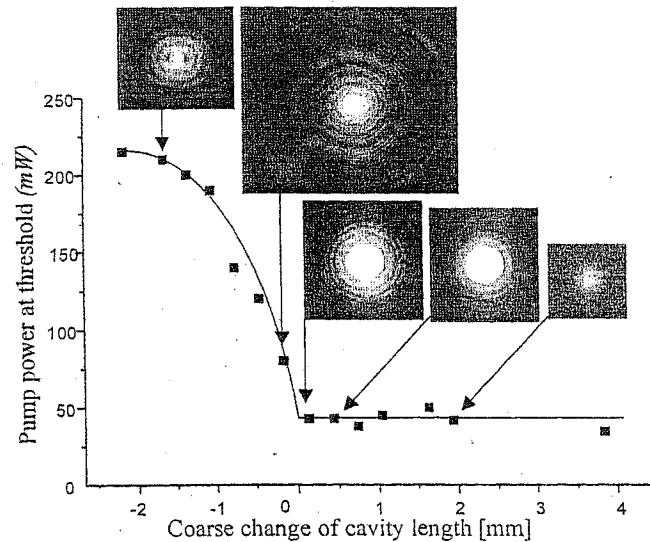


figure 1

Self homodyne Tomography of a Laser Diode

Marco Fiorentino

Università di Napoli, INFN unità di Napoli, Mfiore@na.infn.it

Alessandro Conti

Gianni Giacomelli

Università di Firenze, INO Firenze

INO Firenze

Francesco Marin

Alessandro Zavatta

Università di Firenze, LENS Firenze

Università di Bologna, INO Firenze

Abstract

Considerable interest is growing around self homodyne techniques. Such techniques allow to avoid non unitary detection efficiencies due to inefficient mode matching of the local oscillator. As proposed by Galatola et al. (Opt. Comm. 85 (1991)p.95-103), one possible scheme of self homodyne detection of a field with a strong coherent component involves the use of a Fabry-Perot cavity with a perfectly reflecting mirror. We extend the theory to arbitrary cavities, and we observe a remarkable qualitative agreement between the theory and the observed data. Using the same setup we performed a tomographic measure of the Wigner function of the field emitted by a laser diode

Aim of the present work is to study the self homodyne scheme proposed by Galatola et al. (Opt. Comm. 85 (1991)p.95-103) in presence of losses and to explore the possibility of using such scheme for a tomographic analysis of the field emitted by a laser diode. The set-up used in our experiments is shown in figure 1. The laser is a Mitsubishi ML5415N diode emitting at 830 nm externally feed-backed with an holographic grating. The heart of the experiment is a confocal 10 cm F.P cavity with an high-reflectivity back-mirror ($T < .1\%$) and a measured finesse of 150. We also measure the modulus of coupling coefficient of the cavity $|x|= 0.85$ and infer the negative sign of the coefficient. The homodyne detection system is based on two EG&G FND100 detectors mounted on home made low noise amplifiers followed by passive power combiners which allow to sum/subtract currents from the amplifiers. A photodiode detecting the transmission of the interferometer is used for alignment..

The self homodyne analysis of fields with a strong coherent component used here is based on the possibility of varying the angle between the noise ellipse and the coherent component of the field. This allows to transform any quadrature of the field in the amplitude quadrature thus permitting a direct detection of its fluctuations. As in FM spectroscopy the phase noise is transformed in amplitude noise using a dispersive medium. In our case the dispersive medium is the F.P. cavity. Each Fourier component of the fluctuations undergoes a different phase rotation depending on the ratio Ω of its frequency to the cavity half-linewidth.

Galatola et al. already pointed out that the key feature of the F.P. cavity is the coupling parameter defined as

$$\xi = \frac{T_2 - T_1 + S_1 + S_2}{T_2 + T_1 + S_1 + S_2}$$

In their work they assumed a cavity with a perfectly reflecting rear mirror and loss-less front mirror. For commercial mirrors typical losses are of the order of 0.2 % mainly due to residue reflections on the mirrors' first surfaces. It is easily demonstrated that the effect of losses is dramatic especially for high finesse cavities. In our cavity we measured a coupling factor of -0.85 and a finesse of 150 which are consistent with total losses of a few tenths of percent.

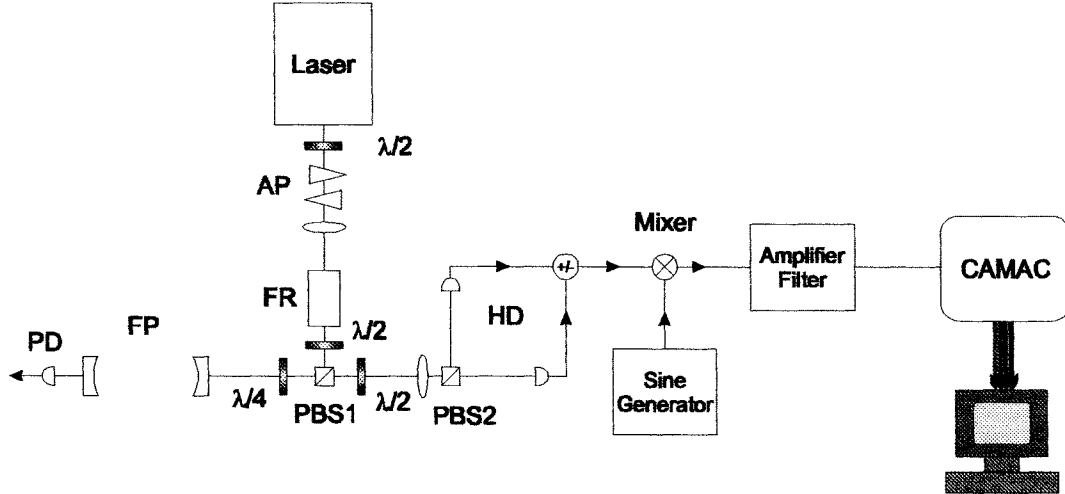


Figure 1: Experimental setup, see text for details

To show the effect of losses on expected signals we plot in figure 2 the variance of the amplitude noise of the field reflected by the cavity as its resonance frequency is scanned for different values of ξ , putting $\Omega=6$, θ is the detuning normalised to the half linewidth of the cavity. We suppose that the input field of the cavity has shot noise limited amplitude fluctuations and phase fluctuations 100 times greater and normalise the variance to the shot noise.

As a check of our extended theory we make a comparison between the theoretical predictions using independently measured parameters and the variance of the amplitude fluctuations measured with a spectrum analyser. We found a remarkable agreement between the theory and the measurement. A systematic deviation is observed on the tails of the curve. This is probably due to a feature of the laser itself.

We explored the possibility of using this self homodyne technique to make a tomographic reconstruction of the Wigner function. The experimental setup is shown in figure 3, we use the mixer and a sine generator (@60 MHz) which allow to analyse the fluctuations of the sum (amplitude fluctuations of the input field) or difference (shot noise calibration) of the photocurrents at a given frequency. The intermediate frequency (IF) signal is amplified and filtered (low pass filter, cutoff frequency 300 kHz) to remove RF components, then it is sent to a Lecroy 6810 CAMAC waveform recorder, which acquires up to 10^6 12-bit points at 5 Msamples/s. The CAMAC is connected via GPIB to a PC for data analysis.

From the data registered by the CAMAC we calculate the variance and fit the variance curve to obtain an experimental evaluation of the cavity and laser parameters (coupling parameter, amplitude and phase noise). The fitted parameters are used to infer the rotation of the quadratures and to obtain the experimental marginal distributions $P(x,\theta)$. The marginal distributions are inverted using a filtered backprojection algorithm to give the Wigner quasidistribution which is plotted in figure 3.

This experiment is still in progress we are willing to demonstrate that also non classical sources of light (i.e. amplitude squeezed laser diodes) maybe successfully analysed with our detection scheme. Moreover some light should be cast on the features appearing in the variance registrations which are shown here. Nevertheless we think that this scheme of self homodyne detection can be useful in all the cases where a strong local oscillator coherent with the field under analysis is not available.

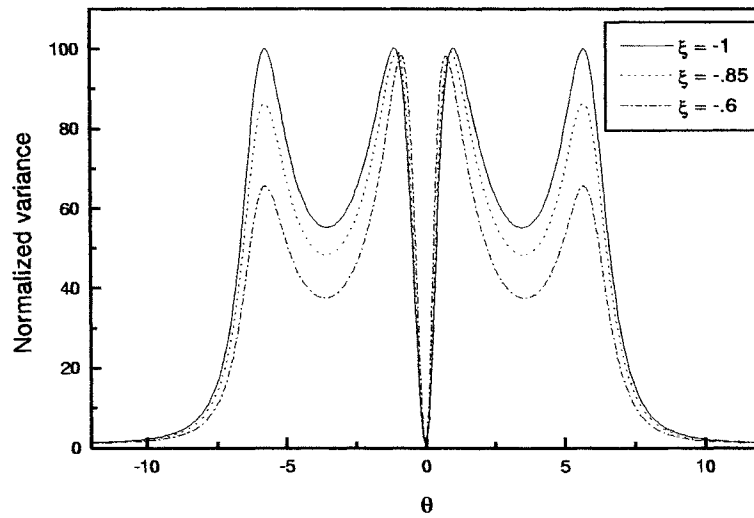


Figure 2: Plot of the normalized variance of the amplitude fluctuations versus cavity detuning

Acknowledgments

M.F. would like to acknowledge the Istituto Nazionale di Ottica and INFN for financial support during the experiment. A special thank to G. Passalaqua for his strong encouragement during the work.

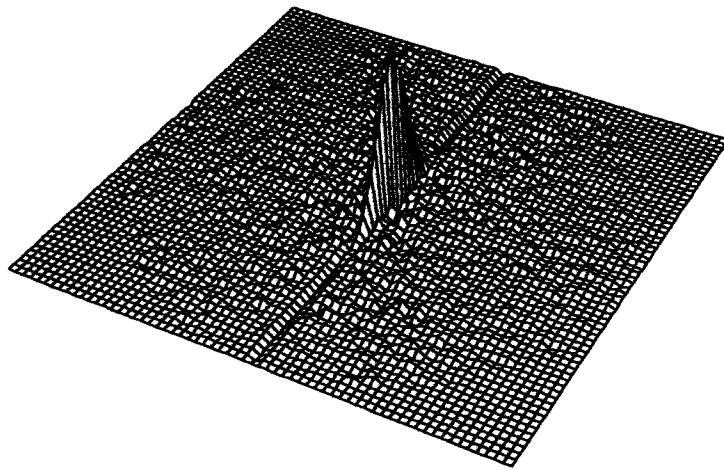


Figure 3: Experimental Wigner function of the fluctuating part of the field emitted by the laser diode

Quantum Tomography Approach in Signal Analysis

Margarita A. Man'ko

P.N. Lebedev Physical Institute, Leninskii Pr. 53, Moscow 117924, Russia

Abstract

Some properties of the fractional Fourier transform, which is used in information processing, are presented in connection with the tomography transform of optical signals. Relation of the Green function of the quantum harmonic oscillator to the fractional Fourier transform is elucidated.

Analysis of signals (electromagnetic, acoustic, seismic, etc.) is based on studying the properties of a complex time-dependent function $f(t)$ (called “analytic signal”) which describes a signal. Signal analysis is an essential ingredient of information processing. The conventional method for studying a signal is Fourier analysis which provides a function $f_F(\omega)$ describing the frequency structure of the signal. Fourier analysis is equivalent to applying invertible map $f(t) \leftrightarrow f_F(\omega)$ of analytic signal on the Fourier component of the signal. Other methods to study signals, in which invertible maps of the analytic signal function onto a function of two variables (time–frequency quasidistributions, for example, the Ville–Wigner quasidistribution [1]) $f(t) \leftrightarrow W(t, \omega)$ are used, were introduced to describe a joint time–frequency distribution of the signal. If one makes the replacement $f \rightarrow \Psi; t \rightarrow x$, formally complex analytic signal $f(t)$ is equivalent to the complex wave function $\Psi(x)$ describing a system’s state in quantum mechanics. In view of this, results of quantum theory can be applied to signal analysis and vice versa.

Recently, in quantum mechanics and quantum optics the invertible tomography map of the wave function on the probability distribution function of a random variable (depending also on extra parameters) was introduced. The application of this map to signal analysis (called “noncommutative” tomography of analytic signal) was developed [2]. Advantages of the proposed tomographic methods of signal analysis consist in the fact that they map a complex function (analytic signal) on the probability distribution that provides the same information on a signal but elucidates the signal properties in more visible appearance.

Fourier transform of optical signals plays an important role in describing the shape and frequency content of optical pulses (for the particular case of interferometric methods of the investigation of output signals in semiconductor lasers, it was successfully applied in [3,4]). Other transforms can be used for an analysis of optical signals for describing both their amplitude and phase; thus, the fractional Fourier transform [5] was intensively employed in optical measurements and information processing [6]. In quantum optics, the symplectic tomography transform was introduced [7] to describe a quantum state, which as well can be conventionally described by the Wigner quasidistribution function. This transform is an

extension of Fourier transform which was also used in the optical tomography procedure [8] to describe a quantum state. The cited transforms can be determined by a kernel of the integral operator. Analogously, in quantum mechanics the Green function, for example, of the quantum harmonic oscillator is the kernel of the quantum time-evolution operator. The aim of this contribution is to discuss the similarity of the Green function of the harmonic oscillator and the kernel of the fractional Fourier transform. We also establish a connection of the fractional Fourier transform to the tomography method suggested for measuring quantum states [7].

The wave function of the harmonic oscillator $\Psi(x, t)$ satisfies the Schrödinger evolution equation (in the coordinate representation)

$$i\hbar \frac{\partial \Psi(x, t)}{\partial t} = -\frac{\hbar^2}{2m} \frac{\partial^2 \Psi(x, t)}{\partial x^2} + \frac{m\omega^2 x^2}{2} \Psi(x, t). \quad (1)$$

The Green function $G_\omega(x, y, t)$ of the Schrödinger equation (1) determines the wave function $\Psi(x, t)$ in terms of the initial wave function $\Psi(y, 0)$ by the relationship

$$\Psi(x, t) = \int G_\omega(x, y, t) \Psi(y, 0) dy. \quad (2)$$

The initial value of the Green function is $G_\omega(x, y, 0) = \delta(x - y)$. The Green function of the harmonic oscillator reads

$$G_\omega(x, y, t) = \sqrt{\frac{m\omega}{2\pi i\hbar \sin \omega t}} \exp \left\{ \frac{im\omega}{2\hbar} \left[(x^2 + y^2) \cot \omega t - \frac{2xy}{\sin \omega t} \right] \right\}. \quad (3)$$

By inserting (3) in (2) one provides the explicit form of the integral transform of the initial wave function $\Psi(y, 0)$

$$\Psi(x, t) = \sqrt{\frac{m\omega}{2\pi i\hbar \sin \omega t}} \int \Psi(y, 0) \exp \left\{ \frac{im\omega}{2\hbar} \left[(x^2 + y^2) \cot \omega t - \frac{2xy}{\sin \omega t} \right] \right\} dy. \quad (4)$$

One can see that for time t satisfying the condition $\cot \omega t = 0$, the integral transform (4) coincides with the usual Fourier transform of the initial wave function, i.e., for $\omega t = (\pi/2) + 2\pi k$, $k = 0, \pm 1, \pm 2, \dots$, one has $\sin \omega t = 1$, and Eq. (4) reads

$$\Psi \left(x, t = \frac{1}{\omega} \left[\frac{\pi}{2} + 2\pi k \right] \right) = \sqrt{\frac{m\omega}{2\pi i\hbar}} \int \Psi(y, 0) \exp \left\{ -\frac{im\omega}{\hbar} xy \right\} dy. \quad (5)$$

For arbitrary time t , relation (4) is the integral transform of the initial wave function with the Gaussian kernel, periodic in time.

In signal analysis and information processing, the fractional Fourier transform $(\mathcal{F}^a q)(u)$ of analytic signal $q(u)$ is used (see, for example, [6])

$$(\mathcal{F}^a q)(u) = \int B_a(u, u') q(u') du'. \quad (6)$$

The kernel of the transform reads

$$B_a(u, u') = \exp \left[-i \left(\frac{\pi \hat{\Phi}}{4} - \frac{\Phi}{2} \right) \right] |\sin \Phi|^{-1/2} \exp \left[i\pi \left(u^2 \cot \Phi - \frac{2uu'}{\sin \Phi} + u'^2 \cot \Phi \right) \right], \quad (7)$$

where the angle variable is determined by the real parameter a , $\Phi = a\pi/2$, $0 < |a| < 2$, and $\hat{\Phi} = \text{sgn}(\sin \Phi)$. For $a = 0$ and $a = 2$, $B_0(u, u') = \delta(u - u')$ and $B_2(u, u') = \delta(u + u')$, respectively. The fractional Fourier transform is the linear transform. For $a = 1$ (the first-order transform), it corresponds to the usual Fourier transform.

Let us now compare relations (6), (7), and (4) using the change of variables

$$u = \frac{x}{\sqrt{2\pi}} \sqrt{\frac{m\omega}{\hbar}}, \quad u' = \frac{y}{\sqrt{2\pi}} \sqrt{\frac{m\omega}{\hbar}}, \quad \omega t = \Phi,$$

and the replacement

$$\left(\frac{\hbar}{m\omega}\right)^{1/4} \Psi\left(\sqrt{\frac{2\pi\hbar}{m\omega}}u, \frac{\Phi}{\omega}\right) \implies (\mathcal{F}^a q)(u), \quad \left(\frac{\hbar}{m\omega}\right)^{1/4} \Psi\left(\sqrt{\frac{2\pi\hbar}{m\omega}}u, 0\right) \implies q(u).$$

We see that (6), (7), and (4) coincide up to the factor $\exp(i\Phi/2) = \exp(i\omega t/2)$; this means that the identity of the oscillator's Green function and the kernel of the fractional Fourier transform takes place, i.e.,

$$B_a(u, u') = \exp\left(\frac{i\omega t}{m\omega}\right) G_\omega(x, y, t), \quad x = \sqrt{\frac{2\pi\hbar}{m\omega}}u, \quad y = \sqrt{\frac{2\pi\hbar}{m\omega}}u', \quad t = \frac{\pi a}{2\omega}.$$

The other phase factor in the kernel of the fractional Fourier transform is equal to the constant phase factor of the Green function $\exp(-i\pi\hat{\Phi}/4) = i^{-1/2}$.

In [2], the procedure of noncommutative tomography of analytic signal was suggested which uses the symplectic tomography approach for measuring quantum states in quantum mechanics proposed in [7]. Below, we show the relation of the fractional Fourier transform to the noncommutative tomography approach. The marginal probability distribution $w(X, \mu, \nu)$ is connected to analytic signal $q(u)$ by means of the relationship [2]

$$w(X, \mu, \nu) = \frac{1}{2\pi|\nu|} \left| \int q(u) \exp\left(\frac{i\mu}{2\nu}u^2 - \frac{iX}{\nu}u\right) du \right|^2. \quad (8)$$

For arbitrary real parameters μ and ν , the probability distribution is normalized $\int w(X, \mu, \nu) dX = 1$, if analytic signal is normalized $\int |q(u)|^2 du = 1$. If one knows $w(X, \mu, \nu)$, analytic signal can be reconstructed, in view of the relationship

$$q(u) q^*(u') = \frac{1}{2\pi} \int w(X, \mu, u - u') \exp\left[i\left(X - \mu \frac{u + u'}{2}\right)\right] dX d\mu. \quad (9)$$

After inserting (8) in (9), one obtains that the product of the analytic signal functions

$$\begin{aligned} q(u) q^*(u') &= \frac{1}{(2\pi)^2} \int \exp\left[i\left(X - \mu \frac{u + u'}{2}\right)\right] [\mu^2 + (u - u')^2]^{-1/2} dX d\mu \\ &\times \frac{1}{|\sin \arctan [(u - u')/\mu]|} \left| \int \exp\left\{\frac{i}{2}\left[\cot\left(\arctan \frac{u - u'}{\mu}\right) y^2\right.\right.\right. \\ &\left.\left.\left. - \frac{2X}{\sqrt{\mu^2 + (u - u')^2}} \frac{y}{\sin[\arctan (u - u')/\mu]}\right]\right\} q(y) dy \right|^2 \end{aligned} \quad (10)$$

is expressed in terms of modulus of the fractional Fourier transform. In fact, let us compare (7) and (10). One can see that the change of the variables $\Phi \rightarrow \arctan [(u - u') / \mu]$ in (7) and $y \rightarrow \sqrt{2\pi}v'$; $X \rightarrow v \sqrt{\mu^2 + (u - u')^2}$ in (10) reduces the term in the two last lines of (10) to the form $|\int B_a(v, v') q(v') dv'|^2$, with $a = (2/\pi) \arctan [(u - u') / \mu]$. Thus, the connection between the noncommutative tomography approach of [2] and employment of the fractional Fourier transform is established. The important aspect of applying the fractional Fourier transform in this context is that, in order to reconstruct analytic signal (up to the constant phase), one needs only the modulus of the transform and this modulus has the meaning of the probability distribution function depending on two real parameters.

In conclusion, we would like to point out that we have demonstrated the formal similarity (better to say even identity) of the fractional Fourier transform used in information processing and signal analysis and the time-evolution transform of the wave function of the quantum harmonic oscillator. The kernel of the fractional Fourier transform is mathematically equivalent to the Green function of the quantum harmonic oscillator. This observation gives the possibility to use physically obvious properties of the Green function, like unitarity of the evolution operator, to describe the properties of the fractional Fourier transform. The experimental realization of the fractional Fourier transform can be done in optical fibers (selfoc) where the signal propagation is described by a Schrödinger-like equation in the Fock–Leontovich approximation [9,10].

We have shown that the fractional Fourier transform is connected with the symplectic tomography approach of measuring quantum states and with noncommutative tomography of analytic signals. The observed relations of quantum problems to some procedures used to analyze different (for example, optical) signals provide the idea to use Green functions of quantum systems with other potentials as kernels of transforms of analytic signals; the kernels being different from the kernel of the fractional Fourier transform related to the harmonic oscillator potential. All these Green functions have the property of unitarity and by inverting time one has the kernel of inverse transform related to the Green functions.

- [1] E. Wigner, *Phys. Rev.*, **40**, 749 (1932); J. Ville, *Cables et Transmission*, **2**, 61 (1948).
- [2] V. I. Man'ko and R. V. Mendes, "Noncommutative time–frequency tomography of analytic signals," E-print LANL Physics/9712022 Data Analysis, Statistics, and Probability; *IEEE Signal Process.* (1999, in press).
- [3] H. Bachert, P. G. Eliseev, M. A. Man'ko, et al., *IEEE Quantum Electron.*, **QE-11/1**, Pt. 2, 510 (1975); *Sov. J. Quantum Electron.*, **45**, 1102 (1975).
- [4] M. A. Man'ko, *Rozprawy Elektrotechniczne*, **425**, 731 (1979).
- [5] V. Namias, *J. Inst. Math. Appl.*, **25**, 241 (1980).
- [6] A. W. Lohmann, *J. Opt. Soc. Am. A: Opt., Image Sci., Vision*, **10**, 2181 (1993).
- [7] S. Mancini, V. I. Man'ko, and P. Tombesi, *Quantum Semiclass. Opt.*, **7**, 615 (1995).
- [8] K. Vogel and H. Risken, *Phys. Rev. A*, **40**, 2847 (1989).
- [9] M. A. Man'ko and G. T. Mikaelyan, *Sov. J. Quantum Electron.*, **416**, 985 (1986); "Modes and mode conversions in active semiconductor waveguides," in: *The Nonlinear Optics of Semiconductor Lasers, Proceedings of the Lebedev Physical Institute*, Nauka, Moscow (1986), Vol. 166. p. 126 [Nova Science, New York (1987), Vol. 166, p. 170].
- [10] M. A. Man'ko, "Some aspects of nonlinear optics of semiconductor lasers," in: M. Bertolotti (Ed.), *ECOOSA-90 Quantum Optics*, IOP Publ. Ltd. (1991), p. 247.

Signal-to-noise ratio in quantum tomography

Marcelo A. Marchioli

*Instituto de Física de São Carlos, Universidade de São Paulo,
Caixa Postal 369, 13560-970 São Carlos, SP, Brazil
e-mail: march@if.sc.usp.br*

Salomon S. Mizrahi and Victor V. Dodonov

*Departamento de Física, Universidade Federal de São Carlos,
Rod. Washington Luiz km 235, 13565-905 São Carlos, SP, Brasil*

Abstract

The operational theory of homodyne detection by nonideal detectors, used in quantum tomography, was recently modified in order to incorporate the preamplification (before homodyne detection) of the input signal, thus enabling to beat the handicap of the lower than 0.5 detector efficiency. In the present work we set an expression for the signal-to-noise ratio in terms of the operational (measured) moments of the preamplified homodyne detection formalism. We illustrate the theory by considering some kinds of fields (for the input signal) and determine the effects of the preamplification on the output signal-to-noise ratios.

I. INTRODUCTION

The *operational theory* of balanced homodyne detection consists in inserting conveniently the efficiency of the detection directly into the measured observables such that the statistical properties of the field can be extracted with the help of the generating operator [1]

$$\mathbf{Z}(\chi; \theta, \epsilon) = \exp \left[-\frac{\chi^2}{4}(1 - \epsilon) + i\chi\sqrt{\epsilon} \mathbf{X}_\theta \right] \quad (-\infty < \chi < \infty), \quad (1)$$

where $\mathbf{X}_\theta = \mathbf{Q} \cos \theta + \mathbf{P} \sin \theta$ ($0 \leq \theta < 2\pi$) is the so-called rotated field quadrature operator, θ is the phase of the local oscillator and ϵ is the efficiency of the photodetectors ($0 \leq \epsilon \leq 1$). The derivatives of $\mathbf{Z}(\chi, \theta, \epsilon)$ at $\chi = 0$ define the *operational observables*

$$\mathbf{x}_\theta^{(n)} \equiv \frac{1}{i^n} \frac{d^n \mathbf{Z}}{d\chi^n} \Big|_{\chi=0} = \epsilon^{n/2} \sum_{k=0}^{[n/2]} \frac{n!}{k!(n-2k)!} \left(\frac{1-\epsilon}{4\epsilon} \right)^k \mathbf{X}_\theta^{n-2k}, \quad (2)$$

where each one is expressed as a polynomial of the *intrinsic observable* \mathbf{X}_θ of the signal. Consequently, this expression permits us to establish a relation between the *operational* and

the *intrinsic moments* for a given state of the field represented by the statistical operator ρ , i.e., $M^{(n)}(\theta, \epsilon) = \text{Tr} \left[\rho \mathbf{x}_\theta^{(n)} \right]$ and $\mathcal{M}^{(n)}(\theta) = \text{Tr} \left[\rho \mathbf{X}_\theta^n \right]$. Note that in an ideal measurement ($\epsilon = 1$), the operational and intrinsic moments coincide.

Formally, a degenerate parametric amplification of a signal is represented by a unitary transformation of the statistical operator $\rho \rightarrow \mathbf{S}^\dagger(\zeta) \rho \mathbf{S}(\zeta)$, where $\mathbf{S}(\zeta)$ is the generalized squeeze operator with $\zeta \equiv y e^{i\phi}$. Applying the same transformation in Eq.(1), one obtains a new generating operator,

$$\mathbf{Z}(\chi; \theta, \epsilon, \lambda, \phi) = \exp \left[-\frac{\chi^2}{4}(1 - \epsilon) + i\chi\sqrt{\epsilon} \left(\lambda^{1/2} \cos \alpha \mathbf{X}_{\frac{\phi}{2}} + \lambda^{-1/2} \sin \alpha \mathbf{X}_{\frac{\phi+\pi}{2}} \right) \right] \quad (3)$$

which takes into account both the effects: *efficiency* and *amplification* [2]. Here $\alpha \equiv \theta - \phi/2$, $\lambda \equiv e^{-2y}$ is the gain parameter for quadrature \mathbf{Q} with $y < 0$ (λ^{-1} is also a gain parameter, $y > 0$, but now it is for \mathbf{P}), and y is proportional to the amplitude of the pump field. So, the operational observables are obtained by a similar procedure [see Eq.(2) for a comparison]

$$\mathbf{x}_\theta^{(n)}(\lambda, \phi) = \epsilon^{n/2} \sum_{k=0}^{\lfloor n/2 \rfloor} \frac{n!}{k!(n-2k)!} \left(\frac{1-\epsilon}{4\epsilon} \right)^k \left(\lambda^{1/2} \cos \alpha \mathbf{X}_{\frac{\phi}{2}} + \lambda^{-1/2} \sin \alpha \mathbf{X}_{\frac{\phi+\pi}{2}} \right)^{n-2k}. \quad (4)$$

Now, our aim is to obtain the generating operator for a preamplified homodyne detection with measurements in a *random local oscillator phase*, which is useful to determine the statistics of both the signal and the difference in photocounts. In order to include the effects of an amplified parametric signal in this framework, we consider initially Eq.(3) with $\alpha = 0$. The generating operator for homodyne detection with random phase is obtained by averaging $\mathbf{Z}(\chi; \theta, \epsilon, \lambda)$ over θ [3],

$$\mathbf{Z}_{\mathcal{R}}(\chi; \epsilon, \lambda) = \int_0^{2\pi} \frac{d\theta}{2\pi} \mathbf{Z}(\chi; \theta, \epsilon, \lambda) = e^{-\chi^2[1+\epsilon(\lambda-1)]/4} : J_0 \left(\chi \sqrt{2\epsilon\lambda\mathbf{a}^\dagger \mathbf{a}} \right) :, \quad (5)$$

where $J_0(z)$ is the Bessel function of the 0th order and $: :$ denotes normal ordering of the creation and annihilation operators. This expression allows to calculate a family of operational observables by means of the derivatives of $\mathbf{Z}_{\mathcal{R}}(\chi; \epsilon, \lambda)$ at $\chi = 0$,

$$\mathbf{x}_{\mathcal{R}}^{(2m)}(\lambda) \equiv [1 + \epsilon(\lambda - 1)]^m m! L_m^{-1/2}(0) : L_m \left(-\frac{2\epsilon\lambda\mathbf{a}^\dagger \mathbf{a}}{1 + \epsilon(\lambda - 1)} \right) :, \quad (6)$$

where $L_m^\alpha(z)$ is the generalized Laguerre polynomial. In order to obtain an expression that relates the normal ordering of the moments coming from photocounts to the operational observables $\mathbf{x}_{\mathcal{R}}^{(2m)}(\lambda)$, it becomes necessary to invert Eq.(6),

$$: \left(\frac{\epsilon\lambda\mathbf{a}^\dagger \mathbf{a}}{1 + \epsilon(\lambda - 1)} \right)^k : = \frac{(-1)^k (k!)^2}{2^k} \sum_{m=0}^k \frac{(-4)^m}{(2m)!(k-m)!} \frac{\mathbf{x}_{\mathcal{R}}^{(2m)}(\lambda)}{[1 + \epsilon(\lambda - 1)]^m}. \quad (7)$$

This result permits to calculate not only the Q parameter but the signal-to-noise (SNR) too [3]. In the following section, we set an expression for the SNR in terms of the operational moments with random phase.

II. THE SIGNAL-TO-NOISE RATIO

The calculation of the signal-to-noise ratio in experiments of homodyne detection represents an important tool for experimental data analysis: It provides a quantitative information on the measured signal and the noise inherent to the experiment. Thus the SNR for the output photocount-difference (OPD) is defined in terms of the mean values of the operational observables $\mathbf{x}_{\mathcal{R}}^{(2m)}(\lambda)$,

$$\mathfrak{R}_{out}^{(\mathcal{R})}(\epsilon, \lambda) = \frac{\left| \langle \mathbf{x}_{\mathcal{R}}^{(2)}(\lambda) \rangle - \frac{1}{2} \right|}{\sqrt{\frac{2}{3} \langle \mathbf{x}_{\mathcal{R}}^{(4)} \rangle - \langle \mathbf{x}_{\mathcal{R}}^{(2)}(\lambda) \rangle^2 - \frac{1}{4}}}. \quad (8)$$

We can figure out what will be the \mathfrak{R}_{out} for different kinds of signals by writing (8) in terms of the photon-number operator

$$\mathfrak{R}_{out}^{(\mathcal{R})}(\epsilon, \lambda) = \frac{\left| \langle \mathbf{n} \rangle + \frac{\lambda-1}{2\lambda} \right|}{\sqrt{\langle (\Delta \mathbf{n})^2 \rangle + \frac{1-\epsilon}{\epsilon\lambda} \langle \mathbf{n} \rangle + \frac{\lambda-1}{4\epsilon\lambda^2} [2 + \epsilon(\lambda-1)]}}, \quad (9)$$

where $\langle \Delta \mathbf{n} \rangle \equiv [\langle \mathbf{n}^2 \rangle - \langle \mathbf{n} \rangle^2]^{1/2}$ is the respective variance. The first term in the numerator is due to the input signal (IS) whereas the second one is due to the pump field, representing the *spontaneous parametric emission*. With respect to denominator, the first term is the signal noise, the second one is the extra noise introduced due to the nonideal detection, and the third term is the noise associated to the pump field. In the absence of pumping $\lambda = 1$, one has a SNR where the numerator is the input signal (IS) and its noise increased due to the nonideal detection. In (9) we see that the deleterious effect coming from a nonideal detection vanishes in the extreme situation $\epsilon\lambda \gg 1$, i.e., high values of λ reduce drastically the handicap $\epsilon < 1$.

III. APPLICATIONS

In Fig. 1 $\mathfrak{R}_{out}^{(\mathcal{R})}(\epsilon, \lambda)$ vs λ is depicted, where there are two separated sets of lines with three lines each; the upper (lower) set stands for $\epsilon = 1$ ($\epsilon = 0.4$). The dashed, solid and dot-dashed lines correspond to the even-coherent, coherent and odd-coherent states, respectively. Analysing first the coherent-state signal (solid line), the SNR is given by [3]

$$\mathfrak{R}_{out}^{(\mathcal{R},c)}(\epsilon, \lambda) = \sqrt{\frac{\epsilon\lambda}{1 + \epsilon(\lambda-1)}} \frac{\langle \mathbf{n} \rangle_c + \frac{\lambda-1}{2\lambda}}{\sqrt{\langle \mathbf{n} \rangle_c + \frac{\lambda-1}{4\lambda} \frac{2+\epsilon(\lambda-1)}{1+\epsilon(\lambda-1)}}}. \quad (10)$$

Note that for a strong signal $\langle \mathbf{n} \rangle_c \gg 1$, one has $\mathfrak{R}_{out}^{(\mathcal{R},c)}(\epsilon, \lambda) \approx C(\epsilon, \lambda) \langle \mathbf{n} \rangle_c^{1/2}$ where $C(\epsilon, \lambda)$ is the first factor in the RHS of Eq.(10). At $\lambda = 1$, the SNR shall depend on ϵ and on the signal amplitude; otherwise, for $\lambda \gg 1$ both curves have the same asymptotic value $\mathfrak{R}_{out}^{(\mathcal{R},c)}(\epsilon, \lambda) \approx (\langle \mathbf{n} \rangle_c + \frac{1}{2}) / (\langle \mathbf{n} \rangle_c + \frac{1}{4})^{1/2}$, without dependence on ϵ . An interesting feature of the amplification is that it is more effective for the lowest value of ϵ . Otherwise, the

quantum nature of the odd-coherent state (dot-dashed line) makes itself evident through the higher values attained by the SNR in comparison to the coherent and even-coherent states, independently of the value of ϵ . This important feature corroborates with the quantum signature of the field. Moreover, for intense fields the SNR for the even- and odd-coherent states go to Eq.(10) since $\langle \mathbf{n} \rangle_{e(o)} \approx \langle \mathbf{n} \rangle_c$.

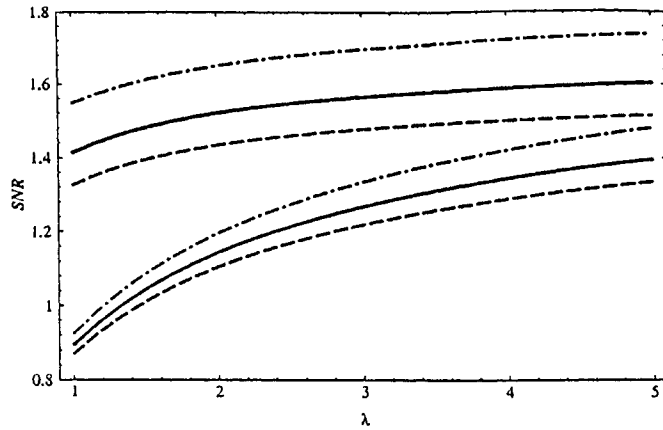


FIG. 1. Plot of $\mathfrak{R}_{out}^{(\mathcal{R})}(\epsilon, \lambda)$ vs λ with $\langle \mathbf{n} \rangle = 2$, where the upper (lower) set of lines stands for $\epsilon = 1$ ($\epsilon = 0.4$). The dashed, solid, and dot-dashed lines correspond to the even-coherent, coherent and odd-coherent states, respectively.

IV. CONCLUSIONS

The present work is an extension of the state reconstruction process of the Husimi function for coherent and number states studied in [2]. Here we also used the operational theory of homodyne detection introduced in [1] to establish a relation between operational and intrinsic observables of a preamplified signal when the local oscillator phase is completely random. The preamplification permits to overcome the deleterious effects of a low efficiency detector. For further details, see the reference [3].

ACKNOWLEDGMENTS

MAM acknowledges financial support from FAPESP, São Paulo, Brazil, project number 97/14551-4. This work has also been partially supported by Convênio FINEP/PRONEX Grant number 41/96/0935/00.

REFERENCES

- [1] K. Banaszek and K. Wódkiewicz, Phys. Rev. A **55**, 3117 (1997).
- [2] M. A. Marchioli, S. S. Mizrahi and V. V. Dodonov, Phys. Rev. A **56**, 4278 (1997).
- [3] M. A. Marchioli, S. S. Mizrahi and V. V. Dodonov, Phys. Rev. A **57**, 3885 (1998).

Realistic pattern functions for tomography revisited and direct sampling of smoothed Wigner function

Th. Richter

*Arbeitsgruppe "Nichtklassische Strahlung", Institut für Physik, Humboldt-Universität
Invalidenstr. 110, D-10115 Berlin, Germany*

Abstract

We present two new representations for the pattern functions f_{kl} needed to reconstruct the density matrix ϱ_{kl} in Fock basis from data measured with an imperfect homodyne detector. We show that smoothed Wigner function and moment generating function can be directly sampled. The sampling functions are shifted and scaled versions of f_{00} and f_{0k} , respectively.

1. INTRODUCTION AND BASIC RELATIONSHIPS

Let us denote by $w(x_\Theta, \Theta, \eta)$ the probability distribution of the quadrature component x_Θ measured with a balanced homodyne detector of overall efficiency η and belonging to a signal field described by the density operator $\hat{\rho}$. Θ is the reference phase of the local oscillator. The density matrix elements ϱ_{kl} in Fock basis follow via the formula

$$\varrho_{kl} = \frac{1}{2\pi} \int_{-\infty}^{\infty} dx_\Theta \int_0^{2\pi} d\Theta w(x_\Theta, \Theta, \eta) f_{kl}(x_\Theta, \eta) \exp[i(k-l)\Theta], \quad (1)$$

where for the so-called pattern function $f_{kl}(x, \eta)$, in particular, for the case $\eta = 1$ different but identical representations exist [1-6]. In this paper we concentrate on the case $\eta < 1$ and present a unified approach to all of them. Moreover, we derive a new expression for the realistic pattern function in the form of a finite weighted sum over scaled ideal pattern functions $f_{kl}(x) \equiv f_{kl}(x, \eta = 1)$ and establish a useful sum relation. With the help of it we show that both smoothed Wigner function and generalized moment generating function can be directly sampled using shifted and scaled versions of f_{00} and f_{0k} , respectively.

The search for the pattern function is facilitated by looking first at the Fourier transform $\tilde{h}(u) = \int_{-\infty}^{\infty} h(x) \exp(-iux) dx$ of the relevant quantities. In Fourier space (1) reads

$$\varrho_{kl} = \frac{1}{4\pi^2} \int_{-\infty}^{\infty} du \int_0^{2\pi} d\Theta \tilde{w}(u, \Theta, \eta) \exp[i(k-l)\Theta] \tilde{f}_{kl}(-u, \eta), \quad (2)$$

where $\tilde{w}(u, \Theta, \eta)$ is the symmetric ordered characteristic function, i.e. the Fourier transformed Wigner function expressed in polar coordinates. A straightforward generalization of our approach [3] to the case $\eta < 1$ yields for $l \geq k$ (note the extra factor π compared to [3])

$$\tilde{f}_{kl}(u, \eta) = \pi (-i)^{l-k} \sqrt{\eta}^{l-k+2} \sqrt{\frac{2^k k!}{2^l l!}} |u| u^{l-k} \exp[-(2\eta-1)u^2/4] L_k^{l-k}(\eta u^2/2). \quad (3)$$

Here $L_m^n(x)$ denotes the generalized Laguerre polynomial. Obviously, $f_{kl}(u, \eta)$ is a well behaved function which, however, is bounded only for $\eta > 1/2$. We note that this intermediate result is of importance by itself since experimental schemes have been devised which allow to measure directly the characteristic function [7,8].

2. ALTERNATIVE REPRESENTATIONS OF THE PATTERN FUNCTION

We now derive several but identical representations of the pattern function itself which result from different ways of evaluation of the inverse Fourier integral $f_{kl}(x, \eta) = (1/2\pi) \int_{-\infty}^{\infty} \tilde{f}_{kl}(u, \eta) \exp(iux) du$. First of all we note that we can rederive the representation of the realistic pattern functions found in [2] by substituting in it the explicit expression of the generalized Laguerre polynomials and integrating term by term.

2.1 $f_{kl}(x, \eta)$ – infinite sum over Hermite polynomials

Next we derive a representations of the realistic pattern functions as a series over even or odd Hermite polynomials. To this end we make use of the generating functions for the Hermite polynomials (Ref.[9], 5.12.1.6) and obtain with $l = k + 2p + \sigma$ and $\sigma = 0, 1$

$$f_{kl}(x, \eta) = f_{kl}^{(mom)}(x, \eta) + \frac{1}{\sqrt{k!l!}} \sum_{n=0}^{p-1} \frac{(-1)^{n+p}}{\sqrt{2\eta}^{2n+\sigma}} \frac{(n+p+\sigma)!}{(2n+\sigma)!} \frac{\Gamma(k+p-n)}{\Gamma(p-n)} H_{2n+\sigma}(x), \quad (4)$$

where $f_{kl}^{(mom)}(x, \eta)$

$$f_{kl}^{(mom)}(x, \eta) = \frac{1}{\sqrt{(2\eta)^{k+l} k!l!}} \sum_{n=0}^{\infty} \left(-\frac{1}{2\eta}\right)^n \frac{(k+n)!(l+n)!}{n!(k+l+2n)!} H_{k+l+2n}(x). \quad (5)$$

This generalizes the result found in [5] to the case $\eta < 1$. Interestingly $f_{kl}^{(mom)}(x, \eta)$ coincides with the form of the pattern function following from a reconstruction of the density matrix via normally ordered moments as proposed in [10] and can be used as pattern function just as well. This is a consequence of the general ambiguity of the pattern functions. Note, however, that $f_{kl}^{(mom)}(x, \eta)$ is not bounded even for $\eta = 1$.

2.2 $f_{kl}(x, \eta)$ – infinite sum over $f_{kl}(x)$

We proceed to derive a representation of the realistic pattern functions as an infinite sum over the ideal ones. To this end we express $L_k^{l-k}(zx)$ as an infinite sum over $L_{k+n}^{l-k}(x)$ (Ref.[9], 5.11.2.8) and find ($f_{kl}(x, \eta = 1) = f_{kl}(x)$)

$$f_{kl}(x, \eta) = \eta^{-\frac{1}{2}(k+l)} \sum_{n=0}^{\infty} \sqrt{\binom{k+n}{k} \binom{l+n}{l}} \left(1 - \frac{1}{\eta}\right)^n f_{k+n, l+n}(x). \quad (6)$$

This representation corresponds to the procedure proposed in [6].

2.3 $f_{kl}(x, \eta)$ – finite sum over scaled versions of $f_{kl}(x)$

Most interesting, however, in particular from the numerical point of view is a representation of the realistic pattern functions as a finite sum over the ideal ones. This time we utilize a finite sum relation for $L_k^\alpha(zx)$ (Ref.[9], 4.4.1.7) and arrive at

$$f_{kl}(x, \eta) = \sqrt{\frac{\eta}{2\eta-1}}^{l+k+2} \sum_{n=0}^k \sqrt{\binom{k}{n} \binom{l}{n}} \left(1 - \frac{1}{\eta}\right)^n f_{k-n, l-n} \left(\frac{x}{\sqrt{2\eta-1}}\right). \quad (7)$$

In particular, the realistic pattern functions $f_{0l}(x_\Theta, \eta)$ are just scaled versions of the corresponding ideal pattern functions

$$f_{0l}(x, \eta) = \sqrt{\frac{\eta}{2\eta-1}}^{l+2} f_{0l} \left(\frac{x}{\sqrt{2\eta-1}}\right). \quad (8)$$

3. DIRECT SAMPLING OF SPECIFIC EXPECTATION VALUES

Equating the right hand sides of Eqs.(6,7) obtain the following identity for $l \geq k$

$$\sum_{n=0}^{\infty} \sqrt{\binom{k+n}{k} \binom{l+n}{l}} \left(\frac{t-1}{t+1}\right)^n f_{k+n, l+n}(x) = \sqrt{t^{k+l}} \left(\frac{1+t}{2t}\right)^{k+l+1} \sum_{n=0}^k \sqrt{\binom{k}{n} \binom{l}{n}} \left(\frac{t-1}{t+1}\right)^n f_{k-n, l-n} \left(\frac{x}{\sqrt{t}}\right). \quad (9)$$

valid for $t > 0$. As a result expectation values of the form

$$Tr \left\{ \hat{\rho} \hat{a}^{\dagger k} \left(\frac{t-1}{t+1}\right)^{\hat{a}^\dagger \hat{a}} \hat{a}^l \right\} = \sqrt{k!l!} \sum_{n=0}^{\infty} \sqrt{\binom{k+n}{n} \binom{l+n}{n}} \left(\frac{t-1}{t+1}\right)^n \varrho_{k+n, l+n} \quad (10)$$

can be determined from quadrature distributions via pattern functions which can be expressed as finite weighted sums of the scaled ideal pattern functions.

3.1 Smoothed Wigner function

We recall that any s-parametrized quasi probability distribution $W(x, p, s)$ can be expressed as an infinite weighted sum in terms of the diagonal density matrix elements $\langle \alpha, n | \hat{\rho} | \alpha, n \rangle$ with $\alpha = (1/\sqrt{2})(x + ip)$ in the displaced Fock-state basis $|\alpha, n\rangle$

$$W(x, p, s) \equiv \frac{1}{2} W\left(\alpha = \frac{1}{\sqrt{2}}(x + ip), s\right) = \frac{1}{\pi(1-s)} \sum_{n=0}^{\infty} \left(\frac{s+1}{s-1}\right)^n \langle \alpha, n | \hat{\rho} | \alpha, n \rangle. \quad (11)$$

These matrix elements can be directly sampled according to [11] (note the extra factor π)

$$\langle \alpha, n | \hat{\rho} | \alpha, n \rangle = \frac{1}{2\pi} \int_{-\infty}^{\infty} dx_{\Theta} \int_0^{2\pi} d\Theta w(x_{\Theta}, \Theta) f_{nn}(x_{\Theta} - x \cos \Theta - p \sin \Theta). \quad (12)$$

Using this in Eq.(11) and in view of Eq.(9) for $k = l = 0$ we readily find for $s < 0$

$$W(x, p, -|s|) = \frac{1}{4\pi^2 |s|} \int_{-\infty}^{\infty} dx_{\Theta} \int_0^{2\pi} d\Theta w(x_{\Theta}, \Theta) f_{00} \left(\frac{x_{\Theta} - x \cos \Theta - p \sin \Theta}{\sqrt{|s|}} \right). \quad (13)$$

Thus any smoothed Wigner function $W(x, p, s < 0)$ can be directly sampled via formula (13). The needed sampling function is just the shifted and scaled ideal pattern function f_{00} [11,12].

3.2 Generalized moment generating function

We introduce the generalized moment generating function $M_k(\mu)$, $0 \leq \mu \leq 2$, [13]

$$M_k(\mu) \equiv Tr \left\{ \hat{\rho} \hat{a}^{\dagger k} (1 - \mu)^{\hat{a}^{\dagger} \hat{a}} \right\} = \sqrt{k!} \sum_{n=0}^{\infty} \sqrt{\binom{k+n}{n}} (1 - \mu)^n \varrho_{n, n+k}, \quad (14)$$

which for $k = 0$ reduces to the widely used ordinary moment generating function $M_0(\mu)$. $M_k(\mu)$ can be directly determined from the quadrature distribution via the formula

$$M_k(\mu) = \int_{-\infty}^{\infty} dx_{\Theta} \left(\frac{1}{2\pi} \int_0^{2\pi} d\Theta w(x_{\Theta}, \Theta) \exp(-ik\Theta) \right) S_k(x_{\Theta}, \mu), \quad (15)$$

where $S_k(x_{\Theta}, \mu)$ is given by

$$S_k(x_{\Theta}, \mu) = \frac{1}{2 - \mu} \frac{\sqrt{k!}}{\sqrt{\mu(2 - \mu)}^k} f_{0k} \left(\sqrt{\frac{\mu}{2 - \mu}} x_{\Theta} \right). \quad (16)$$

We note that $M_k(\mu)$ completely characterizes the quantum state of the system. Indeed, the derivatives of $M_k(\mu)$ evaluated at $\mu = 1$ and $\mu = 0$ are related to the density matrix elements and the normally ordered moments.

-
- [1] G.M. D'Ariano, C. Macchiavello, and M.G.A. Paris, Phys. Rev. **A50**, 4298 (1994)
 - [2] U. Leonhardt, H. Paul, and G.M. D'Ariano, Phys. Rev. **A52**, 4899 (1995)
 - [3] Th. Richter, Phys. Lett. A **211**, 327 (1996)
 - [4] U. Leonhardt et al., Opt. Commun. **127**, 144 (1996)
 - [5] A. Wünsche, J. Mod. Opt. **44**, 2293 (1997)
 - [6] T. Kiss, U. Herzog, and U. Leonhard, Phys. Rev. A **52**, 2433 (1995)
 - [7] M. Wilkens and P. Meystre, Phys. Rev. A **43**, 3832 (1991)
 - [8] S. Wallentowicz and W. Vogel, Phys. Rev. A **54**, 3322 (1996)
 - [9] A. Prudnikov et al., Integrals and Series, (Gordon and Breach, New York, 1986)
 - [10] Th. Richter, Phys. Rev. A **53**, 1197 (1996)
 - [11] Th. Richter, J. Mod. Opt. **46**, 1167 (1999)
 - [12] Z. Kis et al., Phys. Rev. A **59**, R39 (1999)
 - [13] U. Herzog, Phys. Rev. A **53**, 2889 (1996)

Filtering of thermal noise in Wigner tomography

L. K. Stergioulas

*Manchester School of Engineering,
The University of Manchester,
Simon Building, Oxford Road,
Manchester M13 9PL, UK*

S. Chountasis and A. Vourdas

*Department of Electrical Engineering and Electronics,
University of Liverpool, Brownlow Hill,
Liverpool L69 3GJ, UK*

Abstract

A technique for filtering thermal noise in Wigner tomography is presented. The method uses the measured Radon transform of the Wigner function of a quantum state with thermal noise and produces the Wigner function of the corresponding 'clean' (noiseless) state.

There has been a lot of activity recently in the field of Wigner tomography and its use in measuring quantum states. In practice, quantum states always contain some noise and for this reason superpositions of quantum states with thermal noise have been studied. Here we propose a filtering technique which takes the measured Radon transform of the Wigner function of a noisy state and produces the Wigner function of the 'clean' (noiseless) state.

Let us consider a quantum signal described by the density matrix ρ_s . The corresponding noisy signal is known [1] to be described by the density matrix

$$\rho_{sn} = \int \frac{d^2A}{\pi} \frac{1}{\langle N_T \rangle} \exp\left(-\frac{|A|^2}{\langle N_T \rangle}\right) D(A)\rho_s D^\dagger(A), \quad (1)$$

where $\langle N_T \rangle$ is the number of thermal ("noisy") photons and $D(A)$ is the displacement operator with $A = 2^{-1/2}(x + ip)$. Throughout the paper we use the indices s , n and sn for signal, noise and signal with noise, correspondingly.

The Wigner function [2] of a state described by a density matrix ρ is defined as:

$$\begin{aligned} W(x, p) &= \frac{1}{2\pi} \int dX \langle x + \frac{1}{2}X | \rho | x - \frac{1}{2}X \rangle \exp(-iXp) \\ &= \frac{1}{2\pi} \int dP \langle p + \frac{1}{2}P | \rho | p - \frac{1}{2}P \rangle \exp(iPx). \end{aligned} \quad (2)$$

The Weyl function is defined as [3]:

$$\begin{aligned}\tilde{W}(X, P) &= \int dx \langle x + \frac{1}{2}X | \rho | x - \frac{1}{2}X \rangle \exp(-iPx) \\ &= \int dp \langle p + \frac{1}{2}P | \rho | p - \frac{1}{2}P \rangle \exp(ipX) \\ &= \text{Tr}[\rho D(X, P)].\end{aligned}\quad (3)$$

The X, P are position and momentum *increments* and are dual in the Fourier transform sense to the x, p which appear in the Wigner function.

It can be proved that the Weyl function of the noisy signal $\tilde{W}_{sn}(X, P)$ is related to the Weyl function of the clean signal $\tilde{W}_s(X, P)$ through the relation

$$\tilde{W}_{sn}(X, P) = \tilde{W}_s(X, P) \exp\left[-\frac{1}{2}\langle N_T \rangle (X^2 + P^2)\right].\quad (4)$$

The Wigner function can be derived as the two-dimensional Fourier transform of the Weyl function

$$\tilde{W}(X, P) = \iint W(x, p) \exp[-i(Px - pX)] dx dp;\quad (5)$$

therefore Eq.(4) implies that the Wigner function of the noisy signals $W_{sn}(x, p)$ is related to the Wigner function of the clean signal through the convolution

$$W_{sn}(x, p) = \frac{1}{2\pi} \iint W_s(x', p') \frac{1}{\langle N_T \rangle} \exp\left[-\frac{(x - x')^2 + (p - p')^2}{2\langle N_T \rangle}\right] dx' dp'.\quad (6)$$

We now consider an arbitrary quantum state for which the noisy Wigner function $W_{sn}(x, p)$ is measured in Wigner tomography experiments, and explain how we can clean it from noise. The quantity measured is the Radon transform of the Wigner function along the line $x \sin \theta - p \cos \theta = q$, defined as

$$\begin{aligned}P_{sn}(q, \theta) &= \iint W_{sn}(x, p) \delta(x \sin \theta - p \cos \theta - q) dx dp \\ &= \int W_{sn}(q \sin \theta + u \cos \theta, -q \cos \theta + u \sin \theta) du,\end{aligned}\quad (7)$$

where q is a real variable and $0 \leq \theta < \pi$. From the $P_{sn}(q, \theta)$ we can evaluate the Weyl function using the Fourier transform

$$\tilde{W}_{sn}(X = \xi \cos \theta, P = \xi \sin \theta) = \int P_{sn}(q, \theta) e^{-i\xi q} dq.\quad (8)$$

Knowing the 'noisy Weyl function' we can use Eq.(4) to calculate the 'clean Weyl function' as

$$\begin{aligned}\tilde{W}_s(X, P) &= \tilde{W}_{sn}(X, P) \exp\left[\frac{1}{2}\langle N_T \rangle (X^2 + P^2)\right] \\ &= \exp\left[\frac{1}{2}\langle N_T \rangle \xi^2\right] \int P_{sn}(q, \theta) e^{-i\xi q} dq,\end{aligned}\quad (9)$$

where $X = \xi \cos \theta$ and $P = \xi \sin \theta$. In order to proceed we need to know the amount of noise $\langle N_T \rangle$. For a signal in a pure state, we use the relation

$$\frac{1}{2\pi} \int \int |\tilde{W}_s(X, P)|^2 dX dP = 1, \quad (10)$$

which in conjunction with Eq. (9) and in polar coordinates $\xi = [X^2 + P^2]^{1/2}$, $\tan \theta = P/X$ gives

$$\frac{1}{2\pi} \int \int |\tilde{W}_{sn}(\xi \cos \theta, \xi \sin \theta)|^2 \exp[\langle N_T \rangle \xi^2] \xi d\xi d\theta = 1. \quad (11)$$

This equation can be rewritten as

$$\frac{1}{2\pi} \sum [\langle N_T \rangle]^N \mu_N = 1 \quad (12)$$

where

$$\mu_N = \frac{1}{N!} \int \int |\tilde{W}_{sn}(\xi \cos \theta, \xi \sin \theta)|^2 \xi^{2N+1} d\xi d\theta \quad (13)$$

The moments μ_N can be calculated from the data, and Eq.(12) can be solved to give $\langle N_T \rangle$. We can then find the 'clean' Wigner function, using Eq.(9) and a two-dimensional Fourier transform.

We finally point out that we have assumed ideal detectors with unit quantum efficiency. In a realistic experiment we have non-ideal detectors and techniques which correct this error have been studied in [4].

In summary, the method presented in this paper is suitable for filtering noise from noisy signals in Wigner tomography experiments. It uses the measured Radon transform $P_{sn}(q, \theta)$ of a noisy quantum signal, and produces the Wigner function of the clean signal. We first calculate the noisy Weyl function using Eq.(8); then calculate the moments μ_N using Eq.(13); and then we solve Eq.(12) to find the average number of thermal photons $\langle N_T \rangle$. The two-dimensional Fourier transform of the 'clean' Weyl function (Eq. (9)) will give the Wigner function of the clean signal.

ACKNOWLEDGEMENTS

LKS and AV gratefully acknowledge travel grants from the Royal Academy of Engineering. SC gratefully acknowledges financial support from the Alexander S. Onassis Public Benefit Foundation.

REFERENCES

1. V. V. Dodonov, V. I. Man'ko, and V. V. Semyonov, *Nuovo Cimento*, **B 83**, 145 (1984); in *Group-Theoretical Methods in Physics*, edited by M. A. Markov, V. I. Man'ko and A. E. Shabad (Harwood, New York, 1985), Vol. 1.

- A. Vourdas, Phys. Rev. A, **34**, 3466, (1986); **37**, 3890, (1988); **39**, 206, (1989).
- A. Vourdas, R. Weiner Phys. Rev. A, **36**, 5866, (1987).
- H. Fearn and M. J. Collet, J. Mod. Opt. **35**, 553 (1988).
- M. S. Kim, F. A. M. Oliveira, and P. L. Knight, Phys. Rev. A, **40**, 2494 (1989).
- H. Ezawa, A. Mann, K. Nakamura, and M. Revzen, Ann. Phys. (N.Y.)**209**, 216 (1991).
- P. Marian, Phys. Rev. A, **45**, 2044 (1992); P. Marian and T. A. Marian, *ibid.* **47**, 4474 (1993); **47**, 4487 (1993).
- D. Han, Y. S. Kim, M. E. Noz and L. Yeh, J. Math. Phys. **34**, 5493, (1993).
2. M. Hillery, R.F. O'Connell, M. O. Scully, and E. P. Wigner, Phys. Rep., **106**, 121 (1984).
- Y. S. Kim and M. E. Noz, *Theory and Applications of the Poincare Group* (Dordrecht, Reidel 1986)
3. S. Chountasis and A. Vourdas, Phys. Rev. A, **58**, 848 (1998); Phys. Rev. A, **58**, 1794 (1998).
4. G.M. D'Ariano, U. Leonhardt, H. Paul Phys. Rev. A **52**, 1801 (1995)
- T. Kiss, U. Herzog, U. Leonhardt Phys. Rev. A **52**, 2433 (1995)

TOMOGRAPHY OF TWO-PARTICLE SPIN STATES AND THE EINSTEIN-PODOLSKY-ROSEN PARADOX

V.A. Andreev

Lebedev Physics Institute, Leninsky prospect, 53, Moscow 117924, Russia

V.I. Man'ko

Lebedev Physics Institute, Leninsky prospect, 53, Moscow 117924, Russia

Abstract

The new tomographic formulation of quantum mechanics is used to develop a method which can reconstruct the entire density matrix of a 2-particle spin state in terms of positive classical distributions of probabilities of the values of certain observables. It is shown that to obtain a complete description of the mixed spin state it is necessary to know not only the probabilities of the spin projections as functions of the coordinates of the points on a unit sphere but also the probabilities defining the contributions of the pure states to the mixed ones. With the help of this method the Einstein-Podolsky-Rosen paradox is analysed. It is shown that to remove the paradox the observer must strictly fix at every moment the set of observables and describe the transformation of one set into another. Such a description is performed with the help of the technique of selective and nonselective measurements defined by J.Schwinger.

A generic 1-particle j -spin state is described by a $(2j + 1) \times (2j + 1)$ Hermitian density matrix

$$\rho = \|\rho_{mm'}^j\|. \quad (1)$$

The diagonal elements of the density matrix are nonnegative values and their sum is equal to unity. The physical meaning of these elements is that they are the probabilities of observing the value of spin projection on the fixed axis in space. Therefore we introduce the abbreviation

$$\rho_{mm}^j(\theta, \phi) = w(m, \theta, \phi). \quad (2)$$

The angles θ, ϕ define the axis in space. The function $w(m, \theta, \phi)$ is the marginal distribution, i.e. the probability to find the spin projection m on the axis defined by the angles θ, ϕ . If we know the positive, normalized marginal distribution $w(m, \theta, \phi)$, then the matrix elements $\rho_{mm'}^j$ can be reconstructed both for pure and mixed states [1,2].

The situation is different in the case of 2-particle spin states.

We shall analyze the density matrix of 2-particle states with spins $j = 1/2$

$$\rho = \|\rho_{(m_1 m_2)(m'_1 m'_2)}^{\frac{1}{2} \frac{1}{2}}\|. \quad (3)$$

When we go to a different coordinate system, its elements transform as

$$\tilde{\rho}_{(\tilde{m}_1 \tilde{m}_2)(\tilde{m}'_1 \tilde{m}'_2)}^{\frac{1}{2} \frac{1}{2}} = \sum_{m_1, m_2, m'_1, m'_2} D_{\tilde{m}_1 m_1}^{\frac{1}{2}}(\phi, \theta, \psi) D_{\tilde{m}_2 m_2}^{\frac{1}{2}}(\phi, \theta, \psi) \rho_{(m_1 m_2)(m'_1 m'_2)}^{\frac{1}{2} \frac{1}{2}}$$

$$D_{\vec{m}'_1 m'_1}^{\frac{1}{2} *} (\phi, \theta, \psi) D_{\vec{m}'_2 m'_2}^{\frac{1}{2} *} (\phi, \theta, \psi) . \quad (4)$$

The density matrix (3) contains 16 elements. Using the diagonal elements of the transformed matrix (4) one can reconstruct only 6 elements and 5 linear combinations [3,4]

$$\begin{aligned} & \rho_{(\frac{1}{2} \frac{1}{2})(\frac{1}{2} \frac{1}{2})}^{\frac{1}{2} \frac{1}{2}}, \quad \rho_{(\frac{1}{2} \frac{1}{2})(\frac{1}{2} - \frac{1}{2})}^{\frac{1}{2} \frac{1}{2}}, \quad \rho_{(-\frac{1}{2} \frac{1}{2})(-\frac{1}{2} \frac{1}{2})}^{\frac{1}{2} \frac{1}{2}}, \quad \rho_{(-\frac{1}{2} \frac{1}{2})(-\frac{1}{2} - \frac{1}{2})}^{\frac{1}{2} \frac{1}{2}}, \\ & \rho_{(\frac{1}{2} \frac{1}{2})(-\frac{1}{2} - \frac{1}{2})}^{\frac{1}{2} \frac{1}{2}}, \quad \rho_{(-\frac{1}{2} - \frac{1}{2})(\frac{1}{2} \frac{1}{2})}^{\frac{1}{2} \frac{1}{2}}, \quad \rho_{(\frac{1}{2} - \frac{1}{2})(-\frac{1}{2} \frac{1}{2})}^{\frac{1}{2} \frac{1}{2}} + \rho_{(-\frac{1}{2} \frac{1}{2})(\frac{1}{2} - \frac{1}{2})}^{\frac{1}{2} \frac{1}{2}} = \eta, \\ & \rho_{(\frac{1}{2} \frac{1}{2})(\frac{1}{2} - \frac{1}{2})}^{\frac{1}{2} \frac{1}{2}} + \rho_{(\frac{1}{2} \frac{1}{2})(-\frac{1}{2} \frac{1}{2})}^{\frac{1}{2} \frac{1}{2}} = \alpha, \quad \rho_{(\frac{1}{2} - \frac{1}{2})(-\frac{1}{2} - \frac{1}{2})}^{\frac{1}{2} \frac{1}{2}} + \rho_{(-\frac{1}{2} \frac{1}{2})(-\frac{1}{2} - \frac{1}{2})}^{\frac{1}{2} \frac{1}{2}} = \beta, \\ & \rho_{(\frac{1}{2} \frac{1}{2})(\frac{1}{2} - \frac{1}{2})}^{\frac{1}{2} \frac{1}{2}} - \rho_{(\frac{1}{2} - \frac{1}{2})(-\frac{1}{2} - \frac{1}{2})}^{\frac{1}{2} \frac{1}{2}} = \gamma, \quad \rho_{(\frac{1}{2} \frac{1}{2})(-\frac{1}{2} \frac{1}{2})}^{\frac{1}{2} \frac{1}{2}} - \rho_{(-\frac{1}{2} \frac{1}{2})(-\frac{1}{2} - \frac{1}{2})}^{\frac{1}{2} \frac{1}{2}} = \delta . \end{aligned} \quad (5)$$

For pure 2-particle spin states this information permits us to restore the whole density matrix. But if the state is mixed, then in order to reconstruct all the elements of its density matrix one must know three additional quantities [3,4]

$$\rho_{(\frac{1}{2} \frac{1}{2})(-\frac{1}{2} \frac{1}{2})}^{\frac{1}{2} \frac{1}{2}} - \rho_{(-\frac{1}{2} \frac{1}{2})(\frac{1}{2} - \frac{1}{2})}^{\frac{1}{2} \frac{1}{2}} = i\xi, \quad \rho_{(\frac{1}{2} \frac{1}{2})(\frac{1}{2} - \frac{1}{2})}^{\frac{1}{2} \frac{1}{2}}, \quad \rho_{(\frac{1}{2} - \frac{1}{2})(-\frac{1}{2} \frac{1}{2})}^{\frac{1}{2} \frac{1}{2}} . \quad (6)$$

These quantities contain three independent real unknown parameters. These parameters can be found as functions of probabilities w_1, w_2, w_3, w_4 of the pure states, forming the mixed state. In the case of $w_1 = 1, w_2 = w_3 = w_4 = 0$ we have a pure state and therefore formulas (5) give us the whole density matrix.

The result is that for mixed 2-particle spin states, using only the diagonal elements of the density matrix examined merely in terms of a single reference frame common to both spins is inadequate for a complete description of the state. They must be supplemented by the probabilities $w_i, i = 1, \dots$, with which the pure states appear in the mixed one.

The additional parameters (6) can be found with the help of the spin correlation operator

$$\hat{a} \otimes \hat{b} = 4(\vec{a}, \vec{S}^{(1)}) \otimes (\vec{b}, \vec{S}^{(2)}) . \quad (7)$$

Here \vec{a}, \vec{b} are some unit vectors. They determine the axes in the configurational space and $\vec{S}^{(1)}, \vec{S}^{(2)}$ are the spin operators of 1-particle spin states, composing the 2-particle spin state. The measured quantities are the mean values of the spin projections to these axes. The average value of the observable described by the operator (8) at the state defined by a density matrix ρ is

$$E(\vec{a}, \vec{b}) = Sp(\hat{a} \otimes \hat{b} \rho) . \quad (8)$$

If $\vec{a} = \vec{b}$ then the average (8) contains information only about the diagonal elements of the density matrix ρ , but in the case of $\vec{a} \neq \vec{b}$ the average (8) contains information about the offdiagonal elements of the density matrix ρ too. So with the help of some special measurements of the values $E(\vec{a}, \vec{b})$ one can find the unknown parameters (6) and restore the whole density matrix ρ .

All 2-particle spin states can be divided into two classes - the factorisable states and the entangled states. The density matrix ρ_f of a factorisable state can be presented as a sum of direct products of the density matrices of the 1-particle states

$$\rho_f = \sum_i \rho_i^a \otimes \rho_i^b . \quad (9)$$

The density matrix ρ_e of an entangled state can not be presented in a such form. It can be proved that for the factorisable states the Bell's inequality is valid and for the entangled states it is violated.

In the framework of the tomographic formulation of quantum mechanics a quantum state is described by the set of probability distribution functions. This set corresponds to the full set of the independent observables such that their values can be measured simultaneously. A 1-particle 1/2-spin state is described by one probability distribution function (2) $w(1/2; \theta, \phi)$.

The 2-particle factorisable spin state is described by the set of two 1-particle probability distribution functions

$$w_f = \{ w_a(\frac{1}{2}; \theta, \phi), w_b(\frac{1}{2}; \theta, \phi) \} . \quad (10)$$

The 2-particle entangled spin state is described by the set

$$w_e = \{ w(i, j; \theta, \phi); i, j = \pm \frac{1}{2}, w_1, w_2, w_3, w_4 \} . \quad (11)$$

The functions in the set (11) satisfy the conditions

$$\sum_{i,j} w(i, j; \theta, \phi) = 1, \quad \sum_{i=1}^4 w_i = 1 . \quad (12)$$

The quantities forming any probability distribution function can be measured simultaneously. In the case of factorisable spin states one can measure simultaneously the projections of the spins of 1-particle states composing a 2-particle state. In the case of entangled spin states it is possible to measure the common spin (triplet or singlet) of the pair of particles, but it is impossible to find simultaneously both projections of spins of the individual particles and the common spin of the pair. The corresponding measuring procedures are performed by different types of experimental equipment and can not be carried out simultaneously.

We want to stress that according to the principles of quantum mechanics any set of observables can be connected with a given quantum state only after performing the measurements of the values of these observables. The type of a state (either it is factorisable or entangled) isn't the property of a state by itself, but the characteristic of the method of measuring observables that describe the state.

According to J.Schwinger an each quantum mechanical measurement can be divided into two parts - the nonselective measurement and selective measurement. In the process of nonselective measurement we choose the set of observables to be measured and prepare the appropriate measuring equipment. In the process of the selective measurement we carry out the measuring procedures and find the values of chosen observables.

The nonselective measurements describe the subject of measurement and the selective measurements describe the object of measurement.

The nonselective measurements give us the form of a probability distribution functions and the selective measurements provide the values of these functions.

The tomographic formulation of quantum mechanics is adequate to treating the Einstein-Podolsky-Rosen paradox. The essence of the paradox is as follows.

At the moment t_0 we prepare an entangled 2-particle spin state described by the probability distribution function (11). The particles A and B, which compose it, move in opposite directions so that at the moment t_1 they are separated by a macroscopic space interval. During that period the particles A and B form the entangled state and the projections of their individual spins are not defined. Let us measure at the moment t_1 the projection of the spin of the particle A. As the particle B is far from the particle A it does not feel the process of this measurement. Nevertheless after this measurement we know the projection of the spin of the particle B too. The question is whether the particle B had the definite projection of the spin at any moment $t < t_1$?

If the answer is - "YES", then we can construct the Bell's inequality. But this inequality contradicts the assumption that at any moment $t < t_1$ we deal with the entangled state.

So the answer must be - "NO".

The rigorous analysis shows that the measurement of the of the spin of the particle A defines the projection of the spin of the particle B only for the observer connected with the particle A. In order for the observer connected with the particle B to know the projection of the spin of the particle B too, some information must be sent to him from the observer connected with the particle A. Only after this moment the projection of the spin of the particle A and the projection of the spin of the particle B are defined for both observers.

In the framework of the tomographic formulation of quantum mechanics the process of the defining of the projections of the individual spins of the particles A and B can be described as the transformation from a probability distribution function (11) of an entangled state to a probability distribution function (10) of a factorisable state. So at any moment t we know the probability distribution function by which the state is described and know what information about the state it contains and what information it does not contain. We also can connect the transformation from one kind of probability distributions to another with the concrete measuring procedure.

Therefore in this approach the Einstein-Podolsky-Rosen paradox is not present at all.

References

- [1] V.V. Dodonov and V.I. Man'ko, Phys. Lett. A **229**, 335 (1997).
- [2] O.V. Man'ko and V.I. Man'ko, Zh. Eksp. Teor. Fiz. **112**, 796 (1997) [JETP, **85**, 430 (1997)].
- [3] V.A. Andreev and V.I. Man'ko, Zh. Eksp. Teor. Fiz. **114**, 437 (1998) [JETP, **87**, 239 (1998)].
- [4] V.A. Andreev, O.V. Man'ko, V.I. Man'ko and S.S. Safonov, J. Russ. Laser. Res. **19**, 340 (1998).

Quantum theory of cold damping

Jean-Michel Courty, Francesca Grassia and Serge Reynaud
*Laboratoire Kastler Brossel, ENS, CNRS, UPMC case 74,
4 place Jussieu, 75252 Paris Cedex05, France
E-mail: courty@spectro.jussieu.fr*

Abstract

Cold damping is an active method which bypasses the usual thermodynamical limitations on the sensitivity of measurements. We present a quantum treatment of this technique.

We present in this paper a quantum treatment of the sensitivity of a cold damped capacitive accelerometer designed for fundamental physics experiments in space [1–4]. The central element of the capacitive accelerometer is a parallelepipedic proof mass placed inside a box. The walls of these box are electrodes distant from the mass off a hundred micrometers. The proof mass is kept at the center of the cage by an electrostatic suspension. Since a three dimensional electrostatic suspension is instable, an active suspension has to be used. In the cage reference frame, an acceleration is transformed in an inertial force acting on the proof mass. The force necessary to compensate this inertial force is measured. In fact, as in most ultrasensitive measurements, the detected signal the error signal used to compensate the effect of the measured phenomenon.

The essential elements of the accelerometer are presented in figure 1. The proof mass and the cage form two condensators. Any mass motion unbalances the differential detection bridge and provides the error signal. In order to avoid low frequency electrical noise, the electrical circuit is polarized with an AC voltage operating at a frequency of a hundred kilohertz. After demodulation, this signal is used for detection and as an error signal for a servo control loop which allows to keep the mass centered in its cage.

Furthermore, the derivative of this signal provides a force proportional to the mass velocity and simulates a friction force. This active technique is called cold damping since it may be noiseless [5]. More precisely, the limiting fluctuations can be manipulated so that the effective noise temperature of the devices is reduced well below the operating temperature.

The analysis of sensitivity limits in these devices rises questions related to fundamental processes as well as experimental constraints. How far is it possible to reduce the measurement temperature? How are these process related to the fluctuation dissipation theorem? Are there quantum limits to this noise reduction? What about the quantum constraints in sensitivity enforced by Heisenberg inequalities? How do the experimental constraints interplay with the fundamental processes in the ultimate sensitivity?

We show here that quantum network theory allows to address these questions within a rigorous thermodynamical framework able to withstand the constraints of a quantum analysis of the measurement. In the same time, it makes possible a realistic description of

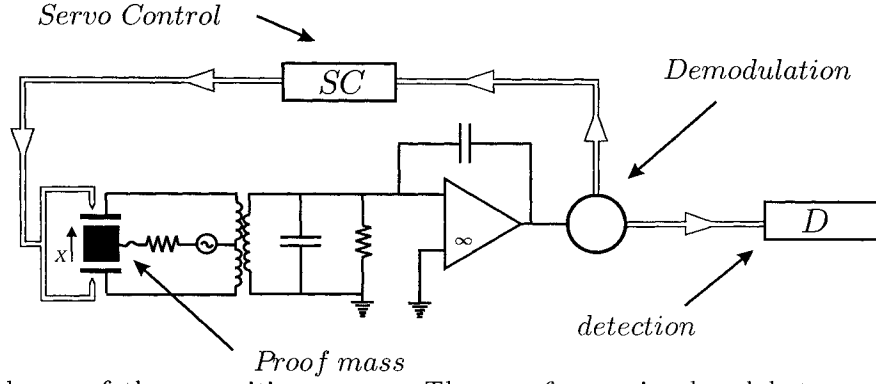


FIG. 1. Scheme of the capacitive sensor. The proof mass is placed between two electrodes formed by the inner walls of the accelerometer cage. The position dependent capacitances are polarized by an AC sinewave source which induces a mean current at a frequency of a hundred kHz in the symmetrical mode. The mass displacement is read as the current induced in the antisymmetric mode. An additional capacitance is inserted to make the antisymmetric mode resonant with the pump frequency. The signal is detected after an ideal operational amplifier with capacitive feedback followed by a synchronous demodulation. The impedance of the detection line plays the role of a further resistance. The detected signal then feeds the servo loop used to keep the mass centered with respect to the cage.

real measurement. In such an approach, the various fluctuations entering the system, either by dissipative or by active elements, are described as input fields in a number of lines. The measurement process is described as a scattering of input quantum fields a_n^{in} towards output fields a_n^{out} with a unitary \mathbf{S} matrix

$$\mathbf{a}^{\text{out}} = \mathbf{S} \mathbf{a}^{\text{in}} \quad (1)$$

Here, $\mathbf{X} = \mathbf{a}^{\text{in}}$, \mathbf{a}^{out} denotes the column vector with components X_n .

The input fields a^{in} as well as the output fields a^{out} obey the same commutation relations

$$[a^{\text{in}}[\omega], a^{\text{in}}[\omega']] = [a^{\text{out}}[\omega], a^{\text{out}}[\omega']] = 2\pi \delta(\omega + \omega') \varepsilon(\omega) \quad (2)$$

$$\langle a^{\text{in}}[\omega] \cdot a^{\text{in}}[\omega'] \rangle = 2\pi \delta(\omega + \omega') \sigma_{aa}^{\text{in}}[\omega] \quad (3)$$

where $\varepsilon(\omega)$ denotes the sign of the frequency ω . The fluctuations of these noncommuting operators are characterized by the correlation function $\sigma_{aa}^{\text{in}}[\omega]$. The dot symbol denotes a symmetrized product for quantum operators. In the case of a thermal bath, the noise spectrum is

$$\sigma_{aa}^{\text{in}}[\omega] = \frac{1}{2} \coth \frac{\hbar |\omega|}{2k_B T_a} \quad (4)$$

Dissipation due to the coupling with the environment is described with single lines. Operational amplifiers can be described with two noise lines [6]. Finally, the accelerometer can be described as a network as depicted on Fig 2.

The detection is performed with the output detection signal r_1^{out} . It is a linear combination of the external force F_{ext} multiplied by some coefficient and of input fields in the various

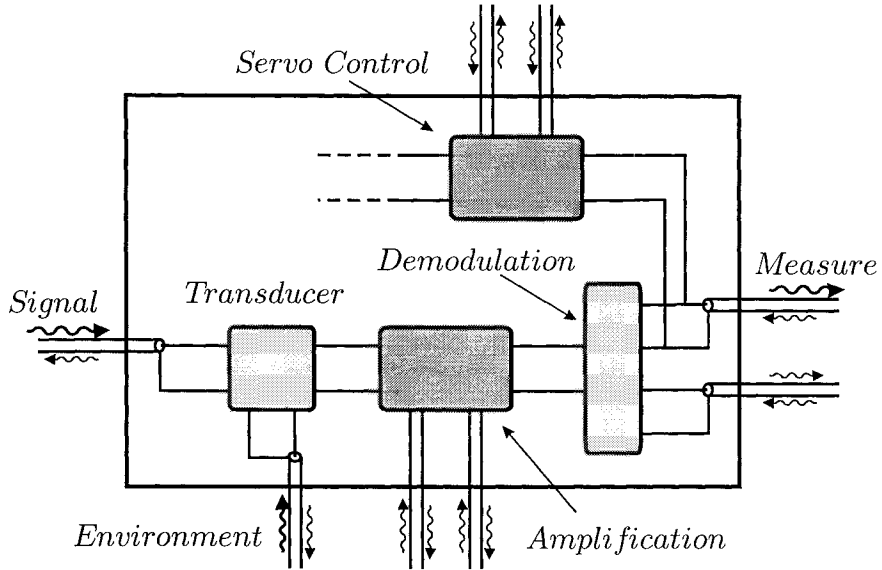


FIG. 2. Description of the accelerometer as a quantum network. The essential elements of the network are represented in this picture. The signal F_{ext} enters the accelerometer with a line and is coupled to the electromechanical transducer. The coupling of the accelerometer with the environment is described with an other line entering the transducer and corresponding to the Langevin force associated with mechanical dissipation. The signal is then amplified with an ideal operational amplifier described with two noise lines. The demoduator provides two output corresponding to the quadratures of the electrical signal, one of them is used for the measurement and as an input to the servo control.

noise lines. When the expression of r_1^{out} is normalized so that the coefficient of proportionality appearing in front of the external force F_{ext} is reduced to unity, a force estimator \hat{F}_{ext} is obtained which is just the sum of the true force F_{ext} to be measured and of an equivalent input force noise. In the absence of feedback, the force estimator reads [4]:

$$\hat{F}_{ext} = F_{ext} + \sum_{\alpha} \mu_{\alpha} \alpha^{in} \quad (5)$$

where α^{in} denote the various input fields corresponding to the active and passive elements in the accelerometer.

With the feedback, the servo loop efficiently maintains the mass at its equilibrium position and the velocity is no longer affected by the external force F_{ext} . The residual motion is interpreted as the difference between the real velocity of the mass and the velocity measured by the sensor. This means that the servo loop efficiently corrects the motion of the mass except for the sensing error. However the sensitivity to external force is still present in the correction signal. In fact, a quite remarkable result is then obtained. In the limit of an infinite loop gain and with the same approximations as above, the expression of the force estimator \hat{F}_{ext} is the same as in the free case [4].

The added noise spectrum Σ_{FF} is obtained as

$$\Sigma_{FF} = \sum_{\alpha} |\mu_{\alpha}|^2 \sigma_{\alpha\alpha}^{in}$$

We have evaluated whole noise spectrum Σ_{FF} for the specific case of the instrument proposed for the μ SCOPE space mission devoted to the test of the equivalence principle. In the

operating conditions of this accelerometer, the added noise spectrum is dominated by the mechanical Langevin forces. This corresponds to a sensitivity in acceleration

$$\frac{\sqrt{\Sigma_{FF}}}{M} = 1.2 \times 10^{-12} \text{ m s}^{-2}/\sqrt{\text{Hz}} \quad (6)$$

Taking into account the integration time of the experiment, this is consistent with the expected instrument performance corresponding to a test accuracy of 10^{-15} .

In the present state-of-the-art instrument, the sensitivity is limited by the residual mechanical Langevin forces. The latter are due to the damping processes in the gold wire used to keep the proof mass at zero voltage [3]. With such a configuration, the detection noise is not a limiting factor. This is a remarkable result in a situation where the effective damping induced through the servo loop is much more efficient than the passive mechanical damping. This confirms the considerable interest of the cold damping technique for high sensitivity measurement devices.

Future fundamental physics missions in space will require even better sensitivities. To this aim, the wire will be removed and the charge of the test mass will be controlled by other means, for example UV photoemission. The mechanical Langevin noise will no longer be a limitation so that the analysis of the ultimate detection noise will become crucial for the optimization of the instrument performance. This also means that the electromechanical design configuration will have to be reoptimized taking into account the various noise sources associated with detection.

REFERENCES

- [1] A. Bernard and P. Touboul, *The GRADIO accelerometer: design and development status*, Proc. ESA-NASA Workshop on the Solid Earth Mission ARISTOTELES, Anacapri, Italy (1991).
- [2] P. Touboul et al., *Continuation of the GRADIO accelerometer predevelopment*, ONERA Final Report 51/6114PY, 62/6114PY ESTEC Contract (1992, 1993).
- [3] E. Willemenot, *Pendule de torsion à suspension électrostatique, très hautes résolutions des accéléromètres spatiaux pour la physique fondamentale*, Thèse de Doctorat de l'université Paris 11 (1997).
- [4] F. Grassia, J-M. Courty, S. Reynaud and P. Touboul , preprint xxx quant-ph/9904073
- [5] J.M.W. Milatz and J.J.Van Zolingen, *Physica XIX* (1953) 181; J.M.W. Milatz, J.J.Van Zolingen and B.B. Van Iperen, *Physica XIX* (1953) 195.
- [6] J-M. Courty, F. Grassia and S. Reynaud, *Europhys. Lett*, **46** (1), pp. 31-37 (1999) [preprint quant-ph/9811062].

Dissipation and Entanglement Swapping

M.O. Terra Cunha*

*Departamento de Matemática, Universidade Federal de Minas Gerais, C.P.
702, Belo Horizonte, MG, 30123-970, Brazil*

K. Furuya

*Instituto de Física Gleb Wataghin, Universidade Estadual de Campinas,
C.P. 6165, Campinas, SP, 13084-970, Brazil*

M.C. Nemes

*DEpartamento de Física, Universidade Federal de Minas Gerais, C.P. 702,
Belo Horizonte, MG, 30123-970, Brazil*

Abstract

We show that entanglement swapping may be induced by dissipation in Optical cavities. An analytical calculation is done in the dispersive approximation of the Jaynes Cummings model with dissipation. We start with an initially entangled atom-field state and show that in the weak coupling (high Q) regime three very distinct time scales are present: firstly a rapid decoherence takes place, followed by the entanglement swapping regime and finally an essentially dissipative dynamics dominates. In the end the initial atom-field entanglement is transferred to atom-cavity system.

It has recently been pointed out that entanglement needs not necessarily arise after some interaction between quantum subsystems [1]. Fundamental aspects of Quantum Mechanics [2,3] which are presently under investigation make use of this phenomenon. Environmental entanglement effects have been shown to play a major role on the description of decoherence [4]. In the past years there has been many proposals for the generation of entangled states of subsystems that have never interacted [5,6]. Crucial for the generation of such states is the phenomenon of entanglement swapping: an auxiliary subsystem is used, entangled with one of the subsystems of interest, and this entanglement is swapped to the other one. The conception of this mechanism was first put forth in ref. [7]. In ref [8] a possible scheme for the generation of a cavity QED entangled atom-field state was devised. In particular the entangled state made up of a (controlled) coherent superposition of even and odd coherent states as follows

*tcunha@mat.ufmg.br

$$|EOC(\alpha, \gamma, \xi)\rangle = \cos \gamma |u\rangle \otimes |e\alpha\rangle + e^{i\xi} \sin \gamma |d\rangle \otimes |o\alpha\rangle, \quad (1)$$

where $|e\alpha\rangle$ and $|o\alpha\rangle$ stands for even and odd coherent states of complex amplitude α :

$$\begin{aligned} |e\alpha\rangle &= \mathcal{N}_e(\alpha) (|\alpha\rangle + |-\alpha\rangle), \\ |o\alpha\rangle &= \mathcal{N}_o(\alpha) (|\alpha\rangle - |-\alpha\rangle), \end{aligned} \quad (2)$$

and $|u\rangle$ and $|d\rangle$ refer to the two Rydberg atomic states considered in the two level atom approximation, can be achieved. The parameters γ and α determine the degree of entanglement of the state.

In the present work we consider the above initial condition evolving according to the dynamics of the dispersive Jaynes Cummings Model (JCM) with dissipation [9]. We show that, once the initial state is prepared, the present experimental device [10] can be used to monitor the transfer of coherence from atom-field state to the atom-cavity system. This process is somehow complementary to cavity loss induced generation of entangled atoms [11], where a pair of disentangled atoms is entangled to a field mode, and dissipation makes the atoms entangle.

The dynamics of the atom-field system is described by the following Liouville-Von Neuman equation

$$\dot{\rho} = \mathcal{L}\rho, \quad (3)$$

with

$$\mathcal{L}\rho = -i[H, \rho] + \mathcal{D}\rho, \quad (4)$$

where H is the dispersive approximation to JCM

$$H = \omega a a^\dagger |u\rangle \langle u| + \omega a^\dagger a |d\rangle \langle d|, \quad (5)$$

with a^\dagger and a being field mode operators, $\omega = \frac{\Omega^2}{\delta}$, Ω the vacuum Rabi frequency and δ the detuning (we use $\hbar = 1$), and \mathcal{D} is the zero temperature RWA dissipator

$$\mathcal{D} = k(2\mathcal{J} - \mathcal{M} - \mathcal{P}), \quad (6)$$

where k stands for dissipation constant and the above (super)operators are defined as

$$\begin{aligned} \mathcal{J}\rho &= a\rho a^\dagger, \\ \mathcal{M}\rho &= a^\dagger a\rho, \\ \mathcal{P}\rho &= \rho a^\dagger a. \end{aligned} \quad (7)$$

If we decompose the atom-field density operator as

$$\rho = \rho_{uu} \otimes |u\rangle \langle u| + \rho_{ud} \otimes |u\rangle \langle d| + \rho_{du} \otimes |d\rangle \langle u| + \rho_{dd} \otimes |d\rangle \langle d|, \quad (8)$$

where ρ_{ij} are operators on field variables only (caution: they are not density operators, despite of our notation). Each ρ_{ij} obeys a Liouville-Von Neuman like equation

$$\dot{\rho}_{ij} = \mathcal{L}_{ij} \rho_{ij}, \quad (9)$$

with

$$\begin{aligned} \mathcal{L}_{uu} &= -i\omega (\mathcal{M} - \mathcal{P}) + \mathcal{D}, \\ \mathcal{L}_{dd} &= i\omega (\mathcal{M} - \mathcal{P}) + \mathcal{D}, \\ \mathcal{L}_{du} &= -i\omega (\mathcal{M} + \mathcal{P} + 1) + \mathcal{D}, \end{aligned} \quad (10)$$

and we can solve these equations as is done in [9]. Considering initial condition

$$\rho(0) = |EOC(\alpha, \gamma, \xi)\rangle \langle EOC(\alpha, \gamma, \xi)|, \quad (11)$$

we obtain

$$\begin{aligned} \rho_{uu}(t) &= \rho_{uuee}(t) |e\alpha(t)\rangle \langle e\alpha(t)| + \rho_{uuoo}(t) |o\alpha(t)\rangle \langle o\alpha(t)|, \\ \rho_{dd}(t) &= \rho_{ddee}(t) |e\alpha^*(t)\rangle \langle e\alpha^*(t)| + \rho_{ddoo}(t) |o\alpha^*(t)\rangle \langle o\alpha^*(t)|, \\ \rho_{ud}(t) &= \rho_{udeo}(t) |e\alpha(t)\rangle \langle o\alpha^*(t)| + \rho_{udoe}(t) |o\alpha(t)\rangle \langle e\alpha^*(t)|, \end{aligned} \quad (12)$$

where $\alpha(t) = \alpha e^{-(i\omega+k)t}$ and

$$\begin{aligned} \rho_{uuee}(t) &= \frac{1}{2} \cos^2 \gamma \left(1 + e^{-2(|\alpha|^2 - |\alpha(t)|^2)} \right) \frac{1 + e^{-2|\alpha(t)|^2}}{1 + e^{-2|\alpha|^2}}, \\ \rho_{uuoo}(t) &= \frac{1}{2} \cos^2 \gamma \left(1 - e^{-2(|\alpha|^2 - |\alpha(t)|^2)} \right) \frac{1 - e^{-2|\alpha(t)|^2}}{1 + e^{-2|\alpha|^2}}, \\ \rho_{ddee}(t) &= \frac{1}{2} \sin^2 \gamma \left(1 - e^{-2(|\alpha|^2 - |\alpha(t)|^2)} \right) \frac{1 + e^{-2|\alpha(t)|^2}}{1 - e^{-2|\alpha|^2}}, \\ \rho_{ddoo}(t) &= \frac{1}{2} \sin^2 \gamma \left(1 + e^{-2(|\alpha|^2 - |\alpha(t)|^2)} \right) \frac{1 - e^{-2|\alpha(t)|^2}}{1 - e^{-2|\alpha|^2}}, \\ \rho_{udeo}(t) &= \frac{1}{2} e^{-i\xi} \sin(2\gamma) e^{-(|\alpha|^2 - |\alpha(t)|^2)} \left(\frac{1 - e^{-4|\alpha(t)|^2}}{1 - e^{-4|\alpha|^2}} \right)^{\frac{1}{2}} \cosh \left[\frac{k |\alpha(t)|^2}{i\omega + k} (e^{2(i\omega+k)t} - 1) \right], \\ \rho_{udoe}(t) &= \frac{1}{2} e^{-i\xi} \sin(2\gamma) e^{-(|\alpha|^2 - |\alpha(t)|^2)} \left(\frac{1 - e^{-4|\alpha(t)|^2}}{1 - e^{-4|\alpha|^2}} \right)^{\frac{1}{2}} \sinh \left[\frac{k |\alpha(t)|^2}{i\omega + k} (e^{2(i\omega+k)t} - 1) \right]. \end{aligned} \quad (13)$$

With this complete solution in hands, some important features become clear. First of all, the atomic density operator defined as

$$\rho_A = tr_F \rho, \quad (14)$$

where tr_F denotes partial trace over the field mode variables, remains constant

$$\rho_A(t) = \cos^2 \gamma |u\rangle \langle u| + \sin^2 \gamma |d\rangle \langle d|, \quad (15)$$

and so the degree of entanglement of atomic state with the rest of the system is conserved. In the initial state all this entanglement is shared with the field mode, with cavity degrees

of freedom factorized, but asymptotically the situation is inverted: field state (vacuum) factorizes out, and all entanglement is shared between atom and cavity.

Now we can investigate how this phenomenon occur in time. As solution given in eq. (12) shows, the density operator has at most four positive eigenvalues, and the maximal cavity-(atom-field) entanglement occurs when all this eigenvalues are equal. Explicit expressions for eigenvalues are given by

$$\begin{aligned}\lambda_1 &= \frac{1}{2} \left\{ \rho_{uuee} + \rho_{ddoo} + [(\rho_{uuee} - \rho_{ddoo})^2 + 4|\rho_{udeo}|^2]^{\frac{1}{2}} \right\}, \\ \lambda_2 &= \frac{1}{2} \left\{ \rho_{uuee} + \rho_{ddoo} - [(\rho_{uuee} - \rho_{ddoo})^2 + 4|\rho_{udeo}|^2]^{\frac{1}{2}} \right\}, \\ \lambda_3 &= \frac{1}{2} \left\{ \rho_{uuoo} + \rho_{ddee} + [(\rho_{uuoo} - \rho_{ddee})^2 + 4|\rho_{udoe}|^2]^{\frac{1}{2}} \right\}, \\ \lambda_4 &= \frac{1}{2} \left\{ \rho_{uuoo} + \rho_{ddee} - [(\rho_{uuoo} - \rho_{ddee})^2 + 4|\rho_{udoe}|^2]^{\frac{1}{2}} \right\}.\end{aligned}\tag{16}$$

Their behaviour depends strongly on the initial state parameters α and γ , and on the ratio $q = \frac{\omega}{k}$. We will focus on the initially maximal entanglement ($\gamma = \frac{\pi}{4}$) and “large α ” ($|\alpha| > 1$) case, but varying q . In case $q \gg 1$ (experimentally feasible, since in Paris experiment [10] $q = \frac{\Omega}{\delta} Q \simeq 10^7$), three distinct time scales can be observed: firstly a rapid decoherence takes place, rather independently of the parameters used; secondly the tripartite system atom-field-cavity evolves and maximally (atom-field)-cavity entangled states takes place; the third and last regime is essentially governed by dissipation alone, and as the field approaches vacuum state it factorizes out and the initial atom-field entanglement is swapped to atom-cavity subsystem. This is illustrated in figure 1, where the second regime is characterized by the flat part of the graphic, and the third by the decay of a pair of eigenvalues.

As dissipation grows, the second regime can be suppressed. No maximally (atom-field)-cavity entangled state take place, but even in this situation entanglement swap is achieved. In figure 2 we show a sequence of intermediate cases.

It is important to emphasize that such behaviour depends dramatically on the model we choose. If atom were allowed to spontaneously decay, or even if a small temperature component were added, the situation would change and entanglement swap would not be complete as in this simple case.

K. Furuya and M.C. Nemes acknowledge the support of CNPq. M.O. Terra Cunha thanks the organizers of 6th ICSSUR for hospitality, and J.G. Peixoto de Faria for fruitful discussions.

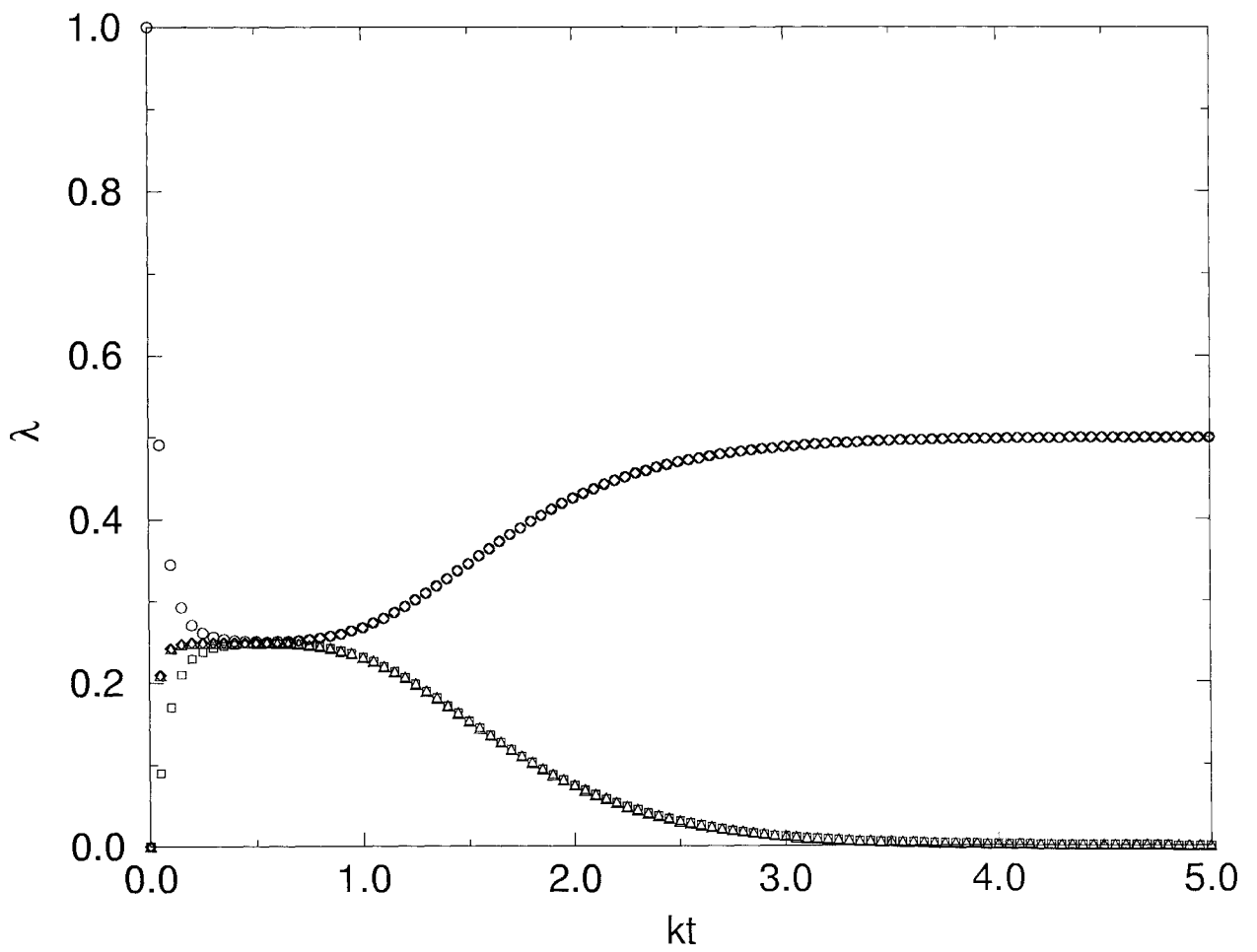
REFERENCES

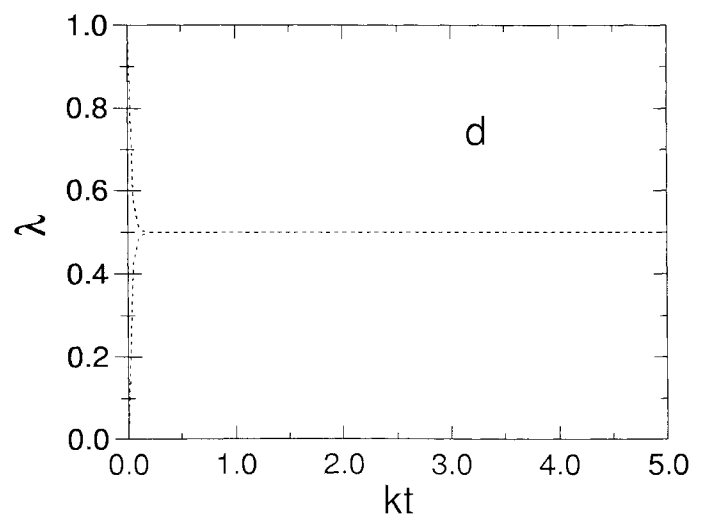
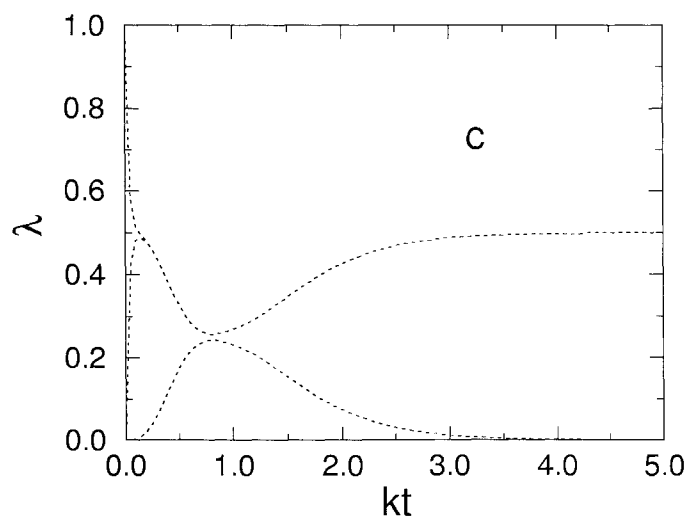
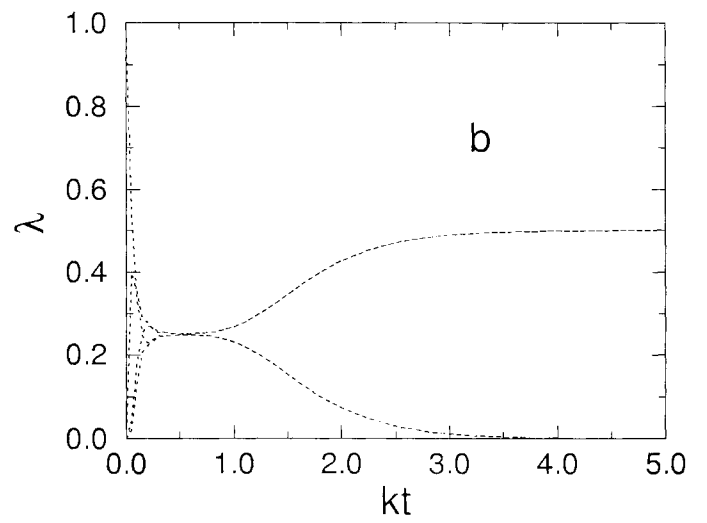
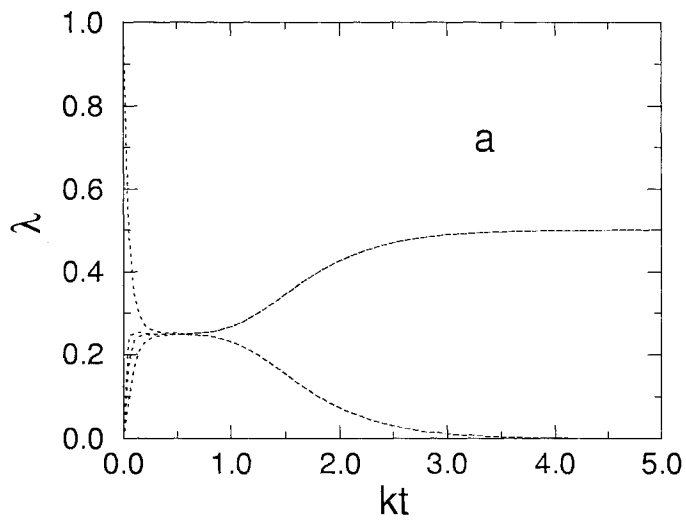
- [1] B. Yurke and D. Stoler, **Phys. Rev. A****46**, 2229 (1992); **Phys. Rev. Lett.** **68**, 1251 (1992).
- [2] A. Einstein, B. Podolsky and N. Rosen, **Phys. Rev.** **47**, 777 (1935).
- [3] J.S. Bell, “*Speakable and Unspeakable in Quantum Mechanics*” (Cambridge University Press, Cambridge, 1988).
- [4] R. Omnès, “*The Interpretation of Quantum Mechanics*” (Princeton University Press, Princeton, 1994), and references therein.
- [5] P.G. Kwiat et al, **Phys. Rev. Lett.** **75**, 4337 (1995).
- [6] S.J.D. Phoenix and S.M. Barnett, **J. Mod. Opt.** **40**, 979 (1993); I.K. Kudrayevtsev and P.L. Knight, **J. Mod. Opt.** **40**, 1673 (1993); J.I. Cirac and P. Zoller, **Phys. Rev. A****50**, R2799 (1994); C.C. Gerry, **Phys. Rev. A****53**, 2857 (1996).
- [7] M. Zukowski et al, **Phys. Rev. Lett.** **71**, 4287 (1993).
- [8] D. Jonathan, MSc Thesis presented at the Universidade Estadual de Campinas (1997); D. Jonathan, K. Furuya and A. Vidiella-Barranco, ‘*Entangled States in the Jaynes-Cummings Model*’, preprint.
- [9] J.G. Peixoto de Faria and M.C. Nemes, **Phys. Rev. A****59**, 3918 (1999).
- [10] M. Brune et al, **Phys. Rev. Lett.** **77**, 4887 (1996).
- [11] M.B. Plenio et al, **Phys. Rev. A****59**, 2368 (1999). Also available as quant-ph/9811003.

Figure captions:

Figure 1: Eigenvalues of ρ for $\gamma = \frac{\pi}{4}$, $\alpha = 3.1$ and $q = 1.2 \times 10^7$ (parameters taken from [10]).

Figure 2: Eigenvalues of ρ for $\gamma = \frac{\pi}{4}$, $\alpha = 3.1$ and (a) $q = 10^2$, (b) $q = 10$, (c) $q = 1$ and (d) $q = 10^{-2}$.





“Golden Rule” for Decoherence and Dissipation: The Emergence of Classicality

M.O.Terra Cunha*

Departamento de Matemática, Universidade Federal de Minas Gerais, C.P. 702, Belo Horizonte, MG, 30123-970, Brazil

S.Geraj Mokarzel

Instituto de Física, Universidade de São Paulo, C.P. 20516, São Paulo, SP, 01317-970, Brazil

M.C. Nemes

Departamento de Física, Universidade Federal de Minas Gerais, C.P. 702, Belo Horizonte, MG, 30123-970, Brazil

Abstract

A perturbative treatment of reduced density operator of quantum subsystems is implemented in the same spirit as Fermi’s Golden Rule for scattering. Analytic expressions for linear entropy (a measure of coherence loss) and subsystem’s energy variation (dissipation) are given. They are applied to the dynamics of a superposition of coherent states in a dissipative cavity. We show that in this example characteristic times for thermalization (τ_{th}), dissipation (τ_{dis}) and decoherence (τ_{dec}) can be formally defined. Explicit expressions for them are obtained in the Markoffian limit and relations among them are explored in several situations.

One of the most remarkable properties of the quantum mechanical description of interacting systems is the entanglement process. It is in the root of a large class of “quantum mysteries” [1]: EPR “paradox”, Schrödinger cats, Bell inequalities and non-locality. Given the remarkable achievements with recent experiments in Quantum Optics [2] and the interest in Quantum Communication [3] we have now the possibility of exploring the dynamics of the entanglement process and its consequences. Theoretical description of parties of large systems, aside from a short list of exactly solvable models [4], is basically given in terms of Master equations [5] which preclude the description of short time regimes, where the dynamics of quantum correlations play decisive roles. Recently a perturbative description of decoherence time scales has been proposed [6], but, to the authors’ knowledge, a well

*tcunha@mat.ufmg.br

founded and practical framework for decoherence and dissipation is still lacking, although many generic arguments on the role of both are available in the literature [7]. The purpose of this contribution is to construct a pragmatic tool to investigate these processes. We work a Dyson Series like expansion for density operators and obtain the Fermi's Golden Rule analog for the quantum interaction of two subsystems in the regime of weak interaction. We also work out a particular example taken from quantum optics (a superposition of coherent states in a dissipative cavity), where similarities and peculiarities of both processes are discussed.

Let us consider a general Hamiltonian (with discrete spectrum) of the form

$$H = H_0 + H_{12}, \quad (1)$$

where $H_0 = H_1 + H_2$, with

$$H_1 = \sum_n |n\rangle \varepsilon_n^{(1)} \langle n| \otimes 1_2, \quad (2)$$

$$H_2 = 1_1 \otimes \sum_s |s\rangle \varepsilon_s^{(2)} \langle s|, \quad (3)$$

and

$$H_{12} = \sum_{m,n,r,s} \gamma_{mrns} |m\rangle \langle n| \otimes |r\rangle \langle s|. \quad (4)$$

In the above expressions $\varepsilon_n^{(i)}$ stands for the eigenenergies of system i whose autonomous dynamics is governed by the Hamiltonian H_i , and γ_{mrns} are the interaction matrix elements in the tensor product basis.

We further assume that the time scales associated with H_{12} are larger than subsystems characteristic times (i.e.: small coupling limit, $\gamma \ll \varepsilon_i$) and the initial state is a factorized one

$$\rho(0) = \rho_1(0) \otimes \rho_2(0). \quad (5)$$

It is in this case convenient to use the interaction picture, in which density operator is given by (we use $\hbar = 1$)

$$\rho_I(t) = \exp(iH_0 t) \rho(t) \exp(-iH_0 t), \quad (6)$$

and the time dependent interaction Hamiltonian becomes

$$\begin{aligned} H_{12}(t) &\equiv \exp(iH_0 t) H_{12} \exp(-iH_0 t) \\ &= \sum \gamma_{12}(t) |m\rangle \langle n| \otimes |r\rangle \langle s|, \end{aligned} \quad (7)$$

where

$$\gamma_{12}(t) = \gamma_{mrns} \exp \left[i \left(\varepsilon_m^{(1)} - \varepsilon_n^{(1)} + \varepsilon_r^{(2)} - \varepsilon_s^{(2)} \right) t \right].$$

It is important to stress that the symbols $\gamma_{12}(t)$ are strongly dependent on m, n, r, s , but we omit such indices for notational convenience. For later convenience we also define the symbols

$$\gamma'_{12}(t) = \gamma_{m'r'n's'} \exp \left[i \left(\varepsilon_{m'}^{(1)} - \varepsilon_{n'}^{(1)} + \varepsilon_{r'}^{(2)} - \varepsilon_{s'}^{(2)} \right) t \right],$$

where the same tacit dependence occur.

Von Neumann's equation takes the form

$$i\dot{\rho}_I(t) = [H_{12}(t), \rho_I(t)]. \quad (8)$$

From now on, we drop the subscript I , but interaction picture must be implied.

A Born like expansion,

$$\rho(t) = \rho(0) - i \int_0^t dt' [H_{12}(t'), \rho(0)] - \int_0^t dt' \int_0^{t'} dt'' [H_{12}(t'), [H_{12}(t''), \rho(0)]] + \dots \quad (9)$$

where we identify

$$\rho = \rho^{0th} + \rho^{1st} + \rho^{2nd} + \dots \quad (10)$$

In this sense we will obtain second order (in interaction) expressions for the reduced density operators

$$\rho_i = \text{Tr}_j \rho, i \neq j, \quad (11)$$

which defines the states of subsystems, in the sense that every prediction about observables of one subsystem alone can be obtained from 11, but says nothing about "non-local" Bell-like observables.

From reduced density operators we can obtain linear entropy (or idempotency deficit) for each subsystem

$$\delta_i = 1 - \text{Tr}(\rho_i^2), \quad (12)$$

which indicates how far from pure states $\rho_\psi = |\psi\rangle\langle\psi|$ density operators ρ_1 and ρ_2 are, and gives an idea of how entangled 1 and 2 are (in case the whole 1-2 system is in a pure state). Also subsystem's energies

$$E_i = \text{Tr}(H_i \rho_i), \quad (13)$$

are obtained. These quantities will allow us to compare the processes of dissipation (energy variation) and decoherence ("purity" variation).

Straight forward calculation gives

$$\rho_j^{1st}(t) = i \sum_{m,n,r,s} \langle s | \rho_i^{0th} | r \rangle [|m\rangle \langle n|, \rho_j^{0th}] \int_0^t d\tau \gamma_{12}(\tau), i \neq j, \quad (14)$$

and

$$\begin{aligned} \rho_j^{2nd}(t) = & \sum_{m,n,r,s} \sum_{m',n',r',s'} \left\{ \delta_{r's} \langle s' | \rho_i^{0th} | r \rangle [|m\rangle \langle n|, |m'\rangle \langle n'| \rho_j^{0th}] + \right. \\ & \left. - \delta_{rs'} \langle s | \rho_i^{0th} | r' \rangle [|m\rangle \langle n|, \rho_j^{0th} |m'\rangle \langle n'|] \right\} \times \\ & \times \int_0^t d\tau \int_0^\tau d\tau' \gamma_{12}(\tau) \gamma'_{12}(\tau'), \end{aligned} \quad (15)$$

At this point the main ingredients of the subsystem's dynamics up to second order become apparent: first notice the manifest symmetry in the subsystem's indices. Moreover, it is easy to see that results will be strongly initial condition dependent. Furthermore the terms involving the integrals will be responsible for the contribution of the particular chosen interaction and for the available phase space just as in Fermi's Golden Rule for scattering. This will become more concrete in the example below.

General expressions for first and second order contributions in $\delta_i(t)$ and $E_i(t)$ can be written as follows

$$\delta_i^{1st}(t) = 0, \quad (16)$$

since it involves a trace of a commutator,

$$\delta_i^{2nd}(t) = -\text{Tr}(\rho_i^{1st}(t))^2 - 2\text{Tr}(\rho_i^{0th}(t)\rho_i^{2nd}(t)), \quad (17)$$

$$E_i^{1st}(t) = \text{Tr}(H_i\rho_i^{1st}(t)), \quad (18)$$

$$E_i^{2nd}(t) = \text{Tr}(H_i\rho_i^{2nd}(t)). \quad (19)$$

In order to gain deeper physical insight into the energy and coherence loss processes we work out an important example in the context of quantum optics. Let us consider two very different subsystems: the first, which we now call S is a harmonic oscillator (i.e. a radiation field mode) of frequency ω initially in the so called even coherent state [8] with amplitude α ,

$$\rho_S^{0th} = |e\alpha\rangle\langle e\alpha|, \quad (20)$$

where $|e\alpha\rangle = N(\alpha)(|\alpha\rangle + |-\alpha\rangle)$, $N(\alpha)$ being a normalization constant and $|\alpha\rangle$ Glauber's coherent state [9]. The other subsystem will represent a dissipative cavity, as modelled by a set of independent harmonic oscillators of frequency Ω^j in thermal equilibrium

$$\rho_R^{0th} = \bigotimes_j \rho_j^{0th}, \quad (21)$$

where $\rho_j^{0th} = Z_j^{-1} \exp(-\beta H_j)$, $\beta = (k_B T)^{-1}$, k_B being Boltzmann's constant, T the temperature and $Z_j = Z_j(\beta)$ partition function of the j th harmonic oscillator.

For the Hamiltonian coupling we consider the Rotating Wave Approximation (RWA) for the interaction between the main oscillator and each j oscillator. In our notation this amounts to consider the following explicit form for the matrix elements

$$\gamma_{mrns}^j = \gamma^j (\delta_{r,s+1}\delta_{m+1,n}\sqrt{rn} + \delta_{r+1,s}\delta_{m,n+1}\sqrt{sm}). \quad (22)$$

In this case first order corrections to energy vanish due to commutativity between ρ_R^{0th} and H_R . Second order contributions, given by eq. 19 becomes

$$\begin{aligned} E_S^{2nd}(t) &= \omega \left(1 + e^{-2|\alpha|^2}\right) \sum_j \frac{e^{-\beta\Omega^j}}{1 - e^{-\beta\Omega^j}} (\gamma^j)^2 \left\{ \frac{\sin[\Delta^j t]}{\Delta^j} \right\}^2 + \\ &\quad -\omega |\alpha|^2 \left(1 - e^{-2|\alpha|^2}\right) \sum_j (\gamma^j)^2 \left\{ \frac{\sin[\Delta^j t]}{\Delta^j} \right\}^2 \\ &\equiv E_{th}^{2nd}(t) - E_{dis}^{2nd}(t). \end{aligned} \quad (23)$$

In the above expression all the essential ingredients previously discussed are present. The initial states of both subsystems (through amplitude α and temperature T), the coupling strength $(\gamma^j)^2$ and

$$\left\{ \frac{\sin [\Delta^j t]}{\Delta^j} \right\}^2, \quad (24)$$

where $\Delta^j = \frac{1}{2}(\Omega^j - \omega)$, which teach us something about very short times when correlations are established. Note that the time-energy uncertainty relation appears in this calculation in the following way: in a time t uncertainty in energy must be of order t^{-1} and all modes with Δ^j up to this order give significant contribution in the summations involved in eq. 23. As times grows a narrow set of oscillators become significative and energy conservation (suitably modified) is achieved. Asymptotically in time, the energy transfer between the system and the reservoir depends just on the later's density of states of frequency ω .

We have separated the energy variation of subsystem S into two parts: one which is temperature dependent E_{th} and the other which will be present even in the $T = 0$ case. We called this the ‘‘dissipative’’ part of E_S^{2nd} . The reason for this will become clear in the sequel.

In the above expression, if we further assume a continuum smooth spectrum for the reservoir and a sufficiently smooth j dependence of γ^j we can convert summations into integrals, change variables to frequency integrals by using the density of states g and the following approximation to such integrals

$$\begin{aligned} \int_0^\infty d\Omega g F \left\{ \frac{\sin(\Delta t)}{\Delta} \right\}^2 &\simeq \int_{\omega - \frac{1}{2t}}^{\omega + \frac{1}{2t}} d\Omega g F \left\{ \frac{\sin(\Delta t)}{\Delta} \right\}^2 \\ &\simeq t^2 \int_{-\frac{1}{2t}}^{\frac{1}{2t}} d\Delta g(\omega + \Delta) F(\omega + \Delta) = \frac{t}{\tau_F}, \end{aligned} \quad (25)$$

where, the first approximation follows from the above discussion on time-energy uncertainty relation and the last one from the required smoothness of g and γ . It is important to stress that the sense of smoothness we are using for g and γ is subtle. For now it means that there is no ubiquitous behaviour like the absence of states in the interval of width t^{-1} around ω . This allows us to consider each term in eq. 23 as defining time scales τ_{th} and τ_{dis} :

$$\tau_{\text{dis}}^{-1} = \frac{|\alpha|^2 (1 - e^{-2|\alpha|^2})}{|\alpha|^2 + \frac{1}{2}} t \int_{-\frac{1}{2t}}^{\frac{1}{2t}} d\Delta g(\omega + \Delta) (\gamma(\omega + \Delta))^2, \quad (26)$$

$$\tau_{\text{th}}^{-1} = \frac{(1 + e^{-2|\alpha|^2})}{|\alpha|^2 + \frac{1}{2}} t \int_{-\frac{1}{2t}}^{\frac{1}{2t}} d\Delta g(\omega + \Delta) \frac{e^{-\beta(\omega + \Delta)}}{1 - e^{-\beta(\omega + \Delta)}} (\gamma(\omega + \Delta))^2. \quad (27)$$

But we must drop out the dependence on t on the right hand side of these equations. There seems to be two ways of doing it: one is to consider both as selfconsistent equations, substituting t by the appropriated τ and solving; the other is to consider asymptotic case $t \rightarrow \infty$, which corresponds to the Markoffian approximation. The first way would be a nice way to go beyond Markoffian approximation, necessary in cases in which g or γ vary drastically around the frequency ω . We will adopt the second, which permits us to obtain

$$\tau_{\text{dis,M}}^{-1} = \frac{|\alpha|^2 (1 - e^{-2|\alpha|^2})}{|\alpha|^2 + \frac{1}{2}} g(\omega) (\gamma(\omega))^2, \quad (28)$$

$$\tau_{\text{th,M}}^{-1} = \frac{(1 + e^{-2|\alpha|^2})}{|\alpha|^2 + \frac{1}{2}} g(\omega) \frac{e^{-\beta\omega}}{1 - e^{-\beta\omega}} (\gamma(\omega))^2, \quad (29)$$

which give us the general time scale relation

$$\frac{\tau_{\text{th,M}}}{\tau_{\text{dis,M}}} = |\alpha|^2 \text{th} |\alpha|^2 \left(\frac{e^{-\beta\omega}}{1 - e^{-\beta\omega}} \right)^{-1} \quad (30)$$

$$\rightarrow \beta\omega |\alpha|^2 \text{th} |\alpha|^2, \quad (31)$$

where the last expression is valid for the large temperature regime $\beta\omega \ll 1$.

The expression for the idempotency deficit of S is given by

$$\begin{aligned} \delta_S^{2nd}(t) = & 2 \left(1 + e^{-2|\alpha|^2}\right) \sum_j \frac{e^{-\beta\Omega^j}}{1 - e^{-\beta\Omega^j}} (\gamma^j)^2 \left\{ \frac{\sin \left[\frac{(\omega - \Omega^j)}{2} t \right]}{\frac{\omega - \Omega^j}{2}} \right\}^2 + \\ & 2 |\alpha|^2 \left(1 - e^{-2|\alpha|^2}\right) \sum_j \frac{1 + e^{-\beta\Omega^j}}{1 - e^{-\beta\Omega^j}} (\gamma^j)^2 \left\{ \frac{\sin \left[\frac{(\omega - \Omega^j)}{2} t \right]}{\frac{\omega - \Omega^j}{2}} \right\}^2. \end{aligned} \quad (32)$$

and the same reasoning defines the time scale τ_{dec} , which in the Markoffian approximation is given by:

$$\tau_{\text{dec,M}}^{-1} = 2 \left[\left(1 + e^{-2|\alpha|^2}\right) \frac{e^{-\beta\omega}}{1 - e^{-\beta\omega}} + |\alpha|^2 \left(1 - e^{-2|\alpha|^2}\right) \frac{1 + e^{-\beta\omega}}{1 - e^{-\beta\omega}} \right] g(\omega) (\gamma(\omega))^2$$

As is clear, in the expressions 23 and 32 the ingredients are the same, but the results are quite distinct. The greater difference is the relative sign and it is easy to understand it in this example. In both cases, the first term is the temperature contribution and the second is still there even for zero temperature. The first term tends to increase E_S (it is a “hot” term), while the second to decrease it (it is a “cold” one), but both add to decoherence. This difference in sign reflects in the difference in behavior and time scales of these processes.

In case $T = 0$ only “cold” terms contribute, and we obtain the relation

$$\frac{\tau_{\text{dis,M}}}{\tau_{\text{dec,M}}} = 2 |\alpha|^2 + 1, \quad (33)$$

and there is no thermalization in the sense which we are using this word. In this case, the time scales are the same for small $|\alpha|$, but can be very different for large $|\alpha|$. This is essentially the relation obtained in [10, eq 2.15], with the extra term +1 given by the zero point energy.

For temperature T we have

$$\frac{\tau_{\text{th,M}}}{\tau_{\text{dec,M}}} = 2 \left(|\alpha|^2 + \frac{1}{2} \right) \left[1 + |\alpha|^2 \text{th} |\alpha|^2 \frac{1 + e^{-\beta\omega}}{e^{-\beta\omega}} \right],$$

which shows that decoherence is even faster than thermalization, unless $\alpha = 0$, in which case they are equal. In the same way

$$\frac{\tau_{\text{dis,M}}}{\tau_{\text{dec,M}}} = 2 \left(|\alpha|^2 + \frac{1}{2} \right) \left[\frac{1}{|\alpha|^2 \operatorname{th} |\alpha|^2} \frac{e^{-\beta\omega}}{1 - e^{-\beta\omega}} + \frac{1 + e^{-\beta\omega}}{1 - e^{-\beta\omega}} \right],$$

where $|\alpha|$ plays its crucial role, and for large temperature we obtain the expected behaviour of linear increasing of decoherence rate with respect to temperature, in complete agreement with expression (20) of [7] and also with [11], but obtained in a very different framework.

Some general consequences of this framework must be pointed. Expressions 13 are also linear in ρ and this has important consequences: subsystem's energy may decrease or may increase, as discussed in the example. In this sense, dissipation is not an adequate term, because a low excited particle in contact with a "hot" reservoir will increase its energy, by the same process that an excited particle will decay. We prefer to call it thermalization. So, by the linearity of 13, interaction will allow energy transfer among subsystems, but not necessarily subsystem's energy variation. On the other hand, expression 12 is nonlinear in ρ . Even more, it has a minimum for pure states. This minimum is generally very unstable. General interaction takes ρ out of pure states. Again in the sense of energy-time uncertainty relation, the equal population of all attainable levels in times extremely short can make energy increase or decrease, but all this terms sum up through decoherence, if we start in a pure state.

In the case that one of the subsystems is a reservoir, the number of levels (density of states, in the continuum limit) allowed in the prekinetic regime grows, and decoherence and thermalization occur even faster. As recurrence times also grow, both processes attain their characteristic irreversibility.

Just as a final word, we point out that it is very striking that entanglement be at the same time in the root of most quantum mysteries, such as EPR "paradox", Schrödinger cats, Bell inequalities and Quantum Communication, and also in the way how classicality emerges from Quantum Mechanics when we insist in treating a part of a whole system as a system itself.

M. C. Nemes acknowledges the support of CNPq. M.O. Terra Cunha thanks the organizers of 6th ICSSUR for hospitality.

REFERENCES

- [1] J.A. Wheeler & W. Zurek (orgs), **Quantum Theory and Measurement** Princeton (1983).
- [2] S. Haroche, **Phys. Today** **51**(7), p. 36, July 1998.
- [3] See special issue of **Physics World**, March 1998.
- [4] A.O. Caldeira & A.J. Legget, **Ann. Phys. (NY)** **149**, p. 374 (1983). W.H. Zurek, **Phys. Rev. D** **26**(8), p. 1862 (1982). K.M. Fonseca Romero & M.C. Nemes, **Phys. Lett. A** **235**, p. 432 (1997).
- [5] R. Omnés, **Phys. Rev. A** **56**(5), p. 3383 (1997).
- [6] J.I. Kim, M.C. Nemes, A.F.R. de Toledo Piza & H.E. Borges, **Phys. Rev. Lett.** **77**(2), p. 207 (1996).
- [7] C. Kiefer & E. Joss, **Decoherence: Concepts and Examples** in P. Blanchard & A. Jadczyk (eds) *Quantum Future* (Springer, Berlin, 1998). Also available as **quant-ph/9803052** (and references therein).
- [8] V.V. Dodonov, I.A. Malkin & V.I. Man'ko, **Physica** **72**, p. 597 (1974).
- [9] R. Glauber, **Phys. Rev.** **131**, p. 2766 (1963).
- [10] L. Davidovich, M. Brune, J.M. Raimond & S. Haroche, **Phys. Rev. A** **53**(3), p. 1295 (1996).
- [11] M.S. Kim and V. Buzek, **Phys. Rev. A** **46**(7), p. 4239 (1992).

Quantum-like Description of a Dissipative Charged-Particle Fluid in a Quadrupole

S. De Nicola

Istituto di Cibernetica del CNR, Arco Felice, Italy

R. Fedele

Dipartimento di Scienze Fisiche, Università "Federico II" and INFN, Napoli, Italy

V.I. Man'ko

Lebedev Physical Institute, Moscow, Russia

Abstract

We show that the dynamics of a classical dissipative charged-particle fluid in a quadrupole-like device (harmonic potential well) can be described in terms of a one-particle Schrödinger-like equation for a complex function. The squared modulus and the gradient of phase of this function are proportional to the fluid density and to the current velocity, respectively. In this quantum-like equation, Planck's constant is replaced by the time-dependent emittance. In this framework, we fully recover the Thermal Wave Model (TWM) description that has been recently applied to the dynamics of an electron bunch in a storage ring in the presence of radiation damping and quantum-excitation.

I. INTRODUCTION

It is well known that a 1-D motion of a dilute charged-particle beam can be described by a fluid model, given by the following set of equations:

$$\left(\frac{\partial}{\partial s} + P \frac{\partial}{\partial x} \right) P = -\frac{\partial U}{\partial x} - \frac{1}{n} \frac{\partial \Pi}{\partial x} \quad , \quad (1)$$

$$\frac{\partial n}{\partial s} + \frac{\partial}{\partial x} (nP) = 0 \quad , \quad (2)$$

where $s = ct$ (c being the speed of light), $P = P(x, s)$ is the current velocity, $n = n(x, s)$ is the particle number density, $\Pi = nk_b T / mc^2$ (k_b is the Boltzmann constant, m is the particle mass, and $T = T(s)$ is the temperature of the system), and the quantity $U = U(x, s)$ is a dimensionless effective potential acting on the system.

In the next section we give a quantum-like description of a dissipative charged-particle fluid in the framework of TWM [1], by assuming that the fluid evolution is governed by a Schrödinger-like equation where instead of \hbar we have an arbitrary function of the timelike variable s . We show that, in the case the fluid is in a quadrupole, this equation is equivalent to the above set of equations (1) and (2) for a classical fluid.

II. QUANTUM-LIKE DESCRIPTION

In the TWM framework, let us assume, in absence of collective effects, that the dynamics of our system is governed by the following Schrödinger-like equation [1]:

$$i\alpha \frac{\partial \psi}{\partial s} = -\frac{\alpha^2}{2} \frac{\partial^2 \psi}{\partial x^2} + U(x, s)\psi \quad , \quad (3)$$

where $\alpha = \alpha(s)$ plays the role of a dispersion parameter and U , x and s have the same meaning as in the previous section. If we write

$$\psi(x, s) = M(x, s) \exp i\varphi(x, s) \quad , \quad (4)$$

and if we substitute the (4) back into the (3) we can easily derive the following dissipative Madelung-like fluid equations, namely

$$\left(\frac{\partial}{\partial s} + P \frac{\partial}{\partial x} \right) P = -\frac{\partial U}{\partial x} + \frac{\alpha'}{\alpha} P + \frac{\alpha^2}{2} \frac{\partial}{\partial x} \left(\frac{1}{M} \frac{\partial^2 M}{\partial x^2} \right) \quad , \quad (5)$$

$$\frac{\partial M^2}{\partial s} + \frac{\partial}{\partial x} (M^2 P) = 0 \quad , \quad (6)$$

where

$$P = \alpha \frac{\partial \varphi}{\partial x} \quad . \quad (7)$$

Note that we can define the fluid density

$$n(x, s) = |\psi(x, s)|^2 = M^2(x, s) \quad , \quad (8)$$

Consequently, under the following condition

$$\frac{\alpha'}{\alpha} P + \frac{\eta}{n} \frac{\partial n}{\partial x} + \frac{\alpha^2}{2} \frac{\partial}{\partial x} \left(\frac{1}{M} \frac{\partial^2 M}{\partial x^2} \right) = 0 \quad , \quad (9)$$

the (5) reduces to the following classical-like form

$$\left(\frac{\partial}{\partial s} + P \frac{\partial}{\partial x} \right) P = -\frac{\partial U}{\partial x} - \frac{\eta}{n} \frac{\partial n}{\partial x} \quad , \quad (10)$$

where $\eta = \eta(s) \equiv \partial \Pi / \partial n$. It is clear that (6) and (10) together with the quantum-like interpretation (8) formally coincide with our starting classical system as given by (1) and (2).

Now we show that a classical-like solution for the dissipative Schrödinger-like equation (3) satisfying (9) can effectively be determined in the case of a quadrupole-like potential, i.e. $U = K(s)x^2/2$, where $K(s)$ is the quadrupole strength. Indeed, in this case the (3) admits the following solution

$$\psi = \left(\frac{1}{\sqrt{2\pi\sigma^2(s)}} \right) \exp \left[-\frac{x^2}{\sigma^2(s)} + \frac{ix^2}{2\alpha(s)\rho(s)} + i\chi(s) \right] . \quad (11)$$

From (11) and (7) we obtain the following expression for the current velocity

$$P(s) = -\frac{x}{\rho(s)} . \quad (12)$$

$\sigma(s)$, $\rho(s)$, and $\chi(s)$ are real functions satisfying the following set of differential equations

$$\frac{1}{\rho} = \frac{1}{\sigma} \frac{d\sigma}{ds} , \quad (13)$$

$$\frac{d\chi}{ds} = -\frac{\alpha(s)}{4\sigma^2(s)} , \quad (14)$$

$$\frac{d^2\sigma}{ds^2} + K(s)\sigma - \frac{1}{\alpha} \frac{d\alpha}{ds} \frac{d\sigma}{ds} - \frac{\alpha^2}{4\sigma^2} = 0 . \quad (15)$$

Up to this point the function $\alpha(s)$ is quite arbitrary in a purely quantum-like context. However, we point out that, by substituting (11) into (9) through (4),(7) and (8), the previous equations (12)-(15) are exactly obtained, provided that the following condition for $\alpha(s)$ is satisfied:

$$\eta(s) = \frac{\sigma}{\alpha} \frac{d\alpha}{ds} \frac{d\sigma}{ds} + \frac{\alpha^2}{4\sigma^2} . \quad (16)$$

This condition clearly shows that $\alpha(s)$ is essentially determined by the temperature $T(s)$ of the fluid through $\eta(s)$.

On the other hand, within the quantum-like framework, the r.m.s of the momentum distribution σ_P is defined as:

$$\sigma_P(s) = \alpha \left[\int_{-\infty}^{+\infty} \left| \frac{\partial\psi(x,s)}{\partial x} \right|^2 dx \right]^{1/2} = \left[\left(\frac{d\sigma}{ds} \right)^2 + \frac{\alpha^2}{4\sigma^2} \right]^{1/2} . \quad (17)$$

Consequently, in agreement with the physical meaning of the TWM description, we assume that

$$\eta(s) = \sigma_P^2(s) . \quad (18)$$

Furthermore, in the classical-like interpretation, $\sigma_P(s)$ is r.m.s. of a Maxwellian-like (Gaussian) distribution in the momentum space, and, consequently, it is proportional to the temperature of the system (see Eq.n (10)). By using (16) and (17) into (18) we obtain the following condition

$$\frac{1}{\alpha} \frac{d\alpha}{ds} = \frac{1}{\sigma} \frac{d\sigma}{ds} . \quad (19)$$

III. CONNECTION BETWEEN α AND THE BEAM EMITTANCE ε

In the classical framework, it is well known that the beam emittance ε can be obtained by the relation [2]:

$$\varepsilon^2 = \langle x^2 \rangle \langle p^2 \rangle - \langle xp \rangle^2 \quad , \quad (20)$$

where $\langle x^2 \rangle = \sigma^2$, $\langle p^2 \rangle = \sigma_P^2$, and $\langle xp \rangle^2 = \sigma^2(d\sigma/ds)^2$; the average operators are taken with respect to the classical phase-space Gaussian distribution whose configuration projection is $|\psi|^2$. Taking into account the above relations, the (20) can be written as

$$\sigma_P^2 = \left(\frac{d\sigma}{ds} \right)^2 + \frac{\varepsilon^2}{4\sigma^2} \quad . \quad (21)$$

Consequently, by comparing (21) and (17) we obtain the following equality:

$$\varepsilon(s) = \alpha(s) \quad , \quad (22)$$

and the envelope equation (15) becomes:

$$\frac{d^2\sigma}{ds^2} + K(s)\sigma - \left(\frac{1}{\varepsilon} \frac{d\varepsilon}{ds} \right) \frac{d\sigma}{ds} - \frac{\varepsilon^2}{4\sigma^2} \quad (23)$$

IV. CONCLUSION

We have proven that a dissipative classical fluid, moving in a quadrupole-like focusing device, can be fully described in terms of a Schrödinger-like equation for harmonic oscillator where the Planck's constant is replaced by the time-varying beam emittance. This result justifies the main assumption of Ref. [3] where the longitudinal dynamics of an electron bunch in a storage ring in the presence of radiation damping and quantum excitation has been described by Eq.s (3) and (22).

Remarkably, note that, in absence of dissipation ($\varepsilon = const$), all the results of Ref. [4], concerning with coherent states of charged-particle beams, are fully recovered by the present fluid treatment. In a forthcoming paper, we investigate the existence of coherent states within the above treatment by taking into account the dissipations.

Finally, we point out that the fluid treatment presented in this paper can be also applied to the e.m. traps [5] with the inclusion of the dissipation.

REFERENCES

1. R. Fedele and G. Miele, *Nuovo Cimento D* **13**, 1527 (1991).
2. J. Lawson *The physics of charged particle beams* (Clarendon Press, Oxford, 1988).
3. R. Fedele, G. Miele and L. Palumbo, *Phys. Lett. A* **194**, 113 (1994).
4. S. De Nicola, R. Fedele, V.I. Man'ko, and G. Miele, *Physica. Scripta* **52**, 191 (1995).
5. R. Fedele, G. Gorini, G. Torelli, and D. Zanello, *Quantum-like Description of Charged-Particle Traps*, these proceedings.

ON A MEASURE OF QUANTUM DECOHERENCE

V. V. Dodonov, S. S. Mizrahi and A. L. de Souza Silva

Depto. de Física, Univ. Federal de São Carlos, 13565-905 São Carlos, SP, Brasil

Abstract

We introduce a decoherence parameter which is proportional to the ‘linear entropy’ at the initial stage of the quantum relaxation process, but goes to 1 for the thermodynamical equilibrium states of any quantum system with an equidistant spectrum, for any temperature $T > 0$. We consider the time evolution of the new parameter in the process of thermal relaxation of the harmonic oscillator, for various initial states: Fock’s, coherent, squeezed, ‘cat’.

Recently, a significant interest to the decoherence processes in quantum mechanics is observed, in particular, due to the problem of stability of quantum superpositions under the influence of an environment. Frequently, a quantitative measure of decoherence is put in a one-to-one correspondence with a degree of ‘purity’ of the quantum state, expressed in terms of the ‘canonical entropy’ $S = -\text{Tr}(\hat{\rho} \ln \hat{\rho})$ or the ‘linear entropy’ $s = 1 - \text{Tr} \hat{\rho}^2$ [1-3]. Although such functionals yield a good insight for high-temperature reservoirs, they seem to suffer from some drawbacks in the low temperature case.

Indeed, let us consider the evolution of an initial *pure* quantum state [$s(0) = S(0) = 0$] due to a weak interaction with a reservoir at low temperature. For $t > 0$, $s(t)$ and $S(t)$ assume positive values, so the initial rate of increase of $s(t)$ or $S(t)$ is often used to give a quantitative measure of the decoherence time [1-3]. However, tracing the evolution of the entropies for the long time interval, we discover that for a small enough temperature of the environment, the entropies, after reaching some maxima, finally decrease to very small values which tend to zero when $T \rightarrow 0$. A typical example is given in figure 1.

Thus one has to make a choice between two possibilities. The first one is to continue to identify the measure of quantum mixing (given by some kind of entropy) with the measure of decoherence. However, in such a case one should accept a strange result that the degree of decoherence of the final *equilibrium* state is almost the same (close to zero) as it was initially, despite that the thermal states are usually believed to be the most ‘decoherent’ ones, in which no quantum interference effects can be observed. Another possibility is to try to find a more adequate definition of the decoherence parameter, which would practically coincide with, say, $s(t)$ for high temperature reservoirs, but will not return to the initial zero value in the low temperature case. Our aim is to show that such a better definition really exists (at least in the special case of systems with equidistant spectra, like a harmonic oscillator). Moreover, it provides a deeper understanding of the final stage of the decoherence process, which appears more diverse and interesting than it was thought before.

The origin of the troubles at low temperatures is connected with the double nature of the ground state, described by the density operator $\hat{\rho}_0 \equiv |0\rangle\langle 0|$. On one hand, this state

is *pure*, with $\text{Tr}\hat{\rho}_0^2 = 1$. On the other hand, it is the limit of the *equilibrium states*, which are conceived to be completely decoherent. It seems reasonable to exclude the state $\hat{\rho}_0$ in some way. Our idea is to take as a basis a simple expression for the linear entropy, but to divide it by a time-dependent factor which would ensure a nonzero limit at $t \rightarrow \infty$. This goal can be achieved, for instance, if one chooses the normalizing factor in the form of the Hilbert-Schmidt distance between the states $\hat{\rho}(t)$ and $\hat{\rho}_0$. Then the measure of decoherence could be written as $\tilde{\mathcal{D}} = (1 - \text{Tr}\hat{\rho}^2) / \sqrt{(\hat{\rho} - \hat{\rho}_0)^2} = (1 - \mu) / (1 + \mu - 2p_0)^{1/2}$, where $\mu \equiv \text{Tr}\hat{\rho}^2$ is the ‘purity’ of the quantum state, and $p_0 \equiv \text{Tr}(\hat{\rho}\hat{\rho}_0) = \langle 0|\hat{\rho}|0\rangle$ is the occupation probability of the ground state. In the low temperature case $T \rightarrow 0$, the equilibrium statistical operator is close to $p_0|0\rangle\langle 0| + p_1|1\rangle\langle 1|$ (where $|1\rangle$ is the first excited state), while the contribution of other states can be neglected (we consider the systems with discrete energy spectra). Then $p_0 + p_1 = 1$ (up to higher order terms), $\mu = p_0^2 + p_1^2$, and $1 + \mu - 2p_0 = 2p_1^2$. As $T \rightarrow 0$, $p_1 \ll 1$, so $1 - \mu \approx 2p_1$. As a result, as $T \rightarrow 0$, the parameter $\tilde{\mathcal{D}}$ tends to the finite value $\sqrt{2}$, which has the same order of magnitude as the equilibrium value in the high temperature case.

Moreover, for the systems with equidistant spectra we can make the equilibrium value of the decoherence measure to be equal to 1, independently of the temperature, introducing an extra normalizing factor and defining the ‘measure of decoherence’ as

$$\mathcal{D} = \frac{1 - \mu}{((1 + \mu - p_f)(1 + \mu - p_0))^{1/2}} \quad (1)$$

where p_f is the occupation probability of the level with the maximal energy. For such systems the equilibrium occupation probabilities read $p_n = \xi^n(1 - \xi) / (1 - \xi^M)$, $n = 0, 1, \dots, M - 1$ (where M is the total number of levels, and $\xi < 1$ is some factor which depends on the temperature). Then $\mu_{eq} = (1 - \xi)(1 + \xi^M) / [(1 + \xi)(1 - \xi^M)]$, $p_0^{(eq)} = (1 - \xi) / (1 - \xi^M)$, $p_f^{(eq)} = \xi^{M-1}(1 - \xi) / (1 - \xi^M)$, so that $\mathcal{D}_{eq} \equiv 1$ for any value $0 < \xi < 1$.

To study a time dependence of the decoherence measure (1) we consider the relaxation of the harmonic oscillator ($M = \infty$, therefore $p_f = 0$ for all states with finite energy) described in the framework of the standard master equation (we assume $\hbar \equiv 1$)

$$d\hat{\rho}/dt = -i[\hat{a}^\dagger\hat{a}, \hat{\rho}] + \gamma(1 + \nu)(2\hat{a}\hat{\rho}\hat{a}^\dagger - \hat{a}^\dagger\hat{a}\hat{\rho} - \hat{\rho}\hat{a}^\dagger\hat{a}) + \gamma\nu(2\hat{a}^\dagger\hat{\rho}\hat{a} - \hat{a}\hat{a}^\dagger\hat{\rho} - \hat{\rho}\hat{a}\hat{a}^\dagger), \quad (2)$$

where \hat{a} and \hat{a}^\dagger are the usual bosonic annihilation and creation operators, ν is the mean photon number of the reservoir, and $\gamma > 0$ is the damping coefficient. Omitting the details of calculations we bring the formulae for $\mu(t)$ and $p_0(t)$ for some interesting quantum states.

For the initial M -photon Fock state $|M\rangle$ we have

$$p_0(t) = \frac{[u(t)(1 + \nu)]^M}{[1 + \nu u(t)]^{M+1}}, \quad \mu(t) = \frac{|1 - 2u(1 + \nu)|^M}{(1 + 2u\nu)^{M+1}} P_M \left(\frac{(1 - u)^2 + u^2(1 + 2\nu)^2}{(1 + 2u\nu)|1 - 2u(1 + \nu)|} \right),$$

where $P_n(x)$ is the Legendre polynomial, and $u(t) \equiv 1 - e^{-2\gamma t}$. The plots of the linear entropy and the decoherence parameter for different initial Fock states are given in figure 1.

For the initial pure *squeezed* state, defined as an eigenstate of the canonically transformed operator $\hat{b} = \cosh \rho \hat{a} + \sinh \rho \hat{a}^\dagger$ with a complex eigenvalue $\alpha \equiv |\alpha| \exp(i\phi)$ and a real ‘squeezing parameter’ ρ (called sometimes as the ‘two-photon state’ [4]) we obtain

$$\mu = \left[(1 + 2u\nu)^2 + 4u(1 - u)(1 + 2\nu) \sinh^2 \rho \right]^{-1/2}, \quad p_0 = A^{-1/2} \exp(-B/A),$$

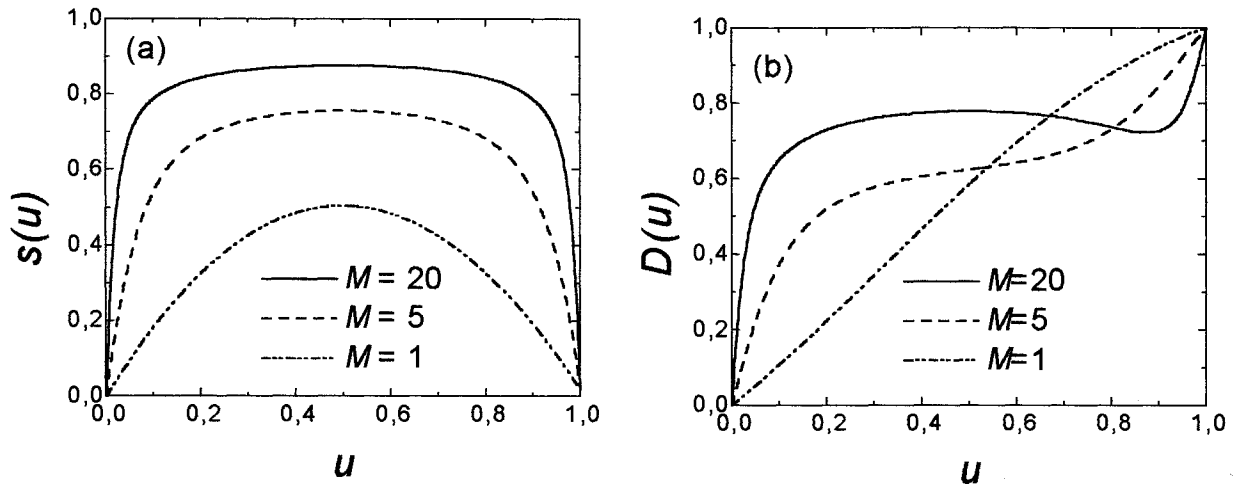


Figure 1: The ‘linear entropy’ (a) $s \equiv 1 - \text{Tr}\hat{\rho}^2$ and the decoherence parameter (b) \mathcal{D} versus the ‘compact time’ $u \equiv 1 - e^{-2\gamma t}$ for $\nu = 0.01$ and different initial Fock states $M = 1, 5, 20$.

$$A = (1 + u\nu)^2 + (1 - u)(1 + u + 2u\nu) \sinh^2 \rho,$$

$$B = |\alpha|^2(1 - u) \{1 + u\nu + (1 + u + 2u\nu) \sinh \rho [\sinh \rho - \cosh \rho \cos(2\phi)]\}.$$

As the last example we consider the family of the initial ‘Schrödinger cat’ states [5,6]

$$|\alpha; \varphi\rangle = \mathcal{N}(|\alpha|, \varphi) (|\alpha\rangle + e^{i\varphi} |-\alpha\rangle), \quad \mathcal{N}(|\alpha|, \varphi) = \left(2 \left[1 + \cos \varphi \exp(-2|\alpha|^2)\right]\right)^{-1/2}.$$

The special cases of this family are even ($\varphi = 0$) and odd ($\varphi = \pi$) coherent states [7], and the Yurke-Stoler states ($\varphi = \pi/2$) [8]. The functions $p_0(u)$ and $\mu(u)$ read

$$p_0 = \frac{2\mathcal{N}^2(\alpha, \varphi)}{1 + u\nu} \exp\left[-\frac{\alpha^2(1-u)}{1+u\nu}\right] \left\{1 + \cos \varphi \exp\left[-\frac{2\alpha^2 u(1+\nu)}{1+u\nu}\right]\right\},$$

$$\mu = \frac{2\mathcal{N}^2(\alpha, \varphi)}{1 + 2u\nu} \left[1 + \cos \varphi e^{-2\alpha^2} (4 + e^{-2\alpha^2}) + \exp\left[-\frac{4\alpha^2(1-u)}{1+2u\nu}\right] + \exp\left[-\frac{4\alpha^2 u(1+2\nu)}{1+2u\nu}\right]\right].$$

Figure 2 demonstrates the dependence $\mathcal{D}(u)$ for the squeezed states and for the even coherent states with different values of $|\alpha|$. If $\alpha^2(1-u) \gg 1$ and $\alpha^2 u \gg 1$, we observe ‘plateaus’, whose widths practically do not depend on α (and u), although they depend on the parameter ρ (but not ϕ) in the case of squeezed states. However, for the ‘cat’ states we have (for $\nu \ll 1$) a *universal* (independent on φ, α, u) ‘plateau’ $\mathcal{D}(u) \approx \frac{1}{3}$.

We see that the decoherence process consists of three distinct stages for highly excited initial states. The first stage is rather short, its characteristic time is determined completely by the initial *energy of quantum fluctuations*, $t_1 \sim (\gamma\mathcal{E})^{-1}$. However, the decoherence parameter does not assume its equilibrium (unit) value at the end of this stage, but it stays approximately constant for a rather long period of time. And only after some ‘ultimate time’ $t_2 \gg t_1$ the coherence is completely destroyed. This time can be evaluated as $t_2 \approx (2\gamma)^{-1} \ln(E/\nu^\beta)$, where E is, approximately, the *total* initial energy, ν is the mean number of thermal photons,

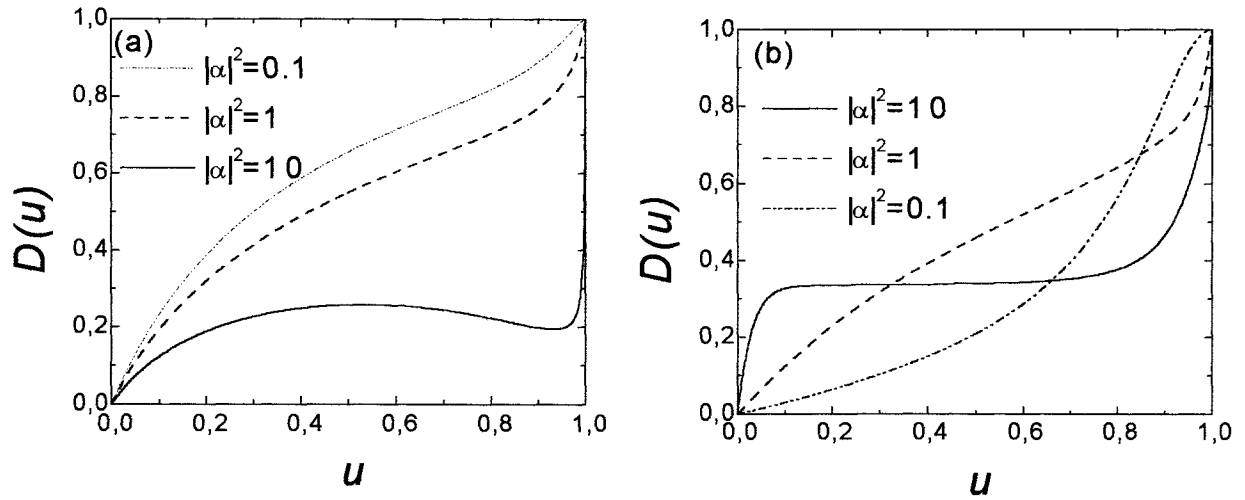


Figure 2: The decoherence parameter $D(u)$ for (a) the squeezed states with $\rho = 1$ and $\phi = 0$ at $\nu = 0.1$, (b) the even coherent states at $\nu = 0.01$; for $|\alpha|^2 = 0.1, 1, 10$.

and β is a positive constant which depends on the type of the initial state. In particular, $\beta = 2$ for the coherent states, $\beta = 1$ for the ‘cat’ and vacuum squeezed states, and $\beta = 1/2$ for the initial Fock states. The value of the ‘ultimate time’ t_2 enables ordering different families of quantum states with respect to their robustness against the decoherence (while the ‘primary time’ t_1 is the same for all states with equal values of the energy of quantum fluctuations). The coherent states are the most robust ones, then follow squeezed and ‘cat’ states, whereas the Fock states, being ‘the most unclassical states’, lose their coherence much faster than all the others (at low temperatures).

We may conclude that the new measure of decoherence permits a sound analysis for the ‘standard’ thermal relaxation of a quantum harmonic oscillator. Moreover, it sheds new light on the details of the decoherence process and shows that this process has three distinct stages for highly excited initial pure states. In particular, we see that at low temperatures the ‘ultimate decoherence time’ may be essentially greater than the relaxation time.

Acknowledgements. VVD thanks the Brazilian agency FAPESP for the travel grant 1999/1098-5. SSM thanks CNPq (Brasil) for partial financial support. ALS thanks CAPES (Brasil) for support.

References

1. P.C. Lichtner and J.J. Griffin, PRL **37**, 1521 (1976).
2. W.H. Zurek, S. Habib and J.P. Paz, PRL **70**, 1187 (1993).
3. J.I. Kim, M.C. Nemes, A.F.R. de Toledo Piza and H.E. Borges, PRL **77**, 207 (1996).
4. H.P. Yuen PRA **13**, 2226 (1976).
5. V. Bužek, A. Vidiella-Barranco and P.L. Knight, PRA **45**, 6570 (1992).
6. C. Brif, Ann. Phys. (NY) **251**, 180 (1996).
7. V.V. Dodonov, I.A. Malkin and V.I. Man’ko, Physica **72**, 597 (1974).
8. B. Yurke and D. Stoler, PRL **57**, 13 (1986).

Langevin Approach to Excess Quantum Noise

S. M. Dutra, K. Joosten, G. Nienhuis, N. J. van Druten, A. M. van der Lee, M. P. van Exter, and J. P. Woerdman
Huygens Laboratory, University of Leiden, P. O. Box 9504, 2300 RA Leiden, The Netherlands

Abstract

To meet recent experimental advances, we develop a quantum theory of excess noise where the dynamics of the gain medium is completely described for the first time. We apply it to the recently discovered colouring of excess noise and to lasers with relaxation oscillations.

Excess quantum noise is an intriguing effect that has been demonstrated recently in several types of lasers [1]. In 1989, Siegman proposed a semiclassical theory that derives excess noise as a universal consequence of mode nonorthogonality [2]. This theory was developed for class A lasers, where the atomic variables relax much faster than the field, within the linear isotropic gain approximation [2]. However, the presence of relaxation oscillations in the lasers (HeXe and $\text{Nd}^{3+}:\text{YVO}_4$) where excess noise was observed so far [1] shows that none of them are strictly class A. Moreover, although Siegman's theory derives excess noise as white noise, it was recently found to be coloured [3]. Here, we present a fully quantum theory that incorporates the dynamics of the gain medium to meet these new experimental challenges.

We adopt a microscopic model consisting of a system of homogeneously broadened two-level atoms embedded in a dielectric host and interacting with the quantized electromagnetic field in a cavity. The atoms are also coupled to reservoirs yielding the decay rates γ_{\parallel} for the inversion and γ_{\perp} for the polarization together with their associated noise fluctuations. Equivalent c-number Langevin equations are obtained from the Heisenberg-Langevin equations by choosing the normal ordering and neglecting thermal noise in the field as in Ref. [4]. This procedure retains quantum correlations but only up to second moments of the dynamical variables [4]. Our c-number Langevin equations describe excess quantum noise in any laser where the inversion can be assumed not to depend on position. When both the inversion and the polarization can be adiabatically eliminated, our theory reduces to Siegman's theory [2]. If only the polarization can be adiabatically eliminated, we obtain rate equations for a class B laser.

It has been discovered recently that the dynamical evolution of the noise-driven nonlasing modes also plays a role in the generation of excess noise. The signature of this dynamical contribution is the colouring of excess noise recently demonstrated in an experiment [3]. Reducing our c-number Langevin equations to a Lamb third-order equation for the electric field, and taking into account the nonlasing modes, we can calculate analytically the non-Lorentzian spectrum due to the colouring of excess noise. In the figure, we plot this spectrum for the case where all but one of the nonlasing modes have a loss rate much larger than

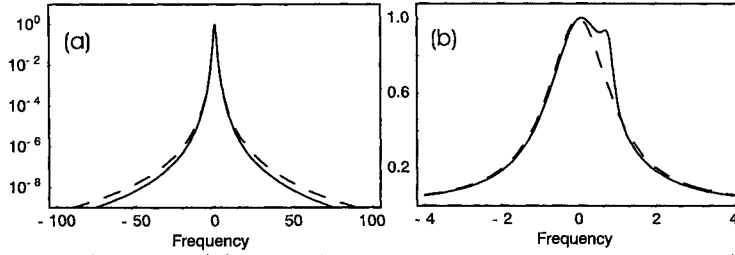


FIG. 1. In (a), we plot the dimensionless spectrum (full line) in a log scale for $\gamma_{nL} = 10$ and $\Delta_{nL} = 1$. In (b), in a linear scale for $\gamma_{nL} = 0.2$ and $\Delta_{nL} = 0.8$. Where Δ_{nL} is the detuning between the lasing and the nonlasing modes. All rates and frequencies are in units of D_{LL}/r^2 . The dotted line corresponds to the ordinary Lorentzian spectrum that one finds in the absence of coloring.

the ordinary K -enhanced laser linewidth, so that only one nonlasing mode contributes to the lineshape. In Fig. (a), the net loss rate, γ_{nL} of the nonlasing mode has been chosen as ten times the ordinary K -enhanced laser linewidth D_{LL}/r^2 . Then deviations from the normal Lorentzian spectrum only start appearing as one moves towards the wings of the spectrum [Fig. (a) is in logarithmic scale] in agreement with the time-domain argument [3]: large frequencies mean small times before the fluctuations in the nonlasing mode become completely damped. One way to bring these deviations closer to the central part of the spectrum is to increase the cavity lifetime of the nonlasing mode. In fact, as we can see from Fig. (b) where we have decreased γ_{nL} by a factor of 50, deviations from the Lorentzian shape become visible even in a normal linear scale in the central part of the spectrum.

REFERENCES

- [1] Y.-J. Cheng, G. Fanning, and A. E. Siegman, *Phys. Rev. Lett.* **77**, 627 (1996); M. A. van Eijkelenborg, A. M. Lindberg, M. S. Thijssen, and J. P. Woerdman, *Phys. Rev. Lett.* **77**, 4314 (1996); O. Emile, M. Brunel, A. Le Floch, and F. Bretenaker, *Europhys. Lett.* **43**, 153 (1998).
- [2] A. E. Siegman, *Phys. Rev. A* **39**, 1264 (1989).
- [3] A. M. van der Lee, M. P. van Exter, A. L. Mieremet, N. J. van Druten, and J. P. Woerdman, *Phys. Rev. Lett.* **81**, 5121 (1998).
- [4] C. Benkert, M. O. Scully, J. Bergou, L. Davidovich, M. Hillery, and M. Orszag, *Phys. Rev. A* **41**, 2756 (1990); M. I. Kolobov, L. Davidovich, E. Giacobino, and C. Fabre, *Phys. Rev. A* **47**, 1431 (1993).

Decoherence Matrices

D. Han, Y. S. Kim, and Marylin E. Noz

*National Aeronautics and Space Administration, Goddard Space Flight Center,
Code 935, Greenbelt, Maryland 20771, Department of Physics, University of Maryland,
College Park, Maryland 20742, and Department of Radiology, New York University,
New York, New York 10016, respectively.*

Abstract

It is known that the Lorentz group is the natural language for a given two-beam system if there are no decoherence effects. This aspect of the two-beam system formulated in terms of the six-parameter representations of the Lorentz group. It is shown that these transformations do not alter the degree of coherence. Thus, the decoherence matrices do not come from the Lorentz group. It is shown therefore that a larger group is needed to accommodate the decoherence effects in the two-beam system. This larger group is isomorphic to $O(3,3)$ or the Lorentz group with three space and three time dimensions.

In our earlier papers [1–5], we have formulated polarization optics in terms of the two-by-two and four-by-four representations of the six-parameter Lorentz group [6,7]. It was shown in our recent paper that this formalism is directly applicable to two-beam interferometers [4,8]. It was shown there that the two-component Jones vector is like the $SL(2, c)$ spinor while the Stokes parameters constitute a four-component Minkowskian four-vector. The two-by-two and four-by-four transformation matrices are formulated from the physical processes of rotations, beam mixtures, phase shifts, and attenuations.

It was noted further that the two-by-two coherency matrix serves also as the density matrix for this two-beam system [9,10]. Let us start with the Jones spinor of the form

$$\Psi = \begin{pmatrix} \psi_1 \\ \psi_2 \end{pmatrix} = \begin{pmatrix} a \exp \{i(kz - \omega t)\} \\ b \exp \{i(kz - \omega t)\} \end{pmatrix}. \quad (1)$$

It was shown in our earlier publications that beam mixtures, phase shifts and attenuations are all combined into the two-by-two matrix of the form [3,4]

$$G = \begin{pmatrix} \alpha & \beta \\ \gamma & \delta \end{pmatrix}, \quad (2)$$

applicable to the column vector of Eq.(1), where all four elements are complex numbers with the condition that the determinant of the matrix be one. The group of these matrices is called $SL(2, c)$ and is locally isomorphic to the Lorentz group applicable to the four-dimensional Minkowskian space. This matrix starts with four complex or eight real parameters. However, there are only six real parameters because of the restriction that their determinants are always one. We call these matrices “unimodular” matrices.

The four-dimensional algebra for the Minkowskian parameters can also be reduced to a two-dimensional algebra. For this purpose, let us introduce the coherency matrix defined as

$$C = \begin{pmatrix} S_{11} & S_{12} \\ S_{21} & S_{22} \end{pmatrix}, \quad (3)$$

with

$$\begin{aligned} S_{11} &= \langle \psi_1^* \psi_1 \rangle, & S_{22} &= \langle \psi_2^* \psi_2 \rangle, \\ S_{12} &= \langle \psi_1^* \psi_2 \rangle, & S_{21} &= \langle \psi_2^* \psi_1 \rangle. \end{aligned} \quad (4)$$

We have shown previously [2] that the four-by-four transformation matrices applicable to the Stokes parameters are like Lorentz-transformation matrices applicable to the space-time Minkowskian vector (t, z, x, y) . The Minkowskian four-vector can be written as

$$X = \begin{pmatrix} z + t & x - iy \\ x + iy & z - t \end{pmatrix}. \quad (5)$$

Instead of writing the Lorentz transformation as a four-by-four matrix applicable to the four-component column vector whose elements are t, z, x , and y , we can write it as

$$X' = G X G^\dagger. \quad (6)$$

Thus, the C matrix is transformed as

$$C' = G C G^\dagger = \begin{pmatrix} S'_{11} & S'_{12} \\ S'_{21} & S'_{22} \end{pmatrix} = \begin{pmatrix} \alpha & \beta \\ \gamma & \delta \end{pmatrix} \begin{pmatrix} S_{11} & S_{12} \\ S_{21} & S_{22} \end{pmatrix} \begin{pmatrix} \alpha^* & \gamma^* \\ \beta^* & \delta^* \end{pmatrix}, \quad (7)$$

where C and G are the density matrix and the transformation matrix given in Eq.(3) and Eq.(2) respectively. As we noted before, the two-by-two G matrix is unimodular. This means that the determinant of the density or coherency matrix has to remain constant. This concept is quite different from the requirement that the trace of the density matrix be one.

Let us start with a pure state with the density matrix with vanishing second component:

$$\begin{pmatrix} 1 & 0 \\ 0 & 0 \end{pmatrix} \quad (8)$$

The trace of this matrix is one, but its determinant is zero. On the other hand, if the phase relation is completely random, and the first and second components have the same amplitude, the density matrix becomes

$$\begin{pmatrix} 1/2 & 0 \\ 0 & 1/2 \end{pmatrix}. \quad (9)$$

Here is the question: Is there a two-by-two matrix which will transform the pure-state density matrix of Eq.(8) into the impure-state matrix of Eq.(9)? The answer within the system of matrices of the form given in Eq.(2) is No, because the determinant of the pure-state density matrix is zero while that for the impure-state matrix is $1/4$.

This is precisely the reason why we need four-by-four transformation matrices applicable to the Stokes parameters defined as

$$S_0 = S_{11} + S_{22}, \quad S_1 = S_{11} - S_{22}, \quad S_2 = S_{12} + S_{21}, \quad S_3 = -i(S_{12} - S_{21}). \quad (10)$$

It is possible to construct four-by-four transformation matrices applicable to these four parameters. We can compute $S'_{11}, S'_{12}, S'_{21}$, and S'_{22} using Eq.(7), and tabulate them in a four-by-four matrix form [11]. Since, as given above, the Stokes parameters are linear combinations of these parameters, it is straight-forward to construct the transformation matrix applicable to the Stokes parameters [11]. It was repeatedly emphasized that resulting four-by-four matrix is like a Lorentz-transformation matrix applicable to the space-time coordinate of (t, z, x, y) , which does not change the determinant of the density matrix.

We are interested in a transformation which will change the density matrix of Eq.(8) to Eq.(9). The corresponding Stokes four-vectors are $(1, 1, 0, 0)$ and $(1, 0, 0, 0)$ up to constant factors respectively. By rotating the coordinate system around the first axis by 45° , it is possible to change the pure-state vector $(1, 1, 0, 0)$ to $(1, 0, 1/\sqrt{2}, 1/\sqrt{2})$. Is it then possible to change this vector into the impure state $(1, 0, 0, 0)$? The answer is No if we insist on Lorentz transformations.

Indeed, we are interested in the mechanism where the off-diagonal elements S_{12} and S_{21} become smaller due to time average or phase-randomizing process [12]. If this happens, we can apply to the Stokes four-vector the following decoherence matrix.

$$\begin{pmatrix} 1 & 0 & 0 & 0 \\ 0 & 1 & 0 & 0 \\ 0 & 0 & e^{-2\lambda} & 0 \\ 0 & 0 & 0 & e^{-2\lambda} \end{pmatrix} = e^{-\lambda} \begin{pmatrix} e^\lambda & 0 & 0 & 0 \\ 0 & e^\lambda & 0 & 0 \\ 0 & 0 & e^{-\lambda} & 0 \\ 0 & 0 & 0 & e^{-\lambda} \end{pmatrix}, \quad (11)$$

where $e^{-\lambda}$ is the overall decoherence factor. For convenience, let us call the four-by-four matrix of the right-hand side the decoherence matrix. This matrix appears to have enough symmetry to fit into the Lorentz group. However, it does not.

If we combine this decoherence matrix with the Lorentz group, the result will be a fifteen-parameter group of four-by-four matrices isomorphic to $O(3,3)$ which is beyond the scope of the present paper [13]. The two-by-two matrix cannot accommodate more than eight real parameters, while the four-by-four matrix can be decomposed into sixteen independent elements. This is how the symmetry group is enlarged, and the Stokes parameters play a much wider role than the Jones vector.

This paper creates a number of new problems. The first problem could be whether the formalism can be extended to three-beam or four-beam systems. This will require mathematics more powerful than the Lorentz group [14]. Another problem could be to examine how the beam dynamics can be formulated in an-isotropic media. This is also a challenging problem in group theory and optics [15].

The word ‘‘decoherence’’ is relatively new in physics. We need a clear understanding of the subject with the most precise mathematical device available to us.

REFERENCES

- [1] D. Han, Y. S. Kim, and M. E. Noz, *J. Opt. Soc. Am. A* **14**, 2290 (1997).
- [2] D. Han, Y. S. Kim, and M. E. Noz, *Phys. Rev. E* **56**, 6065 (1997);
- [3] D. Han, Y. S. Kim, and M. E. Noz, *Phys. Rev. E* **60**, 1036 (1999).
- [4] D. Han, Y. S. Kim, and M. E. Noz, *Phys. Rev. E* (to be published)
- [5] For earlier books and papers on polarization, see W. A. Shurcliff, *Polarized Light* (Harvard Univ. Press, Cambridge, MA, 1962); R. Barakat, *J. Opt. Soc. Am.* **53**(3) 317 (1963); E. Hecht, *Am. J. Phys.* **38**, 1156 (1970). C. S. Brown and A. E. Bak, *Opt. Engineering* **34**, 1625 (1995); J. J. Monzon and L. L. Sánchez-Soto, *Phys. Lett. A* **262** 18 (1999).
- [6] E. Wigner, *Ann. Math.* **40**, 149 (1939).
- [7] Y. S. Kim and M. E. Noz, *Theory and Applications of the Poincaré Group* (Reidel, Dordrecht, 1986); Y. S. Kim and M. E. Noz, *Phase Space Picture of Quantum Mechanics* (World Scientific, Singapore, 1991).
- [8] For earlier papers on applications of $SU(2)$ and $Sp(2)$ symmetries to interferometers, see B. Yurke, S. McCall, and J. R. Klauder, *Phys. Rev. A* **33**, 4033 (1986); R. A. Campos, B. E. A. Saleh, and M. C. Teich, *Phys. Rev. A*, **40**, 1371 (1989); A. Luis and L. L. Sánchez-Soto, *Quantum Semiclass. Opt.* **7**, 153 (1995).
- [9] M. Born and E. Wolf, *Principles of Optics, 6th Ed.* (Pergamon, Oxford, 1980). The first edition of this book was published in 1959.
- [10] R. P. Feynman, *Statistical Mechanics* (Benjamin/Cummings, Reading, MA, 1972); D. Han, Y. S. Kim, and M. E. Noz, *Am. J. Phys.* **67**, 61 (1999).
- [11] From Eq.(7), we can compute

$$\begin{pmatrix} S'_{11} \\ S'_{22} \\ S'_{12} \\ S'_{21} \end{pmatrix} = \begin{pmatrix} \alpha^* \alpha & \beta^* \beta & \alpha^* \beta & \beta^* \alpha \\ \gamma^* \gamma & \delta^* \delta & \gamma^* \delta & \delta^* \gamma \\ \gamma^* \alpha & \delta^* \beta & \gamma^* \beta & \delta^* \alpha \\ \alpha^* \gamma & \beta^* \delta & \alpha^* \delta & \beta^* \gamma \end{pmatrix} \begin{pmatrix} S_{11} \\ S_{22} \\ S_{12} \\ S_{21} \end{pmatrix}. \quad (12)$$

This leads to the four-by-four matrix applicable to the four Stokes parameters:

$$\begin{pmatrix} (a+b+c+d)/2 & (a-b+c-d)/2 & Re(\alpha^* \beta + \gamma^* \delta) & -Im(\alpha^* \beta + \gamma^* \delta) \\ (a+b-c-d)/2 & (a-b-c+d)/2 & Re(\alpha^* \beta - \gamma^* \delta) & -Im(\alpha^* \beta - \gamma^* \delta) \\ Re(\alpha^* \gamma + \beta^* \delta) & Re(\alpha^* \gamma - \beta^* \delta) & Re(\alpha^* \delta + \beta^* \gamma) & -Im(\alpha^* \delta - \beta^* \gamma) \\ Im(\alpha^* \gamma + \beta^* \delta) & Im(\alpha^* \gamma - \beta^* \delta) & Im(\alpha^* \delta + \beta^* \gamma) & Re(\alpha^* \delta - \beta^* \gamma) \end{pmatrix}, \quad (13)$$

with

$$a = |\alpha|^2, \quad b = |\beta|^2, \quad c = |\gamma|^2, \quad d = |\delta|^2. \quad (14)$$

- [12] D. F. McAlister and M. G. Raymer, *Phys. Rev. A* **55**, R1609 (1997).
- [13] D. Han, Y. S. Kim, and M. E. Noz, *J. Math. Phys.* **36**, 3940 (1995).
- [14] D. J. Rowe, B. C. Sanders, and H. de Guise, *J. Math. Phys.* **40**, 3604 (1999).
- [15] R. M. A. Azzam and N. M. Bashara, *Ellipsometry and Polarized Light* (North-Holland, Amsterdam, 1977).

Classical communication and entangled uses of a depolarising channel

G.Massimo Palma

*Dipartimento di Scienze Fisiche ed Astronomiche and INFN-Unità di Palermo,
Via Archirafi 36, I-90123 Palermo, Italy*

Dagmar Bruß,

*Institut für Theoretische Physik, Universität Hannover,
Appelstr. 2, D-30167 Hannover, Germany*

Lara Faoro

Dipartimento di Fisica, Politecnico di Torino, Via Duca degli Abruzzi 24, I-10129 Torino, Italy

Chiara Macchiavello

Dipartimento di Fisica "A.Volta" and INFN-Unità di Pavia, Via Bassi 6, I-27100 Pavia, Italy

Abstract

Quantum Channels are endowed with features which are completely absent in a classical scenario, like the possibility to use entangled transmissions. Having in mind to explore the benefits of the use of entanglement in encoding classical information we analyse the depolarising channel. We will show analytically for the first time that in this case the complete isotropy of the action of the channel prevents the users from gaining by entangling consecutive uses of the channel.

The possibility to use quantum states of a physical carrier to encode bits opens new perspectives in the field of transmission of information. This is true not only in circumstances in which one is concerned with the transmission of *quantum* information, as in the case of quantum teleportation or of quantum cloning, which will be discussed in other proceedings of this conference, but also when the interest is in the efficient transmission of *classical* information. It is on this setting that we will concentrate our attention in this communication [1].

In our scenario the sender uses quantum states of a channel - non necessarily orthogonal - to encode its bits and sends these states to the receiver who will decode the message using the most general form of quantum measurement. During the transmission the channel is exposed to the action of the environment which will in general spoil the unitarity of the

time evolution of the signal states. In the following we will assume that the channel is memoryless, i.e. that the noise affects each use of the channel separately.

If the channel were classical the best the sender could do to achieve reliable transmission is to send its information via block coding of consecutive independent uses of the channel. In the quantum case however it is possible to entangle multiple uses of the channel. For this more general strategy it has been shown that the amount of reliable information which can be transmitted per use of the channel is given by [2,3]

$$C_n = \frac{1}{n} \sup_{\mathcal{E}} I_n(\mathcal{E}) \quad (1)$$

where $\mathcal{E} = \{p_i, \pi_i\}$ with $p_i \geq 0, \sum p_i = 1$ is the input ensemble of states π_i of n - generally entangled - signal qubits, $I_n(\mathcal{E}) = S(\rho) - \sum_i p_i S(\rho_i)$ is the mutual information and $S(\chi) = -\text{tr}(\chi \log \chi)$ is the von Neumann entropy (here ρ_i are the density matrices of the outputs, $\rho = \sum_i p_i \rho_i$ and logarithms are taken to base 2). The advantage of the expression (1) is that it includes an optimisation over all possible POVMs at the output, including collective ones. Therefore no explicit maximisation procedure for the decoding at the output of the channel is needed.

The interest for the possibility of using entangled states as channel input is that it cannot generally be excluded that $I_n(\mathcal{E})$ is superadditive for entangled inputs, i.e. we might have $I_{n+m} > I_n + I_m$ and therefore $C_n > C_1$.

The channel we will consider here is the depolarising channel. If a Bloch vector representation of the signal states is adopted the action of such channel can be easily described as an isotropic shrinking of the Bloch vector of each individual signal qubit by a factor η , known as shrinking factor. For the depolarising channel a lower bound on C is given by the one-shot capacity C_1 (see [2]), while upper bounds are given in [4]. In this communication we will restrict ourselves to the simplest non-trivial case, namely $n = 2$, and we will find the maximal mutual information $I_2(\mathcal{E})$. We will consider as input states the following set, with equal a priori probability [1]

$$\begin{aligned} |\pi_1\rangle &= \cos \vartheta |00\rangle + \sin \vartheta |11\rangle \\ |\pi_2\rangle &= \sin \vartheta |00\rangle - \cos \vartheta |11\rangle \\ |\pi_3\rangle &= \cos \beta |01\rangle + \sin \beta |10\rangle \\ |\pi_4\rangle &= \sin \beta |01\rangle - \cos \beta |10\rangle \end{aligned} \quad (2)$$

where angles θ, β parametrise the degree of entanglement between the two qubit states. To evaluate explicitly I_2 we have to evaluate the eigenvalues of the output density operators, and plug them into the expression for the VonNeumann entropies. This straightforward but lengthy procedure leads to the conclusion that the maximal mutual information is obtained for tensor product signal states ($\theta = \beta = 0$) with the following expression

$$I_2^{max} = (1 + \eta) \log(1 + \eta) + (1 - \eta) \log(1 - \eta) . \quad (3)$$

which is twice I_1 . We have shown in [1] that our choice signal states does not lack of generality. In particular we have shown that no larger I_2 can be achieved with a larger number of signal states or with non orthogonal ones.

Direct inspection of (3) confirms what we have anticipated: the isotropy of the noise of the depolarising channel prevents the users from gaining by encoding information in entangled double uses of the channel. To evaluate the capacity C it would be necessary to evaluate the general expression for C_n for n possibly entangled signal states. This remains still an open problem.

REFERENCES

- [1] D.Bruß,L.Faoro,C.Macchiavello and G.M.Palma, *J.Mod.Opt.* Special issue on *Quantum Information*, in press, also quant-ph/9903033
- [2] B. Schumacher and M.D. Westmoreland, *Phys. Rev. A* **56**, 131 (1997).
- [3] A.S. Holevo, IEEE Trans. Inf. Theory (preprint quant-ph/9611023).
- [4] C.H. Bennett, D.P. DiVincenzo and J. Smolin, *Phys. Rev. Lett.* **78**, 3217 (1997); C.H. Bennett *et al.*, quant-ph/9904023.
- [5] For a recent review see M.B. Plenio and V. Vedral, *Contemp. Phys.* **39**, 431 (1998).
- [6] A. Peres, *Quantum Theory: Concepts and Methods* (Kluwer Academic, Dordrecht, 1993).

SECOND-ORDER DISPERSION IN PULSED ENTANGLED TWO-PHOTON INTERFERENCE

Jan Peřina, Jr.*+,†
Alexander V. Sergienko†
Bahaa E. A. Saleh†
Malvin C. Teich†

+Joint Laboratory of Optics of Palacký University and Institute of Physics of Academy of Sciences of the Czech Republic, 17. listopadu 50, 772 07 Olomouc, Czech Republic

†Quantum Imaging Laboratory, Department of Electrical and Computer Engineering, Boston University, 8 Saint Mary's Street, Boston, MA 02215, USA

Abstract

Interference of entangled two-photon states generated in a short nonlinear crystal pumped by femtosecond pulses is investigated using the polarization analog of the Hong-Ou-Mandel interferometer. The effects of the pump-pulse profile (pulse duration and chirp) as well as those originating in second-order dispersion both in the nonlinear crystal and in the optical elements comprising the interferometer are described. The characteristics of the pump pulse, along with the dispersion, influence the visibility and the symmetry of the coincidence-count interference pattern. Nonlocal dispersion cancellation occurs in some cases.

I. SPONTANEOUS PARAMETRIC DOWN-CONVERSION

A great deal of attention has been recently devoted to the process of spontaneous parametric down-conversion [1] in nonlinear crystals pumped by ultrashort laser pulses. The main reason is that ultrashort pumping may provide time synchronization of several two-photon entangled states and this enables the construction of multiphoton entangled states [2] (GHZ states and their generalizations). The use of femtosecond pump pulses also led to the observation of quantum teleportation [3]. It has been shown that ultrashort pumping causes a loss of visibility of the fourth-order (coincidence-count) interference pattern at a beam splitter [4–6]. Narrowband frequency filters are then required to restore the visibility

*e-mail: perina_j@sloup.upol.cz

[2,5]. The effects of pump-pulse chirp and second-order dispersion (in both the pump and down-converted beams) on the visibility and shape of the fourth-order interference pattern produced at a beam splitter [1] have been studied in [7]. In the contribution we extend the analysis given in [7] to short nonlinear crystals of the length of hundreds μm . Spectra of the down-converted fields are broader in such crystals and thus the influence of intermodal phase changes originating in dispersion on the interference patterns is stronger.

We consider a typical coincidence-count setup, the polarization analog of the Hong-Ou-Mandel interferometer [7]. The fourth-order interference pattern in this setup is described by the normalized coincidence-count rate R_n :

$$R_n(l) = 1 - \rho(l), \quad (1)$$

where

$$\begin{aligned} \rho(l) &= \frac{1}{2R_0} \int_{-\infty}^{\infty} dt_A \int_{-\infty}^{\infty} dt_B \operatorname{Re} \left[\mathcal{A}_{12,l}(t_A, t_B) \mathcal{A}_{12,l}^*(t_B, t_A) \right], \\ R_0 &= \frac{1}{2} \int_{-\infty}^{\infty} dt_A \int_{-\infty}^{\infty} dt_B |\mathcal{A}_{12,l}(t_A, t_B)|^2. \end{aligned} \quad (2)$$

The two-photon amplitude $\mathcal{A}_{12,l}(t_A, t_B)$ describes the entangled two-photon state after it propagated through the delay line of length l (for details, see [7]); Re denotes the real part of its argument.

A Gaussian pump pulse with duration τ_D and chirp parameter a is assumed. The nonlinear crystal (delay line) is characterized by the inverse of group velocity $1/v_j$ ($1/g_j$) and the second-order dispersion coefficient D_j (d_j) for $j = p$ (pump), 1 (signal), and 2 (idler). The symbol σ_j denotes the width of the j th frequency filter.

II. SHORT-LENGTH CRYSTALS

The profile as well as the visibility of the interference pattern described by $R_n(l)$ is determined by the overlap [7] of the two-photon amplitudes $\mathcal{A}_{12,l}(t, \tau)$ and $\mathcal{A}_{12,l}(t, -\tau)$ [$t = (t_A + t_B)/2$, $\tau = t_A - t_B$] which may serve as a measure of photon distinguishability [5]. When the overlap is complete, the detected photons cannot be distinguished and the interference pattern has maximum visibility. Incomplete overlap means that the photons can be “partially” distinguished and thus the visibility is reduced.

A. Role of pump-pulse parameters

The coincidence-count rate $R_n(l)$ forms a triangular dip of width DL [1] ($D = 1/v_1 - 1/v_2$) and with 100% visibility if a cw-pump field is considered. The fourth-order interference pattern depends on the pump-pulse bandwidth $\Delta\Omega_p$ [$\Delta\Omega_p = \sqrt{2(1 + a^2)}/\tau_D$]; the larger the bandwidth $\Delta\Omega_p$, the lower the visibility V (see FIG. 1), but the width of the dip does not change [7]. The fact that the interference pattern is determined only by the pump-pulse bandwidth implies that dispersion between the pump-pulse source and the nonlinear crystal does not change the interference pattern. Frequency filters inserted into the down-converted beams lead to broader dips with higher visibilities; the narrower the spectrum of frequency filters, the wider the dip, and the higher the observed visibility.

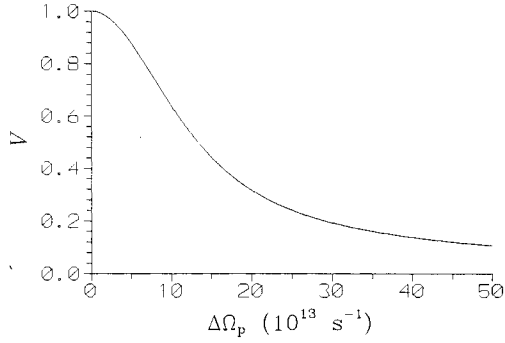


FIG. 1. Visibility V [$V = \rho/(2 - \rho)$] decreases with an increase of the pump-pulse bandwidth $\Delta\Omega_p$; $L = 100 \mu\text{m}$, $\sigma_1 = \sigma_2 = \infty \text{ nm}$, values of the other parameters are zero. In FIGS. 1—3, BBO crystal at the pump wavelength $\lambda_p = 397.5 \text{ nm}$ and down-conversion wavelengths $\lambda_1 = \lambda_2 = 2\lambda_p$ and delay line from quartz are assumed [7].

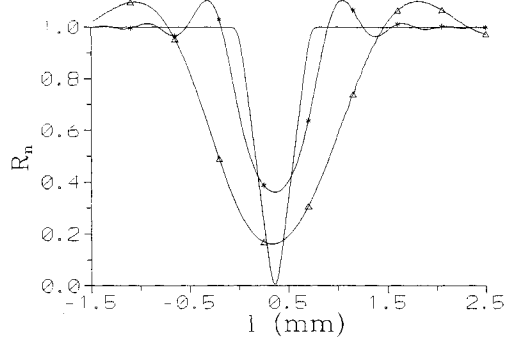


FIG. 2. Coincidence-count rate $R_n(l)$ for various values of the dispersion parameter D_1 ; $D_1 = 0 \text{ s}^2/\text{mm}$ (plain curve without symbols) $D_1 = 2 \times 10^{-26} \text{ s}^2/\text{mm}$ (*), and $D_1 = 1 \times 10^{-25} \text{ s}^2/\text{mm}$ (Δ); $\tau_D = 100 \text{ fs}$; $L = 100 \mu\text{m}$; $\sigma_1 = \sigma_2 = 500 \text{ nm}$; values of the other parameters are zero.

B. Role of second-order dispersion in the nonlinear crystal

An increase of the dispersion parameter D_p of the pump beam results in a lower visibility; the width of the dip does not change. On the other hand, dispersion in the down-converted beams leads to broader dips. They become asymmetric and oscillations occur at their borders (see FIG. 2). Frequency filters suppress asymmetry.

C. Role of second-order dispersion in optical elements comprising the interferometer

Second-order dispersion in an optical material (d_1, d_2) through which the down-converted photons propagate leads to asymmetry of the dip. The dip is particularly stretched to larger values of l as a consequence of the deformation and lengthening of the two-photon amplitude $A_{12,l}$ in a dispersive material. The higher the difference $d_1 - d_2$ of the dispersion parameters, the higher the asymmetry and the wider the dip; moreover its minimum is shifted further to smaller values of l (see FIG. 3).

Asymmetry of the dip caused by second-order dispersion in an optical material can be suppressed in two cases. In the first case, for a pump pulse of arbitrary duration, dispersion cancellation occurs when the magnitude of second-order dispersion in the path of the first photon (given by $d_1 l$) equals that of the second photon (given by $d_2 l$). When the pulse duration is sufficiently long (in the cw regime) dispersion cancellation occurs for arbitrary magnitudes of second-order dispersion present in the paths of the down-converted photons. Dispersion cancellation has its origin in the entanglement of photons.

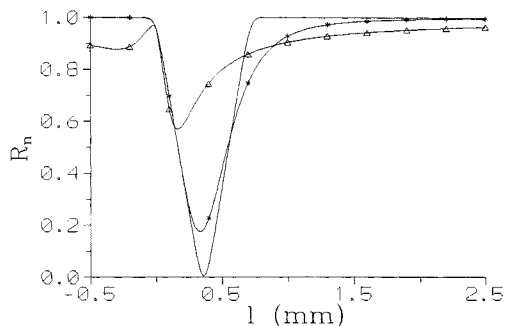


FIG. 3. Coincidence-count rate $R_n(l)$ for various values of the dispersion parameter $d = d_1 - d_2$; $d = 0 \text{ s}^2/\text{mm}$ (plain curve without symbols) $d = 1 \times 10^{-26} \text{ s}^2/\text{mm}$ (*), and $d = 5 \times 10^{-26} \text{ s}^2/\text{mm}$ (Δ); $\tau_D = 100 \text{ fs}$; $L = 100 \text{ }\mu\text{m}$; $\sigma_1 = \sigma_2 = 500 \text{ nm}$; values of the other parameters are zero.

III. CONCLUSION

The fourth-order interference pattern in the polarization analog of the Hong-Ou-Mandel interferometer is determined by the pump-pulse bandwidth; the larger the bandwidth, the lower the visibility. Dispersion between the pump-pulse source and the nonlinear crystal does not influence the interference pattern. Dispersion in the nonlinear crystal and optical elements of the interferometer leads to asymmetry of the interference dip; also oscillations may occur at its borders. These effects can be used for the measurement of dispersion parameters. Dispersion cancellation has been revealed in some cases.

ACKNOWLEDGMENTS

This work was supported by the National Science Foundation under Grant Nos. ECS-9800300 and ECS-9810355. J.P. acknowledges support from Grant No. VS96028 of the Czech Ministry of Education and Grant No. 19982003012 of the Czech Home Department.

REFERENCES

- [1] L. Mandel and E. Wolf, *Optical Coherence and Quantum Optics* (Cambridge Univ. Press, Cambridge, 1995).
- [2] A. Zeilinger, M. A. Horne, H. Weinfurter, and M. Zukowski, *Phys. Rev. Lett.* **78**, 3031 (1997).
- [3] D. Bouwmeester, J.-W. Pan, K. Mattle, M. Eibl, H. Weinfurter, and A. Zeilinger, *Nature* **390**, 575 (1997).
- [4] T. E. Keller and M. H. Rubin, *Phys. Rev. A* **56**, 1534 (1997).
- [5] G. Di Giuseppe, L. Haiberger, F. De Martini, and A. V. Sergienko, *Phys. Rev. A* **56**, R21 (1997).
- [6] W. P. Grice and I. A. Walmsley, *Phys. Rev. A* **56**, 1627 (1997).
- [7] J. Peřina, Jr., A. V. Sergienko, B. M. Jost, B. E. A. Saleh, and M. C. Teich, *Phys. Rev. A* **59**, 2359 (1999).

Quantum Decoherence in the Motion of a Trapped Ion

C. Di Fidio, S. Wallentowitz, Z. Kis, and W. Vogel

*Arbeitsgruppe Quantenoptik, Fachbereich Physik, Universität Rostock, Universitätsplatz 3,
D-18051 Rostock, Germany*

Abstract

The problem of quantum decoherence is studied in the Raman-driven quantized motion of a trapped ion. Using a stochastic wavefunctions approach it is demonstrated that rarely occurring electronic transitions, that are usually ignored, may already cause significant decoherence effects.

In the experimental generation of Schrödinger-cat superposition states of a trapped ion the desired coherent displacements have been performed by a Raman-type drive of the quantized motion of the ion¹. Generally the two lasers are chosen to be close enough to resonance in order to get a significant coupling strength, but also far enough in order to avoid excitations of the upper electronic state. If these conditions are fulfilled, the upper level of the dipole transition can be adiabatically eliminated and the lasers only affect the quantized motion associated with the electronic ground state. However, the more one wants to use this configuration on a larger time scale, the more important become the rarely occurring electronic transitions, or quantum jumps, for the dynamics of the system.

In this contribution we examine the effects of the rarely appearing electronic transitions on the motion of the ion. We intend to present a master equation that includes the effects of laser induced transitions and spontaneous emissions. In the scheme under consideration the strong dipole transition $|1\rangle \leftrightarrow |2\rangle$ (of dipole moment d) is driven by two laser fields far detuned by Δ from the electronic resonance frequency ω_{21} . The frequency difference of the laser fields, $\delta\omega$, can be adjusted to the vibrational frequency ν , so that a Raman vibrational transition is realized.

To derive the desired master equation we start from the standard master equation for the trapped two-level ion under the influence of the two laser fields,

$$\frac{\partial \hat{\rho}}{\partial t} = \frac{1}{i\hbar} [\hat{H}(t), \hat{\rho}] + \frac{\gamma}{2} \left[-\hat{A}_{22} \hat{\rho} - \hat{\rho} \hat{A}_{22} + 2 \int_{-1}^1 dq w(q) \hat{A}_{12} e^{iqk_{21}\hat{x}} \hat{\rho} e^{-iqk_{21}\hat{x}} \hat{A}_{21} \right]. \quad (1)$$

Here $\hat{\rho}(t)$ describes the vibronic quantum state, including the motion in x direction and the electronic degree of freedom. The last term in Eq. (1) describes the recoil effects of

¹C. Monroe, D.M. Meekhof, B.E. King, and D.J. Wineland, *Science* **272**, 1131 (1996).

the spontaneously emitted photons of modulo wavevector $k_{21} = \omega_{21}/c$ with radiation characteristics $w(q) = \frac{3}{8}(1+q^2)$ and dipole relaxation rate $\gamma = \omega_{21}^3 d^2 / (3\pi c^3 \epsilon_0 \hbar)$, where \hat{x} is the center-of-mass position operator of the trapped ion. The Hamiltonian $\hat{H}(t) = \hat{H}_0 + \hat{H}_L(t)$ is given by the free Hamiltonian, $\hat{H}_0 = \hbar\nu\hat{a}^\dagger\hat{a} + \hbar\omega_1\hat{A}_{11} + \hbar\omega_2\hat{A}_{22}$, and the laser interaction, $\hat{H}_L(t) = -\hat{A}_{21}d\hat{E}^{(+)}(\hat{x}, t) + \text{h.c.}$. Here \hat{a} and \hat{a}^\dagger are the annihilation and creation operators of vibrational quanta, respectively, and $\hat{A}_{ij} = |i\rangle\langle j|$ ($i, j = 1, 2$) describe electronic transitions $|j\rangle \rightarrow |i\rangle$. The electric field reads

$$\hat{E}^{(+)}(\hat{x}, t) = \mathcal{E} e^{i(k\hat{x} - \omega t)} + \mathcal{E}' e^{i(k'\hat{x} - \omega' t)}, \quad (2)$$

where \mathcal{E} , \mathcal{E}' are the electric-field amplitudes of the laser beams. Moreover, k, k' are the x -projections of the laser wavevectors and ω, ω' are the laser frequencies that obey $\delta\omega = \nu$ and $\omega \approx \omega' \approx \omega_{21} - \Delta$ ($\delta\omega = \omega - \omega'$). For the further treatment it is convenient to change to a frame rotating with the laser frequency $\omega_{21} - \Delta$ by transforming to the interaction picture with respect to $\hat{H}_0 + \hbar\Delta\hat{A}_{11}$. In this picture the master equation (1) reads

$$\frac{\partial \hat{\rho}}{\partial t} = \frac{1}{i\hbar} [\hat{H}_{\text{int}}(t), \hat{\rho}] + \frac{\gamma}{2} \left[-\hat{A}_{22} \hat{\rho} - \hat{\rho} \hat{A}_{22} + 2 \int_{-1}^1 dq w(q) \hat{A}_{12} e^{iqk_{21}\hat{x}(t)} \hat{\rho} e^{-iqk_{21}\hat{x}(t)} \hat{A}_{21} \right], \quad (3)$$

where now the operator $\hat{x}(t)$ evolves under the free time evolution governed by the free Hamiltonian \hat{H}_0 , and $\hat{H}_{\text{int}}(t)$ is given by

$$\hat{H}_{\text{int}}(t) = -\hbar\Delta\hat{A}_{11} - [\hat{A}_{21}\hat{O}(t) + \hat{A}_{12}\hat{O}^\dagger(t)]. \quad (4)$$

The operator $\hat{O}(t)$ is defined as $\hat{O}(t) = \hbar [\Omega_1 e^{ik\hat{x}(t)} + \Omega_2 e^{ik'\hat{x}(t)} e^{i\nu t}]$, with $\hbar\Omega_1 = d\mathcal{E}$ and $\hbar\Omega_2 = d\mathcal{E}'$.

In the differential equations for the electronic density matrix elements $\langle i|\hat{\rho}|j\rangle$ we insert the adiabatically solved off-diagonal elements ($\partial_t \hat{\rho}_{12} = \partial_t \hat{\rho}_{21} = 0$) into the equations for the diagonal elements. This yields the following master equation for the density operator $\hat{\rho} = \hat{A}_{11} \hat{\rho}_{11} + \hat{A}_{22} \hat{\rho}_{22}$,

$$\frac{\partial \hat{\rho}}{\partial t} = \frac{1}{i\hbar} [\hat{H}'(t) \hat{\rho} - \hat{\rho} \hat{H}'^\dagger(t)] + \int_{-1}^1 dq \hat{J}_q(t) \hat{\rho} \hat{J}_q^\dagger(t) + \hat{J}_\downarrow(t) \hat{\rho} \hat{J}_\downarrow^\dagger(t) + \hat{J}_\uparrow(t) \hat{\rho} \hat{J}_\uparrow^\dagger(t), \quad (5)$$

where the non-Hermitian Hamiltonian $\hat{H}'(t)$ reads

$$\hat{H}'(t) = \hat{A}_{22} \left[\frac{\Delta}{\Delta + i\gamma/2} \hat{H}_{\text{eff}}(t) - i\hbar \frac{\gamma}{2} \right] - \hat{A}_{11} \frac{\Delta}{\Delta - i\gamma/2} \hat{H}_{\text{eff}}(t), \quad (6)$$

with $\hat{H}_{\text{eff}}(t) = \hat{O}^\dagger(t)\hat{O}(t)/\hbar\Delta = \hat{O}(t)\hat{O}^\dagger(t)/\hbar\Delta$. The three different jump operators are defined by

$$\hat{J}_q(t) = \sqrt{\gamma w(q)} \hat{A}_{12} \exp[iqk_{21}\hat{x}(t)], \quad \hat{J}_\downarrow(t) = \sqrt{\Gamma_\downarrow} \hat{A}_{12} \hat{O}(t), \quad \hat{J}_\uparrow(t) = \sqrt{\Gamma_\uparrow} \hat{A}_{21} \hat{O}(t), \quad (7)$$

where $\Gamma_\downarrow = \Gamma_\uparrow = \gamma / \{\hbar^2 [\Delta^2 + (\gamma/2)^2]\}$. The effective Hamiltonian can be expressed in the rotating-wave approximation as²

²S. Wallentowitz and W. Vogel, Phys. Rev. A **55**, 4438 (1997); *ibid.* **58**, 679 (1998); S. Wallentowitz, W. Vogel, and P.L. Knight, *ibid.* **59**, 531 (1999).

$$\hat{H}_{\text{eff}} = \frac{1}{2} [\hbar\Omega(i\eta\hat{a}^\dagger)\hat{f}(\hat{a}^\dagger\hat{a};\eta) + \text{h.c.}] + \hbar\Delta_{AC}, \quad (8)$$

where η is the Lamb–Dicke parameter describing the localization of the ionic center-of-mass wavepacket with respect to the effective wavelength of the beat note of the lasers. The AC Stark shift is given by $\Delta_{AC} = \hbar(|\Omega_1|^2 + |\Omega_2|^2)/\Delta$, and $\Omega = 2\Omega_1\Omega_2^*/\Delta$. The operator function \hat{f} can be expressed in terms of the generalized Laguerre polynomials $L_n^{(1)}(x)$ as

$$\hat{f}(\hat{a}^\dagger\hat{a};\eta) = \sum_{n=0}^{\infty} |n\rangle\langle n| \frac{n!}{(n+1)!} L_n^{(1)}(\eta^2) e^{-\eta^2/2}. \quad (9)$$

It has been formally shown³ that the solution of the master equation (5) can be represented as a sum over all possible realizations, also called stochastic wavefunctions or quantum trajectories, of jump and no-jump evolutions. For the special choice of jump operators (7) we may decompose this solution into conditioned state vectors that evolve with the non-Hermitian Hamiltonian (6) interrupted by these jumps. From the structure it is clear that the non-unitary time evolution between two jumps takes place exclusively in the ground or excited electronic states and the electronic state is only switched by the jumps. The corresponding jumps operators are given in Eq. (7), where $\hat{J}_q(t)$, \hat{J}_\downarrow and \hat{J}_\uparrow describe spontaneous emission, induced emission and absorption, respectively.

Starting with an odd coherent state, $|\psi\rangle \propto (|\alpha\rangle - |-\alpha\rangle)$, the time evolution for the case $\gamma \neq 0$ is shown in Fig. 1 (a). It is readily seen how the initial state with strong interference fringes between the two $\pm\alpha$ peaks evolves towards a state with two incoherent peaks. The initial interferences between the peaks are gradually washed out. The effect of only a few quantum jumps ($\simeq 5$) is already quite significant. If the transitions would have been ignored (setting $\gamma=0$), strong interference fringes would remain. This can be clearly seen in Fig. 1 (b) where we show the Wigner function for a state that starts with the same initial conditions as the state in Fig. 1 (a), but in the absence of electronic transitions.

A particular property of the dynamics of the system when the quantum jumps are included is its non-symmetric character. In Fig. 1 (a) it is seen that the two wings are not symmetric. This phenomenon is in contrast to the perfectly symmetric evolution shown in Fig. 1 (b) where the quantum jumps are ignored. This can be qualitatively understood by looking at the non-Hermitian damping parts of the Hamiltonian, Eqs. (6, 8), that determine the jump probabilities. From the fact that $\langle -x|\hat{H}_{\text{eff}}| -x\rangle = -\langle x|\hat{H}_{\text{eff}}|x\rangle + 2\hbar\Delta_{AC}$, it is immediately seen that the x -representation $\hat{\Gamma}(x) = \langle x|\hat{\Gamma}|x\rangle$ of the damping operator occurring in (6), $\hat{\Gamma} = \text{Re}(i\hat{H}'/\hbar)$, is not symmetric with respect to x . The combined effects of this asymmetric damping and the action of the associated jump operators are responsible for the observed asymmetric evolution of the Wigner function.

³G.C. Hegerfeldt and T.S. Wilser, Procs. of the II. International Wigner Symposium, 1991 (World Scientific, Singapore, 1992), p. 104; C.W. Gardiner, A.S. Parkins, and P. Zoller, Phys. Rev. A **46**, 4363 (1992); J. Dalibard, Y. Castin, and K. Mølmer, Phys. Rev. Lett. **68**, 580 (1992); H.J. Carmichael, *An open systems approach to quantum optics*, Lecture notes in physics (Springer, Berlin, 1993); K. Mølmer, Y. Castin, and J. Dalibard, J. Opt. Soc. Am. B **10**, 524 (1993).

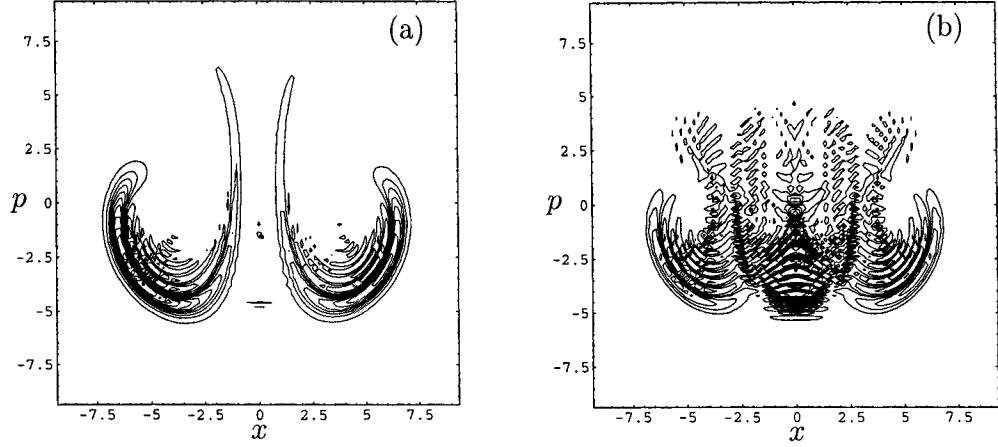


FIG. 1. Wigner function of the time evolved state for an initial odd coherent state, with $\alpha=2$, (x, p are dimensionless). The dimensionless time $\tau = |\Omega|t$ is 500, $\eta=0.2$, $\Omega = |\Omega|e^{i\frac{\pi}{2}}$, $\nu/|\Omega| \simeq 40$. Figure (a): $\gamma \neq 0$, $\Delta/\gamma \simeq 100$. Ensemble average of 10,000 trajectories. Average number of transitions ground-excited-ground: 5.2. The interference fringes between the two peaks have almost completely disappeared. Figure (b): $\gamma=0$, no transitions are possible between the two electronic levels. Strong interference fringes remain between the two peaks.

In the weak field limit⁴ it is possible to obtain a single equation describing solely the nonlinearly driven and damped quantized motion in the ground state. Keeping in Eq. (5) only the leading terms in the Rabi frequencies $\Omega_{1,2}$ and adiabatically eliminating $\hat{\rho}_{22}$, we obtain a master equation of the form

$$\begin{aligned} \frac{\partial \hat{\rho}_{11}}{\partial t} = & \frac{i}{\hbar} [\hat{H}_{\text{eff}}, \hat{\rho}_{11}] - \frac{\gamma}{2\hbar\Delta} (\hat{H}_{\text{eff}} \hat{\rho}_{11} + \hat{\rho}_{11} \hat{H}_{\text{eff}}) \\ & + \frac{\gamma}{\hbar\Delta} \int_{-1}^1 dq \frac{w(q)}{\hbar\Delta} e^{iqk_{21}\hat{x}(t)} \hat{O} \hat{\rho}_{11} \hat{O}^\dagger e^{-iqk_{21}\hat{x}(t)}, \end{aligned} \quad (10)$$

describing the quantized motion in the electronic ground state. In this equation the relaxation part is again of the Lindblad form, so that the norm of $\hat{\rho}_{11}$ is preserved and the solution can be obtained by a quantum trajectory method. The results we get from solving Eqs. (5) and (10) are in good agreement for the chosen parameters.

In summary, we have studied the effects of rarely occurring quantum jumps in the dynamics of a Raman-driven trapped ion. We have shown how the electronic transitions give rise to important effects such as quantum decoherence and an asymmetric evolution of the system. For situations in which one is interested in studying the dynamics of the motional quantum state on long time scales, the effects of these quantum jumps become important.

This research was supported by the Deutsche Forschungsgemeinschaft. Z.K. and S.W. acknowledge support from the National Research Fund of Hungary (OTKA) and from the Studienstiftung des deutschen Volkes, respectively.

⁴J. Dalibard and C. Cohen-Tannoudji, J. Opt. Soc. B **6**, 2023 (1989).

The quantum phase operator in Weyl quantization procedure via Wigner representation of quantum mechanics

Milena D. Davidović

*Electrical engineering faculty, University of Belgrade
Belgrade, Yugoslavia*

Abstract

Equating the expression for average values of dynamical variables, in coherent states, in Wigner representation of quantum mechanics which is classical in structure with Wigner function playing the role of classical phase space probability distribution, and standard quantum mechanical expression for average values of corresponding Weyl quantum operators, matrix elements of the operator corresponding to phase of the oscillator by Weyl procedure, are obtained in the $|n\rangle$ basis.

As the only mathematical technique necessary in the proposed procedure is simple change of variables to polar coordinates in corresponding integrals, this way to introduce Weyl phase operator, and some other operators in Weyl quantization, greatly simplifies necessary derivations and calculations.

I. INTRODUCTION

In Wigner phase space formulation of quantum mechanics every quantum mechanical state is represented by a corresponding function in phase space - its Wigner function. In calculations of quantum mechanical averages the Wigner function plays a role analogous to that of classical distribution function.

More precisely, quantum mechanical average values in some state ψ of the operator $F(\hat{p}, \hat{q})$ which is obtained from a classical function $f(p, q)$ by Weyl procedure may be represented in the form which is classical in structure [1]:

$$\langle \psi | F(\hat{p}, \hat{q}) | \psi \rangle = \int f(p, q) W(p, q) dp dq \quad (1)$$

where $W(p, q) = \int \psi^*(q - x/2) \psi(q + x/2) e^{ipx} dx$ is Wigner function of the state ψ . (Planck constant is taken to be one.)

The essence of Weyl quantization is described by its originator, in Chapter IV of his book [2], as follows: "A quantity f is consequently carried over from classical to quantum

mechanics in accordance with the rule: *replace p and q in the Fourier development of f by the Hermitian operators representing them in quantum mechanics.*"

The great majority of results regarding different aspects of operators in Weyl quantization, is obtained using this characterization of Weyl quantization. In such works the corresponding tools of mathematical analysis, which may be not very transparent, are used.

In the present work it is shown how the derivations of some of these results may be greatly simplified using the characterization of Weyl quantization contained and represented in Eq. (1). This will be done for the operator of the quantum phase and operators of other physical quantities, especially those whose classical expressions in polar coordinates depend only on polar radius or polar angle.

II. THE QUANTUM PHASE OPERATOR

It is well known that an operator is completely defined when its average values, i.e. its diagonal matrix elements, are known in the overcomplete coherent states basis $|\alpha\rangle$. Wigner function for one such state, say $|\beta\rangle$, may be represented in the form $W_\beta(\alpha) = e^{-2|\beta-\alpha|^2}$, where $\alpha = \frac{1}{\sqrt{2}}(q + ip)$ so that (1) becomes

$$\langle\beta|\hat{F}|\beta\rangle = \int f(p, q) e^{-2|\beta-\alpha|^2} d^2\alpha. \quad (2)$$

For the phase operator $\hat{\phi}$ the integral in (2) simplifies in polar coordinates since then $f(p, q) = \phi$.

Expressing the coherent state $|\beta\rangle$ through the $|n\rangle$ states, the left side in Eq.(2) becomes:

$$e^{-|\beta|^2} \sum_{m,n} \frac{\beta^n}{\sqrt{n!}} \frac{\beta^{*m}}{\sqrt{m!}} \langle m|F(\hat{p}, \hat{q})|n\rangle.$$

Developing now the exponential function on the right side in Eq.(2) and identifying the factors multiplying $\beta^m\beta^{*n}$ on both sides, taking into account that $\hat{F} = \hat{\phi}$ and $f(p, q) = \phi$ we get

$$\frac{1}{\sqrt{m!}\sqrt{n!}} \langle m|\hat{\phi}|n\rangle = \int \phi \sum_{k=0}^{\min(m,n)} \frac{\alpha^{*m-k}}{(m-k)!} \frac{\alpha^{n-k}}{(n-k)!} \frac{(-1)^k}{k!} 2^{m+n-k} e^{-2|\alpha|^2} d^2\alpha. \quad (3)$$

As $\alpha = \rho e^{i\phi}$ and $d^2\alpha = \frac{1}{2}\rho d\rho d\phi$ the integration is trivial in polar coordinates. After integration we obtain the matrix elements of the phase operator:

$$\langle m|\hat{\phi}|n\rangle = [1 - \delta_{m,n}] \frac{i^{n-m-1}}{(n-m)} C_{m,n} \quad (4)$$

where

$$C_{m,n} = \sqrt{m!}\sqrt{n!} \sum_{k=0}^{\min(m,n)} \frac{\Gamma(\frac{m+n}{2} + 1 - k)}{(m-k)!(n-k)! k!} (-1/2)^k. \quad (5)$$

The obtained result for matrix elements of the phase operator is algebraically identical with the result obtained in [3] in a very rigorous but quite a long way.

III. OTHER QUANTUM OPERATORS

Another interesting result may be obtained representing Wigner function of the coherent state $|\beta\rangle$ in the form, which follows directly from the definition of the Wigner function:

$$W_\beta(p, q) = \sum_{m,n} e^{-|\beta|^2} \frac{\beta^m}{\sqrt{n!}} \frac{\beta^{*n}}{\sqrt{m!}} \int h_n(q - x/2) h_m(q + x/2) e^{ipx} dx, \quad (6)$$

where $h_n(z)$ are Hermitean functions.

Specifying Eq.(2) to this representation of Wigner function, proceeding in the same way as before, and using the known integral [4]

$$\int_{-\infty}^{+\infty} e^{-c^2 x^2} H_m(a + cx) H_n(b + cx) dx = \frac{2^n \sqrt{\pi} m! b^{m-n}}{c} L_m^{n-m}(-2ab)$$

where $|\arg c| < \pi/4$, $m \leq n$; and $L_n^\lambda(z)$ is the generalized Laguerre polynomial, we can write

$$\langle m | F(\hat{p}, \hat{q}) | n \rangle = \int f(p, q) (-1)^n 2^{n+1} \sqrt{\pi} m! (q - ip)^{n-m} e^{-(p^2+q^2)} L_m^{n-m}(2(q^2 + p^2)) dp dq. \quad (7)$$

The last result is general, it gives matrix elements in the $|n\rangle$ basis of any operator $F(\hat{p}, \hat{q})$ obtained from the classical function of the dynamical variables p and q , $f(p, q)$, using Weyl quantization procedure.

When $f(p, q)$ is such that in polar coordinates it becomes the function of the polar radius or the polar angle only, the integration simplifies and in some case may be done analytically.

So, when the classical dynamical variable is of the form $f(\sqrt{p^2 + q^2})$ the matrix elements of corresponding operator \hat{F} become:

$$\langle m | \hat{F} | n \rangle = \delta_{m,n} \int_0^\infty f(\sqrt{u}) e^{-u} L_n(2u) du \quad (8)$$

where $L_n(u)$ is the Laguerre polynomial.

For the special case when $f(\sqrt{u}) = (\sqrt{u})^k$ the integration may be carried to the end and we obtain:

$$\int_0^\infty u^{k/2} e^{-u} L_n(u) du = \Gamma(k/2 + 1) P_n^{(0, \frac{k}{2} - n)}(-3).$$

Here $P_n^{(\rho, \sigma)}(z)$ are Jacoby polynomials and $[Re\rho, Re\sigma > -1]$.

The case when the function f is function of the polar angle only, may be treated in the same way as for the simple phase angle, the only difference is that corresponding Fourier coefficients should be replaced.

IV. DISCUSSION

Departing from Weyl quantization procedure represented by corresponding Fourier transforms two ways are open [3]. The first is more symbolic approach with bras, kets, delta functions, on more physical level of rigor. Pure mathematicians prefer to recast Weyl's prescription into the form of an integral transform. Both ways may be rather involved.

The point of departure chosen in the present work may make Weyl quantization more broadly accessible, and some related derivations, as the above examples show, much simpler and more transparent.

REFERENCES

- [1] V. I. Tatarski, *Sov.Phys.Usp.* **36**, 311(1983).
- [2] H. Weyl, *The Theory of Groups and Quantum Mechanics* (Dover, New York, 1955).
- [3] D. A. Dubin, M. A. Hennings and T. B. Smith, *Int.J.Mod.Phys.* **9** 2597 (1995).
- [4] A. P. Prudnikov, Yu. A. Brichov, O. I. Marichev, *Integrals and series* (in Russian) (Nauka, Moskva, 1983).

On the nature of number-phase Wigner function for the quantum Kerr-effect

A. Joshi

Laser and Plasma Technology Division, BARC, Trombay, Bombay 400 085, India

John A. Vaccaro

*Department of Physical Sciences, University of Hertfordshire,
College Lane, Hatfield AL10 9AB, United Kingdom*

Abstract

The effect of a Kerr medium on the photon number and phase properties of a single-mode field are examined using the number-phase Wigner function. This function provides a novel description of the Kerr effect in terms of the underlying classical evolution together with a discrete number spectrum.

The study of non-classical states of light has been a topic of great interest for more than two decades and much effort has been focused on their generation and detection. “Schrödinger cat” states are one such class of states exhibiting many non-classical features such as squeezing and sub-Poissonian photon statistics. Non-linear optical interactions can give rise to the production of Schrödinger cat states. For example, a single-mode field that begins in a coherent state can evolve in a Kerr medium [1,2] into a superposition state comprising multiple coherent-states and exhibiting rich phase properties. In contrast, the evolution of the analogous classical system, in simplest terms, exhibits phase diffusion. One notable difference between quantum and classical systems is the nature of the intensity of the field, which is essentially a discrete and continuous quantity, respectively. Taking account of this difference is a key to understanding the origin of the non-classical behaviour of the Kerr medium.

Here, we present the dynamics of a single-mode light field interacting with a Kerr medium in terms of the number-phase Wigner function $W_{NP}(n, \theta)$ [3]. This function gives a direct graphical representation of the photon number and phase properties of the field. Indeed the marginals $\int_{2\pi} W_{NP}(n, \theta) d\theta$ and $\sum_n W_{NP}(n, \theta)$ are the photon number and phase probability distributions, respectively. Number-phase Wigner functions [4,5] have the distinguishing feature of representing photon number as a discrete variable and thus accommodate, in a transparent manner, the fundamental feature that sets the quantum intensity variable apart from its classical counterpart.

The number-phase Wigner function is defined as the expectation of the number-phase Wigner operator $\widehat{W}_{NP}(n, \theta)$, which, in the number state basis, is given by [4]

$$\widehat{W}_{NP}(n, \theta) = \frac{1}{2\pi} \left[\sum_{k=-n}^n e^{2ik\theta} |n+k\rangle \langle n-k| + \sum_{k=-n}^{n-1} e^{i\theta(2k+1)} |n+k\rangle \langle n-k-1| \right] \quad (1)$$

where $n = 0, 1, 2, \dots$ and θ is real. The second sum above is ignored for $n = 0$. $W_{\text{NP}}(n, \theta)$ can be represented graphically in cylindrical coordinates (r, θ, z) as the points $z(r, \theta) = W_{\text{NP}}(r, \theta)$; since n is a non-negative integer this leads to a set of closed curves which lie above circles of (integer) radius $r = n$ in the x - y plane. We refer to the curve for a given value of n as a “ring”.

The action of a Kerr medium on a single-mode cavity field can be conveniently described in the interaction picture by the following Hamiltonian

$$\hat{\mathcal{H}} = \hbar\chi(\hat{a}^\dagger\hat{a})^2 \quad (2)$$

where $\hbar\chi$ is the third-order nonlinear susceptibility, and \hat{a} (\hat{a}^\dagger) is the annihilation (creation) operator of the electromagnetic field sustained in the cavity. The evolution of the cavity field after a time t is given in terms of the number-phase Wigner function by

$$W_{\text{NP}}(n, \theta, t) = W_E(n, \theta, t) + W_O(n, \theta, t) \quad (3)$$

where, for convenience, we have separated the expression for $W_{\text{NP}}(n, \theta, t)$ into the “even” $W_E(n, \theta, t)$ and “odd” $W_O(n, \theta, t)$ parts:

$$W_E(n, \theta, t) \equiv \frac{1}{2\pi} \left\langle \sum_{k=-n}^n e^{2ik(\theta+2n\chi t)} |n+k\rangle\langle n-k| \right\rangle = W_E(n, \theta + 2n\chi t, 0) \quad (4)$$

$$W_O(n, \theta, t) \equiv \frac{1}{2\pi} \left\langle \sum_{k=-n}^{n-1} e^{i(2k+1)[\theta+(2n-1)\chi t]} |n+k\rangle\langle n-k-1| \right\rangle \quad (5)$$

$$= W_O(n, \theta + [2n-1]\chi t, 0) \quad (6)$$

In comparison, the evolution of a classical field in a Kerr medium, written in terms of the analogous intensity-phase probability $P(r, \theta, t)$, is given by [6]

$$P(r, \theta, t) = P(r, \theta + 2r\chi t, 0) \quad (7)$$

which describes a rotational shear. A sufficiently-peaked initial Gaussian distribution $P(r, \theta, 0)$ will shear into a “whorl” structure [6]. This classical evolution is clearly evident in Eq. (4) but not Eq. (6). We can recover the classical rotational-shear evolution in the quantum case by re-expressing the phase-space representation of $W_{\text{NP}}(n, \theta, t)$ so that effectively $W_O(n, \theta, t)$ is moved to half-odd integer values of n . That is, we re-express the number-phase Wigner function as the function $W'_{\text{NP}}(n, \theta)$:

$$W'_{\text{NP}}(n, \theta) = \begin{cases} W_E(n, \theta), & \text{for integer } n \geq 0 \\ W_O(n + \frac{1}{2}, \theta), & \text{for half-odd } n > 0 \end{cases} \quad (8)$$

where now n ranges over $0, \frac{1}{2}, 1, \frac{3}{2}, 2, \dots$. This form of the number-phase Wigner function has been derived by Luks and Perinova [5] using independent means. We should point out that it is only the phase-space representation that has changed and not the Hilbert space of states. Specifically, the half-integer values of n in Eq. (8) index rings (curves) in the phase-space representation of the state of the field whereas the calculation of Eqs. (4) and (5) are based on the photon number states $|m\rangle$ for non-negative integer values of m only. Also, the half-odd values of n do not contribute to the photon number distribution since the marginal

distribution $\int_{2\pi} W'_{NP}(n, \theta, t) d\theta$ is equal to the photon number distribution $\langle n | \langle n |$ for integer n and is zero otherwise. Moreover, all the defining properties of $W_{NP}(n, \theta)$ discussed in [4] also apply to $W'_{NP}(n, \theta)$.

The time evolution of $W'_{NP}(n, \theta)$ is just the classical evolution:

$$W'_{NP}(n, \theta, t) = W'_{NP}(n, \theta + 2n\chi t, 0) \quad (9)$$

In contrast, the position-momentum Wigner function does not give classical evolution for the Kerr-medium [7]. There is clearly an advantage in using the number-phase Wigner function rather than the position-momentum Wigner function for studying the dynamics of the Hamiltonian \mathcal{H} .

We now show how the nonclassical Schrödinger cat states emerge from this classical evolution. Imagine that the cavity is initially in an intense coherent state $|\alpha\rangle$ with mean photon number $\bar{n} = |\alpha|^2$. The number-state amplitudes of this state can be approximated by $\langle n | \alpha \rangle \approx e^{-(n-\bar{n})^2/4\bar{n}} (2\pi\bar{n})^{-1/4}$, where, for convenience, we have set $\alpha = |\alpha|$. Using this approximation we find $W'_{NP}(n, \theta, t)$ is a periodic Gaussian:

$$W'_{NP}(n, \theta, t) \approx \begin{cases} \frac{1}{2\pi} e^{-\frac{(n-\bar{n})^2}{2\bar{n}}} \sum_{m=-\infty}^{\infty} e^{-(\theta+2n\chi t-m\pi)^2 2\bar{n}}, & \text{for integer } n \geq 0 \\ \frac{1}{2\pi} e^{-\frac{(n-\bar{n})^2}{2\bar{n}}} \sum_{m=-\infty}^{\infty} (-1)^k e^{-(\theta+2n\chi t-m\pi)^2 2\bar{n}}, & \text{for half-odd } n > 0 \end{cases} \quad (10)$$

At $t = 0$, $W'_{NP}(n, \theta, t)$ has narrow (positive) peaks at both $\theta = 0$ and $\theta = \pi$ for integer n , whereas it has a narrow (positive) peak at $\theta = 0$ and a narrow (negative) trough at $\theta = \pi$ for half-odd n , as depicted in Fig. 1(a). The peaks at $\theta = 0$ in each ring [i.e. in the curve $z(r, \theta) = W'_{NP}(r, \theta)$ for a fixed value of $r = n$] line up to form a (non-negative) ‘‘hill’’ at a position $(r, \theta) = (\bar{n}, 0)$ in the x - y plane; this is the position where one would expect to find the maximum in the corresponding classical phase space distribution. In contrast, the (positive) peaks and (negative) troughs at $\theta = \pi$ form interference fringes. Such fringes are usually associated with Schrödinger cat states, i.e. superpositions of distinguishable states, and typically occur at a position which is halfway between the superposed states [8]. Their occurrence here is due to the periodic nature of the phase variable: one can regard the coherent state $|\alpha\rangle$ as a superposition of the two states $|\alpha\rangle$ and $|\alpha e^{i2\pi}\rangle$ with the fringes occurring at the half angle $\theta = \pi$ for real α .

For small $t > 0$ the rings of radius n rotate at the angular frequency $2n\chi$ inducing a rotational shear and the beginnings of a whorl structure. However, for χt of the order of $1/\sqrt{\bar{n}}$ the peaks and troughs in adjacent rings no longer overlap and the function appears chaotic. Nevertheless at specific later times the peaks and troughs partially or fully realign. For example, at $\chi t = 2\pi$ each ring has rotated an integral number of 2π radians and the function returns to its $t = 0$ value. At half this time, $\chi t = \pi$, each integer- n ring has rotated an even multiple of π whereas each half-odd- n ring has rotated an odd multiple of π radians and the function, as a whole, is a π -rotated version of its $t = 0$ value. This is the time of the first ‘‘revival’’ where the state evolves to $e^{-i\hat{a}^\dagger \hat{a} \pi} |\alpha\rangle = |-\alpha\rangle$. At $\chi t = \pi/2$ the peaks of the integer- n rings lie along the directions $\theta = 0$ and $\theta = \pi$ having rotated by a multiple of π radians. This gives rise to the two (non-negative) hills at $(r, \theta) = (\bar{n}, 0)$ and $(r, \theta) = (\bar{n}, \pi)$ shown in Fig. 1(b). In contrast, the peaks and troughs of half-odd- n rings have rotated by $\pi/2$ plus a multiple of π radians. These peaks and troughs line up along the directions $\theta = \pm\pi/2$ and form the interference fringes seen in Fig. 1(b). The net result is consistent

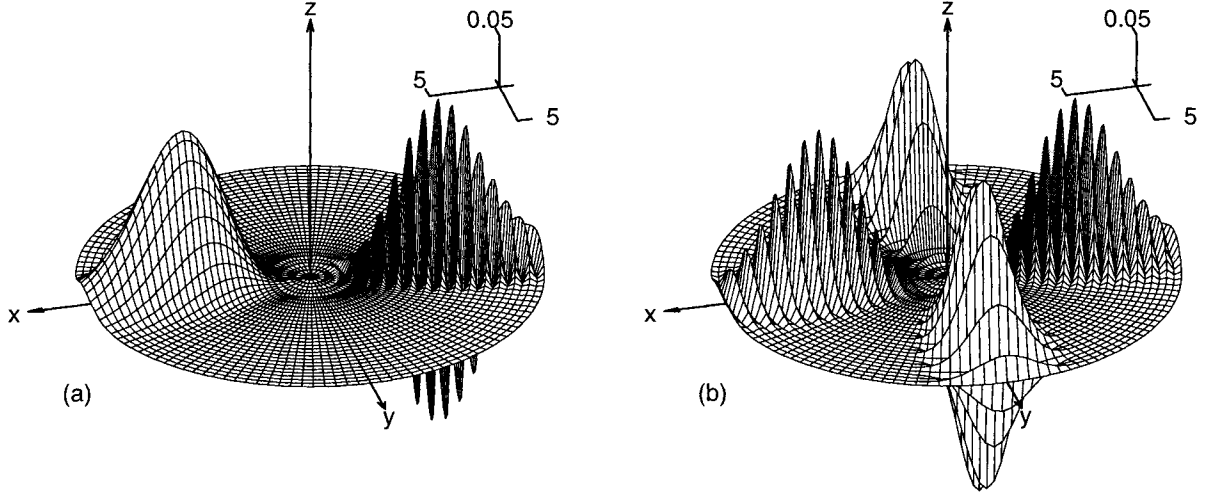


FIG. 1. Polar plots of $W'_{NP}(n, \theta)$ at (a) $\chi t = 0$ and (b) $\chi t = \pi/2$ for a field initially in the coherent state $|\alpha\rangle$ with $\alpha = 3$. The “rings” $z(r, \theta) = W'_{NP}(r, \theta)$ for fixed half-integer $r = n$ are connected with radial lines to help clarify their features.

with the evolved state being the Schrödinger cat state $e^{-i\hat{a}^\dagger \hat{a} \pi/2} |\alpha\rangle \propto (1-i)|\alpha\rangle + (1+i)|-\alpha\rangle$. Similarly, at $\chi t = \pi/4$ another alignment occurs and $W'_{NP}(n, \theta, t)$ displays the characteristics of a four component cat state.

In conclusion, we note that classical evolution alone would lead to a whorl structure; it is the gaps in phase space from the discreteness of the radial variable n in $W'_{NP}(n, \theta, t)$ that leads to re-alignments and the emergence of Schrödinger cat states. In other words, non-classical states emerge from the *classical phase-space evolution* of the Kerr effect and the *discrete photon number spectrum*. This confirms that the number-phase Wigner function, in its various forms [4,5], is a valuable tool for studying the differences between quantum and classical statistics in the spirit that Wigner intended for his celebrated function [9].

REFERENCES

- [1] B. Yurke and D. Stoler, *Phys. Rev. Lett.* **57**, 13 (1986).
- [2] A. Mecozzi and P. Tombesi, *Phys. Rev. Lett.* **58**, 1055 (1987).
- [3] This function was referred to as the “special” number-phase Wigner function S_{NP} in Ref. [4] to distinguish it from other related functions.
- [4] J. A. Vaccaro, *Opt. Comm.* **113**, 421 (1995); *Phys. Rev.* **A52**, 3474 (1995).
- [5] A. Luks and V. Perinova, *Physica Scripta* **T48**, 94 (1993).
- [6] G. J. Milburn, *Phys. Rev.* **A33**, 674 (1986).
- [7] B. M. Garraway and P. L. Knight, *Opt. Comm.* **123**, 517 (1996).
- [8] M. Brune *et al.*, *Phys. Rev. A* **45**, 5193 (1992); A. Vidiella Barranco *et al.*, in *Quantum measurements in optics*, edited by P. Tombesi (Plenum, New York, 1991); W. Schleich *et al.*, *Phys. Rev. A* **44**, 2172 (1991).
- [9] E. P. Wigner, *Phys. Rev.* **40**, 749 (1932).

Wigner and Weyl functions and their use in extended phase space methods

A. Vourdas and S. Chountasis
*Department of Electrical Engineering and Electronics,
University of Liverpool, Brownlow Hill,
Liverpool L69 3GJ, UK*

Abstract

Uncertainty relations between the correlations in the x -direction and the quantum noise in the p -direction (or vice-versa) are studied. They show that small quantum noise is intimately related to large correlations. An extended Wigner function which shows simultaneously the quantum noise and the correlations in the system, is introduced and its properties are studied. The formalism reveals deep connections between correlations and quantum noise.

I. INTRODUCTION

Phase space methods[1] have been used extensively in Quantum Optics. In particular, the Wigner function $W(x, p)$ (where x, p are position and momentum) and the Weyl function, $\tilde{W}(X, P)$ (where X, P are position and momentum increments) have been used in many problems.

In this paper we show that the two-dimensional Fourier transform between the Wigner and Weyl functions, leads naturally to the introduction of an extended phase space $x - p - X - P$, in which (x, P) and also (X, p) are dual variables. In this extended phase space we prove uncertainty relations for $\delta x \delta P$ and for $\delta p \delta X$ and show that the formalism provides a nice description of correlations in the wavefunction. We also introduce an extended Wigner function which is *quartic* function of the wavefunction and describes simultaneously the quantum noise and the correlations in the system. It can be used for a deeper understanding of the interplay between quantum noise and correlations. The results are a continuation of the work presented in ref.[2].

II. WIGNER AND WEYL FUNCTIONS

The Wigner function of a state described by a density matrix ρ is defined as:

$$\begin{aligned} W(x, p) &= \frac{1}{2\pi} \int dX \langle x + \frac{1}{2}X | \rho | x - \frac{1}{2}X \rangle \exp(-iXp) \\ &= \frac{1}{2\pi} \int dP \langle p + \frac{1}{2}P | \rho | p - \frac{1}{2}P \rangle \exp(iPx) \end{aligned} \quad (1)$$

Another related function is the Weyl function which is defined as:

$$\begin{aligned}\tilde{W}(X, P) &= \int dx \langle x + \frac{1}{2}X | \rho | x - \frac{1}{2}X \rangle \exp(-iPx) \\ &= \int dp \langle p + \frac{1}{2}P | \rho | p - \frac{1}{2}P \rangle \exp(ipX) \\ &= Tr[\rho D(X, P)]\end{aligned}\quad (2)$$

The Wigner function is related to the Weyl function through the two-dimensional Fourier transform

$$\tilde{W}(X, P) = \int \int W(x, p) \exp[-i(Px - pX)] dx dp \quad (3)$$

X, P are position and momentum *increments* and are dual in the Fourier transform sense to the x, p which appear in the Wigner function.

III. UNCERTAINTY RELATIONS

We emphasize that the first power of $W(x, p)$ and the density matrix ρ , appear in these uncertainties.

In a recent paper [2] we have introduced the uncertainties:

$$\delta X = \langle \langle X^2 \rangle \rangle^{1/2}, \quad \delta P = \langle \langle P^2 \rangle \rangle^{1/2} \quad (4)$$

where

$$\langle \langle X \rangle \rangle \equiv \frac{1}{2\pi} \int X |\tilde{W}(X, P)|^2 dX dP = 0 \quad (5)$$

$$\langle \langle X^2 \rangle \rangle \equiv \frac{1}{2\pi} \int X^2 |\tilde{W}(X, P)|^2 dX dP = 2Tr[\hat{x}^2 \rho^2] - 2Tr[(\hat{x}\rho)^2] \quad (6)$$

and $\langle \langle P \rangle \rangle = 0$ and $\langle \langle P^2 \rangle \rangle$ are defined in an analogous way. We emphasize that the second power of $W(x, p)$ and the ρ^2 , appear in these uncertainties, in contrast to the usual uncertainties where these quantities appear in the first power. We have proved in [2] that for pure states $\delta X = 2^{1/2} \Delta x$ and $\delta P = 2^{1/2} \Delta p$; and that for mixed states the uncertainties $\delta X, \delta P$ are different from $\Delta x, \Delta p$. The quantities $\delta X, \delta P$ provide a measure for the correlations in the quantum state ρ . Indeed we have explained in [2] that the Weyl function can be interpreted as a generalized correlation function and we have given several mathematical relations that led to interpretation that $|\tilde{W}_s(X, P)|^2$ is a probability density for the correlation function. Therefore the widths $\delta X, \delta P$ which associated to the $|\tilde{W}_s(X, P)|^2$ quantify the correlations in the quantum state ρ .

We have also introduced the uncertainties:

$$\delta x = [\langle \langle x^2 \rangle \rangle - \langle \langle x \rangle \rangle^2]^{1/2}, \quad \delta p = [\langle \langle p^2 \rangle \rangle - \langle \langle p \rangle \rangle^2]^{1/2} \quad (7)$$

where

$$\langle\langle x \rangle\rangle \equiv 2\pi \int x[W(x, p)]^2 dx dp = Tr[\hat{x}\rho^2] \quad (8)$$

$$\langle\langle x^2 \rangle\rangle \equiv 2\pi \int x^2[W(x, p)]^2 dx dp = \frac{1}{2}Tr[\hat{x}^2\rho^2] + \frac{1}{2}Tr[(\hat{x}\rho)^2] \quad (9)$$

and $\langle\langle p \rangle\rangle$ and $\langle\langle p^2 \rangle\rangle$ are defined in an analogous way. The $[W(x, p)]^2$ and the density matrix squared, appear in these uncertainties. The symbol $\langle\langle \cdot \rangle\rangle$ is used to distinguish the above uncertainties from the ordinary uncertainties which we denote as $\Delta x, \Delta p$. The quantities $\delta x, \delta p$ describe quantum noise, like the $\Delta x, \Delta p$. We have introduced them because they play dual role to $\delta X, \delta P$ in the sense that they obey the uncertainty relations. We have proved in [2] that for *pure* states $\delta x = 2^{-1/2}\Delta x$ and $\delta p = 2^{-1/2}\Delta p$; and that for mixed states the uncertainties $\delta x, \delta p$ are different from the uncertainties $\Delta x, \Delta p$.

The uncertainties $\delta X, \delta P, \delta x, \delta p$ have been shown to obey the uncertainty relations

$$\delta X \delta p \geq \frac{1}{2}Tr[\rho^2] \quad ; \quad \delta x \delta P \geq \frac{1}{2}Tr[\rho^2] \quad (10)$$

They show that small quantum noise (i.e., small $\delta x, \delta p$) is intimately related to large correlation:

$$\delta X \geq \frac{Tr[\rho^2]}{2\delta p} \quad ; \quad \delta P \geq \frac{Tr[\rho^2]}{2\delta x} \quad (11)$$

IV. EXTENDED WIGNER FUNCTION

The extended Wigner function is defined as

$$\begin{aligned} W_e(x, p, X, P) &= (2\pi)^2 \int \int dx' dp' W(x + \frac{1}{2}x', p + \frac{1}{2}p') W(x - \frac{1}{2}x', p - \frac{1}{2}p') \\ &\quad \times \exp[i(Xp' - Px')] = \\ &= \int \int dX' dP' \tilde{W}^*(X + \frac{1}{2}X', P + \frac{1}{2}P') \tilde{W}(X - \frac{1}{2}X', P - \frac{1}{2}P') \\ &\quad \times \exp[i(X'p - P'x)] \end{aligned} \quad (12)$$

where the index "e" indicates "extended". It is a *quartic* function of the wavefunction and it is easily seen that it is a real function. The extended Wigner function describes simultaneously the quantum noise and the correlations in the system and provides more detailed information than the uncertainties $(\delta x, \delta p)$ and $(\delta X, \delta P)$. It can be used for a deeper understanding of the interplay between quantum noise and correlations.

We can prove the following properties:

$$\frac{1}{4\pi^2} \int \int W_e(x, p, X, P) dx dp = |\tilde{W}(X, P)|^2 \quad (13)$$

$$\frac{1}{16\pi^4} \int \int W_e(x, p, X, P) dX dP = [W(x, p)]^2 \quad (14)$$

$$\frac{1}{8\pi^3} \int \int \int \int W_e(x, p, X, P) dx dp dX dP = Tr[\rho^2] \quad (15)$$

The extended Wigner function can be constructed from Wigner tomography experimental data. The quantity measured is:

$$\begin{aligned} Q(q, \theta) &= \int \int W(x, p) \delta(x \sin \theta - p \cos \theta - q) dx dp \\ &= \int W(q \sin \theta + u \cos \theta, -q \cos \theta + u \sin \theta) du \end{aligned} \quad (16)$$

From the $Q(q, \theta)$ we can evaluate the extended Wigner function as:

$$\begin{aligned} W_e(x, p, X, P) &= \int \int \int \int dX' dP' dq_1 dq_2 Q \left[q_1, \tan^{-1} \left(\frac{P + \frac{1}{2}P'}{X + \frac{1}{2}X'} \right) \right] \\ &\times Q \left[q_2, \tan^{-1} \left(\frac{P - \frac{1}{2}P'}{X - \frac{1}{2}X'} \right) \right] \exp[i(X'p - P'x)] \\ &\times \exp\{iq_1[(X + \frac{1}{2}X')^2 + (P + \frac{1}{2}P')^2]^{1/2}\} \\ &\times \exp\{-iq_2[(X - \frac{1}{2}X')^2 + (P - \frac{1}{2}P')^2]^{1/2}\} \end{aligned} \quad (17)$$

V. DISCUSSION

We have introduced an extended phase space $x - p - X - P$ and we have proved the uncertainty relations of Eq(10). We have also introduced the extended Wigner function of Eq(15) and studied its properties in Eqs(16)-(18), and its construction from Wigner tomography measurements in Eq(20). The formalism provides a deeper insight into the connection between correlations and quantum noise.

VI. ACKNOWLEDGEMENTS

AV gratefully acknowledges the Royal Academy of Engineering for a travel grant. SC gratefully acknowledges financial support from the Alexander S. Onassis Public Benefit Foundation.

VII. REFERENCES

1. N. L. Balazs and B. K. Jennings, Phys. Rep., **104**, 347 (1984).
M. Hillery, R.F. O'Connell, M. O. Scully, and E. P. Wigner, Phys. Rep., **106**, 121 (1984).
K. E. Cahill and R. J. Glauber, Phys. Rev., **177**, 1857 (1969); **177**, 1882 (1969).
Y. S. Kim, M. E. Noz *Theory and Applications of the Poincare Group* (Dordrecht, Reidel 1986)
2. S. Chountasis and A. Vourdas, Phys. Rev. A, **58**, 848 (1998); Phys. Rev. A, **58**, 1794 (1998).

FEATURES OF S-PARAMETERIZED WIGNER FUNCTION.

Alex Granik

Physics Dept., Univ. of the Pacific, Stockton, CA. 95211
E-mail: galois@ix.netcom.com

George Chapline

c/o Physics Dept., Stanford Univ., Stanford, CA. 94305

Abstract

The generalized Wigner function is derived by considering the Fourier-transform of the probability density in the p-representation. This derivation leads to a natural emergence of the ordering parameter s. Some features of the s-parameterized Wigner function are discussed. The double-parameter associative functional product is introduced and applied to time-independent generalized Wigner function. As an explicit example the generalized Wigner function and the respective eigenvalues are found for the harmonic oscillator.

PACS number(s): 11.15.Tk, 03.65.Db, 04.20.Fy

The generalized Wigner function $W(q,p,s)$ emerges in a very natural way by simply asking the following question: since the wave function in p- and q-representations are Fourier-transforms of each other, what are the respective Fourier-transforms for the probability densities in p- and q-representations? Since the momentum probability density is

$$|\Phi(p)|^2 = \frac{1}{2\pi\hbar} \int dq' e^{-ipq'/\hbar} \Psi(q') \int dq'' e^{ipq''/\hbar} \Psi^*(q'') = \frac{1}{2\pi\hbar} \iint dq' dq'' \Psi(q') \Psi^*(q'') e^{ip(q''-q')/\hbar} \quad (1)$$

we introduce new variables q and τ ($q'' = q + \alpha\tau$, $q' = q + \beta\tau$) such that the respective Jacobian is \hbar and get from (1)

$$|\Phi(p)|^2 = \frac{1}{2\pi} \int d\tau e^{-ip\tau} \int dq \Psi\left(q + \frac{\hbar(1+s)}{2}\tau\right) \Psi^*\left(q - \frac{\hbar(1-s)}{2}\tau\right), \quad (2)$$

where we replace $\alpha = (1-s)\hbar/2$. It is clear that $|\Phi(p)|^2$ is the Fourier-transform of the convolution of the wave function $\Psi(q)$.

On the other hand, $|\Phi(p)|^2$ can be written differently by changing the order of integration in (2)

$$|\Phi(p)|^2 = \frac{1}{2\pi} \int dq \int d\tau e^{-ip\tau} \Psi\left(q + \frac{\hbar(1+s)}{2}\tau\right) \Psi^*\left(q - \frac{\hbar(1-s)}{2}\tau\right) = \int dq F(p, q, s)$$

From this relation follows that function

$$F(p, q, s) = \frac{1}{2\pi} \int d\tau e^{-ip\tau} \Psi\left(q + \frac{\hbar(1+s)}{2}\tau\right) \Psi^*\left(q - \frac{\hbar(1-s)}{2}\tau\right) \quad (3)$$

can be viewed as a mock joint probability distribution (generalized, or s-parameterized Wigner function) in p-q-space whose marginal distributions are $|\Phi(p)|^2$ and $|\Psi(q)|^2$. Interestingly enough, we do not introduce the generalized Wigner function *ad hoc* (as, for example in Ref.1) but arrive at its formulation by using for the Fourier-transform of a product of 2 functions which is equal to the convolution of the originals.

It is easy to see that the generalized Wigner function $F(p, q, s)$ is complex-valued and has the following properties :

1) $F^*(p, q, s) = F(p, q, -s)$, 2) $F^*(p, q, s) = F(p, q, s)$, $\text{Re } s = 0$. Following Moyal [2], one can consider the space-conditional momenta (Wigner averages) based on $F(p, q, s)$: $\langle p^n \rangle_w = \int F(p, q, s) p^n dp / \int \Psi(q) \Psi^*(q)$. The values of these momenta for $n=1$ and $n=2$ provide an intriguing insight into a transition to a classical regime, $\Psi = \sqrt{\rho} \exp(iS/\hbar)$ and a possible relation of the s-parameter to the information transfer at the quantum level:

$$\langle p \rangle_W \Rightarrow \text{grad } S - i\hbar \text{grad} (\text{Ln}\rho)/2 \Rightarrow \text{grad } S,$$

$$\langle p^2 \rangle_W \Rightarrow m[-\partial S/\partial t + (\text{grad} S)^2/2m - V] - ms^2[\partial S/\partial t + (\text{grad} S)^2/2m + V],$$

where $\rho = \Psi\Psi^*$, S is the classical action, and V is the potential energy. From the second of these expressions one can see that $\langle p^2 \rangle_W$ becomes the classical momentum if the last term disappears yielding the Hamilton-Jacobi equation. If $s = \pm 1$ then the Wigner average $\langle p \rangle_W$ corresponds to a complex momentum $\text{grad} S \pm i\hbar \text{grad}(\text{Ln}\rho)$ where the imaginary part $\hbar \text{grad}(\text{Ln}\rho)$ can be presumably interpreted as the "information momentum".

Returning to (3) we see that the Fourier-transform $M(\theta, \tau, s)$ of the generalized Wigner function is

$$M(\theta, \tau, s) \equiv \int dq e^{i\theta q} \Psi(q + \frac{\hbar(1+s)}{2}\tau) \Psi^*(q - \frac{\hbar(1-s)}{2}\tau) = \int dp e^{i\theta p + i\theta q} F(p, q, s)$$

This in turn is nothing more than a quantum average of the s -displacement operator in p - q -space

$$\mathbf{D}(\mathbf{q}, \mathbf{p}, \theta, \tau, s) = e^{-i\hbar s \theta/2} e^{i(\theta \mathbf{q} + \tau \mathbf{p})}, \quad (4)$$

where the bold print denotes an operator. Relation (4) is the generalization of the operators $\Delta_k^+(s=-1)$, $\Delta_k^-(s=1)$, and $\Delta(s=0)$ introduced by N. Balazs & B. Jennings [3]. Using (3) and the relation between $\Psi(q)$ and $\Phi(p)$ it is easy to demonstrate that the alternative expression for $F(q, p, s)$ is

$$F(p, q, s) = e^{-\alpha \hbar i \partial_q} [\Psi^*(q) \Phi(p) e^{i p q / \hbar}],$$

where $\alpha = (1-s)/2$. Interestingly enough, by capitalizing on the Dirac's idea [4] we get the same operator $\exp[-\alpha \hbar \partial^2 / \partial p \partial q]$ by considering the following formal expansion

$$\mathbf{g}(\alpha \frac{\hbar}{i} \partial_q + p + (1-\alpha) \frac{\hbar}{i} \partial_q) = e^{-\alpha \hbar i \partial_q} \mathbf{g}(p, q) e^{(\alpha-1) \hbar i \partial_q} = e^{-\alpha \hbar i \partial_q} \mathbf{g}(p, q)|_{p=q}$$

where $\bar{\partial}$ acts to the right of itself, ∂ acts to the left of itself, and $\mathbf{p} \equiv \partial / \partial p$.

If we use the creation $\mathbf{a}^\dagger = (q+ip)/\sqrt{2}$ and annihilation $\mathbf{a} = (q-ip)/\sqrt{2}$ operators in (4) we arrive at the following

$$\mathbf{D}(\mathbf{a}, \mathbf{a}^\dagger, \alpha, \alpha^*, s) = e^{s(\alpha^2 - \alpha^{*2})/4} e^{\alpha \mathbf{a}^\dagger - \alpha^* \mathbf{a}} \quad (5)$$

where $\alpha = (q+ip)/\sqrt{2}$, $\alpha^* = (q-ip)/\sqrt{2}$, we measure q and p in the same units, and set $\hbar=1$. Let us notice that operator (5) differs from the displacement operator defined in [5]: $\mathbf{D}_G(\mathbf{a}, \mathbf{a}^\dagger, \alpha, \alpha^*, s) = e^{s\alpha\alpha^*/2} e^{\alpha\mathbf{a}^\dagger - \alpha^*\mathbf{a}}$.

Still, the new operator (5) has the same properties as the conventional displacement operator $\mathbf{D}(\mathbf{a}, \mathbf{a}^\dagger, \alpha, \alpha^*) \equiv \mathbf{D}(\alpha) = e^{\alpha\mathbf{a}^\dagger - \alpha^*\mathbf{a}}$. In particular,

$$\mathbf{D}(\mathbf{a}, \mathbf{a}^\dagger, \alpha, \alpha^*, s) \mathbf{D}(\mathbf{a}, \mathbf{a}^\dagger, \beta, \beta^*, s) = e^{2i \text{Im}[\alpha(\beta^* - s\beta)]} \mathbf{D}(\mathbf{a}, \mathbf{a}^\dagger, \alpha + \beta, \alpha^* + \beta^*, s)$$

Since in general, an introduction of any *unimodular* factor $e^{i\phi}$ into the operator $\mathbf{D}_G(\mathbf{a}, \mathbf{a}^\dagger, \alpha, \alpha^*, s) \equiv \mathbf{D}_G(\alpha, s)$ does not change its basic property :

$$e^{i\phi} \mathbf{D}(\alpha, s) |0\rangle = e^{i\phi} e^{s\alpha\alpha^*/2} \mathbf{D}(\alpha) |0\rangle = e^{i\phi} e^{s\alpha\alpha^*/2} |\alpha\rangle$$

(for $s=0$ this expression reduces to an operator in the coset space, cf. Ref. 6), we can introduce a *generalized displacement operator* as follows

$$\mathbf{D}(\alpha, s, r) = e^{r(\alpha^2 - \alpha^{*2})/4} e^{s|\alpha|^2/2} e^{\alpha\mathbf{a}^\dagger - \alpha^*\mathbf{a}} \quad (6)$$

It is easy to see that $\mathbf{D}(\alpha, s, r)$ has the following properties

$$\mathbf{D}^\dagger(\alpha, s, r) = \mathbf{D}(-\alpha, s, -r),$$

$$\mathbf{D}^{-1}(\alpha, s, r) = \mathbf{D}(-\alpha, -s, -r),$$

$$\mathbf{D}^\dagger(\alpha, s, r) \neq \mathbf{D}^{-1}(\alpha, s, r), \text{ and}$$

$$\mathbf{aD}(\alpha, s, r) - \mathbf{D}(\alpha, s, r) \mathbf{a} = \alpha \mathbf{D}(\alpha, s, r)$$

Returning to p - q -space we get from (6) the expression for the generalized displacement operator $\mathbf{D}(p, q, s, r)$:

$$\mathbf{D}(p, q, s, r) = e^{-ir\theta\tau/2} e^{s(\tau^2 + \theta^2)/4} e^{i(\theta q + \tau p)} \quad (7)$$

The form of the operator $\mathbf{D}(p, q, s, r)$ lends itself to the introduction of the following associative two parameter(s and r)-star product

$$\circ \equiv e^{i[(1+r)\bar{\partial}_q \bar{\partial}_p - (1-r)\bar{\partial}_q \bar{\partial}_p]/2} e^{s(\bar{\partial}_q \bar{\partial}_q + \bar{\partial}_p \bar{\partial}_p)/2} \quad (8a)$$

and respectively

$$\circ \equiv e^{i[(1+s)\bar{\partial}_q \bar{\partial}_p - (1-s)\bar{\partial}_q \bar{\partial}_p]/2} e^{r(\bar{\partial}_q \bar{\partial}_q + \bar{\partial}_p \bar{\partial}_p)/2} \quad (8b)$$

The associative \circ -product of any 2 functions $f(q, p)$ and $g(q, p)$ has the following properties:

$$\begin{aligned} \text{i) } f \circ g &= f\left(q + i\frac{1+r}{2}\bar{\partial}_p + s\bar{\partial}_q, p - i\frac{1-r}{2}\bar{\partial}_q + s\bar{\partial}_p\right) g(q, p) \\ &= f\left(q, p - i\frac{1-r}{2}\bar{\partial}_q + s\bar{\partial}_p\right) g\left(q, p + i\frac{1+r}{2}\bar{\partial}_p + s\bar{\partial}_q\right). \end{aligned}$$

$$\text{ii) } \int fg^* dpdq = \int f \circ g dpdq.$$

iii) *Lemma.* A function $\Psi(q)$ satisfies the Schroedinger equation iff the generalized Wigner function

$$F(s, p, q) = \frac{1}{2\pi} \int d\tau e^{-i p \tau} \Psi\left(q + \frac{(1+s)}{2}\tau\right) \Psi^*\left(q - \frac{(1-s)}{2}\tau\right)$$

satisfies one-parameter ($r=0, s \neq 0$) Moyal-Liouville equation

$$\frac{\partial}{\partial t} F = i (F \circ H - H \circ F)$$

where H is the classical Hamiltonian.

For the stationary generalized Wigner function the above lemma yields (cf. Ref.7 where $s=0, r=0$)

$$F \circ H = H \circ F$$

and

$$H \circ F = EF$$

where E is the \circ -eigenvalue of this equation. More generally, for

$$\Psi(q, t) = \sum a_n e^{-iE_n t} u_n(q),$$

$$F(q, p, s) = \sum_n \sum_m a_n a_m^* F_{nm},$$

where

$$F_{nm} = \frac{1}{2\pi} \int e^{-ipy} u_n \left[q + \frac{(1+s)}{2} y \right] u_m^* \left[q - \frac{(1-s)}{2} y \right] dy.$$

Therefore we get

$$H^\circ F_{nm} - F_{nm}^\circ H = (E_n - E_m) F_{nm} \quad (9)$$

and

$$H^\circ F_{nm} = E_n F_{nm} \quad (10)$$

THE SIMPLE HARMONIC OSCILLATOR

The hamiltonian in this case is $H = (p^2 + q^2)/2 = \alpha\alpha^*$. We set in (8b) $r = 0$. Substitution of H into (9) yields then

$$(\alpha\partial_\alpha - \alpha^*\partial_{\alpha^*}) F_{nm} = (E_n - E_m) F_{nm}$$

This means that neglecting a constant coefficient

$$F_{nm} = F(\alpha\alpha^*) \alpha^{*(E_n - E_m)} \quad (11)$$

Inserting this expression in (10) we obtain after some algebra the Whittaker equation

$$zF'' + (sz + 1 + E_n - E_m)F' + \left(\frac{1+s}{2} E_m + \frac{1-s}{2} E_n - \frac{1-s^2}{4} z \right) F = 0, \quad (12)$$

where $z = 4\alpha\alpha^*/(1-s^2)$.

Solution of (12) is given in terms of the confluent hypergeometric function ${}_1F_1$:

$$F = e^{-(1+s)z/2} {}_1F_1\left(\frac{1+s}{2} - E_n, E_m - E_n + 1, z \right)$$

The function F is finite if $\frac{1+s}{2} - E_n$ is equal to a negative integer $(-n)$. Since E_n and E_m symmetric we obtain the following $^\circ$ -eigenvalues of equation (10).

$$E_n = n + \frac{1+s}{2} \quad (13)$$

In this case ${}_1F_1$ is expressed in terms of the Laguerre polynomial $L_n^{(m-n)}$. Therefore returning to the original variables α and α^* we arrive at the unnormalized eigenfunctions F_{nm} corresponding to the $^\circ$ - eigenvalues(13):

$$F_{nm} = (\alpha^*)^{m-n} e^{-\frac{2|\alpha|^2}{1-s}} L_n^{(m-n)}\left(4 \frac{|\alpha|^2}{1-s^2}\right)$$

This result coincides up to a normalization coefficient with the respective expression given in Ref.4.

-
- [1] E.Wigner, Phys.Rev. **40**, 749 (1932).
[2] J.Moyal, Proc.Cambridge Philos.Soc. **45**, 99 (1949).
[3] N.Balazs & B.Jennings, Phys. Reports, **104**, 347 (1984).
[4] P.Dirac, *The Principles of Quantum Mechanics* (Clarendon Press, Oxford,1993).
[5] K.Cahill & R.Glauber, Phys.Rev. **177**, 1882 (1969).
[6] W.Zhang, D.Feng, and R.Gilmore, Rev. Mod.Physics **62**, 867 (1990).
[7] T.Curtright, D.Fairlie, and C.Zachos, Phys.Rev. **58**, 2 (1998).

Direct Measurement of the Wigner Function of Optical Fields

K. Banaszek, C. Radzewicz, and K. Wódkiewicz

Wydział Fizyki, Uniwersytet Warszawski, Hoża 69, PL-00-681 Warszawa, Poland

J. S. Krasinski

Center for Laser and Photonics Research, Oklahoma State University, 413 NCR, Stillwater, OK 74078, USA

Abstract

We present experimental realisation of the photon counting scheme for measuring the Wigner function of a light mode. We also show that generalization of this scheme to the multimode case provides a novel way of testing quantum nonlocality exhibited by correlated states of optical radiation.

One of the most exciting topics studied currently in quantum optics is the complete measurement of the quantum state of microscopic systems. This field has been initiated by the reconstruction of the Wigner function via optical homodyne tomography [1], which combines quantum measurement of field quadratures with a filtered back-projection algorithm used in medical imaging.

In this contribution we briefly review the first experimental realisation of the direct scheme for measuring the Wigner function of light [2]. This method provides complete characterization of the quantum state in the form of the Wigner quasidistribution function without using any numerical reconstruction algorithms. Our experiment is based on the representation of the Wigner function at a complex phase space point denoted by α as the expectation value of the displaced photon number parity operator $(-1)^{\hat{n}}$ [3,4]:

$$W(\alpha) = \frac{2}{\pi} \langle \hat{D}(\alpha) (-1)^{\hat{n}} \hat{D}^\dagger(\alpha) \rangle. \quad (1)$$

The measurement of this observable has been implemented by interfering the signal at a low-reflection beam splitter with an auxiliary coherent probe beam, and subsequent measurement of the photon statistics. Using this scheme, we determined the complete Wigner function by scanning the phase space point-by-point.

The experimental setup was constructed as an unbalanced Mach-Zender interferometer with the beams in the two arms serving as the signal and the probe beams. The signal beam was prepared as the vacuum, a coherent state, or a phase diffused coherent state. Two electrooptic modulators controlled the point of the phase space at which the Wigner function was measured, and a photon counting module was used to collect the photon statistics. Typical experimental results are depicted in Fig. 1.

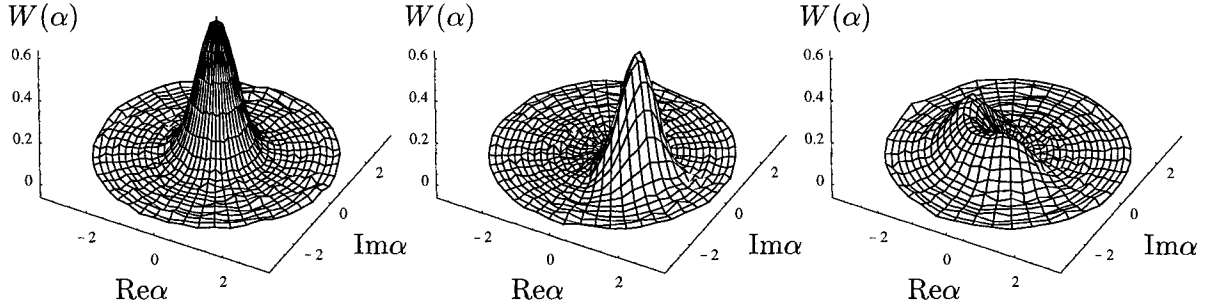


FIG. 1. The measured Wigner functions for the vacuum state (left), a coherent state with approximately one photon (center), and a phase diffused coherent state (right).

The photon counting scheme for measuring the Wigner function has a very elegant generalization to the two-mode case. After applying the displacement transformation to each of the modes, the Wigner function is given by the correlation of the photon number parities measured for both the modes:

$$W(\alpha, \beta) = \frac{4}{\pi^2} \langle \hat{D}_a(\alpha)(-1)^{\hat{n}_a} \hat{D}_a^\dagger(\alpha) \otimes \hat{D}_b(\beta)(-1)^{\hat{n}_b} \hat{D}_b^\dagger \rangle \quad (2)$$

Here the indices a and b refer to the two modes. The above representation of the Wigner function offers a novel way of testing nonlocality of quantum optical correlations [5], in analogy to spin-1/2 measurements: the binary ± 1 outcome is provided by the parity operator, and the coherent displacements α and β play the role of adjustable parameters in each of the spatially separated apparatuses. In particular, this scheme can be applied to test nonlocality of the state produced in the nondegenerate parametric amplification process, which is a quantum optical analog of the original Einstein-Podolsky-Rosen state. Appropriate choice of coherent displacements shows that the corresponding Wigner function, though positive definite, provides a direct evidence for nonlocality [6].

This research was supported by KBN grant 2 P03B 089 16.

1. D. T. Smithey, M. Beck, M. G. Raymer, and A. Faridani, Phys. Rev. Lett. **70**, 1244 (1993).
2. K. Banaszek, C. Radzewicz, K. Wódkiewicz, and J. S. Krasinski, Phys. Rev. A **60**, 674 (1999); see also <http://www.fuw.edu.pl/~kbanasz/QOLab/ExpWigner/>
3. S. Wallentowitz and W. Vogel, Phys. Rev. A **53**, 4528 (1996).
4. K. Banaszek and K. Wódkiewicz, Phys. Rev. Lett. **76**, 4344 (1996).
5. K. Banaszek and K. Wódkiewicz, Phys. Rev. Lett. **82**, 2009 (1999).
6. K. Banaszek and K. Wódkiewicz, Phys. Rev. A **58**, 4345 (1998).

One-Dimensional Representation in Phase-Space

Z. Kis, J. Janszky

Department of Nonlinear and Quantum Optics, Institute for Solid State Physics and Optics, P. O. Box 49, H-1525 Budapest, Hungary

Abstract

A constructive method is derived to represent any state of the harmonic oscillator along an arbitrary, continuous curve in phase-space by a continuous superposition of coherent states. The weight function of the superposition is expressed in terms of the Fock state expansion coefficients of the state in a truncated Hilbert space. This weight function does not necessarily exist as an ordinary function, it can also be a distribution if the dimension of the truncated Hilbert space tends to infinity.

In many applications of quantum mechanics an appropriately chosen basis set simplifies greatly the calculations. In quantum optics coherent states proved to be one of the most efficient one¹. It has been shown, that coherent states on the complex α plane form an overcomplete basis set. It means that even a subset of coherent states could be complete. It was proven by Von Neumann that a set of coherent states on a lattice in phase-space with lattice cell size π is a complete set². Moreover, Cahill has pointed out that for any Cauchy series $\{\alpha_n\}$ the corresponding coherent state set $\{|\alpha_n\rangle\}$ is complete³. Unfortunately, these theorems do not provide a straightforward method to find the expansion coefficients in the coherent state basis.

A further advance in coherent state representations was the discovery of one-dimensional coherent state representation along the real axis of the complex α plane⁴. It was shown that Gaussian superposition of coherent states along the real axis in phase-space yields a quadrature squeezed vacuum state. It has been also pointed out, that any quadrature

¹R. J. Glauber, *Phys. Rev.* **131**, 2766 (1963).

²A. Perelomov, *Generalized Coherent States and Their Applications* (Springer-Verlag, 1986).

³K. E. Cahill, *Phys. Rev.* **138**, B1566 (1965).

⁴J. Janszky and V. Vinogradov, *Phys. Rev. Lett.* **64**, 2771 (1990).

squeezed number state can be represented along the real axis⁵

$$|H_n\rangle = \hat{S}(\zeta) |n\rangle = \mathcal{N}_n \int_{-\infty}^{\infty} dx H_n(ax) e^{-x^2/\gamma} |x\rangle,$$

$$\mathcal{N}_n = \sqrt{\frac{(2+\gamma)^n \sqrt{1+\gamma}}{2^n \pi n! (n+1) \gamma}}, \quad a = \sqrt{\frac{2(1+\gamma)}{\gamma(2+\gamma)}}, \quad (1)$$

where $H_n(x)$ are the Hermite polynomials of order n . This expansion offers a way to find the one-dimensional representation of any state vector in the Hilbert space of the harmonic oscillator

$$|\Psi\rangle = \int_{-\infty}^{\infty} dx F(x) |x\rangle. \quad (2)$$

The expansion function $F(x)$ can be deduced in a straightforward manner

$$F(x) = \sum_{n=0}^{\infty} h_n \mathcal{N}_n H_n(x) e^{-x^2/\gamma}, \quad (3)$$

where

$$h_n = \mathcal{N}_n \int_{-\infty}^{\infty} dx H_n(ax) e^{-x^2/\gamma} \langle x | \Psi \rangle. \quad (4)$$

and a is defined in Eq. (1). There arise two questions in connection with the last formulae: (i) any continuous curve in phase-space could serve as a starting point for a coherent state representation. Is it possible to find a weight function of that representation in a systematic way? (ii) In practical cases the integral in Eq. (4) is difficult to evaluate. Is there a simpler way to find a weight function for a coherent state representation?

In this contribution we propose a method, which possess both the above mentioned properties: in principle it is a representation along an arbitrary curve in phase-space, and it is simpler to evaluate in practical applications. Let us define the general one-dimensional coherent state representation in phase-space:

$$|\psi\rangle = \int_{\Gamma} dz F(z) |z\rangle. \quad (5)$$

where Γ is an arbitrary curve. We truncate the Hilbert space of the harmonic oscillator at a very large, but finite number state $|N\rangle$. Inserting the Fock-state expansion of a coherent state into the previous equation, the one-dimensional coherent state representation in the truncated Hilbert space reads

$$|\psi\rangle = \sum_{n=0}^N \int_{\Gamma} dz G(z) \frac{z^n}{\sqrt{n!}} |n\rangle,$$

$$G(z) = \mathcal{N}_N(z) F(z), \quad \mathcal{N}_N(z) = \left\{ \sum_{n=0}^N \frac{|z|^{2n}}{n!} \right\}^{-1/2}. \quad (6)$$

⁵P. Adam, I. Foldesi, and J. Janszky, Phys. Rev. A **49**, 1281 (1994).

Let us compare this expansion with the fock state representation of the state

$$|\psi\rangle = \sum_{n=0}^N c_n |n\rangle. \quad (7)$$

The Fock-state coefficients and the corresponding integrals should be equal, which implies

$$\tilde{c}_n = \sqrt{n!} c_n = \int_{\Gamma} dz G(z) z^n, \quad n=0\dots N. \quad (8)$$

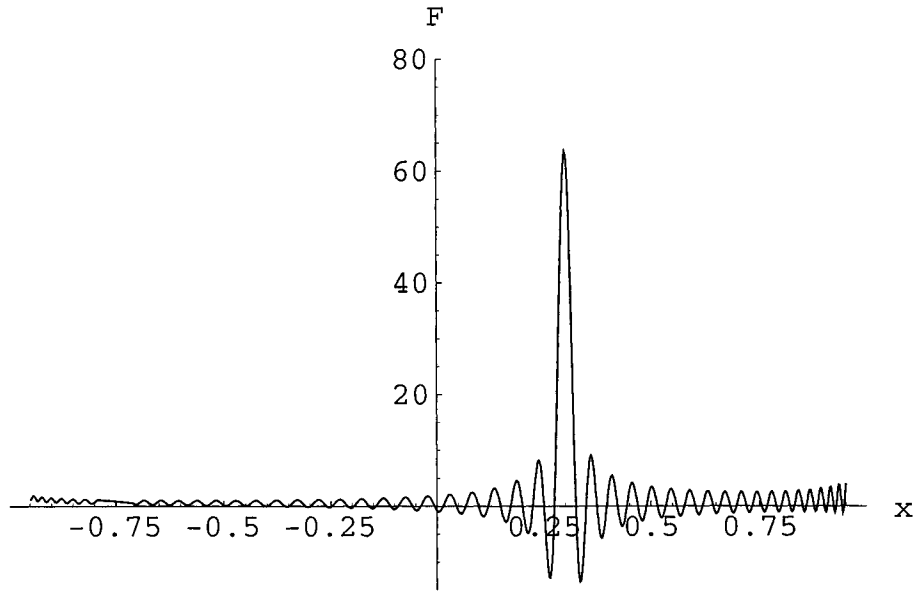


FIG. 1. The graph of the weight function $F(x)$ expanded in the Chebyshev I. polynomial basis for the coherent state $|0.3\rangle$ and the number of polynomials is $N = 120$.

$\{z^n\}$ are polynomials in the domain Γ . They can be orthogonalized with respect to a weight function $w(z)$ which yields the system of orthogonal polynomials $\{P_n(z)\}$. With the aid of these polynomials Eq. (8) can be inverted to find the coherent state expansion function $F(z)$

$$F(z) = w(z) \mathcal{N}_N^{-1}(z) \mathbf{P}(z) \mathbf{P} \tilde{\mathbf{c}}, \quad (9)$$

where

$$\mathbf{P} = \begin{pmatrix} P_{0,0} & 0 & \dots & 0 \\ P_{1,0} & P_{1,1} & \dots & 0 \\ \vdots & \vdots & & \vdots \\ P_{N,0} & P_{N,1} & \dots & P_{N,N} \end{pmatrix}, \quad \mathbf{P}(z) = \begin{pmatrix} P_0(z) \\ P_1(z) \\ \vdots \\ P_N(z) \end{pmatrix}, \quad \tilde{\mathbf{c}} = \begin{pmatrix} c_0 \\ \sqrt{1!} c_1 \\ \vdots \\ \sqrt{N!} c_N \end{pmatrix}. \quad (10)$$

As a first example for the application of the method let us consider the weight function of a coherent state $|x_0\rangle$, with x_0 real. After some straightforward calculations we obtain

$$F(x) = w(x) \mathcal{N}_N^{-1}(x) e^{-x_0^2/2} \mathbf{P}(x) \mathbf{P}(x_0). \quad (11)$$

To be specific, we choose the Chebyshev I. polynomials. The graph of the weight function $F(x)$ for the coherent state $|0.3\rangle$, and summing up the contribution of the first 120 polynomials is depicted in fig. 1. It is readily seen, that the distribution is approximately a Dirac's δ .

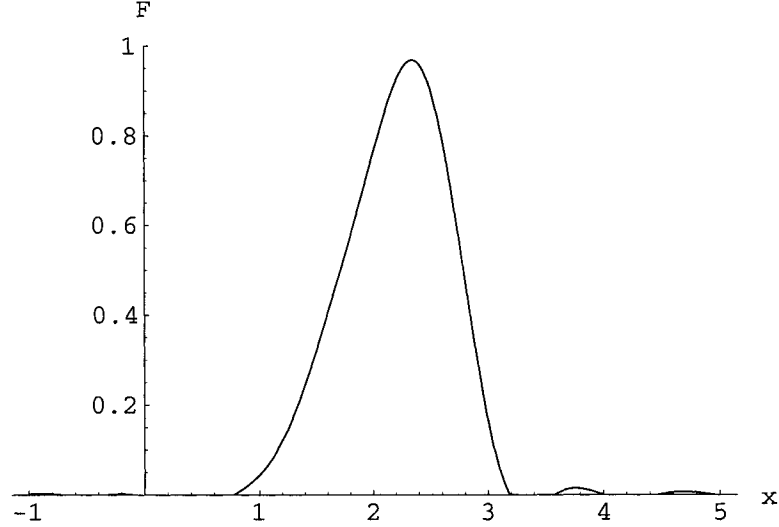


FIG. 2. The graph of the weight function $F(x)$ for the phase optimized state expanded in the Hermite polynomial bases in the $[-\infty, \infty]$ domain.

In the following we determine the weight function $F(x)$ for the Summy-Pegg phase optimized state⁶. The Fock-state expansion of the state is defined by

$$|\psi\rangle = \mathcal{N} \sum_{k=0}^{\infty} \text{Ai}(a[k+b] + b_0) |k\rangle = \sum_{k=0}^N b_k |k\rangle, \quad (12)$$

where $\text{Ai}(x)$ is the Airy function, $b_0 = -2.3381$ is the first zero of the Airy function. We have chosen the parameters $a = 0.271$ and $b = 0.86$. The mean photon number in this state is $\langle \hat{n} \rangle = 4.86$, and the phase variance of the state is $\Delta \hat{\phi} = 0.0574$. In terms of Hermite polynomials the weight function of the coherent state expansion reads

$$F(x) = e^{-x^2/2} \sum_{n,k=0}^N \frac{1}{\sqrt{\pi} 2^n n!} H_n(x) H_{nk} \sqrt{k!} b_k, \quad x \in [-\infty, \infty]. \quad (13)$$

In fig. 2 we plotted $F(x)$ including the first 35 Hermite polynomials into the expansion. We note that for Chebyshev I polynomials this method yields a regular distribution for $F(x)$ as $N \rightarrow \infty$.

This work was supported by the National Research Fund of Hungary (OTKA) under Contract No. F019232.

⁶G. S. Summy, D. T. Pegg, *Opt. Commun.* **77**, 75 (1990).

Phase space localization for trapped atoms

David Vitali, Paolo Tombesi and Stefano Mancini
*Dipartimento di Matematica e Fisica, Università di Camerino
and Istituto Nazionale per la Fisica della Materia, Camerino, Italy*

Abstract

We propose a scheme using feedback from homodyne measurements to cool a trapped particle close to its motional ground state.

In recent years there has been an increasing interest on trapping phenomena and related cooling techniques [1]. Some years ago it has been shown that a single ion can be trapped and cooled down near to its zero-point vibrational energy state [2] and recently, analogous results have been obtained for neutral atoms in optical lattices [3]. The possibility to control trapped particles, indeed, gave rise to new models in quantum computation [4], in which information is encoded in two internal electronic states of the ions and the two lowest Fock states of a vibrational collective mode are used to transfer and manipulate quantum information between them. However the quantum logic operations involving vibrational degrees of freedom cannot be easily performed simultaneously with the standard laser cooling procedures; this implies having heating mechanisms representing, up to now, the dominant source of decoherence which limits the fidelity of quantum logic operations [5]. For this reason it is important to have alternative control schemes for the vibrational modes, able to achieve a significant reduction of thermal noise.

In this paper we present a way to control the motion of a trapped particle, which is able to give a significant phase-space-localisation. This scheme can be applied when the particle is already in the Lamb-Dicke regime, and therefore the scheme assumes that some sort of laser cooling has been already applied. Our scheme will provide therefore further phase space localisation and cooling.

We consider a generic particle trapped in an effective harmonic potential. For simplicity we shall consider the one-dimensional case, even if the method can be in principle generalized to the three-dimensional case. This particle can be an ion trapped by a linear rf-trap [5] or a neutral atom in an optical trap [3]. Our scheme however does not depend on the specific trapping method employed and therefore we shall always refer from now on to a generic trapped “atom”. The trapped atom of mass m , oscillating with frequency ν along the \hat{x} direction and with position operator $x = x_0(a + a^\dagger)$, $x_0 = (\hbar/2m\nu)^{1/2}$, is coupled to a standing wave with frequency ω_b , wave-vector k along \hat{x} and annihilation operator b . We assume that the standing wave can be treated classically and it is resonant with the transition between two internal atomic levels $|+\rangle$ and $|-\rangle$, so that, in the interaction representation with respect to $H_0 = \hbar\omega_b (b^\dagger b + \frac{\sigma_z}{2})$, and making the rotating wave approximation, this Hamiltonian becomes

$$H = \hbar\nu a^\dagger a + \hbar\epsilon|\beta|\sigma_x \sin(kx + \phi) , \quad (1)$$

where $\sigma_x = |+\rangle\langle -| + |- \rangle\langle +|$, ϵ is the coupling constant and $|\beta|$ is the amplitude of the classical standing wave. If we finally set the spatial phase $\phi = 0$ (i.e. the atom is trapped near to a node of the classical standing wave) and assume the Lamb-Dicke regime, we can approximate the sine term at first order and get [7]

$$H = \hbar\nu a^\dagger a + \hbar\chi\sigma_x X, \quad (2)$$

where $\chi = 2\epsilon|\beta|kx_0$ is the effective coupling constant between the internal and the vibrational degrees of freedom, and $X = (a + a^\dagger)/2$ is the dimensionless position operator of the trapped atom. This Hamiltonian shows how one can realize an effective measurement of the atomic position. In fact, the atom displacement away from the electric field node increases the probability of electronic excitation and, hence displacements can be monitored by means of the atomic fluorescence. Therefore, the two-level (sub)system can be used as a meter to measure the position quadrature X .

The evolution equation for the total density operator D for the vibrational degree of freedom and the internal states is determined by Hamiltonian (2) and the dissipative terms describing both the coupling of the vibrations with a thermal environment, and the spontaneous emission from the level $|+\rangle$ responsible for the fluorescence. One has therefore

$$\dot{D} = \mathcal{L}_{th}D - \frac{i}{\hbar} [H, D] + \frac{\kappa}{2} (2\sigma_- D \sigma_+ - \sigma_+ \sigma_- D - D \sigma_+ \sigma_-), \quad (3)$$

where

$$\mathcal{L}_{th}D = \frac{\gamma}{2}(n+1) (2aDa^\dagger - a^\dagger aD - Da^\dagger a) + \frac{\gamma}{2}n (2a^\dagger Da - aa^\dagger D - Daa^\dagger), \quad (4)$$

κ is the spontaneous emission rate, γ is the damping of the center-of-mass motion, and $n = \left[\exp\left(\frac{\hbar\nu}{k_B T}\right) - 1 \right]^{-1}$ is the number of thermal phonons.

It has been recently shown that when excited by a low intensity laser field, a single trapped atom emits its fluorescent light mainly within a quasi-monochromatic elastic peak [8]. The fluorescent light spectrum was measured by heterodyne detection. By improving the technique it does not seem impractical to get a homodyne detection of the single-ion fluorescent light. Thus, by exploiting the resonance fluorescence it could be possible to measure the quantity $\Sigma_\varphi = (\sigma_- e^{-i\varphi} + \sigma_+ e^{i\varphi})$ through homodyne detection of the field scattered by the atom along a certain direction [6]. In fact, the detected field may be written in terms of the dipole moment operator for the transition $|-\rangle \leftrightarrow |+\rangle$ as [6] $E_s^{(+)}(t) = \sqrt{\eta\kappa}\sigma_-(t)$, where η is an overall quantum efficiency accounting for the detector efficiency and the fact that only a small fraction of the fluorescent light is collected and superimposed with a mode-matched oscillator.

The continuous monitoring of the electronic mode performed through the homodyne measurement, modifies the time evolution of the whole system, and the state conditioned on the result of measurement evolves according to an Ito stochastic differential equation. We consider a strong fluorescent transition, i.e. the spontaneous emission rate κ is very large, $\kappa \gg \chi$. This means that the internal two-level system is heavily damped and that it will almost always be in its lower state $|-\rangle$. This allows us to adiabatically eliminate the internal degree of freedom and to perform a perturbative calculation in the small parameter χ/κ , obtaining (see also Ref. [9]) the following equation for the vibrational reduced density matrix ρ_c conditioned to the result of the measurement of the observable $\langle X(t) \rangle_c$,

$$\begin{aligned} \dot{\rho}_c = & \mathcal{L}_{th}\rho_c - i\nu [a^\dagger a, \rho_c] - \frac{\chi^2}{2\kappa} [X, [X, \rho_c]] \\ & + \sqrt{\eta\chi^2/\kappa} \xi(t) \left(ie^{i\varphi} \rho_c X - ie^{-i\varphi} X \rho_c + 2 \sin \varphi \langle X(t) \rangle_c \rho_c \right). \end{aligned} \quad (5)$$

The continuous record of the atom position can be used to control its motion through the application of a feedback loop. We shall use the continuous feedback theory proposed by Wiseman and Milburn [10]: averaging over the white noise $\xi(t)$ and neglecting the feedback delay time, we get the following Markovian master equation [10]

$$\dot{\rho} = \mathcal{L}_{th}\rho - i\nu [a^\dagger a, \rho] - \frac{\chi^2}{2\kappa} [X, [X, \rho]] + \mathcal{K} \left(ie^{i\varphi} \rho X - ie^{-i\varphi} X \rho \right) + \frac{\mathcal{K}^2}{2\eta\chi^2/\kappa} \rho, \quad (6)$$

where \mathcal{K} is a Liouville superoperator describing how the feedback signal acts on the vibrational mode. The second term of the right hand side of Eq. (6) is the usual double-commutator term associated to the measurement of X ; the third term is the feedback term itself and the fourth term is a diffusion-like term, which is an unavoidable consequence of the noise introduced by the feedback itself. The Liouville superoperator \mathcal{K} can only be of Hamiltonian form [10] and we choose it as $\mathcal{K}\rho = g [a - a^\dagger, \rho] / 2$ [9], which means feeding back the measured homodyne photocurrent to the vibrational oscillator with a driving term in the Hamiltonian involving the quadrature orthogonal to the measured one; g is the feedback gain related to the practical way of realizing the loop. Since the measured quadrature of the vibrational mode is its position, the feedback will act as a driving for the momentum. Using the above expressions in Eq. (6) and rearranging the terms in an appropriate way, we finally get the following master equation:

$$\begin{aligned} \dot{\rho} = & \frac{\Gamma}{2} (N + 1) (2a\rho a^\dagger - a^\dagger a \rho - \rho a^\dagger a) + \frac{\Gamma}{2} N (2a^\dagger \rho a - a a^\dagger \rho - \rho a a^\dagger) - \frac{g}{4} \sin \varphi [a^2 - a^{\dagger 2}, \rho] \\ & - \frac{\Gamma}{2} M (2a^\dagger \rho a^\dagger - a^{\dagger 2} \rho - \rho a^{\dagger 2}) - \frac{\Gamma}{2} M^* (2a\rho a - a^2 \rho - \rho a^2) - i\nu [a^\dagger a, \rho], \end{aligned} \quad (7)$$

where $N = \left[\gamma n + \frac{\chi^2}{4\kappa} + \frac{g^2}{4\eta\chi^2/\kappa} + \frac{g}{2} \sin \varphi \right] / \Gamma$, $M = - \left[\frac{\chi^2}{4\kappa} - \frac{g^2}{4\eta\chi^2/\kappa} - i \frac{g}{2} \cos \varphi \right] / \Gamma$. Eq. (7) is very instructive because it clearly shows the effects of the feedback loop on the vibrational mode a . The proposed feedback mechanism, indeed, not only introduces a parametric driving term proportional to $g \sin \varphi$, but it also simulates the presence of a squeezed bath, characterized by an effective damping constant Γ and by the coefficients M and N , which are given in terms of the feedback parameters [9]. Because of its linearity, the solution of Eq. (7) can be easily obtained by using the normally ordered characteristic function $\mathcal{C}(\lambda, \lambda^*, t)$. The stationary state is reached only if the parameters satisfy the stability condition that all the eigenvalues have positive real part. In this case the stationary solution has the following form $\mathcal{C}(\lambda, \lambda^*, \infty) = \exp[-\zeta|\lambda|^2 + m\mu(\lambda^*)^2/2 + \mu^*\lambda^2/2]$, where ζ and μ can be obtained in terms of the parameters of the model (see [11]). Under the stability conditions and in the long time limit ($t \rightarrow \infty$) the variance of the generic quadrature operator $X_\theta = (ae^{i\theta} + a^\dagger e^{-i\theta})/2$ becomes $\langle X_\theta^2 \rangle = \frac{1}{2} \left[\frac{1}{2} + \zeta + \text{Re}\{\mu e^{2i\theta}\} \right]$. If we assume that ν is much greater than any other relevant quantities (as it usually happens), one has $\zeta \approx N$ and $\mu \approx 0$. Then, in absence of feedback ($g = 0$) we have $\zeta \equiv n$, otherwise ζ can be smaller than n , providing a *stochastic localisation* in the phase space. We call it stochastic because it is obtained by feeding back

the fluctuating output of the homodyne measurement. It is worth noting, by virtue of the above assumptions, that the variance $\langle X_\theta^2 \rangle$ is constant over the phase space angle θ ; hence the localisation effect takes place uniformly in all the quadratures. The fact that the feedback action affects all the quadratures is a rather novel result in the quantum theory of feedback, and it is essentially due to the fact that the bare atom Hamiltonian $\hbar\nu a^\dagger a$ mixes the dynamics of the atomic position and momentum, so that the continuous homodyne measurement actually gives informations on both quadratures. This model shares some peculiarities with that one we have proposed in [12] to cool the vibrational motion of a macroscopic mirror of an optical cavity. It is possible to see that the proposed scheme is not able to reduce the noise below the quantum limit, i.e. $\langle X_\theta^2 \rangle < 1/4$ for some θ . The potentiality of this feedback mechanism is clearly shown in Fig.1, where we have sketched the phase space uncertainty contours obtained by cutting the Wigner function at $1/\sqrt{e}$ times its maximum height. We see that the feedback produces a relevant contraction of the uncertainty region. Practically, the feedback mechanism is able to get information from the environment and put it into the system, so to decrease its entropy: in this specific case feedback works as a noise eater.

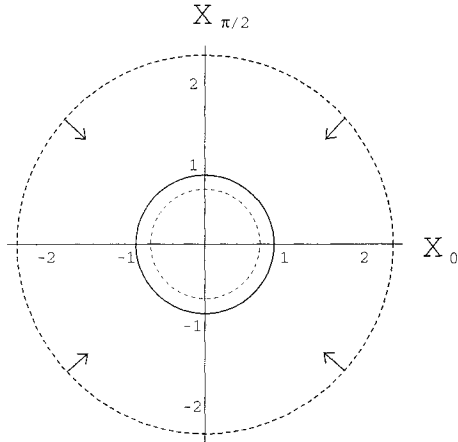


FIG. 1. The phase space uncertainty contours are represented for $\chi = 0$, $g = 0$ (outer dashed line), for $\chi = 5 \text{ s}^{-1}$, $g = 0.3 \text{ s}^{-1}$ (solid line). The values of other parameters are $n = 5$, $\nu = 10^6 \text{ s}^{-1}$, $\gamma = 10^{-2} \text{ s}^{-1}$, $\kappa = 10^2 \text{ s}^{-1}$, $\eta = 0.8$, $\varphi = -\pi/2$. Notice that feedback provides a phase space localisation close to the vacuum state (inner dashed line).

REFERENCES

- [1] see e.g., P. K. Ghosh, *Ion Traps*, (Clarendon, Oxford, 1995), and references therein.
- [2] F. Diedrich *et al*, Phys. Rev. Lett. **62**, 403 (1989).
- [3] S.E. Hamann *et al*, Phys. Rev. Lett. **80**, 4149 (1998);
- [4] J.I. Cirac, P. Zoller, Phys. Rev. Lett. **74**, 4091 (1995).
- [5] D.J. Wineland *et al*, J. Res. Natl. Inst. Stand. Technol. **103**, 259 (1998).
- [6] see e.g., D. F. Walls and G. J. Milburn, *Quantum Optics*, (Springer, Berlin, 1994).
- [7] C.A. Blockley, D. F. Walls and H. Risken, Europhys. Lett. **17**, 509 (1992).
- [8] J. T. Höffges *et al*, Opt. Comm. **133**, 177 (1997).
- [9] P. Tombesi and D. Vitali, Appl. Phys. B **60**, S69 (1995); Phys. Rev. A **51**, 4913 (1995).
- [10] H.M. Wiseman and G.J. Milburn, Phys. Rev. A **49**, 1350 (1994).
- [11] S. Mancini, D. Vitali, and P. Tombesi, quant-ph/9810022.
- [12] S. Mancini, D. Vitali, and P. Tombesi, Phys. Rev. Lett. **80**, 688 (1998); this model has been experimentally implemented by P. F. Cohadon, A. Heidmann and M. Pinard, quant-ph/9903094.

Planck constant and micro–macro scaling laws in complex classical macroscopic systems

Salvatore Capozziello [†], Salvatore De Martino [‡], Silvio De Siena [‡], Fabrizio Illuminati [‡]

[†] *Dipartimento di Scienze Fisiche “E.R. Caianiello”, Università di Salerno,*

[‡] *Dipartimento di Fisica, Università di Salerno,*

INFN Sez. di Napoli, Gruppo Collegato di Salerno, INFN Unità di Salerno,

Via S. Allende, I-84081 Baronissi (SA), Italy.

Abstract

We introduce phenomenological scaling laws relating the characteristic scales of complex macroscopic aggregates to the fundamental quantum scales of the nucleons. These relations allow to predict the observed orders of magnitude of the typical dimensions of stable classical systems.

I. INTRODUCTION

Classical macroscopic systems with many constituents range from charged beams in particle accelerators to astrophysical systems. Although many of the physical aspects of these complex systems are well understood, there are fundamental questions, still unsolved, that in some sense can be seen as preliminary to a truly deeper understanding. A paradigmatic example of such foundational questions is the following: how and why a galaxy, which is a classical system with a large number of components (the stars), is stable on the observed length–scale, with the observed number of stars?

In this note, we present a reformulation of a scheme firstly introduced by Francesco Calogero [1], which provides a possible answer. Calogero suggests that the origin of quantization could be attributed to the universal interaction of every particle with the gravitational force due to all other constituents of the Universe. We replace this hypothesis, introducing general criteria of stability, that hold independently of the nature of the interaction (as long as the latter is attractive). In such a way, the method can be applied, besides gravity, to all the physical situations where a complex system is ruled by an overall effective interaction. More specifically, we show that for any bound and stable aggregate of particles interacting through an overall attractive law of force, there exists a scaling relation between a minimal unit of action per particle (to be defined below), the fundamental constants associated to the interaction, and the dimension of stability of the system. In order of magnitude, such relation always yields the Planck action constant h .

II. SCALING RELATION FOR THE ACTIONS, AND A GENERAL FORM OF THE MINIMAL UNIT OF ACTION

Calogero proposes a model of the Universe as made up of nucleons interacting via the gravitational force [1]. On a sufficiently small scale the overall interaction perturbs the local motion of each single component. This perturbation is described by introducing a characteristic time τ of the local component of the motion, and by assuming normally distributed fluctuations, that scale as $N^{-1/2}$. Hence, Calogero imposes $\tau \cong N^{-1/2}\mathcal{T}$, where \mathcal{T} is the time scale for the mean global deterministic motion of each constituent. One needs to define the global units of energy E and of action A , the unit of energy per particle ϵ , and the minimal unit of action per particle α . By using the above definitions, one obtains the nontrivial scaling relation

$$\alpha \cong N^{-3/2} A. \quad (1)$$

A simple dimensional analysis allows to obtain $\alpha \cong G^{1/2}m^{3/2}R^{1/2}$, where G is the Newton constant, m is the proton mass, and R is the observed radius of the universe. This relation was already known as a numerical coincidence [2]. Inserting experimental values, one gets $\alpha \cong h$, i.e. the Planck action constant. We have generalized this approach by introducing and computing the minimal unit of action for the generic constituent of any bound classical system [3]. These systems, with N elementary constituents, are described by a classical, overall attractive law of force $F(R)$. By introducing the mass m of an elementary constituent, its mean global velocity $v = R/\mathcal{T}$, and a time scale τ , to be determined, we define the minimal action per particle as $\alpha \cong mv^2\tau$. Now, a natural criterion of stability for classical bound systems (virial theorem) requires that, on average, the potential energy of a particle must be of the same order of magnitude of its kinetic energy. Then, if \mathcal{L} denotes the mean characteristic work performed on a generic constituent, one has to impose that $\mathcal{L} \cong mv^2$. On the other hand, $\mathcal{L} \cong NF(R_m)R_m \cong NF(R)R$ where R_m denotes some mean scale of length, which is obviously of the same order of magnitude of the dimension R . We can put together these definitions to obtain, for the minimal unit of action per particle, the relation: $\alpha \cong m\sqrt{NF(R)R}m^{-1}\frac{\tau}{\mathcal{T}} = m^{1/2}R^{3/2}\sqrt{F(R)}\frac{\tau}{\mathcal{T}}\sqrt{N}$. The fluctuative hypothesis of Calogero can be immediately derived by imposing a further criterion of stability, that the minimal action per particle be independent of N . The general form of the minimal action per particle follows:

$$\alpha \cong m^{1/2}R^{3/2}\sqrt{F(R)}. \quad (2)$$

It is essential to stress that the overall law of force $F(R)$ can be associated to any known interaction, also of nongravitational nature. The original scheme of Calogero is of course recovered in the gravitational case.

III. TWO PARADIGMATIC EXAMPLES: ELECTROMAGNETIC SYSTEMS AND GALAXIES

Electromagnetic interactions range, to form bound systems, from the microscopic scale ($\cong 10^{-8}$ cm, atoms) to the intermediate scales ($\cong 10^{-4}$ cm, large molecules), up to the

macroscopic scales (macrocrystals). Screening, photoemission, and absorption effects are accounted for by including the velocity of light c in the laws of force, and by considering combinations of powers of e , m , R , and c , with the other exponents parametrically dependent on γ , the exponent of c : $F(e, m, R, c^\gamma) = (e^2)^{a(\gamma)} m^{b(\gamma)} R^{d(\gamma)} c^\gamma$. For the value $\gamma = 0$ one recovers the Coulomb law in vacuum. Negative values of γ define screened Coulomb forces, which decay faster than R^{-2} . Some examples can be given. a) $\gamma = -1$: in this case $F = e^3 m^{-1/2} c^{-1} R^{-5/2}$; then, the minimal action per particle, from Eq. (2), is $\alpha = m^{1/4} e^{3/2} c^{-1/2} R^{1/4}$. Due to the exponent 1/4 the variation of R over a wide range of values does not modify the result $\alpha \cong h$; the equality is optimized for $R \cong 10^{-4}$ cm (large molecules and molecular clusters). b) $\gamma = -2$: in this case $F = e^4 m^{-1} c^{-2} R^{-3}$ (dipolar interactions, responsible for the binding of molecular crystals). This yields a minimal unit of action $\alpha = e^2 c^{-1}$, independent of R . This fact signals the absence of a specific dimension of stability, since molecular crystals can exist on very different scales of length. Furthermore, the action turns out to be the product $\hbar \alpha_{em}$, where α_{em} is the electromagnetic fine structure constant. Our scheme can be tested in the case of electromagnetic aggregates, whose dynamics is studied in the framework of classical mechanics, for instance charged plasmas, and charged beams in particle accelerators. In the first case, we consider the plasma oscillations, which are described by an effective harmonic force $F = -k_p x$, where x is the displacement inside a double layer of opposite charges. In Ref. [3], we have obtained, for a large class of laboratory controlled plasmas, that the minimal unit of action, Eq. (2), coincides with the Planck action constant. In Ref. [3], we have also considered charged beams in particle accelerators. The latter are kept in a stable state by applying external electromagnetic fields, and by pumping energy from RF cavities. In the comoving frame, one considers the transverse oscillations with respect to the ideal, synchronous orbit. The effective binding force is given, in first approximation, by $F = -k_b x$, where x is the transverse displacement. We have then $\alpha \cong m^{1/2} k_b^{1/2} R^2$, with m the mass of the particles (protons or electrons), and R the transverse dimension of the beam. Taking the most recent experimental data [4], we have that for the Hera proton accelerator $k_b \cong 10^{-9}$ g · sec⁻², $R \cong 10^{-5}$ cm, while for the electron linear collider $k_b \cong 10^{-8}$ g · sec⁻², $R \cong 10^{-5}$ cm. In both cases we get, from Eq. (2), the Planck action constant [5]. Finally, we review the case of galaxies, which are systems that reach stability on proper, characteristic geometric dimensions. The most recent cosmological data [6], give that: the energy per unit of mass is of the order 10^{15} (cm/sec)²; the period of a galactic rotation, is of the order $T_{rot} \cong 10^{15}$ sec; the total mass of a typical galaxy is of the order $M \cong 10^{44}$ g; finally, the total number of nucleons in a galaxy is $N \cong 10^{68}$. Introducing these numbers in Eq. (1), we get, up to at most an order of magnitude, that the minimal unit of action is of the order of the Planck action constant also for nucleons in a galaxy [7]. A micro-macro bridge, analogous to Eq. (1) for actions, can be also imposed for lengths in the form:

$$R \cong \lambda_c \sqrt{N}, \quad (3)$$

where R is the geometrical radius of a typical galaxy, and $\lambda_c = h/mc$ is the Compton wavelength of the proton. Inserting data, we obtain $R \cong 10^{21}$ cm \simeq 1kpc, which coincides with the observed order of magnitude of the galactic radii. It is remarkable that the result (3) can be also obtained working in the standard picture of a galaxy made up of stars, by exploiting a further scaling law in the following way. Let us introduce the number N_s of

stars contained in a typical galaxy, the number N_{ns} of nucleons in a star, and the obvious relation $N \cong N_s N_{ns}$ for the total number of nucleons in a typical galaxy. The following chain of equalities holds:

$$R \cong \lambda_c \sqrt{N} \cong \frac{h}{mc} \sqrt{N_s N_{ns}} \equiv \frac{h N_{ns}^{3/2}}{(m N_{ns})c} \sqrt{N_s} \cong \lambda_s \sqrt{N_s}, \quad (4)$$

where $\lambda_s \cong A_s/Mc$, with $A_s \cong h N_{ns}^{3/2}$, and $M = m N_{ns}$ (the total mass of the star). The length $\lambda_s \cong 10^{15}$ cm coincides with the typical range of interaction for a star. Therefore, the conceptual scheme remains unaltered by identifying, on each scale of length, the proper constituents and their characteristic dimensions.

IV. CONCLUSIONS

We have introduced a general scheme to compute the order of magnitude of a suitably defined minimal unit of action for the particles forming complex macroscopic systems. We have shown that this action is always of the order of magnitude of the Planck action constant, irrespective of the nature of the interactions and of the systems considered. Our scheme allows to introduce phenomenological scaling laws and micro-macro connectivity factors, showing a not negligible role played by quantum mechanics in determining the typical dimensions of macroscopic stable systems.

V. REFERENCES

1. F. Calogero, Phys. Lett. **A 228**, 335 (1997).
2. S. Weinberg, *Gravitation and Cosmology: Principles and Applications of the General Theory of Relativity* (Wiley, New York, 1972).
3. S. S. De Martino, S. De Siena and F. Illuminati, Physica **A** (1999), in press.
4. A.A. V.V., *Review of Particle Physics*, Phys. Rev. **D 54**, 1 (1996).
5. N. Cufaro Petroni, S. De Martino, S. De Siena, and F. Illuminati, in *Quantum Aspects of Beam Physics*, Pisin Chen (ed.) (World Scientific, Singapore, 1999).
6. J. Binney and S. Tremaine, *Galactic Dynamics* (Princeton University Press, Princeton, 1987).
7. S. Capozziello, S. De Martino, S. De Siena, and F. Illuminati, *Quantum Signature of Large Scale Cosmological Structures*, to appear in the Proceedings of the Workshop "The Chaotic Universe", Rome, February 1999.

Description of Quantum Systems by Random Matrix Ensembles of High Dimensions

Maciej M. Duras

Institute of Physics, Cracow University of Technology, ulica Podchorążych 1, 30-084 Cracow, Poland

Abstract

The new Theorem on location of maximum of probability density functions of dimensionless second difference of the three adjacent energy levels for N -dimensional Gaussian orthogonal ensemble $GOE(N)$, N -dimensional Gaussian unitary ensemble $GUE(N)$, N -dimensional Gaussian symplectic ensemble $GSE(N)$, and Poisson ensemble PE , is formulated: *The probability density functions of the dimensionless second difference of the three adjacent energy levels take on maximum at the origin for the following ensembles: $GOE(N)$, $GUE(N)$, $GSE(N)$, and PE , where $N \geq 3$.* The notions of *level homogenization with level clustering* and *level homogenization with level repulsion* are introduced.

Many complex N -level quantum systems exhibiting universal behaviour depending only on symmetry of Hamiltonian matrix of the system are divided into: Gaussian orthogonal ensemble $GOE(N)$, or Gaussian unitary ensemble $GUE(N)$, or Gaussian symplectic ensemble $GSE(N)$. The Gaussian ensembles are used in study of quantum systems whose classical-limit analogs are chaotic. The Poisson ensemble PE (Poisson random-sequence spectrum) is composed of uncorrelated and randomly distributed energy levels and it describes quantum systems whose classical-limit analogs are integrable. The standard statistical measure is Wigner's distribution of the i th nearest neighbour spacing:

$$s_i = \Delta^1 E_i = E_{i+1} - E_i, \quad i=1, \dots, N-1. \quad (1)$$

For i th second difference (the i th second differential quotient) of the three adjacent energy levels:

$$\Delta^2 E_i = \Delta^1 E_{i+1} - \Delta^1 E_i = E_i + E_{i+2} - 2E_{i+1}, \quad i=1, \dots, N-2, \quad (2)$$

we calculated distributions for $GOE(3)$, $GUE(3)$, $GSE(3)$, and PE Refs [1–3].

We formulate the following

Theorem: *The probability density functions of the dimensionless second difference of the three adjacent energy levels take on maximum at the origin for the following ensembles: $GOE(N)$, $GUE(N)$, $GSE(N)$, and PE , where $N \geq 3$.*

We present the idea of proof. For Gaussian ensembles it can be shown that second difference distributions are symmetrical functions for $N \geq 3$. Hence, the first derivatives of the distributions at the origin vanish. For Poisson ensemble the second difference distribution is Laplace one for $N \geq 3$. Therefore, the distribution takes on maximum at zero.

The inferences are the following:

1. The quantum systems show tendency towards the homogeneity of levels (equal distance between adjacent levels). We call it *homogeneization of energy levels*.
2. There are two generic homogeneizations: the first is typical for Gaussian ensembles, the second one for Poisson ensemble. For the former ensembles we define *level homogenization with level repulsion* as follows. Energy levels are so distributed that the situation that both the spacings and second difference vanish:

$$\Delta^2 E_i = s_i = s_{i+1} = 0, \quad (3)$$

is the most probable one. For the latter ensemble *level homogenization with level clustering* is described below. Now it is the most probable that only the second difference is equal to zero but the two nearest neighbour spacings are nonzero:

$$\Delta^2 E_i = 0, s_i = s_{i+1}, s_i \neq 0. \quad (4)$$

3. The assumption of non-zero value by the second difference is less probable than the assumption of zero value. Equivalently, the inequality of the two nearest neighbour spacings is less probable than their equality.
4. The predictions of the Theorem are corroborated by numerical and experimental data Refs [1–3].

The theorem could be extended to other ensembles, *e.g.* circular ones, and it is a direction of future development.

We present on Fig. 1 the second difference probability densities for Gaussian and Poisson ensembles. On Figs 2, 3 we depict comparison between second difference probability densities and experimental nuclear data of ^{181}Ta and ^{167}Er belonging to chaotic systems. We plot these comparison for random sequence spectrum on Fig. 4. Finally, we show it for simulation of GOE(2000) on Fig. 5.

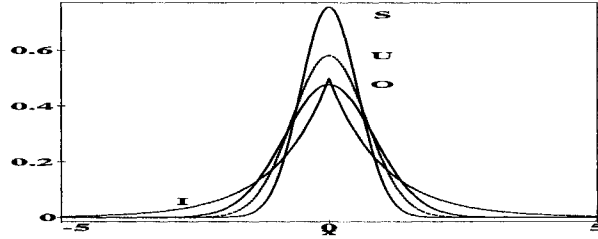


FIG. 1. The probability density function of the dimensionless second difference for Poisson ensemble (P: medium dashed line), for GOE(3) (O: solid line), for GUE(3) (U: medium dashed line), and for GSE(3) (S: short dashed line). The value of x is the ratio of second difference to the mean spacing for GOE(3), GUE(3), GSE(3), and Poisson ensemble, respectively.

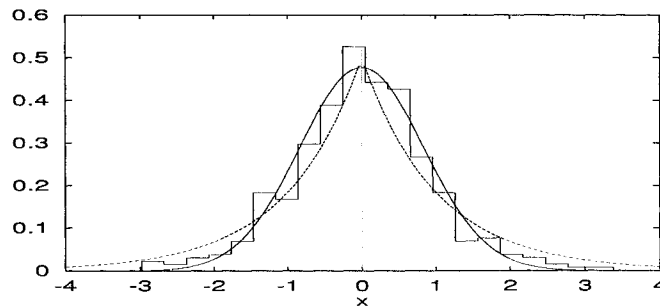


FIG. 2. The probability density function of the second difference for GOE(3) (solid line), for Poisson ensemble (dashed line), and for ^{181}Ta (histogram).

REFERENCES

- [1] M. M. Duras and K. Sokalski, *Phys. Rev. E* **54**, 3142 (1996).
- [2] Maciej M. Duras, *Finite difference and finite element distributions in statistical theory of energy levels in quantum systems*, Ph. D. thesis, Jagellonian University, Cracow, July 1996.
- [3] M. M. Duras and K. Sokalski, *Physica* **D125**, 260 (1999).

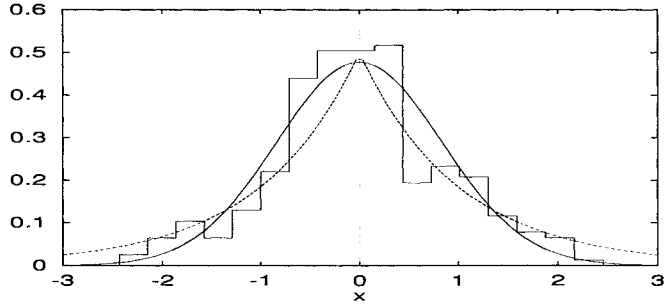


FIG. 3. The probability density function of the second difference for GOE(3) (solid line), for Poisson ensemble (dashed line), and for ^{167}Er (histogram).

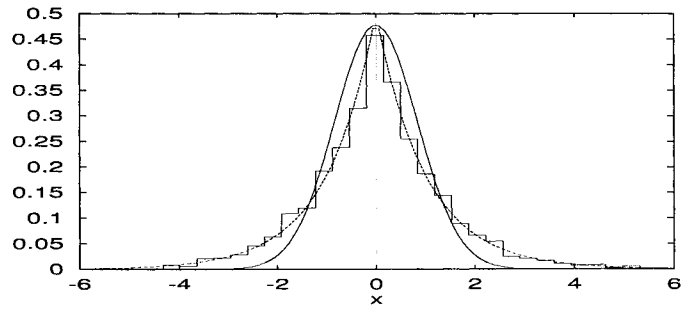


FIG. 4. The probability density function of the second difference for GOE(3) (solid line), for Poisson ensemble (dashed line), and for random-sequence spectrum (histogram).

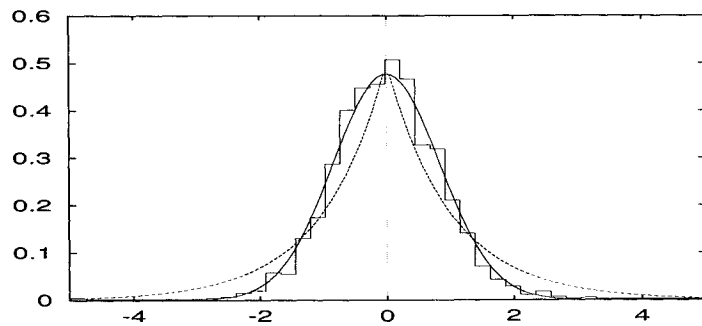


FIG. 5. The probability density function of the dimensionless second difference for GOE(3) (solid line), for Poisson ensemble (dashed line), and for GOE(2000) (histogram).

Quantum-like Description of Charged Particles Traps*

R. Fedele¹, G. Gorini², G. Torelli², D. Zanello³

¹*Dipartimento di Fisica dell'Università "Federico II" di Napoli and INFN, Sezione di Napoli, Italy*

²*Dipartimento di Fisica dell'Università di Pisa and INFN, Sezione di Pisa, Italy*

³*INFN, Sezione di Roma, Italy*

Abstract

This paper reports the results of the application of the Thermal Wave Model (TWM) to the trap dynamics. In particular TWM has been applied to the proposed set-up of the ATHENA experiment to study the trapping conditions that maximize the antiprotons - positrons overlap in the nested trap.

I. INTRODUCTION

Since the first Fedele's presentation in an academic course in Pisa, we were fascinated by the TWM which allowed to write directly an equation for the square root of the beam density, i.e. for the beam envelope, in contrast to the standard single particle approach which forces to look at the phase-space dynamics to get information about the beam envelope. Moreover in the TWM the only crucial condition is the validity of the paraxial approximation. The TWM seems to be the right approach for an unitary reformulation of the accelerator theory, since the model has been recently improved to include non Hamiltonian forces and change in the beam emittance [1,2].

A second reason of interest was the possibility to apply this approach to bunches of charged particles confined in Penning or Pauli traps, the two most used trap structures to measure quantities relevant for the fundamental physics. A set of coaxial electrodes held to suitable DC potentials and immersed in an axial uniform magnetic field constitutes the Penning trap. In the Pauli trap the magnetic field is replaced by suitable RF potentials added to the DC potentials. The time evolution and the equilibrium conditions of a few particles can be studied by means of classical mechanics (quantum effects are usually not relevant), while statistical mechanics is needed when the bunch density approaches the plasma limit.

*Talk presented by G. Torelli

We thought that the TWM could be very useful to study complex situations in these traps, like mixed bunches of positive and negative particles, time or space modulated magnetic field and so on. As a matter of fact we obtained, by means of the TWM [3], the same results of the standard statistical mechanics [4] for the radial density distribution of bunches of charged particles either when the Debye length is much larger (low density) or when it is much shorter (high density) than the bunch dimensions. Since we are interested in the antihydrogen formation at rest in the lab, we included this powerful tool as a new weapon to study the trap dynamics in the ATHENA experiment.

II. THE ATHENA EXPERIMENT

ATHENA [5] is looking at the antihydrogen formation in a trap containing a mixed plasma of antiprotons and positrons. The basic formation process is the radiative recombination, with a rate Γ depending linearly on the positron density and inversely on the positron velocity. Therefore the ATHENA setup has been designed to confine a bunch containing a relevant number of antiprotons overlapping, at least partially, a dense positron bunch at very low temperature.

The set-up is a long array of cylindrical electrodes immersed in a coaxial magnetic field, which provides for the radial confinement of both particles. By acting on the longitudinal distribution of the electrodes potentials positive and negative particle bunches can be confined in different sectors of the array or moved from one sector to another. The section devoted to the recombination process consists of five electrodes which can be connected to DC potentials to form two external traps for antiprotons and a central trap for positrons. If the antiprotons energy is high enough a fraction of them will move through the central trap and will be mixed with the positrons at any time (nested trap).

We applied the TWM formalism to evaluate the efficiency of the antiproton-positron overlap in the nested trap and in this paper we present the first results of the calculations.

III. NESTED TRAP

The fraction of antiprotons overlapping the positron plasma can be derived by a simple integration from the antiprotons axial density function. Using the TWM the axial density function can be calculated solving an unidimensional Schroedinger-like equation with the proper potential distribution. The real axial distribution of the potential due to the five electrodes can be quite well approximated by two symmetric parabolas matched to a central one, oriented in the opposite way (see fig. 1), by imposing the continuity-condition for $U(x)$ and for its derivative at $\mp \bar{x}$, where the concavity of the resultant function changes. Due to the symmetry of the system around the central point it is sufficient to describe the potential function $U(x)$ only on the positive x axis. We can define an "internal region" (labeled 2) for $0 \leq x \leq \bar{x}$ and an "external region" (labeled 1) for $\bar{x} \leq x \leq \infty$:

$$U(x) = \begin{cases} U_1(x) \equiv \frac{1}{2} k_1 (x - x_0)^2 & \bar{x} \leq x \leq \infty \\ U_2(x) \equiv -\frac{1}{2} k_2 x^2 + \frac{1}{2} \frac{k_1 k_2}{k_1 + k_2} x_0^2 & 0 \leq x \leq \bar{x} \end{cases}$$

where k_1 , k_2 and x_0 are positive constants, k_1 and k_2 being the absolute values of the quadrupole-like strengths and x_0 being the absolute value of x where $U(x)$ has the minimum. It turns out to be $\bar{x} \equiv k_1 x_0 / (k_1 + k_2)$. The barrier height that the particles see is $\Delta U \equiv |U_{max} - U_{min}| = \frac{1}{2} \frac{k_1 k_2}{k_1 + k_2} x_0^2$.

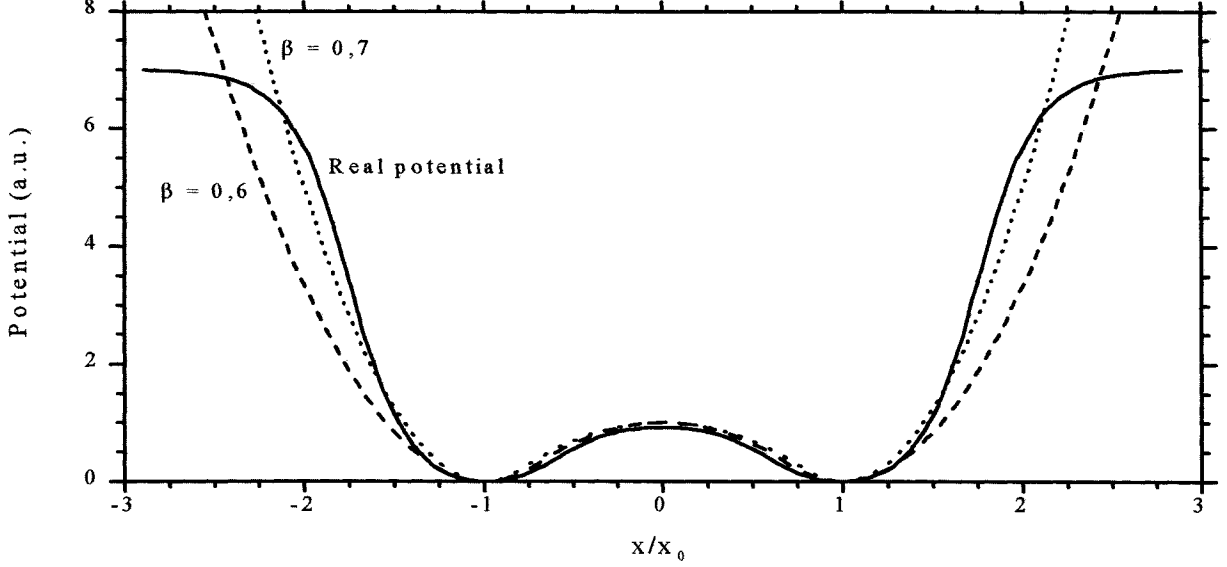


FIG. 1. Comparison between model and real potential for a 5 electrodes nested trap. $\beta = \frac{\bar{x}}{x_0}$

The Schroedinger-like equation is:

$$i\epsilon \frac{\partial \Psi}{\partial s} = - \frac{\epsilon^2}{2} \frac{\partial^2 \Psi}{\partial x^2} + U(x)\Psi$$

where $|\Psi(x, s)|^2 \equiv n(x, s)$ gives the number density along x at each time $t = s/c$, and ϵ is the beam emittance. ϵ is related to the bunch temperature as $\frac{\epsilon^2}{4\sigma_0^2} = \frac{k_B T_p}{mc^2} = \frac{v_{th}^2}{c^2}$ [6], where k_B is the Boltzmann constant, m is the particle rest mass, σ_0 is the r.m.s. particle space distribution, and v_{th} is the thermal velocity. Since the potential is time independent the spatial equation can be solved in semiclassical approximation to obtain for $n(x, s)$:

$$n_1(x, s) = A \exp \left[-\frac{2\sigma_0^2 k_1}{\epsilon^2} (x - x_0)^2 \right] \quad n_2(x, s) = A \exp \left[-\frac{2\sigma_0^2 k_2}{\epsilon^2} (-x^2 + \bar{x}x_0) \right]$$

where the constant A has to be determined by the normalization condition

$$\int_{-\infty}^{\infty} |\Psi(x, s)|^2 dx = \int_{-\infty}^{\infty} n(x, s) dx = N$$

N being the total particle number.

If, as a first approximation, we assume that the positron plasma covers the entire "internal" region ($-\bar{x} \leq x \leq +\bar{x}$), the fraction of antiprotons overlapping the positrons is given by:

$$R_o = \frac{N_2}{N_1 + N_2} = \frac{2 \int_0^{\bar{x}} n_2(x) dx}{2 \int_0^{\bar{x}} n_2(x) dx + 2 \int_{\bar{x}}^{\infty} n_1(x) dx}$$

If we measure the lengths in units of x_0 , the energy in units of ΔU and describe the potential shape through $\frac{\bar{x}}{x_0}$ we obtain:

$$R_o = \frac{N_2}{N_1 + N_2} = \frac{\exp(-\frac{1}{\alpha})\sqrt{\beta} \int_0^{\bar{y}_2} \exp y^2 dy}{\exp(-\frac{1}{\alpha})\sqrt{\beta} \int_0^{\bar{y}_2} \exp y^2 dy + \sqrt{1-\beta} \int_{\bar{y}_1}^{\infty} \exp -y^2 dy}$$

where $\alpha = \frac{k_B T_p}{m_p c^2}$, $\beta = \frac{\bar{x}}{x_0}$, $\bar{y}_1 = -\sqrt{\frac{1-\beta}{\alpha}}$ and $\bar{y}_2 = \sqrt{\frac{\beta}{\alpha}}$. In Fig. 2 R_o is plotted versus α for different values of β .

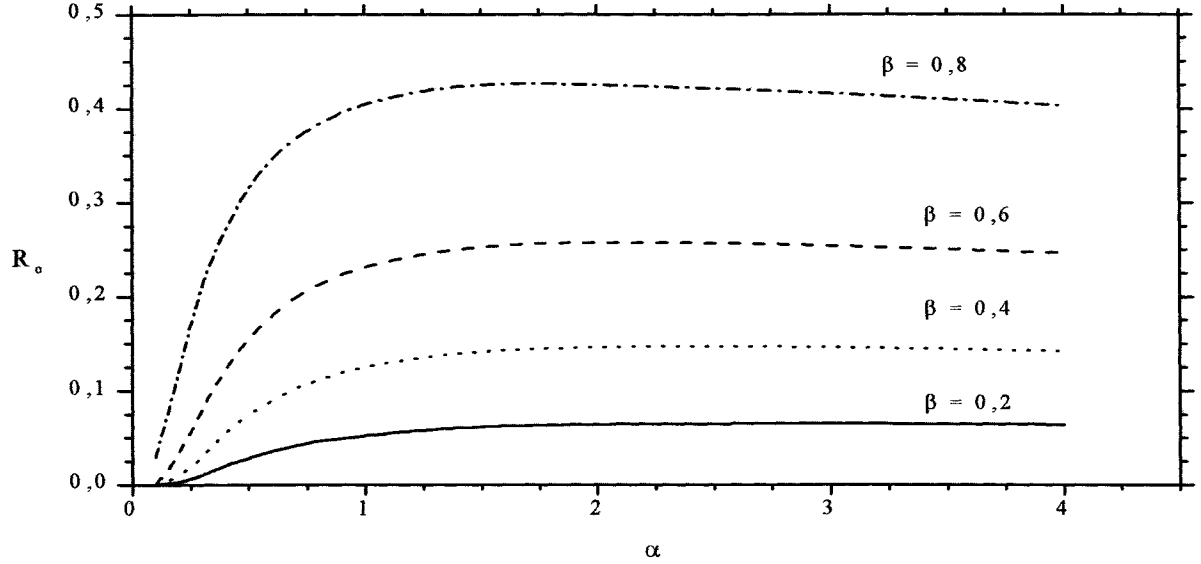


FIG. 2. R_o as a function of α for different values of β

This first approximation shows that with a reasonable choice of β (around 0.6) and for an antiproton thermal energy of the order of magnitude of ΔU about 20 percent of the antiprotons are permanently mixed to the positron plasma and can therefore form antihydrogen. As a matter of fact the efficiency of the nested trap is given by the fraction of antiprotons overlapping the positron plasma, whose length depends on the positrons energy. Calculations are in progress to take into account this correction, which anyway seems to be reasonably small, thus confirming this first positive indication on the efficiency of the nested trap.

REFERENCES

- [1] R. Fedele, G. Miele and L. Palumbo, Phys. Lett. A **194**, 113 (1994).
- [2] S. De Nicola, R. Fedele and V.I. Man'ko, *Quantum like description of a dissipative charged particle fluid in a quadrupole*, these proceedings.
- [3] R. Fedele, R. Poggiani, and G. Torelli, in *Cristalline Beams and Related Issues*, D.M. Maletić and A.G. Ruggiero eds. (World Scientific, Singapore, 1996), pag. 393.
- [4] T.M. O'Neil and C.F. Driscoll, Phys. Fluids **22**, 266 (1979).
- [5] M.H. Holzscheiter et al., Hyperfine interactions **109**, 1 (1997).
- [6] R. Fedele and V.I. Man'ko, Phys. Rev. E **58**, 992 (1998).

Can the charged-particle beam diffusion be described in terms of a diffraction-like process?

R. Fedele

*Dipartimento di Scienze Fisiche, Università
"Federico II" and INFN, Napoli, Italy
Email: renato.fedele@na.infn.it*

A.N. Lebedev, V.I. Man'ko

*P.N. Lebedev Physical Institute, Moscow, Russia
Email: manko@na.infn.it*

L. Palumbo

*Dipartimento di Energetica, Università
"La Sapienza", Roma and INFN-LNF, Frascati, Italy
Email: lpalumbo@frascati.infn.it*

Abstract

We try to deep the concept of diffusion of a charged-particle beam travelling in vacuo. We show that the usual diffusion equation for a given diffusion coefficient (which here is represented by the beam emittance ϵ is not capable of reproducing the envelope motion of the beam. However, under the substitution $\epsilon \rightarrow i\epsilon$, the envelope equation becomes the right one. It results that, according to the experimental results, the above diffusion equation is transformed in a Schrödinger-like equation which explains exactly the beam motion in vacuo with the thermal spreading.

Let us consider a charged-particle beam travelling along the z -axis, and suppose that the beam is relativistic but manifests a transverse thermal spreading which corresponds to a transverse thermal velocity v_{th} much smaller than the speed of light c : $v_{th} \ll c$. In this condition, the beam motion is paraxial. This physical circumstance can be also described saying that the electronic-ray slopes with respect to z are very small. Considering for simplicity a 2-D beam (i.e. with only one transverse extension along, say, x -axis), the paraxial approximation can be written as $dx/dz \ll 1$, where x is the transverse ray location. Let us denote with $p \equiv dx/dz$ the ray slope. Thus x and p constitute a pair of canonical conjugate variables [1,2]. The transverse behavior (diffusion) can be now described statistically by the first- and the second-order moments of the classical phase-space

distribution function $\rho(x, p, z)$ for the electronic rays [3]. In particular, with the second-order moments, $\sigma_x(z) \equiv \langle (x - \langle x \rangle)^2 \rangle$ (beam width or r.m.s. dispersion in the electronic-ray transverse position), $\sigma_p(z) \equiv \langle (p - \langle p \rangle)^2 \rangle$ (r.m.s. dispersion in the electronic ray slopes), and $\sigma_{xp} \equiv \langle (x - \langle x \rangle)(p - \langle p \rangle) \rangle$ (electronic-ray correlation term), we can define the diffusion coefficient ϵ as [4,5]: $\epsilon^2 \equiv 4 \left[\sigma_x^2(z)\sigma_p^2(z) - \sigma_{xp}^2(z) \right]$, which is called *r.m.s. transverse emittance of the beam* [2]. Since the beam is in vacuo, it is well known that ϵ is an invariant [2]. Furthermore, it is possible to show that during the beam motion $\sigma_x(z)$ satisfies to the following envelope equation :

$$\frac{d^2\sigma_x}{dz^2} - \frac{\epsilon^2}{4\sigma_x^3} = 0 \quad . \quad (1)$$

Eq.n (1), which is in full agreement with the experimental observations concerning with the beam propagation in vacuo (f.i., in a final stage of a linear collider) [6], characterizes the behaviour of the beta-function defined as: $\beta(z) \equiv \sigma_x^2(z)/\epsilon$. At this point we are ready to formulate the following question: *Can this diffusion be described, for a given ϵ , with the following diffusion equation:*

$$\frac{\partial f}{\partial z} = \frac{\epsilon}{2} \frac{\partial^2 f}{\partial x^2} \quad , \quad (2)$$

which is written for a probability density distribution $f(x, z)$ in the configurational x -space and giving the experimentally correct envelope equation (1)? In order to give an answer, we observe that, for a Gaussian initial condition of f , (2) has the following non-stationary normalized solution:

$$f(x, z) = \frac{1}{\sqrt{2\pi}\sigma_f(z)} \exp \left[-\frac{(x - \langle x \rangle)^2}{2\sigma_f^2(z)} \right] \quad , \quad (3)$$

where $\sigma_f^2(z)$ satisfies to the following equation: $d\sigma_f^2/dz = \epsilon$, which can be cast in the form

$$\frac{d^2\sigma_f}{dz^2} + \frac{\epsilon^2}{4\sigma_f^3} = 0 \quad . \quad (4)$$

Note that (4) does not coincide with (1). Thus, taking for (1) and (4) the same initial conditions, namely:

$$\sigma_f(z = z_0) = \sigma_x(z = z_0) \equiv \sigma_0 \quad , \quad \left(\frac{d\sigma_f}{dz} \right)_{z=z_0} = \left(\frac{d\sigma_x}{dz} \right)_{z=z_0} \equiv \sigma'_0 \quad , \quad (5)$$

they do not give the same solution. In fact, the envelope equation (1) gives the following solution: $\sigma_x^2(z) = 2\mathcal{E}(z - z_0)^2 + \sigma_0^2$, where $2\mathcal{E} \equiv \epsilon^2/4\sigma_0^2 + (\sigma'_0)^2 > 0$, whilst the envelope equation (4) gives $\sigma_f^2(z) = \sigma_0^2 + \epsilon(z - z_0)$. An important difference between these two solutions is that to determine the latter only the first of (5) is necessary, whilst to determine the former both of (5) are necessary. Another important difference is that, since $\sigma_0 > 0$, for finite emittance ϵ there exist a finite z , say \bar{z} , for which solution of (4) gives the collapse of the beam ($\sigma_f(z = \bar{z}) = 0$, with $\bar{z} = z_0 - \sigma_0^2/\epsilon$). On the other hand, solution of (1) does not predict any collapse (note that $\sigma_x \geq \sigma_0$, for any real z), according to what experimentally

happens in vacuo for finite emittances. We conclude that, even if (2) is a diffusion equation, it does not describe correctly the thermal spreading among the electronic rays in vacuo. The crucial point of this problem is just connected with the fact that to give solution of (1) we need two conditions: one related with the distribution of the transverse electronic ray locations, $\sigma_0\sigma'_0$ included in the initial condition that has given solution (3). Consequently: (i) the parabolic equation (2) is not suitable to describe our beam transport problem; (ii) we need to include in the present diffusion problem the information related to the electronic-ray slope distribution.

In order to include the above second information, we can reasonably keep again a parabolic equation. To understand how to modify the parabolic equation (2), we observe that (4) transforms into (1) by means of the formal substitution:

$$\epsilon \rightarrow i\epsilon \quad (6)$$

where i denote the imaginary unity. Correspondingly, (2) transforms into the following Schrödinger-like equation for the free space ($U = 0$):

$$i \frac{\partial \Psi}{\partial z} = -\frac{\epsilon}{2} \frac{\partial^2 \Psi}{\partial x^2} \quad , \quad (7)$$

where now, instead of f , we have the function Ψ which in principle may be complex. Let us represent Ψ in the following form:

$$\Psi(x, z) = \sqrt{n(x, z)} \exp \left[\frac{i}{\epsilon} \theta(x, z) \right] \quad , \quad (8)$$

with $\theta(x, z)$ real function and $n(x, z)$ positive and real function, satisfying the following normalization condition: $\int_{-\infty}^{\infty} |\Psi(x, z)|^2 dx = \int_{-\infty}^{\infty} n(x, z) dx = 1$. It is immediately clear, following the language of quantum mechanics, that we have now two suitable information: the transverse probability density of the electronic rays, i.e. $|\Psi(x, z)|^2$, and the transverse current velocity, i.e. $V(x, z) = \partial \theta(x, z) / \partial x$. The latter is related to the ray-slopes. In fact:

$$\langle p \rangle \equiv \int_{-\infty}^{\infty} V(x, z) n(x, z) dx = \int_{-\infty}^{\infty} V(x, z) |\Psi(x, z)|^2 dx \quad . \quad (9)$$

It is easy to see that:

$$\frac{d^2 \sigma_x}{dz^2} = 4\mathcal{E} = \text{constant} \quad , \quad (10)$$

where the constant

$$\mathcal{E} = \frac{\epsilon^2}{2} \int_{-\infty}^{\infty} \left| \frac{\partial \Psi}{\partial x} \right|^2 dx \quad , \quad (11)$$

represents the mean total energy of the electronic rays. Obviously, from (10) and (11), we obtain an envelope equation which coincides with the (1) and not with the (4).

Furthermore, it easy to see that, in correspondence to the initial condition for Ψ :

$$\Psi(x, z_0) = \sqrt{n(x, z_0)} \exp \left[\frac{i}{\epsilon} \theta(x, z_0) \right] \quad , \quad (12)$$

with $n(x, z_0) = f(x, z_0)$, and $\theta(x, z_0) = 0$, we obtain the following solution of (7):

$$\Psi(x, z) = \frac{\exp\left[-\frac{x^2}{2\sigma_x^2(z)}\right]}{\sqrt{2\pi\sigma_x^2(z)}} \exp\frac{i}{\epsilon}\theta(x, z) \quad , \quad (13)$$

where σ_x satisfies the (1) and $\theta(x, z) = x^2/2R(z) + \phi(z)$, with $1/R(z) = (1/\sigma_x(z)) (d\sigma_x(z)/dz)$, and $(d\phi/dz) = -(\epsilon/4\sigma_x(z))$. Note that, according to the definition of the current velocity, we have:

$$\frac{dV(x, z)}{dz} = \frac{x}{\sigma_x(z)} \frac{d\sigma_x(z)}{dz} \quad , \quad (14)$$

from which we clearly see that the initial condition $V(x, z_0)$ corresponds to the initial condition (5).

We can conclude that, *the parabolic diffusion equation (2) does not describe the particle beam transport in the presence of thermal spreading among the electronic rays. On the contrary, the Schrödinger-like equation (7) fully describes it.* Eq.n (7) is the starting point of the Thermal Wave Model [7].

Remarkably, the following very important consequence comes from this result. A diffusion process, like the above beam transport, can be described in the real space as a *diffraction-like beam spreading*. In fact, due to the presence of the imaginary unity i , the second derivative in (7) accounts for the quantum mechanical diffraction of a wavepacket as well as the diffraction among the light rays in an e.m. radiation beam in paraxial approximation [8]. Thus, in the real free space, the dispersion of the electronic rays seems to simulate exactly the diffraction of the light rays.

Additionally, we note that $R(z)$, defined above, plays the role of local *curvature radius* of the *wavefront* associated with the *eikonal* $\theta(x, z)$.

REFERENCES

1. P.A. Sturrock, *Static and dynamic electron optics* (Cambridge Univ. Press, Cambridge, 1955).
2. J. Lawson, *The physics of charged particle beams* (Clarendon Press, Oxford, 1988).
3. R. Fedele and V.I. Man'ko, Phys. Rev. E **58**, 992 (1998).
4. P.M. Lapostolle, IEEE Trans. Nucl. Sc. **18**, 1101 (1971).
5. F.J. Sacherer, IEEE Trans. Nucl. Sc. **18**, 1105 (1971).
6. J.J. Su, T. Katsouleas, J. M. Dawson, and R. Fedele, Phys. Rev. A **41**, 3321 (1990).
7. R. Fedele and G. Miele, Nuovo Cimento D **13**, 1527 (1991).
8. S. Solimeno, B. Crosignani, P. Di Porto, *Guiding, Diffraction and Optical Confinement of the Radiation* (Academic Press, London, 1986).

Influence of Spectral Filtering on the Quantum Nature of Light

Krista Joosten

Huygens Laboratorium, Rijksuniversiteit Leiden, Postbus 9504, 2300 RA Leiden, The Netherlands

Gerard Nienhuis

Huygens Laboratorium, Rijksuniversiteit Leiden, Postbus 9504, 2300 RA Leiden, The Netherlands

We study how the bandwidth of a spectral filter influences the spectral correlations of light from a quantum mechanical source. Generally we examine the difference between a classical and a quantum description of a Fabry-Pérot filter. Specifically we apply the results to filtered resonance fluorescence.

The actual presence of a spectral filter, for example in the form of a dielectric slab, can change the statistics of a fluctuating classical field. This was recognized in 1966 by Armstrong [1], who showed that sending laser light through a narrow spectral filter changes the statistics of the light from Poissonian to chaotic. This lead us to question, whether in the case of a quantum mechanical input field also the quantum properties of the spectral correlation function are affected by the presence of the filters. A first off-hand answer would be, that for very narrow filters all quantum properties are lost, seeing that all a spectral filter does is delaying photons for arbitrary times proportional to the inverse of the filter linewidth and thereby mixing the ordering of the photons. We will show in the following that this line of thinking is too simple.

Consider two classical stochastic light fields $E_a^{(\pm)}$ and $E_b^{(\pm)}$ where $(+/-)$ denotes the positive, resp. negative frequency part of the field. We assume that the fields are stationary. The normalized two-time correlation function of these fields is given by

$$g_2(a; b; \tau) = \frac{\langle \hat{E}_a^{(-)}(t) \hat{E}_b^{(-)}(t + \tau) \hat{E}_b^{(+)}(t + \tau) \hat{E}_a^{(+)}(t) \rangle}{\langle \hat{E}_a^{(-)} \hat{E}_a^{(+)} \rangle \langle \hat{E}_b^{(-)} \hat{E}_b^{(+)} \rangle}. \quad (1)$$

For classical fields the mean square deviation is positive, yielding

$$\langle I_a(t)^2 \rangle \geq \langle I_a(t) \rangle^2 \quad \longrightarrow \quad g_2(a; a; 0) \geq 1. \quad (2)$$

In words, the photons are bunched in time. Detecting anti-bunching of photons from a single field thus displays the quantum nature of its source. Furthermore, when we consider the correlation between two fields, Schwarz' inequality leads for classical fields to

$$g_2^2(a; b; \tau) \leq g_2(a; a; 0) g_2(b; b; 0). \quad (3)$$

When the two fields under consideration are the outputs of different spectral filters with the same input field, a violation of this inequality reveals the quantum nature of the source.

Now, using Fourier analysis we find for the spectral correlation function

$$g_2(\omega_a; \omega_b; \tau) \propto \int d\bar{t} e^{-i\omega_a(t_1-t_4)-i\omega_b(t_2-t_3)} \langle \hat{E}_a^{(-)}(t_1) \hat{E}_b^{(-)}(t_2 + \tau) \hat{E}_b^{(+)}(t_3 + \tau) \hat{E}_a^{(+)}(t_4) \rangle, \quad (4)$$

with $\int d\bar{t} = \int \int \int \int dt_1 dt_2 dt_3 dt_4$. This does not satisfy for the description of a physical filter with a finite linewidth though. Firstly the Fourier analysis only holds true for fully stationary fields and infinitely narrow spectral filters [2]. Secondly the right hand side of this equation is an observable quantity, whereas the integrand on the left hand side is not, since it also contains terms that are not ordered in time. For a correct quantum description of the output field, the radiation field needs to be quantized in the presence of the spectral filter [3]. We model the filter by a highly reflective dielectric slab. Several methods have been developed to quantize this system [3,4]. We will not give a complete derivation of the quantization procedure, but just mention the different steps in the procedure, following Knöll et al. [3].

The first step is to quantize the radiation field in the absence of a source, but in the presence of the filter. The electric field can then be written as

$$\hat{E} = \sum_{\lambda} i \sqrt{\frac{\hbar \omega_{\lambda}}{2 \epsilon_0}} \left(\vec{R}_{\lambda} \hat{a}_{\lambda} - \vec{R}_{\lambda}^* \hat{a}_{\lambda}^{\dagger} \right). \quad (5)$$

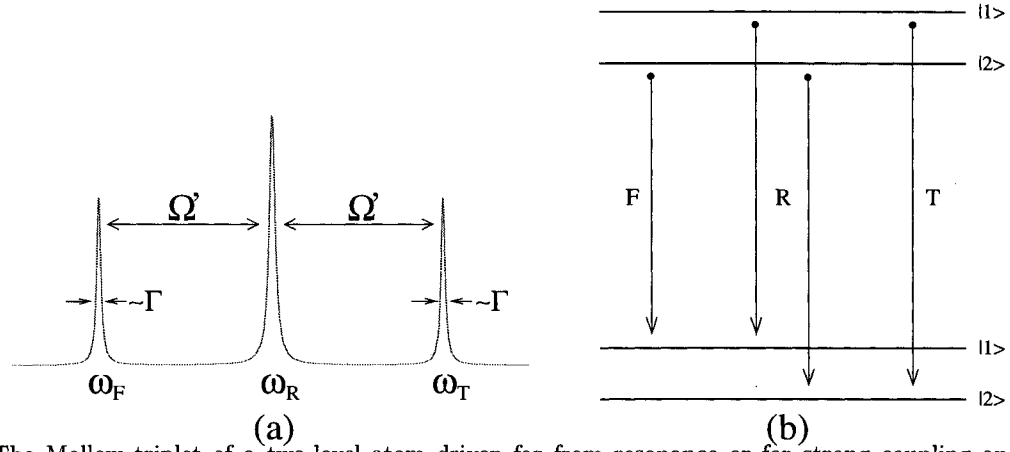


FIG. 1. (a) The Mollow triplet of a two-level atom driven far from resonance or for strong coupling and (b) its dressed eigenstates with the possible transitions for a spontaneous emission event

where $\epsilon_0\epsilon(\vec{r})$ is the dielectric constant of the medium. The operators \hat{a}_λ and \hat{a}_λ^\dagger are annihilation and creation operators that satisfy the standard commutation relations. The time evolution of \hat{a}_λ in the Heisenberg picture is as in the absence of the medium

$$\partial_t \hat{a}_\lambda = -i\omega_\lambda \hat{a}_\lambda. \quad (6)$$

The influence of the filter on the electric field is thus only via the mode functions \vec{R}_λ that are now no longer plane waves, but satisfy

$$\nabla \times (\nabla \times \vec{R}_\lambda) = \frac{\epsilon(\vec{r})\omega_\lambda^2}{c^2} \vec{R}_\lambda. \quad (7)$$

The next step is to include the source. The presence of the source will change the time evolution of the creation and annihilation operators, but not the shape of the mode functions. When the interaction Hamiltonian between the source and the radiation field is linear, the time evolution breaks up in a freely evolving part $\hat{a}_{\lambda,f}$ and a part which is driven by the source $\hat{a}_{\lambda,s}$

$$\hat{a}_\lambda(t) = \hat{a}_{\lambda,f}(t) + \hat{a}_{\lambda,s}(t). \quad (8)$$

Likewise the electric field can be written as $\hat{E}^{(+)} = \hat{E}_f^{(+)} + \hat{E}_s^{(+)}$. Though it is tempting to assume that these two parts commute, they in fact do not. In the case that the source remains evolving freely (this can be established by placing the filter under a slight angle so that no light is reflected back unto the source) we find for g_2 of the output of two filters a and b with frequency setting $\omega_{a,b}$ and linewidth λ

$$g_2(a, \omega_a; b, \omega_b; \tau) \propto \int d\vec{\ell} \lambda^4 e^{-\lambda(t_1+t_2+t_3+t_4)+i\omega_a(t_1-t_4)+i\omega_b(t_2-t_3)} \langle T^{(-)} \left(\hat{S}^{(-)}(-t_1) \hat{S}^{(-)}(\tau-t_2) \right) T^{(+)} \left(\hat{S}^{(+)}(\tau-t_3) \hat{S}^{(+)}(-t_4) \right) \rangle. \quad (9)$$

In this expression $T^{(+)}$ orders the following operators downward in time, $T^{(-)}$ orders them upward in time. This is equivalent to the classical description of the correlation function except for the time ordering in the integrand.

Let us consider resonance fluorescence of a two-level atom driven by a monochromatic field at frequency ω as input for the filters. We assume that the ground and the excited state are non-degenerate and separated in energy by $\hbar\omega_0$. When the detuning $\Delta = \omega - \omega_0$ is large or the coupling Ω is strong, the spectrum is the well-known Mollow triplet (see Fig. 1). Its three components can be easily understood in terms of the ladder of its dressed states $|1\rangle$ and $|2\rangle$, which are mixtures of the state of the radiation field and the state of the atom and are separated in energy by $\hbar\Omega'$ with $\Omega' = \sqrt{\Delta^2 + \Omega^2}$ (see Fig. 1). A spontaneous emission event corresponds to a transition between two successive steps in this ladder. Three transitions with different frequencies are possible. For positive detuning the fluorescence band F has the lowest center frequency, $\omega_F = \omega - \Omega^{prime}$, the middle or Rayleigh band R has a frequency equal to the pump field $\omega_R = \omega$ and the three photon band T has the highest center frequency, $\omega_T = \omega + \Omega^{prime}$. From the ladder of states we see, that the T and F photons alternate in time. The photons within a side band thus violate inequality (2) and the correlation of photons between the two side bands violates inequality (3).

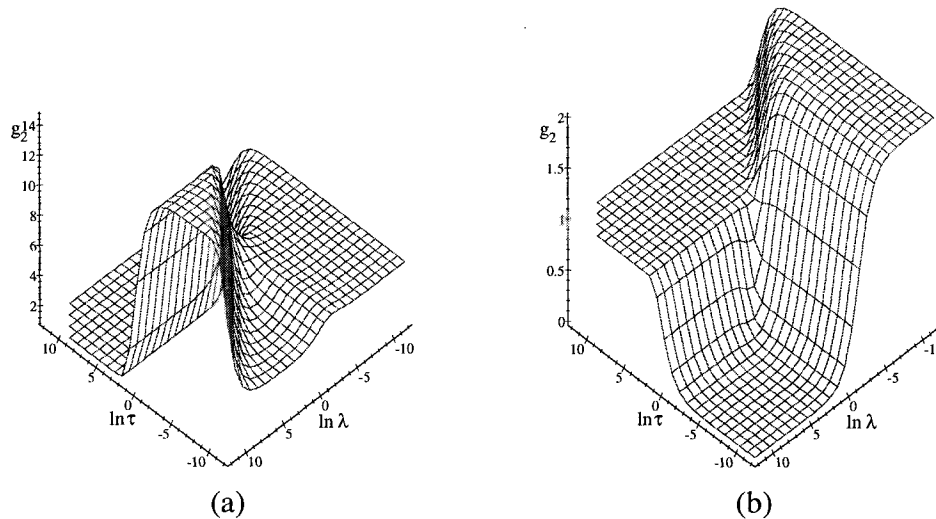


FIG. 2. The spectral correlation functions within and between two side bands plotted against the logarithm of the waiting time τ (in unities Γ^{-1}) and logarithm of the linewidth λ of the filter (in unities Γ) at $\Delta/\Omega = 0.7$. In (a) $g_2(T, \omega_T + \delta; F, \omega_F + \delta; \tau)$ is plotted and in (b) $g_2(T, \omega_T + \delta; T, \omega_T + \delta; \tau)$.

We now have all the ingredients to study the effects of the presence of a spectral filter on the quantum nature of light. The correlation function can be calculated analytically. The resulting expressions however, are in general ill-digested except for the limits where the filter covers a full band ($\lambda \gg \Gamma$) or where the filter is very narrow ($\lambda \ll \Gamma$). For this reason we refrain from giving the analytical expressions, but present the results as Maple plots of g_2 as functions of the waiting time τ and λ (see Fig. 2). For both plots, the two horizontal axes are on a logarithmic scale and λ , τ are given in unities Γ , resp. Γ^{-1} . We have taken $\lambda \ll \Omega'$, so that a filter covers one band at most. The first thing one notices, is that the spectral correlation function depends on the linewidth of the filter. For large filter linewidth and short waiting times the plots show the alternating behaviour of T and F photons: in Fig. 2 (b) $g_2 = 0$ and in Fig. 2 (a) $g_2 > 1$. In Fig. 2 (a) we furthermore see, that as $\lambda \sim \tau^{-1}$, the strength of the bunching is shifted as compared to very short waiting times. This is due to the fact that the probabilities for the transitions $|1\rangle \rightarrow |2\rangle$ and $|2\rangle \rightarrow |1\rangle$ are not equal and that in this region the order of the detection of the F/T photons is not necessarily the order in which they were emitted by the atom.

For narrow filters the anti-bunching behaviour of T photons is lost (see Fig.2 (b)), and so the quantum nature of the source is concealed as expected from our off-hand answer. However, the bunching between photons from different side bands is not lost (see Fig. 2 (a)), no matter how narrow we choose the filter: the quantum nature of the source remains observable. This result can be understood, when we realize that the action of a narrow filter on a stream of in-coming photons is not simply the mixing of these photons in time order. To be precise a filtered photon is better viewed as an average of photons entering the filter at different times, the time span of the average proportional to λ^{-1} . For short waiting times, two filtered photons are constructed from the same set of in-coming photons, so the correlation between successively emitted photons remains present.

ACKNOWLEDGMENTS

This work is part of the research programme of the Stichting voor Fundamenteel Onderzoek der Materie (FOM) which is supported by NWO.

- [1] J. A. Armstrong, *J. Opt. Soc. Am.* **56**, 1024 (1966).
- [2] J. H. Eberly and K. Wódkiewicz, *J. Opt. Soc. Am.* **67**, 1252 (1977).
- [3] L. Knöll, W. Vogel, and D. G. Welsch, *Phys. Rev. A* **36**, 3803 (1987).
- [4] R. Matloob, R. Loudon, S. M. Barnett, and J. Jeffers, *Phys. Rev. A* **52**, 4823 (1995).

p -adic classical and quantum information mechanics

Andrei Khrennikov

*Department of Mathematics, Statistics and Computer Sciences
University of Växjö, S-35195, Sweden*

Abstract

Limits of the use of the standard mathematical model of physical reality (based on the system of real numbers) are discussed. We propose a new mathematical model of physical reality based on the system of so called p -adic numbers. By this model, physical reality is information reality. Basic objects of this reality are transformers of information, basic processes are information processes.

This paper is an attempt to provide a description of reality based only on information objects (so called transformers of information). Material objects give just a particular class, M , of transformers of information. Elements of M can be represented in the real space \mathbf{R}^3 . However, the system of real numbers is a particular system for coding of information. There are many other coding systems which can be used to create new pictures of reality. If instead of the real metric we consider a new metric corresponding to the ability of cognitive systems to form associations, then we obtain systems of p -adic numbers (see, for example, [1]). On the basis of p -adic quantum mechanics we consider a pilot wave theory over information spaces. In fact, already the ordinary pilot (real) wave formalism can be interpreted in the right way only on the information basis [2]. Our general information formalism improves the ordinary pilot wave theory. It gives natural solutions for such problems as non-locality, energy balance for the pilot wave field, information character of this field.

Let us consider some system τ which has the ability to transform information. In the simplest mathematical model we can assume that information strings can be coded by sequences of digits $x = (\alpha_1, \alpha_2, \dots, \alpha_N, \dots)$, where $\alpha_j = 0, \dots, m - 1$ (here $m > 1$ is a fixed natural number). Denote the set of all information strings of this form by the symbol X_m . Suppose that the system τ has the ability to form associations. We introduce a metric ρ_m on the space of information strings X_m which describes such an ability. Let $x = (\alpha_0, \dots, \alpha_n, \dots)$ and $y = (\beta_0, \dots, \beta_n, \dots)$ be two information strings belonging to X_m . The τ 'thinks' that x and y are close with the precision $\epsilon_k = 1/m^k$ ($k = 0, 1, \dots$) if they correspond to the same association (abstract idea) $a = (a_0, \dots, a_{k-1}) : a_0 = \alpha_0 = \beta_0, \dots, a_{k-1} = \alpha_{k-1} = \beta_{k-1}$. We set $\rho_m(x, y) = \frac{1}{m^k}$ if $\alpha_j = \beta_j, j = 0, 1, \dots, k - 1$, and $\alpha_k \neq \beta_k$. This is a metric. It is called m -adic metric. A point $x = (\alpha_n)$ of X_m is identified with the expression: $x = \sum_{k=0}^{\infty} \alpha_k m^k$. We set $|x|_m = m^{-k}$ if $\alpha_j = 0, j = 0, \dots, k - 1$, and $\alpha_k \neq 0$. Then $\rho_m(x, y) = |x - y|_m$. This gives the identification of the information space X_m with the ring \mathbf{Z}_m of m -adic numbers. Therefore

it is natural to use m -adic numbers for a description of information (at least cognitive) processes. Mathematically it is convenient to use prime numbers $m = p > 1$.

We choose the space $X = \mathbf{Z}_p$ (or multidimensional spaces $X = \mathbf{Z}_p^N$) for the description of information. The X is said to be *information space*. Everywhere below we shall use the abbreviation “ I ” for the word information (for example, information space = I -space). Objects which “live” in I -spaces are said to be *transformers of information* (I -transformers). I -transformers are not characterized by localization in information p -adic space (or real space). They are characterized by the ability to transform information and form associations. In particular, the whole universe U is the great I -transformer.

Each I -transformer τ has internal clocks. A state of the clocks is described by an I -vector $t \in T = \mathbf{Z}_p$ which is called *information time*. The I -time can have different interpretations in different I -models. If τ is a conscious system then t is (self-recognized) time of the evolution of this system. We can say about psychological time of an individual or about (collective) social time of a group of individuals. In fact, we have not to image t as an ordered sequence of time counts. This is only information which describes evolution of τ . In principle, there is no direct relation between I -time and “physical” time that is used in the model over the reals. At each instant $t \in T$ of I -time there is defined a *total information state* (I -state) $q(t) \in X$ of τ . It describes the position of τ in the I -space X . The “life”-trajectory of τ can be identified with the trajectory $q(t)$ in X . We use an analogue of the Hamiltonian dynamics on the I -spaces¹. As usual, we introduce the quantity $p(t) = \dot{q}(t)$ ($= \frac{d}{dt}q(t)$) which is the information analogue of the momentum. However, here we prefer to use a psychological terminology. The quantity $p(t)$ is said to be a *motivation* (for changing of the I -state $q(t)$). The space $\mathbf{Z}_p \times \mathbf{Z}_p$ of points $z = (q, p)$ where q is the I -state and p is the motivation is said to be a phase I -space. As in the ordinary Hamiltonian formalism, we assume that there exists a function $H(q, p)$ (I -Hamiltonian) on the phase I -space which determines the motion of τ in the phase I -space:

$$\dot{q}(t) = \frac{\partial H}{\partial p}(q(t), p(t)), \quad q(t_0) = q_0, \quad \dot{p}(t) = -\frac{\partial H}{\partial q}(q(t), p(t)), \quad p(t_0) = p_0. \quad (1)$$

The I -Hamiltonian $H(p, q)$ has the meaning of an *I -energy*. In principle, I -energy is not related to the usual physical energy.

In general case the I -energy is the sum of the I -energy of motivations $H_f = \alpha p^2$ (which is an analogue of the kinetic energy) and potential I -energy $V(q)$: $H(q, p) = \alpha p^2 + V(q)$. The potential $V(q)$ is determined by *fields of information*. In the Hamiltonian framework we can consider interactions between I -transformers τ_1, \dots, τ_N . These I -transformers have the I -times t_1, \dots, t_N and I -states $q_1(t_1), \dots, q_N(t_N)$. By our model we can describe interactions between these I -transformers only in the case in that there is a possibility to choose the same I -time t for all of them. In this case we can consider the evolution of the system of the I -transformers τ_1, \dots, τ_N as a trajectory in the I -space $\mathbf{Z}_p^N = \mathbf{Z}_p \times \dots \times \mathbf{Z}_p$, $q(t) = (q_1(t), \dots, q_N(t))$.

¹In fact, this is an application to the I -theory of the Hamiltonian p -adic formalism developed in [3] (and generalized in [1]).

The above formalism of classical information mechanics can be developed to the formalism of quantum information mechanics (in fact, we need only to use the information interpretation for p -adic quantum mechanics which was developed in [1]). Here the wave function $\psi(x)$ is a function of the information variable x with information values. It is quite natural to interpret such a function as a new *information field* which is associated with an I -transformer or a group of I -transformers. Such a viewpoint to the wave function is very close to the viewpoint of D. Bohm and B. Hiley [2] on the pilot wave theory.

Let us consider a system of N I -transformers, τ_1, \dots, τ_N , with Hamiltonian $H = \sum_k \frac{p_k^2}{2m_k} + \sum_{k>i} V_{ki}(x_k - x_i)$. The wave function $\psi(t, x)$, $x = (x_1, \dots, x_N)$, $x_k \in \mathbf{Z}_p^m$ evolves according to the Schrödinger equation. Thus

$$\frac{\partial}{\partial t} \rho(t) + \sum_k \frac{\partial}{\partial x_k} j_k(x, t) = 0, \quad (2)$$

where $\rho(t, x) = \psi(t, x)\overline{\psi(t, x)}$ is a probability density on the configuration I -space \mathbf{Z}_p^{mN} and $j_k(x, t) = m_k^{-1} \text{Im}(\overline{\psi(t, x)} \frac{\partial}{\partial x_k} \psi(t, x))$. As in the ordinary Bohm's formalism, we assume that a quantum I -transformer τ_k has at any I -time well defined I -state x_k and motivation p_k . I -state x_k evolves according to

$$\dot{x}_k(t) = \frac{j_k(t, x)}{\rho(t, x)}. \quad (3)$$

We describe the work of a brain τ in the framework of the pilot-wave I -theory. The τ has an incredibly complex internal structure (see [4]) which generates a new information field given by brain's wave function $\psi(t, x)$. We claim that the field $\psi(t, x)$ induced by the brain τ is nothing than a conscious field. Thus conscious processes are quantum I -processes. A conscious (quantum) motion in phase I -space differs from an unconscious (classical) motion. This difference is due to a quantum I -potential Q . In the same way we can consider the conscious information dynamics of any group of I -transformers. It is even possible to use the wave function of the universe (conscious field of the universe).

This is the good place to discuss the problem of non-locality of the pilot wave formalism. Some authors consider non-locality as one of the main difficulties of the pilot wave formalism. However, non-locality is not a difficulty in our pilot I -wave formalism. This is non-locality in the I -space. Such non-locality can be natural for some I -systems. For cognitive systems, I -non-locality means that ideas which are separated in a p -adic space can be correlated. However, p -adic separation means only that there are no strong associations between ideas or groups of ideas. But this absence of associations does not imply that these ideas could not interact.

By our model each human society S has a wave function $\psi(t; x)$. This function gives a description of a quantum potential Q . The quantum potential can essentially change I -motions (i.e., evolutions of ideas) of individuals. Different societies are characterized by quantum potentials of different forms. This model provides an explanation of such collective phenomena as religion or political (or national) ideology.

The same considerations can be applied to animals and plants. The only difference is probably that here quantum I -potentials are not so strong. Thus we get the conclusion that there may exist a wave function $\psi_{\text{liv}}(t, x)$ of all living organisms. The wave function $\psi(t, x)_{\text{liv}}(t, x)$ can be represented in the form:

$$\psi(t, x)_{\text{liv}}(t, x) = \sum_f \psi_f(t, x), \quad (4)$$

where $\psi_f(t, x)$ is a wave function of the living form f . An observable F (a living form) can be realized as a symmetric operator in a p -adic Hilbert space, $F\psi_f = f\psi_f$, where $f \in \mathbf{Z}_p$ is the cod of the living form f in the alphabet $\{0, 1, \dots, p-1\}$. By equation (3) the evolution of the fixed form f_0 depends on evolutions of all living forms f .

The process of the evolution of living forms is not just a process based on Darwin's natural selection. This is a process of a quantum I -evolution in that the conscious field of all living forms plays the important role. This model might be used to explain some phenomena which could not be explained by Darwin's theory. For example, the beauty of colours of animals, insects and fishes could not be a consequence of the only process of the natural evolution. This is a consequence of the structure of the conscious field $\psi(t, x)_{\text{liv}}(t, x)$. By the same reasons we can explain some aspects of relations between robbers and victims. It seems that in nature there is a well organized system which gives to robbers a possibility to eat victims. This system is nothing other than a result of the evolution due to (3).

Our formalism improves the ordinary pilot wave theory. One of the delicate problems of this theory is a difference between ordinary fields and ψ -fields. There is no such a problem in the I -theory. All I -fields have no physical energy. Thus we need not discuss the energy balance for the field $\psi(t, x)$ (see [2], p.38). Of course, there is still a difference between classical and quantum rules for computing I -forces. As in the standard pilot wave theory, the increase of the (p -adic) amplitude of $\psi(t, x)$ does not imply the increase of the (p -adic) amplitude of the corresponding I -force. However, even in classical mechanics over p -adic numbers the increase of the amplitude of an I -force does not imply automatically an essential perturbation of a trajectory in phase I -space.

1. A. Yu. Khrennikov, *Non-Archimedean analysis: quantum paradoxes, dynamical systems and biological models*. Kluwer Academic Publ., Dordrecht(1997).
2. D. Bohm and B. Hiley, *The undivided universe: an ontological interpretation of quantum mechanics*. Routledge and Kegan Paul, London (1993).
3. V. S. Vladimirov, I. V. Volovich, and E. I. Zelenov, *p -adic analysis and Mathematical Physics*, World Scientific Publ., Singapore(1994).
4. Khrennikov A.Yu., *J. of Theor. Biology*, **193**, 179-196 (1998).

Classical Propagator for Quadratic Quantum Systems

Olga Man'ko

P.N. Lebedev Physical Institute, Leninskii Pr. 53, 11924 Moscow, Russia

email: omanko@sci.lebedev.ru

Abstract

The classical propagator for tomographic probability (which describes a quantum state instead of the wave function or density matrix) is presented for quadratic quantum systems and its relation to the quantum propagator is considered. The new formalism of quantum mechanics, based on the probability representation of the state, is applied to particular quadratic systems — the harmonic oscillator and particle's free motion; the classical propagator for these system is written in an explicit form.

The quantum propagator (Green function of the Schrödinger equation) contains complete information on a quantum system and can be expressed in terms of the path integral. The quantum propagator can be calculated in different representations. The evolution of quantum systems in different representations is determined by quantum propagators. In view of this, one of the main problems of the theoretical research is to obtain an explicit expression for quantum propagators for given quantum systems.

The quantum propagator for the wave function gives the possibility to obtain also the evolution of the density matrix. Since the density matrix can be expressed in terms of a quasidistribution (e.g., in terms of the Wigner function), the quantum propagator determines the evolution of the quasidistribution. But the quasidistribution is not the joint probability distribution of the quantum system in the phase space. For example, the Wigner function can take negative value and probabilities can take only positive value. Consequently, the quantum propagator cannot be considered as positive transition probability; it has the physical meaning of the complex transition-probability amplitude.

Recently, the symplectic tomography method of measuring quantum states was suggested [1,2]. In this method, a quantum state is described by the conventional probability distribution (marginal distribution or tomographic probability) [3,4]. The evolution of the tomographic probability is described by the classical propagator, which is an analog of the transition probability used in classical statistical mechanics. The quantum propagator is connected with the classical propagator [5,6]. The new formulation of quantum mechanics of [3,4] recently was applied to some physical problems [7,8].

The aim of this study is to construct classical propagators in an explicit form for several interesting systems, which are described by quadratic (in quadrature operators) Hamiltonians, expanding the results of [6,9,10].

It was shown [1] that for generic linear combination of quadratures, which is a measurable observable ($\hbar = 1$)

$$\widehat{X} = \mu \hat{q} + \nu \hat{p}, \quad (1)$$

where \hat{q} and \hat{p} are the position and momentum, respectively, the marginal distribution $w(X, \mu, \nu)$ (normalized with respect to the variable X), which depends on the two extra real parameters μ and ν , is related to the quantum state expressed in terms of its Wigner function $W(q, p)$ as follows

$$w(X, \mu, \nu) = \int \exp[-ik(X - \mu q - \nu p)] W(q, p) \frac{dk dq dp}{(2\pi)^2}. \quad (2)$$

The Wigner function of the state can be expressed in terms of the marginal distribution [1]:

$$W(q, p) = \frac{1}{2\pi} \int w(X, \mu, \nu) \exp[-i(\mu q + \nu p - X)] d\mu d\nu dX. \quad (3)$$

For pure states with the wave function $\Psi(x)$, the nonnegative marginal distribution $w(X, \mu, \nu)$, which describes the quantum state, is given by the relationship [11,8]

$$w(X, \mu, \nu) = \frac{1}{2\pi|\nu|} \left| \int \Psi(y) \exp\left(\frac{i\mu}{2\nu} y^2 - \frac{iX}{\nu} y\right) dy \right|^2. \quad (4)$$

The evolution of the marginal distribution $w(X, \mu, \nu, t)$ can be described by means of the classical propagator $\Pi(X_2, \mu_2, \nu_2, X_1, \mu_1, \nu_1, t_2, t_1)$, in view of the integral relationship [4]

$$w(X_2, \mu_2, \nu_2, t_2) = \int \Pi(X_2, \mu_2, \nu_2, X_1, \mu_1, \nu_1, t_2, t_1) w(X_1, \mu_1, \nu_1, t_1) dX_1 d\mu_1 d\nu_1. \quad (5)$$

Below, we will also use the notation $\Pi(X_2, \mu_2, \nu_2, X_1, \mu_1, \nu_1, t)$ for the classical propagator in the case $t_1 = 0, t_2 = t$.

The classical propagator has the property [6]

$$\Pi(bX, b\mu, b\nu, bX', b\mu', b\nu', t) = \frac{1}{|b|^3} \Pi(X, \mu, \nu, X', \mu', \nu', t) \quad (6)$$

and, in view of [6], is related to the quantum propagator $G(x, y, t)$ by means of the integral transform

$$\begin{aligned} \Pi(X, \mu, \nu, X', \mu', \nu', t) &= \frac{1}{4\pi^2} \int k^2 G\left(a + \frac{k\nu}{2}, y, t\right) G^*\left(a - \frac{k\nu}{2}, z, t\right) \\ &\times \exp\left[ik\left(X' - X + \mu a - \mu' \frac{y+z}{2}\right)\right] \\ &\times \delta(y - z - k\nu') dk dy dz da. \end{aligned} \quad (7)$$

If one introduces the notation

$$K(X, X', Y, Y', t) = G(X, Y, t) G^*(X', Y', t), \quad (8)$$

the inverse of (7) can be found [5]

$$K(X, X', Z, Z', t) = \frac{1}{(2\pi)^2} \int \frac{1}{\nu'} \exp \left\{ i \left(Y - \mu \frac{X + X'}{2} \right) - i \frac{Z - Z'}{\nu'} Y' + i \frac{Z^2 - Z'^2}{2\nu'} \mu' \right\} \times \Pi(Y, \mu, X - X', Y', \mu', \nu', t) d\mu d\mu' dY dY' d\nu'. \quad (9)$$

The classical propagator for free motion obtained in [4,5] has the appearance

$$\Pi_f(X, \mu, \nu, X', \mu', \nu', t) = \delta(X - X') \delta(\mu - \mu') \delta(\nu - \nu' + \mu t). \quad (10)$$

The classical propagator for the harmonic oscillator reads [6]

$$\begin{aligned} \Pi_{os}(X, \mu, \nu, X', \mu', \nu', t) &= |\sin t| \delta(X - X') \delta(\nu \cos t + \mu \sin t - \nu') \\ &\quad \times \delta(\nu' \cos t - \mu' \sin t - \nu) \\ &= \delta(X - X') \delta(\nu \cos t - \mu \sin t - \nu') \delta(\mu \cos t + \nu \sin t - \mu'). \end{aligned} \quad (11)$$

Let us consider the system with the quadratic Hermitian Hamiltonian

$$H = \frac{1}{2} (QBQ) + CQ, \quad (12)$$

where one has the vector-operator $Q = (p, q)$. The symmetric 2×2 -matrix B and real 2-vector C depend on time. The system has linear integrals of motion [12,13]:

$$I(t) = \Lambda(t) Q + \Delta(t), \quad (13)$$

where the real symplectic 2×2 -matrix $\Lambda(t)$ and real vector $\Delta(t)$ satisfy the equations

$$\dot{\Lambda} = i \Lambda B \sigma_y, \quad \dot{\Delta} = i \Lambda \sigma_y C, \quad (14)$$

with the initial conditions

$$\Lambda(0) = 1, \quad \Delta(0) = 0. \quad (15)$$

The classical propagator for quadratic quantum systems reads (see [5])

$$\Pi(X, \mu, \nu, X', \mu', \nu', t) = \delta(X - X' + \mathcal{N} \Lambda^{-1} \Delta) \delta(\mathcal{N}' - \mathcal{N} \Lambda^{-1}), \quad (16)$$

with the vectors $\mathcal{N} = (\nu, \mu)$ and $\mathcal{N}' = (\nu', \mu')$.

The main result of this study consists in the explicit expressions for the classical propagator for two physical systems with quadratic Hamiltonians (harmonic oscillator and particle's free motion) treated in the framework of the new formulation of quantum mechanics based on the symplectic tomography method. The study of the classical propagator and its connection with the quantum propagator for the other particular quadratic systems, namely, for the problems of an ion in a Paul trap and in asymmetric Penning trap and for the process of stimulated Raman scattering one can find in [9, 14–17].

The author is grateful to Dipartimento di Scienze Fisiche, Università di Napoli “Federico II” and Istituto Nazionale di Fisica Nucleare, Sezione di Napoli for kind hospitality.

The work was partially supported by the RF State Programm “Optics. Laser Physics” and the Russian Foundation for Basic Research under Project No. 99-02-17753.

REFERENCES

- [1] S. Mancini, V. I. Man'ko, and P. Tombesi, *Quantum Semiclass. Opt.*, **7**, 615 (1995).
- [2] G. M. D'Ariano, S. Mancini, V. I. Man'ko, and P. Tombesi, *Quantum Semiclass. Opt.*, **8**, 1017 (1996).
- [3] S. Mancini, V. I. Man'ko, and P. Tombesi, *Phys. Lett. A*, **213**, 1 (1996).
- [4] S. Mancini, V. I. Man'ko, and P. Tombesi, *Found. Phys.*, **27**, 801 (1997).
- [5] Olga Man'ko and V. I. Man'ko, *J. Russ. Laser Research* (Plenum), **18**, 407 (1997).
- [6] Olga Man'ko and V. I. Man'ko, *J. Russ. Laser Research* (Plenum/Kluwer), **20**, 67 (1999).
- [7] V. I. Man'ko, L. Rosa, and P. Vitale, *Phys. Rev. A*, **58**, 3291 (1998); *Phys. Lett. B*, **439**, 328 (1998).
- [8] Vladimir Man'ko, Marcos Moshinsky, and Anju Sharma, *Phys. Rev. A*, **59**, 1809 (1999).
- [9] O. V. Man'ko, "Quantum tomography and classical propagator for quadratic quantum systems," Preprint IC/99/16 (The Abdus Salam ICTP, Trieste).
- [10] O. V. Man'ko, "Classical propagators for quadratic quantum systems," *Teor. Mat. Fiz.* (1999, in press).
- [11] V. I. Man'ko and R. V. Mendes, "Noncommutative time–frequency tomography of analytic signals," E-print LANL Physics/9712022 Data Analysis, Statistics, and Probability.
- [12] I. A. Malkin and V. I. Man'ko, *Dynamic Symmetries and Coherent States of Quantum Systems* [in Russian], Nauka, Moscow (1979).
- [13] V. V. Dodonov and V. I. Man'ko, *Invariants and Evolution of Nonstationary Quantum Systems, Proceedings of the P. N. Lebedev Physical Institute*, Nova Science, New York (1989).
- [14] O. V. Man'ko, *Izvestiya Ross. Akad. Nauk, Ser. Fiz.*, **63**, 1095 (1999).
- [15] O. V. Man'ko, "Optical tomography and measuring quantum states of an ion in a Paul trap and in a Penning trap," Contribution to the 16th International Conference on Coherent and Nonlinear Optics (Moscow, June–July 1998), *Proc. SPIE* (1999, in press).
- [16] O. V. Man'ko, "Classical propagator for quadratic quantum systems. Example of a trapped ion," *Fortschritte der Physik* (1999, in press).
- [17] O. V. Man'ko, "Photon distribution function for stimulated Raman scattering," in: V. S. Gorelik (Ed.), *Proceedings of the Conference on 80 Years Anniversary of the Discovery of Raman Scattering* (Moscow, November 1998), [in Russian], P.N. Lebedev Physical Institute Press, Moscow (1999), p. 323.

Quantum-like approaches to the beam halo problem

Sameen Ahmed KHAN

*Dipartimento di Fisica Galileo Galilei Università di Padova
Istituto Nazionale di Fisica Nucleare (INFN) Sezione di Padova
Via Marzolo 8 Padova 35131 ITALY
E-mail: khan@pd.infn.it, <http://www.pd.infn.it/~khan/>*

Modesto PUSTERLA

*Dipartimento di Fisica Galileo Galilei Università di Padova
Istituto Nazionale di Fisica Nucleare (INFN) Sezione di Padova
Via Marzolo 8 Padova 35131 ITALY
E-mail: pusterla@pd.infn.it, <http://www.pd.infn.it/~pusterla/>*

An interpretation of the the “halo problem” in accelerators based on quantum-like diffraction is given. Comparison between this approach and the others based on classical mechanics is discussed

Keywords: Beam Physics, Quantum-like, Beam halo, Beam Losses, Stochasticity.

I. INTRODUCTION

Recently the description of the dynamical evolution of high density beams by using the collective models, has become more and more popular. A way of developing this point of view is the quantum-like approach [1] where one considers a time-dependent Schrödinger equation, in both the usual linear and the less usual nonlinear forms, as a fluid equation for the whole beam. We proceed as follows: A. Linearization of the transversal motion of the beam for a circular accelerator; B. Formal similarities with Schrödinger equation; C. Feynman propagator approach; D. Diffraction through a slit (sharp and Gaussian); E. Differential and Integral probabilities of loss of particles.

We here point out that, after linearizing the Schrödinger-like equation, one can use the whole apparatus of quantum mechanics in beam dynamics, with a new interpretation of the basic parameters (for instance the Planck’s constant $\hbar \rightarrow \epsilon$ where ϵ is the normalized beam emittance) and introduce the propagator $K(x_f, t_f | x_i, t_i)$ of the Feynman theory for both longitudinal and transversal motion [2]. A procedure of this sort seems particularly effective for a global description of several phenomena such as intrabeam scattering, space-charge, particle focusing, that cannot be treated easily in detail by “classical mechanics” and are considered to be the main cause of the creation of the *Halo* around the beam line with consequent losses of particles.

Let us indeed consider the Schrödinger like equation for the beam wave function

$$i\epsilon\partial_t\psi = -\frac{\epsilon^2}{2m}\partial_x^2\psi + U(x, t)\psi \quad (1)$$

in the linearized case $U(x, t)$ does not depend on the density $|\psi|^2$. Here, ϵ is the normalized transversal beam emittance defined as $\epsilon = m_0c\gamma\beta\tilde{\epsilon}$ where, $\tilde{\epsilon}$ being the emittance usually considered, where as we may introduce the analog of the De Broglie wavelength as $\lambda = \epsilon/p$. We now focus our attention on the one dimensional transversal motion along the x -axis of the beam particles belonging to a single bunch and assume a Gaussian transversal profile for a particles injected in to a circular machine. We describe all the interactions mentioned above, that cannot be treated in detail, as diffraction effects by a phenomenological boundary defined by a slit, in each segment of the particle trajectory.

This condition should be applied to both beam wave function and its corresponding beam propagator K . The result of such a procedure is a multiple integral that determines the actual propagator between the initial and the final states in terms of the space-time intervals due to the intermediate segments.

$$\begin{aligned}
& K(x + x_0, T + \tau | x', 0) \\
&= \int_{-b}^{+b} K(x + x_0, \tau | x_0 + y_n, T + (n-1)\tau') K(x + y_n, T + (n-1)\tau' | x_0 + y_{n-1}, T + (n-2)\tau') \\
&\quad \times \cdots K(x + y_1, T | x', 0) dy_1 dy_2 \cdots dy_n, \tag{2}
\end{aligned}$$

where $\tau = n\tau'$ is the total time of revolutions T is the time necessary to insert the bunch (practically the time between two successive bunches) and $(-b, +b)$ the space interval defining the boundary conditions. Obviously b and T are phenomenological parameters which vary from one machine to another and must also be correlated with the geometry of the vacuum tube where the particles circulate. At this point we may consider two possible approximations for $K(n|n-1) \equiv K(x_0 + y_n, T + (n-1)\tau' | x_0 + y_{n-1} + (n-2)\tau')$:

1. We substitute it with the free particle K_0 assuming that in the τ' interval ($\tau' \ll \tau$) the motion is practically a free particle motion between the boundaries $(-b, +b)$.
2. We substitute it with the harmonic oscillator $K_\omega(n|n-1)$ considering the harmonic motion of the betatronic oscillations with frequency $\omega/2\pi$

II. FREE PARTICLE CASE

We may notice that the convolution property (2) of the Feynman propagator allows us to substitute the multiple integral (that becomes a functional integral for $n \rightarrow \infty$ and $\tau' \rightarrow 0$) with the single integral

$$K(x + x_0, T + \tau | x', 0) = \int_{-b}^{+b} dy K(x + x_0, T + \tau | x_0 + y, T) K(x_0 + y, T | x', 0) dy \tag{3}$$

We consequently obtain from equation (3) after introducing the Gaussian slit $\exp\left[-\frac{y^2}{2b^2}\right]$ instead of the segment $(-b, +b)$ we obtain from

$$\begin{aligned}
K(x + x_0, T + \tau | x', 0) &= \int_{-\infty}^{+\infty} dy \exp\left[-\frac{y^2}{2b^2}\right] \left\{ \frac{2\pi i \hbar \tau}{m} \frac{2\pi i \hbar T}{m} \right\}^{-\frac{1}{2}} \exp\left[\frac{im}{2\hbar\tau}(x-y)^2\right] \exp\left[\frac{im}{2\hbar T}(x_0+y-x')^2\right] \\
&= \sqrt{\frac{m}{2\pi i \hbar}} \left(T + \tau + T\tau \frac{i\hbar}{mb^2}\right)^{-\frac{1}{2}} \exp\left[\frac{im}{2\hbar} \left(v_0^2 T + \frac{x^2}{\tau}\right) + \frac{(m^2/2\hbar^2\tau^2)(x-v_0\tau)^2}{\frac{im}{\hbar} \left(\frac{1}{T} + \frac{1}{\tau}\right) - \frac{1}{b^2}}\right] \tag{4}
\end{aligned}$$

where $v_0 = \frac{x_0 - x'}{T}$ and x_0 is the initial central point of the beam at injection and can be chosen as the origin ($x_0 = 0$) of the transverse motion of the reference trajectory in the test particle reference frame. Where as \hbar must be interpreted as the normalized beam emittance in the quantum-like approach.

With an initial Gaussian profile (at $t = 0$), the beam wave function is $f(x) = \left\{\frac{\alpha}{\pi}\right\}^{\frac{1}{4}} \exp\left[-\frac{\alpha}{2}x'^2\right]$ r.m.s of the transverse beam and the final beam wave function is:

$$\phi(x) = \int_{-\infty}^{+\infty} dx' \left(\frac{\alpha}{\pi}\right)^{\frac{1}{4}} e^{-\frac{\alpha}{2}x'^2} K(x, T + \tau; x', 0) = B \exp[Cx^2] \tag{5}$$

with

$$B = \sqrt{\frac{m}{2\pi i\hbar}} \left\{ T + \tau + T\tau \frac{i\hbar}{mb^2} \right\}^{-\frac{1}{2}} \left\{ \frac{\alpha}{\pi} \right\}^{\frac{1}{4}} \sqrt{\frac{\pi}{\left(\frac{\alpha}{2} - \frac{im}{2\hbar T} - \frac{m^2/2\hbar^2 T^2}{\frac{im}{\hbar} \left(\frac{1}{T} + \frac{1}{\tau} \right) - \frac{1}{b^2}} \right)}},$$

$$C = \frac{im}{2\hbar\tau} + \frac{m^2/2\hbar^2 T^2}{\frac{im}{\hbar} \left(\frac{1}{T} + \frac{1}{\tau} \right) - \frac{1}{b^2}} + \frac{\frac{\tau^2}{T^2} \left\{ \frac{m^2/2\hbar^2 T^2}{\frac{im}{\hbar} \left(\frac{1}{T} + \frac{1}{\tau} \right) - \frac{1}{b^2}} \right\}^2}{\left(\frac{\alpha}{2} - \frac{im}{2\hbar T} - \frac{m^2/2\hbar^2 T^2}{\frac{im}{\hbar} \left(\frac{1}{T} + \frac{1}{\tau} \right) - \frac{1}{b^2}} \right)}. \quad (6)$$

The final local distribution of the beam that undergoes the diffraction and the total probability per particle are respectively given by

$$\rho(x) = |\phi(x)|^2 = BB^* \exp[-\tilde{\alpha}x^2], \quad P = \int_{-\infty}^{+\infty} dx \rho(x) = BB^* \sqrt{\frac{\pi}{\tilde{\alpha}}} \approx \frac{1}{\sqrt{\alpha}} \frac{mb}{\hbar T} \quad (7)$$

where $\tilde{\alpha} = -(C + C^*)$. One may notice that the probability P has the same order of magnitude of the one computed in [3] if $\frac{1}{\sqrt{\alpha}}$ is of the order of b .

III. OSCILLATOR CASE

Similarly we may consider the harmonic oscillator case (betatronic oscillations) to compute the diffraction probability of the single particle from the beam wave function and evaluate the probability of beam losses per particle. The propagator $K_\omega(x, T + \tau|y, T)$ in the later case is:

$$\begin{aligned} K(x, T + \tau|x', 0) &= \int_{-\infty}^{+\infty} dy \exp\left[-\frac{y^2}{2b^2}\right] K_\omega(x, T + \tau|y, T) K_\omega(y, T|x', 0) \\ &= \int_{-\infty}^{+\infty} dy \exp\left[-\frac{y^2}{2b^2}\right] \left\{ \frac{m\omega}{2\pi i\hbar \sin(\omega\tau)} \right\}^{\frac{1}{2}} \exp\left[\frac{im\omega}{2\hbar \sin(\omega\tau)} \{ (x^2 + y^2) \cos \omega\tau - 2xy \} \right] \\ &\quad \times \left\{ \frac{m\omega}{2\pi i\hbar \sin(\omega T)} \right\}^{\frac{1}{2}} \exp\left[\frac{im\omega}{2\hbar \sin(\omega T)} \{ (y^2 + x'^2) \cos \omega T - 2x'y \} \right] \\ &= \left\{ \frac{1}{2\pi} \tilde{C} \right\}^{\frac{1}{2}} \exp\left[\tilde{A}x^2 + \tilde{B}x'^2 + \tilde{C}xx' \right] \end{aligned} \quad (8)$$

where

$$\begin{aligned} \tilde{A} &= i \frac{m\omega \cos(\omega\tau)}{2\hbar \sin(\omega\tau)} - \left(\frac{m\omega}{2\hbar} \right)^2 \frac{1}{\sin^2(\omega\tau)} \frac{1}{D}, & \tilde{B} &= i \frac{m\omega \cos(\omega T)}{2\hbar \sin(\omega T)} - \left(\frac{m\omega}{2\hbar} \right)^2 \frac{1}{\sin^2(\omega T)} \frac{1}{D} \\ \tilde{C} &= - \left(\frac{m\omega}{2\hbar} \right)^2 \frac{2}{\sin(\omega\tau) \sin(\omega T)} \frac{1}{D}, & D &= \frac{1}{2b^2} - i \frac{m\omega}{2\hbar} \left(\frac{\cos(\omega\tau)}{\sin(\omega\tau)} + \frac{\cos(\omega T)}{\sin(\omega T)} \right), \end{aligned} \quad (9)$$

$$\phi_\omega(x) = \int_{-\infty}^{+\infty} dx' \left(\frac{\alpha}{\pi} \right)^{\frac{1}{4}} \exp\left[-\frac{\alpha}{2}x'^2\right] K_\omega(x, T + \tau; x', 0) = N \exp[Mx^2] \quad (10)$$

where

$$N = \left(\frac{\alpha}{\pi} \right)^{\frac{1}{4}} \left\{ \frac{\tilde{C}}{(\alpha - 2\tilde{B})} \right\}^{\frac{1}{2}}, \quad M = \tilde{A} + \frac{\tilde{C}^2}{2(\alpha - 2\tilde{B})}, \quad (11)$$

$$\rho_\omega(x) = |\phi_\omega(x)|^2 = N^* N \exp[-(M^* + M)x^2], \quad P_\omega = \int_{-\infty}^{+\infty} dx \rho(x) = N^* N \sqrt{\frac{\pi}{(M^* + M)}} \approx \frac{1}{\sqrt{\alpha}} \frac{mb}{\hbar} \frac{\omega}{\sin(\omega T)}. \quad (12)$$

IV. PRELIMINARY ESTIMATES

Parameters	LHC	HIDIF
Transverse Emittance, ϵ	3.75 mm mrad	13.5 mm mrad
Total Energy E	450 GeV	5 GeV
T	25 nano sec.	100 nano sec.
b	1.2 mm	1.0 mm
ω	4.47×10^6 Hz	1.12×10^7 Hz
P	3.39×10^{-5}	2.37×10^{-3}
P_ω	3.44×10^{-5}	2.96×10^{-3}

V. CONCLUSION

These preliminary numerical results are encouraging because they predict beam losses which seem under control. Indeed the HIDIF scenario gives a total loss of beam power per meter which is about a thousand higher than the LHC. However in both cases the estimated losses appear much smaller than the permissible 1 Watt/m.

The relevant concluding remarks are as follows:

1. The probability calculated from the free and the harmonic oscillator propagators (both in the transversal motion of the particles) appear very close for the two different circular systems such as *LHC* and *HIDIF* rings.
2. In both the machines the beam losses which we consider related with halo are under control because they appear much smaller than 1 Watt/m.
3. The *HIDIF* scenario, as expected has a total loss of beam power which is at least 10^3 times higher than *LHC*.

- [1] See R. Fedele and G. Miele, *Il Nuovo Cimento D* **13**, 1527 (1991); R. Fedele, F. Galluccio, V. I. Man'ko and G. Miele, *Phys. Lett. A* **209**, 263 (1995); Ed. R. Fedele and P.K. Shukla *Quantum-Like Models and Coherent Effects*, Proc. of the 27th Workshop of the INFN Eloisatron Project Erice, Italy 13-20 June 1994 (World Scientific, 1995); R. Fedele, "Quantum-like aspects of particle beam dynamics", in: *Proceedings of the 15th Advanced ICFA Beam Dynamics Workshop on Quantum Aspects of beam Physics*, Ed. P. Chen, (World Scientific, Singapore, 1999).
See also: N. C. Petroni, S. De Martino, S. De Siena, and F. Illuminati, A stochastic model for the semiclassical collective dynamics of charged beams in particle accelerators, in: *Proceedings of the 15th Advanced ICFA Beam Dynamics Workshop on Quantum Aspects of beam Physics*, Ed. P. Chen, (World Scientific, Singapore, 1999); E. Nelson, *Phys. Rev.* **50** 1079 (1966); *Dynamical theories of Brownian motion* (Princeton University Press, Princeton 1967); Francesco Guerra, *Phys. Rep.* **77** 263-312 (1981).
- [2] Sameen A. Khan and Modesto Pusterla, **Quantum mechanical aspects of the halo puzzle** To appear in: *Proceedings of the 1999 Particle Accelerator Conference PAC99* (29 March - 02 April 1999, New York City, NY) Editors A. Luccio and W. MacKay, physics/990405034.
- [3] Formulae (3-33) in R. P. Feynman and A. R. Hibbs, *Quantum Mechanics and Path Integrals*, (McGraw-Hill, New York).
- [4] Ed. P. Lefèvre and T. Pettersson, *Large Hadron Collider (LHC) Conceptual Design CERN/AC/95-05(LHC)* (October 1995).
- [5] Ed. I. Hofmann and G. Plass, *Heavy Ion Driven Inertial Fusion (HIDIF) Study GSI-98-06 Report* (August 1998).

Generation and Application of High Quantum Correlated Twin Beams

Kunchi Peng, Hai Wang, Yun Zhang, Qing Pan, Hong Su, A. Porzio*, Changde Xie
Institute of Opto-Electronics, Shanxi University, Taiyuan 030006, P.R.China
e-mail: kcpeng@mail.sxu.edu.cn

Abstract

The generation and application of high quantum correlated twin beams from cw OPO and OPA will be presented. The applications of twin beams in the QND with nonunity gain and sub-shot-noise optical measurements finished in our lab will be summarized.

1 Introduction

It has been well demonstrated that the intense twin beams generated from CW Optical Parametric Oscillators(OPOS) operating above oscillation thresholds are useful nonclassical light fields in precise optical measurements with sensitivities beyond the Standard-Quantum-Limit (SQL). The two-photon absorption spectroscopy[1] and weak absorption measurement [2] have been accomplished recently, in that the improvements in the Signal-to-Noise Ratio(SNR) with respect to the SQL's of the total light used in experiment are 1.9dB and 7dB respectively, due to employment of quantum correlated twin beams produced from CW nondegenerate OPOs (NOPOs). The quantum measurement of intensity difference fluctuation satisfying all the Quantum Nondemolition(QND) criteria has been achieved with a beam splitter, the dark port of which is injected by the twin beams in 1998 [3].

In this presentation we shall introduce our twin beams generation system at first, then simply present the applications of twin beams on the QND and sub-shot-noise measurements.

2 Continuous wave twin beams generation

As well-known, KTP is a good nonlinear crystal for frequency conversion. Usually the KTP is cut for type-II critical phase-matching (c-cut). In this case, the beams-walk-off effect and polarization mixing will inevitably affect the conversion efficiency. The twin beams with 30% quantum noise reduction below the SQL and intensities of a few milliwatts was generated from a CW NOPO pumped by green light of 200mw for the first time by A.Heidmann et al. in 1987 [4]. Then the result was improved with a larger transmission of the output mirror of NOPO and a better pump source by the same group. A quantum noise reduction of 86% in twin beams with intensities of 6mw was observed at the pump threshold of 390mw[5]. With a pair of c-cut KTP crystals in series to compensate the beam-walk-off effect between signal and idle mode we obtained the twin beams of 50% quantum noise reduction in the intensity difference fluctuation. The total power of the output twin beams is 23mw at the pump power of 300mw[6]. To further increase the conversion efficiency and reduce the pump threshold. We use α -cut KTP which is able to perform the type-II noncritical phase-matching instead of the c-cut one. Due to the collinear transmission of signal and idle mode in the crystal the beams walk -off and

Permanent address : INFN Unitá di Napoli, Italy

polarization mixing effects were minimized, therefore the conversion efficiencies were increased and the threshold power were reduced significantly.

We have established two cw NOPO and a NOPA system consisting of α -cut KTP for nonclassical light generation. One of the NOPOs and the NOPA are the semimonolithic configuration, the front face of crystal was coated to be used as the input coupler for pump field and injected signal a concave mirror was employed as the output coupler for nonclassical light. The pump laser is an intracavity frequency-doubled and frequency-stabilized cw ring Nd:YAP laser [7], the output second-harmonic wave of that is at $0.54\mu\text{m}$ wavelength which is able to perform the degenerate frequency-down-conversion in α -cut KTP. When the NOPO pumped by Nd:YAP laser operated above the oscillation threshold the intensive twin beams of 36 mw with near-degenerate frequency around $1.08\mu\text{m}$ and orthogonal polarization were obtained only at the pump power of 110mw. The intensity difference squeezing was $7\pm 0.1\text{dB}$ [3]. To control the frequencies of twin beams a small signal at $1.08\mu\text{m}$ was injected into the NOPO operated below the threshold from the input coupler. At the NOPA operation scheme the quantum correlated twin beams with exactly degenerate frequency and orthogonal polarization was produced for the first time to our knowledge, the noise in the intensity difference between that was reduced by 3.7dB below the SQL at the measuring frequency of 3MHz shown in Fig.1.

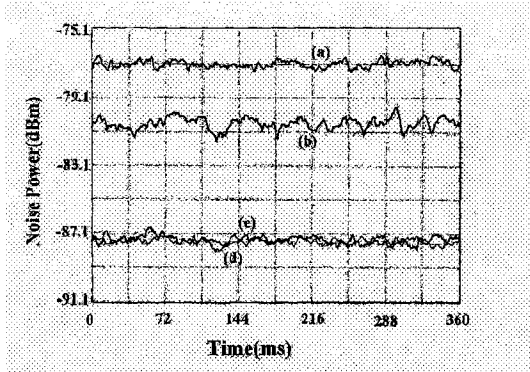


Fig.1

Other system of NOPO is a triply resonant OPO consisting of two concave mirrors coated to be used as the input coupler for pump green light at $0.532\mu\text{m}$ and the output coupler for twin beams at $1.090\mu\text{m}$ and $1.039\mu\text{m}$, respectively, a α -cut KTP of 10mm-long is placed in the center of the NOPO with a cavity length of 38 mm[2].

Due to the higher output coupling efficiency (the transmissions for the output coupler are 7.2% at the range from 1000 to 1100nm) up to 9.2dB (88%) intensity difference squeezing between the frequency nondegenerate twin beam ($1.090\mu\text{m}$ and $1.039\mu\text{m}$) has been accomplished experimentally[2]. All our twin beams generation system are stable which are convenient to be applied into the optical measurements and communications.

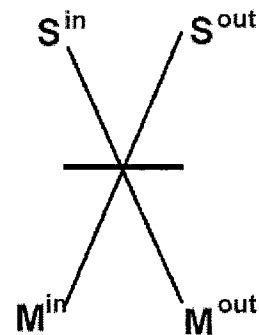


Fig.2

3 Application of twin beams in the optical measurements

We designed a new QND device to measure the intensity difference fluctuation between two orthogonal polarized modes in signal beam. The measured signal is modulated on a polarized component and then is analyzed in the noise spectrum of intensity difference fluctuation.

A 50/50 beam splitter serves as the coupling device of the QND measurement. The input signal (S^{in}) and input meter (M^{in}) both consist of two orthogonal polarized modes (s- and p-polarization) of equal mean intensity. The phase and the frequency of S- and P- polarization modes in S^{in} are same as that in M^{in} , respectively.

The angles of incidence of S^{in} and M^{in} on BS are smaller than 3° to ensure the balance of the reflectivities between S- and P- polarized wave (Fig. 2). The two polarized modes in S^{in} are

uncorrelated, the noise of amplitude difference between that is in the SQL. i.e. $|\delta r_s^{in}| = 1$, while the two modes in M^{in} are quantum correlated twin beams, i.e. $|\delta r_m^{in}| < 1$. The calculated the signal and meter transfer coefficients (T_s and T_m) and the normalized conditional variance ($V_{s/m}$) are[3]:

$$T_s = \frac{R}{R + T \langle |\delta r_m^{in}(\omega)|^2 \rangle + \frac{1-\eta}{\eta}} \quad (1)$$

$$T_m = \frac{T}{T + R \langle |\delta r_m^{in}(\omega)|^2 \rangle + \frac{1-\eta}{\eta}} \quad (2)$$

$$V_{s/m} = \frac{1 - \eta + \eta \langle |\delta r_m^{in}(\omega)|^2 \rangle}{\eta [T + R \langle |\delta r_m^{in}(\omega)|^2 \rangle] + 1 - \eta} \quad (3)$$

Here T and $R=1-T$ are the power transmission and reflectivity of BS. η is the detection efficiency. For our experiments, $R = 50\% \pm 1\%$, $\eta = 89\%$ (All three detectors for detection input meter have nearly identical efficiency). The measured $T_s = 0.66$, $T_m = 0.65$ and $V_{s/m} = -2.1d$ [3]. Since $T_s + T_m = 1.31 > 1$ and $V_{s/m} < 1$ the QND measurement fulfilled all QND criteria in quantum domain[8]. The device has the abilities of quantum signal transfer and quantum state preparation.

Fig.3 is a copy from Fig.3 of the review article in "Nature"[8] to characterize the properties of QND measurement devices, on that open triangles and filled circles represent QND experiments used third- and second-order nonlinearities, respectively. The asterisks represent "quantum-repeater" schemes where the signal is amplified. Our experimental results were published on Feb.1999, two months later than Ref.[8], so it is not on the original figure. For comparing we cite the figure and add our data on it with the symbol of white asterisk.

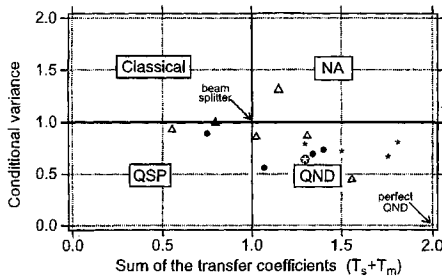


Fig.3

For performing the sub-shot-noise optical measurement with twin beams, we modulate the measured signal on one of the twin beams as an artificial "noise" at the modulation frequency, then observe the noise spectrum of the intensity difference fluctuation between the twin beams. The measured signal emerges from the squeezed noise background and the signal-to-noise ratio (SNR) is improved a factor of the intensity difference squeezing degree. The first experiment on sub-shot-noise measurement of weak absorption to the unmodulated medium was finished with twin beams in 1996. The improvement of SNR was only 2.5dB[9][10]. Then we increased the intensity difference squeezing to 9.2dB and hence the SNR was improved by 7 dB with respect to the SQL of the total light employed in the experiment and by 4dB with respect to that of the signal light.

We have accomplished the QND measurement and the sub-shot-noise measurement with the quantum intensity correlated twin beams produced from NOPO's consisting of α -cut KTP crystals. Since twin beams with high quantum correlation are easier to generate than the quadrature vacuum squeezed state light and in the presented schemes only field intensities are measured,

the designed system is simpler and robust. Combining these measurement systems the twin beams can be developed as a noiseless optical tap to be use in practical optical information and measurement.

Supported by the National Nature Science Foundation of China(No.69837010) and Nature Science Foundation of Shanxi Province.

References

- [1] P.H. Souto Ribeiro et.al., Opt.Lett. **22**, 1983(1997)
- [2] Jiangrui Gao et.al., Opt.Lett. **23**,870(1998)
- [3] Hai Wang et.al., Phys.Rev.Lett. **82**,1414(1999)
- [4] A.Heidmann et.al. , Phys. Rev.Lett. **59**, 2555(1987)
- [5] J.Mertz et.al., Opt.Lett.**16**, 1234(1991)
- [6] Hai Wang et.al., Acta Optica Sinica (in Chinese) **17**, 1002(1997)
- [7] Qing Pan et.al. Appl. Opt. **36**, 2394(1998)
- [8] P. Grangier et.al., Nature, **396**,537(1998)
- [9] Hai Wang et.al., In proceedings of the Third International Conference on Quantum Communication and Measurement (Plenum, New York, 1997) P445
- [10] Hai Wang et.al., Science in China (Series A) **41**, 534(1998)

Figure captions

Fig.1 Noise of the intensity difference of the signal and idler .Trace (a) is the associated shot noise limit. Trace (b) is the noise spectrum of the twin-beam intensity difference. Trace (c) and (d) are the shot noise and intensity difference noise spectrum without the pump. The analysis bandwidth and video bandwidth are 300KHz and 300Hz, respectively.

Fig.2 Principle of QND measurement

Fig3. The different properties used to characterize a QND measurement device

Engineering quantum superpositions of two equally intensity coherent states

A. Napoli

Dipartimento di Scienze Fisiche ed Astronomiche, via Archirafi 36, 90123 Palermo, Italy

A. Messina

Dipartimento di Scienze Fisiche ed Astronomiche, via Archirafi 36, 90123 Palermo, Italy

Abstract

A new and simple way of engineering quantum superpositions of two coherent states of a single-mode quantized electromagnetic field is presented. Our proposal, developed in the context of micromaser theory, exploits the passage of one atom only through a high- Q bimodal cavity supporting two electromagnetic modes of different frequencies.

Quite recently quantum superpositions of two coherent states of light have received a great deal of attention from both experimentalists and theoreticians. The interest toward these states stems from the consideration that, due to probability amplitude interference effects [1], they might exhibit nonclassical features pronounced enough to provide almost ideal conditions to test basic aspects of quantum mechanics and to explore the border between classical and quantum description of nature [2]. In particular it has been shown [1] that squeezing, sub-Poissonian photon statistics and oscillations of the photon number distribution emerge from a superposition of coherent states.

In this paper we present a new and simple way of engineering a class of states obtained as quantum superpositions of two coherent states of a single-mode quantized electromagnetic field. Our proposal, developed in the context of micromaser theory, exploits the passage of one atom only through a high- Q ($Q \approx 5 \times 10^{10}$) bimodal cavity supporting two electromagnetic modes of different frequencies ω_1 and ω_2 such that $\omega_1 \approx \omega_2 \approx 10^{10} Hz$. The atom is a Rydberg atom effectively behaving as a two-level atom whose ground state $|-\rangle$ and excited state $|+\rangle$ are energetically separated by ω_0 ($\hbar = 1$). The cavity mode to be manipulated, hereafter also called mode of interest, is that of frequency ω_1 and is initially prepared in a coherent state $|\alpha\rangle$ where $\alpha \in C$. In the context of our procedure the other mode plays an auxiliary role and at $t = 0$ is left in its empty state. Our experimental scheme relies on the assumption $\omega_0 \approx \omega_1 + \omega_2$ so that the atom-field coupling may be adequately described in accordance with the following effective resonant two-photon Hamiltonian model:

$$H = \sum_{\mu=0}^2 \omega_{\mu} \alpha_{\mu}^{\dagger} \alpha_{\mu} + (\omega_0 + \beta_2 \alpha_2^{\dagger} \alpha_2 - \beta_1 \alpha_1^{\dagger} \alpha_1) S_z + \lambda [\alpha_1 \alpha_2 S_+ + h.c.] \quad (1)$$

well-known in literature after Gou [3]. As usual, the Pauli pseudo spin operators S_z and S_{\pm} describe the atomic internal degrees of freedom and are such that $2S_z|\pm\rangle = \pm|\pm\rangle$ and $S_{\pm}|\mp\rangle = |\pm\rangle$ whereas α_i (α_i^\dagger) is the annihilation (creation) operator relative to the i -th mode of the cavity field. Each atomic excitation (de-excitation) is accompanied by the simultaneous absorption (emission) of one photon from (into) the mode of interest and one photon from (into) the auxiliary mode. The coupling constant λ measures the strength of the atom-field energy exchanges and, as in a typical two-photon micromaser experiment [4], may be taken of the order of $10^3 Hz$. The intensity-dependent detuning is characterized by the two Stark parameters β_1 and β_2 here assumed coincident for simplicity and such that $\beta_1 = \beta_2 \approx 10^3 Hz$ [4]. The Hamiltonian model (1) is exactly solvable and the time evolution of the atom-cavity system has been exactly treated in ref. [5].

Suppose that the Rydberg atom is prepared in its excited state before entering the cavity. The initial condition of atom-field system in our experimental scheme may be represented as

$$|\Psi(0)\rangle = |\alpha\rangle|0\rangle|+\rangle \quad \alpha \in C \quad (2)$$

with the mode of frequency ω_1 in the coherent state

$$|\alpha\rangle = \sum_{p=0}^{\infty} e^{-\frac{|\alpha|^2}{2}} \frac{\alpha^p}{\sqrt{p!}} |p\rangle. \quad (3)$$

Indicate by τ the time spent by the atom inside the cavity. It is possible to demonstrate that, if immediately after leaving the cavity, an appropriate detector of the internal atomic state finds, with a τ -dependent not vanishing probability $P(\tau)$, the atom not excited, then the bimodal cavity field collapses into the factorized state $|\varphi(\tau)\rangle|1\rangle$ where

$$|\varphi(\tau)\rangle = -iN(\tau) \sum_{p=0}^{\infty} e^{-\frac{|\alpha|^2}{2}} \frac{\alpha^p}{\sqrt{p!}} S_p(\tau) |p+1\rangle \quad (4)$$

with

$$S_p(t) = -i \frac{2\sqrt{(p+1)}}{(p+2)} \sin(\Lambda(p+1,1)t) \exp(-i\epsilon_0(p+1,1)t) \quad (5)$$

$$\Lambda(p+1,1) = \frac{\lambda}{2}(p+2) \quad \epsilon_0(p+1,1) = \omega_1(p + \frac{1}{2}) + \omega_2 \quad (6)$$

The positive normalization constant $N(\tau)$ appearing in eq. (4) may be written down as (the phase factor i appears for convenience)

$$N(\tau) = \left| \sum_{p=0}^{\infty} e^{-\frac{|\alpha|^2}{2}} \frac{\alpha^p}{\sqrt{p!}} |S_p(\tau)|^2 \right|^{-\frac{1}{2}} \quad (7)$$

and, of course, in view of eq. (6), is mathematically well defined only when $\lambda\tau \neq 2k\pi$ with $k \in Z$. In order to gain more insight on the properties of the state described by eq. (4),

we exploit the exponential Eulerian representation of the sinusoidal factor appearing in the expression (5), getting:

$$|\varphi(\tau)\rangle = A \left[\sum_{q=0}^{\infty} D_q(\alpha e^{i\gamma_-(\tau)}) |q\rangle - e^{-i\vartheta(\tau)} \sum_{q=0}^{\infty} D_q(\alpha e^{i\gamma_+(\tau)}) |q\rangle \right] \quad (8)$$

where

$$D_q(\alpha e^{i\gamma_{\mp}(\tau)}) = \frac{q}{q+1} e^{-\frac{|\alpha|^2}{2}} \frac{\alpha^q e^{iq\gamma_{\mp}(\tau)}}{\sqrt{q!}} \quad (9)$$

$$A = i \frac{N(\tau)}{\alpha} e^{-i\tau(\omega_2 - \frac{\omega_1}{2} - \frac{\lambda}{2})} \quad (10)$$

$$\gamma_{\mp}(\tau) = \pm \left(\frac{\lambda}{2} \mp \omega_1 \right) \tau, \quad \vartheta = \lambda\tau \quad (11)$$

Since, in view of eq. (9), each probability amplitude $D_q(\alpha e^{i\gamma_{\mp}(\tau)})$ may be obtained multiplying the q -th poissonian amplitude $e^{-\frac{|\alpha|^2}{2}} \frac{\alpha^q e^{iq\gamma_{\mp}(\tau)}}{\sqrt{q!}}$ by $\frac{q}{q+1}$, it is reasonable to guess that, at least in correspondence to not too low values of $|\alpha|^2$, even $D_q(\alpha e^{i\gamma_{\mp}(\tau)})$ exhibits a substantial poissonian character.

We have quantitatively demonstrated that the scalar product between the coherent state $|\alpha e^{i\gamma_{\mp}(\tau)}\rangle$ and the normalized state $|d(\alpha e^{i\gamma_{\mp}(\tau)})\rangle = d \sum_{q=0}^{\infty} D_q(\alpha e^{i\gamma_{\mp}(\tau)}) |q\rangle$ is practically coincident with the unity when the condition $|\alpha|^2 \geq 10$ is satisfied. Thus, appropriately choosing the initial intensity of the mode of interest, we are legitimated to say that at $t = \tau$ it is found in a quantum superposition of the two coherent states $|\alpha e^{i\gamma_-(\tau)}\rangle$ and $|\alpha e^{i\gamma_+(\tau)}\rangle$.

In order to better understand this point, let's consider the normalized state $|\tilde{\varphi}(\tau)\rangle$ defined as

$$|\tilde{\varphi}(\tau)\rangle \equiv \tilde{A} \left[|\alpha e^{i\gamma_-(\tau)}\rangle - e^{-i\vartheta(\tau)} |\alpha e^{i\gamma_+(\tau)}\rangle \right] \quad (12)$$

where the normalization constant \tilde{A} is given by

$$\tilde{A} = \frac{1}{\sqrt{2}} \left[1 - e^{-|\alpha|^2(1 - \cos\vartheta)} \cos(\vartheta + |\alpha|^2 \sin\vartheta) \right]^{-\frac{1}{2}} \quad (13)$$

We have demonstrated that, there exist appropriate conditions, such that the state generated with the help of our scheme is well approximated by the state $|\tilde{\varphi}(\tau)\rangle$ defined in eq. (12). The results obtained are for simplicity showed in figures (1) and (2) where we plot the function $f(\lambda\tau) = |\langle \varphi_-(\lambda\tau) | \tilde{\varphi}(\lambda\tau) \rangle|$ in correspondence to $|\alpha|^2 = 10, 20$ respectively.

Looking at these figures it is immediate to deduce that properly choosing the time τ spent by the atom inside the cavity, the measurement of the internal state of one atom only, after its interaction with the resonator, projects the mode of interest in the desired state if the atom is found in its ground state. In conclusion, it is important to stress that controlling the speed of only one atom is easy to realize and, consequently, it may be tuned to get different

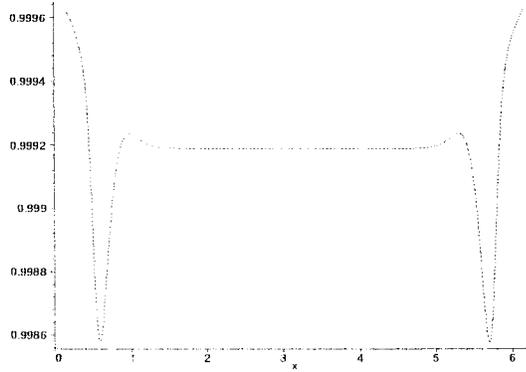


FIG. 1. Plot of the function $f(x) = |\langle \varphi_-(x) | \tilde{\varphi}(x) \rangle|$ against $x = \lambda t$ for $|\alpha|^2 = 10$

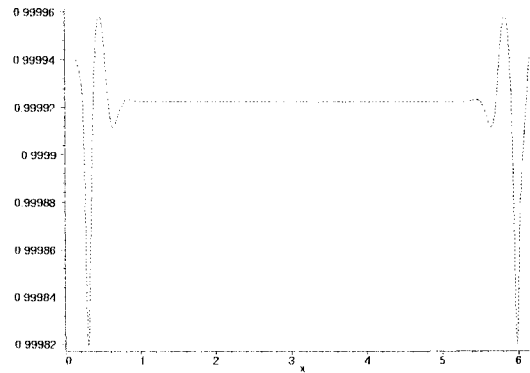


FIG. 2. Plot of the function $f(x) = |\langle \varphi_-(x) | \tilde{\varphi}(x) \rangle|$ against $x = \lambda t$ for $|\alpha|^2 = 20$

desired final states of the mode of interest always in the form of linear superpositions of two equally intensity coherent states as transparently shown by equation (14).

Acknowledgments This research was supported by INFM and MURST co-financial support in the framework of the research project "Amplificazione e Rivelazione di Radiazione Quantistica".

References

- [1] V. Bužek, P.L. Knight, in *Progress in Optics XXXIV*, (Elsevier Science B.V., 1995), **1**
- [2] W.H. Zurek, *Phys. Today*, October 1991, **36**
- [3] S.C. Gou, *Phys. Lett. A* **147**, 218 (1990)
- [4] S. Haroche, *Phys. Today*, July 1998, **36**
- [5] A. Napoli, A. Messina, *J. Mod. Opt.* **43**, 649 (1996).

Hydrodynamical Quantum State Reconstruction

Lars M. Johansen

*Buskerud College, Faculty of Engineering,
P.O. Box 251, N-3601 Kongsberg, Norway*

Abstract

When the density matrix is expressed as Taylor series in the off-diagonal variable, the coefficients in this series are “hydrodynamical” moments of the Wigner distribution. These moments can be obtained both recursively and nonrecursively from the time-dependent probability distribution. The case of a free particle is investigated in particular.

I. INTRODUCTION

In recent years, the subject of quantum state reconstruction has grown into a mature field. Reconstruction methods such as optical homodyne tomography [1,2] and phase space sampling [3,4] have been developed. As regards systems living in infinite-dimensional Hilbert space, most reconstruction methods apply to quantum optical states and to particles in harmonic oscillator potentials. Several interesting experiments have been performed in this field, using for example optical homodyne tomography [5,6] or phase space sampling [7].

The tomographic reconstruction method has been generalized to particles in arbitrary potentials [8,9]. In this case, the density matrix can be reconstructed by measuring the position probability density parametrized over time. The tomographic method has also been generalized to a class of time-dependent potentials [10]. In the generalized version of the tomographical reconstruction method, the position probability density should be measured over an infinite time interval. Experimentally, the tomographic reconstruction method has also been employed to reconstruct the Wigner function of free particles [11]. An unphysical shear of the Wigner function observed in this experiment was attributed to the finite width of the time window used.

Among other reconstruction methods for more general potentials, a method based on least squares approximations can be mentioned [12]. Recently, a general reconstruction method using “hydrodynamical” moments of the Wigner function was found [13]. In this method, the density matrix of a particle in an arbitrary one-dimensional (and possibly time-dependent) potential can be reconstructed. In contrast to the generalized tomographical method, the position probability distribution should ideally be measured over an infinitesimal time interval.

II. HYDRODYNAMICAL MOMENTS

The hydrodynamical reconstruction method is based upon the following Taylor-expansion of the density matrix in the off-diagonal direction [14]

$$\langle x + y | \hat{\rho} | x - y \rangle = \sum_{n=0}^{\infty} \frac{f_n(x, t)}{n!} \left(\frac{2iy}{\hbar} \right)^n, \quad (1)$$

where x is the position and y is the off-diagonal variable. The coefficients f_n are defined in terms of derivatives of the density matrix,

$$f_n(x, t) = \left(\frac{2i}{\hbar} \right)^n \left[\frac{\partial^{(n)} \langle x + y | \hat{\rho} | x - y \rangle}{\partial y^n} \right]_{y=0}. \quad (2)$$

The density matrix is the Fourier-transform of the Wigner distribution

$$\langle x + y | \hat{\rho} | x - y \rangle = \int_{-\infty}^{\infty} dp e^{2ipy/\hbar} W(x, p, t). \quad (3)$$

Therefore, the moments f_n can also be expressed as integrals over the Wigner distribution,

$$f_n(x, t) = \int dp p^n W(x, p, t). \quad (4)$$

The hydrodynamical moments of lowest order have a well known physical interpretation. The zeroth order moment is the position probability density. The zeroth and first order moments are connected by a conservation equation;

$$\frac{\partial f_0(x, t)}{\partial t} + \frac{1}{m} \frac{\partial f_1(x, t)}{\partial x} = 0 \quad (5)$$

Therefore, the second order moment f_1/m is the probability current density.

In certain restricted cases, the state can be described by a finite number of these moments. Thermal states are described by the three lowest order moments [15]. Pure states are described by the two lowest order moments f_0 and f_1 [16]. However, in order to describe arbitrary mixed states, moments of all orders are required.

Higher order moments can be described in terms of those of lower order. To demonstrate this we integrate the conservation equation for the probability density, and obtain

$$f_1(x, t) = -m \int_{-\infty}^x dx' \frac{\partial f_0(x', t)}{\partial t}. \quad (6)$$

Thus, we may reconstruct the probability current density from knowledge of the time derivative of the probability density. Since the two first moment suffice to describe pure states, such states can be reconstructed from the position probability density and the time derivative thereof. This result was first found by Feenberg [17].

For moments of arbitrary order, a recursive reconstruction algorithm can be found [13]

$$\begin{aligned} f_{n+1}(x, t) = & -\mu \frac{\partial}{\partial t} \int_{-\infty}^x dx' f_n(x', t) \\ & - \mu \sum_{k=0}^{[(n-1)/2]} \left(\frac{\hbar}{2i} \right)^{2k} \binom{n}{2k+1} \int_{-\infty}^x dx' \frac{\partial^{2k+1} V(x', t)}{\partial x'^{2k+1}} f_{n-2k-1}(x', t). \end{aligned} \quad (7)$$

We see that every moment is determined from lower order moments. The moments on the r.h.s. in (7) are to be integrated over the space-variable and possibly differentiated over time. This allows one to recursively obtain moments of arbitrary order from lower ones. In this way, the coefficients in the Taylor expansion (1) may be determined.

III. FREE PARTICLE KERNELS

For free particles, the moments can be expressed nonrecursively in terms of the zeroth order moment [18],

$$f_n(x, t) = \frac{m^n}{(n-1)!} \frac{\partial^n}{\partial t^n} \int_{-\infty}^x dx' (x-x')^{n-1} f_0(x', t), \quad n \geq 1. \quad (8)$$

This can be written as a convolution

$$f_n(x, t) = \int dt' \int dx' K_n(x-x', t-t') f_0(x', t'), \quad (9)$$

where the kernel K_n is

$$K_n(x, t) = \frac{(-m)^n}{(n-1)!} \delta^{(n)}(t) x^{n-1} u(x), \quad n \geq 1. \quad (10)$$

$u(x)$ is the step-function, and $\delta^{(n)}(t)$ are n -th order derivatives of Dirac's δ -function.

In a similar manner, we may write the density matrix as a convolution of the probability density with an appropriate kernel function,

$$\langle x+y | \hat{\rho} | x-y \rangle = f_0(x, t) + \int dt' \int dx' K(x-x', t-t', y) f_0(x', t'). \quad (11)$$

Combining Eqs. (1) and (10), we find that the kernel function K is

$$K(x, t, y) = \sum_{n=1}^{\infty} \frac{K_n(x, t)}{n!} \left(\frac{2iy}{\hbar} \right)^n. \quad (12)$$

We may regularize the δ -function derivatives in the kernel in several ways. For example, they may be substituted with gaussian derivatives. It can be shown that

$$\delta^{(n)}(t) = \lim_{a \rightarrow 0} \frac{(-1)^n}{a^{n+1} \sqrt{\pi}} H_n \left(\frac{t}{a} \right) e^{-(t/a)^2}, \quad n \geq 0. \quad (13)$$

Here H_n are Hermite-functions. For regularized kernels, the series (12) can be evaluated to arbitrary order prior to reconstruction.

REFERENCES

- [1] J. Bertrand and P. Bertrand, *Found. Phys.* **17**, 397 (1987).
- [2] K. Vogel and H. Risken, *Phys. Rev. A* **40**, 2487 (1989).
- [3] S. Wallentowitz and W. Vogel, *Phys. Rev. A* **53**, 4528 (1996).
- [4] K. Banaszek and K. Wódkiewicz, *Phys. Rev. Lett.* **76**, 4344 (1996).
- [5] D. Smithey, M. Beck, M. Raymer, and A. Faridani, *Phys. Rev. Lett.* **70**, 1244 (1993).
- [6] G. Breitenbach, S. Schiller, and J. Mlynek, *Nature* **387**, 471 (1997).
- [7] D. Leibfried *et al.*, *Phys. Rev. Lett.* **77**, 4281 (1996).
- [8] M. G. Raymer, M. Beck, and D. F. McAlister, *Phys. Rev. Lett.* **72**, 1137 (1994).
- [9] U. Leonhardt and M. G. Raymer, *Phys. Rev. Lett.* **76**, 1985 (1996).
- [10] U. Leonhardt, T. Kiss, and P. J. Bardroff, *J. Phys. A* **32**, 411 (1999).
- [11] C. Kurtsiefer, T. Pfau, and J. Mlynek, *Nature* **386**, 150 (1997).
- [12] T. Opatrny, D.-G. Welsch, and W. Vogel, *Phys. Rev. A* **56**, 1788 (1997).
- [13] L. M. Johansen, *Phys. Rev. Lett.* **80**, 5461 (1998).
- [14] J. E. Moyal, *Proc. Cambridge Philos. Soc.* **45**, 99 (1949).
- [15] D. Hilbert, *Mathematische Annalen* **72**, 562 (1912).
- [16] E. Madelung, *Z. Phys.* **40**, 322 (1926).
- [17] E. Feenberg, Ph.D. thesis, Harvard University, 1933.
- [18] L. M. Johansen, submitted for publication.

Controlled Quantum Transitions

Nicola Cufaro Petroni

*Dipartimento Interateneo di Fisica dell'Università e del Politecnico di Bari,
INFN, sezione di Bari, INFN Unità di Bari,
Via Amendola 173, I-70126 Bari, Italy.*

Salvatore De Martino, Silvio De Siena, Fabrizio Illuminati

*Dipartimento di Fisica, Università di Salerno,
INFN Sezione di Napoli – Gruppo Collegato di Salerno,
INFN, Unità di Salerno,
via S. Allende, I-84081 Baronissi (Salerno), Italy.*

Abstract

We study controlled transitions of quantum or quantum-like systems from a given initial state associated to a given potential to a final state ruled, in general, by a different potential. An explicit example is supplied in the case of harmonic interactions.

I. INTRODUCTION

In this report we introduce time-dependent potentials which allow to drive, through a controlled and unitary evolution, quantum or quantum-like systems from a given initial state associated to an initial potential, to a preassigned final state (possibly associated to a different potential).

This problem arises in general in quantum mechanics (e.g. quantum optics or controlled chemical reactions), but it can achieve a remarkable interest also for systems whose collective dynamics can be effectively described in a quantum-like formalism (beams in particle accelerators, parametric processes in plasmas, transmission lines etc.).

The controlling potential interpolates between the initial and the final fixed potentials, while the wave function, associated to the controlling potential by the Schroedinger equation, interpolates between the initial and the final fixed states.

We consider here unitary evolutions because, due to the freedom in the choice of controlling potentials, they allow to model the transitions in the more suitable way, depending on the particular case to be considered.

The general idea is to use the hydrodynamic representation of Schroedinger equation [1] as the programming device. In this picture, the Schroedinger equation can be recast in the form of two coupled equations: the Fokker-Planck equation (in the form of a continuity equation),

and the Hamilton-Jacobi-Madelung (HJM) equation (i.e. a dynamical prescription involving the potential). We first exploit the Fokker-Planck part of the Schroedinger equation to drive the state, and we then introduce the so-obtained interpolating wave function in the HJM equation in order to compute the associated controlling potential.

Obviously, the program can be fully accomplished if we are able to compute explicit solutions of the Fokker-Planck equation which (smoothly) interpolate between the initial and the final states. Otherwise, approximations must be implemented.

For sake of clarity, we consider systems in one space dimension, and as a first example we study controlled, smooth transitions between ground states and coherent states associated to different harmonic potentials. This example can be relevant for actual problems of physical interest, for instance the shaping of harmonic atom traps, or the focalization of beams in particle accelerators.

II. FOKKER-PLANCK EQUATION AND QUANTUM SYSTEMS

Let us consider the pair of coupled equations

$$\partial_t \rho = -\partial_x(\rho(\partial_x S/m)); \quad \partial_t S + \frac{(\partial_x S)^2}{2m} - 2mD^2 \frac{\partial_x^2 \sqrt{\rho}}{\sqrt{\rho}} = -V. \quad (1)$$

These equations describe the dynamics of a particle of mass m subject to an external potential V , and whose kinematics is diffusive, with diffusion coefficient D . The first of equations (1) is nothing but the Fokker-Planck equation

$$\partial_t \rho = -\partial_x(\rho v_+) + D\partial_x^2 \rho, \quad (2)$$

written in the form of a continuity equation. If we define the current velocity $v = \partial_x S/m$ and the osmotic velocity $u = D\partial_x \rho/\rho$, the forward drift v_+ in eq. (2) is given by $v + u$. The continuity equation is then semi-sum of the forward Fokker-Planck equation (2), and of its time-reversed (backward) counterpart.

Note that, usually, diffusion processes are associated only to eq. (2), with an *a priori* assigned drift v_+ , which accounts also for the the dynamics. Instead, eqs. (1) are associated to a particular class of diffusion processes (Nelson processes) [2]: in this case, the Fokker-Planck part models the kinematics, while the dynamics is provided by the the HJM equation, which updates at each instant of time the drift, starting by an initial condition.

Contrary to the standard diffusion processes, the ones described by eqs. (1) do not describe dissipative phenomena, but, due to the dynamical updating assured by the HJM equation, preserve time reversal invariance [2].

It is remarkable that Nelson processes can be obtained as extremal solutions of a stochastic variational principle [2]. The latter is a natural extension of the variational principle of classical mechanics, which is obtained by replacing the standard differentiable kinematics by a diffusive kinematics.

Moreover, if one exploits the De Broglie ansatz $\psi = \sqrt{\rho} e^{iS/2mD}$, the pair of equations (1) become equivalent to the linear, Schroedinger-like equation

$$i(2mD)\partial_t \psi = -2mD^2 \partial_x^2 \psi + V\psi. \quad (3)$$

If $D = \hbar/2m$, eqs. (1) or (3) describe a true quantum system. However, eqs. (1), or their linearized version (3), can also provide an effective description for those *classical* systems, where a complex (non dissipative) dynamics is generated by the presence of a very large number of degrees of freedom. Obviously, in these cases the diffusion coefficient is not connected to a fundamental constant, while the function ρ describes the (suitably normalized) spatial density of the elementary constituents of the system; finally, the particle of mass m plays the role of a collective degree of freedom.

The method that we exploit is the following [3]. We select pairs of densities ρ_i, ρ_f such that, inserting ρ_i as initial condition in eq. (2), endowed with a suitable velocity $v_{+,c}$, one obtains ρ_f as the asymptotic solution. In this case, the solution $\rho_c(x, t)$ of the Fokker-Planck equation interpolates between ρ_i and ρ_f . Obviously, this solution is not in general an extremal one in the sense of the stochastic variational principle; however, if one inserts the couple $\rho_c, v_{+,c}$ as input in the HJM equation, one can compute the controlling potential $V_c(x, t)$ so that the solution becomes the extremal solution associated to the potential V_c itself. The interpolating evolution is thus forced to be unitary, and in turn the potential V_c , which supplies the control, interpolates between the potentials associated to the initial and the final conditions.

In the next section, we give a first interesting example of the controlling procedure.

III. TRANSITION BETWEEN HARMONIC WELLS

If the initial and the final densities are both of a gaussian form, with an associated drift field which is linear in the space variable, there always exists an interpolating solution of eq. (2) in the gaussian form [4]

$$\rho_c(x, t) = \frac{e^{-[x-\mu(t)]^2/2\nu(t)}}{\sqrt{2\pi\nu(t)}}. \quad (4)$$

If the initial and final wave functions are ground states or coherent states associated to two harmonic oscillators with different frequencies, eq. (4) allows us to drive smoothly the system from the initial state to the final one by choosing the dispersion $\nu(t)$ and the centre $\mu(t)$ so that they interpolate between the initial and the final values.

In this framework, the definition of the velocities v, u, v_+ , and the relation between the current velocity v and the phase function S give

$$S(x, t) = \frac{m}{2}[\Omega(t)x^2 - 2U(t)x + \Delta(t)], \quad (5)$$

where $\Omega(t), U(t), \Delta(t)$ are functions of $\mu(t), \nu(t)$, and, due to the definition of S , of an arbitrary function of time $\theta(t)$. Note that eq. (5) has the form of the typical quantum phase associated to coherent and/or squeezed states of the harmonic oscillator.

It is possible to show that a suitable choice of the arbitrary part $\theta(t)$ in terms of $\mu(t)$ and $\nu(t)$, allows for a smooth transition from the initial phase to the final one.

Finally, exploiting the HJM equation, one obtains the harmonic, time-dependent controlling potential

$$V_c(x, t) = \frac{m}{2}[\omega^2(t)x^2 - 2a(t)x + c(t)], \quad (6)$$

where

$$\begin{aligned} \omega^2(t) &= \frac{4D^2 - 2\nu(t)\ddot{\nu}(t) + \dot{\nu}^2(t)}{4\nu^2(t)}, \\ a(t) &= \frac{4D^2\mu(t) + 4\nu^2(t)\ddot{\mu}(t) - 2\mu(t)\nu(t)\ddot{\nu}(t) + \mu(t)\dot{\nu}^2(t)}{4\nu^2(t)}, \\ c(t) &= \frac{8D^2\mu^2(t) - 4D\nu(t)\dot{\nu}(t) - 8D^2\nu(t) - (2\nu(t)\dot{\mu}(t) - \mu(t)\dot{\nu}(t) + 2D\mu(t))}{4\nu^2(t)} + \frac{2\dot{\theta}(t)}{m}. \end{aligned} \quad (7)$$

Now, the interpolating functions $\nu(t)$ and $\mu(t)$ can be chosen in an arbitrary number of ways. The choice must then be performed according to the physical goals one wants to achieve [3].

IV. CONCLUSIONS

We have constructed a procedure which, exploiting a stochastic formulation of quantum mechanics, allows for controlled, unitary evolutions of quantum or quantum-like systems. We have provided an explicit example (harmonic wells), and in this case the ample freedom in the choice of the controlling potentials is clearly highlighted. This freedom is of great value, because it can be used to satisfy theoretical or experimental requirements which arise from the specific problems considered. A very interesting development is to introduce optimization criteria by imposing that suitably chosen functionals attain certain extremal values.

Although our general scheme holds in principle for any choice of the pair of initial and final states, the problem of providing explicit examples for nonharmonic potentials is still open. Regarding this point, we are studying both the possibility of exactly solving the problem in particular cases, and of implementing suitable controlled approximation schemes.

A further interesting, and difficult, goal is the extension of these techniques for pure states, to density matrices, in particular with the objective of controlling (reducing) the effects of dissipation and decoherence in quantum optics.

V. REFERENCES

1. E. Madelung, *Z. Physik* **40**, 332 (1926); D. Bohm, *Phys. Rev.* **85**, 166 (1952); D. Bohm, J. P. Vigier, *Phys. Rev.* **96**, 208 (1954).
2. E. Nelson, *Quantum Fluctuations* (Princeton, Princeton U. P.); F. Guerra, *Phys. Rep.* **77**, 263 (1981); F. Guerra, L. Morato, *Phys. Rev.* **D27**, 1774 (1983).
3. N. Cufaro Petroni, S. De Martino, S. De Siena, F. Illuminati, "Controlled quantum evolutions and transitions" (1999), submitted to *J. Phys. A: Math. Gen.*; see also LANL e-print quant-ph/9901054.
4. N. Cufaro Petroni, F. Guerra, *Found. Phys.* **25**, 297 (1995).

“2D-Nonclassical transverse effects in a parametric interaction process”

M. Salvatori, C. Sibilìa, M. Bertolotti

INFN at Dipartimento di Energetica, Università di Roma “La Sapienza”,

via A. Scarpa, 16 – 00161 Rome, Italy – +39-06-49916541, MURST

address: sibilìa@axrma.uniroma1.it

R. Horak

Department of Optics - Palacky University tr 17

listopadu 50, 72146 Olomouc, Czech Republic

Abstract

Non classical spatial effects, such as squeezing, are studied in the transverse domain in the parametric processes of difference frequency generation in travelling plane wave propagation of the field under the hypothesis of low conversion efficiency in a second order nonlinear medium with the assumption of small quantum fluctuations. As expected, we find the spatial quantum effects essentially confined in the instability regions, and with their size being controlled by the initial conditions.

We consider planar propagation of the electric fields, e.g. obtained by means of a waveguide or of a cylindrical lens, in a lossless medium which presents a nonlinear second order susceptibility, in a situation that realizes a DFG process in the slowly varying envelope (SVEA), rotating wave (RW), monochromatic and paraxial approximations at normal incidence [1-5]. Including diffraction, we have the following equations for a collinear interaction ($\omega_3 - \omega_1 = \omega_2$, $\Delta k = k_3 - k_1 - k_2$, being $k = 2\pi / \lambda = \omega / c$)

$$\begin{cases} \left(i \frac{\partial}{\partial Z} - 1 + \frac{\partial^2}{\partial X^2} \right) Q_1 = -Q_3 Q_2^* \\ \left(i \frac{\partial}{\partial Z} - 1 + \frac{k_1}{k_2} \frac{\partial^2}{\partial X^2} \right) Q_2 = -\frac{k_1}{k_2} Q_3 Q_1^* \\ \left(i \frac{\partial}{\partial Z} - 1 + \frac{k_1}{k_3} \frac{\partial^2}{\partial X^2} \right) Q_3 = -\frac{k_1}{k_3} Q_1 Q_2 \end{cases} \quad (1)$$

where the a-dimensional quantities are related to the physical ones by

$$Z = z\Delta k, \quad X = x\sqrt{2k_1\Delta k}, \quad C_j = \frac{16\pi d\omega_j^2}{c^2}, \quad Q_j = E_j \frac{\sqrt{C_i C_k}}{2k_1\Delta k}, \quad (2)$$

(i,j,k=1,2,3 and different from each other), d is the nonlinear tensor component pertinent to the chosen geometry and E_j 's are the amplitudes of the electrical fields of the waves of frequency ω_j .

We can obtain the cascaded $\chi^{(2)}$ effect if we suppose a low conversion efficiency between the input fields (ω_1, ω_3) into the generated field (ω_2) [1,5]

$$|Q_2| \gg \left| \left(i \frac{\partial}{\partial Z} + \frac{k_1}{k_2} \frac{\partial^2}{\partial X^2} \right) Q_2 \right|, \quad (3)$$

so the two coupled equations for the fields at ω , and ω_3 result

$$\begin{cases} \left(i \frac{\partial}{\partial Z} - 1 + \frac{\partial^2}{\partial X^2} \right) Q_1 = -\frac{k_1}{k_2} |Q_3|^2 Q_1 \\ \left(i \frac{\partial}{\partial Z} - 1 + \frac{k_1}{k_3} \frac{\partial^2}{\partial X^2} \right) Q_3 = -\frac{k_1^2}{k_2 k_3} |Q_1|^2 Q_3 \end{cases} \quad (4)$$

and the fields undergo a cross phase modulation in which the nonlinear phase shift of one input field is controlled by the intensity of the other input field.

The hypothesis (3) is equivalent to assume an undepleted regime, i.e. $|Q_j(ZX)| = |Q_j(0, X)|$ ($j=1,3$) and a propagation distance dependence that stays only in the phase factors of $Q_j(ZX) = |Q_j(x)| e^{i\varphi_j(Z)}$, with

$$\begin{aligned} \varphi_1(Z) &= \varphi_1(0) + \left(\frac{k_1}{k_2} |Q_3|^2 - 1 \right) Z \\ \varphi_3(Z) &= \varphi_3(0) + \left(\frac{k_1^2}{k_2 k_3} |Q_1|^2 - 1 \right) Z \end{aligned} \quad (5)$$

Classical solutions are discussed in ref. [5] together with the instability conditions realized during the propagation.

The quantum description can be performed by introducing the operators \hat{Q} 's corresponding to the classical field amplitudes which satisfy the same equations as eqs. (1)

$$\begin{cases} \left(i \frac{\partial}{\partial Z} - 1 + \frac{\partial^2}{\partial X^2} \right) \hat{Q}_1 = -\hat{Q}_2^+ \hat{Q}_3 \\ \left(i \frac{\partial}{\partial Z} - 1 + \frac{k_1}{k_2} \frac{\partial^2}{\partial X^2} \right) \hat{Q}_2 = -\frac{k_1}{k_2} \hat{Q}_1^+ \hat{Q}_3 \\ \left(i \frac{\partial}{\partial Z} - 1 + \frac{k_1}{k_3} \frac{\partial^2}{\partial X^2} \right) \hat{Q}_3 = -\frac{k_1}{k_3} \hat{Q}_1 \hat{Q}_2 \end{cases} \quad (6)$$

and obey boson commutation relations [3,5]

$$\begin{aligned} [\hat{Q}_i(X, Z), \hat{Q}_j^+(X', Z)] &= \delta_{ij} \delta(X - X'), \\ [\hat{Q}_i(X, Z), \hat{Q}_j(X', Z)] &= 0, \\ [\hat{Q}_i^+(X, Z), \hat{Q}_j^+(X', Z)] &= 0. \end{aligned} \quad (7)$$

In terms of photons, eqs. (6) enable us at once to interpret \hat{Q} and \hat{Q}^+ as destruction and creation operators in the Fock space. We assume now that the full quantum character is associated to the small fluctuations of the classical field $Q(Z)$, i.e.

$$\hat{Q}(X, Z) = Q(Z) + \hat{q}(X, Z), \quad (8)$$

where the c-number part is the plane wave stationary solution of the classical equations. The commutation relations for the \hat{q} 's are the same as for the \hat{Q} 's. To study these fluctuations it is well suited the coherent vacuum state $|0\rangle$ (with the normalization $\langle 0|0\rangle = 1$).

We want to discuss the process of DFG in the case of low conversion efficiency. The linearization with respect to the fluctuations excludes operator ordering problems and the development along the Z axis is the same as the classical one. So we have (j=1,3)

$$\hat{q}_j(X, Z) = \frac{e^{i\varphi_j(Z)}}{\sqrt{2\pi}} \int d\sigma e^{-i\alpha X} (t_{j1}(\sigma, Z)\hat{c}_1(\sigma, 0) + t_{j2}(\sigma, Z)\hat{c}_1^*(-\sigma, 0) + t_{j3}(\sigma, Z)\hat{c}_3(\sigma, 0) + t_{j4}(\sigma, Z)\hat{c}_3^*(-\sigma, 0)). \quad (9)$$

The operators \hat{c} at the crystal input follow the commutation relations

$$[\hat{c}_i(\sigma, 0), \hat{c}_j^*(-\sigma', 0)] = \delta_{ij}\delta(\sigma + \sigma'), [\hat{c}_i(\sigma, 0), \hat{c}_j(-\sigma', 0)] = 0, [\hat{c}_i^+(\sigma, 0), \hat{c}_j^*(-\sigma', 0)] = 0 \quad (10)$$

These \hat{c} 's act on the vacuum in the usual manner: $\hat{c}(\sigma, 0)|0\rangle = 0$, $\langle 0|\hat{c}^*(-\sigma, 0) = 0$.

The generated field at ω_2 is found as a function of the other two fields

$$\hat{q}_2 \equiv \frac{k_1}{k_2} \frac{e^{i(\varphi_3 - \varphi_1)}}{\sqrt{2\pi}} \int d\sigma e^{-i\alpha X} (|Q_3|\hat{c}_1^+ + |Q_1|\hat{c}_3). \quad (11)$$

To investigate quantum effects we need observable quantities, i.e. hermitian field operators. Therefore we define the quadrature phase operator

$$\hat{Q}^{(\theta)} = \frac{1}{2}(\hat{Q}e^{i\theta} + \hat{Q}^+e^{-i\theta}).$$

The central second moment of $\hat{Q}^{(\theta)}$, i.e. its variance, on the vacuum field state is

$$\langle (\Delta\hat{Q}^{(\theta)})^2 \rangle = \langle (\hat{Q}^{(\theta)} - \langle \hat{Q}^{(\theta)} \rangle)^2 \rangle = \frac{1}{4}(\langle \hat{q}\hat{q}^+ \rangle + \langle \hat{q}^+\hat{q} \rangle + 2\text{Re}(e^{2i\theta}\langle \hat{q}\hat{q} \rangle)). \quad (12)$$

This quantity measures the deviations of the quadrature operator from its mean value versus Z and X, so it is directly related to the following quantity

$$\langle (\Delta\hat{Q}^{(\theta)})^2 \rangle = \int d\sigma S^{(\theta)} \quad (13)$$

where $S^{(\theta)}$ is the power spatial spectrum of the quantum noise.

We take fields in a coherent input state, the shot-noise level is defined as normalisation parameter: $S^{(\theta)}(\sigma, Z=0)$. Then the spatial noise spectrum normalized to the coherent noise $S^{(\theta)}(\sigma, 0)$ is $S^{(\theta)}(\sigma, Z) = S^{(\theta)}(\sigma, Z)/S^{(\theta)}(\sigma, 0)$. Squeezing effects appear for those angles such that $S^{(\theta)}(\sigma, Z) < 1$.

The other quantity we will utilize is the fourth moment of the field \hat{Q}

$$\langle \hat{Q}^{+2}\hat{Q}^2 \rangle - \langle \hat{Q}^+\hat{Q} \rangle^2 = 2\text{Re}(Q^{*2}\langle \hat{q}\hat{q} \rangle) + 2|Q|^2\langle \hat{q}^+\hat{q} \rangle - 4(\text{Re}(Q^*\langle \hat{q} \rangle))^2 + o(\hat{q}^3). \quad (14)$$

Its significance becomes clear if we introduce the number operator (proportional to the beam intensity) $\hat{n} = \hat{Q}^+\hat{Q}$: the fourth moment is then $\langle \Delta\hat{n}^2 \rangle - \langle \hat{n} \rangle^2$. A nonclassical deviation from the coherent statistics gives negative values (subpoissonian light), while positive values correspond to superpoissonian classical light. To study the variation of the photon correlation on the transverse axis we define the spectrum of bunching $B(\sigma, Z)$ as [5]

$$\langle \hat{Q}^{+2}\hat{Q}^2 \rangle - \langle \hat{Q}^+\hat{Q} \rangle^2 = \int d\sigma B(\sigma, Z), \quad (15)$$

(clearly, if it is negative, it indicates antibunching).

With the aid of these two functions (the spectra of squeezing and bunching), we can analyse the quantum behaviour of the fields at the crystal output after the nonlinear mixing. In the case of the DFG process, the squeezing spectrum

$$\int d\sigma S_j^{(\theta)}(\sigma, Z) = \left\langle \left(\Delta \hat{Q}_j^{(\theta)}(X, Z) \right)^2 \right\rangle = \frac{1}{4} \left(\langle \hat{q}_j(X, Z) \hat{q}_j^+(X, Z) \rangle + \langle \hat{q}_j^+(X, Z) \hat{q}_j(X, Z) \rangle + 2 \operatorname{Re} \left(e^{2i\theta} \langle \hat{q}_j(X, Z) \hat{q}_j(X, Z) \rangle \right) \right) \quad (16)$$

is found by calculating the expectation values in the last member of eq. (16). We see that, in the vacuum state, the unique nonvanishing contributions derive from terms containing the combinations $\langle 0 | \hat{c}_j(\sigma, 0) \hat{c}_j^+(-\sigma, 0) | 0 \rangle$, confirming the fundamental nature of quantum noise, depending on the noncommutativity of the operators rather than on accidental causes, such as instrumental errors, which determine the classical noise. Then it results (j=1,3)

$$S_j^{(\theta)}(\sigma, Z) = \sum_1^4 |t_{j1}(\sigma, Z)|^2 + 2 \operatorname{Re} \left(e^{2i(\varphi_j(Z)+\theta)} (t_{j1}(\sigma, Z)t_{j2}(\sigma, Z) + t_{j3}(\sigma, Z)t_{j4}(\sigma, Z)) \right). \quad (17)$$

For the generated field

$$S_2^{(\theta)}(\sigma, Z) = \frac{1}{|Q_3|^2 + |Q_1|^2} \left(\sum_1^4 \left(|Q_3|^2 |t_{1l}|^2 + |Q_1|^2 |t_{3l}|^2 \right) + |Q_3 Q_1| 2 \operatorname{Re} (t_{11}t_{32} + t_{12}t_{31} + t_{13}t_{34} + t_{14}t_{33}) \right) + 2 \operatorname{Re} \left(e^{2i(\varphi_3 - \varphi_1 + \theta)} \left(|Q_3|^2 (t_{11}t_{12} + t_{13}t_{14})^* + |Q_1|^2 (t_{31}t_{32} + t_{33}t_{34}) + |Q_3 Q_1| \sum_1^4 t_{1l}^* t_{3l} \right) \right). \quad (18)$$

It is important to note that squeezing spectrum $S_j^{(\theta)}(6, Z)$ depends on phase $\varphi_j(Z)$ and on σ . This allows to expect an "optimized" squeezing spectrum for the fields at ω_1 and ω_3 . For the generated field at the frequency ω_2 , we have (see eq. 18) a dependence on the phase difference; therefore we expect for $S_2^{(\theta)}(\sigma, Z)$ a more sensible dependence on the initial conditions. Squeezing spectrum depend strongly on the spatial frequencies at wich modulational instability occurs in the classical propagation for such process.

The bunching spectrum is

$$B_j(\sigma, Z) = \frac{|Q_j|^2}{\pi} \left(|t_{j2}(\sigma, Z)|^2 + |t_{j4}(\sigma, Z)|^2 + \operatorname{Re} (t_{j1}(\sigma, Z)t_{j2}(\sigma, Z) + t_{j3}(\sigma, Z)t_{j4}(\sigma, Z)) \right), \quad (19)$$

(j=1,3); with a coherent input, $B_j(\sigma, 0) = 0$. For the generated field one has

$$B_2(\sigma, Z) = \frac{|Q_3 Q_1|^2}{\pi} \frac{k_1^4}{k_2^4} \left(\operatorname{Re} \left(|Q_3|^2 (t_{11}t_{12} + t_{13}t_{14})^* + |Q_1|^2 (t_{31}t_{32} + t_{33}t_{34}) + |Q_3 Q_1| \sum_1^4 t_{1l}^* t_{3l} \right) + |Q_3|^2 (|t_{11}|^2 + |t_{13}|^2) + |Q_1|^2 (|t_{32}|^2 + |t_{34}|^2) + |Q_3 Q_1| 2 \operatorname{Re} (t_{11}t_{32} + t_{13}t_{34}) \right), \quad (20)$$

$$\text{and } B_2(\sigma, 0) = \frac{|Q_3 Q_1|^2}{\pi} \frac{k_1^4}{k_2^4} |Q_3|^2 > 0.$$

Bunching occurs at spatial frequencies at wich stable classical propagation is realized.

References

- 1 R. De Salvo, D. J. Hagan, M. Sheik-Bahae, G. Stegeman, E. W. Van Stryland, H. Vanherzeele, *Opt. Lett.*, **17**, 28 (1992).
- 2 R. Boyd "Nonlinear Optics", Academic Press (1992).
- 3 A. Buryak, Y.S. Kivshar, *Opt. Lett.* **15**, 1613 (1994)
- 4 C. Sibilia, V. Schiavone, M. Bertolotti, R. Horak, J. Perina, *J. Opt. Soc. Am. B*, **11**, 2175 (1994).
- 5 M.Salvatori, C.Sibilia, M.Bertolotti, R.Horak, Submitted for publication

NEW METHOD FOR SOLVING QUANTUM EQUATION OF SECOND HARMONIC GENERATION OR HIGHER ORDER

Z. S. Sazonova[†], Ranjit Singh[‡]

*[†]Moscow State Automobile & Road Construction Institute (Technical University), 64,
Leningradsky prospect, Moscow 125829, Russia
Tel.: (7-095) 155-0390
E-mail: sazonova@dataforce.net*

*[‡]General Physics Institute of Russian Academy of Sciences, Wave Research Center,
38, Vavilov street, Moscow 117942, Russia
Tel./Fax: (7-095) 135-8234
E-mail: ranjit@dataforce.net*

Abstract

We have applied our method especially for the case of second harmonic generation (SHG) and numerically solved the nonlinear quantum equation of SHG for large number of photons at the input of the nonlinear crystal of second order susceptibility. But our method can be easily applied for the higher order harmonic generation. Also, we have calculated the photon statistics of SHG mode.

1. INTRODUCTION

Theoretically there are not exact methods (see in the monographs: [3-5]) to solve the quantum equation of second harmonic (SH) generation. Numerically, it was solved by [1-2] for the limited number of photons i.e., 20 – 200 at the input of the NLC (nonlinear crystal). To our best knowledge, in quantum optics, the exact solution of nonlinear equation of SH is mathematically unsolved due to the second order operator equations. There are not exact methods, which can be applied to solve the quantum equation of SH.

We have used the matrix method to solve numerically the non-linear equations of SH for the large number of photons at the input of nonlinear crystal. Interaction Hamiltonian of SH is represented in the form of the matrix, which is diagonalized with the help of computer. The eigenvectors and eigenvalues of interaction Hamiltonian are also calculated with the help of computer. Time dependent probability function and average number of photons in the SH are numerically calculated and are shown in the graphics. We have compared our results to the earlier works of [1-2] on the SH.

In paragraph 2, we have diagonalized the interaction Hamiltonian of SH and calculated the time dependent probability function of transformation of photons from fundamental mode to SH numerically. In paragraph 3, we have calculated time dependent average number of photons in the SH.

2. DIAGONALIZING THE HAMILTONIAN OF SHG

The interaction Hamiltonian of SH is well known, which is written as:

$$\hat{H}_{\text{int}} = \hbar (g \hat{a}^2 \hat{b}^+ + g^* \hat{a}^{+2} \hat{b}) \quad (1)$$

Here \hbar Plank's constant, \hat{a} (\hat{a}^+), \hat{b} (\hat{b}^+) are the destruction (creation) operators of fundamental and SH mode, g - is the coupling constant. We are considering the case of perfect phase matching. The coupling constant g is constant. For the simplicity, we have taken $\hbar = 1, g = 1$.

We have taken the interaction Hamiltonian in the matrix form for the Fock states (number states) of the following basis: $|n, m\rangle$. Here n and m are the number of photons in the fundamental and SH modes, n is positive integer and m is also positive integer but runs from 0 to $n/2$. As is well known, in the SH process, we need two photons from the fundamental mode to convert them in one photon of SH. So, the basis $|n, m\rangle$ will take the new form $|n-2m, m\rangle$. Matrix elements of the interaction Hamiltonian are:

$$(H_{\text{int}})_{m,m'} = \langle n-2m, m | \hat{H}_{\text{int}} | m', n-2m' \rangle = \begin{cases} \sqrt{(n-2m)(n-2m-1)(m+1)} & \text{if } m = m' - 1 \\ \sqrt{(n-2m')(n-2m'-1)(m'+1)} & \text{if } m' = m - 1 \end{cases} \quad (2)$$

The matrix of interaction Hamiltonian is symmetric above and below the principal diagonal elements, which is similar to the Jacobi matrix. Dimensions of the interaction Hamiltonian matrix are $(n/2+1) \times (n/2+1)$. The matrix form of the interaction Hamiltonian is:

$$(H_{\text{int}})_{m,m'} = \begin{pmatrix} 0 & (H_{\text{int}})_{12} & 0 & 0 & 0 & 0 & 0 \\ (H_{\text{int}})_{21} & 0 & (H_{\text{int}})_{23} & 0 & 0 & 0 & 0 \\ 0 & (H_{\text{int}})_{32} & 0 & \cdot & 0 & 0 & 0 \\ 0 & 0 & \cdot & \cdot & \cdot & 0 & 0 \\ 0 & 0 & 0 & \cdot & \cdot & \cdot & 0 \\ 0 & 0 & 0 & 0 & \cdot & \cdot & (H_{\text{int}})_{n'/m} \\ 0 & 0 & 0 & 0 & 0 & (H_{\text{int}})_{mm'} & 0 \end{pmatrix} \quad (3)$$

The method of diagonalization of interaction hamiltonain and to calculate eigenvector and eigenvalues of interaction hamiltonain is thoroughly explained in the monographs [6-8]. Interaction hamiltonain is diagonalized with the help of the computer for the large number of photons i.e., 2-20000 and more. Eigenvectors and eigenvalues of the interaction hamiltonain are also calculated and normalized.

The probability of having $n/2$ number of photons in the SHG for the Fock states at time t is as follows:

$$P\left(\frac{n}{2}, t\right) = \left| \langle 0, n/2 | \exp(-i H_{\text{int}} t) | n, 0 \rangle \right| \quad (4)$$

The equation (4) is reduced and will take the following form:

$$P\left(\frac{n}{2}, t\right) = \left| \sum_{l=0}^{n/2} v_{l,0} v_{l,n/2} \exp(-i h_{l,l} t) \right|^2 \quad (5)$$

Here $v_{m,m'}$ are the elements of square eigenvector matrix $V_{m,m'}$ of the dimensions $(n/2+1) \times (n/2+1)$, $h_{m,m}$ are the elements of eigenvalues of the diagonalized matrix H_{int} of the dimensions $(n/2+1) \times (n/2+1)$.

We have numerically diagonalized the interaction hamiltonain and calculated the eigenvecotrs and eigenvalues of the interaction hamiltonain. Time dependent probability of having $n/2$ number of photons in the SH for the different initial number of photons are calculated numerically.

3. AVERAGE NUMBER OF PHOTONS IN THE SH MODE

Average number of photons in the SH is given by:

$$\langle N2(t) \rangle = \sum_{n=0}^{n/2} n P(n, t) \quad (6)$$

We have numerically calculated the (6) for the different initial number of photons at the input of NLC. The fig. 1: (a), (b) and (c) are showing the aperiodicity character of average number of photons in the SH.

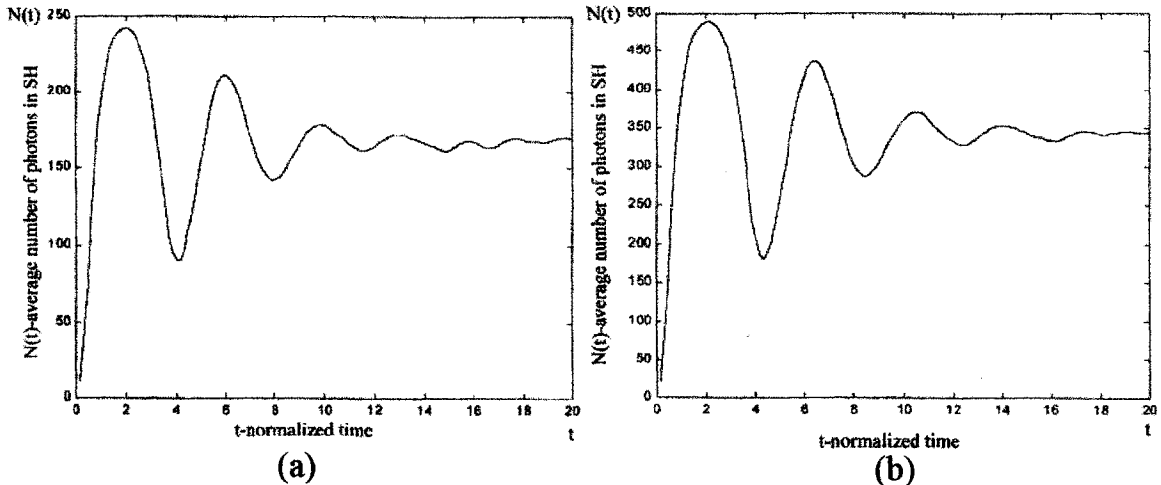
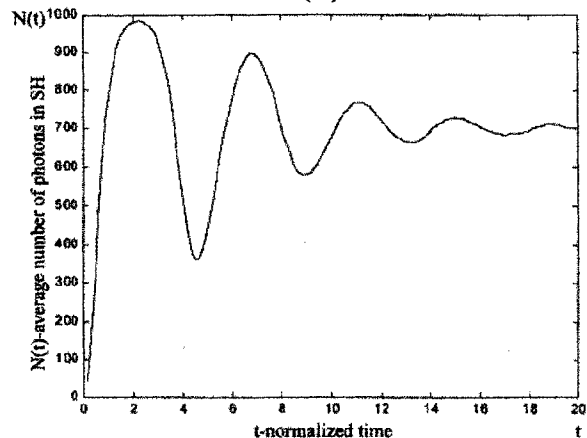


Fig. 1 Average number of photons in the SH mode for the following initial number of photons in the fundamental mode: (a) $n = 500$, (b) $n = 1000$, (c) $n = 2000$.



4. DISCUSSIONS

We have been developing the computer code (program) for the diagonalization of huge Jacobian type matrices (3) and to find the eigenvectors. We have solved numerically the quantum equation of SH for the large number of photons at the input of the NLC, which was unsolved earlier. We have got the aperiodicity in the SH mode, which contradicts the theory and experiment of generation of SHG in the classical optics. From where this aperiodicity arises in SH? What is the reason of this aperiodicity in SHG? Can we detect this aperiodicity in the experiment of SHG? These questions are under study. To our knowledge the aperiodicity in SHG may arise due to the vacuum quantum noise.

This method can be easily applied for the higher order harmonic generation. The quantum solution of third harmonic generation is under process.

ACKNOWLEDGEMENTS

We cordially thank A. S. Chirkin, V. P. Krainov and A. V. Masalov for several useful discussions.

REFERENCES

- [1] Walls D and Barakat R 1970 *Phys. Rev. A* **1** 446-453
- [2] Nikitin S and Masalov A 1991 *Quantum Opt.* **3** 105-113
- [3] Perina J 1991 *Quantum Statistics of Linear and Nonlinear Optical Phenomena* (Dordrecht: Kulwer Academic Publishers)
- [4] Loudon R 1973 *The Quantum Theory of Light* (Oxford: Clarenton Press)
- [5] Walls D and Milburn G 1995 *Quantum Optics* (Heidelberg: Springer-Verlag)
- [6] Bellman, R 1960, *Introduction to Matrix Analysis* (New York: McGraw-Hill Book company, INC.)
- [7] Lankaster P 1969, *Theory of Matrices*, (New York: Academic Press)
- [8] Gantmakher F 1967, *Theory of Matrices*, (Moscow: Nauka) (In Russian)

Theory of Solitary Waves in Synchrotrons

Hans Schamel

Physikalisches Institut, Universität Bayreuth, D-95440 Bayreuth, Germany

Abstract

Observations in stored high-energy beams in circular accelerators show the existence of long-living coherent structures of solitary wave type. The paper focuses on a collective kinetic description of such solitary structures based on an extended Vlasov-Poisson model. Depending on the coupling impedance, on the selected dispersion branch and on the beam energy in relation to the transition energy various solutions of this system can be found. Of special interest is the one, represented by a notch in the thermal range of the distribution function, for which standard wave theory would predict strong Landau damping.

In this paper stationary solitary structures propagating in coasting beams will be constructed [1] which are in favor of recent observations made at the FERMI lab [2]. Concentrating on a perfectly conducting wall situation, we get as the basic set of equations [3]

$$[\partial_t + u\partial_z - \varepsilon\partial_u] f(z, u, t) = 0 \quad (1)$$

$$\varepsilon'' = \alpha g_0 \lambda_1' + \mu \varepsilon \quad (2)$$

where we adopt the normalization of Ref. [1]. The parameter μ is proportional to γ^2 , where γ measures the relativistic beam energy, and α is proportional to η , the slip factor. Both parameters are assumed to be large, g_0 is a geometry factor [1,3]. The beam dynamics in the presence of an electric field $\varepsilon = -\partial_z \phi$ is described by the Vlasov equation (1), whereas the feedback is self-consistently represented by the Poisson-like model equation (2). λ_1 is the perturbed line density. Assuming a solution of (1) of the form of eq. (14) in [1], we get in the small amplitude limit

$$\lambda_1(z) = -\frac{1}{2} Z_r' \left(\frac{\Delta u}{\sqrt{2}} \right) \phi - \frac{4}{3} b(\beta, \Delta u) \phi^{3/2} + \dots \quad (3)$$

where Z_r is the real part of the plasma dispersion function, β a parameter characterizing the trapped particle distribution and Δu is the yet unknown velocity of the solitary structure in the frame moving with the nominal beam velocity.

Inserting (3) into (2) we find after one integration

$$\phi'' = A\phi + B\phi^{3/2} \equiv -V'(\phi) \quad (4)$$

where the parameters A and B are given by

$$A = \mu + g_0\alpha \frac{1}{2} Z'_r(\Delta u/\sqrt{2}) \quad (5a) \quad B = \frac{4g_0\alpha}{3} b(\beta, \Delta u) \quad (5b)$$

where $b(\beta, \Delta u) = \pi^{-1/2}[1 - \beta - (\Delta u)^2] \exp(-\frac{1}{2}\Delta u^2)$. A further integration of (4) yields the “energy law” $\phi'(z)^2 + 2V(\phi) = 0$ with $V(\phi)$ given by

$$-V(\phi) = A\phi^2/2 + \frac{2}{5}B\phi^{5/2} \quad (6)$$

where $V(0) = 0$ was assumed. Two further conditions guarantee the existence of solitary wave solutions

$$\text{i) } V(\psi) = 0 \quad (7a) \quad \text{ii) } V(\phi) < 0, \quad 0 < \phi < \psi \quad (7b)$$

where ψ is the amplitude of the bell-shaped potential, we are looking for.

Condition i) represents the nonlinear dispersion relation (NDR) as it allows the determination of Δu in terms of ψ (and β). Making use of (7a) we can rewrite $V(\phi)$:

$$-V(\phi) = -\frac{2B}{5}\phi^2[\sqrt{\psi} - \sqrt{\phi}] \quad (8)$$

and through a further integration of the “energy law” we find

$$\phi(z) = \psi \operatorname{sech}^4\left(\sqrt{\frac{-B\psi^{1/2}}{20}}z\right) \quad (9)$$

the desired solitary wave solution. The last step, however, requires $B < 0$. To see its consequences, we evaluate the NDR (7a) which becomes

$$-\frac{1}{2}Z'_r(\Delta u/\sqrt{2}) = \frac{\mu}{g_0\alpha} + \frac{16}{15}b\sqrt{\psi} \equiv D \quad (10)$$

Assuming the rhs of (10), D , small, we can make use of the expansion $-\frac{1}{2}Z'_r(x) = 1 - x/x_0$, where $x_0 = 0.924$ and $|x - x_0|$ is assumed to be small. The solution of (10) is then

$$\Delta u = 1.307(1 - D) \quad (11)$$

The phase velocity of the structure is therefore uniquely determined. It lies in the thermal range of the Maxwellian type distribution. Using Δu from (11), we get for b

$$b = \pi^{-1/2}(-\beta - 0.71) \exp(-0.854) \approx 0.24(-\beta - 0.71) \quad (12)$$

and the condition $B = \frac{4g_0\alpha b}{3} < 0$ becomes $\alpha(-\beta - 0.71) < 0$.

For a beam below transition energy, $\alpha < 0$, we thus arrive at the condition $-\beta > 0.71$ i.e. the distribution function must be sufficiently depleted in the resonant region. This corresponds to the observations made in [2], where notches in the beam transfer function reflecting the momentum distribution were found.

On the other hand, a beam above transition energy, $\alpha > 0$, requires $-\beta < 0.71$, satisfied e.g. by a positive β . A $\beta > 0$ corresponds to a hump in the resonant part of the distribution function. This essentially confirms and substantiates the “mass-conjugation theorem” conjectured in [4].

A solitary wave with a smaller speed can be obtained too: Assuming $\Delta u \ll 1$, the lhs of (10) becomes $-\frac{1}{2}Z'_r(x) = 1 - 2x^2 + \dots$ where $|x| \ll 1$, and we get $\Delta u = (1 - D)^{1/2} \ll 1$ from which $-\beta \lesssim \frac{15(g_0\alpha - \mu)}{16g_0\alpha\sqrt{\psi}}$ can be derived. In a beam below transition energy, $\alpha < 0$, the distribution function at resonant velocity appears to be depressed stronger, since $-\beta \sim \psi^{-1/2} \gg 1$. The deeper the notch in the distribution function the slower the solitary wave propagates.

Note that these are extreme states far away from thermal equilibrium, and hence are not accessible by a hydrodynamic description, unlike KdV solitons.

One puzzle remains. Extending the above consideration to periodic wave trains and assuming $|D| \ll 1$ and negligible, we get instead of (10)

$$k^2 - \frac{1}{2}Z'_r\left(\frac{\omega_r}{\sqrt{2}k}\right) = 0 \quad (13)$$

where k is the wave number of the harmonic wave train and $\Delta u = \omega_r/k$. Linearized Vlasov-Poisson theory (Landau theory) on the other hand yields

$$k^2 - \frac{1}{2}Z'\left(\frac{\omega}{\sqrt{2}k}\right) = 0 \quad (14)$$

which is now a complex dispersion relation and has only heavily damped solutions in the thermal range ($\omega = \omega_r + i\gamma$ with $\gamma < 0$). According to the standard linearized wave theory, found in all plasma textbooks, such an undamped mode should not exist at all.

The solution of this discrepancy is that by linearizing the Vlasov-Poisson system and by making use of the Landau contour in handling the wave-particle resonance the above wave solution is lost. Generally speaking, due to the wave-particle resonance the linearization of the Vlasov-Poisson system is not automatically justified even in the infinitesimally small amplitude limit. An appropriate seed distortion which changes the topology in phase space in the resonant range of a width of $O(\psi^{1/2})$ creates such a marginal mode which is hence fundamentally nonlinear even in the infinitesimal wave limit.

Finally we point out the close proximity of the present collective wave description to the thermal wave model (TWM) of [6,7]. In the TWM the beam is described in paraxial approximation by a nonlinear Schrödinger equation which governs the beam wave function. The Planck’s constant is thereby replaced by the transverse beam emittance ϵ and the interaction potential is provided by the wake-potential, a beam particle is surrounded with due its interaction with the image-charges in the wall and its self-interaction potential. Introducing a Wigner-like distribution function $f(z, u, t)$ and performing the semi-classical small emittance limit $|\epsilon| \ll 1$, one obtains a von Neumann-like equation which coincides in the limit $\epsilon \rightarrow 0$ with the Vlasov equation. Quantum-like corrections enter in $O(\epsilon)$, and the interesting question arises, how the present solitary waves are modified by those $O(\epsilon)$ -corrections.

The author acknowledges financial support by INFN and valuable discussions with Dr. R. Fedele.

REFERENCES

- [1] H. Schamel, *Phys. Rev. Lett.* **79**, 2811 (1997)
- [2] P.L. Colestock and L.K. Spentzouris, The Tamara Symposium Proceedings, Austin Texas 1994, AIP Conference Proc. 356 (AIP, Woodbury, N.Y.)
- [3] R. Fedele and H. Schamel (to be published)
- [4] R.A. Dory, *Plasma Phys.* **6**, 511 (1964)
- [5] A.F. Aleksandrov and A.A. Rukhadze, *Plasma Physics Reports* **23**, 442 (1997)
- [6] R. Fedele and G. Miele, *Nuovo Cimento D* **13**, 1527 (1991)
- [7] R. Fedele and V.I. Man'ko, *Phys. Rev. E* **58**, 992 (1998)

QUANTUM PROPERTIES OF POLARIZATION AND QUANTUM PHASE OF ELECTROMAGNETIC RADIATION

Alexander S. Shumovsky

Physics Department, Bilkent University, Bilkent, 06533 Ankara, Turkey

Abstract

For arbitrary multipole radiation of a quantum source the operators of creation and annihilation of polarization are constructed at any space-time point. It is shown that the polarization in the near and intermediate zones is described by the $SU(3)$ algebra of operators which is reduced to the $SU(2)$ algebra in the far zone. A dual representation of these operators, involving the quantum phase properties of the spin states of photons, is considered.

The purpose of this paper is to discuss how the polarization of radiation of a localized quantum source can be described.

The remarkable recent progress in quantum optics gave rise to a strong interest in the quantum polarization measurements. As a particular example of considerable interest, we mention here the quantum entanglement investigation (e.g., see [1]). In the usual treatment of quantum polarization [2,3], the polarization properties of radiation are calculated as though the radiation field consisted of plane waves of photons. It is clear that this picture is incapable of describing the polarization of radiation of a quantum localized source such as an atom or molecule at an arbitrary distance. The point is that the atomic and molecular transitions emit *multipole radiation* represented by *spherical* rather than plane waves of photons [4]. The plane waves of photons correspond to the states with given linear momentum \vec{P} , i.e. with given direction of propagation \vec{k} and two polarizations always orthogonal to \vec{k} . Therefore, the polarization is usually defined to be the measure of the transversal anisotropy of the radiation field [5].

The spherical waves of photons describe the states with given angular momentum \vec{J} . Since $[\vec{P}, \vec{J}] \neq 0$, the spherical waves of photons do not have well defined direction of propagation. In the three-dimensional space they can be specified by three orthogonal unit vectors $\{\vec{\chi}_\mu\}$, describing the states $\mu = 0, \pm 1$ of the spin 1 of photons [6]. It is hence clear that the polarization of radiation of a localized source, both classical and quantum, should be determined as the measure of the *spatial* rather than transversal anisotropy of the field [7,8].

Consider a monochromatic pure (jm) multipole radiation of a quantum source localized at the origin. The vector potential of such a radiation has the form [4,6]

$$\vec{A}(\vec{r}) = \sum_{\mu=-1}^1 \vec{\chi}_{\mu} \sum_{m=-j}^j V_{\mu m}(\vec{r}) a_{jm}. \quad (1)$$

Here $V_{\mu m}(\vec{r})$ are the known functions of position with respect to the source and the operator a_{jm} describes the annihilation of a spherical photon with given j and m . It is clear that the spatial components $A_{\mu}(\vec{r}) = \vec{\chi}_{\mu}^+ \cdot \vec{A}(\vec{r})$ of (1) obey the following commutation relations

$$[A_{\mu}(\vec{r}), A_{\mu'}^{\dagger}(\vec{r})] = \sum_m V_{\mu m}(\vec{r}) V_{\mu' m}^*(\vec{r}) \equiv \mathcal{V}_{\mu\mu'}(\vec{r}). \quad (2)$$

Here the right-hand side determines the entries of the Hermitian (3×3) matrix $\mathcal{V} = ||\mathcal{V}_{\mu\mu'}(\vec{r})||$, which can be diagonalized by a unitary transformation $U(\vec{r})$. This transformation describes the rotation of the basis $\{\vec{\chi}_{\mu}\}$. The same rotation converts (1) into the form

$$\mathcal{A}_{\mu}(\vec{r}) = (W_{\mu})^{-1/2} \sum_{\mu'=-1}^1 U_{\mu\mu'}^*(\vec{r}) A_{\mu'}(\vec{r}) \quad (3)$$

where W_{μ} is the real positive diagonal element of $U^{\dagger} \mathcal{V} U$. The "turned" vector potential (3) obey the commutation relations

$$[\mathcal{A}_{j\mu}(\vec{r}), \mathcal{A}_{j\mu'}^{\dagger}(\vec{r})] = \delta_{\mu\mu'}$$

similar to those for conventional non-local photon operators. Therefore, one can choose to interpret (3) as the annihilation operator of a multipole photon with polarization μ at \vec{r} . Thus, the quantum polarization of radiation of a localized source can be described by the set of three annihilation $\mathcal{A}_{\mu}(\vec{r})$ and creation $\mathcal{A}_{\mu}^{\dagger}(\vec{r})$ operators at any point \vec{r} of the three-dimensional space.

The polarization is usually described in terms of the polarization matrix [5]. In the case of quantum multipole radiation this is the (3×3) Hermitian matrix whose elements are bilinear in the field operators (1) [7]. Instead of finding these elements, one can investigate the generators of the $SU(3)$ algebra, forming the complete set of bilinear forms under consideration [9]. Omitting for the moment the position dependence, the generators of the $SU(3)$ in the representation of operators (3) can be written as

$$\begin{aligned} & (\mathcal{A}_{+}^{\dagger} \mathcal{A}_{+} - \mathcal{A}_{0}^{\dagger} \mathcal{A}_{0}) \quad (\mathcal{A}_{0}^{\dagger} \mathcal{A}_{0} - \mathcal{A}_{-}^{\dagger} \mathcal{A}_{-}) \quad (\mathcal{A}_{-}^{\dagger} \mathcal{A}_{-} - \mathcal{A}_{+}^{\dagger} \mathcal{A}_{+}) \\ & \frac{1}{2}(\mathcal{A}_{+}^{\dagger} \mathcal{A}_{0} + \mathcal{A}_{0}^{\dagger} \mathcal{A}_{+}) \quad \frac{1}{2}(\mathcal{A}_{0}^{\dagger} \mathcal{A}_{-} + \mathcal{A}_{-}^{\dagger} \mathcal{A}_{0}) \quad \frac{1}{2}(\mathcal{A}_{-}^{\dagger} \mathcal{A}_{+} + \mathcal{A}_{+}^{\dagger} \mathcal{A}_{-}) \\ & \frac{1}{2i}(\mathcal{A}_{+}^{\dagger} \mathcal{A}_{0} - \mathcal{A}_{0}^{\dagger} \mathcal{A}_{+}) \quad \frac{1}{2i}(\mathcal{A}_{0}^{\dagger} \mathcal{A}_{-} - \mathcal{A}_{-}^{\dagger} \mathcal{A}_{0}) \quad \frac{1}{2i}(\mathcal{A}_{-}^{\dagger} \mathcal{A}_{+} - \mathcal{A}_{+}^{\dagger} \mathcal{A}_{-}) \end{aligned} \quad (4)$$

The Stokes operators can be constructed as independent linear combinations of (4) and the total number of excitations $S_0(\vec{r}) = \sum_{\mu} \mathcal{A}_{\mu}^{\dagger} \mathcal{A}_{\mu}$. To illustrate the position dependence of the polarization, consider the electric-dipole Jaynes-Cummings model of [10]. Assume that a two-level atom emits a photon with $\mu = 0$, i.e. linearly polarized photon at $\vec{r} = 0$. In view of the explicit form of the coefficients in (1) [4,6], it is a straightforward matter to arrive at the conclusion that the radiation in the near and intermediate zones consists of two circularly polarized components and one component linearly polarized in the radial direction. In the far zone, the radiation consists only of the two linearly polarized components. The polarization at far distance can be specified by the three Stokes operators

$$(\mathcal{A}_+^+ \mathcal{A}_+ - \mathcal{A}_-^+ \mathcal{A}_-) \quad \frac{1}{2}(\mathcal{A}_-^+ \mathcal{A}_+ + \mathcal{A}_+^+ \mathcal{A}_-) \quad \frac{1}{2i}(\mathcal{A}_-^+ \mathcal{A}_+ - \mathcal{A}_+^+ \mathcal{A}_-), \quad (5)$$

out of the nine operators (4). Since operators (5) form a representation of the $SU(2)$ sub-algebra in the Weyl-Heisenberg algebra, one can say that there is a $SU(3) \rightarrow SU(2)$ contraction with the increase of distance from the source.

In the classical picture of transversal radiation, the phase difference between the two components with different polarization is considered. Undoubtedly, the multipole radiation with three spatial components at any space-time point should have more rich phase properties. In the quantum domain they can be described in the following way [11]. At any point \vec{r} , we define the dual representation of the the local photon operators (3)

$$\mathbf{A}_\mu(\vec{r}) = \frac{1}{\sqrt{3}} \sum_{\mu'=-1}^1 e^{i\mu\mu'2\pi/3} \mathcal{A}_{\mu'}(\vec{r}), \quad (6)$$

which effectively represents the polar decomposition of the spin of multipole photons. Note that this polar decomposition cannot be constructed directly in the way proposed in [12]. The point is that the spin and orbital contributions into the total angular momentum of photons cannot, in general, be separated [6]. Moreover, even for the total angular momentum of a photon with well defined representation of the $SU(2)$ sub-algebra in the Weyl-Heisenberg algebra, the polar decomposition cannot be determined because the Casimir operator cannot be represented uniquely in the whole Hilbert space. Nevertheless, transformation (6) introduces the phase states of the spin of a photon. Actually, this transformation diagonalized the operators

$$\begin{aligned} S_1(\vec{r}) &= \mathcal{A}_+^+ \mathcal{A}_0 + \mathcal{A}_0^+ \mathcal{A}_- + \mathcal{A}_-^+ \mathcal{A}_+ + H.c., \\ S_2(\vec{r}) &= -i(\mathcal{A}_+^+ \mathcal{A}_0 + \mathcal{A}_0^+ \mathcal{A}_- + \mathcal{A}_-^+ \mathcal{A}_+ - H.c.), \end{aligned} \quad (7)$$

forming the Cartan algebra in (4). As can be seen from the generalized Jaynes-Cummings model [10], the operators (7) represent the radiation counterpart of the cosine and sine of the quantum phase of the angular momentum of the atomic transition [13]. The quantum phase variable determined in this way has discrete spectrum in $(0, 2\pi)$. Since this variable reflects the spin properties of the radiation, it can be considered as an inherent phase of photons. This is one of the possible quantum phases, which can be determined in the operational way [14].

Let us briefly summarize our results. First, operators (3), describing the polarization of multipole radiation at an arbitrary space-time point, are constructed. In addition to the polarization, they can be used to determine the quantum statistical properties of radiation in the near and intermediate zones as well as in the far zone. Then, the dual representation (6) of these operators describes the quantum phase properties of photons connected with their spin states.

REFERENCES

- [1] Special issue: Proc. Roy. Soc. London, Series A, **459** (1998).
- [2] J.M. Jauch and F. Rohrlich, *The Theory of Photons and Electrons* (Addison-Wesley, Reading MA, 1959).
- [3] A. Luis and L.L. Sánchez-Soto, 1993, Phys. Rev. A **48**, 4702 (1993); A. Luis, A. L.L. Sánchez-Soto, and R. Tanaś, 1995, Phys. Rev. A **51**, 1634 (1995).
- [4] W. Heitler, *The Quantum Theory of Radiation* (Dover Publications, New York, 1984).
- [5] L. Mandel and E. Wolf, *Optical Coherence and Quantum Optics* (Cambridge University Press, New York, 1995).
- [6] V.B. Berestetskii, E.M. Lifshitz, and L.D. Pitaevskii, *Quantum Electrodynamics* (Pergamon Press, Oxford, 1982).
- [7] A.S. Shumovsky and Ö.E. Müstecaplıođlu, Phys. Rev. Lett. **80**, 1202 (1998).
- [8] A.S. Shumovsky and Ö.E. Müstecaplıođlu, Optics Commun. **146**, 124 (1998); J. Mod. Optics **45**, 619 (1998).
- [9] A.S. Shumovsky, Acta Phys. Slovaca **48**, 409 (1998).
- [10] A.S. Shumovsky and Ö.E. Müstecaplıođlu, Phys. Lett. A **235**, 438 (1997).
- [11] A.S. Shumovsky, to be published.
- [12] A. Vourdas, Phys. Rev. A **41** 1653 (1997).
- [13] A.S. Shumovsky, Optics Commun. **136**, 219 (1997).
- [14] J.W. Noh, A. Fougères, and L. Mandel, Phys. Rev. Lett. **67**, 1426 (1991); Phys. Rev. A **45**, 424 (1992); Physica Scripta T **48**, 29 (1993); Phys. Rev. A **47**, 4535 (1993); Phys. Rev. A **47**, 4537 (1993); Phys. Rev. A **48**, 1719 (1993); Phys. Rev. Lett. **71**, 2579 (1993).
- [15] J.R. Torgerson and L. Mandel, Phys. Rev. Lett. **76**, 3939 (1996); Optics Commun. **133**, 153 (1997).

Wavelet-Based Evolution Operators for Quantum Systems and Diffusion

Amaro J. Rica da Silva

*Dep. Física, Instituto Superior Técnico de Lisboa,
Av. Rovisco Pais, 1049-001 Lisboa - Portugal*

Abstract

The construction of a propagator for evolution equations using Laplacian of Gaussian (LOG) wavelets is implemented and studied in analogy with harmonic spectral procedures. What we have done is to generalize the free diffusion solution in wavelet-space to a propagation term for Schrödinger and diffusion type equations. We have applied this method successfully to the construction of spectral correlation functions for the asymmetric well and compared with standard FFT spectral analysis methods, as in [1].

I. INTRODUCTION

We address here the problem of constructing an evolution operator for Schrödinger equations,

$$i\hbar \frac{\partial u}{\partial t} = -\frac{\hbar^2}{2m} \nabla^2 u + \mathcal{V}(x) u \quad (1)$$

using an adequate 'frame' of wavelet transformations called Laplacian of Gaussian (LOG) transforms. Two types of solution will ensue from this approach, one that is meant to be analogous to the split operator algorithm of harmonic analysis, and another based on a Fredholm equation for the propagator kernel in the dual of the wavelet space.

The construction of a propagator $e^{i \mathbb{H} t}$ for the wavefunctions of a Schrödinger equation is, except for a few types of potential function $V(\mathbf{r})$, usually amenable only by numerical methods. Knowledge of a complete orthogonal set of eigenfunctions and eigenvalues is not the most practical way to propagate a given initial state, although formally it could be done, in principle. Numerical methods for solving the time-independent Schrödinger equations have to be used in most cases, and matrix-diagonalization and iterative methods are frequently chosen for the computation of approximated energy eigenvalues and corresponding eigenfunctions. Spectral methods for the solution of potential problems, on the other hand, rely on the computation of the auto-correlation function $\mathcal{P}(t) = \langle \psi_o | \psi_t \rangle$ for determining energy spectra, and thus need to find first a good approximation for the solutions ψ_t of the time-dependent Schrödinger equation given any initial state ψ_o . By using a perturbation

technique based on Fourier transformations, one can obtain good approximations for the solutions ψ_t , and then the numerical Fourier transform $\hat{\mathcal{P}}(\mathcal{E})$ of $\mathcal{P}(t)$ exhibits sharp peaks at the location of the energy eigenvalues.

Since the free evolution can be accurately computed in Fourier space, and we can express that formally as the effect of the operator $e^{i\frac{\hbar}{2m}\delta\tau\nabla^2}$. If we accompany that evolution with a phase change in place $e^{-i\frac{\hbar}{2m}\delta\tau V}$, proportional to the local potential $V(\vec{r})$, we obtain the split operator algorithm for the incremental time evolution of the initial waveform [1].

II. GAUSSIAN WAVELET TRANSFORM DEFINITIONS AND THE LOG TRANSFORM

In analogy with harmonic spectral procedures we studied and implemented the construction of a propagator for evolution equations using Laplacian of Gaussian (LOG) wavelets $g_{\xi}(x)$, with $\xi = (\xi_1, \xi_2) \in \mathbb{R}_+ \times \mathbb{R}$, which are generated in the usual manner from a 'mother-wavelet'

$$g_{\xi}(x) = g^{(2)}(\xi_1 (x - \xi_2)) \quad ; \quad g^{(2)}(x) = (x^2 - 1) e^{-\frac{x^2}{2}} \quad (2)$$

LOG wavelet transforms of a function $u(x)$ are defined here as

$$u(x) \xrightarrow{WT} \hat{u}_{\xi} = \sqrt{\xi_1} \int_{-\infty}^{\infty} u(x) g_{\xi}(x) dx \quad ; \quad \hat{u}_{\xi} \xrightarrow{IWT} u(\xi_2) = -\frac{1}{\sqrt{2\pi}} \int_0^{\infty} \frac{1}{\sqrt{\xi_1}} \hat{u}_{\xi} d\xi_1 \quad (3)$$

III. THE WAVELET TRANSFORM OF DIFFUSION-TYPE EQUATIONS.

As shown in [1], a LOG wavelet transformation of a diffusion equation (1) (of which the Schrödinger equation is a particular case with imaginary diffusion coefficient $\nu = \frac{i\hbar}{2m}$ and potential $V(x) = -i\hbar \mathcal{V}(x)$) yields,

$$\left(\frac{\partial}{\partial t} + \nu \xi_1^3 \frac{\partial}{\partial \xi_1} + \frac{5}{2} \nu \xi_1^2 \right) \hat{u}_{\xi}(t) = \sqrt{\xi_1} \int_{-\infty}^{\infty} V(x) u(x, t) g_{\xi}(x) dx \quad (4)$$

With a change in variable $\xi_1 = \eta_1^{-\frac{1}{2}}$, and defining $\hat{w}_{\eta}(t) = \eta_1^{-\frac{5}{4}} \hat{u}_{\xi}(t)$ we get instead

$$\left(\frac{\partial}{\partial t} - 2\nu \frac{\partial}{\partial \eta_1} \right) \hat{w}_{\eta}(t) = \eta_1^{-3/2} \int_{-\infty}^{\infty} V(x) u(x, t) g_{\eta}(\eta_1^{-3/2} x) dx \quad (5)$$

The time evolution can now be solved approximately in wavelet space.

Using $\boldsymbol{\eta}(t) = (\eta_1 + 2\nu t, \eta_2)$ we obtain, given an initial state $u(x, t_o)$,

$$\begin{aligned} \hat{w}_{\boldsymbol{\eta}}(t_o + \delta t) &\approx \hat{w}_{\boldsymbol{\eta}(\delta t)}(t_o) + \frac{1}{2\nu} \int_{\eta_1}^{\eta_1 + 2\nu\delta t} \tilde{\eta}_1^{-3/2} \int_{-\infty}^{\infty} V(x) u(x, t_o) g_{\boldsymbol{\eta}}(\tilde{\eta}_1^{-3/2} x) dx d\tilde{\eta}_1 \\ u(\eta_2, t_o + \delta t) &\approx -\frac{1}{2\sqrt{2\pi}} \int_0^{\infty} \hat{w}_{\boldsymbol{\eta}(\delta t)}(t_o) d\eta_1 + \frac{1}{4\nu^2} \int_{-\infty}^{\infty} V(x) u(x, t_o) G_{\delta t}(x - \eta_2) dx \end{aligned} \quad (6)$$

where $G_{\delta t}(x) = \sqrt{\pi} x \operatorname{erfc}\left(\frac{x}{2\sqrt{\delta t \nu}}\right) - 2\sqrt{\delta t \nu} e^{-\frac{x^2}{4\delta t \nu}}$.

Notice that the first term in (6) represents free propagation exactly, while the remainder gives an approximation for the potential correction in time δt .

IV. FREDHÖLM INTEGRAL EQUATIONS

An alternative way of solving equation (5) is to introduce the IWT formula for $u(x, t)$ there in terms of $\hat{w}_\eta(t)$ and, by Fourier transforming in all variables $(\eta, t) \rightarrow (\mathbf{k}, \varepsilon)$, obtain a Fredholm equation of the second kind

$$\hat{W}_\mathbf{k}(\varepsilon) = \int_{\hat{\mathcal{D}}'} \hat{K}[\mathbf{k}, -\mathbf{k}'; \varepsilon] \hat{W}_{\mathbf{k}'}(\varepsilon) d\mathbf{k}' \quad (7)$$

where the kernel

$$\hat{K}[\mathbf{k}, -\mathbf{k}'; \varepsilon] = \frac{i(2\pi)^{-\frac{5}{2}}}{2(\varepsilon - 2\nu k_1)} \int_{\mathcal{D}' \times \mathcal{D}} \eta_1^{-3/2} V(\eta_2') g_\eta(\eta_1^{-3/2} \eta_2') e^{-i(\mathbf{k} \cdot \boldsymbol{\eta} - \mathbf{k}' \cdot \boldsymbol{\eta}')} d\boldsymbol{\eta}' d\boldsymbol{\eta}. \quad (8)$$

can be computed to be

$$\hat{K}[\mathbf{k}, -\mathbf{k}'; \varepsilon] = \frac{i}{2\pi(\varepsilon - 2\nu k_1)} \delta(-k_1') \hat{V}(k_2 - k_2') \hat{\mathcal{G}}(\mathbf{k}) \quad (9)$$

with

$$\hat{\mathcal{G}}(\mathbf{k}) = -\frac{1}{\sqrt{2\pi}} \int_{\mathbb{R}_+ \eta_1} \frac{1}{\sqrt{\eta_1}} g^{(2)}(\sqrt{\eta_1} k_2) e^{-i k_1 \eta_1} d\eta_1 \quad (10)$$

This is not a separable kernel in k_2, k_2' , but it is interesting to note that any discrete wavelet transform (DWT) of the potential's $\hat{V}(k_2 - k_2')$ provides the means to approximate this kernel by a separable one. Specifically, if we select $h_\zeta(k)$ as a convenient wavelet frame (chosen e.g. to provide a convenient multi-resolution analysis), we could write

$$\hat{V}(k_2 - k_2') = \sum_{\zeta'} \mathcal{C}_{\zeta'}(k_2) h_{\zeta'}(k_2') \quad (11)$$

and $\mathcal{C}_{\zeta'}(k_2) = \int_{-\infty}^{+\infty} \hat{V}(k_2 - x) h_\zeta(x) dx$. Applying such a transformation to both sides of the Fredholm equation (7) will generate the algebraic problem

$$Z_\zeta(k_1, \varepsilon) = \sum_{\zeta'} \mathcal{K}_{\zeta \zeta'}(k_1, \varepsilon) Z_{\zeta'}(0, \varepsilon). \quad (12)$$

V. CONCLUSIONS

LOG wavelet transforms have been used by J.Lewalle [2] to study diffusion and Burger's equations and incompressible 3-dimensional fluid equations. The relevance of these equations in the context of quantum mechanical motion has been previously noted in connection with nonlinear Schrödinger equations. Burger's equations and Hamilton-Jacobi theory, which is interesting in itself since the connection with the 'classical' trajectories seems to be after all needed to make sense of a notion of quantum chaos.

As compared with usual Fast-Fourier transform methods, the evolution of a wave packet solution exhibits greater stability in a LOG method with lower resolution. The method is also stable with potential term evolution $e^{-i \Delta t V}$, and in fact the wavelet transform of the equation with potential terms leads to a Fredholm integral equation.

Since the free evolution can be also be accurately computed in (LOG) wavelet space, we can express the sequence of WT, evolution and IWT, as the effect of the operator $e^{i \frac{\hbar}{2m} \delta \tau \nabla^2}$ on an initial condition. The technique for the conventional harmonic split operator algorithm for incremental time evolution can also be used instead of (6) if we modify the free evolution with a phase change in place $e^{-i \frac{1}{\hbar} \delta \tau V}$, proportional to the local potential $V(\vec{r})$.

The issue of effectiveness is also of importance: since the LOG method is a continuous wavelet decomposition it does not automatically yield a fast pyramidal algorithm for a multi-resolution analysis, although proposals exist to associate scale discretizations of the mother wavelet with low- and high-pass filters resulting from an 'integrated wavelet'[3]. A scale analysis can be performed which shows how initial conditions details can affect the numerical solution.

VI. BIBLIOGRAPHY

- [1]. Feit, Fleck & Steiger, "Solution of the Schrödinger equation by a Spectral Method", Jour. Comput. Physics, 47, 412-433 (1982)
- [2]. J.Lewalle, "Wavelet Transforms of some equations of fluid mechanics", Acta Mechanica 104, 1-25 (1994)
- [3]. Torresani & al. "Continuous Wavelet Decompositions, Multiresolution and Contrast Analysis", SIAM Jour. Math. Anal., vol.24, 3,739-755 (1993)

Quantum Solitons in Fibers - Recent Experimental Progress and Perspectives

A. Sizmann, S. Schmitt, F. König, and G. Leuchs

*Universität Erlangen-Nürnberg, Physikalisches Institut, Lehrstuhl für Optik, Staudtstraße 7/B2,
D-91058 Erlangen, Germany*

Optical solitons in fibers are an experimentally readily accessible system for studying the quantum dynamics of the nonlinear Schrödinger equation. Recent experiments show strong photon-number noise reduction below shot-noise and a complex internal quantum structure of spectral photon-number correlations, unraveling new perspectives in experimental quantum optics.

Optical solitons in glass fibers are an attractive system for quantum measurements. Despite their large photon number of $n \approx 10^9$, solitons showed unique nonclassical behavior in a number of experiments, producing strong quadrature-amplitude and photon-number squeezed light with large bandwidth [1].

Studying the quantum properties of fiber-optic solitons gives insight into a variety of fundamental phenomena and application-related problems. The fiber-optic soliton is an experimentally easily accessible system for studying the quantum dynamics of the nonlinear Schrödinger equation, a fundamental nonlinear field theory that models many phenomena in nonlinear physics [2–5]. Furthermore, the nonlinear Schrödinger equation governs pulse propagation in fiber-optic communication links. Here, the quantum nature of light and in particular the noise behavior of solitons impose a fundamental upper limit on bit rate and distance of a communication channel. Quantum noise reduction techniques are useful in extending these limits beyond the limits presently perceived because these techniques are applicable to broadband noise reduction of both quantum and technical noise. Finally, a third motivation for studying the quantum nature of light and fiber nonlinearities is the unique opportunity that quantum entanglement offers for quantum information processing beyond the capabilities of information processing in a classical world [6].

This paper summarizes recent progress and promising trends of experiments that exploit the quantum nature of fiber-optic solitons. Recent experimental progress covers mainly photon-number squeezing of solitons with the methods of spectral filtering and nonlinear interferometers. The questions to be addressed here are:

- what has been and what can be achieved in terms of noise reduction,
- what are the underlying squeezing mechanisms, and
- which promising new developments may originate from this work?

In the history of fiber-optic quantum noise reduction, four generations of experiments can be identified [1]. The first generation of experiments with continuous-wave laser light demonstrated the principle of quadrature-amplitude squeezing based on the optical Kerr effect. The second generation used ultrashort pulses to achieve a larger nonlinear phase shift with less Brillouin scattering noise in shorter fibers. Ultrashort pulses that propagate

as solitons are free of chirp. Therefore, the local oscillator phase can easily be optimized for the entire pulse in the phase-sensitive detection of quadrature-amplitude squeezing.

Recent experimental progress in fiber-optic quantum noise reduction was achieved with spectral filtering and asymmetric nonlinear interferometers, the third and fourth generation of experiments, respectively, using picosecond and sub-picosecond solitons. These new kinds of experiments produced directly detectable photon-number squeezing, where no phase-matched local oscillator was needed and where higher-power solitons may be used for further enhancement of the nonlinear effects.

The method of spectral filtering gave new insight into the quantum structure of the soliton. Spectral filtering of coherent solitons was unexpectedly found to produce photon-number squeezed states [7,8] in 1995. The experimental method was fairly simple: a pulse launched into a fiber was spectrally band-pass filtered after emerging from the fiber end and was then detected. A variable bandpass filter allowed for optimizing the high and low cut-off frequencies. From the first observation of 2.3 dB squeezing with 2.7-ps solitons, bandpass filtered after $\zeta = 4.5$ soliton periods of propagation [7,8], the method was further investigated with sub-picosecond solitons and a variety of filter functions, fiber lengths, pulse energies below and above the fundamental soliton energy [9,10] and in the normal dispersion regime [11]. When optimized in the experiment, up to 3.8(± 0.2) dB of photocurrent noise reduction below shotnoise were achieved in direct detection. If corrected for linear losses, a reduction in the photon-number uncertainty by 6.4 dB below the Poisson limit can be inferred [9].

Predictions for what can be achieved in terms of noise reduction by spectral filtering show that up to 6.5 dB of photon-number noise reduction can be expected when an optimized bandpass filter removes the outlying sidebands of a fundamental soliton and transmits 82 % of the pulse energy [12]. With pulses of more than the fundamental soliton energy up to 8.1 dB of quantum noise reduction were predicted [13].

The underlying squeezing mechanism can be understood in terms of the multimode quantum structure of solitons [14–17]. Spectrally resolved quantum noise measurements showed that anticorrelations in photon number fluctuations emerge within the spectrum as the soliton propagates down the fiber [16]. If these anticorrelated modes are transmitted through a spectral filter and then detected simultaneously and coherently, their fluctuations cancel each other. This anticorrelation produces a photocurrent noise reduction far below shotnoise, similar to earlier predictions for squeezing by twin-beam correlations in fibers [18].

Nonlinear interferometers seem to be the most promising and most successful method of quantum noise reduction with solitons so far. The continuous-wave [19] and soliton-pulse analysis [20–22] show that the interferometer must be highly asymmetric in order to produce strong photon-number noise reduction, in contrast to earlier experiments with symmetric nonlinear fiber interferometers that produced a squeezed vacuum. Noise reduction in excess of 10 dB was predicted.

After the first experimental demonstration with 130-fs solitons [23], the method was optimized and observation of more than 5 dB of photocurrent noise reduction was reported [24,25]. This was the strongest noise reduction observed for solitons to date. When corrected for linear losses, the inferred photon-number squeezing was 7.3(+1.3/ – 1.0) dB [24]. More squeezing can be expected with pulse durations around one picosecond where Raman scattering noise is much reduced.

The squeezing mechanism can be understood in terms of number-phase correlations induced by the Kerr nonlinearity [22], similar to the continuous-wave case studied by Kitagawa and Yamamoto [19]. This squeezing mechanism implies that noise reduction grows with nonlinear phase shift in one arm of the nonlinear interferometer. This is in contrast to spectral filtering, where noise reduction originates from multimode photon-number correlations, which does not grow with propagation distance [22]. However, spectral filtering may play a role because the multimode structure of the output pulse of the asymmetric interferometer will be different from that of the strong pulse before interference with the weak pulse [2,24].

To summarize the experimental progress, there has been significant advancement towards developing multimode broadband quantum optics and fiber-integrated sources of classical and quantum noise reduction.

Worthwhile perspectives for further developments can be derived from the following current trends: Firstly, higher-order solitons [26,27] and/or femtosecond high-peak-power solitons show strong internal correlations and enhanced nonclassical effects. Unexpectedly, femtosecond pulses which experience strong Raman scattering showed more photon-number squeezing in the strongly Raman-shifted regime (110 soliton periods of fiber length) than in the weakly Raman-shifted case of shorter propagation distances (3 soliton periods fiber length, the predicted optimum propagation distance without Raman scattering) [9]. Therefore, experiments in the femtosecond regime of pulse propagation can be expected to give insight into a novel Raman-assisted squeezing mechanism. Secondly, spectrally resolved quantum measurements will be rewarding when applied to photon-number-squeezed solitons, such as the solitons emerging from a nonlinear interferometer, and to strongly Raman-shifted solitons. Spectrally resolved quantum measurements give insight into the multimode quantum correlation pattern of the pulse and therefore into the squeezing mechanism. Open questions concerning the squeezing mechanism of nonlinear interferometers and Raman-shifted pulses can be addressed with this method. Thirdly, demonstrating a source of bright entangled beams [28] based on the successful quantum noise reduction method in fibers, the nonlinear interferometer, will be rewarding towards realizing quantum information processing capabilities with solitons. Furthermore, extending recent quantum measurements to the case of interacting solitons will open up new opportunities for quantum-nondemolition measurements and entanglement of beams. As an example, spectral filtering in the center of a soliton collision has been proposed as a novel method for back-action evading detection of the photon number, allowing for direct detection in the probe beam. The interpulse photon-number correlations were found to be strong enough to predict a conditional variance of 0.7 or better by spectral filtering of the probe soliton [26]. Last, but not least, the methods for quantum noise reduction discussed here are relevant for optical communication links. Spectral filters and nonlinear interferometers are already being investigated as key elements in system design. They are promising for stabilizing the soliton against Gordon-Haus jitter, resonance radiation and amplified spontaneous emission noise. With these nonlinear elements in the fiber-optic link, the quantum limits need to be investigated for a better understanding of the ultimate bounds of terabaud communications.

With these perspectives in mind, significant experimental as well as theoretical developments with quantum solitons can be expected in the near future.

- [1] A. Sizmann, and G. Leuchs, Progress in Optics **XXXIX**, E. Wolf (Ed.), p. 373 (Elsevier, Amsterdam 1999)
- [2] M.J. Werner, Phys. Rev. Lett. **81**, 4132 (1998)
- [3] W. Zhang, D.F. Walls, and B.C. Sanders, Phys. Rev. Lett. **72**, 60 (1994)
- [4] M.J. Werner and P.D. Drummond, J. Opt. Soc. Am. B **10**, 2390 (1993), Opt. Lett. **19**, 613 (1994)
- [5] P.A. Ruprecht, M.J. Holland, and K. Burnett, Phys. Rev. A **51**, 4704 (1995)
- [6] A. Furusawa, J.L. Sorensen, S.L. Braunstein, C.A. Fuchs, H.J. Kimble, and E.S. Polzig, Science **282**, 706 (1998)
- [7] S.R. Friberg, S. Machida, and A. Levanon, CLEO/Pacific Rim'95, Chiba, Japan, 1995
- [8] S.R. Friberg, S. Machida, M. J. Werner, A. Levanon, and Takaaki Mukai, Phys. Rev. Lett. **77**, 3775 (1996)
- [9] S. Spälter, M. Burk, U. Ströbner, A. Sizmann, and G. Leuchs, Opt. Expr. **2**, 77 (1998)
- [10] S. Spälter, M. Burk, U. Ströbner, M. Böhm, A. Sizmann, and G. Leuchs, Europhys. Lett. **38**, 335 (1997)
- [11] F. König, S. Spälter, I. Shumay, A. Sizmann, T. Fauster, and G. Leuchs, J. Mod. Opt. **45**, 2425 (1998)
- [12] A. Mecozzi and P. Kumar, Opt. Lett. **22**, 1232 (1997)
- [13] M.J. Werner, private communication, 1997
- [14] M. Werner, Phys. Rev. A **54**, R2567 (1996)
- [15] M. J. Werner and S. R. Friberg, Phys. Rev. Lett. **77**, 4143 (1997)
- [16] S. Spälter, N. Korolkova, F. König, A. Sizmann, and G. Leuchs, Phys. Rev. Lett. **81**, 786 (1998).
- [17] D. Levandovsky, M.V. Vasilyev, and P. Kumar, Opt. Lett. **24**, 43 (1999).
- [18] T.A.B. Kennedy, Phys. Rev. A **44**, 2113 (1991).
- [19] M. Kitagawa and Y. Yamamoto, Phys. Rev. A **34**, 3974 (1986).
- [20] M.J. Werner, OSA Annual Meeting, Long Beach, CA (Optical Society of America, Washington D.C, 1997)
- [21] S. Schmitt, J. Ficker, M. Wolff, F. König, A. Sizmann, and G. Leuchs, Phys. Rev. Lett. **81**, 2446 (1998)
- [22] D. Levandovsky, M.V. Vasilyev, and P. Kumar, Opt. Lett. **24**, 89 (1999).
- [23] S. Schmitt, F. König, B. Mikulla, S. Spälter, A. Sizmann, and G. Leuchs, IQEC, San Francisco, CA, OSA Technical Digest Series **7**, 195 (Optical Society of America, Washington D.C, 1997)
- [24] S. Schmitt, F. König, R. Merk, M. Wolff, A. Sizmann, and G. Leuchs, EQEC, Glasgow, UK, p. 110 (IEEE Piscataway, NJ, 1998)
- [25] D. Krylov and K. Bergman, Opt. Lett. **23**, 1390 (1998)
- [26] M.A. Zielonka, Diploma thesis, Friedrich-Alexander-Universität Erlangen-Nürnberg, Physikalisches Institut (5/1999)
- [27] E. Schmidt et al., in preparation
- [28] G. Leuchs, T.C. Ralph, C. Silberhorn, and N. Korolkova, J. Mod. Opt., in press (1999)

Macroscopic Quantum Systems and Point Interactions

Colin Trueman and K K Wan,

School of Physics and Astronomy,

University of St. Andrews, Fife, KY16 9SS, Scotland, UK

May 16, 1999

Abstract

We present systematic quantization scheme for dealing with single point interactions in one dimension. The scheme is very general and is capable of treating macroscopic quantum systems like superconducting circuits.

Traditionally, point interaction problems in quantum mechanics are treated in the physics literature by solving the Schrödinger equation containing an appropriate δ -function potential. In this paper we discuss a systematic quantization scheme, known as the method of *quantization by parts* [1, 2, 3, 4, 5, 6, 7], which provides a general method for dealing with single point interactions in one dimension, namely by reducing the problem to boundary conditions. Our method can also be applied to superconducting systems like those concerning Josephson and the recently discovered π -junctions, and single electron circuit systems, amongst others.

An important aspect of operator theory, i.e., symmetric operators and their extensions, a subject not normally encountered in standard quantum mechanics, plays a key role here. Take the simple example of a one-dimensional case. In the absence of any potential a particle of mass m moving in one-dimension along the real line \mathbf{R} has associated with it the Hilbert space of square-integrable functions $L^2(\mathbf{R})$ on \mathbf{R} . A normalized wave function ϕ , describing the state of the particle, is a member of $L^2(\mathbf{R})$. To define an operator in $L^2(\mathbf{R})$ it is not enough just to give an operator expression. One must also specify the domain on which the operator acts in order to define the operator.

Let $C_0^\infty(\mathbf{R})$ denote the set of infinitely differentiable functions on \mathbf{R} , each of which vanishes outside a closed and bounded interval in \mathbf{R} . Note that $C_0^\infty(\mathbf{R})$ is a subset of $L^2(\mathbf{R})$. Now, consider

quantum mechanical operators acting in $L^2(\mathbf{R})$. When the given operator expression is a differential expression the standard procedure is to let the differential expression act on $C_0^\infty(\mathbf{R})$ first. Let the resulting operator be denoted by \widehat{A}_0 . Such an operator is usually symmetric and not selfadjoint [8]. Hopefully \widehat{A}_0 will have a unique selfadjoint extension. In other words there exists one and only one selfadjoint operator \widehat{A} acting on domain $\mathcal{D}(\widehat{A})$ such that $\mathcal{D}(\widehat{A})$ contains $C_0^\infty(\mathbf{R})$ and that on $C_0^\infty(\mathbf{R})$ the operator \widehat{A} is equal to \widehat{A}_0 , i.e., $\widehat{A}\phi = \widehat{A}_0\phi$ if $\phi \in C_0^\infty(\mathbf{R})$. One then concludes that the appropriate quantized operator is \widehat{A} . In this paper we shall come across a new situation when \widehat{A}_0 possesses many different selfadjoint extensions.

Mathematically the geometry of a one-dimensional system with a point interaction may be idealised as the real line $\mathbf{R} = \{x \in (-\infty, \infty)\}$ broken into two half lines $\mathbf{R}_0^- = (-\infty, 0)$ and $\mathbf{R}_0^+ = (0, \infty)$. The point at which the potential abruptly changes being at $x = 0$. This is referred to as the branch point which separates the real line into two branches $\mathcal{B}_1 = \mathbf{R}_0^-$ and $\mathcal{B}_2 = \mathbf{R}_0^+$. A particle being scattered by this potential is represented by a wave function ψ on the interrupted line $\mathbf{R}_0 = \mathbf{R}_0^- \cup \mathbf{R}_0^+$. The wave function on \mathbf{R}_0^- is denoted by $\psi_1(x)$ and by $\psi_2(x)$ on \mathbf{R}_0^+ . Classically, for point interactions, the particle is free when it is on \mathcal{B}_1 or on \mathcal{B}_2 and when restricted to these branches the Hamiltonian would agree with the kinetic energy. The method of quantization by parts starts by setting up the kinetic energy for the particle on the branches separately in terms of operators defined on $C_0^\infty(\mathbf{R}_0^-)$ and $C_0^\infty(\mathbf{R}_0^+)$. These operators are generally symmetric. We then combine the results and find all the selfadjoint extensions to obtain the kinetic energy, and the Hamiltonian for the system as a whole. Different selfadjoint extensions of the kinetic energy operators on the combined system correspond to different domains. That is, each selfadjoint extension gives rise to different boundary conditions at the point corresponding to different domains and this leads to a characterisation of different types of point interactions.

We then use the concept of a transfer matrix [9, 10] to help us describe the boundary conditions that arise from this method. Generally, let $\phi(x_1), \phi'(x_1)$ be the values of the wave function ϕ and its spatial derivative ϕ' at the point x_1 , and let $\phi(x_2), \phi'(x_2)$ be their values at x_2 . The transfer matrix linking the values of ψ and ψ' at two points x_1, x_2 is defined to be the matrix $\mathcal{M}(x_1, x_2)$ satisfying

$$\mathcal{M}(x_1, x_2) \begin{pmatrix} \psi(x_1) \\ \psi'(x_1) \end{pmatrix} = \begin{pmatrix} \psi(x_2) \\ \psi'(x_2) \end{pmatrix}. \quad (1)$$

It is apparent that a transfer matrix is just a convenient way of rewriting boundary conditions, but it is an extremely useful tool. We find that by using these transfer matrices we can find limiting

families of potentials that give rise to the boundary conditions associated with each selfadjoint extension of the kinetic energy of our system. For example there exists a selfadjoint extension \widehat{K}_{ex} corresponding to the boundary conditions¹:

$$-\left(\frac{2m}{\hbar^2} V_0\right) (\psi_1(0) - \psi_2(0)) = \psi_1'(0), \quad \psi_1'(0) - \psi_2'(0) = 0. \quad (2)$$

The transfer matrix at $x = 0$ is

$$\mathcal{M}_{ex, V_0} = \begin{pmatrix} 1 & \frac{\hbar^2}{2mV_0} \\ 0 & 1 \end{pmatrix}. \quad (3)$$

We then find that a family of four δ -function potentials located at regular intervals from the origin can be limited in such a way as to produce the same boundary conditions at a point as the selfadjoint extension. Let us introduce some notation to aid the discussion of this potential. Let a be a small positive number much less than 1, n be a positive integer, and following Pearson [9] let

$$v_{na}^+(x) = g_a^+ \delta(x - na), \quad g_a^+ = \frac{\hbar^2}{2ma} \left(\frac{\hbar}{\sqrt{2mV_0}} \frac{1}{\sqrt{a}} - 1 \right). \quad (4)$$

For sufficiently small a , g_a^+ is positive and hence $v_{na}^+(x)$ represents a repulsive δ -potential at $x = na$, and let

$$v_{na}^-(x) = g_a^- \delta(x - na), \quad g_a^- = \frac{\hbar^2}{2ma} \left(\frac{\sqrt{2mV_0}}{\hbar} \sqrt{a} - 1 \right). \quad (5)$$

For sufficiently small a , g_a^- is negative and hence $v_{na}^-(x)$ represents a attractive potential at $x = na$. Note that the coefficients g_a^+ and g_a^- are dependent on a but not on n .

Now consider combining these δ -potentials to form a new potential $V_{+,a}^{(3)}(x)$

$$V_{+,a}^{(3)}(x) = v_a^-(x) + v_{2a}^+(x) + v_{3a}^+(x) + v_{4a}^-(x). \quad (6)$$

The transfer matrices for each of the elements of this family, may be multiplied together² and we can show that in the limit as $a \rightarrow 0$, this potential does indeed realise the transfer matrix and hence boundary conditions for \widehat{K}_{ex} .

We find that there are eleven more boundary conditions that give rise to selfadjoint extensions and each of them can be attributed a potential in this way. Let us summarize our results as follows:

¹From conditions (86,87) in [1].

²This method has a strong analogy with the ray transfer matrix analysis in optics. Each element has its own matrix and by multiplying together the matrices corresponding to the elements of a system we get the effective matrix for the whole system.

1. Intuitively the basic building block for a point interaction is the δ -function. First, we derive the limit of a family of four δ -function potentials. We then derive most of the rest of point interactions in terms of a finite family of δ -function potentials and this limiting family.
2. Each type of point potential shows a distinct physical characteristic, determined by the boundary conditions.
3. Some of the point interactions that are included in this theory are: the step potential, δ -function, δ' -function, 'open end' potentials, full π -phase shifter, high-pass π -phase shifter, low-pass π -phase shifter, mid-pass $\frac{1}{2}\pi$ -phase shifter, tunable partial mid-pass filter, tunable mid-pass phase shifter and the Josephson junction.

Hopefully the theoretical possibility of these potentials will find applications, e.g., in identifying some of these point interactions with known phenomena as well as in prompting new experiments to verify their existence. Full details will be published elsewhere.

References

- [1] K K Wan and R H Fountain, *Found. Phys.* **26**, 1165 (1996).
- [2] K K Wan and R H Fountain, *Int J Theor Physics* **37**, 2153 (1998).
- [3] K K Wan and F E Harrison, *J. Phys. A: Math. Gen.* **30**, 4731 (1997).
- [4] P Exner and P Seba, *J. Math. Phys.* **28**, 386 (1987).
- [5] P Exner and P Seba, *Rep. Math. Phys.* **28**, 7 (1989).
- [6] P Exner and P Seba, *Quantum Junctions and the Self-Adjoint Extensions Theory*, also P Exner, P Seba and P Stovicek, *Quantum Waveguides*, both in *Applications of Self-Adjoint Extensions in Quantum Physics* (Eds. P. Exner and P. Seba) (Springer-Verlag, Berlin, 1989).
- [7] J Blank, P Exner and M Havlicek, *Hilbert Space Operators in Quantum Physics* (American Institute of Physics Press, New York, 1994) p 60, pp 471- 489, p145, p149, p137, p122.
- [8] R D Richtmyer, *Principles of Advanced Mathematical Physics Vol 1* (Springer-Verlag, New York, 1978) p155, p141, p157.
- [9] D B Pearson, *Quantum Scattering and Spectral Theory* (Academic Press Ltd, London, 1988) pp490-497.
- [10] Merzbacher, *Quantum Mechanics* (Wiley, New York, 1970) Ch 6.
- [11] K K Wan, R H Fountain and Z Y Tao, *J. Phys. A: Math. Gen.* **28**, 2379 (1995).

A variational approximation for the ground states of Bose-Einstein condensates as described by the Gross-Pitaevskii equation

D.Anderson, F. Cattani, B.Hall and M.Lisak
Chalmers University of Technology, SE-41296 Göteborg, Sweden

Yu.Kivshar, E. Ostrovskaya and T.Alexander,
Optical Sciences Centre, Australian National University, Canberra, Australia.

Abstract

An analysis, based on direct variational methods, is made of the properties of two-dimensional ground state Bose-Einstein condensates as described by the Gross-Pitaevskii equation. Convenient analytical approximations are found for the wave function and the concomitant properties of the condensate. The results are compared and shown to be in good agreement with numerical results.

Introduction. In experimental studies of Bose-Einstein condensates (BEC) in ultracold and dilute atomic gases, the BEC atoms are trapped in a generally anisotropic external potential created by a magnetic trap and their collective dynamics in the trap can be described by the Gross-Pitaevskii (GP) equation

$$i\hbar \frac{\partial \psi}{\partial t} = -\frac{\hbar^2}{2m} \nabla^2 \psi + V_{ex}(r) + U |\psi|^2 \psi = 0 \quad (1)$$

where ψ is the macroscopic wave function of the condensate, V_{ex} is a parabolic trapping potential and the parameter $U = 4\pi\hbar^2 a / m$ characterizes the two particle interaction, which is proportional to the scattering length a . Although V_{ex} is always a confining potential, the nonlinear potential may be deconfining or confining depending on whether the scattering length, a , is positive or negative respectively.

The purpose of the present analysis is to investigate the properties of stationary two dimensional radially symmetric solutions of eq.(1). This will be done using direct variational methods involving trial functions and Rayleigh-Ritz optimization. The analytical approximations are compared and showed to be in good agreement with results of numerical calculations. For the present analysis, eq.(1) can be rewritten as

$$\frac{1}{r} \frac{d}{dr} \left(r \frac{d\rho}{dr} \right) + \mu \rho - r^2 \rho \pm \rho^3 = 0 \quad (2)$$

where μ plays the role of eigenvalue and \pm refer to confining (+) and deconfining (-) two-particle interactions. The properties of the ground state solutions of eq.(2) will be investigated.

A variational approach to the GP equation. Approximate solutions of eq.(2) can be obtained using a variational approach based on trial functions and Rayleigh-Ritz optimization. For this purpose, eq.(2) is rewritten as the variational problem

$$\delta \int_0^{\infty} L(r, \rho, \frac{d\rho}{dr}) dr = 0 \quad (3)$$

where the Lagrangian, L , is given by

$$L = r \left[\left(\frac{d\rho}{dr} \right)^2 - \mu \rho^2 + r^2 \rho^2 \mp \frac{1}{2} \rho^4 \right] \quad (4)$$

A convenient and flexible trial function to be used in the Rayleigh-Ritz optimization procedure is super-Gaussian functions i.e. $\rho(r) = \rho_T(r) = \rho_0 \exp[-(r/a)^{2m} / 2]$, where the profile width - a ,

the super Gaussian index - m and the maximum amplitude - ρ_0 , are to be related to the eigen value - μ using variational optimization. Inserting the ansatz into the variational integral we obtain

$$\langle L \rangle \equiv \int_0^{\infty} L(\rho = \rho_T) dr = \rho_0^2 I_0 - \mu \rho_0^2 a^2 I_1 + \rho_0^2 a^4 I_2 + \frac{1}{2} \rho_0^4 a^2 I_3 \quad (5)$$

where $I_0 = m/2$; $I_1 = \Gamma(1+1/m)/2$; $I_2 = \Gamma(1+2/m)/4$; $I_3 = 2^{-\frac{1}{m}} \Gamma(1+1/m)$ and $\Gamma(x)$ is the Gamma function. The integrated Lagrangian $\langle L \rangle$ is a function of a, ρ_0 and m and the corresponding variational equations can be manipulated into the following form

$$\rho_0^2 a^2 = \pm \frac{mp(m)}{I_3} \quad ; \quad a^4 = \frac{m[1-p(m)]}{2I_2} \quad ; \quad \mu = \frac{m[2-3p(m)]}{2a^2 I_1} \quad (6)$$

where the characteristic function $p(m)$ is given by

$$p \equiv \frac{m + 2[\psi(1 + \frac{1}{m}) - \psi(1 + \frac{2}{m})]}{\ln 2 + 2[\psi(1 + \frac{1}{m}) - \psi(1 + \frac{2}{m})]} \quad (7)$$

and $\psi(x)$ is the logarithmic derivative of the Gamma function. The function $p(m)$ changes sign at $m = 1$ and only the branches where $\pm p(m)$ is positive has physical significance i.e. $m < 1$ for (+) and $m > 1$ for (-).

BEC for negative scattering length. Since in this case the nonlinear potential is focusing, the condensate will ultimately collapse when the nonlinearity (i.e. the number of particles in the condensate) becomes sufficiently large. The threshold for collapse can easily be shown to be $p = 1$. When $p = 0$ (the linear case), the condensate ground state wave function is Gaussian ($m = 1$), as it should, and for increasing p , the waveform becomes increasingly peaked and at collapse ($p = 1$), the super Gaussian index is $m = \ln 2$. A comparison between the variationally obtained super Gaussian approximations and the results of numerical solutions of the eigen value equation (2) are shown in Figs. 1a,b. The agreement is seen to be very good over the whole allowable range of p . A corresponding comparison is also made in Figs. 2a,b for the eigenvalue and the number of particles of the condensate as functions of ρ_0 .

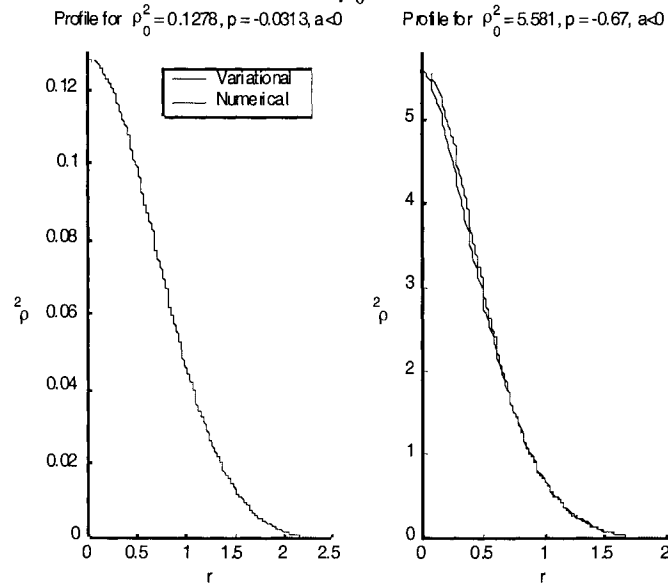


Fig.1 Comparison between normalized stationary condensate profiles for different number of particles. The dashed lines are variational approximations and solid lines are numerical result.

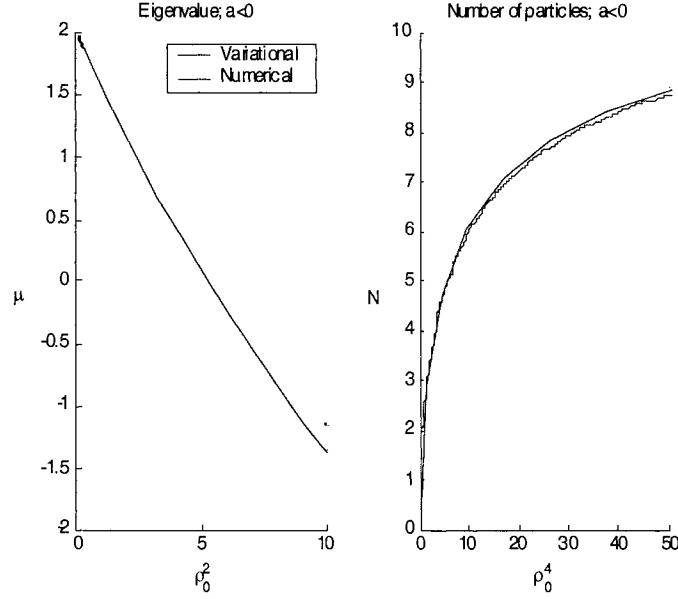


Fig.2 Comparisons between variational and numerical results for the eigenvalue μ (2a) and the particle number N (2b). The dashed lines are variational approximations and solid lines are numerical result.

BEC for positive scattering length. In this case the external potential and the nonlinearity are counteracting each other and stationary solutions exist for arbitrary number of particles in the condensate. A classical approximation in this case is obtained by balancing the defocusing nonlinearity against the linear focusing potential - the Thomas-Fermi approximation - which yields simply $\rho^2(r) = \mu - r^2$ implying that $\mu = \rho_0^2$ and $N = \rho_0^4 / 2$. It is clear that the Thomas-Fermi approximation can be expected to do best for strongly nonlinear situations, but also that the parabolic approximation for the condensate density profile can be expected to be less good in this case - the actual shape of the solution should be broader than a parabola.

The variational approximation predicts correctly these features: the profile of the condensate density (ρ^2) is not parabolic, it does depend on amplitude i.e. on the number of particles in the trap and it becomes increasingly rectangular for large values of N (or ρ_0). As a comparison we note that for large ρ_0 , the variational predictions, expanded in this limit, yield $\mu \approx 1.14\rho_0^2$ and $N \approx 0.24\rho_0^4$ in close agreement with the Thomas-Fermi approximation.

The analytical predictions obtained by the variational approach and the Thomas-Fermi approximations for the condensate profiles are compared with numerical solutions of eq.(2) in Fig.3a,b. The variational approximation is very good for small and moderate values of ρ_0 , but tends to overestimate the condensate profile for large ρ_0 . On the other hand, the Thomas-Fermi approximation is less good for small ρ_0 (as expected) and straddles the numerical curve for large ρ_0 . This has the consequence that the Thomas-Fermi approximation provides very good approximations for $\mu \approx \mu(\rho_0^2)$ and $N \approx N(\rho_0^4)$ for large ρ_0 , in fact even better than the variational approximation, cf Figs.4a,b

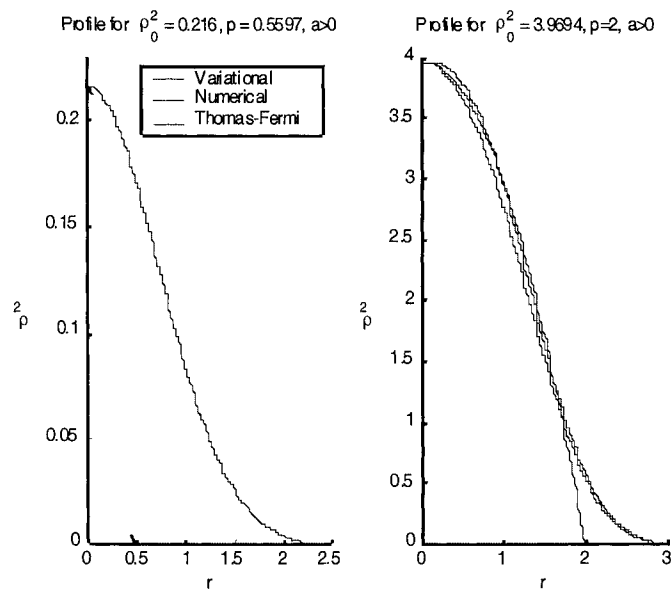


Fig.3 Comparison between normalized stationary condensate profiles for different number of particles. The dashed lines are variational approximations and solid lines are numerical results, while the dotted lines are the Thomas-Fermi approximations.

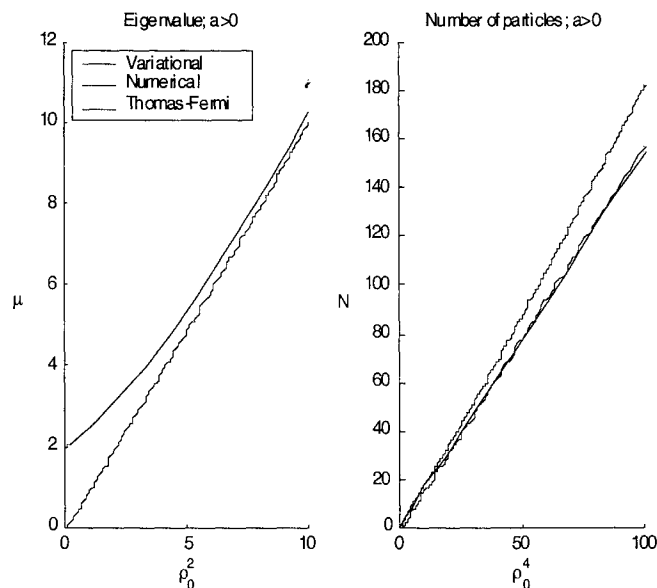


Fig.4 Comparisons between variational and numerical results for the eigen value μ (2a) and the particle number N (2b). The dashed lines are variational approximations and solid lines are numerical results, while the dotted lines are the Thomas-Fermi approximations.

Conclusion. It has been shown that direct variational methods based on super-Gaussian trial functions and subsequent Rayleigh-Ritz optimization provide excellent approximations of the profiles and other properties of Bose-Einstein condensates in parabolic traps and in the presence of two-body interaction with positive as well as negative scattering length.

References. [1] M.Edwards, R.J.Dodd, C.W.Clark, P.A. Ruprecht and K. Burnett, Phys.Rev.A 53 (1996) R1950

[2] M. Karlsson and D.Anderson, J.Opt.Soc.Am.B9 (1992) 1558

States of a General Quantum System which Behave Classically

Dušan Arsenović
Institute of Physics,
PO Box 57, Beograd, Yugoslavia

Nikola Burić
Department of Mathematics and Physics, Faculty of Pharmacy, Vojvode Stepe 490, Beograd,
Yugoslavia

Dragomir M. Davidović
Laboratory of Theoretical Physics, The institute of Nuclear Sciences "Vinča", PO Box 522, 11001
Beograd, Yugoslavia

Abstract

We present a consistent definition of classical-like states of a quantum system, and provide an explicate construction of such states, irrespective of whether the system has or has no classical analogue. We show that the definition singles out a unique set of states of the quantum system which behave classically up to an arbitrary prescribed accuracy.

I. INTRODUCTION

A mixture of many pure states could suppress the typically quantum properties of the single pure state. There could be such quantum states, represented by mixtures of pure states, that the predictions of quantum mechanics can be obtained with the tools of classical statistical mechanics. We shall formulate natural conditions to characterise the quantum probability distributions, which behave as classical statistical distributions up to any desired accuracy. The classical-like states, fixed by these conditions, are not localised on a classical orbit of a single system. Furthermore, there need not be any classical system like in the case of the spin. The approximate equality of the quantum and the classical formalisms is achieved only in the statistical sense.

The coherent states are the most natural framework to study the possibility of the classical description of a quantum system. Among all pure states, they are those which minimise the uncertainty relations for the corresponding dynamical variables. The phase-space picture for a large class of quantum systems is obtained in the theory of generalised

coherent states [2], [3]. The phase space of a quantum system is obtained as a manifold which parameterises the states which minimise the uncertainty relations among the basic quantum dynamical variables of the considered system. For example, the quantum phase-space of a one dimensional (1D) quantum particle is the complex plane \mathbb{C} , and that of the spin is the sphere S^2 . We shall explain the ideas using the spin $s = 1/2$ as an example of a typically quantum system.

As in the case of 1D particle, there are various prescriptions which can be used to assign functions on S^2 to the quantum states and observables. The Husimi function ρ_Q of the state $\hat{\rho}$ is a real probability distribution on S^2 , while the Wigner function ρ_W of the state $\hat{\rho}$ can have negative values, so that, like in the 1D case, it is not a proper probability distribution. Notice that only the W representation can be used to represent both the states and the observables on an equal footing (i. e. using the same formulas on the corresponding operators $\hat{\rho}$ and \hat{B}).

Like in the 1D particle case, the Heisenberg dynamics of the spin components can be described by the Hamiltonian dynamics of points on S^2 . The Hamilton's function $H(\alpha)$ is Q representation of the corresponding Hamilton operator \hat{H} .

II. CLASSICAL-LIKE STATES FOR THE SPIN

A quantum state of the spin $s = 1/2$, represented by a statistical operator $\hat{\rho}$, is called classical-like to a degree $0 \leq 1 - \lambda \leq 1$ if the following conditions are satisfied:

- 1) The quantum phase space distribution ρ describing the state is non-negative.
- 2) The mean value of an observable represented by an operator \hat{B} in the classical-like state is up to a given accuracy equal to the classical mean value:

$$\text{Tr}[\hat{\rho}\hat{B}] \approx \int \rho(\theta, \psi) B(\theta, \psi) \sin \theta d\psi d\theta, \quad (1)$$

where the functions $B(\theta, \psi)$ and $\rho(\theta, \psi)$ are obtained from the operators \hat{B} and $\hat{\rho}$ by the same procedure.

- 3) Up to a given accuracy, the quantum phase-space distribution of the classical-like state evolve in time according to the classical Liouville equation, with the Hamilton function H corresponding to the Hamilton operator \hat{H} given by the condition 2.

The first condition is restrictive only together with the second condition. Namely, any state $\hat{\rho}$ generates a well defined positive function, given by the Q representation. If the Q representation is taken to define the functions which represent a physical observable \hat{B} than, in general, the classical average and the quantum average are different. However, the difference might be relatively small or large as compared to the actual values of the averages, and this depends on the properties of the states $\hat{\rho}$. The condition 2 selects such states for which this difference is relatively small. Thus the degree of classically $0 \leq 1 - \lambda \leq 1$ of a given quantum state is measured by the following ratio:

$$\lambda \approx \frac{\text{Tr}[\hat{\rho}\hat{B}] - \int_{S^2} \rho_Q B_Q \sin \theta d\theta d\psi}{\text{Tr}[\hat{\rho}\hat{B}]}.$$

The smaller is λ the states are more classical-like.

In order to explicitly construct and study the classical-like states of the spin, we shall now introduce, the so called, Λ -transformation of the states. The transformation is obtained using the representations of the operators and the corresponding functions on S^2 in terms of the irreducible tensor operators and the spherical harmonics respectively. This transformation maps a given state $\hat{\rho}$ into the classical-like state $\hat{\rho}^\lambda$ which satisfies the conditions 1, 2, and 3, with an error proportional to $0 \leq \lambda \leq 1$.

A statistical operator $\hat{\rho}$ can be represented by the corresponding ρ_Q or ρ_W functions. We expect the classical like states to be represented by functions with small derivatives on the relevant phase-space. Also, in order to satisfy both of the conditions 1) and 2) the difference between the two representations of $\hat{\rho}$ by functions ρ_Q and ρ_W should be small everywhere on S^2 . Both of these goals are achieved by the following transformation:

$$\Lambda : \hat{\rho}(c_{0,0}, c_{1,0}, c_{1,1}, c_{1,-1}) \rightarrow \hat{\rho}(c_{0,0}, \lambda c_{1,0}, \lambda c_{1,1}, \lambda c_{1,-1}) \equiv \hat{\rho}^\lambda \quad (2)$$

where $0 \leq \lambda \leq 1$ is a real number, and $c_{i,j}$ are complex parameters which uniquely fix the quantum state [4].

Given a state $\hat{\rho}$ we can always associate with it a state which satisfies the first two conditions up to a desired accuracy. The Λ -transformed states also satisfy the third condition

$$[\hat{H}, \hat{\rho}^\alpha]_Q - \{H_Q, \rho_Q^\alpha\} \approx \lambda, \quad (3)$$

since the difference on the left side is given as a product of a bounded function on S^2 by a small λ . We conclude that the Λ -transformed states, with a proper values of λ , will satisfy all the three conditions on the classical-like states.

Let us now briefly state a few properties of the Λ -transformed states. Some of these are common to the 1D particle and the case of spin, but others are typical for the spin, and come essentially from the finite dimensionality of the space of states, or from the compactness of S^2 .

First notice that the Λ -transformed states can not be pure states. Any mixed state of the spin can be understood formally also as a Λ -transformed state of some other state, and is, up to a certain accuracy, a classical-like state. This is not so in the 1D case, where mixtures of a finite number of pure states are not classical-like to any accuracy at least with respect to some variables. When λ is small all Λ -transformed states of the spin are close to each other, and in all such states an observable has similar measured values. This is also quite different from the case of the 1D particle, which can be in many classical-like states satisfying the classicallity conditions up to the same accuracy, but with large differences in the measured values of an observable. All Λ -transformed states of the spin system converge when $\lambda \rightarrow 0$ to a unique mixed state, known as the unpolarised state. This unique, exactly classical-like state, is a well defined quantum state i. e. it is represented by an admissible statistical operator. This is not true for the one-dimensional particle, where the would-be exactly classical-like state, with $\lambda = 0$, has an infinite norm, and thus is not permitted.

An example of application of the Λ -trnsformed states has been provided in [5], using the most quite phase-insensitive amplifier of Glauber [6].

REFERENCES

- [1] D. M. Davidović and Lalović D, J. Phys. A: Math. Gen. **31** 2281 (1998).
- [2] A. Perelomov, *Generalized Coherent States and Their Applications* (Berlin: Springer-Verlag) (1986).
- [3] W.M. Zhang, D.H. Feng and R. Gilmore, Rev. Mod. Phys. **62** 867 (1990).
- [4] D. Arsenović, N. Burić and D.M. Davidović, to appear in Phys.Rev A (1999).
- [5] D.M. Davidović and D. Lalović, J. Phys. A: Math. Gen. **29** 3787 (1996).
- [6] R. Glauber, Ann. NY Acad. Sci. **480** 115 (1987).

Random Motion of Quantum Harmonic Oscillator. Thermodynamics of Nonrelativistic Vacuum

A.V. Bogdanov, A.S. Gevorkyan, A.G. Grigoryan
Institute for High-Performance Computing and Data Bases,
P/O Box 71, 194291, St-Petersburg, Russia
 bogdanov@hm.csa.ru, ashot@fn.csa.ru, ara@fn.csa.ru

Abstract

The new nonperturbative theory of quantum system interacting strongly with thermostat (or physical vacuum) is developed on example of randomly moving quantum parametric oscillator (RMQPO) problem. Mathematically the problem of closed "oscillator+thermostat" system is formulated in terms of complex probability process on extended space $\Xi = R^1 \otimes R_{\{\xi\}}$, where R^1 designates the Euclidean space and $R_{\{\xi\}}$ – the space of some functional $\xi(t) \equiv \{\xi\}$. The representation for "ground state-ground state" transition probability is obtained and investigated in detail. The thermodynamics potentials of nonrelativistic physical vacuum is constructed exactly.

It must be noted, that chaos may be caused not only by the complicated dynamics of the quantum system [1], but also by the strong interaction of simple quantum system with thermostat or mesoscopic system. The quantum chaos can arise also in nonlinear optics during a light ray movement through waveguide with nonideal or stochastic borders.

In the case of the 1D RMQPO the equation for the wave function can be written in following form:

$$id_t \Psi_{stc} = \left[-\frac{1}{2} \partial_x^2 + \frac{1}{2} (\Omega_0(t) + \Omega_1(t; \{W\}))^2 x^2 \right] \Psi_{stc}, \quad (x, t) \in (-\infty, +\infty), \quad (1)$$

where the $\Omega_1(t; \{W\})$ and the wave state $\Psi_{stc}(x, t; \{\xi\})$ are functionals of some real process $W(t) \equiv \{W\}$, $\xi(t; \{W\}) \equiv \{\xi\}$ is some stochastic differential equation (SDE) (1). The $\Omega_1(t; \{W\})$ satisfies the following limit expression $\lim_{t \rightarrow -\infty} \Omega_1(t; \{W\}) = 0$. In particular case of frequency being the regular function of t , i.e. $\Omega_1(t; \{W\}) \equiv 0$, with boundary conditions $\lim_{t \rightarrow \mp\infty} \Omega_0(t) = \Omega_{in(out)}$ the equation (1) has exact solution (see [2]).

So in our new approach the SDE (1) for complex stochastic process $\Psi_{stc}^+(n|x, t; \{\xi\})$ determined in the extended space $\Xi = R^1 \otimes R_{\{\xi\}}$, where $n = 0, 1, \dots$ is a vibration quantum number.

The wave functional in the limit $t \rightarrow -\infty$ must pass to wave function of autonomous quantum oscillator with n -th vibrational quantum state.

Let us start from the equation of classical oscillator under Brownian motion

$$\ddot{\xi} + \Omega^2(t; \{W\}) \xi = 0, \quad \xi(t; \{W\}) \Big|_{t \rightarrow -\infty} \rightarrow \exp(i\Omega_{in}t), \quad \dot{\xi} = d_t \xi. \quad (2)$$

The solution of model equation (2) can be represented in following form:

$$\xi(t; \{W\}) = \xi_0(t) \exp\left(\int_{-\infty}^t \Phi(t'; \{W\}) dt'\right), \quad (3)$$

where $\xi_0(t)$ is the solution of equation (2) with regular frequency $\Omega_0(t)$. Substituting (3) into (2) one gets the nonlinear SDE of Langevin type

$$\chi_t + \chi^2 + \Omega_0^2(t) + F(t; \{W\}) = 0, \quad \Phi(t; \{W\}) = \chi(t; \{W\}) - \dot{\xi}_0 \xi_0^{-1}, \quad \chi_t = \partial_t \chi, \quad (4)$$

with boundary condition $\lim_{t \rightarrow -\infty} \chi = i\Omega_{in}$.

Now we can pass to solving the equation (1) for complex probability process.

Theorem (see [2]): *If the model SDE (2) can be reduced to SDE of Langevin type (4), then the SDE (1) has exact solution*

$$\Psi_{stc}^+(n|x, t; \{\xi\}) = \left[\frac{(\Omega_{in}/\pi)^{1/2}}{2^n n! |\xi|}\right]^{1/2} \exp\left\{-i\left(n + \frac{1}{2}\right)\Omega_{in} \int_{-\infty}^t \frac{dt'}{|\xi|^2} + i\frac{\xi_t}{2\xi} x^2\right\} H_n\left(\sqrt{\Omega_{in}} \frac{x}{|\xi|}\right). \quad (5)$$

It is easy to see that the complex wave functionals (5) forms the full orthonormalized basis set in Hilbert space $L_2(R^1 \otimes R_{\{\xi\}})$.

Let us pass to derivation of the evolutional equation for condition probability $P(\vec{\theta}, t | \vec{\theta}', t')$. We shall study the functional of the form

$$P(\vec{\theta}, t | \vec{\theta}', t') = \langle \delta[\vec{\theta}(t) - \vec{\theta}(t')] \rangle, \quad \vec{\theta} \equiv \{\theta, \varphi\}, \quad \theta = \text{Re } \chi, \quad \varphi = \text{Im } \chi, \quad (6)$$

where $\vec{\theta}(t)$ is the solution of SDE (4). After differentiating (6) over the time, using (4) and taking into account, that stochastic force is given by correlator of "white noise"

$$\langle F(t) F(t') \rangle = 2\varepsilon \delta(t - t'), \quad \langle F(t) \rangle = 0, \quad \varepsilon > 0, \quad (7)$$

one can obtain the expression for Fokker-Plank equation for conditional probability:

$$\left\{ \partial_t - \partial_\theta \left[(\theta^2 - \varphi^2 + \Omega_0^2(t)) + \varepsilon \partial_\theta \right] + 2\partial_\varphi [\theta \varphi] \right\} P(\vec{\theta}, t | \vec{\theta}', t') = 0. \quad (8)$$

One can derive from (8) the solution for small time intervals and construct the total Fokker-Plank measure of the functional space $R_{\{\vec{\theta}\}}$

$$D\mu\{\vec{\theta}\} = \lim_{\varepsilon_0 \rightarrow 0} \lim_{N \rightarrow \infty} \left(\frac{1}{2\pi} \sqrt{\frac{N}{\varepsilon_0 \varepsilon t}} \right)^N \prod_{k=0}^N d\theta_{k+1} d\varphi_{k+1} \exp\left\{-\frac{N}{2\varepsilon t} [\theta_{k+1} - \theta_k - \right.$$

$$- \left(\theta_{k+1}^2 - \varphi_{k+1}^2 + \Omega_0^2 (t_{k+1}) \right) \frac{t_{k+1}}{N} \Big]^2 - \frac{N}{2\varepsilon_0 t} \left[\varphi_{k+1} - \varphi_k + 2\theta_{k+1}\varphi_{k+1} \frac{t_{k+1}}{N} \right]^2 \Big\} \quad (9)$$

Now we can construct the full wave function of 1D RMQPO:

$$\Psi_{br}^+(n|x, t) = \int D\mu \{ \vec{\theta} \} \tilde{\Psi}_{stc}^+(n|x, t; \{ \vec{\theta} \}), \quad \tilde{\Psi}_{stc}^+(n|x, t; \{ \vec{\theta} \}) = \Psi_{stc}^+(n|x, t; \{ \xi \}). \quad (10)$$

The transition matrix will be evaluated as a limit $t \rightarrow +\infty$ of the projection of the total averaged wave function (10) on the asymptotic wave function $\Psi_{out}(m|x, t)$ (see [2]).

Taking the wave function of autonomous quantum harmonic oscillator (see [2]) as a $\Psi_{out}(m|x, t)$ and taking into account expressions (9)-(10) one can obtain the following expression for "vacuum-vacuum" transition probability [2]

$$\Delta_{00}(\lambda, \gamma) = (1 - \rho)^{1/2} \{ I_1^2(\lambda, \gamma) + I_2^2(\lambda, \gamma) \}, \quad \lambda = \left(\frac{\Omega_{in}}{\varepsilon^{1/2}} \right)^2, \quad \gamma = \left(\frac{\Omega_{out}}{\Omega_{in}} \right)^2, \quad (11)$$

where ρ is a coefficient of reflection from barrier in the corresponding one-dimensional quantum problem and

$$I_{1,2}(\lambda, \gamma) = \int_{-\infty}^{+\infty} dx \frac{1}{a} \sqrt{\frac{a \pm 1}{2}} Q_s^{(1)}(\lambda, \gamma; x), \quad a = \left(1 + \frac{x^2}{\lambda\gamma} \right)^{1/2}.$$

The $Q_s(\lambda, \gamma; x)$ satisfies to the following second order differential equation

$$d_x \left[(x^2 + \lambda\gamma) + d_x \right] Q_s^{(p)} - \frac{p}{2} x Q_s^{(p)} = 0, \quad \lim_{|x| \rightarrow \infty} Q_s^{(p)} = \lim_{|x| \rightarrow \infty} d_x Q_s^{(p)} = 0, \quad p = 0, 1. \quad (12)$$

Let's consider the case when frequency $\Omega_0(t)$ has following form:

$$\Omega_0^2(t) = \frac{1}{2} (\Omega_{in}^2 + \Omega_{out}^2) + \frac{1}{2} (\Omega_{out}^2 - \Omega_{in}^2) \tanh(\alpha t), \quad (13)$$

where α characterizes the area of frequency changes. In this case parameter γ can be obtained as follow:

$$\gamma = \begin{cases} b^{-2} \ln^2 \left[(e^b + \rho^{1/2}) (1 + \rho^{1/2} e^b)^{-1} \right], & \gamma \leq 1, \quad \rho \in [0, 1] \\ b^{-2} \ln^2 \left[(e^b - \rho^{1/2}) (1 - \rho^{1/2} e^b)^{-1} \right], & \gamma > 1, \quad \rho \in [0, 1] \end{cases} \quad (14)$$

where $b = 2\frac{\pi}{\alpha}\Omega_{in}$.

Using the wave functionals the theory of generalized density matrix is constructed that is not limited by value of "thermostat-quantum system" interaction. In the framework of new representation [2] the expression for ground state energy of 1D RMQPO is obtained

$$E_{osc}(\lambda_+, \Omega_+) = \frac{1}{2} \Omega_+ \left\{ 1 + \int_{-\infty}^{\infty} dx x^2 \Delta Q(\lambda_+, x) + \frac{i}{\sqrt{\lambda_+}} \int_{-\infty}^{\infty} dx x \Delta Q(\lambda_+, x) \right\}, \quad \lambda_+ = \frac{\Omega_+}{\varepsilon_+^{1/3}}, \quad (15)$$

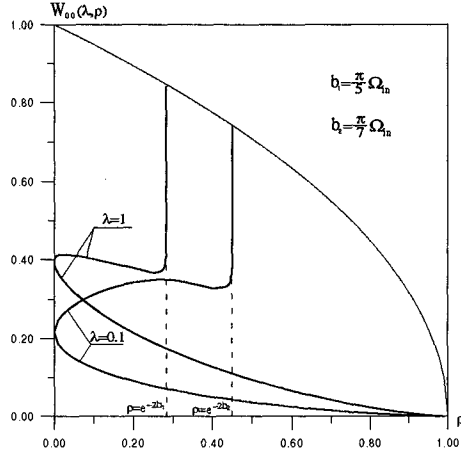


Figure 1. One can see from this figure that the probability of "vacuum-vacuum" transition has two branches. The first branch has monotonous behaviour and corresponds to a case, when the γ varies in an $[0, 1]$ interval. In this case the transition to a curve, that corresponds to a regular problem, takes place at $\lambda \rightarrow +\infty$. The second branch corresponds to a case when depending on ρ parameter γ varies in an $[1, \infty]$ interval. In this case when ρ aspires to e^{-2b} value then probability goes to its regular limit.

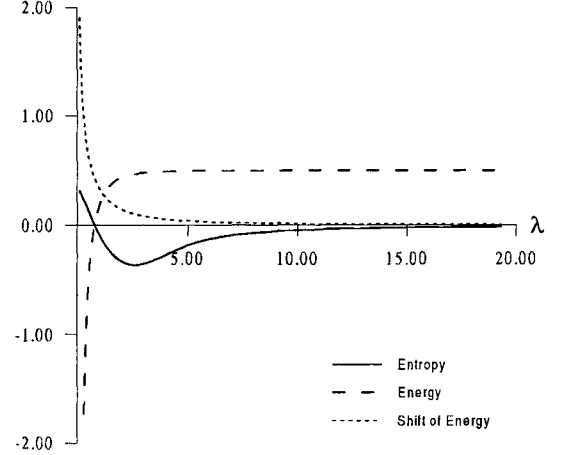


Figure 2. The curves 1 and 2 show dependences of oscillator's energy and its broadening in a vacuum state over fluctuation parameter λ_+ . The behaviour of entropy of nonrelativistic physical vacuum from λ_+ parameter is shown by a curve 3. One can see that since certain value of λ_+ parameter (from value at which the entropy becomes positive) it is necessary to consider the oscillator as a vacuum state.

where Ω_+ and ε_+ are constant frequency and diffusion coefficient, $\Delta Q(\lambda_+, x) = Q_s^{(0)}(\lambda_+, 1; x) - Q_s^{(2)}(\lambda_+, 1; x)$.

One can obtain the following expression for the entropy of nonrelativistic physical vacuum

$$S^{(0)}(\lambda_+) = -\frac{2}{3}k\lambda_+\partial_{\lambda_+}\vartheta_s^{(0)}(\lambda_+) + k\ln\vartheta_s^{(0)}(\lambda_+), \quad (16)$$

where $\vartheta_s^{(0)}(\lambda_+)$ is states distribution function in vacuum and given by following expression

$$\vartheta_s^{(0)}(\lambda_+) = J_+ [I_1^2(\lambda_+; 1) + I_2^2(\lambda_+; 1)], \quad J_+ = \int_{-\infty}^{\infty} dx Q_s^{(0)}(\lambda_+, 1; x). \quad (17)$$

REFERENCES

1. A.V. Bogdanov, A.S. Gevorkyan, *Three-body multichannel scattering as a model of irreversible quantum mechanics*, in Proceedings of Int. Symposium on Nonlinear Theory and its Applications, Hilton Hawaiian Village, 1997, V.2, pp.693-696.
2. A.V. Bogdanov, A.S. Gevorkyan, A.G. Grigoryan, *Random Motion of Quantum Harmonic Oscillator. Thermodynamics of Nonrelativistic Vacuum*, in Proceedings of Int. Workshop "Trends in Mathematical Physics", University of Tennessee, Knoxville, October 14-17, 1998

Cooling and trapping of potassium isotopes: perspectives for quantum degeneracy

F. S. Cataliotti, C. Fort, F. Minardi, M. Prevedelli, and M. Inguscio
*INFM–European Laboratory for Non Linear Spectroscopy (L.E.N.S.) and Dipartimento di Fisica,
Università di Firenze, Largo E. Fermi, 2, I-50125 Firenze, Italy*

Abstract

Cooling and trapping of potassium bosonic isotopes in a double MOT apparatus has been studied. Density and temperature limitations due to the peculiar laser cooling process are investigated and collisional parameters are estimated in a magneto-static trap. Trapping of the fermionic isotope in a single MOT is reported and perspectives for the achievement of quantum degeneracy of this atoms are discussed.

Potassium has three “stable” isotopes: ^{39}K , ^{40}K , ^{41}K with a relative abundance of 93.26%, 0.012% and 6.73%, respectively. ^{40}K is a fermion, therefore potassium is a good candidate to study a degenerate dilute Fermi gas and bosons-fermions mixtures.

The well established experimental method to achieve quantum degeneracy in a sample of alkali-metal bosons [1], consists of two different cooling stages. In the first one laser cooling techniques allow to gain many orders of magnitude in the phase space density ρ obtaining a sample with $\rho \sim 10^{-7}$ starting from a dilute gas with $\rho \sim 10^{-23}$. The final gap in the phase space density is covered by evaporative cooling in a magnetic trap. To be effective this cooling process requires a high enough ratio between elastic and inelastic collision rates $\gamma_{el}/\gamma_{inel}$. In the case of potassium the laser cooling stage is affected by the peculiar features of the levels structure and, at the time we started to investigate potassium, little was known on the collisional properties of the potassium isotopes. Something more must be said regarding the possibility to evaporate a sample of fermions. The Pauli exclusion principle inhibits s-wave collisions (the predominant collisional channel which is active at very low temperature) between spin polarized fermion atoms. As a consequence for a sample of spin polarized fermions in a magnetic trap the evaporative cooling will stop at low temperature preventing from reaching quantum degeneracy. This problem can be circumvented using a mixtures of fermions in different spin states [2,3] or taking advantage of sympathetic cooling [4] in a mixture bosons-fermions. In spite of the experimental complication and the uncertainties on the collisional properties of the mixture, this scheme would also provide an efficient diagnostic of quantum degeneracy of the fermion sample [5].

As a preliminary step to use the potassium bosons as collisional partners to cool down via sympathetic cooling the fermionic isotope, we studied cooling and trapping of ^{39}K and ^{41}K in a double-MOT set-up [6].

The laser cooling process for ^{39}K and ^{41}K is complicated by the structure of the D_2 transition. The hyperfine spacing of the upper level is comparable with the natural linewidth making not possible to isolate a single cooling transition. The first relevant consequence is that two laser frequencies are needed, separated by the hyperfine splitting of the ground state, both intense and red detuned with respect to the whole hyperfine structure of the excited state [7]. A detailed description of our studies on the laser cooling process in a MOT both for ^{39}K and ^{41}K can be found in [8] [9]. In this context, we would like to give only the relevant results concerning the minimum temperature and the maximum density observed. As a direct consequence of the high intensity regime necessary to capture atoms in the MOT, the typical temperature during the loading phase is relatively high: few mK. In order to cool further the cloud we found a regime (“cooling phase”) of reduced intensity and detuning applied for few ms after the loading, allowing to decrease the temperature by one order of magnitude. The coldest observed temperature is $\sim 150\mu\text{K}$ corresponding roughly to the Doppler limit. We were never able to observe sub-Doppler temperatures, in agreement with the theoretical analysis predicting a sub-Doppler component of the cooling force only in presence of very stable laser light (both in frequency and in amplitude) [8]. During the “cooling phase” an increase of density is also observed. The peak density ($\sim 10^8\text{ cm}^{-3}$) is however still lower than those obtained in a standard MOT with effective sub-Doppler cooling. We also tried well established techniques to increase the density in conventional MOTs, like CMOT [10] or darkSPOT [11] without any result.

To summarize, at the end of the laser cooling cycle we are able to collect in the second MOT $10^8 - 10^9$ atoms with a maximum density of 10^8 cm^{-3} and a minimum temperature of $150\mu\text{K}$. This gives a phase space density $\rho = 10^{-9}$. This numbers have to be compared with typical numbers at the end of the laser cooling stage in a rubidium BEC experiment where one can collect 10^9 atoms with a density of 10^{11} cm^{-3} and a temperature of few tens of μK ($\rho \sim 10^{-6}$).

In order to assess the effectiveness of evaporative cooling, one has to evaluate the elastic collisions rate $\gamma_{el} = n\sigma v$ (where n is the density, σ is the elastic collision cross section and v is the relative velocity of two colliding atoms) at the end of the laser cooling cycle. At low temperature, where s-wave collisions are the predominant collisional channel left, $\sigma = 8\pi a^2$ (a is the scattering length). At the time we were facing this problem, theoretical predictions of a based on photoassociative spectra of ^{39}K were contradictory (see table I [12,13]). We estimated experimentally the collisional rate loading a cloud of cold ^{39}K or ^{41}K in a quadrupole magnetic trap. We measured $\gamma_{el}/\gamma_{inel} \sim 10$, which is too small to start an efficient evaporation. Our very preliminary results have found confirmation in recent works (see Table I [14,3]). In [14] a new analysis of photoassociation spectra of ^{39}K gives a relatively small value for the scattering length a for ^{41}K and an even smaller one for ^{39}K . Furthermore the expected sign the ^{39}K scattering length is negative. Ref. [3] reports the first direct measurement of $|a|$ for the fermionic isotope (^{40}K) in a magnetic trap, from which values for the bosonic isotopes are predicted and found in good agreement with [14].

We conclude that having a relatively low density and high temperature at the end of the laser cooling stage and collisional parameters not favorable, an efficient evaporation of potassium bosons would need a very long trapping lifetime (at least 1000 s). Therefore it seems a reasonable choice to try to use a “simpler” atom like ^{87}Rb as partner for the sympathetic cooling of the potassium fermionic isotope. Following this plan we converted

our double-MOT apparatus actually observing the condensation in rubidium [?].

Regarding the fermionic isotope (^{40}K) we realized the first MOT for this atoms in a natural abundance sample [15]. As a consequence of the very low natural abundance of this isotope, we observed a MOT with only $\sim 10^4$ atoms estimating a temperature $T \sim 50\mu\text{K}$, well below the Doppler limit. As a matter of fact the levels scheme of ^{40}K is very different from the one for ^{39}K and ^{41}K . The hyperfine spacing is bigger and, more important, the hyperfine structure is inverted. A better measurement of temperature both in a MOT and in a molasses of ^{40}K has been done in our group very recently [16] loading the MOT from an enriched sample (3%). Using the enriched sample we were able to capture 10^7 atoms in the MOT having high enough signal to measure the temperature with the Time Of Flight (TOF) method. The measured temperature confirmed that sub-Doppler mechanisms are effective in a MOT of ^{40}K . This results on the laser cooling of the fermionic isotope of potassium are very encouraging giving less stringent requirement for the magnetic trapping of this atom. Moreover the low temperature attainable let one think to be able to capture the cold potassium ^{40}K directly in an optical trap having no constrains in populating different magnetic levels.

isotopes	H. Boesten et al. [12]	R. Côté et al. [13]	J. Bohn et al. [14]	B. DeMarco et al. [3]
39-39	$-1200 < a_T < -60$	81.1 ± 2.4	-17 ± 25	$-80 < a_T < -28$
40-40		1.7 ± 4.4	194_{-35}^{+114}	$136 < a_T < 176$
41-41	$25 < a_T < 60$	286 ± 36	65_{-8}^{+13}	$49 < a_T < 62$
39-40		47.5 ± 2.3	$-460_{-\text{inf}}^{+330}$	$a_T > 500$ or $a_T < -900$
39-41		5.1 ± 4.1	-205_{-10}^{+140}	$140 < a_T < 185$
40-41		-162 ± 36	104_{-11}^{+20}	$83 < a_T < 99$

TABLE I. Comparison of scattering lengths values.

REFERENCES

- [1] M. H. Anderson, J. R. Ensher, M. R. Matthews, C. E. Wieman, and E. A. Cornell, *Science* **269**, 1989 (1995). K. B. Davis, M.-O. Mewes, M. R. Andrews, N. J. van Druten, D. S. Durfee, D. M. Kurn, and W. Ketterle, *Phys. Rev. Lett.* **75**, 3969 (1995). C. C. Bradley, C. A. Sackett, and R. Hulet, *Phys. Rev. Lett.* **78**, 985 (1997)
- [2] B. DeMarco and D. S. Jin, *Phys. Rev. A* **58**, R4267 (1998)
- [3] B. DeMarco, J. L. Bohn, J. P. Burke, M. Holland, and D. S. Jin *Phys. Rev. Lett.* **82**, 4208 (1999)
- [4] C. J. Myatt, E. A. Burt, R. W. Ghrist, E. A. Cornell, and C. E. Wieman, *Phys. Rev. Lett.* **78**, 586 (1997). W. Geist, L. You, and T. A. B. Kennedy, *Phys. Rev. A* **59**, 1500 (1999)
- [5] L. Vichi, M. Inguscio, S. Stringari, and G. M. Tino. *J. Phys. B* **31**, L899 (1998)
- [6] C. J. Myatt, N. R. Newbury, R. W. Ghrist, S. Loutzenhiser, and C. E. Wieman, *Opt. Lett.* **21**, 290 (1996)
- [7] R. S. Williamson III, and T. Walker, *J. Opt. Soc. Am. B* , **12**, 1393 (1995). M. S. Santos, P. Nussenzeig, L. G. Marcassa, K. Helmerson, J. Flemming, S. C. Zilio, and V. S. Baginato, *Phys. Rev. A* , **R4340** (1995). H. Wang, P. L. Gould, and W. C. Stwalley, *Phys. Rev. A* **53**, R1216 (1996)
- [8] C. Fort, A. Bambini, L. Cacciapuoti, F. S. Cataliotti, M. Prevedelli, G. M. Tino, and M. Inguscio, *Eur. Phys. J. D***3**,113 (1998)
- [9] M. Prevedelli, F. S. Cataliotti, E. A. Cornell, J. R. Ensher, C. Fort, L. Ricci, G. M. Tino, and M. Inguscio, *Phys. Rev. A* **59**, 886 (1999)
- [10] W. Petrich, M. H. Anderson, J. R. Ensher, and E. A. Cornell, *J. Opt. Soc. Am. B* **11**, 1332 (1994)
- [11] W. Ketterle, K. B. Davis, M. A. Joffe, A. Martin, and D. E. Pritchard *Phys. Rev. Lett.* **70**, 2253 (1993)
- [12] H. M. J. M. Boesten, J. M. Vogel, J. G. C. Tempelaars, B. J. Verhaar, *Phys. Rev. A* **54**, R3726 (1996)
- [13] R. Côté, A. Dalgarno, H. Wang, W. C. Stwalley, *Phys. Rev. A* , **57**, 4118R (1998)
- [14] J. L. Bohn, J. P. Burke, C. H. Green, H. Wang, P. L. Gould, and W. C. Stwalley, *Phys. Rev. A* **59**, 3660 (1999)
- [15] M. Prevedelli, C. Fort, F. Minardi, F. S. Cataliotti, L. Ricci, G. M. Tino, and M. Inguscio to be published.
- [16] F. S. Cataliotti, E. A. Cornell, C. Fort, M. Inguscio, F. Marin, M. Prevedelli, L. Ricci, and G. M. Tino *Phys. Rev. A* **57**, 1136 (1998)
- [17] G. Modugno, C. Benkő, G. Roati, and M. Inguscio *submitted to Phys. Rev. A*

Quantum Solitons in Fibers - Internal Structure, Entanglement, and Cats

Natalia Korolkova

*Lehrstuhl für Optik, Physikalisches Institut der Universität Erlangen Nürnberg,
Staudtstr. 7/B2, D-91058 Erlangen, Germany*

R. Loudon

*Physics Department, University of Essex, Wivenhoe Park,
Colchester CO4 3SQ, United Kingdom*

M. W. Hamilton

Department of Physics and Mathematical Physics, University of Adelaide, SA 5005, Australia

G. Gardavsky, and G. Leuchs

*Lehrstuhl für Optik, Physikalisches Institut der Universität Erlangen Nürnberg,
Staudtstr. 7/B2, D-91058 Erlangen, Germany*

Abstract

We study quantum interference effects and internal entanglement of fiber optical solitons associated with their multi-particle nature. Such effects are of interest as fundamental macroscopic quantum-optical phenomena but also as practical mechanisms for noise reduction.

Solitons in optical fibres are uniquely stable macroscopic excitations that can be employed for the undistorted propagation of information over long distances. At a more basic level, the propagation of optical solitons is accompanied by unavoidable quantum effects that progressively modify the stability of the excitations [1]. Such effects are of interest not only as fundamental macroscopic quantum-optical phenomena but also as practical mechanisms for noise reduction in optical signal detection. The purpose of this presentation is to assess the development of these quantum effects in soliton dynamics, with particular emphasis on phenomena that occur over distances no greater than the attenuation length.

We consider the propagation of the optical pulse with a mean frequency ω in a single-mode polarization-preserving optical fibre. On the quantum level, it is described by the quantum nonlinear Schrödinger equation (QNSE) including both the effects of the group velocity dispersion (GVD) and the Kerr nonlinearity:

$$i \frac{\partial}{\partial t} \hat{\phi}(t, x) = -\frac{\partial^2}{\partial x^2} \hat{\phi}(t, x) - 2C \hat{\phi}^\dagger(t, x) \hat{\phi}(t, x) \hat{\phi}(t, x), \quad (1)$$

where x is the normalized deviation from pulse center, t is the normalized propagation distance, $\hat{\phi}(t, x)$, $\hat{\phi}^\dagger(t, x)$ are the annihilation and creation operators of photons at a “point” x and “time” t , and the nonlinear coefficient C characterizes the ratio between Kerr nonlinearity and GVD. We address the problem in Schrödinger picture using Bethe ansatz (see also [2]). The system is analogous to that of the one-dimensional Bose gas in an attractive δ -function potential. It results in the formation of the photon number - momentum bound states, and the attractive binding force is the Kerr nonlinearity of the fibre. We consider the evolution of the soliton state, which is a superposition of these bound states, in the frame of the time - dependent Hartree approximation. This means that in the limit of a large number of particles each of the particles (photons in the case of a soliton) experiences the same attractive δ - potential.

To visualize the evolution of the quantum state of the fundamental soliton $|\psi(t)\rangle$ we calculate the Q-function

$$Q = |\langle \psi(0) | \psi(t) \rangle|^2, \quad |\psi(t)\rangle = U(t) |\psi(0)\rangle \quad (2)$$

which is the anti-normally ordered quasiprobability distribution in phase space. $U(t)$ is the evolution operator determined by the interaction Hamiltonian of the system. For the soliton pulse with the average photon number \bar{n} , the parameter Δ defined as $n = \bar{n} + \Delta$ and the nonlinear parameter $\gamma = C^2 t / 2$ soliton Q-function takes the form:

$$Q(\alpha, \alpha^*, t) = e^{-|\alpha_0|^2 - |\alpha|^2} \times \left| \sum_n \frac{(\alpha^* \alpha_0)^n}{n!} \exp[in(n^2 - \bar{n}^2) \frac{\gamma}{2}] \right|^2, \quad (3)$$

or, equivalently:

$$Q(\alpha, \alpha^*, t) = e^{-|\alpha_0|^2 - |\alpha|^2} \times \left| \sum_{\Delta=-\bar{n}}^{\Delta=\infty} \frac{(\alpha^* \alpha_0)^{\bar{n}+\Delta}}{(\bar{n} + \Delta)!} U(t) \right|^2. \quad (4)$$

$$U(t) = \exp i[\Phi_1 \Delta + \Phi_2 \Delta^2 + \Phi_3 \Delta^3]. \quad (5)$$

The term $\Phi_1 \Delta = \bar{n}^2 \gamma \Delta$ in the exponential phase factor (5) is the linear phase shift, which leads merely to a rotation in phase space. The quadratic nonlinear term $\Phi_2 \Delta^2 = \bar{n} \frac{3\gamma}{2} \Delta^2$ has the same form as the evolution factor for the single-mode field in a Kerr medium. Figure 1 (a,b) shows the main features of the time-development of the quantum soliton Q-function in a regime where the effects of the quadratic phase $\Phi_2 \Delta^2$ are more important than those of the third-order nonlinear phase $\Phi_3 \Delta^3 = \frac{\gamma}{2} \Delta^3$. Although the dynamics follows the single-mode behaviour only approximately, it is an interesting aspect of the evolution, because the quantum effects in the dynamics emerge here at the distances by a factor of \bar{n} shorter as usually considered in optical experiments [3]. Figure 1(a) displays the formation of crescent-shaped squeezing contours, corresponding to a state with reduced number uncertainty, which is also a characteristic of the single-mode coherent state evolution in a Kerr medium [4].

Further propagation of the optical field results in spreading of the Q-function contours in a ring, with the formation of quasi-periodic multi-component quantum interference patterns. Figure 1(b) shows the Q-function for Φ_2 equal to $\pi/2$, with the form of an approximate two-component superposition, which we call a quasi-cat-state. In comparison with the dynamics of the single-mode pulse in a Kerr medium, the additional structures and shifts in peak positions are caused by the smaller third-order nonlinear phase term $\Phi_3\Delta^3 = \frac{1}{2}\Delta^3$. For longer propagation distances, where the third-order phase $\Phi_3\Delta^3$ plays a more important role, the Q-function (Fig. 1(c)) breaks up into multi-component interference structures (multiple Schrödinger cat states). In contrast to the typical single-mode superposition states produced in various nonlinear optical processes, the peak amplitudes of the individual components differ and their phase separations lie at unequal intervals around the ring of radius $\sqrt{\bar{n}}$.

As it is seen from Eq.3,4,5 and Fig.1 the nonlinear dynamics of the quantum fundamental soliton state in an optical fibre differs essentially from that of the single mode case. Mathematically, the quantum soliton acquires an extra factor n in the relevant equations and the evolution factors and the phase shift due to the Kerr interactions are nonlinear in n_2 by reference to the linear dependence in a single mode case. These reflect the stronger interaction of the photons in the pulse with each other and the medium (in comparison with a single mode case) and lead to the development of the internal entanglement in a soliton pulse. One of the evidences of this intrapulse entanglement is the recent observation of the quantum spectral correlations in femtosecond soliton pulses [5] providing the additional mechanism for noise reduction. In the case of fibre solitons, the conventional Kerr-type squeezing [4] due to the phase - photon number correlations is efficient at the earlier stages of squeezing development. With the propagation distance, the quantum spectral correlations [5], i.e. the photon number - photon number correlations, come into play and turn to the main noise reduction mechanism.

It is worthwhile to estimate the feasibility of the experimental observation of quantum interference effects, like the superposition states (for details see [6]). The presence of the single-mode-like dynamics, though exhibited approximately only, is associated with the periodicity in the evolution of the quantum state in phase space, and the formation of the coherent superposition states (Fig. 1b). These features come into play at distances shorter, by a factor of order \bar{n} , than the quantum interference structures due to the characteristic soliton dynamics (Fig. 1c). This may allow for the possibility of experimental observation of the intrinsic quantum effects in the evolution of the macroscopic quantum objects, soliton pulses.

The authors (NK, RL and MWH) greatly appreciate the financial support of the Alexander von Humboldt Foundation and the hospitality of Prof. Dr. Gerd Leuchs and his group.

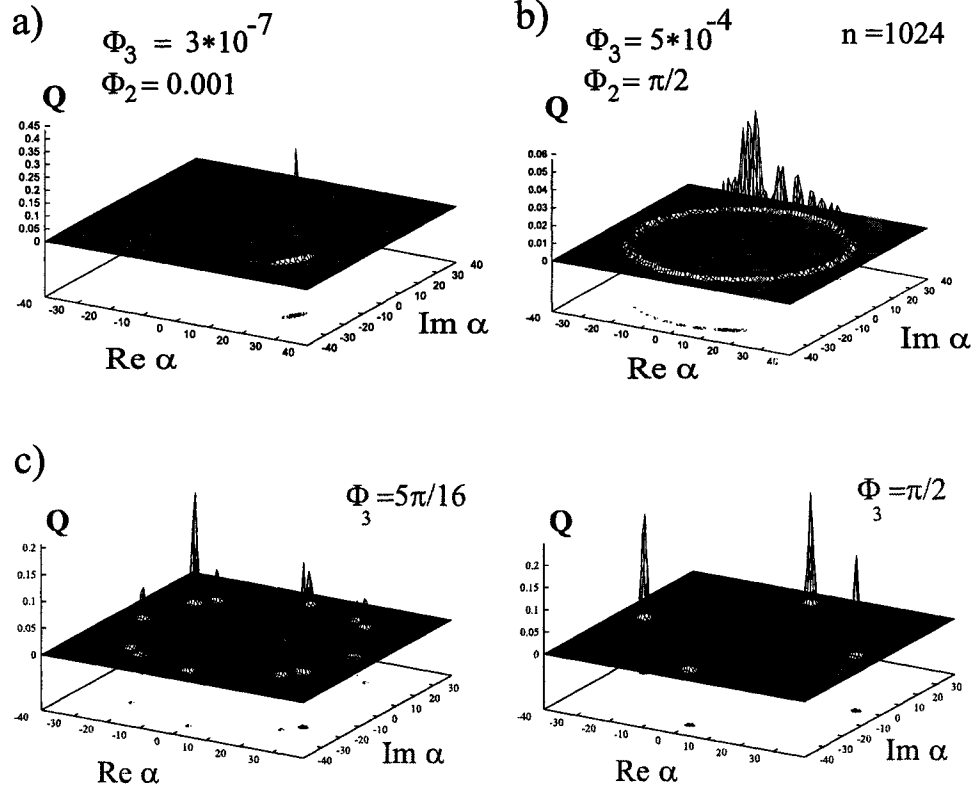


FIG. 1. Q-function of the fundamental quantum soliton at different stages of the evolution, characterized by the nonlinear phase shifts Φ_2, Φ_3 : a) squeezing; b) quasi-cat-like-state; c) multi-component interference structures. Parameter α is the complex amplitude of the field, n is the average photon number per pulse.

REFERENCES

- [1] Drummond P. D., Shelby R. M., Friberg S. R., and Yamamoto Y., 1993, *Nature*, **365**, 307-313.
- [2] Lai Y., and Haus H. A., 1989, *Phys. Rev.*, **A 40**, 844-853; Lai Y., and Haus H. A., 1989, *Phys. Rev. A* **40**, 854-866.
- [3] Gerry C. C., and Knight P. L., 1997, *Am. J. Phys.*, **65**, 964-973.
- [4] Kitagawa M., and Yamamoto Y., 1986, *Phys. Rev. A* **34**, 3974-3988.
- [5] Spälter S., Korolkova N., König F., Sizmman A., and Leuchs G., 1998, *Phys. Rev. Lett.*, **81**, 786-789.
- [6] Korolkova N., Loudon R., Gardavsky G., Hamilton M. W., and Leuchs G. Time evolution of a quantum soliton in a Kerr medium. In preparation.

Optical Displacement Sensor in Pulsed Regime for Experiments with Probe Bodies

Victor V. Kulagin

Sternberg Astronomical Institute, Moscow State University, Universitetsky prospect 13, 119899, Moscow, Russia, e-mail: kul@sai.msu.su

Abstract

The displacement transducer pumped with a train of high-intensity laser pulses is considered. An expression for the minimal detectable external classical force resembles those for the continuous wave pumping with substitution of the laser power by a time averaged power of pulsed laser. Possible scheme for back action noise compensation for such transducers is considered.

The sensitivity of modern longbase laser interferometric gravitational wave detectors to metric perturbation will be about $h \approx 10^{-21}$ that corresponds to the classical regime of operation. However for future installations with projected sensitivity $10^{-22} \div 10^{-23}$ the quantum features of the measurement process can play a significant role. At the same time there are no principal limits on the accuracy of measurement of external classical force. Therefore the methods and schemes which allow to overcome the quantum measurement limitations [1] (or the so called standard quantum limit, SQL) is of vital importance for future generation of gravitational wave experiments.

The pumping with a train of high-intensity laser pulses for gravitational wave detectors can be technically advantageous over a continuous wave pumping for practical realization of the schemes overcoming the SQL. In this contribution a sensitivity of a displacement transducer illuminated with a train of high-intensity laser pulses is considered and the algorithm of optimal signal processing for such transducer is revealed.

Let consider the most simple case of optical displacement transducer - a mirror attached to a mass of a mechanical oscillator and illuminated with a train of high-intensity laser pulses. An external force displaces an equilibrium position of mechanical oscillator changing the phase of reflected wave. The variation of the reflected field phase is measured by a homodyne detector. This model is easy to calculate and it contains at the same time all features of displacement transducers with pulsed pump. For the incident E_i and reflected E_r waves one can use the quasimonochromatic approximation

$$\begin{aligned} E_i &= (A(t - x/c) + a_1) \cdot \cos \omega_p(t - x/c) - a_2 \cdot \sin \omega_p(t - x/c) \\ E_r &= (B(t + x/c) + b_1) \cdot \cos \omega_p(t + x/c) - b_2 \cdot \sin \omega_p(t + x/c) \end{aligned} \quad (1)$$

where $A(t - x/c)$ and ω_p are an amplitude (mean value) and a frequency of the pump wave, a_1 and a_2 are the operators of the quadrature components (fluctuations) of the pump wave

(vacuum for coherent state), $B(t + x/c)$ is an amplitude (mean value) of the reflected wave, b_1 and b_2 are the operators of the quadrature components (fluctuations) of the reflected wave. The periodic envelope function $A(t - x/c)$ consists of a train of equally spaced pulses with period T and the duration of each pulse is considerably larger than the period of light wave but considerably smaller than the period of the mechanical oscillator. The spectrum of the pump has the form of a train of pulses in frequency domain with the distance between neighbour pulses $\omega_q = 2\pi T^{-1}$. For the amplitude of the pump $A(t)$ one can use the expansion into the Fourier series

$$A(t) = \sum_{n=-\infty}^{\infty} g_n \exp(-in\omega_q t) \quad (2)$$

and the particular form of $A(t)$ is defined by the set of Fourier amplitudes g_n .

To obtain the equation coupling the amplitudes of the incident and reflected waves for the moving mirror one can use a transformation of electromagnetic field for moving reference frame. Then in linear approximation in V/c and for not very large frequencies one can obtain the following expression for the transformation of the quadrature components of the field

$$\begin{aligned} b_1(t) &= -a_1(t) \\ b_2(t) &= -a_2(t) + 2\omega_p A(t)X(t)/c \end{aligned} \quad (3)$$

where for simplicity the reflection coefficient of the mirror is taken to be $r \approx -1$ and X is the position of the mirror.

For the motion of the mirror one has the following equation

$$\ddot{X}(t) + 2\delta_\mu \dot{X}(t) + \omega_\mu^2 X(t) = M^{-1}(F_s(t) + F_p(t) + F_{th}(t)) \quad (4)$$

where M and δ_μ are the mass and the damping coefficient of mechanical oscillator, $F_s(t)$ is a signal force, $F_p(t)$ is a radiation pressure force and $F_{th}(t)$ is a force associated with the damping of the oscillator. Let suppose for simplicity that δ_μ tends to zero. Then the displacement $X(t)$ of the mirror will consist of two parts - a signal displacement $X_s(t)$ and a radiation pressure displacement $X_p(t)$. For $F_p(t)$ one has

$$F_p(t) = SA(t) \cdot a_1(t)/(4\pi) \quad (5)$$

where S is a cross section of the laser beam.

The response of the displacement transducer have many frequency components at $\omega = n\omega_q, n = 0, 1 \dots$ according to the equations (3) and each frequency component contains the signal part besides the radiation pressure force $F_p(t)$ have also wide spectrum (cf. (5)). So there are two problems: how to collect the signal parts from the whole spectral band of the output and how to achieve the compensation of the radiation pressure noise in the output to circumvent the SQL. It occurs that two problems can be overcome by the use of the pulsed local oscillator with the amplitude time dependence resembling that for the pump.

For the radiation pressure displacement X_p of the mechanical oscillator one has from equations (2), (4) and (5) the following expression

$$X_p(\omega) = G(\omega)F_p(\omega) = \lambda G(\omega) \sum_{n=-\infty}^{\infty} g_n a_1(\omega - n\omega_q) \quad (6)$$

where $G(\omega) = [M(-\omega^2 - 2\delta_\mu i\omega + \omega_\mu^2)]^{-1}$ is oscillator transfer function and $\lambda = S/(4\pi)$.

For the quadrature transformation in frequency domain one can obtain the following equations from (2) and (3)

$$\begin{aligned} b_1(\omega) &= -a_1(\omega) \\ b_2(\omega) &= -a_2(\omega) + 2\omega_p c^{-1} \sum_{k=-\infty}^{\infty} g_k (X_p(\omega - k\omega_q) + X_s(\omega - k\omega_q)) \end{aligned} \quad (7)$$

Let suppose the local oscillator field in the form of $E_L(t) = A_L(t) \cos(\omega_p t + \phi)$ where the dependence of the amplitude $A_L(t)$ on t is much slower than $\cos \omega_p t$. Then for the envelope of the local oscillator field $A_L(t)$ the Fourier expansion similar to (2) is valid

$$A_L(t) = \sum_{n=-\infty}^{\infty} e_n \exp(-in\omega_q t) \quad (8)$$

The photodetector current has the following form

$$I_{pd} \propto A_L(t)(b_1(t) \cos \phi + b_2(t) \sin \phi) \quad (9)$$

and in the frequency domain one has

$$I_{pd}(\omega) \propto \cos \phi \cdot \sum_{n=-\infty}^{\infty} e_n b_1(\omega - n\omega_q) + \sin \phi \cdot \sum_{n=-\infty}^{\infty} e_n b_2(\omega - n\omega_q) \quad (10)$$

Let consider different parts in the photodetector output. The first term in equation (10) depends only on the amplitude fluctuations of the input field according to (7)

$$\cos \phi \cdot \sum_{n=-\infty}^{\infty} e_n b_1(\omega - n\omega_q) = -\cos \phi \cdot \sum_{n=-\infty}^{\infty} e_n a_1(\omega - n\omega_q) \quad (11)$$

The second term in equation (10) contains the signal and the noise parts. The noise part I_{2n} consists of the additive noise and the back action noise and has the following expression according to (6) and (7)

$$\begin{aligned} I_{2n} &= -\sin \phi \cdot \sum_{n=-\infty}^{\infty} e_n a_2(\omega - n\omega_q) + 2\omega_p c^{-1} \sin \phi \cdot \lambda \cdot \\ &\sum_{n=-\infty}^{\infty} \sum_{k=-\infty}^{\infty} e_n g_k G(\omega - k\omega_q - n\omega_q) \left\{ \sum_{m=-\infty}^{\infty} g_m a_1(\omega - k\omega_q - n\omega_q - m\omega_q) \right\} \end{aligned} \quad (12)$$

Let consider only the photocurrent at small frequencies $\omega \approx \omega_\mu$. Then the main input into the photocurrent will be given by the resonant terms for which $k + n = 0$. With this supposition one has from equation (12) ($\xi(\omega) = 2\omega_p G(\omega) c^{-1}$)

$$I_{2n} = -\sin \phi \sum_{n=-\infty}^{\infty} e_n a_2(\omega - n\omega_q) + \sin \phi \cdot \lambda \xi(\omega) \sum_{m=-\infty}^{\infty} e_m g_{-m} \sum_{n=-\infty}^{\infty} g_n a_1(\omega - n\omega_q) \quad (13)$$

Comparing equations (11) and (13) one can conclude that full compensation of back action noise in the photocurrent is possible only for $e_n = \alpha g_n$, where α is the same for all

numbers n so the forms of pump and local oscillator fields have to be the same (apart from the scale factor α).

Let now consider the signal part I_{2s} of the second term in the r.h.s. of equation (10). From equations (4), (7) and (10) one has for $k + n = 0$

$$I_{2s} = \sin \phi \cdot \xi(\omega) F_s(\omega) \sum_{n=-\infty}^{\infty} e_n g_{-n} \quad (14)$$

Combining equations (10), (13) and (14) and supposing that the back action noise is compensated in the output of the photodetector one can obtain for the signal-to-noise ratio μ the following expression

$$\mu \propto N_0^{-1} P \int_{-\infty}^{\infty} |\xi(\omega) F_s(\omega)|^2 d\omega = \mu_{cw} \quad (15)$$

where it is supposed that fluctuations at frequencies $\omega - n\omega_q, n = 0, 1 \dots$ are uncorrelated and have the same spectral density N_0 (this assumption is valid for not very small duration of pump pulses), P is proportional to the time averaged power of the pulsed pump, μ_{cw} is the signal-to-noise ratio for continuous wave pump with a power P and correlative processing of the output [2]. Note that the sensitivity here is not limited by the SQL like in the case of correlative processing of quadratures for the monochromatic pump [2] and is increasing with the increase of P .

It is worth to mention that the condition for the back action noise compensation for the pulsed pump is just the same as for the monochromatic pump [2] with substitution of the A^2 with the time averaged value P . Therefore the compensation of the back action noises for the finite frequency band can be possible for the time varying phase of the local oscillator [2].

In conclusion the pumping of the displacement transducer with a train of a short high-intensity laser pulses can be advantageous over the single frequency pumping because in this case the energy of the pump is spread over the large frequency band and high intensities can be produced relatively easy. At the same time the amplitude and frequency stability of the pulsed pump in the case of a mode locked laser can be at the same level as for the monochromatic pump [3]. Besides the perspectives of squeezed states generation with high nonclassicality for the case of short laser pulses seem more realistic allowing the use of squeezed pulsed pump in displacement transducers [4].

REFERENCES

- [1] Caves C. M., Thorne K. S., Drever R. W. P., Sandberg V. D., Zimmerman M. *Rev. Mod. Phys.* **52** (1980) 341.
- [2] Gusev A. V., Kulagin V. V. *Appl. Phys.* **B64** (1997) 137.
- [3] Spence D. E., Dudley J. M., Lamb K., Sleat W. E., Sibbett W. *Opt. Letters* **19** (1994) 481.
- [4] Kulagin V. V. *Proc. 5th Int. Wigner Symp.* ed. P. Kasperkovitz, D. Grau (Singapore: World Scient. Publ. Co.) (1998) p. 509.

An Operator Formulation of Classical Mechanics and Semiclassical Limit

Slobodan Prvanović

Institute of Physics, P.O. Box 57, 11001 Belgrade, Yugoslavia

Zvonko Marić

Institute of Physics, P.O. Box 57, 11001 Belgrade, Yugoslavia

Abstract

The generalized h -dependent operator algebra is defined ($0 \leq h \leq h_o$). For $h = h_o$ it becomes equivalent to the quantum mechanical algebra of observables and for $h = 0$ it is equivalent to the classical one. We show this by proposing how the main features of both mechanics can be defined in operator form.

I. INTRODUCTION

There have been many investigations concerning the algebraic structures of classical and quantum mechanics with different epistemological horizons [1-4 and references therein]. Here, our interest is to study the semiclassical limit of quantum mechanics (QM) in the algebraic framework. For that reason an operator formulation of classical mechanics (CM) is proposed, which is very similar to the standard QM one. Our intention is the formulation in which all the characteristics of QM and CM are preserved. Therefore, the mathematical arena for that purpose has to be wider than the one usually used in the representation of QM. In some sense, it could be seen as a direct product of coordinate and momentum representations of QM, so it mimics phase space formulation of CM.

II. BASIC DEFINITIONS

Firstly, we introduce the generalized operator h -dependent algebra of observables which is defined as the algebra of polynomials with real coefficients over the operators \hat{Q} , \hat{P} and $\hat{\mathcal{I}}$, which are defined as:

$$\tilde{Q} = \hat{Q} \otimes \hat{I} \otimes \left[\hat{R}_q + \left(1 - \frac{h}{h_o} \right) \hat{R}_p \right] + \hat{I} \otimes \hat{Q} \otimes \hat{R}_p, \quad (1)$$

$$\tilde{P} = \hat{P} \otimes \hat{I} \otimes \hat{R}_q + \hat{I} \otimes \hat{P} \otimes \left[\left(1 - \frac{h}{h_o} \right) \hat{R}_q + \hat{R}_p \right], \quad (2)$$

and

$$\hat{\mathcal{I}} = \hat{I} \otimes \hat{I} \otimes \hat{I}. \quad (3)$$

These operators act in $\mathcal{H}_q \otimes \mathcal{H}_p \otimes \mathcal{H}_r$ where q, p and r are indices, the first two spaces are rigged Hilbert spaces and the third is, at least, a two dimensional Hilbert space. More concretely, \mathcal{H}_q and \mathcal{H}_p are formally identical to the rigged Hilbert space of states which is used in nonrelativistic QM of a single particle with the one degree of freedom when spin is neglected. The indices q and p serve only to denote that the choice of a basis in these spaces is *a priori* fixed. For the basis in $\mathcal{H}_q \otimes \mathcal{H}_p$ we take $|q\rangle \otimes |p\rangle$. Here $|q\rangle$ and $|p\rangle$ are eigenvectors of \hat{Q} and \hat{P} , respectively. Then, $\mathcal{H}_q \otimes \mathcal{H}_p$ can be seen as an analogue of the phase space. The third space is introduced only for the formal reasons. The parameter h takes values from 0 to h_o where h_o is related to QM (the nonvanishing Planck constant) while for $h = 0$ the above algebra will be related to CM. The operators \hat{Q} and \hat{P} are as the operators representing coordinate and momentum in standard QM: they do not commute ($[\hat{Q}, \hat{P}] = i\hbar\hat{I}$), they are Hermitian *etc.*

For projectors \hat{R}_q and \hat{R}_p the following relations should hold: $\hat{R}_q\hat{R}_p = 0$, $\hat{R}_q\hat{R}_q = \hat{R}_q$, $\hat{R}_p\hat{R}_p = \hat{R}_p$, $\hat{R}_q^\dagger = \hat{R}_q$, $\hat{R}_p^\dagger = \hat{R}_p$ and $\hat{R}_q + \hat{R}_p = \hat{I}$. They have no physical meaning and are introduced to ensure desired formal properties. This becomes obvious when one forms polynomials over \hat{Q} and \hat{P} .

III. QUANTUM MECHANICS

When the above algebra of operators is represented in the basis $|q\rangle \otimes |p\rangle \otimes |r_i\rangle$, where $i = \{q, p\}$ and $|r_i\rangle$ is the eigenvector for \hat{R}_i , for $h = h_o$ it becomes equivalent to the representation (in the same basis) of:

$$\hat{Q}_{qm} = \hat{Q} \otimes \hat{I} \otimes \hat{R}_q + \hat{I} \otimes \hat{Q} \otimes \hat{R}_p, \quad (4)$$

$$\hat{P}_{qm} = \hat{P} \otimes \hat{I} \otimes \hat{R}_q + \hat{I} \otimes \hat{P} \otimes \hat{R}_p, \quad (5)$$

and

$$\hat{\mathcal{I}} = \hat{I} \otimes \hat{I} \otimes \hat{I}. \quad (6)$$

This algebra and the appropriate eigenvectors are in one-to-one correspondence with the standard formulation of QM (defined in one rigged Hilbert space). Namely, for these representations of QM, for the coordinate and momentum, it holds: $[\hat{Q}_{qm}, \hat{P}_{qm}] = i\hbar\hat{\mathcal{I}}$, as it is necessary. Moreover, due to the mentioned properties of \hat{R}_q and \hat{R}_p , the standard representation of QM observable, *e.g.*, $f(\hat{Q}, \hat{P})$, is now translated to

$$f(\hat{Q}_{qm}, \hat{P}_{qm}) = f(\hat{Q}, \hat{P}) \otimes \hat{I} \otimes \hat{R}_q + \hat{I} \otimes f(\hat{Q}, \hat{P}) \otimes \hat{R}_p. \quad (7)$$

The ordering problem for operators is here inherited from the standard QM. This we shall discuss elsewhere. If $|\Psi_i\rangle$ were eigenstates of $f(\hat{Q}, \hat{P})$, then

$$|\tilde{\Psi}_i\rangle = c_q|\Psi_i\rangle \otimes |a\rangle \otimes |r_q\rangle + c_p|b\rangle \otimes |\Psi_i\rangle \otimes |r_p\rangle, \quad (8)$$

are eigenstates of $f(\hat{Q}_{qm}, \hat{P}_{qm})$ with the same eigenvalues. The coefficients c_q and c_p has to satisfy only the condition $|c_q|^2 + |c_p|^2 = 1$, and vectors $|a\rangle$ and $|b\rangle$ are fixed at the beginning of all considerations, they are arbitrarily picked and they only have to be normalized. The quantities like the mean values, the spectrum, and all relations and properties among eigenstates of the same or different observables are the same as in the standard formulation of QM (what can be easily seen). Obviously, $\mathcal{H}_q \otimes \mathcal{H}_p \otimes \mathcal{H}_r$ is much wider than it is necessary for representing just the QM. Only a subspace of $\mathcal{H}_q \otimes \mathcal{H}_p \otimes \mathcal{H}_r$, which depends on the choice of $|a\rangle$, $|b\rangle$, c_q and which is formed over the basis $|\tilde{\Psi}_i\rangle$, has the QM interpretation.

IV. CLASSICAL MECHANICS

On the other hand, for the above representation of (1-3), but for $\hbar = 0$, the above algebra (1-3) becomes equivalent to the representation of:

$$\hat{Q}_{cm} = \hat{Q} \otimes \hat{I} \otimes \hat{I}, \quad (9)$$

$$\hat{P}_{cm} = \hat{I} \otimes \hat{P} \otimes \hat{I}, \quad (10)$$

and

$$\hat{\mathcal{I}} = \hat{I} \otimes \hat{I} \otimes \hat{I}. \quad (11)$$

This algebra and the appropriate eigenstates are in 1-1 correspondence with the standard formulation of CM (defined in the phase space). Namely, to the c -number formulation of a CM observable, *e.g.*, $h(q, p)$, now corresponds $h(\hat{Q}_{cm}, \hat{P}_{cm})$. Such an algebra is manifestly a commutative one. The vectors $|q_0\rangle \otimes |p_0\rangle \otimes (c_q|r_q\rangle + c_p|r_p\rangle)$ are eigenstates of all CM observables for the eigenvalues $h(q_0, p_0)$. These vectors are the analogs of the points in phase space for a CM system with one degree of freedom. For these pure states it holds:

$$\begin{aligned} & |q_0\rangle\langle q_0| \otimes |p_0\rangle\langle p_0| \otimes (c_q|r_q\rangle + c_p|r_p\rangle) (c_q^*\langle r_q| + c_p^*\langle r_p|) = \\ & = \int \int \delta(q - q_0)\delta(p - p_0) |q\rangle\langle q| \otimes |p\rangle\langle p| dq dp \otimes (c_q|r_q\rangle + c_p|r_p\rangle) (c_q^*\langle r_q| + c_p^*\langle r_p|) = \\ & = \delta(\hat{Q} - q_0) \otimes \delta(\hat{P} - p_0) \otimes (c_q|r_q\rangle + c_p|r_p\rangle) (c_q^*\langle r_q| + c_p^*\langle r_p|). \end{aligned} \quad (12)$$

Motivated by this, the mixed CM states now can be defined as $\rho(\hat{Q} \otimes \hat{I}, \hat{I} \otimes \hat{P}) \otimes (c_q|r_q\rangle + c_p|r_p\rangle)(c_q^*\langle r_q| + c_p^*\langle r_p|)$. All CM states will be Hermitian, non-negative operators and normalized to $\delta^2(0)$ if $\rho(q, p)$ is real, non-negative and normalized to 1 as in the standard phase space formulation of CM. The mean values of both QM and CM observables are now calculated by the Ansatz: $\langle \hat{A} \rangle = Tr(\hat{\rho}\hat{A})/Tr\hat{\rho}$, so the norm $\delta^2(0)$ does not affect anything in the theory.

There will be a complete correspondence between the c -number formulation and the above given operator formulation of CM if the dynamical equation (Lie bracket) is defined as the Liouville equation, where the partial derivations within the Poisson bracket are done with respect to the operators \hat{Q}_{cm} and \hat{P}_{cm} .

V. CONCLUDING REMARKS

The semiclassical limit of QM is established through the generalized operator algebra, since for the one extreme value of \hbar it expresses QM properties while for the other value of \hbar it has CM ones, and only for $\hbar \in \{0, \hbar_0\}$ operators \tilde{Q} and \tilde{P} have a physical meaning. This holds for each polynomial with real coefficients over coordinate and momentum no matter of how these operators are ordered. The ordering problem we shall discuss elsewhere together with the semiclassical limit of generalized Lie bracket. We have not expressed the above operators explicitly after representing them only for the sake of simplicity. It could be easily done having in mind that $[\hat{Q}, \hat{P}] = i\hbar\hat{I}$ and that $|q\rangle$ and $|p\rangle$ are eigenstates of \hat{Q} and \hat{P} , respectively.

Acknowledgement

We are very grateful to the organizer for allowing us to present this work at the conference without being there personally, caused by the circumstances in our country. This article is our minimal protest against the war.

1. G. Folk, Zeit. Phys. **130**, (1951) 51.
2. T. Jordan and E. C. G. Sudarshan, Rev. Mod. Phys. **33**, (1961) 515.
3. G. Ludwig, Zeit. Phys. **181**, (1964) 233.
4. A. Petersen and E. Grgin, Phys. Rev. **5**, (1972) 300.

General Uncertainty-Like Relationships.

E. Romera, J. C. Angulo, J. S. Dehesa
*Departamento de Física Moderna
and Instituto Carlos I de Física Teórica y Computacional,
Facultad de Ciencias, Universidad de Granada,
18071-Granada, Spain.*

and J. Sánchez-Ruíz
*Departamento de Matemáticas, Universidad Carlos III de Madrid, Avda. de la Universidad 30,
28911-Leganés, Madrid, Spain
and Instituto Carlos I de Física Teórica y Computacional,
Facultad de Ciencias, Universidad de Granada,
18071-Granada, Spain.*

Abstract

Model independent uncertainty-like relationships for D -dimensional quantum-mechanical systems are obtained using the concept of information entropy. Numerical comparisons employing accurate Hartree-Fock atomic densities are done in the whole Periodic Table.

The electron densities in position $\rho(\mathbf{r})$ and momentum $\gamma(\mathbf{p})$ spaces play a significant role in the modern quantum theory of N -particle systems, as in the Density Functional Theory [1]. Some radial expectation values of the aforementioned densities for a D -dimensional system, defined as $\langle r^a \rangle \equiv \int r^a \rho(\mathbf{r}) d^D \mathbf{r}$, $\langle p^a \rangle \equiv \int p^a \gamma(\mathbf{p}) d^D \mathbf{p}$, are experimentally accessible and/or physically meaningful in different systems (see references in [2]). More recently, the so-called logarithmic expectation values $\langle r^a \ln r \rangle$ and $\langle p^a \ln p \rangle$ have been shown to be also relevant in the description of some features of this kind of systems [3].

The Heisenberg uncertainty principle can be expressed in terms of the best known relation involving radial expectation values of conjugate spaces

$$\langle r^2 \rangle \langle p^2 \rangle \geq \frac{D^2}{4} N^2. \quad (1)$$

There are other known uncertainty expressions involving radial expectation values, obtained by using different techniques [4], namely:

$$\langle r^2 \rangle \langle p^{-1} \rangle^{-2} \geq N^{-1}; \quad (2)$$

$$\langle r^{-2} \rangle^{-1} \langle p^2 \rangle \geq \frac{1}{4}. \quad (3)$$

Inequality (3) is a particular case of the Pitt-Beckner inequality [5]

$$\langle p^{-a} \rangle \leq 2^{-a} \left(\frac{\Gamma((D-a)/4)}{\Gamma((D+a)/4)} \right)^2 \langle r^a \rangle \quad (4)$$

In this work we show how the concept of information entropy allows us to obtain uncertainty relations which generalize and improve the above mentioned ones. To study the accuracy of such inequalities, a numerical analysis has been carried out for neutral atoms within a Hartree-Fock framework.

UNCERTAINTY RELATIONS

The so-called Fisher entropy and Shannon entropy of a D -dimensional density function can be considered, in an information-theoretical context, as two different and complementary measurements of the degree of spatial delocalization of such distribution. Several sets of uncertainty relations expressed in terms of radial and logarithmic expectation values can be obtained, based on the concepts of Fisher and Shannon information entropy, and on i) the use of a known uncertainty principle for each entropy, and ii) bounds to these entropies derived variationally and/or using different classical inequalities [6].

The Fisher information entropy I_f of a D -dimensional density function $f(\mathbf{r})$ is defined as [7]

$$I_f \equiv \int \frac{|\nabla f(\mathbf{r})|^2}{f(\mathbf{r})} d\mathbf{r} \quad (5)$$

The Stam uncertainty principle [8] establishes an upper bound to the entropy I_ρ of the one-particle density $\rho(\mathbf{r})$ in position space in terms of the mean square momentum $\langle p^2 \rangle$ (related to the kinetic energy of the system) in the form

$$I_\rho \leq 4 \langle p^2 \rangle \quad (6)$$

and similarly for the entropy I_γ associated to the momentum space distribution $\gamma(\mathbf{p})$ in terms of the mean square value of the conjugate variable.

Using this uncertainty principle together with the D dimensional bounds to the Fisher entropy [9] (which have been derived in a similar way to that of Ref. [2]) the following expressions are obtained:

$$\langle p^2 \rangle \langle r^{-2} \rangle^{-1} \geq \frac{1}{4} \left[(D-2)^2 + \frac{(\beta+1)^2 \langle r^{\beta-1} \rangle^2}{\langle r^{2\beta} \rangle \langle r^{-2} \rangle - \langle r^{\beta-1} \rangle} \right] = B_1(\beta); \quad \beta > -1 \quad (7)$$

$$\langle p^2 \rangle \langle r^{-2} \rangle^{-1} \geq \frac{1}{4} \left[(D-2)^2 + \frac{\langle r^{-2} \rangle^2}{\langle r^{-2} (\ln r)^2 \rangle \langle r^{-2} \rangle - \langle r^{-2} \ln r \rangle^2} \right] = B_2 \quad (8)$$

$$\langle p^2 \rangle \leq \left(\frac{\beta + D - 1}{2} \right)^2 \frac{\langle r^{\beta-1} \rangle^2}{\langle r^{2\beta} \rangle} = B_3 \quad \text{if } D \geq 2 \text{ and } \beta > \frac{-3}{2} \quad (9)$$

$$\langle p^2 \rangle \leq \left(\frac{\beta - D + 3}{2} \right)^2 \frac{\langle r^{\beta-1} \rangle^2}{\langle r^{2\beta} \rangle} = B_4 \quad \text{if } D \leq 2 \text{ and } \beta > \frac{-3}{2} \quad (10)$$

These inequalities improve Eq.(3) accordingly to the fact that $\langle r^b \rangle \langle r^{-2} \rangle - \langle r^{b/2-1} \rangle^2 \geq 0$, as Hölder inequality establishes.

The Shannon Information Entropy of a density function $f(\mathbf{r})$ in a D -dimensional space is defined by

$$S_f \equiv - \int f(\mathbf{r}) \ln f(\mathbf{r}) d\mathbf{r} \quad (11)$$

Concerning this entropy, the key inequality to obtain uncertainty expressions between radial and logarithmic expectation values is the inequality of Bialynicki-Birula and Mycielski [10]

$$S_\rho + S_\gamma \geq DN(1 + \ln \pi) - 2N \ln N \quad (12)$$

Angulo uses that concept and several variational relations [11] between the Shannon entropy and the expectation values $\langle r^\alpha \rangle$, $\langle \ln r \rangle$, $\langle (\ln r)^2 \rangle$ to obtain:

$$\langle r^{D/\alpha} \rangle^\alpha \langle p^{D/\beta} \rangle^\beta \geq \alpha^\alpha \beta^\beta \frac{\Gamma^2(1 + \frac{D}{2})}{\Gamma(1 + \alpha)\Gamma(1 + \beta)} e^{D-\alpha-\beta} N^{\alpha+\beta} \quad (13)$$

$$\Delta(\ln r) \Delta(\ln p) \geq \frac{N^2 \Gamma^2(D/2)}{8\pi} \exp \left(D - 1 - D \frac{\langle \ln r \rangle + \langle \ln p \rangle}{N} \right) \quad (14)$$

where $\Delta(a) = \sqrt{\langle a^2 \rangle - \langle a \rangle^2}$.

The relations (7)-(10) and (13) and (14) connect different sets of expectation values so they are complementary inequalities. In addition these expressions generalized the known relations (1) to (3). The uncertainty relations (7) and (8) improve the expression (3) using more information, i. e. , by means of more expectation values.

A numerical analysis of the quality of some of these inequalities have been done using the NHF atomic wave functions of Refs. [12]. The analysis have been done to see how the inequality (3) is improved with the new relations (7) and (8). We can observe in table 1 that in general the best inequality is B_2 , and that all the new relations improve the relation (3).

N	B_2	$B_1(1)$	$B_1(0)$	Eq.(1)
2	83.1	86.7	66.4	52.4
10	61.0	44.6	40.7	40.3
15	54.4	37.5	36.6	36.4
30	44.3	31.0	30.4	30.3
48	38.1	26.9	26.5	26.5
65	34.7	24.6	24.3	24.3
92	30.9	22.0	21.9	21.9
103	29.7	21.3	21.1	21.1

Table 1 Numerical analysis of the accuracy of some of the bounds to $\langle r^{-2} \rangle^{-1} \langle p^2 \rangle$ by means of the accurate Koga-Hartree-Fock wavefunctions [12] for some neutral atoms with N electrons.

SUMMARY

The concepts of Fisher and Shannon information entropies allow us to reach two sets of D -dimensional uncertainty relations. The keys to obtain these sets are the Stam and the Bialynicki-Birula uncertainty principles, and several bounds to these entropies. The analysis of the different relations reveals a large improvement in some cases respect to the previously known ones.

ACKNOWLEDGMENTS

We acknowledge partial financial support from the Spanish DGICYT under Project No. PB95-1205, and the Junta de Andalucía (Grant No. FQM-0207), and from the European Project No. INTAS-93-219-EXT.

REFERENCES

- [1] R. G. Parr y W. Yang, *Density Functional Theory of Atoms and Molecules* (Oxford University Press, Oxford, 1994).
- [2] E. Romera, J. C. Angulo, and J. S. Dehesa, *Phys. Rev. A* **59**, 4064 (1999).
- [3] J. C. Angulo and J. S. Dehesa, *J. Chem. Phys.* **97**, 6485 (1992); erratum **98**, 1 (1993); F. Lenz y R. Rosenfelder, *Nucl. Phys. A* **176**, 513 (1971).
- [4] B. Tsapline, *Chem. Phys. Lett.* **6**, 596 (1970); S. R. Gadre y R. J. Pathak, *Adv. Quantum Chem.* **22**, 1 (1991).
- [5] W. Beckner, *Proc. Amer. Math. Soc.* **123**, 1897 (1995).
- [6] J. C. Angulo and J. S. Dehesa, *J. Chem. Phys.* **97** 6485 (1992); E. Romera and J. S. Dehesa, *Phys. Rev. A* **50**, 256 (1994)
- [7] R. A. Fisher, *Theory of Statistical Estimation*, *Proc. Cambridge Philos. Soc.* **22** (1925), 700.
- [8] A. Stam, *Inf. Control.* **2**, 101 (1959).
- [9] J. Sánchez-Ruíz, E. Romera, J. C. Angulo and J. S. Dehesa, Preprint, 1999.
- [10] I. Bialynicki-Birula y J. Mycielski, *Comm. Math. Phys.* **44**, 129 (1975).
- [11] J. C. Angulo, *Phys. Rev. A* **50**, 311 (1994).
- [12] T. Koga, K. Kanayama, S. Watanabe, and A. J. Thakkar, to be published; T. Koga, K. Kanayama, T. Watanabe, T. Imai, and A. J. Thakkar, to be published.

Nonclassical correlations in damped N -solitons

Eduard Schmidt, Ludwig Knöll, and Dirk–Gunnar Welsch
*Friedrich-Schiller-Universität Jena, Theoretisch-Physikalisches Institut
Max-Wien Platz 1, D-07743 Jena, Germany*

The quantum statistics of damped higher-order optical solitons are analyzed numerically, using cumulant-expansion techniques in Gaussian approximation. A detailed analysis of nonclassical properties in both the time and the frequency domain is given, with special emphasis on the role of absorption. Highly nonclassical broadband spectral correlation is predicted.

From classical optics it is well known that nonlinearities can compensate for the dispersion-assisted pulse spreading [1,2] or for diffraction-assisted beam broadening (see, e.g., [3]). In the two cases, the undamped motion of the (slowly varying) bosonic field variables $\hat{a}(x, t)$ is governed by the Hamiltonian

$$\hat{H} = \hbar \int dx \left[\frac{1}{2} \omega^{(2)} (\partial_x \hat{a}^\dagger) (\partial_x \hat{a}) + \frac{1}{2} \chi \hat{a}^\dagger \hat{a}^\dagger \hat{a} \hat{a} \right], \quad (1)$$

$$\left[\hat{a}(x, t), \hat{a}^\dagger(x', t) \right] = \delta(x - x') \quad (2)$$

[t , propagation variable; x , “transverse” coordinate; $\omega^{(2)}$, second order dispersion or diffraction constant; χ nonlinearity constant; see, e.g., [4,5]]. Note that bright temporal solitons can be formed either in focusing media with anomalous dispersion ($\chi < 0$, $\omega^{(2)} > 0$) or in defocusing media with normal dispersion ($\chi > 0$, $\omega^{(2)} < 0$), whereas spatial solitons require always focusing nonlinearity. The effect of absorption is described in terms of ordinary Markovian relaxation theory resulting, in the low temperature limit, in the master equation

$$i\hbar \partial_t \hat{\rho} = [\hat{H}, \hat{\rho}] + i\gamma \hbar \int dx \left(2\hat{a} \hat{\rho} \hat{a}^\dagger - \hat{\rho} \hat{a}^\dagger \hat{a} - \hat{a}^\dagger \hat{a} \hat{\rho} \right) \quad (3)$$

(γ , damping constant).

The master equation (3) is converted, after spatial discretization, into a pseudo-Fokker-Planck equation for an s -parametrized multi-dimensional phase-space function, which is solved numerically using cumulant expansion in Gaussian approximation [5]. The initial condition is realized by a multimode coherent state without internal entanglement, and it is assumed that the field expectation value corresponds to the classical N -soliton solution, $\langle \hat{a}(x, t_0) \rangle = N a_0 \operatorname{sech}(x/x_0)$, $N = 1, 2, \dots$ (a_0 and x_0 , mean amplitude and width of the fundamental soliton, respectively).

Spectral properties can be studied introducing the Fourier-component operators

$$\hat{a}(\omega, t) = (2\pi)^{-\frac{1}{2}} \int_{-\infty}^{\infty} dx e^{i\omega x} \hat{a}(x, t). \quad (4)$$

Here we restrict our attention to correlations of photon number fluctuations. In the case of fiber soliton pulses the correlations in the ω -domain can be measured using appropriate spectral filtering (see, e.g., in [6]). In the case of spatial solitonic beams the correlations in both the x and ω -domains, respectively, can be measured by filtering the field in the near- and far-field zones of the output beam (see, e.g., [4]).

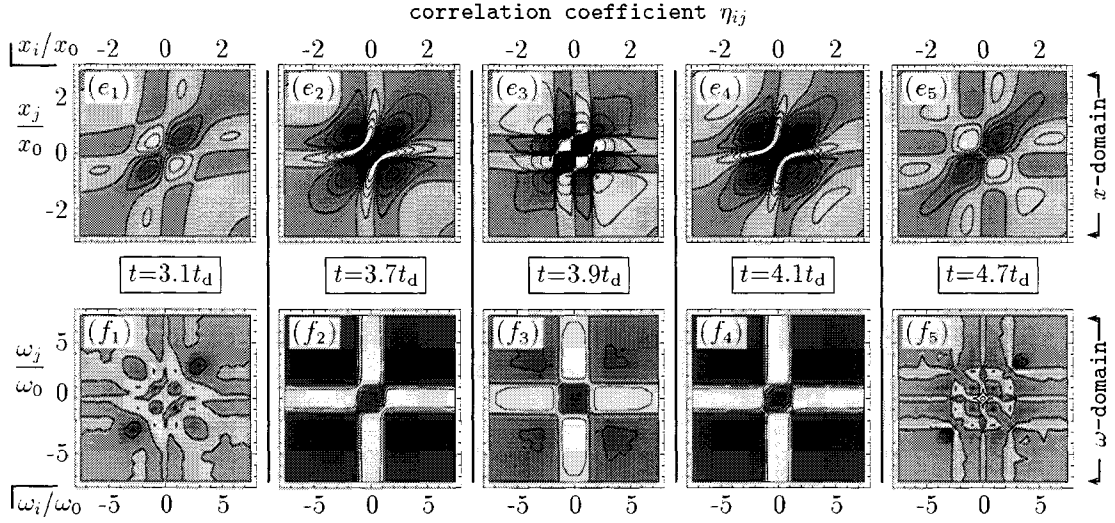
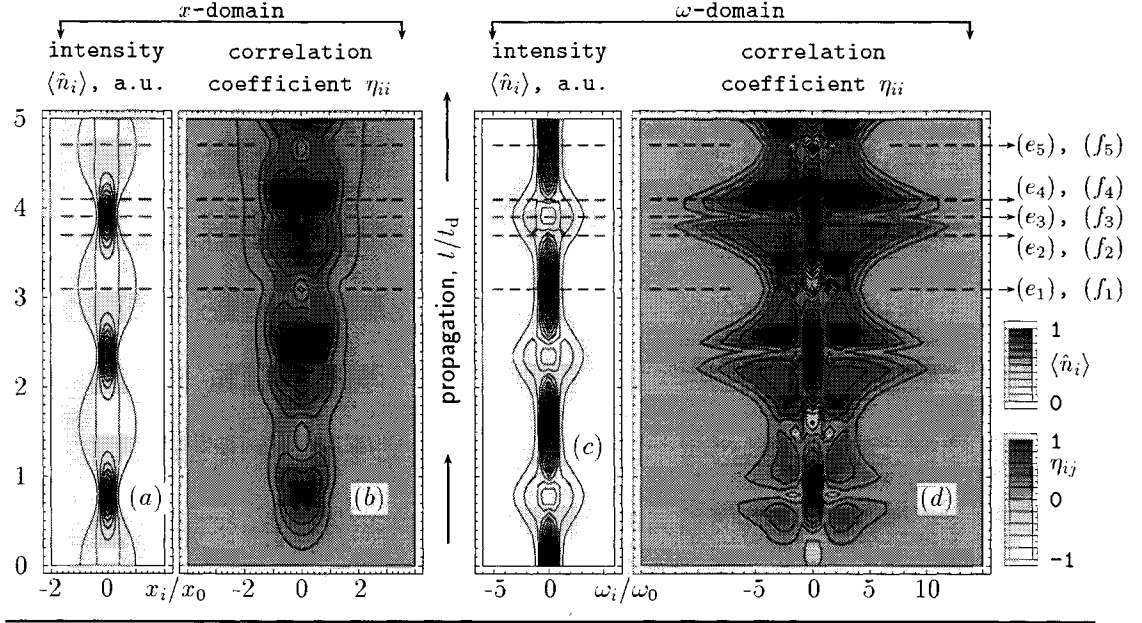


FIG. 1. The evolution of the mean photon number $\langle \hat{n}_i \rangle$ and the correlation coefficient η_{ii} of an undamped soliton, $N = 2$, is plotted in the x -domain, $\Delta x = 0.05 x_0$ [(a),(b)], and the ω -domain, $\Delta \omega = 0.25 \omega_0$ [(c),(d)]. The plots (e₁)–(e₅) (x -domain) and (f₁)–(f₅) (ω -domain) show the correlation coefficient η_{ij} for typical propagation lengths ($\omega_0 = 1/x_0$, $t_d = |x_0^2/\omega^{(2)}|$, $\int dx \hat{a}^\dagger(x, 0)\hat{a}(x, 0) = 8 \times 10^9$).

The output can be given by (see, e.g., [7])

$$\hat{b}(\nu, t) = G(\nu, t)\hat{a}(\nu, t) + \sqrt{1 - |G(\nu, t)|^2} \hat{f}(\nu, t), \quad (5)$$

where, according to the domain considered, ν stands for x or ω , and $G(\nu, t)$, $|G(\nu, t)| \leq 1$, is the (complex) transmittance of the filter and $\hat{f}(\nu, t)$ is a bosonic noise operator. The photon number operator of the detected light is $\hat{n} = \int d\nu \hat{b}^\dagger(\nu, t)\hat{b}(\nu, t)$. Assuming square bandpass filters with $G_i(\nu, t) = 1$ if $|\nu - \Omega_i| \leq \Delta\Omega$ and $G_i(\nu, t) = 0$ otherwise, we consider the correlation coefficient

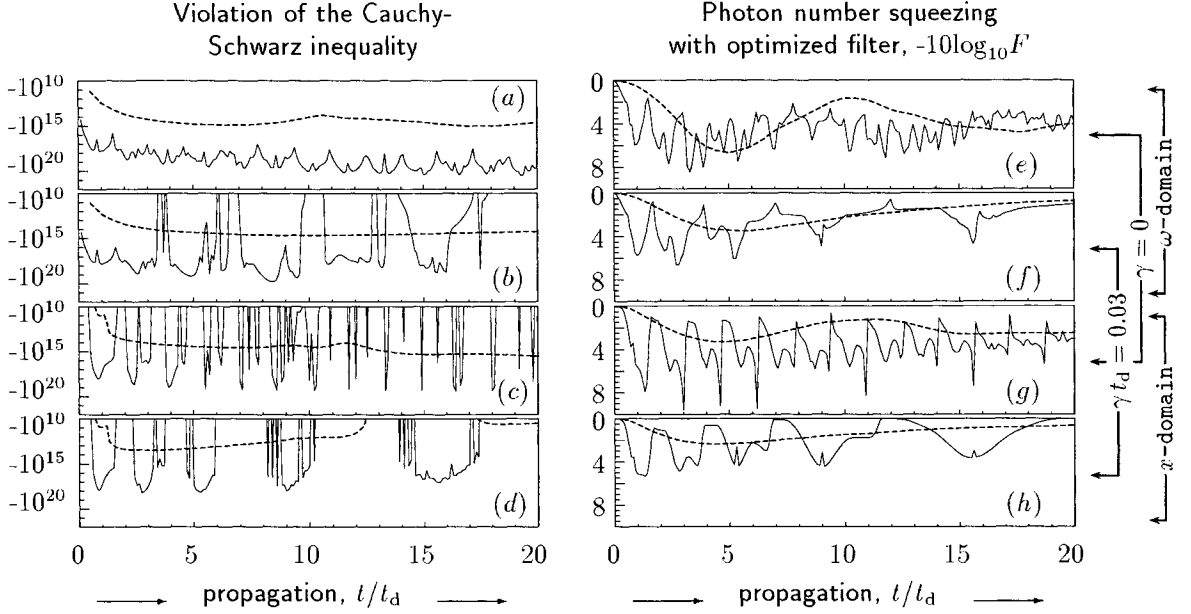


FIG. 2. The maximal violation of the Cauchy–Schwarz inequality for the photon number fluctuation [plots (a)–(d)] and the smallest Fano factor $F = \langle \Delta \hat{n}^2 \rangle / \langle \hat{n} \rangle$ (strongest photon number squeezing) achievable with optimized filters [plots (e)–(h)] are shown for the fundamental soliton, $N = 1$, (dotted line) and the soliton with $N = 2$ (full line) [x -domain: plots (a), (b), (e), (f), ω -domain: plots (c), (d), (g), (h); $\gamma = 0$: plots (a), (c), (e), (g), $\gamma t_d = 0.03$: plots (b), (d), (f), (h); other parameters as in Fig. 1].

$$\eta_{ij} = \frac{\langle : \Delta \hat{n}_i \Delta \hat{n}_j : \rangle}{\sqrt{\langle \Delta \hat{n}_i^2 \rangle \langle \Delta \hat{n}_j^2 \rangle}} = \frac{c_{ij}}{\sqrt{(c_{ii} + m_i)(c_{jj} + m_j)}} \quad (6)$$

($m_i = \langle \hat{n}_i \rangle$, $c_{ij} = \langle : \Delta \hat{n}_i \Delta \hat{n}_j : \rangle$, $\Delta \hat{n}_i = \hat{n}_i - m_i$), where $:$ introduces normal ordering. It can be shown that $\eta_{ii} \leq 1$, and $|\eta_{ij}| \leq 1$ for nonoverlapping intervals. A negative sign of the coefficient η_{ii} or a value smaller than unity of the Fano factor $F_i = \langle \Delta \hat{n}_i^2 \rangle / \langle \hat{n}_i \rangle = (1 - \eta_{ii})^{-1}$ indicates photon number squeezing of the filtered light.

From Fig. 1 it is seen that typical changes in the evolution of $\langle \hat{n}_i \rangle$ [Figs. 1(a), (c)] and those of η_{ii} [Figs. 1(b), (d)] and η_{ij} [Figs. 1(e₁)–(e₅), (f₁)–(f₅)] are closely related to each other. Near the points of soliton compression [maxima of $\langle \hat{n}_i \rangle$ in Fig. 1(a)] the formation of strong-correlation patterns is observed [Figs. 1(e₂)–(e₄), (f₂), (f₄)]. In contrast to the x -domain [Fig. 1(b)], sub-Poissonian statistics is observed in the ω -domain [Fig. 1(d)]. Moreover, the correlation in the ω -domain extends over a larger interval (relative to the corresponding initial pulse width) than the correlation in the x -domain. One possible explanation of such strong, almost perfect correlation ($|\eta_{ij}| \rightarrow 1$) can be seen in the instability of the classical N -soliton solution. From a linearization approach [8], the internal noise of a quantum soliton should be associated with interferences [9] between the soliton components and the continuum part of the solution to the classical nonlinear Schrödinger equation, as obtained by means of inverse scattering method (see, e.g., [10]). The qualitative changes observed for turning from the fundamental soliton to higher-order solitons ($N = 1 \rightarrow N = 2, 3, \dots$) are due to the presence of *more than one* soliton component. Discrepancies between the parameters

(amplitude, group velocity, etc.) of the soliton components of the N -soliton solution play the central role in establishing very strong internal correlations.

Nonclassical correlation can be detected, e.g., by testing the Cauchy-Schwarz inequality for the normally ordered photon number variances. When it is violated, i.e.,

$$c_{ii}c_{jj} - c_{ij}^2 < 0, \quad (7)$$

then the photon number noise in the intervals i and j is nonclassically correlated. Figures 2(a)–(d) reveal that the nonclassical correlation of the 2-soliton is substantially stronger than that of the fundamental soliton even for an absorbing fiber. Such an increase cannot be explained by a simple intensity scaling. The effect is obviously related to the mentioned instability of higher-order solitons. It is remarkable that there exist propagation distances for which the nonclassical correlation is stronger for an absorbing fiber than a nonabsorbing one.

The strongest photon number squeezing (smallest Fano factor) achievable with an optimized broadband filter is illustrated in Figs. 2(e)–(h). Compared with the fundamental soliton, only a small increase of the effect is observed for the 2-soliton in the ω -domain [Fig. 2(e), 6.6 \rightarrow 8.4dB]. On the contrary, a rather strong increase of the effect can be observed in the x -domain [Fig. 2(g), 3.3 \rightarrow 9.6dB], provided that losses can be disregarded. It is worth noting that the best photon number squeezing is achieved in the ω -domain for the fundamental soliton and in x -domain for the 2-soliton. The results show that the degree of squeezing sensitively depends on the domain considered. Hence, replacing the Fourier transformation in Eq. (4) [including Eq. (5)] with more general transformation that relates the fields in the two domains, may offer possibilities of further optimization. In particular, when we restrict our attention to linear transformations which can be realized experimentally by passive linear optical elements, then we are left with a two-dimensional integral kernel function to be optimized. In this way we may hope that also for other nonlinear quantum objects a considerable improvement of nonclassical features can be achieved.

Acknowledgment

This work was supported by the Deutsche Forschungsgemeinschaft.

-
- [1] A. Hasegawa, *Optical Solitons in Fibers* (Springer-Verlag, Berlin, 1989).
 - [2] S. A. Akhmanov, V. A. Vysloukh, and A. S. Chirkin, *Optics of Femtosecond Laser Pulses* (AIP, New York, 1992).
 - [3] J. S. Aitchison, Y. Silberberg, A. M. Weiner, D. E. Leaird, M. K. Oliver, J. L. Jackel, E. M. Vogel, and P. W. E. Smith, *J. Opt. Soc. Am. B* **8**, 1290 (1991).
 - [4] A. Mecozzi and P. Kumar, *Quantum Semiclass. Opt.* **10**, L21 (1998).
 - [5] E. Schmidt, L. Knöll, and D.-G. Welsch, *Phys. Rev. A* **59**, 2442 (1999).
 - [6] S. Spälter, N. Korolkova, F. König, A. Sizmann, and G. Leuchs, *Phys. Rev. Lett.* **81**, 786 (1998).
 - [7] D. Levandovsky, M. Vasilyev, and P. Kumar, *Opt. Lett.* **24**, 43 (1999).
 - [8] H. A. Haus and Y. Lai, *J. Opt. Soc. Am. B* **7**, 386 (1990).
 - [9] A. Mecozzi and P. Kumar, *Opt. Commun.* **22**, 1232 (1997).
 - [10] A. Hasegawa and Y. Kodama, *Solitons in Optical Communications* (Clarendon Press, Oxford, 1995).

Quantum noise versus classical noise: phase dependent spectra in a squeezed vacuum

Stuart Swain

*Department of Applied Mathematics and Theoretical Physics,
The Queen's University of Belfast, Belfast BT7 1NN, United Kingdom.*

Peng Zhou

*Department of Applied Mathematics and Theoretical Physics,
The Queen's University of Belfast, Belfast BT7 1NN, United Kingdom.*

We show that the resonance fluorescence spectra emitted from a two-level atom driven by a strong, coherent field and a weak, amplitude-fluctuating field are qualitatively similar to those produced by a driven two-level atom in a squeezed vacuum. This prompts a comparison of the behaviour of atoms interacting with classical and quantum noise sources.

In 1987, Carmichael et al. [1] showed that a monochromatically driven two-level atom interacting with a squeezed vacuum exhibits strongly phase-dependent features in resonance fluorescence. The relative heights and widths of the spectral triplet vary greatly with the phase of the squeezed vacuum relative to that of the driving field. In addition, some peaks may show subnatural linewidths. Although these effects were predicted over a decade ago, their experimental verification remains a major challenge in quantum optics. The principal difficulty is that the squeezed field modes must occupy the whole 4π solid angle of space.

The squeezed vacuum is a quantum field, and it is tempting to attribute the features described to the quantum nature of the squeezed vacuum. However, in this paper we describe an arrangement using only classical fields which leads to very similar spectra. The only real difference is that subnatural linewidths do not occur, at least in this parameter range, if the fields are all classical¹. Details may be found in the reference [2].

We consider a two-level atom driven by a strong, coherent laser, and in addition, by a weak, amplitude-fluctuating field of wide bandwidth which replaces the squeezed vacuum. The experiment should be feasible with current technology, and avoids the problem of the 4π angle of squeezing. We study the modification of the Mollow triplet as controlled by the phase difference between applied coherent and stochastic fields. The coherent field has a constant amplitude E_c , and the stochastic field a randomly fluctuating amplitude $E_s(t)$. The atom is also damped in the usual way by the electromagnetic vacuum. The frequencies of the atomic transition, of the coherent laser and of the stochastic field are assumed to be identical for simplicity.

¹Subnatural linewidths do occur with classical fields in other parameter ranges (W. S. Smyth and S. Swain, *J. Mod. Opt.* **46**, 1233 (1999)).

The master equation for the density operator ρ of the system is

$$\begin{aligned}\dot{\rho} = & -i[H_{a-c} + H_{a-s}, \rho] \\ & + \gamma(2\sigma_- \rho \sigma_+ - \sigma_+ \sigma_- \rho - \rho \sigma_+ \sigma_-),\end{aligned}\quad (1)$$

where

$$H_{a-c} = \frac{\Omega}{2}(\sigma_+ + \sigma_-), \quad (2)$$

$$H_{a-s} = \frac{x(t)}{2} [e^{i\phi} \sigma_+ + e^{-i\phi} \sigma_-]. \quad (3)$$

H_{a-c} and H_{a-s} describe the interaction of the atom with the coherent field and the stochastic field, respectively, γ is the atomic decay constant, ϕ is the relative phase of the two fields, $\Omega = 2|\mathbf{d} \cdot \mathbf{e}E_c|/\hbar$ is the Rabi frequency of the coherent field, and $x(t) = 2|\mathbf{d} \cdot \mathbf{e}E_s(t)|/\hbar$ represents the stochastic amplitude of the atom/stochastic-field interaction, which is assumed to be a real Gaussian-Markovian random process with zero mean value and correlation function,

$$\langle x(t)x(t') \rangle = D\kappa e^{-\kappa|t-t'|}, \quad (4)$$

where D is the strength of the stochastic process and κ can be associated with the bandwidth of the stochastic field. The correlation function (4) describes a field undergoing amplitude fluctuations, which result in a finite laser bandwidth κ .

For simplicity, we assume that the intensity of the coherent part is much greater than that of the stochastic field, and the bandwidth κ of the stochastic field is much greater than the atomic linewidth (in other words, the correlation time κ^{-1} of the stochastic field is very short compared to the radiative lifetime γ^{-1} of the atom). That is,

$$\Omega \gg \sqrt{D\kappa} \quad \text{and} \quad \kappa \gg \gamma. \quad (5)$$

One can then invoke standard perturbative techniques to eliminate the stochastic variable $x(t)$. The resultant master equation for the reduced density operator ρ in the particular case where $\phi = 0$ is

$$\begin{aligned}\dot{\rho} = & -i[H_{a-c}, \rho] \\ & + \gamma(N+1)(2\sigma_- \rho \sigma_+ - \sigma_+ \sigma_- \rho - \rho \sigma_+ \sigma_-) \\ & + \gamma N(2\sigma_+ \rho \sigma_- - \sigma_- \sigma_+ \rho - \rho \sigma_- \sigma_+) \\ & + 2\gamma M \sigma_+ \rho \sigma_+ + 2\gamma M \sigma_- \rho \sigma_-, \end{aligned}\quad (6)$$

where $M = N = D/4\gamma$.

The master equation (6) is the formally the same as that of a coherently driven two-level atom interacting with a squeezed vacuum. However, the ideal squeezed vacuum (ISV) satisfies $|M| = \sqrt{N(N+1)}$ whereas here we have $M = N$. This value of M corresponds to a reservoir in which there is the maximal *classical* correlation between pairs of photons. Such a reservoir is sometimes called a ‘‘classically squeezed field’’ (CSF).

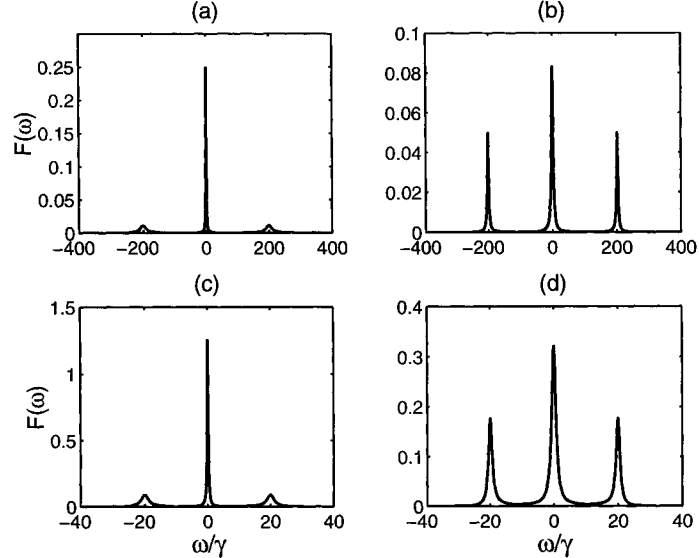


FIG. 1. Resonance fluorescence spectrum $F(\omega)$ for $\Omega = 200\gamma$, $\kappa = 100\gamma$, $D = 10\gamma$, with (a) $\phi = 0$ and (b) $\phi = \pi/2$. Frames (c) and (d) are for an ideal squeezed vacuum with $\Omega = 20\gamma$ and $N = 0.25$, $\Phi = \pi$ in (c) and $N = 0.05$, $\Phi = 0$ in (d).

For $\phi = \pi/2$, we again obtain an equation of the form (6), but now with $N = -M = D/4\gamma \times \kappa^2 / (\Omega^2 + \kappa^2)$. For $\phi \neq 0, \pi/2$ our stochastic system does not correspond exactly to that of a classically squeezed field.

In Figure 1 we present the resonance fluorescence spectra for the stochastic system with $\Omega = 200\gamma$, $\kappa = 100\gamma$ and $D = 10\gamma$ in frames (a) and (b) for $\phi = 0$ and $\pi/2$ respectively, where the strong phase dependence is evident. In frames (c) and (d) we give the spectra for the corresponding ideal squeezed vacuum, with $\Omega = 20$ and $N = 0.25$ in (c), and $N = 0.05$ in (d). (For the squeezed vacuum case we have divided the parameters by a factor of ten, in order to obtain experimentally reasonable values for N .) The comparison between the spectra for the stochastic system and the system with a squeezed vacuum is most striking.

It is the modification of the atomic decay rates by the weak, amplitude-fluctuating field that strongly affects the physical properties of the atom. For example, the two quadratures, $\sigma_x = \sigma_- + \sigma_+$ and $\sigma_y = i(\sigma_- - \sigma_+)$, of the atomic polarization decay at the different rates

$$\begin{aligned}\gamma_x &= \gamma + \frac{D\kappa^2}{\kappa^2 + \Omega^2} \sin^2 \phi, \\ \gamma_y &= \gamma + D \cos^2 \phi,\end{aligned}\tag{7}$$

whilst the population inversion σ_z decays at the rate $\gamma_z = \gamma_x + \gamma_y$. All these decay rates are dependent upon the relative phase and intensities of the driving fields. Clearly, when the coherent field is in-phase with the amplitude-diffusing one, *i.e.* when $\phi = 0$, the decay of the dipole quadrature σ_x is suppressed ($\gamma_x = \gamma$), while the other decay rate is enhanced ($\gamma_y = \gamma + D$). When both the fields are $\pi/2$ degrees out of phase, however, the situation is reversed. The suppression or enhancement of the polarization decays gives rise to rich spectral features.

FIG. 2. 3D fluorescence spectrum $F(\omega)$ against ω/γ and ϕ/π , for $\Omega = 200\gamma$, $\kappa = 100\gamma$, $D = 40\gamma$.

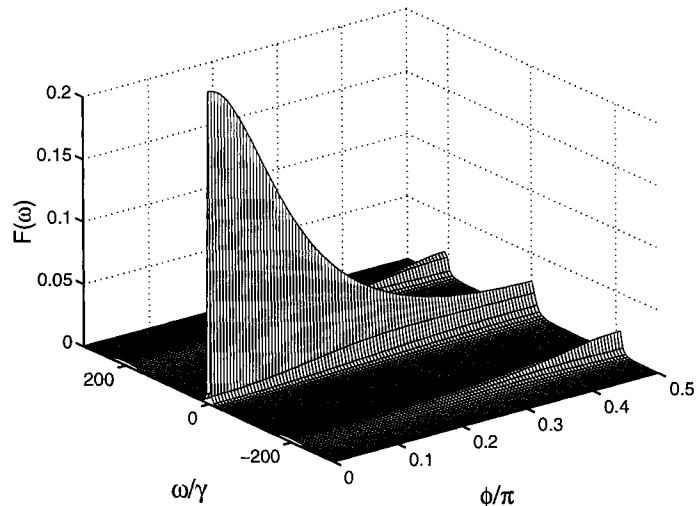


FIG. 3. 3D fluorescence spectrum $F(\omega)$ against ω/γ and ϕ/π , for $\Omega = 200\gamma$, $\kappa = 100\gamma$, $D = 40\gamma$.

In conclusion, we have reported a scheme to modify the Mollow fluorescence and absorption spectra by means of the relative phase of a coherent field and a stochastically amplitude-diffusing field interacting with a two-level atom. The phase-sensitive spectral features, which are qualitatively similar to those of a driven atom in a squeezed vacuum, are revealed. We have demonstrated that the atomic spectra produced by quantum and classical fields may be qualitatively very similar. Noting that relevant experiments of the phase-control of the two-photon excitation spectrum of atoms by a field with coherent and real Gaussian components [3], and of the transient dynamics of bichromatically driven two-level atoms [4] have already been demonstrated, the present model is experimentally accessible. Such experiments would demonstrate our ability to tailor reservoirs so as to modify atomic radiative properties in fundamental ways.

This work is supported by the United Kingdom EPSRC.

-
- [1] H. J. Carmichael *et al.*, Phys. Rev. Lett. **58**, 2539 (1987); S. Swain, *ibid.* **73**, 1493 (1994); S. Swain and P. Zhou, Phys. Rev. A **52**, 4845 (1995).
 - [2] Peng Zhou and S. Swain, Phys. Rev. Lett. **82**, 2500 (1999)
 - [3] C. Chen *et al.*, Phys. Rev. A **49**, 461 (1994).
 - [4] Q. Wu *et al.*, Phys. Rev. A **49**, R1519; **50**, 1474 (1994).

Spatial Structure of Quantum Noise in Spatial Solitons

N.Treps, C.Fabre

Laboratoire Kastler Brossel, Université Pierre et Marie Curie, Case 74, 75252 Paris Cedex 05, France

Abstract

We study the transverse distribution of the quantum noise inside a spatial soliton. The most interesting case is the $\chi^{(2)}$ medium, as two fields interact, the $\chi^{(3)}$ case is studied as a comparison. We demonstrate that the quantum information moves from the intensity squeezing to the correlation between quantum fluctuations in different regions of the transverse plane.

A lot of intensive studies has been done on the quantum aspects of the interaction between an electromagnetic field and a nonlinear media [1]. However, they have mainly been restricted to the study of quantum fluctuations integrated over all the transverse plane. It is interesting to go further and look at the spatial distribution of quantum noise in simple cases. Working here in simple propagation (without cavities), we study the propagation and the correlations of this noise in a situation where diffraction and nonlinearity play balanced roles : the case of spatial solitons either in $\chi^{(2)}$ or $\chi^{(3)}$ media.

In order to present the method, we will consider the $\chi^{(2)}$ media as an example. Let us first set up the notation and the geometry : z designates the propagation direction, r represents the one dimensional position in the transverse plane. \mathcal{E}_l is the envelope of the field, slowly varying along the propagation direction. We will call 1 the fundamental field at frequency ω and 2 the second harmonic at frequency 2ω . The propagation equations become :

$$\begin{aligned}i\frac{\partial\mathcal{E}_1}{\partial z} + \frac{1}{2k_1}\Delta_t\mathcal{E}_1 + \chi_1\mathcal{E}_1^*\mathcal{E}_2e^{-i\Delta k.z} &= 0 \\i\frac{\partial\mathcal{E}_2}{\partial z} + \frac{1}{2k_2}\Delta_t\mathcal{E}_2 + \chi_2\mathcal{E}_1^2e^{-i\Delta k.z} &= 0\end{aligned}$$

Where $\Delta k = 2k_1 - k_2$ is the phase mismatch, and χ_1 and χ_2 are proportional to the nonlinear coefficient for each field.

The spatial soliton is a state of the field whose envelope does not depend on time and position. It has been studied for a long time and recently observed experimentally [2]. For a certain value of the parameter, we can find an analytical solution for such a soliton. This solution is given here with non-dimensional variables [3], u being the fundamental and v the second harmonic in a rotating frame.

$$\bar{u}(r) = \frac{3\sqrt{2}}{2 \cosh^2 \frac{r}{2}} \quad \bar{v}(r) = \frac{3}{2 \cosh^2 \frac{r}{2}}$$

Assuming that the quantum fluctuations are small, we can linearise the classical equations around the classical solution in order to get the propagation equations of these fluctuations [4,5]. We define $u = \bar{u} + \delta u$ and $v = \bar{v} + \delta v$ and obtain the equations :

$$\begin{aligned} i \frac{\partial \delta u}{\partial \zeta} + \frac{\partial^2 \delta u}{\partial r^2} - \delta u + (\delta u)^* \bar{v} + \bar{u}^* \delta v &= 0 \\ 2i \frac{\partial \delta v}{\partial \zeta} + \frac{\partial^2 \delta v}{\partial r^2} - \delta v + \bar{u} \delta u &= 0 \end{aligned}$$

As these equations are linear, we can solve them in term of Green functions. For instance, we can write input/output relations like :

$$\delta u(\zeta^{out}, r) = \int G_u^u(r, r') \delta u(z^{in}, r') dr' + \int G_u^v(r, r') \delta v(z^{in}, r') dr'$$

The method consists in using stochastic variables for the fluctuations. At $z^{in} = 0$, the fluctuations of the input beam verify :

$$\langle \delta u(r) \delta u^*(r') \rangle = C_1 \delta(r - r') \quad \langle \delta v(r) \delta v^*(r') \rangle = C_2 \delta(r - r') \quad \langle \delta u(r) \delta v^*(r') \rangle = 0$$

So that, using the solution in terms of Green functions, we can derive the correlation functions at the output of the crystal. One has for instance:

$$\langle \delta u(z^{out}, r) \delta v^*(z^{out}, r') \rangle = \sum_{w=\delta u, \delta v} C_i \int G_u^w(r, r_1) G_v^w(r', r_1) dr_1$$

The spatial distribution of the fluctuations only depends on the Green functions which are evaluated numerically. In the $\chi^{(3)}$ case, the same method is implemented, with only one field.

Let us now give the main results obtained by our method. Fig.(1) gives the correlation function between the amplitude quadrature of the fundamental field and the phase quadrature of the second harmonic ($\chi^{(2)}$). The size and the position of the soliton is given above the figure. One notices that there exists non zero quantum correlations between the local fluctuations of these quadratures, especially between the centre of one field and the outer part of the other. These normalised correlations are rather small on the left side picture corresponding to very small pixel sizes. They increase appreciably if one takes much larger pixels of the order of a quarter of the soliton size. This gives an idea of the coherence area of quantum fluctuations in this problem.

Our approach allows us to determine the quantum noise in any partial measurement of the soliton intensity distribution. Let us consider for example the situation where one uses a diaphragm of radius r at the output of the crystal, centred on the soliton axis. Fig.(2a) gives the intensity noise in this measurement as a function of r : one notices that the strongest intensity squeezing effect is obtained when one measures only the centre part of the soliton. The dashed line gives as a comparison the intensity noise variation of a single mode field

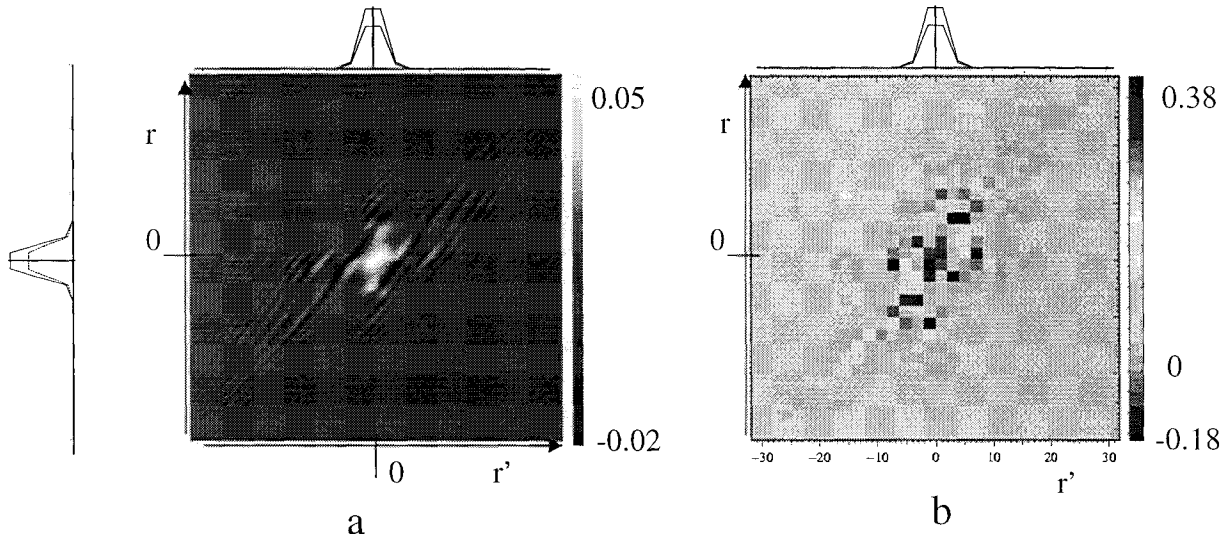


FIG. 1. Normalised quantum correlation between the local fluctuations of the fundamental amplitude quadrature and second harmonic phase quadrature. The size of the soliton mean intensity is given on the sides of the figures. Each dot represents the correlation between an area of the fundamental and an area of the second harmonic. The only difference between the two is the size of the pixel. In figure b we are only interested in the amplitude of the correlations

having the same transverse intensity distribution and same squeezing measured over the whole transverse plane.

The two lower traces of Fig.(2b) give values of conditional variances in the same configuration : they give a quantitative evaluation of the knowledge about the quantum fluctuations of the measured quantity drawn from the simultaneous knowledge of other fluctuations, because of the quantum correlations existing between the two. The very low value of this conditional variance that can be obtained for a diaphragm size equal to the soliton radius indicates that the effect of diffraction on the quantum fluctuations is to build strong quantum correlations between the different local field quadratures, much more than to locally reduce the fluctuations of some observable.

In the $\chi^{(3)}$ medium we have just to consider two quadratures of the same field. By a rotational operation, we can find the most squeezed one, its conjugate being the noisiest one. The correlation function of each of these quadrature does not depend on the parameter of the system and this is also the case when one consider one field in the $\chi^{(2)}$ case. This demonstrates that the picture we get using two fields is very peculiar and more interesting on the correlations point of view than with only one field (for instance, the symmetry breaking of Fig.1a cannot be seen with one field) [6].

Acknowledgements

This work has been supported by the European Union TMR network "QSTRUCT".

REFERENCES

- [1] Z.Y. Ou, Phys. Rev. A **49**, 4902 (1994).
- [2] Torruellas W.E., Wang Z., Hagan D.J., VanStryland E.W., Stegeman G.I., Torner L. and Menyuk C.R. (1995) Phys. Rev. Letters, **74**, 5036-39.
- [3] Yuri S. Kivshar, in Advanced Photonics with Second-order Optically Nonlinear Processes, Edited by A.D. Boardman, L.Pavlov and S.Tanev, NATO Science Series, 3. Vol.61, 1997.
- [4] S. Reynaud, A. Heidman, E. Giacobino, C. Fabre, Progress in Optics **30** (1992) 1.
- [5] C. Fabre, S. Reynaud (course 11), in *Fundamental systems in quantum optics*, J. Dalibard, J.-M. Raimond and J. Zinn-Justin, eds (Elsevier Science Publishers, Amsterdam, 1992).
- [6] N. Treps, C.Fabre, "Transverse distribution of quantum fluctuations and correlations in spatial solitons", preprint.

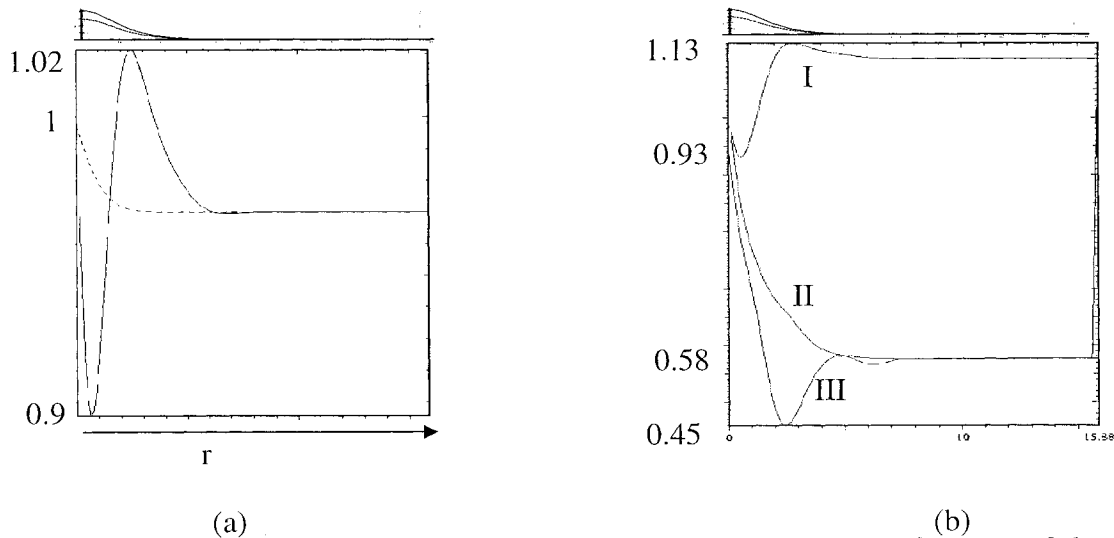


FIG. 2. Partial photodetection of the soliton intensity noise as a function of detector radius r . a) full line : actual measurement on the soliton; dashed line : measurement on a single mode field of same mean intensity and same total squeezing. b) I : same as a) for a longer propagation length. II : conditional variance of the second harmonic field intensity knowing the fundamental field intensity fluctuations in the same area. III : same as II, but with the knowledge added of the second harmonic field intensity fluctuations in the complementary region of the transverse plane.

Observing the nonclassicality of a quantum state

W. Vogel

*Arbeitsgruppe Quantenoptik, Fachbereich Physik, Universität Rostock, Universitätsplatz 3,
D-18051 Rostock, Germany*

Abstract

An observable criterion is proposed that allows one to distinguish nonclassical quantum states of the harmonic oscillator from those having classical counterparts. It is shown that a quantum state is nonclassical if measurable quadrature or phase-space distributions display structures that are narrower than the corresponding distributions in the oscillator ground-state.

I. INTRODUCTION

The study of nonclassical properties of quantum systems has been a subject of increasing interest. Pioneering experiments have demonstrated nonclassical effects of light, such as photon antibunching, sub-Poissonian statistics and squeezing¹. More recently, it became possible to prepare in various systems quantum superposition states of the Schrödinger-cat type². Until now, however, there exists no criterion for the nonclassicality of a quantum state that is of general validity and that can be observed.

II. MEASURABLE NONCLASSICAL EFFECTS

The nonclassical effects observed so far are typically based on one particular observable. For the example of quadrature squeezing, let consider the phase sensitive quadrature,

¹H.J. Kimble, M. Dagenais, and L. Mandel, *Phys. Rev. Lett.* **39**, 691 (1977); R. Short and L. Mandel, *Phys. Rev. Lett.* **51**, 384 (1983); R.E. Slusher, L.W. Hollberg, B. Yurke, J.C. Mertz, and J.F. Valley, *Phys. Rev. Lett.* **55**, 2409 (1985).

²M.W. Noel and C.R. Stroud Jr., *Phys. Rev. Lett.* **77**, 1913 (1996); C. Monroe, D.M. Meekhof, B.E. King, and D.J. Wineland, *Science* **272**, 1131 (1996); M. Brune, E. Hagley, J. Dreyer, X. Maitre, A. Maali, C. Wunderlich, J.M. Raimond, and S. Haroche, *Phys. Rev. Lett.* **77**, 4887 (1996).

$$\hat{x}(\varphi) = \hat{a}e^{i\varphi} + \hat{a}^\dagger e^{-i\varphi}, \quad (1)$$

for arbitrary but fixed phase $\varphi = \varphi'$. A quantum state is squeezed, if the variance of $\hat{x}(\varphi')$ is below that in the oscillator ground-state, $\langle [\Delta\hat{x}(\varphi')]^2 \rangle < \langle (\Delta\hat{x})^2 \rangle_{\text{gr}}$.

Why does this condition define a nonclassical property? This may be surprising since the variance of any classical variable may be vanishing. However, one may argue that the quantum noise in the ground-state is the minimal one desired to fulfill the Heisenberg uncertainty relation, for which there is no classical counterpart at all. Thus it is useful to seek for a correspondence to a classical state after “subtracting” the noise effects in the oscillator ground-state by considering normally-ordered expectation values, denoted by the “:” symbol. In this form the condition for squeezing reads

$$\langle : [\Delta\hat{x}(\varphi')]^2 : \rangle < 0. \quad (2)$$

In classical physics operator orderings are meaningless, thus one may establish the following correspondence between quantum and classical fluctuations:

$$\langle : [\Delta\hat{x}(\varphi')]^2 : \rangle \Leftrightarrow \langle [\Delta x(\varphi')]^2 \rangle_{\text{cl}}. \quad (3)$$

Since $\langle [\Delta x(\varphi')]^2 \rangle_{\text{cl}} \geq 0$, the property (2) is a signature of nonclassicality.

Note that the choice of a particular observable in such a criterion can only incompletely characterize a quantum system. The quadrature operator for the chosen phase φ' in general does not commute with the quadratures for other phases, $[\hat{x}(\varphi'), \hat{x}(\varphi'')] \neq 0$. Moreover, the restriction to second-order statistical moments is incomplete.

III. CRITERION BASED ON THE P FUNCTION

The most commonly accepted criterion for a nonclassical state is the one based on the P representation of the density operator,

$$\hat{\rho} = \int d^2\alpha P(\alpha) |\alpha\rangle\langle\alpha|. \quad (4)$$

Mean values of normally ordered operators can be written in close analogy to classical ones,

$$\langle : \hat{F}(\hat{a}^\dagger, \hat{a}) : \rangle = \int d^2\alpha P(\alpha) F(\alpha^*, \alpha). \quad (5)$$

An observable \hat{F} behaves like a classical one if two conditions are fulfilled. First, the ground-state noise is “subtracted” by normally ordering, $\hat{F} \rightarrow : \hat{F} :$. Second, the P function has the properties of a classical probability measure, $P(\alpha) \equiv P_{\text{cl}}(\alpha)$.

Thus we conclude that a state is nonclassical, if:

- (a) The ground-state noise is substantial for its characterization.
- (b) The P function fails to be interpreted as a classical probability measure, $P(\alpha) \neq P_{\text{cl}}(\alpha)$.

This criterion has been broadly accepted, see for example³. It ensures a complete characterization of the quantum states. However, the P function may become strongly singular and thus it can hardly be measured. What one needs is a general, measurable criterion.

IV. CRITERION BASED ON QUADRATURE DISTRIBUTIONS

Let consider the quadrature operator $\hat{x}(\varphi)$ defined in Eq. (1), including its dependence on the phase parameter φ . For formulating a criterion on nonclassicality the use of this quantity has several advantages. First, the statistics of this observable is measurable. Second, knowing the probability distribution $p(x, \varphi)$ for a φ interval of size π implies the complete information on the quantum state of the oscillator⁴. Third, the observable $\hat{x}(\varphi)$ is closely related to the classical trajectory of the oscillator, which plays a key role in the classical theory.

The quadrature distribution $p(x, \varphi)$ can be derived from its characteristic function $G(k, \varphi)$ via

$$p(x, \varphi) = \frac{1}{2\pi} \int dk e^{-ikx} G(k, \varphi), \quad G(k, \varphi) = \langle e^{ik\hat{x}(\varphi)} \rangle. \quad (6)$$

We may subtract the ground-state noise to obtain a noise-subtracted distribution $\tilde{p}(x, \varphi)$, by replacing $G(k, \varphi)$ with its normally ordered version, $\tilde{G}(k, \varphi) = \langle : e^{ik\hat{x}(\varphi)} : \rangle$. Using the Baker-Campbell-Hausdorff formula for relating both characteristic functions to each other, the measured distribution is obtained as the convolution,

$$p(x, \varphi) = \int dx' \tilde{p}(x', \varphi) p_{\text{gr}}(x - x'), \quad (7)$$

of the noise subtracted distribution with the (phase-insensitive) distribution of the ground state, $p_{\text{gr}}(x) = (2\pi)^{-1/2} e^{-x^2/2}$.

The noise-subtracted distribution can be related to the P function by evaluating the characteristic function $\tilde{G}(k, \varphi)$ by applying Eq. (5). After some algebra this yields

$$\tilde{p}(x, \varphi) = \int d^2\alpha P(\alpha) \delta[x - x_\alpha(\varphi)], \quad (8)$$

the function $x_\alpha(\varphi) = \alpha e^{i\varphi} + \alpha^* e^{-i\varphi}$ corresponds to the classical trajectory. Equation (8) yields the noise subtracted quadrature distribution in terms of a classical stochastic process,

$$\tilde{p}(x, \varphi) \equiv p_{\text{cl}}(x, \varphi), \quad (9)$$

³U.M. Titulaer and R.J. Glauber, Phys. Rev. **140**, B 676 (1965); L. Mandel, Phys. Scr. T **12**, 34 (1986).

⁴For a review on measurements and reconstruction of quantum states, see D.-G. Welsch, W. Vogel, and T. Opatrny, *Homodyne Detection and Quantum State Reconstruction*, in: *Progress in Optics*, Vol. 39, ed. by E. Wolf.

provided that the P function has the properties of a classical probability, $P(\alpha) \equiv P_{\text{cl}}(\alpha)$. There is a one-to-one correspondence between the classical behaviors of the P function and of the noise-subtracted quadrature statistics.

The classical low-noise limits of these distributions consists in a deterministic behavior, $P(\alpha) = \delta(\alpha - \beta)$ and $\tilde{p}(x, \varphi) = \delta[x - x_\beta(\varphi)]$. From Eq. (7), the low-noise limit of the measured distribution is given by

$$p(x, \varphi) = p_{\text{gr}}[x - x_\beta(\varphi)]. \quad (10)$$

Consequently, if the P function behaves like a classical probability, the measured quadrature statistics cannot exhibit structures that are narrower than the quadrature distribution of the ground state.

We may formulate a new criterion for nonclassicality that replaces the criterion (b) with:

- (b*) There exist structures in $p(x, \varphi)$ that are narrower than $p_{\text{gr}}(x)$. Or equivalently, the characteristic function $G(k, \varphi)$ decays more slowly than $G_{\text{gr}}(k) = e^{-k^2/2}$.

This criterion is fulfilled for typical nonclassical states such as Fock states, squeezed states, Schrödinger-cat states, and others.

V. CRITERION BASED ON QUASIDISTRIBUTIONS

A measurable criterion for nonclassicality can also be based on the s -parameterized quasidistributions $P(\alpha, s)$. The latter can be given as the convolution of the P function with the s -parameterized distribution $P_{\text{gr}}(\alpha; s)$ in the ground state⁵,

$$P(\alpha; s) = \int d^2\beta P(\beta)P_{\text{gr}}(\alpha - \beta; s). \quad (11)$$

Based on this relation and on similar arguments as in the preceding section, the criterion (b*) for a nonclassical state can be reformulated as follows: There exist structures in the phase-space distribution $P(\alpha; s)$ that are narrower than the ground-state distribution $P_{\text{gr}}(\alpha; s)$. Equivalently, the decay of the related characteristic function may survive the decay of the characteristic function of $P_{\text{gr}}(\alpha; s)$.

VI. SUMMARY AND CONCLUSIONS

A new criterion has been proposed for the nonclassicality of quantum states of the harmonic oscillator. It is based on measurable distributions such as quadrature or phase-space distributions. A quantum state has no classical counterpart when these functions show structures that are narrower than the corresponding distributions of the ground state of the oscillator. This criterion is closely related to the commonly used one that is based on the P function. An extension to include effects of nonideal detection is straightforward.

⁵K.E. Cahill and R. Glauber, Phys. Rev. **177**, 1882 (1969); for measurement principles see footnote 4.

Automatic feedback as a tool to preserve Schrödinger-cat states

M. Fortunato, P. Tombesi, D. Vitali

*Dipartimento di Matematica e Fisica, Università di Camerino, via Madonna delle Carceri
I-62032 Camerino
and INFN, Unità di Camerino, Italy*

J. M. Raimond

*Laboratoire Kastler Brossel, Département de Physique de l'École Normale Supérieure,
24 rue Lhomond, F-75231 Paris Cedex 05, France*

Abstract

We briefly sketch a scheme for contrasting the decoherence of a Schrödinger-cat state in a high-Q microwave cavity. It is based on the injection of appropriately prepared “probe” and “feedback” atoms, whereby the information transmission from the probe to the feedback atom is mediated by a second auxiliary cavity. The decoherence time of the superposition state can be significantly increased using presently available technology.

Schrödinger-cat states [1] lie both at the heart and at the foundations of quantum mechanics, as their understanding would give us a deeper insight in the most important issue of how the classical macroscopic world emerges from the quantum substrate [2,3]. These rather paradoxical states are very difficult to observe, and the currently (almost generally) accepted explanation of this fact is provided by *decoherence*, i.e., the rapid transformation of these linear superpositions into the corresponding classical statistical mixture, caused by the unavoidable entanglement of the system with uncontrolled degrees of freedom of the environment [2]. The decoherence time depends on the form of system-environment interaction [4] but, in most cases, it is inversely proportional to the squared “distance” between the two states forming the superposition [5]. For macroscopically distinguishable states, the decoherence process becomes thus practically instantaneous [2]. Decoherence is therefore experimentally accessible only in the *mesoscopic* domain. In this case, one is able to monitor the progressive emergence of classical properties from the quantum ones. Schrödinger-cat states of the vibrational motion of a trapped ion and of the electromagnetic field in a cavity have been experimentally obtained recently by Monroe *et al.* [6] and by Brune *et al.* [7], respectively.

In some recent publications [8,9] it has been shown that a possible way to control decoherence in optical cavities is given by appropriately designed feedback schemes. In [9] the photodetection-mediated scheme has been adapted to the microwave experiment of Ref. [7]

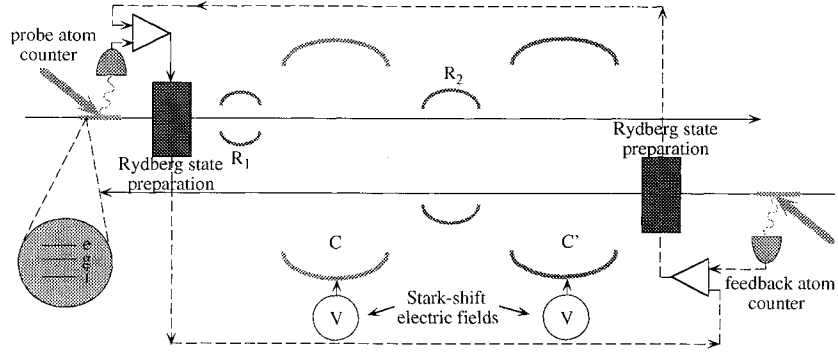


FIG. 1. Schematic diagram of the autofeedback scheme proposed in this paper. R_1 and R_2 are the two cavities in which classical microwave pulses can be applied, C is the microwave cavity of interest and C' is the cavity automatically performing the needed correction. Electric fields can be applied at the superconducting mirrors of C and C' to Stark shift the Rydberg levels in order to tune the interaction times in C' and realize adiabatic transfer in C .

in which photodetectors cannot be used, and the cavity state can only be indirectly inferred from measurements performed on probe atoms which have interacted with the cavity mode. Under ideal conditions, this adaptation to the microwave cavity case leads to a significant increase of the lifetime of the Schrödinger cat generated in [7]. It suffers however from two important limitations, making it very inefficient when applied under the actual experimental situation. It first requires the preparation of samples containing *exactly* one Rydberg atom sent through the apparatus. Up to now, the experimental techniques allow only to prepare a sample containing a random atom number, with a Poisson statistics. Two-atom events are excluded only at the expense of a low average atom number, lengthening the feedback loop cycletime [10]. The original scheme requires also a near unity atomic detection efficiency, which is extremely difficult to achieve even with the foreseeable improvements of the experimental apparatus.

Here we present a significant improvement of the microwave feedback scheme described in [9]. This new version, using a direct transmission of the quantum information from the probe to the feedback atom, does not require a large detection efficiency, removing one of the main difficulties of the previous design. It also circumvents the problem of one-atom packets, implementing an atom counter.

The original “stroboscopic” feedback scheme for microwave cavities proposed in [9] is based on a very simple idea: whenever the cavity loses a photon, a feedback loop supplies the cavity mode with another photon, through the injection of an appropriately prepared atom. However, since there are no good enough photodetectors for microwaves, one has to find an indirect way to check if the high-Q microwave cavity has lost a photon or not. In the experiment of Brune *et al.* [7], information on the cavity field state is obtained by detecting the state of a circular Rydberg atom which has dispersively interacted with

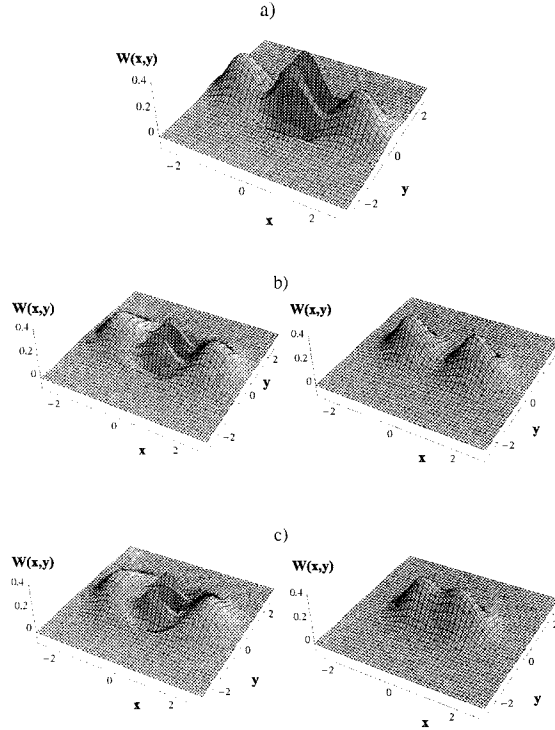


FIG. 2. Wigner function of the initial odd cat state, $|\psi\rangle = N_{-}(|\alpha\rangle - |-\alpha\rangle)$, with $|\alpha|^2 = 3.3$ (a, top). Wigner function of the same cat state after 13 feedback cycles (b), corresponding to a mean elapsed time $\bar{t} \simeq 1/\gamma \simeq 6.6t_{\text{dec}}$, and after 25 feedback cycles (c) corresponding to a mean elapsed time $\bar{t} \simeq 2/\gamma \simeq 13t_{\text{dec}}$ (left). Wigner function of the same cat state after one relaxation time $t = 1/\gamma$ (b), and after two relaxation times $t = 2/\gamma$ (c), in absence of feedback (right).

the superconducting microwave cavity. This provides an “instantaneous” measurement of the cavity field and suggests that continuous photodetection can be replaced by a series of *repeated* measurements, performed by non-resonant atoms regularly crossing the high-Q cavity.

The limitations due to the non-unit efficiency of the atomic detectors could be avoided if we eliminate the measurement step in the feedback loop and replace it with an “automatized” mechanism preparing the correct feedback atom whenever needed. This mechanism can be provided by an appropriate conditional quantum dynamics. This conditional dynamics can be provided by a second high-Q microwave cavity C' , similar to C , replacing the atomic detectors, crossed by the probe atom first and by the feedback atom soon later, as described in Fig. 1.

Instead of preparing a random atom number at a given time, one thus prepares with a high probability a single Rydberg atom after a random delay. However, after a full quantum mechanical calculation and lengthy algebra, it is possible to determine the map of a generic feedback cycle, that is, the transformation connecting the states of the cavity field in C soon after the passage of two successive feedback atoms in C , which also takes into account

the non-unit efficiency of the Rydberg state preparation. This map, which is reported elsewhere [11], allows us to study the dynamics of the Schrödinger-cat state in the presence of feedback, and to compare it with the corresponding dynamics in absence of feedback.

In Fig. 2 we show the Wigner function of the initial odd cat state (top) and its dynamics in presence (left) and in absence (right) of feedback. The comparison between the two performances is striking: in absence of feedback the Wigner function becomes quickly positive definite, while in the presence of feedback the quantum aspects of the state remain well visible for many decoherence times.

REFERENCES

- [1] E. Schrödinger, *Naturwiss.* **23**, 807 (1935). B. Yurke and D. Stoler, *Phys. Rev. Lett.* **57**, 13 (1986). W. Schleich, M. Pernigo, and Fam Le Kien, *Phys. Rev. A* **44**, 2172 (1991).
- [2] W.H. Zurek, *Phys. Today* **44**(10), 36 (1991), and references therein.
- [3] D. Giulini, E. Joos, C. Kiefer, J. Kupsch, I.O. Stamatescu, and M.D. Zeh, *Decoherence and the appearance of classical world in quantum theory*, (Springer, Berlin 1996).
- [4] J. Anglin, J.P. Paz, and W.H. Zurek, *Phys. Rev. A* **55**, 4041 (1997).
- [5] A.O. Caldeira and A.J. Leggett, *Phys. Rev. A* **31**, 1059 (1985); D.F. Walls and G.J. Milburn, *ibid* **31**, 2403 (1985).
- [6] C. Monroe, D.M. Meekhof, B.E. King, and D.J. Wineland, *Science* **272**, 1131 (1996).
- [7] M. Brune, E. Hagley, J. Dreyer, X. Maitre, A. Maali, C. Wunderlich, J.M. Raimond, and S. Haroche, *Phys. Rev. Lett.* **77**, 4887 (1996).
- [8] P. Tombesi and D. Vitali, *Phys. Rev. A* **51**, 4913 (1995); P. Goetsch, P. Tombesi and D. Vitali, *Phys. Rev. A* **54**, 4519 (1996).
- [9] D. Vitali, P. Tombesi, and G.J. Milburn, *Phys. Rev. Lett.* **79** 2442 (1997). D. Vitali, P. Tombesi, and G.J. Milburn, *J. Mod. Opt.* **44** 2033 (1997). D. Vitali, P. Tombesi, and G.J. Milburn, *Phys. Rev. A* **57** 4930 (1998).
- [10] E. Hagley *et al.*, *Phys. Rev. Lett.* **79**, 1 (1997).
- [11] M. Fortunato, D. Vitali, P. Tombesi, and J.M. Raimond, *Phys. Rev. A* (August 1999).

Testing Quantum Mechanics by means of entangled photon pairs

M.Genovese

*Istituto Elettrotecnico Nazionale Galileo Ferraris, Str. delle Cacce 91, I-10135 Torino,
genovese@ien.it*

G.Brida, C.Novero

Istituto Elettrotecnico Nazionale Galileo Ferraris, Str. delle Cacce 91, I-10135 Torino

E. Predazzi

Dip. Fisica Teorica Univ. Torino e INFN, via P. Giuria 1, I-10125 Torino

Abstract

We study the realisation of a new test of Bell inequalities using the superposition of type I parametric down conversion produced in two different non-linear crystals pumped by the same laser, but with different polarisations.

We discuss the feasibility and the advantages of this configuration.

A new procedure for the alignment, which constitutes the major improvement permitting the realisation of this scheme, is suggested.

The technique of parametric down-conversion (PDC) has been employed, since its discovery, for generations of "entangled" photon pairs, i.e. pairs of photons described by a common wave function which by no means can be factored up into the product of two distinct wave functions pertaining to separated photons. It is due essentially to L. Mandel and collaborators [1] the idea of using such a state of the electromagnetic field to perform tests of quantum mechanics, more specifically to test Bell's inequalities which discriminate between standard quantum mechanics and local realistic theories.

The generation of entangled states by parametric down conversion is alternative to other techniques, such as the radiative decay of atomic excited states, as it was in the celebrated experiment of A. Aspect et al. [2], and overcomes some former limitations in the propagation direction of the conjugated photons. In fact the poor angular correlation of atomic cascade photons is the origin of a small total efficiency of this set up, leading to a selection of the small subsample of the produced photons; this is responsible of the efficiency loophole [3] which does not permit a definitive test of the non locality in quantum mechanics in such experiments. On the other hand a very good angular correlation (better than 1 mrad) of the two photons of the pair is obtained in the PDC process, permitting, in principle, to overcome the previous problem.

The entanglement on phase and momentum, which is directly produced in Type I parametric down conversion can be used for a test of Bell inequalities using two interferometers spatially separated [4], as realized by [5]. The use of beam splitters however strongly reduces the total quantum efficiency.

In alternative, one can generate a polarisation entangled state [6]. It appears, however, that the creation of couples of photons entangled from the point of view of polarisation, which is by far the most diffuse case due to the easy experimental implementation, still suffers severe limitations, as it was pointed out recently in the literature. The essence of the problem is that in generating this state, half of the initial photon flux is lost (in most of the used configurations), and one is, of-necessity, led to assume that the photon's population actually involved in the experiment is a faithful sample of the original one, without eliminating the efficiency loophole.

A scheme which allows no postselection of the photons [7] has been realised recently, using Type II PDC, where a polarisation entangled state is directly generated. This scheme has effectively permitted, paying the price of delicate compensations for having identical arrival time of the ordinary and extraordinary photon, a much higher total efficiency than the previous ones. It is, however, still far from the value 0.67 [8], which is required for an efficiency-loophole free experiment for non maximally entangled pairs (for maximally entangled pairs this limit rises to 0.81).

Some recent experiments using entanglement among three photons [9] are also far by solving these problems [10]. A large interest remains therefore for new experiments increasing total quantum efficiency in order to reduce and finally overcome the efficiency loophole.

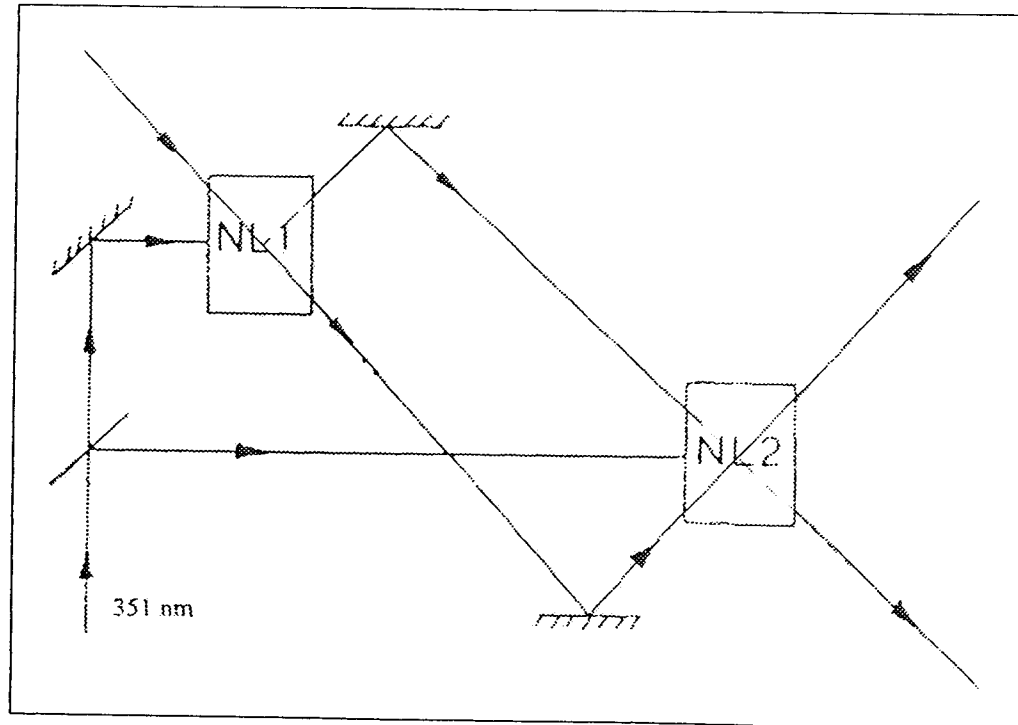


Figure 1. The amplification scheme for aligning PDC produced in the two non-linear crystals.

Our proposal follows and develops an idea of Hardy [11] and contemplates the creation of a polarisation entangled state of the form

$$|\psi\rangle = \frac{|H\rangle|V\rangle + |V\rangle|H\rangle}{\sqrt{2}} \quad (1)$$

(where H and V indicate horizontal and vertical polarisations respectively) via the superposition of the spontaneous fluorescence emitted by two non-linear crystals driven by the same pumping laser (at 351 nm). The crystals will be put in cascade along the propagation direction of the pumping laser and the superposition will be obtained by using an appropriate optics.

The alignment (which is of fundamental importance for having a high visibility and in principle constitutes the main problem of such a configuration) can be profitably improved using of an optical amplifier scheme, where a solid state laser is injected in the crystals together with the pumping laser (see fig.1): such a technique has already proved its validity and it is of strong help in the recognition of the directions of propagation of correlated photon wavelengths and applied to metrological studies in our laboratory [12].

A very preliminary study of the problem and computer simulations of the optical group to be used in the experiment proves the feasibility of the set-up. In particular, the main difficulty concerning the alignment derives from the fact that the PDC produced in the first crystal enters the second crystal as extraordinary rays. This leads to a non perfect superposition with the PDC produced in the second crystals.

We have studied the compensation of the different paths by a computer simulation for the degenerate PDC at 702 nm. This simulation has shown that for a crystal of 1 cm length with two conjugated rays with angles of 6.8 and -6.8 degrees with respect to the normal and contained with the pump (propagating along the z axis) in a plane (xy) forming an angle of 53 degrees with the optical axis, the deviation with respect to the rays produced inside this crystal is of 0.07 cm on the y axis (larger than the ordinary ones) and 0.76 cm on the x axis (both acquiring a positive x component). The symmetry of the effect (due to the choice of the pair inside a plane orthogonal to the one containing the pump and the optical axis) permits an easier compensation.

This compensation does not require further optical elements (aside from those necessary to focus the PDC of the first crystal on the second one) as it is the case for experiments using type II PDC.

A first practical attempt to superimpose the PDC produced in the two crystals has been successful, showing the feasibility of the scheme, which will be realised soon.

The proposed scheme will lead to a further step toward a conclusive experimental test of non-locality in quantum mechanics. The analysis of the experiments realised up to now [3] shows in fact that visibility of the wanted effect (essentially visibility of interference fringes) and overall quantum efficiency of detection are the main parameters in such experiments. One first advantage of the proposed configuration with respect to most of the previous experimental set-ups is that all the entangled pairs are selected (and not only 50% as with beams splitters); furthermore, we hope to be able to obtain rather high efficiencies thanks to developments in photo-detectors. Finally, the elimination of the space-like separation loophole could be obtained in a second time using rapid switch optical devices.

Altogether our aim is to obtain an experiment with high efficiency as well as high visibility.

Acknowledgements

We would like to acknowledge support of ASI under contract LONO 500172.

References

1. see L. Mandel, and E. Wolf, *Optical Coherence and Quantum Optics*, Cambridge University Press, 1995 and references therein.
2. A. Aspect et al., *Phys. Rev. Lett.* 49 , 1804, (1982).
3. E. Santos, *Phys. Lett. A* 212, 10 (1996); L. De Caro and A. Garuccio *Phys. Rev. A* 54, 174 (1996) and references therein.
4. J. P. Franson, *Phys. Rev. Lett.* 62, 2205 (1989).
5. J. G. Rarity, and P. R. Tapster, *Phys. Rev. Lett.* 64, 2495 (1990); J. Brendel et al. *Eur.Phys.Lett.* 20, 275 (1992); P. G. Kwiat et al, *Phys. Rev. A* 41, 2910 (1990); W. Tittel et al, quant-ph 9806043
6. Z.J. Ou and L. Mandel, *Phys. Rev. Lett.* 61, 50, (1988); Y.H.Shih et al., *Phys. Rev. A*, 1288, (1993).
7. T.E. Kiess et al., *Phys. Rev. Lett.* 71, 3893, (1993); P.G. Kwiat et al., *Phys. Rev. Lett.* 75, 4337, (1995).
8. P. H. Eberhard, *Phys. Rev. A* 47, R747 (1993).
9. J.R.Torgerson et al., *Phys. Lett. A* 204, 323 (1995); G.Di Giuseppe, F.De Martini and D.Boschi, *Physical Review A* 56, 176 (1997); D.Boschi, S.Branca, F.De Martini and L.Hardy, *Phys. Rev. Lett.* 79, 2755 (1998).
10. A. Garuccio, *Phys. Rev. A* 52, 2535 (1995).
11. L. Hardy, *Phys. Lett. A* 161, 326 (1992).
12. G. Brida, S. Castelletto, C. Novero and M. L. Rastello, *Metrologia* 35 247 (1998).

p -adic probability point of view to Bell's inequality

Andrei Khrennikov

*Department of Mathematics, Statistics and Computer Sciences
University of Växö, S-35195, Sweden*

Abstract

We demonstrate that Bell's inequality has nothing to do with such things as nonlocality or death of reality. Arguments based on Bell's inequality could not be used to choose 'right interpretation' of quantum mechanics (statistical or orthodox Copenhagen). In fact, Bell's mystification has purely probabilistic roots: identification of probability distributions for hidden variables with respect to different statistical ensembles. In principle, these distributions need not be reproduced in quantum measurements. So called p -adic probability theory gives a large class of such probabilistic distributions fluctuating from ensemble to ensemble.

Experimental violations of Bell's inequality [1] are typically interpreted in one of two ways: (1) **nonlocality**: by changing the state of one particle in the EPR pair we change the state of the other particle; (2) **death of reality**: realism could not be used as the philosophic base of quantum mechanics ('properties' of quantum systems are not objective properties, i.e., the properties of an object). In particular, (2) implies that the statistical interpretation of quantum mechanics (via L. Ballentine) must be denied in favour of the orthodox Copenhagen interpretation. The aim of this note is to demonstrate that Bell's inequality implies neither nonlocality nor death of reality. This is just a mistake in quite trivial chain of probabilistic considerations.

We reproduce now the proof of Bell's inequality. Let $\mathcal{P} = (\Omega, \mathcal{F}, \mathbf{P})$ be a Kolmogorov probability space: Ω is a space of elementary events, \mathcal{F} is an algebra of events, \mathbf{P} probability measure.

Theorem 1. *Let $A, B, C = \pm 1$ be random variables on \mathcal{P} . Then Bell's inequality*

$$| \langle A, B \rangle - \langle C, B \rangle | \leq 1 - \langle A, C \rangle \quad (1)$$

holds true.

Proof. Set $\Delta = \langle A, B \rangle - \langle C, B \rangle$. By linearity of Lebesgue integral we obtain

$$\Delta = \int_{\Omega} A(\omega)B(\omega)d\mathbf{P}(\omega) - \int_{\Omega} C(\omega)B(\omega)d\mathbf{P}(\omega) = \int_{\Omega} [A(\omega) - C(\omega)]B(\omega)d\mathbf{P}(\omega). \quad (2)$$

As $A(\omega)^2 = 1$,

$$|\Delta| = \left| \int_{\Omega} [1 - A(\omega)C(\omega)]A(\omega)B(\omega)d\mathbf{P}(\omega) \right| \leq \int_{\Omega} [1 - A(\omega)C(\omega)]d\mathbf{P}(\omega). \quad (3)$$

Of course, this is the rigorous mathematical proof of (1) for Kolmogorov probabilities. However, abstractness of Kolmogorov's probability model could induce serious problems, if we do not control carefully dependence of probabilities on corresponding statistical ensembles of physical systems. Bell's did not control this dependence. In fact, the symbol \mathbf{P} used in the proof must be regarded to different statistical ensembles.

To simplify our considerations, we suppose that the set of hidden variables is finite: $\Lambda = \{\lambda_1, \dots, \lambda_M\}$. For each physical observable U , the value λ of hidden variables determines the value $U = U(\lambda)$. Let U and V be physical observables, $U, V = \pm 1$. We start with the consideration of the frequency (experimental) covariation $\langle U, V \rangle_{x_{UV}}$ with respect to a collective ('random sequence') $x_{UV} = (x_1, x_2, \dots, x_N, \dots)$, where $x_i = (u_i, v_i)$, which is induced by measurements of the pair (U, V) . The x_{UV} is obtained by measurements for an ensemble S_{UV} of physical systems (for example, pairs of correlated quantum particles). Our aim is to represent experimental covariation $\langle U, V \rangle_{x_{UV}}$ as ensemble covariation $\langle U, V \rangle_{S_{UV}}$. Then we shall demonstrate that in the general case it is impossible to perform for ensemble covariations Bell's calculations which have been performed for Kolmogorov covariations. Let $S_{UV} = \{d_1, \dots, d_N\}$, where i th measurement is performed for the system d_i . Define a function $i \rightarrow \lambda(i)$, the value of hidden variables for d_i . We set $n_k(S_{UV}) = |\{d_i \in S_{UV} : \lambda(i) = \lambda_k\}|$ and $\mathbf{p}_k^{UV} = \mathbf{P}_{S_{UV}}(\lambda = \lambda_k) = \frac{n_k(S_{UV})}{N}$. These are probabilities of hidden variables $\lambda_k, k = 1, 2, \dots, M$, in the statistical ensemble S_{UV} . We have $\langle U, V \rangle_{x_{UV}} = \frac{1}{N} \sum_{i=1}^N U(\lambda(i))V(\lambda(i)) = \sum_{k=1}^M \mathbf{p}_k^{UV} u_k v_k = \langle U, V \rangle_{S_{UV}}$, where $u_k = U(\lambda_k), v_k = V(\lambda_k)$. Thus

$$\begin{aligned} \Delta &= \langle A, B \rangle_{x_{AB}} - \langle C, B \rangle_{x_{CB}} \\ &= \langle A, B \rangle_{S_{AB}} - \langle C, B \rangle_{S_{CB}} = \sum_k (\mathbf{p}_k^{AB} a_k - \mathbf{p}_k^{CB} c_k) b_k \end{aligned}$$

and

$$\langle A, C \rangle_{x_{AC}} = \langle A, C \rangle_{S_{AC}} = \sum_k \mathbf{p}_k^{AC} a_k c_k.$$

We suppose now that *probabilities of λ_k do not depend on statistical ensembles*:

$$\mathbf{p}_k = \mathbf{p}_k^{AB} = \mathbf{p}_k^{CB} = \mathbf{p}_k^{AC} \quad (4)$$

(later we shall modify this condition to obtain statistical coincidence of probabilities, instead of the precise coincidence). Hence $\Delta = \sum_{k=1}^M \mathbf{p}_k (a_k - c_k) b_k$ and $\langle A, C \rangle_{x_{AC}} = \sum_{k=1}^M \mathbf{p}_k a_k c_k$. We can now apply Theorem 1 for the discrete probability distribution $\{\mathbf{p}_k\}_{k=1}^M$ and obtain Bell's inequality.

However, if condition (4) does not hold true, then equality (2) and, as a consequence, Bell's inequality can be violated. The violation of condition (4) is the exhibition of unstable (with respect to the real metric) statistical structure on the level of hidden variables of (at least some) quantum ensembles. In particular, the principle of the statistical stabilization ('the law of the large numbers') can be violated for hidden variables: $\lim_{N \rightarrow \infty} \nu_N(\lambda_i)$ do not exist. Thus we could not introduce the probability distribution on the set of hidden labels Λ .

All our considerations were based on the statistical stabilization with respect to the real metric. In [2] we considered the statistical stabilization with respect to a p -adic metric.

The field of p -adic numbers \mathbf{Q}_p , where $p > 1$ is a prime number, can be constructed (as the field of real numbers \mathbf{R}) as a completion of the field of rational numbers \mathbf{Q} . The p -adic metric differs strongly from the real one. As for finite ensembles S , ensemble probabilities $\mathbf{P}_S(a) = \frac{n(a)}{N}$ are rational numbers, we can study their behaviour not only with respect to the real metric on \mathbf{Q} , but also with respect to the p -adic metric. p -adic probability theory gives numerous examples of ensemble probabilities fluctuating in the real metric and stabilizing in the p -adic metric. However, the p -adic stabilization of probabilities does not imply the possibility to repeat Bell's proof for p -adic probabilities: these probabilities may be negative rational numbers, see [2].

We introduce now a statistical analogue of the precise coincidence of ensemble probabilities for hidden variables. Let $\mathcal{E}_1, \mathcal{E}_2$ be two ensembles of physical systems and let π be a property of elements of these ensembles. The π has values $(\alpha_1, \dots, \alpha_m)$. We define

$$\delta_\pi(\mathcal{E}_1, \mathcal{E}_2) = \sum_{i=1}^M |\mathbf{P}_{\mathcal{E}_1}(\alpha_i) - \mathbf{P}_{\mathcal{E}_2}(\alpha_i)|,$$

where $\mathbf{P}_\mathcal{E}(\alpha_i) = \frac{|\{d \in \mathcal{E} : \pi(d) = \alpha_i\}|}{|\mathcal{E}|}$ are ensemble probabilities. We remark that the function δ_π is a pseudometric on the set of all ensembles which elements have the property π . In our model we set $\pi = \lambda$, hidden variables. The precise reproducibility of the probability distribution of hidden variables (4) can be written as $\delta(S_{AB}, S_{CB}) = \delta(S_{AB}, S_{AC}) = 0$, where $\delta = \delta_\lambda$. Of course, we need not use such a precise coincidence in probabilistic considerations.

Theorem 2. *Let statistical ensembles satisfy condition*

$$\delta(S_{AB}, S_{CB}), \delta(S_{AB}, S_{AC}) \leq \epsilon.$$

Then Bell's inequality

$$| \langle A, B \rangle_{S_{AB}} - \langle C, B \rangle_{S_{CB}} | \leq (1 + 2\epsilon) \langle A, C \rangle_{S_{AC}} \quad (5)$$

holds true.

However, the constant ϵ is unknown. Thus the 'right Bell's inequality' (5) could not be experimentally verified.

1. J.S. Bell, On the problem of hidden variables in quantum mechanics. *Rev. Mod. Phys.*, **38**, 447–452 (1966).
2. A.Yu. Khrennikov, *Non-Archimedean analysis: quantum paradoxes, dynamical systems and biological models*. Kluwer Acad.Publ., Dordrecht, The Netherlands, 1997.

Classical Distinguishability and Schrödinger Cat States

K K Wan, R Green and C Trueman

School of Physics and Astronomy,

University of St. Andrews, Fife, KY16 9SS, Scotland, UK

May 22, 1999

Abstract

The Schrödinger's cat paradox [1] is to do with possible coherent superpositions of classical-like states of quantum systems. The object of this paper is to explore various possible Schrödinger Cats, their states and their separability. The commonly cited coherent states fail our definition of separability.

1 Classical cats and their states

A classical cat is assumed to have only two pure states: being alive and being dead, and there are no coherent superpositions of a live and a dead state (limbo state). We can describe such a cat with a 2d Hilbert space \mathcal{H}_{cc} spanned by two orthonormal vectors $|L\rangle$ and $|D\rangle$, with $|L\rangle$ for the state of being alive and $|D\rangle$ for the state of being dead. The absence of any limbo state can be achieved by a superselection rule [2] which forbids any coherent superposition of $|L\rangle$ and $|D\rangle$. This is the same as to require all observables of a classical cat to be of the form $\hat{A} = a|L\rangle\langle L| + b|D\rangle\langle D|$, $a, b \in \mathbf{R}$. Operators of this form are unable to correlate the live and dead states, i.e., $\langle D | \hat{A} | L \rangle = 0$, so that a linear combination $\alpha |L\rangle + \beta |D\rangle$ is equivalent to a mixture of the live and dead states with weightings $|\alpha|^2$ and $|\beta|^2$.

Note that a coherent superposition of states is a physical statement implying the existence of observables capable of correlating the constituent states. In contrast, a linear combination of states is just a mathematical expression for a sum. For a system admitting a superselection

rule, the Hilbert space \mathcal{H} is divided into certain subspaces \mathcal{H}_n such that states Φ_1, Φ_2, \dots from these subspaces $\mathcal{H}_1, \mathcal{H}_2, \dots$ cannot form coherent superpositions [2]. These subspaces are known as *supersectors*. We call states from different supersectors *separable*. For a classical cat the two states $|L\rangle$ and $|D\rangle$ are separable.

2 Quantum cats and their states

A quantum cat is assumed to have two pure states $|L\rangle$ and $|D\rangle$ which span a 2d Hilbert space \mathcal{H}_{qc} . These are not assumed to be the only pure states. No superselection rules are assumed so that all selfadjoint operators on \mathcal{H}_{qc} represent observables, i.e., there are observables to correlate $|L\rangle$ and $|D\rangle$. So, any linear combination $\alpha|L\rangle + \beta|D\rangle$ represents a new pure state describing a state of limbo, i.e., the cat being partially alive and partially dead.

A quantum cat is no different from any 2-level orthodox quantum system, and the two states $|L\rangle$ and $|D\rangle$ are not separable.

3 Separable states

Our primary interest is in cases which lie in between the two extremes of being classical and being quantum. We look for what may be called quasi-separable states. Intuitively we seek states whose behaviour is classical sometimes, i.e., definitely alive or definitely dead as far as one can tell, and quantum at some other times, i.e., having a state of limbo of being partially alive and partially dead.

There have been many attempts to construct what may be called *classical-like* states of a quantum system. The best known examples are perhaps the coherent states of a quantized harmonic oscillator [3]. The motion of a classical oscillator is

$$x_c(t) = A \cos \omega t, \quad p_c(t) = -m\omega A \sin \omega t.$$

A coherent state is the following solution of the time-dependent Schrödinger equation of the quantized oscillator:

$$\begin{aligned} \Phi_z(x, t) &= C(t) \exp\left(\frac{i}{\hbar} p_c(t)x - \frac{m\omega}{2\hbar}(x - x_c(t))^2\right), \quad z = \left(\frac{m\omega}{2\hbar}\right)^{\frac{1}{2}} \left(\frac{i}{m\omega} p_c(t) + x_c(t)\right) \\ C(t) &= \left(\frac{m\omega}{\pi\hbar}\right)^{\frac{1}{4}} \exp\left[i\left(\frac{m\omega}{4\hbar} A^2 \sin 2\omega t - \frac{1}{2}\omega t\right)\right] \end{aligned}$$

with an oscillating spatial probability density

$$|\Psi_z(x, t)|^2 = \left(\frac{m\omega}{\pi\hbar}\right)^{1/2} \exp\left[-\frac{m\omega}{\hbar}(x - x_c(t))^2\right].$$

The magnitude of oscillation can be as big as one likes by increasing A . This solution represents a wave packet which oscillates without distortion like a classical oscillator. A coherent state is therefore considered classical-like. Linear combinations of classical-like states are referred to as Schrödinger cat states in the literature, e.g., a linear combination of coherent states Φ_z and Φ_{-z} .

A quantized harmonic oscillator is a pure quantum system with no superselection rules so that observables \hat{A} , in the form of selfadjoint operators, exist to correlate Φ_z and Φ_{-z} , e.g., we have the parity operator $\hat{\rho}$ such that $\langle \Phi_z | \hat{\rho} \Phi_{-z} \rangle = 1$ for all z and t . Clearly the traditional Schrödinger cat states represented by coherent states Φ_z and Φ_{-z} are not separable by our definition.

To proceed further we have to resort to a concept of **equivalence FAPP**¹ based on the following assumption on measurement:

Any experiment \mathcal{E}^n is performed within a finite time and is capable of measuring only a finite number n of bounded observables $\hat{A}_1, \dots, \hat{A}_n$ with some finite resolution of interference terms.

Suppose that the experiment cannot tell the existence of the interference terms when they are less than a certain small number, when the system is in state $\Psi = (\phi + \psi)/\sqrt{2}$. Then,

$$\begin{aligned} & \text{linear combination } \frac{1}{\sqrt{2}} (\phi + \psi) \\ \equiv & \text{mixture } \hat{\rho} = \frac{1}{2} (|\phi\rangle\langle\phi| + |\psi\rangle\langle\psi|) \quad \text{FAPP}\mathcal{E}^n. \end{aligned}$$

Generally let ϕ_z, ψ_z be a one-parameter family of pairs of states of a system at time $t = 0$. At a later time the states evolve to ϕ_{zt}, ψ_{zt} . Suppose that given any experiment \mathcal{E}^n , there is a finite time interval Δ and a value z_0 such that for all $z > z_0$ and for all times $t \in \Delta$ we have

$$\Psi_{zt} = a\phi_{zt} + b\psi_{zt} \equiv \hat{\rho} = |a|^2 |\phi_{zt}\rangle\langle\phi_{zt}| + |b|^2 |\psi_{zt}\rangle\langle\psi_{zt}| \quad \text{FAPP}\mathcal{E}^n .$$

Then we call ϕ_{zt}, ψ_{zt} **separable FAPP** \mathcal{E}^n for $z > z_0, t \in \Delta$. It turns out that many standard quantum systems admit separable states in this sense.

Take for example a general scattering system which possesses bound states ϕ_b and scattering states ϕ_s in \mathcal{H} . As time goes on ϕ_s evolves to ϕ_{st} which moves to a region far away from the origin, while ϕ_b evolves to ϕ_{bt} which remains around the origin at all times. The

¹FAPP means *for all practical purposes*, an abbreviation proposed by John Bell [4]. We shall denote FAPP for experiment \mathcal{E}^n by FAPP \mathcal{E}^n .

overlap between ϕ_{bt} and ϕ_{st} over any finite region tends to zero $t \rightarrow \infty$. We can establish vanishing correlation

$$\lim_{t \rightarrow \infty} \langle \phi_{bt} | \hat{A} \phi_{st} \rangle = 0$$

for every bounded operator \hat{A} in \mathcal{H} . So, for any finite set of bounded observables \hat{A}_j , $j = 1, \dots, n$ we have correlations $\langle \phi_{bt} | \hat{A}_j \phi_{st} \rangle$ becoming arbitrarily small as $t \rightarrow \infty$. Hence ϕ_{bt} and ϕ_{st} are separable FAPP at large times, leading to a resolution of the de Broglie Paradox.

Finally let us return to the quantized oscillator. Let φ_n be the normalized eigenfunctions of the Hamiltonian. Then a coherent superposition $\eta_t = (\varphi_0 + \varphi_1)/\sqrt{2}$ represents a wave packet with oscillating position expectation value, i.e.,

$$\langle \eta_t | \hat{x} \eta_t \rangle = \left(\frac{\hbar}{2m\omega} \right)^{\frac{1}{2}} \cos \omega t.$$

It can be shown that for any given bounded operator \hat{A} the correlation term $\langle \Phi_z | \hat{A} \eta_t \rangle$ tends to zero as $z \rightarrow \infty$. So Φ_z and η_t are separable FAPP for sufficiently large z .

It is common to use the terms *classical-like* and *classical distinguishable* interchangeably. We have avoided referring to classical distinguishability altogether. When classical waves meet and interfere the constituent waves may become indistinguishable!

This idea of separable states can be developed a lot further, e.g., periodic separability (separable in a periodic manner). Full details of this development will be published elsewhere.

References

- [1] E Schrödinger *Naturwissenschaften* **23** 807-812 (1935), J A Wheeler, W. Zurek, *Quantum Theory of Measurement* (Princeton U. P., Princeton, N. J.,1983).
- [2] K K Wan, *Can. J. Phys.* **58** 976 (1980). B. Beltrametti and G. Cassinelli, *The Logic of Quantum Mechanics* (Addison-Wesley, Reading, MA,1981).
- [3] B Yurke and D Stoler, *Phys Rev Lett* **57** 13 (1986) S. Howard and S K Roy *Am. J. Phys.* **55** 1109 (1987). C. Monroe, D M Meekhof, B. E. King and D. J. Wineland *Science* **272** 1131 (1996). C C . Gerry and P L Knight *Am. J. Phys* **65** 964 (1997).
- [4] J S Bell, *Against "Measurement"* in *Sixty-Two Year of Uncertainty* edited by A I Miller (Plenum, New York, 1990).

An experiment on Bell's inequality and quantum cryptography using ultrafast random switches

G. Weihs, T. Jennewein, C. Simon, A. Zeilinger

Institut für Experimentalphysik, Universität Wien, Boltzmannngasse 5, 1090 Wien, Austria

H. Weinfurter

Sektion Physik, Ludwig-Maximilians-Universität München Schellingstr. 4/III, 80799 München, Germany

Abstract

We present an experiment testing Bell's inequality under strict Einstein locality conditions using ultrafast random switches. At the same time the experimental setup can be used to generate quantum cryptographic keys.

The inequality derived by J. S. Bell in 1964 [1], which puts limits on the strength of correlations of two-particle systems, rests upon the assumptions of realism and locality. In the experiments that followed to test the theorem locality could not be guaranteed by the apparatus. In fact in most of the experiments the analyzers had been at rest for several hours so that any hypothetical communication between the two observing stations could in principle explain the strong correlations that had been observed [2].

The first attempt to close this so-called Einstein locality loophole was the impressive experiment by Aspect and coworkers [3] who used acousto-optic modulators to switch the basis of polarization analysis on a time scale that was shorter than the flight time of the



FIG. 1. Photograph of the Innsbruck science campus. The parametric down-conversion source was approximately centered between the two observer station called "Alice" and "Bob". Optical fibers connected the different locations.

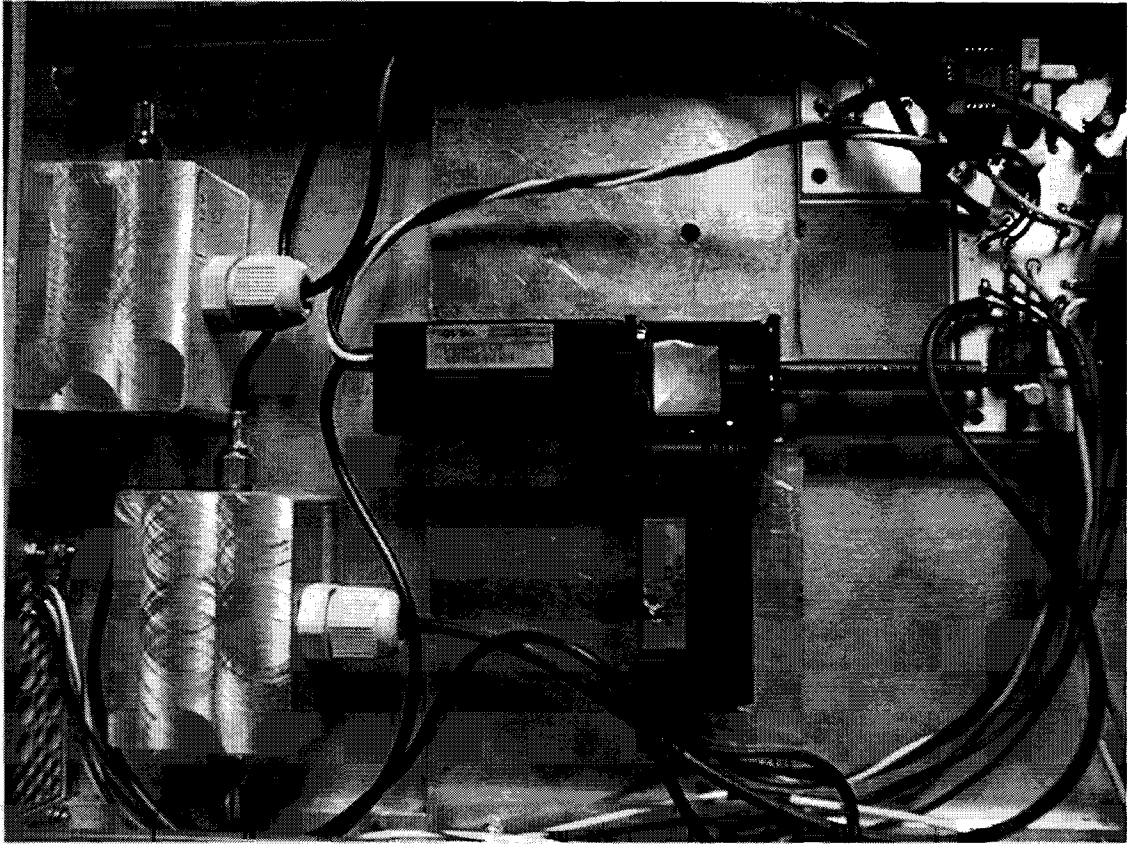


FIG. 2. A physical random bit generator. This device produces an output signal that toggles randomly between “0” and “1” triggered by the detections of photons in either output of a beamsplitter.

photons. However, the switching was performed only in a periodic, predictable manner. A conclusive test of Bell’s inequality should involve fast random switching. Random switching requires high bandwidth in all the components used and is therefore much more difficult.

Recently we completed an experiment [4] where the random switching and spacelike separation conditions could be fulfilled. Further we were able to utilize the apparatus to perform quantum cryptographic key distribution. This was possible because the data were collected independently at the observer stations.

To achieve the timing conditions it was necessary to spatially separate the observers, in our case by 360 m across the Innsbruck university science campus (Fig. 1), which gave us $1.2 \mu\text{s}$ to have each observer complete his individual measurement. Near the geometric center between the two observers we placed our type-II parametric down-conversion source, which emits polarization entangled photon pairs.

Each of the observers switched the direction of local polarization analysis using a transverse electro-optic modulator with DC to 30 MHz bandwidth. The actual orientation for local polarization analysis was determined independently by binary physical random number generators with a maximum toggle speed of 500 MHz (Fig. 2). With the random number generator and the fast switch we made sure that the whole measurement process was short-

er than 100 ns. This is much shorter than the $1.2\mu\text{s}$ that any information about the other observer's measurement is necessarily retarded.

In our experiment a typically observed maximum value of the function was $S = 2.73 \pm 0.02$ corresponding to a violation of the CHSH inequality of 30 standard deviations assuming only statistical errors. Such a measurement took 10 s and is in good agreement with the quantum theoretical prediction. The correlations had 97% visibility (less than 3% Bit Error Rate) and were thus appropriate for efficient quantum key distribution by EPR-pairs. The Bit Error Rate could be enhanced to less than 0.5% by classical lossy error correction.

REFERENCES

- [1] J. Bell, *Physics* **1**, 195 (1964).
- [2] S. J. Freedman and J. F. Clauser, *Phys. Rev. Lett.* **28**, 938 (1972).
- [3] A. Aspect, J. Dalibard, and G. Roger, *Phys. Rev. Lett.* **49**, 1804 (1982).
- [4] G. Weihs *et al.*, *Phys. Rev. Lett.* **81**, 5039 (1998).

Low Quantum Efficiency of Detectors In Recent Experimental Tests Of Bell's Inequality

V. Berardi

*INFN - Unità di Bari, and Dipartimento Interateneo di Fisica,
Università di Bari, Via E. Orabona 4, 70126 Bari (ITALY)*

A. Garuccio, V. L. Lepore

*Dipartimento Interateneo di Fisica and INFN - Sezione di Bari,
Università di Bari, Via E. Orabona 4, 70126 Bari (Italy)*

Abstract

In this communication we will derive a new form of Bell's inequality to carefully take into account the detectors efficiency. By this approach we will show that, although the two most recent experiments on Bell's inequality can be considered a huge improvement in the direction of testing quantum mechanics predictions, the loophole of the low quantum efficiency of detector is not yet solved.

I. INTRODUCTION

Is Quantum Mechanics non-local? Addressing this question has been the subject of a huge amount of work, starting from the very first paper by Einstein, Podolsky and Rosen (EPR) [1]. In 1965, J. S. Bell [2] set a milestone in this subject by proving that Quantum Mechanics (QM) is not compatible with the existence of *elements of reality* (according with the definition given by EPR), introducing the well known Bell's inequality. Unfortunately, his analysis was based on two assumptions that are hardly achievable in experiments: i) it is possible to get total correlation ; ii) the measurements always yield well defined results. Later, several attempts were made to derive testable Bell's inequalities by introducing supplementary assumptions [3,4], though none of them gave any justification for making such assumptions. However, all experiments to date showed a remarkable agreement with QM predictions giving a very strong evidence that QM has a non-local character. Notwithstanding the agreement reached by all the experiment with QM, if for no other reason than the great importance of the question, the experimental results must be carefully analyzed in order to elucidate the role of supplementary assumptions. In particular a common problem for all the experiments appears to be the detection efficiency, namely the ratio between the number of detected events and that of tested quantum systems. This, often referred as detection loophole (DL), is recognized as the major problem in the two most recent experiments

too [5,6], and will be the central issue of the this report. The DL consists in the following trivial (under the point of view of QM) assumption: the sample over which the statistic is measured is fair (fair sampling assumption, FSA). Of course such assumption is unavoidable in any experiment where the finite value of the detection efficiency limits the number of tested events in comparison with the overall number of quantum system. However, as already pointed out by Clauser, Horne, Shimony, and Holt [3], who wrote that, in view of the difficulty of an experimental check, the assumption could be challenged by an advocate of hidden variable theories in case the outcome of the proposed experiment favors quantum mechanics, the FSA is not so trivial under the point of view of a Local Hidden Variables (LHV) theory. It is, in fact, possible to postulate that there exists some actual value of a hidden variable affecting the probability to trigger a detector. Several attempts have been done to develop a LHV advocate proof version of Bell's inequality, in particular Ebherard [7] deduced a supplementary assumption free inequality, proving that it can be violated on condition that the detection efficiency is greater than 66% assuming null background noise (that is visibility equal to unity) and highly asymmetric entangled states. Moreover, De Caro and Garuccio [8] proved that in case of trichotomic observables the detection efficiency lower bound is 81%. Recently Larsson [9] showed that, within the framework of GHZ states, the lower bound for detection efficiency drops down to 75%.

II. DERIVATION OF BELL'S INEQUALITY

If $A(a)$ and $B(b)$ are two observables assuming the values $[+1,0,-1]$ and if the result of a measurement on $A(a)$ and $B(b)$ is dependent on the experimental parameters a and b respectively, and on the element of reality λ variable over the set Λ with normalized density $\rho(\lambda)$, the correlation function of $A(a)$ and $B(b)$ is defined as [10]:

$$P(a, b) = \frac{\int_{\Lambda} A(a, \lambda)B(b, \lambda)\rho(\lambda)d\lambda - \int_{\Lambda} A(a, \lambda)\rho(\lambda)d\lambda \cdot \int_{\Lambda} B(b, \lambda)\rho(\lambda)d\lambda}{\sqrt{\int_{\Lambda} A^2(a, \lambda)\rho(\lambda)d\lambda} \cdot \sqrt{\int_{\Lambda} B^2(b, \lambda)\rho(\lambda)d\lambda}} \quad (1)$$

We define the Bell observable as $\bar{\Delta} = |P(a, b) - P(a, b')| + |P(a', b) + P(a', b')|$. If the quantum state is symmetric $\int_{\Lambda} A(a, \lambda)\rho(\lambda)d\lambda = \int_{\Lambda} B(b, \lambda)\rho(\lambda)d\lambda = 0$ and, after a few mathematics we have:

$$\begin{aligned} \bar{\Delta} \leq & \frac{1}{\sqrt{\sigma_A^2(a)}} \int_{\Lambda} |A(a, \lambda)| \left| \frac{B(b, \lambda)}{\sqrt{\sigma_B^2(b)}} - \frac{B(b', \lambda)}{\sqrt{\sigma_B^2(b')}} \right| \rho(\lambda)d\lambda + \\ & + \frac{1}{\sqrt{\sigma_A^2(a')}} \int_{\Lambda} |A(a', \lambda)| \left| \frac{B(b, \lambda)}{\sqrt{\sigma_B^2(b)}} + \frac{B(b', \lambda)}{\sqrt{\sigma_B^2(b')}} \right| \rho(\lambda)d\lambda \end{aligned} \quad (2)$$

where $\sigma_A^2(a) = \int_{\Lambda} A^2(a, \lambda)\rho(\lambda)d\lambda$ and $\sigma_B^2(b) = \int_{\Lambda} B^2(b, \lambda)\rho(\lambda)d\lambda$. Now, let $\Lambda_A(a)$ and $\Lambda_A(a')$ be subsets of Λ in which $A(a, \lambda) = 0$ and $A(a', \lambda) = 0$, respectively; if $\lambda \in \Lambda' = \Lambda_A(a) \cap \Lambda_A(a')$ the integrals vanish and we can evaluate them in the subset $\Lambda - \Lambda'$. Moreover, since $|A(a, \lambda)| \leq 1$ as well as $|A(a', \lambda)| \leq 1$, we can replace the above quantities with their maximum value. The same argument can be applied to observable $B(b)$ for which subsets

$\Lambda_B(b)$ and $\Lambda_B(b')$ of Λ in which $B(b, \lambda) = 0$ and $B(b', \lambda) = 0$ respectively, can be defined. For all the values of $\lambda \in \Lambda'' = \Lambda_B(b) \cap \Lambda_B(b')$ we have:

$$\left| \frac{B(b, \lambda)}{\sqrt{\sigma_B^2(b)}} - \frac{B(b', \lambda)}{\sqrt{\sigma_B^2(b')}} \right| + \left| \frac{B(b, \lambda)}{\sqrt{\sigma_B^2(b)}} + \frac{B(b', \lambda)}{\sqrt{\sigma_B^2(b')}} \right| = 0 \quad (3)$$

Now, let's assume that: i) $\Lambda_A(a)$, $\Lambda_A(a')$, $\Lambda_B(b)$, $\Lambda_B(b')$, are completely randomly determined, i.e. the non detection process is independent of the value of the hidden variables; ii) the probability of non-detection does not depend on the values of a , a' , b and b' ; iii) the measuring apparatuses are identical, i.e. channel A and B are identical. In these conditions $\sqrt{\sigma_A^2(a)} = \sqrt{\sigma_A^2(a')}$ and $\sqrt{\sigma_B^2(b)} = \sqrt{\sigma_B^2(b')}$. As a consequence for $\lambda \in \Lambda' \cap \Lambda''$, it holds:

$$\left| \frac{B(b, \lambda)}{\sqrt{\sigma_B^2(b)}} - \frac{B(b', \lambda)}{\sqrt{\sigma_B^2(b')}} \right| + \left| \frac{B(b, \lambda)}{\sqrt{\sigma_B^2(b)}} + \frac{B(b', \lambda)}{\sqrt{\sigma_B^2(b')}} \right| \leq \frac{2}{\sqrt{\sigma_B^2(b)}} \quad (4)$$

And finally we get:

$$\bar{\Delta} \leq \frac{2}{M} \int_{\Lambda' \cap \Lambda''} \rho(\lambda) d\lambda = \frac{2}{M} \mu(\bar{\Lambda}) \quad (5)$$

where $M = \min(\sqrt{\sigma_A^2(a)}, \sqrt{\sigma_B^2(b)})$. If $\mu_A(a, a') = \int_{\Lambda'} \rho(\lambda) d\lambda$, $\mu_B(b, b') = \int_{\Lambda''} \rho(\lambda) d\lambda$ and $\mu_{AB}(a, a', b, b') = \int_{\Lambda' \cap \Lambda''} \rho(\lambda) d\lambda$, Eq.(5) turns to be:

$$\bar{\Delta} \leq \frac{2}{M} (1 - \mu_A(a, a') - \mu_B(b, b') + \mu_{AB}(a, a', b, b')) \quad (6)$$

Owing to hypothesis i), we have $\mu_{AB}(a, a', b, b') = \mu_A(a, a') \cdot \mu_B(b, b')$, $\mu_A(a, a') = \mu_A(a) \cdot \mu_A(a')$ and $\mu_B(b, b') = \mu_B(b) \cdot \mu_B(b')$. Moreover, hypothesis ii) allows us to state that $\mu_A(a) = \mu_A(a') = \mu_A$ and $\mu_B(b) = \mu_B(b') = \mu_B$. Finally hypothesis iii) allows us to write $\mu_A = \mu_B = \mu$. As a consequence Eq.(6) becomes:

$$\bar{\Delta} \leq \frac{2}{M} (1 - \mu^2)^2 \quad (7)$$

Remembering that if η is the detection efficiency, $\eta = 1 - \mu$, and $M = (1 - \mu) = \eta$ we finally have:

$$\bar{\Delta} \leq 2 \eta (2 - \eta)^2 \quad (8)$$

whereas it is well known that the Quantum Mechanics prediction (Δ_{QM}) gives for maximally entangled states (as the singlet state):

$$\Delta_{QM} = 2 \sqrt{2} \frac{\eta^2}{\eta} \quad (9)$$

As long as $\Delta_{QM} \leq \bar{\Delta}$ it is impossible to distinguish between a LHV theory and QM predictions. The comparison between Eq.(8) and (9) gives a lower bound for the detection efficiency,

$$\eta_{min} = 2 - \sqrt[4]{2} = 0.811 \quad (10)$$

This number is in total agreement with the a previous one, deduced by De Caro and Garuccio [8] in the framework of a Bell's inequality using expectation values (instead of correlation functions) and assuming a random non-detection process. We would moreover note that the result of Eq.(10) can only be partially compared with the that one, obtained by Eberhard [7], who derived an inequality without using any supplementary assumption which could be violated by QM predictions if the detection efficiency exceeds 66%. Since, as already pointed out in the Introduction, he got his result by using extremely asymmetrical quantum-states and in the limit of visibility equal to 1.

III. CONCLUSION

Up to now, all the experimental tests aiming to investigate the non-local character of QM carried out by using photon-pairs show a remarkably good agreement with QM itself. Notwithstanding, in all the experiments the detection efficiency was far below 20%. Moreover, in all the experiments, the comparison between QM and LHV theories have been performed by using the CHSH inequality. In this short communication we introduce a *probabilistic* form of Bell's Inequality, i.e. we propose to use a very general approach entirely based on the *probability* definition of correlated variables. In summary we showed that assuming the validity of **Random selection hypothesis** and in the case of **symmetric quantum state** any discrepancy between a LHV theory and QM prediction can be evidenced by a clever experimental physicist if and only if the detection efficiency is greater that 0.811%.

REFERENCES

- [1] A. Einstein, B. Podolsky and N. Rosen, Phys. Rev. **47**, 777 (1935).
- [2] J. S. Bell, Physics **1**, 195 (1965).
- [3] J. F. Clauser, M. A. Horne, A. Shimony, and R. A. Holt, Phys. Rev. Lett. **23**, 880 (1969).
- [4] J. F. Clauser, M. A. Horne, Phys. Rev. **D10**, 526 (1974).
- [5] G. Weihs, T. Jennewein, C. Simon, H. Weinfurter, and A. Zeilinger, Phys. Rev. Lett. **81**, 5039 (1998).
- [6] W. Tittel, J. Brendel, N. Gisin, H. Zbinden, Phys. Rev **A59**, 4150 (1999).
- [7] Ph. H. Eberhard, Phys. Rev **A47**, R747 (1993).
- [8] L. De Caro and A. Garuccio, Phys Rev. **A54**, 176 (1996).
- [9] Jan-Ake Larsson, Phys. Rev. **A57**, R3145 (1998).
- [10] M.H. DeGroot, *Probability and Statistics*. Addison-Wesley, Reading, MA (1988).

Detection of mesoscopic entanglement

Matteo G. A. Paris *

*Theoretical Quantum Optics Group – INFN Unitá di Pavia
Dipartimento di Fisica 'Alessandro Volta' – Università di Pavia
via Bassi 6, I-27100 Pavia, ITALY*

Abstract

We suggest a feasible method, based on a homodyne-like detection scheme, to detect the degree of entanglement obtainable by mixing a couple of excited squeezed coherent states in a balanced beam splitter.

In the novel field of quantum technology, entanglement is a resource that can be exploited for the transmission and the manipulation of information. Actually, the entanglement between two photons has been widely investigated, both theoretically and experimentally. Entangled photon pairs have been used to test nonlocality of quantum mechanics, and to explore potential applications such as secure quantum key distribution and teleportation [1]. More recently, the experimental realization of continuous teleportation [2] raised attention to mesoscopic entanglement, namely the quantum correlations that can be established between two radiation beams containing many photons. Indeed, the continuous teleportation protocol relies on the mesoscopic entanglement obtained by mixing a couple of squeezed states in a balanced beam splitter. For these reasons, it is a matter of interest to quantify the entanglement between excited beams, and to devise detection schemes capable of revealing their degree of entanglement.

In experiments involving correlated photon pairs, entanglement is revealed by measuring the coincidence counting rate at the output, namely the fourth-order correlation function $K(\phi) = \langle \psi_{\text{OUT}} | a^\dagger a b^\dagger b | \psi_{\text{OUT}} \rangle$, where ϕ is a phase-shift between the two photon paths. However, when many photons are present, namely when we are dealing with mesoscopic entanglement, this corresponds to low fringes visibility, and thus we need a more sensitive kind of measurement. The homodyne-like detection of the output difference photocurrent $\langle \psi_{\text{OUT}} | a^\dagger a - b^\dagger b | \psi_{\text{OUT}} \rangle$ is widely used in interferometry and generally results in a very sensitive measurement scheme [3]. Starting from this consideration, here we suggest the squared difference photocurrent $H(\phi) = \langle \psi_{\text{OUT}} | (a^\dagger a - b^\dagger b)^2 | \psi_{\text{OUT}} \rangle$ as a suitable fourth-order quantity to be measured at the output. Apart from the very low signals regime (the photon-pair regime) homodyne-like detection shows very high fringes visibility, thus providing a reliable detection scheme to reveal mesoscopic entanglement.

*paris@pv.infn.it

In order to present explicit calculations, and to compare the two different measurement schemes, we focus our attention on the specific setup depicted in Fig. 1. First, a couple of degenerate optical parametric amplifiers (DOPAs) is employed to generate a couple of uncorrelated identical squeezed coherent state [4]

$$|\Psi_{in}\rangle = |\alpha, r\rangle_a |\alpha, r\rangle_b = \hat{D}_a(\alpha)\hat{D}_b(\alpha)\hat{S}_a(r)\hat{S}_b(r)|0\rangle$$

where $\hat{D}(\alpha) = \exp\{\alpha a^\dagger - \bar{\alpha}a\}$ is the displacement operator, and $\hat{S}(r) = \exp\{1/2r^2(a^{\dagger 2} - a^2)\}$ the squeezing operator.

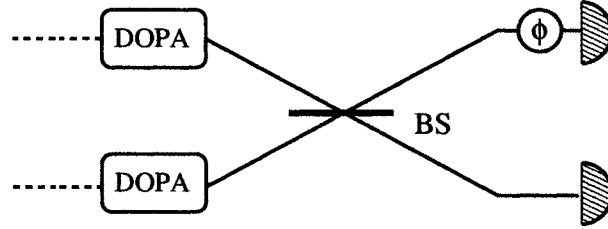


FIG. 1. Schematic diagram of the setup to generate and reveal states with different degree of mesoscopic entanglement.

The two squeezed states are then mixed in a balanced beam splitter, and the resulting output state, $\hat{U} = \exp\{i\pi/4(a^\dagger b + ab^\dagger)\}$ being the evolution operator of the balanced beam splitter,

$$|\Psi_{out}\rangle = \hat{U}|\Psi_{in}\rangle$$

ranges from a totally disentangled state to a maximally entangled state, depending on the squeezing fraction γ of each of the input state. This is defined as the fraction of the total number of photons engaged in squeezing $\gamma = \sinh^2 r/N$, $N = |\alpha|^2 + \sinh^2 r$ being the total number of photons of the state. In particular, for a couple of squeezed vacuum at the input ($\gamma = 1$) the output state is given by the so-called twin-beam state

$$|\chi\rangle = \sqrt{1 - |\chi|^2} \sum_{n=0}^{\infty} \chi^n |n, n\rangle \quad (1)$$

where $\chi = \tanh r$. Twin-beam $|\chi\rangle$ represents a maximally entangled state that may contain a mesoscopic number of photons, we have

$$N_\chi = \langle \chi | a^\dagger a + b^\dagger b | \chi \rangle = 2|\chi|^2 / (1 + |\chi|^2)^2.$$

In general, a measure of the entanglement for pure state is provided by the normalized entropy of entanglement [5,6]

$$\epsilon = \frac{S[\hat{\rho}_a]}{S[\hat{\rho}_{th}]}$$

where $S[\hat{\rho}] = -\text{Tr}\{\hat{\rho} \log \hat{\rho}\}$ is the Von-Neumann entropy of the quantum state $\hat{\rho}$, $\hat{\rho}_a = \text{Tr}_b\{|\Psi_{out}\rangle\langle\Psi_{out}|\}$ is the partial trace of the output state, and $\hat{\rho}_{th}$ describes a thermal state (a maximum entropy state) with the same number of photon of the partial trace $\hat{\rho}_a$. The degree

of entanglement ϵ ranges from zero for uncorrelated states to unit for maximally entangled states. After some algebra we obtain for the degree of entanglement of $|\Psi_{out}\rangle$

$$\epsilon = \frac{\log(1 + \gamma N) + \gamma N \log(1 + \frac{1}{\gamma N})}{\log(1 + N) + N \log(1 + \frac{1}{N})}. \quad (2)$$

From Eq. (2) it is apparent that the degree of entanglement is an increasing function of the squeezing fraction, and that a maximum entangled state ($\epsilon = 1$) at the output is reached for a couple of squeezed vacuum ($\gamma = 1$) at the input. For highly excited states the entanglement is given by the asymptotic formula

$$\epsilon \stackrel{N \gg 1}{\simeq} 1 + \frac{\log \gamma}{\log N}. \quad (3)$$

We now study the visibility of the interference fringes that are observed, by varying the phase-shift ϕ between the two signals, in intensity measurements at the output. Besides being originated by interference effects, the variations in the quantities measured at the output also reflect the variations in the quantum correlations between the two output signals. In analogy with experiments involving correlated photon pairs, we may consider the detection of the coincidence counting rate at the output, namely of the fourth-order correlation function $K(\phi)$. However, as we will show in the following, this corresponds to low fringes visibility, and thus we sought for a more sensitive kind of measurement. Here, we consider the squared difference photocurrent $H(\phi) = \langle \Psi_{out} | (a^\dagger a - b^\dagger b)^2 | \Psi_{out} \rangle$ as a suitable fourth-order quantity to be measured at the output of the interferometer. The fringes visibilities of both detection schemes are given by

$$V_K = \frac{K_{max} - K_{min}}{K_{max} + K_{min}} \quad V_H = \frac{H_{max} - H_{min}}{H_{max} + H_{min}}. \quad (4)$$

In Fig. 2 we report V_K and V_H as a function of the intensity N for different values of the input squeezing fraction γ . The H-measurement visibility V_H is larger than V_K in almost all situations, with the exception of the very low signals regime, where very few photons are present. The behavior of fringes visibility versus intensity N also confirms that V_H represents a good measure of the entanglement at the output. As it happens for the degree of entanglement, in fact, a couple of squeezed vacuum at the input corresponds to maximum visibility $V_H = 1$ independently on the intensity. On the other hand, the coincidence counting rate shows a visibility V_K that rapidly decreases versus N , and saturates to a value well below $1/2$. For non unit squeezing fraction, and moderate input intensities ($N < 10$), the behavior of V_H looks qualitatively similar to that of the degree of entanglement, whereas again V_K rapidly decreases. Remarkably, for highly excited states $N > 10$, the visibility V_H has the same asymptotic dependence of the degree of entanglement ϵ , in formula

$$\epsilon \stackrel{N \gg 1}{\simeq} 1 + \frac{A(\gamma)}{\log N}, \quad (5)$$

where the proportionality constant $A(\gamma) \simeq 1/5 \log \gamma$ is roughly proportional to that appearing in Eq. (3).

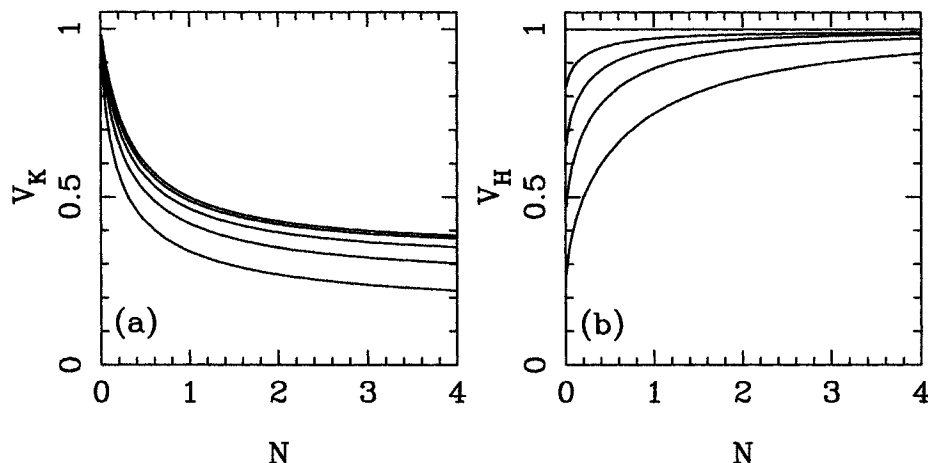


FIG. 2. Fringes visibility as a function of the intensity N for different values of the input squeezing fraction γ . In (a) the visibility of K-measurement V_K , and in (b) the visibility of H-measurement V_H . In both plots we report the visibility versus N for five values of the input squeezing fraction. From bottom to top we have the curves for $\gamma = 0.2, 0.4, 0.6, 0.8$, and 1.0 . As it is apparent, V_H is larger than V_K in almost all situations, with the exception of the very low signals regime.

In conclusion, we have analytically evaluated the degree of entanglement at the output of a balanced beam splitter fed by a couple of squeezed coherent states. By varying the input energy, we can produce entangled states of arbitrary large intensity, whereas the degree of entanglement can be tuned by varying the input squeezing fraction. We have suggested an effective experimental characterization of the output entanglement through the measurement of the squared difference photocurrent between the output modes. The interference fringes that are observed by varying the phase-shift between the signals show, in fact, high visibility for the whole range of input squeezing parameter.

REFERENCES

1. D. Boschi, S. Branca, F. De Martini, L. Hardy, S. Popescu, Phys. Rev. Lett. **80**, 1121 (1998).
2. S. L. Braunstein, H. J. Kimble, Phys. Rev. Lett. **80**, 869 (1998).
3. M. G. A. Paris, Phys. Lett A **201**, 132 (1995).
4. M. G. A. Paris Phys. Lett. A **225**, 28 (1997).
5. S. Popescu, D. Rohrlich, Phys. Rev. A **56**, R3319 (1997).
6. M. G. A. Phys. Rev. A **59**, 1615 (1999).

Uncertainty relations based on Geometry of Quantum State Space

Arun Kumar Pati

SEECs, Dean Street, University of Wales, Bangor LL 57 1UT, UK.

and

Theoretical Physics Division, 5th Floor, Central Complex

BARC, Mumbai-400 085, India

Abstract

Quantum states move in the projective Hilbert space because there are quantum fluctuations (uncertainties) in the observables. We investigate the uncertainty relations based on the geometry of the projective Hilbert space of the quantum system. We do not need *any* Hermitian operator to represent an observable to study the associated uncertainty.

Section: (a) Uncertainty Relations .

1. Introduction:

Though the dynamical aspects of the quantum theory have been well studied, the geometric aspects have been appreciated much later. The study of geometry of quantum states and its implications have gained much importance in recent years [1–7]. One of the outcome of the geometric approach is the parameter-based uncertainty relation (PBUR) in quantum theory [2,8]. This is often useful when we do not have a Hermitian operator canonical conjugate to another operator which represent a physical quantity of our interest. The vivid example is the quest for time-energy uncertainty relation, when we do not have a Hermitian time operator canonical conjugate to energy.

In this paper we discuss the geometric uncertainty relations when we have one Hermitian operator and when we do not have any Hermitian operator. We present a new form of energy-time uncertainty relation without any recourse to time operator. We argue that one may not need any Hermitian operator to define an uncertainty in the physical quantity. We find the intelligent states [9,10] for non-orthogonal initial and final states. From a quantum information processing point of view keeping track of intelligent states are important.

2. Geometric Uncertainty Relation:

Let us consider a quantum state $|\psi(t)\rangle \in \mathcal{H} = \mathcal{C}^N$ which evolves in time. Geometrically the state is represented by a point in the projective Hilbert space $\mathcal{P} = \mathcal{H} - \{0\}/\mathcal{C}^*$. The time evolution of the system gives us a curve C in \mathcal{H} . The Hilbert space curve can be projected onto a curve $\hat{C} = \Pi(C)$ via a projection map $\Pi : \mathcal{H} \rightarrow \mathcal{P}$. The projected curve \hat{C} has a length which is induced from the inner product of the Hilbert space and is given by the Fubini-Study metric [2–5] $S = \frac{2}{\hbar} \int_{t_1}^{t_2} \Delta H(t) dt$, where $\Delta H(t) = \left[\langle \psi(t) | H(t)^2 | \psi(t) \rangle - \langle \psi(t) | H(t) | \psi(t) \rangle^2 \right]^{\frac{1}{2}}$ is the usual uncertainty in the energy of the system. This distance is independent of a

particular Hamiltonian used to evolve the quantum system and is invariant under a gauge transformation. On the other hand if S_0 is the shortest distance between the initial and final states joining the points $\Pi(|\psi(t_1)\rangle)$ and $\Pi(|\psi(t_2)\rangle)$ then the distance measured by Fubini-Study metric is always greater than the geodesic distance connecting the initial and final points, where S_0 is given by the Bargmann angle [5] formula $\cos^2 \frac{S_0}{2} = |\langle \psi(t_1) | \psi(t_2) \rangle|^2$. This gives $S \geq S_0$ and the equality holds only for those states that evolve along a geodesic in \mathcal{P} . The Anandan-Aharonov uncertainty relation for time-energy is given by

$$\langle \Delta H(t) \rangle \Delta t \geq \frac{\hbar}{4} \quad (1)$$

where $\langle \Delta H(t) \rangle = \frac{1}{(t_2 - t_1)} \int_{t_1}^{t_2} \Delta H(t) dt$ is the time average of the energy uncertainty and $\Delta t = \frac{\pi}{S_0} (t_2 - t_1)$ is the ‘‘uncertainty in time’’. When the initial and final states are orthogonal (which are distinguishable by quantum mechanical tests) then the shortest distance is π . In this case time-energy uncertainty relation takes a simple form (for a time-independent Hamiltonian) as $\Delta H \Delta t \geq \frac{\hbar}{4}$, where $\Delta t = (t_2 - t_1)$ is the ordinary time difference that is required to make a transition to a orthogonal state. There are various approaches to time-energy uncertainty relation and to estimate the time required to make a transition to orthogonal states in the literature [11]. The advantage of the geometric uncertainty relation is that we do not have to look for a Hermitian operator for time. It can remain just as a parameter and uncertainty in the parameter would mean how good we can estimate it given a certain amount of uncertainty in the conjugate variable. This fact can be grounded by the observation that we can go beyond the time-energy uncertainty relation. If we have any continuous parameter λ and any Hermitian observable $A(\lambda)$ which is the generator of the parametric evolution, then the Fubini-Study distance is given by

$$S = \frac{2}{\hbar} \int_{\lambda_1}^{\lambda_2} \Delta A(\lambda) d\lambda \quad (2)$$

where $\Delta A(\lambda)$ is the uncertainty in the observable (the quantum fluctuation) of the system. The speed of the system point in \mathcal{P} is $V(\lambda) = \frac{2}{\hbar} \Delta A(\lambda)$. This means if we regards position as a parameter then $V(X) = \frac{2}{\hbar} \Delta P$ is the speed of the system point in \mathcal{P} . On the other hand if we regard momentum as a parameter then $V(P) = \frac{2}{\hbar} \Delta X$ is the speed of the system point in \mathcal{P} . This suggests us a *new meaning to the Heisenberg uncertainty relation*. Thus, $\Delta X \Delta P \geq \frac{\hbar}{2}$ can be expressed as

$$V(X)V(P) \geq \frac{2}{\hbar} \quad (3)$$

which means *in the projective Hilbert space we can not trace two curves parametrised by X and P (whose quantum parts do not commute) with an arbitrary speed*. The product of two speeds must have a lower bound fixed by Planck’s constant.

Now coming to geometric uncertainty relation a similar geometric reasoning (as for time-energy case) would give us $\langle \Delta A(\lambda) \rangle \Delta \lambda \geq \frac{\hbar}{4}$, where $\langle \Delta A(\lambda) \rangle = \frac{1}{(\lambda_2 - \lambda_1)} \int_{\lambda_1}^{\lambda_2} \Delta A(\lambda) d\lambda$ is the parameter average of the observable uncertainty and $\Delta \lambda = \frac{\pi}{S_0} (\lambda_2 - \lambda_1)$ is the scaled displacement in the space of the conjugate variable of A . This generalised uncertainty relation would hold for position-momentum, phase-number or any possible combinations. Recently, Yu [12] has discussed the PBUR for position-momentum case.

If the Hermitian generator A of the parametric evolution can be split into two parts $A_0 + A_1$ such that A_0 has a complete basis of normalised eigenstates $\{|\psi_i\rangle\}_{i \in I}$ with degenerate spectrum $\{a_0\}$, with I a set of quantum numbers and A_1 has matrix elements $(A_1)_{ii} = 0 = (A_1)_{jj}$ and $(A_1)_{ij} = (A_1)_{ji} = a_1$, then all states of the form

$$|\psi(\lambda)\rangle = e^{\frac{-i}{\hbar}a_1\lambda}(\cos(a_1\frac{\lambda}{\hbar})|\psi_i\rangle - i\sin(a_1\frac{\lambda}{\hbar})|\psi_j\rangle), \quad i \neq j \quad (4)$$

are intelligent states for non-orthogonal initial and final states.

The proof can be found in [13]. The uncertainty in the operator $\Delta A^2 = a_1^2$. The shortest distance along the geodesic $S_0 = 2\cos^{-1}(|\langle\psi(\lambda_1)|\psi(\lambda_2)\rangle|) = \frac{2}{\hbar}a_1\lambda_2$. The rhs of the PBUR of Anandan-Aharonov becomes $\Delta A\Delta\lambda = a_1 \cdot \frac{\pi}{2a_1}\hbar = \frac{\hbar}{4}$. This proves that the states (4) are indeed intelligent states.

3. Uncertain Relation without Hermitian operator:

In the preceding section we discussed geometric uncertain relation when we have a Hermitian operator which is the generator of the parameter evolution. Suppose we do not have any Hermitian generator corresponding to a particular parametric evolution. All that is known about a quantum system is that the state vector evolves in the Hilbert space continuously when certain parameters are changed in an arbitrary manner. We argue that even in this case we can talk of a geometric uncertainty relation. This suggest us that we may not need a time operator at all in quantum theory. We can define an uncertainty in the time without a time operator. The idea is as follows.

Let us imagine a quantum system which evolves in the Hilbert space through the variation of a continuous parameter λ . The state may not necessarily obey some linear and unitary evolution law. In fact, it can obey some non-linear and non-unitary equation. In such situations the norm of the state may not be preserved during a parametric evolution. Given the Hilbert space structure of the quantum system, we know that we can define the inner product between any two vectors. This inner product induces a generalised Fubini-Study metric [14] on the projective Hilbert space of the quantum system \mathcal{P} . The Fubini-Study metric is given by

$$dS^2 = \left[\left\langle \frac{d}{d\lambda} \left(\frac{\psi(\lambda)}{\|\psi(\lambda)\|} \right) \middle| \frac{d}{d\lambda} \left(\frac{\psi(\lambda)}{\|\psi(\lambda)\|} \right) \right\rangle - \left(i \left\langle \frac{d}{d\lambda} \left(\frac{\psi(\lambda)}{\|\psi(\lambda)\|} \right) \middle| \frac{d}{d\lambda} \left(\frac{\psi(\lambda)}{\|\psi(\lambda)\|} \right) \right\rangle \right)^2 \right] d\lambda^2 \quad (5)$$

Therefore, during an arbitrary evolution the total distance travelled by the system point in \mathcal{P} is given by

$$S = \int_{\lambda_1}^{\lambda_2} V(\lambda) d\lambda. \quad (6)$$

Since the actual distance S is always greater than the geodesic distance S_0 we can write the following inequality

$$\langle V(\lambda) \rangle \Delta\lambda \geq 1 \quad (7)$$

where $\langle V(\lambda) \rangle$ is the parameter average of the speed of transportation of the system point in \mathcal{P} and $\Delta\lambda = \frac{1}{S_0}(\lambda_2 - \lambda_1)$. The above inequality is most general geometric uncertainty

relation for pure quantum states. When we have a Hermitian operator A corresponding to the parameter translation, the the Anandan-Aharonov uncertain relation can be thought of as a special case of the present one. Since the system point moves in \mathcal{P} because there is some kind of uncertainty in the system, we might intereprete $V(\lambda)$ as an inherent uncertainty in the quantum system without an associated operator. For example, if we have quantum state labelled by energy (a continuous variable) for unbounded systems, then the parameter λ can play the role of energy. Then the the quantity $V(E)$ may be called an uncertainty in the time (on dimensiaonal ground also $V(E)$ has dimension of time), where $V(E)$ is given by

$$V(E) = \sqrt{\left[\left\langle \frac{d}{dE} \left(\frac{\psi(E)}{\|\psi(E)\|} \right) \middle| \frac{d}{dE} \left(\frac{\psi(E)}{\|\psi(E)\|} \right) \right\rangle - (i \left\langle \left(\frac{\psi(E)}{\|\psi(E)\|} \right) \middle| \frac{d}{dE} \left(\frac{\psi(E)}{\|\psi(E)\|} \right) \right\rangle)^2 \right]} \quad (8)$$

Then the generalised uncertainty relation takes the form

$$\langle V(E) \rangle \Delta E \geq 1 \quad (9)$$

This is new form of energy-time uceratinty relation treating energy as a parameter unlike the Anadan-Aharonov case, where time was a parameter.

4. Conclusion:

We have discussed geometric uncertainty relations in quantum theory without any recourse to Hermitian operators. We provided a new meaning to Heisenebrg uncertainty relation. We found the explicit form of intelligent states when the initial and final states are *non-orthogonal*.

I acknowledge the financial support from EPSRC.

REFERENCES

- [1] J. P. Provost and G. E. Valle, *Commun. Math. Phys.* **76**, 289 (1980).
- [2] J. S. Anandan and Y. Aharonov, *Phys. Rev. Lett.* **65**, 1697 (1990).
- [3] J. S. Anandan, *Phys. Lett. A* **147**, 3 (1990).
- [4] A. K. Pati, *Phys. Lett. A* **159**, 105 (1991).
- [5] A. K. Pati, *J. Phys. A* **25**, L1001 (1992).
- [6] J. S. Anandan, *Found. Phys.* **21**, 1265 (1991).
- [7] S. L. Braunstein and C. M. Caves, *Phys. Rev. Lett.* **72**, 3439 (1994).
- [8] S. L. Braunstein, C. M. Caves and G. J. Milburn, *Ann. Phys.* **247**, 135 (1996).
- [9] C. Aragone, G. Guerri, S. Salamo and J. L. Tani, *J. Phys. A* **7**, L149 (1974).
- [10] N. Horesh and A. Mann, *J. Phys. A* **31**, L609 (1998).
- [11] L. Vaidman, *Am. J. Phys.* **60**, 182 (1992).
- [12] T. Yu, *Phys. Lett. A* **223**, 9 (1996).
- [13] A. K. Pati, [quant-ph/9901033](#).
- [14] A. K. Pati, *Phys. Lett. A* **202**, 40 (1995).

Finite time measurements of entangled states

Morton H. Rubin

Department of Physics, University of Maryland, Baltimore County, Baltimore, MD 21250

In this paper, I discuss how the duration of the measurement of a subsystem of an entangled state determines the state of the unmeasured subsystem. We derive an integral equation that must be satisfied for perfect teleportation of a broadband qubit state. This type of measurement is important in quantum computing, quantum information theory and in the preparation of entangled states such as the Greenberger, Horne, and Zeilinger state [1].

I. A simple example: Quantum teleportation of qubit states

We begin with a simple example of the effect of finite time measurements on quantum teleportation. Following the usual teleportation protocol [2], Alice and Bob each receive one of two identical particles prepared in an entangled singlet state $|\Psi\rangle_{ab}$. Alice is then given a qubit in an arbitrary state, $|\phi\rangle_c = \alpha|+\rangle_c + \beta|-\rangle_c$, that she wishes to send to Bob. We suppose that the computational states of the qubits are not degenerate, $H|+\rangle = -\frac{\epsilon}{2}|+\rangle$. $H|-\rangle = \frac{\epsilon}{2}|-\rangle$. Consequently, $|\phi\rangle_c$ is time dependent.

Alice performs a measurement of duration T_m at the time T on the pair of particles a, c . Her measurement projects out one of the Bell states

$$|\Phi^{(\pm)}\rangle_{ac} = \sqrt{\frac{1}{2}}(|++\rangle_{ac} \pm |--\rangle_{ac}) \quad |\Psi^{(\pm)}\rangle_{ac} = \sqrt{\frac{1}{2}}(|+-\rangle_{ac} \pm |-+\rangle_{ac}). \quad (1)$$

Suppose the outcome of the measurement is $|\Phi^{(+)}\rangle_{ac}$, then the state in Bob's laboratory is given by

$$\rho(t) = \begin{pmatrix} |\beta|^2 & -\alpha^*\beta(t) \\ -\alpha\beta^*(t) & |\alpha|^2 \end{pmatrix} \quad (2)$$

where $\beta(t) = \beta e^{-i\epsilon t}$. Since the measurement is not performed instantaneously, but is of finite duration T_m , Bob's density matrix must be time averaged which leads to the replacement $\beta(t) \rightarrow \beta(T) \text{sinc}(\epsilon T_m/2)$ in eq(2).

To complete the protocol Alice performs the unitary transformation, conditioned on the outcome of her measurement, $\bar{\rho}_f = \sigma_y \bar{\rho} \sigma_y$. The fidelity, correcting for the time T , is

$$F = \langle \phi(T) | \bar{\rho}_f | \phi(T) \rangle_b = 1 - 2|\alpha|^2 |\beta|^2 (1 - \text{sinc}(\epsilon T_m/2)) \quad (3)$$

where $|\phi(T)\rangle = \alpha|+\rangle + \beta(T)|-\rangle$. The same result hold for the other three possible outcomes. For $\epsilon = 0$ or $T_m = 0$ we get perfect fidelity. If $\epsilon T_m \gg 1$ then the fidelity reduces to $F = 1 - 2|\alpha|^2 |\beta|^2 \geq \frac{1}{2}$, which depends on the state that is teleported.

II. Finite time measurements of photons

We now examine the effect of finite time measurements on photon entangled states. We

define a detection operator [3] $E = \sum_{\omega} p(\omega) e^{-i\omega(t-x)} a(\omega, \mathbf{e})$, where $a(\omega, \mathbf{e})$ is the annihilation operator for a photon of angular frequency ω and polarization \mathbf{e} , and $p(\omega)$ is the spectral function of the detector. The function $p(\omega)$ is determined, in part, by placing filters and polarizers in front of the photodetector. We restrict ourselves to a point detector located at x . The instantaneous counting rate for an input state Ψ is proportional to $R(t) = \langle \Psi | E^\dagger E | \Psi \rangle$. If Ψ is the single photon state $|\phi\rangle = \sum_{\omega} f(\omega) a^\dagger(\omega, \mathbf{e}') |0\rangle$, $R(t)$ can be written in terms of the single photon amplitude, $\langle 0 | E | \phi \rangle = \sum_{\omega} f(\omega) p(\omega) e^{-i\omega(t-x)} (\mathbf{e} \cdot \mathbf{e}')$. The detector actually measures a quantity proportional to the time averaged intensity. Introducing the retarded time $\tau = t - x$, we find

$$\begin{aligned} I &= \frac{1}{T_m} \int_{T-T_m/2}^{T+T_m/2} d\tau |\langle 0 | E | \phi \rangle|^2 \\ &= \sum_{\omega, \omega'} f(\omega')^* p(\omega')^* f(\omega) p(\omega) e^{i(\omega' - \omega)T} \text{sinc}[(\omega - \omega')T_m/2] |(\mathbf{e} \cdot \mathbf{e}')|^2. \end{aligned} \quad (4)$$

The outcome of the measurement depends on the duration of the measurement T_m , f , and p . T_m is the fundamental resolving time of the detector.

We shall restrict ourselves to the case that the spectral amplitude $f(\omega)$ is peaked at $\omega = \Omega$ with width of $\Delta\omega \ll \Omega$ and to broadband detectors so the width of the p is large compared to that of f . The characteristic quantity for the detector is $\theta = \Delta\omega T_m = T_m/T_\omega$, where T_ω is the coherence time of the single photon wave packet.

There are two extreme cases that we shall consider, fast and slow detectors. Fast detectors are characterized by the condition $\theta \ll 1$ so the sinc function can be replaced by 1 over the range of summation giving $I = |p(\Omega) \sum_{\omega} f(\omega) e^{-i\omega T} (\mathbf{e} \cdot \mathbf{e}')|^2$, (fig.1). This means that the envelope of the wave packet can be resolved by the detector. For slow detectors, which is the usual case for photodetectors, $\theta \gg 1$. The sinc function restricts the integration region to $\omega \approx \omega'$ and we find $I = \pi |p(\Omega)|^2 \sum_{\omega} |f(\omega)|^2 |(\mathbf{e} \cdot \mathbf{e}')|^2$, (fig.1). In this case the average intensity is measured.

A. Preparation of a one particle state from a two particle entangled states

For an entangled pure state, neither photon is in a definite state [4]. When one of particles is detected, then the undetected particle acquires a definite state. Consider the two photon entangled state with one photon moving to the right and the other to the left,

$$|\Psi\rangle = \sum_{\omega, \omega'} f(\omega, \omega') (\xi_+ |\omega, \mathbf{e}_+\rangle_R |\omega', \mathbf{e}_-\rangle_L + \xi_- |\omega, \mathbf{e}_-\rangle_R |\omega', \mathbf{e}_+\rangle_L), \quad (5)$$

where \mathbf{e}_+ and \mathbf{e}_- are orthogonal linear polarization states, and ξ_{\pm} are phase factors. We assume that $f(\omega, \omega')$, is peaked around ω_0 and ω'_0 with widths $\Delta\omega \ll \omega_0$ and $\Delta\omega' \ll \omega'_0$.

If the right-moving photon, R, is detected at time t_1 and the left-moving photon is not detected, the density matrix for the system reduces to a one photon state. The subsequent detection of the second photon is determined by

$$C_1 = N \text{tr} (\rho_L E_2^\dagger E_2) \quad \rho_L = \sum_{\omega', \Omega'} |\omega', \tilde{\mathbf{e}}_1\rangle_L \rho_L(\omega', \Omega')_L \langle \Omega', \tilde{\mathbf{e}}_1| \quad (6)$$

$$\rho_L(\omega', \Omega') = \frac{1}{N} \sum_{\omega, \Omega} p_R(\omega) p_R(\Omega)^* f(\omega, \omega') f(\Omega, \Omega')^* e^{-i(\omega - \Omega)T_1} T_m \text{sinc}[(\omega - \Omega)T_m/2] \quad (7)$$

$\rho_L(\omega', \Omega')$ is a density matrix element of the L particle. N is the normalization constant.

For a slow detector the sinc function is non-negligible when $|\omega - \Omega| < \Delta\omega/\theta \ll \Delta\omega$. We may set $\omega \approx \Omega$ in f giving the mixed state $\rho_L(\omega', \Omega') = \sqrt{\frac{1}{N'}} \sum_{\omega} |p_R(\omega)|^2 f(\omega, \omega') f(\omega, \Omega')^*$. For a fast detector $|\omega - \Omega| < \Delta\omega/\theta \gg \Delta\omega$ and the sinc function may be set equal to 1 over the entire range of the summation over ω and Ω , giving the pure state

$$\rho_L(\omega'; \Omega') = \chi(\omega') \chi(\Omega')^* \quad \chi(\omega') = \sqrt{\frac{1}{N}} \sum_{\omega} p_R(\omega) f(\omega, \omega') e^{-i\omega T_1}. \quad (8)$$

B. Teleportation of qubit wave packets

In this section we outline the calculation for the teleportation of qubit wave packets. For the initial three particle state $|\Psi\rangle = |\Psi\rangle_{ab} |\Phi\rangle_c$, where $|\Psi\rangle_{ab} = \sum_{\omega_a \omega_b} f(\omega_a, \omega_b) (|\omega_a, \mathbf{e}_+\rangle_a |\omega_b, \mathbf{e}_-\rangle_b + |\omega_a, \mathbf{e}_-\rangle_a |\omega_b, \mathbf{e}_+\rangle_b)$, $|\Phi\rangle_c = \sum_{\omega_c} g(\omega_c) |\phi; \omega_c\rangle_c$ and $|\phi; \omega_c\rangle_c = \alpha_+ |\omega_c, \mathbf{e}_+\rangle_c + \alpha_- |\omega_c, \mathbf{e}_-\rangle_c$ is a normalized plane wave state. $|\Phi\rangle_c$ is the state to be teleported. We shall use the notation $|B\rangle$, $B = 1, 2, 3, 4$, respectively, for the Bell states $|\Phi^{(+)}\rangle$, $|\Phi^{(-)}\rangle$, $|\Psi^{(+)}\rangle$, $|\Psi^{(-)}\rangle$ and define the Bell state detector

$$E^{(B)} = \sum_{\omega_1 \omega_2} p^{(B)}(\omega_1, \omega_2) e^{-i(\omega_1 + \omega_2) \tau_B} \sum_{\sigma_1 \sigma_2} \zeta_{\sigma_1 \sigma_2}^{(B)} a(\omega_1, \mathbf{e}_{\sigma_1}) a(\omega_2, \mathbf{e}_{\sigma_2}), \quad (9)$$

where the non-zero elements of the ζ 's are $\zeta_{++}^{(1)} = \zeta_{--}^{(1)} = 1$, $\zeta_{++}^{(2)} = -\zeta_{--}^{(2)} = 1$, etc.

As before, $\tau_B = t_B - x_B$, where x_B is the coordinate normal to the detector and t_B is the time the detector registers the pair. The three particle correlation is $C_B = \langle \Psi | E^{(B)\dagger} E_b^\dagger E_b E^{(B)} | \Psi \rangle = |A_{bB}|^2$ where the amplitude A_{bB} is given by

$$A_{bB} = \langle 0 | E_b E^{(B)} | \Psi \rangle = \sum_{\omega_a \omega_b \omega_c} U_B(\omega_a, \omega_b, \omega_c) e^{-i(\omega_a + \omega_c) T_B} \langle 0 | E_b | \phi^{(B)}(\omega_b) \rangle_b \quad (10)$$

with $U_B(\omega_a, \omega_b, \omega_c) = f(\omega_a, \omega_b) g(\omega_c) p^{(B)}(\omega_a, \omega_c)$. The procedure is now the same as above, we must integrate C_B over the detection time T_B , giving the density matrix in Bob's laboratory:

$$\rho_B(\omega_b, \omega'_b) = \frac{1}{N} \sum_{\omega_a \omega_b \omega'_a \omega'_b} \text{sinc}(\omega_a + \omega_c - \omega'_a - \omega'_c) \frac{T_m}{2} e^{-i(\omega_a + \omega_c) T_B} U_B(\omega_a, \omega_b, \omega_c) e^{i(\omega'_a + \omega'_c) T_B} U_B(\omega'_a, \omega'_b, \omega'_c)^*. \quad (11)$$

For a fast detector so that the sinc is approximately equal to one over the range of integration. This requires that $(\Delta\omega_a + \Delta\omega_c) T_m \ll 2\pi$, where $\Delta\omega_a$ is the width of $f(\omega_a, \omega_b)$ in the first variable and $\Delta\omega_c$ is the width of $g(\omega_c)$. With these assumptions, $\rho_B = |\chi^B\rangle_b \langle \chi^B|$ where the state produced in Bob's laboratory is $|\chi^B\rangle_b = \sqrt{\frac{1}{N}} \sum_{\omega_b} \left[\sum_{\omega_a \omega_c} U(\omega_a, \omega_b, \omega_c) e^{i(\omega_a + \omega_c) T_B} \right] |\phi^{(B)}; \omega_b\rangle_b$. This is a pure state but, in general, it does not have the same spectral properties as the state given to Alice. Consequently, for perfect teleportation there is an additional condition that must be satisfied by the state to be teleported. The spectral function g must satisfy the integral equation

$$\sum_{\omega_c} \left(\sum_{\omega_a} f(\omega_a, \omega_b) p^{(B)}(\omega_a, \omega_c) e^{i(\omega_a + \omega_c) T_B} \right) g(\omega_c) = \lambda g(\omega_b). \quad (12)$$

That is, g must be an eigenvector of the operator, K , in brackets which depends on the input entangled state, f , and the nature of the Bell state detector, $p^{(B)}$. The fidelity of the teleportation is $F = |(g, Kg)/(g, g)|^2 \leq \lambda_{max}$.

III. Conclusion

When a system composed of subsystems is an entangled state, the subsystems are in general not in any definite state. The effect of measuring a subsystem is to project the unmeasured subsystem into a definite state. The precise nature of this state depends on the initial entangled state and the nature of the measurement. In particular, there is a time scale set by the initial entangled state and the subsystem measured. If the duration of the measurement is long on this time scale, then the state prepared will be a mixed state. If the duration is short, then the state prepared is a pure state, otherwise, the prepared state is mixed. We have illustrated the effect of finite time measurements on teleportation but similar results hold for any process in which a subsystem of an entangled state is measured in order to generate a state of the unmeasured subsystem.

IV. Acknowledgements

The author wishes to express his thanks to Mark Heiligman, Keith Miller, Arthur Pittenger, and Yanhua Shih for their comments on this work. This work was supported in part by ONR and NSA/ARO.

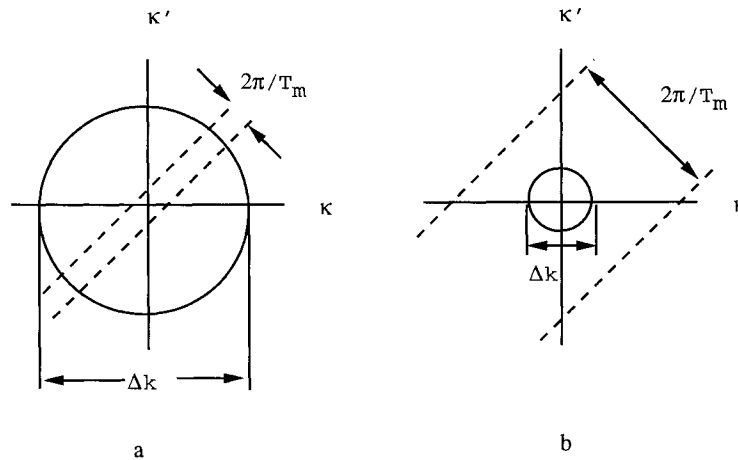


figure 1: Illustration of the case a) slow detector, $\theta \gg 1$ and b) fast detector, $\theta \ll 1$

References

1. D. M. Greenberger, M. Horne, and A. Zeilinger, in *Bell's Theorem, Quantum Theory, and Conceptions of the Universe*, M. Kaftos ed., (Kluwer, Dordrecht, 1989); D. M. Greenberger, M. Horne, A. Shimony, and A. Zeilinger, *Am. J. Phys.* **58**, 1131 (1990).
2. C. H. Bennett, et. al., *Phys. Rev. Lett.* **70**, 1895 (1993).
3. R. J. Glauber, *Phys. Rev.* **130**, 2529 (1963).
4. E. Schrödinger, *Naturwissenschaften* **23**, 807, 823, 844 (1935) Translation in J. A. Wheeler and W. H. Zurek, ed. *Quantum Theory of Measurement*.

Atomic State Reduction in Resonance Fluorescence with Spectral Resolution

Vyacheslav Shatokhin and Sergei Kilin
*B. I. Stepanov Institute of Physics,
National Academy of Sciences of Belarus,
F. Skaryna Avenue 70, Minsk 220602, Belarus*

Abstract

A general expression is found for the instantaneous atomic state following detection of a photon passed through an interference filter. For its derivation, the second-order correlation function of filtered and unfiltered photons has been used. Properties of the reduced atomic state are discussed.

“Quantum state reduction”, or “collapse of the wavefunction”, is an inherently quantum mechanical phenomenon which can be regarded as a back-action of a measuring device on a quantum system during measurement [1]. This notion also becomes useful for physical interpretation of many experiments in quantum optics, for example, of those related to resonance fluorescence. It is known [2] that when the atomic radiation is detected without spectral resolution, each photodetection event is accompanied by atomic state reduction onto the ground state for zero time delay. Now, let us suppose that we have detected a photon transmitted through a spectral (Fabry-Perot) filter with the bandwidth Γ_f and resonance frequency ω_f . Then what the atomic state is? In this paper we present an answer to this question. The answer is based on the use of the fact that the second-order coherence of resonance fluorescence contains explicit information about the reduced atomic state.

For derivation of the expression for the atomic state following a detection of a transmitted photon, we propose to use, apart from the detector D_1 placed behind the filter, an additional broadband detector D_2 . We associate the narrowband and broadband detection channels with these detectors. Earlier, an identical scheme was used in connection with the study of two-photon wave-packets [3]. A similar setup but with two narrowband channels was extensively studied as applied to the problem of spectral correlations in resonance fluorescence [4–6]. In the problem of atomic state reduction being considered, the detector D_2 is used monitor the atom in instants when clicks are produced by the detector D_1 . Then, based on an analysis of time delays between clicks at D_1 and D_2 , the atomic state can be deduced. In terms of the quantum measurement theory, detection of the filtered photon is regarded as preparation of an atomic state, whereas detection of an unfiltered photon is considered as measurement of this atomic state.

In the stationary regime, statistics of delayed coincidences at the detectors D_1 and D_2 can be described by the second-order temporal coherence $g^{(2)}(\tau)$. This is the joint probability $p_{fu}(\tau)$ for detection of a filtered photon at some time followed after delay τ by detection of

an unfiltered photon, normalized by the probability for two independent counts of filtered and unfiltered photons $p_f(\infty)$ and $p_u(\infty)$, respectively,

$$g^{(2)}(\tau) = \frac{p_{fu}(\tau)}{p_f(\infty)p_u(\infty)}. \quad (\tau \geq 0) \quad (1)$$

Under assumption that optical paths from the atom to both detectors D_1 and D_2 are the same equal to l , and that the field reflected from the filter does not affect the atom and photon flux at D_2 , expressions for the probabilities in the right-hand side are given by

$$\begin{aligned} p_{fu}(\tau) &\propto \lim_{t \rightarrow \infty} \text{Tr} \left[\hat{\sigma}_+^f(t_R) \hat{\sigma}_+(t_R + \tau) \hat{\sigma}_-(t_R + \tau) \hat{\sigma}_-^f(t_R) \hat{\rho}_{AF}(0) \right], \\ p_f(\infty) &\propto \lim_{t \rightarrow \infty} \text{Tr} \left[\hat{\sigma}_+^f(t_R) \hat{\sigma}_-^f(t_R) \hat{\rho}_{AF}(0) \right], \\ p_u(\infty) &\propto \rho_{22}(\infty), \end{aligned} \quad (2)$$

where $\hat{\rho}_{AF}(0)$ is the initial density operator,

$$\hat{\sigma}_-^f(t) = \int_0^t dt' T_f(t-t') \hat{\sigma}_-(t') \quad (3)$$

is the convolution of the atomic lowering operator $\hat{\sigma}_-(t)$ and the filter transmission function [7,8] $T_f(t) = \Theta(t) \Gamma_f e^{-(i\omega_f + \Gamma_f)t}$, $\hat{\sigma}_+^f(t) = \left(\hat{\sigma}_-^f(t)\right)^\dagger$, $t_R = t - l/c$, and $\rho_{22}(\infty)$ is the steady-state population of the atomic excited state. The joint probability $p_{fu}(\tau)$ can be expressed as the conditional probability of a click at D_2 at time τ given a click at D_1 at time 0. Then $g^{(2)}(\tau)$ reads

$$g^{(2)}(\tau) = \frac{\rho_{22}(\tau) |_{\hat{\rho}(0)=\hat{\rho}^c(\infty)}}{\rho_{22}(\infty)}, \quad (\tau \geq 0) \quad (4)$$

where $\hat{\rho}^c(\infty)$ is the reduced atomic state following detection of filtered photon. The superscript “c” means that this state is conditioned by a count in the narrowband channel. The conditioned atomic state is given by

$$\hat{\rho}^c(\infty) = \lim_{t \rightarrow \infty} \frac{\hat{\chi}(t - l/c)}{\text{Tr} \hat{\chi}(t - l/c)} \quad (5)$$

where

$$\hat{\chi}(t - l/c) = \text{Tr}_F \left[\hat{U}(t_R) \hat{\sigma}_-^f(t_R) \hat{\rho}_{AF}(0) \hat{\sigma}_+^f(t_R) \hat{U}(t_R)^\dagger \right], \quad (6)$$

$\hat{U}(t) = \exp(-i\hat{H}t/\hbar)$ is the evolution operator, and the Hamiltonian $\hat{H} = \hat{H}_{\text{atom}} + \hat{H}_{\text{field}} + \hat{H}_{\text{int}}$.

Equations (5) and (6) allow to calculate the atomic state just after detection of the transmitted photon, provided that the parameters of the atom, exciting field and filter are known. For large filter bandwidths $\Gamma_f \gg \gamma$, where γ is the spontaneous decay rate, the conditioned state slightly differs from the ground atomic state, and in the limit $\Gamma_f \rightarrow \infty$ we have $\hat{\rho}^c(\infty) = |1\rangle\langle 1|$. On the other side, when $\Gamma_f \ll \gamma$ the distribution of emission times has the width $\sim \Gamma_f^{-1}$ which is much larger than the lifetime of the atom in the excited state.

The atom after collapse to the ground state evolves to its steady state, before the emitted photon reaches the detector D_1 . Therefore, in the limit of a very narrow filter, $\hat{\rho}^c(\infty)$ tends to the unconditional atomic state $\hat{\rho}(\infty)$. In the intermediate case, when $\Gamma_f \sim \gamma$, we can expect that detection of the transmitted photon occurs when the atom is still in the transient regime. It is well known that for large Rabi frequencies the excited state population in the transient regime oscillates and may be $> 1/2$, although the steady state population of the excited atomic state cannot exceed $1/2$. So, we can expect that for particular bandwidths and setting frequencies of the filter the conditioned atomic state can be inverted, that is, $\langle \hat{\sigma}_z \rangle^c = \text{Tr}[\hat{\rho}^c(\infty) \hat{\sigma}_z] > 0$. And this is indeed so. The calculations of the expectation value of the inversion operator in the stationary conditioned state has been performed for several filter parameters at the Rabi frequency $\Omega = 10\gamma$. For $\Gamma_f = 3\gamma$ we found that for any setting frequencies $\langle \hat{\sigma}_z \rangle^c < 0$. For $\Gamma_f = 0.01\gamma$ the sign of $\langle \hat{\sigma}_z \rangle^c$ is the same. However, we obtained positive $\langle \hat{\sigma}_z \rangle^c = 8 \cdot 10^{-4}$ for $\Gamma_f = 0.5\gamma$ and $\omega_f = \omega_L$ (ω_L is the laser frequency) and the larger value $\langle \hat{\sigma}_z \rangle^c = 0.0246$ for the filter set in between the central and sideband components of the fluorescence triplet $\omega_f = \omega_L \pm \Omega/2$. Although the reason of the inversion in $\hat{\rho}^c(\infty)$ can be explained approximately as the transient regime of the atom at the instant of transmitted photon detection, the influence of the filter resonance frequency and role of the wings of the transmission function should be clarified in a more rigorous consideration. Obviously, it is incorrect to identify $\hat{\rho}^c(\infty)$ and the unconditional atomic state at any time. The state $\hat{\rho}^c(\infty)$ explicitly depends on the filter parameters and cannot be expressed as resulting from the atomic evolution alone.

It is interesting that, given a measured intensity correlation function $g^{(2)}(\tau)$ defined by Eq. (4), it is possible to find the conditioned state in the case of the unknown filter parameters, provided the parameters of the exciting field are known. Moreover, the diagonal elements of the state $\hat{\rho}^c(\infty)$ can be obtained from the value $g^{(2)}(0)$ alone:

$$\rho_{22}^c(\infty) = \tilde{g}^{(2)}(0); \quad \rho_{11}^c(\infty) = 1 - \tilde{g}^{(2)}(0), \quad (7)$$

where $\tilde{g}^{(2)}(0) = g^{(2)}(0) \rho_{22}(\infty)$.

In conclusion, we considered spectrally-resolved resonance fluorescence of a single atom and showed that a simple scheme with two detectors allows to express the second-order intensity correlation function at the detectors in terms of the instantaneous atomic state $\hat{\rho}^c(\infty)$ conditioned by detection of a spectrally resolved photon. That makes it possible (i) to calculate $\hat{\rho}^c(\infty)$, provided that the atomic, filter and exciting field parameters are known; (ii) to reconstruct the conditioned atomic state from the measured second-order coherence. The steady-state $\hat{\rho}^c(\infty)$ can be found inverted indicating that on average, transmitted photons are detected at instants corresponding to the transient regime of the atomic evolution.

ACKNOWLEDGMENTS

V.N.S. is grateful to Eugene Petrov and Dmitry Horoshko for remarks and fruitful discussions. This work was partially supported by INTAS under grant # 0167.

REFERENCES

- [1] J. A. Wheeler and W. H. Zurek, *Quantum Theory of Measurements*, Princeton Univ. Press, 1983.
- [2] H. J. Carmichael and D. F. Walls, *J. Phys. B* **9**, 1199 (1976).
- [3] A. V. Belinsky and D. N. Klyshko, *Laser Phys.*, **4**, 663 (1994).
- [4] C. Cohen-Tannoudji and S. Reynaud, *Phil. Trans. R. Soc. London, Ser. A* **293**, 223 (1979).
- [5] P. A. Apanasevich and S. Ya. Kilin, *J. Phys. B* **12**, L83 (1979).
- [6] C. Schrama, G. Nienhuis, H. A. Dijkerman, C. Steijsiger, H. G. M. Heideman, *Phys. Rev. A* **45**, 8045 (1992); G. Nienhuis, *Phys. Rev. A* **47**, 510 (1993).
- [7] J. H. Eberly and K. Wódkiewicz, *JOSA B* **67**, 1252 (1977).
- [8] L. Knöll, W. Vogel, and D. -G. Welsch, *Phys. Rev. A* **42**, 503 (1990).

RANDOM PATH APPROACH TO QUANTUM MECHANICS

M. RONCADELLI

INFN, Sezione di Pavia, Via A. Bassi 6, I-27100 Pavia, Italy

E-mail: roncadelli@pv.infn.it

We discuss the motivations as well as the structural aspects of the random path approach to quantum mechanics.

In spite of the fact that *probabilities* get replaced by *amplitudes* in the transition from classical to quantum mechanics, a very remarkable *structural similarity* between classical and quantum physics exists. Indeed, in the coordinate representation amplitudes satisfy (up to the normalization condition) the *same calculus* that probabilities obey in the theory of classical diffusion processes defined in the *configuration space* \mathcal{M} of the dynamical system in question. That is, in either case one has a first-order time evolution with a semigroup structure. As a consequence, quantum mechanics *ought* to be formulated in (at least) *three different ways* – as it is the case for classical diffusion processes (see below). In addition, these formulations of quantum mechanics are expected to be *structurally very similar* to those of classical diffusion processes in \mathcal{M} .

What is the actual import of these facts? We all know that the wave function $\psi(x, t)$ is an arbitrary solution of the Schrödinger equation, while the transition amplitude $\langle x, t | x_0, t_0 \rangle$ is the associated propagator. Similarly, the probability density $P(x, t)$ is an arbitrary solution of the Fokker-Planck equation in \mathcal{M} , and again the transition probability $P(x, t | x_0, t_0)$ is the associated propagator. In fact, both equations have the *same* mathematical structure. Therefore, the Schrödinger formulation of the quantum theory can be regarded as the quantum counterpart of the the Fokker-Planck approach to classical diffusion processes in \mathcal{M} . Alternatively, $\langle x, t | x_0, t_0 \rangle$ is supplied by the Feynman path integral and analogously $P(x, t | x_0, t_0)$ can be represented by a Wiener-Onsager-Machlup path integral. In reality, the two treatments are *almost indistinguishable*, and so the Feynman formulation can be viewed as the quantum counterpart of the Wiener-Onsager-Machlup description of classical diffusion processes in \mathcal{M} . Although all this is well known since a long time, a *crucial point* nevertheless emerges. Indeed – as far as classical diffusion processes in \mathcal{M} are concerned – $P(x, t | x_0, t_0)$ can also be expressed as a noise average involving the solutions of a Langevin equation with a gaussian white noise. *So, what the present discussion implies is that even in quantum mechanics a similar representation of $\langle x, t | x_0, t_0 \rangle$ should exist.* Actually, such

a representation is provided by the *random path quantization*¹, which looks like the quantum counterpart of the Langevin approach to classical diffusion processes in \mathcal{M} .

As we shall see, the strategy upon which the random path approach is based consists in modifying classical mechanics by putting a certain white noise into play, so that every classical dynamical trajectory in \mathcal{M} gets replaced by a set of *quantum random paths* which fluctuate about it. Any solution of the Schrödinger equation – and in particular the propagator – then arises as a noise average involving a set of quantum random paths. As a result, quantum mechanics can be analyzed *explicitly* in terms of

- classical mechanics,
- quantum fluctuations^a.

We consider throughout a point particle \mathcal{S} (mass m , spin 0) with $\mathcal{M} = \mathcal{R}^N$ and described classically by a lagrangian of the form^b $L(x, \dot{x}, t) = \frac{1}{2}m\dot{x}_i\dot{x}_i + \Omega_i(x, t)\dot{x}_i - \Phi(x, t)$. As is well known, the Hamilton-Jacobi equation reads in this case

$$\frac{\partial}{\partial t}S(x, t) + \frac{1}{2m} \left(\frac{\partial}{\partial x_i}S(x, t) - \Omega_i(x, t) \right)^2 + \Phi(x, t) = 0. \quad (1)$$

Corresponding to *any* particular integral $S(x, t)$ of eq. (1), a family of trajectories in \mathcal{M} is provided by the *first-order* equation

$$\frac{d}{dt}q_i(t) = \frac{1}{m} \left(\frac{\partial}{\partial x_i}S(x, t) - \Omega_i(x, t) \right) \Big|_{x=q(t)}. \quad (2)$$

We denote by $q(t; x', t'; [S(\cdot)])$ the solution of eq. (2) with initial condition $q(t') = x'$ and controlled by $S(x, t)$. Then $q(t; x', t'; [S(\cdot)])$ happens to be just the classical dynamical trajectory of \mathcal{S} in \mathcal{M} selected by the initial data $q(t') = x'$, $p(t') = (\nabla S)(x', t')$ in phase space.

Starting point of the random path quantization is classical mechanics in the Hamilton-Jacobi form. Central to the present strategy is the idea – naturally suggested by the similarity between quantum mechanics and classical diffusion processes in \mathcal{M} – that *all* quantum fluctuations can be simulated by a certain white noise $\eta(t)$ which perturbs the classical time evolution in \mathcal{M} . Moreover,

^aAlthough this statement might give the impression that the random path quantization strongly resembles Nelson's stochastic mechanics, it will become apparent that the two formulations are totally different.

^bRepeated indexes are summed over.

such an analogy also implies that the white noise variables $\eta(t)$ should merely be *added* in eq. (2) without altering the already-present terms. Observe that this fact entails in turn that the Hamilton-Jacobi eq. (1) remains *unchanged* within this setting. So, *quantization* is presently accomplished by turning eq. (2) into the following *Langevin equation*

$$\frac{d}{dt}\xi_i(t) = \frac{1}{m} \left(\frac{\partial}{\partial x_i} S(x, t) - \Omega_i(x, t) \right) \Big|_{x=\xi(t)} + \left(\frac{\hbar}{m} \right)^{1/2} \eta_i(t) \quad (3)$$

where $\eta(t) \equiv \{\eta_i(t)\}_{1 \leq i \leq N}$ is a *Fresnel white noise* – first introduced by Itô – defined by the functional (pseudo) measure

$$\mathcal{D}\mu[\eta(\cdot)] = \mathcal{D}\eta(t) A[\eta(\cdot)] \equiv \mathcal{D}\eta(t) \exp \left\{ (i/2) \int_{-\infty}^{\infty} dt \eta_i(t) \eta_i(t) \right\}. \quad (4)$$

Quite analogously to the case of classical diffusion processes, the Fresnel noise average of any $\eta(t)$ -dependent quantity (\dots) is defined by

$$\langle (\dots) \rangle_{\eta} \equiv \int \mathcal{D}\mu[\eta(\cdot)] (\dots). \quad (5)$$

We stress that the Fresnel white noise variables $\eta(t)$ are *real*, while $\mathcal{D}\mu[\eta(\cdot)]$ is manifestly *complex* – this circumstance prevents a standard probabilistic interpretation of eq. (4). Still – given that classical probabilities get replaced by quantum amplitudes – we are to regard $\mathcal{D}\mu[\eta(\cdot)]$ as an *amplitude* (pseudo) measure, so that $A[\eta(\cdot)]$ has to be understood as the *amplitude distribution* for the Fresnel white noise realizations $\eta(t)$. As either $\hbar \rightarrow 0$ or $m \rightarrow \infty$ the noise decouples away and the classical behaviour of \mathcal{S} shows up.

Coming back to the Langevin eq. (3), we denote by $\xi(t; x', t'; [S(\cdot), \eta(\cdot)])$ its solution with initial condition $\xi(t') = x'$ and controlled by *any* particular integral $S(x, t)$ of eq. (1). These solutions describe the set of *quantum random paths* controlled by $S(x, t)$, which are the basic objects in the present approach. They are *fluctuating curves* (fractals with Hausdorff dimension *two*) analogous to the erratic trajectories so characteristic of macroscopic brownian motion.

Within this context, we obviously expect the quantum mechanical propagator to arise as a noise average involving the quantum random paths, indeed much in the same manner as the transition probability of a classical diffusion process in \mathcal{M} arises within the Langevin treatment (namely, as a noise average involving the solutions of a Langevin equation). What is its explicit form? Surely, $\langle x, t | x_0, t_0 \rangle$ should not depend on any further variable besides those

indicated. Therefore, the desired representation of $\langle x, t | x_0, t_0 \rangle$ should *not* depend on the particular solution $S(x, t)$ of eq. (1) which controls the quantum random paths. Remarkably enough, this requirement yields

$$\langle x, t | x_0, t_0 \rangle = \exp\left\{ (i/\hbar)[S(x, t) - S(x_0, t_0)] \right\} \cdot \left\langle \delta(x - \xi(t; x_0, t_0; [S(\cdot), \eta(\cdot)])) \Delta(t; x_0, t_0; [S(\cdot), \eta(\cdot)])^{1/2} \right\rangle_\eta \quad (6)$$

where the definition

$$\Delta(t''; x', t'; [S(\cdot), \eta(\cdot)]) \equiv \det \left| \frac{\partial}{\partial x'_j} \xi_i(t'', x', t'; [S(\cdot), \eta(\cdot)]) \right| \quad (7)$$

is employed. We stress that the overall $S(x, t)$ -independence of eq. (6) – besides making the random path representation of $\langle x, t | x_0, t_0 \rangle$ quite flexible in practical applications – also explains why the dependence on the classical initial momentum $p(t_0) = (\nabla S)(x_0, t_0)$ gets washed out on going over to the quantum theory. As a consequence, we understand why “phase space gets squeezed into configuration space” in the transition from classical to quantum mechanics. Moreover, an *arbitrary* solution $\psi(x, t)$ of the Schrödinger equation for \mathcal{S} – arising from a given initial wave function $\psi(x, t_0) \equiv |\psi(x, t_0)| \exp\{iS(x, t_0)/\hbar\}$ – enjoys the following random path representation

$$\psi(x, t) = e^{iS_0(x, t)/\hbar} \left\langle \Delta(t_0; x, t; [S_0(\cdot), \eta(\cdot)])^{1/2} |\psi(\xi(t_0; x, t; [S_0(\cdot), \eta(\cdot)]), t_0)| \right\rangle_\eta, \quad (8)$$

where $S_0(x, t)$ denotes that particular solution of eq. (1) which arises from $S(x, t_0)$.

Manifestly, the strategy outlined above – which is characterized by the fact that *all* quantum corrections to the classical behaviour are brought about by a *noise* – provides a *new way* to handle and solve quantum dynamical problems by exploiting techniques developed in the field of classical diffusion processes.

Although it would be out of place to describe here the technical advantages of the random path quantization, we would like to mention that this approach leads most easily to a full quantum generalization of the semiclassical Gutzwiller formula, and proves more effective than other formulations in performing numerical simulations of certain dynamical systems which exhibit a chaotic behaviour in the classical limit².

1. M. Roncadelli, *Random Path Approach to Quantum Mechanics*, in *Quantum-like Models and Coherent Effects*, ed. by R. Fedele and P. K. Shukla (World Scientific, Singapore, 1995).
2. G. Vattay and P. E. Rosenqvist, *Phys. Rev. Lett.* **76**, 335 (1996).

Interference Effect between Two Squeezed State Light Fields

Junxiang Zhang, Lingxiang He, Tiancai Zhang, Changde Xie, Kunchi Peng
Institute of Opto-Electronics, Shanxi University, Taiyuan, 030006, China

0.1 INTRODUCTION

With the development of the optical Quantum measurement and communication, there is a great demand for the high measurement sensitivity in the processing of the optical information. It has been demonstrated that the squeezed light has a broadly application in the measurement of weak absorption, interferometry and spectroscopy[1, 2, 3], in the quantum measurement and communication, the nonlocality study of photos[4, 5] and the newly emerging field of quantum information processing [6, 7], the superposition and interference of quantum state of light from independent sources are involved.

A number of optical interference experiments[8, 9, 10, 11] have recently been performed in which the fields are in nonclassical states, and the resulting interference patterns exhibit certain explicitly quantum-mechanical features. Several proposals have also been made to investigate quantum interference between two independent sources among which the demonstration of nonlocal phase correlation in a parametric down-conversion process[12], quantum state teleportation[13], and the realization of multi-photon entangled states are[14]. These phenomena rely on interference between a quantum state and a classical coherent state or between two independent quantum states.

In this paper, the interference of the squeezed lights derived from two independent OPO's will be discussed. First, the basic equations of the OPO's are presented, then the second and fourth order interference of the two overlapped squeezed lights are analyzed.

0.2 THE MODEL OF THEORY

The squeezed lights generated in OPO1 and OPO2 through type II parametric downconversion are superposed at 50% beam splitter; then the intensity of the resultant field is detected by detectors D_1 and D_2 .

We use the semiclassical approach proposed by Fabre et al.[15] to calculate the interference of the output fields from the OPO cavities and the fluctuations. We consider these field fluctuations to be driven by the vacuum fluctuations entering the cavity through the coupling mirror. Treating the pump light as a classical field and neglecting the dissipation of the pump field and the detuning of the OPO cavities, we can write the C-number Langevin equation of the system as:

$$\tau \dot{\alpha}_1 + (\gamma_1 + \gamma'_1)\alpha_1 = g\varepsilon_0\alpha_2^* + \sqrt{2\gamma_1}\alpha_1^{in} + \sqrt{2\gamma'_1}\alpha_1'^{in} \quad (1a)$$

$$\tau \dot{\alpha}_2 + (\gamma_2 + \gamma'_2)\alpha_2 = g\varepsilon_0\alpha_1^* + \sqrt{2\gamma_2}\alpha_2^{in} + \sqrt{2\gamma'_2}\alpha_2'^{in} \quad (1b)$$

where α_i ($i=1,2$) represent the intracavity signal and idler field amplitudes associated with their annihilation operators, ε_0 is proportional to the amplitude of the classical pump field, τ is the cavity round-trip time for the signal and idler modes, g is the nonlinear coupling parameter that depends on the second order nonlinear coefficient $\chi^{(2)}$ of the intracavity medium, γ_i is related to the losses of the output mirror of the cavity, and γ'_i depends on the absorption and scattering losses of the crystal as well as on the losses of the other cavity mirrors. In the following calculations we assume that $\gamma_1 = \gamma_2 = \gamma$ and $\gamma'_1 = \gamma'_2 = \gamma'$, and we take g, γ and γ' as real quantities, i.e., the phase shift of the light field in the cavities is not considered. and α_i^{in} and $\alpha_i'^{in}$ are the field amplitudes of the injected noise from the output and the input mirrors respectively.

Taking $\alpha_i^{in} = \alpha_i'^{in} = 0$, we easily obtain the threshold pump power from Equ.(1):

$$|\varepsilon_0| = (\gamma - \gamma')/g \quad (2)$$

Solving Equ.(1) in frequency space and using boundary condition, we obtain the output fields of the signal and idler lights:

$$\alpha_1^{out}(\Omega) = \frac{A_1 \alpha_1^{in}(\Omega) + A_1' c_1^{in}(\Omega)}{B} + \frac{A_2^* \alpha_2^{*in}(-\Omega) + A_2'^* c_2^{*in}(-\Omega)}{B} + \frac{A_2' \varepsilon_1^* + A_1' \varepsilon_1}{B} \quad (3a)$$

$$\alpha_2^{out}(\Omega) = \frac{A_1 \alpha_2^{in}(\Omega) + A_1' c_2^{in}(\Omega)}{B} + \frac{A_2^* \alpha_1^{*in}(-\Omega) + A_2'^* c_1^{*in}(-\Omega)}{B} + \frac{A_2' \varepsilon_1^* + A_1' \varepsilon_2}{B} \quad (3b)$$

where, $A_1 = \gamma^2 - (\gamma' - i\Omega\tau)^2 + g^2 |\varepsilon_0|^2$, $A_1' = 2[(\gamma + \gamma') - i\Omega\tau] \sqrt{\gamma\gamma'}$,
 $A_2 = 2g\varepsilon_0\gamma$, $A_2' = 2g\varepsilon_0\sqrt{\gamma\gamma'}$, $B = [(\gamma + \gamma') - i\Omega\tau]^2 - g^2 |\varepsilon_0|^2$

We assume that the configuration for OPO1 and OPO2 are completely identical, so all expressions obtained for OPO1 can be used for OPO2 if we replace α by β , while the injected signal and noise obeys the following relations:

$$\begin{aligned} [\alpha_i^{in}(\Omega), \alpha_j^{*in}(-\Omega')] &= \delta_{ij} \delta(\Omega + \Omega'), [\alpha_i'^{in}(\Omega), \alpha_j'^{*in}(-\Omega')] = |\varepsilon_0|^2 \delta_{ij} \delta(\Omega + \Omega'), \\ [\alpha_i^{in}(\Omega), \alpha_j^{in}(\Omega')] &= 0, [\alpha_i'^{in}(\Omega), \alpha_j'^{in}(\Omega')] = 0, [\alpha_i^{*in}(-\Omega), \alpha_j^{*in}(-\Omega')] = 0, \\ [\alpha_i^{*in}(-\Omega), \alpha_j'^{*in}(-\Omega')] &= 0, \end{aligned}$$

The output fields from OPO1 and OPO2 are

$$c = \frac{\alpha_1^{out} + \alpha_2^{out}}{\sqrt{2}}, d = \frac{\beta_1^{out} + \beta_2^{out}}{\sqrt{2}} \quad (4)$$

The superposition field of the two output fields from OPO1 and OPO2 through beam splitter M2 can be expressed as

$$D_1 = \frac{ce^{-i\omega t} + id}{\sqrt{2}}, D_2 = \frac{ice^{-i\omega t} + d}{\sqrt{2}} \quad (5)$$

The average photon flux at the detector is

$$R = \langle D_1^* D_1 \rangle = \frac{g^2 |\varepsilon_0|^2 \gamma}{\tau [(\gamma + \gamma')^2 - g^2 |\varepsilon_0|^2]} + \frac{1}{\tau^2} \left\{ 8\pi\gamma\gamma' |\varepsilon_1|^2 + 8\pi\gamma\gamma' |\varepsilon_1|^2 \cos(\omega t + \Delta\Psi) \right\} \quad (6)$$

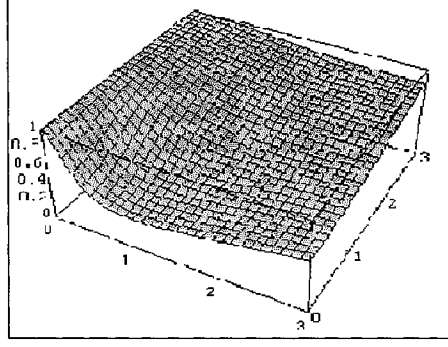


Figure 1:

It is obviously seen that there is no interference in the usual sense when there is no injected signals ($|\varepsilon_1|^2 = 0$).

Next, we show the spectral analyses of the fourth order interference without the injected signals. In this case, the coincidence measurement of two photons is applied to detect the effect. The coincidence rate is then propotional to the quantity:

$$R_4(\Omega) = \langle D_1^* D_1 D_2^* D_2 \rangle = \frac{1}{|B|^4} \{ 32g^4 |\varepsilon_0|^4 \gamma^2 (\gamma + \gamma')^2 + 4g^2 |\varepsilon_0|^2 \gamma^2 [(\gamma + \gamma')^2 + \Omega^2 \tau^2 + g^2 |\varepsilon_0|^2]^2 + 4g^2 |\varepsilon_0|^2 \gamma^2 [(\gamma + \gamma')^2 + \Omega^2 \tau^2 + g^2 |\varepsilon_0|^2]^2 \cos 2\omega t \} \quad (7)$$

The fourth-order interference is just defined by the phase delay (ωt) between two squeezed lights, but not depend on the phase of pump power, which is good matched with the result in the literature[16].

The visibility as a function of normalized pump power and analyzed frequency is depicted in Fig. 1. It is shown that the visibility takes the minimum value of 33.3% at the frequency of zero and the threshold pump power. The visibility increase along with the pump power taking the value of away from the threshold and at the high analysis frequency. This effect is in accordance with the descriptions in the Ref.[17], in which it is shown that the maximum intensity correlation exists between two perfect random lights. The phase squeezed light is a photon bunched state in which the randomness is smaller, so the intensity correlation between them reduces. The maximum degree of quadrature phase squeezing is obtained at the threshold and the zero analysis frequency, in the mean while the maximum bunching of photon numbers happens, that lead to the minimum intensity correlation between the two outputs from OPO1 and OPO2. The forth-order interference depends on the intensity correlation, so the visibility reduces to the minimum.

0.3 SUMMARY

We have studied the second and forth-order interference effect between two squeezed lights produced by two OPOs pumped by a common laser source. The calculation results show:

1. Without the injected signal the second-order interference is not present. There is fourth-order quantum interference between the two squeezed state light fields, at the oscillation threshold of OPOs the squeezing of two output fields is highest but the fringe visibility is lowest. When the pump power is away from the threshold the squeezing decreases while the visibility increases. 2. When two coherent subharmonic signals are injected respectively into the two OPOs, the output squeezed fields interfere in the usual sense. The interference pattern depends only on the phase difference between the propagation times from two OPOs to the observing point.

References

- [1] M.Xiao, L.A.Wu and H.J.Kimble, Phys. Rev.Lett., **59**,278(1987).
- [2] P.Grangier, R.E.Slusher, B.Yurke et al, Phys.Rev.Lett, **59**, 2153(1987).
- [3] K.C.Peng, Q. Pan, H.Wang et al., Appl.Phys.B, **66**, 755(1998).
- [4] M.Tan, D.F.Walls and M.J.Collett, Phys.Rev.Lett., **66**, 252(1991).
- [5] L. Hardy, Phys.Rev.Lett., **73**, 2279(1994).
- [6] S.C.H.Bennett, Phys.Today, **48**,24(1995).
- [7] C.H.Bennett, G.Prassard, Phys.Rev.Lett., **70**, 1895(1993).
- [8] R.Ghosh and L.Mandel, Phys.Rev.Lett., **59**,1903(1987).
- [9] Z.Y.Ou and L.Mandel, Phys.Rev.Lett., **62**,2941(1989).
- [10] P.G.Kwiat, W.A.Vareka, C.K.Hong et al, Phys.Rev.A, **41**, 2910(1990).
- [11] Z.Y.Ou, X.Y.Zou, L.J.Wang et al, Phys.Rev.A, **42**, 2957(1990).
- [12] P.Grangier, M.J.Potasek and B.Yurke, Phys.Rev.A, **38**, 3132(1988).
- [13] S.L.Braunstein and A.Mann, Phys.Rev.A, **51**, R1727(1995).
- [14] B.Yurke and D.Stoler, Phys.Rev.Lett., **68**, 1251(1992).
- [15] C.Fabre, E.Giacobino, A.Heidmann et al, J.Phys. **50**, 1209(1989).
- [16] Z.Y.Ou, Phys.Rev.A, **37**, 1607(1988).
- [17] K.Saxena, D.S.Metha, H.C.Kandpal et al., Opt. Commun., **111**, 423(1994)

Figure caption

Fig.1 The visibility vs the normalized pump power and analysis frequency

The Low Frequency Facility: present status and near future plan

*F. Benabid, V. Chickarmane, A. Di Virgilio, A. Gaddi, A. Giazotto, P. La Penna,
D. Passuello and Z. Zhang*

INFN-Pisa, San Piero a Grado (Pisa), Italy.

Abstract

The Low Frequency Facility (LFF), an R&D VIRGO project experiment, plans to measure the thermal noise of two mirrors suspended to the last stage of the R&D super-attenuator (SA), with a similar suspension performance to that of Virgo. The expected displacement sensitivity is 10^{-18} m/Hz^{1/2}. Present status and near future plan are described.

Introduction and sketch of the experiment

Direct thermal noise measurement is doubly important and its direct observation is a topic of current interest¹. Firstly, because suspension and mirror internal thermal noise is the ultimate fundamental noise of the Laser Interferometric Gravitational Waves (LIGW) detectors in the intermediate frequency range². Secondly, it will allow us to have a wide spectrum of thermal noise, which represents by itself a considerable scientific breakthrough³. In VIRGO, Low Frequency Facility project (LFF)⁴ is under progress. It aims to study the thermal noise of suspension systems as well as of mirror substrates. It consists of suspending a Fabry-Perot cavity to the R&D SA, which is identical to the VIRGO super-attenuator. It has already been built, and is being used for Virgo tests. It will become part of the Low Frequency Facility in a very short time.

The VIRGO suspension⁵ system, which works by suspending a cascade of several mechanical filters, is expected to considerably reduce the seismic noise above a few Hz. The SA has been designed with three roles in mind: to isolate the test mass from environmental noise, to exhibit the minimum possible thermal noise level and finally to control the test mass position in order to keep the interferometer at its working point.

The highest noise source in the frequency range up to a few hundred Hz is the seismic noise, which are reduced by the SA by more than a factor 10^{12} . There have recently been many proposals to improve the sensitivity of the suspension due to thermal noise, such as cryogenic cooling, low loss test mass materials and novel noise cancellation techniques³. A very high sensitivity experiment devoted to studying methods to reduce the thermal noise level is therefore of enormous importance.

In Figure 1 we show a design of the apparatus: the R&D SA supporting the two mirrors of the Fabry-Perot cavity, and the table with the optical components from which a stabilized laser is injected into the cavity. The injection table is only 1m diameter in order to put the whole experiment set-up under vacuum.

The thermal noise measured at the mirror depends⁶ on the last stage of the suspension and the mirror itself. Finally the control of the mirror position is handled by special parts of the SA: the inverted pendulum⁷, the marionetta and the reference mass. These two last elements of the SA

can be important for the thermal noise itself since they are very close to the test mass. The essential idea is to suspend to the SA a very high finesse Fabry-Perot cavity in which one of the mirrors is the standard VIRGO mirror (VM), suspended and controlled by the SA, and the other mirror, which we call auxiliary (AX), will also be suspended to the SA⁸. The AX mirror will be much smaller than the VM, so in order to reduce the displacement noise due to the radiation pressure of the stored light in the cavity, it will be loaded with an extra mass, thus forming a double pendulum. It will be attached to the last seismic filter of the R&D SA in a similar way as the VM. The F-P cavity will act as a displacement transducer and allow the measurement of the combined thermal noise of the VM and the AX; the expected displacement power spectrum sensitivity is 10^{-18} m/Hz^{1/2}. The planned cavity has 1 cm length and finesse 3000, while the frequency stabilization has to be at the level of 10^{-1} Hz/Hz^{1/2}.

The LFF is composed of two main parts: the R&D SA and the optics. The tests concerning the R&D SA are described in different papers and in Virgo Notes in preparation. For a detailed description of this experiment the reader should take a look to reference⁴. In the present paper we focus on the experimental results obtained so far for the optical lay-out⁹ and the laser stabilization, and we outline the very near future plan.

Tests of the optical lay-out

Figs. 2a and 2b show the optical lay-out, composed of a frequency stabilised laser injected into a Fabry-Perot cavity. Excluding the displacement transducer cavity, which is suspended to the SA, all the optics sit on a round table of 1m diameter in order to fit inside a vacuum tank, and machined from a single piece of steel.

There are two main independent optical circuits: the Fabry-Perot transducer and the frequency stabilisation circuits, they have been separately assembled and tested so far.

Transducer cavity:

Fig. 3 shows the experimental set-up: a 2 cm long plane-concave cavity, with plane input mirror. The radius of curvature of the curved mirror was 3.8 cm, so the waist was about 80 μ m. The F of this cavity was about 2,000. The mirrors, of 1/2 inches diameter, were mounted in a steel cage of INVAR bars. The curved mirror was fixed on a mirror mount for laser cavity (Oriel). The plane mirror was mounted on a piezo (PZT) tube, also on a laser mount, on which the longitudinal feedback was applied. Two steering mirrors mounted before the cavity on three piezo actuators (Physik Instrumente) controlled the input beam. The laser source was a Nd:YAG 500 mW MISER (LightWave), $\lambda=1.064$ μ m. The frequency jitter $\delta\nu(f)$ of the laser had been separately measured by locking it on a ULE (Ultra Low Expansion) triangular cavity and extracting the correction signal inside the locking bandwidth (more than 200 kHz). It yielded about 1.4 kHz/ $\sqrt{\text{Hz}}$ at 10 Hz, with a $1/f$ trend from at least 0.1 Hz to 10 kHz. The well-known Pound-Drever-Hall¹⁰ technique has been used to extract the longitudinal signal. The phase modulation frequency for the locking on the 2 cm cavity was 11 MHz, with about 4% of power in each side band.

The digital filters developed in the INFN-Virgo laboratories in Pisa⁵ has been used for signal acquisition, processing and feedback generation; controlled by computer. The bandwidth of the loop was about 1700 Hz and the open loop gain was about 10^4 at 10 Hz. The power spectrum of the correction signal is a measure of the cavity displacement sensitivity $\delta x_{\text{cav}}(f)$: the value at 10

Hz is about 3×10^{-13} m/ $\sqrt{\text{Hz}}$. This value is in agreement with the expected sensitivity limit imposed by the laser frequency jitter ($\delta x_{\text{LAS}}(f) = x_0 \times \delta v(f) / v_0$, where x_0 is the cavity length and v_0 is the laser frequency).

The transducer cavity has to be kept aligned using signal extracted by the cavity itself. This is called wave-front sensing, a detailed theoretical analysis of the behavior of signals in function of the Gouy phase shift has been done and compared with the experimental results⁹. For the experimental test the same cavity used in the longitudinal control experiment has been used. It has been locked by using signal extracted with the so called Ward method¹³.

We performed the locking of the translation degree of freedom of the 2 cm cavity (see fig. 4). The quadrant photodiode was situated at $\Phi \approx 90^\circ$, where only the translation signal is detected. The feedback was actuated on the two steering mirrors. The displacement sensitivity in the error signal was measured sending a known modulation to the piezo and detecting the peak in the error signal at the same frequency with a spectrum analyzer. The same results were obtained for the horizontal degree of freedom. In both cases the unitary gain of the closed loop gain was about few hertz. The noise reduction was more than one order of magnitude, and the residual translation between cavity axis and beam results about 10^{-7} times w_0 . The noise level of the power spectrum at 10 Hz was about 3×10^{-14} m/ $\sqrt{\text{Hz}}$.

Frequency stabilization

Our experimental set-up for laser frequency stabilization is fully described in¹¹. A 400 mW Nd:Yag MISER is locked to a high finesse ring cavity (19000) using P-D-H technique. The frequency fluctuations is corrected using a servo which drives the Laser PZT and thermal control as well as an electro-optic modulator to cover a wide frequency range (>1 MHz). Figure 4 shows the frequency stabilization level, measured relatively to the U.L.E. reference cavity. A level of less than 10^{-3} Hz/ $\sqrt{\text{Hz}}$ is achieved which is compatible with the expected shot noise level.

Moreover, we measured the power fluctuation while the laser is locked, and shows a level of 10^{-6} / $\sqrt{\text{Hz}}$.

Near Future plan and Conclusions

We have reported the main principle of the Low Frequency Facility and summarized the results obtained in our laboratory to build the optical part of the experiment.

We have extracted all the control signal (longitudinal, angular and translation), from a 2 cm cavity (Finesse 2000), the longitudinal signal has been extracted with the Pound-Drever technique; and the wave-front sensing (Ward technique) has been applied to extract all the other signals to keep the cavity in its working point. Moreover a full control of the cavity has been done using the digital filter which will be used in our experiment. It has been checked that the displacement sensitivity of the Fabry-Perot transducer is limited by the frequency jitter of the laser, and is 10^{-13} m/Hz^{1/2}. Frequency stabilization of the laser relative to the reference cavity has been measured to be below 10^{-1} Hz/Hz^{1/2}.

In the near future, we plan to complete and study the whole optical layout, before installation in front of the R&D SA. This test, together with the tests on the control of the R&D SA, will give detailed information on the control procedure of the whole experiment.

At present the R&D SA is being used for tests on the control of the suspended test mass. At a later stage, it will be wholly dedicated to the LFF (approximately spring 2000).

The LFF expected displacement sensitivity 10^{-18} m/ $\sqrt{\text{Hz}}$ is enough to probe the thermal noise of the test mass suspension. In order to reach the mirror substrate itself thermal noise it will be necessary to improve the sensitivity. Since the transducer is limited by the frequency noise of the Laser, a possibility to improve the sensitivity will be to make the cavity very short. The theory of a very short cavity has been studied in ref. ¹².

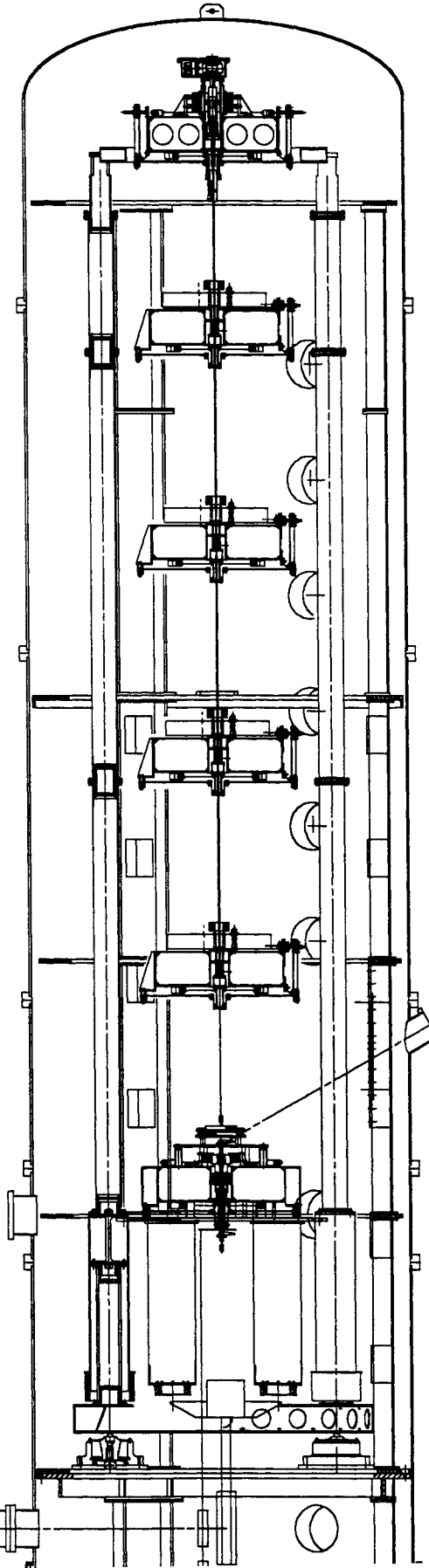
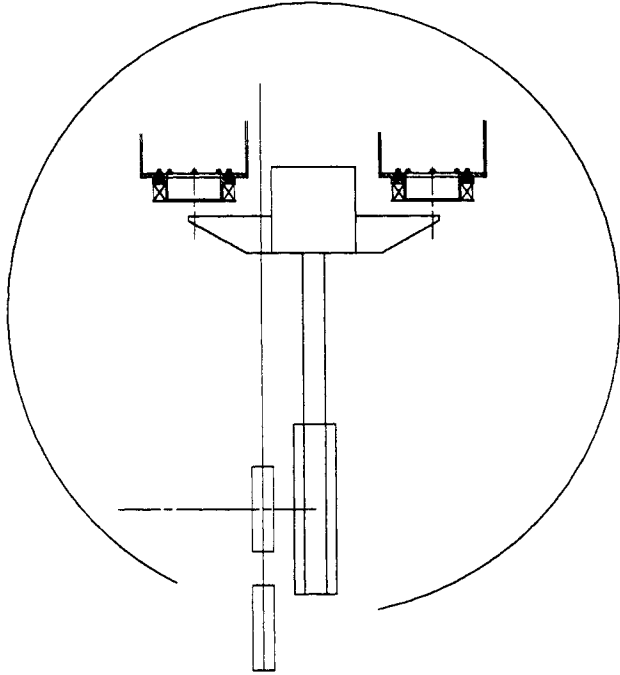
We expect that such an accurate measurement of the thermal noise of the suspension, will throw light on the fundamental dissipation processes in suspension systems, and will help in the future development of suspension for large gravitational wave interferometric detectors, based on Earth.

REFERENCES:

- 1) see articles in: ", in Gravitational Waves, second Edoardo Amaldi Conference (Geneva 1-4 July 1997), Vol. 4, editors: E. Cocchia, G. Veneziano and G. Pizzella, World Scientific.
- 2) A. Giazotto, "Interferometric detection of gravitational waves", Physics Report, 182(6), November 1989.
- 3) see for example:
N. Mio and K. Tsubono, Appl. Optics, 34 n.1m pg. 186,(1995)
L. Conti *et al.*, Rev. Sc. Instr. 69, 554-558 (1998)..
Y. Hadjar, quant-ph/990/56.
T. Uchiyama *et al.*, ICRR-410-98-6, Feb 1998. 8pp.
L. Ju *et al.*, Phys.Lett.A218:197-206,1996
F. Bondu *et al.*, Phys.Lett.A246:227-236,1998
V.B. Braginsky *et al.*, e-Print Archive: gr-qc/9805031
- 4) see for example:
Virgo note: "Proposal R&D in suspension for interferometric gravitational wave detection", VIR-NOT-PIS-8000-101
A. Di Virgilio *et al.*: "A facility to measure the displacement noise of mirrors suspended as in the Virgo antenna", in Gravitational Waves, Vol. 4, pg. 339-350, editors: E. Cocchia, G. Veneziano and G. Pizzella, World Scientific.
F. Benabid *et al.*, "The Low Frequency Facility, R&D experiment of the Virgo Project", Submitted paper
- 5) Virgo Collaboration, FCD (Final Conceptual Design), May 1997.
- 6) Gammaitoni, Kovalik, Punturo, "The Virgo sensitivity curve", NOT-PER-1390-84, 30-3 1997
- 7) G. Losurdo *et al.*: "Review of Scientific Instruments, 70 (5), p.2507-2515 (May 1999)
- 8) G. Cella *et al.*, "Suspension for the Low Frequency Facility", submitted paper
- 9) A. Di Virgilio *et al.*, "Reflected wave front sensing signal computation and experimental digital control of a plane-concave cavity", submitted for publication.
- 10) R.W.P. Drever *et al.*, App. Phys. B 31, 97-105 (1983)
- 11) F. Bondu *et al.*, Optics Letters 21 (8), 582-584 (1996)
- 12) P. LaPenna *et al.*, "Transmittivity profile of high finesse PPF cavities illuminated by Gaussian beam", Opt. Comm., accepted for publication.
- 13) E. Morrison, B. J. Meers, D. I. Robertson *et al.*, Applied Optics 33 (2), 5037-5049 (1994).

R&D SuperAttenuator

enlarged view
of the suspended
Fabry-Perot



Injection Bench

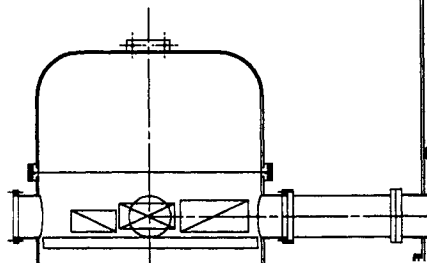


FIG 1

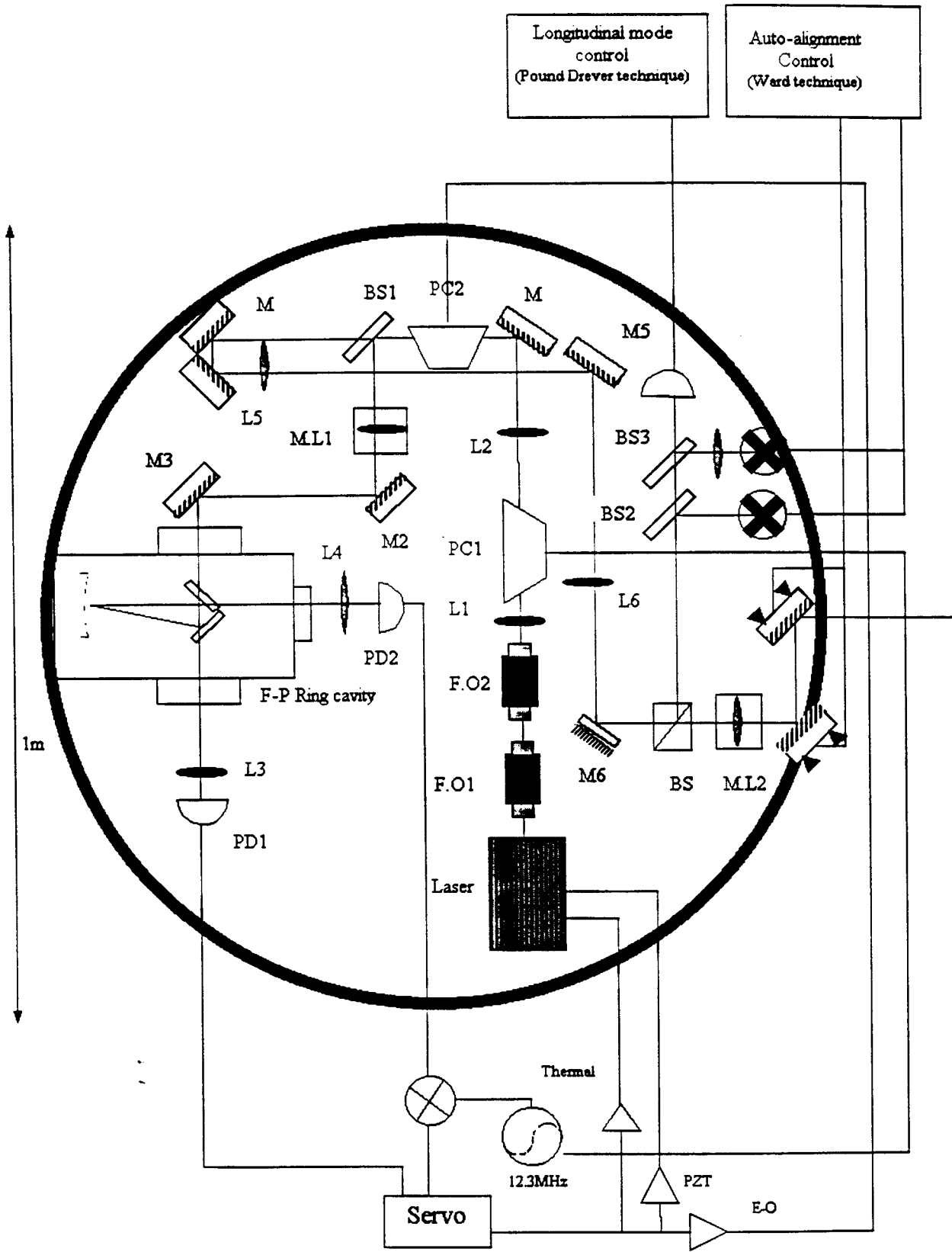
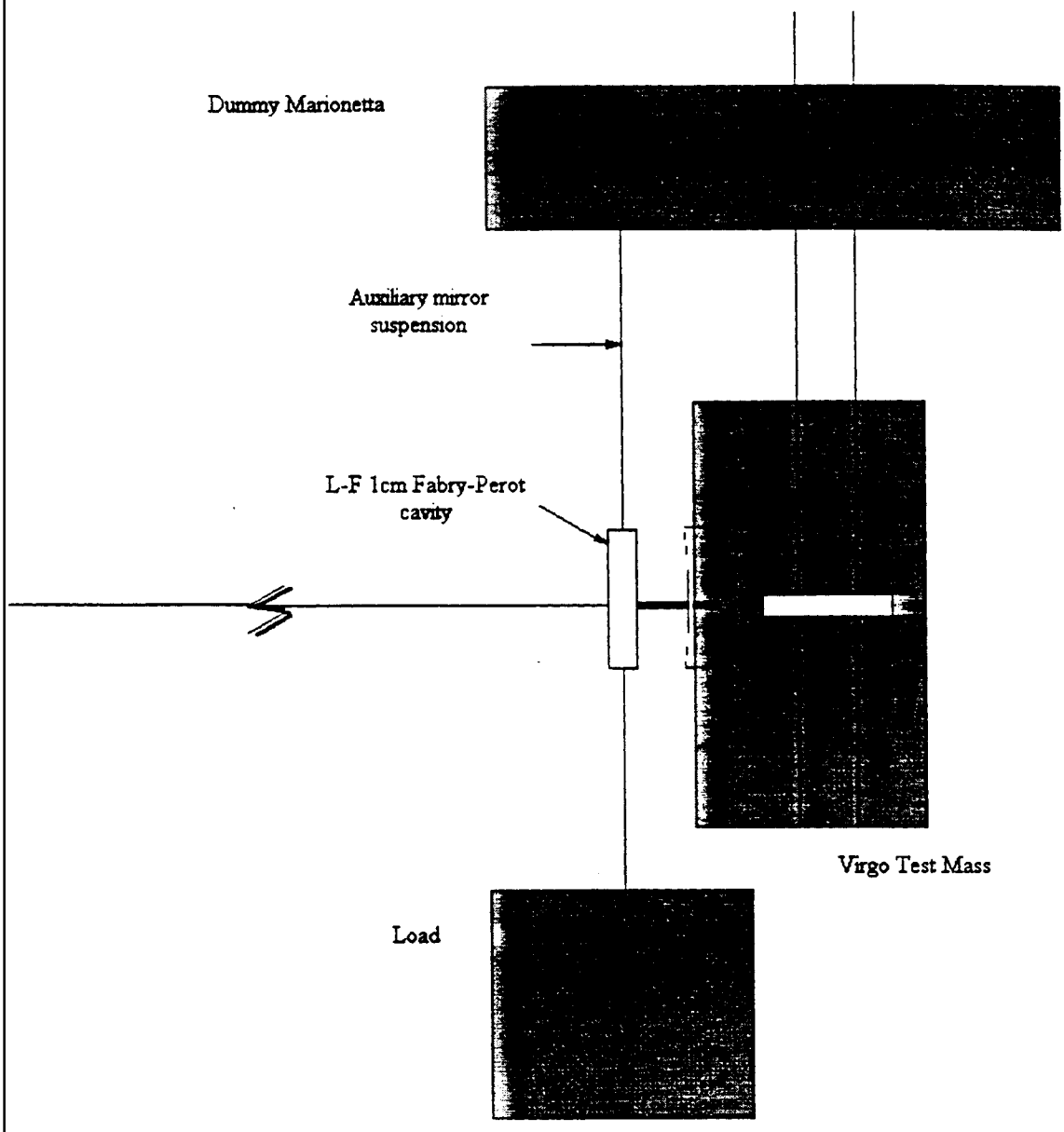


Fig 2a



Dummy Marionetta

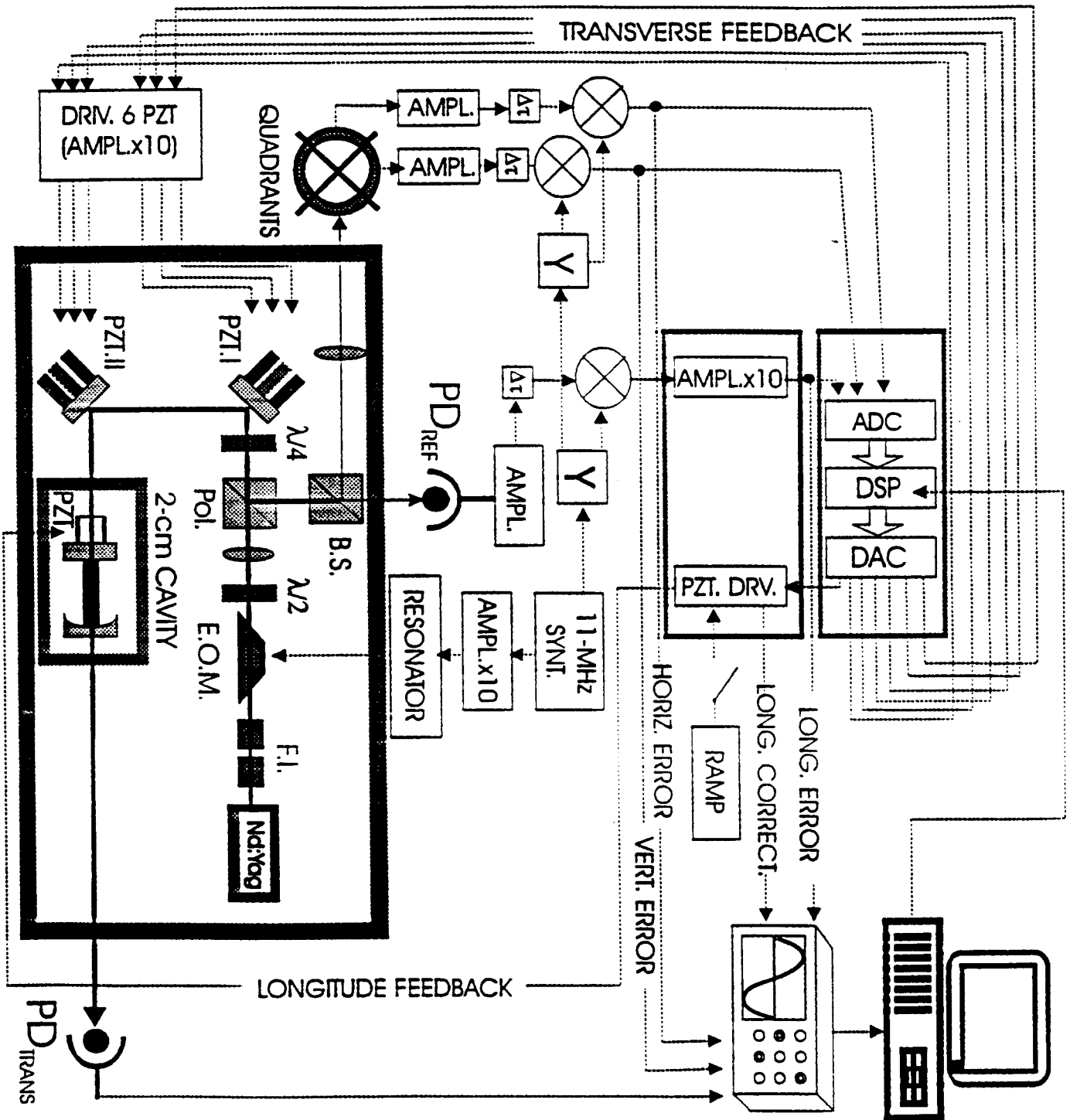
Auxiliary mirror suspension

L-F 1cm Fabry-Perot cavity

Virgo Test Mass

Load

Fig 2b



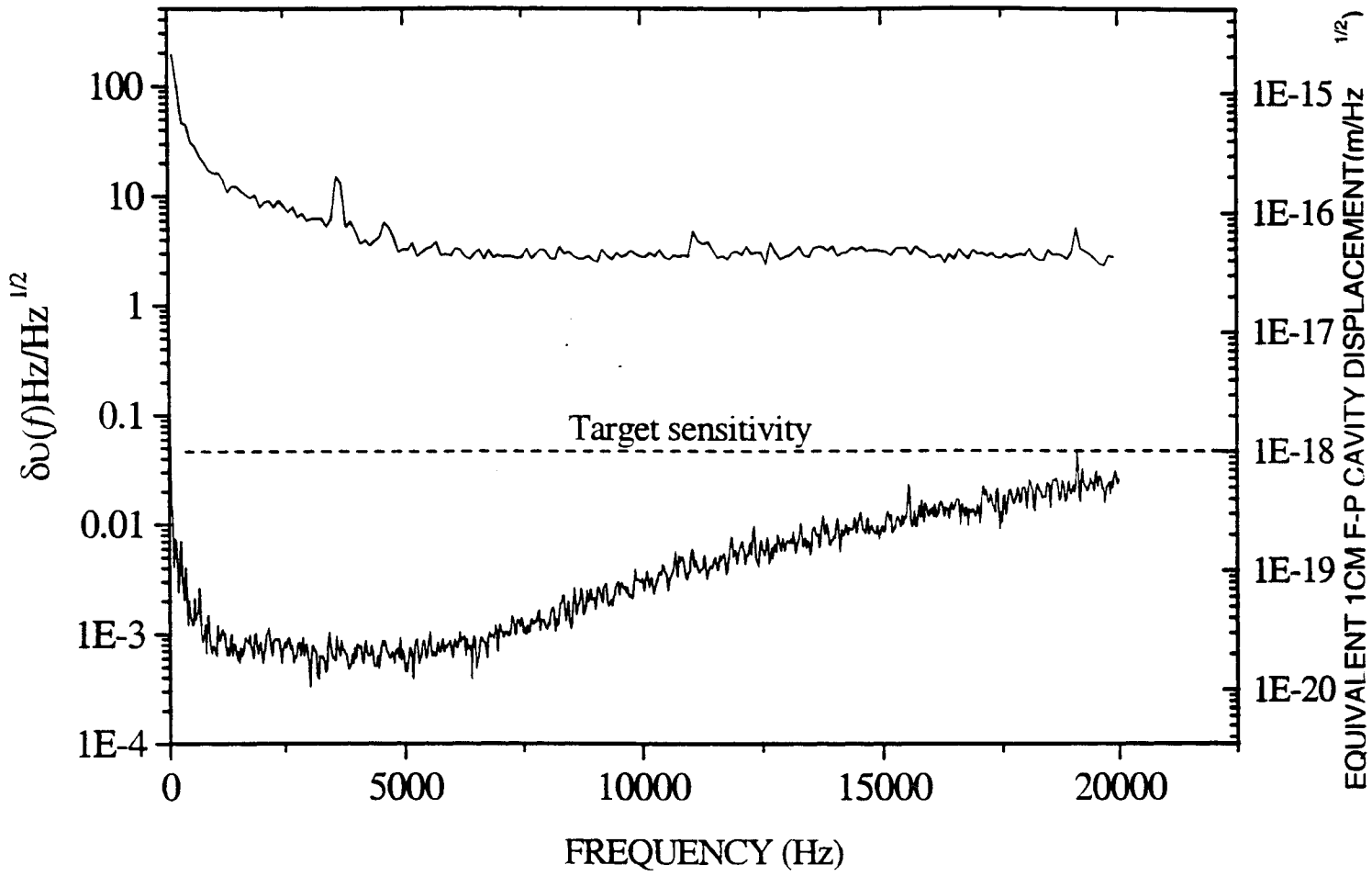


Fig 4

REPORT DOCUMENTATION PAGEForm Approved
OMB No. 0704-0188

Public reporting burden for this collection of information is estimated to average 1 hour per response, including the time for reviewing instructions, searching existing data sources, gathering and maintaining the data needed, and completing and reviewing the collection of information. Send comments regarding this burden estimate or any other aspect of this collection of information, including suggestions for reducing this burden, to Washington Headquarters Services, Directorate for Information Operations and Reports, 1215 Jefferson Davis Highway, Suite 1204, Arlington, VA 22202-4302, and to the Office of Management and Budget, Paperwork Reduction Project (0704-0188), Washington, DC 20503.

1. AGENCY USE ONLY (Leave blank)		2. REPORT DATE July 2000	3. REPORT TYPE AND DATES COVERED Conference Publication	
4. TITLE AND SUBTITLE Sixth International Conference on Squeezed States and Uncertainty Relations			5. FUNDING NUMBERS 930	
6. AUTHOR(S) D. Han, Y.S. Kim, and S. Solimeno, Editors				
7. PERFORMING ORGANIZATION NAME(S) AND ADDRESS (ES) Goddard Space Flight Center Greenbelt, Maryland 20771			8. PERFORMING ORGANIZATION REPORT NUMBER 2000-03479-0	
9. SPONSORING / MONITORING AGENCY NAME(S) AND ADDRESS (ES) National Aeronautics and Space Administration Washington, DC 20546-0001			10. SPONSORING / MONITORING AGENCY REPORT NUMBER CP—2000—209899	
11. SUPPLEMENTARY NOTES Y.S. Kim: University of Maryland, College Park, Maryland; S. Solimeno, Universita di Napoli, Naples, Italy				
12a. DISTRIBUTION / AVAILABILITY STATEMENT Unclassified—Unlimited Subject Category: 74 Report available from the NASA Center for AeroSpace Information, 7121 Standard Drive, Hanover, MD 21076-1320. (301) 621-0390.			12b. DISTRIBUTION CODE	
13. ABSTRACT (Maximum 200 words) <p>These proceedings contain contributions from about 200 participants to the 6th International Conference on Squeezed States and Uncertainty Relations (ICSSUR'99) held in Naples May 24–29, 1999, and organized jointly by the University of Naples “Federico II,” the University of Maryland at College Park, and the Lebedev Institute, Moscow. This was the sixth of a series of very successful meetings started in 1990 at the College Park Campus of the University of Maryland. The other meetings in the series were held in Moscow (1992), Baltimore (1993), Taiyuan P.R.C. (1995) and Balatonfuered, Hungary (1997). The present one was held at the campus Monte Sant’Angelo of the University “Federico II” of Naples. The meeting sought to provide a forum for updating and reviewing a wide range of quantum optics disciplines, including device developments and applications, and related areas of quantum measurements and quantum noise.</p>				
14. SUBJECT TERMS Squeezed states, uncertainty relations, quantum optics, group theory, information theory.			15. NUMBER OF PAGES 592	
			16. PRICE CODE	
17. SECURITY CLASSIFICATION OF REPORT Unclassified	18. SECURITY CLASSIFICATION OF THIS PAGE Unclassified	19. SECURITY CLASSIFICATION OF ABSTRACT Unclassified	20. LIMITATION OF ABSTRACT UL	